Cast-in-Place Concrete Connections for Precast Deck Systems

DETAILS

AUTHORS

ACKNOWLEDGMENT

This work was sponsored by the American Association of State Highway and Transportation Officials (AASHTO), in cooperation with the Federal Highway Administration, and was conducted in the National Cooperative Highway Research Program (NCHRP), which is administered by the Transportation Research Board (TRB) of the National Academies.

COPYRIGHT INFORMATION

Authors herein are responsible for the authenticity of their materials and for obtaining written permissions from publishers or persons who own the copyright to any previously published or copyrighted material used herein.

Cooperative Research Programs (CRP) grants permission to reproduce material in this publication for classroom and not-for-profit purposes. Permission is given with the understanding that none of the material will be used to imply TRB, AASHTO, FAA, FHWA, FMCSA, FTA, Transit Development Corporation, or AOC endorsement of a particular product, method, or practice. It is expected that those reproducing the material in this document for educational and not-for-profit uses will give appropriate acknowledgment of the source of any reprinted or reproduced material. For other uses of the material, request permission from CRP.

DISCLAIMER

The opinions and conclusions expressed or implied in this report are those of the researchers who performed the research. They are not necessarily those of the Transportation Research Board, the National Research Council, or the program sponsors.

The information contained in this document was taken directly from the submission of the author(s). This material has not been edited by TRB.

THE NATIONAL ACADEMIES
Advisers to the Nation on Science, Engineering, and Medicine

The **National Academy of Sciences** is a private, nonprofit, self-perpetuating society of distinguished scholars engaged in scientific and engineering research, dedicated to the furtherance of science and technology and to their use for the general welfare. On the authority of the charter granted to it by the Congress in 1863, the Academy has a mandate that requires it to advise the federal government on scientific and technical matters. Dr. Ralph J. Cicerone is president of the National Academy of Sciences.

The **National Academy of Engineering** was established in 1964, under the charter of the National Academy of Sciences, as a parallel organization of outstanding engineers. It is autonomous in its administration and in the selection of its members, sharing with the National Academy of Sciences the responsibility for advising the federal government. The National Academy of Engineering also sponsors engineering programs aimed at meeting national needs, encourages education and research, and recognizes the superior achievements of engineers. Dr. Charles M. Vest is president of the National Academy of Engineering.

The **Institute of Medicine** was established in 1970 by the National Academy of Sciences to secure the services of eminent members of appropriate professions in the examination of policy matters pertaining to the health of the public. The Institute acts under the responsibility given to the National Academy of Sciences by its congressional charter to be an adviser to the federal government and, on its own initiative, to identify issues of medical care, research, and education. Dr. Harvey V. Fineberg is president of the Institute of Medicine.

The **National Research Council** was organized by the National Academy of Sciences in 1916 to associate the broad community of science and technology with the Academy's purposes of furthering knowledge and advising the federal government. Functioning in accordance with general policies determined by the Academy, the Council has become the principal operating agency of both the National Academy of Sciences and the National Academy of Engineering in providing services to the government, the public, and the scientific and engineering communities. The Council is administered jointly by both Academies and the Institute of Medicine. Dr. Ralph J. Cicerone and Dr. Charles M. Vest are chair and vice chair, respectively, of the National Research Council.

The **Transportation Research Board** is one of six major divisions of the National Research Council. The mission of the Transportation Research Board is to provide leadership in transportation innovation and progress through research and information exchange, conducted within a setting that is objective, interdisciplinary, and multimodal. The Board's varied activities annually engage about 7,000 engineers, scientists, and other transportation researchers and practitioners from the public and private sectors and academia, all of whom contribute their expertise in the public interest. The program is supported by state transportation departments, federal agencies including the component administrations of the U.S. Department of Transportation, and other organizations and individuals interested in the development of transportation. **www.TRB.org**

www.national-academies.org

Acknowledgments

Abstract

This report contains recommended design specifications, construction specifications, and five illustrative examples of durable CIP reinforced concrete connections for precast deck systems that emulate monolithic construction, considering issues including speed of construction, durability, and fatigue. Included in the report is the supporting research that led to these recommendations. This research focused on systems that reduce the need to place and remove formwork thus accelerating on-site construction and improving safety. The three systems considered to accomplish these objectives were: (1) a precast composite slab span system (PCSSS) for short to moderate span structures, (2) full-depth prefabricated concrete decks, and (3) deck joint closure details (e.g., decked-bulb-tee (DBT) flange connections) for precast prestressed concrete girder systems for long span structures. Depending on the system, the connections are either transverse (i.e., across the width of the bridge) or longitudinal (i.e., along the length of the bridge). The first system, PCSSS, is an entire bridge system; whereas the other two systems investigated in the project represented transverse and longitudinal joint details to transfer moment and shear in precast deck panels and flanges of decked bulb tees. Two types of connection concepts were explored with these details, looped bar details and two layers of headed bar details.

Contents

v

List of Tables

x

xiii

List of Figures

xiv

xv

xvii

xviii

xxiii

Executive Summary

Introduction

The aging highway bridge infrastructure in the United States is subjected to increasing traffic volumes and must be continuously renewed while accommodating traffic flow. Speed of construction, especially for the case of bridge replacement and repair projects, is a critical issue. Disruption of traffic and inconvenience to motorists, let alone major safety issues arising from detours, has encouraged the development of rapid construction methods. The issue of speed of construction, combined with higher labor costs and more variable quality control associated with on-site concrete casting, construction and motorist safety issues, political pressures, and environmental concerns, has paved the way for further increase in the use of precast elements to speed construction.

Depending on the specific site conditions, the use of prefabricated bridge systems can minimize traffic disruption, improve work-zone safety, minimize impact to the environment, improve constructability, increase quality, and lower life-cycle costs. This technology is applicable and needed for both existing bridge replacement and new bridge construction. For many deficient bridges in the United States on the waiting list for replacement, it is imperative that new bridge construction be as economical as possible and yet be long lasting and nearly maintenance free.

The focus of this study was to develop design specifications, construction specifications, and examples for the design and construction of durable CIP reinforced concrete connections for precast deck systems that emulate monolithic construction, considering issues including durability and fatigue, while increasing speed of construction. The typical sequence of erecting bridge superstructures in the United States is to erect the precast prestressed concrete or steel beams, place either temporary formwork or stay-in-place formwork such as steel or concrete panels, place deck reinforcement, cast deck concrete, and remove formwork if necessary. This project focused on systems that reduce the need to place and remove formwork thus accelerating on-site construction and improving safety.

The three systems considered to accomplish these objectives were identified during a 2004 Prefabricated Bridge Elements and Systems International Scanning tour. These systems included: (1) a precast composite slab span system (PCSSS) for short to moderate span structures based on the French Poutre Dalle system, (2) full-depth prefabricated concrete decks, and (3) deck joint closure details (e.g., decked-bulb-tee (DBT) flange connections) for precast prestressed concrete girder systems for long-span structures. Each system uses precast elements that are brought to the construction site ready to be set in place and quickly joined together. Depending on the system, the connections are either transverse (i.e., across the width of the bridge) or longitudinal (i.e., along the length of the bridge). The first system, PCSSS, is an entire bridge system; whereas the other two systems investigated in the project represented transverse and longitudinal joint details to transfer moment and shear in precast deck panels and flanges of decked bulb tees. Because of the similarities in the latter two types of systems, they are grouped together in the report. Two types of connection concepts were explored with these details, looped bar details and two layers of headed bar details. Although both types of systems performed adequately in initial tests, the looped bar systems were deemed to be more practical for construction purposes and were investigated in the subsequent tests.

Because this report covers two very different systems: (1) the precast composite slab-span system (PCSSS), which is an entire bridge system, and (2) transverse and longitudinal cast-in-place connection concepts to transfer moment and shear between precast deck panels and the flanges of precast decked bulb-Ts. The executive summary, as well as the report, is separated accordingly.

Precast Composite Slab Span System: Introduction

Precast composite slab span systems (PCSSS) are a promising technology for the implementation of accelerated construction techniques for bridge construction. The bridge systems are composed of precast, inverted-T sections, fabricated off-site and delivered to the jobsite ready for erection. The inverted-T sections are assembled such that no formwork is required prior to the placement of the CIP deck, which considerably reduces construction time related to the placement and removal of formwork. Transverse load transfer is achieved through the development of transversely oriented reinforcement protruding from the precast members. Furthermore, improved quality of the main superstructure can be achieved due to the rigid quality control associated with the fabrication of precast members, which may be difficult to achieve in cast-in-place (CIP) bridge construction.

Precast Composite Slab Span System: Research Methodology and Findings

Several numerical and experimental investigations were completed and reviewed during the project related to issues of importance to the design and performance of precast composite slab span system (PCSSS) bridges. Included in this review was the work completed during a study commissioned by the Minnesota Department of Transportation which was the first Department of Transportation in the United States to implement this technology. The laboratory bridge specimen utilized during the Minnesota Department of Transportation study was subsequently made available for use with the project described herein.

Numerical studies included an investigation of bursting and spalling stresses in the end zones of precast inverted-T sections, effects of spacing of transverse reinforcement in the joint region, and an investigation of the applicability of current design specifications for slab-type bridges to the design of PCSSS bridges for live load distribution factors and for consideration of effects of skewed supports. The two primary considerations that distinguish PCSSS bridges from slab-span bridges are (1) the required reinforcement to control reflective cracking above the longitudinal joint between the precast flanges, and (2) the effect of time-dependent restraint moments due to the composite nature of the system. With regard to the issue of reflective crack control, in addition to a numerical investigation regarding the effect of the transverse reinforcement, the issue was also studied in laboratory investigations of two large-scale laboratory specimens (i.e., Concept 1 and 2 bridges), as well as in subassemblage test specimens specifically designed to investigate crack control.

The Concept 1 laboratory bridge was a two-span continuous bridge that included variations in a number of parameters including precast flange depth and end zone reinforcement details. It had been instrumented in the study for the Minnesota Department of Transportation to investigate the effects of restraint moment and potential development of reflective cracking. The Concept 1 specimen included No. 6 transverse hooked reinforcement embedded into the precast webs to provide load transfer and crack control in the joint region, as well as No. 5 cage stirrups which contributed to the crack control reinforcement. The nominal maximum spacing between transverse reinforcement was 12 in., similar to the detail of one of the first implementations of PCSSS bridges in the State of Minnesota, the Center City Bridge. The Concept 2 bridge was a simply-supported structure that included variations in the transverse reinforcement details across the precast joint. The horizontal shear reinforcement between the precast web and cast-in-place topping was eliminated in this structure. In the Concept 2 specimen, No. 4 embedded hooked reinforcement was used in the west half of the simple span, while No. 4 straight embedded bars mechanically connected to reinforcement in the precast webs were provided in the east half span. No. 3 cage stirrups were staggered in the Concept 2 laboratory bridge relative to the transverse reinforcement spaced at 18 in. to provide a maximum spacing of 9 in. between transverse reinforcement.

In the research described herein, the performance of both bridge specimens was investigated under various types of loading, including cyclic loading to simulate traffic, loading to simulate environmental effects, and loading to investigate load transfer between adjacent precast panels (both longitudinally and transversely). To simulate environmental effects, the structures were loaded to impose transverse strains above the longitudinal joint between the precast flanges that were observed due to thermal gradient effects in the Center City Bridge which was instrumented in the Minnesota Department of Transportation study. The structures were cycled at these strain levels to simulate more than 100 years of service life due to thermal gradient effects which were found to be much more significant than strains due to traffic loading. Following the cyclic load tests, the bridges were loaded above the nominal design flexural strengths to the limiting capacities of the actuators to investigate the effectiveness of composite action. Following the tests, cores and slices of the bridge were examined to investigate any residual cracks.

In addition to the two large-scale laboratory bridge specimens, six subassemblage specimens were tested to investigate the relative performance of various reflective crack control reinforcement details. The subassemblage specimens were loaded to flexurally induce cracking above the longitudinal joint between the precast flanges. The size, quantity, and location of cracking were documented through a range of quasi-static and cyclic load tests. The subassemblages were instrumented internally to investigate the location of the crack along the depth and through the thickness of the structure. The results obtained from the internal instrumentation were compared to visual observations of crack initiation, width and depth observed on the faces of the specimen.

There were a few considerations not included in the laboratory research or numerical study such as the connection between the precast elements and the substructure. These details were investigated primarily by means of examination of structural plans for existing PCSSS structures.

Precast Composite Slab Span System: Conclusions and Recommendations

The conclusions and recommendations are summarized by topic.

Bursting, Splitting and Spalling Stresses - Significant changes have been made to the bridge design specification since 2007 with regard to end zone stresses, specifically in the terminology. Up to and including the 2007 specifications, the term "bursting" was used to describe the end zone stresses, and were associated with design requirements likely developed specifically for I-girders, but applied to other shapes. The 2008 Interim specifications relaxed the placement requirements for wide-shallow sections, by allowing the designer to spread the end zone reinforcement, termed "splitting" reinforcement over a larger distance. In the case of pretensioned solid or voided slabs, the designer can substitute the section width for "*h,*" rather than using the section depth for "*h*." According to this study, this may not be appropriate when trying to control spalling stresses. In addition, the terminology for the reinforcement described in this section of the design specifications is more correctly termed "spalling" reinforcement rather than "splitting" or "bursting" reinforcement.

Experimental and numerical studies were completed to investigate the effects of end zone stresses on the precast prestressed inverted-T sections used in the PCSSS. The experimental results from the Concept 1 and 2 laboratory bridge investigations indicated that the 12 in. deep concrete sections had sufficient strength to resist tensile stresses induced in the transfer zone of the precast inverted-T sections at the time of release. Four unique end regions of the Concept 1 laboratory bridge specimen precast members, did not exhibit any evidence of cracking in those regions, even where vertical reinforcement was not provided in the end zones of those specimens. These findings were corroborated with the results of numerical studies that showed certain inverted-T members did not require spalling reinforcement, specifically those members with depths less than 22 in. for which the expected concrete

tensile strength was larger than the expected vertical tensile stresses due to the development of prestress.

It was also found through numerical studies that the existing design requirements may not be conservative for deep inverted-T sections (i.e., greater than 22 in.). Larger amounts of spalling reinforcement than specified by the 2010 design specifications were found to be required. It was also found that the reinforcement should be placed as close to the end of the member as possible (i.e., within *h/*4 of the end of the member, where "*h*" represents the depth of the member). The end region was the most critical region for the reinforcement to be located to address spalling stresses, even for the case of wide sections.

Restraint Moment - It is important to consider the effects of restraint moments in the design of PCSSS bridges made continuous, or they should be designed as a series of simple spans. The current specification allows that, when the age of the girder is at least 90 days at the time of continuity, the computation of restraint moments is not required. The reasoning lies in the fact that, when the girder has aged beyond 90 days, the positive restraint moments caused by the precast beams due to time-dependent effects are minimal, and the negative restraint moments that may be generated can be accommodated by the negative moment reinforcement over the piers.

In the case of PCSSS bridges made continuous by casting the CIP concrete on relatively young girders (e.g., 7 to 14 days old) to complete the continuous composite bridge system, the effects of positive restraint moments should be considered. In these cases the positive restraint moments due to time-dependent effects are typically dominated by the creep of the precast sections. It is recommended that the resulting positive time-dependent restraint moments developed at the piers be computed using the P-method.

Research completed during the Minnesota Department of Transportation study and the current study has shown that restraint moments that develop due to thermal gradients can be significant, and should be considered in either case (i.e., whether or not time-dependent effects generate positive or negative restraint moments). The positive restraint moment effects attributed to the design thermal gradients can be an order of magnitude larger in some climates than the positive restraint moments due to time-dependent effects. The thermal gradients provided by the bridge design specification should be taken into consideration by calculating the resulting expected curvatures of each span treated as simply supported and then determining the moment required to overcome the end rotations and provide continuity. There may be little or no economic gain in continuity because of the large thermal restraint moments that develop and in some cases, continuity may require additional reinforcement in the precast sections (i.e., larger than would be required for a simply-supported design). As a consequence it is not conservative to design the PCSSS bridges as simply supported and add positive moment reinforcement across the piers for integrity reinforcement without considering the effects of the restraint moments that can be generated due to the thermal gradient effects.

Live Load Distribution Factors - Numerical modeling was combined with observations from a live load truck test on the field-instrumented Center City Bridge along with load distribution tests on the laboratory bridge specimens (i.e., Concept 1 and Concept 2) to determine the applicability of current live load distribution factors in the bridge design specification for slab-type bridges to the PCSSS.

The numerical models illustrated that the longitudinal curvatures measured in the precast slab span system with a reflective crack extending to within 3 in. of the extreme compression fiber and a tandem load greater than that which could be physically applied in the field resulted in longitudinal curvatures which were only 84 percent of the longitudinal curvatures predicted using the AASHTO LRFD (2010) load distribution factors for monolithic concrete slab span bridges, suggesting that PCSSS-type

superstructures could reasonably and conservatively be designed using the current live load distribution factors for monolithic slab-type bridges.

Furthermore, the live load truck tests on the Center City Bridge suggested that the measured longitudinal curvatures were approximately three times less than those calculated using monolithic slab span equations. In addition, the measured longitudinal curvatures were consistently conservative when compared to monolithic slab span FEM models. The conservatism in the factors for monolithic slab span bridges was sufficient to cover the cases of the PCSSS bridges even considering the potential effects of reflective cracking as discussed above.

Load distribution tests on Span 2 of the Concept 1 laboratory bridge and the Concept 2 laboratory bridge included an investigation of the transverse load distribution between adjacent precast panels. Both spans showed good load transfer capabilities across the longitudinal joint during intermittent tests conducted throughout the investigation of the laboratory bridge specimens to extend the reflective crack. In both cases, little variation in the measured longitudinal curvatures with crack growth was observed in the unloaded panels, which suggested that load was effectively transferred across the longitudinal joint from the loaded panel despite the presence and increase in the size of reflective cracking induced in/near the joint.

In summary, the numerical and experimental studies in regards to live load distribution factors indicated that the PCSSS was well represented by monolithic FEM models, suggesting that the discontinuity at the precast joint did not significantly affect the load distribution characteristics of the system. Also, the performance of the large-scale laboratory bridge specimens reinforced the notion that the system provided sufficient transverse load distribution, with and without the presence of reflective cracking near the joint region.

Skew - Numerical modeling was applied to simply-supported monolithic and jointed (to simulate the PCSSS discontinuity at the adjacent precast flange interface) bridge models with skewed supports ranging up to 45 degrees. Three independent load cases were investigated, which included a 35 kip load individually applied over a 12 by 12 in. patch at both quarter points and at midspan for each model. For each load case, the largest horizontal shear stress in the plane above the precast joint nearest the loading was determined. The small variation and consistency between the models considering a joint between precast sections with a 3 in. flange and a monolithic structure suggested that the effect of the joint in precast composite slab span construction was not expected to significantly affect the performance of the system in skewed applications, and the design of skewed PCSSS bridges could be completed assuming a monolithic slab span system.

Composite Action and Horizontal Shear Strength - To conclude the laboratory tests, the large-scale bridge specimens were loaded above the nominal flexural capacities to the limiting capacities of the actuators to investigate the ability for the precast slab span sections to remain composite with the CIP concrete topping. Placement of reinforcement for horizontal shear was observed to be difficult and time consuming for the fabricator, especially when finishing the top web surfaces. Furthermore, the reinforcement extending from the precast webs for horizontal shear extended out of the precast section with minimal clearance between the hook and the precast web surface to avoid interference with placement of the deck reinforcement in the field. In initial field applications of the PCSSS, the low clearance of this horizontal shear reinforcement may have limited its effectiveness because aggregate was unable to flow below the returned stirrups. Span 2 of the Concept 2 laboratory bridge was designed with the same horizontal shear layout utilized in the Center City Bridge, which satisfied the 2005 bridge design requirements. Span 1 of the Concept 1 laboratory bridge was designed with fewer horizontal shear ties than were used in Span 2 and in the Center City Bridge, and which did not satisfy the

xxix

minimum horizontal shear reinforcement requirements of the 2005 bridge design requirements. The Concept 2 laboratory bridge was designed and constructed with no horizontal shear ties. In both bridges, the surface condition of the precast member was roughened to a surface consistent with a 1/4 in. rake.

In the tests on both spans of the Concept 1 laboratory bridge and on the Concept 2 laboratory bridge, the sections were observed to remain composite well beyond service load levels, through the full range of loading to the maximum capacity of the loading system, which was in excess of the predicted nominal capacity of the Concept 1 and 2 bridges. The horizontal shear stress estimated in the Concept 2 system at the precast-CIP interface was subsequently calculated to be 135 psi. As the bridge had not yet been loaded to failure due to the limited capacity of the actuators, it may have been possible to generate even larger horizontal shear stresses.

The results of the laboratory tests suggest that the bridge design specification should allow for the design of precast slab span structures without horizontal shear ties, and allow for the development of a maximum factored horizontal shear stress of 135 psi in sections with intentionally roughened surfaces (i.e., 1/4 in. rake) unreinforced for horizontal shear.

Reflective Crack Control Across the Longitudinal Joint between Precast Flanges - Reflective cracking was intentionally induced in the Concept 1 and Concept 2 large-scale laboratory specimens to investigate the performance of the PCSSS through a range of loading that was designed to simulate both fatigue performance due to vehicular loading, as well as the influence of environmental effects. The performance of both spans of the Concept 1 laboratory bridge and the Concept 2 laboratory bridge was observed to adequately control cracking in the precast joint region throughout loading to simulate traffic and environmental effects related to the thermal gradient.

Reflective cracking was also monitored throughout the range of testing for seven subassemblage specimens to quantify the relative performance of the respective design details for reflective crack control in each specimen. The ability for each specimen to control the width of cracking was desirable, as large cracks were expected to cause degradation of the longitudinal joint region including providing a potential avenue for the ingress of moisture and chlorides.

Each of the subassemblage specimens performed adequately throughout the range of loading, though variations in the extent of cracking indicated some relative differences. The two specimens with the largest reinforcement ratios for crack control, SSMBLG5-No.6Bars (ρ_{cr}=0.0061) and SSMBLG6-Frosch (ρ_{cr}=0.0052), performed well relative to the remaining specimens. In these two specimens, measured crack widths were consistently smaller than the remaining specimens. SSMBLG7-Control2 also indicated better than average performance through visual observations; however the analysis of the embedded instrumentation suggested that the behavior of this specimen was similar to the specimens in the group not including SSMBLG5-No.6Bars and SSMBLG6-Frosch. The behavior of SSMBLG7-Control2 was attributed to a relatively smooth precast flange surface achieved prior to the placement of the CIP concrete (which was done in anticipation of studying a debonded flange surface, which was abandoned to allow for a second control specimen to be tested). The relatively smooth flange surface was expected to better distribute transverse stresses across the precast flanges in the joint region, thereby reducing the potential stress concentration at the interface between the adjacent precast flanges which created a longitudinal joint, however it was observed via an analysis of the horizontal crack propagation using the concrete embedment resistive strain gages that a single crack was present internally in the specimen, suggesting that the smooth flange surface did not distribute the transverse stress adequately well so as to promote the development of multiple cracks. A completely debonded surface, however, was not expected to be desirable, as it would likely promote delamination of the horizontal precast flange-CIP

xxx

interface, which was expected to promote cracking at the vertical precast web, where cage reinforcement was not present to aid in the control of cracking.

In the subassemblage study, the maximum transverse 9 in. spacing for crack control appeared to be sufficient as long as enough reinforcement was provided to ensure that the reinforcement did not yield upon cracking. This was evident through the good performance of the SSMBLG5-No.6Bars and SSMBLG6-Frosch specimens.

The maximum transverse reinforcement spacing was further investigated by evaluating the performance of the Concept 1 and 2 laboratory bridges which provided more realistic boundary conditions in the longitudinal joint region above the precast flanges. In this study, it was found that the 9 in. maximum transverse reinforcement spacing provided in the Concept 2 laboratory bridge did not correlate with an improvement in the control of cracking near the longitudinal trough area relative to the 12 in. maximum spacing provided in the Concept 1 spans, and therefore an economical design may favor 12 in. transverse reinforcement spacing to 9 in. spacing with no expected reduction in performance. An increase in the maximum transverse reinforcement spacing to 18 in. is not recommended, primarily because cracking in SSMBLG2-NoCage (which was reinforced with only transverse No. 4 bars spaced at 18 in.) was generally largest. The crack widths in SSMBLG2-NoCage increased with the least increase in the applied load relative to the other subassemblage specimens which had transverse reinforcement spacings no larger than 9 in. The subassemblage specimen with transverse reinforcement spacing no larger than 9 in. was observed to provide acceptable crack control.

Furthermore, little difference was observed between the performance of the sections of the Concept 1 laboratory bridge where reflective cracking was observed, with No. 6 transverse hooked bars, and the performance of the Concept 2 laboratory bridge where reflective cracking was observed, with No. 4 transverse hooks. There was, however, a noticeable increase in the relative performance of SSMBLG5-No.6Bars compared to SSMBLG1-Control1, in which the only nominal difference was the larger bars in the former specimen. Because the increased performance observed in SSMBLG5-No.6Bars, which performed similar to SSMBLG6-Frosch, was achieved with larger bars and a maximum transverse reinforcement spacing of 9 in., it was suggested that a design with No. 6 bars and less cage reinforcement was likely to be more economical and easier to implement in the field than the closely spaced reinforcement cage provided in SSMBLG6-Frosch, which had a 4.5 in. bar spacing.

Design Recommendations and Examples – Recommended changes to the bridge design and construction specifications are proposed to implement this promising new system. The PCSSS bridge design guidelines cover both component and system issues including "spalling" reinforcement, load distribution, effect of restraint moments, composite action, and reinforcement to control reflective cracking. Two MathCAD® examples were created to illustrate the design issues associated with a simply-supported PCSSS and a three-span system made continuous. Because of the effects of thermal gradients in generating large restraint moments, it is recommended that the PCSSS bridges be designed as a series of simply-supported spans.

Longitudinal and Transverse Joints in Decked Bulb-T (DBT) and Full-Depth Precast Panel on Girder Systems: Introduction

Two issues that limited the PCSSS bridge concept with regard to the potential for accelerated bridge construction applications were (1) the significant use of CIP to complete the composite system, which would slow the construction process, and (2) the limitation of the system to short- to moderate- span lengths. As a consequence, the study included CIP connection concepts that minimized the use of CIP by

limiting its application to the joints between the flanges of decked bulb-T's or between full-depth precast deck panels on girders. The investigated joints used two layers of reinforcement to provide the ability to transfer moment as well as shear through the deck. Two types of details were investigated to reduce the width of the joint: U-bar details (with deformed wire reinforcement (DWR) and stainless steel (SS)) and headed reinforcement details.

Longitudinal and Transverse Joints in Decked Bulb-T (DBT) and Full-Depth Precast Panel on Girder Systems: Research Methodology and Findings

Two types of details were investigated to reduce the width of the joint: U-bar details (with deformed wire reinforcement (DWR) and stainless steel (SS)) and headed reinforcement details. Initial tests were conducted using monolithic specimens that contained these details to simulate longitudinal and transverse joint connection concepts (i.e., flexural and tension test specimens, respectively). Based on the performance of the initial tests, the most promising connection concept in terms of behavior, constructability and cost, was investigated in additional tests where parameters were varied to refine the proposed connection concepts.

Effects of variables including overlap lengths, rebar spacings, and concrete strengths were investigated. Based on capacity, service level crack widths, constructability, and cost, the U-bar detail, with No. 5 equivalent deformed wire reinforcement at 4.5 in. spacing with 6 in. overlap length and two transverse lacer bars was recommended for the longitudinal and transverse joints. The tests were based on uncoated reinforcement. If epoxy-coated reinforcement was used, larger joint widths may be required to develop the reinforcement across the joint. An alternative is to use stainless steel reinforcement which performed well in the initial study, but was an expensive alternative.

The investigation included the development of performance specifications to achieve high performance durable closure pour (CP) materials for both overnight cure and 7-day cure applications. Based on extensive literature reviews and the experimental investigation, performance criteria for selecting durable CP materials were developed as listed in Tables 1 and 2.

Table 1: Proposed performance criteria of CP materials

Performance Characteristic	Test Method	Performance Criteria		
Compressive Strength (CS), ksi	ASTM C39 modified	6.0≤CS @ 8 hours (overnight cure) @ 7 days (7-day cure)		
Shrinkage[a](S), (Crack age, days)	AASHTO PP34 modified	20<S		
Bond Strength (BS), psi	ASTM C882 modified	300<BS		
Chloride Penetration[b](ChP), (Depth for Percent Chloride of 0.2% by mass of cement after 90-day ponding, in)	ASTM C1543 modified	ChP<1.5		
Freezing-and-thawing Durability (F/T), (relative modulus after 300 cycles)	ASTM C666 Procedure A modified	Grade[c] 1 / 70%≤F/T	Grade 2 / 80%≤F/T	Grade 3 / 90%≤F/T

a: No S criterion need be specified if the CP material is not exposed to moisture, chloride salts or soluble sulfate environments.

b: No ChP criterion need be specified if the CP material is not exposed to chloride salts or soluble sulfate environments.

c: Grades are defined in Table 2.

Table 2: Application of CP material grades for freezing-and-thawing durability

Freezing-and-thawing Durability (F/T)	Is the concrete exposed to freezing-and-thawing environments?	Yes	Is the member exposed to deicing salts?	Yes	Will the member be saturated during freezing?	Yes. Specify F/T-Grade 3
						No. Specify F/T-Grade 2
				No. Specify F/T- Grade 1		
		No. F/T grade should not be specified.				

Numerical studies of bridge systems were conducted with a number of variations to investigate service static and fatigue loadings that might be expected in the longitudinal and transverse joint connection concepts. The analytical parametric study considered parameters such as different loading locations, effect of bridge width, design truck and lane loading versus design tandem and lane loading, girder geometry (depth, spacing and span), bridge skew, single-lane loading versus multi-lane loading, and impact of cracking of the joints. Through this investigation, a database of maximum forces to be expected in the joint was developed. These forces were subsequently used to determine the fatigue loading demand for the large-scale longitudinal joint specimen (flexure and shear-flexure) tests and the large-scale transverse joint specimen (tension) tests.

Large-scale longitudinal and transverse jointed specimens were fabricated to investigate the flexure and flexure-shear behavior of the longitudinal joints and the tension behavior of the transverse jointed specimens. The tension tests on the transverse jointed specimens were intended to simulate continuity provided by the joints over the piers, where it was assumed that the deck would transmit tension

equilibrated by compression in the girder. The large-scale specimens were fabricated with the most promising connection detail which was a U-bar connection concept fabricated with deformed wire reinforcement (DWR). The specimens were subjected to static and fatigue tests with the loads determined in the numerical parametric study. The tests were evaluated in terms of load-deformation response, strain distribution, crack control, and strength.

The studies indicated that the proposed longitudinal joint detail had sufficient strength, fatigue characteristics, and crack control for the maximum service loads determined from the analytical studies and was deemed to be a viable connection system to provide continuity in jointed deck systems over piers. The tests also confirmed that the U-bar detail was a viable connection system for the transverse joint. The joint with the 7-day cure material was able to achieve higher strengths which might be attributed to the section with the lower strength overnight cure material being unable to fully develop the reinforcement. To reduce the crack sizes in the joints, it is proposed to reduce the service stresses in the joints. This could be accommodated economically by using more lower-grade reinforcement (i.e., Grade 60 rather than Grade 75 bars).

Longitudinal and Transverse Joints in Decked Bulb-T (DBT) and Full-Depth Precast Panel on Girder Systems: Conclusions and Recommendations

The research completed during the NCHRP 10-71 study resulted in the development of a comprehensive design guide for the design and construction of longitudinal and transverse joints for full depth deck panels and decked bulb T's (DBTs). The design guide covers the detailing requirements for both loop bar and headed bar details. Adequate performance of these systems requires the use of lacer bars which improve the mechanical anchorage of these systems. Tests were conducted to investigate the behavior of these systems in shallow decks to emulate the flanges of DBTs. These shallow deck thicknesses required the use of tighter bends than presently allowed by the bridge design specifications and thus the recommendations are restricted to wire reinforcement and stainless steel reinforcement which may accommodate tighter bends due to their higher levels of ductility. Another important feature of these joints is the performance of the closure pour materials, which was also investigated through a series of laboratory tests that included an evaluation of the shrinkage and freeze-thaw durability characteristics of candidate overnight-cure and 7-day cure materials which might be considered in accelerated construction applications. Three MathCAD® examples were developed to illustrate the proposed detailing for longitudinal joints between decked bulb-Ts, longitudinal joints in full-depth precast panels on girders, and transverse joints.

Chapter 1 Introduction and Research Approach

1.0   Introduction

The aging highway bridge infrastructure in the United States is subjected to increasing traffic volumes and must be continuously renewed while accommodating traffic flow. Speed of construction, especially for the case of bridge replacement and repair projects, is a critical issue. Disruption of traffic and inconvenience to motorists, let alone major safety issues arising from detours, has encouraged the development of rapid construction methods. The issue of speed of construction, combined with higher labor costs and more variable quality control associated with on-site concrete casting, construction and motorist safety issues, political pressures, and environmental concerns, has paved the way for wider acceptance for the use of precast elements to speed construction.

Depending on the specific site conditions, the use of prefabricated bridge systems can minimize traffic disruption, improve work-zone safety, minimize impact to the environment, improve constructability, increase quality, and lower life-cycle costs. This technology is applicable and needed for both existing bridge replacement and new bridge construction. Over the past 50 years, thousands of short to medium span bridges have been built using precast concrete elements. Replacing an entire highway bridge including the substructure over a weekend has been accomplished through intense planning (Merwin 2003). In 1993, four bridges, each with spans ranging from 700 to 900 ft., were erected in less than 36 hours each including the substructures (Endicott 1993). Interestingly, the finished cost of the replacement project was significantly lower than the competing cast-in-place (CIP) alternatives. For many deficient bridges in the United States on the waiting list for replacement, it is imperative that new bridge construction be as economical as possible and yet be long lasting and nearly maintenance free (Tokerud 1979, Anderson 1972).

There are a large number of papers on the use of precast concrete elements in bridge systems including research on the use of precast elements such as deck panels for rapid deck replacement. On deck elements alone, there are nearly 200 references. The papers include research studies conducted at a number of universities including the University of Illinois, Chicago (Issa, 1995), and University of Nebraska (Tadros, 1998). Strong momentum exists for the growing use of precast construction; two recent projects to investigate precast decked systems include NCHRP 12-65 *Full-Depth, Precast-Concrete Bridge Deck Panel Systems* and NCHRP 12-69 *Design and Construction Guidelines for Long-Span Decked Precast, Prestressed Concrete Girder Bridges*. The present project NCHRP 10-71 *Cast-in-Place Reinforced Connections for Precast Deck Systems* complements the work that was developed under those studies.

NCHRP 12-65 addressed the development of transverse and longitudinal connections between full-depth, precast-concrete bridge deck panels, with emphasis on systems without overlays and without post tensioning through the connection. NCHRP 12-69 addressed I-beam, bulb-tee, or multi-stemmed girders with integral decks cast and prestressed with the girder. The girders are erected abutting flanges of adjacent units, and load is transferred between the adjacent units using connections developed in the project.

The focus of the present project, NCHRP 10-71, was to develop specifications, guidelines, and examples for the design and construction of durable CIP reinforced concrete connections for precast deck systems that emulate monolithic construction, considering issues including speed of construction, durability, and fatigue. The typical sequence of erecting bridge superstructures in the United States is to erect the precast prestressed concrete or steel beams, place either temporary formwork or stay-in-place

1

formwork such as steel or concrete panels, place deck reinforcement, cast deck concrete, and remove formwork if necessary. This project focused on systems that reduce the need to place and remove formwork thus accelerating on-site construction and improving safety.

The three systems considered in NCHRP 10-71 to accomplish these objectives were identified during the 2004 Prefabricated Bridge Elements and Systems International Scanning tour (International Scanning Study Team (2005)). The scanning tour visited France, Belgium, Japan, and the Netherlands with eleven participants representing FHWA, State Departments of Transportation, National Association of County Engineers, industry, and academia. The study team developed a series of recommendations related to prefabricated elements and systems to be used for superstructure systems, along with substructure systems and movement systems for rapid replacement and construction. Examples of these systems include a French precast slab superstructure (Poutre Dalle) with overlapping looped reinforcement that extends into the longitudinal CIP connections, a Japanese full-depth deck panel system with similar looped reinforcement in the transverse CIP connections, and a Japanese full-depth deck flange system with similar looped reinforcement in the longitudinal CIP connection. Additionally, other deck connection details were identified for development through this research. Three of the superstructure systems were specifically addressed in this project.

These systems included: (1) a precast composite slab span system (PCSSS) for short to moderate span structures based on the French Poutre Dalle system, (2) full-depth prefabricated concrete decks, and (3) deck joint closure details (e.g., decked-bulb-tee (DBT) flange connections) for precast prestressed concrete girder systems for long span structures. Each system uses precast elements that are brought to the construction site ready to be set in place and quickly joined together. Depending on the system, the connections are either transverse (i.e., across the width of the bridge) or longitudinal (i.e., along the length of the bridge). The first system, PCSSS, is an entire bridge system; whereas the other two systems investigated in the project represented transverse and longitudinal joint details to transfer moment and shear in precast deck panels and flanges of decked bulb tees. Because of the similarities in the latter two types of systems, they are grouped together in this report. Two types of connection concepts were explored with these details, looped bar details and two layers of headed bar details. Although both types of systems performed adequately in initial tests, the looped bar systems were deemed to be more practical for construction purposes and were investigated in the subsequent tests.

To implement these promising new systems, design guidelines and standard details were established. The developed guidelines also address the durability of the connection concepts including crack control. The PCSSS bridge design guidelines cover both component and system issues including "spalling" reinforcement, load distribution, effect of restraint moments, composite action, and reinforcement to control reflective cracking. Critical goals for the precast panel and decked-bulb-tee flange connections included minimizing the required connection depth to accommodate the loop bar while ensuring concrete cover, achieving durable material properties for the CIP concrete, and preventing moisture from penetrating the interface between the precast and CIP concrete.

The research team included individuals with expertise in structural analysis and testing, materials testing, bridge design, precast concrete fabrication, bridge construction, specification development, and examples and tools development. The researchers at the University of Minnesota had been involved with the first PCSSS bridge implementations in the State of Minnesota, for which they instrumented one of the first two bridges constructed for the Minnesota Department of Transportation (Mn/DOT). In addition, they conducted an investigation on a two-span PCSSS laboratory bridge specimen to investigate a number of variations with the system. Following that study, Mn/DOT agreed to make the two-span bridge available for testing in association with the NCHRP 10-71 project.

The following sections summarize the objective and list of tasks associated with the NCHRP 10-71 project, *Cast-in-Place Concrete Connections for Precast Deck Systems*.

1.1. Scope of Study

The objective of this project was to develop guidance for the design and construction of durable CIP reinforced concrete connections for precast deck systems that emulate monolithic construction. This was accomplished through the following ten tasks.

1.1.1. Task 1 – Review relevant practice, performance, data, and research findings

Reviewed relevant practice, performance data, research findings, physical test results, and other information related to the design, fabrication, and installation of CIP reinforced concrete connections for precast deck systems that emulate monolithic construction. This information was gathered from technical literature and from unpublished experiences of engineers, bridge owners, and others. This review included the looped reinforcement details identified in Japan and France during the 2004 Prefabricated Bridge Elements and Systems International Scan.

1.1.2. Task 2 – Develop detailed design, fabrication, construction, and performance criteria

Developed detailed design, fabrication, construction, and performance criteria that were selected to provide durability, strength, fatigue resistance and rapid construction.

1.1.3. Task 3 – Develop conceptual designs for CIP reinforced concrete connections

Developed several conceptual designs for CIP reinforced concrete connections, including a comprehensive longitudinal connection detail for precast slab superstructures and three connection concepts for longitudinal or transverse connections between full-depth deck panels or deck flanges. The connection concepts were developed to not require overlays or post-tensioning. Emphasis was placed on increasing construction speed while achieving durability and ride quality.

1.1.4. Task 4 – Develop an updated and detailed work plan

Developed an updated and detailed work plan for numerical and experimental evaluation of the conceptual designs based on the results of Tasks 2 and 3, including the development of large-scale connection test specimens.

1.1.5. Task 5 – Submit an interim report

The interim report was completed and submitted to seek approval to move forward with the work plan.

1.1.6. Task 6 – Execute the approved work plan for evaluation of the connections

This task represented the bulk of the effort for this project during which the approved work plan was executed for the evaluation of the connections.

1.1.7. Task 7 – Prepare a connection design, detailing guide, and construction guide

Prepared a comprehensive connection design and detailing guide, including a listing of all design steps with examples as needed for the connections that met the criteria established in Task 2.

1.1.8. Task 8 – Develop specification language and commentary

Developed specification language and commentary for recommended changes to the *AASHTO LRFD Bridge Design Specifications* and the *AASHTO LRFD Bridge Construction Specifications* as necessary to implement the recommended connection details.

1.1.9. Task 9 – Submit the products of Tasks 7 and 8 and the Draft Final Report

The products of Tasks 7 and 8 were submitted for panel review and comment.

1.1.10. Task 10 – Final Report

The research study has been documented in this final report. It includes the design and detailing guide with recommended modifications to the design specifications and a list of design steps and examples.

1.2.   Introduction to Precast Composite Slab Span Systems (PCSSS)

Precast composite slab span systems (PCSSS) are a promising technology for the implementation of rapid construction techniques for bridge construction. The bridge systems are composed of precast, inverted-T sections, fabricated off-site and delivered to the jobsite ready for erection. The inverted-T sections are assembled such that no formwork is required prior to the placement of the CIP deck, which considerably reduces construction time related to the placement and removal of formwork. Transverse load transfer is achieved through the development of transversely oriented reinforcement protruding from the precast members. Furthermore, improved quality of the main superstructure can be achieved due to the rigid quality control associated with the fabrication of precast members, which may be difficult to achieve in cast-in-place (CIP) bridge construction.

The current study included an investigation of the literature related to precast composite slab span bridge systems and other relevant topics valuable in the development of PCSSS bridges. Included in this review was the work completed during a study commissioned by Mn/DOT (Smith et al., 2008) regarding a field and laboratory implementation of a PCSSS bridge. The laboratory bridge specimen utilized during the Mn/DOT study was subsequently made available for use with the NCHRP 10-71 project. The research conducted during the NCHRP 10-71 study included numerical parametric studies and further experimental studies of variables deemed to be important from the Mn/DOT study including the effects of reinforcement to control spalling, connection details for crack control, cyclic loading effects on crack development, and composite action between the precast and CIP.

4

Because of its similarity to slab-span bridge systems, the applicability of the AASHTO design provisions for slab-span systems were investigated in the study. The two primary considerations that distinguish PCSSS bridges from slab-span bridges are (1) the required reinforcement to control reflective cracking above the longitudinal joint between the precast flanges, and (2) the effect of restraint moments due to the composite nature of the system. With regard to the issue of reflective crack control, in addition to a numerical investigation regarding the effect of the transverse reinforcement, the issue was also studied in laboratory investigations of two large-scale laboratory specimens (i.e., Concept 1 and 2 bridges), as well as in subassemblage test specimens specifically designed to investigate crack control. The effect of restraint moments in the PCSSS were investigated numerically and experimentally in a previous study by the researchers, the results of which can be found in Smith et al. (2008) and Eriksson (2008).

Other considerations for the design of the PCSSS investigated in the study included the composite action of the precast and CIP which was investigated through ultimate load tests of the Concept 1 and 2 bridges and the spalling reinforcement detail of the precast section. Current design requirements to control the end zone stresses in prestressed concrete members were developed for I-sections and are not directly applicable to the PCSSS precast inverted-T sections. The current design recommendations were found to be conservative for shallow inverted-T sections and unconservative for deeper inverted-T sections.

There were a few considerations not included in the laboratory research or numerical study such as the connection between the precast elements and the substructure. These details were investigated primarily by means of examination of structural plans for existing PCSSS structures.

1.3. Introduction to Longitudinal and Transverse Joints in Decked Bulb-T (DBT) and Full-Depth Precast Panel on Girder Systems

Two issues that limited the PCSSS bridge concept with regard to the potential for accelerated bridge construction applications were (1) the significant use of CIP to complete the composite system, which would slow the construction process, and (2) the limitation of the system to short- to moderate- span lengths. As a consequence, NCHRP 10-71 included the study of CIP connection concepts that minimized the use of CIP by limiting its application to the joints between the flanges of decked bulb-T's or between full-depth precast deck panels on girders. The investigated joints used two layers of reinforcement to provide the ability to transfer moment as well as shear through the deck. Two types of details were investigated to reduce the width of the joint: U-bar details (with deformed wire reinforcement (DWR) and stainless steel (SS)) and headed reinforcement details. Tests were included to evaluate the effectiveness of the different connection concepts, and the most promising connection concept in terms of behavior, constructability and cost was subjected to a series of parametric tests to further refine the joint details.

The investigation included the development of performance specifications to achieve high performance durable closure pour (CP) materials for both overnight cure and 7-day cure applications. Numerical studies were conducted with a number of variations to investigate service static and fatigue loadings that might be expected in the longitudinal and transverse joint connection concepts.

Large-scale longitudinal and transverse jointed specimens were fabricated to investigate the flexure and flexure-shear behavior of the longitudinal joints and the tension behavior of the transverse jointed specimens. The large-scale specimens were fabricated with the most promising connection detail which was a U-bar connection concept fabricated with deformed wire reinforcement (DWR). The specimens were subjected to static and fatigue tests with the loads determined in the numerical parametric study.

5

The tests were evaluated in terms of load-deformation response, strain distribution, crack control, and strength.

1.4. Organization of Report

As mentioned in Section 1.0, this report covers two very different systems: (1) the precast composite slab-span system (PCSSS), which is an entire bridge system, and (2) transverse and longitudinal cast-in-place connection concepts to transfer moment and shear between precast deck panels and the flanges of precast decked bulb-Ts. The report is separated accordingly. The research contained in Chapters 2 through 7 includes the documentation associated with Tasks 1 through 8 related to the development of PCSSS bridges. Chapters 8 through 14 include the documentation associated with Tasks 1 through 8 related to the development of longitudinal and transverse connection concepts between full-depth deck panels and decked bulb-T flanges.

The chapters associated with the PCSSS bridge system are organized as follows. Chapter 2 provides a literature review of the system and associated parameters of interest including literature on crack control, composite action of cast-in-place (CIP) and precast systems, and spalling design requirements. Chapter 3 provides background on the system which was initially implemented in the U.S. by the Minnesota Department of Transportation (Mn/DOT). The chapter contains the results of a field and laboratory investigation sponsored by Mn/DOT which included an investigation of live load distribution and the effects of restraint moments. Chapter 4 presents a summary of a parametric study to investigate the range of applicability of PCSSS bridges. Numerical studies are summarized in this chapter, which were conducted to investigate a number of parameters including transverse reinforcement spacing for crack control, applicability of slab-span design recommendations for PCSSS in terms of live load distribution factors and skew effects. The chapter also summarizes the numerical and experimental results associated with end zone stresses in the inverted-T precast sections used to fabricate the PCSSS, and a review of support conditions that have been used for the systems in the field. The chapter concludes with the results of a numerical study used to determine the magnitude of the patch load to be applied in the laboratory investigations of the PCSSS Concept 1 and Concept 2 bridges. Chapter 5 presents a summary and results of the tests on the Concept 1 and 2 laboratory bridges. Subassemblage tests used to investigate detailing of the joint region for crack control are summarized in Chapter 6. Conclusions of the PCSSS investigation are provided in Chapter 7.

As mentioned above, the investigation of the longitudinal and transverse connection concepts between decked bulb-Ts or full-depth precast deck panels is summarized in Chapters 8 through 14. Chapter 8 contains a brief introduction. Rather than having a separate chapter on literature review for the longitudinal and transverse connection concepts, the literature is summarized in the respective chapters where appropriate. Chapter 9 summarizes the preliminary tests on monolithic specimens containing the U-bar (deformed wire reinforcement (DWR) and stainless steel (SS)) and headed reinforcement to determine the most promising connection detail; it presents the results of parametric tests used to further refine details of the connection concept. Chapter 10 detailed the numerical parametric study conducted to determine loads to be applied to large-scale longitudinal and transverse joint specimens described in later chapters. Chapter 11 details the development of performance specifications for overnight-cure and 7-day-cure closure pour (CP) materials considered for the joints. The chapter also presents the results of tests on a number of prospective CP materials used to determine the most promising CP candidate materials in each category (i.e., for overnight cure and 7-day cure) that were subsequently used in the fabrication of the large-scale longitudinal and transverse joint specimens. Chapters 12 and 13 summarize the static and fatigue loading tests on the large-scale longitudinal and

6

transverse joint specimens, respectively, and Chapter 14 presents a summary of the conclusions of the study.

Appendix A contains the recommended design recommendations including suggested changes to the AASHTO LRFD Bridge Design code and commentary that were developed during the study, in accordance with Task 8. Appendix B contains detailed design examples in accordance with Task 7. The results of the phone survey conducted at the initial stages of the project to gather information including the respondents' experience with similar systems, their input on important performance criteria, and their feedback on proposed connection concepts are contained in Appendix C. Appendix D contains information on the instrumentation of one of the early implementations of the PCSSS in the State of Minnesota. Appendices E and F contain the information on the instrument locations in the two laboratory PCSSS bridge specimens. The coring analysis of the PCSSS laboratory bridge and subassemblage test specimens are contained in Appendix G. The subassemblage sectional design calculations and information on the instrumentation locations are contained in Appendices H and I, respectively.

Chapter 2 PCSSS: Literature Review

2.0 Introduction to Literature Review

The design and implementation of the experimental and numerical studies regarding precast composite slab span systems (PCSSS) associated with the NCHRP 10-71 project were completed after consideration of available previous research. Because the PCSSS was a relatively new concept, the existing literature associated with the system was limited. The system was based on the Poutre Dalle bridge system developed in France, but there were no published results regarding the performance of that system. The designs associated with the original implementation of the PCSSS in the U.S. were based on the AASHTO provisions for slab-span systems because of their many similarities. Major differences exist, however, between the PCSSS and slab-span bridge systems including the composite precast / cast-in-place (CIP) nature of the PCSSS which can result in the development of restraint moments in continuous bridges due to the different time-dependent properties of the component materials. In addition, the precast portion of the PCSSS had issues to be resolved regarding the applicability of AASHTO reinforcement provisions to control end cracking due to spalling stresses, and issues associated with the development of details to control reflective cracks that might develop above the interface between the precast flanges or the CIP-precast web interface.

2.1. Poutre Dalle System

During the FHWA/AASHTO 2004 International Scan Tour, rapid construction techniques used for prefabricated bridges in Europe were investigated (Hagen, 2005). The Poutre Dalle system used in France showed promise for rapid construction of short to moderate span bridges, shown in Figure 2.1.1. The system was designed to provide longitudinal moment capacity through the longitudinally oriented precast beams made composite with a CIP deck surface. Transverse load distribution was achieved through the development of transversely oriented reinforcement protruding from the precast section in the CIP concrete placed in the trough region created by adjacent panels.

The Minnesota Department of Transportation developed a precast composite slab span system (PCSSS), described in Chapter 3, that was based on the Poutre Dalle concept. Mn/DOT implemented the first two PCSSS bridges in 2005, both of which had been previously planned for CIP slab construction. One of them was instrumented to be monitored in two ways: to investigate the magnitude and location of reflective cracking between adjacent inverted-T sections and to examine the conitnuity over the piers. Additionally four Mn/DOT PCSSS secctions were delivered to the University of Minnesota structures laboratory for additional study for possible refinements to the design and detailing of the system, described in Chapter 4.

Figure 2.1.1: Photograph of precast section used in Poutre Dalle System (Hagen, 2005)

2.2.   Crack Control Reinforcement, Frosch et al., 2006

Cracking in bridge systems must be adequately controlled for aesthetic as well as performance and durability considerations. The presence of cracking in bridge superstructures introduces a means of ingress for chlorides and other contaminants which can be detrimental to the performance of the embedded reinforcement. This concern is especially applicable in regions with harsh environments, such as those with freeze-thaw cycles, which are also usually coupled with the application of large amounts of salt to bridge superstructures. Crack control requires the use of adequately sized and spaced reinforcement.

Frosch et al. (2006) provided an extensive investigation of cracking in bridge decks and developed associated design recommendations for reinforcement to control cracking. Although Frosch's application was focused on the crack control of bridge decks, the findings of his research were applied to the NCHRP 10-71 study to investigate their applicability in the control of potential reflective cracking above the longitudinal joint between the precast flanges.

Frosch et al. (2006) completed an experimental research program through the observation of four highway bridge decks in Indiana, three of which were instrumented by the researchers. The fourth bridge was instrumented in a previous research study by Radabaugh (2001), the primary objective of

9

which was to observe early age behavior of bridge decks exposed to field conditions. The bridges selected for the study included three two-span continuous bridges, with equal spans of 76, 101, and 123 ft. The fourth bridge was a five span bridge with spans of 39, 63, 77, 63, and 39 ft. The decks in the three two-span bridges were constructed with two layers of steel reinforcement for crack control, while the five span bridge was built with GFRP for the top layer of reinforcement and steel bars for the bottom layer of deck reinforcement. Characteristics of the four bridges selected for the field investigation are given in Table 2.2.1.

Table 2.2.1: Characteristics of Bridges in Field Investigation (Frosch et al., 2006)

Bridge	No. of Spans	Length of Spans (ft.)	Girder Type	Abutment Type	Skew (deg.)
I 65 over SR 25	2	76, 76	Steel	Integral	25
SR 18 over I 65	2	123, 123	Steel	Semi-Integral	30
SR 23 over US 20	2	101, 101	Precast/Prestressed Concrete	Integral	11
Thayer Rd over I 65	5	39, 63, 77, 63, 39	Steel	Rockers	5

The reinforcement selected in the bridge decks provided a range of longitudinal bar spacing values, between 6 and 18 in. The reinforcement size consisted of No. 4 or No. 5 bars. To facilitate the development of design recommendations related to crack control, the SR 18 bridge was constructed with different reinforcement details in the eastern and western spans, as illustrated in Table 2.2.2.

Table 2.2.2: Characteristics of deck reinforcement in field investigation (Frosch et al., 2006)

Bridge	Type of Reinforcement		Bar Size		Longitudinal Reinforcement Spacing (in.)	
	Top	Bottom	Top	Bottom	Top	Bottom
I 65 over SR 25	Steel	Steel	4	5	12	12
SR 18 over I 65 (Purdue Span)	Steel	Steel	4	4	6	6
SR 18 over I 65 (AASHTO Span)	Steel	Steel	5	5	18	12
SR 23 over US 20	Steel	Steel	5	5	6	6
Thayer Rd over I 65	GFRP	Steel	5	5	6	9

The Purdue span of the SR 18 bridge contained the reinforcement detail proposed by Frosch et al. for crack control, while the AASHTO Span was designed to conform to the requirements in the *Standard Specifications for Highway Bridges, 16th Edition* (AASHTO 1997) and the *INDOT Standard Specifications* dated 1999 (INDOT 1999).

Visual crack mapping, beginning as early as 15 days after the placement of the CIP deck with subsequent mappings completed as late as 799 days after the placement of the CIP deck, was utilized in conjunction with measured strains to evaluate the performance of each bridge deck. Table 2.2.3 compares the crack statistics for the two spans of SR18, as well as the results of the Thayer Road bridge, which had five shorter spans. Both of these structures were wet-cured for seven days.

As expected, for SR18 with the two different reinforcement details, the closer-spaced reinforcement tended to produce smaller cracks in greater numbers. The Purdue span was observed to have the most number of cracks; however the average crack width was the smallest, with a magnitude of 0.007 in., which was 30 percent less than the average crack width measured in the AASHTO span. Furthermore, less variation was observed in the crack widths, with a standard deviation of 0.005 in. compared to 0.008 in. for the AASHTO and Thayer Road spans. Finally, the maximum crack width observed in the Purdue span was 28 and 31 percent smaller than that measured in the AASHTO and Thayer Road spans, respectively. The approximately 30 percent improvement in both the average and maximum crack widths, in combination with the reduction in variability among the crack widths, suggested that the design parameters utilized to develop the Purdue span in the SR 18 bridge should be considered as a superior alternative, in terms of performance, to the AASHTO (1997) and INDOT (1999) design parameters. Furthermore, the authors suggested that the performance of the Thayer Road spans, which was similar to that observed in the AASHTO span, was due to increased slip between the concrete and FRP reinforcement.

11

Table 2.2.3: Comparison of crack width statistics (Frosch et al., 2006)

Crack Statistics	SR 18		Thayer Rd
	AASHTO	Purdue	
Number of Cracks (Total)	15	22	19
Number of Cracks (per 100 ft.)	12.2	17.9	6.8
Average Crack Widths (in.)	0.010	0.007	0.010
Standard Deviation (in.)	0.008	0.005	0.008
Maximum Crack Width (in.)	0.025	0.018	0.026
Variance	3.11×10^{-5}	2.53×10^{-5}	5.56×10^{-6}

In addition to the experimental results obtained during the study, the researchers completed a numerical parametric study to further investigate the expected effects of various bridge design characteristics on the performance of bridge decks. The finite element method (FEM) model was developed using ANSYS (SAS Inc. 2004) and was calibrated using the results of the Radabaugh (2001) study to investigate the effects of restrained shrinkage. Radabaugh (2001) constructed two laboratory specimens to study the effects of shrinkage restraint due to stay-in-place (SIP) deck pans. The specimens were 9 ft. by 9 ft. square, and represented the positive moment region of the bridge decks in the I-65 bridge span over SR 25. The specimens were developed in an effort to investigate the level of restraint based on the type of formwork, where one specimen had SIP steel deck forms, and the second was constructed with plywood forms and two layers of 10-mil Teflon as a barrier between the plywood and concrete. The second specimen was expected to provide little shrinkage restraint and therefore was developed to represent a state of free-shrinkage. Four layers of solid elements were selected to model the deck, which provided insight into the behavior of the deck through its depth, while reinforcement was discretely modeled using link elements. The materials were modeled as linear elastic, with the elastic modulus of the steel reinforcement and concrete of 29,000 ksi and 3,610 ksi, respectively. Uniform and linear concrete shrinkage profiles were considered, which were developed from the literature (Radabaugh, 2001 and Blackman, 2002).

The calibrated FEM model was utilized to complete a numerical parametric study to investigate the effects of a range of variables on cracking in bridge decks, outlined in Table 2.2.4. The variables considered included reinforcement type, size, and spacing, the girder superstructure depth and spacing, and the thickness and material strength of the CIP deck.

12

Table 2.2.4: Range of variables considered in parametric study (Frosch et al., 2006)

Variable		Range	Control
Reinforcement	Area (Bar Size)	#3-#7	#5
	Top Mat Spacing (in.)	3-18	12
	Bottom Mat Spacing (in.)	3-18	12
	Reinforcement Type	Steel, FRP	Steel
Girder	Depth (in.)	12-51	51
	Spacing (ft.)	6-10	7
Deck	Thickness (in.)	6-12	8
	f'$_c$ (psi)	3,000-10,000	4,000

The results of the parametric study generally corroborated the results anticipated by the researchers, such as increasing the area of reinforcement in a section tended to reduce the crack widths and reinforcement stresses under a given load. The effects of reinforcement spacing were investigated by varying the spacing while simultaneously maintaining a constant reinforcement ratio among models. Using this method, the reinforcement spacing was observed to control two aspects of the behavior of the models: (1) the crack width was observed to be larger as the reinforcement spacing increased, and (2) the variation in the crack width between adjacent reinforcement was highly dependent on the bar spacing (i.e., an "unzipping" effect was observed between adjacent reinforcing bars).

For example, in the case of uniform shrinkage, with a steel reinforcement ratio of 0.65 percent, the following results were obtained. For the largest reinforcement spacing (i.e., 18 in.) considered in the study, the maximum difference between the crack width near a bar and half the distance to an adjacent bar was approximately 1.5 mils. Furthermore, the unzipping effect was dependent on the 3 in. mesh size, which was evinced by the fact that a change in crack width of approximately 1/2 mil was observed between measurements near and away from a bar in the 6 in. spacing model, while virtually no variation in the crack width was observed between adjacent bars in the model representing a 9 in. reinforcement spacing. A comparison of the performance of the different models was made by considering the maximum crack widths in each model, which subsequently corresponded to the crack width measured equidistant from adjacent reinforcement if a variation was observed between bars. A maximum crack width of approximately 2.4 mils was observed in the model with a 3 in. reinforcement spacing, while a maximum crack width of approximately 6.3 mils was observed in the model with an 18 in. reinforcement spacing; where the increase in the crack widths was observed to be linearly proportional to the bar spacing between these limits.

The authors suggested that if no slip is assumed to occur between the reinforcement and concrete, then when cracking occurs, the tensile stresses previously restrained by the concrete will be transferred to the reinforcement. If the concrete tensile strength is taken to be $6\sqrt{f'_c}$, then the stress in the reinforcement upon cracking can be determined as shown in Eqn. (2.2.1).

$$f_s = \frac{6\sqrt{f_c}}{\rho_g}$$

(2.2.1)

13

where f_c is the concrete compressive strength at the initiation of cracking in psi (and the units of $\sqrt{f_c}$ are in psi), and ρ_g is the gross reinforcement ratio. The researchers plotted the average reinforcement stresses versus the ratio $\sqrt{f_c} / \rho_g$, and found that a linear fit yielded a line with a slope of approximately 3, indicating that the average stress in the reinforcement bridging the crack was numerically determined to be about half of what would be expected if no slip occurred. The slip length utilized in the model was 2 in.

Furthermore, the authors discovered that, on average, the reinforcement stresses increased by approximately a factor of two between the simulated initial and final shrinkage states, where the initial state was when cracking first occurred ($6\sqrt{f_c}$) and the final was considered to be after a free shrinkage "load" of 1000 με was applied.

The researchers provided a recommended gross reinforcement ratio for crack control reinforcement based on the results from the FEM parametric study, outlined above. Because the concrete compressive strength at the time of cracking was unlikely to be known by the designer, the authors conservatively substituted the 28-day concrete compressive strength in the calculation. The recommended reinforcement ratio proposed by Frosch et al. (2006) is given in equation 2.2.2).

$$\rho_g = \frac{6\sqrt{f_c'}}{f_y} \tag{2.2.2}$$

Furthermore, the reinforcement spacing required to restrain crack growth was developed during the study and based on previous work. The reinforcement spacing, s, for Grade 60 bars is given as

$$s \leq 9\left(2.5 - \frac{c_c}{2}\right) \leq 9 \ in. \tag{2.2.3}$$

where s is the reinforcement spacing (in.) and c_c is the depth of concrete cover measured from the extreme tensile fiber of the concrete to the face of reinforcement (in.).

2.3. Horizontal Shear Capacity of Composite Concrete Beams without Ties, Naito et al., 2006

Composite precast construction increases the efficiency of precast sections because it may reduce the section depth, as well as increase the load capacity, and the geometric stiffness of the system. A composite concrete system must be designed such that the horizontal compression and tension forces developed in the system can be transferred between the precast and CIP interface. Two design documents for concrete construction in the United States, AASHTO (2010) and ACI (318-08), include design parameters for horizontal shear transfer. ACI (318-08) allows for the design of composite sections without the use of horizontal shear reinforcement, and permits a maximum factored horizontal shear stress of 80 psi to be developed by a clean, roughened, surface with no ties crossing the shear plane. AASHTO (2010) requires that horizontal shear reinforcement be present in all sections in which composite action is to be achieved; however AASHTO provides a cohesion factor that may be interpreted, for the purpose of discussion, as a maximum allowable horizontal shear strength (Naito et al., 2006). The 2006 AASHTO LRFD design specification provided a cohesion factor of 100 psi for a clean, intentionally roughened surface to an amplitude of 1/4 in., while AASHTO (2010) increased the cohesion factor for a clean, intentionally roughened surface to 240 psi; which was not published at the time of designing the NCHRP 10-71 Concept 1 laboratory bridge specimen. Furthermore, research by Naito et al. (2006) suggests that sections without vertical ties for horizontal shear reinforcement can develop adequately large and reliable horizontal shear capacities.

14

The calculation of the horizontal shear demand in a section can be completed using many different methods. The researchers investigated three of these methods: (1) global force equilibrium, (2) simplified elastic beam behavior, and (3) classic elastic methods (Naito et al., 2006). Global force equilibrium considers a change in the compression force resultant over a distance along the length of the beam, l. The horizontal shear strength is simply the change in the compression force divided by the horizontal shear area, or b_v $*l$, where b_v is the width of the horizontal shear plane. For simply-supported systems, the horizontal shear stress can be calculated using this method by dividing the total compressive force at midspan by half of the span length and the width of the horizontal shear plane. The second method considers flexural beam theory, which equates the horizontal shear demand to the vertical shear acting at a given section and is calculated as $V/(b_v\,d)$, where d is defined differently in ACI and AASHTO. ACI (318-08) defines d as the distance from the centroid of the longitudinal tension reinforcement to the extreme compression fiber of the section, while AASHTO (2010) defines d as the distance from the longitudinal tension reinforcement to the mid-thickness of the slab. The third method presented by the authors, the classic elastic method, considers the section properties of the beam; however, the method is applicable to uncracked sections only. The horizontal shear stress calculated using the classical elastic method is illustrated in Eqn. (2.3.1).

$$v_h = {VQ}/{Ib_v} \qquad\qquad (2.3.1)$$

Naito et al. (2006) investigated the horizontal shear stress developed in composite girders without horizontal shear reinforcement. The researchers completed an experimental program with 19 test specimens to investigate the effects of surface roughness, concrete strength, and loading type (i.e., point loading versus uniform loading). Four variations in the surface roughness were considered, including as-placed (A), broom finish (B), 1/4 in. rake (R), and sheepsfoot (Sh). The concrete compressive strength in the flange was varied within a wide range of reasonably expected values, with measured concrete strengths of 3.11, 5.67, 8.75, and 9.71 ksi. Two-point and 5-point loading configurations were utilized during the study to simulate point loading and uniform loading, respectively. Load was applied through 12 in. neoprene bearing pads in an effort to reduce the localized bearing stress near the applied load. A summary of the research parameters and specimen characteristics is outlined in Table 2.3.1 (Naito et al., 2006).

The researchers provided instrumentation to determine the horizontal shear stress at the interface as well as to measure the slip that may occur along predicted failure planes. Two horizontally oriented strain gages were mounted on the surface of the CIP flange along the depth, to allow for the measurement of the horizontal shear stress with the use of known stress-strain relationships for the CIP concrete.

Table 2.3.1: Research parameters and specimen characteristics considered during the study (Naito et al., 2006)

Beam	Interface Finish	Loading Method	Interface Width (in.)	Web Steel Area (in.^{2})	Flange Strength (ksi)	Effective Prestress (ksi)
1	As-Placed	5 Point	5	0.2	5.67	141.3
2	Broom	5 Point	5	0.2	5.67	142.1
3	Monolithic	5 Point	5	0.0	9.71	139.9
4	Rake	5 Point	5	0.2	3.11	141.5
5	Rake	5 Point	5	0.2	5.67	143.1
6	Rake	5 Point	5	0.2	8.75	140.3
7	Sheepsfoot	5 Point	5	0.2	5.67	140.3
8	As-Placed	2 Point	2	0.2	5.67	140.2
9	As-Placed	2 Point	2	0.2	5.67	140.1
10	Broom	2 Point	2	0.2	5.67	140.2
11	Monolithic	2 Point	2	0.0	9.71	140.2
12	Monolithic	2 Point	2	0.0	9.71	140.2
13	Rake	2 Point	2	0.2	3.11	140.2
14	Rake	2 Point	2	0.2	3.11	140.2
15	Rake	2 Point	2	0.2	5.67	140.2
16	Rake	2 Point	2	0.2	5.67	140.2
17	Rake	2 Point	2	0.0	8.75	140.2
18	Rake	2 Point	2	0.0	8.75	140.2
19	Smooth	2 Point	2	0.2	5.67	140.2

Relatively large horizontal shear stresses were measured during both the 2-point and 5-point loading cases, and were always above the 80 psi allowed for sections without horizontal shear ties as specified by ACI (318-08) and the 240 psi cohesion value provided by AASHTO (2010). During the 5-point load tests, the horizontal shear stress was measured at the first indication of cracking in the section, generally flexure shear cracking, in an effort to investigate the shear stress developed before cracking, which would generally be the case for a service condition, where cracking is generally avoided. The results of the 5-point load tests are illustrated in Table 2.3.2, with an average horizontal shear stress at cracking of 340.2 psi using the classic elastic method of calculation. The smallest average horizontal shear stress was 275.4 psi, calculated using the simplified elastic method provided by ACI (318-08).

Table 2.3.2: Horizontal shear stress at cracking (psi) during 5-point load tests (Naito et al., 2006)

Beam	Interface Finish	Elastic VQ/Ib_v	ACI V/b_vd_p	AASHTO V/b_vd_v
1	As-Placed	341.1	276.0	334.5
2	Broom	341.1	276.0	334.5
3	Monolithic	350.1	280.0	339.4
4	Rake	321.6	266.0	322.4
5	Rake	341.1	276.0	334.5
6	Rake	345.6	278.0	337.0
7	Sheepsfoot	341.1	276.0	334.5
	Average	340.2	275.4	333.9

The horizontal shear stresses developed during the 2-point load tests were calculated at the ultimate capacity of each specimen, and were subsequently considerably larger than those measured during the five-point load configurations. As illustrated in Table 2.3.3, the average horizontal shear stress measured at ultimate ranged from 828.4 psi to 1022.3 psi, depending on the method of calculation.

17

Table 2.3.3: Horizontal shear stress at ultimate (psi) during two-point load tests (Naito et al., 2006)

Beam	Interface Finish	From Strain C/Lb_v	Elastic VQ/Ib_v	ACI $V/b_v d_p$	AASHTO $V/b_v d_v$
8	As-Placed	482.2	863.2	698.4	846.6
9	As-Placed	814.0	1060.8	860.7	1043.2
10	Broom	915.6	993.2	804.6	975.3
11	Monolithic	1075.0	1067.0	848.4	1028.4
12	Monolithic	1288.0	1248.1	981.1	1189.2
13	Rake	639.0	850.6	703.7	852.9
14	Rake	1182.0	1015.1	840.2	1018.4
15	Rake	1348.0	1001.0	811.1	983.2
16	Rake	1245.0	1165.9	948.1	1149.2
17	Rake	1054.0	1141.3	934.3	1132.5
18	Rake	1194.0	1073.6	873.1	1058.3
19	Smooth	787.4	787.9	637.5	772.7
	Average	1002.0	1022.3	828.4	1004.1

The experimental results indicated that composite girders without horizontal shear reinforcement can develop significant horizontal shear stresses. The authors suggested that, with an average horizontal shear stress of 340.2 psi at the service state, which was more than three times the least conservative design estimate, the requirement for horizontal shear reinforcement in all sections by AASHTO (2005) be waived.

2.4.   AASHTO (2007) Bursting Design Requirements

The AASHTO (2007) specifications required vertical reinforcement to resist four percent of the prestressing force in the end regions of precast beams over a horizontal distance of *h/4* from the face, where *h* is the section height. The provisions are for pretensioned anchorage regions and do not provide any distinction based on cross section. The AASHTO (2007) specifications resulted in the requirement of a large amount of vertical steel over a short distance for wide shallow members, such as the shallow inverted T sections used in PCSSS bridges. This created congestion of the vertical reinforcement in the end zones and provided an impetus for a review of the requirements and the end zone force demands for the case of shallow inverted-T sections.

 In reviewing the literature, the origin of the AASHTO bursting requirements likely resulted from a Marshall and Mattock (1962) study on horizontal end zone cracking of pretensioned I-girders. The 1961 Interim AASHTO Specifications introduced bursting reinforcement requirements (in the AASHTO (2010) LRFD Bridge Design Specifications this is labeled "splitting resistance") for pretensioned I-beams stating, "Vertical stirrups acting at 20,000 psi to resist 4 percent of the prestressing force shall be placed within

18

d/4 from the end of the beam with the end stirrup placed as close to end of beam as practicable," where *d* is the effective depth. By 1969, the above requirements were not limited to just I-beams, and instead were made applicable to end zones of all pretensioned beams. The AASHTO LRFD Bridge Design Specifications 1st edition (1994) had the same requirements as the 1969 version, but the 2nd edition (1998) stated that the vertical steel should be placed within *h/5* from the end face, where *h* is the height of the member. This specification was changed to *h*/4 from the end face in the 3rd edition (2004). The only difference between the 1969 provisions and the 4th edition (2007) of the AASHTO LRFD Bridge Design Specifications was that vertical steel could be placed within *h*/4 from the end face, rather than *d*/4. The 2008 Interim specifications relaxed the requirements for wide-shallow sections, by allowing the designer to spread the end zone reinforcement, termed "splitting" reinforcement over a larger distance. In the case of pretensioned solid or voided slabs, the designer can substitute the section width for "*h*," rather than using the section depth for "*h*."

Because the original AASHTO provisions were likely developed as a result of experimental testing performed on I-beams by Marshall and Mattock (1962), it is not clear whether the AASHTO requirements, developed for I-beam members, are applicable to other cross sections, particularly slab-span systems.

2.4.1. Bursting, Splitting and Spalling Stresses

The end regions of prestressed concrete sections have complicated states of stress. Beam theory is not applicable in the end regions of prestressed concrete beams because the longitudinal strain is not linearly distributed through the depth of the cross section due to the introduction of the prestress force. As the prestress force distributes through the section, various zones of compression and tension are created over a region assumed to extend a distance approximately equal to the depth of the section, in accordance with St. Venant's principle. The tensile stresses that develop in this region have been identified as bursting or spalling stresses, depending on their location. Splitting stresses are circumferential tensile stresses resulting from the radial compressive stresses caused by bond. Splitting stresses occur along the transfer length and locally around the prestressing strand.

Bursting and spalling stresses are vertical tensile stresses that develop in the concrete from the distribution of the prestressing force as the force is transferred from the prestressing strand to the concrete at the ends of the member and can result in cracking at different locations in the beam. Spalling stresses are a maximum at the end face of the member, typically near the centroid of the section and result in cracking at the end face, which can propagate further into the member (Gergely et al., 1963). Bursting stresses occur along the line of the prestressing force, beginning a few inches into the beam and extending through the transfer length. Bursting and splitting stresses can result in strand slippage as cracking at the strand can eliminate bond between the strand and the concrete. Figure 2.4.1 shows the location of the bursting and spalling stresses in the end region of a section. Note that the AASHTO (2007) provisions (incorrectly labeled as bursting provisions) and the AASHTO (2010) provisions (incorrectly labeled as splitting provisions) are intended to resist spalling forces (i.e., vertical tensile forces occurring near the end face at the centroid of the member). AASHTO (2010) does not explicitly include provisions for vertical steel to resist bursting and splitting forces (i.e., vertical forces occurring along the line of the prestress in the transfer length region); however the AASHTO confinement reinforcement provisions fill this role.

Distribution of tensile stresses in the end region depends on the eccentricity of the prestressing force in the member, where eccentricity is the distance between the centroid of the prestressing force and the centroid of the member. In a centrally loaded member, forces distribute symmetrically through the

19

vertical member height. Small spalling forces develop on the end face and a bursting force starts further into the member, as shown in Figure 2.4.1-a. In members with large eccentricity, there is greater area above the prestressing force in which the stresses need to distribute. This allows the prestressing force to spread through a greater vertical distance, making the curvature of the flow of stresses greater, creating a larger spalling force near the end region, as shown in Figure 2.4.1-b. This is consistent with previous experimental work which related the maximum tensile stress location to eccentricity. Gergely's (1963) study on post-tensioned I-girders and rectangular sections found members with small eccentricities had maximum tensile stresses in the bursting zone and members with large eccentricities had maximum tensile stresses in the spalling zone. Hawkins (1960) corroborated Gergely's findings and also found as eccentricity increased so did the magnitude of maximum tensile stress in the spalling zone.

The 12 in. deep precast inverted tee sections of the laboratory bridge specimen had slight eccentricities of 2.4 in. for the 3 in. flanged section and 2.5 in. for the 5.25 in. flanged section. Because it was unclear whether this shallow section would have a maximum tensile force in the bursting or spalling zone, tensile stresses in both zones were investigated.

    (a) Centrally prestressed member   (b) Eccentrically prestressed member
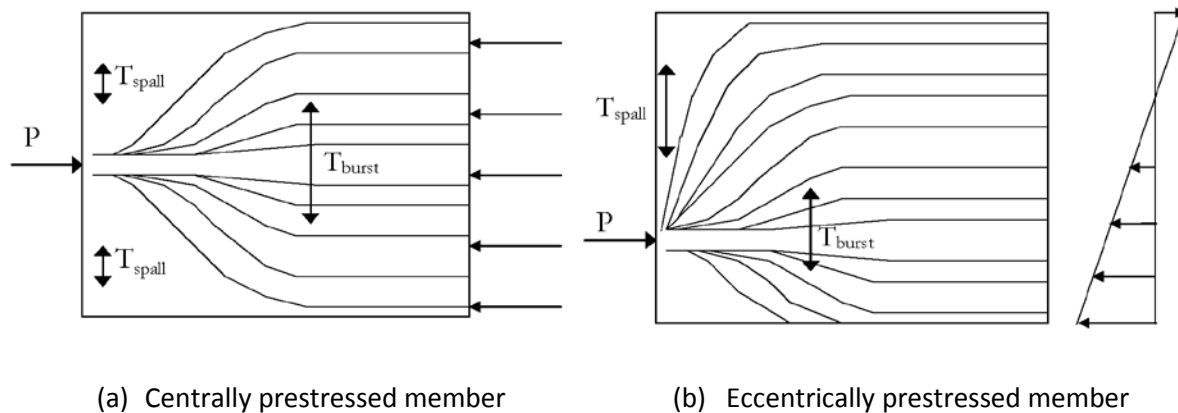
Figure 2.4.1: Effects of eccentricity of distribution of compression and spalling forces

2.4.2. Stresses in End Regions of Post-Tensioned and Pretensioned Sections

Many previous studies investigated the effects of bursting and spalling stresses in post-tensioned members (Gergely et al., 1963; Hawkins, 1960). Only a few examined pretensioned members. The primary difference between post-tensioned and pretensioned systems is the means of introducing the distribution of the prestress force into the members. Post-tensioned systems transfer stress from the steel to the concrete at the end face, through bearing at the end plate, which spreads the force over the end of the member. In pretensioned systems, where the transfer of stress occurs through bond, the stress transfer is often assumed to vary linearly or uniformly until full transfer occurs. The distance needed to transfer the stress from steel to concrete is defined as the transfer length.

Research has shown that tensile stresses in end zones are affected by the transfer length (Base, 1958). Longer transfer lengths in pretensioned systems result in smaller bursting and spalling stresses. Shorter transfer lengths concentrate the transfer of forces, which result in larger bursting and spalling stresses, more similar to the case of post-tensioned systems (Uijl, 1983). Many theories developed from post-

20

tensioned experiments can provide conservative estimates of the spalling and bursting stresses in pretensioned members, because they simulate the case of a very short transfer length.

Chapter 3 PCSSS: Background

3.0   Introduction to Background

Interest in the development of precast composite slab span system (PCSSS) bridges in Minnesota led to research on the topic at the University of Minnesota prior to the initiation of the NCHRP 10-71 project. The results were valuable in selecting appropriate design parameters for the laboratory portion of the NCHRP 10-71 project, and provided important information considered in the development of the comprehensive design guide for PCSSS bridges as part of the NCHRP project.

The first section of this chapter includes a summary of a phone survey that was completed at the outset of the current study. The primary focus of the survey was to identify the principle behaviors and concerns that engineers, contractors, fabricators, and researchers had with the precast slab span bridge system. The results of the phone survey proved very useful in the development of specific characteristics that the PCSSS should be expected to satisfy.

In addition, this chapter includes observations of an existing three-span PCSSS bridge (i.e., Bridge No. 13004) constructed in Center City, Minnesota, by the Minnesota Department of Transportation (Mn/DOT). This bridge was one of the initial implementations of the PCSSS in Minnesota, and was instrumented during construction to measure the load distribution and the potential for the development of reflective cracking. Near midspan of the center span of the bridge, three adjacent longitudinal joints were instrumented to investigate reflective cracking using a series of strain gages placed transversely above the joint. The instruments were monitored for several years following construction. The data collected from this bridge provided a useful data set regarding the behavior of an in-service PCSSS bridge, which was analyzed and utilized during the NCHRP 10-71 study to correlate the laboratory results with measured field data.

In addition to the Center City Bridge, Mn/DOT sponsored the construction and testing of a two-span laboratory specimen located at the University of Minnesota, referred to as the Concept 1 laboratory bridge elsewhere in the report. The Mn/DOT study included the investigation of the development of restraint moments in the Concept 1 laboratory bridge specimen. In addition, Eriksson (2008) completed a numerical and parametric study of restraint moments as part of the Mn/DOT investigation. Because of the previous research conducted regarding restraint moments on the PCSSS, no further investigation on the topic was conducted during the NCHRP 10-71 study, however the experimental data and other available resources from the previous studies were analyzed to provide guidance regarding restraint moments that is included in the design guide developed during the NCHRP 10-71 study.

3.1.   Introduction to Survey Results

This section provides a summary of the comments received from the individual respondents who participated in the phone survey that was used to gather information including the respondents' experience with similar systems, their input on important performance criteria, and their feedback on proposed connection concepts. A more extensive summary of the comments received is included in Appendix C.

Nearly 60 people were interviewed during the phone surveys which were conducted in partial fulfillment of project Tasks 1 and 2. The individuals interviewed were selected through consultation with the project team, David Beal (Senior Program Officer, NCHRP), and interviewees who recommended

others who should be contacted. The respondents represent bridge engineers (including many individuals who serve as State Bridge Engineers), consulting engineers, fabricators, material suppliers, industry representatives, and technical committee contacts. The distribution is presented in Table 3.1.1.

Table 3.1.1: Distribution of phone survey respondents

Bridge Engineer	Material Specialist	Fabricator	Researcher	Industry Rep	Contractor	Other
37	9	6	13	3	0	3

A few survey respondents were identified under multiple categories in Table 3.1.1, so the total number in the table (71) exceeds the number of survey respondents (59). Also note, that although there are no individuals listed under the "contractor" category, a number of bridge engineers and fabricators were able to provide firsthand experience on constructability issues encountered in the field. Attempts were made to include contractors in the survey, but because of the high level of activity with the contractors in the field towards the end of the construction season, and the difficulty in reaching the individuals in the field, this was not possible. The contractor on site during construction of the Mn/DOT implementation of the Poutre Dalle (PD) concept was queried by members of the project team regarding constructability issues, which influenced some of the decisions made in the concept development implemented in the University of Minnesota laboratory specimens described in Chapters 5 and 6. A complete list of the phone survey participants is included in Appendix C.

The phone survey was primarily developed to provide insight into what the respondents considered to be the most important aspects and behaviors that should be considered for a rapid construction bridge system. In addition, respondents were provided with an overview and figure of the Poutre Dalle system as well as the modifications considered in the development o f the Mn/DOT PCSSS, and were asked to share their comments, concerns, and any changes they might consider if they were to implement a similar composite slab span system.

Some respondents (44) provided insight into the relative importance and prioritization of certain characteristics in regards to the PCSSS. The participating respondents were asked to provide a rank ordering, from one to eight (one being the most important), of the following categories: durability, strength, fatigue, seismic, constructability, rapid construction, serviceability/performance, and economy. Some participants did not rank all eight performance categories, and only ranked the one or two criteria considered to be most important. The category that received the highest number of votes was durability, with 91 percent of the 44 participants providing a ranking. A total of 75 percent of the respondents that provided a ranking in the durability category selected it as being the most important, with a ranking of one. The second and third most ranked categories were constructability and rapid construction, with a total of 68 and 57 percent of the respondents providing a ranking. Economy, serviceability/performance, and strength were the fourth, fifth, and sixth most ranked categories, with 45, 43, and 34 percent of the respondents providing a ranking, respectively. The two performance categories least likely to be ranked at all were fatigue and seismic, both with a total of 20 percent of the respondents providing a ranking. A complete breakdown of the rank ordering is provided in Appendix C.

The vast majority of the respondents considered durability to be the primary issue that must be considered with the PCSSS. Many respondents provided additional comments suggesting that reflective cracking between the precast panels would likely be a primary issue with the system. A primary concern among the respondents was in regards to the development of cracking and subsequent ingress of chlorides and the potential for corrosion of the reinforcement. One respondent suggested that the joints between the precast elements would be the weak link of the system, and should therefore be well

23

designed and thought out. The overwhelming consensus that durability was a primary concern regarding the PCSSS was a major driver in the fact that the control of reflective cracking was an essential objective of the project.

3.1.1. Mn/DOT PCSSS and Poutre Dalle System

The survey respondents provided insightful comments and suggestions regarding the original PD system as well as the first implementation of the Mn/DOT PCSSS. Most, if not all, respondents liked the overall concept of the PCSSS, and furthermore thought it could be implemented by their DOT's. Some however, considered the system to be economical only in shorter spans, and did not envision the system as a highway bridge. Several respondents commented specifically on the applicability of the system in locations with vertical clearance requirements. The use of 90 degree hooked transverse reinforcement over the precast joint was favored strongly to the 180 degree version in the French Poutre Dalle system, especially as this allowed for the cage reinforcement to be pre-tied and dropped into position as one piece. A few respondents commented on the use of embedded transverse hooked bars, as it would require perforations of the formwork, which may not be favored by fabricators. One solution to perforated formwork would be the use of threaded bars, where the hooked reinforcement was threaded on after casting, which could therefore be done on-site. One respondent suggested that, if the embedded bars were selected for this system, that a standard bar spacing be selected. The bar spacing should either be constant, or an even multiple, thereby allowing fabricators to perforate their formwork in a given pattern which would not be expected to change.

The use of voids in the precast elements was brought up by a majority of the respondents, both for and against. Proponents of incorporating voids into the system suggested that the large dead weight of the system would be a hindrance, and that fabricating precast beams with voided elements had been successfully completed in the past (Grafton; Hyzak; Khalegi; Tadros). Several respondents however were opposed to the use of voids primarily due to previous performance issues, including durability issues reported by Minnesota and South Dakota.

The use of CIP concrete was discouraged by a number of respondents, primarily because they felt it would be difficult to achieve a significant benefit in terms of rapid construction, and can be costly and difficult to procure in rural areas. The use of CIP concrete in only the trough between each panel was suggested, where the top of the precast web could then be used as the driving surface, however limiting the quantity of CIP concrete was not expected to provide a significant savings. Furthermore, the use of a CIP deck overlay was favored by many respondents because it provided a uniform driving surface, regardless of differential camber in the precast elements, as well as covered the longitudinal joints and ensured the entire driving surface was a uniform color, which was considered to be important to several respondents.

3.2. Center City PCSSS Bridge

The first implementations of the Mn/DOT PCSSS began in 2005 with the design and construction of two precast composite slab-span structures. The first was in Beltrami County, Minnesota with three 45 ft. spans and a precast section depth of 16 in. The second implementation was Mn/DOT Bridge No. 13004 in Center City, Minnesota about 40 miles northeast of Minneapolis. The Center City Bridge was also a three-span bridge with 22, 27, 22 ft. spans and had a 12 in. precast section depth. The depth of the CIP concrete over the webs of the precast elements was 6 in. in both implementations. The CIP above the

webs was reinforced with typical deck reinforcement in both the longitudinal and transverse directions. The plan view and construction stages of the Center City Bridge are shown in Figure 3.2.1.
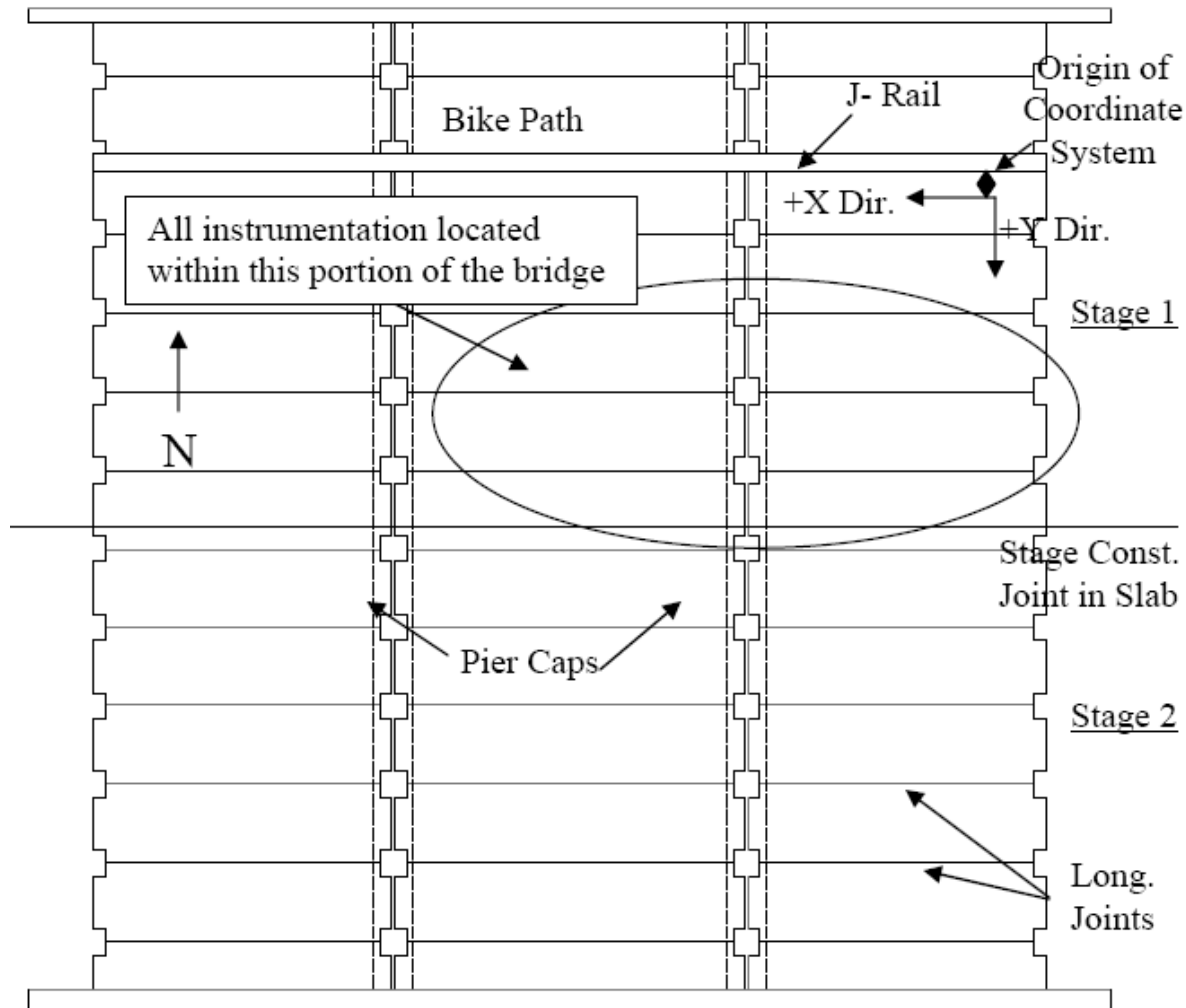
Figure 3.2.1: Plan view and construction stages of Mn/DOT Bridge No. 13004 in Center City, Minnesota (Bell et al. 2006)

The Center City Bridge was instrumented to investigate two primary behaviors, reflective cracking and live load distribution over a continuous pier. Reflective cracking was anticipated to originate from the discontinuity created by the joint between precast panels and/or at the corners of the precast webs near the top of the section, as illustrated in Figure 3.2.2. To facilitate the monitoring of reflective cracking and the overall performance of the structure, the bridge was instrumented with a total of 45 transversely oriented concrete embedment vibrating wire (VW) strain gages and 21 transversely oriented spot-weldable VW strain gages in the trough area between precast panels. The instrumentation to investigate reflective cracking was located solely in the center span of the bridge constructed during Stage 1, as shown in Figure 3.2.1. The instrumentation was distributed over three adjacent longitudinal joint regions, shown in Figure 3.2.3, to provide insight into the performance of each joint as well as the interaction between precast panels.

25
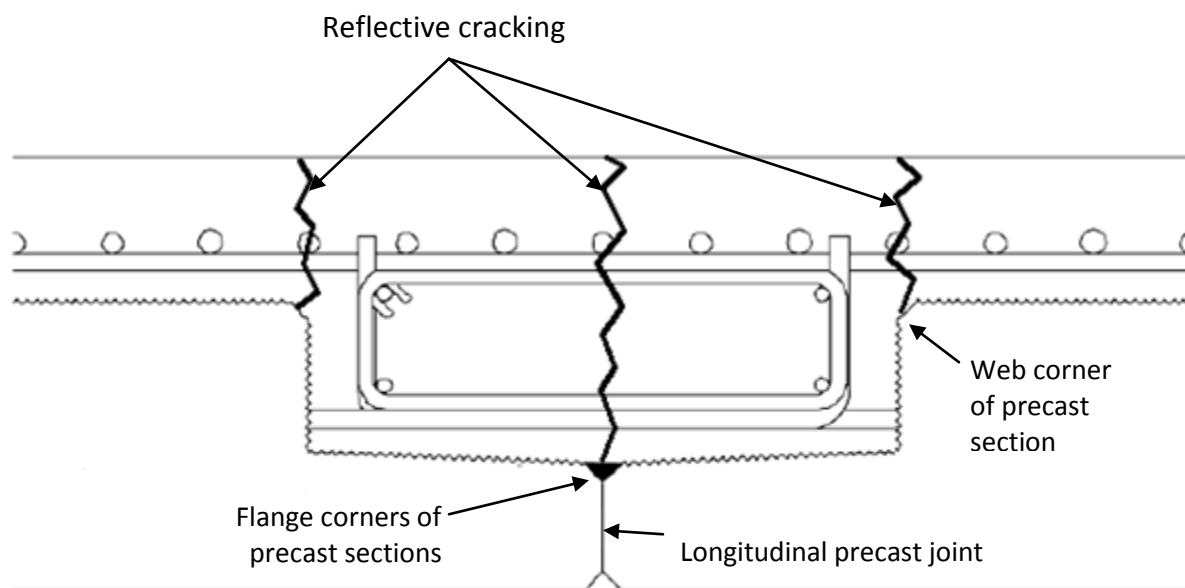
Figure 3.2.2: Anticipated locations of reflective cracking in Mn/DOT PCSSS (Bell et al. 2006)
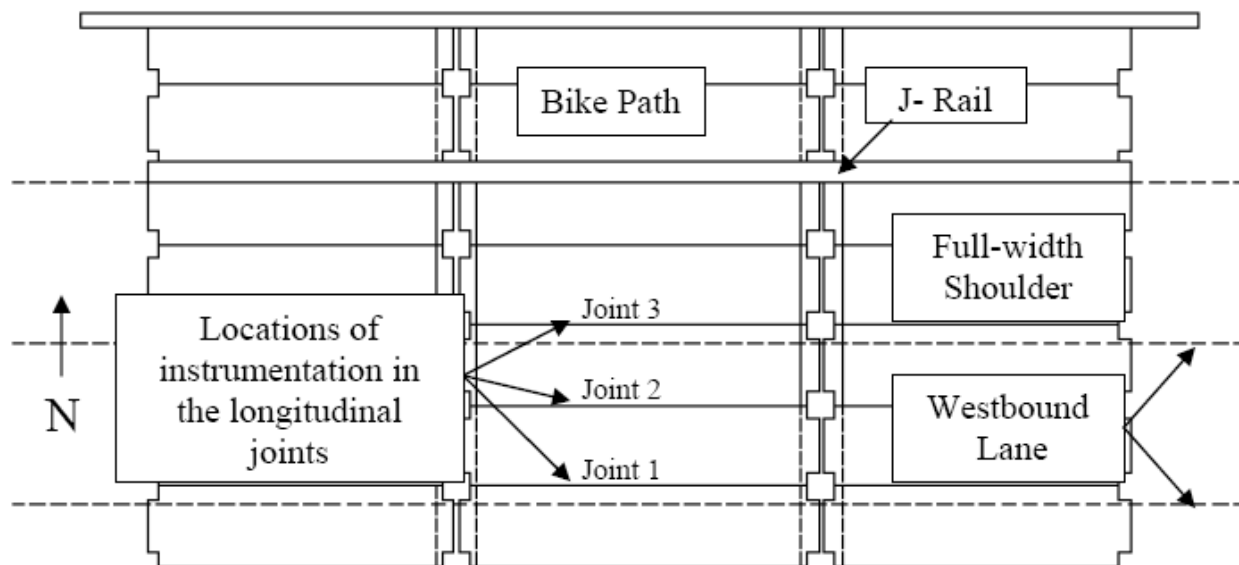
Figure 3.2.3: Location of instrumented joints in the Center City Bridge (Bell et al. 2006)

The concrete embedment gages provided a useful means of exploring the condition of the CIP concrete in the longitudinal trough region and were the primary instrumentation investigated during the NCHRP 10-71 study. All concrete embedment gages in the field bridge were nominally located at midspan of the center span in each of the three instrumented joints. The gages were oriented transversely in the precast trough in two vertical rows. The lower row, nominally placed at the same vertical location as the

26

transverse hooks, contained five gages, while the upper row, placed just above the precast web consisted of ten gages. The instrumentation layout, which was identical at each of the instrumented joints, is shown in Figure 3.2.4. As shown in the figure, the instrumentation was overlapped to better determine the crack location to within a 2 in. region (i.e., gage length was 6 in., gage overlap was 2 in.). If an increase in strain was observed in two adjacent gages, it could be deduced that the crack developed in the region where the gages overlapped. The lower row of gages was embedded only in the CIP concrete and therefore cracking or separation along the vertical precast web interface could not be observed by the instrumentation, unless such a crack extended into the CIP topping.
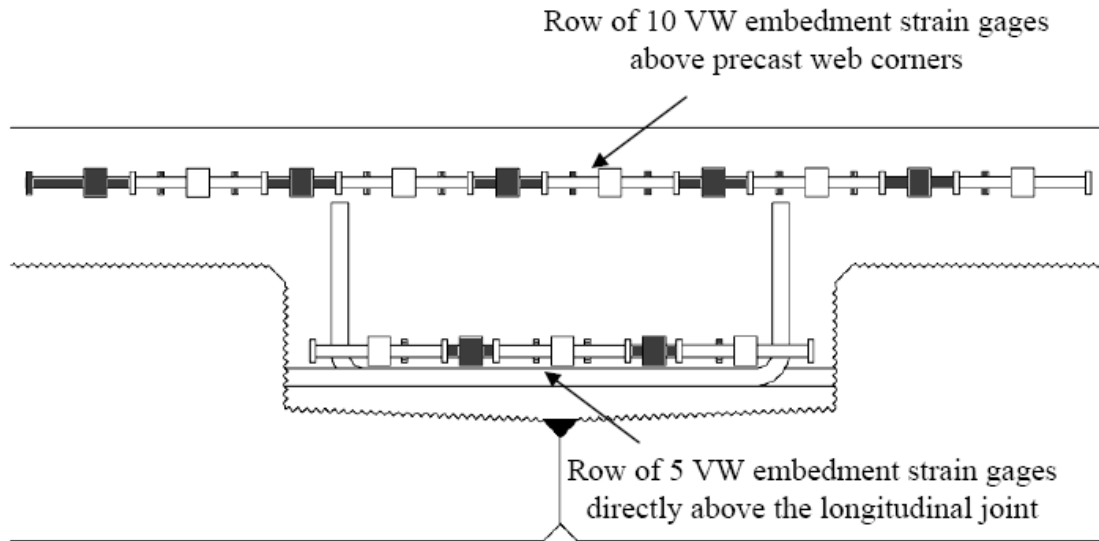
Figure 3.2.4: Location of transverse concrete embedment gages in each of the three instrumented joints at midspan of the center span of the Center City Bridge (Bell et al. 2006)

In addition, seven transversely oriented spot-weldable strain gages were included in each joint to provide insight into the stress demands on the reinforcement bridging the joint between adjacent precast members. The seven gages were installed on two immediately adjacent transverse hooked bars near the group of concrete embedment gages, as shown in Figure 3.2.5.

27

Figure 3.2.5: Lower level of concrete embedment and spot-weldable VW gages utilized in observation of reflective cracking in the Center City Bridge

Furthermore, the bridge was instrumented with longitudinally oriented spot-weldable gages to investigate the behavior of the structure in terms of longitudinal live load distribution over a continuous pier. Because of symmetry, only one pier was considered, as shown in Figure 3.2.1. The longitudinal instrumentation was selected to provide for the calculation of the longitudinal curvature at various cross sections on either side of the continuous pier. The longitudinal instrumentation layout is shown in Figure 3.2.6, where the vertical groups of gages are represented by either a diamond or circle. The gage groups represented by a diamond include three gages vertically distributed through the depth, with one gage on the lower No. 5 longitudinal cage bar, the second gage on the top No. 5 longitudinal cage bar, and the third was attached to the deck reinforcement. At cross sections near the pier, where the longitudinal cage reinforcement was not continuous, only two gages were present through the depth of the section, which is represented by the circle symbols. At these locations, the bottom gage was located on the longitudinal No. 8 bar that was provided near the precast flanges for positive restraint moments, and the top gage was located on the deck reinforcement. In addition, the deck reinforcement above two of the webs on the center span side of the pier were instrumented with single longitudinally oriented spot-weldable strain gages, represented by the triangle symbols in Figure 3.2.6.

28
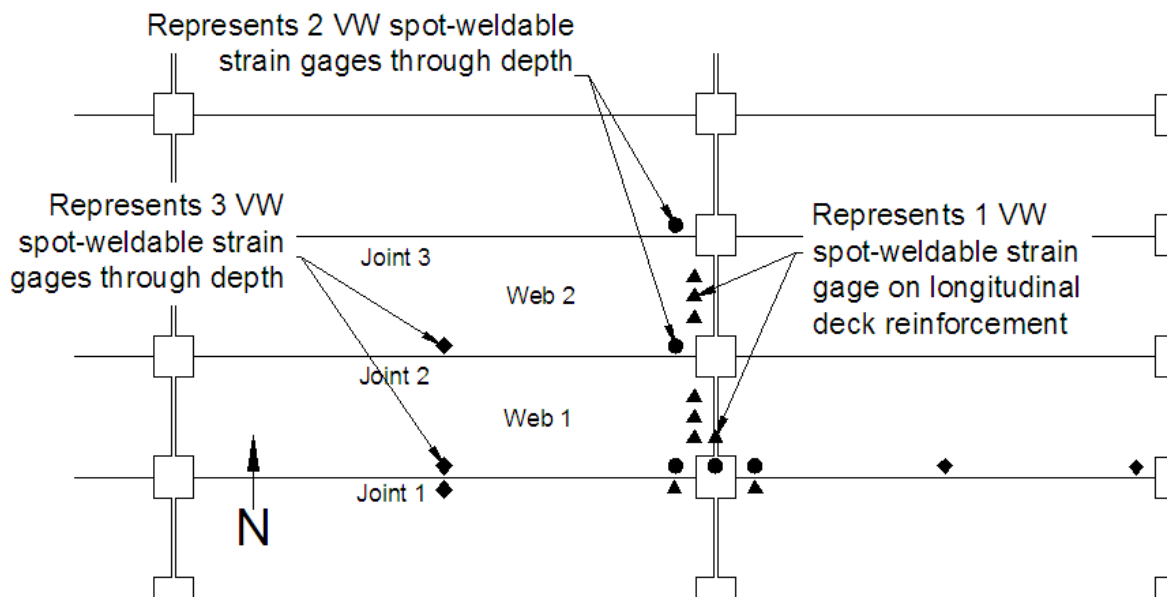
Figure 3.2.6: Plan view of longitudinal instrumentation locations for investigation of live load distribution over the continuous pier (Bell et al. 2006)

The Center City Bridge was constructed with a 5-1/4 in. thick precast flange, which controlled the depth of the transverse hooks and subsequently the vertical location of the instrumentation. The lower level of instruments were installed at a nominal depth, measured from the bottom of the section, of 8.5 in., while the upper row of instrumentation for monitoring reflective cracking was located at a nominal depth of 13.5 in. The nominal and measured instrumentation locations were tabulated by Smith et al. (2008). The nominal and as measured gage locations in the Center City Bridge are included in Appendix D.

The instrumentation naming scheme was described in detail by Smith et al. (2008), and is summarized here. The first two letters of the name refer to the type of gage and general location, "CJ" refers to a concrete embedment gage near the precast joint. The third digit refers to the joint number; therefore "CJ1" refers to instrumentation in joint 1. The fourth digit refers to the longitudinal location of the gage, "5" corresponds to midspan of the center span, which is where all concrete embedment gages were located to monitor the potential for developing reflective cracks (in conjunction with spot-weldable gages on transverse reinforcement). The fifth digit refers to the vertical depth of the gage, with "1" corresponding to the lower row of gages, and "3" corresponding to the top level of gages. Finally, the sixth digit corresponds to the individual gage number in a given row of instruments, and is incremented between one and five for the lower row of gages, and between one and ten for the top row of gages. Therefore, "CJ1-51-3" refers to a concrete embedment gage near the joint region in Joint 1 at midspan of the center span of the bridge, in the bottom layer of instruments and is the third gage in the row of five gages, which was centered directly over the joint.

The data from the instruments was recorded every two hours starting at 10:00am on October 1, 2005. The transverse strains measured at the three instrumented joints at midspan of the center span were monitored over the initial 24 month observation period during the study commissioned by Mn/DOT, as well as afterwards to augment data for the NCHRP 10-71 study. To provide insight into the mechanical strains observed in the bridge, the data collected from the concrete embedment gages was further

29

analyzed. Due to the different values of the coefficient of thermal expansion between the concrete itself and the steel wire inside of the concrete embedment VW gages, taken to be 5.67 με/°F and 6.78 με/°F, respectively, a correction based on the difference between the values of the coefficients of thermal expansion was required to determine the mechanical strain, which was calculated as shown in Eqn. (3.2.1).

$$\varepsilon_{mechanical} = \varepsilon_{measured} + (6.78\ \mu\varepsilon/°F - 5.67\ \mu\varepsilon/°F) * \Delta T \tag{3.2.1}$$

where ΔT is the change in temperature, in degrees Fahrenheit, measured from the base temperature recorded when the initial readings of the strain gages were taken. No correction was necessary for the spot-weldable gages, as they measured the mechanical strain directly.

Large changes in strain observed in Joints 1 and 3 of the structure during the first spring after construction indicated reflective cracking initiated in Joints 1 and 3 on April 25, 2006. Figure 3.2.7 shows the data obtained for Joint 1 which was representative of the behavior of Joint 3 as well. The strain measured in the blue and red gages, which were located directly over and immediately next to the joint, show a large increase and divergence from the other gages starting on April 25, 2006. The blue and red gages correspond with a "3" and "2" as the last number in their name shown in the legend in Figure 3.2.7, respectively; the red gage data series is completely hidden from view by the blue gage data series. The behavior observed in Joints 1 and 3 suggested that cracking was initiated in these joints on April 25, 2006, which was attributed to the effects of solar radiation. Because the bridge was constructed in September of 2005, the bridge was not subjected to significant effects of solar radiation until the spring of 2006. Because the superstructure had been in service and instrumented for a total of 206 days before an increase in the transverse strain was observed, it is unlikely that traffic loading initiated the crack. In fact, strains measured in the transverse joints during subsequent truck load tests conducted in April 2007, as discussed in Section 3.2.1.1, were an order of magnitude smaller than those generated due to the solar radiation effects. Consequently, the reflective cracking was attributed to the effects of large daily variations in the thermal gradient encountered during the spring season due to solar radiation which produced large transverse tensile stresses between the precast panels. Also shown in the figure are the approximate changes in strain over the course of a day during a given summer, with values of 150με and 220με measured during the summers of 2008 and 2009, respectively.

A similar pattern of large measured strains and divergence of Gages 3 and 4 was observed in Joint 3 of the bridge. The approximate relative changes in transverse strain measured in Joint 3 during the summers of 2008 and 2009 were 230με and 300με, respectively. No sudden increase or divergence of the transverse strain was measured in any of the gages located in Joint 2 for the period between October 1, 2005 and July 14, 2009. The presence of cracking in both Joints 1 and 3 was expected to relieve the tensile stresses in the structure which may explain why cracking was not observed in Joint 2; that is, reflective cracking was not originally observed to develop in the adjacent joint.
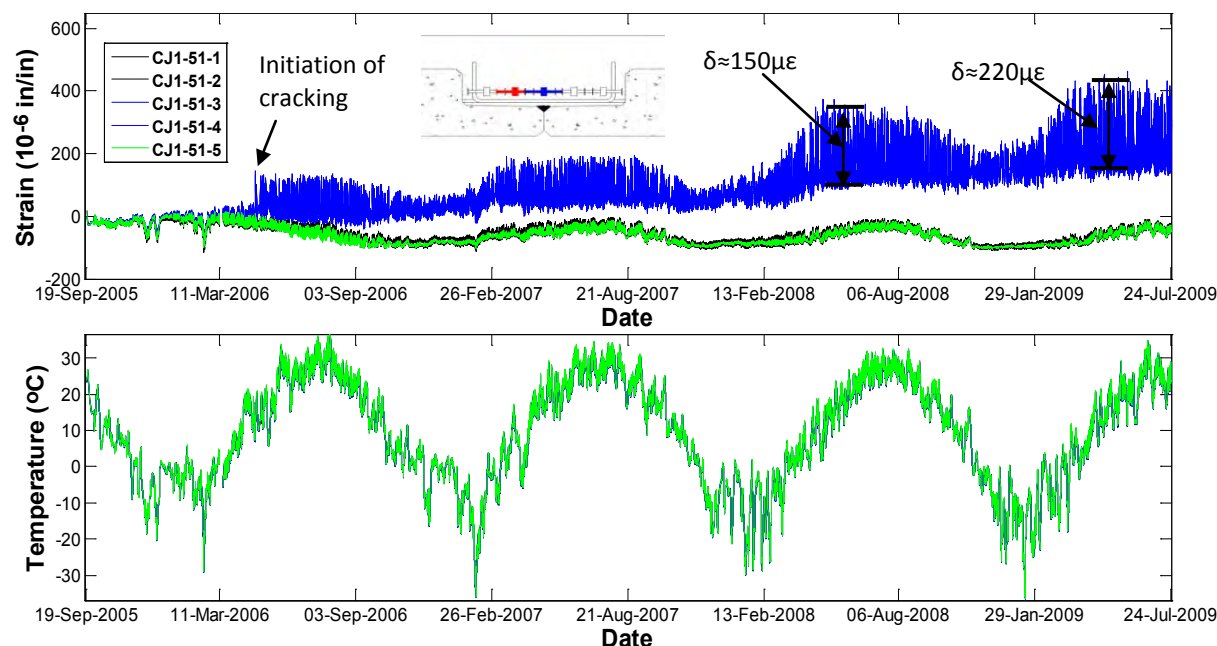
Figure 3.2.7: Measured transverse mechanical strain and temperature in Joint 1 of Center City Bridge [note results of red gage (black dashed line) are obscured by those of the blue gage (blue line) in the figure]

The transverse mechanical strains measured in the Center City Bridge, primarily the relative changes in the strain during a given summer outlined above, provided a quantitative measurement of the performance of an existing bridge in terms of reflective cracking. The measured transverse strains were utilized during the laboratory tests of the NCHRP 10-71 study as a means of determining adequate loading parameters in the laboratory and qualifying the results. The application of the data extracted from the Center City Bridge to the laboratory research specimens is discussed further in Chapters 4 and 5.

Smith et al. (2008) also observed large longitudinal strain readings on the reinforcement near mid-depth of the section at the east pier, which suggested that cracking due to positive restraint moment was present at that location. The daily strain changes of approximately 45 $\mu\varepsilon$ prior to cracking increased to more than 700 $\mu\varepsilon$ on April 23, 2006, which was two days before large increases in the daily strain fluctuations were observed in the transverse directions near the longitudinal precast joints at midspan of the center span. The crack at the east pier was monitored for a little over a year, however the monitoring did not continue past June 21, 2007, when the gage measuring the large daily strain changes began to malfunction. Two longitudinally oriented strain gages located near the top of the section failed to record any large increases in strain over this period, which suggested that the crack had not propagated to the top of the section.

3.2.1. Live Load Distribution Tests at the Center City Bridge

A live load truck test at the Center City Bridge was completed by Smith et al. (2008). The objectives of the live load truck test were to evaluate the response of the structure to known static vehicle loads using the embedded instrumentation, which was subsequently analyzed to determine the applicability

31

of the design assumptions made with respect to transverse live load distribution and continuity over the shared piers. A total of seven single truck and five paired truck configurations were selected for the truck tests, however due to time constraints associated with the single night test, the various configurations were prioritized, with the authors designating the primary test configurations with numbers, and the secondary configurations with letters. The locations of the centroid of the rear truck axles are shown in Figures 3.2.8a and 3.2.8b. The width of the truck axles was measured to be 6 ft.

As shown in Figure 3.2.8a, configurations 1, 2, 3, 4, A, and B were located at midspan of the center span of the bridge, and consisted only of single truck configurations, where the rear tandem of the single truck was centered at midspan of the center span for various lateral positions. The primary purpose of these test locations was to provide several load points across the width of the bridge, which would be useful in calculating longitudinal curvature profiles for many locations along the width of the bridge.

Furthermore, data from the transverse instrumentation collected during these test configurations was utilized to measure the transverse tensile strains in the trough region between the precast panels, where the potential for reflective cracking was a concern. The six truck configurations were selected such that the centroid of the wheels were located either over the precast web (i.e., configurations 2, 4, and A) or directly over the precast joint (i.e., configurations 1, 3, and B), which was expected to represent practical bounds for the minimum and maximum transverse tensile stress demands near the precast joint, respectively. An additional truck position was located at midspan of the outer span (configuration 6) to provide further insight into longitudinal continuity over the pier.

32
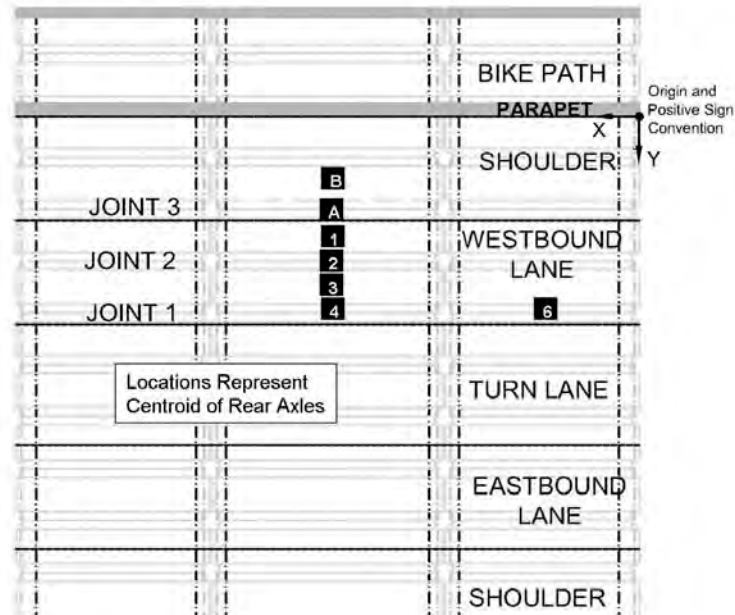
(a) Single truck positions
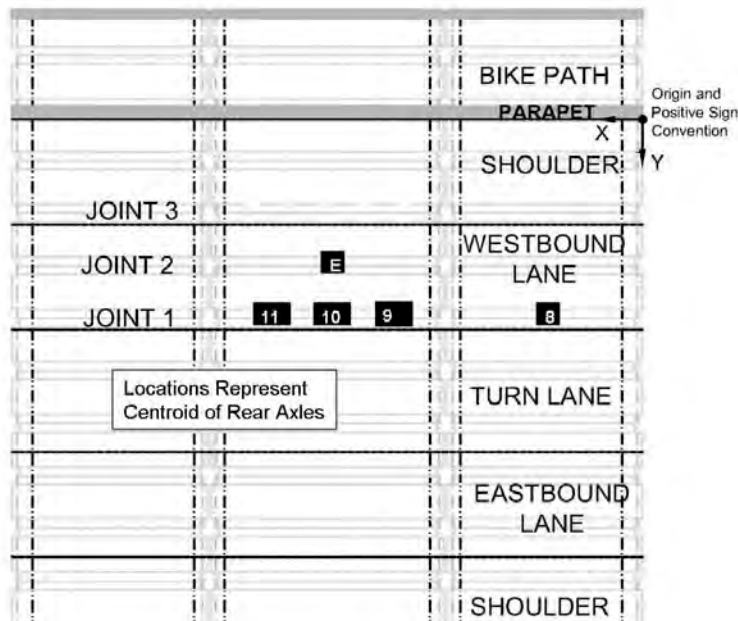
(b) Paired truck positions

Figure 3.2.8: Single and paired truck positions during live load truck tests at the Center City Bridge (Smith et al. 2008)

Paired truck configurations are shown in Figure 3.2.8b which included configurations 8, 9, 10 and 11, in which cases, the two trucks were parked side by side as closely as possible. These configurations were centered over Joint 1, due to the abundance of longitudinal instrumentation near that joint, and were primarily used to investigate longitudinal continuity over the pier. A fifth configuration, designated E,

33

had the rear tandem of the two trucks spaced laterally at 12 ft. on center at midspan of the center span. This orientation located the centroid of one truck directly over Joint 1 and the centroid of the other paired truck directly over Joint 3, thereby loading all three joints by wheel loads transversely located 3 ft. to either side of the three instrumented longitudinal joints. This configuration enabled evaluation of the transverse strains due to global plate bending without the effects of concentrated loads directly over the joints.

The researchers completed the live load tests overnight on April 18, 2007. A total of two tandem sand trucks were utilized, with measured gross vehicle weights of 52.0 and 51.7 kips, which were measured by the contractor away from the test site. Drive-on scales were utilized at the test site to determine the rear axle weights of the individual trucks, however fluctuations in the readings were observed during various weigh-ins due to the fact that the scales elevated the wheels being measured. Therefore, an average rear axle weight was calculated, which was estimated to be 18.6 kips and was applicable to both trucks. Complete tabulated strain measurements from the live load truck tests are given by Smith et al. (2008).

3.2.1.1. Observation of Reflective Cracking during Live Load Truck Tests

The transverse instrumentation located in the three joint regions at midspan of the center span was monitored while wheel loads were individually placed above each joint to investigate the effects of the static loading on the joint regions. When wheel loads were placed above each joint, an increase in the transverse mechanical strains of 19, 7, and 32 με were measured in Joints 1, 2, and 3, respectively. The results obtained for Joints 1 and 2 were calculated as an average over two tests, while three tests were completed over Joint 3. In all cases, the maximum transverse strain was recorded by the middle of the five concrete embedment gages that were located in the lower layer of instrumentation. The increase in the transverse mechanical strains observed during the various test configurations are shown in Table 3.2.1. Instrumentation designation and measured gage locations are given in Appendix D.

Table 3.2.1: Increases in transverse mechanical strains immediately over longitudinal joint during static live load truck tests on the Center City Bridge (Smith et al. 2008)

	Truck Configuration	Strain Value(s) (με)
Joint 1	3	19, 19
Joint 2	1	6, 6
Joint 2	3	8, 8
Joint 3	1	30, 31
Joint 3	B	34

When wheel loads were located directly above the longitudinal joints, the change in transverse strain was positive, indicating that there was an induced tensile stress in each joint, and therefore that loading tended to open the joint. Due to the fact that the three instrumented joints were designed identically, it was expected that each of the three joints should see similar increases in transverse strains under similar loading. Therefore, the results of the live load truck tests suggested that pre-existing cracking was likely to be present in Joints 1 and 3, because of the larger increases in transverse strain observed in those locations. This conclusion was also supported by the long term strain monitoring described in Section 3.2, where it was suggested that reflective cracking was observed in Joints 1 and 3. Furthermore

34

the relative values of transverse strain observed during the live load truck tests were significantly less than the daily strain fluctuations observed in the same Joints during the long term observation, where, as discussed in Section 3.2, daily transverse strain fluctuations of more than 220 $\mu\varepsilon$ were observed. This suggests that transverse strains induced due to thermal gradients can be an order of magnitude larger than those observed due to traffic loading, and therefore should be considered carefully in the design of precast composite slab span systems.

Smith et al. also investigated the strains measured in the transverse hooked bars using seven spot-weldable strain gages placed on two adjacent hooked bars (i.e., three on one hooked bar and four on an immediately adjacent hooked bar) at midspan of the center span in each of the three Joints. The researchers observed that the strains measured in the transverse hooked bars were slightly smaller than those measured in the concrete embedment gages, despite the fact that the spot-weldable gages were located 1-¼ in. lower in the section. The authors suggested that the reduction in the measured strain in the transverse hooked bars may be due to slip between the transverse hooked bar and CIP concrete due to the size of the bar (No. 6) and epoxy coating. Another potential reason for the reduction in the measured strain may be due to localized slip due to reduced bond immediately near the strain gage as a result of the strain gage cover.

The measured increases in transverse mechanical strains in the adjacent hooked bars observed in Joint 1 under a wheel load during the live load tests are shown in Figure 3.2.9. It can be seen in the figure that each of the adjacent transverse hooked bars shared the load approximately equally, and the strain profile for each hooked bar was similar, regardless of the hook orientation, which suggested that the hooked end was equally effective as the embedded end of each bar.

35
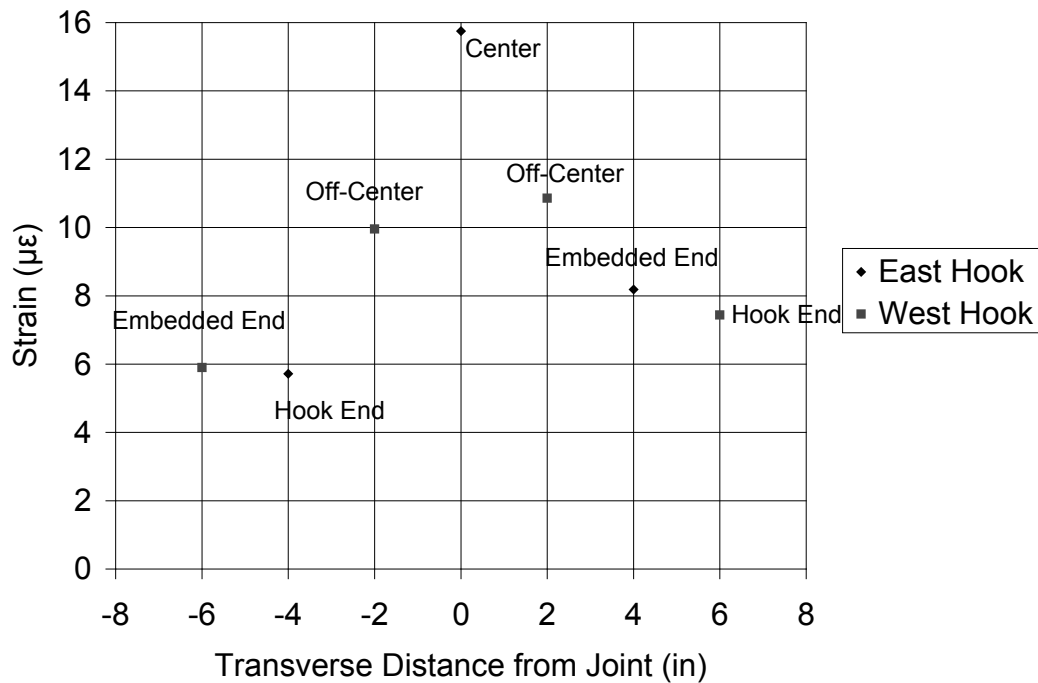
Figure 3.2.9: Change in mechanical tensile strain in transverse hooked bars at Joint 1 immediately under wheel load during live load truck tests on the Center City Bridge (Smith et al., 2008)

3.2.1.2.   Transverse Load Distribution During Live Load Truck Tests

Smith et al. (2008) utilized the longitudinal curvature data collected during the live load truck tests to investigate the ability for the Center City Bridge to transfer live loads transversely to adjacent precast panels. In addition, the researchers were interested in the applicability of the AASHTO 2004 Specification Article 4.6.2.3 slab-type bridge load distribution factors, which were utilized in the design of the Center City Bridge (note that the AASHTO Article numbering and content has not changed between the 2004 and 2010 specifications). The authors subsequently utilized the effective width calculations for slab-type bridges to analyze the performance of the Center City Bridge during the truck tests. Configurations 1, 2, 3, 4, A, and B of the truck test were utilized to investigate live load distribution. In each case, longitudinal curvatures calculated at midspan of the center span were measured using the spot-weldable gages located on the longitudinal reinforcement in Joints 1 and 2. Using this procedure, the longitudinal curvature at each joint was calculated as the distance from the joint to the center of the truck load was varied from 0 in. when the center of the truck was immediately over the joint, to as much as 180 in., which was the distance from the center of the truck to Joint 1 in Configuration B.

The longitudinal curvatures were estimated as the slope of the best fit line through three spot-weldable gages nominally located at 9, 12.5, and 15.5 in. from the bottom of the precast section, though measured locations were utilized in the calculation of the curvatures. The longitudinal curvatures measured as a function of the distance from the center of the truck load to Joints 1 and 2 are shown in Figure 3.2.10. Also included in the figure are the results of a finite element analysis assuming an isotropic flat plate with a smeared stiffness representing the composite section stiffness of the Center

36

City Bridge. The authors included the parapets in their model, however found that the results were affected only locally by the parapets, and therefore were able to superimpose the data for each of the six configurations onto the single plot. Also included in the figure is a simple-span model, which was calculated assuming that the center span was modeled alone on roller bearings located at the center of each pier, thus providing a center to center of bearing simple span of 306 in. Finally, Figure 3.2.10 also illustrates the design equations provided by AASHTO LRFD (2004) Article 4.6.2.3, which provided the effective width factors for slab-type bridges.
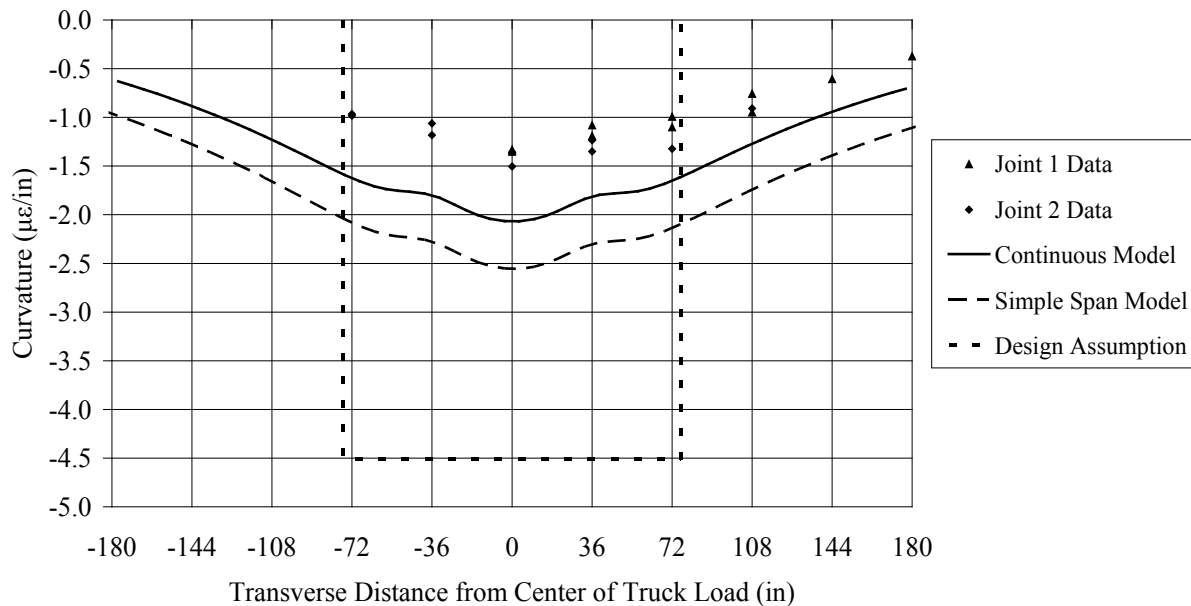
Figure 3.2.10: Longitudinal curvatures at midspan due to a single truck located at midspan of the center span of the Center City Bridge (Smith et al. 2008)

It is evident from Figure 3.2.10 that the measured longitudinal curvatures in the Center City Bridge followed the continuous isotropic model predictions well. Also observed from the figure are the relative similarities in the magnitudes of longitudinal curvatures at common distances from the center of the truck loads. This suggested that loads applied at various distances from Joints 1 and 2 tended to affect each joint similarly, despite suspected reflective cracking in Joint 1 (see Section 3.2). For this reason, the authors suggested that the PCSSS could be adequately modeled using an isotropic plate, which was expected to be simpler because it removed the need to model the discontinuity created by the longitudinal precast joint. Furthermore, the simple span model was found to be more conservative than the continuous model, and would also adequately serve as a method for numerical analysis of the PCSSS.

These results also provided significant insight into the applicability of the current design equations provided for slab-type bridges in the AASHTO (2004) LRFD Specification. As shown in the figure, the curvatures determined via the slab-type design equations were approximately three times larger than the curvatures measured in the Center City Bridge when the wheel load was centered directly over the longitudinal joint. For this reason, the slab-type effective lane widths presented in the AASHTO LRFD Specifications (2004) were deemed to be adequate and conservative for the design of precast composite

37

slab span systems. It can be assumed that longer spans would behave similarly because they would have a deeper overall section, and the height of the gap at the flange tips would be unchanged, so longer span bridges should behave more like monolithic systems than shorter ones.

3.2.1.3.   Continuity over the Continuous Piers during Live Load Truck Tests

Another behavior of interest considered by Smith et al. (2008) was the level of continuity achieved between the piers. For this case, midspan of the center span was loaded directly over Joint 1 and the longitudinal strains in the deck reinforcement of the adjacent span were recorded and compared to the values calculated using the isotropic continuous finite element model. When the center span was loaded, changes in longitudinal strains in the deck steel of the adjacent span were 1.2 and 1.5 με for single and double truck configurations, respectively. These values were slightly smaller than those predicted by the continuous FEM model, where values of 1.9 and 3.7 με were predicted for single and double truck configurations, respectively. A likely reason for the discrepancy between the measured and predicted values was attributed to moment transferred into the pier cap, whereas idealized rollers were assumed in the finite element model. In addition, the midspan curvatures in the center span were observed to be smaller than those predicted in the model, as discussed in Section 3.2.1.2. The overall performance of the Center City Bridge during the truck tests suggested that the assumption of full continuity appeared to be conservative for the precast composite slab span system.

3.3.   Restraint Moment

Multi-span precast composite bridge structures made continuous with CIP concrete develop time-dependent and thermal restraint moments at the continuous piers. The sign and magnitude of restraint moments are affected by shrinkage, creep, age of the precast members at the time of continuity, and thermal gradients. Positive and negative restraint moments are illustrated in Figure 3.3.1.

Negative restraint moments are caused by differential shrinkage of the CIP concrete, where the rate of shrinkage of the CIP concrete is larger than the rate of shrinkage and creep of the precast member. When the precast member is at a relatively old age, defined as greater than 90 days in AASHTO (2010) Article 5.14.1.4.4, the shrinkage of the newly placed CIP concrete will tend to "shorten" the top fiber of the bridge structure and subsequently induce longitudinal tensile stresses in the top of the bridge at the piers. The reinforcement included in the deck of the structure over the piers in continuous systems provides the tension ties necessary to counteract negative restraint moments.
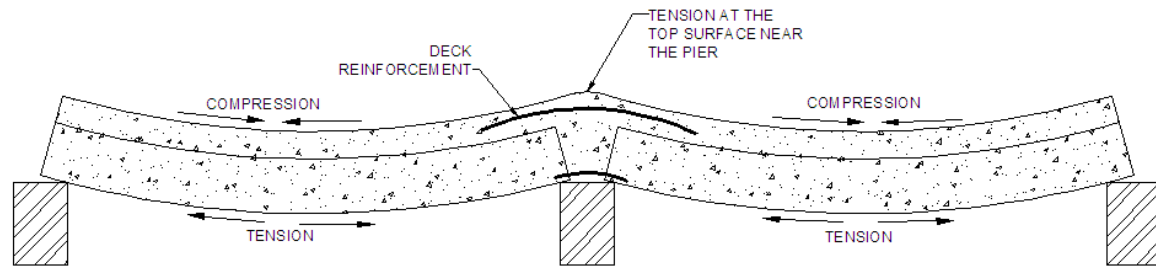
(a) Negative restraint moment induces tension near the top surface at the pier
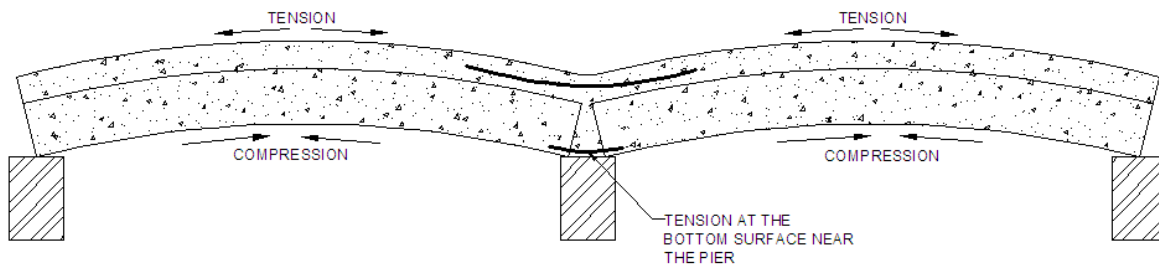
(b) Positive restraint moment induces tension near the bottom surface at the pier

Figure 3.3.1: Positive and negative restraint moments in continuous bridge superstructures (Molnau 2007)

Positive restraint moments at the piers in continuous systems may be due to both time-dependent and thermal effects. When the precast member is at a relatively young age at the time of continuity, the rate of shrinkage of the precast member and the CIP may be similar, however, the precast member would also undergo creep. The creep of the precast section would tend to "shorten" the bottom fiber of the bridge structure and subsequently induce longitudinal tensile stresses in the bottom of the bridge at the pier. In addition, thermal gradients in the section cause the top surface of the structure to expand, again inducing a positive restraint moment in the structure. For this reason, both time-dependent and thermal gradient effects must be considered in the design of positive restraint moments. Because positive restraint moments induce longitudinal tensile stresses near the bottom of the section, reinforcement must be provided to carry the tensile force at the piers. Because of the sectional geometry of the PCSSS, all reinforcement provided for positive restraint moments must be located within the longitudinal trough regions between precast panels. Consequently, this reinforcement must be placed in groups centered between panels, generally six feet apart, thereby prohibiting the distribution of the reinforcement along the face of the bottom surface.

Smith et al. (2008) monitored the Center City Bridge for evidence of cracking due to restraint moment. Gages located at the pier indicated that cracking initiated due to the effects of positive restraint moment. The crack was believed to develop as the bridge underwent its first large thermal gradient effects due to solar radiation in the spring. As a consequence, it was suspected that the behavior was driven by thermal gradients in the bridge superstructure where the solar radiation heated the top of the bridge. This caused the individual spans of the bridge to camber which generated positive restraint moments. Eriksson (2008, pp. 56) stated, "Because [the] time-dependent effects on [the day the crack

39

was observed] should not have varied significantly from the previous day, researchers speculated thermal effects may have played a role in the crack development. Based on this conjecture, both time-dependent and thermal gradient effects on restraint moment were investigated analytically." Eriksson (2008) completed a parametric study to investigate the effects of differential shrinkage, creep, and thermal gradient effects on the development of restraint moments.

In an effort to predict the restraint moment in a section based on the time-dependent properties of the system, Eriksson completed a numerical parametric study using Pbeam, which is a fiber-based finite element code developed by Suttikan at the University of Texas in 1978 (Suttikan, 1978). The program allows for inputs including material strength, age, creep, shrinkage, steel relaxation, dead loads and support conditions. The program provides output in the form of stresses, strains, reactions and deformations at user specified time intervals (Suttikan 1978). Furthermore, Eriksson utilized a modified version of Pbeam created by Le (1998), called TPbeam, which enables incorporation of thermal gradient effects in the analysis. After finding that, when using functions based on measured quantities for the input values (i.e., creep, shrinkage, concrete strength gain with age, etc.), Pbeam predicted restraint moments that corresponded reasonably well with the measured results from the Concept 1 laboratory specimen, Eriksson utilized both Pbeam and TPbeam to conduct a parametric study to determine reasonable bounds for expected restraint moments in PCSSS bridges. In general, the purpose of the parametric study was to predict the maximum positive and negative restraint moments that would be expected in PCSSS bridges. Precast strengths of 6 ksi and 12.9 ksi were used with assumed continuity dates of 7, 28, 60, and 90 days to develop an expected envelope of the positive and negative restraint moments.

Because of the difficulty in providing reinforcement for positive restraint moment due to the geometry of the PCSSS, the necessity to design for such moments was of interest. Eriksson found that, "positive restraint moment cracking due to time-dependent effects is not expected for [PCSSS] for spans between 20 and 50 ft" as seen in Figure 3.3.2 where the ratio of positive restraint moment to cracking moment is always less than one when only time-dependent effects were included. Also, positive restraint moment generally induced at the pier was due to creep of the precast member, therefore increasing the age of the precast member at continuity will reduce the positive restraint moment due to time-dependent effects in the section. The thermal gradient due to solar radiation has the same effect as placing CIP on a young precast section. The results from TPbeam substantiate NCHRP 519 findings that state restraint moments due to thermal effects are significant (Miller et al. 2004). Eriksson (2008) found that the positive restraint moments caused by thermal effects induced restraint moments that were two to seven times larger than the positive restraint moments caused by time-dependent effects as shown in Figure 3.3.3. As a consequence, positive restraint moment cracking due to thermal gradient effects was expected to occur in nearly all of the designs studied, and therefore should be considered by the designer.
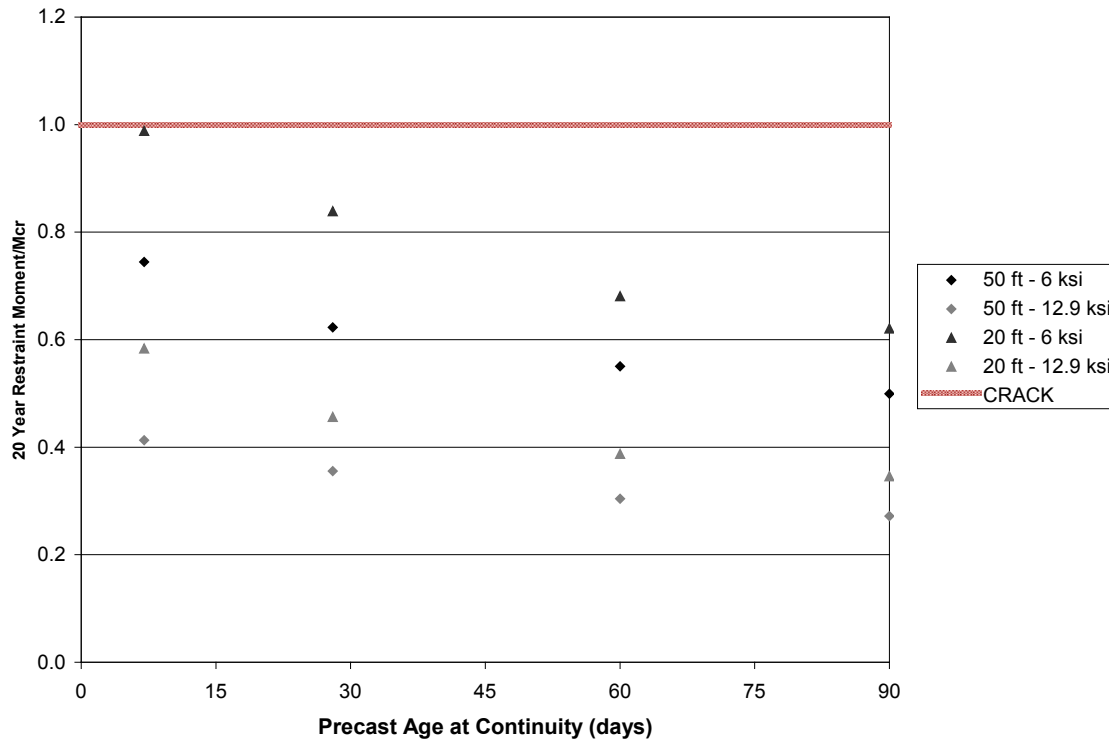
Figure 3.3.2: Ratio of 20-year positive restraint moment (due to time-dependent effects only) to cracking moment comparison
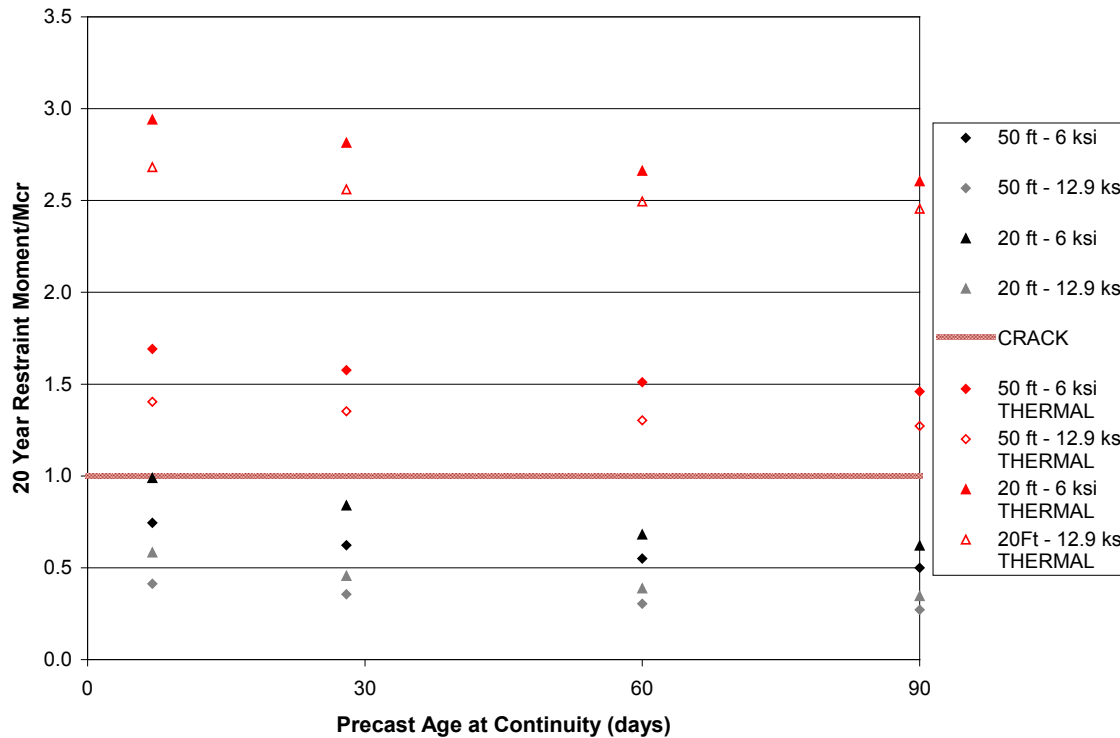
Figure 3.3.3: Ratio of 20-year positive restraint moment (due to time-dependent and thermal effects) to cracking moment comparison

AASHTO (2010) Article 3.12.3 provides general guidelines for design of thermal gradients based on regional zones, but indicates temperature gradient should be evaluated on a project specific basis. Judgment is reserved for experienced designers indicating thermal gradient can be neglected if previous structures have not experienced distress. These basic guidelines provide little guidance regarding when thermal gradients are important. Based on the fiber-based finite element model results from Pbeam and TPbeam and the suspected positive moment crack in the Center City Bridge, thermal effects have a significant effect on the development of positive restraint moments and should be considered in the restraint moment design.

Restraint moment design for time-dependent properties is complicated by the need to investigate the interaction of the variation in time-dependent effects over time. The PCA and P-method both provide options for how to design for restraint moments due to time-dependent effects. However, design for restraint moments caused by thermal effects does not include the time variation and should be summed with restraint moments due to time-dependent effects.

Barker and Puckett (2007) provide a hand calculation for determining the restraint moment due to thermal effects. Assuming the beam is a simple span between supports, the design thermal gradient is applied to the section and used to calculate the resulting curvature in the beam. The curvature from a temperature gradient can be expressed as

$$\phi = \frac{\alpha}{I} \cdot \int T(y) \cdot y \cdot dA \qquad (3.3.1)$$

42

where α is the coefficient of thermal expansion, $T(y)$ is the temperature gradient (°F) through the depth y of the member (in.), and I is the moment of inertia of the entire cross section (in.[4]) (Barker and Puckett, 2007). This equation is also found in AASHTO (2010) Article C4.6.6.

The end rotation (θ) can be found by integrating the curvature from midspan to the end of the span. Then, the restraint moment, or the moment restraining the rotation, can be found using the three-moment equation. The equation assumes pinned-end supports and is expressed as

$$M = 3 \cdot \theta \cdot \frac{E \cdot I}{L} \qquad\qquad (3.3.2)$$

where θ is the rotation, E is the elastic modulus (for the composite system), and L is the span length.

The moment, M, is the restraint moment at the pier of a continuous system to resist the rotations induced by the thermal gradient. If the span lengths on each side of the pier are not equal, then the different spans will induce different moments at the pier (i.e., the rotation would be different, leading to different moments).The restraint moments induced by thermal gradients in each span can be calculated using Eqn. (3.3.2) and the design thermal gradient should be for the largest restraint moment. The effects of thermal gradients and time-dependent effects can be calculated independently and then combined with the appropriate load factors.

Using the above methodology for prediction of the thermally-induced restraint moments in the 20 and 50 ft. span beams in the parametric study conducted by Eriksson (2008) provided conservative results as compared to the TPbeam results, as shown in Figure 3.3.4. The hand calculations over-predicted the calculated positive restraint moment by a range of 20 to 40 percent. The calculations agreed with TPbeam results that the highest ratio of positive restraint moment induced by a thermal gradient to the cracking moment (i.e., 2.9) was for the 20 ft. span with 12.9 ksi concrete. The shorter span with greater concrete strength had the greatest stiffness and the least flexibility of the sections studied. The 50 ft. span with 6 ksi concrete, the most flexible section studied, had the lowest ratio of positive restraint moment induced by thermal gradient to cracking moment (i.e., 0.95).

43
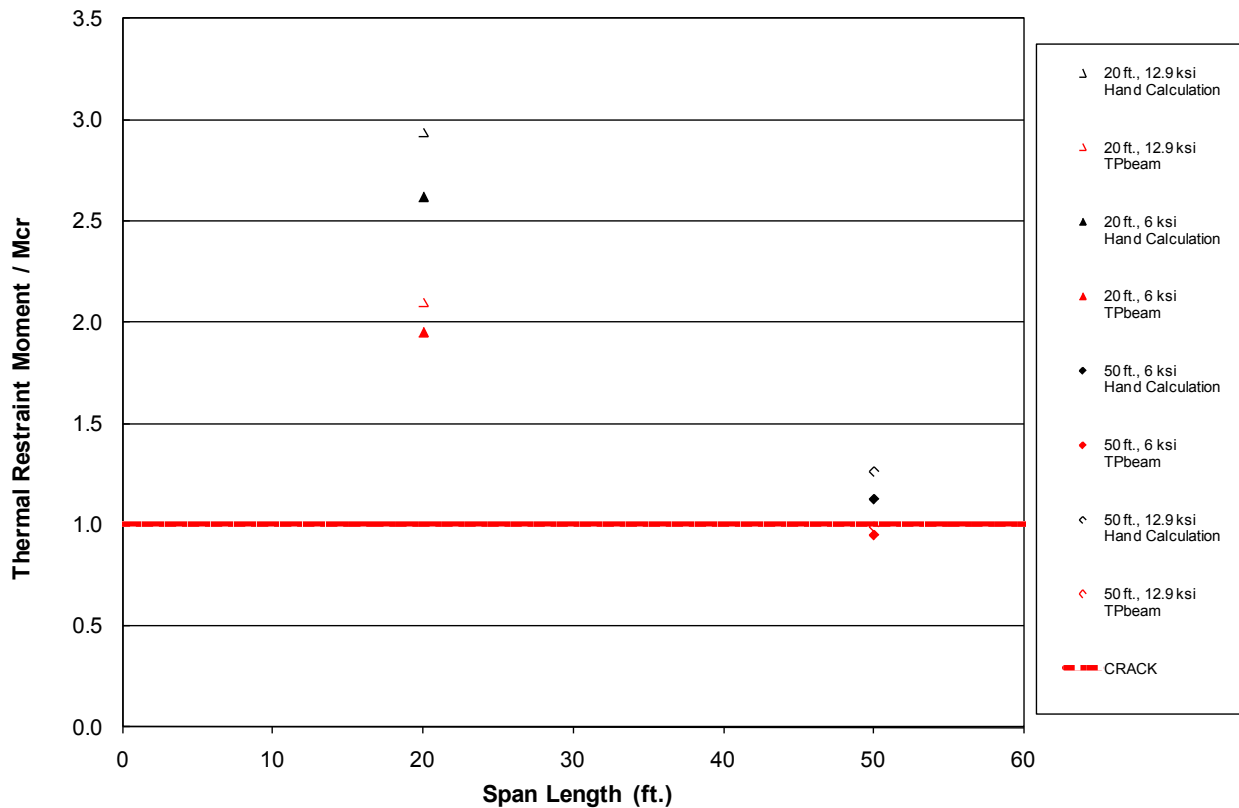
Figure 3.3.4: Comparison of calculated and TPbeam results for ratio of 20-year restraint moment (due to thermal effects only) to cracking moment

The magnitude of the positive restraint moments, with the inclusion of the effects of thermal gradient, may negate any benefit from continuity at service. In this case, if positive moment reinforcement steel is placed at the pier to tie the structure together, the possibility of developing a positive moment at the pier cannot be neglected and the restraint moment should be taken as the lesser of the calculated restraint moments and the moment that can be developed using the positive moment reinforcement placed at the pier.

44

Chapter 4 PCSSS Numerical Studies: Practical Span Ranges, Applicability of Design Recommendations, and Other Issues

4.0   Introduction and Organization

A combined numerical and experimental approach was used to investigate issues associated with the development of design recommendations for the precast composite slab span system. In a few cases, where appropriate, design recommendations for the PCSSS were based on information obtained from the literature or previous studies conducted by the researchers (Smith et al. 2008, Eriksson 2008). Issues of interest included:

- Determination of range of applicability for PCSSS bridges (Section 4.1)
- Control of reflective cracking across the longitudinal joint between precast flanges
    - Effect of transverse reinforcement spacing (Section 4.2)
- Applicability of slab-span design recommendations to PCSSS bridges
    - Live load distribution factors (Section 4.3)
    - Skew effects (Section 4.4)
- Composite action between the precast and CIP
- Effect of restraint moment due to time-dependent and thermal gradient effects
- End zone stresses in precast inverted tee sections (Section 4.5)
- Support conditions (Section 4.6)
- Determination of appropriate magnitude of patch load to be applied to laboratory specimens to represent range of possible span lengths (Section 4.7)

This chapter primarily focuses on the numerical investigations associated with these issues.

Regarding the range of applicability for the PCSSS, it was expected to be most efficient for relatively short to moderate span bridges. A parametric study was conducted over a range of span lengths for both simply-supported and continuous PCSSS models to provide greater insight into the range of spans that could be efficiently bridged using the PCSSS. Because of the shallow member depths associated with this type of superstructure, the service behavior and effective moment capacity of the section was largely dependent on the amount of prestress force, due to the fact that the moment arm is relatively short in comparison to traditional girder-type bridges. For this reason, one of the primary limiting components of the precast inverted-T design was the level of prestress that could be achieved, while the appropriate stress limits in the specification were satisfied. The parametric study therefore was utilized to identify the appropriate span lengths that could be efficiently achieved, and the corresponding prestress force and member depths that would be required, which is summarized in Section 4.1.

A primary issue of importance for the NCHRP 10-71 study was the development of durable connection concepts. In the case of PCSSS bridges, the control of the development of potential reflective cracking is key to the achievement of a durable system. There is the potential for the development of reflective cracks in the CIP from stress raisers associated with the precast portion of the section (i.e., above the joint between the precast flanges and near sharp corners of the precast section). With regard to the issue of reflective crack control, numerical studies summarized in this chapter were used to investigate the effect of the transverse reinforcement spacing on reflective crack control, as well as on transverse load transfer. These studies are described in Section 4.2. Reflective crack control was also investigated extensively through the laboratory studies described in Chapters 5 and 6 which detail the results of the laboratory bridge and subassemblage tests, respectively.

PCSSS bridges are very similar to slab-span systems, with two exceptions. First, the adjacent flanges of the precast inverted-Ts used to create the PCSSS bridges cause discontinuities in the system along the interface of the adjacent flanges; and second, the composite nature of the PCSSS requires additional design considerations. To investigate the applicability of slab-span design recommendations to PCSSS bridges which feature the discontinuity along the adjacent flanges, numerical studies were conducted as described in Sections 4.3 and 4.4 regarding live load distribution and skew effects. Numerical models of the PCSSS featured discontinuities along the adjacent flanges which were compared to the results of models of monolithic systems. In some cases, additional models were developed to investigate the influence of potential reflective cracking on the performance of the systems. The PCSSS was expected to provide live load distribution in a similar manner to that of traditional monolithic slab-span superstructures, a conclusion that was supported by the numerical modeling. Furthermore, the effects of skew were expected to increase the magnitude of longitudinal shear stress in the region between the tips of the precast flanges, especially in the exterior joints between the members. Several FEM models were utilized to provide insight into the behavior of the system and the potential increases in stress at various locations of the system due to skew, and to determine the applicability of the current specifications to the PCSSS.

The composite nature of the PCSSS required an investigation of the detailing requirements across the interface between the precast and CIP. In addition, the composite nature of the system required investigation of the potential for the development of restraint moments due to the time-dependent effects of creep and shrinkage. The required detailing across the interface between the precast and CIP to ensure composite action was investigated through a review of the literature, as well as through laboratory studies of the PCSSS Concept 1 and 2 bridges which were subjected to ultimate load tests as described in Chapter 5. The effect of restraint moments in the PCSSS were investigated numerically and experimentally in a previous study by the researchers, the results of which can be found in Smith et al. (2008) and Eriksson (2008). These results summarized in Section 3.3 provided the basis for the associated design recommendations in this study.

The precast inverted-T sections of the PCSSS also required review of associated design recommendations for the precast prestressed elements particularly for the development of detailing requirements associated with end zone stresses because current requirements were found to be developed considering I-sections rather than panel systems. This aspect was investigated numerically and experimentally as described in Section 4.5.

The connection between the precast elements and the substructure was investigated primarily by means of examination of structural plans for existing PCSSS structures. This review is summarized in Section 4.6.

Numerical analyses were also used to determine the patch load to be used for the laboratory investigations conducted on the Concept 1 and 2 PCSSS bridges discussed in Chapter 5. These analyses are summarized in Section 4.7.

4.1. Parametric Study to Investigate Practical Span Ranges and Associated Precast Sections

The weight associated with the precast composite slab span system, like most slab bridges, was expected to limit the range of applicable spans to what may be considered short to moderate spans. The PCSSS was expected to be a practical system for bridges with spans up to approximately 60 ft. In an effort to clearly identify and document the range of spans and associated section dimensions and design details for the PCSSS, a parametric study was completed. The study aimed to identify efficient span

lengths, as well as the required prestress forces and to ensure that the compression and tension stress limits were satisfied in the inverted-T sections.

Span lengths of 20, 30, 50, and 65 ft. were identified as practical and efficient for the precast slab span system. The 20 ft. span length was chosen to represent the shortest practicable span length; the span range between 30 and 50 ft. was selected because of the large applicability of this system, while the 65 ft. span was chosen as a maximum feasible span length for the PCSSS. In addition, with the recommendation from K. Molnau (Mn/DOT), more representative configurations were considered, which included 20-30-20 ft., 30-50-30 ft., and 50-50-50 ft. three-span continuous systems. Because it was expected that a two-span 50-50 ft. would not differ significantly from the behavior of the 30-50-30 ft. three span bridge, a sole 65-65 ft. configuration was selected to investigate two-span systems.

Moment envelope curves were developed for the configurations listed above, and were considered for two dynamic load situations as specified by the AASHTO (2010) LRFD specifications, HL-93 and Tandem vehicles, in addition to a static uniformly distributed lane load of 640 lb/ft.^{2} patterned along the length of the system. A dynamic allowance factor equal to 0.33 was selected for the moving load cases. Live load distribution factors were calculated according to a modified version of the AASHTO (2010) specifications (Article 4.6.2.3), *Equivalent Strip Widths for Slab-Type Bridges,* as shown in Eqn. (4.1.1). The effective lane width was considered with two or more lanes loaded, and the limiting lane width factor of 12.0W/N_L was not considered.

$$\overline{}$$

$$(4.1.1)$$

where E is the equivalent lane width when two or more lanes are loaded (in.), L_1 is the modified span length taken equal to the lesser of the span length or 60.0 (ft.), and W_1 is the modified edge-to-edge width of the bridge taken to be equal to the lesser of the width or 60.0 (ft.).

Initially positive and negative restraint moments were assumed to be zero during this portion of the study, which corresponded with the assumption that the CIP concrete was placed after the precast members were at a relatively old age. When the casting of the bridge deck is completed much later than the casting of the precast elements (i.e., 90 days as specified by the specification) the time-dependent drivers of positive restraint moments can be neglected (however the effects of thermal gradients should be considered).

Later consideration included the calculation of the restraint moments for two configurations, the 50-50-50 ft. and 65-65 ft. systems. In both cases, the age of the precast members was taken to be 14 days when continuity was established. The moments were calculated using the PCA method (Freyermuth, 1969). Depending on the age of the precast at which continuity is made and the amount of time since continuity, the PCA method is considered to predict accurate magnitudes for the maximum positive moments but generally overestimates the negative restraint moments. The method is based on both structural mechanics concepts and creep/shrinkage experimental data.

In this study, the positive restraint moments were more thoroughly considered because they were expected to influence the design of the system more significantly than the negative restraint moments. The positive restraint moments increase the magnitude of the positive moment at midspan at service, and are difficult to resist because of the limited locations available to include continuous reinforcement near the bottom of the section at the piers (i.e., in the troughs between the precast webs).

The material properties utilized in each model were identical. The concrete compressive strength of the CIP and precast concrete was taken to be 4 and 6 ksi, at 28-days, respectively. The precast concrete strength was assumed to be 5 ksi at transfer. A 6 in. thick composite CIP deck was identical in each model. The strands were assumed to be 0.5 in. diameter Grade 270 low relaxation strands pulled to a

47

stress of 202.5 ksi (75 percent of f_{pu}). The flange thickness was kept constant at 3 in., and the standard width inverted-T sections of 6 ft. were used. The increased stiffness associated with the deck reinforcement was ignored during this study, which was consistent with similar calculations used by Mn/DOT during the design of bridge systems, and was conservative. Losses were calculated using the Zia method (1979).

The primary metrics utilized to determine the appropriate design parameters for each configuration were the stress limits specified by AASHTO (2010). Two limit states were investigated, transfer and service. The compression and tension stress limits for each are shown in Table 4.1.1.

Table 4.1.1[1]: Concrete stress limits utilized during parametric study

	PC Concrete	
	Limit	Value
Transfer		
Compression	$-0.6 \cdot f_{ci}$	-3 ksi
Tension	$0.24 \cdot \sqrt{f_{ci}}$	0.537 ksi
Service		
Compression	$-0.45 \cdot f'_c$	-2.7 ksi
Tension	$0.19 \cdot \sqrt{f'_c}$	0.465 ksi

[1]All units in Table 4.1.1 are in units of ksi, i.e., f_c is entered into the equations in units of ksi (regardless of whether there is a square root function or not) and the results of each stress limit are in ksi

The design process was found to be governed by the stress limits at transfer at the ends of the beams, and the stress limits at service at midspan. In most cases, the tension limit for the bottom fiber at midspan at the service state was found to control.

Table 4.1.2 presents a summary of selected optimized sections for the individual span lengths. For each of the optimized sections, the table summarizes the total precast section depth; the assumed flange thickness, which was taken as 3 in. (76 mm) except in the case of one of the spans which was designed to replicate the short spans in the Center City field implementation of the bridge; cross-sectional area; required number of strands to meet the service stress limits; required concrete compressive strengths at transfer and service to meet the required stress limits; total prestress force assumed immediately after transfer; span configuration in which the section was assumed; and the limiting stress ratios in the design of the sections. In cases where the design stresses were exceeded, recommended changes were provided to alleviate the limit exceedance. In cases where the compressive stress limits were exceeded, the design concrete compressive strengths at release were increased; in cases where the tensile stress limits were exceeded, the required mild reinforcement to carry the full tensile force is listed.

As mentioned above, the bottom fiber tension stress limits controlled at service in most of the cases. Satisfying the bottom fiber tensile stress limits at service required increasing the number of tendons (total prestressing force) or increasing the depth of the section. An increase in the value of the maximum positive moment at midspan (longer spans), required a larger number of tendons to satisfy the stress limits and, when this was not feasible, the depth of the section was increased. When considering the effect of the positive restraint moments, the total positive moment acting at midspan was increased and so it was necessary to increase the amount of prestress for the same section.

In considering the feasibility of the systems according to the different configurations described above, important issues were identified associated with the weight of the precast section that might be

controlled by truck load capacities in transport or crane capacities at erection. For the truck load limits, the sections should be limited to 80 kips (350 kN) without requiring a special permit. Typical crane capacities can readily handle the 80 kip (350 kN) capacity (this value could be as high as 130 kips (580 kN) in some cases).

As an example, in the case of the 65 ft. (19.8 m) span section, an initial minimum depth of 20 in. (500 mm) was considered for the precast section, but it required three rows of tendons. The amount of prestress caused problems with the tensile and compressive stress limits at the ends at release and compressive stress limits at midspan at service. Increasing the depth of the precast section to 22 or 24 in. alleviated these issues to an extent. Using a 22 in. deep precast section with 54 tendons, required a concrete compressive strength at transfer of 6 ksi rather than the nominal value of 5 ksi. Using a 24 in. deep precast section with 46 prestressing tendons alternatively solved the problem but with this depth the weight of the precast section exceeded 80 kips, which could be an issue with transport.

Table 4.1.2: Precast section dimensions and results of parametric study

Span Length [ft.]	20	30	22[1]	22[1]	45	50	62	65
Depth of Precast [in.]	8	10	12	12	14	16	20	22
Flange Thickness [in.]	3	3	5.25	3	3	3	3	3
Cross-Sectional Area [in.^{2}]	460	560	710	650	750	840	1000	1100
Number of Strands	10	16	16	16	36	38	46	54
Concrete Strength at Transfer [ksi]	5	5	4.5	4.5	5.5	5.4	5.6	6
Concrete Strength at Service (ksi)	6	6	6	6	6	6	6	6
Prestress Force [kip]	306	500	500	500	1100	1200	1400	1700
Span Combination [ft.]	**20**[2]-30-**20**	20-**30**-20	**22-22**	**22-22**	45-**62**-45	**50-50-50**	45-**62**-45	**65-65**
Limiting Ratios in Design of Sections								
End stresses at transfer including mild reinforcement and f_{ci} modifications required to satisfy end stresses								
$f_t /(0.24\sqrt{f_{ci}}$ ksi)	<1	<1	<1	<1	1.51	1.73	2.04	2.11
Solution, A_s [in.^{2}]	--	--	--	--	6-#5	9-#5	10-#6	12-#6
$f_c /(0.6f_{ci}$ ksi)	<1	<1	<1	<1	1.08	1.08	1.12	1.20
Solution, f_{ci} [ksi]	--	--	--	--	$f_{ci}'=5.4$	$f_{ci}'=5.4$	$f_{ci}'=5.6$	$f_{ci}'=6$
Midspan stresses at service Section depth and number of strands were chosen to satisfy end stresses								

[1]Represents the precast sections used in the Center City Bridge and Concept 1 and Concept 2 large scale laboratory specimens
[2]Bolded span lengths indicate the span utilized for the sectional design parameters in that column

In summary, the range of span lengths considered during this study was found to provide a reasonable bound for applicable span lengths for the PCSSS. The 65 ft. simply supported system would require 54

0.5 in. diameter strands. Because the prestressed strand is concentrated within the 4 ft. web width of the inverted-T section, it would take more than two layers of strands at 2 in. centers to accommodate 54 tendons. This would not be the most efficient use of the system because the short member depths require that the longitudinal reinforcement is grouped as low in the member as possible to increase the eccentricity and moment arm. Also, at the lower bound, the 20 and 30 ft. spans provide a relatively economical design with the moderate member depth and number of tendons.

4.2.   Parametric Study to Investigate Effect of Transverse Hook Spacing on Reflective Cracking

Finite element parametric modeling was used to investigate the influence of the spacing between transverse hooked reinforcement on the transverse load transfer and reflective crack controlling capabilities of the PCSSS. The geometry of the bridge specimen was similar to that used in the large-scale Concept 1 laboratory bridge, consisting of a two-span continuous bridge, however each span utilized in the model was 30 ft. Each span consisted of two adjacent 6 ft. wide precast panels. Several models were developed to investigate the range of transverse hooked bar spacing between 6 and 18 in. Each model was constructed using 20 node quadratic continuum elements with reduced integration. The boundary conditions were roller supports at the ends of the bridge and a perfectly frictionless pin at the continuous pier. Loading was applied to correspond with the magnitude and patch size utilized in the laboratory study, which was 35 kip and 10 by 20 in., respectively. The load was oriented such that the long direction of the patch was perpendicular to the direction of the longitudinal precast joint. Two load cases were considered, the first was with loading centered at midspan directly over the precast joint and the second was at midspan with the edge of the load aligned with the edge of the vertical precast web, as illustrated in Figure 4.2.1. A summary of the FEM test cases is given in Table 4.2.1.
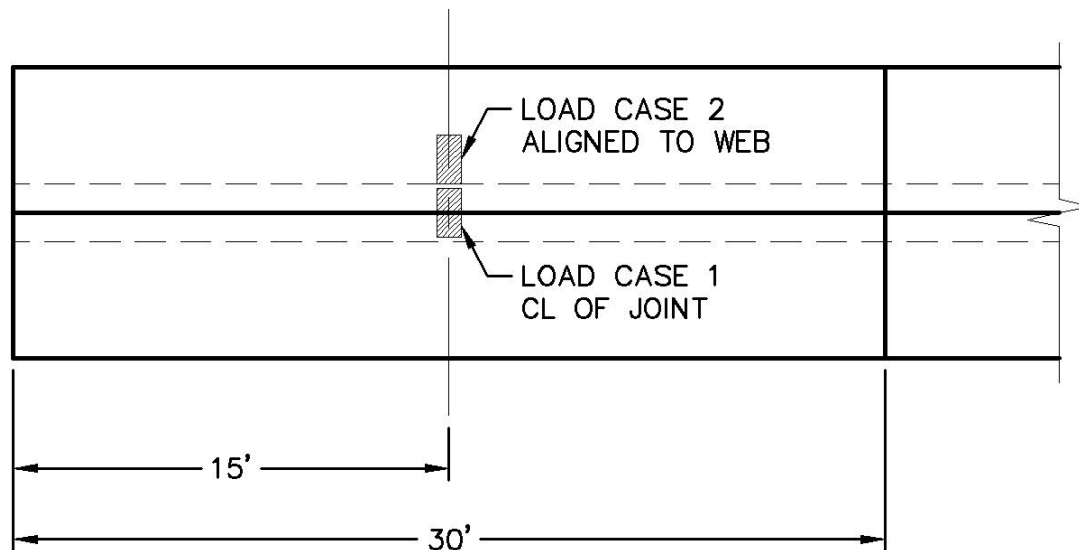
Figure 4.2.1: Location and orientation of loading in the loaded span of the two-span bridge model

Except for the transverse hooked bars crossing the longitudinal joint, rebar and prestressing strands were approximated as plates with negligible stiffness in all directions except axially in the orientation of the rebar. The transverse hooked bars were modeled as beam members with a 3/4 in. diameter circular

50

cross section. The transverse hooked bars were debonded for 1-1/2 in. on either side of the longitudinal joint for a total debonded length of 3 in., which was selected as an approximation of the bond condition between the rebar and concrete in the joint area.

Four materials were used throughout the model. All CIP concrete was assumed to have an elastic modulus of 3,600 ksi, which was determined using AASHTO LRFD Article C5.4.2.4-1, assuming normal weight concrete with a compressive strength of 4,000 psi and Poisson's ratio of 0.2. All precast concrete was modeled assuming an elastic modulus of 4,600 ksi, which was calculated using the above equation and normal weight concrete with strength of 6.5 ksi and Poisson's ratio of 0.2. The plates used for modeling the rebar were assumed at have a modulus of elasticity of 1 psi and Poisson's ratio of 0.2; the low elastic modulus of the plates was selected to ensure that they did not contribute to the section stiffness globally. All rebar layers embedded within the plates (including mild steel and prestressing strands) were modeled with a modulus of elasticity of 29,000 ksi and Poisson's ratio of 0.3.

In model Runs 1, 2, and 3 the cast-in-place was bonded only to the sides and top of the precast panel webs. The precast flanges were assumed to be unbonded from the CIP concrete. The unbonded flanges were selected to simulate the separation of the flanges from the CIP above the longitudinal joints. These runs assumed reflective cracking to approximately the depth of the elastic neutral axis in transverse bending for the 12 in. hooked bar spacing. The crack was assumed to extend vertically a distance of 9 in. from the bottom of the section. The fourth run depicted a fully bonded slab, where the CIP was completely bonded to the precast panels and the joint between the tips of the precast panels was eliminated through the use of tied elements between the adjacent members. This fourth run simulated a monolithic slab span.

Table 4.2.1: Summary of FEM runs to investigate effects of transverse hooked bar spacing

	Run Number	1	2	3	4
Description	*Run configuration*	*PCSSS w/crack (6in. hook spacing, hooks lapped w/1in. stagger)*	*PCSSS w/crack (12in. hook spacing, hooks lapped w/1in. stagger)*	*PCSSS w/crack (18in. hook spacing, hooks lapped w/1in. stagger)*	*Solid slab, no crack (12in. hook spacing, hooks lapped w/1in. stagger)*
Geometry	*Spans:*	*2*	*2*	*2*	*2*
	#Panels wide	*2 (no outside flange) - 10ft wide*	*Same*	*Same*	*Same*
	Length	*30ft-30ft*	*Same*	*Same*	*Same*
	Depth of precast section	*3in.flange; 12in. web*	*Same*	*Same*	*Same*
	Depth of deck above precast web	*6in. CIP*	*Same*	*Same*	*Same*
	Supports	*Pin at center support, rollers on ends*	*Same*	*Same*	*Same*
Crack	*Simulated "crack" using contact elements.*	*Bottom of section to 9in. from bottom (half depth).*	*Same*	*Same*	*No Crack*
Material strength	*CIP Concrete*	*4ksi*	*Same*	*Same*	*Same*
	Precast Concrete	*6.5ksi*	*Same*	*Same*	*Same*
	Reinforcement	*60ksi*	*Same*	*Same*	*Same*
Reinforcement	*Deck steel*	*#8-#7-#7 @ 4in. oc* *Run along entire span length*	*Same*	*Same*	*Same*
	Transverse hooks in each direction (offset transversely by 1in.)	*#6@6in. (1" offset over joint)*	*#6@12in. (1" offset over joint)*	*#6@18in. (1" offset over joint)*	*#6@12in. (1" offset over joint)*
	Vertical location of transverse reinforcement	*4-5/8" center of #6 from bottom of form*	*Same*	*Same*	*Same*
	Prestressing strands	*16 in each PCSSS*	*Same*	*Same*	*Same*
	Transverse cage	*None*	*None*	*None*	*None*

In each model run, it was enforced that at least one solid element along the length of the bridge was unfilled with transverse hooked bars (i.e., in the case of the 18 in. spacing, two elements were often unfilled per transverse hooked bar). This causes the plots to appear "spiky", as elements without rebar were free to open more than the reinforced elements. Figure 4.2.2 shows a comparison of the crack opening of runs where all elements were reinforced versus runs where at least every other element was unreinforced. The crack opening was measured directly above the precast joint, in the tension fiber of the CIP concrete. The case with all elements reinforced tended to fall between the bounds defined by the spikes in the plot for the case where not all elements had reinforcement. It was assumed that the case where not every element was reinforced better approximated the variations in the joint opening

52

for a physical bridge, so the method of leaving every other element void of rebar was used throughout the analyses.
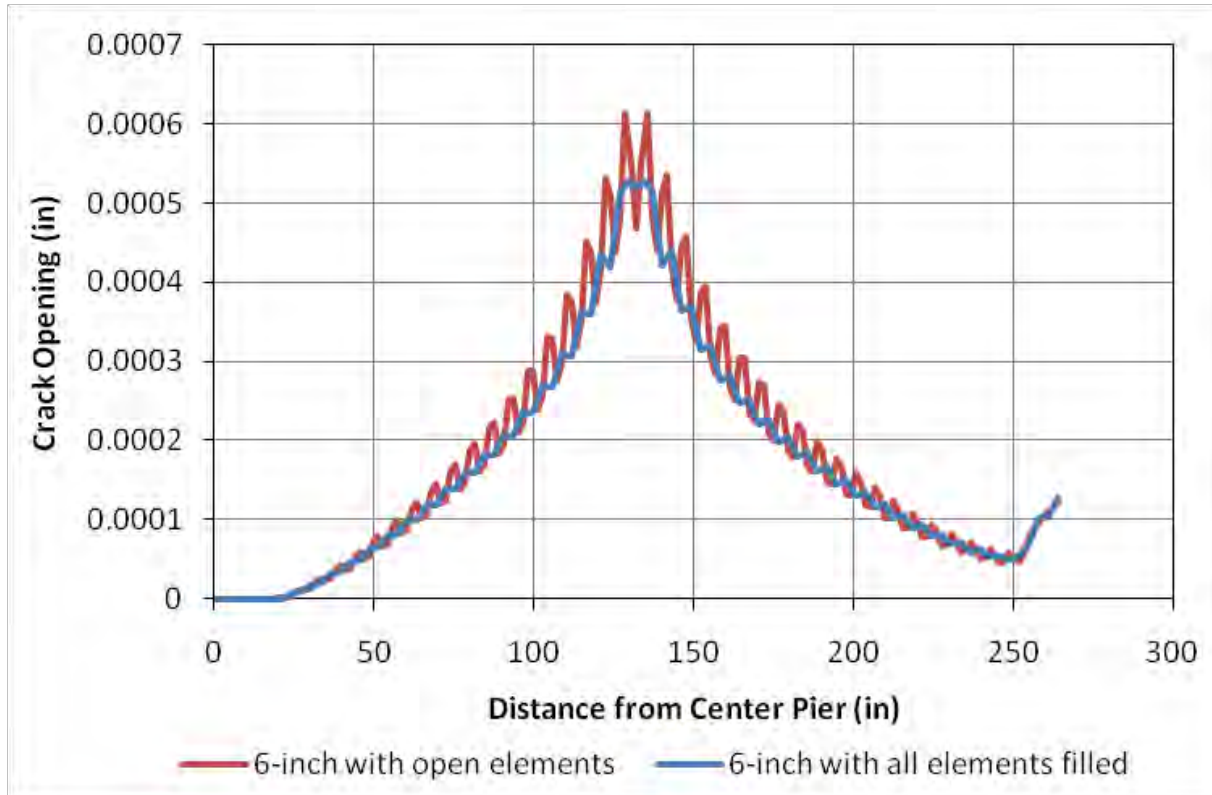
Figure 4.2.2: Crack opening in loaded span for 6 in. hooked bar spacing with or without one rebar per solid element

The measured bar stress and maximum crack opening in the loaded span for load case 1 (i.e., load at midspan with the edge of the load aligned with the edge of the vertical precast web) is plotted as a function of the transverse hooked bar spacing in Figure 4.2.3. A strong linear relationship was observed between the stress in the bar and the measured crack opening at the precast flange-CIP interface and the spacing between the transverse reinforcement, with a correlation coefficient between the three data points of 0.999 and 0.993, respectively. The linear relationship between the bar spacing and both the stress in the reinforcement and maximum opening suggests that the effectiveness of the reinforcement is not degraded as more reinforcement is added. The proportional constant between the amount of reinforcement and the crack size/bar stress remained constant for the range of reinforcement spacing values considered during this study.

53
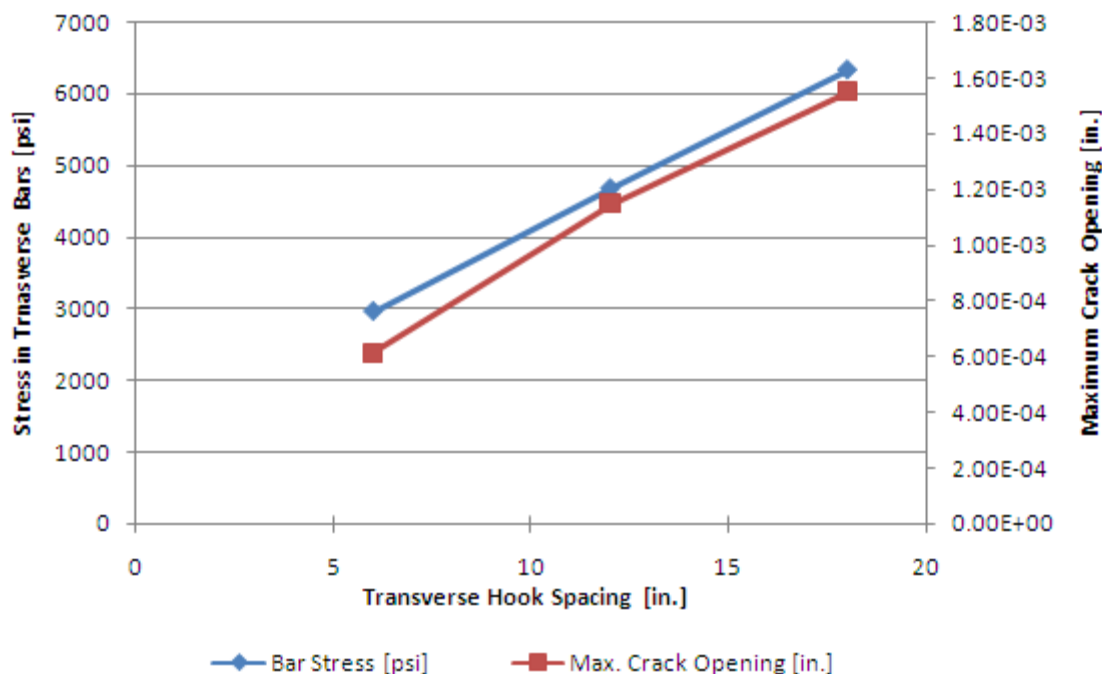
Figure 4.2.3: Maximum crack opening and transverse bar stress versus transverse hooked bar spacing in loaded span for load case 1

The effect of the spacing of the transverse hooked bars on transverse and longitudinal load distribution was also investigated during the parametric study. The transverse and longitudinal stress fields created by loading due to both load cases provided insight into the ability for each model to distribute the load throughout the structure. The transverse and longitudinal stress fields observed during the FEM runs for both load cases are shown in Figures 4.2.4-4.2.7. For the 6 and 12 in. spacing cases, the centerline of the patch load was centered over a pair of transverse hooks, while in the 18 in. spacing case the patch load straddles the hooks such that the edge of the patch load was relatively near the adjacent hooks. The center pier is illustrated in each model with the thick white line at the middle of each contour plot. Contour scales, which represent stress in units of psi, are also provided for each plot. For all cracked analyses (i.e., Runs 1 through 3), there was little variation in the overall distribution of the stresses, suggesting that the spacing of the transverse reinforcement had little effect on the ability for the PCSSS to distribute localized loading between adjacent panels and spans, which might be attributed to the proximity of the load to the reinforcement in all cases. As expected, noticeable variation in the transverse stress fields was observed between the cracked and uncracked model.

54

(a) 6 in. spacing (run 1)

(b) 12 in. spacing (run 2)

(c) 18 in. spacing (run3)
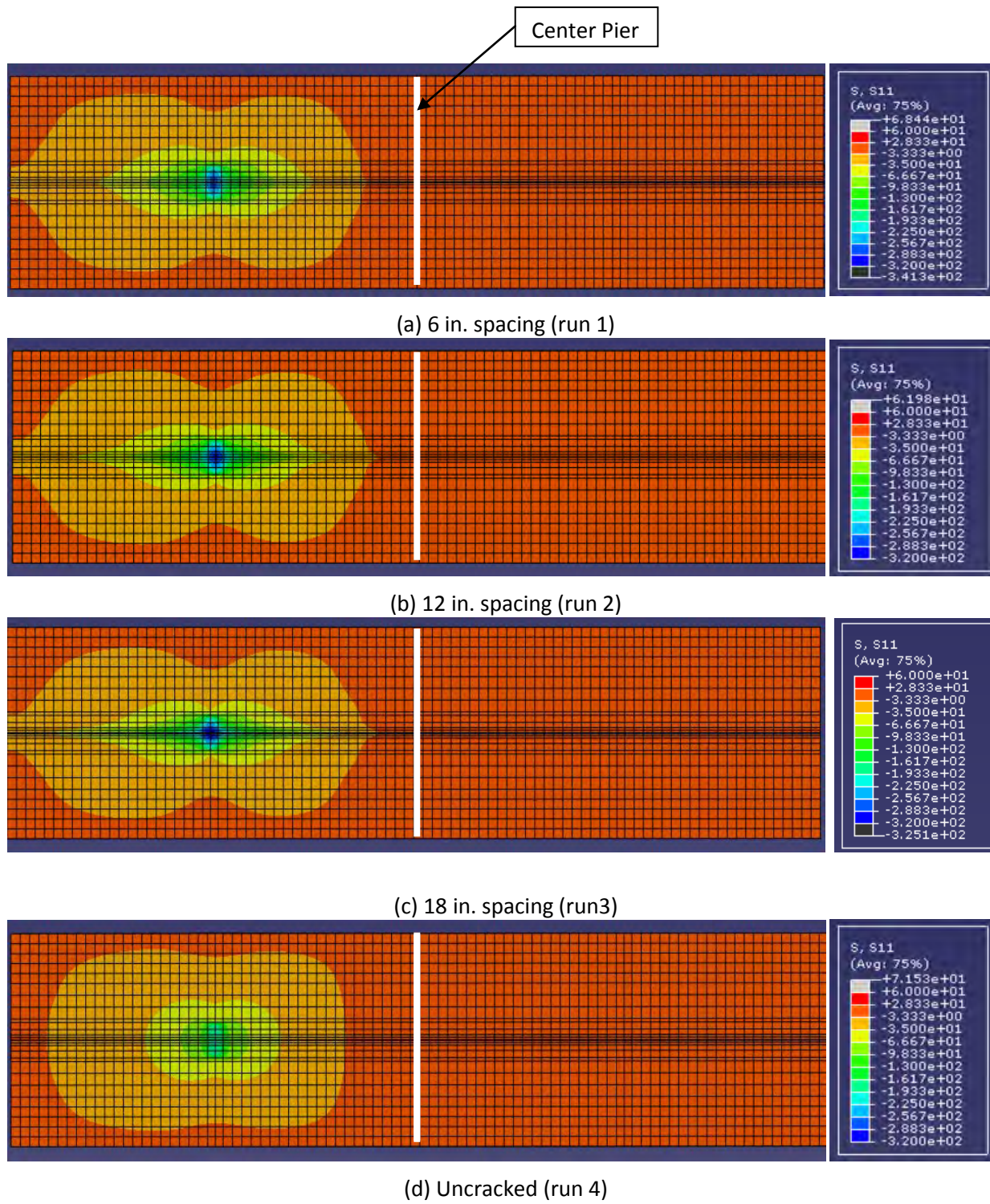
(d) Uncracked (run 4)

Figure 4.2.4: Transverse stress distribution in the compression (i.e., top) concrete fiber for load case 1 (units of stress are in psi)

55
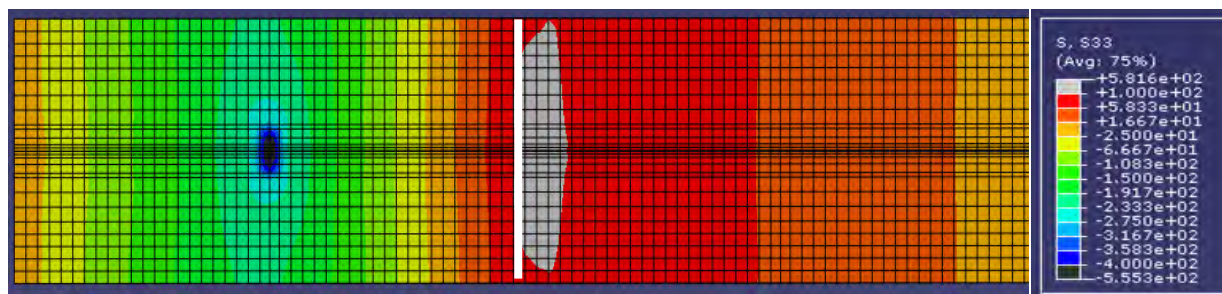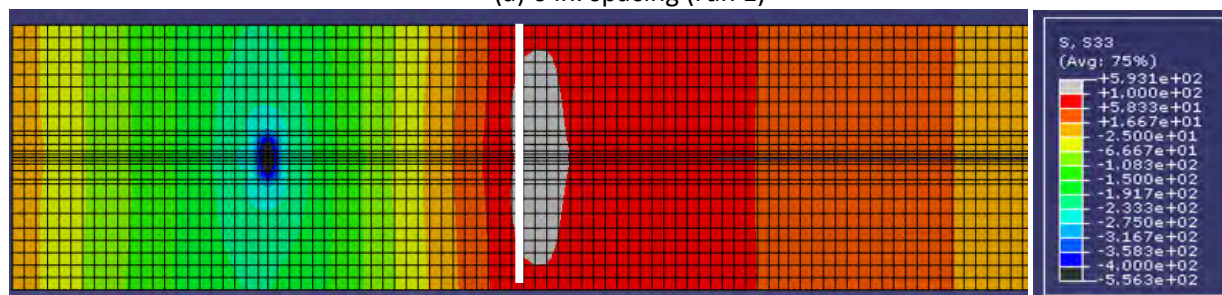
(a) 6 in. spacing (run 1)
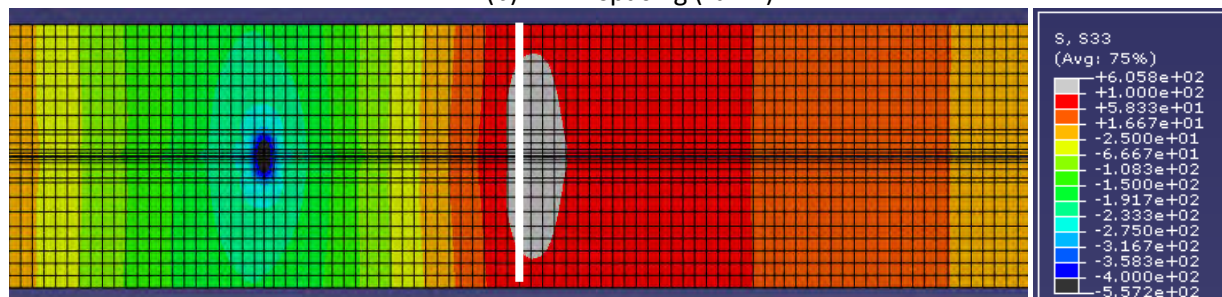
(b) 12 in. spacing (run 2)
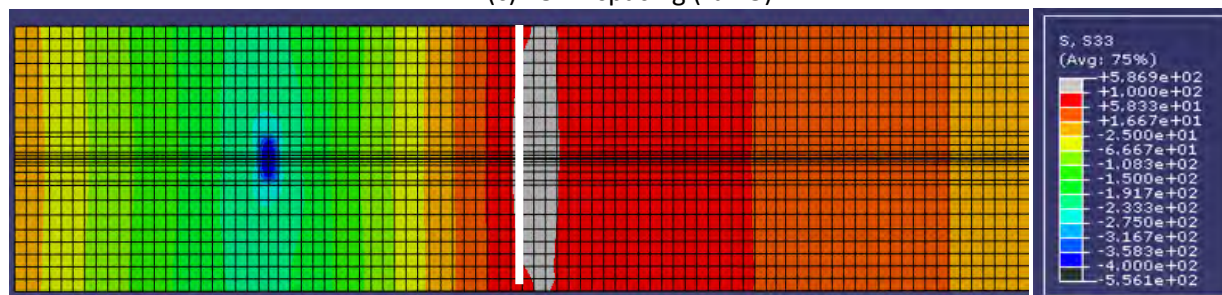
(c) 18 in. spacing (run 3)

(d) Uncracked (run 4)

Figure 4.2.5: Longitudinal stress distribution in the compression (i.e., top) concrete fiber for load case 1 (units of stress are in psi)

56
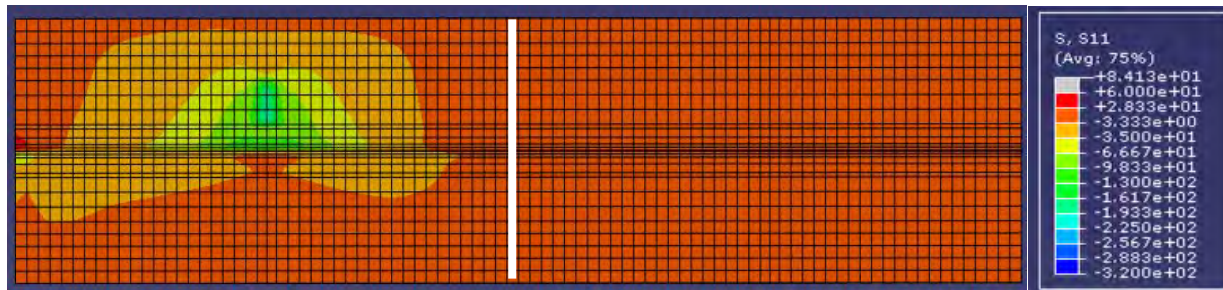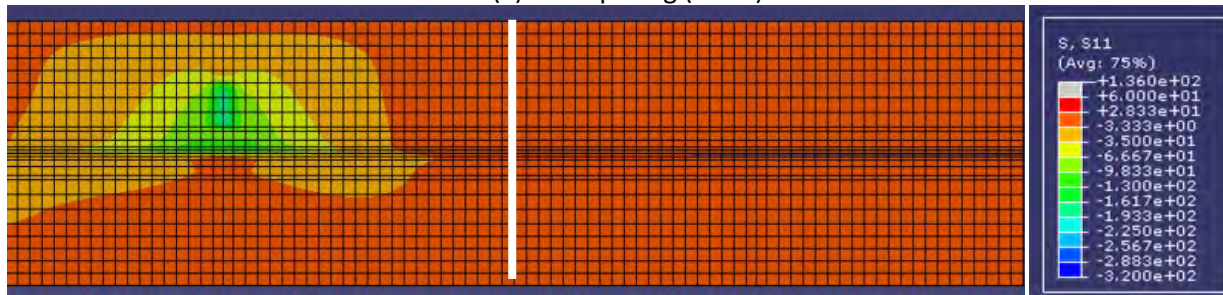
(a) 6 in. spacing (run 1)
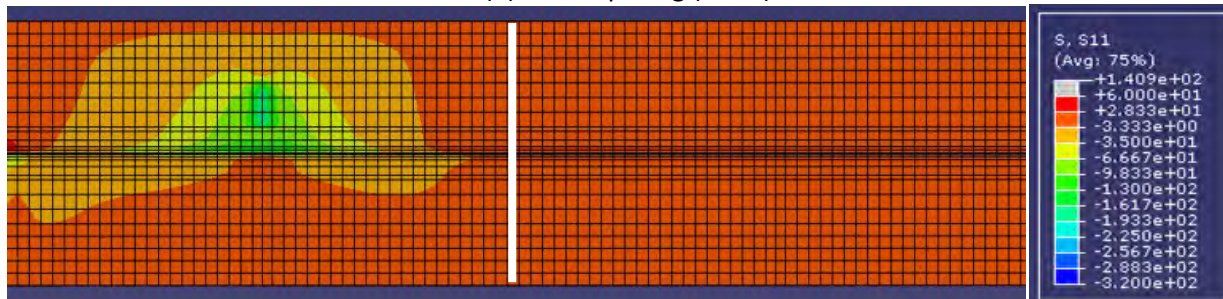
(b) 12 in. spacing (run 2)
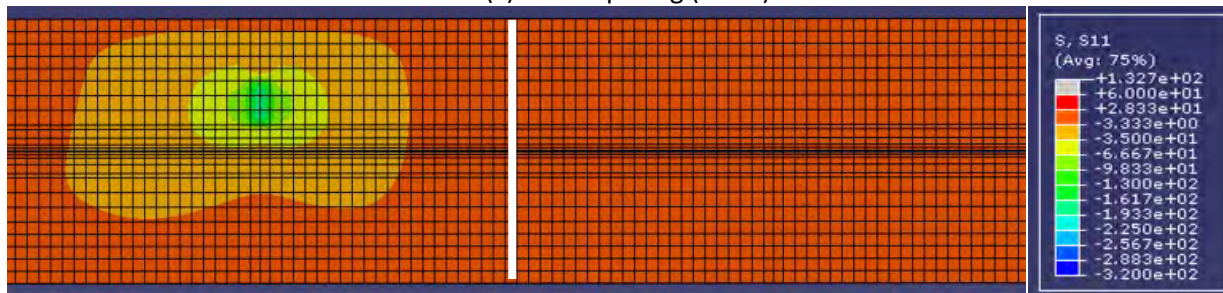
(c) 18 in. spacing (run 3)

(d) Uncracked (run 4)

Figure 4.2.6: Transverse stress distribution in the compression (i.e., top) concrete fiber for load case 2 (units of stress are in psi)

57
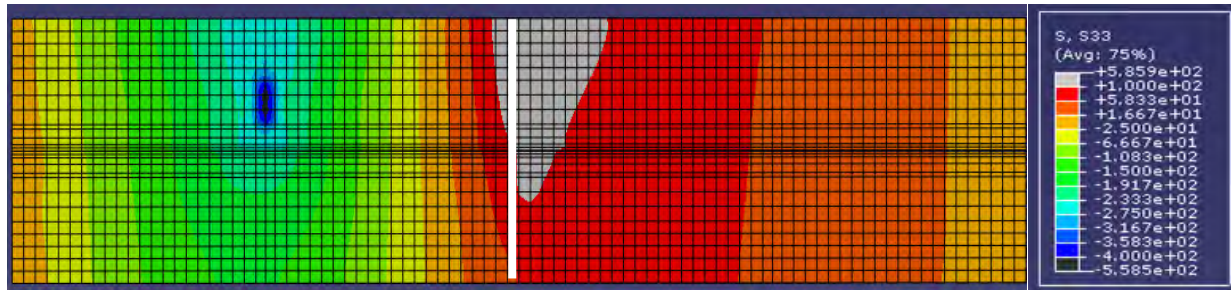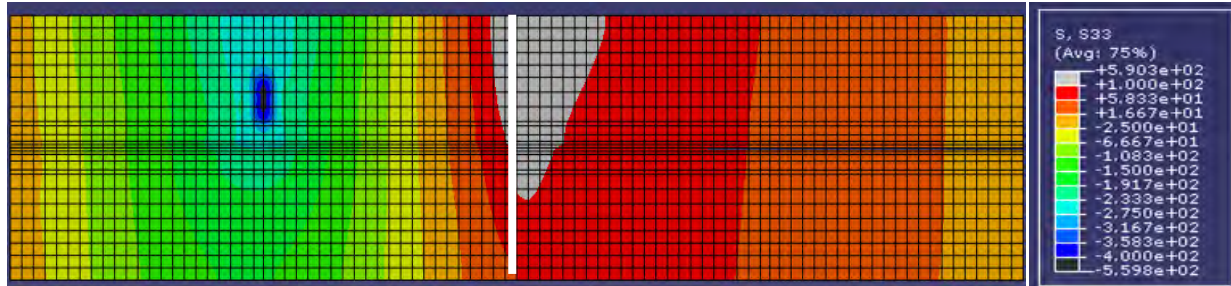
(a) 6 in. spacing (run 1)
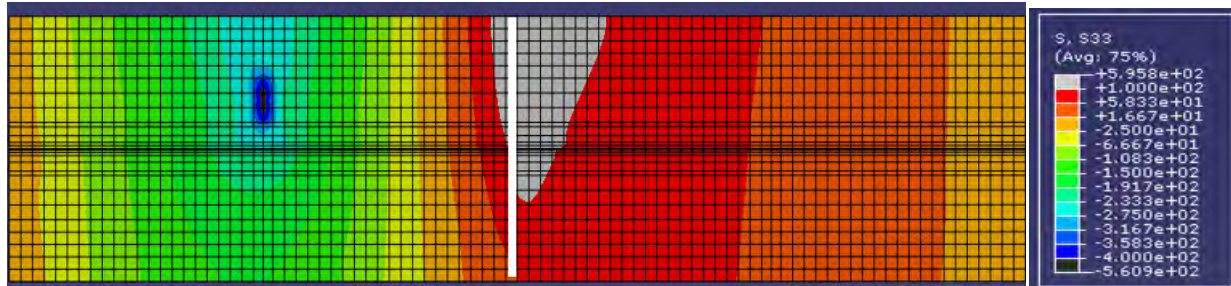
(b) 12 in. spacing (run 2)

(c) 18 in. spacing (run 3)
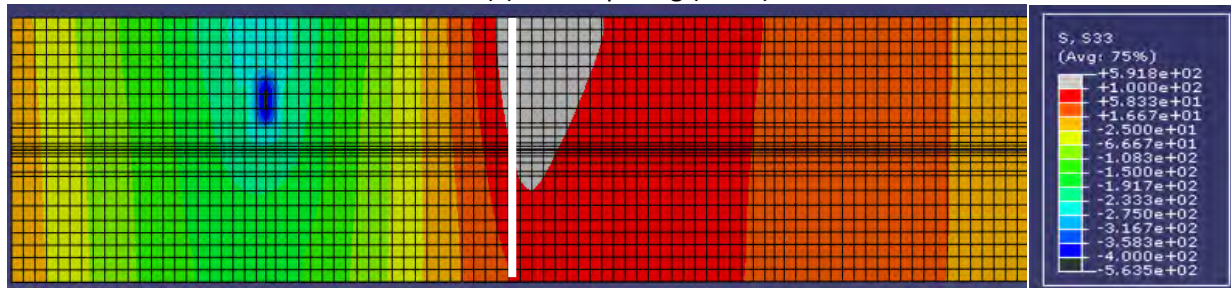
(d) Uncracked (run 4)

Figure 4.2.7: Longitudinal stress distribution in the compression (i.e., top) concrete fiber for load case 2 (units of stress are in psi)

58

4.3.   Parametric Study to Investigate Live-Load Distribution Factors for PCSSS

The *Interim 2010 AASHTO LRFD Design Specification* provided design equations to determine the appropriate longitudinal moment demand for a given slab bridge system based on an effective lane width. The designer is then responsible for determining the proper amount and location of the longitudinal reinforcement and section geometry to satisfy the load demands. The specification provides further guidance in the design of the transverse reinforcement for slab bridges as a simple proportion of the total longitudinal tension reinforcement based on the span length of the structure, however the validity of this relationship when applied to the PCSSS was unknown.

A total of nine finite element models were constructed to investigate the effects of the longitudinal discontinuity between precast members on the longitudinal and transverse distribution of load. The models were constructed using the same material and modeling assumptions as stated in Section 4.2, however symmetry was utilized in this case to minimize computation time. Four unique specimen geometries were investigated, including two three-span bridges with equal spans of 30 and 50 ft., as well as two simply-supported bridges also with spans of 30 and 50 ft. Each of the specimens had ten 6 ft. precast panels across the width to accommodate four 12 ft. lanes and two 6 ft. shoulders. Several variations in the state of the specimen near the precast discontinuity were considered, including both a bonded and unbonded interface between the precast flange and CIP concrete, as well as a monolithic slab with no precast discontinuity present. The parameters of each of the nine models are given in Table 4.3.1. A tandem load was utilized for all models, with a total load of 12.5 kip distributed over a 10 by 20 in. patch, as shown in Figure 4.3.1. The 12.5 kip load represents the tire load from the AASHTO tandem load of 25 kip axles spaced 4 ft. apart, with the transverse spacing taken to be 6 ft., as specified in Article 3.6.1.2.3 (AASHTO 2010), and assuming that the axle load is equally distributed to each tire. No dynamic load allowance (per AASHTO 2010 Article 3.6.2) was used to magnify the loading, which was consistent with the assumed loading for the design moments that were used for comparison. The center spans were loaded in the continuous models. The joint and panel numbering is shown in Figure 4.3.2, which represents the center span of the continuous models as well as the simple span. Five variations in the applied tandem loading were considered for each run, as described below:

- Tandem 1 – tandem loading centered over webs of panels 5 and 6
- Tandem 2 – tandem loading centered over precast joints 4 and 5
- Tandem 3 – double tandem loading centered over webs of panels 4,5,6,7
- Tandem 4 – double tandem loading centered over precast joints 3,4,5,6
- Tandem 5 – double tandem loading with 12.5 kip patch loads over joints 4 and 6 and a double patch load (i.e., 25 kips) over joint 5

59

MIDSPAN OF LOADED SPAN

PATCH LOAD
12.5 kip (62.5 psi)

20 in.

10 in.

2 ft.

6 ft.
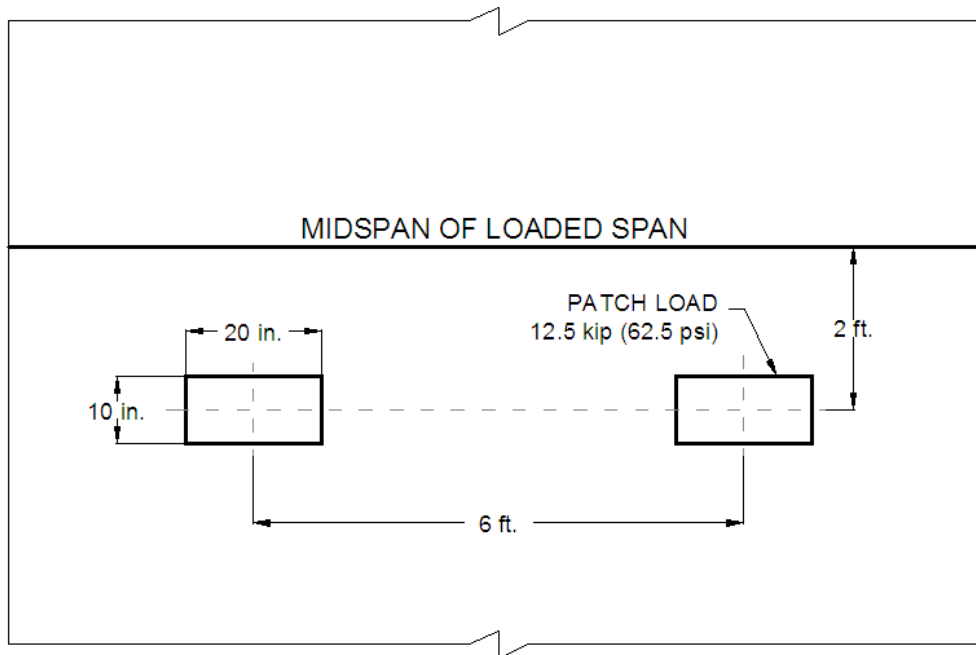
Figure 4.3.1: Tandem loading located 2 ft. from midspan utilized for FEM live-load distribution study
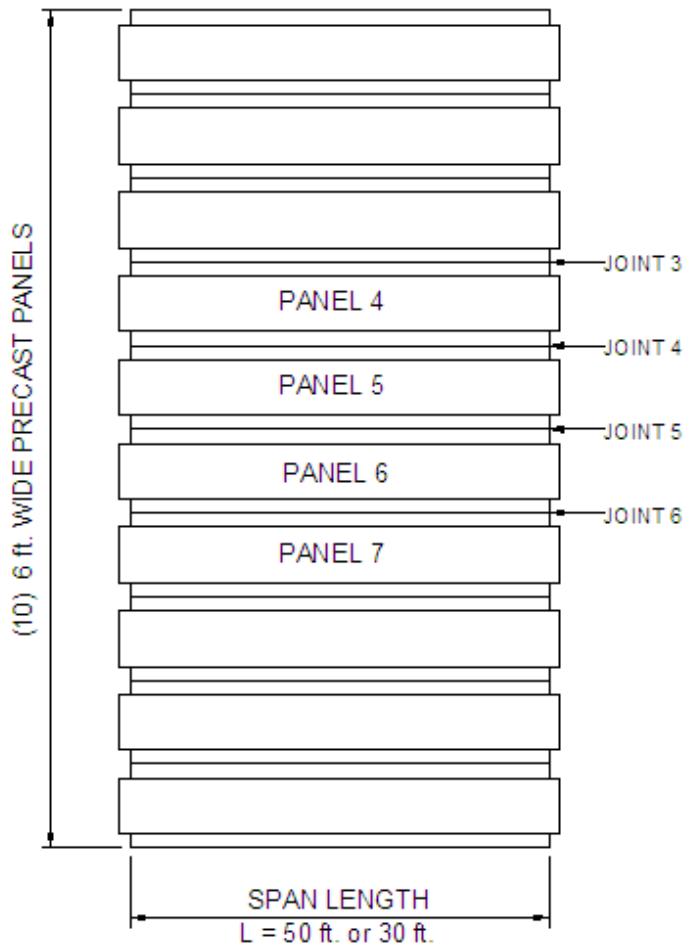
Figure 4.3.2: Panel and joint numbering used in the placement of tandem loading for the center span of the continuous models and the simple-span models

61

Table 4.3.1: Summary of FEM runs to investigate longitudinal and transverse live-load distribution factors

	Run Number	1	2	3	4	5	6	7	8	9
Description	Run configuration	PCSSS w/ 3" crack	PCSSS w/ 3" crack	PCSSS w/ 3" crack	PCSSS w/o crack	PCSSS w/ 3" crack	PCSSS w/ 3" crack	PCSSS w/ 3" crack	PCSSS w/o crack	PCSSS w/ 15" crack
Geometry	Spans:	3	Single	Single	Single	3	Single	Single	Single	Single
	#Panels wide	10—4lane bridge (12 ft. lanes + 6 ft. shoulders)\60ft.wide	Same	Same	Same	Same	Same	Same	Same	Same
	Length	30ft-30ft-30ft	30ft	30ft	30ft	50ft-50ft-50ft	50ft	50ft	50ft	30ft
	Depth of precast section	3in.flange; 12in. web	3in.flange; 12in. web	3in.flange; 12in. web	3in.flange; 12in. web	3in.flange; 16in. web	3in.flange; 16in. web	3in.flange; 16in. web	3in.flange; 16in. web	3in.flange; 12in. web
	Depth of deck above precast web	6in. CIP	Same	Same	Same	Same	Same	Same	Same	Same
	CIP to precast interface above flange	Unbonded	Unbonded	Bonded	Monolithic	Unbonded	Unbonded	Bonded	Monolithic	Unbonded
	Supports	Rollers	Same	Same	Same	Same	Same	Same	Same	Same
Crack	Simulated "crack" using contact elements.	Bottom of section to 3in. from bottom (precast joint).	Bottom of section to 3in. from bottom (precast joint).	Bottom of section to 3in. from bottom (precast joint).	No crack, monolithic	Bottom of section to 3in. from bottom (precast joint).	Bottom of section to 3in. from bottom (precast joint).	Bottom of section to 3in. from bottom (precast joint).	No crack, monolithic	Bottom of section to 15in. from bottom.
Mat'l strength	CIP Concrete	4ksi	Same	Same	Same	Same	Same	Same	Same	Same
	Precast Concrete	6.5ksi	Same	Same	Same	Same	Same	Same	Same	Same
	Reinforcement	60ksi	Same	Same	Same	Same	Same	Same	Same	Same
Reinforcement	Deck steel	#8-#7-#7 @ 4in. oc Run along entire span length	Same	Same	Same	Same	Same	Same	Same	Same
	Transverse hooks in each direction (offset transversely by 1in.)	#6@12in. Model as a continuous bar across the section rather than as lapped steel	Same	Same	Same	Same	Same	Same	Same	Same
	Location of transverse reinforcement	4-5/8" center of #6 from bottom of form	Same	Same	Same	Same	Same	Same	Same	Same
	Prestressing strands	16 in each PCSSS	16 in each PCSSS	16 in each PCSSS	16 in each PCSSS	38 in each PCSSS	38 in each PCSSS	38 in each PCSSS	38 in each PCSSS	16 in each PCSSS
	Transverse cage	None	None	None	None	None	None	None	None	None

62

In Runs 1, 2, 5, and 6 the CIP was bonded only to the sides and top of the panel webs while in Runs 3 and 7 the CIP was also bonded to the top of the precast flanges. In Runs 4 and 8 the system was assumed to be a monolithic slab with the discontinuity from the joint between the precast panels absent. Finally, Run 9 was similar to Run 2, except the crack was extended up to approximately the elastic neutral axis in transverse bending. In Run 9, the rebar crossing the cracked plane was debonded from the concrete a distance of 3 in. to either side of the cracked face.

The longitudinal design moments for slab bridges are calculated by applying the design load over an effective lane width, which is dependent on whether loading is applied to a single lane or multiple lanes, per AASHTO (2010) Article 4.6.2.3. The two variations of effective lane widths account for multiple presence factors in that the effective strip width for single lane loading has been divided by a factor of 1.20. The factors do not represent a physical change in loading, but instead account for the likelihood of multiple vehicles traveling together; they are statistical factors to promote conservative design (in the case of single lane loading). The multiple presence factors were ignored in the modeled scenarios. The longitudinal design moments and associated curvatures are shown in Table 4.3.2 for both single and multiple lane loadings for the various runs.

Table 4.3.2: AASHTO (2010) longitudinal design moments and curvatures

Run	Moment (kip-ft./ft. span)		Curvature (με/in.)	
	Single[1]	Multiple[2]	Single	Multiple
1	16.1	17.7	7.37	8.13
2	24.4	26.9	11.17	12.32
3	24.4	26.9	11.17	12.32
4	24.4	26.9	11.17	12.32
5	22.9	28.6	5.64	7.05
6	33.9	42.4	8.34	10.43
7	33.9	42.4	8.34	10.43
8	33.9	42.4	8.34	10.43
9	24.4	26.9	11.17	12.32

[1]"Single" is associated with all loading applied to a single lane
[2]"Multiple" is associated with loading applied to two or more lanes

The maximum longitudinal curvatures obtained from the FEM model with the Tandem 2 loading (patch load applied over joints 4 and 5) and Tandem 5 loading (patch load applied over joints 4 and 6 and double patch load applied over joint 5) are compared with the design curvatures in Table 4.3.3. The Tandem 5 loading was considered to be a worst case loading scenario with respect to expected lane loading because the tandems were spaced much closer than would be physically possible.

In comparing the results of the FEM to design ratios, the PCSSS resulted in slightly higher values in comparison to those of the monolithic systems (e.g., for the Tandem 2 Load Case: 0.43 [Run 2] for PCSSS vs. 0.39 [Run 4] for the monolithic 30 ft. span sections, and 0.41 [Run 6] for the PCSSS vs. 0.39 [Run 8] for the monolithic 50 ft. span); however the results were still conservative. The ratio of the maximum longitudinal curvature to the design curvature among the nine runs loaded with the Tandem 5 load case ranged from 0.57 to 0.84 for run 8 and 9 respectively. This suggests that, even when reflective cracking

was assumed to have progressed vertically to within 3 in. of the extreme compression fiber, as in run 9, the design effective lane widths provided by AASHTO (2010) Article 4.6.2.3 prove to be conservative, and should therefore be utilized for the design of precast composite slab span bridge systems.

Table 4.3.3: FEM and design longitudinal curvatures under Tandem 2 and Tandem 5 load cases

Run	Tandem 2 Load Case Curvature ($\mu\varepsilon$/in)			Tandem 5 Load Case Curvature ($\mu\varepsilon$/in)		
	Max FEM	Design	FEM/Design	Max FEM	Design	FEM/DESIGN
1	3.72	7.37	0.50	6.76	8.13	0.83
2	4.76	11.17	0.43	8.81	12.32	0.72
3	4.41	11.17	0.39	8.25	12.32	0.67
4	4.35	11.17	0.39	8.14	12.32	0.66
5	2.68	5.64	0.48	NM[1]	7.05	NM
6	3.4	8.34	0.41	NM	10.43	NM
7	3.26	8.34	0.39	6.03	10.43	0.58
8	3.23	8.34	0.39	5.97	10.43	0.57
9	5.18	11.17	0.46	10.38	12.32	0.84

[1]Not measured
Shaded rows indicate monolithic models

4.4. Parametric Study to Investigate Skew Effects

Several additional challenges are present in the design of bridges with skewed supports, such that the primary axis of the substructure is not aligned perpendicularly to the longitudinal axis of the superstructure. The primary effects of skewed bridge construction are geometric, with some effect on moments, shears, and live-load distribution. A plan view of the pier details for a skewed PCSSS bridge is shown in Figure 4.4.1. According to the PCI Bridge Manual (2001), in solid slab-span bridge systems with skewed supports, the load tends to take a "short cut" between the obtuse corners of the span, while the load in skewed bridges supported by longitudinal I-girders tends to flow along the length of the supporting members (PCI 2001). The PCSSS was expected to be bounded by these behaviors, and would subsequently tend to exhibit the characteristics of longitudinal stringer bridges as the precast joint is degraded due to reflective cracking.

Another primary concern regarding skewed PCSSS bridges was the effect of the skew angle on the maximum horizontal shear induced above the precast joint. Several FEM models were developed to investigate the relationship between the skew angle and the resulting magnitude of this stress.

A total of eight FEM models were constructed for this portion of the study, with skew angles ranging from 0 to 45 degrees. For each of the skew angles selected, two corresponding FEM models were created, one with the presence of the 3 in. discontinuity between the precast joints and an unbonded surface between the top of the precast flanges and the CIP concrete and a second with a monolithic thickness and the absence of the precast joint. Each model was constructed as a single 30 ft. simple-span bridge structure. The material and other modeling parameters were identical to the previous runs, described in Section 4.2. The parameters of each of the eight FEM models are given in Table 4.4.1.

Three load cases were considered for this portion of the study, outlined below. Each load case included a 35 kip load applied over a 12 by 12 in. patch. An illustration of the model and applied load cases is shown in Figure 4.4.2.

- Load Case 1 – loading applied at quarter span at center of outside panel near acute angle support
- Load Case 2 – loading applied at midspan at center of outside panel
- Load Case 3 – loading applied at quarter span at center of outside panel near obtuse angle support
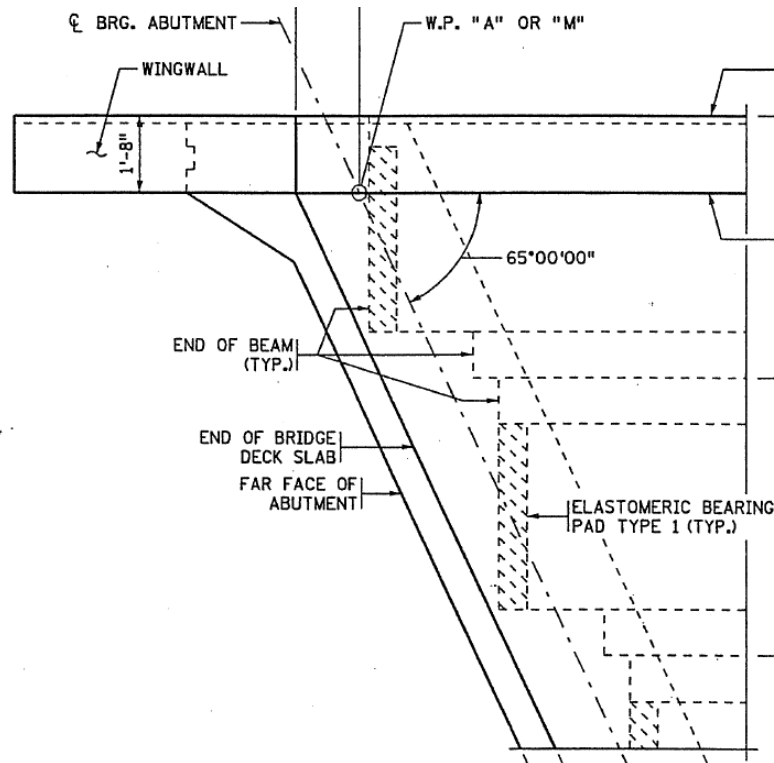
Figure 4.4.1: Placement of precast slab span panels at a skewed support

65

Table 4.4.1: Summary of FEM runs to investigate performance of skewed PCSSS

Description	Run Number	1	2	3	4	5	6	7	8
	Run configuration	PCSSS w/ 3" crack - 0 skew	PCSSS w/ 3" crack - 15 skew	PCSSS w/ 3" crack - 30 skew	PCSSS w/ 3" crack - 45 skew	PCSSS w/o crack - 0 skew	PCSSS w/o crack - 15 skew	PCSSS w/o crack - 30 skew	PCSSS w/o crack - 45 skew
Geometry	Spans:	Single	Single	Single	Single	Single	Single	Single	Single
	#Panels wide	3 panels /18ft.wide	Same	Same	Same	Same	Same	Same	Same
	Length	30ft	Same	Same	Same	Same	Same	Same	Same
	Skew Angle	0 deg	15 deg	30 deg	45 deg	0 deg	15 deg	30 deg	45 deg
	Depth of precast section	3in.flange; 12in. web	Same	Same	Same	Same	Same	Same	Same
	Depth of deck above precast web	6in. CIP	Same	Same	Same	Same	Same	Same	Same
	CIP to precast interface above flange	Unbonded	Unbonded	Unbonded	Unbonded	Monolithic	Monolithic	Monolithic	Monolithic
	Supports	Rollers	Same	Same	Same	Same	Same	Same	Same
Crack	Simulated "crack" using contact elements.	Bottom of section to 3in. from bottom (precast joint).	Bottom of section to 3in. from bottom (precast joint).	Bottom of section to 3in. from bottom (precast joint).	Bottom of section to 3in. from bottom (precast joint).	No crack, monolithic	No crack, monolithic	No crack, monolithic	No crack, monolithic
Mat'l strength	CIP Concrete	4ksi	Same	Same	Same	Same	Same	Same	Same
	Precast Concrete	6.5ksi	Same	Same	Same	Same	Same	Same	Same
	Reinforcement	60ksi	Same	Same	Same	Same	Same	Same	Same
Reinforcement	Deck steel	#8-#7-#7 @ 4in. oc Run along entire span length	Same	Same	Same	Same	Same	Same	Same
	Transverse hooks in each direction (offset transversely by 1in.)	#6@12in. Model as a continuous bar across the section rather than as lapped steel	Same	Same	Same	Same	Same	Same	Same
	Location of transverse reinforcement	4-5/8" center of #6 from bottom of form	Same	Same	Same	Same	Same	Same	Same
	Prestressing strands	16 in each PCSSS	Same	Same	Same	Same	Same	Same	Same
	Transverse cage	None	None	None	None	None	None	None	None

66

Figure 4.4.2: Simply supported, three panel wide bridge and location of loading used for FEM models

For all cases, the horizontal shear stress in the cast-in-place concrete was measured along the entire length and depth of the structure in the plane of the precast joint adjacent to the loading. The maximum horizontal shear stress in this plane was investigated for a range of skew angles for each of the load cases. The maximum horizontal shear stress measured in the models with a 3 in. deep precast joint and the associated monolithic models are shown in Figure 4.4.3 (a) and (b), respectively.

(a) 3 in. precast joint   (b) Monolithic
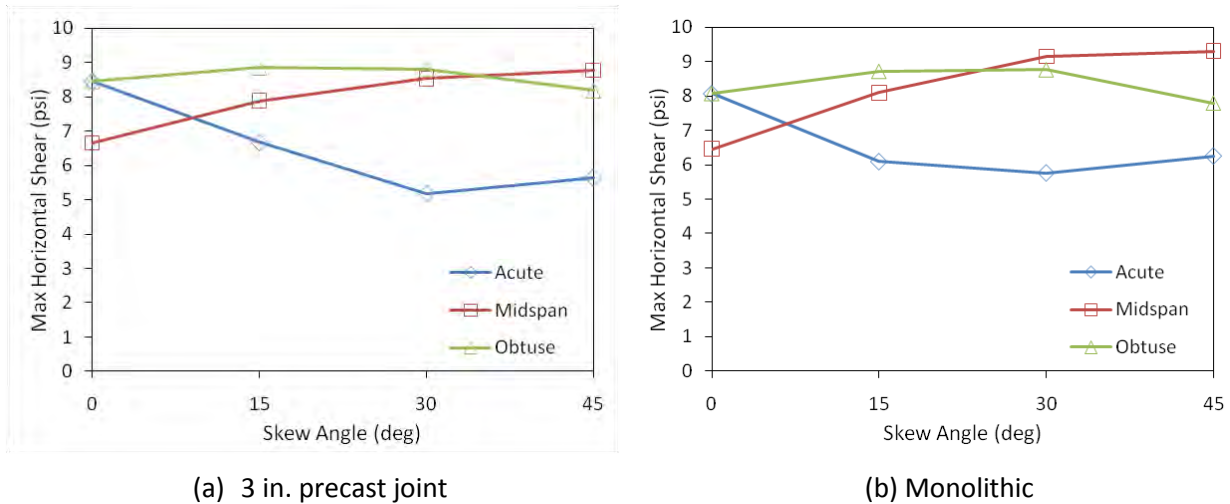
Figure 4.4.3: Maximum horizontal shear stress measured in the cast-in-place concrete above the precast joint measured under the acute, midspan, and obtuse load cases

67

The horizontal shear stress in the models considered with load case 1, which had load applied near the acute pier connection, was observed to be reduced with increasing skew angles for both the section with the 3 in. flange joint as well as the monolithic model. The horizontal shear stress caused by load case 3, representing loading near the obtuse pier connection, for both the jointed and monolithic models remained relatively constant through the range of skew angles considered. For both model types, the midspan load case produced the most significant increase in horizontal shear stress, with an approximately 1/3 increase in the stress observed in both the jointed and monolithic models.

The maximum shear stress from these three load cases defined stress envelopes for the jointed and monolithic models that varied with skew angle, shown in Figure 4.4.4. This maximum horizontal shear stress envelope remained relatively constant through the range of skew angles considered for both jointed and monolithic models. With increasing skew angle, the shear stress envelope increased by approximately 15% for the monolithic models and by less than 10% for the jointed models. The small variation and consistency between the models considering a 3 in. precast joint and a monolithic structure suggested that the effect of the precast joint in precast composite slab span construction was not expected to significantly affect the performance of the system in skewed applications.
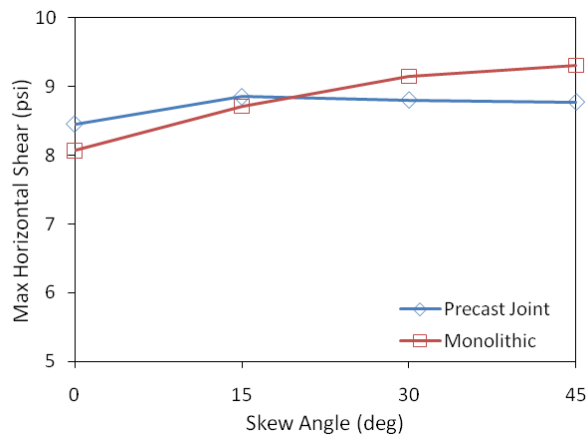
Figure 4.4.4: Maximum horizontal shear stress envelope above longitudinal precast joint considering all load cases for precast joint models and monolithic slab models.

4.5. End Zone Stresses in Precast Inverted Tee Sections

Horizontal cracking frequently forms in the end region of prestressed concrete members when the prestressing strand is released and the prestress force is transferred to the concrete section. These cracks, which result from the vertical tension created by the transfer of prestress force, are defined as "spalling" cracks, though often incorrectly labeled as "bursting" or "splitting" cracks (Gergely et al., 1963). If unrestrained, these cracks can extend into the precast member and may negatively impact both the flexural and shear strength and durability of the section.

Previous studies have suggested that these cracks cannot be eliminated, however vertically oriented reinforcing steel can limit crack width and propagation (Fountain, 1963). The first design parameters related to end zone stresses in prestressed members were introduced in the 1961 AASHTO Design Specification (AASHTO, 1961), that specified a minimum vertical reinforcement requirement for

68

pretensioned member end regions. This specification remained virtually unchanged since its introduction until the 2008 interim AASHTO LRFD specification incorporated changes to the specification, which included a change in the terminology of the end zone stresses from "bursting" to "splitting" resistance of the pretensioned anchorage zones.

The placement of large amounts of vertical reinforcement in the end regions of shallow inverted-T precast members caused congestion and difficulty in the placement of prestressing strand and concrete when 4 percent of the total prestressing force was used (i.e., AASHTO LRFD 2010). A historical study of the development of reinforcement designs for vertical end zone stresses indicated that the original design parameters were likely developed from a Marshall and Mattock (1962) study on horizontal end zone cracking in pretensioned I-girders, suggesting that design parameters provided in the specification may not be applicable to precast inverted-T sections. Also included in the modifications to the 2008 interim AASHTO LRFD specification was specific language for solid and voided slabs, as well as pretensioned box and tub girders.

Variations in the spalling reinforcement details were investigated experimentally with the Concept 1 and 2 laboratory bridge specimens by varying the vertical end region reinforcement in the ends of the precast panels used in the laboratory bridges, which are discussed under the unnumbered heading "experimental study," included in this section.

Because of the complicated state of stress near the end regions of prestressed members, two similar but unique modes of cracking may be observed. To limit the ambiguity regarding these stresses, the vertical tensile stresses which occur along the line of the prestressing forces were labeled as bursting stresses, while the vertical tensile stresses located away from the line of the prestressing force were labeled as spalling stresses, as illustrated in Figure 4.5.1.
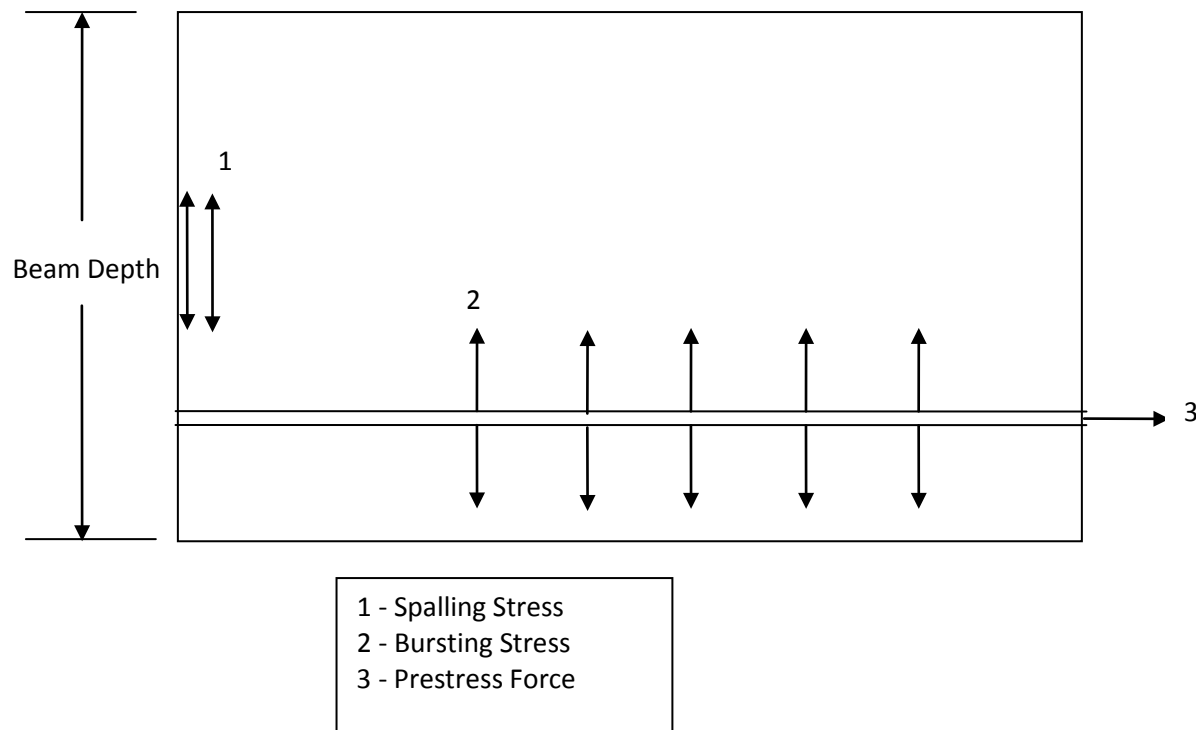
Figure 4.5.1: Spalling and bursting stresses near the end zone of prestressed members

69

Beam theory is not applicable in the end regions of prestressed concrete beams because the longitudinal strain is not linearly distributed through the depth of the cross section due to the introduction of the prestress force. Spalling stresses are a maximum at the end face of the member, typically near mid-height of the section and result in cracking at the end face which can propagate further into the member (Gergely et al., 1963). Bursting stresses occur along the line of the prestressing force, beginning a few inches into the beam and extending throughout the transfer length. Bursting stresses can result in strand slippage as cracking along the strand can eliminate bond between the strand and the concrete.

Distribution of tensile stresses in the end region depends on the eccentricity of the prestressing force within the member. When the prestress acts at the centroid of the section, force is distributed symmetrically through the vertical member depth; in members with large eccentricity there is greater area above the prestressing force for stresses to distribute. This prestressing force is allowed to spread through a greater vertical distance which subsequently increases the spalling force near the end region. This is consistent with previous experimental work which related the maximum tensile stress location to eccentricity. Gergely's (1963) study on post-tensioned I-girders and rectangular sections found members with small eccentricities had maximum tensile stresses in the bursting zone and members with large eccentricities had maximum tensile stresses in the spalling zone. Hawkins (1960) corroborated Gergely's findings and also found that the eccentricity of the prestressing strand and the magnitude of maximum tensile stress in the spalling zone were positively related.

Numerical Study

FEM modeling was also performed to determine the magnitude and location of spalling and bursting stresses in the end region of precast inverted-T sections. Several simplifications were considered during the analysis to reduce the complexity and computational requirements of the model. The flanges were neglected to allow for the system to be modeled as a two-dimensional (2D) rectangular slab. Furthermore, the concrete was modeled as perfectly linearly elastic, which was appropriate up to the initiation of cracking. The transfer of the prestressing force was simulated by incrementing the force in the strand, from zero at the face of the section to the full magnitude at the transfer length (L_t), in 1/4 in. increments. Slip occurring between the strand and concrete was ignored. The transfer length was conservatively taken as 40 strand diameters (i.e., 20 in. for 1/2 in. strand), which was two-thirds of the transfer length specified by AASHTO (2010). The reduction in the transfer length from the AASHTO (2010) specification was selected to be conservative, as shorter transfer lengths are associated with higher vertical end zone stresses. Uniform and linear bond stress models were utilized, with the linear distribution decreasing with distance from the end face of the member. A total of 57 runs were completed during the numerical study, as documented in Table 4.5.1.

Although the FEM model was not verified with experimental results from pretensioned beams, the models were compared to the results from Gergely's (1963) experimental study on a 6 by 12 in. post-tensioned rectangular beam. A 2D elastic model was created to simulate the physical experiment, with adequate correlation between the experimental and FEM model results, as shown in Figure 4.5.2, where the vertical axis represents the vertical tensile strains measured at midheight along the edge of the section and the horizontal axis corresponds to the distance from the end face of the specimen.

70
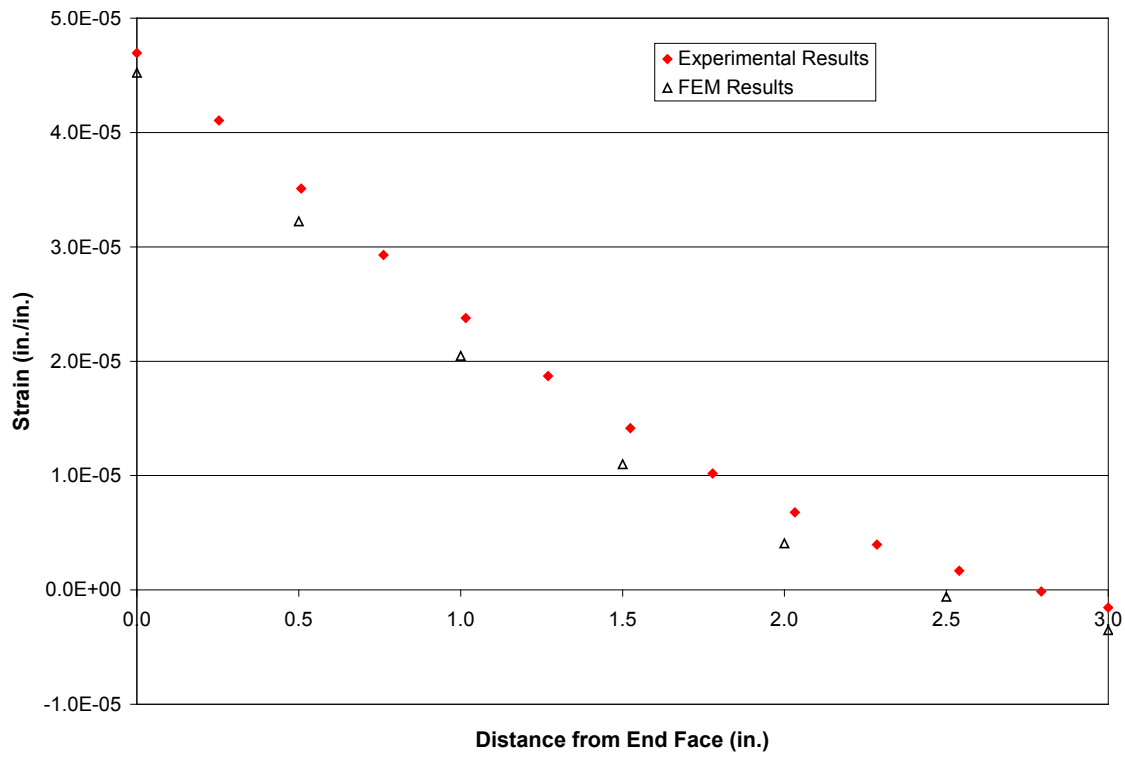
Figure 4.5.2: Validation of FEM model with experimental results from Gergely (1963)

71

Table 4.5.1: Description of models run during parametric study

Run #	h (in.)	L_t (in.)	e (in.)	e/h	Bond Stress Distribution	Run #	h (in.)	L_t (in.)	e (in.)	e/h	Bond Stress Distribution
1	12	20	5	0.42	Uniform	30	6	20	2	0.33	Uniform
2	12	20	4	0.33	Uniform	31	18	20	6	0.33	Uniform
3	12	20	3.5	0.29	Uniform	32	24	20	8	0.33	Uniform
4	12	20	3	0.25	Uniform	33	30	20	10	0.33	Uniform
5	12	20	2.5	0.21	Uniform	34	36	20	12	0.33	Uniform
6	12	20	2	0.17	Uniform	35	42	20	14	0.33	Uniform
7	12	20	0	0.0	Uniform	36	6	20	2	0.33	Linear
8	12	20	5	0.42	Linear	37	18	20	6	0.33	Linear
9	12	20	4	0.33	Linear	38	24	20	8	0.33	Linear
10	12	20	3.5	0.29	Linear	39	30	20	10	0.33	Linear
11	12	20	3	0.25	Linear	40	36	20	12	0.33	Linear
12	12	20	2.5	0.21	Linear	41	42	20	14	0.33	Linear
13	12	20	2	0.17	Linear	42	8	20	1.6	0.20	Uniform
14	12	20	0	0.0	Linear	43	10	20	2.5	0.25	Uniform
15	12	6	4	0.33	Uniform	44	12	20	2.5	0.21	Uniform
16	12	10	4	0.33	Uniform	45	12	20	2.4	0.20	Uniform
17	12	12	4	0.33	Uniform	46	14	20	3.7	0.26	Uniform
18	12	16	4	0.33	Uniform	47	16	20	4.6	0.29	Uniform
19	12	20	4	0.33	Uniform	48	20	20	6.3	0.31	Uniform
20	12	24	4	0.33	Uniform	49	22	20	6.8	0.31	Uniform
21	12	28	4	0.33	Uniform	50	8	20	1.6	0.20	Linear
22	12	0	4	0.33	End[1]	51	10	20	2.5	0.25	Linear
23	12	6	4	0.33	Linear	52	12	20	2.5	0.21	Linear
24	12	10	4	0.33	Linear	53	12	20	2.4	0.20	Linear
25	12	12	4	0.33	Linear	54	14	20	3.7	0.26	Linear
26	12	16	4	0.33	Linear	55	16	20	4.6	0.29	Linear
27	12	20	4	0.33	Linear	56	20	20	6.3	0.31	Linear
28	12	24	4	0.33	Linear	57	22	20	6.8	0.31	Linear
29	12	28	4	0.33	Linear						

[1]All force assumed to be applied at the end face to simulate post-tensioned case

The spalling force magnitude and stress distribution into the beam was found to depend on many factors. The assumption of linear bond distribution (where bond stress decreases linearly into the section) creates larger spalling stresses which extend a shorter distance into the member than uniform bond distribution. As the ratio of eccentricity (e) and height (h) increases, the magnitude of the spalling stresses increase and extend further into the member. A shorter transfer length distributes the prestress over a shorter distance resulting in larger spalling stresses extending over a shorter distance into the member. As height increases, the spalling force increases and the distribution of the stress extends further into the member because of the greater vertical area over which to distribute the prestress.

Bursting force magnitude and location is affected by eccentricity, transfer length, and height. Bursting forces increase with smaller e/h ratios and start further into the member. Shorter transfer lengths distribute forces over a shorter distance which results in larger bursting stresses and a smaller length

over which bursting stresses act. As member height increases, the magnitude of the bursting forces increase and the length over which the bursting stress acts is increased slightly. The length which bursting stresses extend is mostly based on transfer length but larger heights and smaller *e/h* values also increase the ratio of the length over which bursting stresses act to height.

For smaller *e/h* values, bursting force is significantly larger than the spalling force. However, although the total force generated from the bursting stresses is larger than the total force generated from the spalling stresses, the bursting force acts over a much larger area. This provides a greater amount of concrete to resist the tensile forces.

Figure 4.5.3 compares the bursting and spalling stresses for a member 12 in. in height with 2.4 in. eccentricity and a 20 in. transfer length. The maximum stress is larger for spalling than for bursting. Also, the maximum spalling stress occurs on the end face which is only restrained on one side making it more likely for a crack to form there. In the majority of historical studies on end zone cracking, detrimental cracking initiates on the end face of members. If cracks are found along the line of load, they are likely caused by a combination of bursting and radial stresses, as expressed in Uijl's (1983) hollow core slab study.
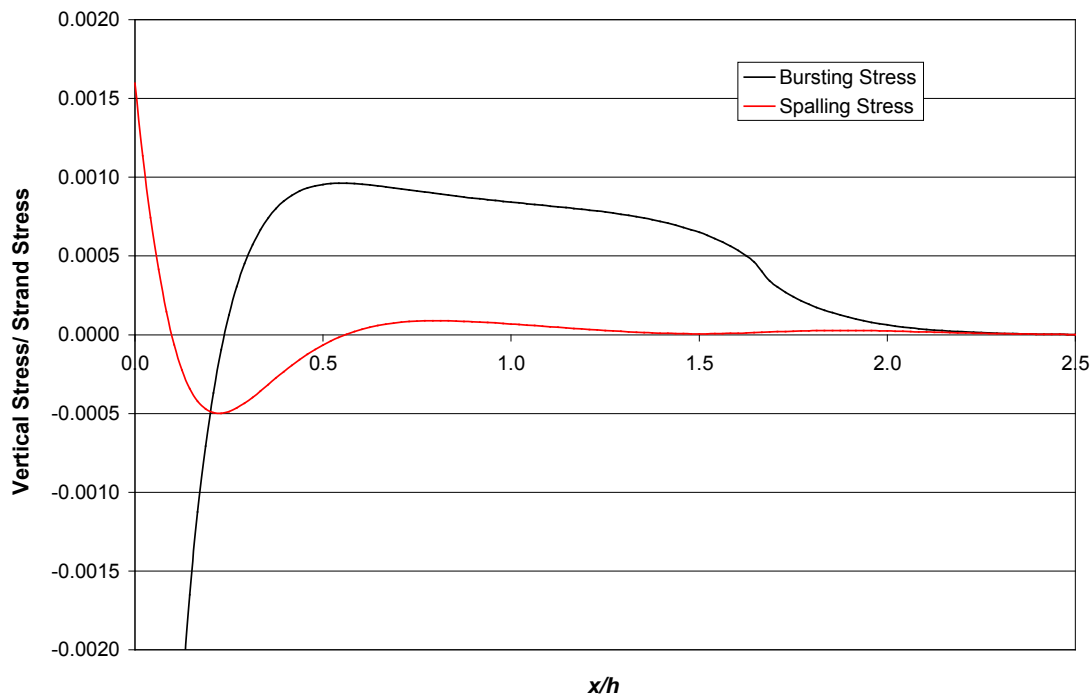
Figure 4.5.3: Comparison of Bursting and Spalling Stresses for Member *e/h*=0.20

The ratio of the predicted spalling force to the prestress force of slabs with a constant depth of 12 in. is shown in Figure 4.5.4. Table 4.5.2 shows the ratio of predicted spalling force to strand force as found through FE modeling of slabs with the same *e/h* ratio as the feasible precast inverted tee sections in Table 4.1.2. The spalling force ranged from 0.3 to 8.5 percent of the prestressing force.

73
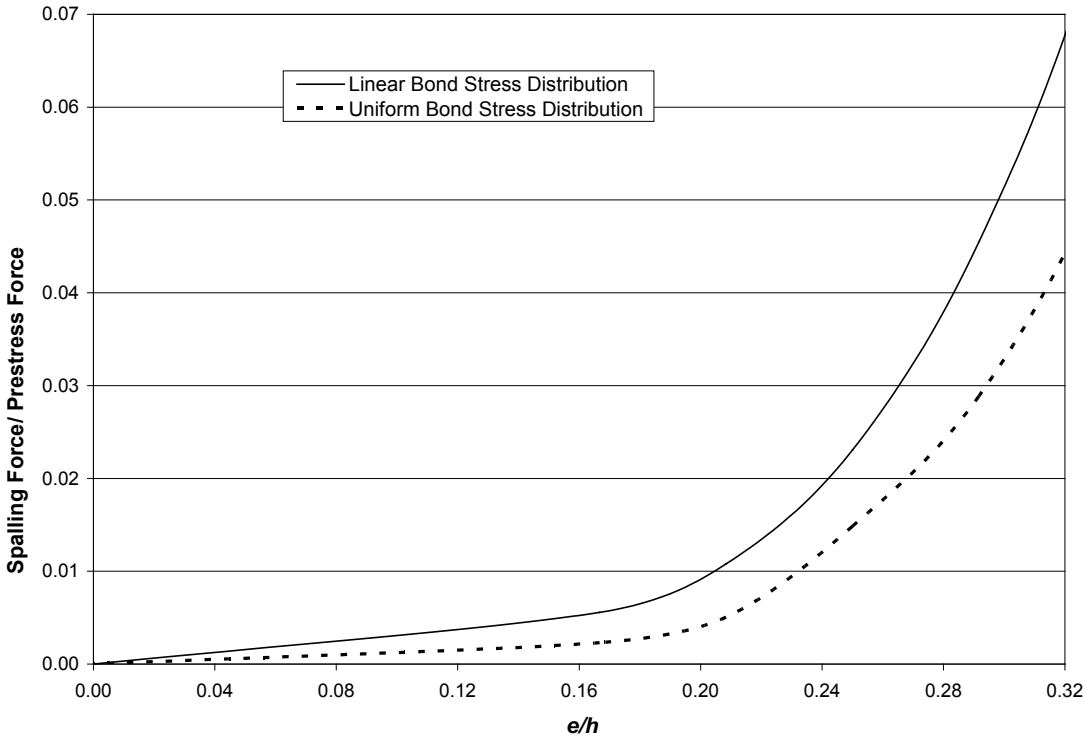
Figure 4.5.4: Ratio of spalling force to prestress force as a function of ratio of eccentricity to precast member depth for linear and uniform bond stress distributions, with h= 12 in and L_t = 20 in.

Table 4.5.2: Ratio of Spalling Forces to Prestress Forces as Predicted by FE Models for Slabs with Equivalent e/h as Feasible Precast Inverted Tee Sections, using both Uniform and Linear Bond Stress Distributions, varying h and e/h and constant L_t=20 in.

Depth of Precast (in.)	8	10	12^1	12^2	14	16	20	22
e/h (in.)	0.20	0.25	0.20	0.21	0.26	0.29	0.31	0.31
Spalling Force assuming uniform bond stress distribution/ Total Strand Force	0.003	0.011	0.004	0.005	0.019	0.033	0.065	0.067
Spalling Force assuming linear bond stress distribution/ Total Strand Force	0.006	0.021	0.009	0.011	0.030	0.052	0.085	0.085

[1]Laboratory Bridge Specimen with 5.25 in. flange height
[2]Laboratory Bridge Specimen with 3.0 in. flange height
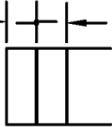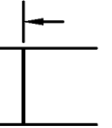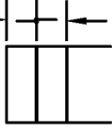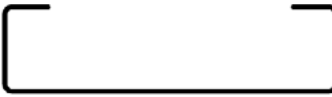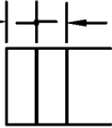
Experimental Study

Four different variations in the vertical steel configurations were considered during the laboratory study, with each configuration repeated twice. The reinforcement details for each configuration are shown in

74

Table 4.5.3. The vertical reinforcement in configurations 1 and 2 provided less than half of the 1.0 in.[2] required by the AASHTO (2010) specification. The area of vertical reinforcement provided in configuration 4 was sufficient according to the specification; however it did not meet the placement requirements because the reinforcement extended farther into the section than the larger of 3 in. or one quarter of the total member depth (i.e., the reinforcement was not adequately grouped near the end of the beam). The vertical reinforcement in configuration 3 met all requirements of the specification, and consisted of No. 5 four legged stirrups spaced at 2 in. An additional No. 5 four legged stirrup was also placed a distance of 4 in. from the face in configuration 3.

Table 4.5.3: Vertical reinforcement in configurations 1-4 of the precast members utilized in experimental study

Configuration	Description of Vertical End Zone Reinforcement	Cross Section View of Stirrup	Elevation View of Reinforcement Spacing
1	#3 stirrup at 2 and 4 in. total area = 0.44 in^2		2 spaces @ 2 in.
2	#4 stirrup at 2 in. total area = 0.40 in.^{2}		1 space @ 2 in.
3	#5 four legged stirrup at 2 and 4 in. total area = 2.5 in.^{2}		2 spaces @ 2 in.
4	#5 stirrup at 2 and 4 in. total area = 1.2 in.^{2}		2 spaces @ 2 in.

The end regions of the panels used in the Concept 1 laboratory bridge were well instrumented to investigate the state of stress immediately after release. On the side face of each section, rosettes were placed at midheight, 2 in. from the end face. A single strain gage was attached to each vertical stirrup with vertical placement ranging from 5.5 in. to 7.5 in. from the bottom of the precast section. The concrete and steel gages were monitored before, during, and after transfer. Readings were taken every minute, starting at 56 minutes before release and until 88 minutes after release. The average of the strain readings taken in the fifteen minutes before release was used to zero the remaining measurements.

The measured strains in each end section of the precast members used for the Concept 1 laboratory bridge are recorded in Table 4.5.4. The magnitudes of the strains observed in the end sections of the inverted-T sections were negligible, and no signs of cracking were detected, visually or via the instrumentation. The results from the experimental study suggested that the precast concrete at the

time of transfer, which was measured to have a compressive strength of 7410 psi at an age of 1 day (Smith et al., 2008), was sufficient to resist vertical tensile stresses in the end zones regardless of the reinforcement details.

Table 4.5.4: Maximum of the measured strain values in end regions of precast members used for Concept 1 laboratory bridge in the 88 minutes after transfer of prestress force

	Span 1		Span 2	
Stirrup Location from End Face	2 in.	4 in.	2 in.	4 in.
Northwest				
Vertical Stirrup Size	#3	#3	#3	#3
Steel Gages ($\mu\varepsilon$)	3.5	-3.6	19	-4.8
Concrete Gages (Vertical Leg of Rosette) ($\mu\varepsilon$)	-21	n/a	7.2	n/a
Northeast				
Vertical Stirrup Size	#4	n/a	#4	n/a
Steel Gages ($\mu\varepsilon$)	-1.1	n/a	16	n/a
Concrete Gages (Vertical Leg of Rosette) ($\mu\varepsilon$)	3.0	n/a	35	n/a
Southwest				
Vertical Stirrup Size	2 - #5	2 - #5	2 - #5	2 - #5
	Inner[1] | Outer[2]	Inner | Outer	Inner | Outer	Inner | Outer
Steel Gages ($\mu\varepsilon$)	-3.7 | 16	-4.2 | 0.8	-8.7 | 6.2	-7.2 | -1.9
Concrete Gages (Vertical Leg of Rosette) ($\mu\varepsilon$)	0.4	n/a	17	n/a
Southeast				
Vertical Stirrup Size	#5	#5	#5	#5
Steel Gages ($\mu\varepsilon$)	-1.1	-7.1	-20	-8.6
Concrete Gages (Vertical Leg of Rosette) ($\mu\varepsilon$)	1.4	n/a	24	n/a

[1] Inner – inner stirrup of four-legged stirrup
[2] Outer – outer stirrup of four-legged stirrup

Summary and Application to Design

Results from the finite element study revealed that the relationship between $e^2/(h*d_b)$ to the ratio of tensile spalling force to prestress force is reasonably approximated by a straight line as shown in Figure 4.5.5. Because the true bond stress distribution is somewhere between uniform and linear bond stress,

an average between these two assumptions was developed, as shown in Figure 4.5.5. The equation for this straight line approximation is

$$\frac{\quad}{\quad} \qquad ,$$ (4.5.1)

where T is the spalling force and P is the strand force.
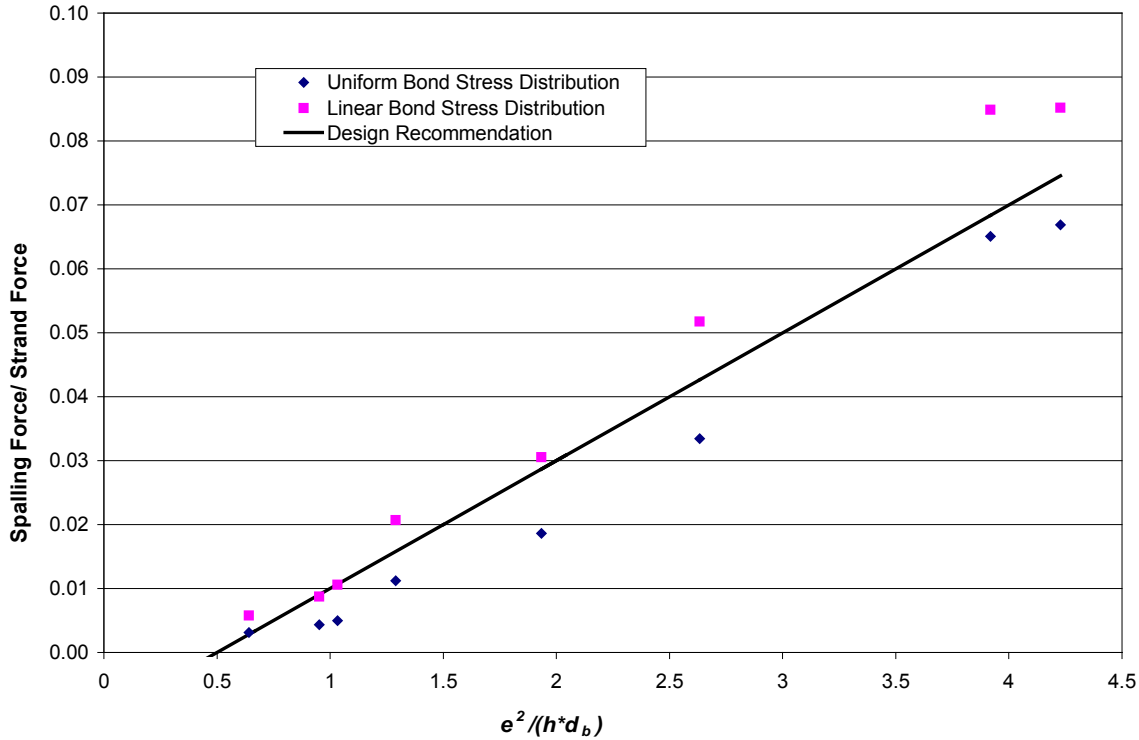
Figure 4.5.5: Ratio of Spalling Force to Prestress Force for varying $e^2/(h*d_b)$

Vertical steel reinforcement does not carry the vertical tensile stress until the concrete cracks. If the spalling stresses are small enough in a member for the concrete tensile strength to prevent cracking, vertical tensile steel is not necessary for the member.

To calculate the concrete area to be considered in providing tensile resistance, the area over which spalling forces act must be determined. Based on the slab span sections studied, the shortest distance into the member the spalling stress extends is $h/12$. This becomes a conservative estimate as the section increases in height and e/h. The area of concrete to resist this tensile strength is conservatively estimated as the product between $h/12$ and the distance between the outermost prestress strands (b_s) and can be written as

$$\frac{\quad}{\quad} \qquad ,$$ (4.5.2)

where T_c is the tensile force that can be resisted by the concrete, f_c is the concrete compressive strength at 28 days, h is the height of the member, and b_s is the distance between the outermost pretension strands. If the design tensile force is smaller than the tensile force resisted by concrete ($T < T_c$), it is reasonable to assume cracking will not occur and vertical tensile steel is not needed in the end region to resist the spalling force. Otherwise, steel must be placed within the end region of the member to resist

77

the tensile force found in Eqn. (4.5.1). The area of steel needed to resist the predicted spalling force is given by

$$- \, , \qquad\qquad\qquad\qquad\qquad\qquad\qquad\qquad\qquad (4.5.3)$$

where A_s is the area of steel and f_s is the allowable working stress of vertical reinforcement.

Application of these recommendations to the designs resulting from the parametric study described in Section 4.1 result in the end zone reinforcement identified in Table 4.5.5. The last line of the table includes the AASHTO 2010 requirements for comparison, which are incorrectly referred to as splitting resistance rather than spalling resistance requirements in AASHTO.

Table 4.5.5: Spalling reinforcement for Precast Inverted-T Sections

Height (in.)	8	10	12	12	14	16	20	22
Number of Strands	12	16	16	16	36	38	46	54
Strand Diameter (in.)	0.5	0.5	0.5	0.5	0.5	0.5	0.5	0.5
Total Prestress Force at Jacking (k)	370	500	500	500	1100	1200	1400	1700
Concrete Compressive Strength at Transfer (ksi)	5.0	5.0	4.5	4.5	5.5	5.5	5.6	6.0
e (in.)	1.6	2.5	2.4	2.5	3.7	4.6	6.3	6.8
T (k) (Eqn. 4.5.1)	1.0	7.5	4.6	5.4	32	51	97	126
T_c (k) (Eqn. 4.5.2)	17	21	24	24	32	36	45	51
Vertical Steel Needed?	No	No	No	No	No	Yes	Yes	Yes
A_s (in.^{2}) (Eqn. 4.5.3)	--	--	--	--	--	2.6	4.9	6.3
$h/4$	--	--	--	--	--	4.0	5.0	5.5
Stirrup Bar Size	--	--	--	--	--	#6	#6	#6
A_s (in^2) per AASTHO Article 5.10.10.1	0.74	1.0	1.0	1.0	2.2	2.4	2.8	3.4

4.6.   Connection Details between Superstructure and Substructure

The bearing and connection details between the bridge superstructure and the supporting substructure were investigated by a review of existing PCSSS bridges constructed by the Minnesota Department of Transportation. Because no problems have been encountered in the existing field bridges, the same details may be deemed appropriate in future applications of PCSSS bridges. Some modifications are recommended to reduce the potential for restrained shrinkage in the transverse direction.

Figure 4.6.1 shows an elevation view of the bearing detail at one of the two continuous supports for the Center City Bridge, one of the original field implementations of the PCSSS. The pile caps in this particular

bridge were precast, and the elevation view is shown through one of the sections featuring a vent hole through the pile cap into which dowels were placed prior to casting the CIP concrete.

As shown in the figure, the main bearing support was provided by a 6 in. wide by 1/2 in. thick neoprene bearing pad, with the center of bearing located 12 in. from the edge of the pier. Polystyrene was utilized in the 9 in. between the edge of the pier and the neoprene, as well as the 4 in. between the neoprene and the end of the beam; the polystyrene was selected because it would prevent the egress of concrete during the closure pour and was crushable and would therefore not significantly affect the bearing geometry of the system.
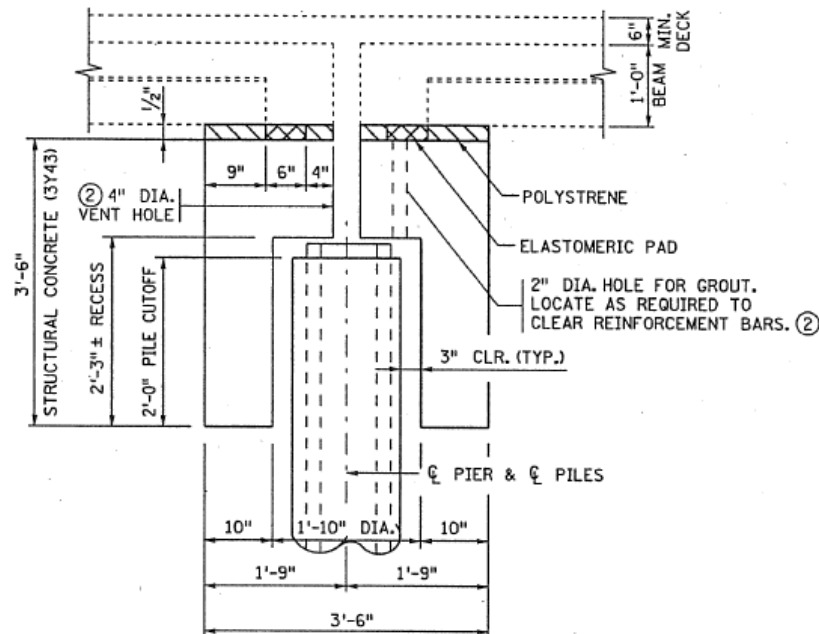
Figure 4.6.1: Bearing detail at continuous pier in Mn/DOT Bridge No. 13004 in Center City, Minnesota

The neoprene and polystyrene were not located in the transverse joint between the precast sections nor in the regions beneath the flange cutouts. This enabled the CIP concrete to fill those regions to facilitate the negative moment resistance of the bridge by enabling the transfer of compressive forces low in the section across the pier.

Vertical dowels were provided in the Center City Bridge to ensure that a mechanical connection was present between the substructure and superstructure. The vertical reinforcement was epoxied into holes drilled between the ends of the adjacent precast members at the continuous piers, and were subsequently embedded in the CIP closure pour. The vertical dowels consisted of No. 5 bars at 12 in.

The placement of the vertical reinforcement in these locations was found to be difficult in some of the subsequent applications of PCSSS bridges, because the 4 in. gap between the ends of the precast panels does not always provide sufficient tolerance for the precast panel span lengths. For this reason, the placement of the vertical dowels in the 10 in. flange cutout region may be preferred; however eccentricity of the vertical dowels from the centerline between precast panels will allow for the introduction of a moment between the superstructure and substructure in plan, and should therefore be avoided. It is recommended that the vertical dowels be oriented along a single line bisecting the area

79

between adjacent precast panels at continuous piers. Because the reinforcement is not provided to prevent cracking, and is simply to provide dowel action in the case of differential displacement between the superstructure and substructure, it may be acceptable to place the reinforcement as a group in the 24 in. space between precast webs, however still along the line bisecting the specimens.

A method considered by the Minnesota Department of Transportation to reduce the potential for the restraint of transverse shrinkage was to encase the vertical dowels in foam. The foam will likely only be beneficial if the CIP is debonded from the pier via a bond breaker. Consequently, in future applications of PCSSS bridges, it is recommended that a debonding material, such as a sheet of plastic be used, to prevent the CIP concrete from bonding to the substructure.

4.7.   Numerical Determination of Laboratory Loading

Mechanical loading was utilized in the laboratory to simulate traffic loading on the laboratory specimens (i.e., Concept 1 and Concept 2), described in Chapter 5. The Concept 1 specimen was developed based on the Center City Bridge, with some parameter variations (e.g., investigation of different flange thicknesses: 3 in. flange thickness in one span versus the 5-¼ in. flange thickness in the other span which emulated the Center City Bridge). The laboratory bridge specimens were fabricated with 12 in. thick precast panels and 6 in. cast-in-place topping. The approximately 22 ft. span lengths represented the outer spans of the Center City Bridge, which were a lower practical bound of PCSSS bridge spans. The same 18 in. deep section was used in all three spans (22-27-22 ft.) of the Center City Bridge, and could be used in even longer spans as indicated by Table 4.1.2. The use of the 18 in. deep section led to relatively low service stresses particularly in the end spans.

In an effort to improve the relevance of the laboratory tests to longer spans, the magnitude of the patch load was selected after a numerical analysis of longer PCSSS bridges. The 35 kip value was expected to induce the same levels of transverse tensile stress in the joint region of the 22 ft.-5 in. laboratory bridge span as would be expected in a 30 ft. three-span continuous system. The 30 ft. continuous bridge was selected because it represented a reasonable value for the design span of a slab span system with 12 in. deep precast panels (although as shown in Table 4.1.2, it might be possible to use something as shallow as a 10 in. deep precast section for a 30 ft. span). The 35 kip patch load was applicable to both the two-span Concept 1 and simply-supported Concept 2 laboratory bridges, coincidentally, because loading was applied at the quarter points of the simply-supported Concept 2 specimen, which featured different transverse reinforcement details in each half of the bridge span.

The numerical model was developed assuming an unbonded constraint between the precast flanges and CIP concrete, as illustrated in Figure 4.7.1. This was done to ensure that convergence would be achieved at the interface immediately above the precast joint. Figure 4.7.2 illustrates a modified four point AASHTO tandem design load on the three span 30 ft. continuous bridge, which consists of four 25 kip patch loads spaced in a 4 by 6 ft. grid. This modified tandem load pattern was based on twice the design tandem load, as specified in Article 3.6.1.2.3 (AASHTO 2010). The design tandem was doubled to provide an expected worst case scenario near the joint region, which represented two truck wheel loads placed as closely as possible directly over a longitudinal joint. The image is shown from the end span looking in the direction of traffic. The 6 ft. wide patch loads are placed directly above the precast joints, which represented the worst load case for the system.

Separation of precast flange and CIP concrete
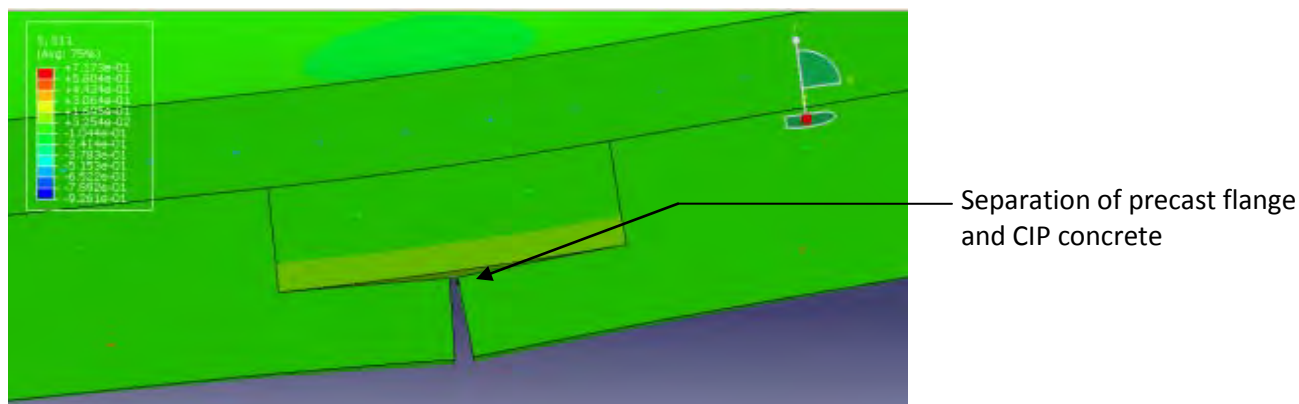
Figure 4.7.1: Separation of top of precast joint from CIP concrete in 30 ft. continuous and laboratory bridge models

Center Span

End Span

4 sets of 25 kip patch loads

6 ft. section
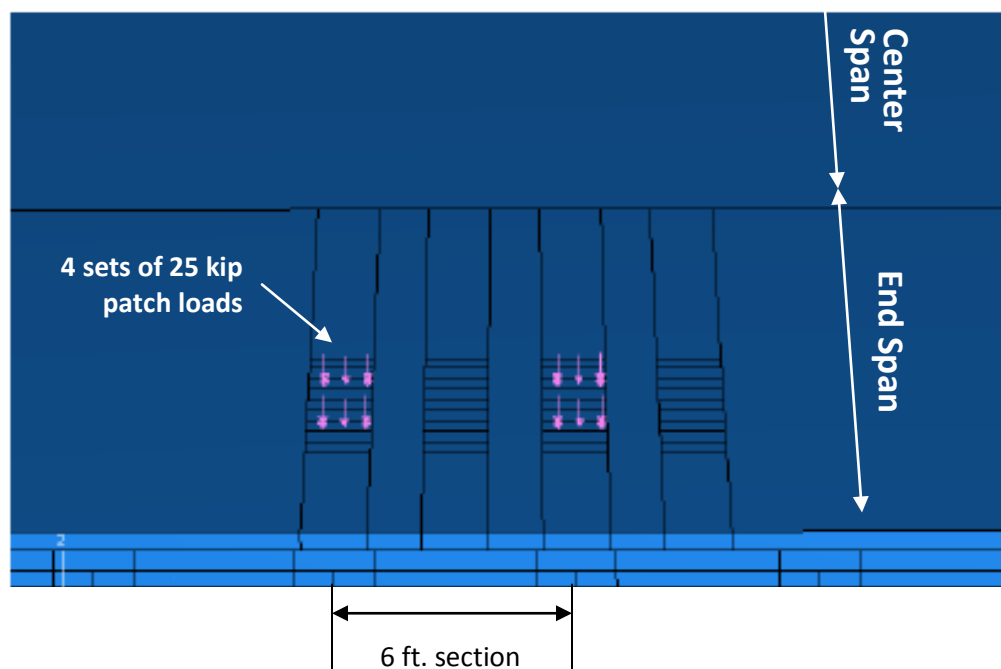
Figure 4.7.2: Three span 30-30-30 ft. continuous bridge with AASHTO tandem loading, increased by a magnitude of two to account for two trucks side by side with adjacent wheels applied over the joint, applied for the numerical calculation of a patch load demand in laboratory bridge.

The numerical models utilized for the Concept 1 and Concept 2 laboratory specimens are shown under deformation in Figure 4.7.3a-b, respectively. The Concept 1 model was analyzed with the patch load centered at midspan of both spans, while the Concept 2 model was loaded at the quarter points. The same numerical model was utilized to analyze the effect of the patch load for both specimens. For the Concept 2 bridge, which was a simply-supported span, the same two-span model was used with an assumed modulus of elasticity of the CIP and precast concrete in the span with the 5-¼ in. thick flange

81

set to be 1/100 of the modulus of elasticity of the CIP used in the loaded span modeled with a 3 in. flange, effectively creating a simply-supported boundary condition at the end of the bridge connected to the adjacent span.
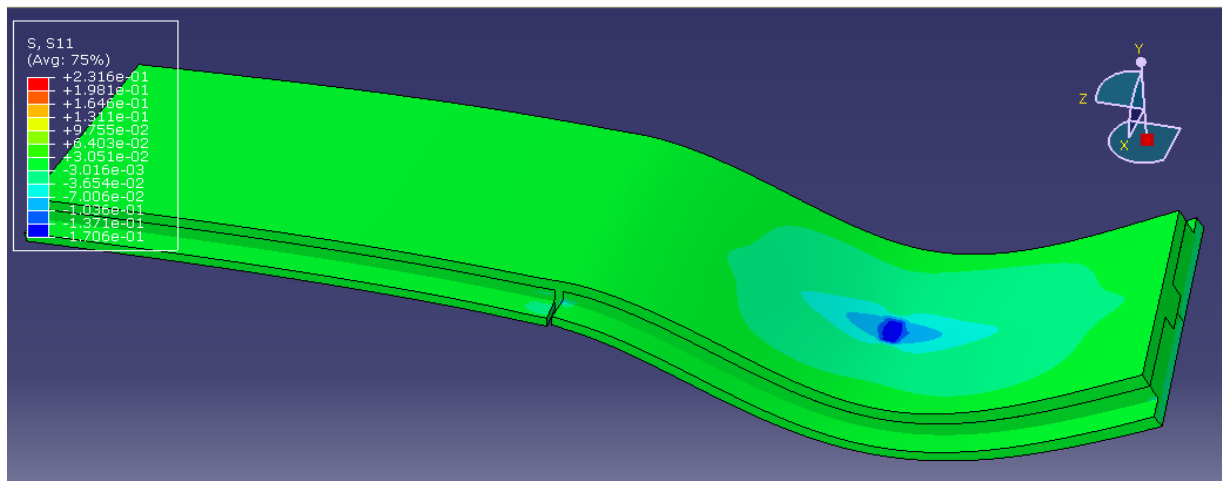
a) Concept 1 laboratory specimen – patch loading at midspan
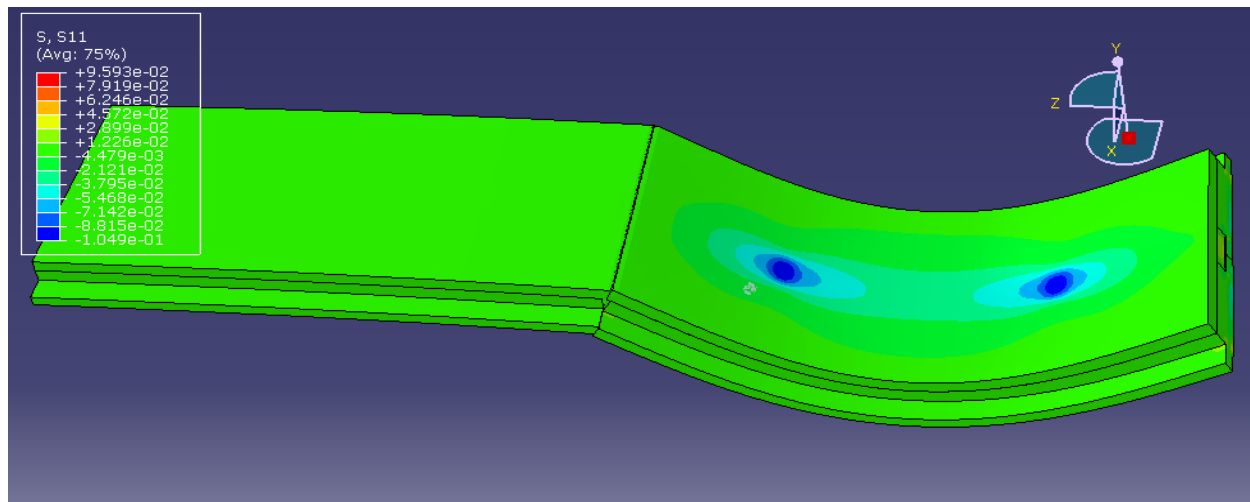
b) Concept 2 laboratory specimen – patch loading at quarter points. Second span modeled with modulus of elasticity of CIP equal to 1/100 CIP modulus of elasticity of loaded span

Figure 4.7.3: Deflected numerical models of (a) Concept 1 specimen and (b) Concept 2 specimen for determination of patch loading in laboratory specimens

The analyses suggested that the load required to induce similar levels of transverse tensile stresses in the 30 ft. continuous bridge and the loading cases of the laboratory bridge varied by less than two kips, and therefore, with a patch load of 26.7 kips required to induce similar levels of transverse stress in the laboratory bridge as the 30 ft. continuous bridge. Furthermore, the dynamic loading effects were considered through the use of a 33 percent increase in the static load, as specified in Article 3.6.2.1 of the AASHTO specification (2010). Therefore, the calculated load to be applied to the laboratory bridge to simulate a tandem vehicle loading on a 30 ft. continuous bridge was determined to be 35 kips (26.7 kips * 1.33).

82

Chapter 5 PCSSS: Large-Scale Laboratory Bridge Investigation of System Behavior

5.0   Introduction

The performance of the precast composite slab span system in a global sense depends on the interaction between neighboring precast panels as well as panels in the adjacent spans. This interaction between components of the PCSSS warranted the development of two large-scale laboratory test specimens constructed and tested in the University of Minnesota Structures Laboratory. The first bridge, Concept 1, was developed as a continuous two-span system with two adjacent precast panels per span. A number of variables were investigated with this bridge, which are discussed in detail in Section 5.1.1. A portion of the Concept 1 specimen emulated one of the first implementations of PCSSS bridges in the State of Minnesota, Mn/DOT Bridge 13004 built in Center City. The second bridge, designated as the Concept 2 specimen, was a simply-supported bridge with two adjacent precast panels. The Concept 2 laboratory bridge was developed to augment the information obtained from testing of the Concept 1 laboratory bridge specimen, and is discussed in detail in Section 5.1.2. This chapter discusses the development, testing, and results of the large-scale laboratory testing.

5.1.   Selection and Design of Laboratory Bridge Specimens

The Concept 1 specimen which was based on the Center City Bridge with modifications as required to investigate variations in some of the parameters, was constructed as part of a Mn/DOT research project which consisted of a companion field and laboratory investigation described by Smith et al. 2008. The results of the field study are summarized in Section 3.2. At the conclusion of the Mn/DOT study, the Concept 1 laboratory bridge was made available to the NCHRP 10-71 study, which included cyclic tests to simulate fatigue, investigation of initiation of reflective cracking simulated to emulate observed crack initiation in the Center City field bridge, as well as tests to investigate the ultimate strength of the system and composite action. The Concept 2 laboratory bridge, developed at the conclusion of laboratory testing on the Concept 1 laboratory bridge, was designed to incorporate information accrued from the Concept 1 tests, as well as to investigate variations in additional parameters. Relevant design details for both specimens are discussed in the following sections.

Many of the design details associated with the Concept 1 and Concept 2 large-scale laboratory bridge specimens, as well as the subassemblage specimens discussed in Chapter 6, include variations in the size and spacing of the transverse reinforcement traversing the longitudinal precast joint in the trough region created by adjacently abutted precast sections. To provide a means of qualifying the reinforcement in this region, a transverse reinforcement ratio was defined. The presence of transverse reinforcement for both transverse load transfer and reflective crack control warranted separate definitions for the reinforcement ratio in each case.

In the case of transverse load transfer, the area of reinforcement considered was only that which was embedded or mechanically anchored through the precast web in the lowest region of the CIP trough such that all load developed in the reinforcement could be adequately transferred through the adjacent panels. For a given longitudinal joint, the reinforcement protruding from a single precast panel was considered (i.e., for each pair of transverse embedded bars, only one was considered in the reinforcement ratio). It was assumed that the load was transferred from the bars protruding from one panel to the bars protruding from the adjacent panel through lap splices. Furthermore, the area of

concrete considered in the calculation was taken as that between the top of the precast flanges and the top of the section. An illustration of the area of steel and concrete considered for the calculation of the reinforcement ratio for transverse load transfer is highlighted in yellow in Figure 5.1.1.
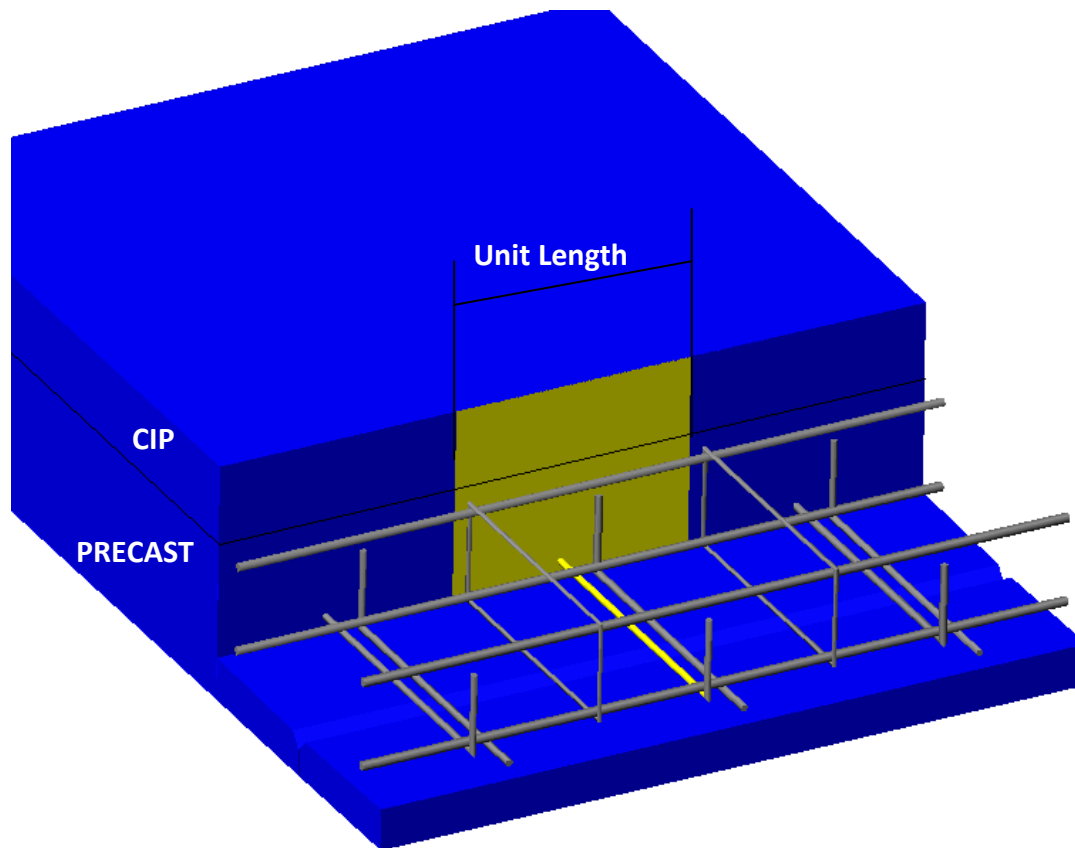
Figure 5.1.1: Reinforcement and depth of concrete considered in the calculation of the reinforcement ratio for transverse load transfer (highlighted in yellow)

The reinforcement ratio for crack control, on the other hand, considered the area of all reinforcement crossing the precast joint near the bottom of the CIP trough. Therefore, the bottom leg of the cage stirrups and all of the embedded transverse reinforcement was included in the calculation (i.e., for each pair of transverse embedded bars, both were included in the calculation because both were assumed to be effective above the longitudinal joint between the adjacent flanges). Furthermore, the area of concrete used in the calculation was only that which was located between the top of the precast flanges and the top of the precast webs. An illustration of the area of steel and concrete considered in the calculation of the reinforcement ratio for crack control is highlighted in yellow in Figure 5.1.2. It should be noted that this crack control reinforcement would only be effective in the region above the longitudinal joint between adjacent precast panels. For potential cracks that may develop at the precast web-CIP interface, only the reinforcement protruding from the precast webs would be effective.

84
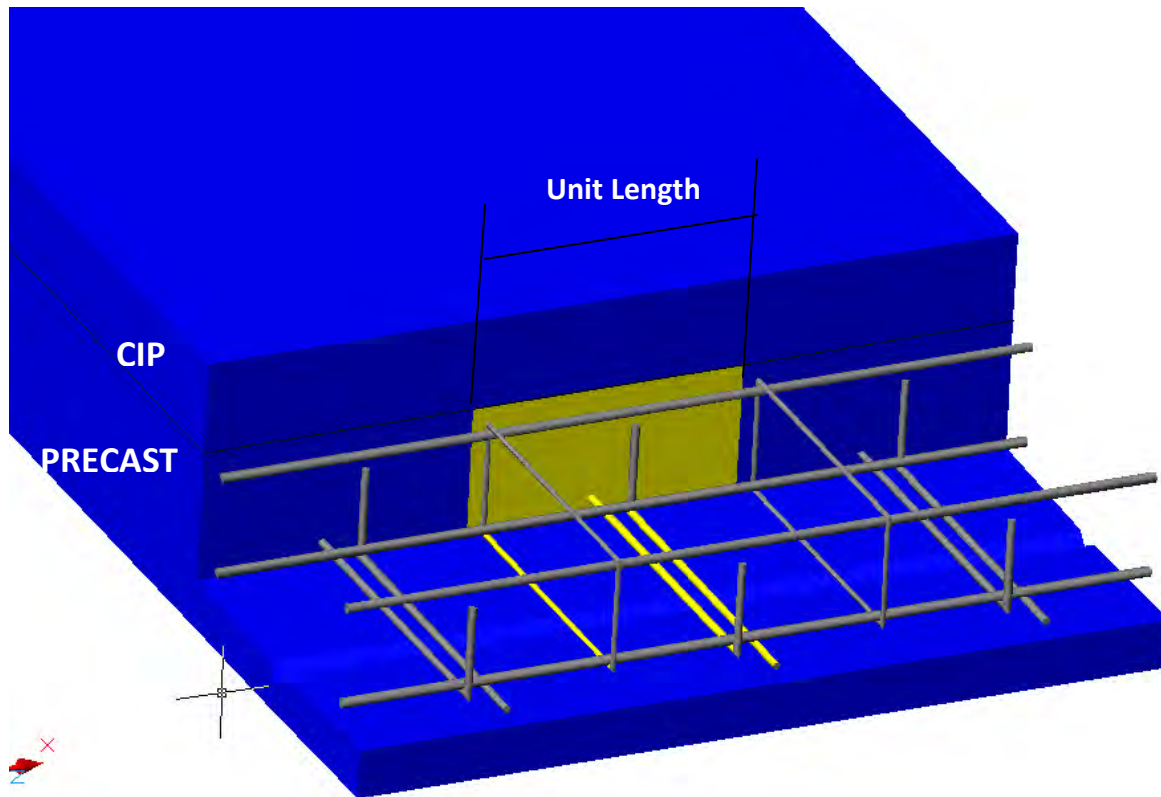
Figure 5.1.2: Reinforcement and depth of concrete considered in the calculation of the reinforcement ratio for reflective crack control (highlighted in yellow)

5.1.1. Concept 1 Laboratory Bridge

The continuous two-span Concept 1 laboratory bridge specimen was selected to provide insight into the effects of restraint moment developed at the pier, load distribution, and the effect of a number of variations in parameters. Restraint moments will develop at continuous piers due to both time-dependent effects (i.e., creep and shrinkage) and thermal gradients. Because the laboratory bridge was constructed and tested within the temperature-controlled environment of the University of Minnesota Structures Laboratory, restraint moments due to thermal effects were not experimentally studied in the laboratory specimen, however an effort to induce a longitudinal curvature due to a uniformly applied thermal heat source was implemented on Span 2 of the Concept 1 laboratory bridge, which is discussed later in this chapter.

Variables investigated in the two-span Concept 1 laboratory bridge are summarized in Table 5.1.1. The variables included the precast flange thickness, flange surface roughness, and reinforcement detailing, in addition to the amount of CIP deck reinforcement. Span 2 of the bridge was constructed identically to the exterior spans of the Center City Bridge, allowing for a relative comparison between observed results in the field and laboratory bridges. Span 1 of the bridge specimen was constructed with the application of the variables of interest, such as a reduced flange depth; the reduction in flange depth from 5.25 to 3 in. was introduced in an effort to reduce the distance between the transverse hooked bars and the precast flange, which would help to intercept a potential reflective crack at the precast joint region at a lower depth as well as increase the transverse moment capacity. Additionally, a smooth

85

flange surface was used in Span 1. The smooth flange was designed to reduce the stress concentration above the flanges directly at the joint, as well as aid in the removal of the formwork during fabrication. The stirrup spacing for horizontal shear reinforcement was increased to 24 in. on center in Span 1, primarily because the 12 in. stirrup spacing utilized in Span 2 was expected to be overly conservative. The horizontal shear reinforcement was also detailed with increased clear spacing below the hooked bars in Span 1, as the 1/4 in. nominal clear spacing provided in Span 2 was expected to inhibit bond development between the CIP concrete and the stirrup hook. The longitudinal and transverse deck reinforcement was also considered during the study, with the north half of the bridge consisting of a reduced longitudinal reinforcement scheme. The transverse deck reinforcement was reduced to No. 4 bars at 12 in. in Span 1, from No. 5 bars at the same spacing in Span 2. The four precast panels used in the Concept 1 laboratory bridge provided eight regions (i.e., one region at each end of each precast panel) that were used in the end zone stress study, discussed in Section 4.5. The bursting reinforcement locations in the Concept 1 laboratory bridge are shown in Figure 5.1.3, and were identical for Spans 1 and 2.

The behaviors of interest to this study are discussed herein; additional results pertinent to the Concept 1 laboratory bridge have been documented by Smith et al. (2008) in association with the previous Mn/DOT study.

Table 5.1.1: Original and modified design criteria in Spans 1 and 2 of the Concept 1 laboratory bridge

Span 1 (Modified Section)	Span 2 (Original Section)
Decreased flange thickness (3 in.)	Original flange thickness (5-¼ in.)
Smooth flange surface	Original roughened flange surface
Increased stirrup spacing for horizontal shear reinforcement (No. 5 Stirrups at 24 in.)	Original stirrup spacing for horizontal shear reinforcement (No. 5 Stirrups at 12 in.)
Increased clear spacing under hooks (1-3/8 in. nominal clear spacing between horizontal shear reinforcement stirrups and precast section)	Original clear spacing under hooks (1/4 in. nominal clear spacing between horizontal shear reinforcement stirrups and precast section)
Decreased transverse deck reinforcement (No. 4 bars at 12 in.)	Original transverse deck reinforcement (No. 5 bars at 12 in.)
The longitudinal deck steel in the south half of the bridge was two No. 7 and one No. 8 bars per 12 in. at the continuous pier (Original design)	
The longitudinal deck steel in the north half of the bridge was reduced to No. 6 bars at 6 in. spacing at the continuous pier (Modified design)	

NW	1N	NE	NW	2N	NE
SW	1S	SE	SW	2S	SE

SPAN 1 | SPAN 2

BURSTING CONFIGURATION (Both Spans):
CONFIG 1: NW Ends - Minimum Configuration I (No. 3 @ 2,4 in.)
CONFIG 2: NE Ends - Minimum Configuration II (No. 4 @ 2 in.)
CONFIG 3: SW Ends - Original Design (No. 5 four legged stirrup @ 2, 4 in.)
CONFIG 4: SE Ends - AASHTO Design (No. 5 stirrup @ 2,4 in.)
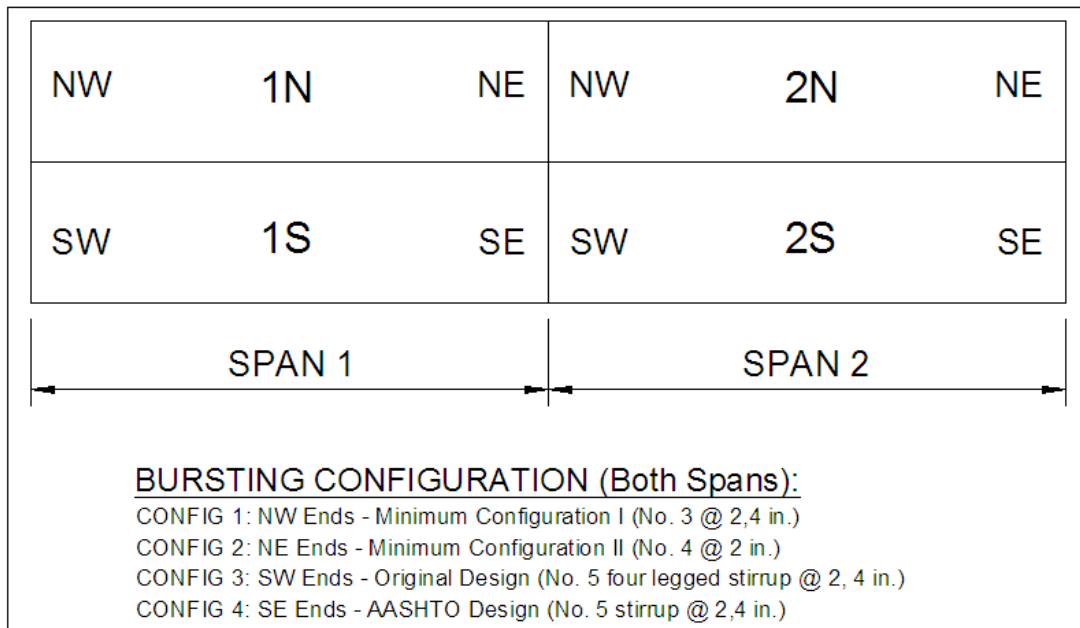
Figure 5.1.3: Bursting reinforcement details used in the Concept 1 laboratory specimen. Configuration numbers correspond to the discussion on bursting in Section 4.5

A simplified plan view of the Concept 1 laboratory bridge, including support locations and relevant dimensions is included in Figure 5.1.4; the transverse reinforcement near the longitudinal precast joint region is not shown for clarity. The reinforcement present in each unique cross section (i.e., east, west, or midspan) of each precast panel (i.e., 1N, 1S, 2N, 2S), as well as an elevation and layout views illustrating the location of reinforcement along the length of each beam are shown in Figures 5.1.5 through 5.1.20; four figures are included for each precast panel, in the following order: east cross section, west cross section, midspan cross section, and elevation/plan. A photograph of the Concept 1 laboratory bridge shortly after the completion of the continuity deck pour is shown in Figure 5.1.21.
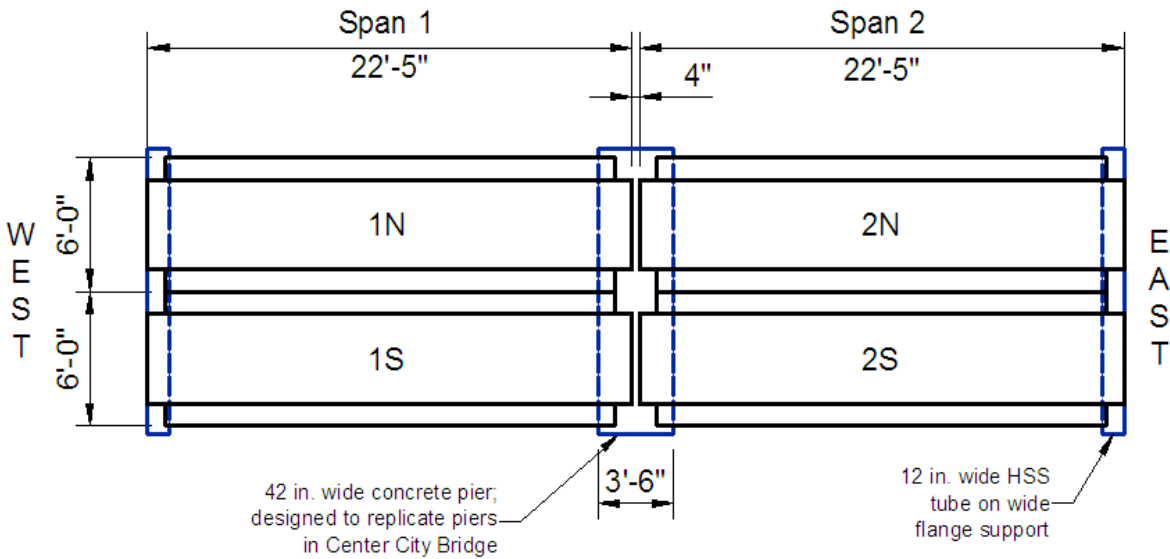
Figure 5.1.4: Plan view of the Concept 1 laboratory bridge, including support locations and relevant dimensions. Transverse reinforcement near longitudinal precast joint is not included for clarity

88
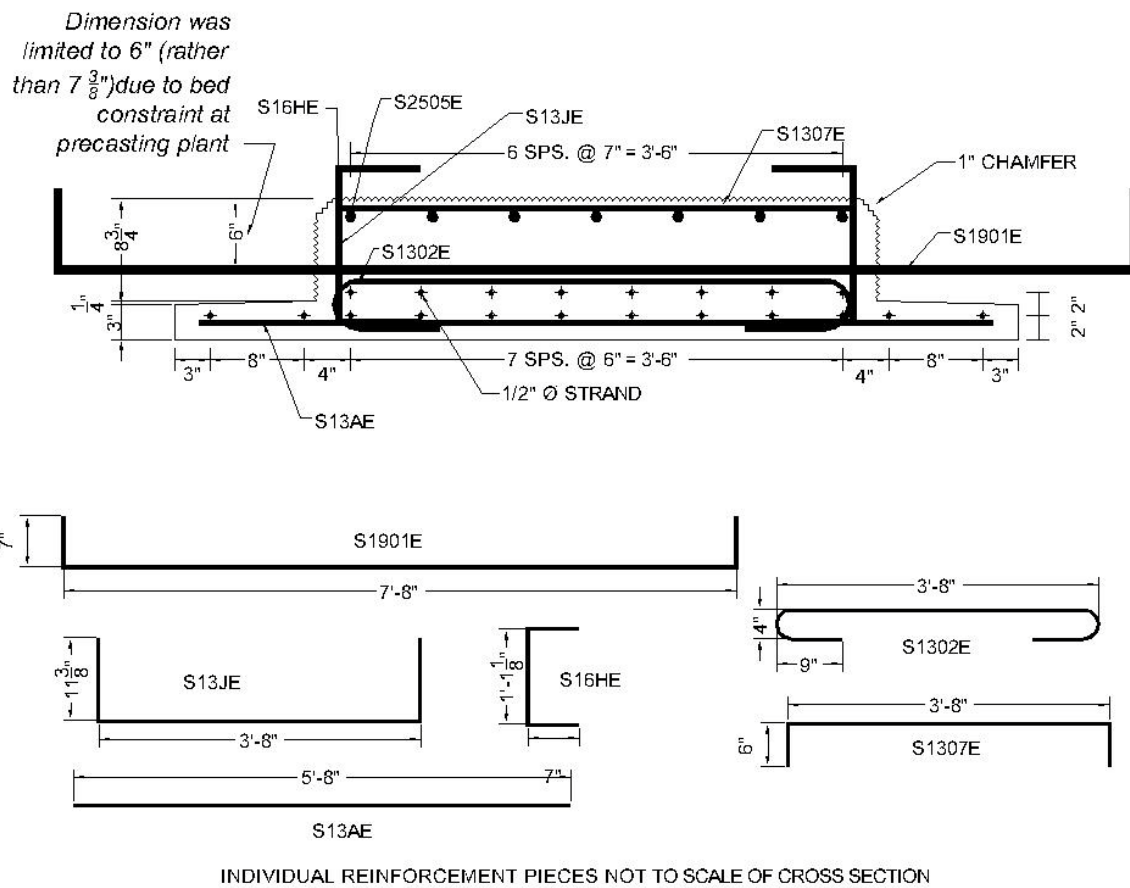
Figure 5.1.5: Cross section and individual reinforcement details for the east end of precast beam 1N
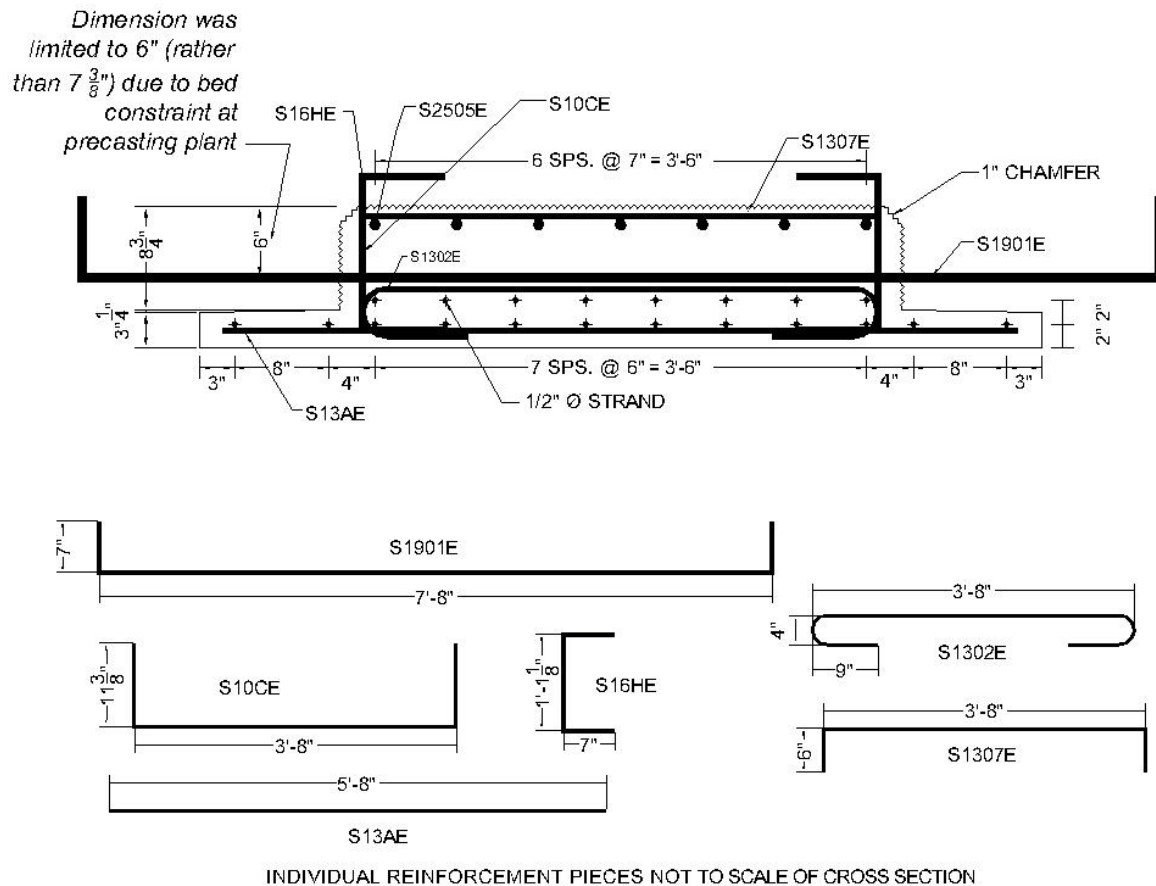
Figure 5.1.6: Cross section and individual reinforcement details for west end of precast beam 1N
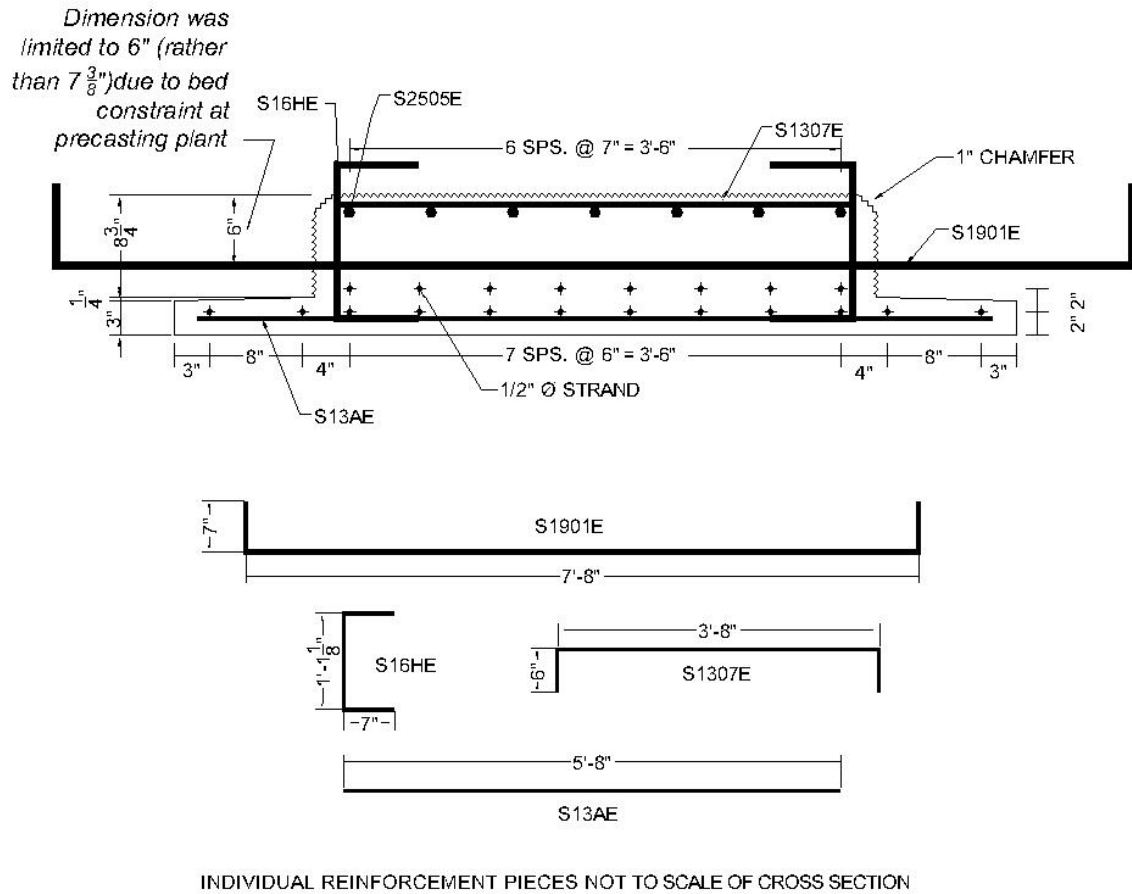
Figure 5.1.7: Cross section and individual reinforcement details for midspan of precast beam 1N

91
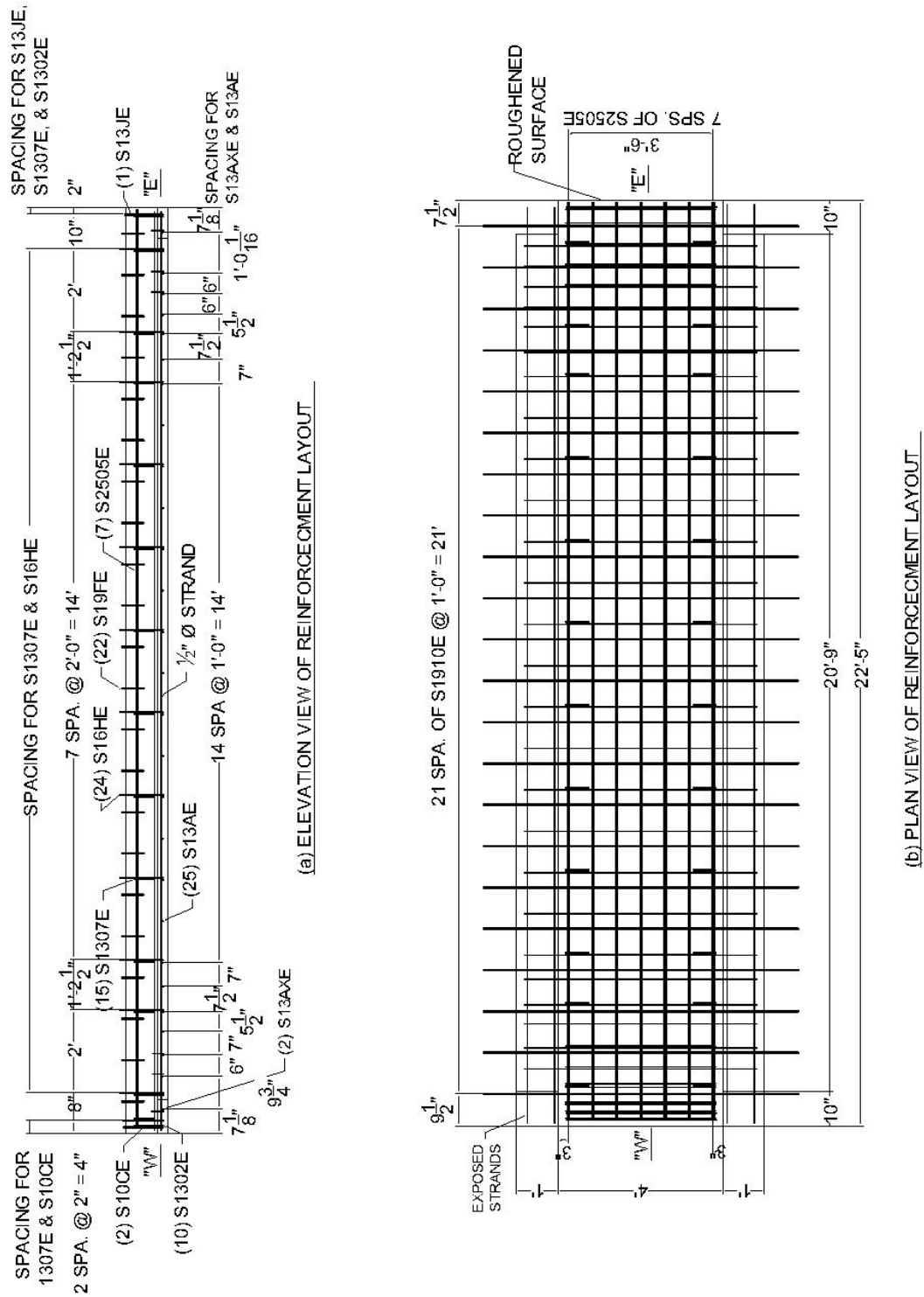
Figure 5.1.8: Elevation and plan views of reinforcement layout for precast beam 1N

92

Figure 5.1.9: Cross section and individual reinforcement details for east end of precast beam 1S

93

Figure 5.1.10: Cross section and individual reinforcement details for west end of precast beam 1S

94
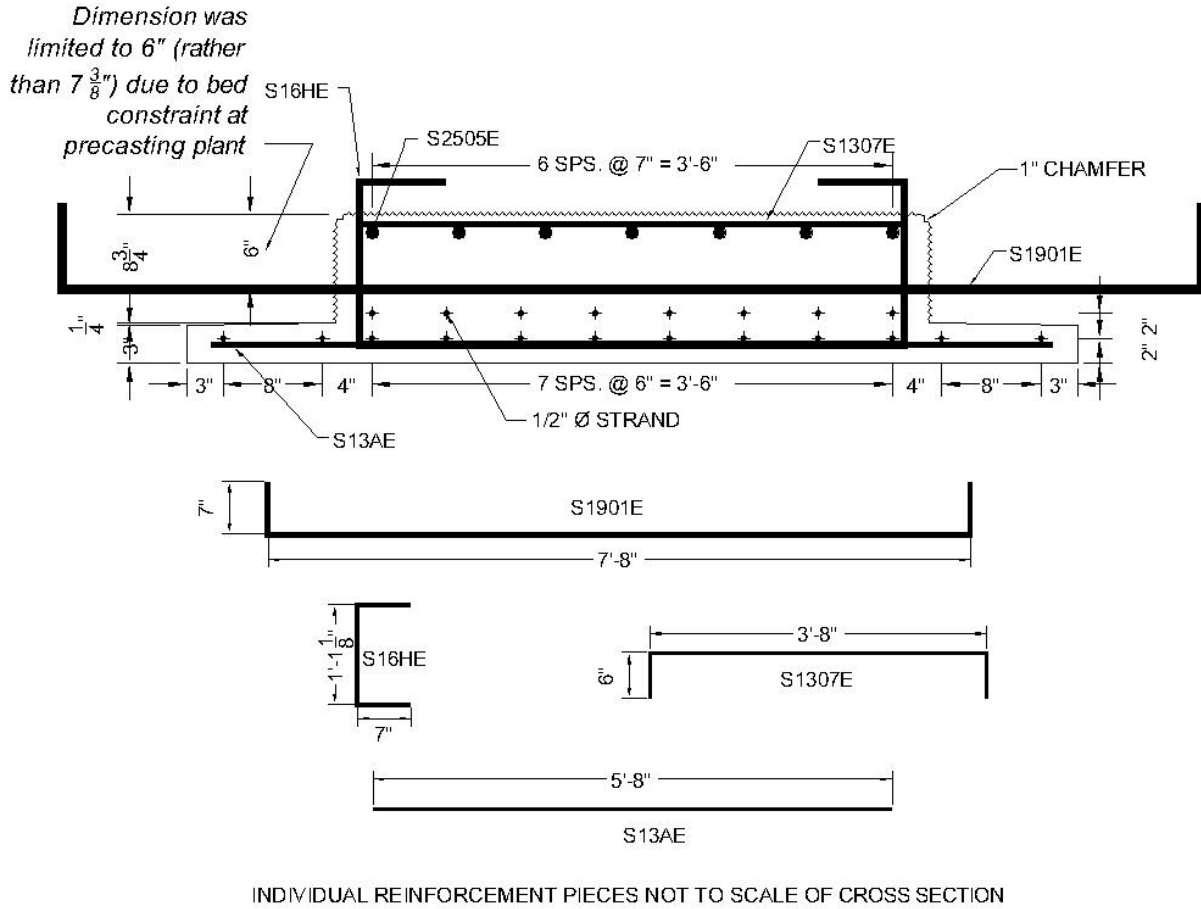
Figure 5.1.11: Cross section and individual reinforcement details for midspan of precast beam 1S

95
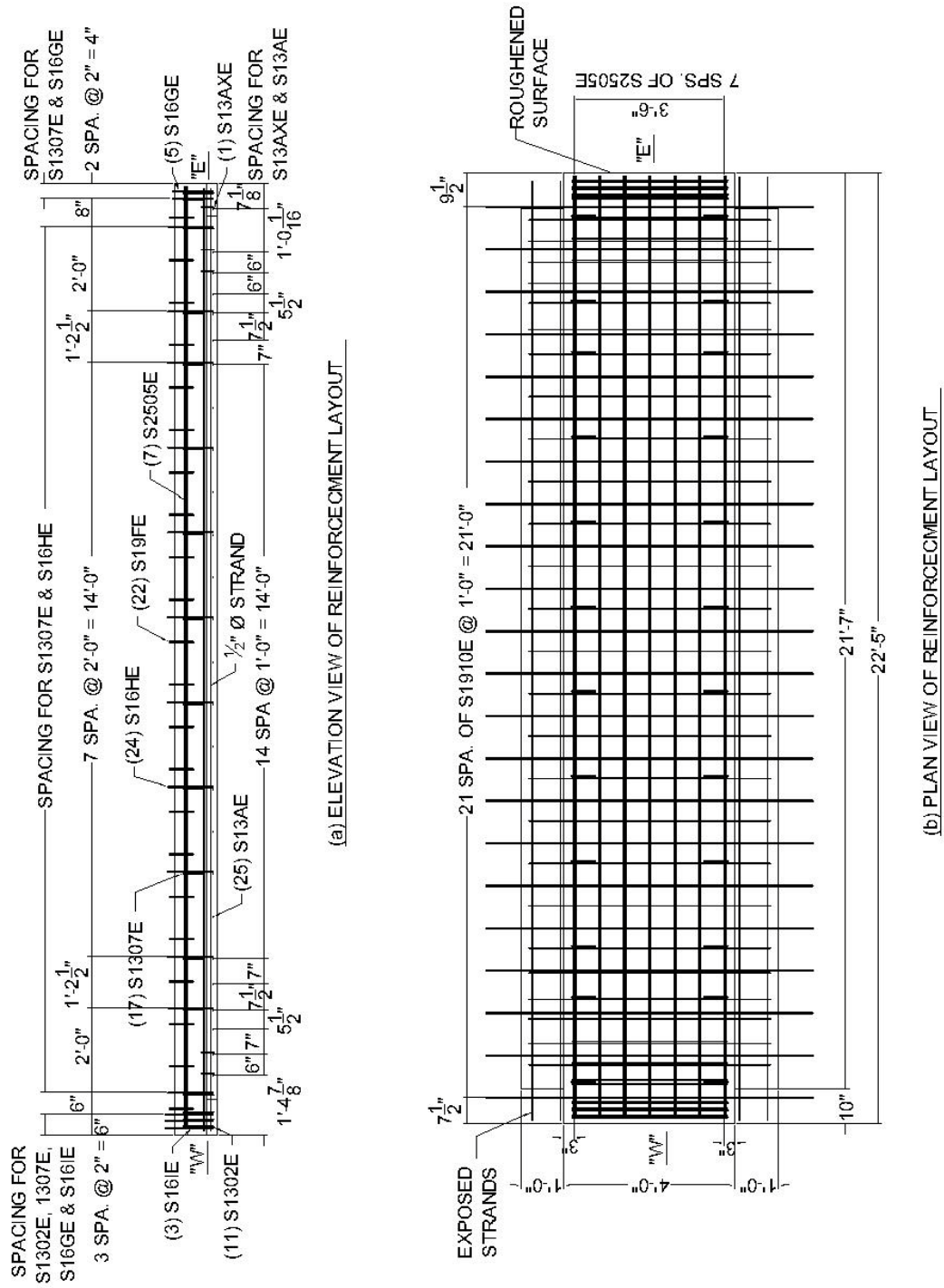
Figure 5.1.12: Elevation and plan views of reinforcement layout for precast beam 1S

96
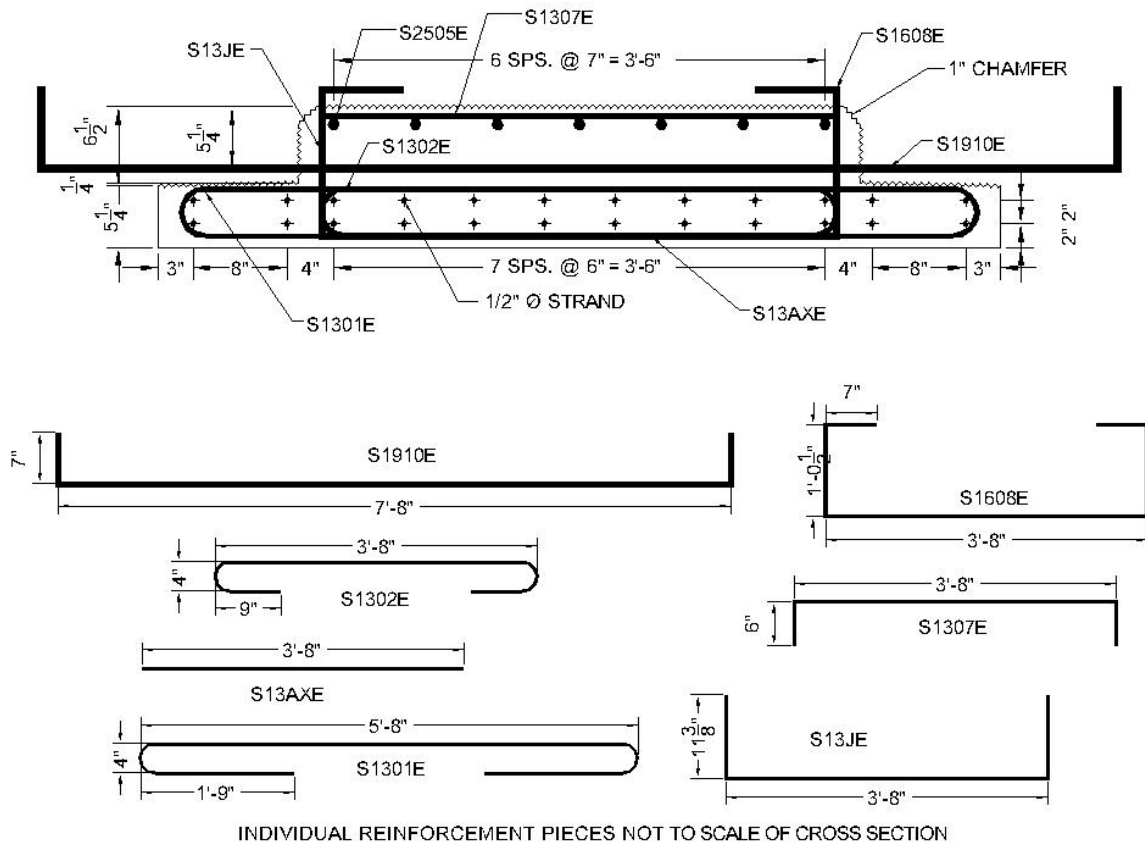
Figure 5.1.13: Cross section and individual reinforcement details for east end of precast beam 2N

97

INDIVIDUAL REINFORCEMENT PIECES NOT TO SCALE OF CROSS SECTION
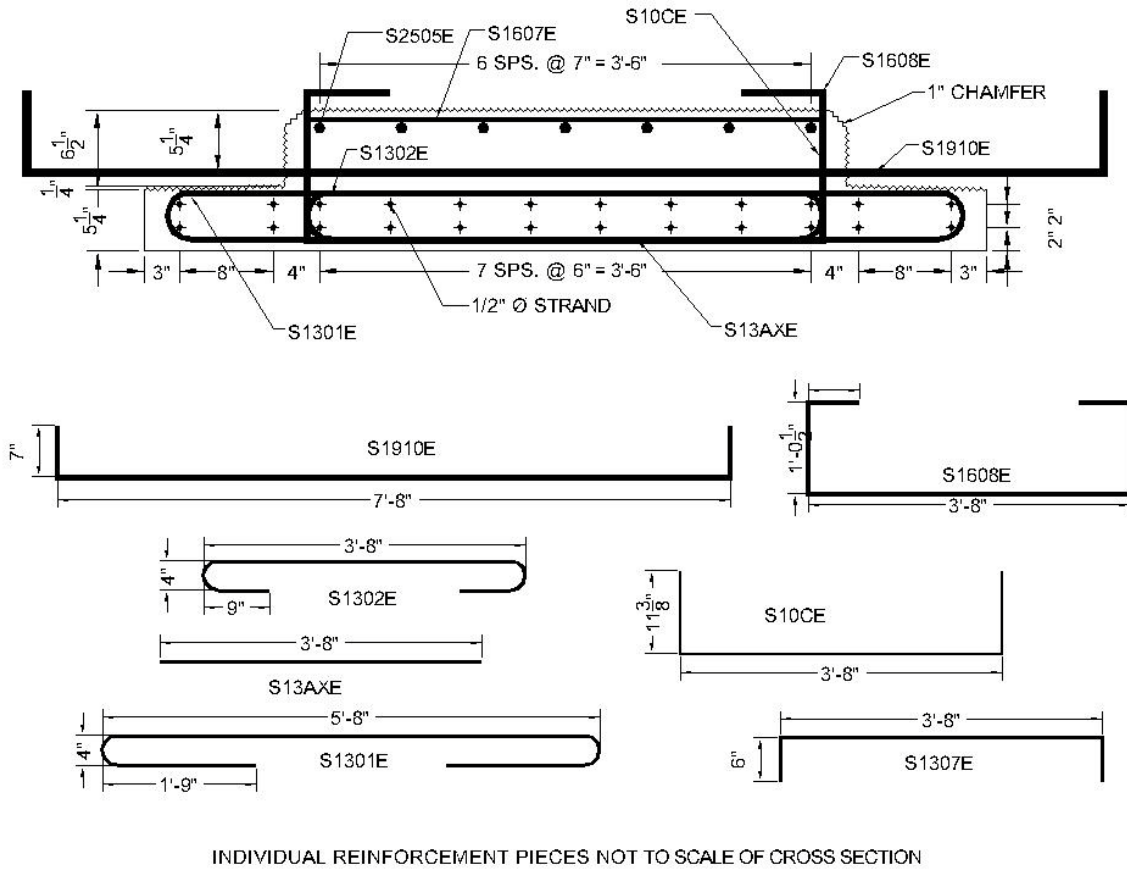
Figure 5.1.14: Cross section and individual reinforcement details for west end of precast beam 2N

98
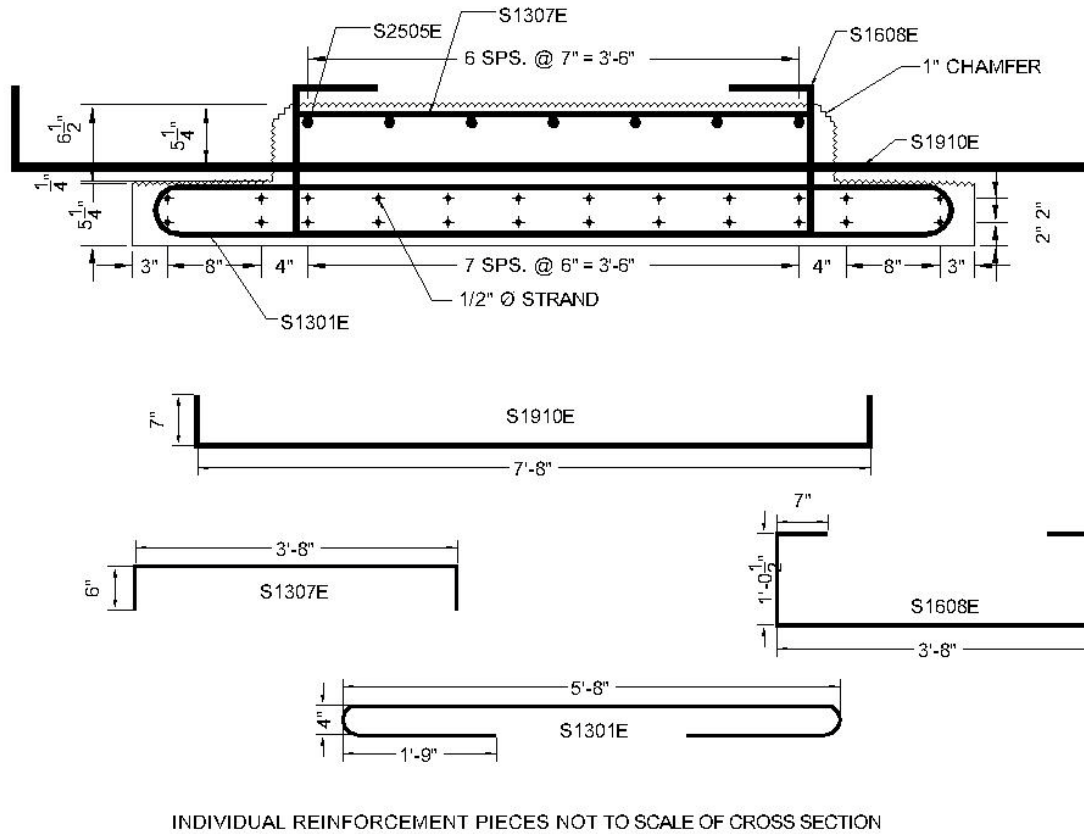
Figure 5.1.15: Cross section and individual reinforcement details for midspan of precast beam 2N

99
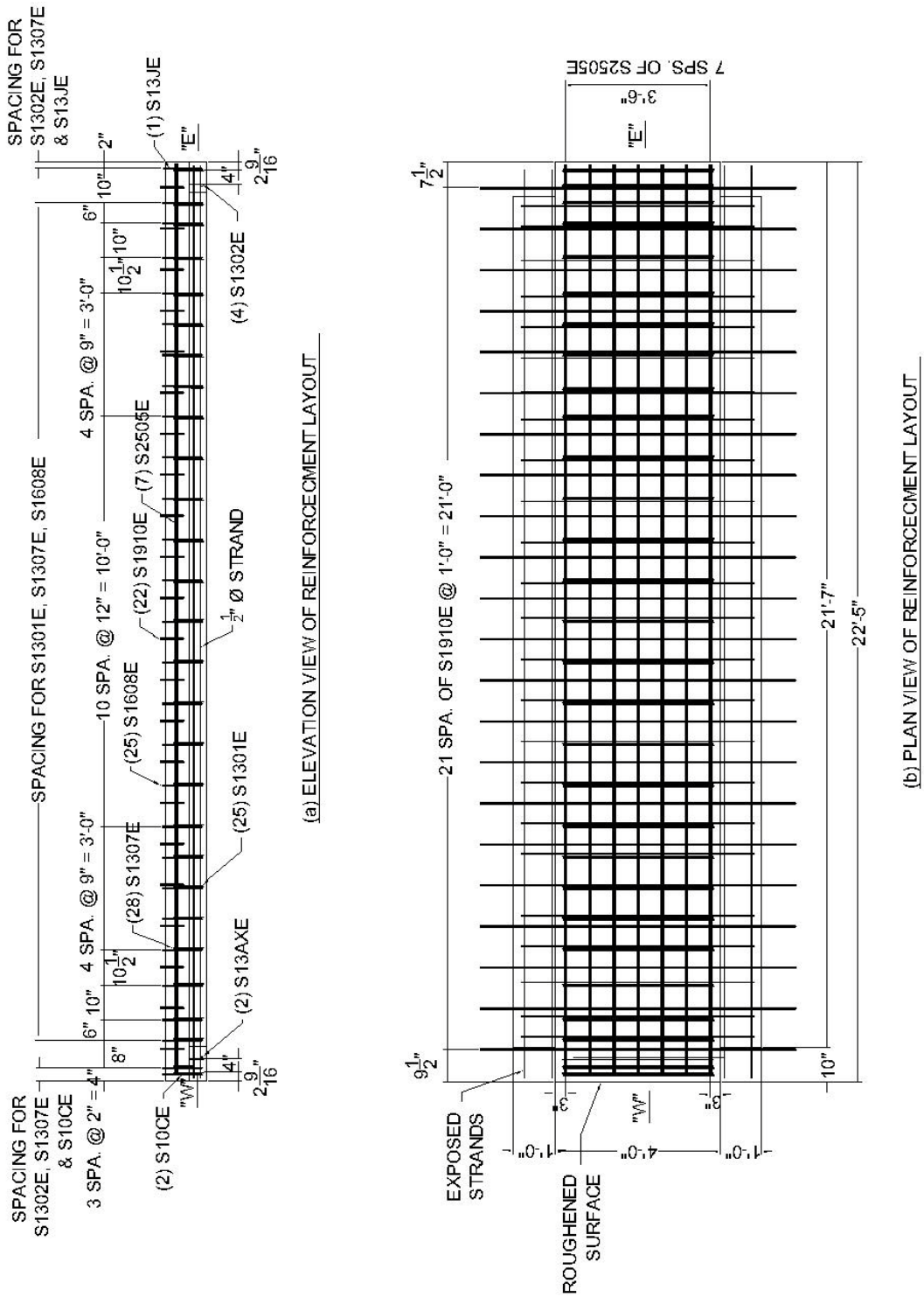
Figure 5.1.16: Elevation and plan views of reinforcement layout for precast beam 2N

100
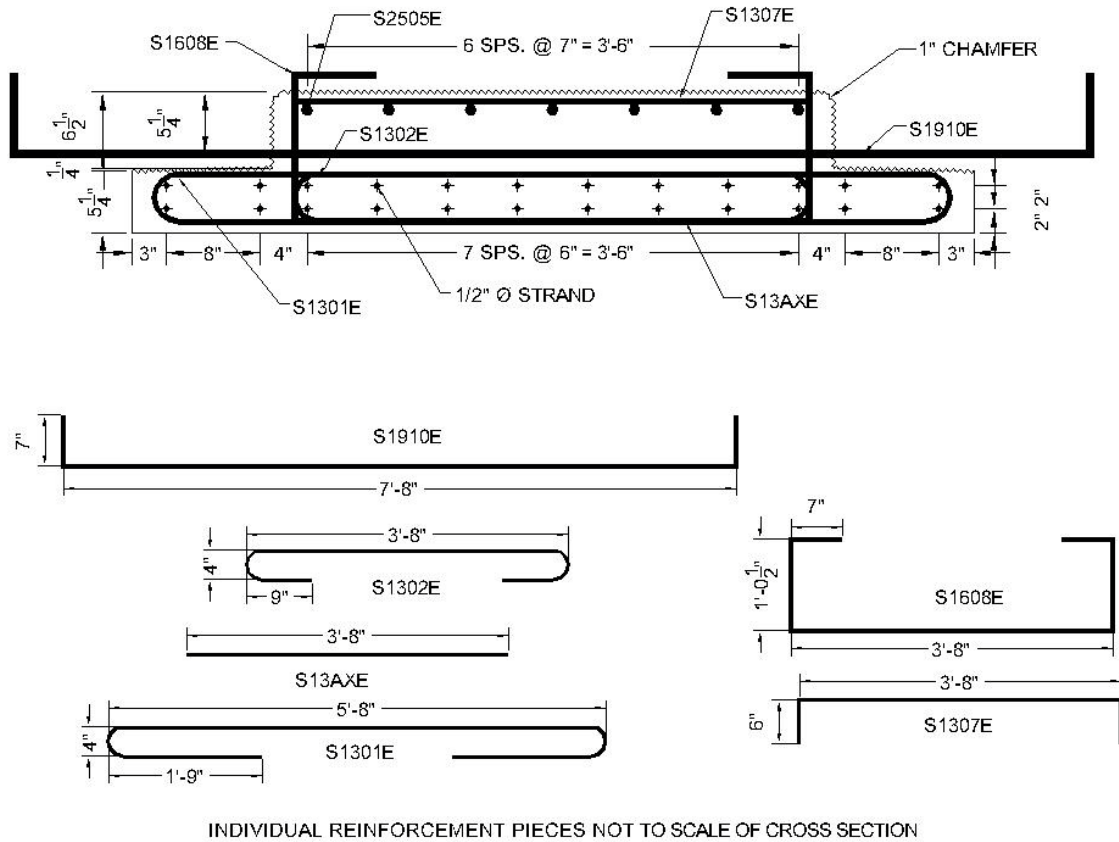
Figure 5.1.17: Cross section and individual reinforcement details for east end of precast beam 2S

101
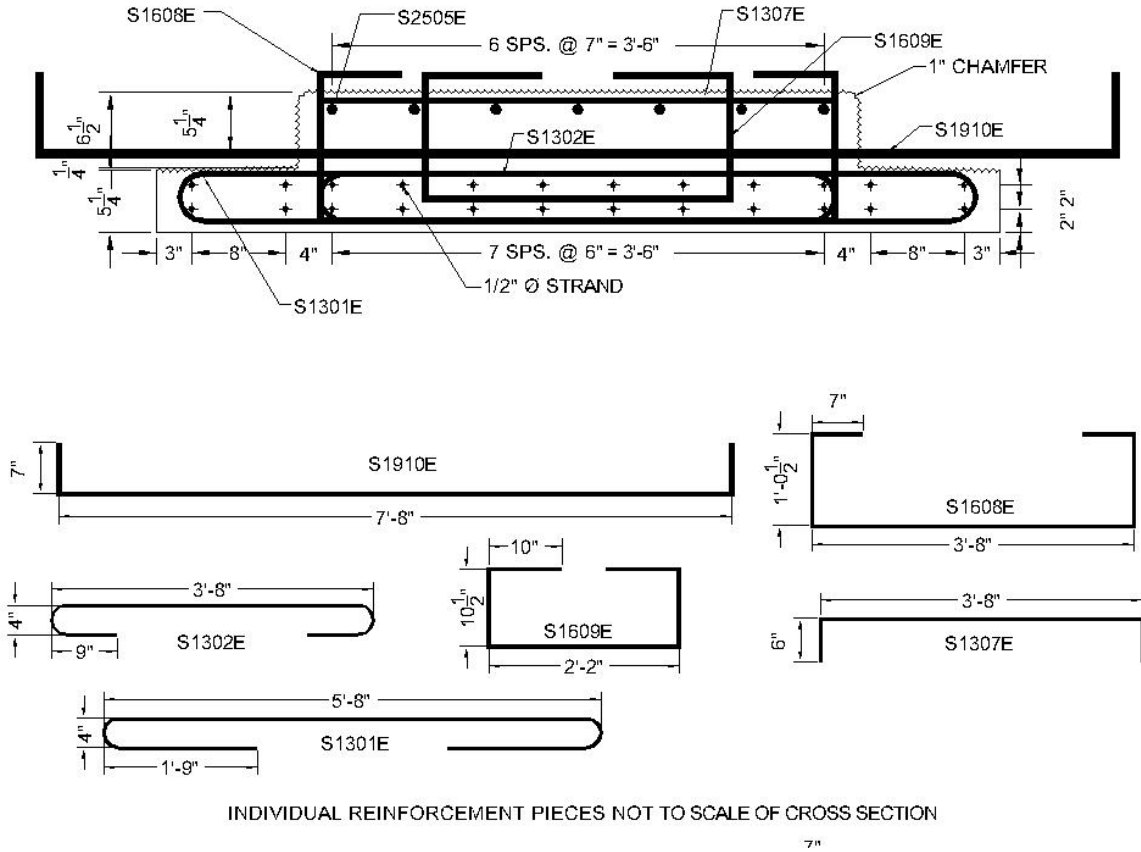
Figure 5.1.18: Cross section and individual reinforcement details for west end of precast beam 2S

102
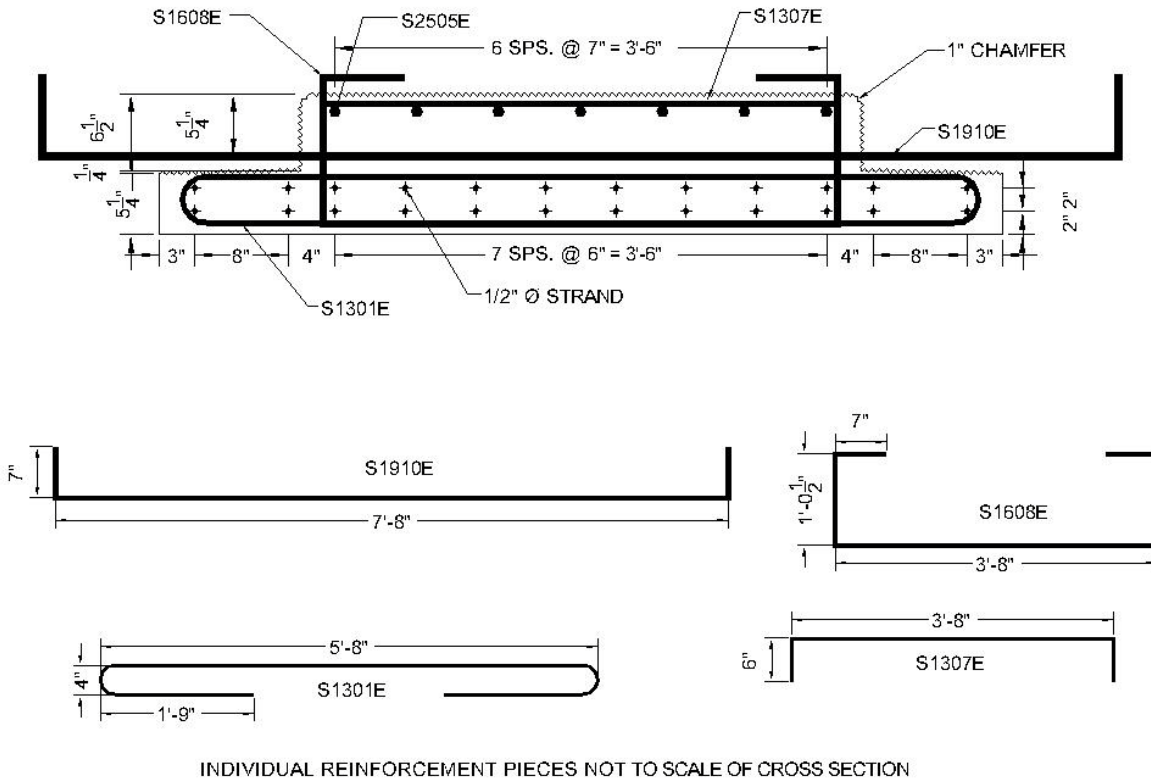
Figure 5.1.19: Cross section and individual reinforcement details at midspan of precast beam 2S
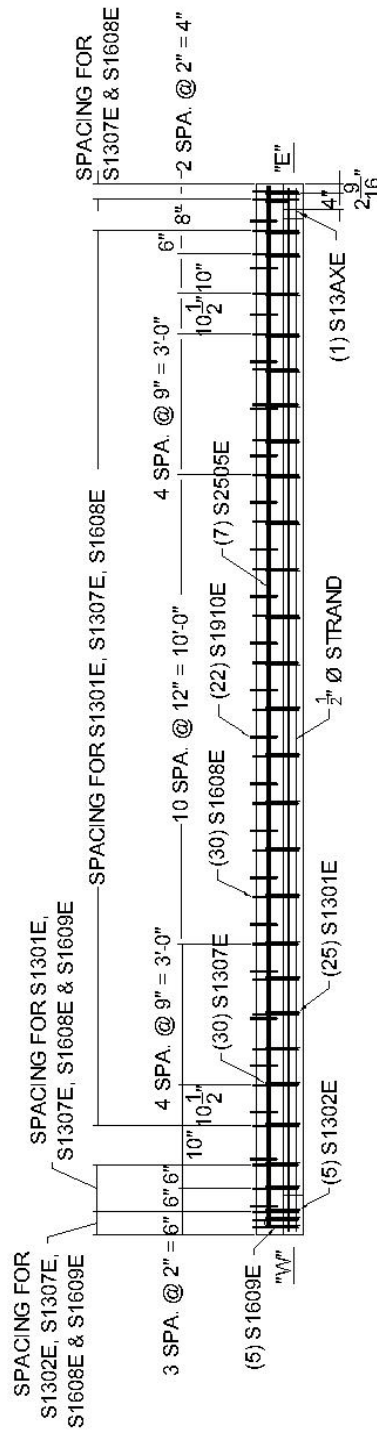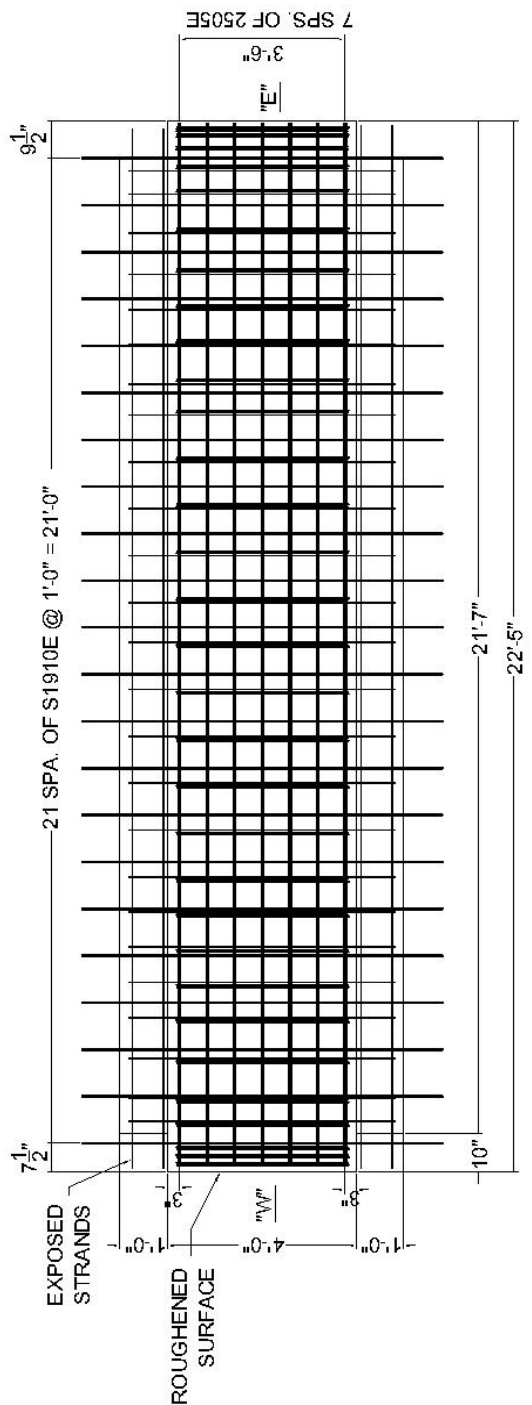
Figure 5.1.20: Elevation and plan views of reinforcement layout for precast beam 2S

104
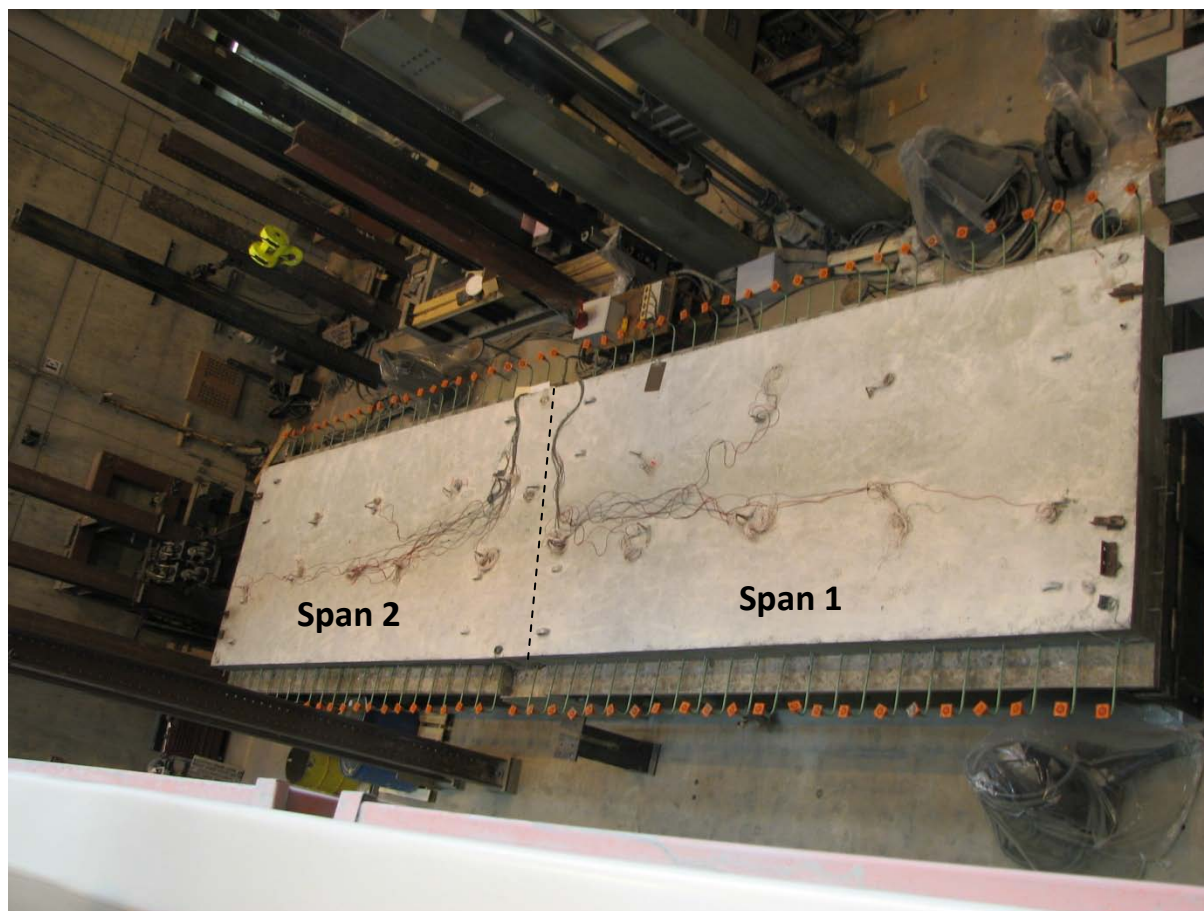
Figure 5.1.21: Photograph of the Concept 1 laboratory bridge shortly after completion of the continuity pour

The reinforcement ratios for each span were not identical because of the reduction in the flange thickness in Span 1. The reinforcement ratio for transverse load transfer and crack control in Span 2 (which was similar to the Center City Bridge) was 0.0029 and 0.0147, respectively; whereas the reinforcement ratio for transverse load transfer and crack control in Span 1 was 0.0024 and 0.0110, respectively.

The center pier supporting the Concept 1 laboratory bridge was designed to replicate the piers present in the Center City Bridge (see Figure 4.6.1 for the bearing and pier detail in the Center City Bridge). The pier cap extended 42 in. in the direction corresponding to the longitudinal direction of the bridge, identified hereafter as the width of the pier. A 6 in. wide by 1/2 in. thick elastomeric bearing pad provided the primary bearing at the pier, with the bearing pad occupying the area between 4 and 10 in. from the ends of the precast beams. The remaining area between the pier cap and precast beams was filled with 1/2 in. polystyrene foam, which was selected to prevent the egress of CIP concrete during the closure pour, while also remaining relatively crushable to allow the elastomeric bearing pad to act as the primary means of bearing.

The supports at the free ends of the bridge were constructed with a 12 in. wide HSS tube section resting on a wide flange section. A 1/2 in. thick by 12 in. wide elastomeric bearing pad was provided between the HSS tube and precast inverted-T. The end support detail was selected to provide little rotational

105

restraint, and therefore simulate a roller connection. Lateral stability at the end supports was provided via bracing between the wide flange sections and the strong floor, as shown in Figure 5.1.22.
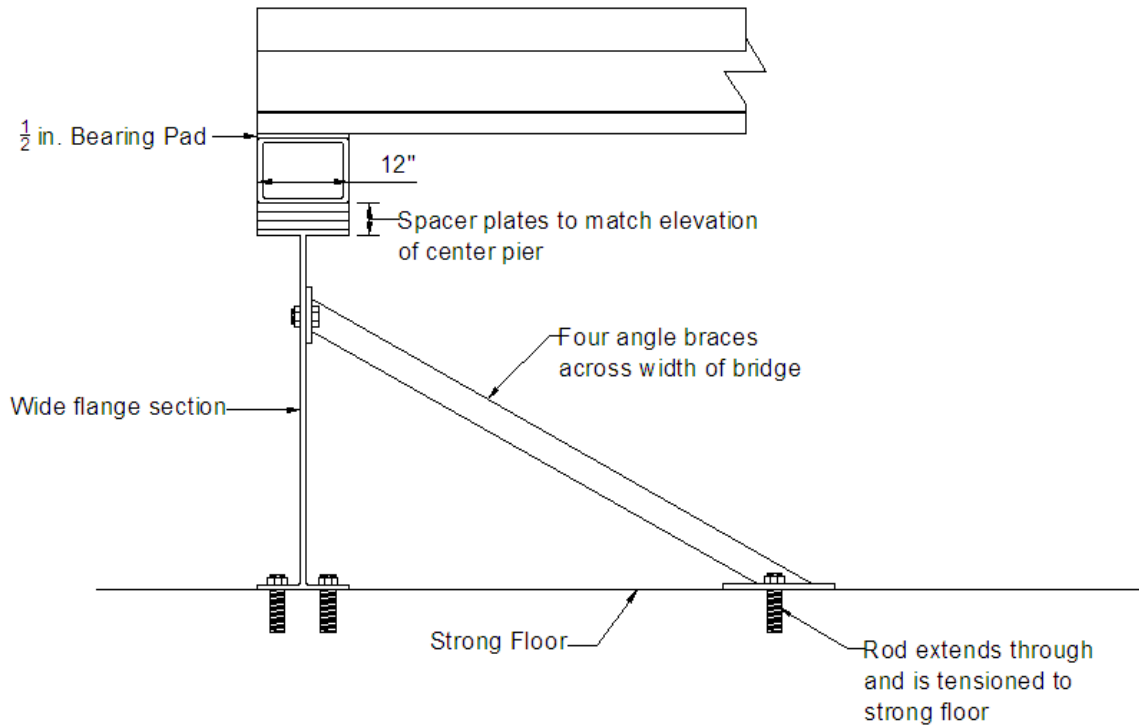
Figure 5.1.22: Support and bearing detail of the end supports of the laboratory bridge specimens

5.1.2. Concept 2 Laboratory Bridge

The Concept 2 laboratory bridge was developed to address issues that remained unanswered at the conclusion of the Concept 1 tests. A statically determinate simply-supported bridge specimen was selected to provide a direct means of determining the applied moment during testing. The symmetrical nature of the simply-supported structure enabled investigation of two unique design parameters in each half span of the bridge. Table 5.1.2 highlights the variations in parameters in the Concept 2 laboratory bridge relative to those of Span 1 of the Concept 1 laboratory bridge.

Both half spans of the Concept 2 laboratory bridge were constructed with No. 4 transverse bars spaced at 18 in. protruding from the precast sections. The west half span of the bridge was constructed using traditional hooked bars as defined by AASHTO (2010) Article 5.10.2.1. The east half span of the Concept 2 laboratory bridge was constructed with threaded transverse bars without a hook return or headed feature, as shown in Figure 5.1.23, extending approximately 22.5 in. from the face of the web, which left approximately 1.5 in. clear to the face of the adjacent precast web. The use of hooked threaded bars were deemed impractical due to the difficulty in ensuring the hooked portion of the bar would be oriented vertically upward when the threaded portion of the bar was fully tightened into the anchor; positional threaded inserts that could resolve this issue would be costly. Headed bars were considered as an alternative to hooked bars, but the clearance required around the head would require the transverse bars to be raised higher in the section to accommodate the required clearance of the head to the horizontal precast flange face. As a consequence, it was decided to use straight transverse bars

106

threaded into the anchors embedded in the precast sections. The development length of the straight bars was calculated to be 28.5 in. using ACI 318-08 Section 12.2.2, with an assumed concrete compressive strength of 4,000 psi and ψ_t=1.2, suggesting that approximately 80 percent of the yield strength of the straight bars would be developed over the distance between the free end of the bar and the vertical precast web.

The transverse reinforcement (both the hooked and straight bars) in the trough region provided the primary mechanism for transverse load transfer between adjacent precast panels. For this reason, it is imperative that the transverse reinforcement be continuous through the precast member. In the case of the mechanically anchored reinforcement, continuity was provided using straight bars embedded in the web region of each precast member, which were threaded half way into the mechanical anchor at the interior longitudinal precast joint, as shown in Figure 5.1.24; a vertical hook was maintained over the outside precast flange to assist with the location of the internal reinforcement during the study. When mechanical anchors are used in a real world application, the embedded continuous reinforcement could be connected to mechanical anchors at the vertical web faces on both sides of the precast member. Note that in Figure 5.1.24 the transverse reinforcement to be mechanically anchored across the joint region is not shown for clarity.

Table 5.1.2: Comparison of design parameters between Span 1 of Concept 1 and Concept 2 laboratory bridge specimen

Span 1 of Concept 1 Laboratory Bridge	Concept 2 Laboratory Bridge
No 6 transverse hooks spaced at 12 in.	No. 4 transverse bars spaced at 18 in.
No. 5 cage spaced at 12 in., in line with hooks	No. 3 cage spaced at 18 in., offset 9 in. from bars
2 1/2 in. clear from face of flange to bottom of transverse hook	1 in. clear from face of flange to bottom of transverse bar
All transverse bars embedded into web and terminated with a standard hook	East half span included threaded straight bars West half span included embedded hooked bars
No. 5 stirrups at 24 in. for horizontal shear reinforcement	No reinforcement for horizontal shear transfer
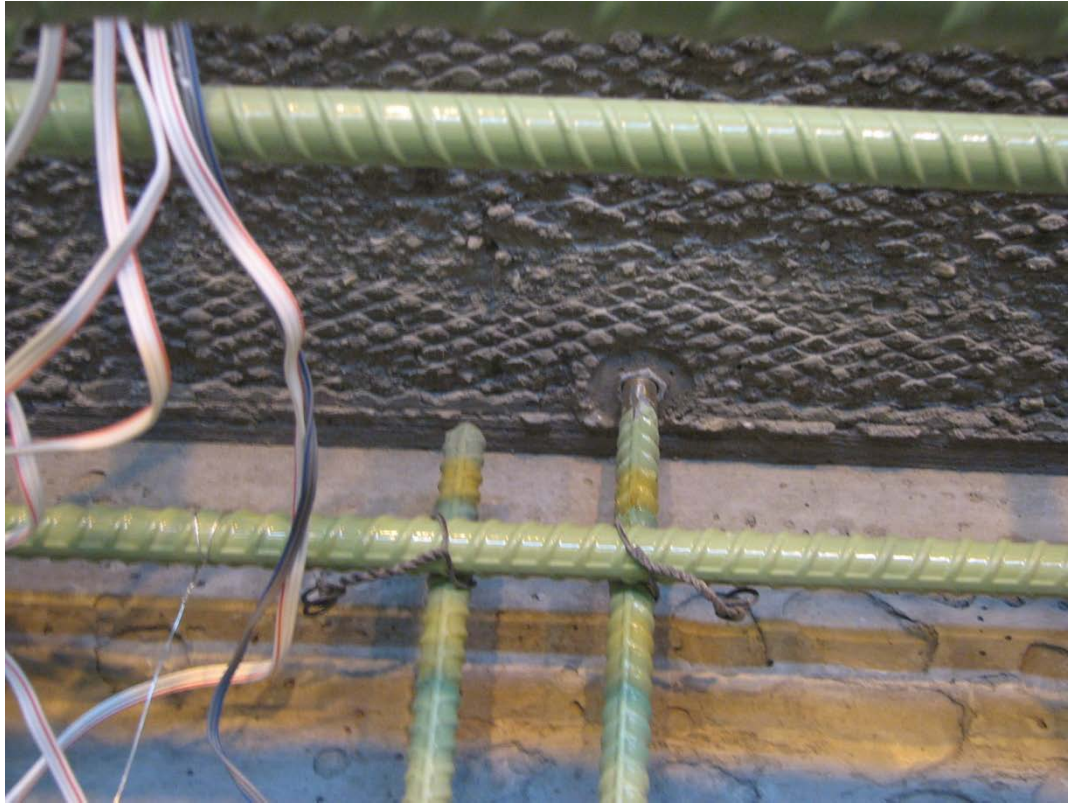
Figure 5.1.23: Threaded connection and adjacent termination detail of straight bars in east half span of the Concept 2 laboratory bridge specimen
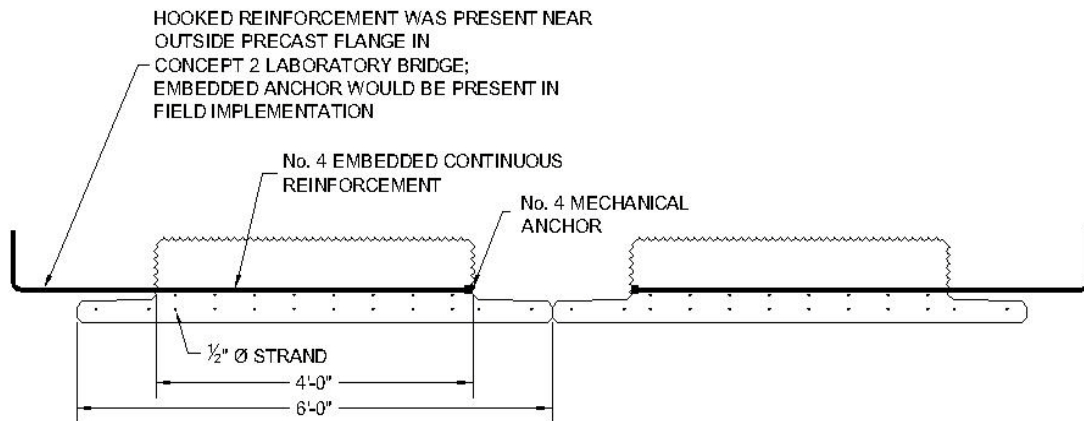
Figure 5.1.24: Conceptual section illustrating continuous nature of embedded reinforcement utilized in conjunction with mechanical anchors when threaded transverse reinforcement is present; figure shown represents configuration in east half span of the Concept 2 laboratory bridge specimen (transverse reinforcement in joint region to be mechanically anchored to reinforcement in precast web is not shown)

108

As for the Concept 1 specimen, a supplementary cage was used in the joint region to control potential reflective cracks that could originate over the longitudinal joint between the adjacent precast flanges. The reinforcement cage in the Concept 2 laboratory bridge was reduced in size to No. 3 stirrups and increased in spacing to 18 in. in comparison with that of the Concept 1 laboratory bridge. The cage reinforcement was offset from the protruding transverse bars by 9 in. to ensure that the maximum spacing of the transverse reinforcement across the joint did not exceed 9 in. The reinforcement ratio of the transverse section for crack control was 0.0031. The specimen was intended to provide a lower bound design based on the ACI (318-08) and AASHTO (2010) specifications for potential crack control reinforcement, specifically satisfying a spacing limit of 18 in. and a minimum reinforcement ratio of 0.0018. The reinforcement ratio of the section for transverse load transfer was 0.0007. The reinforcement ratios for both the Concept 1 and Concept 2 laboratory bridges are summarized in Table 5.1.3.

Table 5.1.3: Transverse load transfer and crack control reinforcement ratios for the Concept 1 and Concept 2 large-scale laboratory bridge specimens

Specimen description	Reinforcement ratio for crack control	Reinforcement ratio for transverse load transfer
Concept 1, Span 1	0.0110	0.0024
Concept 1, Span 2	0.0147	0.0029
Concept 2	0.0031	0.0007

Another modification implemented in the Concept 2 laboratory bridge included the removal of all horizontal shear reinforcement, leaving only the roughened surface of the precast web to provide all necessary horizontal shear transfer. This modification was selected to address the required minimum horizontal shear reinforcement in the AASHTO (2010) LRFD specification, as the literature suggested that requirement was overly conservative (see review of work by Naito et al. (2006) in Section 2.3). Furthermore, the large horizontal interface between the top of the precast webs and the CIP deck provided a horizontal shear interface area that was considerably larger than is generally provided by traditional girder bridges, where the width of the top flange is relatively narrow. The sectional capacity of the Concept 2 laboratory bridge was calculated using the measured concrete compressive strength of 5,800 psi, which resulted in the determination of the largest expected internal compression and tension forces for the specimen, which were equal to approximately 2450 kips. Using the global force equilibrium method for calculating the horizontal shear demand, the total change in compression force was divided by the area over which that change occurs. Because the Concept 2 laboratory bridge was simply supported, the compression force was assumed to be a maximum of 2450 kips at midspan, and 0 kips at the center of bearing. The shear area was therefore calculated as the product of half of the center to center of bearing (256 in. / 2 = 128 in.) multiplied by the full width of the web in compression, or 10 ft.; the area over the longitudinal trough region was included in the width of the shear area, as this area was expected to provide horizontal shear resistance as effectively as the horizontal precast-CIP interface [Note that CIP was not placed over the exterior flanges, only in the trough region between the two adjacent precast sections.]. Using this method, the horizontal shear demand at the predicted ultimate capacity of the Concept 2 laboratory bridge was calculated to be approximately 160 psi. The cohesion factor for a horizontal shear interface that is clean and intentionally roughened provided in Article 5.8.4.3 of the AASHTO LRFD specification (2010) was 240 psi, suggesting that the largest

horizontal shear stress that was expected to be developed in the Concept 2 laboratory bridge was unlikely to result in loss of composite action.

A simplified plan view of the Concept 2 laboratory bridge specimen, including support locations and relevant dimensions is included in Figure 5.1.25; the transverse reinforcement near the longitudinal precast joint region is not shown for clarity. The Concept 2 laboratory bridge was designed with the same overall dimensions as a single span in the Concept 1 laboratory bridge. Therefore, the Concept 2 laboratory bridge was placed to the east of the center pier, with the west bearing being located on the concrete pier, and the east bearing located on the 12 in. HSS tube. Based on the work outlined in Section 4.5, no bursting reinforcement was necessary in the precast elements utilized in the Concept 2 specimen. The reinforcement present in each cross section (i.e., east, west, and midspan), as well as elevation and layout views documenting the location of reinforcement along the length of each beam is shown in Figures 5.1.26 through 5.1.32. A photograph of the Concept 2 laboratory bridge specimen is shown in Figure 5.1.33.
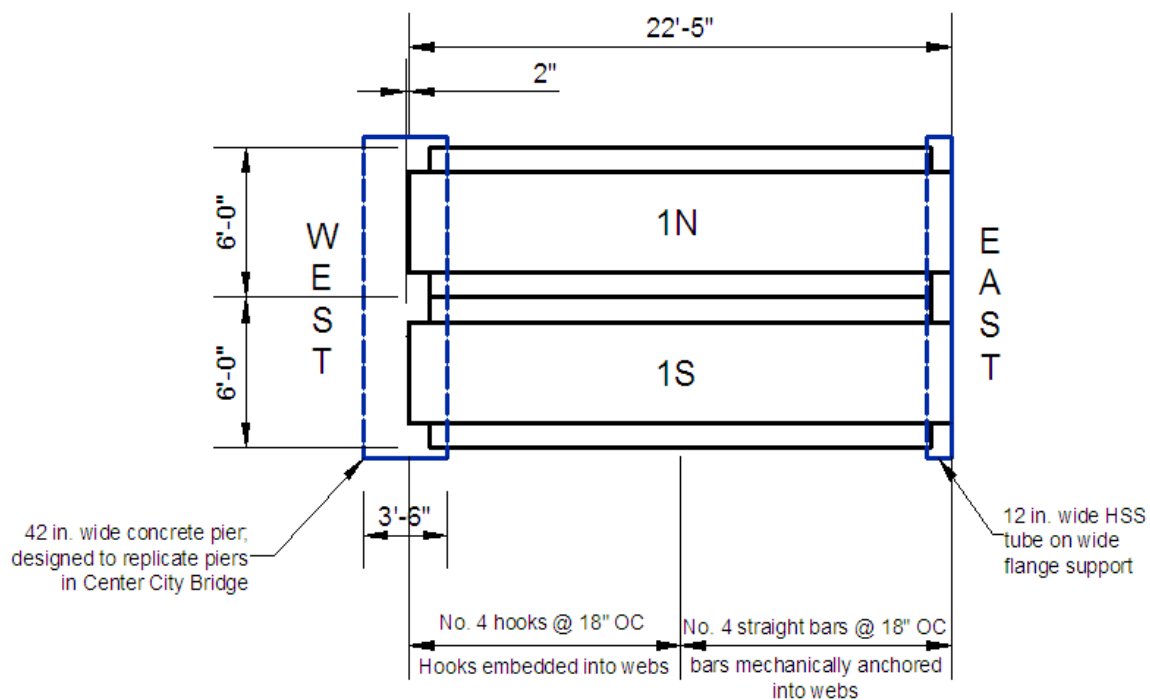
Figure 5.1.25: Plan view of the Concept 2 laboratory bridge specimen, including support locations and relevant dimensions. Transverse reinforcement near longitudinal precast joint is not included for clarity

110
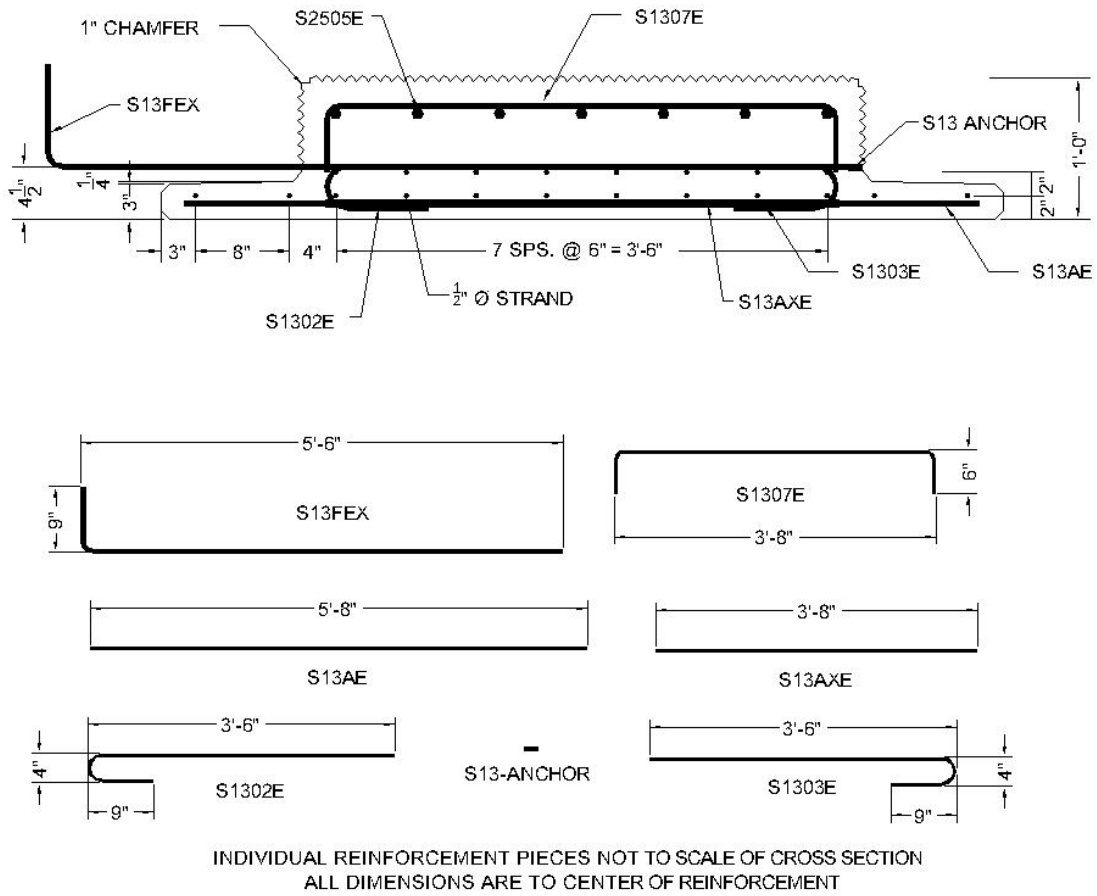
Figure 5.1.26: Cross section and individual reinforcement details for the east end of the precast beam 1N in the Concept 2 laboratory bridge specimen

111
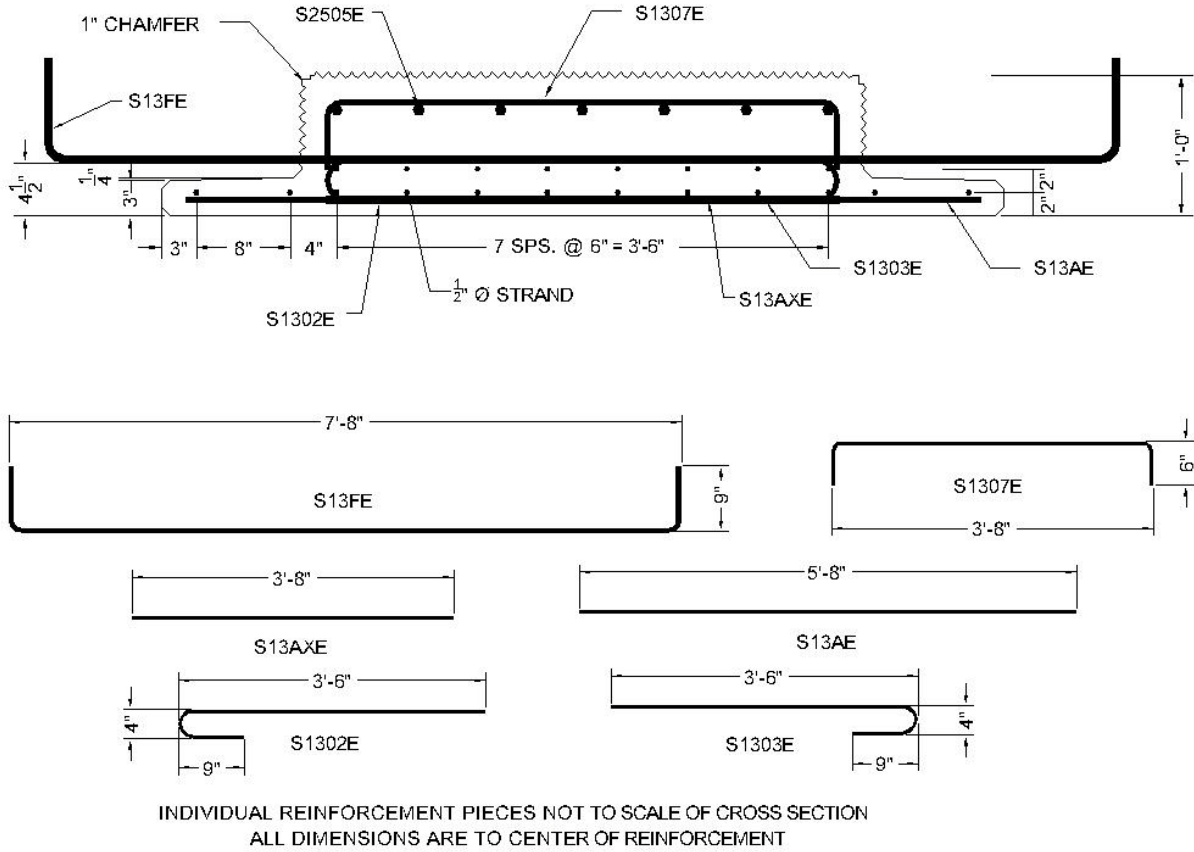
Figure 5.1.27: Cross section and individual reinforcement details for the west end of the precast beams 1N and 1S in the Concept 2 laboratory bridge specimen
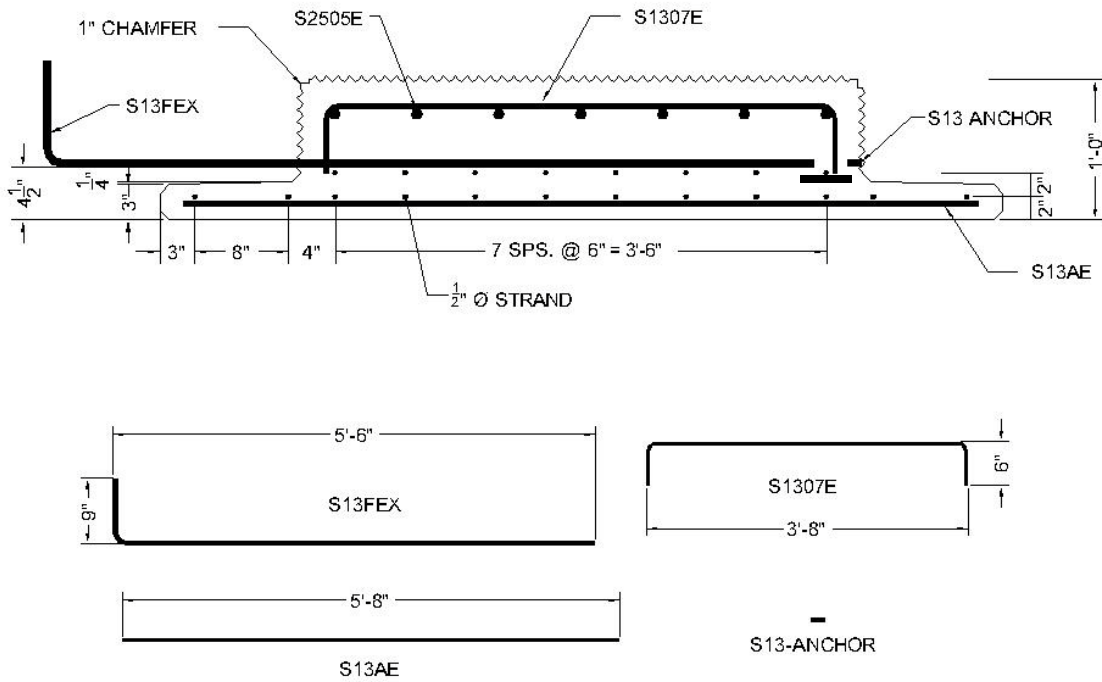
112

Figure 5.1.28: Cross section and individual reinforcement details at midspan of precast beam 1N in the Concept 2 laboratory bridge specimen

113

Figure 5.1.29: Elevation and plan views of the reinforcement layout for precast beam 1N in the Concept 2 laboratory bridge specimen

114
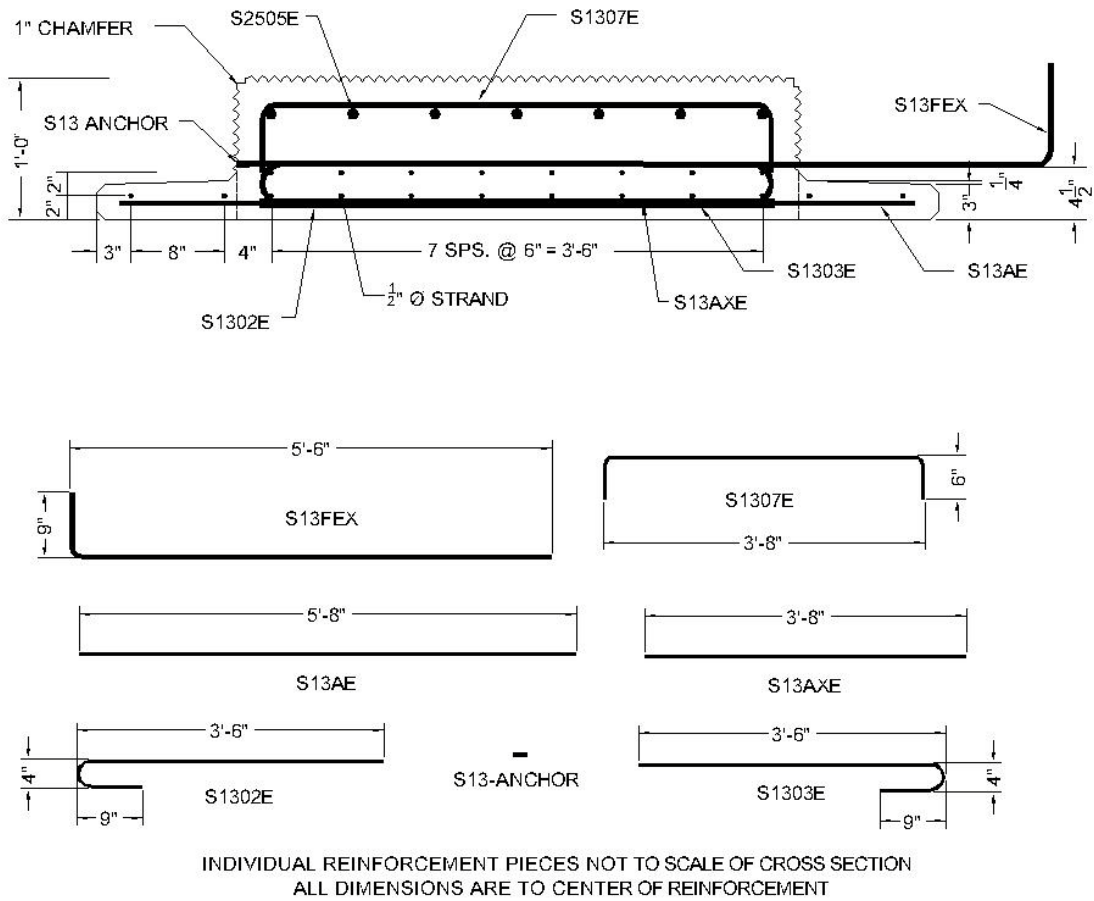
Figure 5.1.30: Cross section and individual reinforcement details for the east end of the precast beam 1S in the Concept 2 laboratory bridge specimen
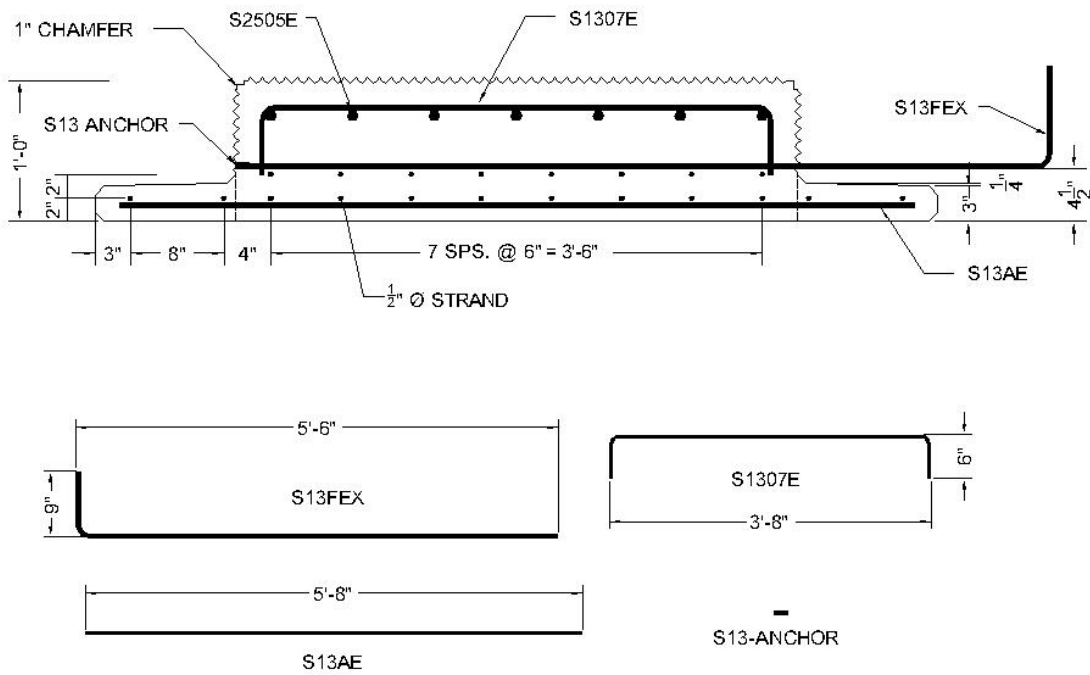
115

Figure 5.1.31: Cross section and individual reinforcement details at midspan of precast beam 1S in the Concept 2 laboratory bridge specimen

116
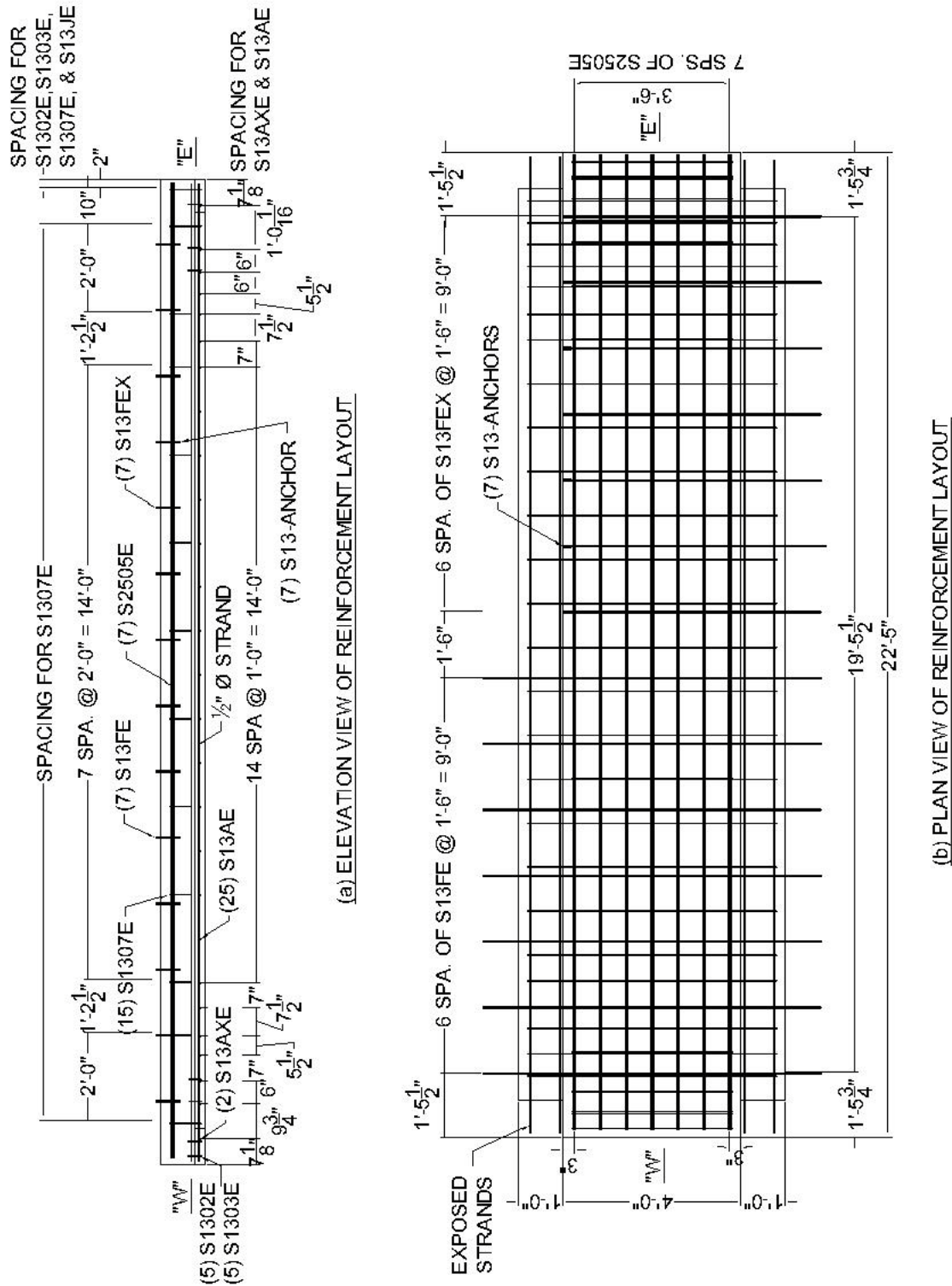
Figure 5.1.32: Elevation and plan views of the reinforcement layout for precast beam 1S in the Concept 2 laboratory bridge specimen

117

Figure 5.1.33: Photograph of the Concept 2 laboratory bridge specimen prior to placement of CIP concrete

The Concept 2 laboratory bridge specimen occupied the same space in the University of Minnesota Structures Laboratory as Span 2 of the Concept 1 laboratory bridge specimen. The west end of the Concept 2 laboratory bridge specimen was located a distance of 2 in. from the center of the concrete pier, with the east end of the specimen bearing completely on the 12 in. HSS tube/wide flange support. See Figure 4.6.1 and 5igure 5.1.22 for details on the concrete and steel supports, respectively.

5.1.3. Instrumentation of Concept 1 and Concept 2 Laboratory Bridge Specimens

The instrumentation schemes used in the Concept 1 and Concept 2 laboratory bridge specimens facilitated the monitoring of the transverse behavior and health of the joint region between precast panels. In addition, vertical sets of longitudinally oriented instrumentation were provided as a means of calculating the longitudinal curvature during load transfer and ultimate tests. The primary instrumentation type was concrete embedment resistive strain gages due to their relatively inexpensive cost, which allowed for an adequately dense instrumentation field. A small number of longitudinally oriented concrete embedment VW strain gages were also used to allow for the measurement of prestress losses, as well as to provide an estimate of the absolute levels of strain in the section without the effects of gage drift. Transversely oriented concrete embedment VW and spot-weldable VW strain gages were also included to provide an estimate of the strain due to transverse shrinkage near the precast joint, as well as to provide an estimate of the absolute levels of transverse strain throughout the laboratory tests.

118

The instrumentation layout for the Concept 1 laboratory bridge specimen is shown in Figure 5.1.34 (Smith et al. 2008). Each span had a set of transversely oriented instruments at each end, each quarter point, and at midspan. At each section, five transversely oriented concrete embedment resistive gages were located near the precast flange equally dispersed between adjacent precast webs. Some cross sections had an additional ten transversely oriented concrete embedment resistive gages located above the precast web corners. The presence of the gages above the precast web is indicated by the longer transverse line extending over the webs in Figure 5.1.34. A representative cross-sectional view of the fully instrumented section is shown in Figure 5.1.35; the aspect ratio of the instrumentation has been modified for clarity. In addition, adjacent transverse gages overlapped (not shown in figure) to provide redundancy and a means to better refine the determination of crack locations by investigating whether a crack may have intersected a single gage or two adjacent gages. The nominal and measured gage locations in the Concept 1 laboratory bridge are given in Appendix E.
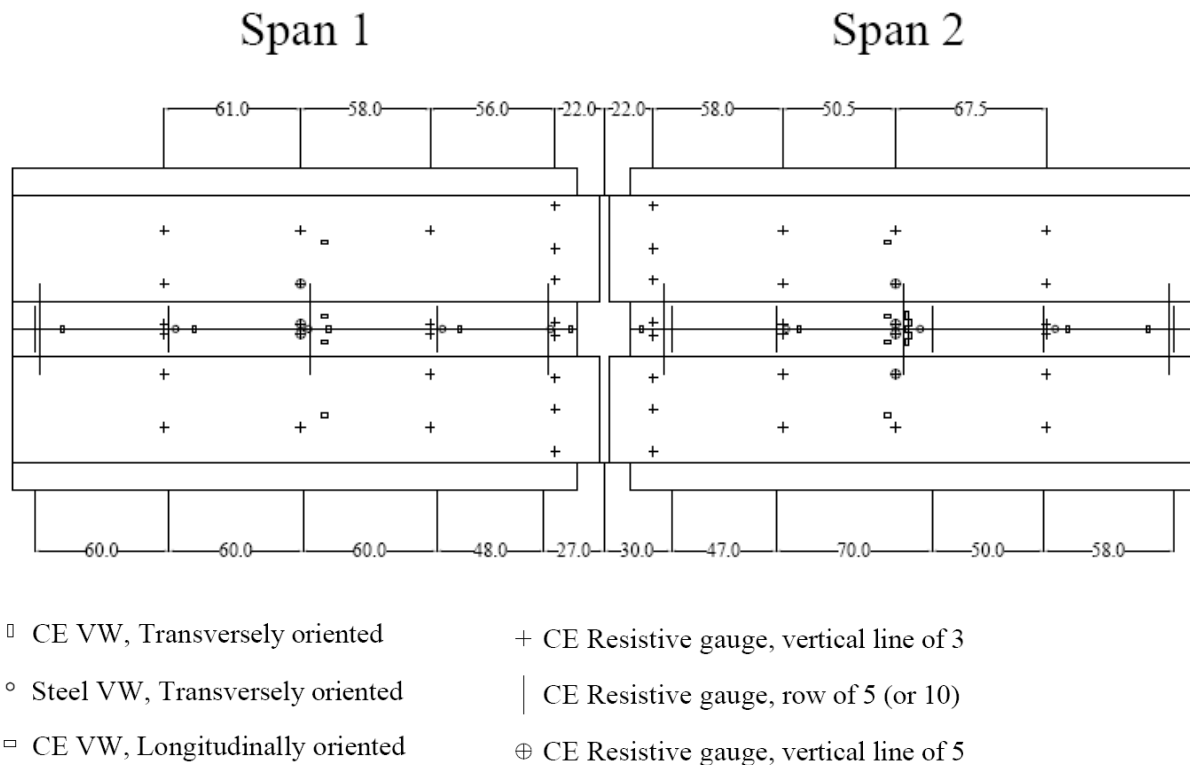
Figure 5.1.34: Instrumentation layout for Concept 1 laboratory bridge specimen (Smith et al. 2008)

119
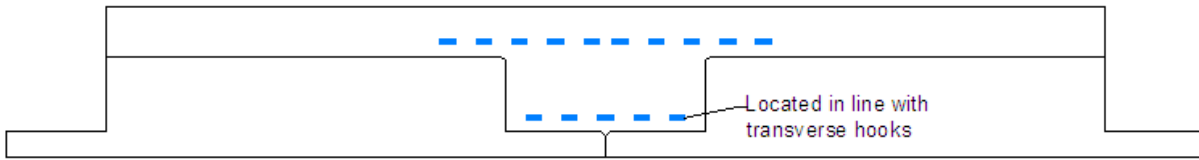
15 GAGE TRANSVERSE LAYOUT

Figure 5.1.35: Typical instrumentation layout near precast joint in the Concept 1 laboratory bridge specimen

The instrumentation layout developed for the Concept 2 laboratory bridge closely followed the original instrumentation plan for the Concept 1 laboratory bridge. Additional transversely oriented instruments were added at the eighth points to allow for increased refinement in detection of the extent of longitudinal reflective cracking. Similarly, an additional layer of transversely oriented concrete embedment strain gages was added through the depth of the cross section to improve the accuracy of the measurement of the depth of the crack in the section. The number of gages across the width of the joint region was reduced in response to the localized behavior of the crack observed in the Concept 1 laboratory bridge near the precast joint. Furthermore, fewer vertical sets of instruments were selected for longitudinal instrumentation, while five gages were included in each vertical set to improve the accuracy of the curvature calculation, especially in the case of faulty or broken instrumentation due to construction. The instrumentation layout for the Concept 2 laboratory bridge and the standard cross sections are shown in Figure 5.1.36 and Figure 5.1.37, respectively. The nominal and measured gage locations for the Concept 2 laboratory bridge are given in Appendix F.

The origin and positive x and y ordinate directions for the placement of the instrumentation for the Concept 1 and Concept 2 laboratory bridges is shown in Figure 5.1.38. The origin was located at the center of the concrete pier for both bridges. The positive x ordinate was directed towards the east wall of the lab, with the positive y ordinate towards the north. The vertical ordinate, z, was measured from the bottom of the precast sections.

120
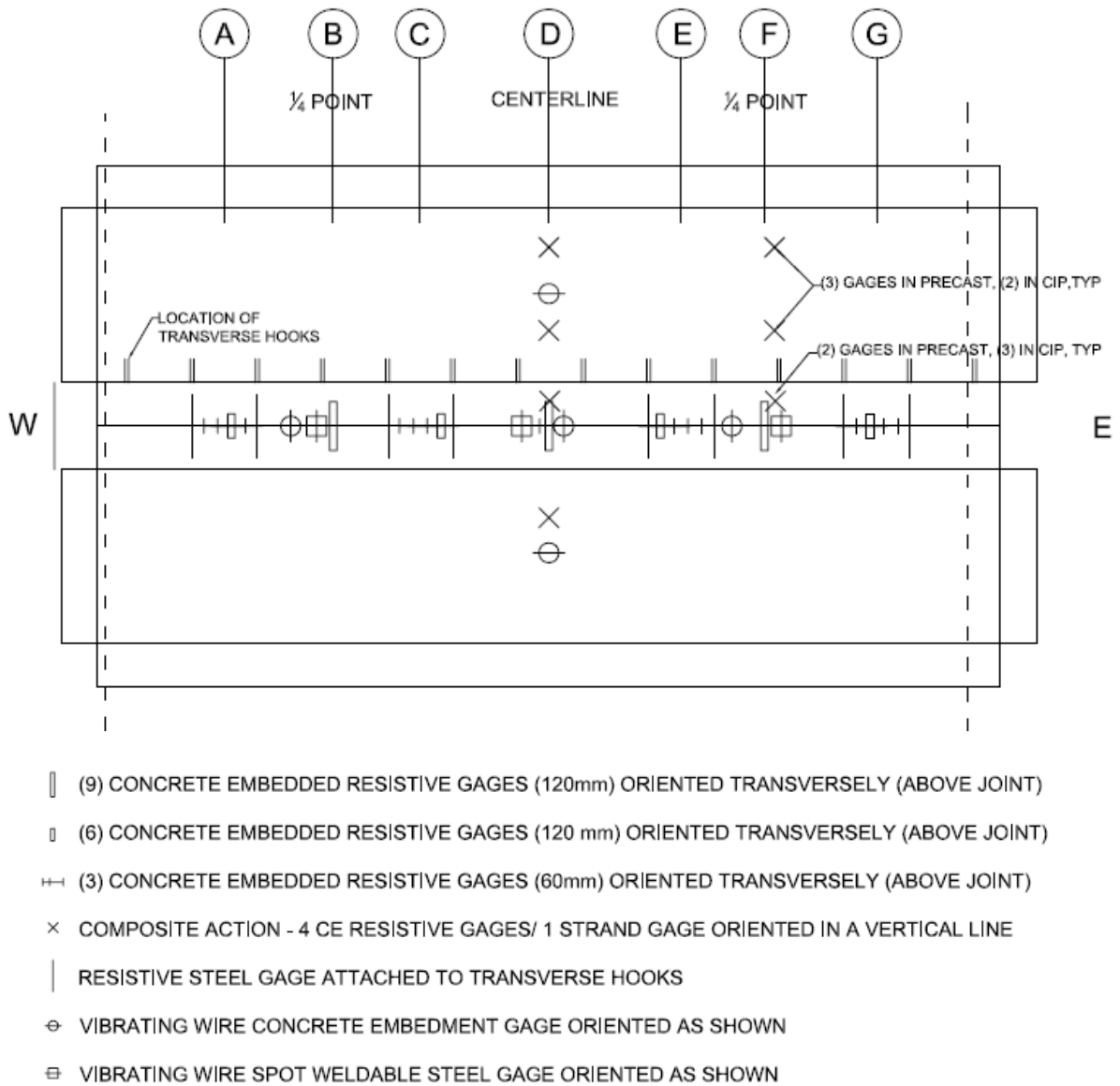
Figure 5.1.36: Instrumentation layout for the Concept 2 laboratory bridge specimen

121
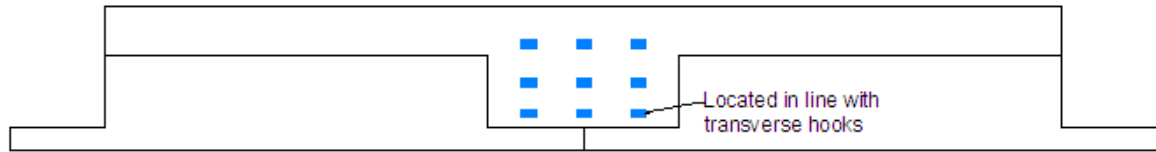
9 GAGE TRANSVERSE LAYOUT
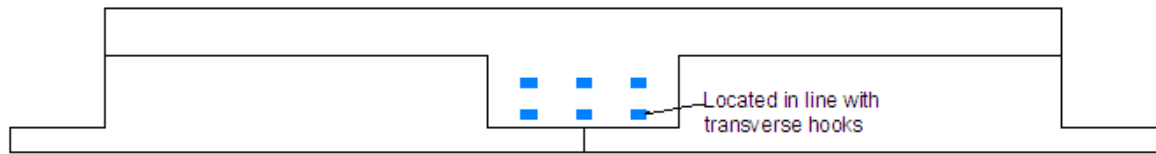
6 GAGE TRANSVERSE LAYOUT

Figure 5.1.37: Typical 9 and 6 gage transverse instrumentation layout in Concept 2 laboratory bridge specimen
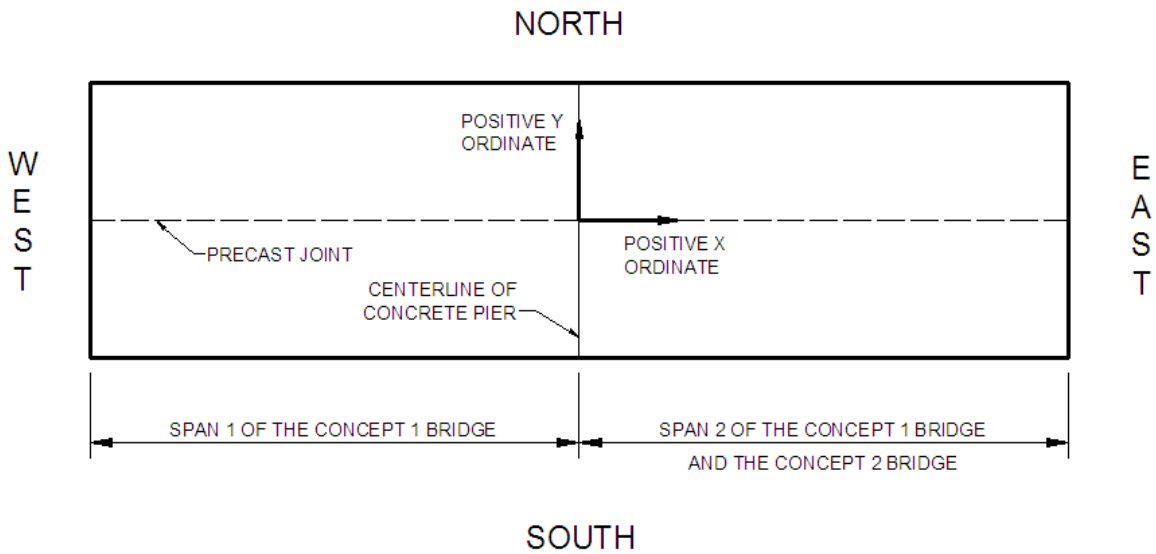
Figure 5.1.38: Location of origin and definition of positive x and y ordinates for instrumentation layout in the Concept 1 and Concept 2 laboratory bridge specimen

122

5.2. Construction of Laboratory Bridge Specimens and Material Properties

Fabrication of the precast panels for both bridges was completed at County Materials in Roberts, Wisconsin. The CIP concrete selected for the project was a standard Mn/DOT bridge design mix, designated as 3Y33H68, with a nominal compressive strength of 4,000 psi at 28 days. Due to the interest in the effects of restraint moment on the system, the CIP concrete was placed on the Concept 1 laboratory bridge when the precast panels were at a young age of 7 days. Material testing was completed on the Concept 1 laboratory bridge to determine measured concrete compressive strengths, tensile strengths, and elastic modulus, and was tabulated by Smith et al. (2008), which is summarized in Table 5.2.1 and Table 5.2.2 for the CIP and precast concrete, respectively.

A more relaxed construction schedule was sufficient for the Concept 2 laboratory bridge because of the simply-supported design. The CIP concrete for the Concept 2 laboratory bridge was poured when the precast panels had reached an age of 83 days. The concrete 28-day CIP concrete compressive strength was measured to be 5750 psi, measured according to ASTM C36 *Test Method for Compressive Strength of Cylindrical Concrete Specimens* (ASTM C36, 2009). The CIP concrete tensile strength was measured to be 640 psi at an age of 28 days, measured according to ASTM C78 *Standard Test Method for Flexural Strength of Concrete (Using Simple Beam with Third-Point Loading)* (ASTM C78, 2009). The elastic modulus of the CIP concrete at an age of 28 days was measured to be 4,020 ksi, which was measured in accordance with ASTM C469 *Standard Test Method for Static Modulus of Elasticity and Poisson's ratio of Concrete in Compression* (ASTM C469, 2002). The measured material properties are summarized in Table 5.2.1 and Table 5.2.2 for the CIP and precast concrete, respectively.

Table 5.2.1: Measured CIP material properties at an age of 28 days

Specimen Description	Compressive Strength, f_c'	Modulus of Rupture, f_r	Elastic Modulus, E
Concept 1, Span 1	4160 psi	411 psi	3540 ksi
Concept 2, Span 2	4590 psi	457 psi	3780 ksi
Concept 2	5750 psi	640 psi	4020 ksi

Table 5.2.2: Measured precast concrete material properties for the Concept 1 and Concept 2 bridges

Specimen Description	Compressive Strength, f_c'	Modulus of Rupture, f_r	Elastic Modulus, E
Concept 1, both spans	12,900 psi	927 psi	6160 ksi
Concept 2	12,150 psi	783 psi	6029 ksi

The surfaces of the precast panels were not pre-wetted prior to the placement of the CIP concrete for either of the bridge specimens. No deleterious behavior appeared to result in casting the CIP on non-wetted precast surfaces; however, it is recommended in future applications of constructing PCSSS bridges in the field, that the precast surfaces be pre-wetted prior to casting the CIP. Both specimens were moist-cured for 8 days based on the ACI 308.1-98 *Standard Specification for Curing Concrete*.

The yield strength of the No. 4 hooked bars that provided transverse reinforcement continuity and crack control reinforcement above the longitudinal joint between the precast panels in the Concept 2 laboratory bridge specimen was found to be approximately 70 ksi through the testing of three representative samples.

5.3. Laboratory Testing Program and Results

An extensive laboratory testing program was developed for each specimen. The requirements for the testing plan included simulated fatigue loading, reproducing levels of strain in the precast joint region as observed in the Center City Bridge, as well as the introduction of reflective cracking, monitoring load transfer between precast panels in common spans, and loading to the ultimate capacity of the bridge specimens or the maximum capacity of the load frame. Because the tests used on the Concept 1 and Concept 2 laboratory bridges were similar, the testing plans and results of the laboratory tests are discussed below based on the controlling behavior, rather than by laboratory specimen. The results of the tests presented herein were all associated with the NCHRP 10-71 study. The previous tests conducted on the Concept 1 laboratory bridge specimen as part of a Mn/DOT study are summarized in Smith et al. (2008).

5.3.1. Simulated Traffic Loading

Good fatigue performance of any highway structure is essential to ensure stable behavior over extended periods of time. Traffic loading was simulated on the Concept 1 and 2 bridge specimens using a representative patch load of dimensions 10 by 20 in. oriented with the long direction perpendicular to the joint. Two million cycles of fatigue loading were completed on each span of the laboratory bridge specimens. The loading was placed at midspan of both spans of the Concept 1 laboratory bridge. The complete two million cycles of fatigue loading were completed on Span 2 prior to the implementation of fatigue loading on Span 1, while equal patch loads were cycled at the quarter points of the Concept 2 laboratory bridge using a spreader beam. The nominal patch load used for all fatigue loading was 35 kips (i.e., Concept 1 laboratory bridge: 35 kips was applied to midspan; Concept 2 laboratory bridge: 35 kips was applied to each quarter point simultaneously); the development of the magnitude of the laboratory patch loading was discussed in Section 4.7.

The magnitude of the patch load was developed to replicate the magnitude of transverse stress at the precast flange-CIP interface in the laboratory specimen as was expected in a 30-30-30 ft. three-span continuous bridge with twice the AASHTO (2010) tandem design load applied. A magnitude of twice the AAHSTO tandem load was selected to account for the possibility of two truck wheel loads being located directly above a longitudinal joint and situated immediately adjacent to one another. As discussed in Section 4.7, the stress developed near the precast flange at midspan of the Concept 1 laboratory bridge and at the quarter points of the Concept 2 laboratory bridge were nearly identical, which accounts for the equal patch loads used in both specimens. Also note that the maximum moment developed due to a single patch load at midspan was equal to the maximum moment developed due to two equal patch loads placed at the quarter points.

During the fatigue and all associated patch loading, the load was cycled between 2 and 35 kips. A minimum load of 2 kips was maintained during all tests to prevent the actuator from "walking" during cycling. Steel angles were also adhered to the surface of the deck to help constrain the movement of the actuators during testing. Load distributed to the quarter points of the Concept 2 laboratory bridge using the spreader beam was cycled between 4 and 70 kips.

124

As discussed in Section 3.2 reflective cracking was observed in two of the three instrumented joints in the Center City Bridge via transversely oriented concrete embedment VW strain gages located at midspan of the center span. Furthermore, cracking in the field bridge was observed to occur during the first spring after construction was completed, revealing the potential for reflective cracking to be present during the majority of the service life for the precast composite slab span system (PCSSS) bridge. In an effort to investigate the fatigue performance of the PCSSS both with and without the presence of reflective cracking, the fatigue study for each specimen was conducted in two parts. As mentioned above, the fatigue study for each span of the Concept 1 laboratory Bridge (Span 2 first, followed by Span 1) was conducted in series; followed by the tests of the Concept 2 laboratory bridge after completion of the Concept 1 laboratory bridge tests. The subsequent discussion of the fatigue testing is relevant to each span separately.

The first portion of fatigue loading consisted of the completion of one million cycles of fatigue loading on the virgin laboratory specimens, with no reflective cracking observed prior to the initiation of fatigue loading. At the conclusion of each 100,000 cycles, fatigue loading was suspended to allow for a quasi-static 35 kip patch load to be applied to the section at the same location as the fatigue patch load (i.e., Concept 1 laboratory bridge: 35 kips was applied to midspan; Concept 2 laboratory bridge: 35 kips was applied to each quarter point simultaneously).

During the quasi-static loading, data from the complete set of transversely oriented strain gages was collected. A minimum of three quasi-static cycles were completed during this process to provide redundancy. This process provided a sample of the condition of the longitudinal joint in 100,000 cycle increments.

At the completion of the first million cycles of loading, a longitudinal reflective crack was introduced near the precast joint by increasing the applied loads until target strain values were reached to replicate the levels of transverse strain measured via concrete embedment VW strain gages located near the precast flange in the Center City Bridge. The target transverse strain value of 160 µε was selected to represent the maximum daily change in strain observed in Joint 1 during the first summer after construction. The target strain value of 160 µε is hereafter referred to as part of the environmental effect simulation, which is discussed in further detail in Section 5.3.2.

During the initiation of the reflective crack in the laboratory study, mechanical loading was applied to the same 10 by 20 in. patch dimension utilized during the fatigue study while the transverse strains measured via the concrete embedment resistive strain gages located nearest the precast flanges were monitored in real time, until a change in strain of approximately 160 µε was observed, which was also generally associated with observed nonlinearity in the strain measurements, suggesting that a crack was generated. For Span 2 of the Concept 1 laboratory bridge, the crack was initiated at midspan (i.e., same location as during fatigue tests). In Span 1 of the Concept 1 laboratory bridge and the Concept 2 laboratory bridge, the crack was first initiated at the same longitudinal location as the fatigue tests (i.e., midspan of Span 1 and at the quarter points of the Concept 2 laboratory bridge, though cracking at the west quarter of the Concept 2 laboratory bridge was not clearly observed, which is discussed in Section 5.3.2. For these two spans, the crack was extended longitudinally using a 10 ft. long spreader beam, as it was expected that the uniform nature of a thermal gradient induced in a field bridge would tend to extend the crack along the length of the span. Bearing plates were placed a distance of 2.5 and 5 ft. to either side of midspan (corresponding with an effective 5 and 10 ft. spreader length). The locations of the applied patch loads for fatigue loading and locations of the patch loads used to extend the length of the reflective crack, where applicable, are shown in Figures 5.3.1 and 5.3.2 for the Concept 1 and Concept 2 laboratory bridge specimens, respectively.

125
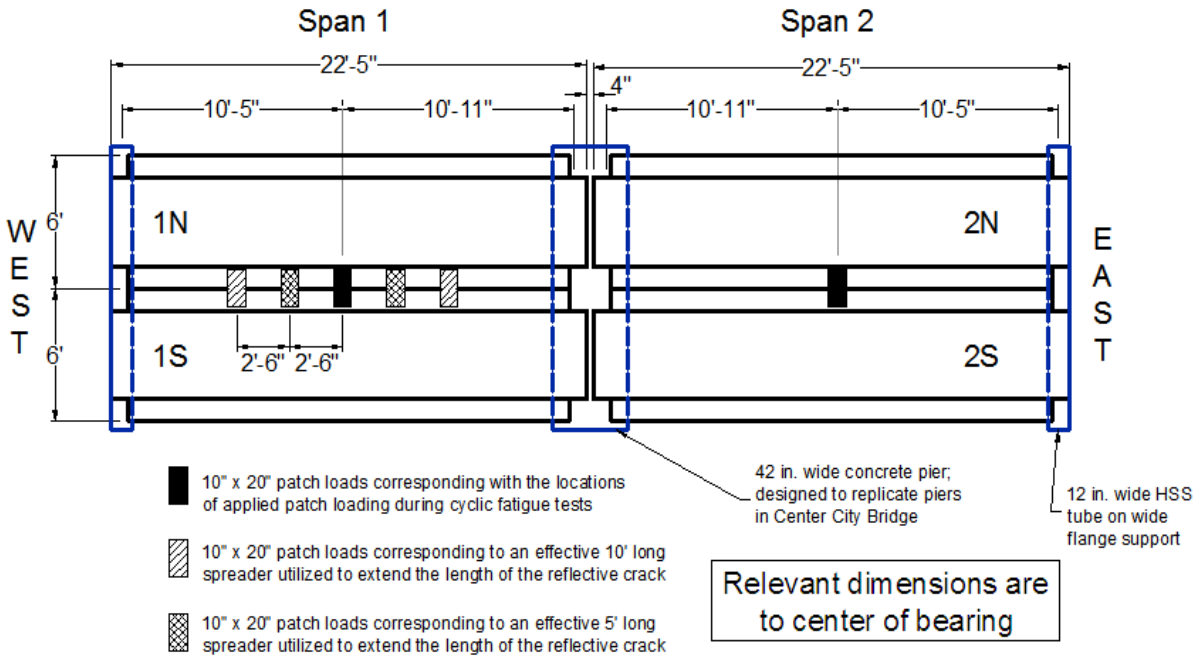
Figure 5.3.1: Placement of patch loads during fatigue loading and extension of longitudinal reflective cracking (applicable in Span 1 only) for the Concept 1 laboratory bridge specimen
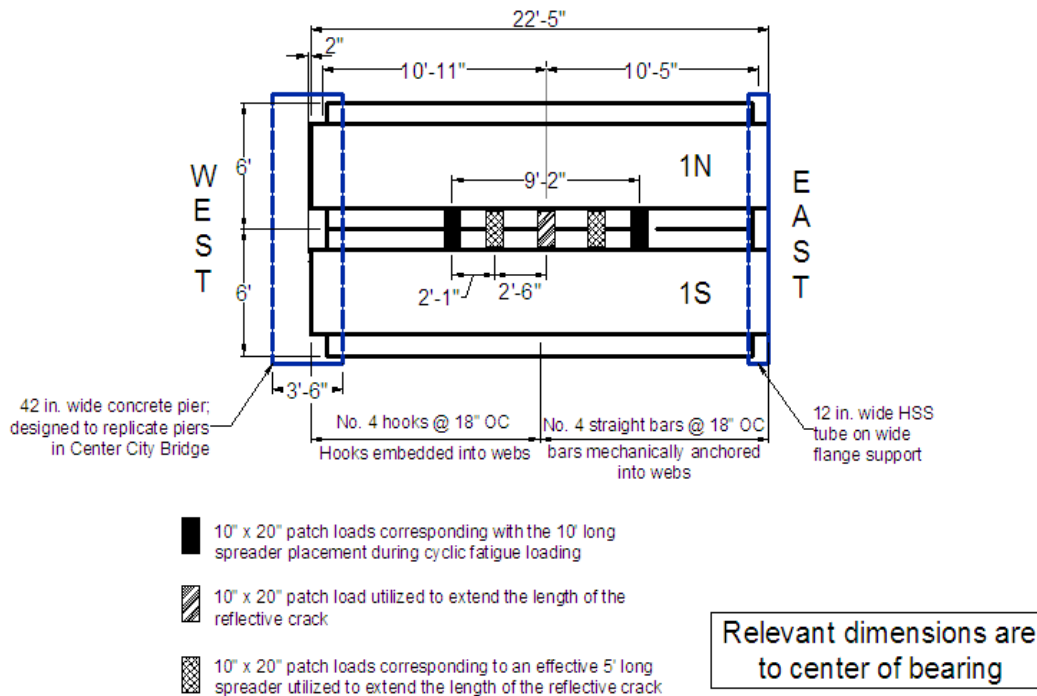
Figure 5.3.2: Placement of patch loads during fatigue loading and extension of longitudinal reflective cracking for the Concept 2 laboratory bridge specimen

126

The vertical location of the transversely oriented concrete embedment resistive strain gages varied between each span of the Concept 1 laboratory bridge and the Concept 2 laboratory bridge due to the variations in the thickness of the precast flange and the vertical depth of the transverse reinforcement traversing the longitudinal precast joint. The measured vertical locations of the bottommost layers of transversely oriented strain gages that were monitored during initiation of cracking in the laboratory bridge specimens, as well as the relative instrumentation in the Center City Bridge, are given in Table 5.3.1. Because of the variations in the depths of the instrumentation, the transverse strain observed in the Center City Bridge was not simulated exactly in the laboratory specimens. The target strain was not modified for each span based on the relative depth of the instrumentation because a relatively consistent magnitude of strain was desired to be induced in the transverse reinforcement (which was vertically collocated with the instrumentation).

The transverse strains measured during the introduction of reflective cracking in each span are shown in Table 5.3.2, along with the total applied load required to achieve each level of strain. The transverse strains reported here were the largest strains measured at the cross sections associated with fatigue loading (i.e., midspan for Concept 1 laboratory bridge, and quarter points for the Concept 2 laboratory bridge). When cracking was completed using the spreader load, the applied load shown in Table 5.3.2 represents the total load applied to the spreader. The distribution of load to symmetrically placed patch loads was measured via load cells and was found to be approximately equal.

Table 5.3.1: Measured vertical locations of transversely oriented strain gages that were utilized in the observation of reflective cracking in the Center City Bridge and laboratory bridge specimens

Specimen Description	Type of Instrumentation	Vertical depth of instrumentation, measured from the bottom of precast section
Center City Field Bridge	Concrete embedment VW strain gage	8.25 in.
Concept 1, Span 1 laboratory bridge	Concrete embedment resistive strain gages	6 in.
Concept 1, Span 2 laboratory bridge	Concrete embedment resistive strain gages	7.25 in.
Concept 2 laboratory bridge	Concrete embedment resistive strain gages	4 in.

Table 5.3.2: Measured transverse strains during introduction of reflective cracking after the completion of one million fatigue cycles in each specimen

Specimen Description	Load applied to patch or spreader	Measured transverse strain	Associated applied load
Concept 1, Span 1	Patch load	161 με	89 kip
Concept 1, Span 2	Patch load	200 με	95 kip
Concept 2, east quarter point (straight bars)	Spreader load	150 με	210 kip
Concept 2, west quarter point (hooked bars)	Spreader load	85με	210 kip

The largest strain that was developed in the west quarter point of the Concept 2 laboratory bridge was 85 με, when a total load of 210 kips was applied to a spreader beam and a transverse strain of 150 με was measured at the east quarter point.

A second million cycles of fatigue loading were subsequently completed on each specimen after reflective cracking was introduced in each section. As before, cyclic loading was suspended every 100,000 cycles to investigate the condition of the longitudinal precast joint via the measurement of the transversely oriented strain gage data during application of a quasi-static 35 kip patch load.

The behavior of the large-scale bridge specimens subjected to the fatigue loading is summarized in Table 5.3.3, which illustrates the change in strain measured under the quasi-static 35 kip patch load at relevant points during the two million cycles of loading. The first column of the table identifies the specimen designation. For the Concept 2 specimen, fatigue loading was completed at the quarter points using a spreader beam; in addition, a 35 kip quasi-static load was applied at midspan to investigate the performance of the joint at that location, and is included in the table. The initial strain was the strain measured prior to the fatigue tests (at zero cycles). Because little variation in the transverse strain was observed during the first and second million cycles, only the end points of these loading periods are shown.

The transverse instrumentation used to ascertain the results in Table 5.3.3 was determined after the introduction of cracking at one million cycles. During and after cracking, only one or two transversely oriented concrete embedment resistive strain gages located at the loaded cross section recorded a crack with a significant permanent strain increase, suggesting that, at those cross sections, the crack traversed those gages. For all cases, this instrumentation was located in the lowest level of gages, near the precast flanges, and was coincident with the location of loading (i.e., at midspan if loading was applied at midspan or at the quarter points when loading was applied there). Figure 5.3.3 illustrates the gages that were used to create Table 5.3.3 for each specimen. Note that for the Concept 1 specimen, gage number 3 corresponded to the gage centered over the precast joint; whereas, in the Concept 2 specimen, gage number 2 corresponded to the gage centered over the precast joint.

Table 5.3.3[1]: Change in transverse strain measured at 35 kips throughout the course of 2M cycles of fatigue loading in each span of Concept 1 and Concept 2 laboratory specimens

Specimen	Initial Strain (με)	Change from initial strain (με)[2]		
		Before Cracking	After Cracking	After 2M Cycles
Concept 1, Span 1	18	0	24	25
Concept 1, Span 2	23	1	26	24
Concept 2, Midspan	33	-2	9	9
Concept 2, East Quarter span (straight bars)	33	-1	32	30
Concept 2, West Quarter span (hooked bars)	30	-3	5	6

[1]The instrumentation used to measure the values in this table is illustrated in Figure 5.3.3
[2]The initial strain was measured at zero cycles. The data taken to represent the before cracking state was recorded immediately after the completion of one million cycles. The data representing the after cracking state was recorded immediately after cracking with no cycling completed between.

(a) Concept 1 Span 1; patch load at midspan

(b) Concept 1 Span 2; patch load at midspan

(c) Concept 2; patch load at midspan

(d) Concept 2; patch load at west quarter point

(e) Concept 2; patch load at east quarter point
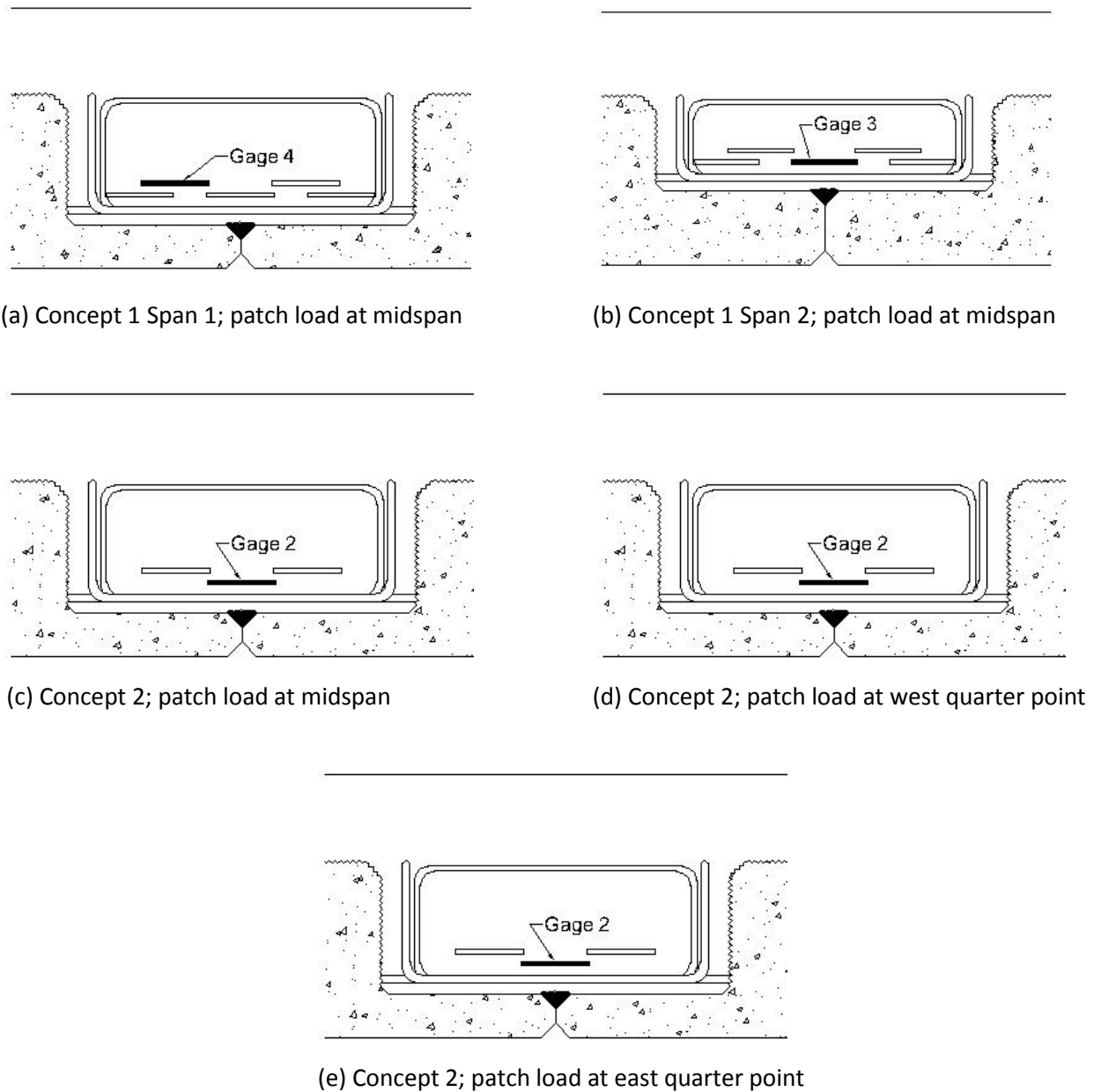
Figure 5.3.3: Transversely oriented concrete embedment resistive gages located nearest the precast flange[1]. Instrumentation locations which detected reflective cracking and were used for measurement of transverse strain values during fatigue loading are highlighted in black and annotated

[1]The instrumentation is shown in two layers to illustrate the overlap between gages, however the gages were nominally located in the same vertical layer and at the same depth as the horizontal legs of the embedded transverse reinforcement. Extent of overlap between gages is shown to scale

Good fatigue behavior was observed for both the Concept 1 and Concept 2 laboratory bridge specimens. No significant degradation of the joint was observed. The transverse strains remained stable throughout the two million cycles of load regardless of the presence of the longitudinal reflective crack that was imposed near the precast joint. The performance of each specimen during the second million cycles of fatigue loading can be inferred from Table 5.3.3 by subtracting the measured strain values in the two rightmost columns. The largest increase in the strain measured during the second million cycles of loading was observed to be 2 με in both Span 2 of the Concept 1 laboratory bridge and the east quarter of the Concept 2 laboratory bridge. Because the resistive gages were considered accurate to approximately +/- 6με, this small increase in strain was considered negligible. Furthermore, the increase in the transverse strain due to the introduction of the longitudinal reflective crack (calculated by subtracting the after cracking strain value from the before cracking strain value in Table 5.3.3) varied slightly depending on the specimen. The increase in strain in Span 1 and 2 of the Concept 1 laboratory bridge was 24με and 25με, respectively, while the increase under the spreader load in the Concept 2 laboratory bridge was approximately 33με and 8με for the east and west quarters, respectively. The increase in strain due to cracking under the midspan patch load in the Concept 2 laboratory bridge was approximately 11με. The similar performance level attributed to the Concept 1 laboratory bridge and Concept 2 laboratory bridge in regards to reflective crack control under traffic loading suggested that the reinforcement details from either span were adequate for the design of PCSSS bridges.

5.3.2. Environmental Effect Simulation

As mentioned in Section 5.3.1, transverse strain measurements in the Center City Bridge suggested that a reflective crack initiated in the joint region during the first spring after construction. Of the three adjacent instrumented joints at midspan of the center span of the field bridge, the two outermost joints showed evidence of cracking. The transverse strains measured in the bridge immediately after construction in October 2005 until July 2009 are shown in Figure 3.2.7. The instruments directly over the joint and in the position immediately next to the joint (blue and red series, respectively) illustrated the presence of a reflective crack, initiating on April 25th, 2006. The ranges of strains observed during the summer of 2008 and summer of 2009 were approximately 150με and 220με respectively. The seasonal fluctuation of the strain measurements, in addition to the fact that the 35 kip patch load used for fatigue testing had induced a transverse strain of only approximately 40με in the laboratory bridge, further substantiated that the large strains observed in the transverse joints of the field bridge were likely due to environmental effects rather than due to traffic load.

The increase in transverse strains from the summer of 2008 to the summer of 2009 warranted the investigation of the degradation of the joint region under large strains. It was expected that the increase in strains was caused by one of three sources: (1) fatigue traffic loading on the cracked system caused the degradation of the joint, (2) the cyclic influence of the thermal gradient change between day and night caused the increase in transverse strain, or (3) a larger thermal gradient may have been experienced that caused the crack to extend. Therefore, as mentioned in Section 5.3.1, a crack was induced in the laboratory bridge at the conclusion of one million traffic fatigue cycles to allow for the investigation of traffic fatigue loading on the cracked system.

At the conclusion of the second million cycles of traffic fatigue loading, additional cyclic loading was applied to the laboratory bridge specimens at larger strain levels to simulate cyclic strains due to environmental effects observed in the Center City Bridge. The strain cycles simulated the large daily strain fluctuations observed in the field bridge that occurred during the seasons that experienced the largest effects of solar radiation. For each level of strain considered, a total of 15,000 cycles were applied. The 15,000 cycles were selected to simulate approximately 100 years of significant temperature

130

fluctuations, assuming that a total of 150 days a year were expected to induce considerable thermal gradients. Each of the three test spans were subjected to similar levels of transverse strains throughout the testing procedure. Two qualitative levels of transverse strain were considered during the environmental study, specified from here forward as environmental simulation strain level A, which corresponded to a target strain of approximately 180 µε, and environmental simulation strain level B, which corresponded to a target strain of approximately 300 µε. Target level A was selected based on the observed daily fluctuations in the transverse strain in Joints 1 and 3 of the Center City Bridge soon after reflective cracking was observed. Target level B was defined during the environmental simulation tests on Span 1 of the Concept 1 specimen; a strain of approximately 300 µε was measured in the transverse instrumentation near the precast joint when a total patch load of 210 kips, which was the maximum practically available load to the 210 kip actuators, was applied at midspan of Span 1. This magnitude of transverse strain was comparable to the daily transverse strain fluctuations observed in Joint 3 of the Center City Bridge during the summer of 2008.

At both levels of strain to simulate environmental effects, quasi-static and cyclic loading was applied. As with the initiation of reflective cracking in the specimens after the first million fatigue cycles, quasi-static loading was applied to each specimen, while the instrumentation designated in Figure 5.3.3 (same instrumentation that was utilized during the fatigue tests) was monitored in real time, until a change in strain approximately equal to the target levels was reached. The full range of transversely oriented instrumentation was also monitored during this process, however only the gages that had previously indicated cracking exhibited large increases in strain with load, suggesting that no new cracks developed during this process. Quasi-static loading was applied using a load controlled program, with load applied at a rate of approximately 6 kips per minute until a strain of 80 percent of the target strain was observed, at which point load was applied at a rate of 1 kip per minute. All quasi-static and cyclic loading associated with environmental simulation strain level A was completed prior to the initiation of quasi-static and cyclic loading to strain level B. A spreader beam was also employed in each of the spans to help increase the longitudinal extent of the reflective crack. Because the methodology utilized in the environmental effect simulation evolved during the tests, the specific spreader orientation for each span is discussed later in this section.

Cyclic loading during the environmental simulation was completed using a displacement-controlled test program, which effectively ensured that the level of strain induced near the precast joint during each cycle was approximately equal to the target strain level. Displacement limits were determined during the preceding quasi-static load-control tests at both target levels. The displacement limits were selected such that each cycle ranged from a maximum displacement which approximately induced the level of strain selected, while the minimum displacement was selected to ensure that a compressive force of no less than 2 kips was present at each patch load, which was primarily to keep the loading actuator from "walking" during testing. The magnitude of strain in the selected instrumentation (i.e., Figure 5.3.3) and the minimum load was monitored throughout each test. The displacement limits were modified in real time as necessary to maintain the desired values, though this process was seldom required.

The maximum levels of strain achieved in the joint region in each of the specimens throughout the environmental effect simulation are tabulated in Table 5.3.4. For both spans of the Concept 1 specimen, the cyclic loading to induce the target strain levels was applied at midspan through a single patch load, though both quasi-static patch and spreader loads were first utilized to induce and extend the longitudinal crack. For the Concept 2 laboratory bridge, the cyclic environmental loading to induce the target-level strains was applied using a spreader beam, with the patch loads placed at the quarter points of the span, though both quasi-static patch and spreader loads were utilized to induce and extend the crack prior to cyclic loading. The column designated by 'P/S' in Table 5.3.4 represents the use of a patch

131

load, spreader load, or both (in which case the order shown is that applied to the specimen) during the quasi-static cracking process. Generally, the use of the spreader test did not affect the strains measured at midspan, and vice-versa, which indicated that the effects of loading were relatively localized and did not affect the measurements 1/4 span away. The number of cycles completed at each load, if applicable, is represented in parentheses immediately following the respective strain level to which the sections were cycled. The column headers in Table 5.3.4 represent the target environmental simulation strain levels. Deviations from the measured strain and target strain at each level were generally due to limitations in the capacities of the loading actuators used during the study, as was observed for the Concept 2 specimen at the 300με target strain.

Table 5.3.4: Maximum transverse strains and number of cycles completed at given strain level during laboratory environmental effect simulation

Max. strain observed in joint regions and (number of cycles completed at that strain)	Prior to cracking at 1M cycles[1]	P/S[2]	Cracking at 1M Cycles	P/S[1]	Environmental simulation strain level A	P/S[1]	Environmental simulation strain level B	P/S[1]
Approximate target strain value			160 με		180 με		300 με	
Concept 1, Span 1	18με	P	161με	S,P	213με (15,000)	S,P	303με (15,000)	S,P
Concept 1, Span 2	23με	P	200με	P	183με (15,000)	S,P	233με (15,000)	S,P
Concept 2, east quarter	33με	S	150με	S,P	177με (15,000)	S,P	253με (15,000)	S,P
Concept 2, west quarter	30με	S	85με	S,P	81με (15,000)	S,P	104με (15,000)	S,P
Concept 2, midspan	33με	P	174με	S,P	176με (15,000)	S,P	256με (15,000)	S,P

[1]Measured strain was induced due to applied 35 kip patch load at midspan of the Concept 1 laboratory bridge spans, and at each quarter span, simultaneously, in the Concept 2 laboratory bridge
[2]Patch (P) or spreader (S) load orientation utilized to apply initial quasi-static cracking load, prior to cyclic loading

Span 2 of the Concept 1 laboratory bridge (which emulated the Center City Bridge section) was the first specimen to undergo loading to simulate environmental effects and as a result was subjected to the most unique loading procedure of all of the bridge specimens. Specifically, the use of a 110 kip capacity actuator initially limited the loading capabilities on the specimen. Also unique to the environmental simulation history on Span 2 of the Concept 1 laboratory bridge was that a preliminary load test was completed which induced a transverse strain of approximately 160με near the joint at which 200 cycles were completed. This process was completed to investigate the performance of the joint to the 160με level after the completion of the second million cycles of fatigue load. The specimen was subsequently cycled for an additional 15,000 cycles to the environmental simulation levels A and B each. The reflective crack introduced in the section after the completion of the first million cycles of fatigue load was developed using a quasi-static patch load at midspan, and was not extended with use of a spreader beam. Cracking induced in the section to correlate with the environmental simulation strain levels A and B was generated with the use of both spreader and patch loading. The reflective crack was extended to

132

the outer (i.e., east) quarter point of Span 2, however the crack was not observed to have extended to the instrumentation at the interior quarter point, which may have been attributed to transverse restraint provided by the proximity to the nearby interior support. Figure 5.3.4 illustrates the performance of Span 2 of the Concept 1 laboratory bridge during the environmental loading simulation. The diamond, square, and triangle data series represent strain measurements at midspan, the outer quarter point and the inner quarter point, respectively, with the data measured from the gages centered over the precast joint at each cross section. The vertical axis represents the magnitude of the transverse strain measured under a 35 kip patch load applied at midspan. The number of cycles completed, the strain that was induced in the section and the load required to induce that strain has been tabulated for Span 2 of the Concept 1 laboratory bridge in Table 5.3.5.
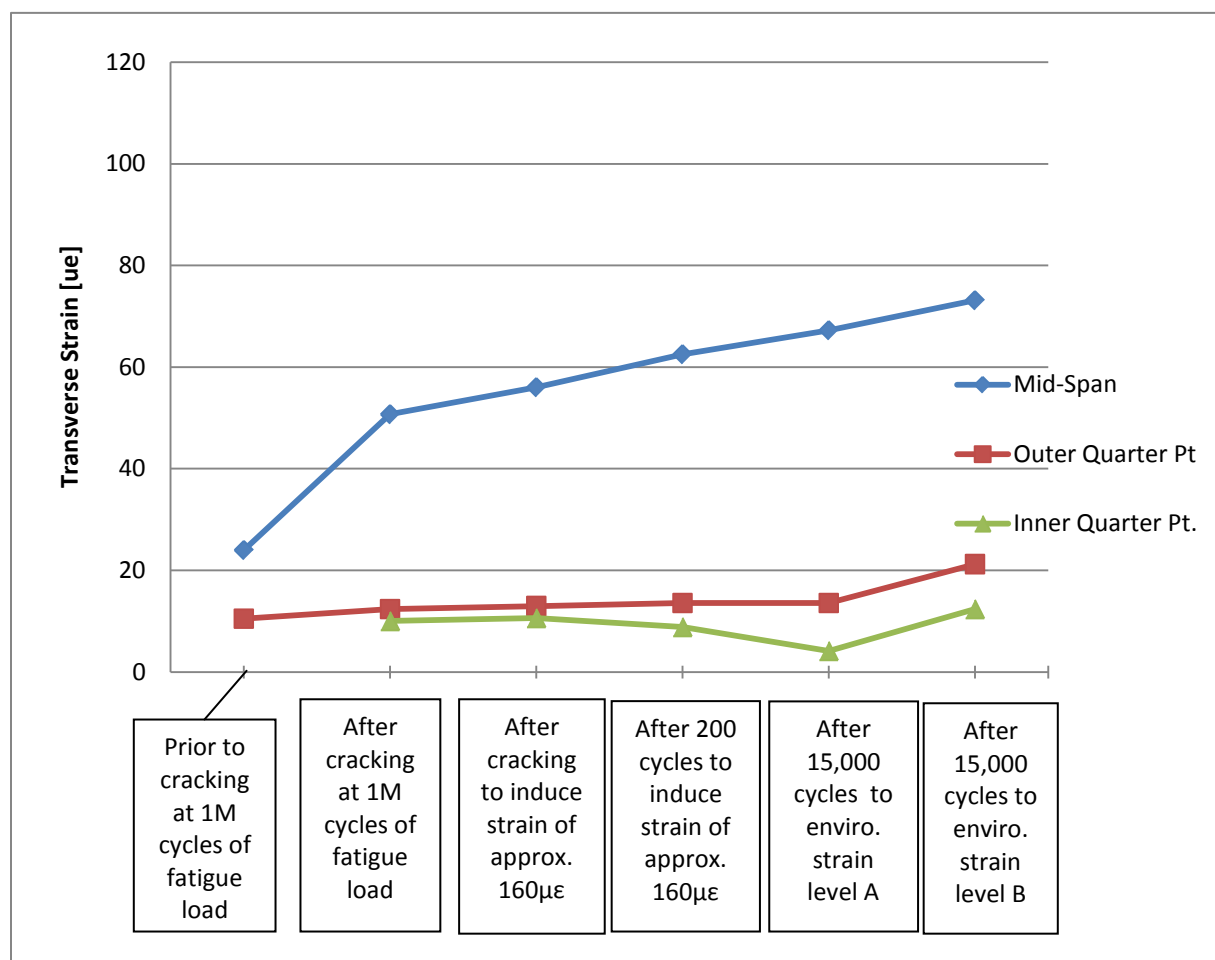
Figure 5.3.4[1]: Transverse strains measured with a 35 kip patch load applied at midspan during environmental effect simulation in Span 2 of Concept 1 laboratory bridge

[1]Figure 5.3.4 shows the transverse strain measured at midspan, the outer quarter point and the inner quarter point under a 35 kip patch load applied at midspan of Span 2. The horizontal axis contains a description of the behavior and qualitative target strain values. For example, the data points labeled "After 15,000 cycles to enviro. strain level A" represent the transverse strain measured with a 35k patch load applied at midspan after a load to induce a strain of $183\mu\varepsilon$ (from Table 5.3.4) was applied quasi-statically, and a spreader beam was utilized to extend the crack.

133

Table 5.3.5: Measured load and transverse strain, and number of cycles completed during environmental effect simulation on Span 2 of the Concept 1 laboratory bridge specimen

Concept 1, Span 2	Prior to cracking at 1M cycles of fatigue load	After cracking at 1M cycles of fatigue load	After cracking to target strain of 160µε	After cycling to target strain of 160µε	After cycling to enviro. strain level A	After cycling to enviro. strain level B
Magnitude of target strain	NA[1]	160µε	160µε	160µε	180µε	300µε
Number of cycles completed at each stage	3	3	3	200	15000	15000
Max. transverse strain achieved	23µε	200µε	160µε	160µε	183µε	233µε
Load required to achieve strain	35k[2]	95k[2]	95k[2]	95k[2]	108k[2]	155k[3]

[1]The first column of Table 5.3.5 represents the strain measured during the fatigue loading. Fatigue loading was not based on strain levels, but rather was based on an applied patch load of 35 kip, therefore no target strain was applicable to fatigue loading

[2]The load recorded represents the patch load applied at midspan.

[3]The load recorded represents the total load applied to the 10 ft. longitudinal spreader beam. The load applied at each quarter point was half of this value.

Span 2 of the Concept 1 laboratory bridge indicated degradation of the joint due to the static and cyclic application of loads after reflective cracking was first introduced into the span (which corresponds to the data point labeled as "After cracking at 1M cycles of fatigue loading"). Degradation of the joint is evident in Figure 5.3.4 in that the transverse strain measured at midspan with a 35 kip patch load applied at midspan increased as the environmental effect simulation progressed from initially cracking the joint after the first million cycles of fatigue load to the last environmental simulation test of applying cyclic loading to induce strains on the order of the environmental simulation strain level B. The increase in strain under the 35 kip patch load applied at midspan, however was relatively small after the crack was first introduced in the section. The increase in transverse strain at midspan under the 35 kip patch load due to the initiation of the crack after the first million cycles was approximately 25µε (i.e., 50µε - 25µε). Increases in the transverse strain due to cracking and cyclic loading to induce strains on the order of the environmental target levels A and B were observed to be between 5-8µε (i.e., difference in measured strains between the second and third data points, the third and fourth data points, etc.). Furthermore, a total increase in strain at the 35 kip patch load of about 15µε at midspan due to the application of 30,000 cycles to simulate environmental loading (i.e., 77µε after cycling to strain level B - 62µε after 200 cycles to strain level A), suggests a relatively stable joint region when loaded to strains on the order of 200µε. Recall that the application of 15,000 cycles was assumed to represent approximately 100 years of thermal effect loading, where there was assumed to be 150 days in a year with a significant thermal gradient.

A similar environmental simulation process was completed on Span 1 of the Concept 1 laboratory bridge. The primary difference in testing Span 1 involved the early use of an actuator with a 220 kip capacity. The reflective crack introduced in the section after the completion of the first million cycles of fatigue load was developed using a quasi-static patch load at midspan, and was also extended with use

134

of a spreader beam during two separate load cycles, the first with bearing points symmetrically located 2.5 ft. from midspan, and the second with bearing points symmetrically located 5 ft. from midspan (referred to as 5 and 10 ft. spreader tests, respectively). Cracking induced in the section to correlate with the environmental simulation strain levels A and B was generated with the use of both the 5 and 10 ft. spreader layout as well as patch loading; however, cyclic loading was always applied through a patch load at midspan. The reflective crack was extended to the outer (i.e., west) quarter point of Span 2, however the crack was not observed to have extended to the instrumentation at the interior quarter point, which was attributed to the transverse restraint provided by proximity to the nearby interior support, and was similar to the observed results from Span 1 of the Concept 1 laboratory bridge.

The results of the environmental effect laboratory test on Span 1 are shown in Figure 5.3.5. In addition, Table 5.3.6 outlines the number of cycles completed, the strain that was induced in the section and the load required to induce that strain for Span 1 of the Concept 1 laboratory bridge.
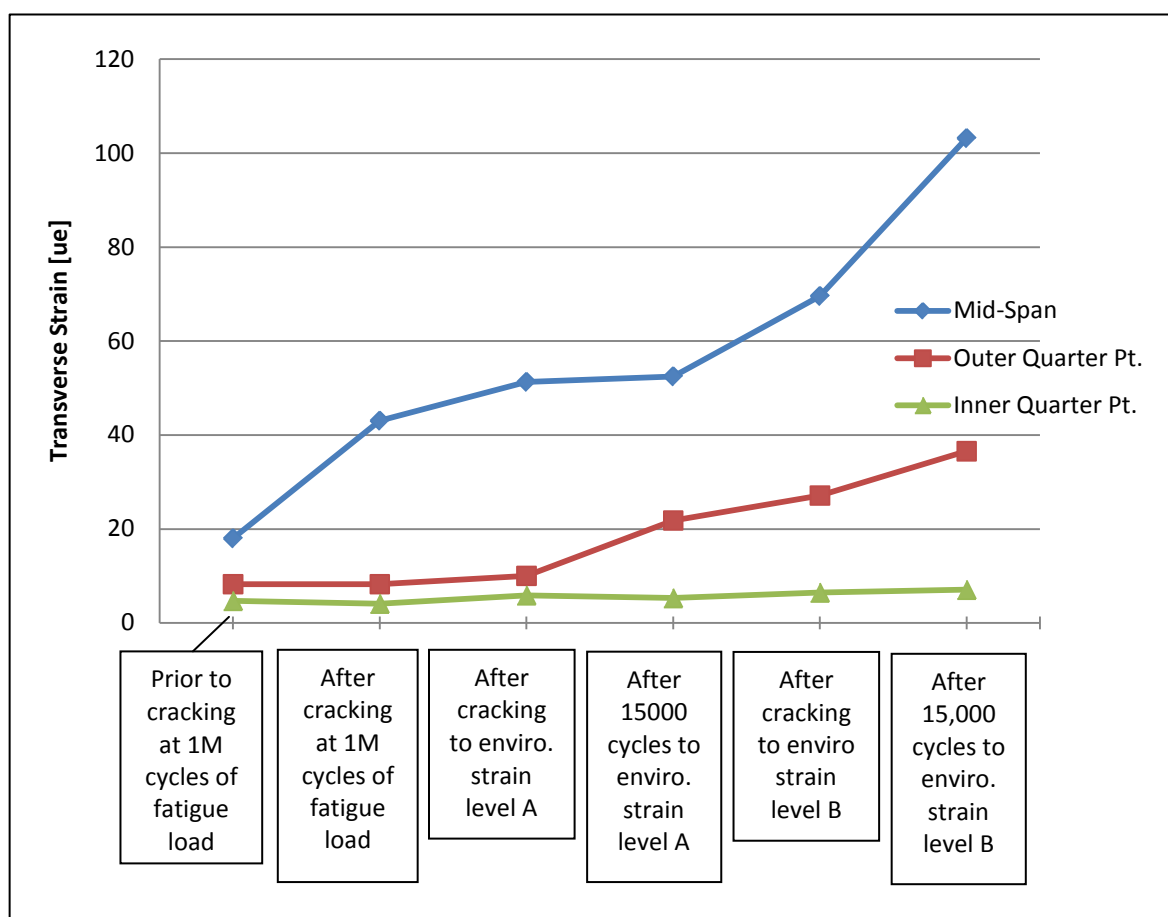
Figure 5.3.5: Transverse strains measured with 35 kip patch load applied at midspan during environmental effect simulation in Span 1 of Concept 1 laboratory bridge

135

Table 5.3.6: Measured load and transverse strain, and number of cycles completed during environmental effect simulation on Span 1 of the Concept 1 laboratory bridge specimen

Span 1, Concept 1	Prior to cracking at 1M cycles of fatigue load	After cracking at 1M cycles of fatigue load	After cracking to enviro. strain level A	After cycling to enviro. strain level A	After cracking to enviro. strain level B	After cycling to enviro. strain level B
Magnitude of target strain	NA[1]	160με	180με	180με	300με	300με
Number of cycles completed	3	3	3	15000	3	15000
Max. transverse strain achieved	18με	161με	213με	213με	280με	303με
Load required to achieve strain	35k[2]	89k[2]	160k[3]	105k[3]	206k[3]	210k[3]

[1]The first column of Table 5.3.6 represents the strain measured during the fatigue loading. Fatigue loading was not based on strain levels, and but rather was based on an applied patch load of 35 kip, therefore no target strain was applicable to fatigue loading
[2]The load recorded represents the patch load applied at midspan.
[3]The load recorded represents the total load applied to the 10 ft. longitudinal spreader beam setup.

Somewhat significant degradation of the joint with the application of the 35 kip patch load was observed due to both cracking and cycling at approximately 210 kips, or a measured strain of approximately 300με. Furthermore, degradation of the outer quarter point at the environmental strain level A and above suggested that the use of the 10 and 5 ft. spreader beam for the application of the quasi-static patch loads reduced the stiffness toward the exterior support along the joint. It should be noted that although degradation was observed under the application of loading, a forensic examination of the specimen discussed in Section 5.4 indicated negligible residual damage in the unloaded specimen.

The Concept 2 laboratory bridge consisted of two half spans of interest. For this reason, simulation of environmental effects was completed at the quarter points and at midspan separately, with the tests for environmental simulation strain level A completed first at the quarter points and then at midspan, with the same order of testing used at environmental simulation strain level B. The spreader setup consisted of load applied quasi-statically and dynamically through a 10 ft. long spreader beam centered at midspan. The reflective crack introduced in the section after the completion of the first million cycles of fatigue load was developed using a quasi-static patch load at the quarter points through the use of the 10 ft. spreader beam, and was also extended to midspan via a single patch load at that location, though cracking was observed only between midspan and just beyond the east quarter point, which corresponded to the half span constructed with straight transverse reinforcement in the trough region. Cracking induced in the section to correlate with the environmental simulation strain levels A and B was generated with the use of both a 5 and 10 ft. spreader layout as well as patch loading at midspan, though for all tests cracking was not observed in the instrumentation in the west half span of the specimen. An additional load test was designed with a spreader beam bearing a distance of 2.5 ft. towards the west half span, and 5 ft. towards the east half span, in an effort to increase the reaction force in the west half span and subsequently induce cracking near that location. Loading was applied in

136

a quasi-static load controlled load test, however the transverse strains measured at the midspan cross section reached the target values prior to the indication of the cracking at the west quarter point, and therefore no additional load was applied in this modified setup.

The lack of observed cracking was attributed to three possible explanations. The west half span corresponded to the half span of the bridge bearing on the concrete pier (i.e., corresponding to the interior half spans in the Concept 1 laboratory bridge), in which cracking was also not observed attributed to transverse restraint provided by the support. The natural roughness of the concrete pier may have provided additional restraint to the transverse expansion of the joint at the pier, which may have reduced the transverse stress demands in the CIP concrete near the joint. The west half span was also constructed with hooked reinforcement rather than the straight bars in the adjacent half span, though cracking was observed in the previous specimens where larger diameter hooked bars at closer spacing were used. A third possibility was that a potential reflective crack in the west half span was not observed by the instrumentation. This may have been the case especially if the crack propagated along the precast flange-CIP interface to the vertical web interface of the precast section, where instrumentation was not present (A forensic examination of the specimen following testing did not reveal a crack at the vertical web interface; however, the forensic exam was conducted under no load such that cracks that had opened under loading may have closed upon unloading.).

Figure 5.3.6 illustrates the behavior of the Concept 2 laboratory bridge under a 35 kip quasi-static patch load applied at the quarter points (i.e., a load of 70 kips applied to a 10 ft. spreader beam from midspan) at various times during the environmental simulation. Even though the Concept 2 laboratory bridge specimen had a single simply-supported span, the three data series in Figure 5.3.6 are named in the same way as for the Concept 1 laboratory bridge: the inside quarter was located nearest the concrete pier (i.e., west end of the Concept 2 laboratory bridge), while the outside quarter was located nearest the steel pier (i.e., east end of the Concept 2 laboratory bridge). Table 5.3.7 outlines the number of cycles completed, the strain that was induced in the section at both the east and west quarter points, and the associated load required to induce that strain for the Concept 2 laboratory bridge specimen.

137
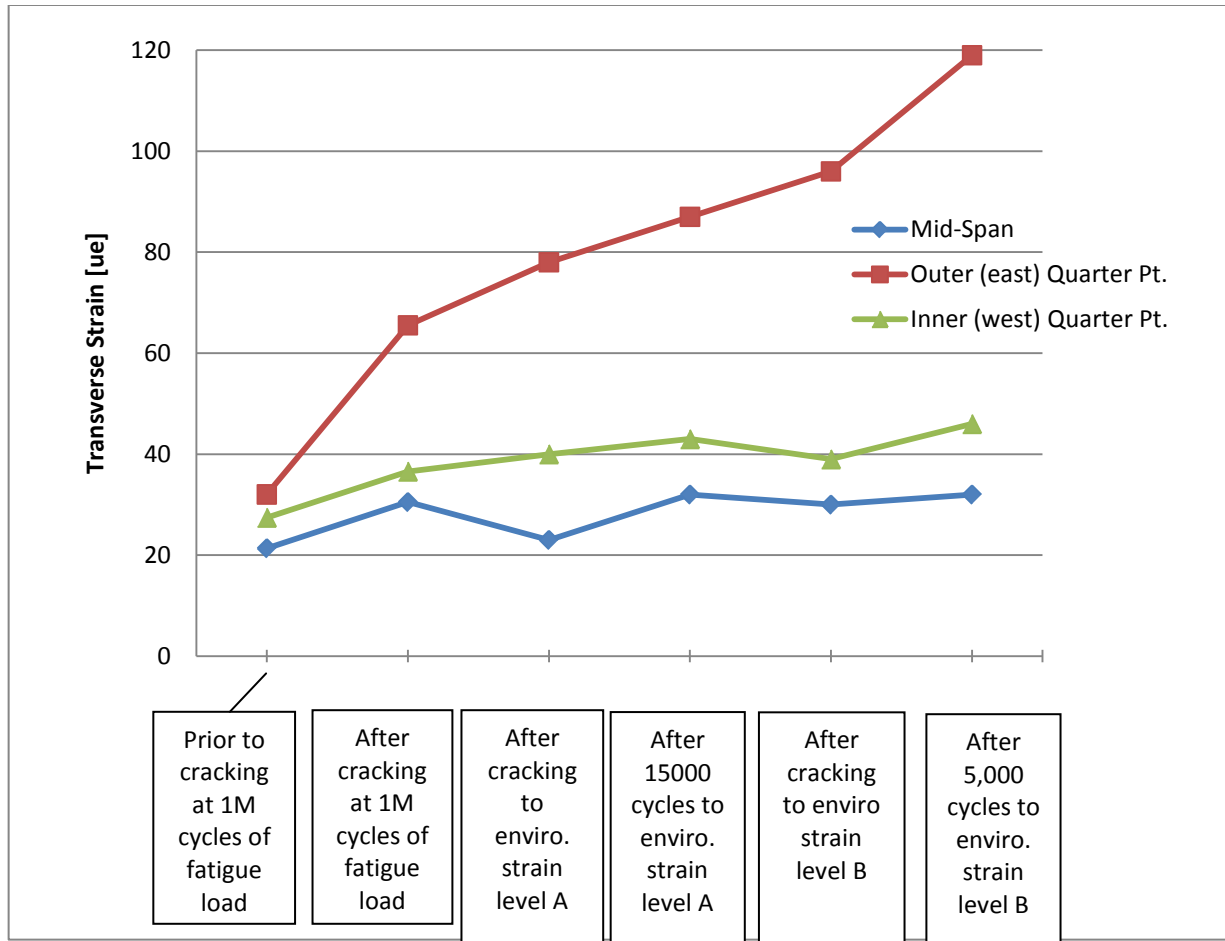
Figure 5.3.6: Transverse strains measured with 35 kip patch load applied at quarter points during environmental effect simulation in the Concept 2 laboratory bridge

Table 5.3.7: Measured load and transverse strain, and number of cycles completed during environmental effect simulation at the quarter points of the Concept 2 laboratory bridge specimen

Concept 2, load applied at quarter points	Prior to cracking at 1M cycles of fatigue load	After cracking at 1M cycles of fatigue load	After cracking to enviro. strain level A	After cycling to enviro. strain level A	After cracking to enviro. strain level B	After cycling to enviro. strain level B
Magnitude of target strain	NA[1]	160µε	180µε	180µε	300µε	300µε
Number of cycles Completed	3	3	3	15000	3	5000
Max. transverse strain measured at the east quarter point	33µε	150µε	177µε	177µε	253µε	253µε
Max. transverse strain measured at the west quarter point	30µε	85µε	81µε	81µε	104µε	104µε
Load required to achieve strain[2]	70k	210k	195k	153k	210k	207k

[1]The first column of Table 5.3.7 represents the strain measured during the fatigue loading. Fatigue loading was not based on strain levels, but rather was based on an applied patch load of 35 kip, therefore no target strain was applicable to fatigue loading
[2]The load recorded represents the total load applied to the 10 ft. longitudinal spreader beam setup

Relatively similar levels of degradation were observed in the Concept 2 laboratory bridge compared to Span 1 of the Concept 1 laboratory bridge. At the conclusion of cracking and cycling to a load that induced a strain representative of the environmental target strain level A, the strain measured when a 35 kip patch load was applied to each quarter point had increased by 22µε (i.e., 87µε - 65µε), compared to 9µε (i.e., 52µε - 43µε) and 17µε (i.e., 67µε - 50µε) for Spans 1 and 2 of the Concept 1 laboratory bridge, respectively. Furthermore, when loaded to the maximum capacity of the 220 kip actuator, which was limited to 210 kips due to the available system hydraulic pressure at the time of testing, and cycling to induce a strain of 253µε at the east quarter point, the strain measured with an applied 35 kip quasi-static patch load at each quarter point increased by 32µε (i.e., 119µε - 87µε), compared to a 51µε (i.e., 103µε - 52µε) increase in Span 1 of the Concept 1 laboratory bridge. Note however that the Concept 2 bridge only underwent 5000 cycles at that strain level as opposed to the 15000 cycles subjected to the Concept 1 bridge spans and the magnitude of strain induced in each span during the environmental simulation varied. The absence of cracking near the west quarter span was further supported by the minimal increase in the strain measured at that location over the duration of the environmental simulation.

Cyclic loading was applied at midspan of the Concept 2 laboratory bridge after the completion of loading at the quarter points for both environmental simulation strain levels A and B (i.e., cyclic loading to level A was applied at quarter points, then midspan, followed by cyclic loading to level B at the quarter points, then midspan). The target strain level at the environmental simulation level B was modified for the

139

midspan tests, with the revised target strain to be the maximum transverse strain measured at the quarter points (i.e., 253με at the east quarter point). The behavior of the specimen under a 35 kip quasi-static patch load at midspan through the duration of the environmental simulation is shown in Figure 5.3.7. The three data series in Figure 5.3.7 are named in the same way as for the Concept 1 laboratory bridge (i.e., the inside quarter is located nearest the concrete pier (west end of the Concept 2 laboratory bridge), while the outside quarter was located nearest the steel pier (east end of the Concept 2 laboratory bridge)). Table 5.3.8 outlines the number of cycles completed, the strain that was induced in the section at midspan, and the associated load required to induce that strain for the Concept 2 laboratory bridge.
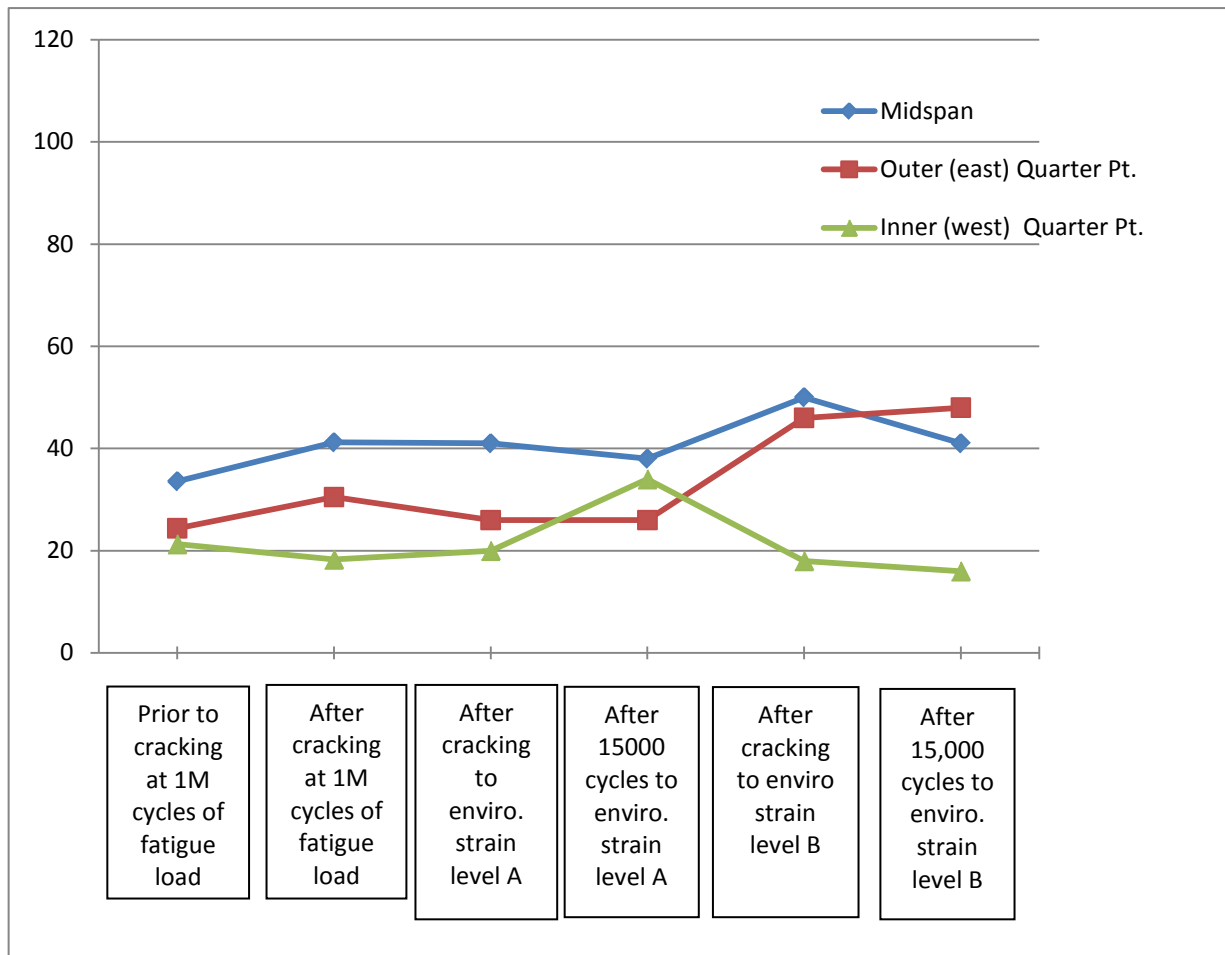
Figure 5.3.7: Transverse strains measured with 35 kip patch load applied at midspan during environmental effect simulation in the Concept 2 laboratory bridge

140

Table 5.3.8: Measured load and transverse strain, and number of cycles completed during environmental effect simulation at midspan of the Concept 2 laboratory bridge specimen

Concept 2, load applied at midspan	Prior to cracking at 1M cycles of fatigue load	After cracking at 1M cycles of fatigue load	After cracking to enviro. strain level A	After cycling to enviro. strain level A	After cracking to enviro. strain level B	After cycling to enviro. strain level B
Magnitude of target strain	NA[1]	160με	180με	180με	300με	300με
Number of cycles Completed	3	3	3	15000	3	15000
Max. transverse strain measured at midspan	33με	174με	176με	176με	256με	256με
Load required to achieve strain	35k	136k	116k	116k	124k	134k

[1]The first column of Table 5.3.8 represents the strain measured during the fatigue loading. Fatigue loading was not based on strain levels, but rather was based on an applied patch load of 35 kip; therefore no target strain was applicable to fatigue loading.

Little degradation of the longitudinal joint was observed at midspan of the Concept 2 laboratory bridge during the environmental effect simulation. Note that despite the fact that loading was applied at midspan in Figure 5.3.7, a larger increase in the transverse strain was measured at the outer (east) quarter point than at midspan after cracking and cycling to simulate the environmental strain target level B, which suggested that the level of degradation achieved near the east quarter point was more severe than that at midspan. The resiliency of the joint region at midspan was likely due to the limited success in extending the reflective crack into the west half span of the specimen.

The rate of degradation of the joint during cycling was also monitored during the environmental simulation on the Concept 2 laboratory bridge. Figure 5.3.8 illustrates the strain measured at midspan periodically with the 35 kip patch load located at midspan throughout the 15000 cycles that were completed to the maximum capacity of the actuator.

The cycling portion of the environmental simulation to induce a strain to the target level B was ended at after the completion of 5,000 cycles because of a fracture failure of the steel spreader beam used for the test. The rate of degradation of the joint at the outside quarter point was observed to be larger during the early cycles and tended to taper off between 2,000 and 5,000 cycles. The increase in strain at the outer quarter point measured with the application of the 35 kip patch load over the first 2,000 cycles was 22με, while an additional 3,000 cycles increased the strain by only 10με. This suggested that the 5,000 cycles applied for the environmental simulation of the Concept 2 specimen provided an adequate estimate of the degradation that might be expected under the cyclic loads to a given strain condition.

141
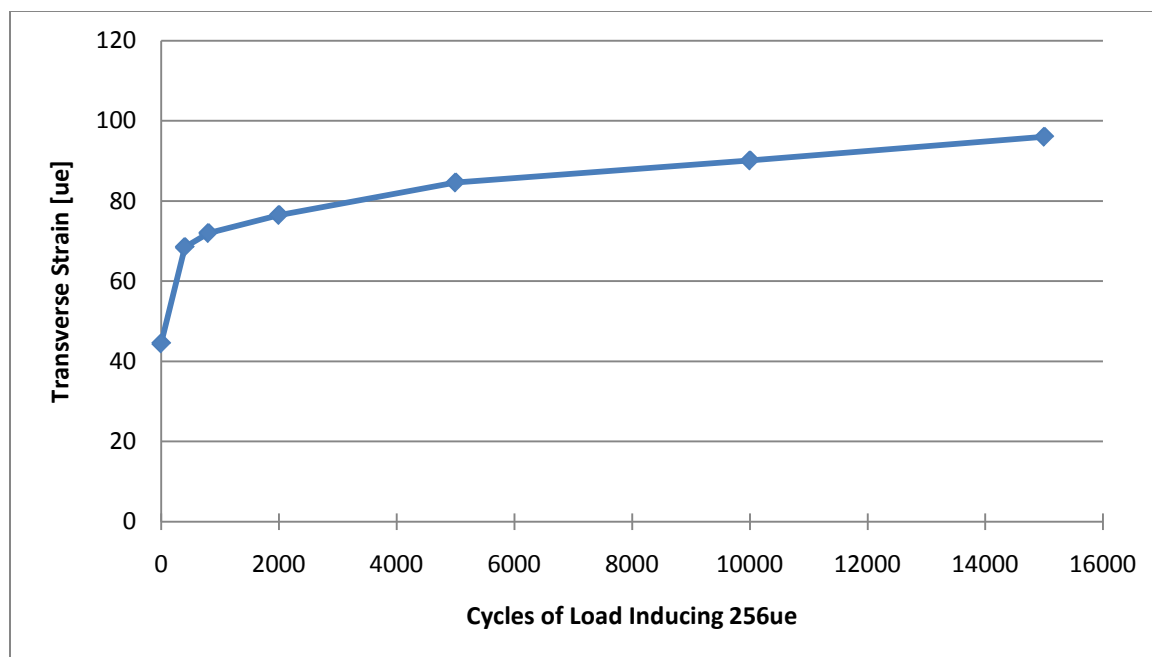
Figure 5.3.8: Transverse strains measured at midspan under the 35 kip patch load applied at midspan during the 15,000 cycles completed during the environmental effect simulation

In summary, Span 2 of the Concept 1 laboratory bridge showed excellent crack control during the cycling procedure at the environmental simulation strain level B, which corresponded to a measured value of approximately 233µε. Span 1 of the same bridge, which would be expected to have superior crack control capabilities because of the reduced flange depth, showed a degradation of the joint under the same target strain level, which corresponded to an approximate transverse strain of 303µε. Finally, the Concept 2 laboratory bridge, which was cycled to a maximum strain level of approximately 256µε, measured at the east quarter point, also showed degradation of that portion of the joint region during cycling. The Concept 2 span was constructed with less total reinforcement, however with a tighter spacing. In addition, the Concept 2 laboratory bridge was constructed with a 3 in. flange, which would be expected to outperform Span 2 of the Concept 1 laboratory bridge. Because of the similarity in the performance of the two bridge concepts, the details from either were expected to be acceptable for PCSSS bridge construction. Furthermore, the adequate performance of the Concept 1 laboratory bridge (with 12 in. maximum transverse reinforcement spacing) indicated that a maximum spacing of 12 in. was suitable for the design of PCSSS bridges based on this research. Recall that the variations in the depths of the instrumentation utilized to measure the transverse strains (see Table 5.3.1) in each specimen prevented direct comparison of the relative magnitudes of measured strain among the specimen. Assuming that the transverse strain varied linearly between the compression and tension fibers of the section, instrumentation that was located lower in the section was associated with a smaller transverse curvature than instrumentation that was located higher in the section when both gages measured identical strains. A forensic exam was completed on each of the laboratory bridge specimens in an effort to visually identify reflective cracking by means of an investigation of core samples. After saw cutting the specimens into several sections, as discussed in detail in Section 5.4, negligible evidence of reflective cracking was observed in the forensic exam, despite the fact that many locations selected for core samples coincided with the location of concrete embedment instrumentation which reported large,

142

inelastic strains during the load tests. Because the forensic exam was conducted following the tests, the cracks may have closed due to the load removal.

In addition to the environmental effect simulation using the procedures described above with the application of mechanical loading, a setup using commercial grade heated thermal blankets was applied to Span 2 of the Concept 1 laboratory bridge in an attempt to induce the same thermal gradient in the laboratory bridge as measured in the Center City Bridge. This method was found to be incapable of inducing the required thermal gradient in the specimen, and was not considered feasible in the future.

5.3.3. Load Transfer Between Precast Panels

The ability of the section to effectively transfer load between adjacent precast panels was expected to depend on the condition of the longitudinal joint and therefore was expected to change throughout the extent of laboratory testing as cracking was induced along the longitudinal joint. To investigate the load transfer between adjacent panels, patch loading was applied at the middle of the south precast panel, approximately 36 in. from the precast joint, directly at midspan of Span 2 of the Concept 1 laboratory bridge as well as separate tests at midspan and the quarter points of the Concept 2 laboratory bridge. The locations of the applied load for the load transfer tests are shown in Figure 5.3.9. Load transfer was not investigated during testing of Span 1 of the Concept 1 laboratory bridge. Load transfer tests were completed on Span 2 prior to traffic fatigue or introduction of cracking, as well as at the conclusion of all fatigue loading and environmental simulations. Several load transfer tests were completed on the Concept 2 laboratory bridge throughout the series of traffic fatigue cycles as well as intermittently during the environmental simulation. Monitoring of the longitudinal instrumentation during the load transfer tests allowed for the calculation and comparison of the longitudinal curvature in the loaded and unloaded panels.

Span 2 of the Concept 1 laboratory bridge was first loaded on the south panel prior to any fatigue or cracking loading in November 2007. The second load test on the south panel was completed at the conclusion of all fatigue, cracking, and environmental simulation on both spans in October 2008 at the completion of roughly 2,030,200 cycles of fatigue and environmental loading on Span 2. Figure 5.3.10 illustrates the measured longitudinal curvature in the north and south panels at midspan in Span 2 of the Concept 1 laboratory bridge. The gages utilized through the depth in both panels were nominally located at midspan approximately 21 in. from the precast joint.
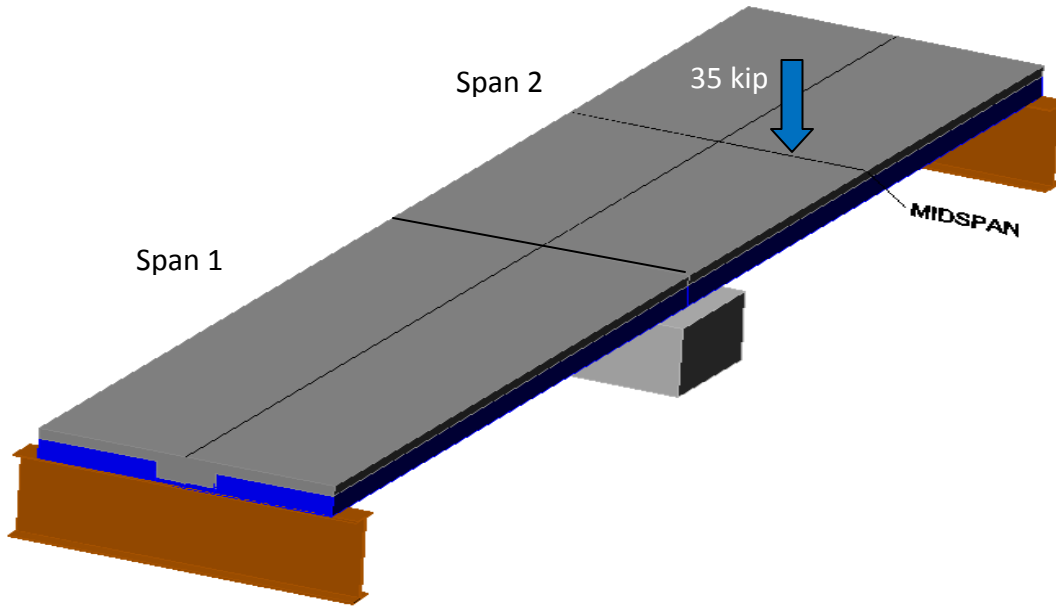
(a) Load placement during transverse load distribution tests for Concept 1 laboratory bridge
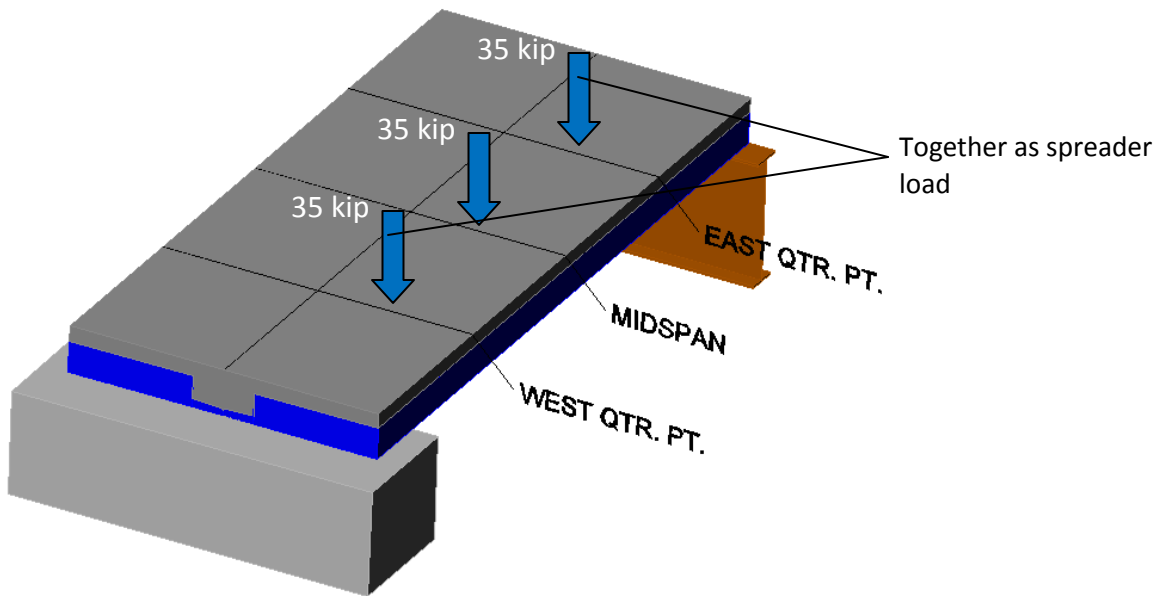
(b) Load placement during transverse load distribution tests for Concept 2 laboratory bridge

Figure 5.3.9: Load placement during transverse load distribution tests for Concept 1 and Concept 2 laboratory specimens

144
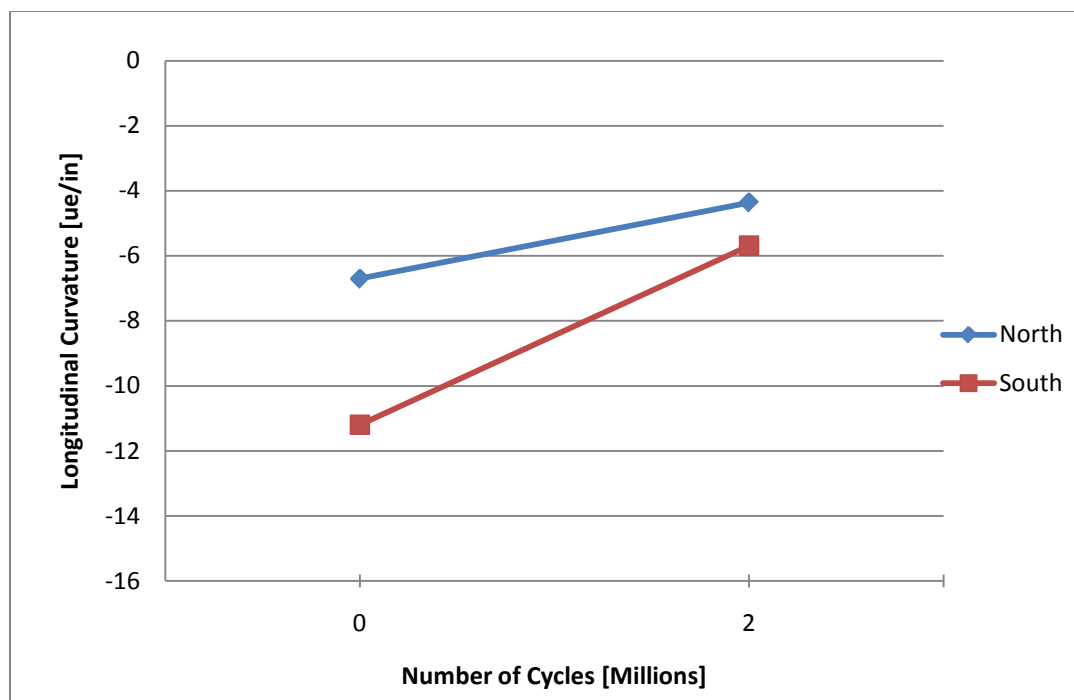
Figure 5.3.10: Longitudinal curvature in north and south panels in Span 2 of Concept 1 laboratory bridge under 35 kip patch load applied at midspan centered over south panel

The curvature at each data point was calculated using three longitudinally oriented strain gages in a vertical line. The coefficient of variation (R^2) value for the curvature ranged from 0.961 to 0.988 for the four data points shown in Figure 5.3.10. The reduction in measured curvature between the tests at zero and two million cycles might be attributed to variations in the loading and instrumentation setup between the two measurements, as the zero and two million cycles were completed by different personnel.

Load transfer was more thoroughly investigated in the Concept 2 laboratory bridge, with the longitudinal curvature measured several times throughout the laboratory tests conducted by the same personnel. As for the tests on Span 2 of the Concept 1 laboratory bridge, the south panel of the Concept 2 laboratory bridge was loaded both at midspan as well as at the quarter points with a 35 kip patch load at each location. Figure 5.3.11 illustrates the curvature calculated throughout the fatigue and environmental cycles with a 35 kip patch load applied to each quarter point through a longitudinal spreader. The last data points in the figure were taken after completion of environmental cycling to the 160με strain level. The longitudinal curvature was not obtained after the environmental simulation cycles to the 250με strain level due to failure of the spreader beam during those tests.

145
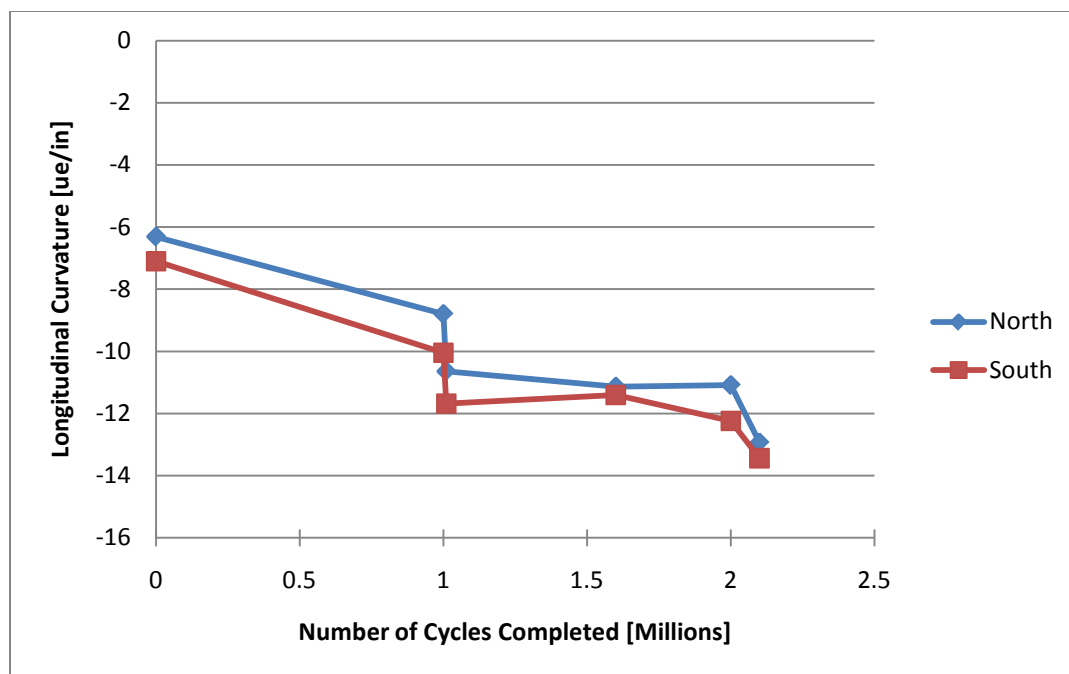
Figure 5.3.11: Longitudinal curvature in north and south panels in Concept 2 laboratory bridge under 35 kip patch load applied at the quarter points centered over south panel.

The longitudinal curvatures were observed to increase in the Concept 2 laboratory bridge. The increase in curvature observed in the Concept 2 laboratory bridge was not suspected to be a result of longitudinal flexural cracking, as the predicted cracking loads for Span 2 of the Concept 1 laboratory bridge and the Concept 2 laboratory bridge were 271 and 224 kips, respectively, while the largest loads applied to Span 2 of the Concept 1 laboratory bridge and the Concept 2 laboratory bridge were 155 and 210 kips, respectively.

It was expected that the longitudinal curvatures measured in the north precast panels would decrease as reflective cracking was introduced and extended near the precast joint because of reduced ability for the section to transfer load across the joint region, though this was not observed. Rather, good transverse load transfer was observed across the longitudinal joint regardless of the application of fatigue loading to simulate traffic loads, the introduction of reflective cracking, or even the application of cyclic loading to simulate the large daily strain fluctuations observed in the Center City field bridge due to environmental effects.

5.3.4. Composite Action

Each of the three bridge spans (i.e., Concept 1 Span 1 and 2, and Concept 2) provided an opportunity to investigate the effects of variations in horizontal shear reinforcement on composite action. Span 2 of the Concept 1 laboratory bridge was constructed with horizontal shear ties spaced at 12 in., though the hook returns provided a nominal 1/4 in. of clearance to the top of the precast web, which was unlikely to provide adequate clearance for proper bond. The horizontal shear reinforcement in this span reflected that used in the Center City Bridge, where, according to Article 5.8.4.1 of the AASHTO LRFD

146

specification (2004), the maximum stirrup spacing at the ends of the precast beam was 15 in., which could be reduced to 24 in. at locations away from the ends (where the shears were smaller). The horizontal shear reinforcement spacing was doubled to 24 in. in Span 1 of the Concept 1 laboratory bridge and the clearance between hook returns and the top of the precast web was increased to 1-3/8 in., while no horizontal shear reinforcement was provided in the Concept 2 laboratory bridge. The 2010 AASHTO LRFD specification required the presence of a minimum area of horizontal shear reinforcement, though Naito et al. (2006) suggested that this requirement was overly conservative (see Section 2.3), which prompted the investigation of the performance of the PCSSS in the absence of horizontal shear reinforcement. In all three cases, a roughened surface was provided by means of raking, which created a surface roughness amplitude of approximately 1/4 in, and was provided on the horizontal top web surface as well as both vertical web faces in each specimen. The top surface of the precast flanges was also roughened in Span 2 of the Concept 1 laboratory bridge. A photograph of the surface condition of one of the precast members utilized in the Concept 2 laboratory bridge is shown in Figure 5.3.12.

Figure 5.3.12: Intentionally roughened surface, by means of raking, of top web of precast beam used for the construction of Concept 2 laboratory bridge specimen

The ability of the precast slab span system to maintain composite action throughout all loading scenarios warranted investigation of composite action at the largest possible load levels available in the

147

laboratory. For this reason, load tests were conducted on each span to determine the maximum capacity of each specimen, and subsequently to determine whether composite action was maintained throughout each test. A total of between 3 and 6 longitudinally oriented concrete embedment resistive gages aligned vertically in the CIP and precast concrete at several cross sections in each specimen were utilized to calculate the longitudinal curvature during the ultimate tests. An analysis of the curvatures provided an assessment of the state of continuity between the precast and CIP concrete.

The application of load during the ultimate tests was expected to create an artificially compressed region near the location of applied load, which was likely to increase the horizontal shear friction (due to the localized increase in the normal force) at that location. Therefore, the location of the applied loading during the ultimate tests was modified in an effort to reduce the artificial effects of loading on the longitudinally oriented instrumentation. In both spans of the Concept 1 laboratory bridge, the instrumentation utilized for the investigation of composite action was located within a longitudinal distance of 3 in. from the application of load at midspan. The load frame was therefore modified, and relocated 20 in. closer to the center pier, which provided a center to center distance of 17 in. from the load beam to the instrumentation. The longitudinally oriented instrumentation in the Concept 2 laboratory bridge was designed to allow for the load frame to remain in the same position for the ultimate loading as was utilized for the fatigue and environmental studies, with a center to center distance of 21 in. between the instrumentation and load beam.

Each test was preceded by the construction of an even grouted surface between the top of the bridge and the loading beam, which extended across the entire width of the bridge and had a flange width of 12 in. Three actuators, a 220 kip in the center with a 110 kip actuator to each side, were used to apply load to the transverse load beam. Load was applied to each specimen using a displacement-controlled program, primarily to prevent the rapid collapse of the specimens, if applicable. The displacement rate was selected such that the load was increased by approximately 2 kips per minute. A photograph of the loading system utilized for the ultimate tests is provided in Figure 5.3.13.

148
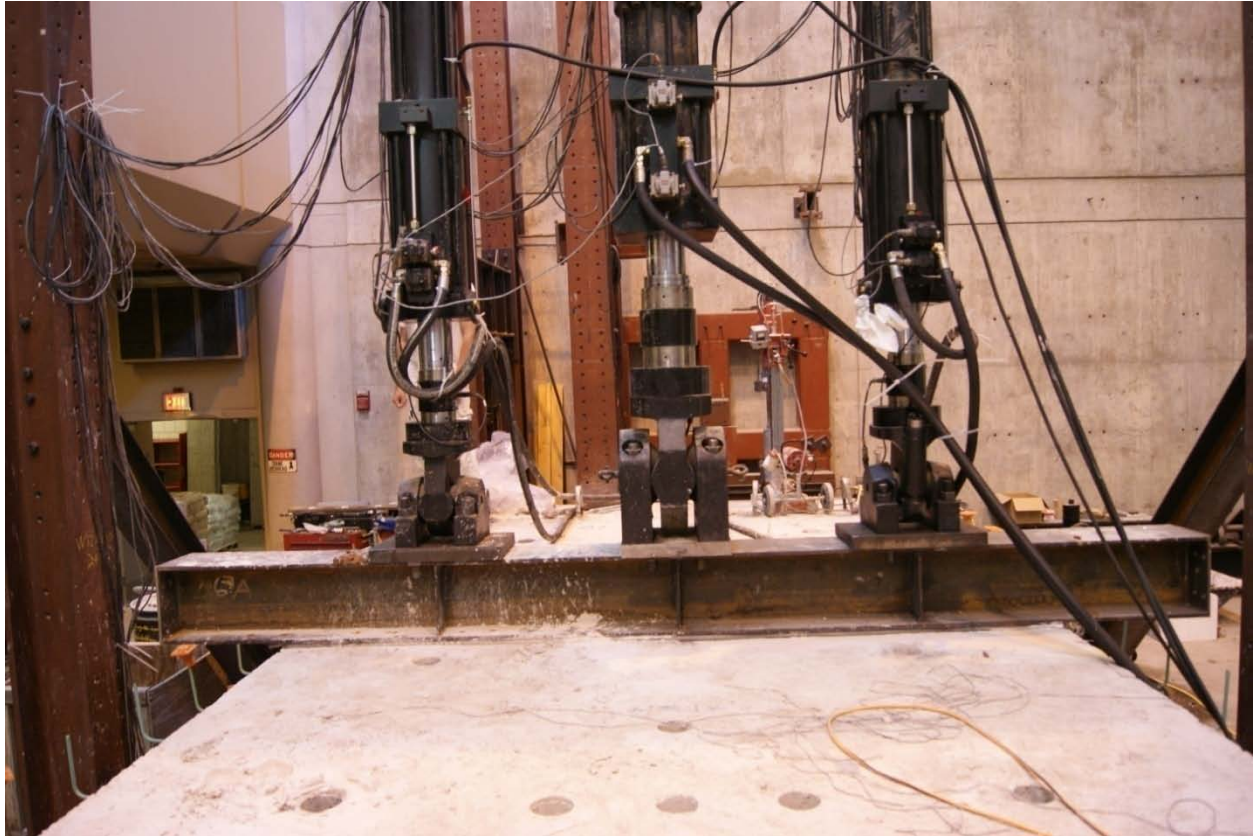
Figure 5.3.13: Photograph of tri-actuator load setup and transverse loading beam utilized during ultimate load tests; shown for the Concept 2 laboratory bridge test

The calculation of the sectional ultimate moment capacity for each span was completed using Response-2000. The assumed tensile strength of the prestressing strand was taken to be 270 ksi, the yield strength of the mild reinforcement as 60 ksi, and the concrete compressive strain at crushing was assumed to be 0.003.

The ultimate sectional moment capacity of each section varied slightly, due to the depths of the longitudinal cage reinforcement based on the flange thickness, number of strands in each span, as well as variations in the CIP concrete compressive strength and the finished depth of each span due to construction tolerances. The maximum measured depth of the Concept 1 laboratory bridge was 19.25 in., with concrete compressive strengths of 4.47 ksi and 4.55 ksi at an age of 432 days in Spans 1 and 2, respectively. The measurement of the compressive strength at 432 days suggests that the value should reasonably represent the maximum strength and reasonably predict the strength during ultimate loading, which occurred when the CIP concrete was 855 and 784 days old in Spans 1 and 2, respectively. The maximum measured section depth in the Concept 2 laboratory bridge was 18.5 in. with a CIP concrete compressive strength of 6.9 ksi measured 10 days prior to ultimate loading on the Concept 2 laboratory bridge.

The ultimate sectional moment capacity of Span 2 of the Concept 1 laboratory bridge was calculated to be 2544 ft.-kip, and the calculated capacity of Concept 1 Span 1 was 2256 ft.-kip. The sectional capacity of the Concept 2 laboratory bridge was calculated to be 2313 ft.-kip.

149

A numerical analysis of the continuous two-span Concept 1 laboratory bridge suggested that the ultimate capacity of the specimen would not be reached, as the maximum load available during the Concept 1 ultimate tests was approximately 420 kips, which corresponded to an applied maximum moment of 1272 ft.-kips, which was considerably less than the ultimate sectional capacities of either Span 1 or 2. The continuous bridge was modeled as a three-span system, with the center span modeled with an 18 in. span length (i.e., the distance between the center of bearing of Spans 1 and 2 at the center pier). The center span was modeled with a moment of inertia that was an order of magnitude larger than that of the exterior spans, to simulate the stiffness provided by the pier.

Ultimate loading was initiated on Span 2 of the Concept 1 laboratory bridge, with a maximum applied load of approximately 420 kips. The ultimate capacity of the section was not observed to be imminent, which corresponded with the previously stated predictions. In an effort to reach the ultimate capacity of Spans 1 and 2, saw cutting was completed at the center pier in an attempt to reduce the continuity in the bridge (i.e., create approximately simple-support conditions) to reach the maximum flexural capacity of the laboratory bridge specimens with the available actuators. The cutting blade had a usable cutting radius of approximately 5 in, and therefore only the longitudinal deck reinforcement was severed, while the longitudinal reinforcement for continuity at the bottom of the reinforcing cage through the joint remained intact. Spans 1 and 2 of the Concept 1 laboratory bridge after continuity was modified at the center pier are referred to as semi-simple spans hereafter.

The ultimate capacities of the two semi-simple spans in the Concept 1 laboratory bridge and the simple span in the Concept 2 laboratory bridge were not achieved during testing due to limitations of the actuators. The maximum load available during the Concept 1 tests was approximately 420 kips, while an applied load of 458 kips was achieved during the Concept 2 test, due to an increase in available hydraulic pressure. The applied loads and respective moments, as well as the calculated sectional capacities of each specimen are given in Table 5.3.9.

Table 5.3.9: Maximum loads applied to laboratory bridge specimens during ultimate loading, calculated applied moments, and predicted moment capacities

Specimen	Max. applied load	Calculated max. applied moment	Predicted ultimate sectional capacity
Concept 1, continuous span	420 kip	1272 ft.-kip	2256 ft.-kip for Span 1 2544 ft.-kip for Span 2
Concept 1, Span 1, semi-simple span	420 kip	2158 ft.-kip	2256 ft.-kip
Concept 1, Span 2, semi-simple span	420 kip	2158 ft.-kip	2544 ft.-kip
Concept 2	458 kip	2450 ft.-kip	2313 ft.-kip

In all cases, ultimate failure of the specimens was not observed to be imminent. Loading was conducted at a displacement controlled rate; no reduction in applied load was observed during the tests, suggesting that composite action was maintained throughout the applied load range. In addition, visual inspections of the CIP-precast interface did not reveal any indication of slippage between the CIP and precast section on the external faces.

A composite section should experience linearly varying strains through the full depth of the section, while loss of composite action would be evinced if distinct curvatures were observed in each section

150

(i.e., the CIP top section and the precast bottom section). Therefore, an analysis of the longitudinal curvatures in each section was conducted.

The Concept 2 laboratory bridge specimen was well instrumented for the calculation of longitudinal curvature. At least three longitudinally oriented instruments were included in both the precast and CIP concrete. Good linear correlation through the section was observed among the instruments used to calculate the curvature at most locations. The change in curvature, measured between an applied load of 0 kips and 458 kips, and correlation coefficients, among other quantities determined during the ultimate test on the Concept 2 laboratory bridge are summarized in Table 5.3.10.

Table 5.3.10: Longitudinal curvature and relevant values during ultimate loading on Concept 2 laboratory bridge specimen

Location[1]	Number of Gages	Load [kip]	Curvature [1/in.]	NA Depth [in.]	R^2
N-Mid-40"	7	458	-454.5	14.0	0.991
N-Mid-20"	6	458	-341.3	12.8	0.977
N-Mid-3"	6	458	-476.2	14.3	0.930
S-Mid-20"	6	458	-416.7	12.9	0.975
N-Qtr-20"	6	458	-201.0	13.0	0.995
N-Qtr-40"	7	458	-196.1	13.0	0.981
N-Qtr-3"	5	458	-213.2	12.4	0.954

[1]The instrumentation location was designated as follows: North/South precast panel – Mid-span/Quarter point – Distance to gage set from precast joint

As an example, the longitudinal curvature measured at midspan of the north panel, 20 in. from the precast joint (i.e., N-Mid-20") is shown in Figure 5.3.14. The curvature measured at this location reasonably represents the results of the ultimate load test at all locations. The linear trend line appears to provide a good fit to the instrumentation both above and below a vertical depth of 12 in. measured from the bottom of the precast, the location of the top of the precast web-CIP interface, suggesting that composite action was maintained at the applied load of 458 kips. The measured curvature was calculated based on the linear trend line, where the curvature was the reciprocal of the slope of the line.
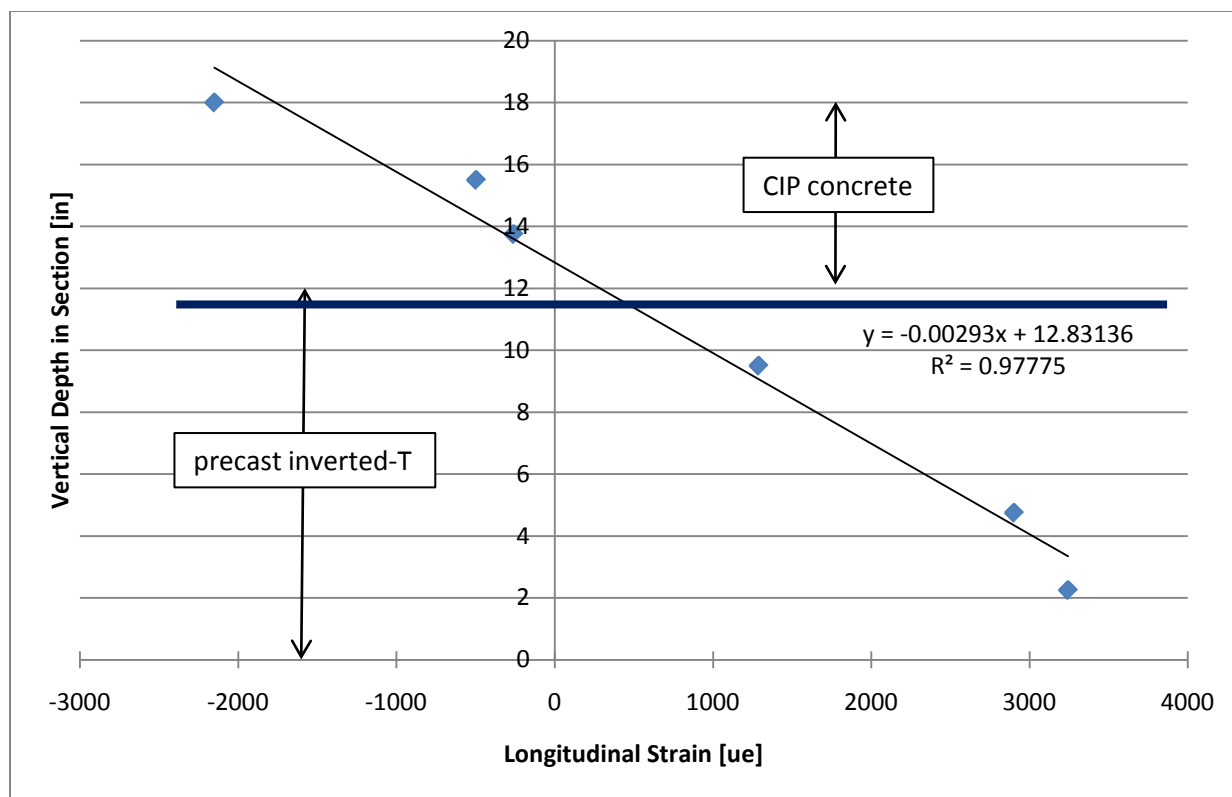
Figure 5.3.14: Longitudinal strains measured through the section depth at midspan of north panel 20 in. from precast joint with 458 kip applied Load in Concept 2 laboratory bridge specimen

The compression force developed in the section was calculated by integrating the stress profile using the measured strain profile and assuming the modified Kent and Park (Park et al., 1982) concrete stress-strain model with a nominal concrete compressive strength, f'_c, of 5865 psi, which was equal to 85 percent of the measured concrete compressive strength of 6.9 ksi, and $\varepsilon_0 = 0.002$. Eighty-five percent of the measured concrete compressive cylinder strength was utilized to provide an estimate of the unconfined concrete compressive strength in a structural member. Integrating the compressive stress above the neutral axis and multiplying by the deck width, the total compressive stress developed in the Concept 2 laboratory bridge was 2134 kips. The reduction in compressive force transferred through the composite surface due to the concrete in tension must also be considered. Using the measured modulus of rupture, the uncracked concrete in tension was assumed to provide a tensile force of 46 kips in the CIP. Therefore, the compressive force transferred between the CIP and precast concrete was 2088 kips. Dividing the total force by the width of the deck, including the area above the longitudinal trough, and half of the center to center of bearing span length, the measured stress transferred through the unreinforced composite surface was determined to be 135 psi. Because the unreinforced Concept 2 laboratory bridge span provided good horizontal shear capacity throughout loading to the maximum load of the actuators, which was nearly the ultimate capacity of the section, it was recommended that AASHTO Article 5.8.4 be modified to allow sections unreinforced for horizontal shear to develop a nominal horizontal shear strength of up to 135 psi.

152

5.4. Destructive Testing of Large-Scale Laboratory Specimens

At the conclusion of the tests, cores were taken at locations of interest through the laboratory bridge specimens to investigate the location and extent of cracks that were believed to have developed during the tests based on the strain measurements. The information obtained from the cores is summarized in Section 5.4.1. The specimens were also sliced into segments small enough such that they could be removed from the laboratory with the overhead crane. The information obtained from a visual inspection of the sliced surfaces to determine the extent of any residual cracking is summarized in Section 5.4.2.

5.4.1. Inspection of Cores taken from Laboratory Bridge Specimens

At the conclusion of laboratory testing a series of cores were removed from both the Concept 1 and Concept 2 laboratory bridges to provide a means of physical investigation of the cracking behavior near the precast joint. The cores were utilized to document a maximum crack width and length in each core, the magnitude of the crack width was dependent on the maximum loading and specific boundary conditions in each span, and therefore would not be directly comparable between spans.

The diameter of cores ranged between 2, 3, and 4 in. Each of the core specimens was examined both with the naked eye and the aid of an Olympus SZX12 stereo-microscope to find cracks on the core surface. The level of magnification used to examine the cores ranged between 2.1X to 27X, which was the full capacity of the microscope. All cracking that was identified in each core was tabulated, regardless of the size or anticipated origin. The observed crack widths were documented in classification categories, defined in Table 5.4.1. The vertical depth of the cracking identified in the cores was referenced from the line created by the horizontal precast flange-CIP interface, as shown in Figure 5.4.1. A complete description of the characteristics and measured values obtained from each core sample is tabulated in Appendix G.

Table 5.4.1: Crack width classification categories for analysis of core specimens

Crack Classification	Crack Width (W)
0.002	W < 0.002 in.
A	0.002 in. ≤ W < 0.008 in.
B	0.008 in. ≤ W < 0.023 in.
C	0.023 in. ≤ W < 0.200 in.
D	W ≥ 0.200 in.
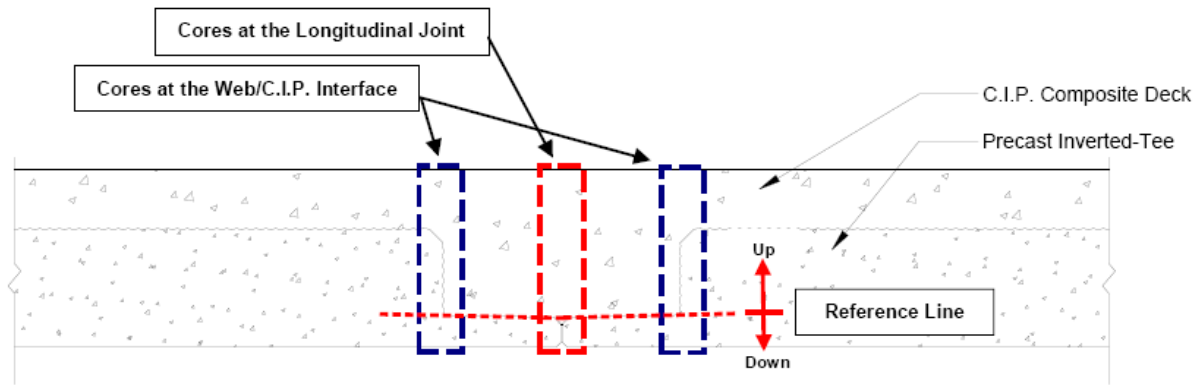
Figure 5.4.1: Location of reference line for measurement of vertical location of cracking in core specimens

Core samples were extracted from both spans of the Concept 1 large-scale laboratory bridge. A total of five cores were removed from Span 1, while four cores were extracted from Span 2. All the cores from the Concept 1 laboratory bridge specimen were nominally located directly over the longitudinal precast joint (corresponding to the red core outline in Figure 5.4.1), at various locations along the length of each span. Table 5.4.2 shows the core description and location, as well as observed crack width and depth. The specimen identification consists of the bridge concept number-span number-core number. The x-coordinate of the core location corresponds to the coordinate system with the origin at the center of the pier, in accordance with the locations of the instrumentation; a negative x-coordinate corresponds to Span 1; while a positive x-coordinate corresponds with Span 2. After the first core was removed from Span 1 of the Concept 1 laboratory bridge, a saw cut was completed along the entire length of the bridge near the precast joint, after which specimens C1-S1-2 through C1-S1-5 were removed from the span. These cores therefore consisted of two half cylinders. The thickness of the cylinder removed due to the saw cut was approximately 1/8 in. wide through the length of the core near where the precast joint was located. Because of this, evidence of cracking in these specimens may have been removed from the saw cut, however the only core from the Concept 1 laboratory bridge where a crack was clearly measured was in a core specimen that had been cut. The other potential cracks were too small to be seen even with the magnification of the microscope.

Table 5.4.2: Summary of maximum height and width of cracks measured in core specimens from the Concept 1 laboratory specimen

Specimen	x-Coordinate of Core (in.)	Saw Cut?	Diameter of Core (in.)	Maximum height of crack[1] (in.)	Maximum width of crack[2] (in.)
C1-S1-1	-194.5	No	1.75	Undefined[4]	Undefined
C1-S1-2	-26	Yes	2.75	NO[3]	NO
C1-S1-3	-134	Yes	2.75	NO	NO
C1-S1-4	-192	Yes	2.75	NO	NO
C1-S1-5	-197.5	Yes	2.75	2.75 (up)	A
C1-S2-1	74	No	1.75	NO	NO
C1-S2-2	146	No	1.75	NO	NO
C1-S2-3	195.5	No	1.75	NO	NO
C1-S2-4	198	No	1.75	NO	NO

[1]The height of crack was measured from the reference line, defined in Figure 5.4.1; only "upward" values are recorded in this table

[2]The width of crack was documented by crack classification, as defined in Table 5.4.1

[3]"NO" represents "No reflective cracks observed"

[4] "Undefined" represents that the reflective crack was continuous with a shrinkage crack from the deck surface, therefore beginning and end points were undefined

The only evidence of internal cracking observed via the investigation of the core samples was in specimen C1-S1-5, which was in the outer quarter of Span 1, despite clear evidence from the instrumentation that cracking occurred at several other locations. Strain increases as large as 303 $\mu\varepsilon$ and 233 $\mu\varepsilon$ were measured in Spans 1 and 2, respectively, via the concrete embedment resistive gages under loading. Considering the 4.7 in. gage length, a maximum associated crack width of 0.0011 and 0.0014 inches might be expected in all the core samples except C1-S1-2 because of the proximity to the continuous pier. While the expected crack widths of approximately 0.001 inches were smaller than the 0.002 inch minimum reading on the crack gage, the use of the microscope allowed for significantly smaller cracks to be identified, especially those on the order of 0.001 inches. From the forensic examination, it appears that the cracks may have closed upon unloading.

The Concept 2 laboratory bridge was similarly cored at the conclusion of testing. In this case, eight cores were removed from the specimen, four from each quarter point. At each quarter point, two cores were removed from above the joint, 4 in. apart, while the remaining two were centered over the vertical precast webs. Cores were taken from the web areas to document any cracks or separation at the CIP-precast web interface at those locations, which should be avoided because the cage reinforcement provides no benefit near the vertical web interfaces. Table 5.4.3 includes a summary of the measured crack widths and depths in the cores from the Concept 2 specimen. No saw cutting was present in the Concept 2 laboratory bridge specimen prior to the removal of the core samples. The measured core locations in the Concept 2 laboratory bridge corresponded with the origin and sign convention utilized for the placement of the instrumentation.

155

Table 5.4.3: Summary of maximum height and width of cracks measured in core specimens from the Concept 2 laboratory specimen

Specimen	x-Coordinate of Core (in.)	y- Coordinate of Core (in.)	Diameter of Core (in.)	Maximum height of crack[1] (in.)	Maximum width of crack[2] (in.)
C2-S1-1	193	0	3.75	NO[3]	NO
C2-S1-2	189	0	3.75	2.25	0.003
C2-S1-3	193	+12	3.75	3.5	A
C2-S1-4	193	-12	3.75	NO	NO
C2-S1-5	76	0	3.75	NO	NO
C2-S1-6	80	0	3.75	NO	NO
C2-S1-7	76	+12	3.75	NO	NO
C2-S1-8	76	-12	3.75	NO	NO

[1]The height of crack was measured from the reference line, defined in Figure 5.4.1; only "upward" values are recorded in this table
[2]The width of crack was documented by crack classification, as defined in Table 5.4.1
[3]"NO" represents "No reflective cracks observed"

Reflective cracking was observed in one of the four cores located over the joint in the Concept 2 laboratory bridge specimen, and was located in the east half span (C2-S1-2). In addition, a vertical crack was also observed at the vertical CIP-precast web interface (C2-S1-3), also located in the east half span. It is unclear if the discontinuity observed at this location was truly a crack, or was separation of the precast web and CIP concrete due to poor bond, or was simply an illusion due to the interface between the two types of concrete, however it was expected that cracking or separation at the vertical web interface would relieve transverse stresses at the longitudinal joint, which would likely hinder crack growth over the joint, however cracking was measured extensively near the east quarter point of the span, suggesting that the vertical web face cracking was unlikely. Furthermore, the fact that no cracking or separation of vertical CIP-precast web interface at the west quarter point suggested that it was unlikely that the lack of observed cracking indicated by the instrumentation over the joint in the west half span of the Concept 2 specimen was due to cracking at the vertical web interface and subsequent relief of transverse stresses near the longitudinal precast joint.

The largest transverse strain measured during load testing on the Concept 2 laboratory bridge was approximately 256 με, measured near midspan, which over the 4.7 in. gage length of the concrete embedment resistive gage would correspond to a maximum crack width of approximately 0.0014. This was a strain measured under loading to simulate the environmental effects. A likely reason that the cracks were not identifiable with the microscope was because the cores were removed from the bridge upon unloading and examined under no load conditions.

156

5.4.2. Visual Inspection of Internal Surfaces after Sectioning the Laboratory Bridge Specimens by Means of Saw Cutting

Capacity constraints of the overhead crane system present in the University of Minnesota Structures Laboratory necessitated that both the Concept 1 and Concept 2 laboratory specimens be split into segments of no more than 30,000 lbs in total weight for removal. This created an opportunity to visually inspect the internal cut faces of the specimens for signs of cracking. For this reason, the laboratory bridge specimens were segmented such that the locations of the cuts were near locations of expected cracking, as determined via the data analyses.

The two span Concept 1 laboratory bridge specimen was cut into a total of eight sections, as shown in Figure 5.4.2.

NORTH
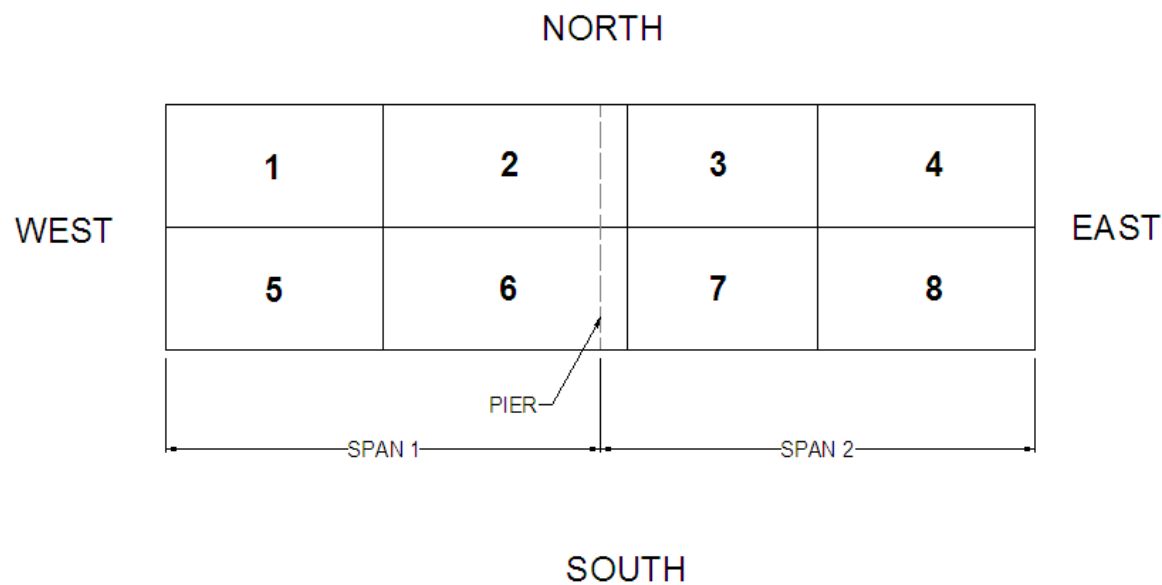
Figure 5.4.2: Concept 1 laboratory bridge specimen partitioning for saw cutting procedure

The longitudinal saw cut, which ran the length of the Concept 1 laboratory bridge specimen was nominally located directly through the precast joint, though drift of the saw during the cutting process caused the cut to vary between +/- 1 in. to either side of the precast joint. Unfortunately, the location of the cut line near the precast joint allowed for the possibility of the saw kerf to remove the evidence of reflective cracking in the section.

No signs of reflective cracking were observed on any of the cut faces in the Concept 1 laboratory bridge specimen, despite the use of a wetting and drying process in the region where reflective cracking was expected (i.e., the precast trough region) in which water was sprayed on the surface and allowed to air dry. This process was expected to highlight small cracks, where the ingress of water into the cracks would emphasize any cracking on the cut surfaces.

The vertical and horizontal interfaces between the precast concrete and CIP concrete however tended to feature unique characteristics. In the case of the horizontal precast – CIP interface, delamination of the PC flanges from the CIP concrete was observed, as shown in Figure 5.4.3. This documented evidence

157

of delamination at the horizontal interface was observed in all cross-sectional cuts, regardless of the presence of the smooth or roughened precast flange. No evidence of delamination or cracking was observed at the vertical PC web interface on any of the cut surfaces of the Concept 1 laboratory bridge.
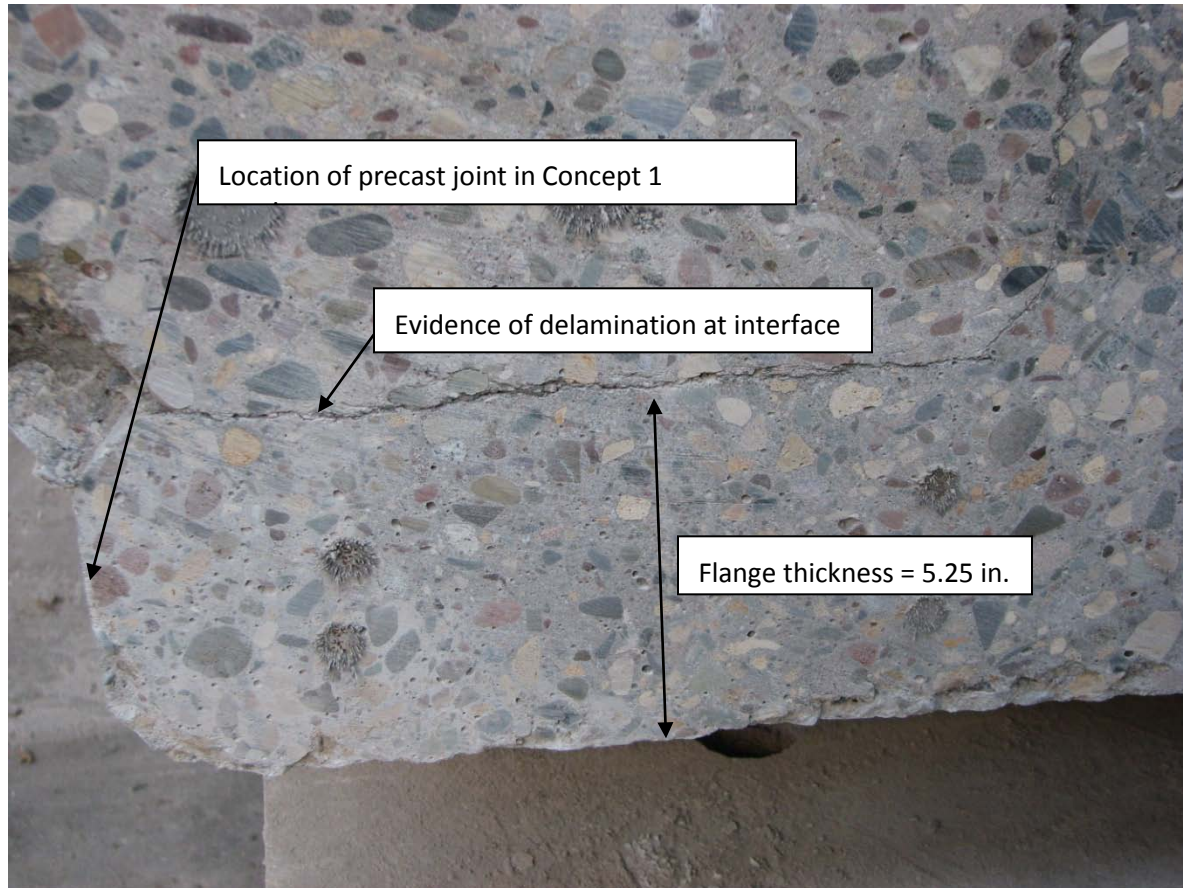
Figure 5.4.3: Delamination at the PC – CIP interface in the East transverse face of section number 7 of the Concept 1 Laboratory bridge specimen

The Concept 2 laboratory bridge specimen was similarly sectioned to accommodate removal from the laboratory. The cutting plan for this specimen included a total of three transverse cuts, at each quarter point of the span. Recall that the quarter points of the span coincided with the locations of the loading during the tests. The cutting plan and numbering convention is shown in Figure 5.4.4.

158
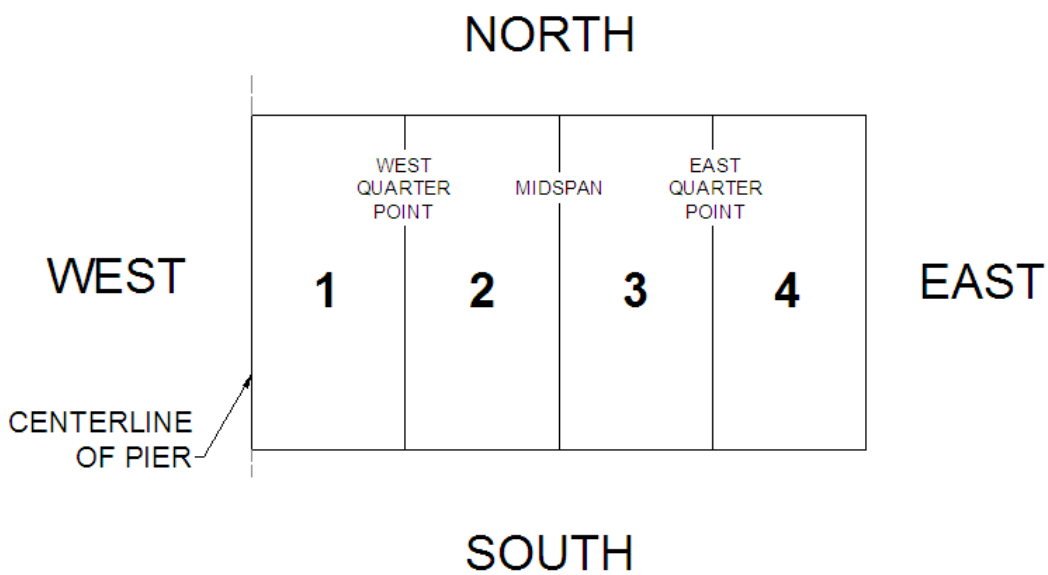
Figure 5.4.4: Concept 2 laboratory bridge specimen partitioning for saw cutting procedure

Evidence of reflective cracking was not observed in any of the cross sections in the Concept 2 laboratory bridge specimen. As observed in the Concept 1 laboratory bridge specimen, some delamination of the horizontal PC – CIP interface was observed at midspan on both the west face of panel 3 and the east face of panel 2, as illustrated in Figure 5.4.5. In addition, a diagonal crack was observed on the east face of panel 2 originating near the precast flange interface and propagating towards the corner of the precast section, as shown in Figures 5.4.6 and 5.4.7. The crack was measured to be approximately 0.006 in. As discussed in Section 5.4, cracking was observed in the east quarter of the Concept 2 laboratory bridge north of the joint via the core analysis, though was not detected via the analysis of the cut faces at the corresponding location.
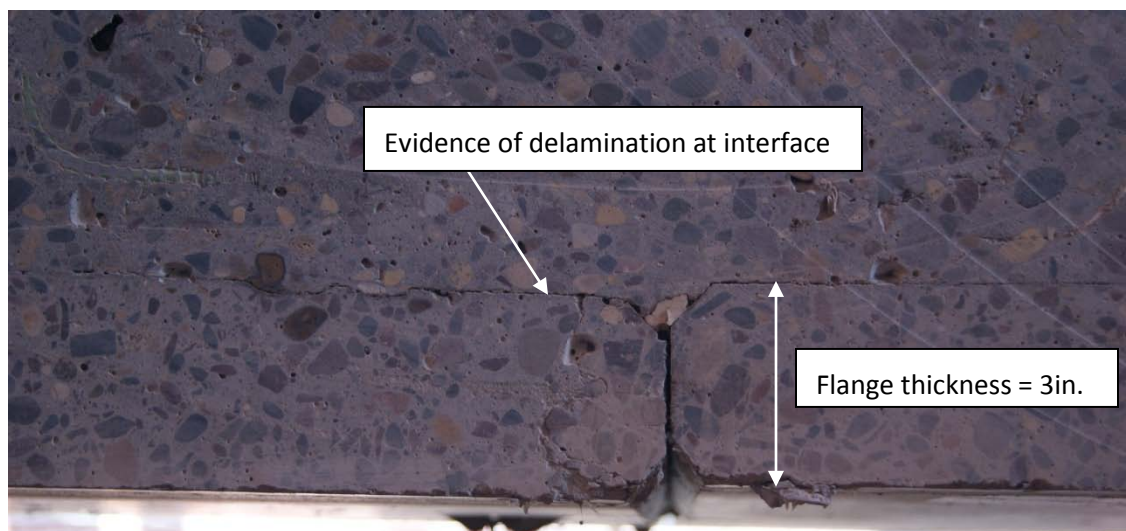
Figure 5.4.5: Delamination at the PC – CIP interface observed on the West face of section number 3 of the Concept 2 laboratory bridge specimen

159
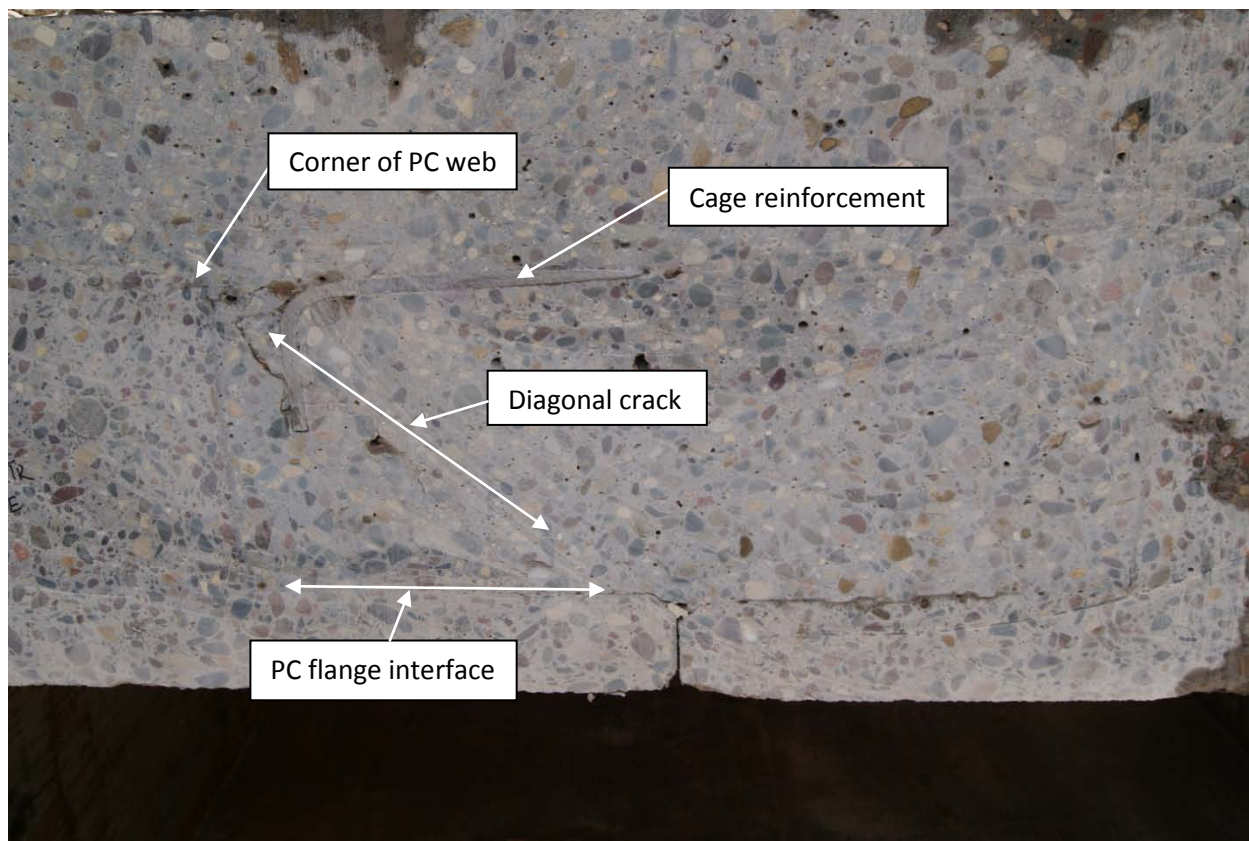
Figure 5.4.6: Evidence of diagonal cracking in the trough region on the east face of panel 2 in the Concept 2 laboratory bridge
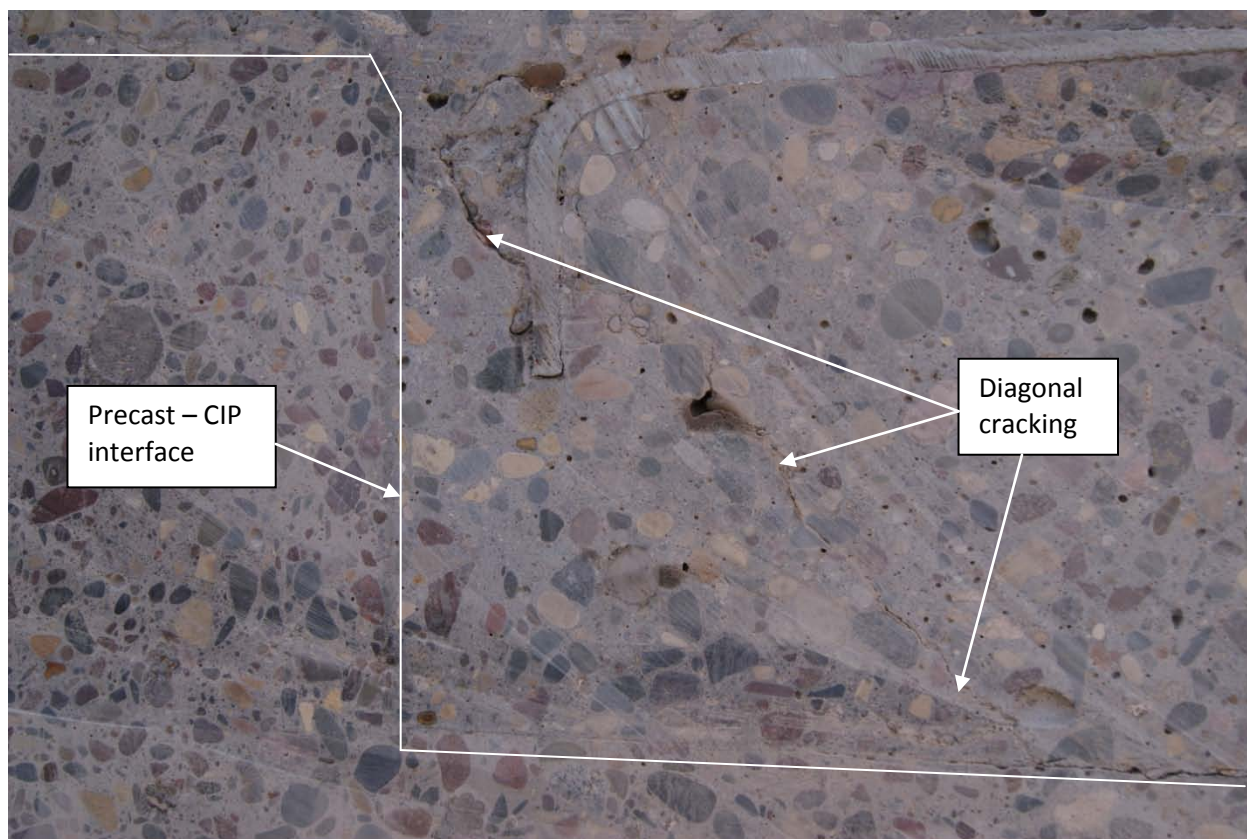
Figure 5.4.7: Close up view of diagonal crack identified on east face of panel 2 in the Concept 2 laboratory bridge

Chapter 6 PCSSS: Subassemblage Investigation of Crack Control Reinforcement

6.0   Introduction

Seven specimens were designed to investigate the effect of spacing, size, and placement of transverse reinforcement on the development and propagation of reflective cracking in the precast composite slab span system. This chapter describes the design and cracking behavior of these seven subassemblage specimens. Each specimen in this section is generally referenced by the specimen number and representative design parameter, i.e., Specimen 1, the first control specimen, is commonly referenced as: SSMBLG1-Control1.

6.1.   Selection and Design of Laboratory Subassemblage Specimens

Each subassemblage specimen was selected to investigate a single attribute (e.g., spacing of transverse reinforcement, bar size, absence of reinforcement cage, specimen depth) that was expected to influence the crack control performance of the system. The specimens were designed as simply-supported panel elements with a 10 ft. span with the precast joint located at midspan, as illustrated in Figure 6.1.1. The widths of the specimens (i.e., in the direction parallel to the precast joint) ranged from 62.75 to 67.25 in. and was dependent on the transverse reinforcement spacing. Each specimen was designed such that the center of the transverse reinforcement closest to one face was located a distance of 3.5 in. from that face, defined as the origin face, except for in SSMBLG6-Frosch where the center of the hoop reinforcement was located 3.25 in. from the face. The specimen width was selected such that the opposite face, designated as the end face, was located a distance of half of the transverse reinforcement spacing from the center of the nearest transverse hooked pair, or in the case of SSMBLG6-Frosch it was the distance from the end face to the center of the nearest cage hoop. This configuration enabled the investigation of crack width both at a constant distance from the interior reinforcement, as well as an estimate at the maximum crack width, which was expected to occur at midpoint between adjacent bars.

 The specimen supports were parallel to the longitudinal joint between the precast elements, rather than transverse to the joint, in order to flexurally crack the specimens along the joint. It was found during the testing of the first specimen, that the stiff flanges of the precast section rotated and caused delamination between the precast flange and CIP concrete, resulting in propagation of a crack at the precast-CIP concrete interface. The test setup was modified to clamp the precast flanges to the CIP concrete a distance of approximately 1.25 in. from the longitudinal joint in both directions. This test setup with the clamping system was believed to more realistically emulate the field conditions because in a bridge system, the pier supports are normal to the longitudinal joint and would constrain the relative rotation between the precast flange tips and the CIP at the ends of the span.

 The selection of the reinforcement details for each specimen was completed using a range of sources, primarily Frosch (2006), AASHTO (2010), and ACI (318-08). The design parameters of each subassemblage specimen are summarized in Table 6.1.1. The reinforcement ratio shown in Table 6.1.1 is the reinforcement ratio defined for crack control. This value accounts for all reinforcement traversing the longitudinal joint located near the bottom of the trough area near the precast flanges, which accounts for contribution from both the transverse hooked bars and the reinforcing cage. The reinforcement ratios for load transfer and crack control are discussed in detail in Section 5.1.

The subassemblage specimens were designed to provide insight into the relative performance of variations in the transverse reinforcement details for crack control and load transfer. For this reason, the specimen designs were limited to the transverse reinforcement selection. The primary depth of the precast members used for the subassemblage specimens was selected to be 12 in. to maintain consistency with the bridge specimens. The depth of the deck was minimized in an effort to reduce the transverse cracking moment of the specimens so that yielding of the transverse reinforcement immediately at cracking could be avoided. A minimum deck thickness of 2 in. was used to provide concrete cover over the deck reinforcement placed to resist potential shrinkage cracking at the surface. The reinforcement to control shrinkage cracking consisted of a total of five No. 3 bars, oriented perpendicular to the precast joint, in the deck region of each of specimen, in addition to eight No. 3 bars oriented parallel to the precast joint. The deck reinforcement was placed a clear distance of 1/4 in. from the precast members in all specimens except for SSMBLG3-HighBars, where the deck reinforcement was placed a clear distance of 3/4 in., due to a localized increase in the section depth away from the joint, which is discussed in more detail in Section 6.1.3. A photograph illustrating the deck reinforcement is shown in Figure 6.1.2.

Each subassemblage specimen was designed to include four sets of transverse hooked bars to ensure at least two sets of interior transverse hooked bars were present, while the cage reinforcement design and placement was varied among the specimens. The specific design parameters of each subassemblage specimen are described in the following sections. The design and section calculations for each of the subassemblage specimens are given in Appendix H, which utilize the measured material properties, as documented in Section 6.4. Two spatial relationships were used throughout the construction and testing of the subassemblage specimens. The North direction was defined to originate from the origin face and point in the direction of the precast joint. In addition, a three-dimensional grid, with the origin located at the bottom of the section, at the precast joint, on the origin face, was used. The x-direction corresponded to the north direction and pointed along the direction of the precast joint and was therefore always positive. The y- and z- directions followed the right hand rule, thus y pointed in the west direction, with zero at the precast joint, and z pointed upwards, with zero at the bottom of the section.

163

Table 6.1.1: Subassemblage specimen design details

Specimen Identification	Width [in]	Depth [in]	Transverse Bars (Load Trans.)			Cage (Crack Control)			Max Spacing[2]	R/F Ratio[3]
			Size	Spacing	Depth[1]	Presence	Size	Spacing		ρ_{cr}
SSMBLG1-Control1	62.75	14	#4	18 in. OC	4 1/2 in.	Cage	#3	18 in. OC	9	0.0031
SSMBLG2-NoCage	67.25	14	#4	18 in. OC	4 1/2 in.	No Cage	0	0	18	0.0025
SSMBLG3-HighBars	62.75	14	#4	18 in. OC	7 in.	Cage	#3	18 in. OC	9	0.0031
SSMBLG4-Deep	62.75	18	#4	18 in. OC	4 1/2 in.	Cage	#3	18 in. OC	9	0.0022
SSMBLG5-No.6Bars	62.75	14	#6	18 in. OC	4 1/2 in.	Cage	#3	18 in. OC	9	0.0061
SSMBLG6-Frosch	64	14	#4	18 in. OC	4 1/2 in.	Cage	#3	4.5 in. OC	4.5	0.0052
SSMBLG7-Control2	62.75	14	#4	18 in. OC	4 1/2 in.	Cage	#3	18 in. OC	9	0.0031

[1]The depth of the transverse reinforcement was taken from the bottom of the precast section to the center of the reinforcement
[2]The maximum spacing was the maximum nominal distance between reinforcement traversing the longitudinal joint, regardless of type (i.e., transverse hooked bars or cage)
[3]The reinforcement ratio shown is that corresponding to crack control, see above and Section 5.1

164
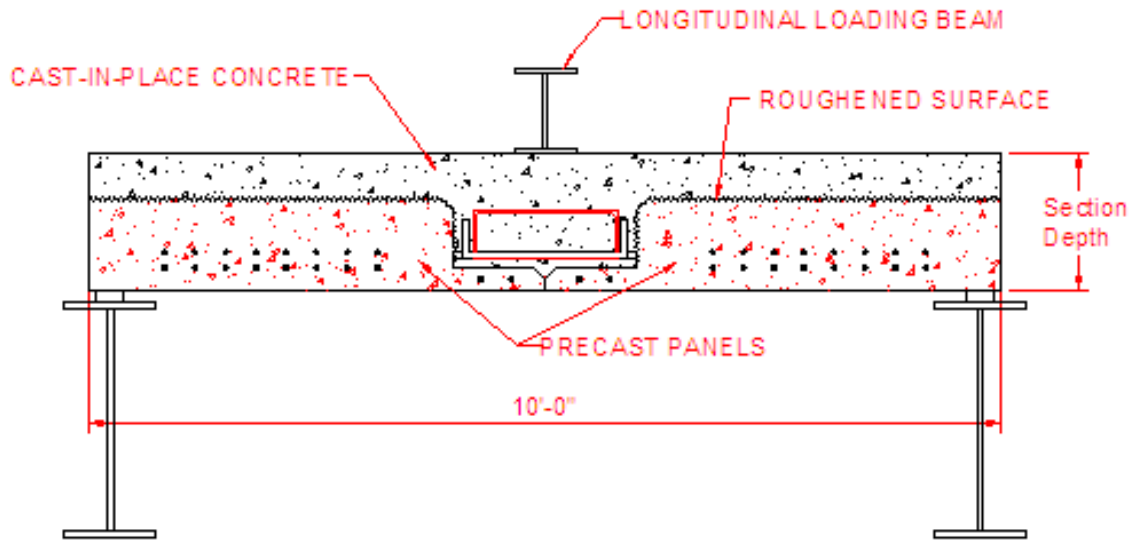
(a) Elevation view of subassemblage specimens
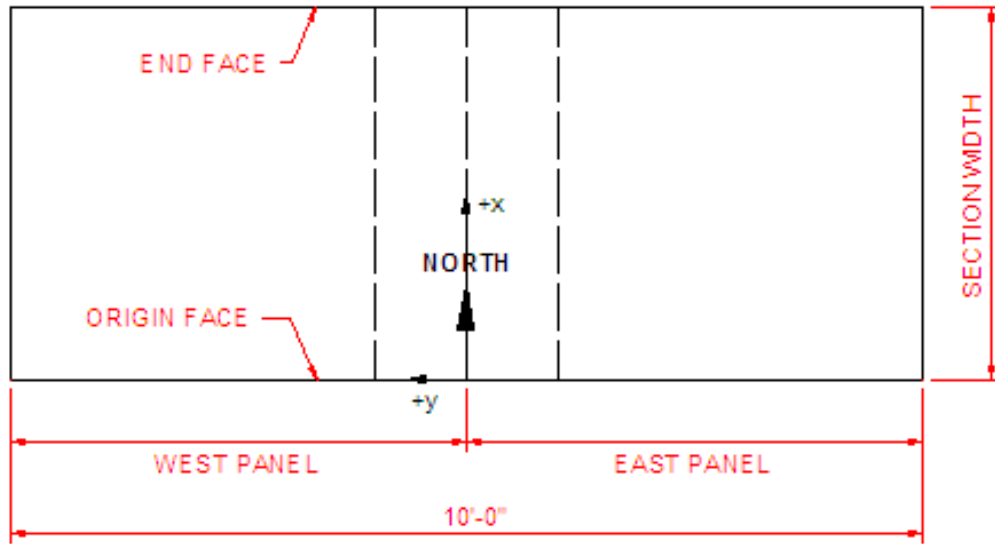
(b) Plan view and directional orientation of subassembalge specimens

Figure 6.1.1: Elevation and plan views of subassemblage specimen. The *x*-axis was aligned along the North direction and corresponded with the longitudinal joint. Positive *x* pointed North, positive *y* pointed West, positive *z*, was vertically upward

165
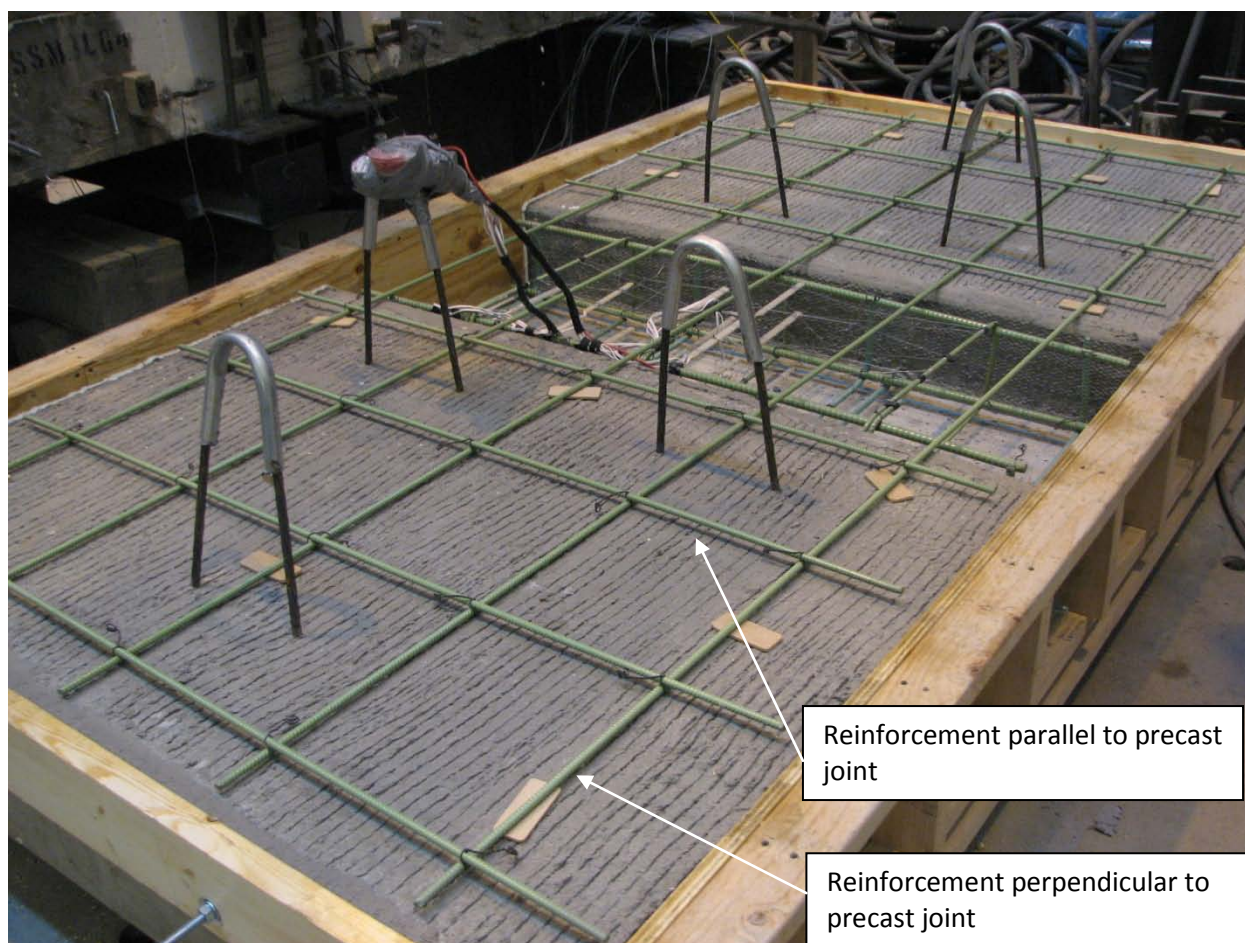
Figure 6.1.2: Photograph of deck reinforcement utilized for the subassemblage specimens

6.1.1. Subassemblage 1 – Control Specimen 1

The first subassemblage was deemed the control specimen because it had detailing similar to that of the transverse hooked reinforcement in the Concept 2 laboratory bridge specimen. The control specimen had a reinforcement ratio for transverse load transfer of 0.0010, while the cage and additional transverse hooked bar provided a reinforcement ratio of 0.0031 for crack control. This crack control reinforcement ratio was considered a practical lower bound value for the system when constructed with a cage, as constructability issues may arise if reinforcement smaller than No. 4 transverse hooked bars and No. 3 cage hoops are selected. The maximum spacing between transverse reinforcement was reduced to 9 in. by offsetting the cage reinforcement from the transverse hooked bars. The reinforcement layout for SSMBLG1-Control1 is shown in Figure 6.1.3. The cage reinforcement is shown in green. The portion of the transverse hooked bars protruding into the CIP concrete is shown in blue. For simplicity, the part of the hooked bars embedded in the precast elements is not shown.

166
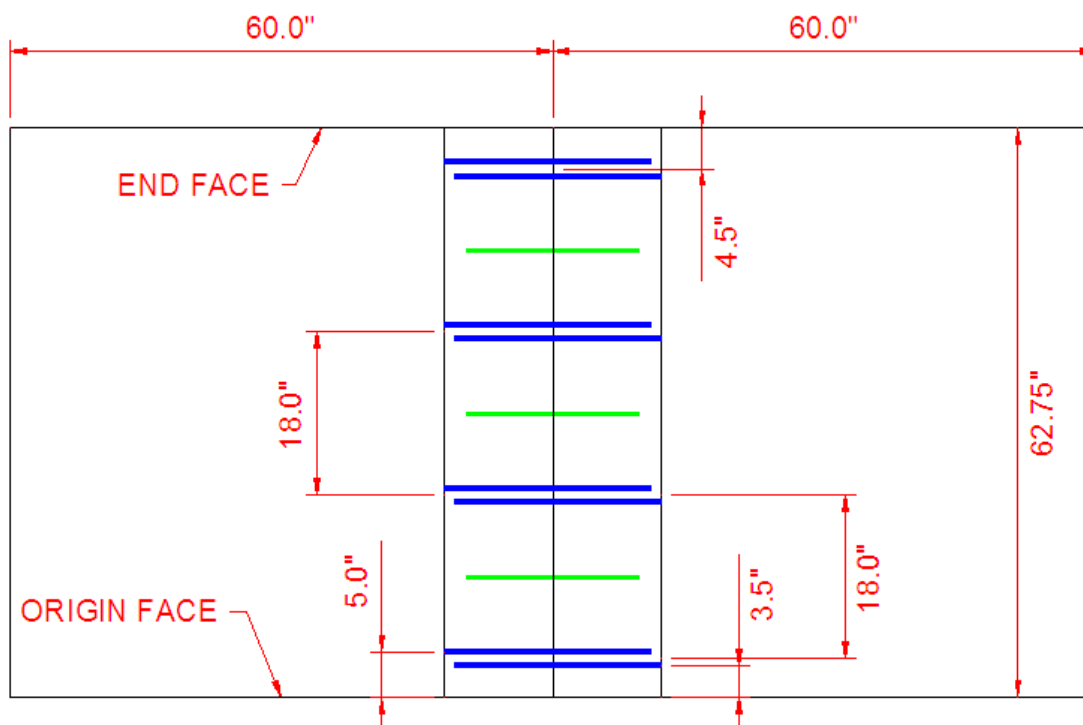
Figure 6.1.3: Layout for SSMBLG1-Control1, SSMBLG3-HighBars, SSMBLG4-Deep, SSMBLG5-No.6Bars, and SSMBLG7-Control2. Transverse hooked bars are shown in blue; cage reinforcement is shown in green

6.1.2. Subassemblage 2 – No Cage Reinforcement

The reinforcement cage was intended to provide additional reinforcement for reflective crack control above the longitudinal joint. In order to be able to evaluate the effectiveness of the presence of the cage with the test series, one of the specimens, SSMBLG2-NoCage, was designed without cage reinforcement. The overall width of the specimen was increased to 67.25 in. to allow for the end transverse hooked bar to be half of the maximum spacing (9 in.) away from the end face. The reinforcement ratio for transverse load transfer was equal to 0.0010, while the reinforcement ratio for crack control was equal to 0.0025, which corresponded to the lower bound reinforcement ratio for crack control investigated during the study. The absence of the reinforcement cage increased the maximum spacing to 18 in. The specimen layout is shown in Figure 6.1.4.

167
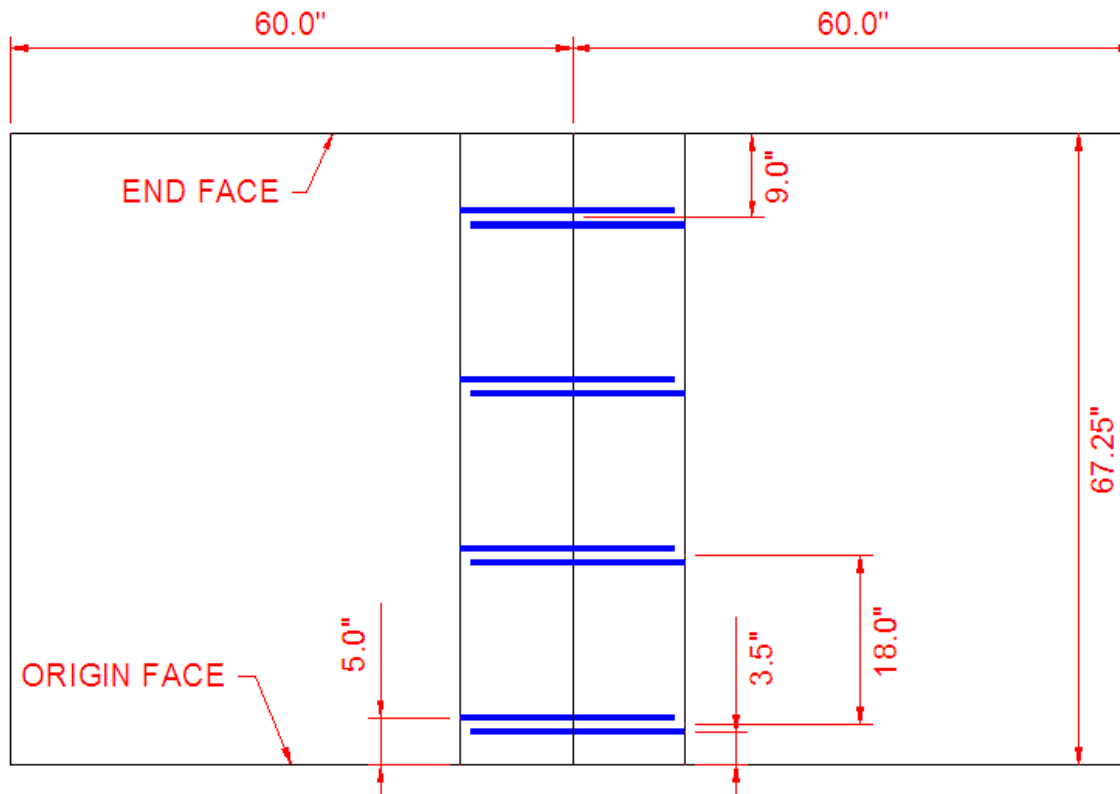
Figure 6.1.4: Layout for SSMBLG2-NoCage. Transverse hooked bars are shown in blue

6.1.3. Subassemblage 3 – Increased Distance Between Transverse Hooks and Precast Flange

The third subassemblage specimen was designed with the centroid of the transverse hooked bars located higher in the section than for the other specimens. In SSMBLG3-HighBars, the reinforcement was located 7 in. from the bottom of the section, which placed the hooked bars 55 percent higher than those in the other specimens. The proximity of the transverse hooked bars to the precast flange was expected to alter the performance of the system in two primary ways. The transverse moment of inertia of the cracked section decreased as the distance between the compression fiber and the reinforcement was decreased. The reduced moment of inertia of SSMBLG3-HighBars was expected to increase the curvature, and subsequently the stress demands on the transverse reinforcement of the section relative to the control specimen. Secondly, the lower in the section that the transverse reinforcement intercepts the reflective crack, the more effective that reinforcement was expected to be in controlling the crack. As a consequence, it was expected that SSMBLG3-HighBars would be less effective in controlling the crack than the control specimen. The specimen layout for SSMBLG3-HighBars was identical to that shown in Figure 6.1.3 for the control specimen. The only difference was the vertical position of the transverse hooked bars and cage.

Because SSMBLG3-HighBars was constructed and tested first, and the capability of the 2 in. deep deck to develop adequate bond for the shrinkage reinforcement used in the deck was unknown, this specimen was constructed with an increased section depth away from the precast joint. The depth of the section near the joint was maintained at 14 in., and increased to 15-½ in. starting at 15 in. from the joint in both directions.

168

An elevation view of SSMBLG3-HighBars with the increased depth of the deck is shown in Figure 6.1.5. The reinforcement ratios for crack control and load transfer were equal to 0.0031 and 0.0010, respectively.

Figure 6.1.5: Elevation view of SSMBLG3-HighBars and increased deck depth to provide additional cover for the shrinkage reinforcement in the deck

As previously noted, SSMBLG3-HighBars was tested first, and delamination of the precast-CIP interface was observed early in the test, before cracking was observed near the precast joint. Though subsequent use of a clamping assembly was anticipated to better emulate the expected restraint of a real structure, the presence of delamination at those locations greatly influenced the behavior near the precast joint, and subsequently, data collected during testing on this section is not considered to be reliable, and therefore is not included in the analysis of the data from the remaining specimens. Because little information was expected to be learned from the specimen after delamination of the joint, SSMBLG3-HighBars was utilized as a general test specimen to investigation the behavior of the overall subassemblage concept in the load frame. Therefore, the specimen was loaded in a wide range of sequences and load levels, so much so that the specimen failed by fracturing of the transverse hooks near the CIP - precast web interface at an applied load of approximately 111 percent of the predicted cracking load, or 32 kips. The specimen after failure is shown in Figure 6.1.6.

169
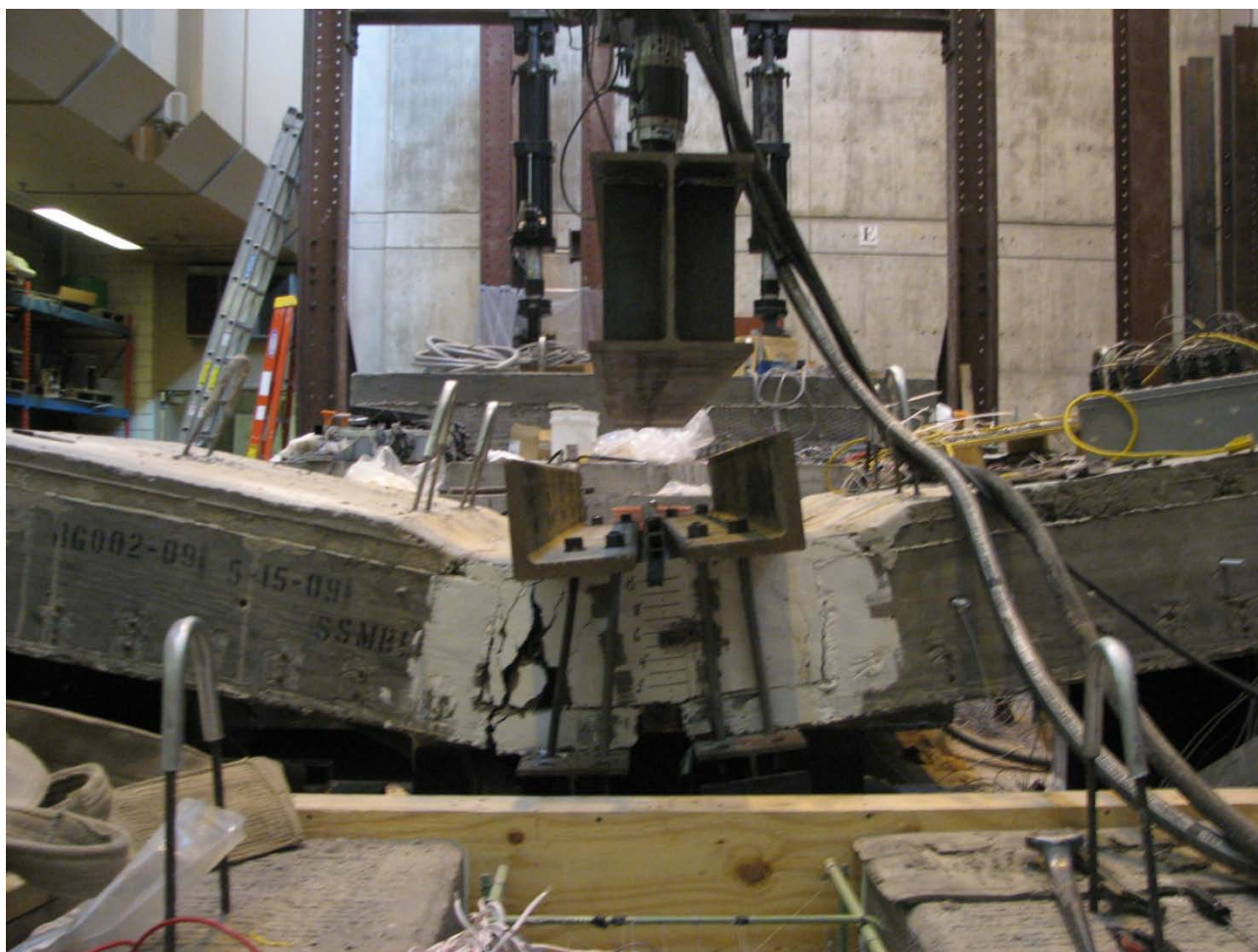
Figure 6.1.6: Failure of SSMBLG3-HighBars due to fracture of the transverse hooked reinforcement near the CIP - precast web interface

6.1.4. Subassemblage 4 – Increased Depth of Precast Section

As the span length of the PCSSS increases, the depth of the precast section also needs to increase in order to meet stress requirements at transfer and service. The 12 in. deep precast section was expected to perform well for moderate spans. The maximum practical span of the system was estimated to be approximately 65 ft., requiring a precast section depth of approximately 22 in. SSMBLG4-Deep was designed with an identical reinforcement plan as that of the control specimen, such that the effects of the deeper section could be investigated with an unchanged reinforcement design, although the depth of the cage stirrups was increased to the same relative depth as in the 12 in. deep precast sections (i.e., the top of the cage stirrup was aligned with the top of the precast web). The load transfer and crack control reinforcement ratios of the section were reduced to 0.0007 and 0.0012, respectively, due to the increase in the area of concrete considered in the calculation. The specimen layout of SSMBLG4-Deep was identical to that shown in Figure 6.1.3 for the control specimen.

170

6.1.5. Subassemblage 5 – Increased Transverse Hook Size

The size of the reinforcement used for transverse load transfer must be sufficient to provide adequate flexural capacity after cracking. Article 5.7.3.3.2 of the *2010 AASHTO LRFD Design Specification* requires that the nominal flexural moment capacity of the section be at least 120 percent of the cracking moment. No. 6 transverse hooked bars represented the minimum bar size that could satisfy this requirement while maintaining a hook spacing of 18 in. The specimen layout of SSMBLG5-No.6Bars was also identical to that shown in Figure 6.1.3. The cage remained unchanged from the control specimen; the only difference was that No. 6 hooked bars were used rather than No. 4 hooked bars. The reinforcement ratio for crack control and load transfer was 0.0033 and 0.0061, respectively, both of which represented the upper bounds investigated during the study.

6.1.6. Subassemblage 6 – Frosch Design Recommendations

Frosch et al. (2006) provided relevant design recommendations for crack control reinforcement in bridge decks which is summarized in Section 2.2. Frosch et al. provided guidelines for both the spacing and reinforcement ratio required for crack control via an experimental and numerical parametric study. The spacing limits were developed to provide sufficient reinforcement such that the crack widths would remain less than 0.021 in. The crack width selected represented a 1/3 increase in the maximum crack width of 0.016 in. suggested by ACI 224 (2001) for aesthetics. The authors stated that the increase in the selected maximum crack width was done due to the wide scatter generally observed in crack widths. The reinforcement spacing design proposed by Frosch et al. when grade 60 mild steel reinforcement was used is given in Eqn. (6.1.1).

$$\qquad -$$ (6.1.1)

where c_c is the depth of concrete cover from the extreme tensile fiber of the concrete to the center of reinforcement in inches.

The depth of cover, c_c, considered in Eqn. (6.1.1) was calculated to the bottom of the CIP concrete above the flanges, thus disregarding the depth of the precast flange. This was deemed a reasonable assumption because of the discontinuity between the precast flanges along the longitudinal joint where the flanges in the adjacent precast panels abutted. The precast flanges themselves were reinforced as part of the design of the precast inverted-T sections.

Frosch provided a recommended reinforcement ratio for crack control reinforcement, as given in Eqn. (6.1.2). The reinforcement ratio was developed to ensure that sufficient reinforcement is present upon the introduction of cracking such that all tensile loads can be transferred through the reinforcing bars.

$$-$$

$$\qquad -$$ (6.1.2)

where fc' is the specified concrete strength and f_y is the specified reinforcement yield strength.

With the depth of cover assumed to be 1.5 in., the maximum spacing was determined to be the 9 in. bound of Eqn. (6.1.1), and with grade 60 reinforcement and a 28-day concrete compressive strength of 4000 psi, the reinforcement ratio for crack control reinforcement was determined to be 0.0063 from Eqn. (6.1.2).

171

The reinforcement design for SSMBLG6-Frosch was selected such that the transverse reinforcement for load transfer (i.e., hooked bars protruding from the precast webs) was identical to that of the control specimen. Therefore, the cage reinforcement was modified to meet the above limits; however the cage bar size was maintained at No. 3 hoops to provide consistency among the specimens. The hoop spacing for the SSMBLG6-Frosch specimen was provided at 4.5 in. because an even multiple of 18 in. (i.e., the hook spacing) was desired, primarily to avoid interference between the cage and transverse hooked reinforcement, and a cage design requiring closer spacing, or spacing that caused intermittent interference between the cage and hooked bars, would be expensive and difficult to implement in the field. The 4.5 in. spacing was well within the maximum 9 in. spacing recommended by Frosch et al. (2008), but because of the design constraints associated with spacing the cage reinforcement to facilitate constructability, the reinforcement ratio for crack control provided in the SSMBLG6-Frosch specimen (i.e., 0.0052) was smaller than that strictly required by Frosch et al. (2008) (i.e., 0.0063 for Grade 60 steel and a concrete compressive strength of 4,000 psi). The specimen reinforcement ratio was considered sufficient to explore the increased benefit of the design recommendations provided by Frosch et al. (2008). The reinforcement ratio for load transfer was 0.0010. The specimen layout of SSMBLG6-Frosch is shown in Figure 6.1.7. It should be noted that the specimen SSMBLG5-No.6Bars had a reinforcement ratio (i.e., 0.0061) that was closer to that of the Frosch requirements.
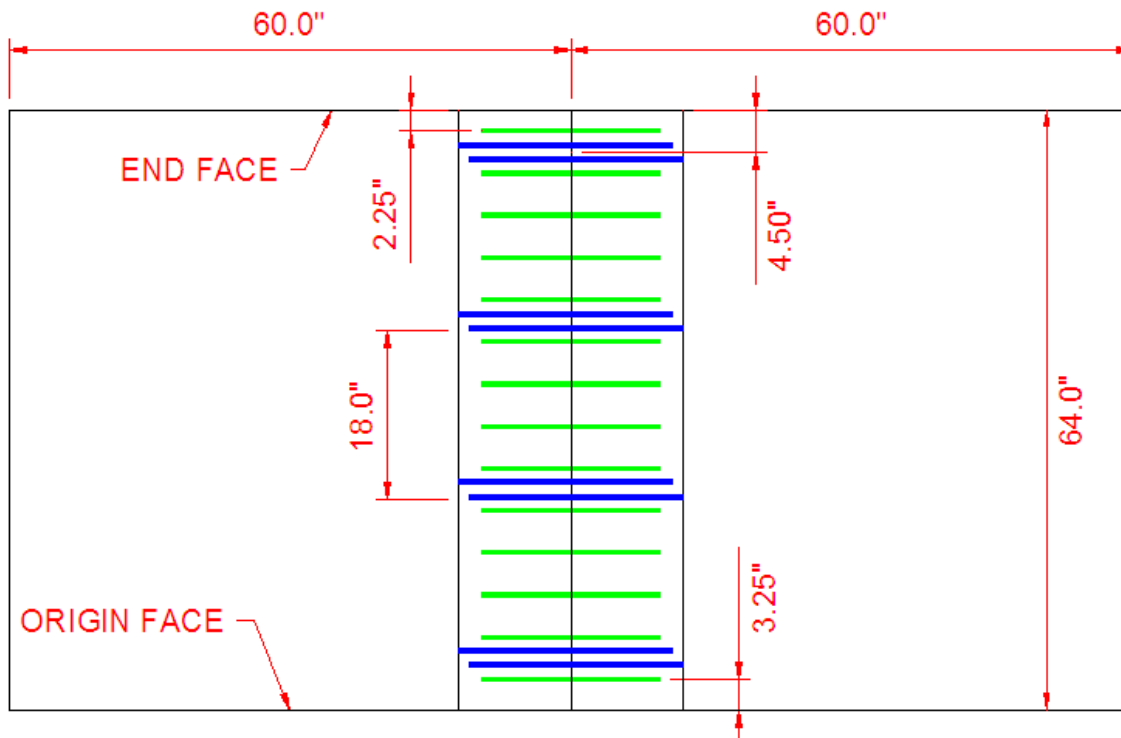
Figure 6.1.7: Specimen layout for SSMBLG6-Frosch. Transverse hooked bars are shown in blue; cage reinforcement is shown in green

172

6.1.7. Subassemblage 7 – Control Specimen 2

The seventh subassemblage specimen was originally designed to provide means to investigate a debonded flange surface. Observations of the performance of SSMBLG3-HighBars and SSMBLG5-No.6Bars, which were constructed and tested prior to the construction of the remaining five specimens, suggested that inadequate bond of the precast flange and CIP concrete could hinder the performance of the subassemblage specimens and limit their value by promoting the formation of a crack at the CIP-precast web interface. The intent of the subassemblage specimens was to investigate the crack control characteristics of the transverse reinforcement and cage above the longitudinal joint above the interface of the adjacent precast flanges. No instrumentation was located across the CIP-precast web interface, and only the transverse hooked bars could provide crack control at that location rather than the combined effect with the cage. For these reasons, the seventh subassemblage specimen was developed as a redundant control specimen. The reinforcement ratios for crack control and load transfer were identical to SSMBLG1-Control1, with values of 0.0031 and 0.0010, respectively.

The specimen geometry of SSMBLG7-Control 2 was identical to SSMBLG1-Control1, however the flange surfaces of this specimen had been patched to provide a smooth surface in an effort to minimize the bond at the interface before the decision to abandon the debonded specimen was made. This represented the only difference in the design and construction between SSMBLG7-Control2 and SSMBLG1-Control1. The specimen layout for SSMBLG7-Control2 is shown in Figure 6.1.3. The flange surface before and after the surface irregularities were patched is shown in Figure 6.1.8, which illustrates the representative level of smoothness present in this specimen.

(a) Prior to patching	(b) After patching
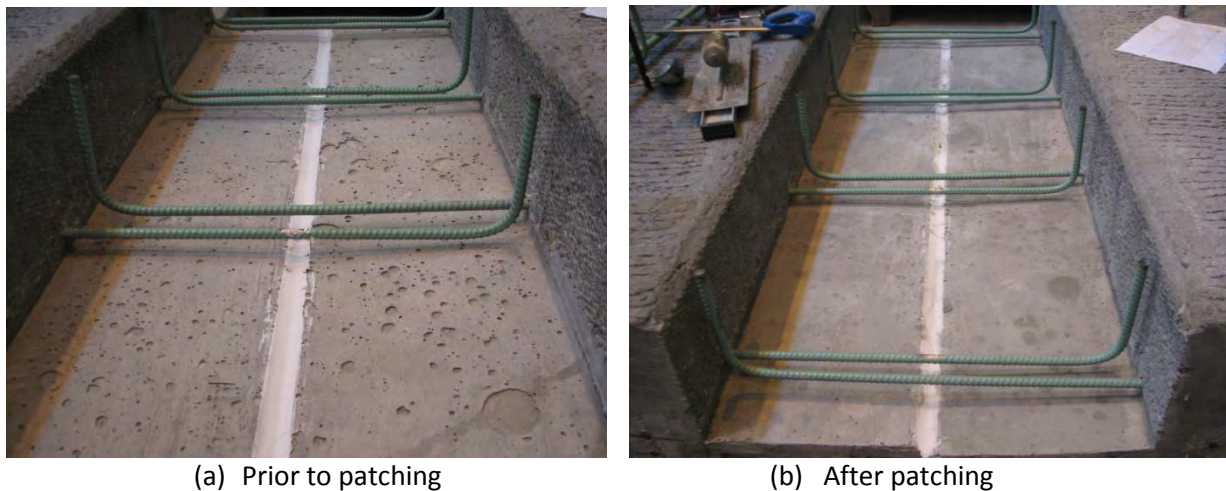
Figure 6.1.8: Precast flange surface condition in SSMBLG7-Control2 before and after patching of the flange to provide a smooth surface condition

A manufacturing error was observed after the fabrication of the precast elements for SSMBLG7-Control2 was completed. The second set of transverse hooked bars, measured from the origin face, was constructed with the bars protruding from the adjacent precast members in reverse order, as shown in Figure 6.1.9. Because of this, two adjacent bars protruding from one precast member were spaced slightly larger than 18

173

in., and the two respective bars from the opposite member were spaced at slightly less than 18 in., however the center to center distance between adjacent sets of transverse hooked bars remained constant, at 18 in.
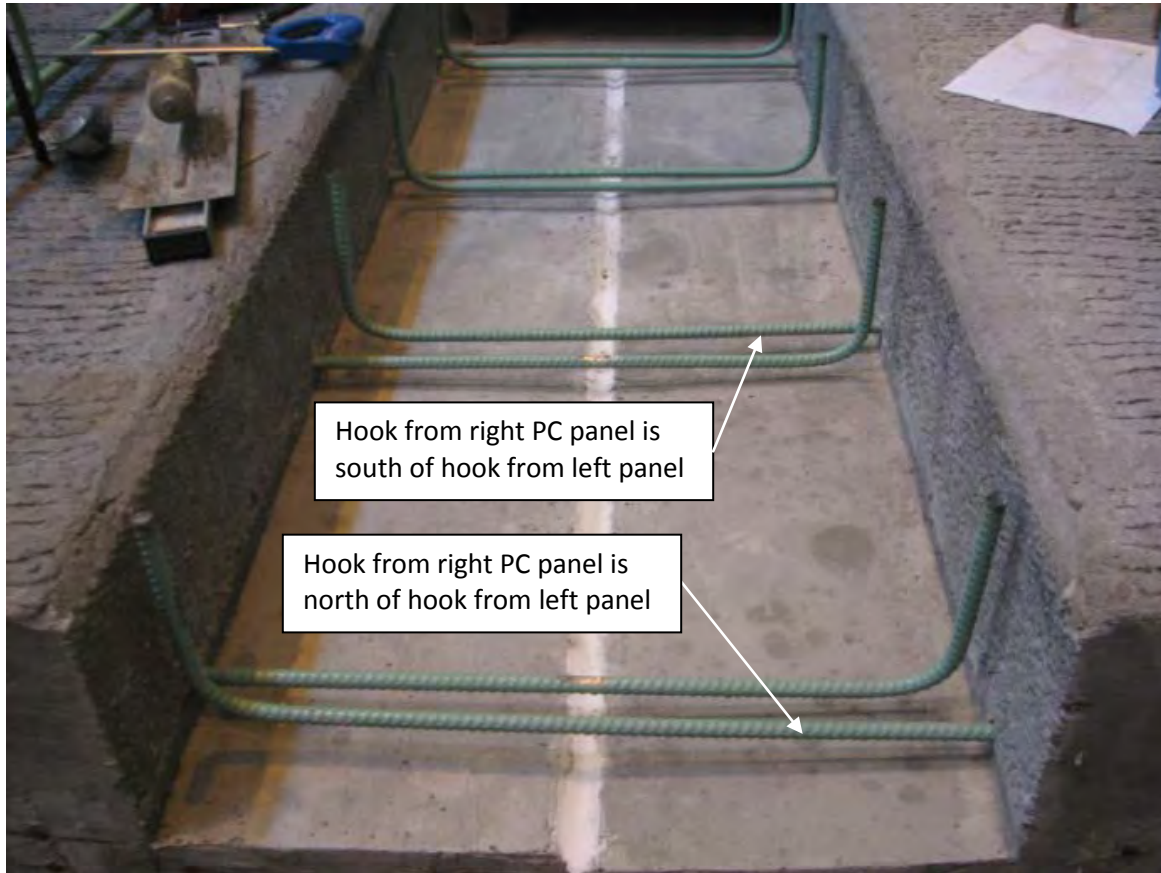
Figure 6.1.9: Photograph of SSMBLG7-Control2 to illustrate manufacturing error in placement of transverse hooked bars

6.2.   Instrumentation of Subassemblage Specimens

Each of the seven subassemblage specimens were instrumented similarly, with the only exception being the presence of additional instrumentation in SSMBLG3-HighBars to provide adequate comparison among specimens. Each specimen had a concrete embedment VW strain gage oriented perpendicular to the joint near the middle of the specimen directly over the precast joint at the same vertical depth as the transverse hooked bars (i.e., a nominal distance of 4.5 in. from the bottom of the precast section). Because vibrating wire gages do not drift over time, these were selected to monitor the effects of shrinkage as well as provide an absolute value of strain at the joint to quantify any potential shrinkage or cracking during handling of the specimens in the laboratory (see Section 6.6). An analysis of the shrinkage strains measured via the concrete embedment VW strain gages is included in Section 6.6.1.

Each specimen contained a total of 17 concrete embedment resistive strain gages oriented perpendicular to the joint, near the joint. The 17 gages were split between two cross sections. Nine of the gages were located near the middle of the specimen, with the remaining eight gages located near the origin face of the

174

specimen. The instrumentation layout for the subassemblage specimens is shown in Figure 6.2.1. Each vertical layer of gages consisted of three concrete embedment resistive gages, with one centered over the precast joint and the remaining two centered 4.5 in. to either side of the precast joint.
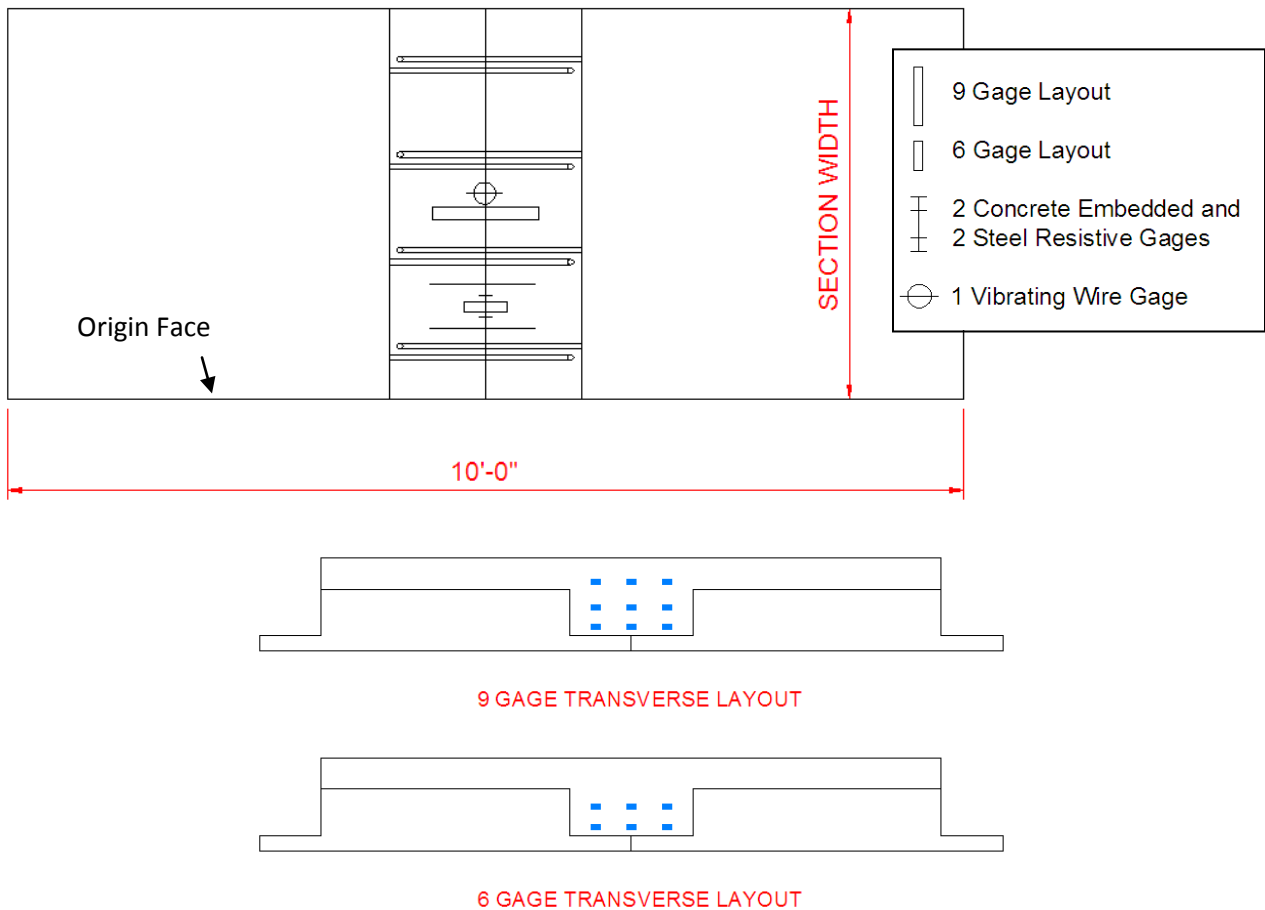
Figure 6.2.1: Instrumentation layout for subassemblage specimens. Overlap of gages not shown for clarity

The nine and six gage layouts were installed to track the height of the crack from the precast – CIP concrete interface above the flange. All instruments in the nine and six gage layouts were 120 mm concrete embedment resistive strain gages. The bottom three strain gages were located at the same depth as the transverse hooked bars. The second layer was located midway through the depth of the reinforcement cage, while the third layer, where present, was located at the top of the reinforcement cage. The additional instrumentation near the origin face included two 60 mm concrete embedment resistive strain gages oriented perpendicular to the joint, one to either side of the six gage layout; 60 mm gages were chosen for this location because they were available from a past project. A 1 mm strain gage was attached to the transverse hooked bar nearest the origin face with a second gage attached to the hooked bar located 18 in. away; both were located directly over the precast joint. The two resistive steel gages and three concrete embedment resistive gages across the joint allowed for the transverse strain to be measured at five

175

locations between adjacent transverse hooked bars. The instrumentation at the origin face of SSMBLG7-Control2, which was representative of all specimens, is shown in Figure 6.2.2.
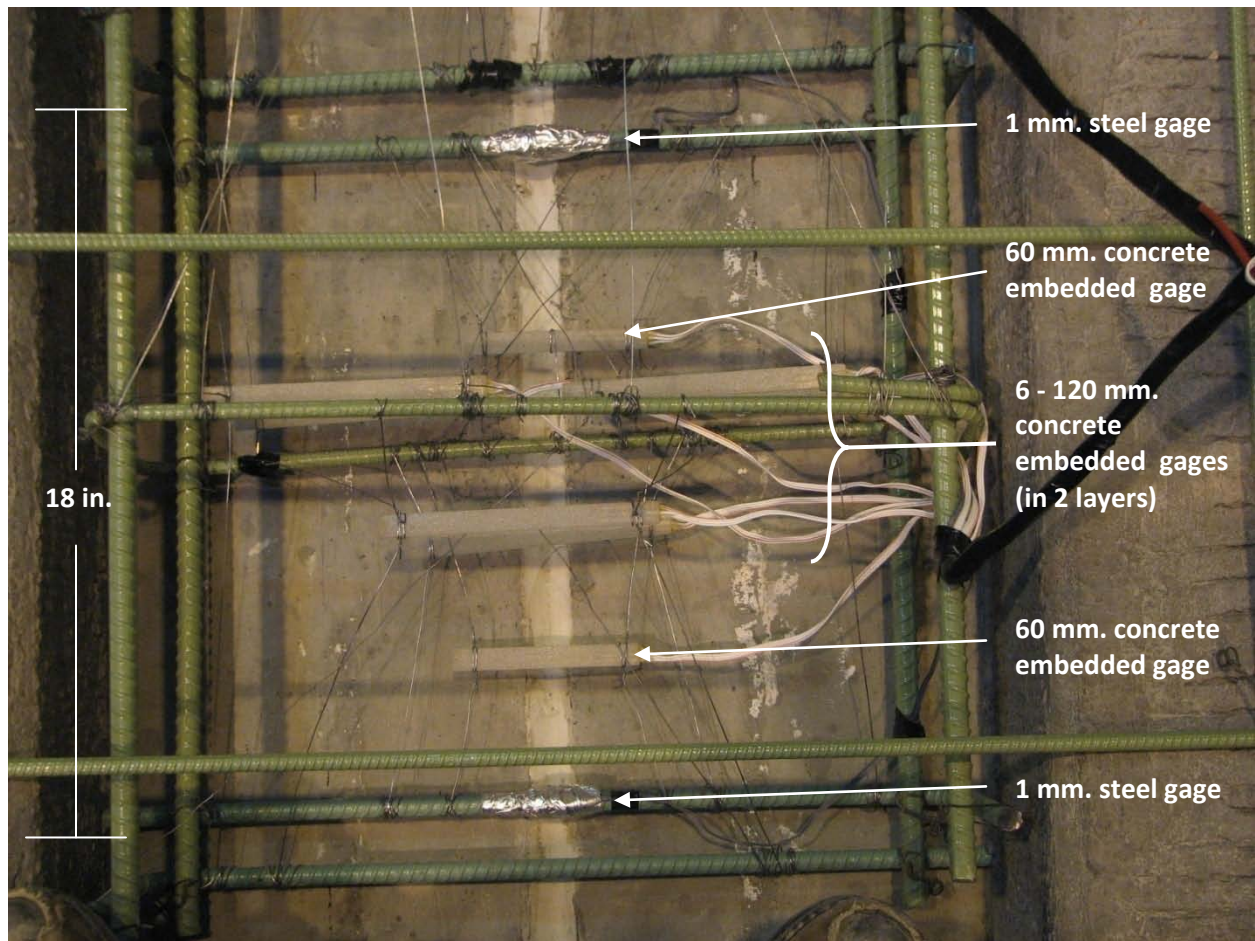
Figure 6.2.2: Plan view of instrumentation near origin face of subassemblage specimens

Two additional strain gages were added to SSMBLG3-HighBars to facilitate comparison among the specimens. The two additional strain gages were located 1.5 in. up from the precast flange centered over the joint, one at each instrumented cross section, to correspond with the lower level of gages in the other specimens. The instrumentation naming scheme and nominal and as-placed locations for the instrumentation in each specimen are tabulated in Appendix I.

In addition to the embedded instrumentation, external LVDT's were utilized to monitor the joint opening. Four LVDTs were placed on both the origin and end faces of the specimen, and were located such that the center of the gage length of each LVDT was vertically aligned with the precast joint. The vertical locations of the LVDT instrumentation was measured from the bottom of the 45 degree, 1 in. chamfer near the horizontal precast-CIP interface, as shown in Figure 6.2.3. Three LVDTs were utilized to measure displacement locally near the precast joint, each with a nominal range of ±0.050 in., except for SSMBLG5-

No.6Bars, which was instrumented with LVDTs with a nominal range of ±0.1 in. (referred to as LVDT050 or LVDT100 hereafter) and a relatively constant gage length of 9.5 in, which was measured from the center of the anchor block that secured the LVDT to the center of the corresponding anchor block to which the core was attached, and varied by no more than 1/4 in. The three LVDT050s were located a distance of -0.75 in. (Low LVDT), 2 in. (Mid LVDT), and 5 in. (High LVDT) from the bottom of the 1 in. precast chamfer. A fourth LVDT spanned between the adjacent vertical precast webs, which was selected to provide a measurement of the total opening associated with the vertical web interfaces, as well as entire CIP region. The fourth LVDT had a nominal range of ±0.5 in. (referred to as LVDT500 hereafter), a gage length of 30 ±1/4 in., and was located a nominal distance of 3 in. from the bottom of the precast chamfer.

Also included on both the origin and end faces was a vertical grid to assist with the documentation of cracking expected on those faces. The grid was also measured from the bottom of the precast chamfer, and consisted of solid horizontal lines in increments of 1 in., along with dots in increments of 1/2 in. The dots were located along a vertical projection of the precast joint. The LVDT layout and vertical grid on the origin face of SSMBLG6-Frosch, which was representative of both faces on all of the specimens, is shown in Figure 6.2.4.
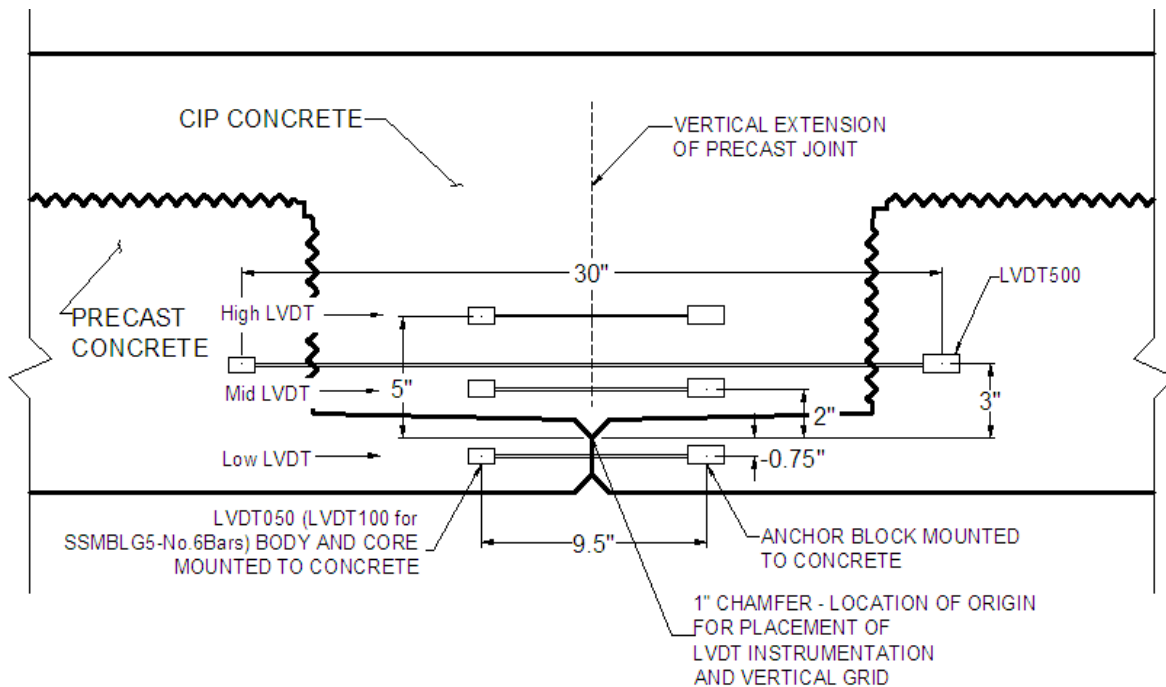
Figure 6.2.3: Location of LVDT instrumentation utilized for subassemblage tests. Vertical measurements for placement of instrumentation originated from bottom of 1 in. precast chamfer

177
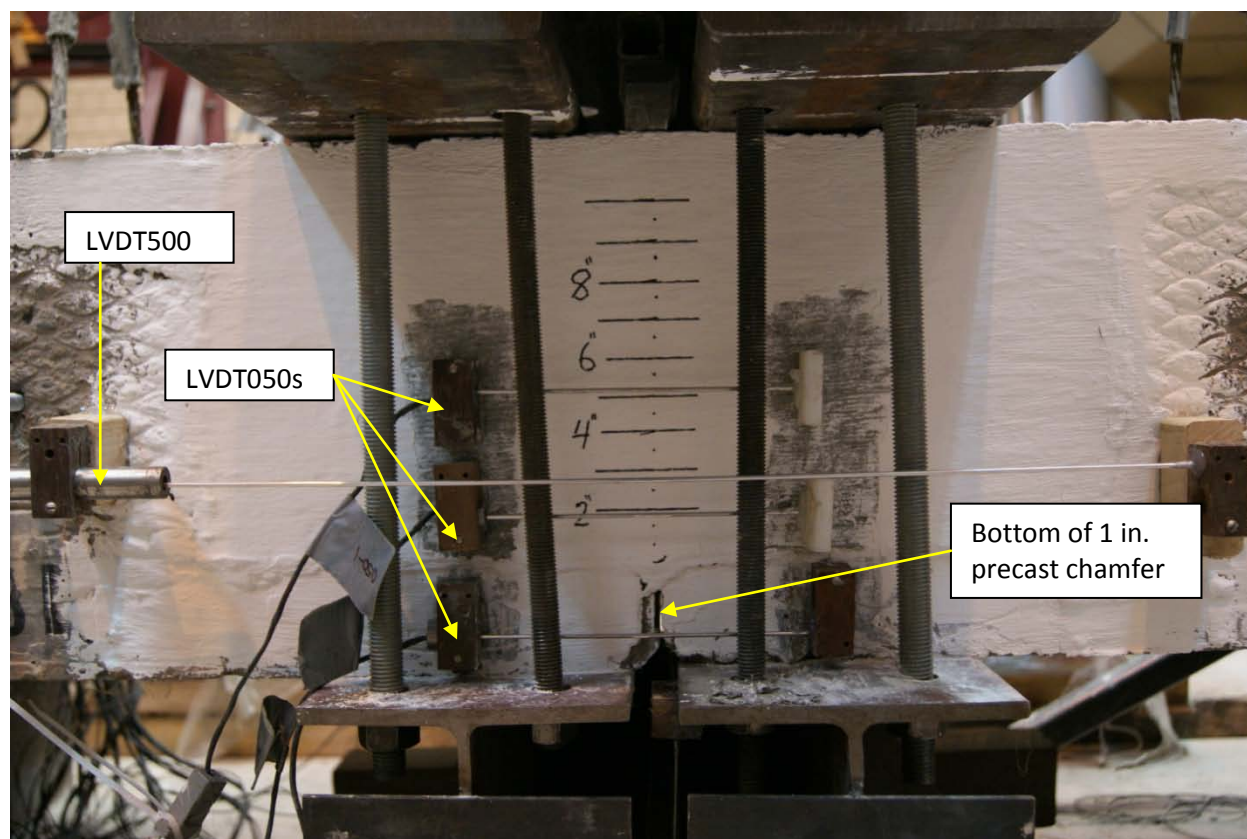
Figure 6.2.4: LVDT layout on origin face of SSMBLG6-Frosch. Vertical line above precast joint is shown by series of dots; measurements were taken from bottom of the precast chamfer

6.3.   Clamping System

Each subassemblage specimen was considered to represent a portion of a PCSSS bridge. The specimens were essentially 5 ft. "long" bridge sections, two panels "wide"; however the panels were supported parallel to the longitudinal joint between the precast panels to facilitate investigation of the effectiveness of the transverse reinforcement in controlling flexural cracks that could be induced along the longitudinal joint with the test setup.

As described in Section 6.1, it was found during the testing of the first specimen, that the stiff flanges of the precast section rotated and caused delamination between the precast flange and CIP concrete, resulting in propagation of a crack at the precast-CIP concrete interface. The test setup was subsequently modified by developing a system to clamp the precast flanges to the CIP concrete on either side of the longitudinal joint. Although the test setup induced compressive forces through the depth of the section at the faces, it was believed to better emulate the field conditions because in a bridge system, the pier supports would be normal to the longitudinal joint, preventing the relative rotation of the precast flanges with respect to the CIP in the trough above the precast flanges at the ends of the sections.

The vertical rods that connected the top and bottom steel members used to clamp the section were located a clear distance of between 2 and 3 in. from the face of the specimen. Consequently, curvature was induced

178

in the longitudinal clamping members, which tended to concentrate the compressive force at the ends of the members. This served to better simulate the effects of restraint in the bridge system (i.e., clamping the subassemblage specimens near the ends simulated the effect of the bridge supports transverse to the longitudinal joint, and relieved the compressive stress across the subassemblage). An illustration of the clamping system, viewed in elevation perpendicular to the precast joint, is shown in Figure 6.3.1, while a cross section (i.e., section AA in Figure 6.3.1) parallel to the precast joint with the curvature of the clamping system shown exaggerated, is shown in Figure 6.3.2.
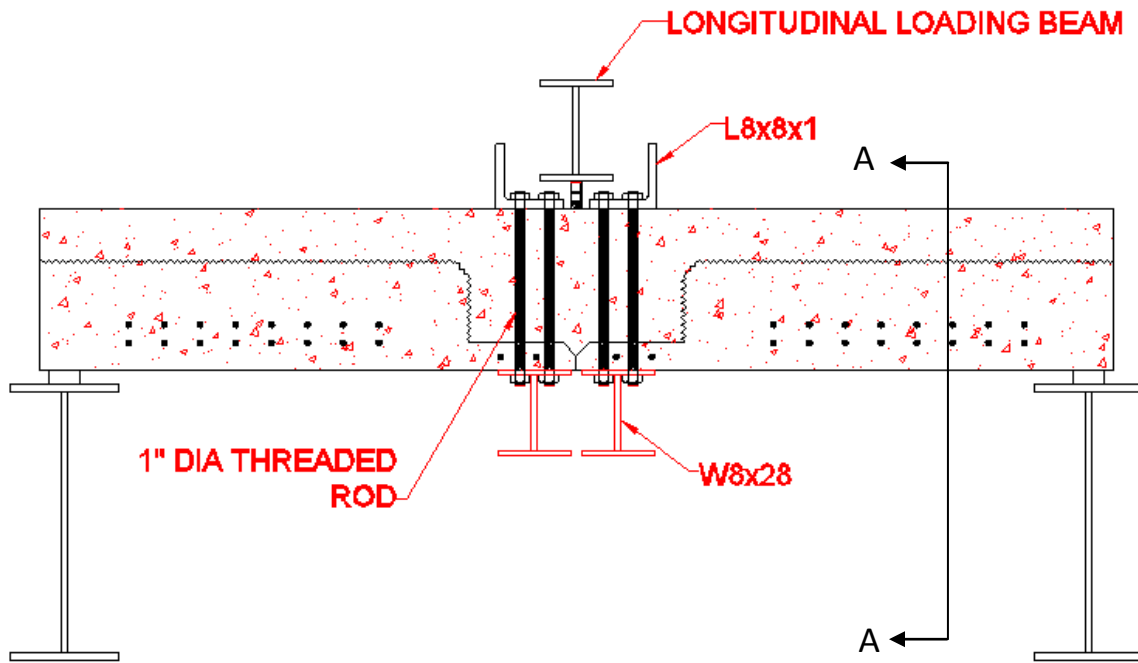
Figure 6.3.1: Clamping system developed to simulate restraint near joint region on subassemblage specimens. Section AA is shown in Figure 6.3.2
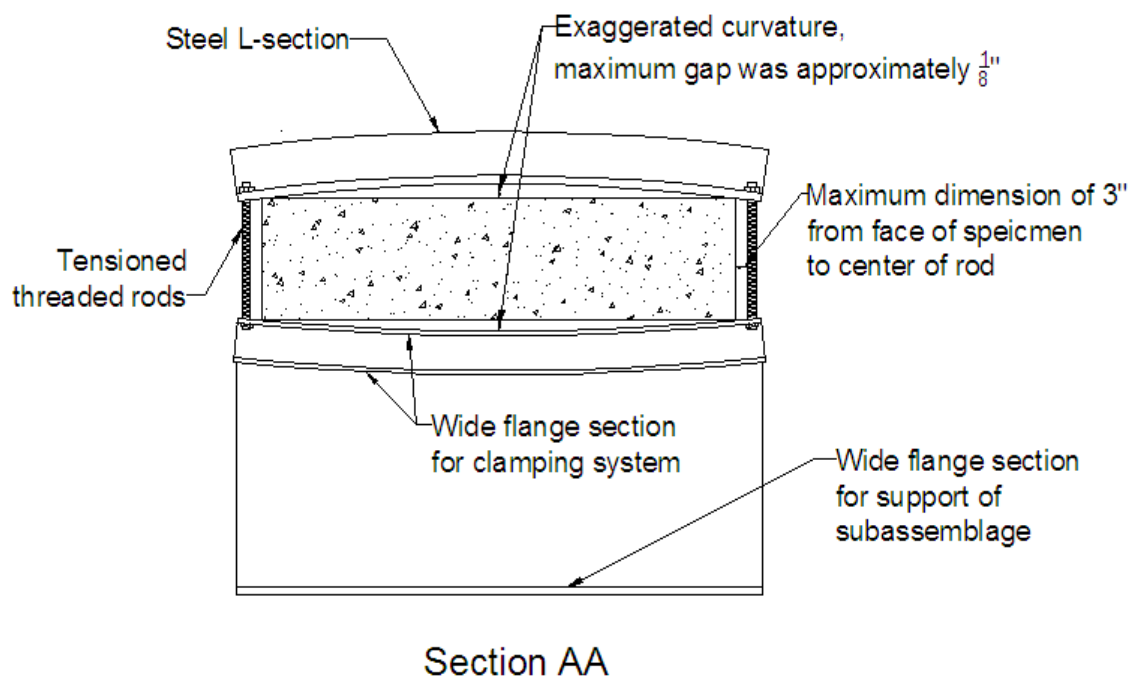
Section AA

Figure 6.3.2: Section view of clamping assembly and subassemblage specimen, parallel to joint, illustrating exaggerated curvature of L-section (top) and wide flange section (bottom) due to eccentricity of tensioned threaded rods

The clamping system was developed with structural steel members, as shown in Figure 6.3.1 placed as near the precast joint as possible, while providing sufficient clearance for the loading strip between the clamps. A total of four 1 in. diameter threaded rods connected the upper and lower steel members near each face. The rods were tightened using an 18 in. long standard spud wrench. The concrete surfaces at the top and bottom of the specimens were adequately smooth and level such that the longitudinal steel clamping members were placed directly on the specimens as constructed without the addition of a grout bed.

As mentioned previously, the clamping assembly was not initially utilized during the testing of the first specimen, SSMBLG3-HighBars. The necessity for the clamping system was quickly realized, as the separation of the horizontal precast flange – CIP concrete interface and the vertical web interface was observed early in the test, shown in Figure 6.3.3. Cracking and/or separation at these locations greatly reduced the applicability and value of the tests because the crack was not able to develop above the longitudinal joint where the crack control reinforcement and instrumentation was located. In the field study of Center City PCSSS bridge (No. 13004) documented in Smith et al. (2008), instrumentation had indicated the initiation of reflective cracking above the longitudinal joint between the precast flanges. While instrumentation was not present in that bridge at the vertical CIP-precast web interface, it would be unlikely that a crack would be present both at the joint and web face, because the presence of one crack would tend to relieve tensile stresses at the other locations. For these reasons, it was necessary to provide the clamping system to ensure that the boundary conditions imposed on the subassemblages were adequately representative of the conditions observed in the implementation of the PCSSS in the field. The clamped assembly fully installed with the HSS sections and neoprene bearing pad in place is shown in Figure 6.3.4.

180
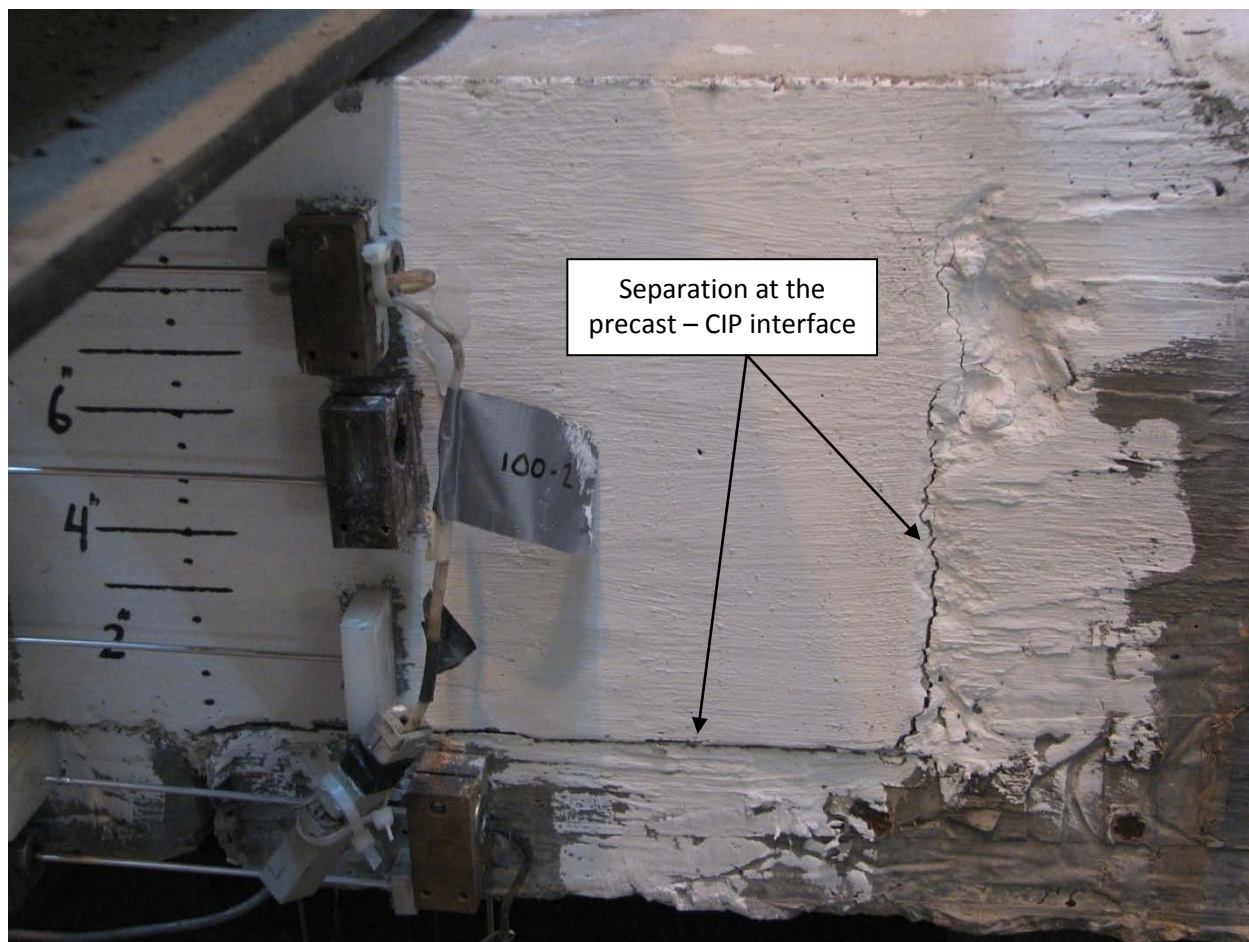
Figure 6.3.3: Separation of East precast section from CIP concrete during testing of SSMBLG3-HighBars before the implementation of the vertical clamping assembly
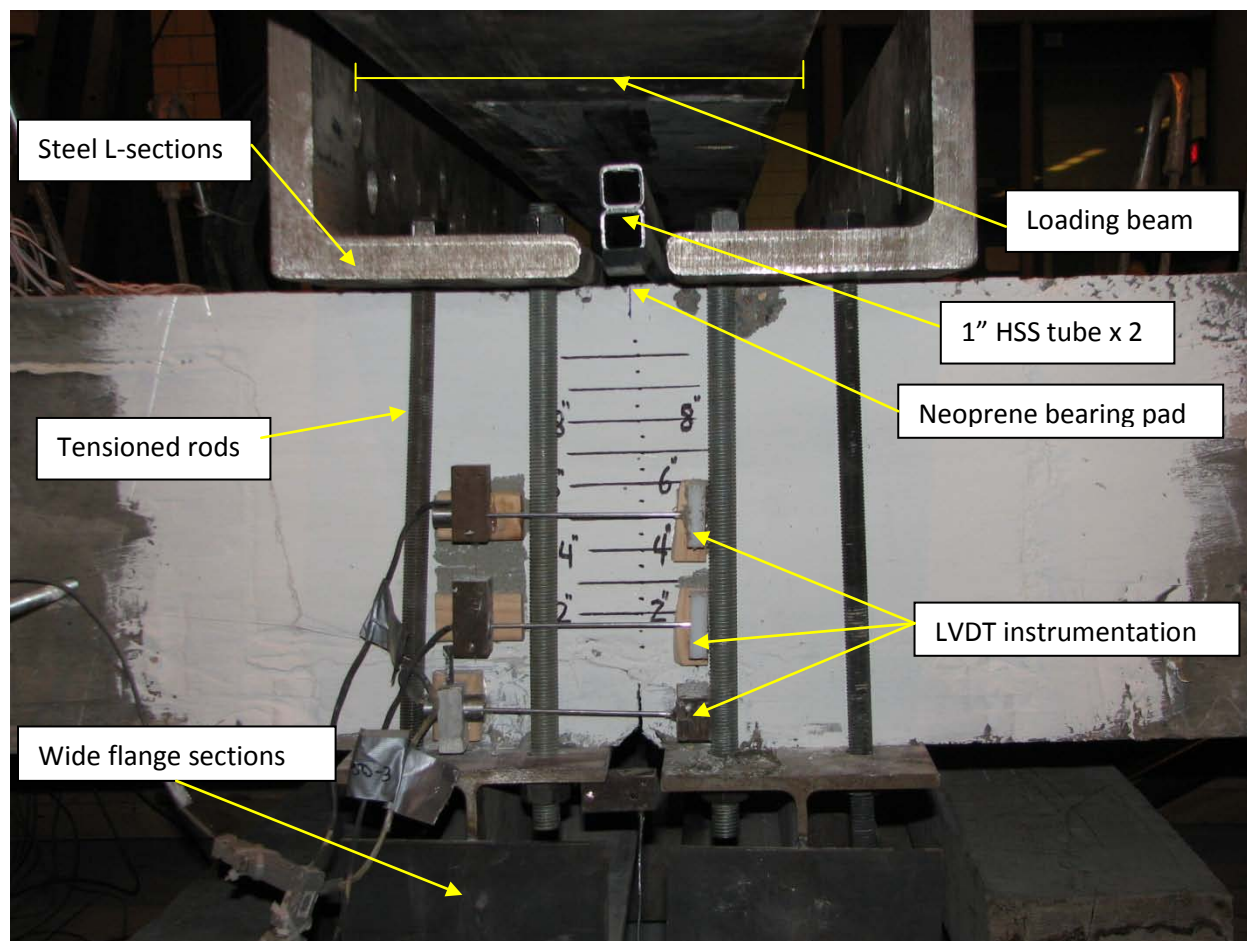
Figure 6.3.4: Clamping system used to provide rotational restraint of the precast members from the CIP concrete during the subassemblage tests and loading apparatus consisting of 1 in. HSS and neoprene bearing pad

6.4. Construction of Subassemblage Specimens and Material Properties

The seven subassemblage specimens were constructed in two groups. The CIP concrete for SSMBLG3-HighBars and SSMBLG5-No.6Bars was placed on July 27th, 2009. The remaining five specimens were cast on October 1st, 2009. The CIP concrete used in all specimens was Mn/DOT state mix 3Y33HE, which had a nominal 28-day strength of 4,000 psi and was provided by a single supplier.

The two specimens constructed during the first pour were built with concrete from two separate ready-mix trucks to allow for sufficient time between pours to finish each specimen. The vertical precast webs near the joint were not prewetted prior to placement of the CIP concrete.

The five specimens constructed during the second pour used concrete from a total of three ready-mix trucks. SSMBLG2-NoCage and SSMBLG6-Frosch used concrete from the same truck, while SSMBLG1-Control1 and SSMBLG7-Control2 used concrete from the second truck, and SSMBLG4-Deep used concrete

182

from the third truck. All the specimens were prewetted with water and allowed to reach a surface dry condition prior to the placement of the CIP concrete.

All seven specimens were moist cured for 8 days immediately after placement of the CIP concrete according to ACI 308.1-98 *Standard Specification for Curing Concrete* (ACI 308.1-98). The curing process consisted of the placement of prewetted burlap against the concrete surface, with a 4 mil plastic sheet above. The burlap was wetted in 12 hour increments to ensure the surface was continuously moist during the 8 day period.

The material properties of each specimen were measured at two key times. The concrete compressive strength was measured via 4x8 in. concrete cylinders 28 days after the concrete was placed and on the day testing was initiated for each specimen. Furthermore, the tensile strength of the concrete was measured both via 6x6x24 in. beams and 6x12 in. concrete cylinders on the first day of testing for each specimen. In addition, the modulus of elasticity of the concrete was measured on the first day of testing using 4x8 in. concrete cylinders. The measured material properties for the specimens when the CIP concrete was at an age of 28 days are included in Table 6.4.1. Note that the order of the specimens listed in the table is the order in which the specimens were cast; consequently, they are not listed in numerical order. For the sets of specimens cast with the same batch of concrete (i.e., specimens 1 and 7, and specimens 2 and 6), a single value is listed in the table for the 28-day strength. The material properties measured on the first day of testing for each specimen are given in Table 6.4.2. The order in which the specimens were tested was: SSMBLG3-HighBars, SSMBLG5-No.6Bars, SSMBLG1-Control1, SSMBLG6-Frosch, SSMBLG7-Control2, SSMBLG2-NoCage, and lastly SSMBLG4-Deep.

Table 6.4.1: Measured subassemblage CIP concrete material properties at an age of 28 days

Specimen #	Description	f_c' [psi]
3	High Bars	4714
5	No. 6 Bars	5201
1	Control 1	5670
7	Control 2	5670
2	No Cage	6238
6	Frosch	6238
4	Deep Section	6326

183

Table 6.4.2: Measured subassemblage CIP concrete material properties on first day of specimen testing

Specimen #	Description	CIP age on 1st day of testing	f_c [psi]	f_t -Beam [psi]	f_t – Split Cylinder [psi]	E_c [ksi]
1	Control 1	95 days	6552	840	594	4740
2	No Cage	122 days	6577	746	521	5633
3	High Bars	37 days	4726	678	497	3933
4	Deep Section	127 days	7151	757	546	4703
5	No. 6 Bars	53 days	5204	609	501	4112
6	Frosch	103 days	6898	806	529	5270
7	Control 2	113 days	7005	732	548	4194

The transverse hooked reinforcement utilized in the subassemblage specimens was tested using the exterior transverse hooks in the Concept 2 laboratory bridge. The No. 4 reinforcing bars embedded in the precast panels for the Concept 2 bridge and subassemblage tests was procured by County Materials at the same time, was of the same bar size, and was epoxy coated; therefore it was expected that the embedded reinforcement in the Concept 2 bridge adequately represented the embedded #4 bars in the subassemblage specimens. Three tensile tests were completed to measure the yield strength of the reinforcement, with average yield strength of approximately 70 ksi. Note that the reinforcing bars were specified as standard Grade 60 steel. Tensile tests were not conducted on the No. 6 bars.

6.5.   Laboratory Testing Program

An extensive laboratory testing program was developed to investigate the performance of each subassemblage specimen. The primary concern regarding the design of the testing program was to create a testing plan that would not be heavily influenced by the age of the specimen or the differences in the material strengths and properties of each specimen at the time of testing. The primary objective of the testing plan was to provide a means to investigate the effectiveness of the transverse reinforcement above the longitudinal joint between the precast flanges in controlling the crack growth generated through both static and cyclic load tests. Therefore, the test plan was constructed to monitor crack growth, especially at loads above those which initiated flexural cracking near the joint.

In an effort to minimize the variations of the concrete strengths and other material properties on the results of the tests, the modulus of rupture of the CIP concrete in each specimen, measured on the first day of testing, according to ASTM C78-09 *Standard Test Method for Flexural Strength of Concrete (Using Simple Beam with Third-Point Loading)* (ASTM C78-09), was used to determine the predicted transverse cracking moment of the subassemblage specimen. The modulus of rupture of each specimen is repeated in Table 6.5.1 along with the respective predicted cracking moment, M_{crack} , and predicted cracking load, P_{crack} , for each specimen.

184

Table 6.5.1: Subassemblage specimen measured modulus of rupture and predicted cracking moment and load

Specimen #	Description	f_t [psi]	$M_{CR\text{-}pred}$ [in-kip]	$P_{CR\text{-}pred}$ [kip]
1	Control 1	840	1117	33.0
2	No Cage	746	1050	30.8
3	High Bars	678	872	28.9
4	Deep Section	757	1855	56.9
5	No. 6 Bars	609	851	22.7
6	Frosch	806	1121	32.2
7	Control 2	732	972	28.2

The testing plan for the subassemblage specimens was based on the load at which cracking was observed to occur. Because effects such as restrained shrinkage in the test specimens may have reduced the cracking load from the predicted value, loading was conducted in small increments, followed by cyclic loading, in order to capture the initiation of visual cracking. After the specimen was taken to each increased load level and held at the peak, the specimen was examined at each face (i.e., origin and end face) for evidence of visual cracking. After cracking was observed, the specimens were subjected to cyclic loading at a lower load level to investigate the stability of the crack (i.e., potential durability of the test specimens) under repeated loads. The specimens were subsequently subjected to increased levels of static load to grow the crack, and the process of cycling the specimen at a lower load level continued.

The specific testing plan, which was consistent for each specimen (with the exception of SSMBLG3-HighBars), consisted of an initial load to 15 percent of the predicted cracking load, $P_{CR\text{-}pred}$, followed by an increase of 5 percent of the predicted cracking load during each subsequent load step. At each load step, the load was applied and removed at a quasi-static rate three times; followed by 1,000 cycles to the displacement that occurred concurrent with load applied at the current load step at a dynamic rate of 0.7 Hz via a displacement-controlled test. The displacement limits were selected such that the range of load that was applied at each load step was initially between 2 kips at the lower bound up to the load applied during the quasi-static loading at each step. A quasi-load controlled testing scheme was used in the initial cracking phases of the tests to better control the crack propagation. Upon observation of a visual crack at either the origin or end faces, the load was recorded as the observed cracking load, $P_{CR\text{-}meas}$, after which the specimen was subjected to 5,000 cycles of displacement-controlled loading to the displacement that occurred concurrent to the load level previously reached. As previously mentioned, displacement limits were selected such that the applied load was cycled between 2 kips and the target load at that particular load step. The specimens were subsequently subjected to an additional 2,000 displacement-controlled load cycles with the displacement limits selected such that they initially occurred concurrent with the "base" level load. The displacement limits were periodically adjusted during the completion of cyclic loading at each load step such that the applied load range was kept relatively constant; thereby producing a load-controlled type testing environment with the benefit of a controlled lower bound displacement to prohibit sudden collapse of the specimens. The base load was taken as approximately 55 percent of $P_{CR\text{-}meas}$ (i.e., "BASE" $\approx 0.55 * P_{CR\text{-}meas}$), rounded to the nearest 5 percent of $P_{CR\text{-}pred}$, because the applied load values were

185

tabulated and plotted as percentages of the predicted cracking load. The use of 55 percent of the observed cracking load was selected to provide an adequately small base level (i.e., small enough such that initial cracking was reasonably expected not to have occurred prior to exceeding the base level load) which would allow for the investigation of degradation of the specimen due to cyclic loading at the base load while not inducing large levels of strain.

The load was incremented above the observed cracking load, $P_{CR\text{-}meas}$, in load step increments of 5 percent of $P_{CR\text{-}pred}$ consisting of both quasi-static and 1,000 cycles of quasi-load-controlled fatigue load at each load step, until the crack length observed on either the origin or end face reached a length of 8 in., measured from the origin of the vertical grid on each face (i.e., the bottom of the chamfer at the precast joint, see Figure 6.2.3 for additional details). A total of 5,000 quasi-load-controlled cycles were then completed at a displacement consistent with the load required to grow the crack to a length of 8 in., and the base-level load was repeated. Load was then incremented until the maximum load, P_{max}, was achieved, which was selected as the lesser of: (1) a proportion of the predicted cracking load, taken as approximately 195 percent of $P_{CR\text{-}meas}$ (i.e., $P_{max} \approx 1.95*P_{CR\text{-}meas}$), rounded to the nearest 5 percent of the predicted cracking load, or (2) when delamination was observed at the vertical precast – CIP web interface. Because the subassemblage tests were designed to induce a maximum moment at the longitudinal precast joint, data measured near the precast joint after the observation of cracking or delamination at the vertical precast-CIP web interface was considered to be irrelevant. Therefore, P_{max} was selected based on when cracking was observed at the vertical precast-CIP web interface during testing on SSMBLG5-No.6Bars, which was at an applied load of approximately 195 percent of $P_{CR\text{-}meas}$. The maximum applied load, P_{max}, was then followed by 2,000 cycles of quasi-load-controlled loading at the base level. The loading procedure for an example specimen with a predicted cracking load of 40 kips is given in Table 6.5.2. The only specimen to deviate from this plan was the first one tested, SSMBLG3-HighBars, where the initial load step was 50 percent of the predicted cracking load, and the lack of the clamping assembly allowed separation at the precast flange-CIP concrete interface.

During each load step, visual observations were recorded. The crack width and general observations were documented after the application of the third quasi-static load cycle with the load applied. In addition, after the completion of all cyclic loading at a given load step, the crack widths and other observations were again recorded with the magnitude of load equal to that which was applied during the cyclic tests at that load step.

186

Table 6.5.2: Subassemblage loading plan for example specimen with predicted cracking load of 40 kips

Predicted Cracking Load		Applied load when cracking was observed	
$P_{CR\text{-}pred}$ = 40 k		$P_{CR\text{-}meas}$= 24 k (= 60% of $P_{CR\text{-}pred}$)	
Base ≈ 0.55*$P_{CR\text{-}meas}$ = 0.55(24 k) = 13.2 k = 33% of $P_{CR\text{-}pred}$ rounded to 35% of $P_{CR\text{-}pred}$ = 14 k			
Reflective crack width reached length of 8 in. during load step to 105% of $P_{CR\text{-}meas}$			
Maximum Load ≈ 1.95*$P_{CR\text{-}meas}$ = 47 k = 117% of $P_{CR\text{-}pred}$ rounded to 120% of $P_{CR\text{-}pred}$ = 48 k			
Load Step	Applied Load [% of $P_{CR\text{-}pred}$]	Applied Load [kip]	# Cycles Completed at applied load
1	15	6	1000
2	20	8	1000
3	25	10	1000
4	30	12	1000
5	35	14	1000
6	40	16	1000
7	45	18	1000
8	50	20	1000
9	55	22	1000
10[1]	60 (100% of $P_{CR\text{-}meas}$)	24	5000
11 "base" load	35 (≈55% of $P_{CR\text{-}meas}$)	14	2000
12	65	26	1000
13	70	28	1000
14	75	30	1000
15	80	32	1000
16	85	34	1000
17	90	36	1000
18	95	38	1000
19	100	40	1000
20	105	42	5000
21 "base" load	35 (≈55% of $P_{CR\text{-}meas}$)	14	2000
22	110	44	1000
23	115	46	1000
24	120 (≈195% of $P_{CR\text{-}meas}$)	48	1000
25 "base" load	35 (≈55% of $P_{CR\text{-}meas}$)	14	2000

[1]cracking visually observed at this load level

187

6.5.1. Data Acquisition

The primary instrumentation utilized during the subassemblage tests were resistive-type concrete embedment strain gages and LVDTs, and also included a single transversely oriented concrete embedment VW gage. All data from the resistive and LVDT instrumentation were collected via a single National Instruments data acquisition (DAQ) system. The DAQ collected data at all times during the testing process at a rate of 15 Hz. The DAQ was equipped with a low pass filter which produced readings of satisfactory quality, with an approximate total gage noise of ±6 µε for the 120 mm concrete embedment resistive strain gages at a steady state condition. Data from the concrete embedment VW gages was collected via a CR10X data logger from Campbell Scientific at 2 minute intervals. The approximate noise of the concrete embedment VW gages instrumentation was approximately ±0.5 µε.

6.6. Results of Laboratory Testing

A thorough analysis of the data collected both visually and via the DAQ was completed at the conclusion of the laboratory testing of each specimen. Seven metrics were developed in an effort to quantitatively and qualitatively characterize the performance of the subassemblage specimens relative to each other. Three of the seven metrics were defined based on visual observations and crack measurements during each test, which consisted of the documentation of general observations related to cracking observed during testing, and the measurement of the width and length of the crack observed on the origin and end faces of each specimen. Three metrics were determined through analysis of the data collected with the DAQ during the tests, and included an analysis of the strain due to shrinkage and placement of the subassemblage specimens in the load frame, width of opening of the joint measured via the LVDT instrumentation, and an analysis to investigate the vertical and horizontal generation and propagation of reflective cracking internally. The seventh metric consisted of the investigation of the predicted transverse reinforcement stress demands in the specimens. In all cases, the results were tabulated in terms of the predicted cracking load, $P_{CR-pred}$. The section is organized as follows:

- Investigation of transverse strain due to shrinkage and handling of the specimens (Section 6.6.1)
- General observations regarding cracking observed during load tests (Section 6.6.2)
- Analysis of visually observed crack widths on the origin and end faces of each specimen (Section 6.6.3)
- Analysis of opening of joint region measured at the origin and end faces via LVDT instrumentation (Section 6.6.4)
- Analysis of the rate of increase in the vertical length of cracking measured with a crack gage on the origin and end faces of each specimen (Section 6.6.5)
- Investigation of the vertical and horizontal generation and propagation of reflective cracking near the longitudinal joint between the precast flanges measured via concrete embedment resistive strain gages (Section 6.6.6)
- Predicted transverse reinforcement stress demands through range of loading (Section 6.6.7)

6.6.1. Transverse Strains Near Joint Region due to Shrinkage and Handling of Subassemblage Specimens

The transverse strain near the joint region was monitored during the curing process, as well as during handling of the specimens, to provide an estimate of the state of strain near the joint at the initiation of load testing. A single transversely oriented concrete embedment VW strain gage was installed near the middle of each section (measured along the precast joint), as shown in Figure 6.2.1. The strain in each gage was recorded in two hour increments from 1 hour after placement of the CIP concrete until the conclusion of all load testing.

The initial state of strain, defined to be the strain at the initiation of load testing, was of interest because the introduction of cracking due to applied load was a critical element of the testing plan, and therefore a record of existing cracking present prior to the start of testing was of interest. The transverse mechanical strains measured via the concrete embedment VW strain gages as a function of the number of days after placement of the CIP concrete, up until the first day of laboratory testing for each specimen, is shown in Figure 6.6.1. The horizontal axis represents the number of days between the placement of the CIP concrete and the first day of load testing for each specimen, and ranged from 37 days (SSMBLG3-HighBars) to 127 days (SSMBLG4-Deep). The transverse strains given in the figure originate at zero strain, and increase quickly over a short period of time, giving the illusion that the initial strain was nonzero. In addition, the DAQ was initiated at the same absolute time for all of the specimens, therefore there was a variation of several hours between when the CIP concrete was placed in the first and last specimen of the day, resulting in a small relative difference in the age of the specimens at what is referred to as zero time (when the DAQ was initiated). The vertical offsets among the readings may be attributed to the different stages of hydration occurring in the different specimens when the DAQ was initiated. Each specimen was transferred from a construction staging area (where the CIP concrete was placed) to a loading frame, which is shown in the figure by the positive (i.e., tensile) increase in strains near the rightmost point of most of the data series.

The specimens were cured and stored in the University of Minnesota Structures Laboratory. The maximum temperature variation measured via the thermistors in the concrete embedment vibrating wire gages was +/- 7 degrees Fahrenheit. No sudden change in temperature was observed during the time between casting and testing of the specimens, which suggested that the mechanical strains reported in Figure 6.6.1 were primarily due to shrinkage.

189
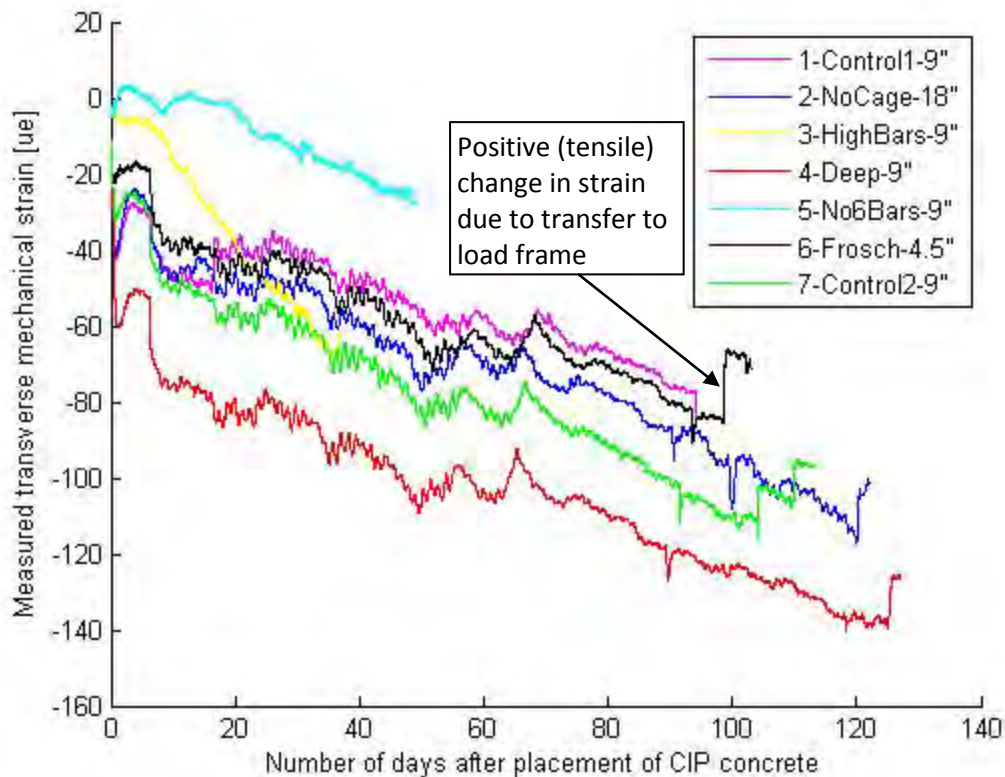
Figure 6.6.1: Measured transverse mechanical strains in the subassemblage specimens based on the number of days after the placement of the CIP concrete

The sign of the transverse strain data remained "compressive" indicating shortening or shrinkage throughout the curing and handling periods for each specimen. No evidence of cracking was visually observed on either the origin or end faces of the specimens after placement of each subassemblage into the load frame.

6.6.2. General Observations of Cracking Behavior during Load Testing

Cracking was induced in the CIP region near the precast joint in each of the seven subassemblage specimens as a result of applied mechanical loading in accordance with the testing program. In addition, cracking was also observed at the vertical precast web-CIP interface, and occurred after the initiation of cracking near the joint in each of the specimens except SSMBLG3-HighBars, due to the absence of the clamping assembly on that specimen. Of the remaining six specimens, a single primary vertical crack was observed on both the origin and end faces throughout the range of applied loads on all but SSMBLG6-Frosch, where two distinct vertical cracks were observed on both faces. For this specimen, a second vertical crack was observed at an applied load of approximately 49.0 k (152 percent of $P_{CR-pred}$) and 41.9 k (130 percent of $P_{CR-pred}$) on the origin and end faces, respectively. A photograph of the dual vertical cracks observed on the origin face of SSMBLG6-Frosch, which is representative of both faces, is shown in Figure

190

6.6.2. In the discussion regarding visually measured crack widths and lengths in the following sections, the crack width was taken to be equal to the largest observed crack on each face when two cracks were present (i.e., when the load was large enough such that a second crack had formed), and the recorded crack length was taken to be the longest crack among the two, though little variation was observed in either the crack widths or crack lengths after the second 5 percent increase in applied load above the load step in which the secondary cracks were initiated.
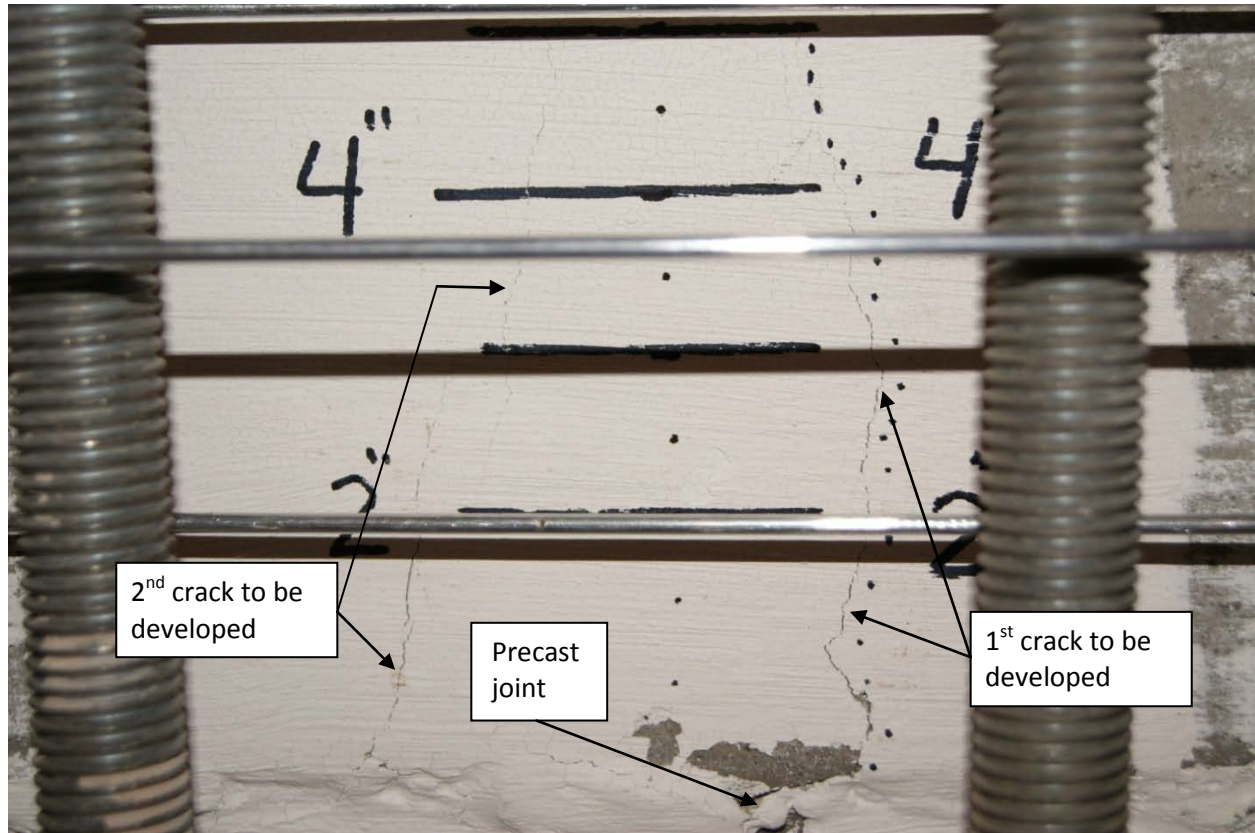
Figure 6.6.2: Photograph of development of two primary vertical cracks near the precast flange on origin face of SSMBLG6-Frosch. Applied load was 49.0 k (152 percent of $P_{CR\text{-}pred}$)

Cracking was also observed near the vertical precast web-CIP interface at large levels of applied load. Cracking at these locations generally initiated at the bottom of the precast section, near the embedded end of the precast flange, as illustrated in Figure 6.6.3. The observed cracking near the bottom of the precast flanges was likely primarily due to the added restraint provided by the clamping assembly, whereas if the clamps were not present delamination of the horizontal precast flange-CIP interface was expected, as observed during testing of SSMBLG3-HighBars before the installation of the clamping mechanism. The introduction of cracking was generally observed at the vertical web interfaces on both sides of the precast joint, and tended to initiate at roughly the same applied load.

191

In some cases, at loads near the maximum applied to each specimen, diagonal cracking was also observed in the CIP region, initiating at the outside edge of the bottom wide flange section of the clamping assembly, and extending to the vertical precast web-CIP interface, as noted in Figure 6.6.3.
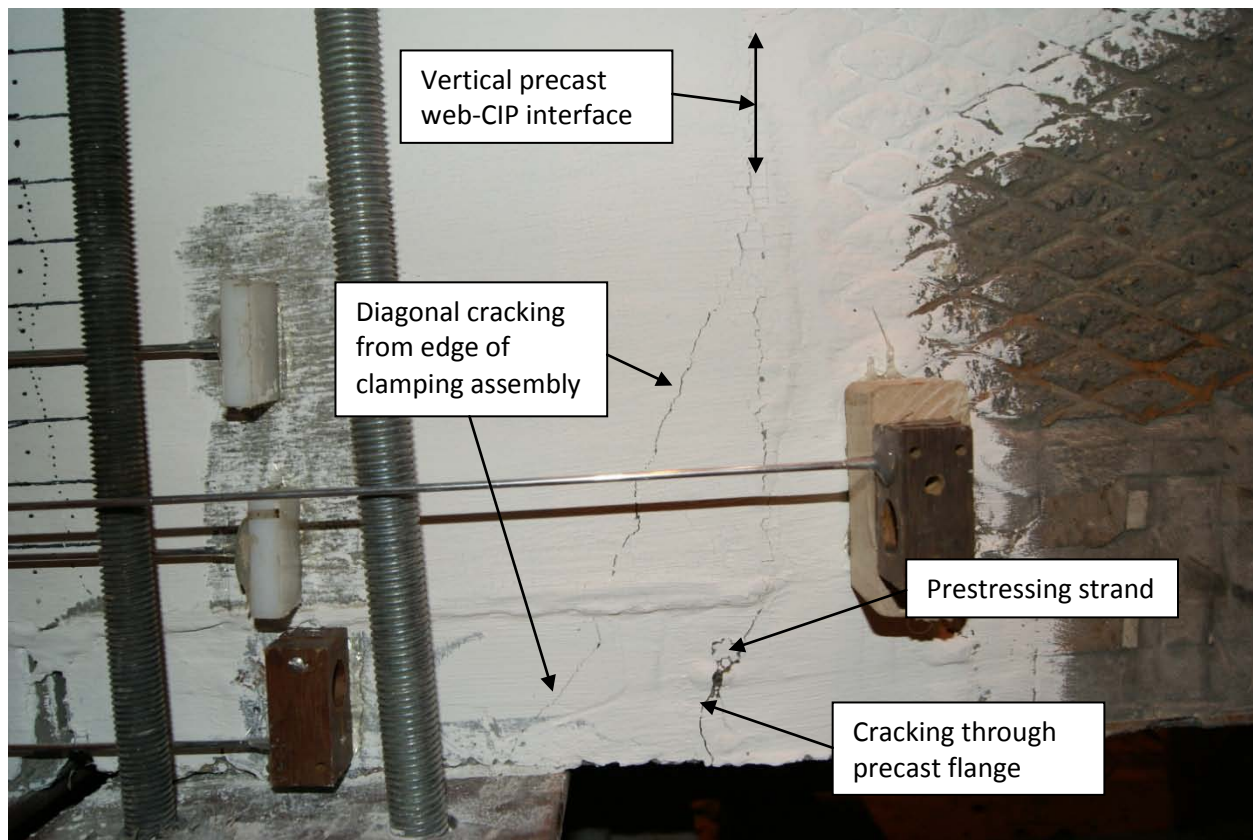
Figure 6.6.3: Photograph of cracking near the vertical precast web-CIP interface, including cracking through the precast flange and diagonal cracking due to the clamping assembly in SSMBLG6-Frosch

6.6.3. Width of Cracking Near Joint Region Measured with Crack Gage

The crack widths observed on both the origin and end faces of each subassemblage were documented throughout the majority of the tests. The procedure for visually documenting the crack growth in the subassemblage specimens was finalized during testing of the second specimen, or SSMBLG5-No.6Bars. For this reason, crack widths obtained for the SSMBLG3-HighBars test and crack widths from the origin face of SSMBLG5-No.6Bars are not compared with those of the other specimens. For the remaining specimens, the crack width was measured at each 5 percent increment relative to the predicted cracking load on both faces. A standard crack gage with a range of 0.002 to 0.032 in., inclusive, was used to measure the crack width at the lowest possible location in the CIP concrete in each specimen. The crack width was measured directly at the interface between the silicone caulk and CIP concrete, or as close as possible, and was recorded in association with the loading that corresponded to the respective load step applied to the section. The width of observed cracking on the faces of the specimens generally tended to be reduced with the removal of the applied load.

192

The detail near the joint and location of crack measurement is shown in Figure 6.6.4. A representative image of the crack width measurement is shown in Figure 6.6.5.
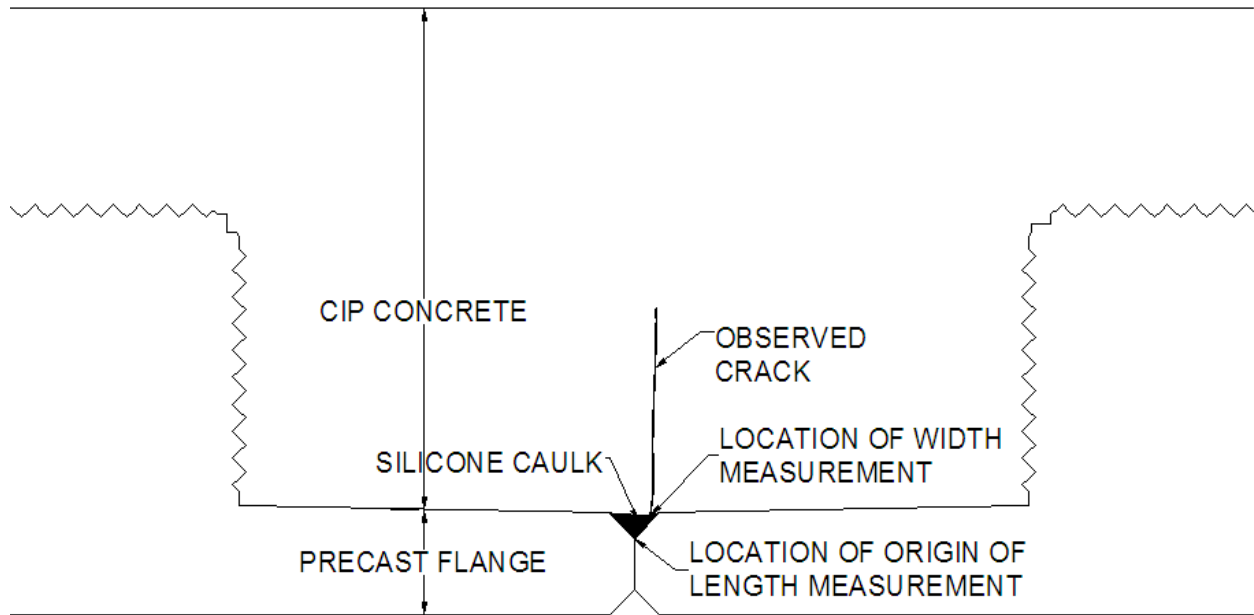
Figure 6.6.4: Location of measurement of width and length of crack observed on origin and end faces of subassemblage specimens

193
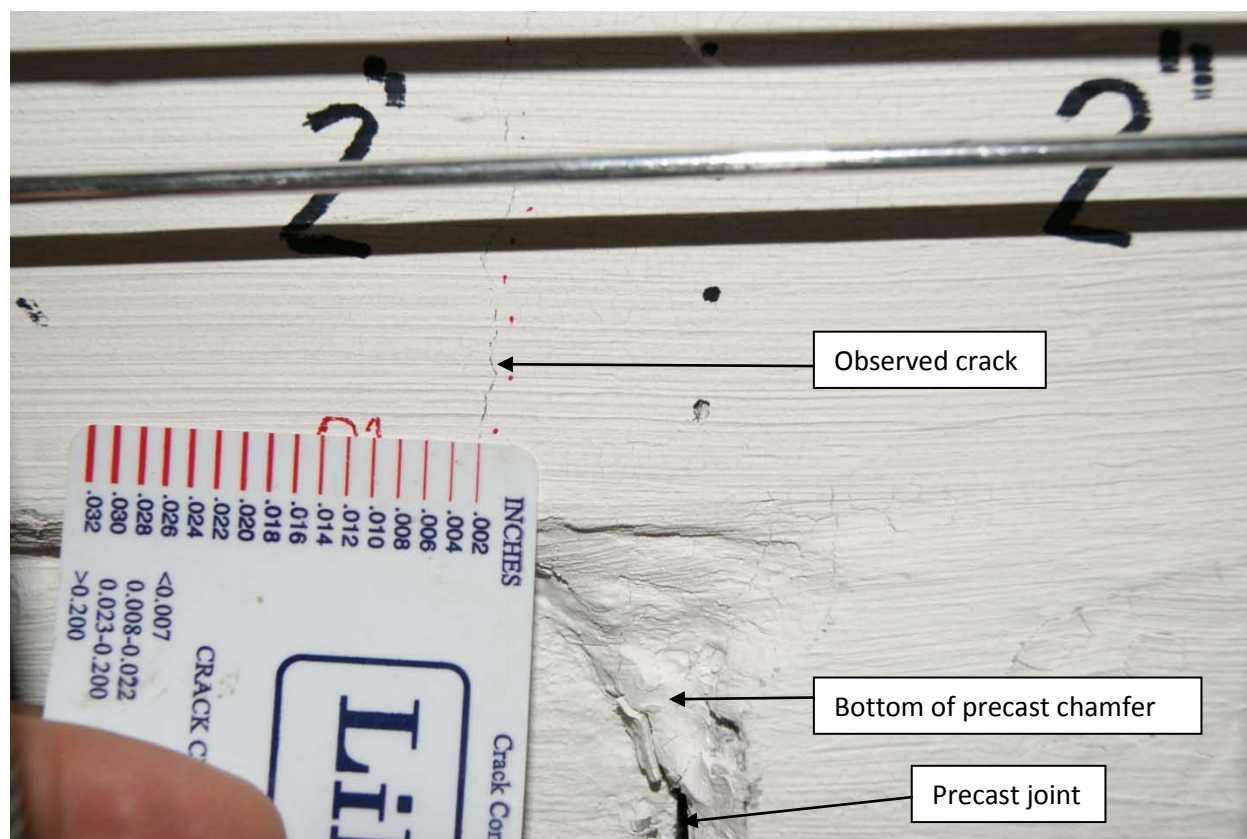
Figure 6.6.5: Measurement of crack width during subassemblage testing

Because the performance of the transverse hooked bars and cage reinforcement was of primary interest in the subassemblage specimens, and the presence of cracking near the vertical precast web face was undesirable and could have an influence on the crack width measurement above the longitudinal joint between the precast flanges, the observed crack widths were tabulated up to and including the load step in which the first crack or separation of the vertical precast web was observed. Figure 6.6.6 shows the width of the crack observed near the joint on the origin face before each set of cycles in the selected specimens. Each specimen is labeled in the legend using the specimen number, descriptive name, and transverse reinforcement spacing (considering both the transverse hooked bars and cage as transverse reinforcement). The horizontal axis illustrates the measured crack width in inches, while the percent of predicted cracking load is shown on the vertical axis. It is to be noted, that the percent of the predicted cracking load at which the crack width is indicated as "0 in." corresponds to the visually observed cracking load. In other words, for 6-Frosch-4.5", visual cracking was observed at 65% of the predicted cracking load. One of the reasons for the observed cracking load being less than the predicted cracking load was attributed to potential restrained shrinkage effects in the subassemblages. The crack was observed to originate at roughly the same percentage of predicted cracking load, with the exception of SSMBLG6-Frosch, which required an additional increase of approximately 15 percent of the predicted cracking load before cracking was first observed. Subsequent analysis of the internal strain data (see Section 6.6.6) suggested that small crack widths of SSMBLG6-Frosch hindered early visual detection of the crack, which caused the observed results to be inaccurately recorded at higher loads. Because of the larger perceived measured cracking load,

194

SSMBLG6-Frosch was consistently loaded to higher levels of load in comparison with some of the other test specimens. This was also the case for the SSMBLG5-No.6Bars, for which results are not present in Figure 6.6.6 because crack width measurements were not recorded on the origin face of that specimen.
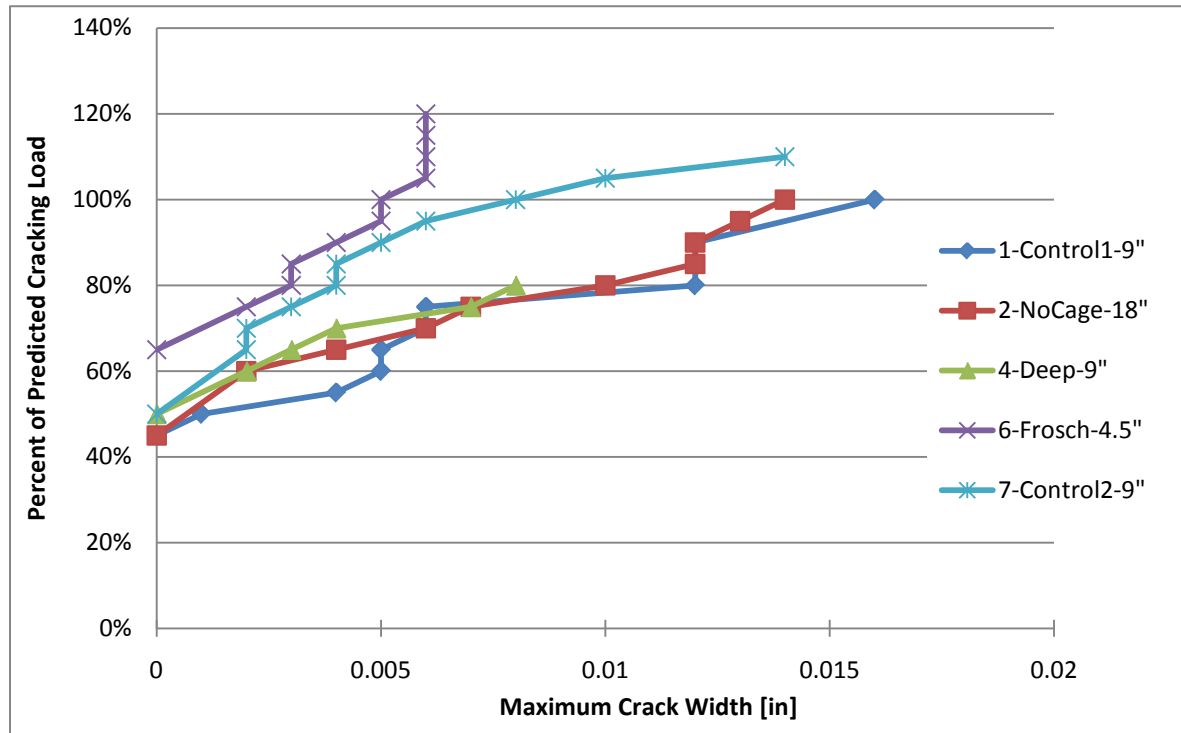
Figure 6.6.6: Maximum[1] crack widths measured on the origin face[2] of selected specimens[3] before each set of cycles

[1]Maximum crack width was measured at the horizontal precast-CIP flange interface
[2]Clear distance from origin face to first transverse bar was approximately 3.1 in. for SSMBLG5-No.6Bars and SSMBLG6-Frosch, and 3.25 in. for the other specimens
[3]SSMBLG5-No.6Bars is not shown because crack widths were not measured on the origin face of that specimen. SSMBLG3-HighBars is also not shown because the clamping apparatus was not installed prior to testing and therefore those results are not comparable to the remaining specimens

The performance of each specimen can be deduced from Figure 6.6.6 by selecting a value for the percent of the predicted cracking load and comparing the measured crack widths at that load. As expected, the observed crack widths tended to be bounded by the specimens with the closest (Frosch) and sparsest (No Cage) maximum reinforcement spacing. The variation in the observed crack widths between the two control specimens, SSMBLG1-Control1 and SSMBLG7-Control2 might be attributed to the smooth surface condition achieved in the SSMBLG7-Control2 specimen. The smooth flange surface was expected to better distribute the tensile stresses across the width of the CIP concrete in the trough between the precast webs (transverse to the longitudinal joint) reducing the effect of the discontinuity created by the interface between the adjacent precast flanges. A smooth or debonded surface however may not support an

195

improved overall PCSSS because if a reflective crack would initiate at the vertical precast web-CIP concrete interface, the cage reinforcement would not contribute to the crack control resistance. The only reinforcement crossing such a crack would be the transverse hooked bars protruding from the precast webs. Figure 6.6.6 clearly shows that SSMBLG6-Frosch outperformed the other specimens at high loads.

The crack widths on the end face of the specimens were documented at increased load levels prior to the subsequent cycling, and the values are plotted in Figure 6.6.7 with respect to the percentage of the cracking load applied. The crack widths measured on the end face followed a similar trend to those documented on the origin face. The transverse reinforcement terminated a distance of half of the maximum spacing from the end face of each specimen, essentially providing an estimate of the crack width at the point farthest from adjacent transverse reinforcement in the specimen; whereas on the origin face, the clear distance to the transverse reinforcement was approximately 3.1 in. for SSMBLG5-No.6Bars and SSMBLG6-Frosch and 3.25 in. for the remaining specimens. As observed near the origin face, the Frosch and Control2 specimens performed well, however the inclusion of the results from SSMBLG5-No.6Bars also showed very good performance of this specimen. As stated earlier in this section, the relatively higher initial visual cracking loads recorded for SSMBLG5-No.6Bars and SSMBLG6-Frosch were found to be much larger than those identified with the embedded instrumentation which was attributed to the relatively smaller crack widths generated in these specimens (see Section 6.6.6). The SSMBLG5-No.6Bars and SSMBLG6-Frosch were subjected to relatively higher levels of subsequent loads than the other specimens because the applied load history was associated with the visual crack initiation.
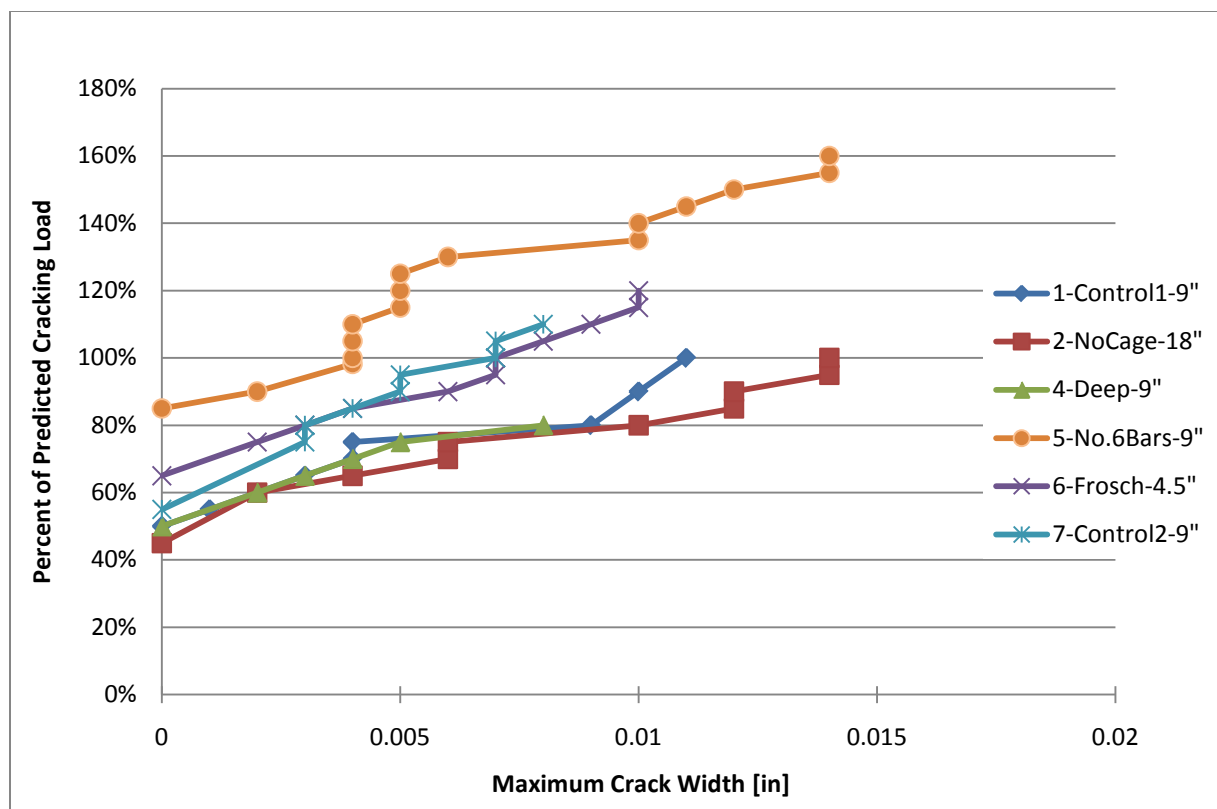
Figure 6.6.7: Maximum[1] crack widths measured on the end face[2] of selected specimens before each set of cycles

[1]Maximum crack width was measured at the horizontal precast flange -CIP interface; and in the case of SSMBLG6-Frosch, where two vertical cracks were observed at high loads, the largest crack width was recorded
[2]Reinforcement spacing from end face of specimen was half of the maximum reinforcement spacing

According to Figure 6.6.7, SSMBLG5-No.6Bars, SSMBLG6-Frosch, and SSMBLG7-Control2 appeared to outperform the other specimens, especially at higher levels of load in the case of SSMBLG6-Frosch and SSMBLG7-Control2. Also, in the case of SSMBLG6-Frosch, recall two vertical cracks were observed on each face of the specimen, which was generally preferred because the development of many, smaller cracks is often favored to the development of few, larger cracks, especially when the ingress of water and corrosive materials are of concern. Also observed from the figure, SSMBLG2-NoCage showed large increases in the measured crack width with each 5 percent increase in the applied load, especially at higher levels of load, highlighting the faster rate of degradation of this specimen compared to the others that were well reinforced for crack control. Furthermore, it is evident that an increased area of reinforcement can also provide satisfactory crack control performance, as shown by SSMBLG5-No.6Bars.

The section constructed with a deeper precast beam, SSMBLG4-Deep, was observed to perform relatively well, especially considering that the reinforcement ratio for crack control in this section was smaller than

197

the other specimens due to the increase in member depth while the section contained similar reinforcement details as were used in the control specimens.

The overall performance of the six subassemblage specimens based on the crack widths measured using a crack gage was good. Note that at an applied load of 100 percent of $P_{CR\text{-}pred}$, the worst performing specimen was SSMBLG2-NoCage, with a measured crack width of approximately 0.014 in. An estimate of acceptable crack widths was determined based on recommendations from ACI Committee 224, which recommended a maximum crack width of 0.007 in. for structures exposed to corrosive environments, and 0.016 in. as a maximum limit for aesthetics (ACI 224, 2001). Also recall that Frosch et al. selected a target maximum crack with of 0.021 in. during their study (Frosch et al., 2006).

The crack widths were also measured after the completion of all cyclic loading at each load step. The potential durability of each specimen subjected to cyclic loading might be inferred by examining the change in measured crack width on the end face before and after the completion of cyclic loading at a given load step, as illustrated in Table 6.6.1. Negligible to small increases in measured crack widths after cyclic loading at each load step indicated good performance. Many specimens showed no increase or only small increases in crack width (i.e., 0.001 in.) due to the application of cyclic loading. The four largest increases in the measured crack widths are highlighted in yellow.

Table 6.6.1: Increase in the measured crack width on the end face as a result of cyclic loading at each load step

Increase in measured crack width (in.)	Subassemblage Specimen					
Percent of $P_{cr\text{-}pred}$	1-Control1	2-NoCage	4-Deep	5-No.6Bars	6-Frosch	7-Control2
45	NCO[1]	0	NCO	NCO	NCO	NCO
50	0	0	0			
55	0	0.001	0.001			
60	0.001	0.002	0.001			0
65	0.001	0.002	0		0	0
70	0	0	0.003		0	0
75	0.004	0.002	0.003		0	0.001
80	0.001	0	0.002		0.001	0
85	NA[2]	0	Delam	0	0.001	0.001
90	0	0.001		0	0	0
95	NA	0		0	0	0
100	0.002	0.001		0	0	0.002
105	Delam[3]	Delam		0	0.001	0.001
110				0	0	0.002
115				0	0	Delam
120				0	0	
125				0.001	Delam	
130				0.003		
135				0		
140				0.001		
145				0.001		
150				0		
155				0		
160				0		

[1]No cracking was visually observed at associated load step
[2]Measurements were not available at given load step due to error in data collection
[3]Delamination was observed at vertical precast web – CIP interface

The relative performance between each face of a given specimen was also of interest. Each face had reinforcement located a specified distance away. The reinforcement near the origin face was a clear distance of 3.1 in. away in SSMBLG5-No.6Bars and SSMBLG6-Frosch and 3.25 in. in the remaining specimens, while the center of the reinforcement or paired hooks near the end face was half of the maximum spacing away, ranging from ideally 2.25 to 9 in. Figure 6.6.8 shows the difference in the measured crack widths between the origin face and the end face; a positive value in Figure 6.6.8 indicates that the crack width measured on the origin face was larger than that measured on the end face. For all

199

specimens shown other than SSMBLG6-Frosch, the proximity of the reinforcement to the origin face (3.1 in.) was smaller than the proximity of the reinforcement to the end face, and therefore the crack widths on the origin face would be expected to be smaller than those on the end face, resulting in negative values in Figure 6.6.8. On the contrary, SSMBLG6-Frosch data showed a negative trend, suggesting that the crack width at the end face, where the reinforcement was nearest the face of the specimen was larger than on the origin face; however, there was very little difference in the distance from the reinforcement to the origin and end faces in the SSMBLG6-Frosch specimen. Both control specimens showed a trend towards positive differences in the crack widths, again suggesting that the face with the reinforcement located closer exhibited larger crack widths. Furthermore, contrary to expected results, SSMBLG2-NoCage, which had the largest difference between the proximity of the reinforcement on each face at 5.75 in. (9 in. on end face – 3.25 in. on origin face), showed the least variation in the crack widths measured between the faces.

Because the crack width could only be measured at the external faces, and only one measurement was taken on each face, potential variations in the measured crack widths with respect to the distance from the reinforcement were expected, which may correspond to some of the unexpected trends documented in Figure 6.6.8.
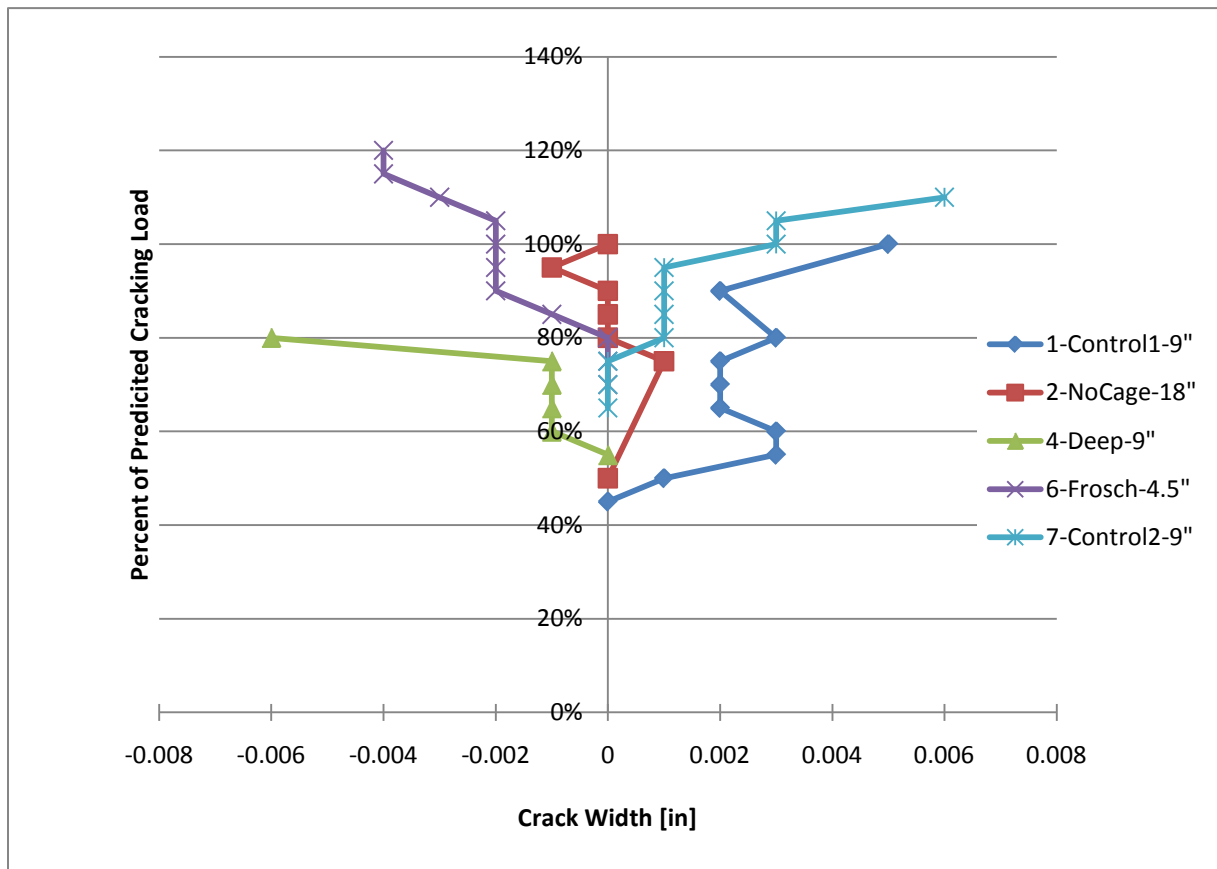
Figure 6.6.8[1]: Difference in crack width between the origin and end face (origin minus end)

[1]Measured crack widths were not available on the origin face of SSMBLG5-No.6Bars

200

6.6.4. Width of Cracking Near Joint Region Measured with LVDTs

The origin and end face of each specimen was instrumented with LVDTs oriented across the joint to measure the total displacement, or opening, within their gage lengths. The placement and LVDT size used was included in Section 6.2.

The Mid LVDT displacement measurements (from LVDT050, or LVDT100 for SSMBLG5-No.6Bars) located a distance of 2 in. from the bottom of the precast chamfer on the origin and end faces are shown in Figures 6.6.9 and 6.6.10, respectively. The figures illustrate the measured LVDT displacement as a function of the applied load; therefore improved performance can be identified by data closer to the upper left corner of the plot, and steeper slope. As before, the specimens exhibiting smaller crack widths were SSMBLG6-Frosch, SSMBLG7-Control2, and SSMBLG5-No.6Bars, especially at larger levels of load, which was especially evident by the steeper slopes of those three data series, compared to the slopes of the SSMBLG1-Control1, SSMBLG2-NoCage, and SSMBLG4-Deep data series.

The displacements measured with the Mid LVDTs correlated relatively well with the visually recorded crack widths measured with a crack gage at the intersection of the chamfers at the joint, documented in Section 6.6.3. It was generally expected that the displacements measured with the LVDTs would be slightly larger than the crack widths measured with a crack gage because the LVDT measurements included the concrete strains across the gage length, as well as the widths of each of the vertical cracks, where multiple cracks were present (i.e., SSMBLG6-Frosch), though this was not generally observed. Note however that the Mid LVDTs were located a vertical distance of 2 in. above the horizontal precast – CIP interface (which is where the visual observations were recorded). Because the specimens were subjected to flexural stresses, it was expected that the strain would vary linearly with the depth, which suggested that the Mid LVDTs could measure a smaller crack width than what was visually observed, depending on the amount of straining and additional cracking occurring between the gage blocks of the LVDT instrumentation. The maximum crack width measured with a crack gage and maximum displacement measured with the LVDT instrumentation are given for both the origin and end faces in Table 6.6.2. The measured LVDT displacements correlated relatively well to the crack widths measured visually using a crack gage.

201
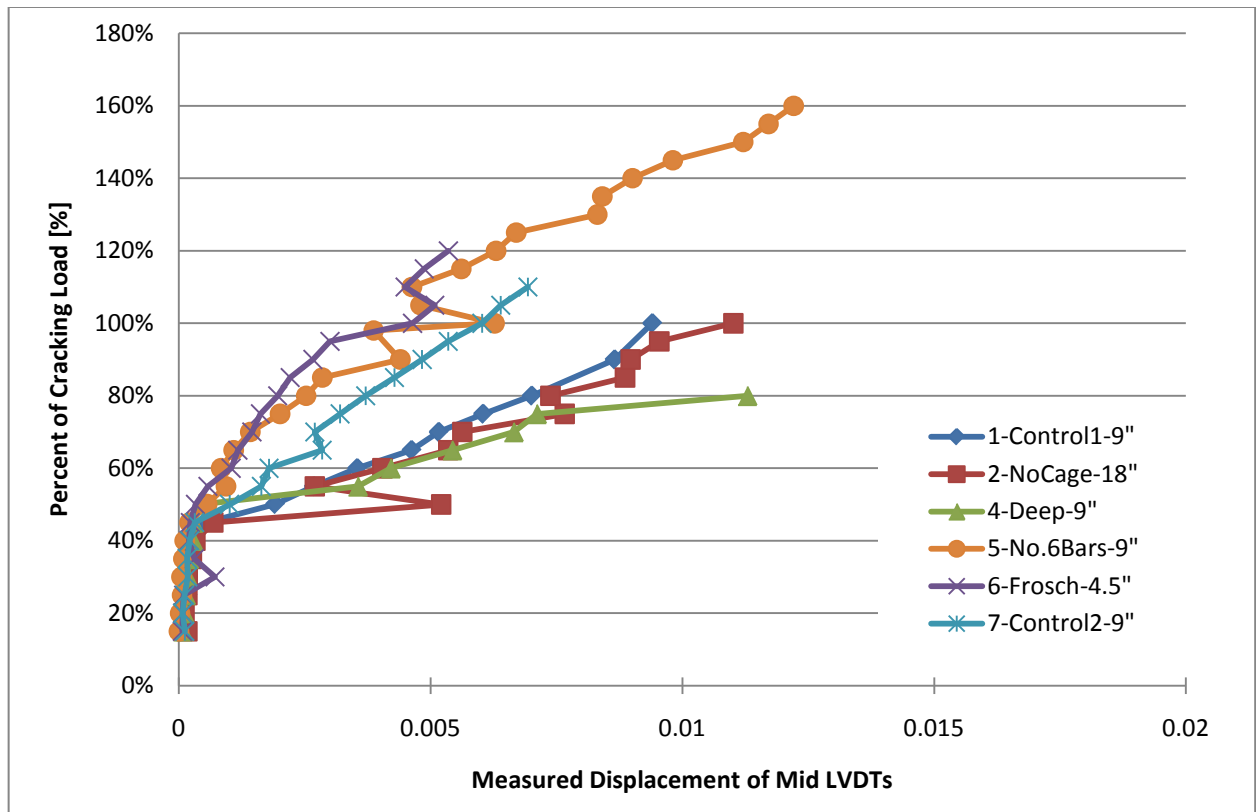
Figure 6.6.9: LVDT displacement measured via the Mid LVDT at the origin face
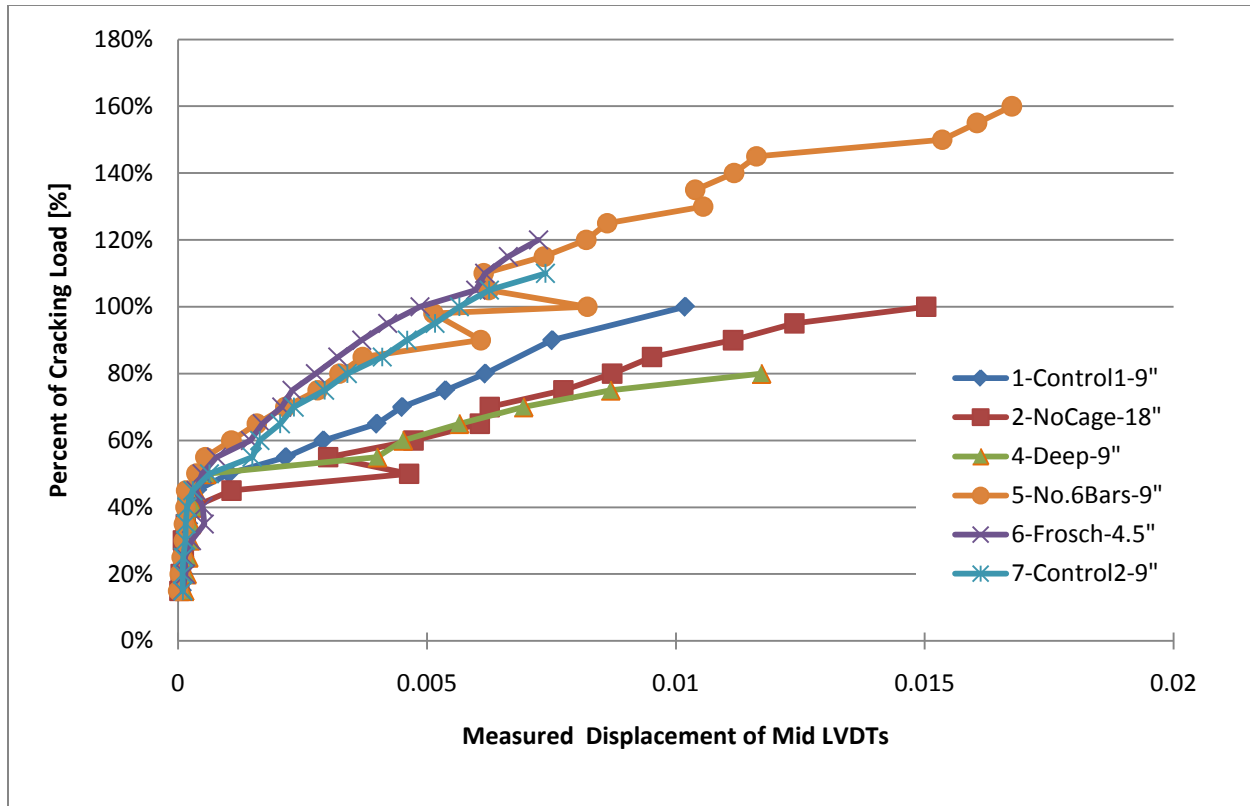
Figure 6.6.10: LVDT displacement measured via the Mid LVDT at the end face

Table 6.6.2: Maximum crack widths via crack gage (from Section 6.6.3) and LVDT displacements measured on the origin and end faces[1]

Specimen Description	Percent of predicted cracking load applied[2]	Origin Face		End Face	
		Measured with crack gage	Measured with LVDTs	Measured with crack gage	Measured with LVDTs
1-Control1-9"	100%	0.016 in.	0.009 in.	0.011 in.	0.010 in.
2-NoCage-18"	100%	0.014 in.	0.011 in.	0.014 in.	0.015 in.
4-Deep-9"	80%	0.008 in.	0.011 in.	0.008 in.	0.012 in.
5-No.6Bars-9"	160%	NA[3]	0.012 in.	0.014 in.	0.017 in.
6-Frosch-4.5"	110%	0.006 in.	0.005 in.	0.01 in.	0.007 in.
7-Control2-9"	120%	0.014 in.	0.007 in.	0.008 in.	0.007 in.

[1]Note that the locations of measurements were inconsistent between the crack gage and LVDT measurements (see Section 6.2)
[2]The tabulated applied percentage of the predicted cracking load was the largest applied load prior to cracking at the vertical precast web-CIP interface
[3]Crack widths measured with a crack gage were not available on the origin face of SSMBLG5-No.6Bars

The difference in the measured LVDT displacements between the origin and end faces at each load step was investigated in a similar method to that used in Section 6.6.3. Recall that all reinforcement near the origin face was a clear distance of 3.1 in. away from the face in SSMBLG5-No.6Bars and SSMBLG6-Frosch and 3.25 in. from the face in the remaining specimens, while the center of the hooked pair or center of the cage hoop reinforcement was half of the maximum spacing away from the end face, nominally ranging from 2.25 to 9 in. Figure 6.6.11 shows the difference in the LVDT displacements between the origin face and the end face; a positive value in Figure 6.6.11 indicates that the LVDT displacement measured on the origin face was larger than that measured on the end face. For all specimens other than SSMBLG6-Frosch, the proximity of the reinforcement to the origin face was less than that to the end face, therefore, it was expected that the results for these specimens would have a negative sign because crack widths were expected to increase as the distance from the nearest reinforcement increased, which generally corresponded with the observed results. Also note that SSMBLG6-Frosch was expected to have the least variation in the measurements from opposite faces because the difference in the proximity to the reinforcement to the exterior faces was the smallest for that specimen. Furthermore, the observed relative LVDT displacements between the origin and end faces matched the expected results better than the same analyses of the crack widths measured with a crack gage, which highlighted the variability in those measurements.

204
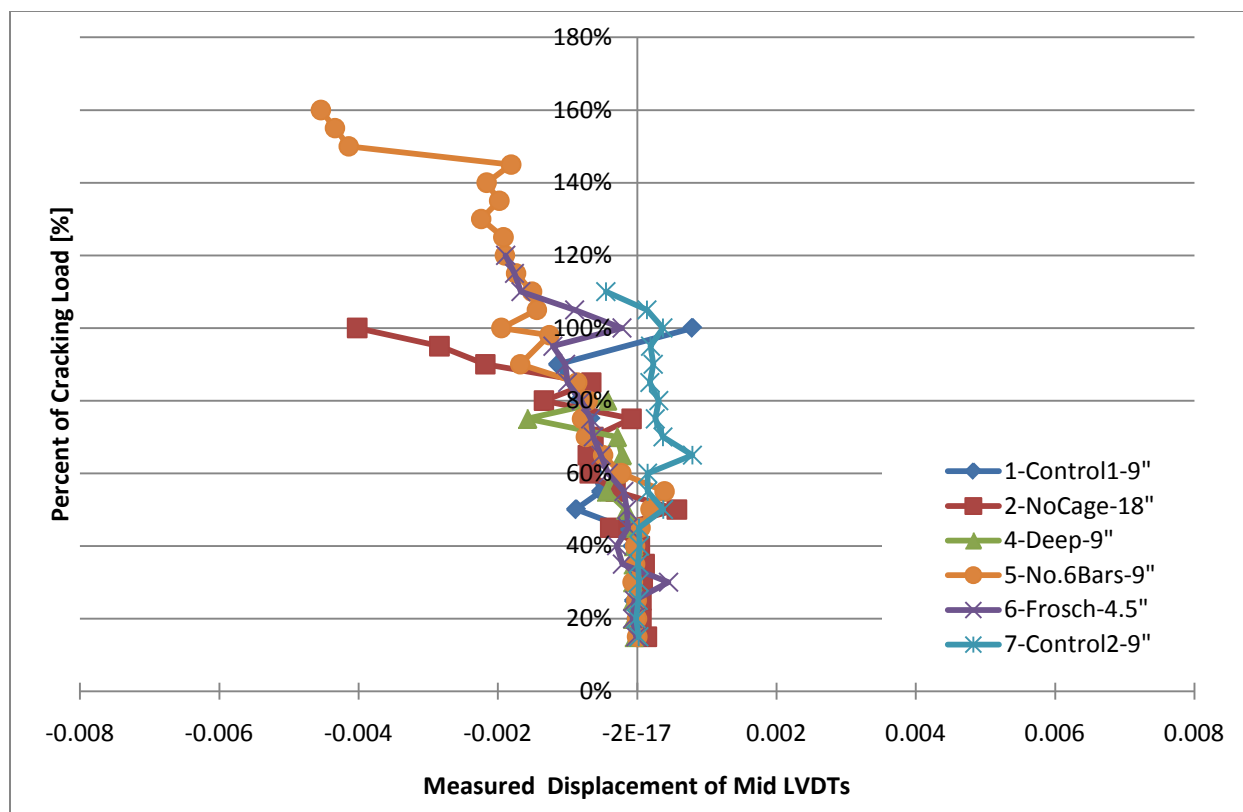
Figure 6.6.11: Difference in LVDT displacements between the origin and end face (origin minus end)

6.6.5. Rate of Increase in the Length of Cracking Near Joint Region via Visual Observation

The vertical length of the reflective crack near the joint region was also recorded during the subassemblage tests. The origin of the measured crack length was taken at the intersection of the chamfers at the joint in the precast flanges, as shown in Figure 6.6.4. As before, crack lengths were not documented for SSMBLG3-HighBars (which underwent delamination between the precast flange and the CIP concrete without the clamping system rather than developing a crack above the adjacent precast flange tips); crack lengths were also not documented on the origin face of SSMBLG5-No.6Bars using the same methodology as for the other specimens; therefore, those locations are not included in the specimen comparison. The length of the crack was measured using either the grid that was transferred onto each specimen, a tape measure, or both. Measurements were generally taken with a precision to within ¼ in. A representative image of the measurement of the length of the crack is shown in Figure 6.6.12. The measured crack length, normalized by the total section depth of each specimen (to include analysis of the deep section in the comparison), versus the applied load in terms of a percent of the predicted cracking load before each set of cycles measured on the origin and end face is shown in Figure 6.6.13 and Figure 6.6.14, respectively. Also included is the range of the predicted cracked neutral axis locations for the specimens shown in the figures, with the specimens representing the upper and lower bounds annotated on the plots. The predicted cracked neutral axis locations are also tabulated in Table 6.6.3. The location of the cracked neutral axis was calculated using measured concrete compressive strengths and the measured modulus of rupture for each specimen.

205
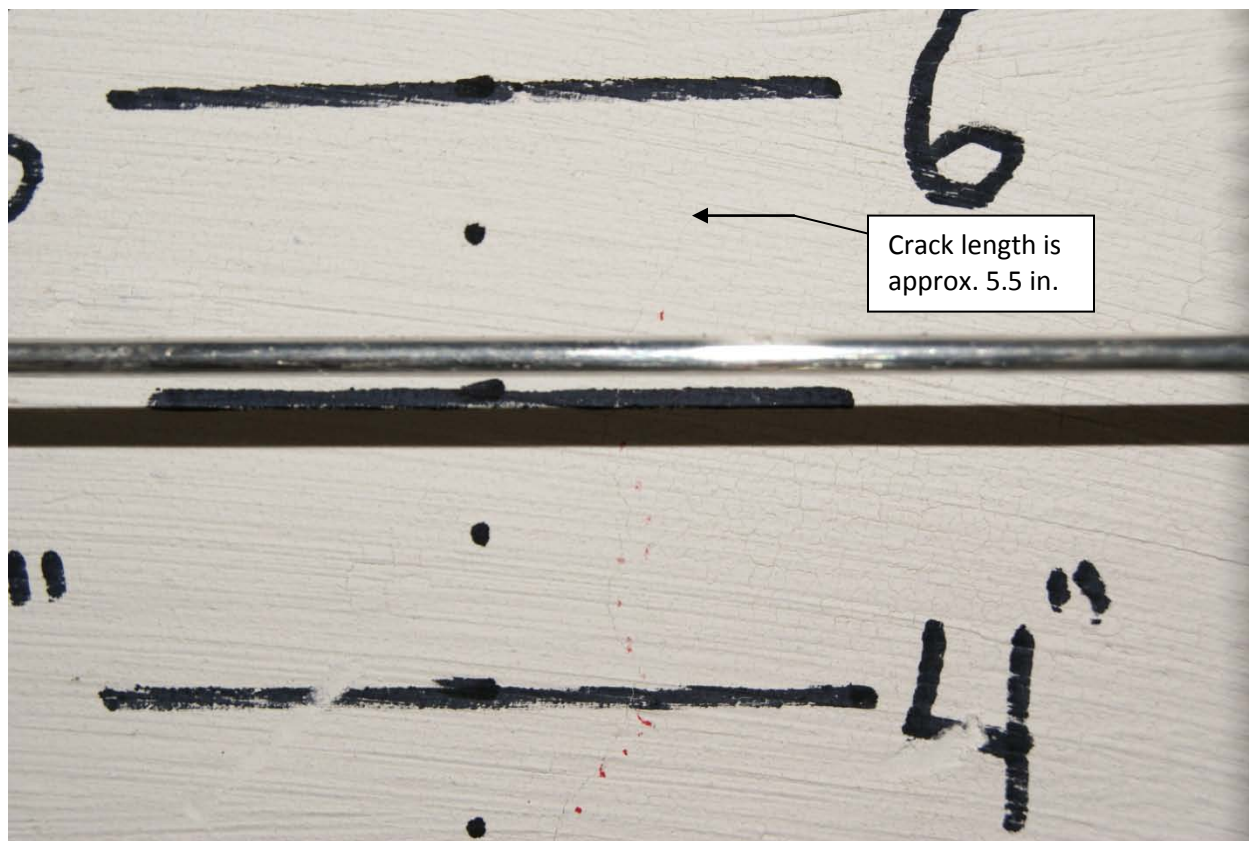
Figure 6.6.12: Measurement of the length of crack during subassemblage testing. Red dots illustrate path of crack
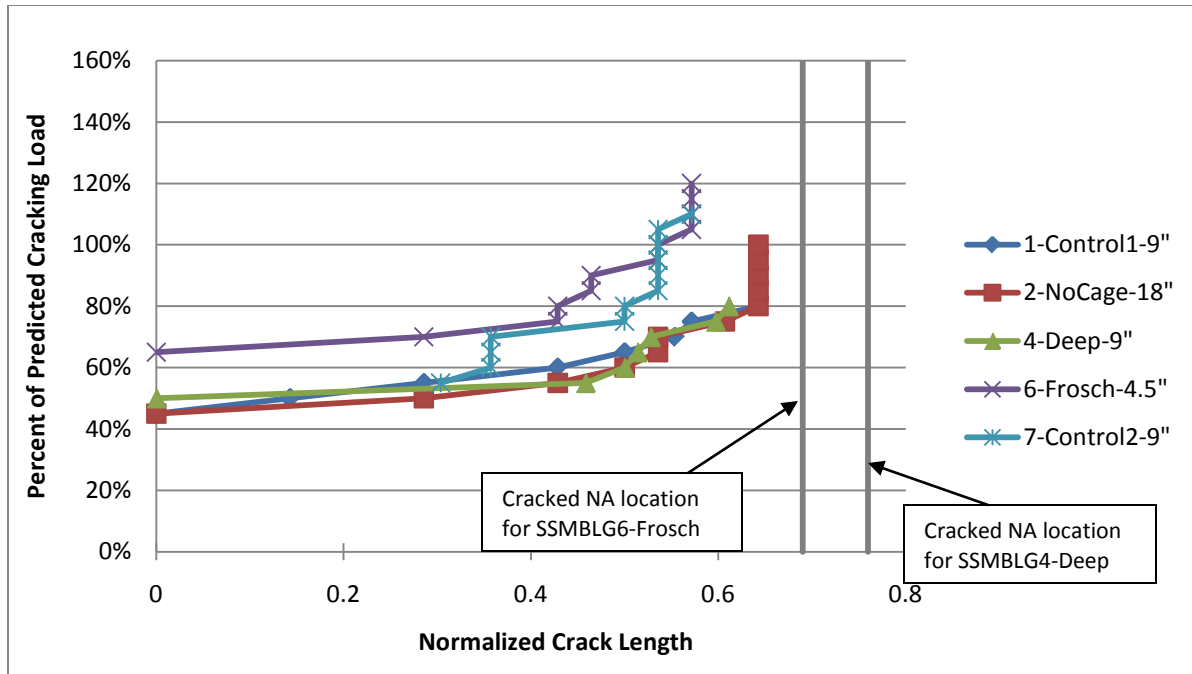
Figure 6.6.13: Normalized crack length on the origin face of selected specimens before each set of cycles
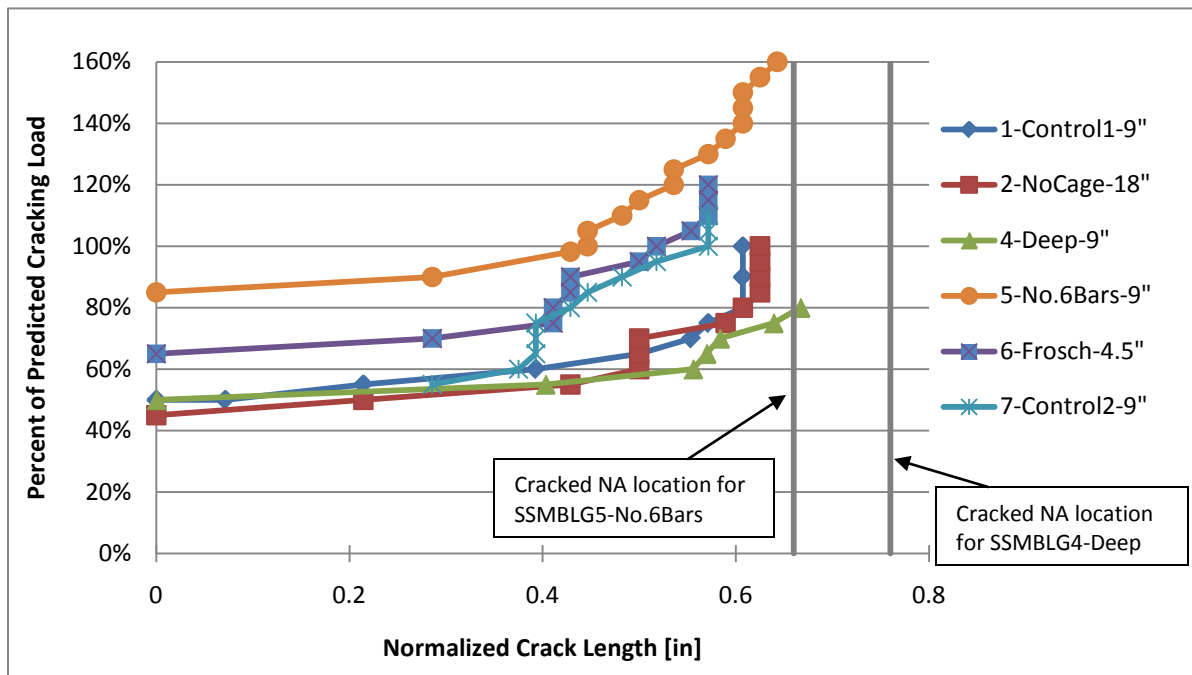
Figure 6.6.14: Normalized crack length on the end face of selected specimens before each set of cycles

207

Table 6.6.3: Predicted locations of the subassemblage cracked section neutral axes

Specimen	Cracked Section Neutral Axis Depth measured from the compression fiber	Normalized Depth of Cracked Section Neutral Axis (measured from bottom of section)
1-Control1	1.74 in.	0.71
2-NoCage	1.43 in.	0.73
4-Deep	2.09 in.	0.76
5-No.6Bars	2.48 in.	0.66
6-Frosch	2.01 in.	0.69
7-Control2	1.84 in.	0.71

For each of the specimens, normalized crack length increased to a maximum of between 50 and 65 percent of the total section depth (i.e., precast depth plus depth of the deck). The primary behavior of interest regarding the length of the crack was its rate of increase relative to increases in the applied load, or the slope of each data series, particularly over a select range of applied loads. The final, or maximum, crack length was of little significance because the crack length was expected to be driven up to the cracked neutral axis (NA) in each case, though the results for each specimen showed that the maximum visually observed length of the crack did not reach the location of the cracked neutral axis As illustrated in Figures 6.6.13 and 6.6.14, the well reinforced sections (i.e., SSMBLG5-No.6Bars and SSMBLG6-Frosch controlled the length and rate of increase in the length of the crack, especially at high loads. Note however, that the predicted neutral axis locations suggest that the maximum length of the crack in the well reinforced sections would be lower than in the remaining specimens.

The variation in the crack length measured on the origin face and end face before each set of cycles provided further insight regarding the effect of reinforcement spacing. The difference in the normalized crack length on the origin and end faces (origin minus end face) is illustrated in Figure 6.6.15; a positive value implies that the crack length on the origin face was greater than that on the end face at a given load step. As before, all specimens other than SSMBLG6-Frosch had reinforcement located closer to the origin face (3.1 in. clear from face) than the end face (2.25 in. from center of reinforcement to end face), suggesting that the difference in the normalized crack length should be negative for these specimens. However, for the majority of the specimens, the difference in the crack length between the origin and end faces was almost always positive, suggesting that the proximity of transverse reinforcement to a face for the situations investigated did not directly affect the length of the crack. This further supports the notion that the crack length is better controlled by the amount of reinforcement for crack control as opposed to the spacing of the reinforcement for the spacings included in this study.
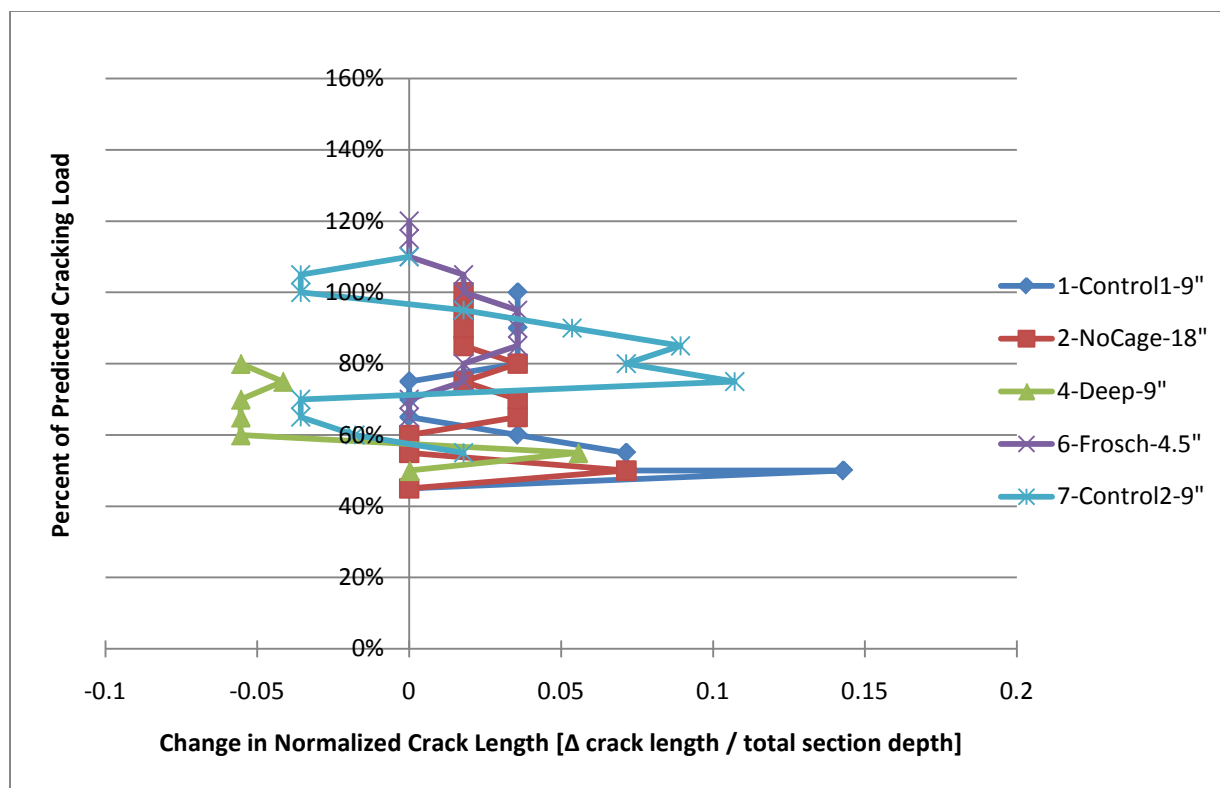
Figure 6.6.15: Difference in normalized crack length between the origin and end face (origin minus end) of selected specimens

6.6.6. Investigation of the Vertical and Horizontal Generation and Propagation of Reflective Cracking near the Precast Joint Measured via Concrete Embedment Resistive Strain Gages

The concrete embedment resistive strain gages provided a quantitative means to determine the internal crack initiation and propagation within the subassemblage specimens. The presence of cracking at a particular gage was identified based on the slope of the load versus strain relationship for each gage, which is illustrated in Figures 6.6.16 through 6.6.20. Using this method, the location of the crack could be determined using an "on-off" type of metric. Furthermore, when the load was small (i.e., when the percent of cracking load was on the order of 40 or 45 percent) large increases in the measured strain were also considered to be representative of cracking. As an example, consider the slope of the load versus strain data for SSMBLG1-Control1, as shown in Figures 6.6.16 through 6.6.20. Each figure illustrates the slope of the load versus strain data for each of the three transversely oriented concrete embedment resistive gages across the width of the CIP region near the precast joint at each vertical level (i.e., 1.0, 1.5, and 2.0). The figures are also annotated with the load at which load cracking was assumed to have occurred, which included some level of subjectivity.

209
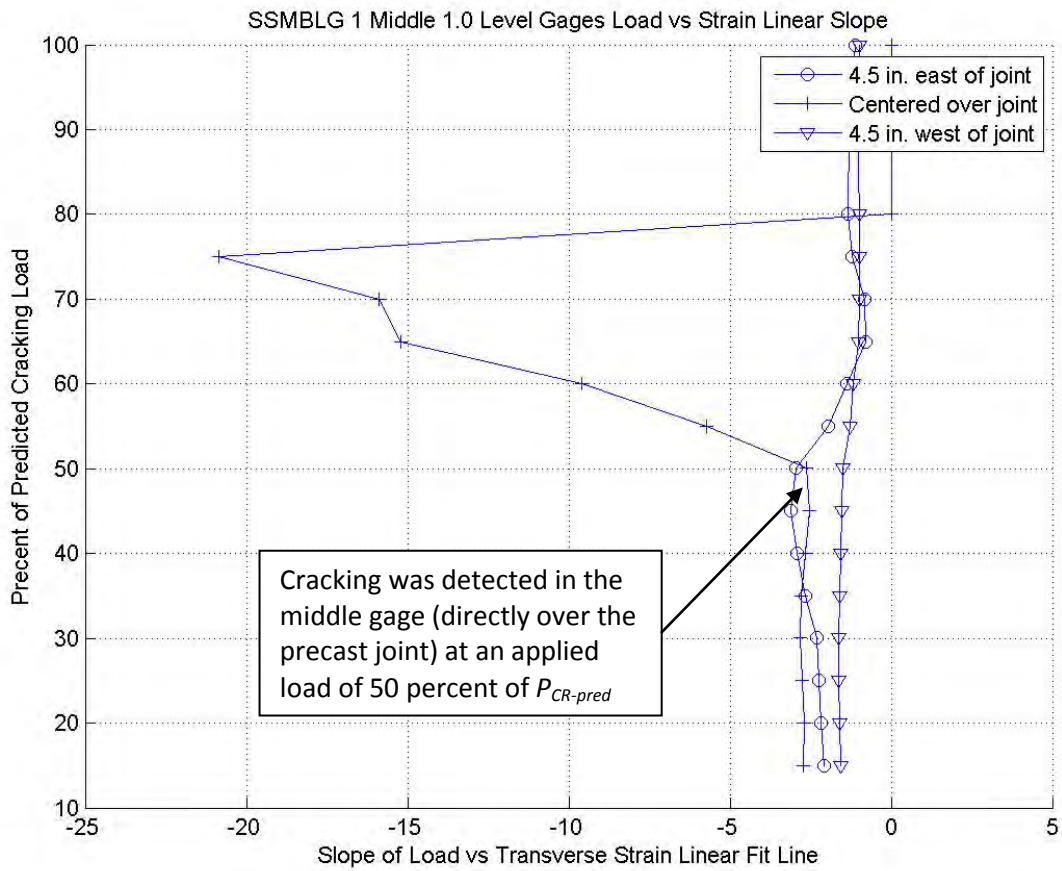
Figure 6.6.16: Slope of linear fit line for load versus 1.0 level strain data at middle cross section in SSMBLG1-Control1

210
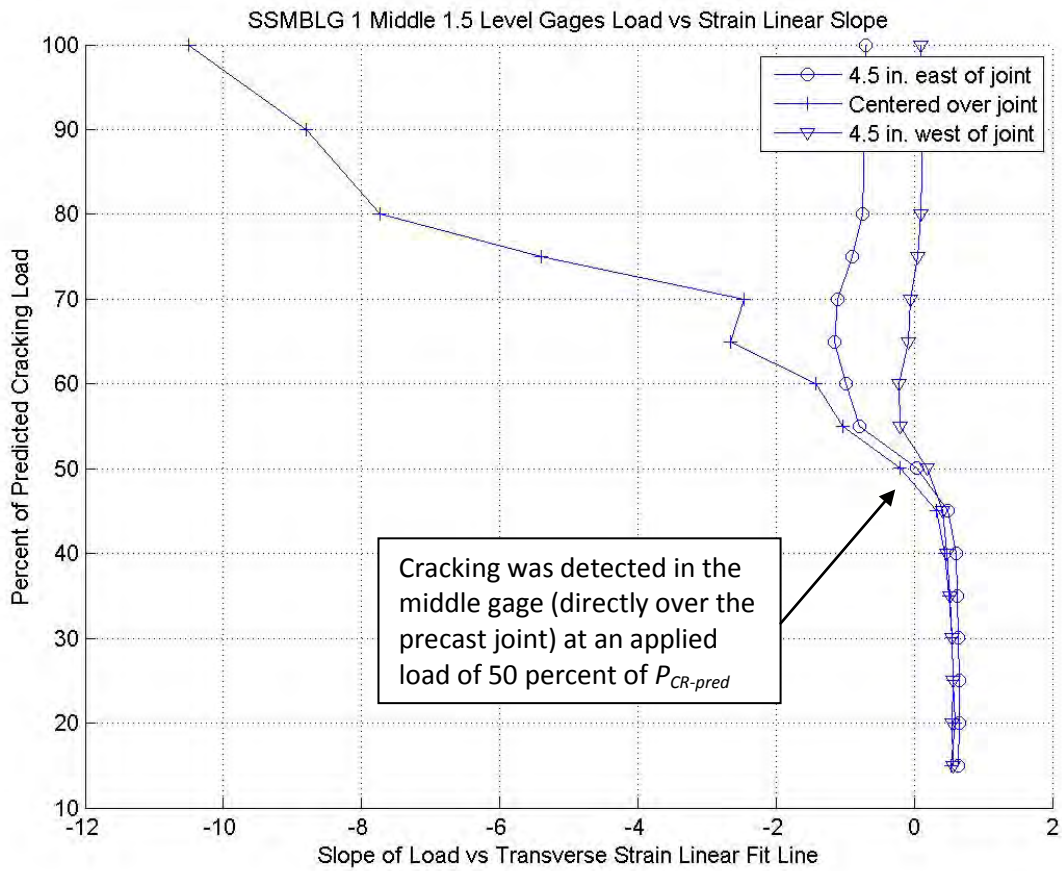
Figure 6.6.17: Slope of linear fit line for load versus 1.5 level strain data at middle cross section in SSMBLG1-Control1

211
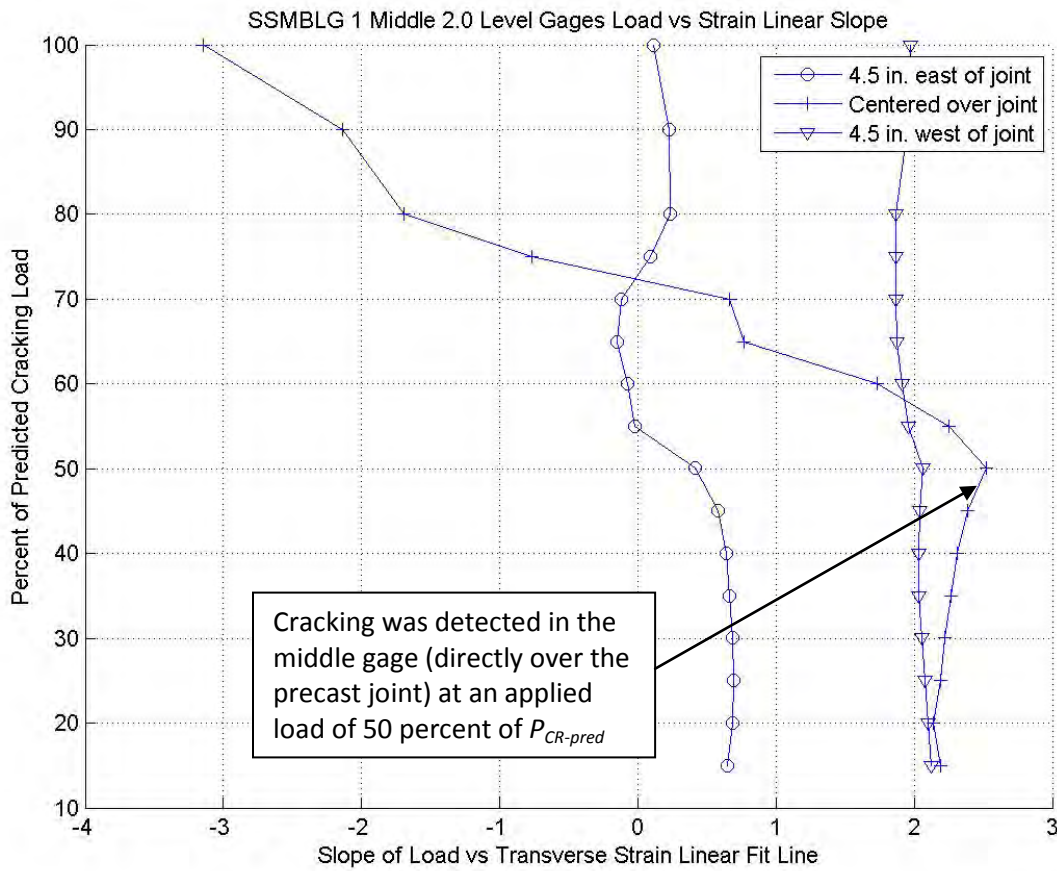
Figure 6.6.18: Slope of linear fit line for load versus 2.0 level strain data at middle cross section in SSMBLG1-Control1
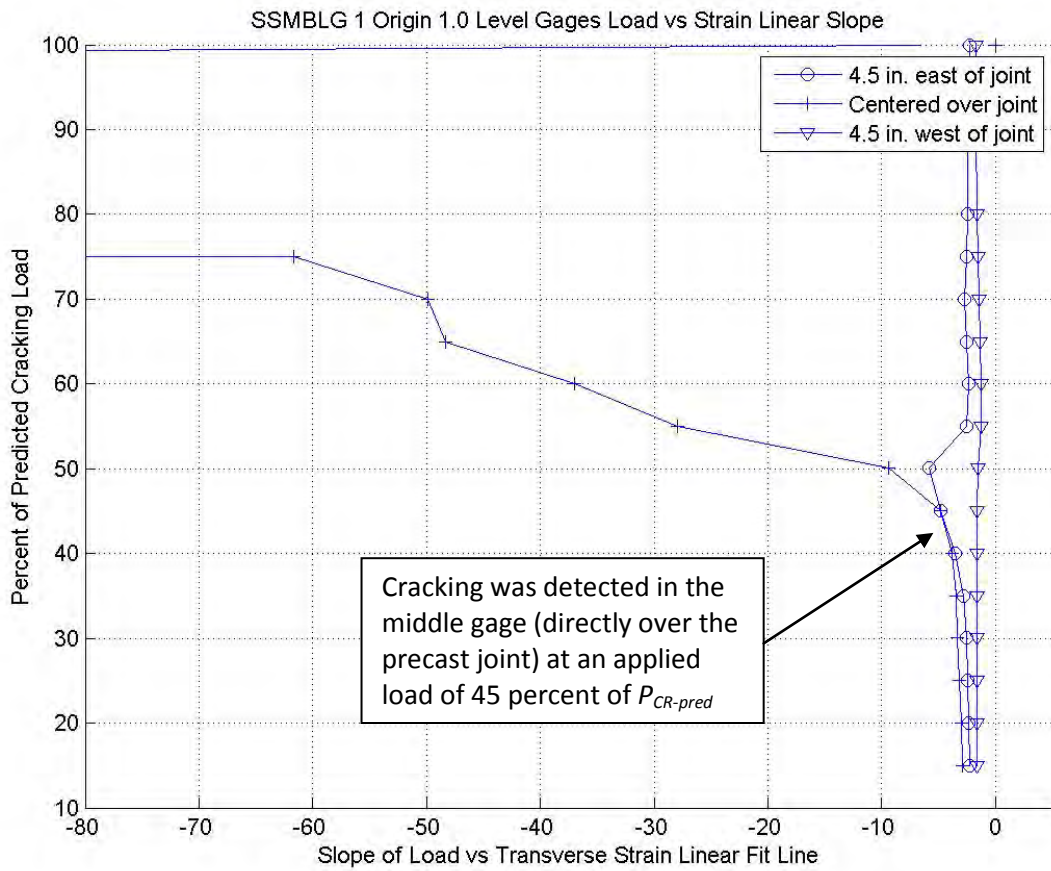
Figure 6.6.19: Slope of linear fit line for load versus 1.0 level strain data at origin cross section in SSMBLG1-Control1

213
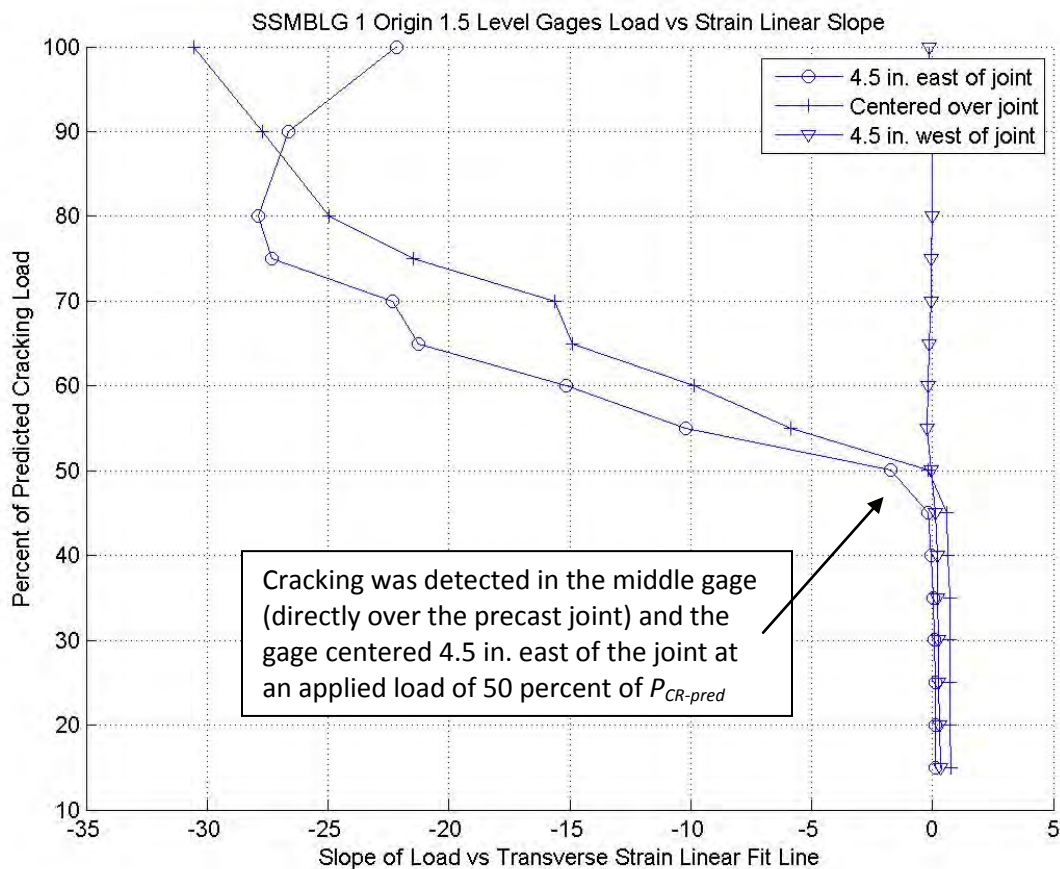
Figure 6.6.20: Slope of linear fit line for load versus 1.5 level strain data at origin cross section in SSMBLG1-Control1

The load at which cracking was first observed was taken as the first data point where a clear difference in the slope of the data occurred. For example, in Figure 6.6.16, the crack was assumed to be present at the 1.0 location at the midspan cross section at a load of 50% of the cracking load, with cracking observed only in the gage centered over the joint. Furthermore, when cracking was observed in two adjacent gages at similar levels of applied load, it was more likely that a single crack was developed in the region of overlap between the gages as opposed to two independent cracks.

Using this process, the load required to drive a crack to the various vertical levels of each specimen was determined. Recall (from Section 6.2) that the concrete embedment resistive gages were placed at three vertical locations designated 1.0, 1.5 and 2.0. The 1.0 level gages coincided with the depth of the transverse hooked bars which were nominally located 4-½ in. from the bottom of the specimen (for all but SSMBLG3-HighBars). The 1.5 level gages were located 8 in. from the bottom of the section (10 in. for SSMBLG4-Deep), and the 2.0 level gages coincided with the top of the cage (i.e., top of the precast web) at 12 in. from the bottom of the section (16 in. for SSMBLG4-Deep). The middle cross section contained the 1.0, 1.5, and 2.0 level gages, while the origin cross section contained only the 1.0 and 1.5 level gages.

214

Figure 6.6.21 and Figure 6.6.22 illustrate the load at which cracking was observed for each specimen at the gages through the depth at the midspan and origin cross sections, respectively.

A specimen exhibiting superior performance would have a steeper slope at each gage level, that is, larger levels of load would be required to drive a crack to a given depth. Better performance was observed in SSMBLG6-Frosch and SSMBLG5-No.6Bars, which corresponded with expected results, as the transverse reinforcement details of these two specimens included an increased area of reinforcement (achieved either through tighter spacing or larger bars, respectively). Also pertinent to these specimens was the fact that the cracked section neutral axis was slightly lower in the section than in the other members, as outlined in Table 6.6.3, though the variation in cracked neutral axis depth normalized to the total section depth was relatively small. An analysis of the remaining four specimens suggested that little to no increase in load was required to drive a crack from the lowest level of gage to the highest, indicating a less than ideal reinforcement design. As with the other analyses, SSMBLG3-HighBars were not included in this analysis because this specimen was initially tested with the absence of the clamping system.
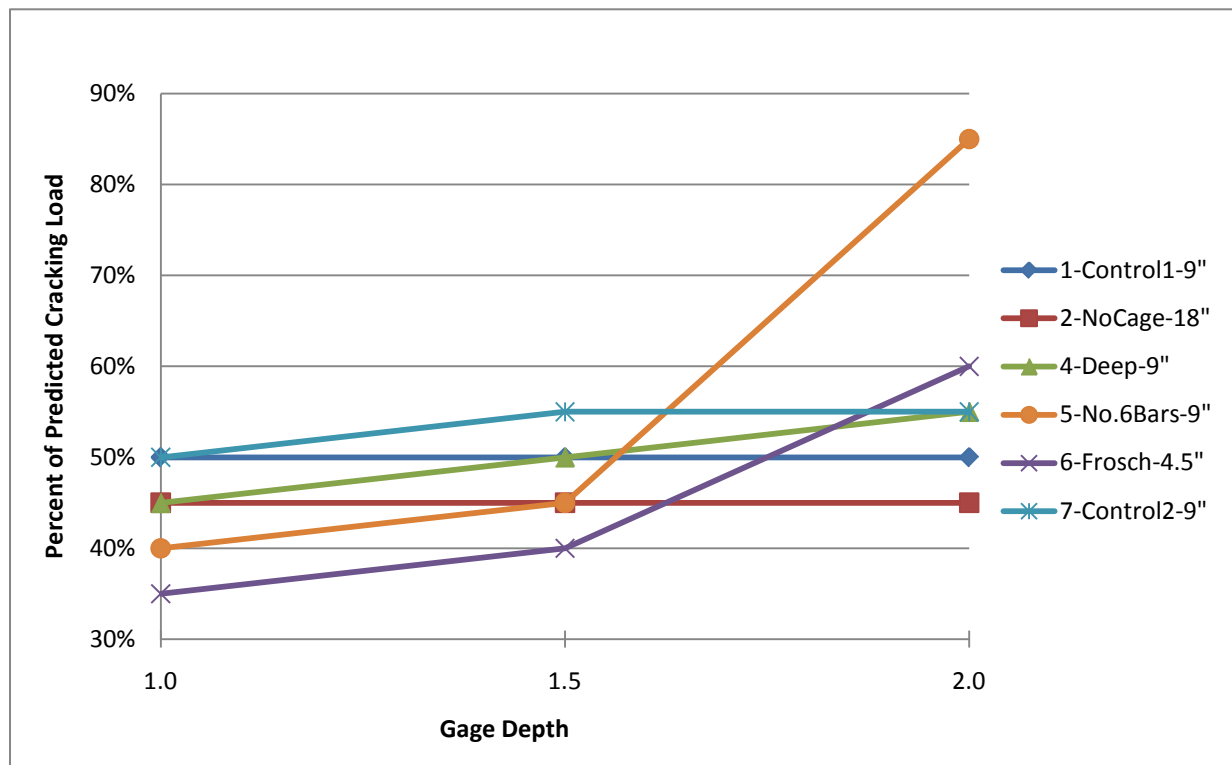
Figure 6.6.21: Load at which cracking was first observed in gages at middle cross section as determined from concrete embedment resistive strain gages

215
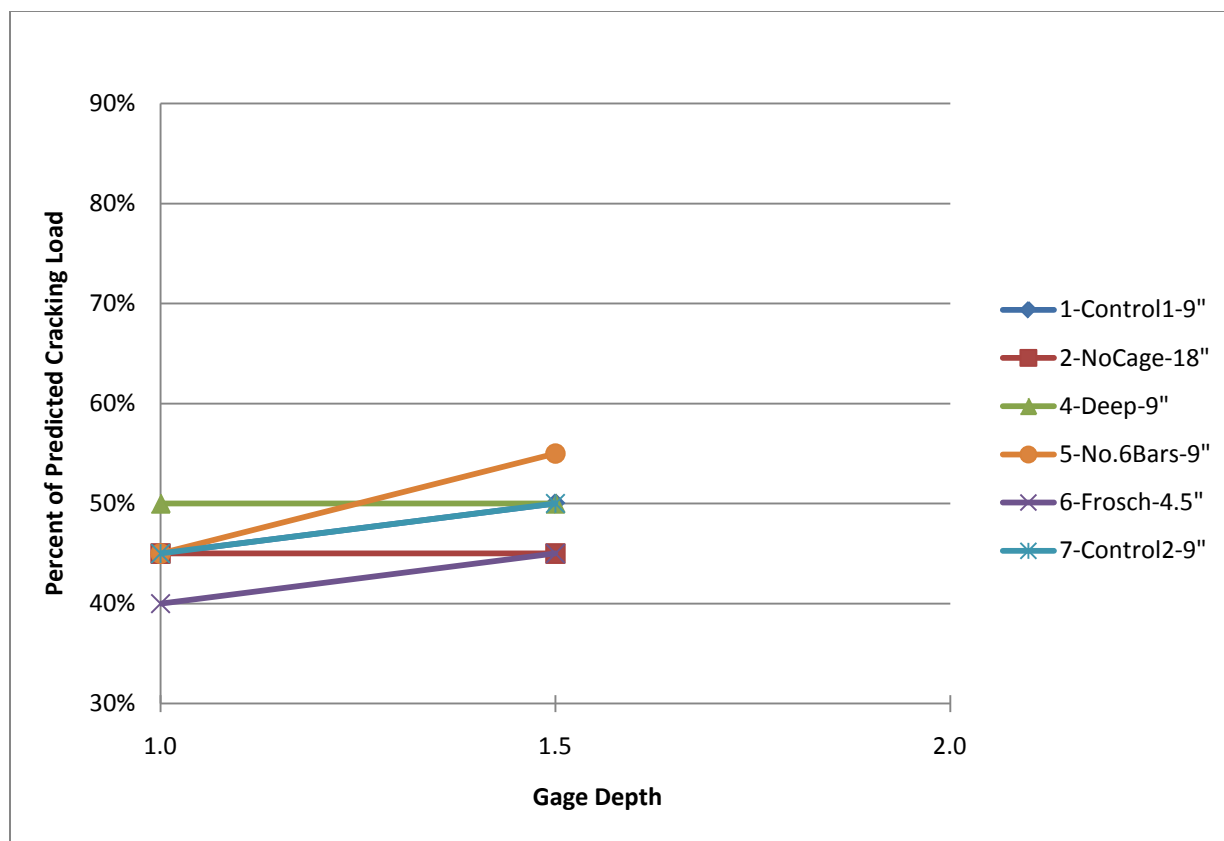
Figure 6.6.22: Load at which cracking was first observed in gages at origin cross section as determined from strain gages

The improved performance of SSMBLG5-No.6Bars and SSMBLG6-Frosch based on the analysis of the strain gage data supported the results from the previous sections. Furthermore, SSMBLG5-No.6Bars outperformed the Frosch specimen as larger levels of load were applied as the crack was driven up towards the top level of instrumentation. The specimen with larger reinforcing bars, which had a slightly larger overall reinforcement ratio for crack control, at 117 percent of the crack control reinforcement ratio of the Frosch specimen, further supported the notion that increased reinforcement area was superior to reduced reinforcement spacing when working to limit the depth of reflective cracking in the sections studied (although the reinforcement ratio provided in SSMBLG5-No.6Bars was closer to that specified by Frosch et al., 2006, because of the desire to maintain the same transverse bar sizes and hook spacing among the specimens). This may have resulted because the reinforcement spacings used in the study were all no larger than 9 in. with the exception of SSMBLG2-NoCage. With adequate reinforcement spacing, the dominant factor observed in controlling the cracking was the amount of reinforcement.

In addition to the investigation of the vertical propagation of cracking, the horizontal propagation was also considered. A longitudinally oriented spreader beam (i.e., parallel to the precast joint) was utilized to apply load during the subassemblage tests to provide a relatively uniform transverse stress gradient (i.e., stresses perpendicular to the precast joint) along the length of the precast joint. The spreader loading was designed

to provide a stress field that was constant along the length of the precast joint over which the reinforcement details of each particular specimen could be investigated. Furthermore, uniform loading applied along the structure above the longitudinal joint between the precast elements was necessary to provide an unbiased investigation of the crack mapping completed on the origin and end faces of each specimen, where the influence of the proximity of the embedded reinforcement on surface cracking was monitored. In addition, the investigation of horizontal crack propagation (both along the joint and transverse to the joint) provided a useful metric to identify details that promoted the development of more cracks, which were expected to be smaller in size.

Several transversely oriented concrete embedment and steel resistive strain gages were installed in each subassemblage specimen at various locations along the precast joint, as outlined in Section 6.2. The largest number of gages in a single layer were vertically located at approximately 1.5 in. from the horizontal precast – CIP interface, which corresponded to the vertical location of the center of the transverse hooked bars (in all cases except SSMBLG3-HighBars). A total of ten transversely oriented gages were located at this depth, and were distributed between the middle of the section near the precast joint, and towards the origin face. The behavior of cracking along the length of the precast joint was investigated using these ten gages, which provided insight into the uniformity of loading as well as a means of comparing the results from the visual observations and DAQ analysis. A plan view of the ten strain gages discussed in this section is shown in Figure 6.6.23. The 120 mm concrete embedment resistive strain gages over the joint, and to the east or west of the joint are illustrated using a square, circle and x symbol, respectively. The 60 mm concrete embedment resistive strain gages over the joint are shown with a star. The steel resistive strain gages are illustrated using a diamond symbol, while cracks observed visually on the end and origin faces of each specimen are denoted by a triangle.

The results of the analysis for each subassemblage specimen are presented in two complementary plots. In both plots, only gages in which cracking was detected are shown, and subsequently the number of data points in each plot varied. The first plot illustrates the load at which cracking was detected by the internal instrumentation or visually on each face versus the location along the precast joint where each of the ten strain gages of interest were located. The horizontal axis corresponds with the "x" axis dimension utilized for the duration of the subassemblage tests, and therefore a distance of zero corresponded to the origin face and the end face was located at either 67.25 in. (SSMBLG2-NoCage), 64 in. (SSMBLG6-Frosch), or 62.75 in. (remaining specimens). The first plot provides a means of identifying how uniform cracking was along the length of the precast joint in terms of the level of applied load required to induce cracking, and also provided insight into the uniformity of applied loading using a spreader beam.

The second plot presented for each specimen provides a means of visualizing the geometric location of the crack in terms of approximate lateral distance from the longitudinal joint between the precast flanges. The horizontal axis matches the previously described plot, and corresponds with the length of the precast joint. The vertical axis represents the width of the precast trough region, which is 24 in. Both plots also indicate the transverse hook and cage reinforcement in blue and green vertical lines, respectively. In this case, the gages near the middle and origin face of the specimen provided insight into where the crack was detected internally. The reported location of the crack represents the center of the gage in which cracking was detected, and therefore the location of the crack was given as the nominal "y" dimension for the gages, which corresponded to +/- 4.5 in. and 0 in. for the three gages located at each of the two cross sections. Also because of the overlap between adjacent gages, cracking detected in two adjacent gages at similar levels of load suggested that the crack was located in the region of overlap.

217

The results of the above analysis for each of the subassemblage specimens are shown in Figures 6.6.24 – 6.6.29.
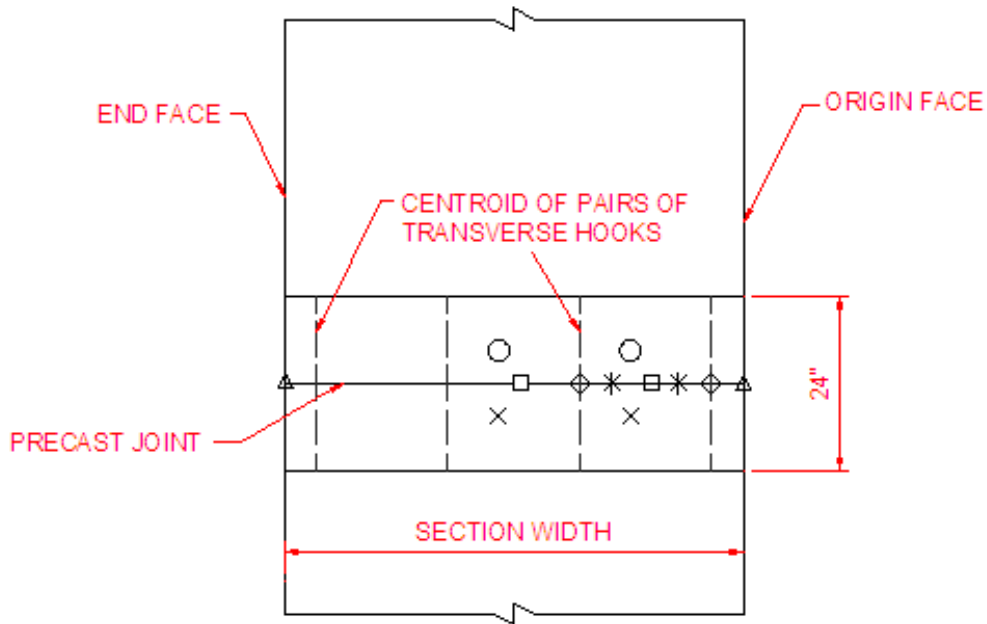
○	120 mm EMBEDMENT GAGE EAST OF JOINT (POSITIVE Y COORD.)
□	120 mm EMBEDMENT GAGE LOCATED DIRECTLY OVER JOINT
✕	120 mm EMBEDMENT GAGE WEST OF JOINT (NEGATIVE Y COORD.)
✳	60 mm EMBEDMENT GAGE LOCATED DIRECTLY OVER JOINT
◇	1 mm STEEL GAGE LOCATED DIRECTLY OVER JOINT
△	CRACKING DETECTED BY VISUAL OBSERVATION

Figure 6.6.23: Strain gage identification utilized for investigation of uniformity of cracking along the length of the precast joint. Pairs of hooks spaced at 18 in. and the cage reinforcement are not shown in the drawing for clarity
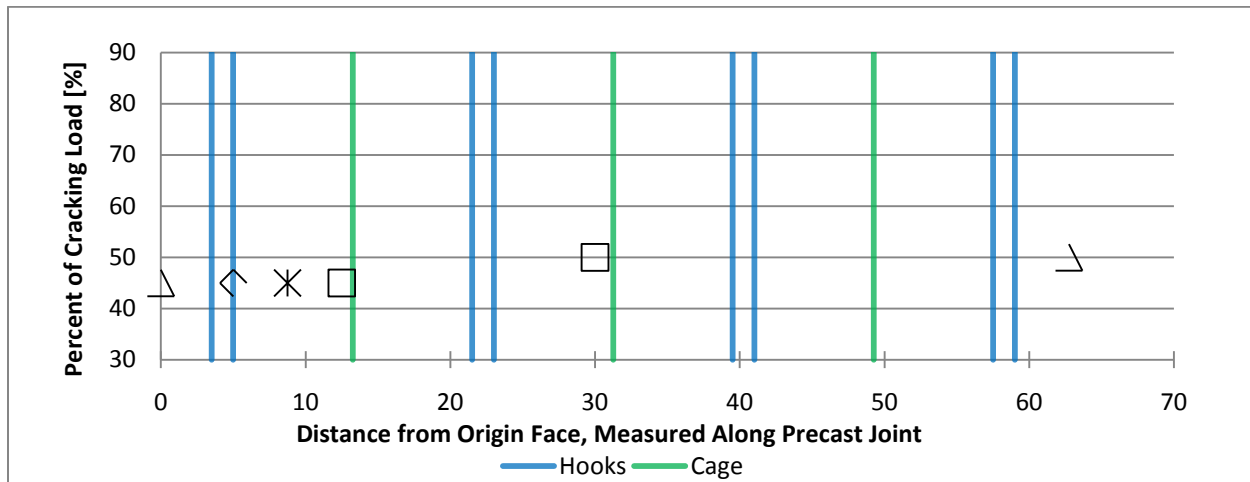
218

(a) Load at which cracking was detected at various locations along the length of the precast joint
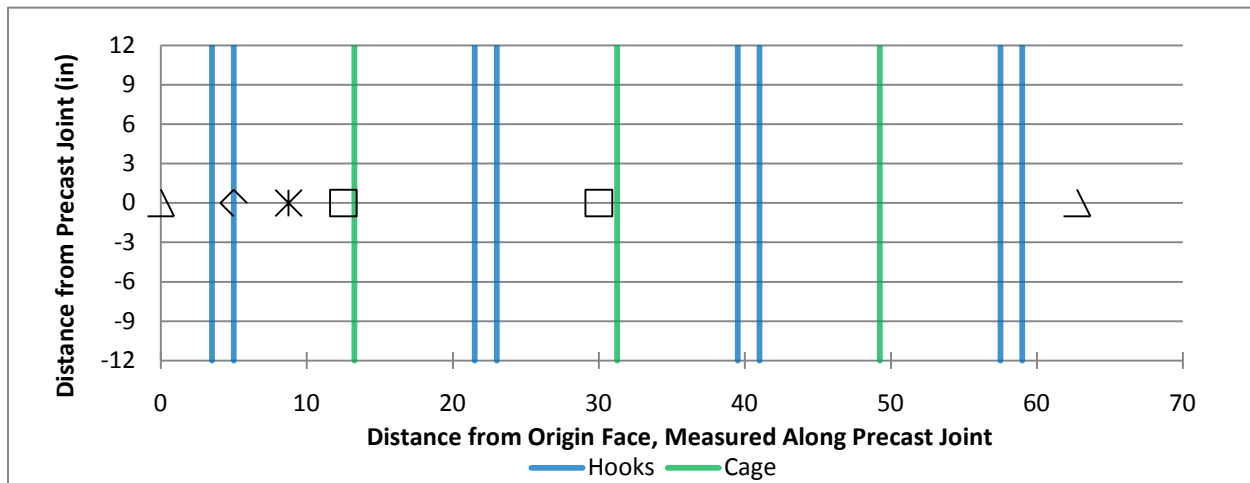
(b) Lateral location of instrumentation in which cracking was detected at various locations along the length of the precast joint

Figure 6.6.24: Load and location at which cracking was detected for SSMBLG1-Control1

The results from SSMBLG1-Control1 showed relatively good uniformity in the location and load at which cracking was observed. The load at which cracking was detected near the origin cross section and the middle cross section varied by only one load step or 5 percent of the predicted cracking load. Cracking was detected internally near the origin cross section at 45 percent of the predicted cracking load, while not visually observed on the origin or end face until the following load step, at 50 percent of the predicted cracking load. Also, as shown in Figure 6.6.24(b), the instrumentation in which the crack was detected was that which was centered over the longitudinal joint between the precast flanges.
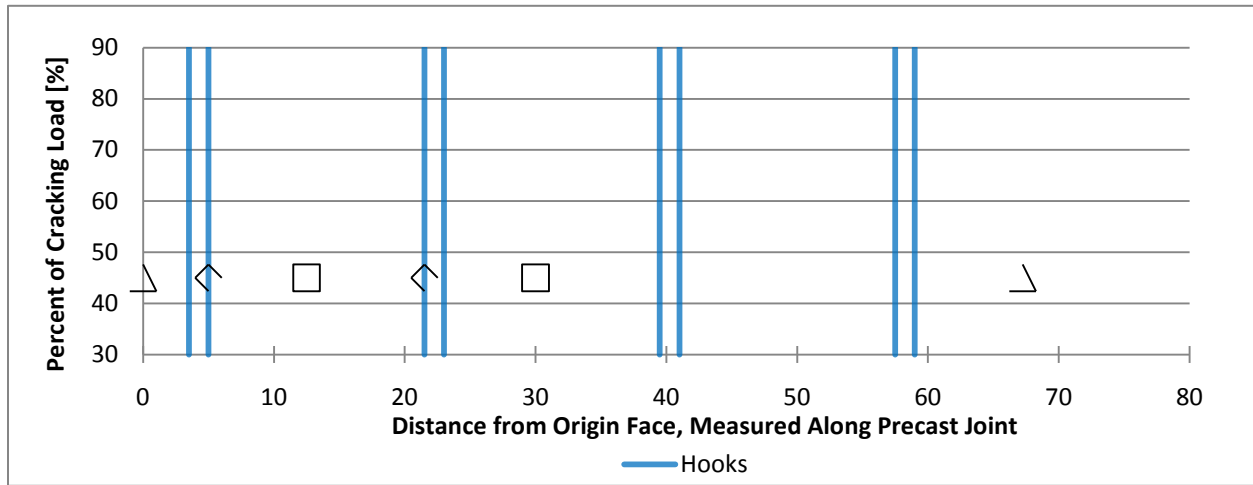
219

(a) Load at which cracking was detected at various locations along the length of the precast joint
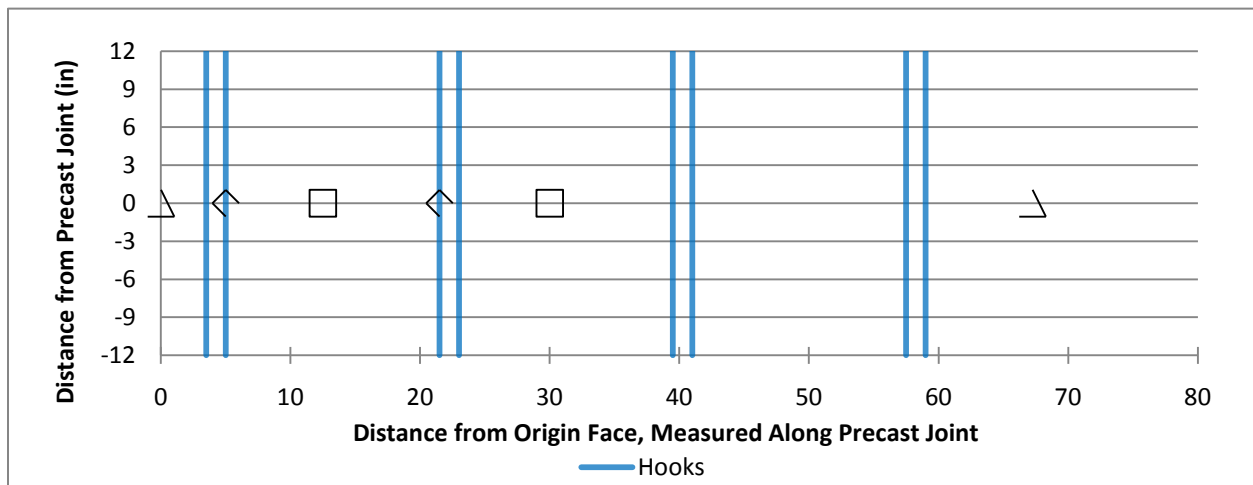
(b) Lateral location of instrumentation in which cracking was detected at various locations along the length of the precast joint

Figure 6.6.25: Load and location at which cracking was detected for SSMBLG2-NoCage

Relatively good uniformity in the location and load at which cracking was detected was also observed for SSMBLG2-NoCage. As with the first specimen, cracking was observed via the embedment instrumentation one load step prior to the visually observed cracking load. Also, cracking was detected solely in the instrumentation which was centered directly over the longitudinal joint between the precast flanges.
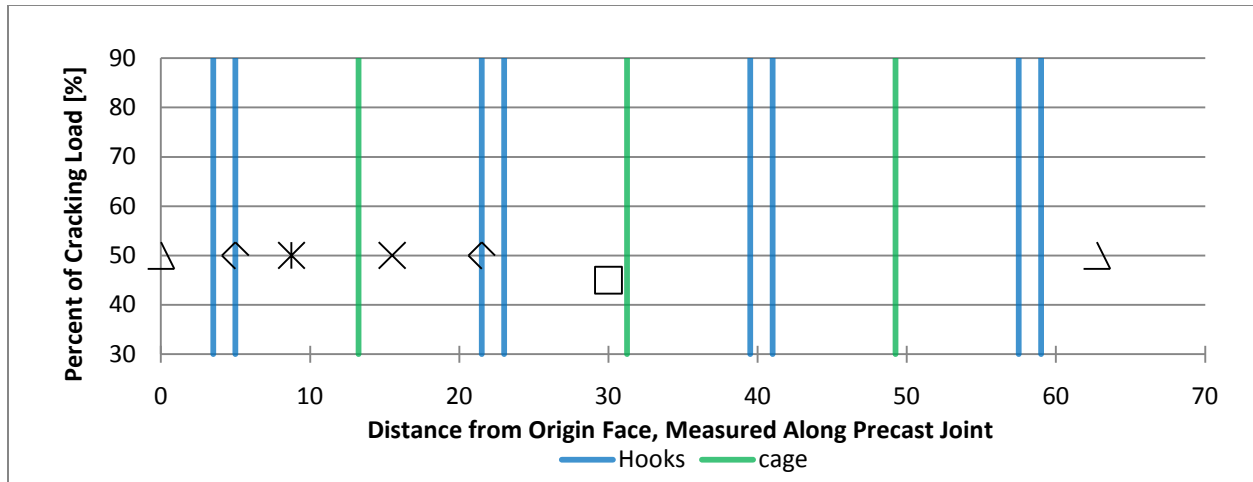
220

(a) Load at which cracking was detected at various locations along the length of the precast joint
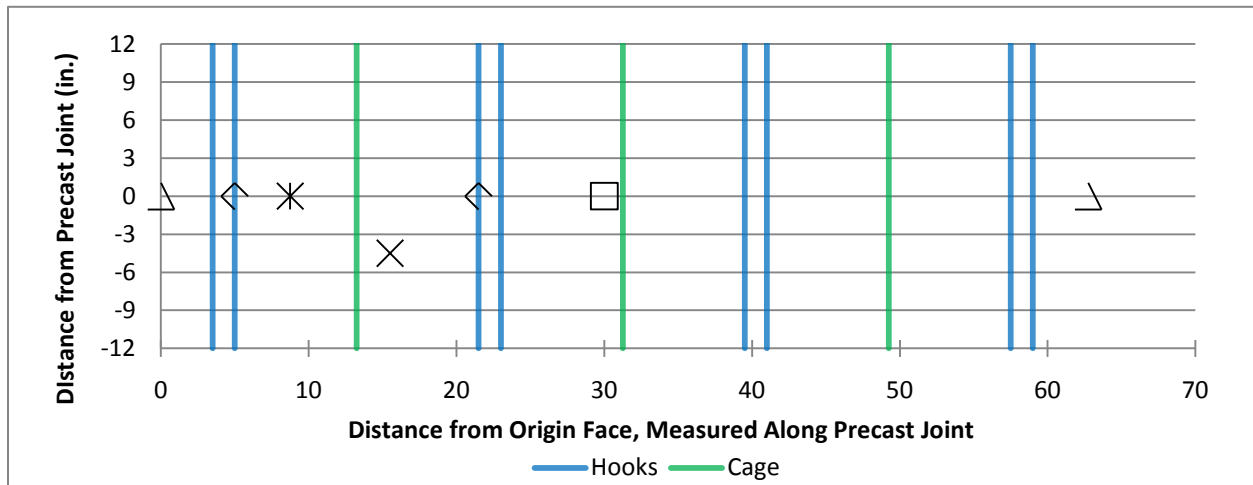
(b) Lateral location of instrumentation in which cracking was detected at various locations along the length of the precast joint

Figure 6.6.26: Load and location at which cracking was detected for SSMBLG4-Deep

As observed in the previous two specimens, the visually observed cracking load was larger than the load at which cracking was detected via the embedded instrumentation for SSMBLG4-Deep. Cracking was relatively uniform along the length of the longitudinal joint between the precast flanges, and varied by 10 percent of the predicted cracking load between the internal and visually observed results. Cracking at the set of three concrete embedment resistive strain gages near the origin face was detected in the gage centered 4.5 in. west of the precast joint, though the remaining gages near the origin face (which were all centered over the precast joint) also detected the crack.
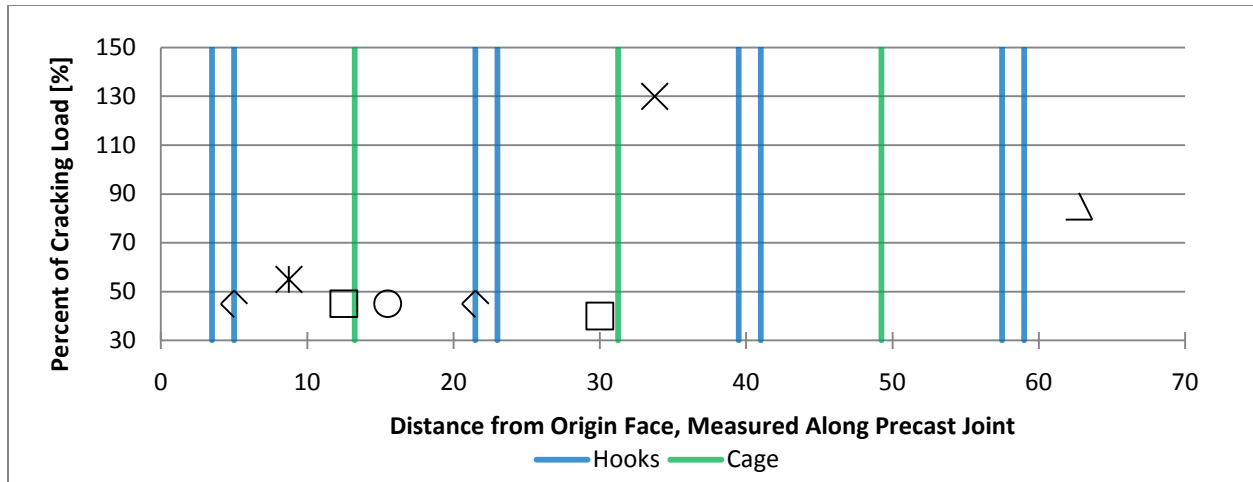
221

(a) Load at which cracking was detected at various locations along the length of the precast joint
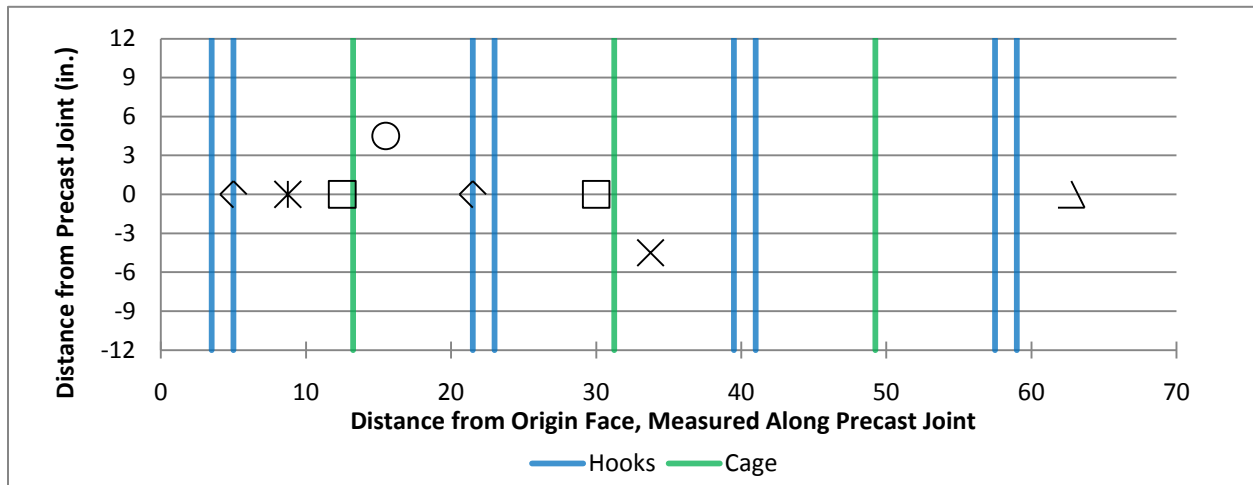
(b) Lateral location of instrumentation in which cracking was detected at various locations along the length of the precast joint

Figure 6.6.27: Load and location at which cracking was detected for SSMBLG5-No.6Bars

The results for SSMBLG5-No.6Bars are shown in Figure 6.6.27. For this specimen, visual observations were not recorded on the origin face of the specimen, and are therefore not present in the figure. Cracking was first detected in SSMBLG5-No.6Bars with the internal instrumentation at an applied load of approximately 45 percent of the predicted cracking load, which was observed at both the origin and middle cross sections; however the load at cracking detected by the internal gages did not correlate with the load at which cracking was visually observed on the end face, which was approximately 85 percent of the predicted cracking load. The discrepancy between the DAQ and visually observed data is likely due to an error in the load at which cracking was visually observed, possibly as a result of the crack not being immediately identified. This might be attributed to crack widths being smaller in this specimen than those of other

222

specimens where the internal instrumentation and external visual measurements better correlated in terms of crack initiation.

Also observed in SSMBLG5-No.6Bars was that the crack traversed two gages at each of the two multi-instrumented cross sections. Near the origin face, the crack traversed the gage centered over the joint first, and then at the next load step was detected in the gage 4.5 in. west of the joint. This may have indicated that the crack was slightly offset from the longitudinal joint between the precast flanges. At the middle cross section the crack was detected in the gage centered over the joint at roughly the same load as other locations in the section, and then cracking was detected in the gage 4.5 in. east of the joint at a significantly higher load (i.e., a approximately 130 percent of the predicted cracking load). The indication of cracking on the opposite side of the joint compared to the other gage that had previously indicated cracking, at a much later time in the test after the load had been increased significantly, suggests that multiple cracks developed in the section. The presence of multiple cracks was expected to be a beneficial characteristic of PCSSS bridges, because more cracks near the joint suggested that the crack widths may be smaller, and cracks located in the region of the cage reinforcement was preferred to cracking occurring near the vertical precast web, where the cage provided no benefit.
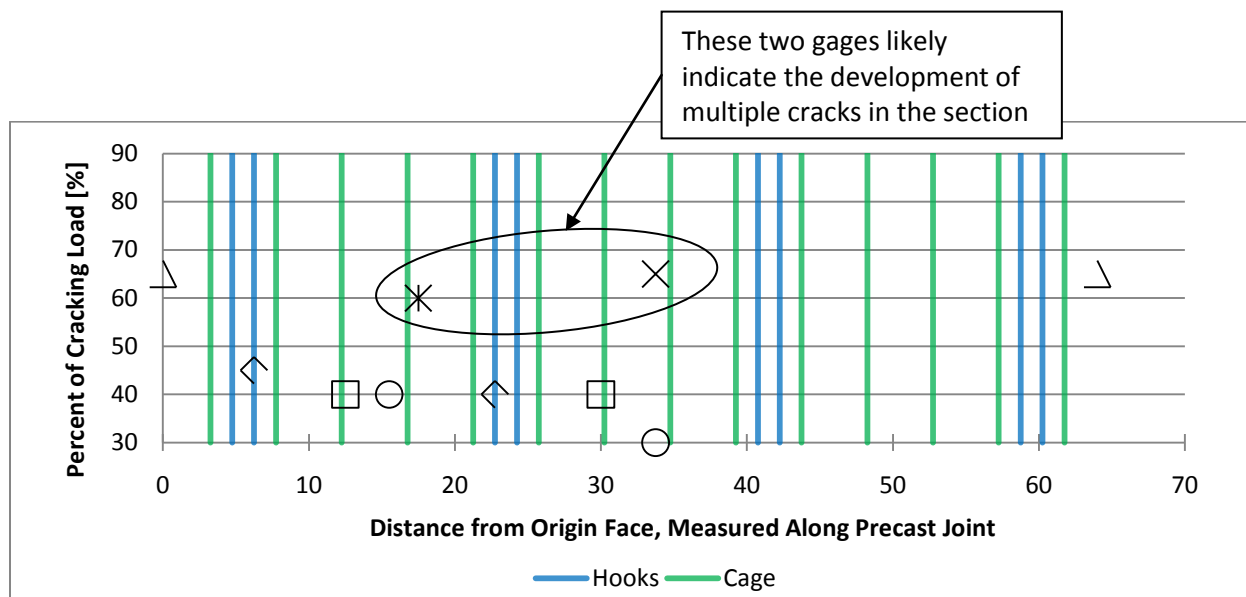
223

(a) Load at which cracking was detected at various locations along the length of the precast joint
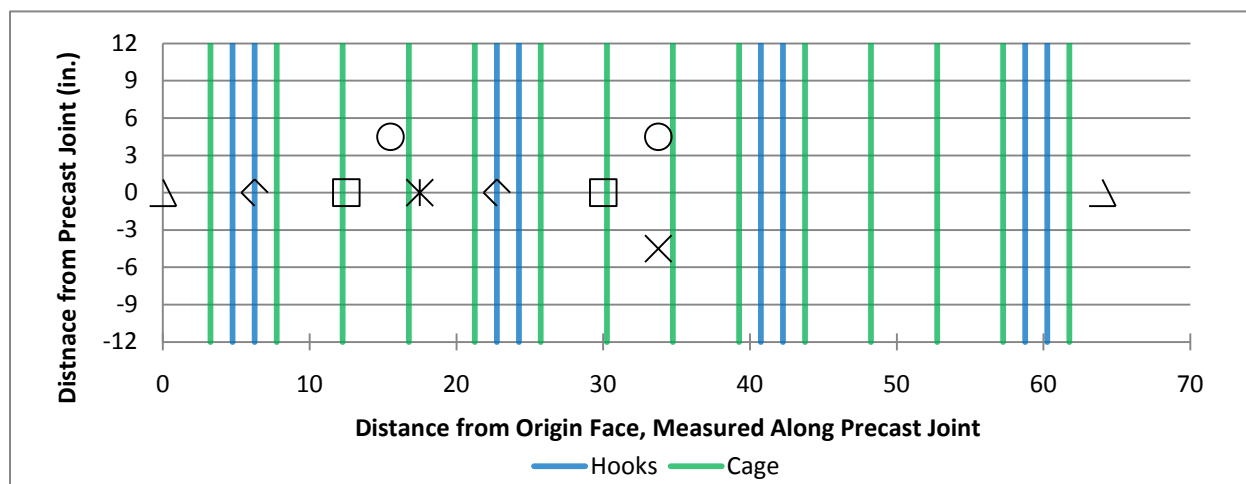
(b) Lateral location of instrumentation in which cracking was detected at various locations along the length of the precast joint

Figure 6.6.28: Load and location at which cracking was detected for SSMBLG6-Frosch

Cracking in SSMBLG6-Frosch was detected in the most number of gages, a total of eight, among the specimens. There was a relatively large variation in the load at which cracking was detected, though the grouping of data points near 40 and 65 percent of the predicted cracking load suggested that multiple cracks were present in the section. Also, as discussed in Section 6.6.2, two cracks were observed near the longitudinal joint between the precast flanges on both the origin and end faces of this specimen, with the secondary cracks observed visually at approximately 140 percent of the predicted cracking load. These

224

observations suggest that the relatively large reinforcement ratio provided in SSMBLG6-Frosch (which was accomplished through a tight spacing of No. 3 cage stirrups) encouraged the development of more, smaller cracks, as for the case of SSMBLG5-No.6Bars. The presence of multiple cracks was further supported by the results shown in Figure 6.6.28, specifically at the middle cross section, where cracking was detected in the gages centered directly over the joint, as well as the gages centered 4.5 in. in either direction of the joint at different load levels.
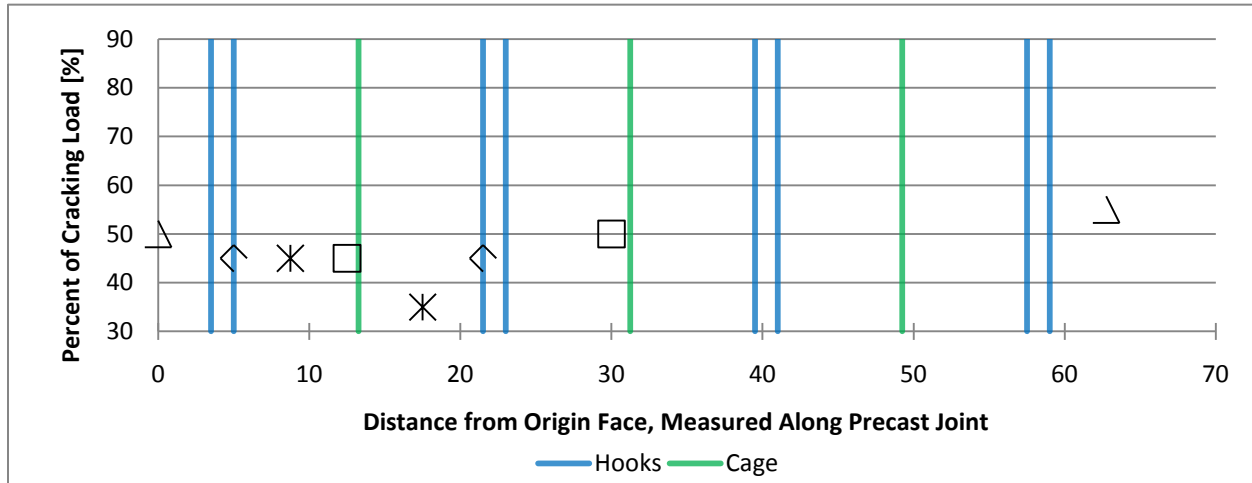
(a) Load at which cracking was detected at various locations along the length of the precast joint
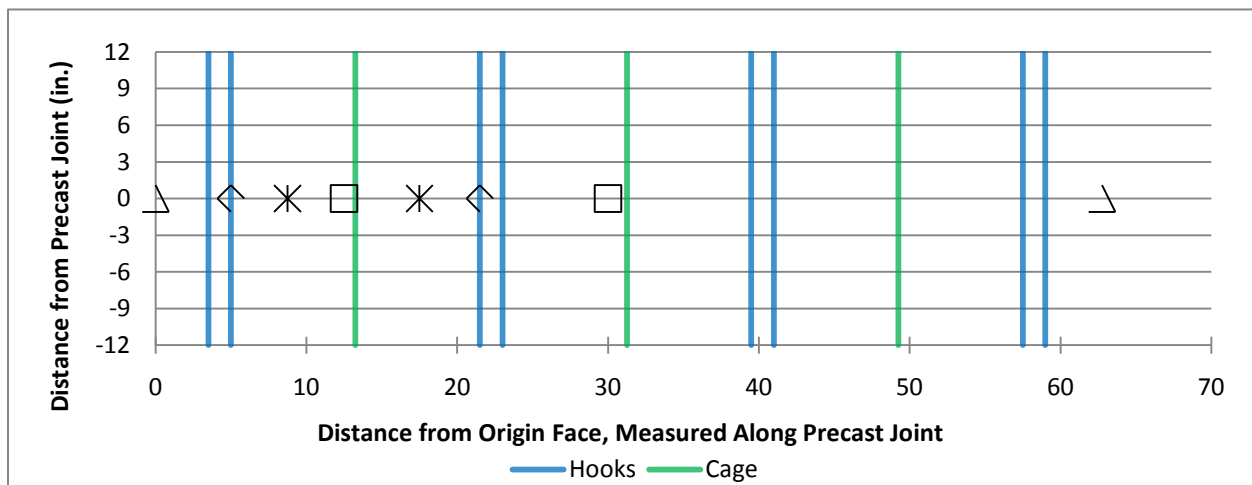
(b) Lateral location of instrumentation in which cracking was detected at various locations along the length of the precast joint

Figure 6.6.29: Load and location at which cracking was detected for SSMBLG7-Control2

The second control specimen exhibited behavior similar to SSMBLG1-Control1, SSMBLG2-NoCage, and SSMBLG4-Deep, in that a single crack was detected along the length of the longitudinal joint between the

225

precast flanges, as shown in Figure 6.6.29(b), at roughly the same applied load despite the presence of the smooth surface condition.

In general, the behavior of the specimens as categorized in this section can be divided into two categories, based on the relative area of reinforcement provided for crack control. SSMBLG1-Control1, SSMBLG2-NOCage, SSMBLG4-Deep, and SSMBLG7-Control2, which had similar amounts of reinforcement for crack control, had cracking that was observed at nearly the same applied load at the various locations along the longitudinal joint between the precast flanges. Furthermore, cracking was generally detected in the gages that were centered over the precast joint. Visual cracking loads observed for these specimens also correlated well with the internal strain measurements. This behavior provided confirmation that the loading setup shown in Figure 6.3.4 adequately induced a region of maximum moment uniformly along the precast joint.

The two specimens with relatively larger reinforcement areas for crack control, SSMBLG5-No.6Bars and SSMBLG6-Frosch appeared to develop multiple cracks in the precast joint region based on the results from the embedded instrumentation. In the case of SSMBLG6-Frosch, this was confirmed with the visual observation of two unique cracks observed on both the origin and end faces of the specimen, as discussed in Section 6.6.2. The introduction of more cracks, each of which was expected to have smaller crack widths, was expected to provide an improved system because the smaller crack widths tend to be more resistant to the ingress of chlorides. The visual cracking loads recorded for these specimens were significantly larger than the cracking loads identified with the embedded instrumentation, which indicates that the crack widths generated in these more heavily reinforced specimens were much smaller than those generated in the more lightly reinforced specimens (SSMBLG1-Control1, SSMBLG2-NOCage, SSMBLG4-Deep, and SSMBLG7-Control2).

6.6.7. Calculation of Expected Tensile Reinforcement Stress in Subassemblage Specimens

An analytical investigation of the stress demands on the tensile reinforcement in each subassemblage specimen was conducted to investigate the expected reinforcement stress ranges among the specimens during loading. The sectional analysis tool BIAX (Wallace, 1989) was utilized to construct moment-curvature diagrams for each specimen. Two models were constructed for each specimen, one with the concrete tensile strength included in the analysis – which was utilized to identify the cracking moment and stress in the reinforcement before cracking, while the second model neglected the effects of the concrete tensile strength and was utilized to model the behavior after cracking. The stress-strain model for the reinforcement included the effects of strain hardening, which was based on the equation presented by Saenz (1964). The ultimate strength of the reinforcement was assumed to be 100 ksi, with a fracture strength of 90 ksi. The strain at the onset of strain hardening was assumed to be 1 percent. The strain at the ultimate stress was assumed to be 8 percent, with an assumed fracture strain of 10 percent. The initial modulus of elasticity for the strain hardening region was assumed to be 1500 ksi. The measured 28-day concrete compressive strengths, concrete tensile strengths, and reinforcement yield strengths were utilized in the program inputs. The reinforcement yield strength was measured to be approximately 70 ksi for the No. 4 bars, and was assumed to be similar for the No. 6 bars. The reinforcement stress was calculated for increasing moment until a concrete compressive strain of 0.003 (inclusive) was achieved, which was assumed to represent the maximum available concrete compressive strain before crushing occurred.

226

The predicted tensile reinforcement stress in each specimen is shown in Figure 6.6.30. The vertical axis represents the applied loading, and is given as the ratio of the applied load to the predicted cracking load.
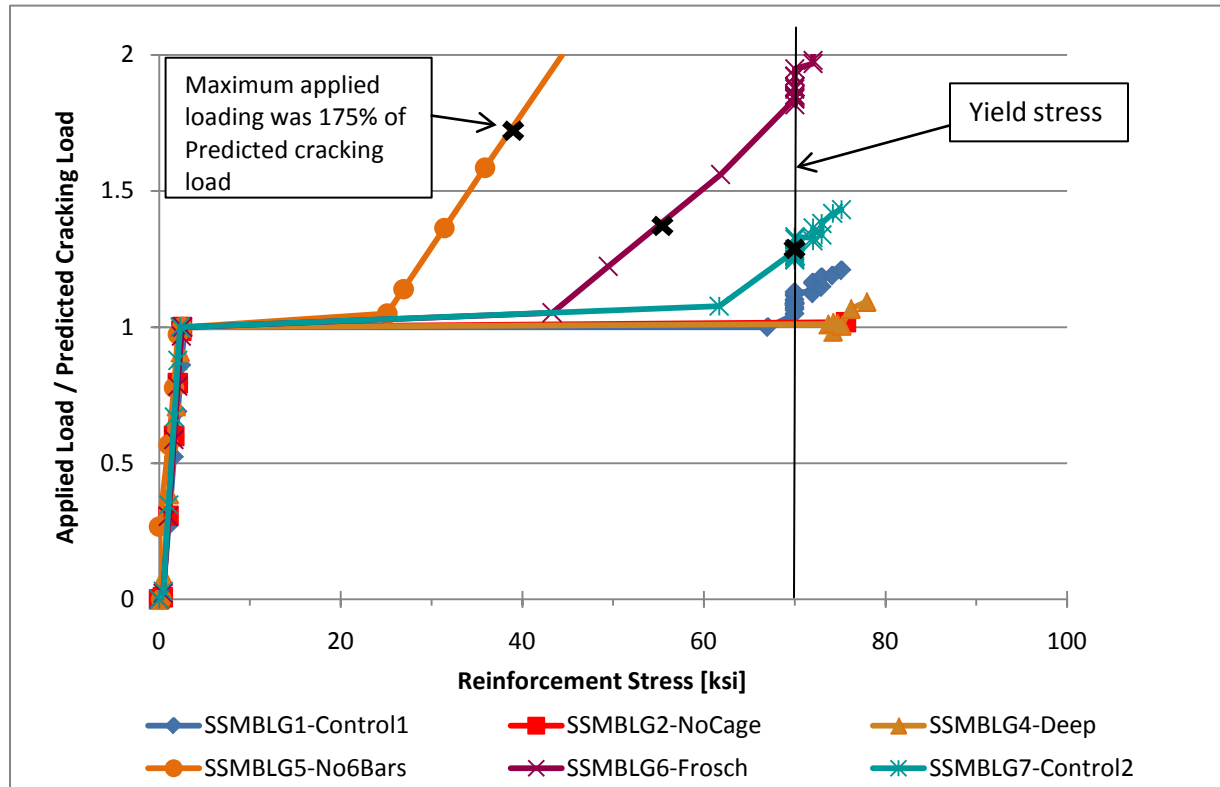
Figure 6.6.30: Predicted tensile reinforcement stress demands as a function of applied loading in subassemblage specimens[1]

[1]The black 'x' symbols indicate the maximum applied load for each specimen during testing. The 'x' symbol was not shown for each specimen for clarity; the maximum applied load for each specimen is given in Table 6.6.4.

The plot shown in Figure 6.6.30 represents the expected tensile reinforcement stress range in each subassemblage specimen for increasing load up to when concrete crushing in compression was expected according to the analysis. The plot is truncated at a ratio of applied load to predicted cracking load of 2, which cuts off the load at which crushing would have been observed for SSMBLG5-No.6Bars. All of the tests were terminated before concrete crushing was observed. Test terminations are denoted by the black "x" symbols for three of the specimens. For clarity, these symbols were left off the plot for the specimens that were expected to undergo concrete crushing near the cracking load.

Table 6.6.4 summarizes the maximum tensile reinforcement stress predicted for each of the specimens associated with the maximum loads applied during each of the tests.

Table 6.6.4: Maximum applied loading and associated predicted tensile reinforcement stresses in subassemblage specimens

Specimen	Tensile Reinforcement Area, including cage [in²]	Ratio of Maximum Applied Load/Predicted Cracking Load	Predicted Tensile Reinforcement Stress [ksi]
SSMBLG1-Control1	1.93	1.0	67.0
SSMBLG2-NoCage	1.60	1.0	75.7
SSMBLG4-Deep	1.93	1.05	76.0
SSMBLG5-No6Bars	3.85	1.75	39.3
SSMBLG6-Frosch	3.03	1.35	54.1
SSMBLG7-Control2	1.93	1.25	70.0

As illustrated in Table 6.6.4, the tensile reinforcement was expected to yield in subassemblage specimens 2 (NoCage), 4 (Deep), and 7 (Control2). As shown in Figure 6.6.30, the reinforcement stresses immediately after cracking in the two specimens with the significantly larger tensile reinforcement areas, SSMBLG5-No6Bars and SSMBLG6-Frosch, were expected to be considerably smaller than yield. This is consistent with the conclusions of the previous sections that the more heavily reinforced specimens exhibited smaller crack widths.

6.7. Destructive Testing of Subassemblage Specimens

At the conclusion of the testing program, three or more cores were removed from each specimen to investigate the physical crack length. Three total cores were taken from each specimen, unless more were deemed necessary to locate a crack. The three cores were removed from the middle of the specimen on a line perpendicular to the joint, with one core centered over the joint, and the remaining two centered over each vertical precast web, as illustrated in Figure 6.7.1. The core locations were selected to facilitate measurement of the reflective crack at the joint and the depth of cracking or separation at the vertical precast web-CIP concrete interface.

228
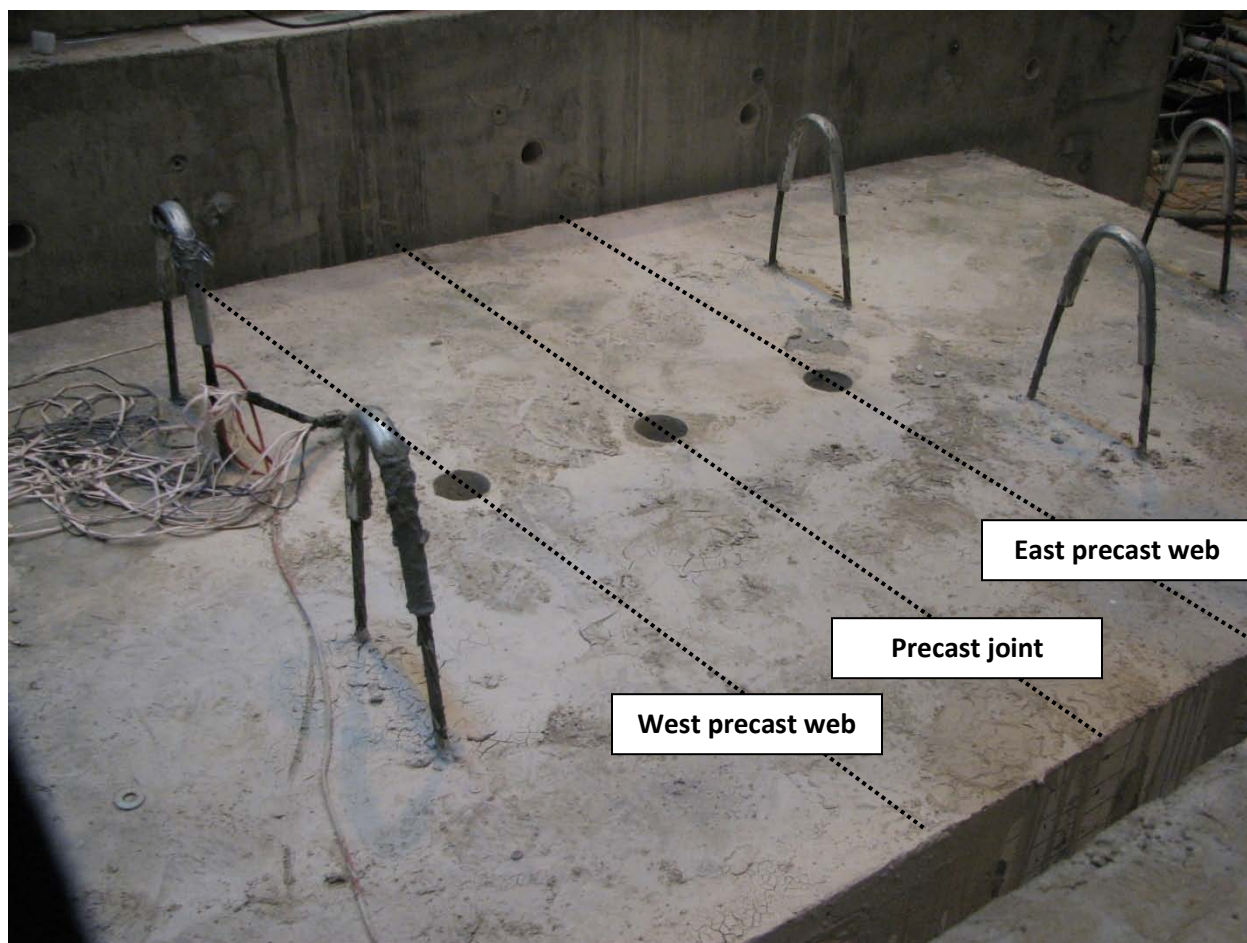
Figure 6.7.1: Coring locations in subassemblage specimens

Each of the core specimens was examined both with the naked eye and the aid of an Olympus SZX12 stereo-microscope to identify the extent of cracking on the core surface. The level of magnification used to examine the cores ranged between 2.1X to 27X, which was the full capacity of the microscope. Any and all cracking that was identified in each core was tabulated, regardless of the size or anticipated origin. The observed crack widths were documented in classification categories, defined in Table 6.7.1. The vertical depth of cracking identified in the cores was referenced from the line created by the horizontal precast flange-CIP concrete interface, as shown in Figure 6.7.2. The characteristics of each core specimen and the measured crack widths and locations for each subassemblage specimen are tabulated in detail in Appendix G.

Table 6.7.1: Crack width classification categories for analysis of core specimens

Crack Classification	Crack Width (W)
0.002	W < 0.002 in.
A	0.002 in. ≤ W < 0.008 in.
B	0.008 in. ≤ W < 0.023 in.
C	0.023 in. ≤ W < 0.200 in.
D	W ≥ 0.200 in.
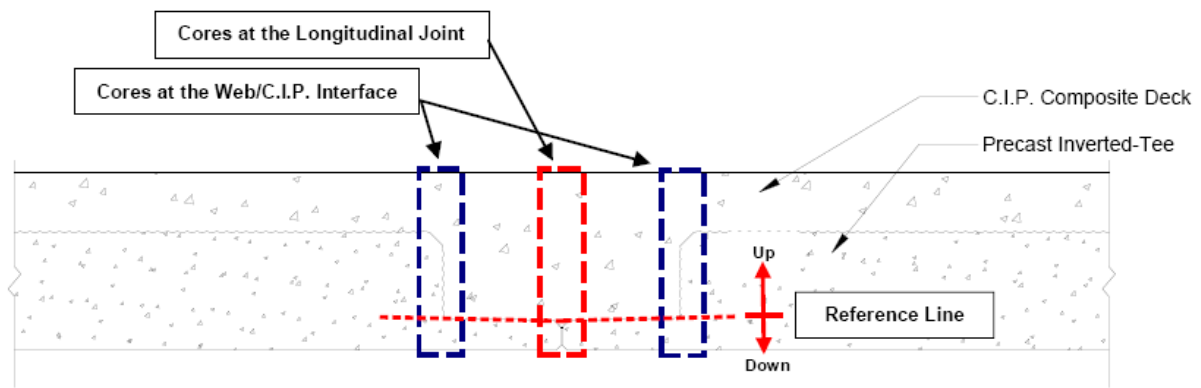
Figure 6.7.2: Location of reference line for measurement of vertical location of cracking in core specimens

The maximum height of the crack, measured vertically upwards from the reference line, and the maximum width of the crack are summarized in Table 6.7.2. Also shown in the table are the maximum crack length and width that were measured on the origin and end faces of the specimens during the tests. The crack length and width correspond to the length and width of the cracks under the applied load in the load step immediately preceding the first observed cracks at the vertical web interface. The maximum values recorded here are the largest of the measured crack widths and lengths documented in Appendix G. Because the cores were removed after the completion of all loading, the observed cracked condition of the core specimens corresponded to the maximum level of loading applied to each subassemblage specimen. Because the cores were subsequently examined under no load, the potential cracks present in the cored samples may have been reduced in size in comparison with the maximum lengths and widths measured at the origin and end faces under load. This was corroborated by the fact that the observed crack widths on the faces of the specimens were reduced after the removal of load.

230

Table 6.7.2: Summary of maximum height and width of crack measured in core specimens

Specimen	Location of Core	Maximum height of crack[1]	Maximum width of crack[2]	Crack length measured on face[3]		Crack width measured on face[4] (class designation)	
				Origin Face	End Face	Origin Face	End Face
1-Control1-9"	Joint	7.5 in.	C	8.3 in	7.8 in.	0.016 in. (B)	0.011 in. (B)
	East Web	7 in.	B				
	West Web	NO[5]	NO				
2-NoCage-18"	Joint	7.25 in.	B	8.3 in.	8.1 in.	0.014 in. (B)	0.014 in. (B)
	East Web	NO	NO				
	West Web	NO	NO				
3-HighBars-9"	Joint	9.5 in.	B	Values not relevant because clamping assembly was not utilized during the test of this specimen			
	East Web	NO	NO				
4-Deep-9"	Joint	11.5 in.	B	10.3 in	11.3 in.	0.008 in. (B)	0.014in. (B)
	East Web	10.75 in.	B				
	West Web	10.75 in.	A				
5-No.6Bars-9"	Joint	7.5 in.	B	NA	8.3 in	NA	0.014 in. (B)
	East Web	7 in.	<0.002				
	West Web	NO	NO				
6-Frosch-4.5"	Joint	8 in.	B	7.3 in.	7.3 in	0.006 in. (A)	0.010 in. (B)
	East Web	2.25 in.	A				
	West Web	0.75 in.	<0.002				
7-Control2-9"	Joint	NO	NO	7.3 in.	7.3 in.	0.014 in. (B)	0.008 in. (B)
	Joint	NO	NO				
	East Web	NO	NO				
	West Web	NO	NO				

[1]The height of crack was measured from the reference line, defined in Figure 6.7.2; only "upward" values are recorded here
[2]The width of crack was documented by crack classification, as defined in Table 6.7.1
[3]The crack length measured on the face of the specimens was taken as the maximum crack length observed prior to cracking at the vertical web interface, see Section 6.6.5. Values are adjusted to match reference line defined in Figure 6.7.2
[4]The crack width measured on the face of the specimen was taken as the maximum crack width observed prior to cracking at the vertical web interface, see Figures 6.6.6-6.6.7
[5]"NO" represents "No reflective cracks observed"

Most of the specimens with a total section depth of 14 in. had a maximum observed crack height of approximately 7- ½ in., which corresponded to a crack length of 8.2 in. once the chamfer length was taken into account as discussed in Section 6.6.5, which correlated well with the visually observed data on the two faces of the specimens. Cracking was visually identified in all of the subassemblage specimens with the exception of SSMBLG7-Control2. The width of the crack near the joint region was generally a Class B crack, which has a relatively wide range of crack widths (i.e.: 0.008 in. ≤ W < 0.023 in.) and corresponded well to the crack widths observed on the origin and end faces of the subassemblages during testing. The only core

231

to develop a Class C crack, crack width larger than 0.023 in., was SSMBLG1-Control1, in which no specific perturbation in the history of the specimen was known to be the cause.

Cracking or separation of the CIP concrete at the vertical precast web interface was observed on nearly every specimen. The presence of cracking at these locations was not known to exist in field applications of the PCSSS, and was attributed to the subassemblage test setup which induced flexural stresses in the joint region. The results discussed in Section 6.6 do not include measurements or recorded data after the presence of cracking at the vertical web interface was detected, therefore the introduction of cracking at the vertical web was not expected to influence the results in Section 6.6.

An additional core specimen was removed near the joint of SSMBLG7-Control2 after no cracking was identified in any of the three original cores. Investigation of the fourth core did not reveal any cracking in the subassemblage specimen, however cracking was visible on the end faces of the specimen during laboratory testing.

Chapter 7 PCSSS: Conclusions and Recommendations

7.0 Introduction

Several numerical and experimental investigations were completed and reviewed during the NCHRP 10-71 project related to issues of importance to the design and performance of precast composite slab span system (PCSSS) bridges. The results from each of these parts of the study were synthesized to develop a relevant design guide for precast composite slab span bridges. The following sections provide a brief summary of the results that were obtained during these studies.

Numerical studies included an investigation of bursting and spalling stresses in the end zones of precast inverted-T sections, effects of spacing of transverse reinforcement in the joint region, and an investigation of the applicability of the AASHTO (2010) specifications for slab-type bridges to the design of PCSSS bridges for live load distribution factors and for consideration of effects of skewed supports.

Experimental studies were completed on two large-scale laboratory bridge specimens, including a Concept 1 two-span continuous bridge and a Concept 2 simply-supported bridge specimen. The Concept 1 laboratory bridge included variations in a number of parameters including precast flange depth and end zone reinforcement details. It was also instrumented in a study by the Minnesota Department of Transportation (Mn/DOT) to investigate the effects of restraint moment and potential development of reflective cracking (Smith et al. 2008). The Concept 1 laboratory bridge was made available to the NCHRP 10-71 project for further study. In the NCHRP 10-71 study, the performance of both bridge specimens was investigated under various types of loading, including cyclic loading to simulate traffic, loading to simulate environmental effects, as well as to investigate load transfer between adjacent precast panels (both longitudinally and transversely).

One of the keys to the effectiveness of the PCSSS bridge, which also makes it unique relative to slab-type bridges, is the need to control potential reflective cracking in the cast-in-place (CIP) concrete above the longitudinal joint between the adjacent precast flanges. A significant effort in the project was devoted to the investigation of crack control reinforcement and the simulation of potential crack development which was noted in a field instrumented PCSSS in Center City Minnesota. The Concept 1 specimen included No. 6 transverse hooked reinforcement embedded into the precast webs to provide load transfer and crack control in the joint region, as well as No. 5 cage stirrups which contributed to the crack control reinforcement. The nominal maximum spacing between transverse reinforcement was 12 in. (similar to the detail of the Center City Bridge). The Concept 2 specimen included No. 4 embedded hooked reinforcement in the west half of the simple span, while No. 4 straight embedded bars mechanically connected to reinforcement in the precast webs were provided in the east half span. No. 3 cage stirrups were staggered in the Concept 2 laboratory bridge relative to the transverse reinforcement spaced at 18 in. to provide a maximum spacing of 9 in. between transverse reinforcement.

In addition to the two large-scale laboratory bridge specimens, six subassemblage specimens were tested to investigate the relative performance of various reflective crack control reinforcement details. The subassemblage specimens were loaded to flexurally induce cracking above the longitudinal joint between the precast flanges. The size, quantity, and location of cracking were documented through a range of quasi-static and cyclic load tests.

233

The culmination of the NCHRP 10-71 was the development of a design guide and examples which is included in Appendices A and B for application to PCSSS bridges. The following sections provide a summary of the investigation and conclusions from the components of the study. The order of the topics focuses on issues related to the precast inverted-T element of the bridge and progresses to system issues.

7.1. Bursting, Splitting and Spalling Stresses

The AASHTO (2007) specification included design procedures to address bursting stresses at the ends of precast prestressed concrete beams due to the effects of the development of prestress, which were likely developed specifically for I-girders. These guidelines required large amounts of vertical reinforcement to be placed within a distance of $h/4$ from the end of the member. The shallow section depths of inverted-T precast beams resulted in limited area for the placement of vertical reinforcement, which led to significant congestion.

Significant changes to the specification in regards to end zone stresses have been incorporated since 2007, specifically in the terminology related to end zone stresses. The 2008 interim AASHTO LRFD specification indicate that "bursting" has been replaced with "splitting" in terms of the resistance of pretensioned anchorage zones, and also represented a wider range of precast member shapes (i.e., not necessarily developed specifically for I-girders), as opposed to the specifications up to and including the 2007 LRFD specifications. The 2008 Interim specifications relaxed the placement requirements for wide-shallow sections, by allowing the designer to spread the end zone reinforcement, termed "splitting" reinforcement over a larger distance. In the case of pretensioned solid or voided slabs, the designer can substitute the section width for "h," rather than using the section depth for "h." According to the NCHRP 10-71 study, this may not be appropriate when trying to control spalling stresses. In addition, the terminology for the reinforcement described in this section of the AASHTO specifications should be termed "spalling" reinforcement rather than "splitting" or "bursting" reinforcement.

Experimental and numerical studies were completed in the NCHRP 10-71 study to investigate the effects of end zone stresses on the precast prestressed inverted-T sections used in the PCSSS. The experimental results from the Concept 1 and 2 laboratory bridge investigations indicated that the 12 in. deep concrete sections had sufficient strength to resist tensile stresses induced in the transfer zone of the precast inverted-T sections at the time of release. Four unique end regions of the Concept 1 laboratory bridge specimen precast members, did not exhibit any evidence of cracking in those regions, even where vertical reinforcement was not provided in the end zones of those specimens. These findings were corroborated with the results of numerical studies that showed certain inverted-T members did not require spalling reinforcement, specifically those members with depths less than 22 in. for which the expected concrete strength was larger than the expected vertical tensile stresses due to the development of prestress.

It was also found that for deep inverted-T sections, in particular, the existing requirements specified by the LRFD specification (AASHTO 2010) may be unconservative. Larger amounts of spalling reinforcement than specified by AASHTO 2010 were found to be required through a numerical study. It was also found that the reinforcement should be placed as close to the end of the member as possible (i.e., within $h/4$ of the end of the member, where "h" represents the depth of the member). The end region was the most critical region for the reinforcement to be located to address spalling stresses, even for the case of wide sections.

234

7.2. Restraint Moment

It is important to consider the effects of restraint moment in the design of PCSSS or design the systems as a series of simple spans. The current specification allows that, when the age of the girder is at least 90 days at the time of continuity, the computation of restraint moments is not required (AASHTO 2010 Article 5.14.1.4.4). The reasoning lies in the fact that, when the girder has aged beyond 90 days, the positive restraint moments caused by the precast beams due to time-dependent effects are minimal, and the negative restraint moments that may be generated can be accommodated by the negative moment reinforcement over the piers.

In the case of PCSSS bridges made continuous by casting the CIP concrete on relatively young girders (e.g., 7 to 14 days old) to complete the continuous composite bridge system, the effects of positive restraint moments should be considered. In these cases the positive restraint moments due to time-dependent effects are typically dominated by the creep of the precast sections. It is recommended that the resulting positive time-dependent restraint moments developed at the piers be computed using the P-method.

Research completed during the Mn/DOT study by Smith et al. (2008) and the current study has shown that restraint moments that develop due to thermal gradients applied to the section are significant, and should be considered in either case (i.e., whether or not time-dependent effects generate positive or negative restraint moments). The positive restraint moment effects attributed to the design thermal gradients can be an order of magnitude larger in some climates than the positive restraint moments due to time-dependent effects. The thermal gradients provided by the AASHTO 2010 specification should be taken into consideration by calculating the resulting expected curvatures of each span treated as simply supported. Subsequent derivation of the resulting restraint moments due to the thermal gradient effects is summarized in Section 3.3. The development of positive restraint moments due to thermal gradient effects would also be expected to be significant in continuous monolithic slab span systems, and should be considered during design.   There may be little or no economic gain in continuity because of the large thermal restraint moments that develop and in some cases, continuity may require additional reinforcement in the precast sections (i.e., larger than would be required for a simply-supported design).

7.3. Live Load Distribution Factors

Numerical modeling was combined with observations from a live load truck test on the Center City Bridge along with load distribution tests on the laboratory bridge specimens (i.e., Concept 1 and Concept 2) to determine the applicability of current live load distribution factors in the AASHTO LRFD (2010) specification for slab-type bridges to the PCSSS.

The numerical models illustrated that the longitudinal curvatures measured in the precast slab span system with a reflective crack extending to within 3 in. of the extreme compression fiber and a tandem load greater than that which could be physically applied in the field resulted in longitudinal curvatures which were only 84 percent of the longitudinal curvatures predicted using the AASHTO LRFD (2010) load distribution factors for monolithic concrete slab span bridges, suggesting that PCSSS-type superstructures could reasonably and conservatively be designed using the current live load distribution factors for monolithic slab-type bridges.

Furthermore, the live load truck tests on the Center City Bridge suggested that the measured longitudinal curvatures were approximately three times less than those calculated using monolithic slab span equations. In addition, the measured longitudinal curvatures were consistently conservative when compared to

235

monolithic slab span FEM models. The conservatism in the factors for monolithic slab span bridges was sufficient to cover the cases of the PCSSS bridges even considering the potential effects of reflective cracking as discussed above.

Load distribution tests on Span 2 of the Concept 1 laboratory bridge and the Concept 2 laboratory bridge included an investigation of the transverse load distribution between adjacent precast panels. For each specimen, loading was applied to the south precast panel, and the longitudinal curvatures in the north and south precast panels were calculated based on measured longitudinal strains located throughout the depth of each section. The longitudinal curvatures were measured at various times throughout the range of testing that occurred on each specimen, and therefore provided an estimate of the curvatures of the sections before cracking was induced near the precast joint, as well as after traffic fatigue loading and loading to simulate cracking along the longitudinal precast joint due to environmental effects. The test was designed such that a reduction in the ability of the PCSSS to transfer load to adjacent precast panels would be indicated by a relative reduction in the measured longitudinal curvature of the unloaded panel.

Both Span 2 of the Concept 1 laboratory bridge and the Concept 2, laboratory bridge showed good load transfer capabilities across the longitudinal joint during intermittent tests conducted throughout the investigation of the laboratory bridge specimens to extend the reflective crack. In both cases, little variation in the measured longitudinal curvatures was observed in the unloaded panels, which suggested that load was effectively transferred across the longitudinal joint from the loaded panel despite the presence and increase in the size of reflective cracking induced in/near the joint.

In summary, the numerical and experimental studies in regards to live load distribution factors indicated that the PCSSS was well represented by monolithic FEM models, suggesting that the discontinuity at the precast joint did not significantly affect the load distribution characteristics of the system. Also, the performance of the large-scale laboratory bridge specimens reinforced the notion that the system provided sufficient transverse load distribution, with and without the presence of reflective cracking near the joint region.

7.4. Skew

Numerical modeling was applied to simply-supported monolithic and jointed (to simulate PCSSS discontinuity at the adjacent precast flange interface) bridge models with skewed supports ranging from 0 to 45 degrees. Three independent load cases were investigated, which included a 35 kip load individually applied over a 12 by 12 in. patch at both quarter points and at midspan for each model. For each load case, the largest horizontal shear stress in the plane above the precast joint nearest the loading was determined. The maximum shear stress from these three load cases defined envelopes for the monolithic and jointed models that varied with skew angle. This maximum horizontal shear stress envelope remained relatively constant through the range of skew angles considered for both jointed and monolithic models. With increasing skew angle, the shear stress envelope increased by approximately 15% for the monolithic models and by less than 10% for the jointed models. The small variation and consistency between the models considering a joint between precast sections with a 3 in. flange and a monolithic structure suggested that the effect of the joint in precast composite slab span construction was not expected to significantly affect the performance of the system in skewed applications, and the design of skewed PCSSS bridges could be completed assuming a monolithic slab span system.

236

7.5. Composite Action and Horizontal Shear Strength

To conclude the laboratory tests, the large-scale bridge specimens were loaded to near ultimate levels of load to investigate the ability for the precast slab span sections to remain composite with the CIP concrete topping. Placement of reinforcement for horizontal shear was observed to be difficult and time consuming for the fabricator, especially when finishing the top web surfaces. Furthermore, the reinforcement extending from the precast webs for horizontal shear extended out of the precast section with minimal clearance between the hook and the precast web surface to avoid interference with placement of the deck reinforcement in the field. In initial field applications of the PCSSS, the low clearance of this horizontal shear reinforcement may have limited its effectiveness because aggregate was unable to flow below the returned stirrups. In addition, past research by Naito et al. (2006) suggested that concrete girders loaded to induce positive moments in the section without horizontal shear ties were observed to achieve sufficiently large levels of horizontal shear stress and remain composite.

Span 2 of the Concept 2 laboratory bridge was designed with the same horizontal shear layout utilized in the Center City Bridge, which satisfied the design requirements of AAHSTO (2005). Span 1 of the Concept 1 laboratory bridge was designed with fewer horizontal shear ties than were used in Span 2 and in the Center City Bridge, and which did not satisfy the minimum horizontal shear reinforcement requirements of the LRFD specification (AASHTO 2005). The minimum horizontal shear reinforcement requirements have not been modified between the 2005 and 2010 versions of the AASHTO specification. The Concept 2 laboratory bridge was designed and constructed with no horizontal shear ties. In both bridges, the surface condition of the precast member was roughened to a surface consistent with a 1/4 in. rake.

In the tests on both spans of the Concept 1 laboratory bridge and on the Concept 2 laboratory bridge, the sections were observed to remain composite well beyond service load levels, through the full range of loading to the maximum capacity of the loading system, which was in excess of the predicted nominal capacity of the Concept 1 and 2 bridges.

The longitudinal strains measured during the tests on the Concept 2 laboratory bridge (which had no horizontal shear ties) indicated linear distributions through the cross sections. The Kent and Park model (1971) was used to determine the corresponding compressive stress distribution in the CIP section assuming unconfined concrete models. Integrating the nonlinear stress distribution, resulted in an estimate of the maximum compression force achieved in the slab during loading to the ultimate capacity. The horizontal shear stress estimated in the system at the precast-CIP interface was subsequently calculated by dividing the total compression force by half of the center to center of bearing span length and the total width of the bridge structure, and was determined to be 135 psi.

The results of the laboratory tests suggest that the AASHTO LRFD specification should allow for the design of precast slab span structures without horizontal shear ties, and allow for the development of a maximum factored horizontal shear stress of 135 psi in sections with intentionally roughened surfaces (i.e., 1/4 in. rake) unreinforced for horizontal shear.

7.6. Control of Reflective Cracking across Longitudinal Joint between Precast Flanges

Control of reflective cracking was investigated through the development and testing of two large-scale laboratory bridge specimens (Concept 1 and Concept 2 laboratory bridges), as well as through a series of subassemblage tests.

237

Reflective cracking was intentionally induced in the Concept 1 and Concept 2 large-scale laboratory specimens to investigate the performance of the PCSSS through a range of loading that was designed to simulate both fatigue performance due to vehicular loading, as well as the influence of environmental effects. Two million cycles of fatigue loading were applied near the longitudinal precast joint with a patch load to simulate tire traffic on both spans of the Concept 1 laboratory bridge, as well as on the Concept 2 simply-supported laboratory bridge. The magnitude of measured transverse strain under loading to simulate traffic was on the order of 30με, which was much less than the strains measured in the Center City field bridge after cracking was observed. Therefore, in each case, a reflective crack was introduced near the precast joint region by inducing transverse strains above the horizontal precast flange-CIP interface to replicate strain measurements (i.e., approximately 160 με) observed in a field application of a PCSSS bridge in Center City, Minnesota, that were attributed to reflective cracking resulting from thermal gradient effects. Reflective cracking was induced in each specimen after the completion of one million fatigue cycles and then the laboratory bridge specimens were subjected to an additional one million cycles of simulated traffic loading. This enabled investigation of the fatigue performance of the virgin and cracked systems. In the Concept 2 laboratory bridge, reflective cracking was induced only in the east half span (i.e., associated with straight embedded transverse bars), despite equal loading simultaneously applied at the quarter points of both half spans.

During both the first (i.e., uncracked) and second (i.e., after cracking to approximately 160 με) million cycles of traffic loading, little degradation of the joint was observed in either of the large-scale bridge specimens. The resiliency of the system under simulated traffic load suggested that the PCSSS would provide a durable bridge solution even with the presence of reflective cracking.

Because traffic loading was observed to promote little to no degradation of the system, additional tests were conducted to simulate the large increases in transverse strains that had been measured in the Center City Bridge suspected to be the result of daily fluctuations due to thermal gradient effects. To simulate thermal gradient effects in the laboratory, mechanical loading was applied over the precast joint to induce nominal strains on the order of 180με (target level A) and 300 με (target level B), which corresponded to approximate magnitudes measured in the Center City Bridge. To simulate the repeated yearly effects of daily fluctuations of the thermal gradients, a total of 15,000 cycles of load were applied to induce each of the target level strains (except in the Concept 2 laboratory bridge, where the loading beam fractured after 5000 cycles of load to target level B). The 15,000 cycles at the target strain levels (A and B) each corresponded to approximately 100 years of environmental effects, conservatively assuming thermal gradients large enough to induce the target strain levels would be expected to occur 150 days a year.

Transverse strains measured under a 35 kip patch load, to simulate the adjacent wheel loads of two truck tires, were documented at various times during the environmental effect simulation for both spans of the Concept 1 laboratory bridge, as well as the Concept 2 laboratory bridge to investigate potential degradation of the joint during these tests. For each specimen, measured increases in the transverse strains under the 35 kip patch load were observed as an increasing number of cycles to induce the target-level strains were completed. After the cycles to the target-level strain B (i.e., 300 με) were completed (i.e., 15,000 cycles for the Concept 1 bridge and 5000 cycles for the Concept 2 bridge), the increases in strains due to the application of the 35 kip patch load were approximately 34, 6, and 23 percent for Spans 1 and 2 of the Concept 1 laboratory bridge, and the east (i.e., straight embedded transverse bars) quarter point of the Concept 2 laboratory bridge, respectively. Degradation of the joint in Span 2 of the Concept 1 laboratory bridge was expected to be most severe because the precast flange was thicker than the remaining specimens causing the transverse reinforcement to be located higher in the section and therefore intercept

238

the reflective cracking at a higher depth, and also because the instrumentation was located higher in the section, and therefore strains measured in Span 2 would have been larger if they had been measured lower in the section, at the same approximate depths as in Span 1 of the Concept 1 laboratory bridge and the Concept 2 laboratory bridge. Also documented during the environmental effect simulation was the rate of degradation of the joint under the loads required to induce strains of target-level strain B (approximately 300 με). It was observed that the increase in the strain occurred quickly during the first few thousand cycles, and then tended to stabilize.

The performance of both spans of the Concept 1 laboratory bridge and the Concept 2 laboratory bridge was observed to adequately control cracking in the precast joint region throughout loading to simulate traffic and environmental effects related to the thermal gradient.

Reflective cracking was also monitored throughout the range of testing for seven subassemblage specimens to quantify the relative performance of the respective design details for reflective crack control in each specimen. A primary metric recorded during these tests was the width and stability of the observed cracks throughout the range of applied loads. The ability for each specimen to control the width of cracking was desirable, as large cracks were expected to cause degradation of the longitudinal joint region including providing a potential avenue for the ingress of moisture and chlorides.

Each of the subassemblage specimens performed adequately throughout the range of loading, though variations in the extent of cracking indicated some relative differences. The two specimens with the largest reinforcement ratios, SSMBLG5-No.6Bars (ρ_{cr}=0.0061, as defined in Figure 5.1.2) and SSMBLG6-Frosch (ρ_{cr}=0.0052), performed well relative to the remaining specimens. In these two specimens, measured crack widths were consistently smaller than the remaining specimens. SSMBLG7-Control2 also indicated better than average performance through visual observations; however the analysis of the embedment instrumentation suggested that the behavior of this specimen was similar to the specimens in the group not including SSMBLG5-No.6Bars and SSMBLG6-Frosch. The behavior of SSMBLG7-Control2 was attributed to a relatively smooth precast flange surface achieved prior to the placement of the CIP concrete (which was done in anticipation of studying a debonded flange surface, which was abandoned to allow for a second control specimen to be tested). The relatively smooth flange surface was expected to better distribute transverse stresses across the precast flanges in the joint region, thereby reducing the potential stress concentration at the interface between the adjacent precast flanges which created a longitudinal joint, however it was observed via an analysis of the horizontal crack propagation using the concrete embedment resistive strain gages that a single crack was present internally in the specimen, suggesting that the smooth flange surface did not distribute the transverse stress adequately well so as to promote the development of multiple cracks. A completely debonded surface, however, was not expected to be desirable, as it would likely promote delamination of the horizontal precast flange-CIP interface, which was expected to promote cracking at the vertical precast web, where cage reinforcement was not present to aid in the control of cracking.

In the subassemblage tests, the best performing specimens, SSMBLG5-No.6Bars and SSMBLG6-Frosch, had the largest amounts of steel as noted above (ρ_{cr} of 0.0061 and 0.0052, respectively). Although SSMBLG6-Frosch was named after the Frosch et al. (2006) recommendations, the reinforcement ratio of the SSMBLG5-No.6Bars specimen more closely correlated with that of the Frosch recommendations for crack control. SSMBLG5-No.6Bars had No. 6 transverse hooks spaced at 18 in., which was supplemented with No. 3 bars spaced at 18 in. in a cage that was staggered relative to the transverse hooks such that the maximum spacing was 9 in. to provide crack control over the longitudinal joint region between the precast flanges.

239

SSMBLG6-Frosch was fabricated with No. 4 transverse hooks spaced at 18 in., supplemented with No. 3 bars spaced at 4.5 in. in a cage that was offset around the transverse bars. The maximum spacing in the SSMBLG6-Frosch specimen was 4.5 in., and narrowed in the region where the cage reinforcement bounded the transverse hooks. The tight spacing of the SSMBLG6-Frosch specimen required careful construction tolerances. In the subassemblage study, the maximum transverse 9 in. spacing for crack control appeared to be sufficient as long as enough reinforcement was provided to ensure that the reinforcement did not yield upon cracking. This was evident through the good performance of both of these specimens.

The maximum transverse reinforcement spacing was further investigated by evaluating the performance of the Concept 1 and 2 laboratory bridges which provided more realistic boundary conditions in the longitudinal joint region above the precast flanges. In this study, it was found that the 9 in. maximum transverse reinforcement spacing provided in the Concept 2 laboratory bridge did not correlate with an improvement in the control of cracking near the longitudinal trough area relative to the 12 in. maximum spacing provided in the Concept 1 spans, and therefore an economical design may favor 12 in. transverse reinforcement spacing to 9 in. spacing with no expected reduction in performance. An increase in the maximum transverse reinforcement spacing to 18 in. is not recommended, primarily because cracking in SSMBLG2-NoCage (which was reinforced with only transverse No. 4 bars spaced at 18 in.) was generally largest and crack widths increased with the least increase in the applied load relative to the other subassemblage specimens which had transverse reinforcement spacings on the order of 9 in. (except for the SSMBLG6-Frosch which had the 4.5 in. spacing), which were observed to provide acceptable crack control.

Furthermore, little difference was observed between the performance of the sections of the Concept 1 laboratory bridge where reflective cracking was observed, with No. 6 transverse hooked bars, and the performance of the Concept 2 laboratory bridge where reflective cracking was observed, with No. 4 transverse hooks. There was, however, a noticeable increase in the relative performance of SSMBLG5-No.6Bars and SSMBLG1-Control1, in which the only nominal difference was the larger bars in the former specimen. Because the increased performance observed in SSMBLG5-No.6Bars, which was on the order of SSMBLG6-Frosch, was achieved with larger bars and a maximum transverse reinforcement spacing of 9 in., it was suggested that a design with No. 6 bars and less cage reinforcement was likely to be more economical and easier to implement in the field than the closely spaced reinforcement cage provided in SSMBLG6-Frosch.

7.7. PCSSS Design Recommendations

The research completed during the NCHRP 10-71 study resulted in the development of a comprehensive design guide for the design and construction of precast composite slab span system bridges. The design guide in reference to PCSSS was developed based on previous work by the researchers (Smith et al. 2008, Eriksson 2008) summarized in Chapter 3; numerical studies to investigate the performance of the PCSSS details, as well as considering the system as a whole as described in Chapter 4; and an extensive large-scale laboratory research program summarized in Chapters 5-6. The design guide includes proposed modifications to the AASHTO LRFD 2010 Bridge Design Specification, as well as the AASHTO LRFD Bridge Construction Specifications.

The design guide developed during the NCHRP 10-71 study is included in Appendix A, and corresponding design examples of PCSSS bridges are included in Appendix B.

Chapter 8 Flange/Deck Connection: Concept Development of Joint Details for Accelerated Bridge Construction

8.0   Introduction

Speed of construction, particularly for bridge replacement and repair projects, has become a critical issue to minimize disruption of traffic and commerce. Promising systems for rapid construction include precast bridge systems fabricated using decked bulb-T (DBT) concrete girders or precast deck panels on girders. This project focused on the development of cast-in-place (CIP) longitudinal and transverse joints between the flanges of the DBTs or between the precast panels. Because of the similarity in these systems, the discussion herein focuses primarily on DBTs which generally have greater constraints on deck thickness than precast panel systems.

The bridge deck in DBTs consists of the girder flange, which is precast and prestressed with the girder. DBTs are manufactured in the precast plant under closely monitored conditions, transported to the construction site, and erected such that the flanges of adjacent units abut. Load transfer between adjacent units is provided by longitudinal joints (parallel to traffic direction). Figure 8.0.1 shows a DBT bridge being constructed.
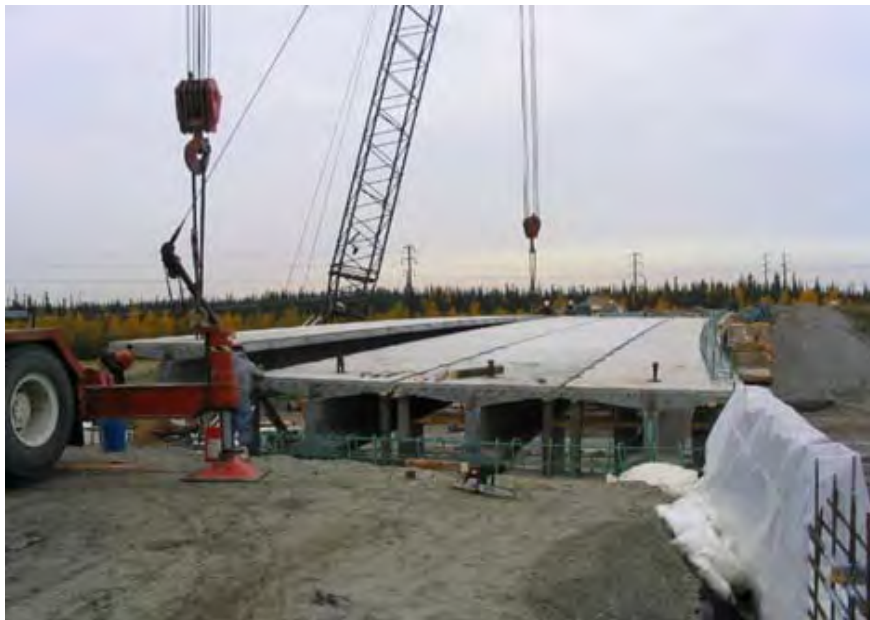
Figure 8.0.1: A DBT concrete bridge being constructed

Depending on the specific site conditions, the use of other prefabricated bridge systems can also minimize traffic disruption, improve work-zone safety, minimize impact to the environment, improve constructability, increase quality, and lower life-cycle costs. This technology is applicable and needed for both existing and new bridge construction. Over the past 50 years, thousands of short to medium span bridges have been built using precast concrete elements. There are a large number of papers on the use of precast concrete

241

elements in bridge systems including research on the use of precast elements such as deck panels for rapid deck replacement. There are both longitudinal joints and transverse joints in prefabricated bridge systems.

The DBT bridge system eliminates the time necessary to form, place, and cure a concrete deck at the bridge site. In addition, the wide top flange provided by the deck; improves construction safety due to ease of installations, enhances durability because the deck is fabricated with the girder in a controlled environment, and enhances structural performance with a more efficient contribution of the deck in stress distribution. Despite the major benefits of this type of bridge, use has been limited to isolated regions of the U.S. because of concerns about certain design and construction issues. One of the hurdles that must be overcome to enable a wider use of this technology is the development of design guidelines and standard details for the joints used in these systems, which must produce full strength joints, but still allow for accelerated construction.

Figure 8.0.2 shows a typical DBT bridge consisting of five DBTs connected by four longitudinal joints with welded steel connectors and grouted shear keys (Stanton and Mattock 1986, Ma et al 2007). In order to reduce the total DBT weight, the thickness of the deck is typically limited to 6 in. Welded steel connectors are typically spaced at 4 ft. To make the connection, as shown in Figure 8.0.2, two steel angles are anchored into the top flange of the DBT and a steel plate is welded to steel angles in the field. Between two connectors, a shear key is provided at the vertical edge of the top flange. Grout is filled into the pocket of the connector and in the voids of the shear key to tie the adjacent girders together. A joint backer bar is placed at the bottom of the shear key to prevent leakage when grouting.
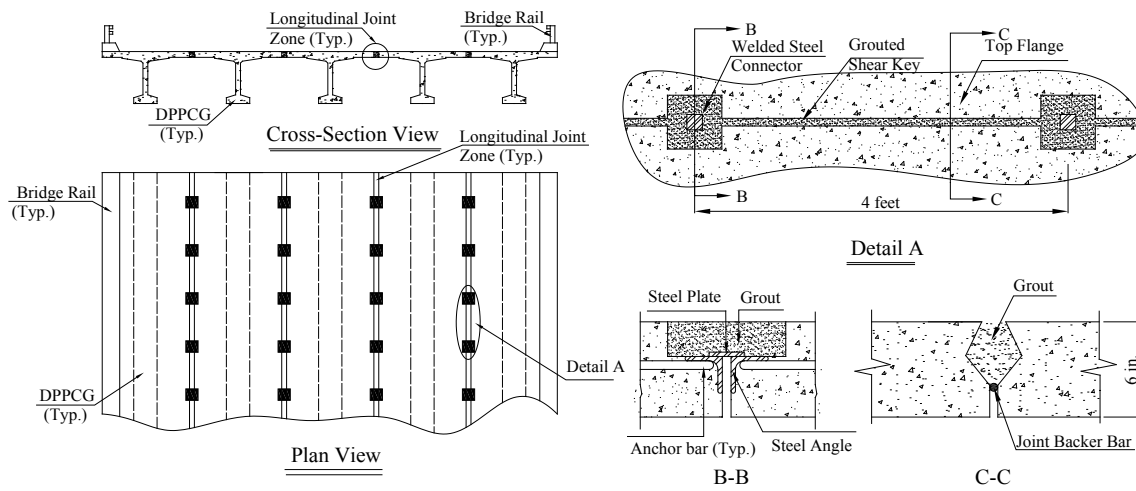
Figure 8.0.2: A typical DBT bridge connected by longitudinal joints with welded steel connectors

The typical longitudinal joint shown in Figure 8.0.2 has the strength needed to transfer shear and limited moment from one girder to adjacent girders. The width of the joint zone is small so that it facilitates accelerated construction. However, because the welded steel plates are located 4 ft from each other and at mid-depth of the flange, they cannot help to control flexural cracks along the longitudinal joint. Although the performance of this type of joint was reported as good to excellent in a survey of current users, problems with joint cracking in these systems have been reported in the literature (Stanton and Mattock 1986; Martin and Osborn 1983). This joint cracking along with joint leakage is perceived to be an issue

242

limiting wider use of this type of bridge. The State of Washington limited the use of DBTs for roads with high ADT and for continuous bridges. As part of a research project to address issues that influence the performance of DBT bridges, a specific objective was defined to develop improved joint details which allow DBT bridge systems to be more accepted as a viable system for accelerated bridge construction.

As mentioned in Chapter 1, the focus of NCHRP 10-71 was to develop specifications, guidelines, and examples for the design and construction of durable cast-in-place (CIP) reinforced concrete connections for precast deck systems that emulate monolithic construction, considering issues including speed of construction, durability, and fatigue. This project focused on systems that eliminate the need to place and remove formwork thus accelerating on-site construction and improving safety. The three systems considered in NCHRP 10-71 to accomplish these objectives were identified during the 2004 Prefabricated Bridge Elements and Systems International Scanning tour (International Scanning Study Team, 2005). These systems included: (1) precast composite slab-span systems (PCSSS) for short- to moderate-span structures, (2) full-depth prefabricated concrete decks, and (3) deck joint closure details (e.g., DBT flange connections) for precast prestressed concrete girder systems for long-span structures. Each system uses precast elements that are brought to the construction site ready to be set in place and quickly joined together. Depending on the system, the connections are either transverse (across the width of the bridge) or longitudinal (along the length of the bridge); however, practices differ in detailing the transverse and longitudinal connections.

Chapters 2 through 7 summarized the research effort conducted by the University of Minnesota research team, which was associated with the development of design recommendations for PCSSS bridges. These remaining chapters, Chapters 8 through 14, summarize the research effort conducted by the University of Tennessee at Knoxville (UTK) research team, which was associated with the development of longitudinal and transverse connection concepts between full-depth deck panels and decked bulb-T flanges including the development of durable closure pour materials for accelerated bridge construction. As noted in Chapter 1, Appendix A contains the recommended design recommendations including suggested changes to the AASHTO LRFD Bridge Design code and commentary that were developed during the study, and Appendix B contains detailed design examples developed by Roy Eriksson and his team from Eriksson Technologies, Inc. The first two design examples are associated with the PCSSS bridge concepts, and the latter three examples provide guidance on the detailing of longitudinal and transverse joints between precast panels and decked bulb-T flanges.

8.1. Longitudinal and Transverse Connection Concepts between Precast Panels and Decked Bulb-T (DBT) Flanges

This section summarizes the conceptual designs proposed and evaluated for the longitudinal and/or transverse connections between full-depth deck panels or deck flanges. Five different connection details were originally presented to phone survey respondents for comment (see Appendix C), the results of which are briefly summarized in Section 8.1.1. Issues considered in finalizing the connection details and description of connection details further investigated in the NCHRP 10.71 study are summarized in Section 8.1.2.

8.1.1. Summary of Phone Survey in Association with Longitudinal and Transverse Connection Concepts between Precast Panels and Bulb-T Flanges

Survey respondents provided feedback and insight on the longitudinal and transverse connection concepts in general, as well as regarding the five specific joint connection details outlined in a handout that was distributed prior to the phone survey conducted by the research team (see Appendix C). The five connection concepts that were addressed were: loop bar (U-bar) detail, straight bar detail with spiral to reduce lap length, headed bar detail, welded wire reinforcement (WWR) detail, and structural tube detail.

In general many respondents considered all five of the connection concepts to be potentially useful in bridge construction, and especially when rapid construction was critical. A common concern regarding the connection of each of the precast elements was that of differential camber, and many respondents who voiced this concern suggested that the use of a steel plate or haunch should be included to assist with the leveling of adjacent precast panels.

Many of the respondents preferred the U-bar detail over the other options, and noted that a loop bar detail has been successful in Japan and Korea. Some expressed that although the U-bar detail was the most promising, it could require a thicker deck to accommodate the bend radius of the loop detail, which would add weight to the structure. It was suggested by another, that the key to the U-bar detail would be to obtain a waiver on the minimum bend radius of the looped bar. Experience of a similar detail used in Nebraska four years indicated exceptional performance of the system; it was emphasized that the connection must be either nonshrink or expansive to prevent cracking. Some respondents commented that the loop detail would require perforations in the formwork, and therefore the bar spacing should be standardized as much as possible.

The straight bar with spiral reinforcement to reduce the lap length detail was also favored by many of the respondents. A common concern regarding the connection was that it was expected to be more expensive, and would also require additional field labor to complete the connection. In addition, it was suggested that the spiral reinforcement may create alignment issues during construction, which could add to the amount of time required for construction.

The headed bar detail was often praised for the fact that it would come to the field site nearly completed, which would reduce construction labor as well as the time required to construct the system. Many respondents conceded little experience with the headed bar details and suggested that testing would be required, though many said that they expected that the detail would work adequately. Some respondents also suggested that the detail may be difficult to fabricate, and that the alignment and placement of the longitudinal steel could be complicated.

The welded wire reinforcement detail was generally liked by most of the respondents, especially because the wire reinforcement detail was expected to promote rapid construction in the field. A few respondents voiced concern regarding the ability for the welded wire reinforcement to be adequately developed in the space available. In California, it was noted that welded wire reinforcement was not permitted, and that it may be due to a fatigue concern, though manufacturers are promoting its use.

Many of the respondents viewed the structural tube detail as being exceptionally robust, with one respondent describing it as being "bomb proof." A common concern regarding the structural tube detail was the potential for alignment and other constructability issues. Also of concern was the potential for sloppy field work to degrade the connection, especially if the tube were not correctly and completely filled with grout.

8.1.2. Criteria Considered and Finalization of Longitudinal and Transverse Connection Concepts Investigated in NCHRP 10-71

In further developing the connection concepts, the following criteria were considered:

- The connection detail should not only be able to transfer shear but also provide moment continuity across the joint. Where possible, two layers of steel should be used in the joint.
- The connection detail must allow the precast units to be joined together quickly to minimize disruption to traffic. For the joint connections, it is desirable to minimize or eliminate forming of the joint to expedite construction and reduce cost. Field placement of reinforcement within the longitudinal joint area after erection should be minimized. In joints where forming is required, provide sufficient room to facilitate connection completion and use CIP rather than special grout mixes.
- The closure pour (CP) material to precast unit interface is an area of concern for durability. The focus in this area must be on minimizing cracking in this location to reduce intrusion of water that may result in corrosion. Place the reinforcement as close as practicable to the top and bottom surfaces to help control cracking.
- Cumulative fabrication and erection tolerances, particularly differential camber in deck flanges, will result in some degree of vertical flange mismatching. A temporary welded connector detail should be considered for leveling flange mismatching before the permanent connection is placed.

When selecting CP materials, performance-based specifications for durability need to be developed to proportion concrete mixtures or other grouting materials that are capable of protecting structures against a given degradation for a specified service life in given environmental conditions.

To improve the current joint detail (Figure 8.0.2), the proposed new details should control joint cracking better, and maintain the accelerated construction features. One concept was to replace the current welded steel connectors with distributed reinforcement to provide moment transfer as well as shear transfer across the joint. Well-distributed reinforcement can control cracks much better than widely spaced welded steel connectors. However, straight lap-spliced reinforcement requires a much wider joint to develop its strength. It is very important for the proposed joint width to be as narrow as possible. Joint width minimization will reduce the required expensive grout which results in a reduction of cost and faster construction time. As a result, options to reduce the joint width were explored. Such options included bars with hooks (U-bar), bars with headed terminations, and bars with spirals. To allow for accelerated construction, the details were also developed to minimize deck thickness which would reduce the weight of DBT girders. As a result, the U-bar detail and the headed bar detail were selected as the most viable candidates for this research.

U-bar details are oriented vertically in the joint to provide two layers of reinforcement fabricated with a single rebar. The U-bars provide continuity of the deck reinforcement across the joint by lapping with the U-bars from the adjacent flanges. The 180° bend of the U-bar, embedded in the joint, provides mechanical anchorage to the detail necessary to minimize the required lap length. The extended reinforcement of the U-bar details is staggered (i.e., out of phase) with the adjacent lapped U-bar to facilitate constructability in

245

the field. The stagger cannot be too large, or the transfer of forces across the joint would be difficult to achieve.

To minimize deck thickness, the U-bar detail was designed to utilize an extremely tight bend. The inside bend diameter that was used was three times the diameter of the bar ($3d_b$), thus with No. 5 bars used, the inside diameter of the bend was 1-7/8 in. ACI Committee 318-08 (2008) set minimum bend diameters for different rebar sizes and materials. For a No.5 bar made of conventional steel, the minimum bend diameter, per ACI 318-08 (2008), was six times the diameter of the bar ($6d_b$), and for D31 deformed wire reinforcement (DWR) the minimum bend diameter was four times the diameter of the bar ($4d_b$) when used as stirrups or ties. Clearly the U-bar bend diameter that was used ($3d_b$) violated the minimum allowable bend diameters established by ACI 318-08 (2008). The minimum bend diameters were established primarily for two reasons: feasibility of bending the reinforcement without breaking it and possible crushing of the concrete within the tight bend. To ensure that the reinforcement would not be broken while bending, two ductile reinforcing materials were used: deformed wire reinforcement and stainless steel reinforcement. Concrete crushing in the tight bend was closely observed in the experimental investigation to determine if it would occur.

As an alternative to the U-bar details, two layers of headed bars were considered to provide continuity of the top and bottom deck steel through the joint. The previous NCHRP 12-69 project explored the use of single large-headed bars to provide continuity across the joint (Li et al. 2010, Li et al. 2010a). In that project, Headed Reinforcement Corporation (HRC) provided the headed reinforcement, which consisted of a No. 5 bar with a standard 2 in. diameter circular friction welded head with a head thickness of 0.5 in. Large-headed bars such as these with the bearing area (A_{brg}) exceeding nine times the area of the bar (A_b), are assumed to be able to develop the bar force through bearing at the head. Bars with smaller heads, (e.g., $A_{brg}/A_b \geq 4$) are assumed to be able to develop the force in the bar through a combination of mechanical anchorage and bond, where the development length for these bars is less than that required to develop a hooked bar (ACI 318-08). In the current study, the headed reinforcement used was No. 5 bar with Lenton Terminator® bearing heads. The diameter of the head was 1.5 in., and the thickness of the head was 7/8 in., which gave A_{brg}/A_b of 4.76. The smaller head dimension was necessary in order to fit the two layers of reinforcement within the deck while minimizing the deck thickness. The large-headed bars in two layers would have resulted in a much thicker, uneconomical deck system.

Both longitudinal joints (parallel to the traffic direction) and transverse joints (perpendicular to the traffic direction) were designed and tested in the NCHRP 10-71 study utilizing each joint detail. Both joint directions were investigated so that the results of this experimental program could apply to several precast deck systems (e.g., DBT systems and full-depth precast deck systems). Figure 8.1.1 shows the two joint directions tested and the specimen orientations used to represent the joints.

246
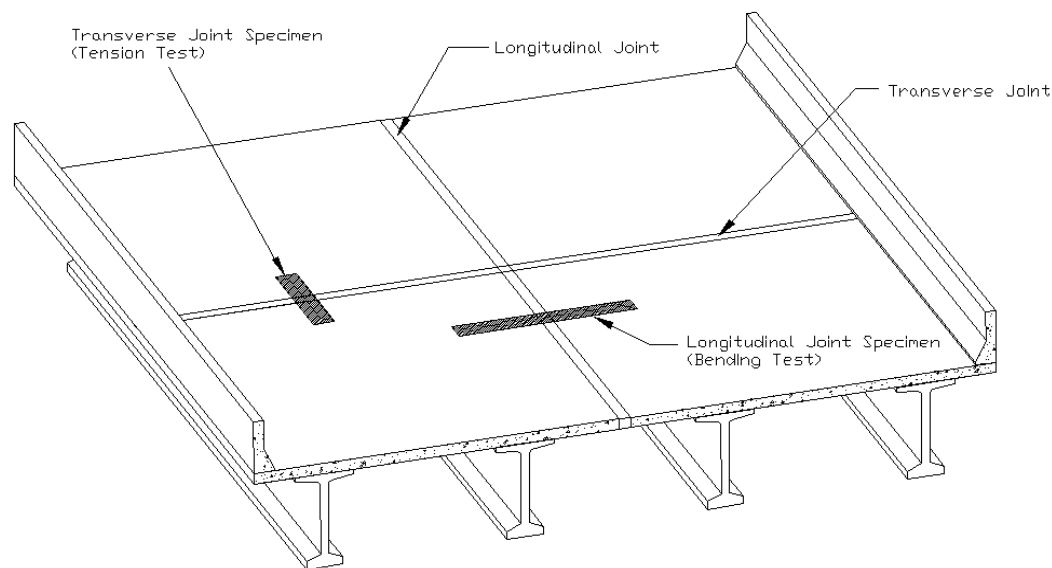
Figure 8.1.1: Orientation of joints and corresponding test specimens

8.2. Organization of Report Regarding Investigation of Longitudinal and Transverse Connection Concepts between Precast Panels and Bulb-T Flanges

Chapter 9 describes the process of selection of trial longitudinal and transverse joint systems and the laboratory testing of trial selected joints. The performance of different joint details was compared in Phase I experiments. In Phase II experiments, additional tests were conducted on the most promising connection detail from Phase I to investigate parameters including overlap lengths, rebar spacings, and concrete strengths. In all of these tests conducted to select the most viable joint details, the details were cast in monolithic concrete specimens. Chapter 10 presents the parametric studies conducted to determine live load forces to be applied in the connection tests. Parameters investigated included girder depth, girder span, girder spacing, single- and multi-lane loading, skew, diaphragm spacing and stiffness, and location of wheels relative to the joints in the precast deck for the panel-to-panel and/or flange-to-flange connections for fully continuous transverse or longitudinal deck behavior. Chapter 11 describes the selection of two closure pour materials (overnight and 7-day cures) based on the specified performance criteria for freeze thaw, shrinkage, bond strength and permeability. Chapters 12 and 13 summarize the slab tests to determine serviceability (including crack control), static load strengths, and fatigue characteristics for the selected longitudinal and transverse joints, respectively, fabricated with durable grout material in the connection region, selected through research described in Chapter 11. A brief summary and conclusions are provided in Chapter 14.

Chapter 9 Flange/Deck Connection: Selection of Most Promising Connection Detail through Two-Phase Experimental Investigation

9.0 Introduction to Two-Phase Experimental Investigation to Finalize Connection Concept Detail for Further Study

The headed bar detail and deformed wire reinforcement (DWR) and stainless steel (SS) U-bar details described in Section 8.1.2 were investigated and compared in the first phase of a two-phase experimental program conducted to finalize the best-performing connection detail for further study. The detail with the best performance as deemed from the Phase I experiments was subjected to additional testing in Phase II to investigate variations in parameters including overlap lengths, rebar spacings, and concrete strengths. The two-phase study was conducted on representative longitudinal (flexure) joint specimens and transverse (tension) joint specimens cast monolithically. The detailed connection concept, which was the outcome of the two-phase study, was subsequently investigated in jointed test specimens which included overnight-cure and 7-day cure closure pour (CP) materials (see Chapter 11) in the joint subjected to static and fatigue loadings as described in Chapters 12 and 13 for the longitudinal and transverse connection concepts, respectively. This chapter presents the results of the initial two-phase experimental investigation.

9.1. Test Phase I

9.1.1. Specimen Design

As shown in Figure 8.1.1, in a real bridge, the longitudinal joint specimen is representing the specimen across the longitudinal joint and transverse joint specimen is representing the specimen across the transverse joint. The longitudinal and transverse reinforcement are the directions in the real bridge. Therefore, the main reinforcement in the longitudinal joint specimen is transverse reinforcement. And the main reinforcement in the transverse joint specimen is longitudinal reinforcement.

Based on typical deck design practice and the desired deck thickness (e.g., DBT top flange thickness is 6 in.), the maximum bar size was limited to #5 bars. This size of reinforcement represented the maximum possible bar size to achieve the required tight bend diameters and clearance requirements for the head. It was assumed that the transverse reinforcement would always be located as the outer reinforcement layers in the deck to provide the largest moment couple to resist flexure of the deck in the transverse direction. Consequently, the specimens were detailed to give the transverse rebar the largest moment arm without violating cover requirements. To simulate the most demanding case to achieve flexural capacity across the longitudinal joint, the deck was minimized in those specimens to represent a situation where a transverse joint may not be required (e.g., a relatively short span, simply-supported bridge). In such cases, it may be possible to achieve thinner decks because there may not be a need to provide headed or U-bars in the longitudinal direction. In such a situation, the deck thickness was controlled by the outer layer of reinforcement achieving the tightest bend diameter. The resulting deck thickness for the longitudinal joint specimens was 6-¼ in. The most demanding load case for a transverse joint is to resist a high tension force (e.g., a transverse joint over the pier in the negative moment region). In such cases, headed or U-bars in the longitudinal direction can be placed inside of the outer reinforcement layers which can also be headed or U-

248

bars in the transverse direction. The resulting deck thickness for the transverse joint only (or the combined transverse and longitudinal joints) was 7-¼ in. to accommodate the required reinforcement clearances.

Due to two joint directions being investigated, two design methods were used to determine a realistic spacing for the reinforcement of the joint details. The spacing of the rebar in the longitudinal joint was designed utilizing the AASHTO strip method of deck design (AASHTO LRFD 2010). This method takes into account the largest positive and negative moments that would be experienced by the longitudinal joint. However, to determine the controlling load case for a transverse joint, the transverse joint should be positioned over an interior support in a continuous span bridge system. In this case, if the deck was compositely connected to the girder, the deck would have to resist large tensile forces that would be produced by the negative moment developed there. So, the rebar spacing for the transverse joint was determined using flexural analysis of the deck-girder composite section, conservatively assuming that all the tension force created by the negative moment would be resisted by the deck. The spacing of the rebar in each joint direction was determined by its corresponding deck design.

Two PCI design examples were used to design the reinforcement spacings for the joint details. The longitudinal joint spacing was designed using design example 9.8 in the PCI Bridge Design Manual (PCI 2003). The spacing for the transverse joint reinforcement was designed using design example 9.6 in the PCI (2003). Both examples used the same bridge cross section and longitudinal section. The bridge cross section consisted of four BT-72 girders that were spaced at 12 ft on center. The longitudinal section of the bridge consisted of a center span of 120 ft and two side spans of 110 ft. The PCI design examples were used, so that the steel areas determined would represent the amount of steel in a typical bridge deck.

An 8 in. deck was first designed for the interior portion of the deck. This design was carried out to obtain an estimate of the area of steel used in decks with a conventional thickness. Table 9.1.1 shows the results of the design for the U-bar detail assuming Grade 75 steel, and Table 9.1.2 shows the design results for the headed bar detail assuming Grade 60 steel for the 8 in. deck thickness. Two different values of exposure factors, class one and class two, were used in the designs to show where the service limit state controlled the design. Exposure factors are directly proportional to the crack widths expected at service level loading. So, the larger the exposure factor the larger the expected crack widths.

In order to minimize the deck thickness, two other thicknesses were also investigated. A 6-¼ in. deck was designed for the longitudinal joint direction utilizing both joint details, and a 7-¼ in. deck was designed for the transverse joint direction utilizing both joint details. The transverse joint required a larger deck thickness in order to keep the transverse deck rebar, required to cross the longitudinal joint, as the outer reinforcement layer, as discussed earlier. The 6-¼ in. and 7-¼ in. deck thicknesses were the thinnest deck sections possible when considering the joint details and cover requirements.

The 6-¼ in. thick deck section was then designed. The results from this design were used for the design of the reinforcement for the longitudinal joint direction for both joint details. Both yield strengths and exposure classes were used. Table 9.1.3 shows the results of the design for the U-bar detail, and Table 9.1.4 shows the design results for the headed bar detail.

249

Table 9.1.1: Reinforcement required for the U-bar detail in an 8 in. deck

Locations		f_y = 60 ksi			
		γ_e = .75		γ_e = 1	
		Bars Size	Spacing (in)	Bars Size	Spacing (in)
M+ (Bottom)	Transverse	# 5	8.0	# 5	8.0
	Longitudinal	# 5	11.5	# 5	11.5
M- (Top)	Transverse	# 5	7.0	# 5	8.5
	Longitudinal	# 4	18.0	# 4	18.0

Table 9.1.2: Reinforcement required for the headed bar detail in an 8 in. deck

Locations		f_y =75 ksi			
		γ_e = .75		γ_e = 1	
		Bars Size	Spacing (in)	Bars Size	Spacing (in)
M+ (Bottom)	Transverse	# 5	8.0	# 5	9.5
	Longitudinal	# 5	11.5	# 5	11.5
M- (Top)	Transverse	# 5	7.0	# 5	8.5
	Longitudinal	# 4	18.0	# 4	18.0

Table 9.1.3: Reinforcement required for the U-bar detail in a 6-¼ in. deck

Locations		f_y =75 ksi			
		γ_e = .75		γ_e = 1	
		Bars Size	Spacing (in)	Bars Size	Spacing (in)
M+ (Bottom)	Transverse	# 5	4.5	# 5	4.5
	Longitudinal	# 5	6.5	# 5	6.5
M- (Top)	Transverse	# 5	4.0	# 5	4.5
	Longitudinal	# 4	12.0	# 4	12.0

250

Table 9.1.4: Reinforcement required for the headed bar detail in a 6-¼ in. deck -

| Locations | | f_y = 60 ksi | | | |
| | | γ_e = .75 | | γ_e = 1 | |
		Bars Size	Spacing (in)	Bars Size	Spacing (in)
M+ (Bottom)	Transverse	# 5	4.0	# 5	4.0
	Longitudinal	# 5	5.5	# 5	5.5
M- (Top)	Transverse	# 5	4.0	# 5	4.0
	Longitudinal	# 4	12.0	# 4	12.0

Tables 9.1.3 and 9.1.4 show that the service limit state had little impact on the rebar spacing for the 6-¼ in. deck section. The only case that the service limit state governed was the top layer of transverse reinforcement of the U-bar detail design. Also, when comparing the amount of reinforcement required for the 6-¼ in. and 8 in. thick deck sections (see Tables 9.1.3 and 9.1.4 compared to 9.1.1 and 9.1.2), it was found that the 8 in. thick deck required approximately half the reinforcement that was required for the 6-¼ in. thick deck. Although the area of steel required for the 6-¼ in. thick deck was larger than that required for the 8 in. thick deck, the decrease in weight of the slimmer deck section and the labor costs saved by the possibility of accelerated construction provided the incentive to investigate the slimmer deck section.

The required steel area for the transverse joint was then determined. The reinforcement in the transverse joint was designed as if the joint was located over an interior pier of a continuous span bridge system with the deck compositely connected to the girder. The negative moment developed in these locations would create large tensile forces in the deck, which would require more longitudinal steel in these regions. The composite cross section and the negative moment used in the flexural calculations were taken from example 9.6 of PCI (2003). The negative moment value that was used in the flexural calculations was 4837 kip-ft.

The amount of longitudinal deck reinforcement was determined by a conventional flexural design using the composite section. The centroid of the reinforcement was assumed to be at mid-height of the deck and the required amount of reinforcement was determined for both the 60 ksi and 75 ksi yield strengths. Table 9.1.5 contains the results of the designs.

251

Table 9.1.5: Negative moment longitudinal reinforcement

f_y (ksi)	rebar size	spacing (in)
Longitudinal Reinforcement (MU- region)		
60.9	#5	4.5
75.4	#5	5.5

To facilitate comparison of the results of the different joint details and joint directions, the deck designs were used to develop a rebar spacing configuration that was used for the construction of all specimens. The reinforcement in both the longitudinal (flexure) joint specimens and transverse (tension) joint specimens was selected to be the same for both specimens (across the joint and perpendicular to the joint). The reinforcement spacing was conservatively selected from the tables above to provide the same detailing across the joint in the specimens that used the Grade 75 reinforcement as was used in those that used the Grade 60 reinforcement. Due to the use of the U-bar detail, the top and bottom layers of primary joint reinforcement had to have the same spacing (because by the very nature of the U-bar, it consists of two layers of reinforcement). In summary, the reinforcement that crossed the joint consisted of a top and bottom layer of #5 rebar spaced at 4.5 in. (see Table 9.1.5). The top layer of reinforcement transverse to the joints consisted of #4 rebar spaced at 12 in. and the bottom layer of reinforcement transverse to the joint was determined to be #5 rebar spaced at 6 in.

The joint overlap length, which is defined herein as the distance between the reinforcement bearing surfaces, was determined based on the expected development length of a U-bar. The ACI equation for determining the development length of a standard hook in tension was used to calculate the approximate development length of a U-bar. This equation does not directly apply to the U-bars that were used, because the U-bars do not meet the dimensional requirements for a standard hook, namely the $3d_b$ bend diameter used in the U-bar fabrication violated the minimum $6d_b$ bend diameter specified in ACI 318-08. Eqn. (9.1.1) shows the ACI development length equation for a standard hook in tension.

$$l_{dh} = \left[\frac{.02 \Psi_e \lambda f_y}{\sqrt{f'_c}} \right] d_b$$

(ACI 12.5.2) $\hspace{4cm}$ (9.1.1)

where l_{dh} represents the development length from the tail of the hook, in.; Ψ_e is the epoxy coating factor; λ is the lightweight concrete factor; f_y is the reinforcement yield strength; $\sqrt{(f'_c)}$, the square root of the concrete compressive stress, is expressed in psi; and d_b is the diameter of the bar, in. The terms, Ψ_e and λ, were both set equal to one in Eqn. (9.1.1), because the rebar that was used was not epoxy coated and the concrete was not lightweight. It should be noted that a number of states do not use epoxy-coated reinforcement in their decks, 4 of 38 states surveyed by Russell (2004) indicated that they do not specify epoxy-coated deck reinforcement. In addition, 14 of the 38 states surveyed, indicated that they specify a

metallic coating for the deck reinforcement, and 7 of the 38 states indicated that they were beginning to use solid stainless steel. In order to minimize the joint width between the precast flanges or panels, it is desirable to avoid epoxy-coated reinforcement because that may require a longer lap length to develop the reinforcement. In addition, tighter bend diameters are feasible with stainless steel reinforcement than with ordinary mild reinforcement.

Using Eqn. (9.1.1), the development length was calculated for a No. 5 bar, assuming a concrete compressive strength of 6 ksi and a steel yield strength of 75 ksi, because deformed wire reinforcement and stainless steel were materials used for this joint detail. The ACI 318-08 development length modification factor of 0.7 was used, because the specimens met the bar cover perimeters of having not less than 2.5 in. of side cover and not less than 2 in. of cover beyond the extension of the bar. The development length of a standard hook bar in tension for this situation was calculated to be 8.5 in. In the testing program, an overlap length of 6 in. was used for the U-bar detail. Where the overlap length is taken from the inside bend of the adjacent hooks. This would be 7-¼ in. to the outside of the hooks, less than the 8.5 in. specified by ACI 318-08, but lacer bars were also used in the connection to enhance the mechanical anchorage.

Based on Li et al. (2010), one-layer of headed bars with varying overlap lengths, 2.5 in., 4 in. and 6 in., were tested and compared, and the lap length for the headed bar detail was recommended to be 6 in. Although the head was larger in the Li study (Li et al. 2010) as discussed earlier, for the case of the No. 5 headed bars in this study, with the small head size, the overlap length was also taken to be 6 in.

Because the behavior of the specimens with both joint details was to be compared, the overlap lengths for the U-bar and headed bar joint details were made the same, i.e., 6 in. Two transverse lacer bars were added to each joint detail to provide continuity and confinement of the joints. The inclusion of lacer bars in both joint types was due to previous research conducted by Gordon and May (2005) on loop bar joints in tension. In their experimental program a loop bar specimen was tested in tension without transverse lacer bars, which resulted in a sudden brittle failure. The transverse lacer bars were installed in the center of the bend in the U-bar detail and in the middle of the headed bar detail.

The specimens and connection details designed for the longitudinal joint direction are shown in Figures 9.1.1 and 9.1.2. The specimens and connection details designed for the transverse joint direction are shown in Figures 9.1.3 and 9.1.4.
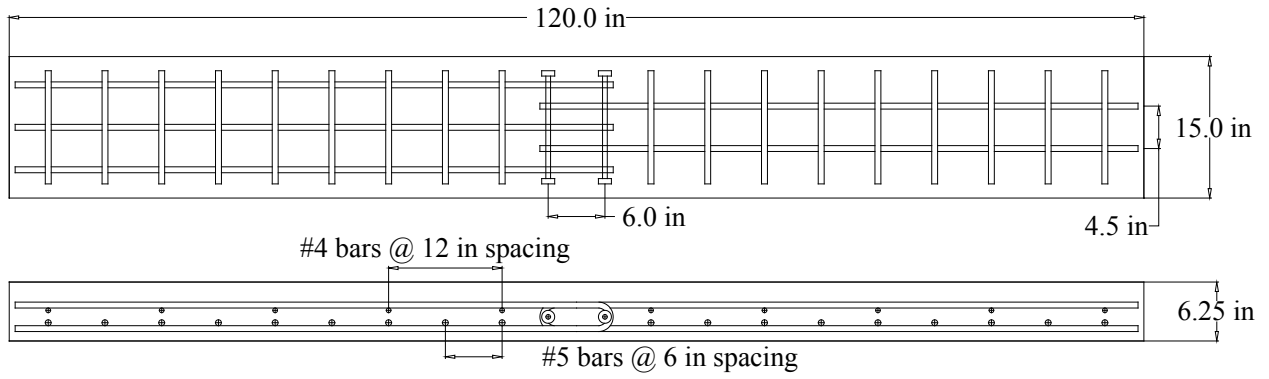
Figure 9.1.1: U-bar longitudinal joint specimen
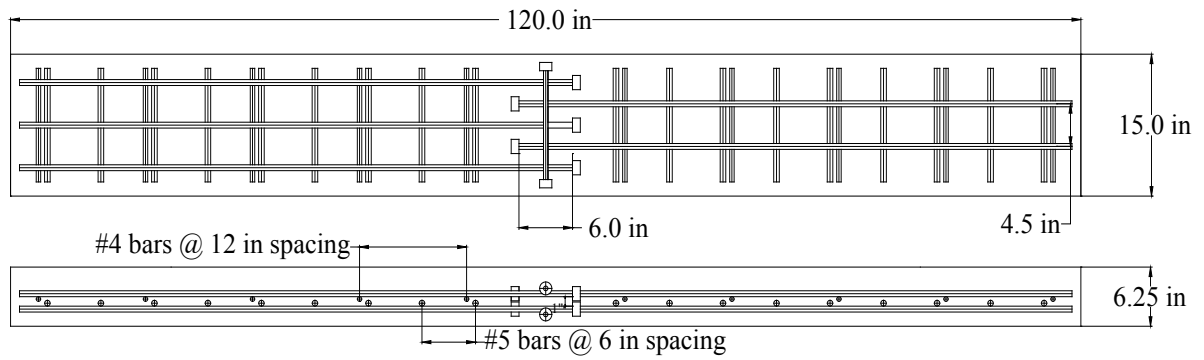
Figure 9.1.2: Headed bar longitudinal joint specimen

254
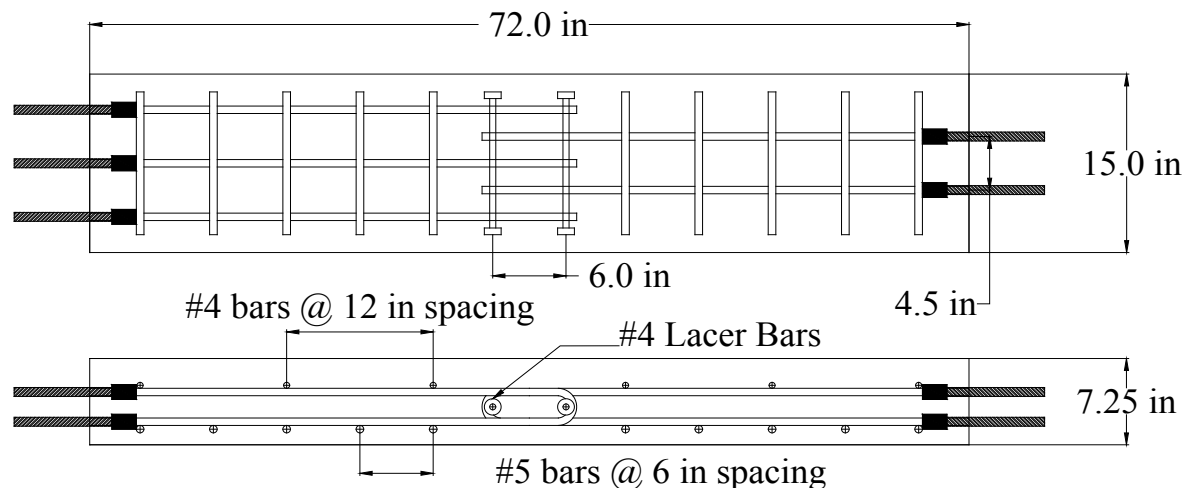
Figure 9.1.3: U-bar transverse joint specimen
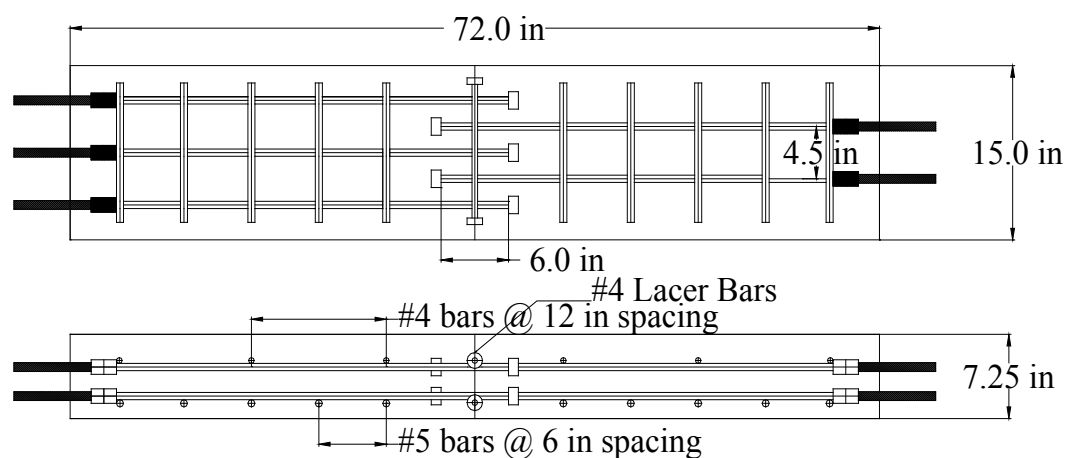
Figure 9.1.4: Headed bar transverse joint specimen

9.1.2. Experimental Setup and Instrumentation

Experimental Set-up

Simple static tests were performed for both the longitudinal connections and transverse connections. The specimens representing the longitudinal joint direction were tested in bending. The specimens representing the transverse joint direction were tested in tension, because of the tensile forces assumed to be generated in the deck created by negative moment regions of the bridge system. Both joint details (i.e., U-bar and headed bar) were tested in both joint directions.

255

As stated previously, the specimens representing the longitudinal joint direction were tested in bending. A modified version of the four point bending tested was used for the flexural test set-up. The actuators used to apply force were located on the outside of the supports; this set-up produced upward deflection in the specimen producing tension on the top surface of the specimen. Tension on the top surface of the specimen produced safer conditions for observing cracks and crack propagation. This set-up, like the four point bending test, produced a constant maximum moment between the supports where the joint was located. Figure 9.1.5 shows the experimental set up used to test the longitudinal joint specimens (Flexural Test Set-Up).
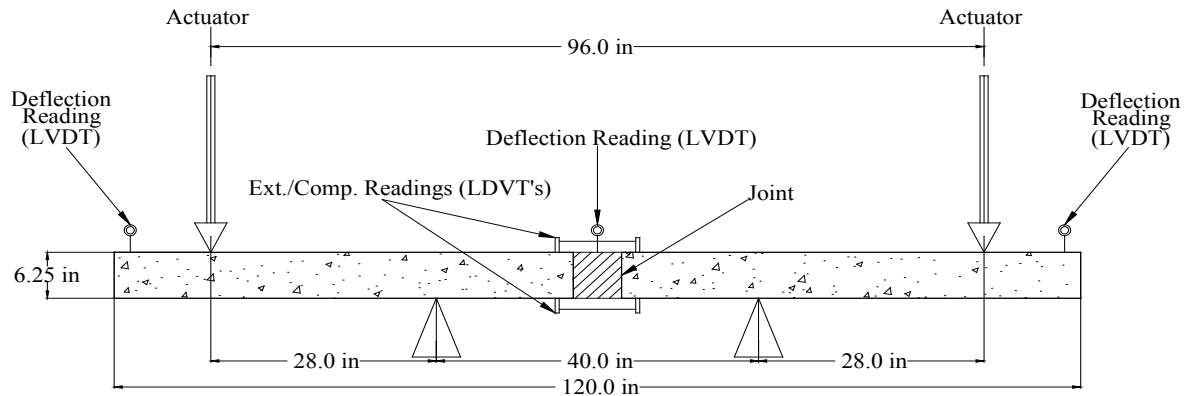
Figure 9.1.5: Flexural test set-up (Longitudinal Joint Test)

256

As stated previously the specimens representing the transverse joint direction were tested in tension. The tension test set-up was slightly more complicated than the flexural test set-up. The longitudinal reinforcement in the transverse joint specimens was welded to ¾ in. threaded rods. These threaded rods were used to bolt the tension specimen to the support and loading beams. The support beam was connected to the specimens and then placed on top of the load frame. The support beam was then braced and clamped into position, so it would remain stationary. The loading beam was then connected to the specimen and the actuators. The actuators pushed the loading beam down, which applied a tension force to the specimens. Figure 9.1.6 shows the tension test set-up.

257
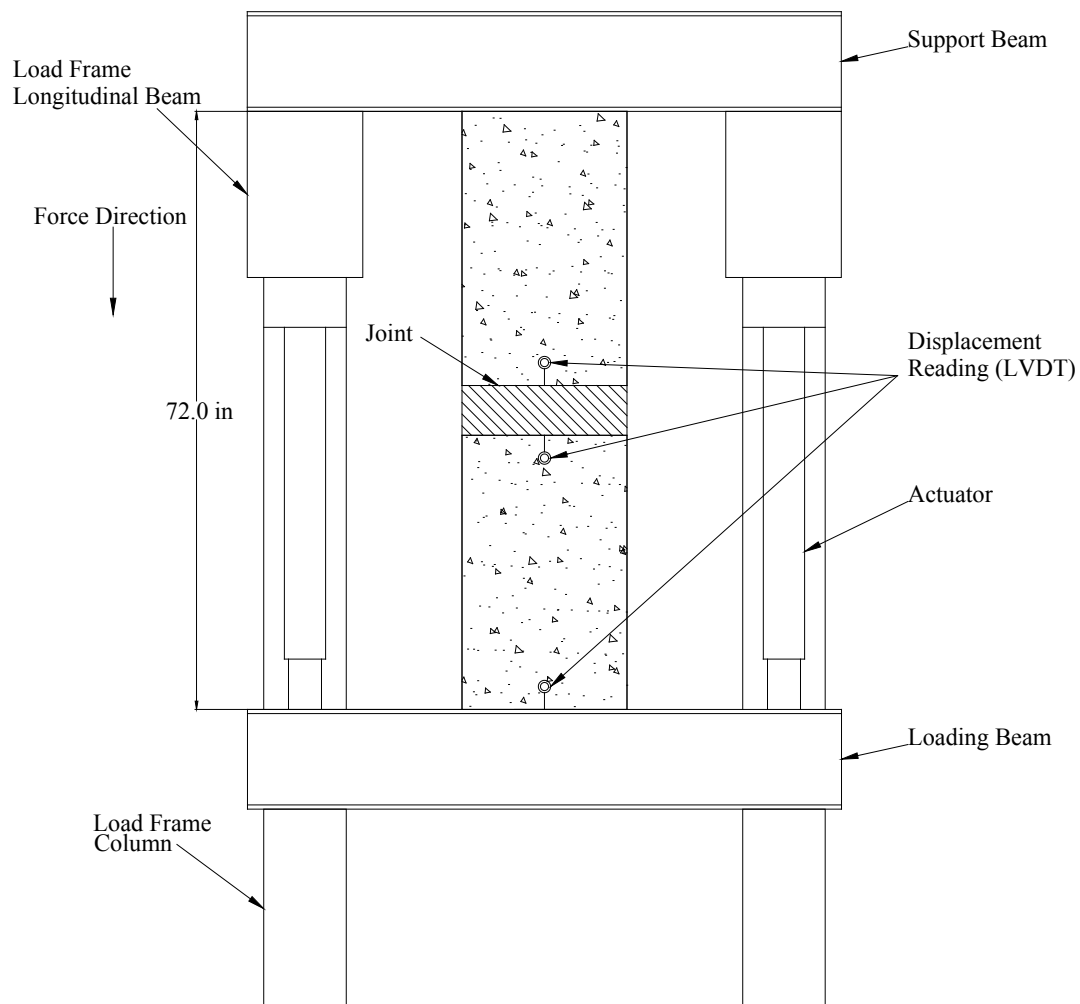
Figure 9.1.6: Tension test set-up (Transverse Joint)

Instrumentation

The specimens were instrumented to achieve an understanding of the U-bar and headed bar details in bending and tension in the longitudinal and transverse joint tests, respectively. Loads cells were used to measure the loads applied to the specimens. Linear motion transducers (LMT's) were used to measure the deflection of the specimens. Also, horizontally placed LMT's were used to determine the curvature of the longitudinal joint specimens tested in flexure. The strain in the joint reinforcement was measured using strain gages. The main purpose of the strain gages was to determine whether the reinforcement could achieve yielding in the joint, which would indicate that the joint details could produce a precast deck system that would emulate monolithic behavior. For the U-bar detail, strain gages were installed on the top and bottom of the three interior U-bars. These gages were installed 2, 6, 8, and 10 in. away from the bend of the bar. Also, a strain gage was installed on the outside apex of the bend on each gaged U-bar. For the headed bar joint detail, strain gages were installed on the top and bottom headed bars on the three interior sets of headed bars. The term headed bar set refers to the top and bottom headed bars at a specific location. These gages were installed 1, 4, 6, and 8 in. away from the bearing surface of the head on headed bar sets 2 and 3. Strain gages were installed 4, 6, 8 and 10 in. away from the bearing surface of the head on headed bar set 4. Figures 9.1.7 and 9.1.8 show the strain gage configurations used for the U-bar and headed bar details, respectively.

258
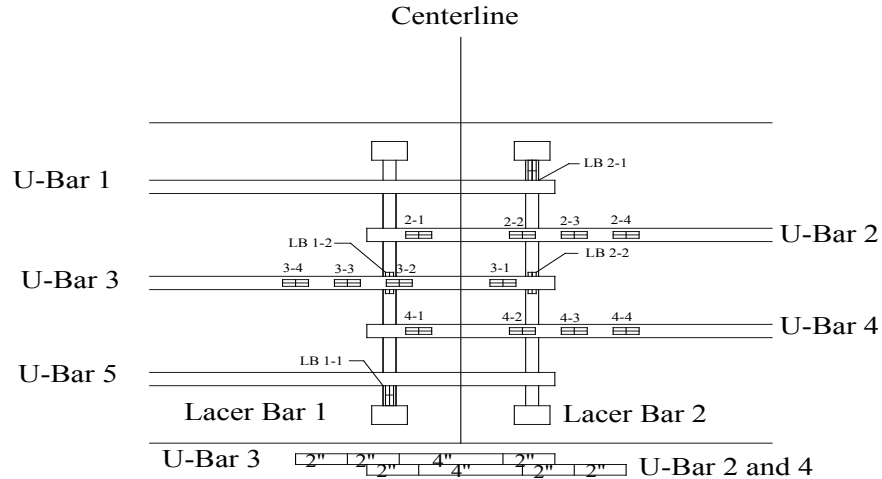
Figure 9.1.7: U-bar joint detail strain gage configuration
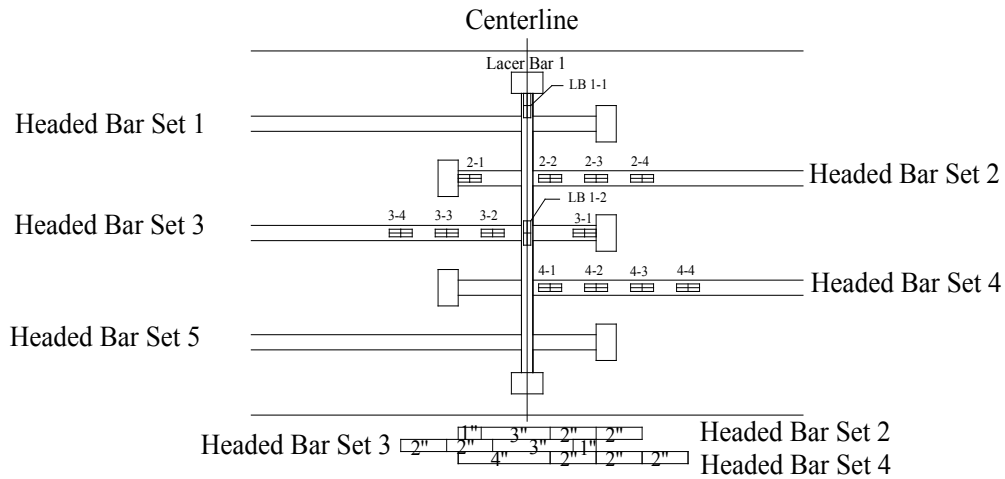
Figure 9.1.8: Headed bar joint detail strain gage configuration

The strain gage notation used in Figures 9.1.7 and 9.1.8 indicates the U-bar or the headed bar set where the gage was located and the relative position of that gage. For example, strain gage 2-3 indicated that the gage was located on U-bar 2 or headed bar set 2 and that it was the third gage away from the bearing surface of that bar. In the strain gage results section of this paper, the strain gages are labeled additionally with a "T" or "B" indicating that they are located on the top or bottom of a U-bar or located on the top or bottom bar of a headed bar set. The distances to the centerlines of the strain gages are given at the bottom of Figures 9.1.7 and 9.1.8 in inches. The first length given for each bar is the distance from the centerline of the first gage to the bearing surface of the reinforcement. The other distances shown in the figures represent the center to center spacing between consecutive strain gages in inches.

259

Strain gages were also installed on the transverse lacer bars. A strain gage was installed 1 in. away from the bearing surface of the head, and another strain gage was installed in the center. All lacer bars used for the construction of the specimens were gaged. Figure 9.1.9 shows the strain gage configuration of the lacer bars.
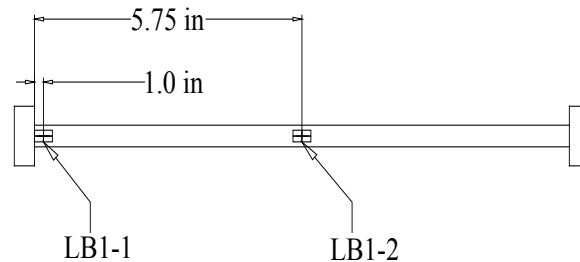
Figure 9.1.9: Lacer bar strain gage configuration

LMT's were used to determine specimen deflections at various locations. For the longitudinal joint bending specimens, LMT's were installed at the center of the specimen and at both ends. For the transverse joint tension specimens, LMT's were installed on the top and the bottom of the joint to measure joint elongation and at the bottom of the specimen to measure the total deflection of the specimens.

The curvature of the longitudinal joint bending specimens was also measured using LMT's. The LMT's were installed parallel to the specimen on the top and bottom of the joint zone. Top and bottom surface strains could then be calculated based on the initial gage length of the LMT wire and the change in the readings taking into consideration the distance between LMTs and concrete surface. These surface strains were then used to determine the curvature of the specimens throughout the duration of the test. Figures 9.1.5 and 9.1.6 show the positions of all previously discussed LMT's.

9.1.3. Specimen Construction, Reinforcement Cost and Fabrication

Specimen Construction

Figure 9.1.10 shows several specimens during the construction process. As can be seen in the photos, the specimens were monolithically cast. In practice the joint would consist of precast deck panels with staggered, protruding reinforcement that would then be anchored into a cast-in-place joint. In this experimental program the behavior of the reinforcement of the different joint details was of main concern. The monolithic specimens allowed the behavior of the joint details to be observed without the additional variable of a grouted joint. Additional testing with the best performing detail contained the grouted joint between the precast panel sections. These tests are described in Chapters 12 and 13.

260

(a) Reinforcement in the forms

(b) Plate used to ensure proper layer separation

(c) Threaded rods extending through the form

(d) Casting concrete

(e) Vibrator use in the joint zone

(f) Concrete finishing

Figure 9.1.10: Specimen construction

261

Comparing the constructability of the U-bar and the headed bar joint details, the U-bar detail seemed to be the easiest to construct for two reasons. The U-bar detail produces a joint that is less congested than the headed bar detail and therefore allows for easier placement of precast deck components. The headed bar detail is more congested due to the bearing heads. Instead of considering just the diameter of the bar in considering clearances, which is the case for the U-bar detail, the outside diameter of the bearing head must be accommodated. The head reduces the construction tolerances, which may lead to placement problems in the field. The reinforcement of the U-bar detail was also easier to tie and set in place compared to the headed bar detail. After the top and bottom of the U-bars were set to the correct height by tack welding a thin plate between the free ends, the U-bars acted as a single reinforcement cage, which made the installation of the rebar easier than the two separate layers of reinforcement produced by the headed bar detail.

During shipment, storage, and placement of precast deck components, unintentional bending of the protruding joint reinforcement due to handling is a concern. The U-bar detail provides benefits considering this aspect. In the headed bar detail, one headed bar could be accidentally bent at a time, but for the U-bar detail two bars would have to be bent at one time, because the top and bottom layer of reinforcement consists of one bent bar. The bending of two bars at once would require a greater force and would therefore be more unlikely to happen. With the U-bar detail, it may be possible to bend a mesh of reinforcement to prepare the rebar cage for placement. This would reduce construction time in the precast plant, which would reduce overall project cost.

Reinforcement Cost and Fabrication

In February 2009, reinforcement suppliers were contacted to determine an approximate cost of reinforcing materials and their fabrication. The cost information received from the suppliers was a representative snap shot of the reinforcement prices at that particular time for construction scale orders. The ease of fabrication of the U-bars was also discussed with the suppliers.

The lowest price quote was given for conventional A615 rebar with attached Lenton Terminator® bearing heads. The price per ton of this reinforcement was 800 dollars with an additional cost of 25 dollars for the application of each Lenton Terminator® bearing head. Deformed wire reinforcement was very competitive with the headed bar price. Two price ranges were given for fabricated deformed wire reinforcement, the first price of 850-950 dollars a ton was given for single cut and fabricated wires. The second price range of 900-1000 dollars a ton was given for fabricated wire mesh. The highest price was the price of fabricated stainless steel reinforcement. The price quote given was for Enduramet 32 stainless steel, which was 5000 dollars a ton. The stainless steel price also included fabrication in a stainless steel only production line which eliminated contamination from black carbon dust. Even though stainless steel had the largest initial material cost, the life cycle cost of a deck using this material could offset the high initial cost.

The ease of the U-bar fabrication process was also discussed with the reinforcement distributors. The U-bar fabrication process was of concern, because of the tight bends that were required in the U-bar detail so the deck thickness could be minimized. The stainless steel supplier stated that the tight bends were not a problem for the stainless steel material, because of its high ductility. The stainless steel supplier also stated that it may be possible to reduce the bend diameter to less than three times the diameter of the bar ($3d_b$) without breaking the material. The deformed wire reinforcement supplier stated that the tight bend was

also not a problem for the material. After determining the best fabrication method for the bends, no deformed wire reinforcement was broken during fabrication.

9.1.4. Material Testing

Concrete Testing

Tables 9.1.6 and 9.1.7 show the results of the concrete compressive strength tests.

Table 9.1.6: Concrete compressive strengths, U-bar specimens

U-Bar Specimens (Four Specimens, Cast on July 24, 2008)			
7 Day Test		28 Day Test	
Cylinder #	Stress (psi)	Cylinder #	Stress (psi)
1	8710	1	10350
2	9753	2	11651
3	9820	3	11575
Average	**9428**		**11192**

Table 9.1.7: Concrete compressive strengths, headed bar specimens

Headed Bar Specimens (Two Specimens, Cast on August 28, 2008)			
7 Day Test		28 Day Test	
Cylinder #	Stress (psi)	Cylinder #	Stress (psi)
1	8301	1	9948
2	8068	2	9383
3	8114	3	9416
Average	**8161**		**9582**

Reinforcing Materials Testing

Tension tests were performed on the deformed wire reinforcement and stainless steel reinforcement to obtain accurate material properties. The conventional Grade 60 reinforcement used for the headed bars was not tested. Four samples of each reinforcing material were tested. An Instron Universal Testing Machine (UTM) was used to test the reinforcement and to obtain the data necessary to construct stress versus strain curves for both reinforcement types.

263

An extensometer with the required 2 in. gage length was used to determine the strain in the deformed wire reinforcement (DWR) and the stainless steel reinforcement (SS) materials. When the yield strength of the reinforcing materials was approached, the extensometer was removed as a precautionary measure. The remainder of the strain readings was determined using an initial gage length of the entire specimen and the position of the moving platen of the UTM. The stress in the specimens was calculated by using the force readings taken from the load cell in the UTM divided by the area of the #5 bars tested. This allowed for the construction of a stress versus strain curve for both the deformed wire reinforcement and the stainless steel reinforcement.

The modulus of elasticity for the materials was taken as the slope of the stress-strain trend line using the extensometer data. As shown in Table 9.1.8, the modulus of elasticity of the DWR and SS was determined to be 29918 ksi and 26802 ksi, respectively. A modulus of elasticity of 29000 ksi was used in all theoretical calculation. The ultimate strength data is also given in Table 9.1.8. The stress versus strain curves for the DWR and the SS reinforcement is plotted in Figure 9.1.11, which shows that stainless steel reinforcement was extremely ductile, compared to the deformed wire reinforcement.

Table 9.1.8 Modulus of elasticity and ultimate strength

	Modulus (ksi)		Ultimate strength (ksi)	
	DWR	SS	DWR	SS
Sample1	31536.0	26913.0	117.0	117.0
Sample 2	28621.0	28537.0	115.0	116.9
Sample 3	28781.0	24902.0	116.4	117.0
Sample 4	30734.0	26856.0	113.7	117.0
Average	**29918.0**	**26802.0**	**115.5**	**117.0**
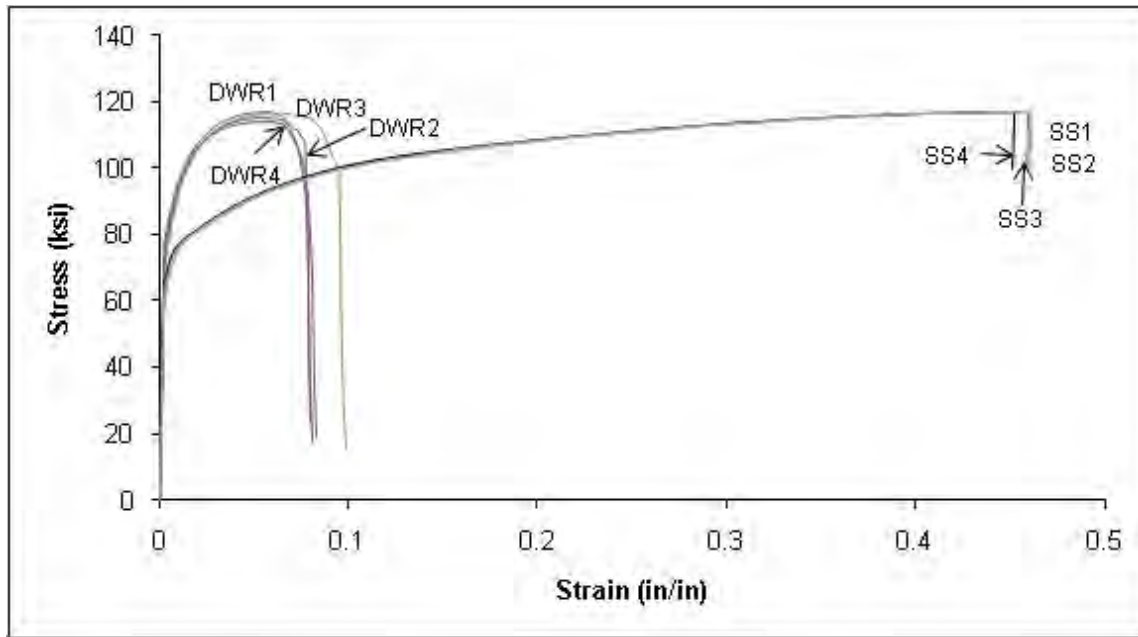
Figure 9.1.11: Stress versus strain curves for Deformed Wire Reinforcement (DWR) and Stainless Steel (SS)

Weld Testing

A preliminary concern of the tension test set-up was the strength of the welds between the longitudinal rebar in the specimens and the threaded rods that were used to connect the specimens to the loading and support beams. If the welds were to fail before the specimen, then the test would terminate before valuable information about the connection behavior could be ascertained. Tension tests were performed on the rebar to threaded rod welds to ensure that the weld strengths were greater than the rebar yield strengths. The top connection detail used in the tension test set-up is shown in Figures 9.1.12 and 9.1.13. Figure 9.1.14 shows the weld test set-up.

265
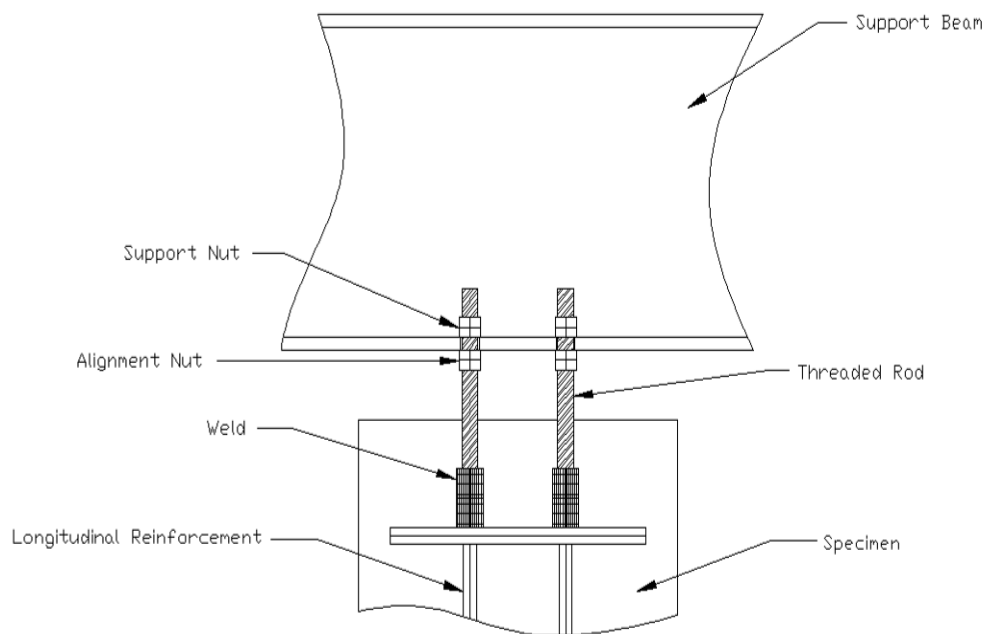
Figure 9.1.12: Connection detail, conceptual drawing

Figure 9.1.13: Photo of the top connection detail

266
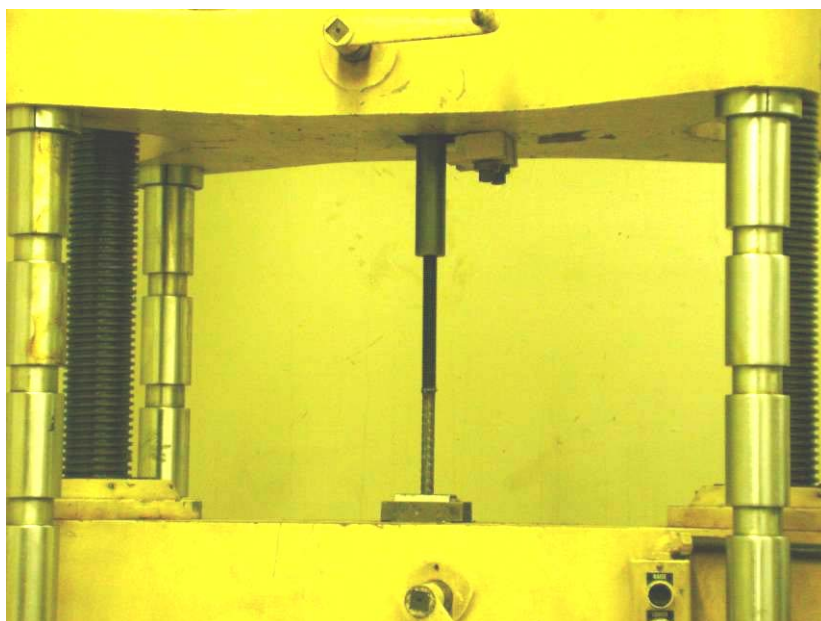
Figure 9.1.14: Weld test set-up

The welds tested were made using the Metal Inert Gas, Tungsten Inert Gas and Shielded Metal Arc Welding (MIG, TIG and SMAW) welding methods on all rebar materials. Again, conventional reinforcement had a yield strength of 60 ksi, and deformed wire reinforcement and stainless steel reinforcement had a yield strength of 75 ksi. The threaded rods that were used in the experimental program had a diameter of ¾ in. and a minimum yield strength of 110 ksi.

The first set of weld tests placed were one pass welds made by both MIG and TIG welding methods with a 70 ksi carbon welding wire. This welding method produced a small ring of weld material around the outside of the threaded rod and the rebar, and did not fuse the threaded rod and reinforcement together in the center. This welding method produced small cross-sectional areas in the weld region, which led to small capacities. The desired capacity for each of the welds was the capacity of the #5 bar (i.e., $0.31in.^2 \times 60ksi$ (or 75ksi)=18.6(or 23.3)kip). Table 9.1.9 shows the testing results of the one pass weld tests and Figure 9.1.15 shows the typical failure of the one pass weld specimens.

267

Table 9.1.9: Weld test results, one pass welds

Material	Welding Method	Capacity (kips)	Failure Mode
Stainless Steel, fy = 75 ksi	MIG	15.5	Weld Broke
Deformed wire Reinforcement, fy = 75 ksi	MIG	13	Rebar Pulled Out of Weld
Conventional Rebar, fy = 60 ksi	MIG	13.7	Rebar Pulled Out of Weld
Stainless Steel fy = 75 ksi	TIG	11.8	Weld Broke
Deformed wire Reinforcement fy = 75 ksi	TIG	15	Weld Broke
Conventional Rebar fy = 60 ksi	TIG	15.8	Weld Broke
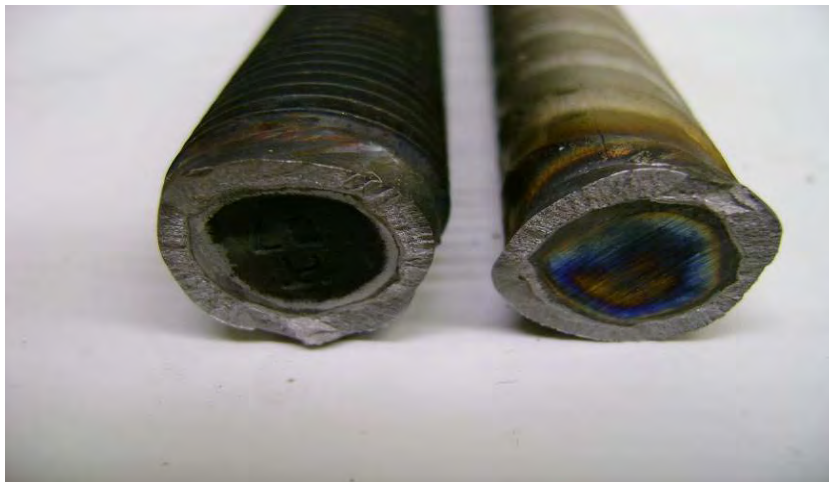
Figure 9.1.15: One pass weld failure

The second set of weld tests consisted of the same welding methods and materials, but the threaded rods and rebar were beveled, so larger weld areas and capacities could be produced. This set of weld tests all produced capacities that were larger than the 23.3 kip force required to yield a #5 bar with a yield strength

268

of 75 ksi. These results indicated that the welds could yield the reinforcing material, but to account for any unforeseen forces in the experiment, larger weld capacities were preferred. Table 9.1.10 shows the results of the second set of weld tests using the beveled weld geometry.

The third set of weld tests used a 110 ksi welding stick and the beveled weld geometry. The welding method was also changed to shielded metal arc welding (SMAW). These welds were tested on all reinforcing materials. The results of the third set of welding tests are given in Table 9.1.11.

Table 9.1.10: Weld test results, Beveled Welds

Material	Welding Method	Capacity (kips)	Failure Mode
Stainless Steel, fy = 75 ksi	MIG	23.8	Weld Broke
Deformed wire Reinforcement, fy = 75 ksi	MIG	26.7	Weld Broke
Conventional Rebar, fy = 60 ksi	MIG	26.5	Weld Broke
Stainless Steel fy = 75 ksi	TIG	25.9	Weld Broke
Deformed wire Reinforcement fy = 75 ksi	TIG	24.5	Weld Broke
Conventional Rebar fy = 60 ksi	TIG	23.8	Weld Broke

Table 9.1.11: Weld test results, beveled welds and 110 ksi welding stick

Material	Welding Method	Capacity (kips)	Failure Mode
Stainless Steel, fy = 75 ksi	SMAW	21.4	Weld Broke
Deformed wire Reinforcement, fy = 75 ksi	SMAW	33.5	Weld Broke
Conventional Rebar, fy = 60 ksi	SMAW	29.5	Weld Broke

Table 9.1.11 shows that the 110 ksi welding sticks and the SMAW welding method produced very strong welds with the deformed wire reinforcement and the conventional rebar, but the strength of the weld decreased for the stainless steel reinforcement. The decrease in weld strength for the stainless steel reinforcement may have been because of a weld incompatibility between the 110 ksi welding stick and the stainless steel reinforcement. So the threaded rod to stainless steel weld was tested again using a stainless steel welding stick.

The SMAW welding method using a 308 stainless steel welding rod was used in conjunction with the beveled weld geometry to increase the weld strength between the threaded rod and the stainless steel reinforcement. Only one weld test was conducted using these parameters, due to time constraints and an adequate result. The capacity of the weld using the previously described parameters produced a strength of 28.4 kips, which was adequate strength for the transverse joint (tension) tests.

The results of the weld tests indicated that the previously described tension test set-up was feasible and that the weld strength between the threaded rod and the longitudinal reinforcement was not a limiting factor.

9.1.5. Results and Discussion

Flexural Capacity (Longitudinal Joint Behavior)

The flexural test specimens were designated as HB-1, SB-1 and WB-1, where the first letter corresponds to H=headed bar, S=stainless steel U-bar or W=deformed wire reinforcement U-bar; and the second letter, "B," stands for "bending." The numerical designation, "1," represents the first specimen.

The AASHTO strength I and service limit states were used in the determination of both the positive and negative moments. A 2 in. future wearing surface, 6-¼ in. deck thickness, and the live load determined from AASTHO Table A4-1, were used to calculate the following moment demands. Table 9.1.12 and Table 9.1.13 show the service and strength I moments for the specimens. It should be noted that the original design was based on the Strip Method using Grade 60 reinforcement; however, the size and spacing of the

270

reinforcement was kept the same when the Grade 75 reinforcement was used. Considering the specimens with the Grade 75 reinforcement could resist a higher moment, a reinforcement ratio was used to adjust the loading demands to reflect this difference.

Table 9.1.12: Moment demands for specimens containing the U-bar detail

U-Bar Detail Specimens (SB-1 and WB-1)		
	M^+ (kip-ft)	M^- (kip-ft)
Service	10.1	8.3
Strength I	16.9	13.6

Table 9.1.13: Moment demands for specimens containing the headed bar detail

Headed Bar Detail Specimen (HB-1)		
	M^+ (kip-ft)	M^- (kip-ft)
Service	9.5	7.8
Strength I	16.0	13.1

All specimens produced similar flexural capacities. Specimen HB-1, which contained the headed bar joint detail, produced the lowest flexural capacity, which was 29.1 kip-ft. Specimen WB-1, which contained the U-bar detail made of deformed wire reinforcement, produced a flexural capacity of 31.0 kip-ft. The largest flexural capacity was produced by specimen SB-1, which contained the U-bar joint detail made of the stainless steel material; the flexural capacity of this specimen was 31.9 kip-ft. Comparing the flexural capacities of the specimens to the required capacities (Strength I) shown in Tables 9.1.12 and 9.1.13, it can be seen that all specimens produced capacities that were much greater than the required Strength I limit state moments. These results show that both the U-bar and headed bar joint details are capable of creating precast deck systems that can emulate the behavior of cast-in-place deck systems in terms of strength requirements.

Moment versus deflection and moment-versus-curvature curves were constructed for each specimen. The total applied moment was determined from the actuator load cell. The deflection data were taken from the LMT located in the center of the joint. The curvature data were taken from the horizontally placed LMT's located above and below the joint. Figure 9.1.16 shows the moment versus deflection curves and Figure 9.1.17 shows the moment-versus-curvature curves for all of the flexural specimens. Also plotted in the figures is the Strength I limit state moment requirements for the U-bar (UB) and headed bar (HB) cases.
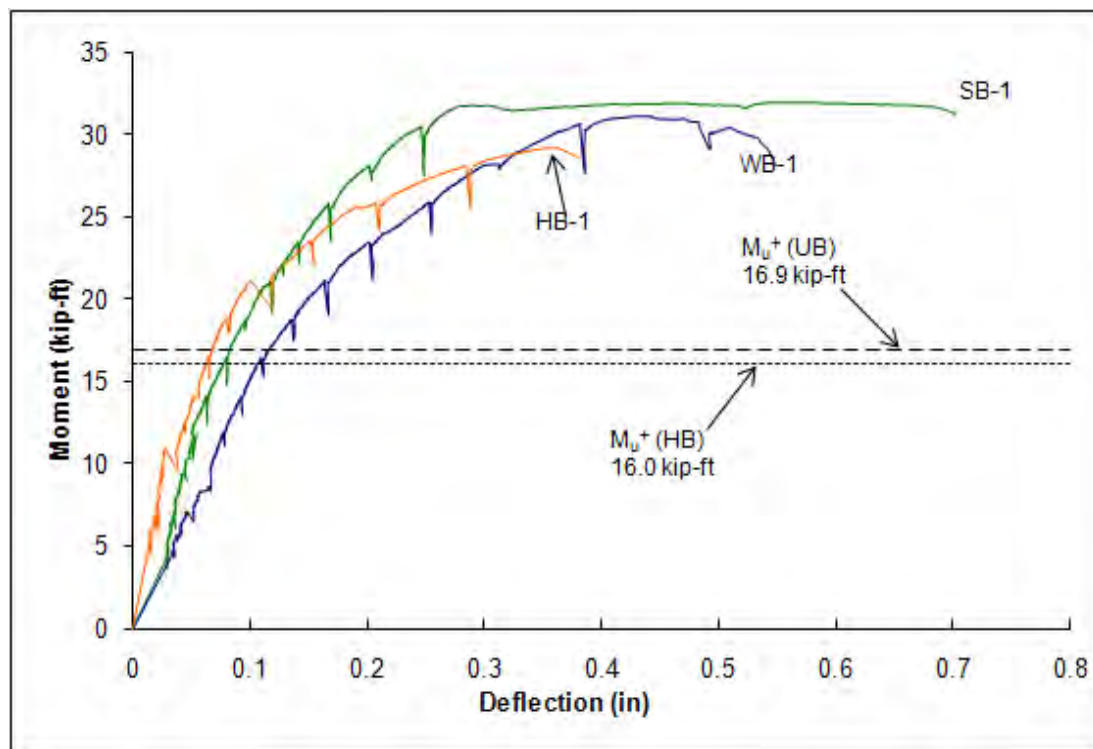
Figure 9.1.16: Moment versus deflection curves

272
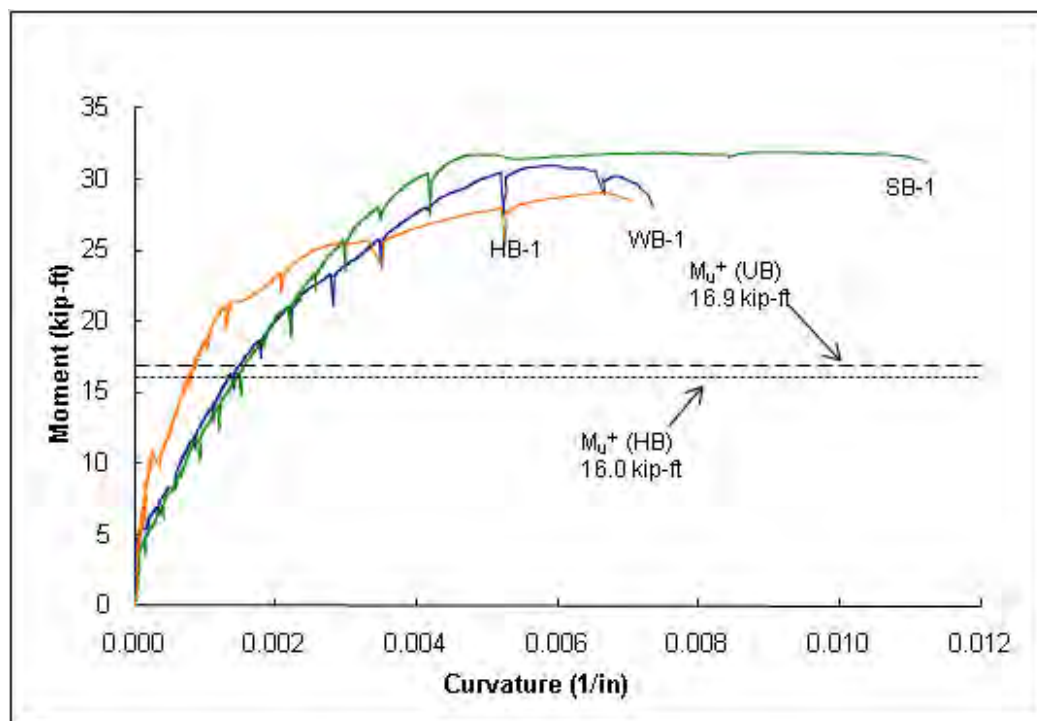
Figure 9.1.17: Moment-versus-curvature curves

From Figures 9.1.16 and 9.1.17, the ductility of the specimens can be seen. Figure 9.1.16 shows that the U-bar specimens, SB-1 and WB-1, produced larger deflections than the headed bar detail contained in specimen HB-1. The same trend is also shown in Figure 9.1.17. Specimens SB-1 produced larger curvatures than HB-1 and WB-1. Even though specimens SB-1 and WB-1 were more ductile then HB-1, they did not sacrifice capacity.

Although the concrete age at structural testing was older than 28 days for all six specimens, the concrete strength test at 28 days, shown in Tables 9.1.6 and 9.1.7, was used to determine the calculated section capacities discussed below. The respective nominal yield strength of either 60ksi or 75ksi was used to determine the calculated section capacities. The higher capacities of SB-1 and WB-1 can be attributed to the joint detail, the higher reinforcement yield strength, and the higher compressive strength of the concrete. The higher ductility produced by the U-bar specimens compared with the headed bar specimen may have been due to the U-bar joint detail: U-bars can deform (bent around lacer bars) while the head of headed bars bears against concrete.

When comparing the ductilities of SB-1 and WB-1, it can be seen that specimen SB-1 had a significantly larger deflection and curvature. Specimens SB-1 and WB-1 had the same measured concrete strength, rebar yield strength, and joint detail; the only difference was the reinforcing materials used in them. SB-1 consisted of the stainless steel reinforcing material and WB-1 consisted of deformed wire reinforcement. Stainless steel is extremely ductile compared to deformed wire reinforcement as shown in Figure 9.1.11.

Theoretical moment-versus-curvature curves were constructed, so that the behavior of the longitudinal joint (flexural) specimens could be compared to theoretical values. The theoretical moment-versus-

273

curvature curves were constructed for both the U-bar detail and the headed bar detail. Two separate moment-versus-curvature curves had to be determined because of the different concrete strengths, assumed rebar yield strengths and reinforcement configurations used in the specimens. The cracking moment was calculated considering the modulus of concrete rupture stated in ACI 318-08, the additional stiffness added to the cross sections by the rebar and the uncracked moment of inertia. The moment at yield was calculated considering the cracked section moment of inertia and a steel strain equal to the yield strain. The steel yield strain was determined by dividing the yield stress by a modulus of elasticity of 29,000ksi. The nominal moment capacity was calculated based on ACI 318-08 procedures, which considered an equivalent rectangular concrete stress block and no strain hardening of the reinforcement. Both layers of reinforcement were considering during the calculation of all moments. The specimen cross sections used for the theoretical calculations consisted of the six bar side shown in Figure 9.1.18 (U-bar specimens) and Figure 9.1.19 (headed bar specimens). The calculated theoretical moments and corresponding curvatures are given in Table 9.1.14 for the six bar (three loop) configuration. The actual behavior of the specimen was controlled by the joint zone where the steel changed from six bars (three loop bars) to four bars (two loop bars) in the loop splice region.
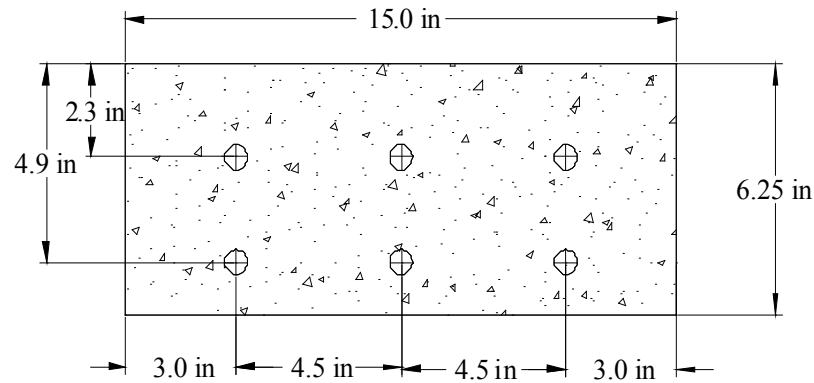
Figure 9.1.18: Cross Section used for theoretical calculations of the U-bar specimens
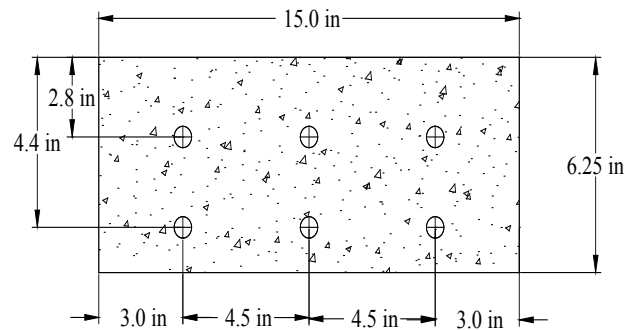
Figure 9.1.19: Cross section used for the theoretical calculations of the headed bar specimen

Table 9.1.14: Calculated moments and curvature (six-bar side)

Headed Bar Detail (f_y=60ksi)				U-bar Detail (f_y=75ksi)			
Moment (kip-ft)		Curvature (10^{-5}/in)		Moment (kip-ft)		Curvature (10^{-5}/in)	
M_{cr}	6.19	Φ_{cr}	4.27	M_{cr}	6.82	Φ_{cr}	4.27
M_y	20.7	Φ_y	73.15	M_y	25.82	Φ_y	76.96
M_n	20.7	Φ_n	213.87	M_n	25.82	Φ_n	214.44

When comparing the tested specimen moment capacities and the calculated moment capacities, it can be seen that the specimens behaved better than expected. The theoretical calculations were based on 60ksi and 75 ksi nominal yield strengths and tested concrete 28-day compressive strengths. For HB-1, the calculated moment, when the nominal design yield strength was used, was 20.7 kip-ft, but the measured capacity was 29.1 kip-ft. The measured capacity of HB-1 was 41 percent greater than the calculated value. SB-1 and WB-1 both had the same theoretical nominal moment capacity because they had the same nominal design yield strength of 75 ksi and reinforcement configurations; the calculated moment capacity was 25.8 kip-ft. The measured moment capacities of SB-1 and WB-1 were 31.9 kip-ft and 31.0 kip-ft respectively. The measured moment capacities of SB-1 and WB-1 were 23.5 and 20.4 percent greater than the calculated value. The main point shown here was that although reinforcement was not continuous across the joint zone (i.e., the U-bars were spliced), the specimen resisted a moment capacity as if continuous reinforcement was provided across the joint with bars that had the nominal design yield strength.

The theoretical moment-versus-curvature curves are plotted with the corresponding measured moment-versus-curvature curves obtained from experimental data in Figures 9.1.20 and 9.1.21 for the U-bar and headed bar details, respectively.
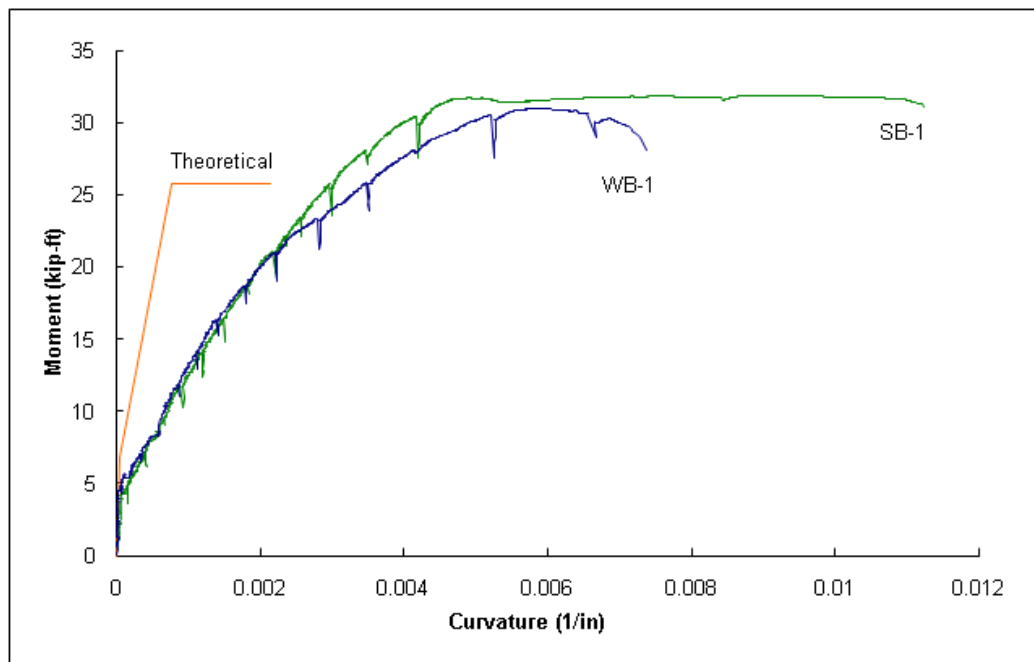
Figure 9.1.20: Measured and theoretical moment-versus-curvature curves for the U-bar details
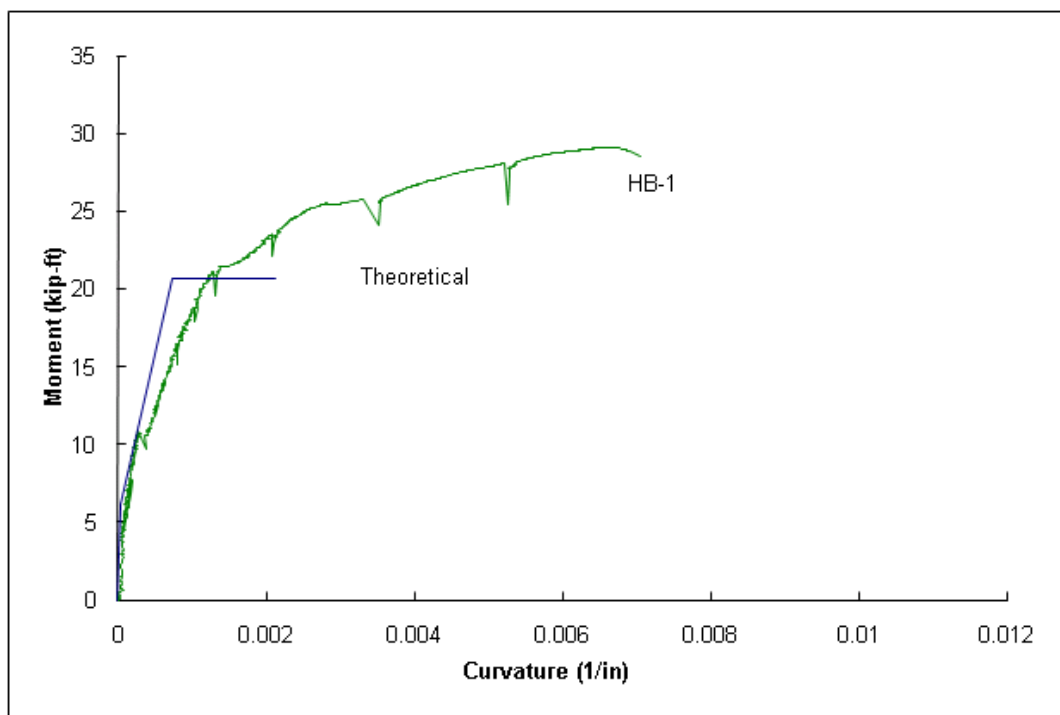
Figure 9.1.21: Measured and theoretical moment-versus-curvature curves for headed bar details

276

Figures 9.1.20 and 9.1.21 show that all specimens produced a larger capacity than the theoretical capacity. Also, the specimens were more ductile than predicted by the theoretical curvature calculations based on nominal properties; the detailed explanation for this difference is provided later in reference to Figure 9.2.22. The behavior of the specimens shows that the U-bar and headed bar joint details produced joints deemed to emulate the behavior of a cast-in-place bridge deck.

Flexural Specimen Behavior (Longitudinal Joint Behavior)

The first cracks to appear in all of the flexural specimens were transverse cracks uniformly spaced along the length of the specimens. In the joint zone the transverse cracks formed at the ends of the longitudinal reinforcement. The transverse cracks formed in the top tension face of the specimens first (see Figure 9.1.5 for test set-up) and then propagated deeper into the specimens as the loading progressed. At higher moments, lateral cracks formed in the direction of the longitudinal reinforcement, which corresponded to the direction of transverse reinforcement in an actual bridge deck. These lateral cracks formed over the longitudinal reinforcement that comprised the lightly reinforced half of the specimens. Diagonal cracks then formed from the longitudinal rebar comprising the lightly reinforced half of the specimens and extended to the outside edge of the specimen. Figure 9.1.22 shows the crack patterns of specimens SB-1, WB-1 and HB-1 at failure.

277

(a) Specimen SB-1

(b) Specimen WB-1

(c) Specimen HB-1

Figure 9.1.22: Flexural crack patterns at failure

278

The numbers written next to the cracks shown in Figure 9.1.22 represent the total force, in kips, applied to the specimen when the cracks formed. All flexural specimen failures were ductile, producing yielding in the reinforcement and crushing of the concrete on the compression face of the specimens, under the joint zone.

Flexural Crack Widths at Service Level Loading (Longitudinal Joint Behavior)

Flexural crack widths were visually measured systematically throughout the testing of all bending specimens using a crack width gage. The crack width gage contained numerous lines of labeled widths. The cracks in the specimens were compared to the lines on the crack width gage; the width of the line that most accurately represented the crack was recorded as the crack width.

The positive service level moments given in Tables 9.1.12 and 9.1.13 were used to compare the crack widths of the specimens because the flexural specimens represented a longitudinal joint that would primarily resist positive moment. The positive service moments for the U-bar detail and the headed bar detail were 10.1 kip-ft and 9.5 kip-ft, respectively. For specimens SB-1 and WB-1, crack widths were measured at 9.29 kip-ft and 11.65 kip-ft. For specimen HB-1, the crack widths were measured at 8.11 kip-ft and 10.47 kip-ft. Because the crack widths were not measured at the corresponding service moments, the crack widths at the service-level loading were found by interpolating between the measured values. SB-1 was found to have an average crack width of 0.0075 in. at service level loading. The average crack width at service level loading for specimen HB-1 was found to be 0.0083 in. WB-1 was found to have an average crack width of 0.01 in. at service level loading. So the U-bar detail produced both the largest and the smallest crack widths at service level loading, which were 0.01 in and 0.0075 in. The headed bar detail produced the mid-range crack widths.

Strain Gage Data (Longitudinal Joint Behavior)

Strain gages were installed on the specimen reinforcement in the configurations shown in Figures 9.1.7 and 9.1.8. The purpose of the strain gage data was to verify the required overlap length needed to develop the yield strength of the reinforcement. The strain gage data were expected to show increasing strain as the distance away from the bearing surface of the reinforcement increased (i.e., as the spliced bars transferred the tension across the joint region). The strain gage data did not show this trend because of the effect of the cracks. The strain gage locations that were crossed by a crack produced high strain readings, while the other gage locations had smaller strain readings. The joint cracking patterns produced scattered results that could not be used to verify the required overlap length; however, the strain gage data do show that both joint details allowed the reinforcement to develop large strains, and the required forces were transferred across the joints. Figures 9.1.23, 9.1.24 and 9.1.25 show the moment versus reinforcement strain curves for specimens SB-1, WB-1 and HB-1, respectively.

279
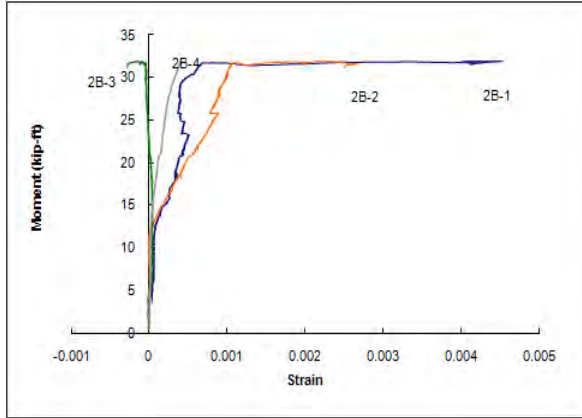
(a) Bottom of U-bar 2 (Specimen SB-1)
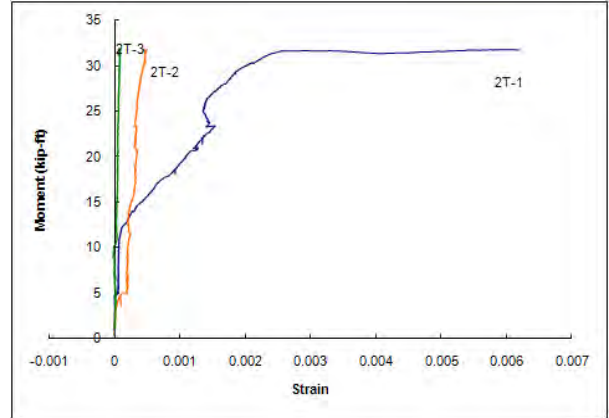
(b) Top of U-bar 2 (Specimen SB-1)
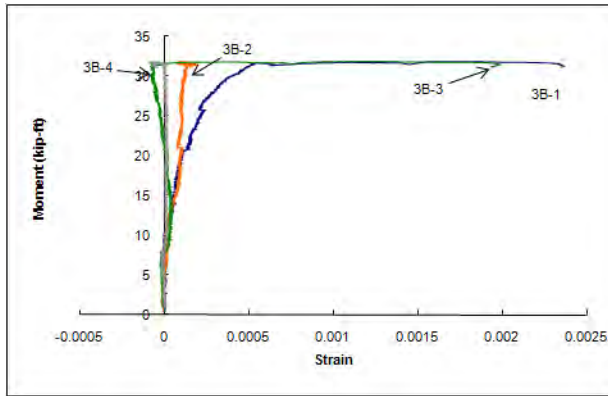
(c) Bottom of U-bar 3 (Specimen SB-1)
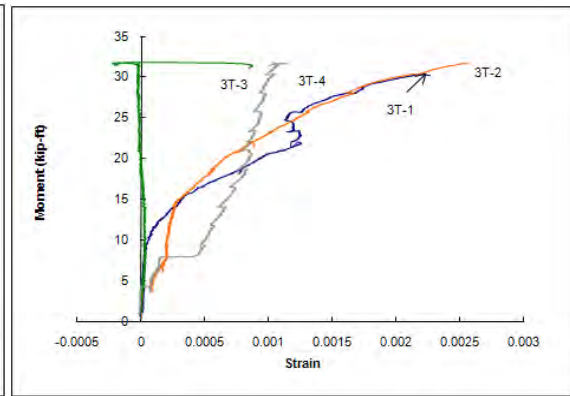
(d) Top of U-bar 3 (Specimen SB-1)
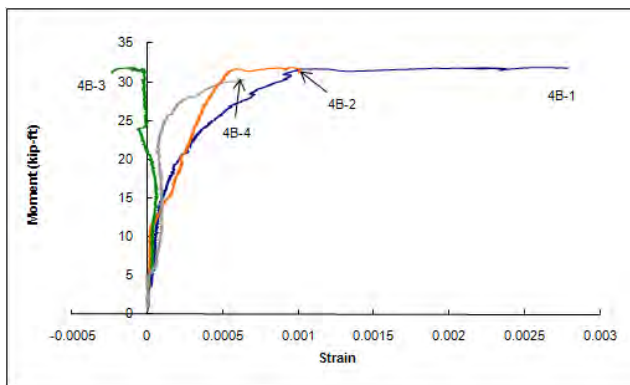
(e) Bottom of U-bar 4 (Specimen SB-1)
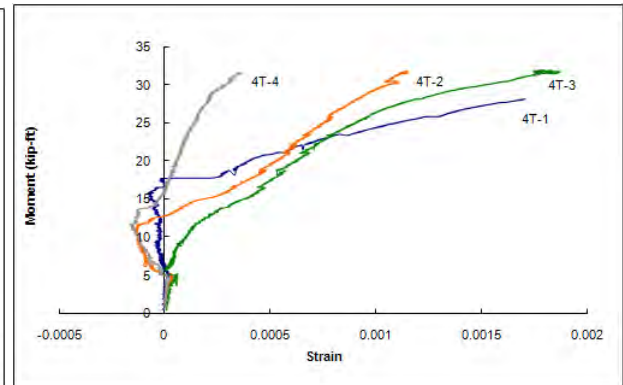
(f) Top of U-bar 4 (Specimen SB-1)
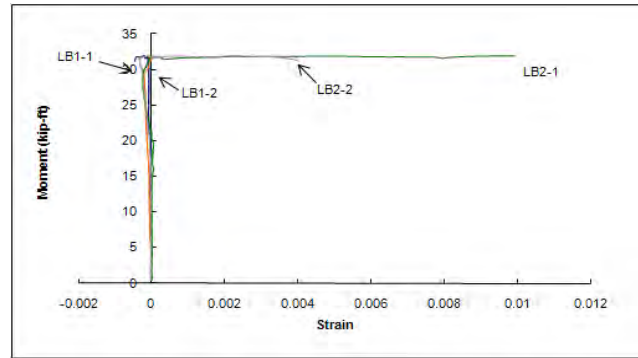
(g) Lacer Bars 1 and 2 (Specimen SB-1)

Figure 9.1.23: Moment versus rebar strain curves for SB-1
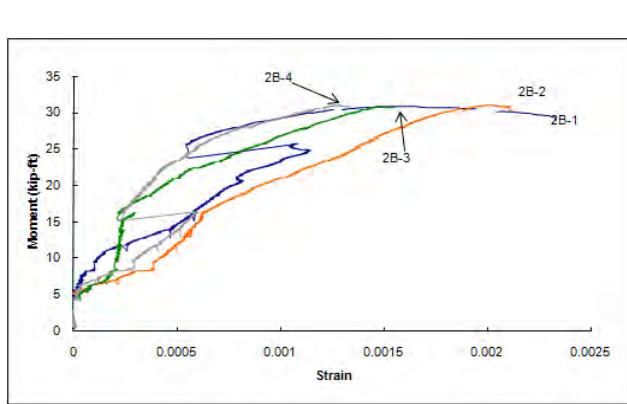
(a) Bottom of U-bar 2 (Specimen WB-1)
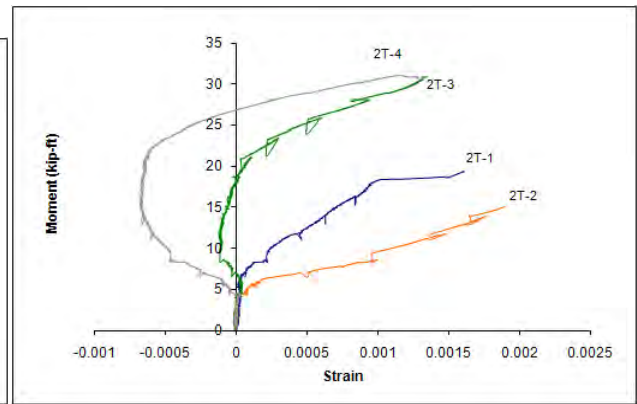
(b) Top of U-bar 2 (Specimen WB-1)
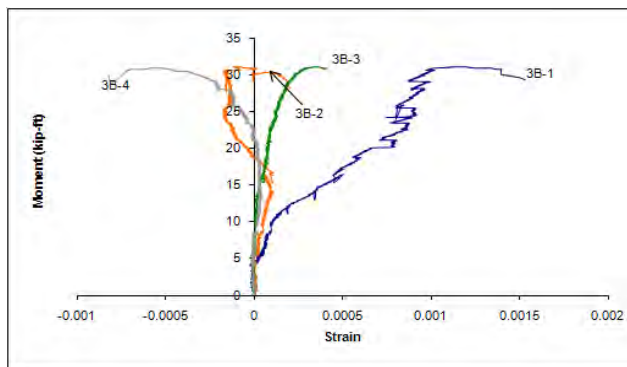
(c) Bottom of U-bar 3 (Specimen WB-1)

(d) Top of U-bar 3 (Specimen WB-1)

281
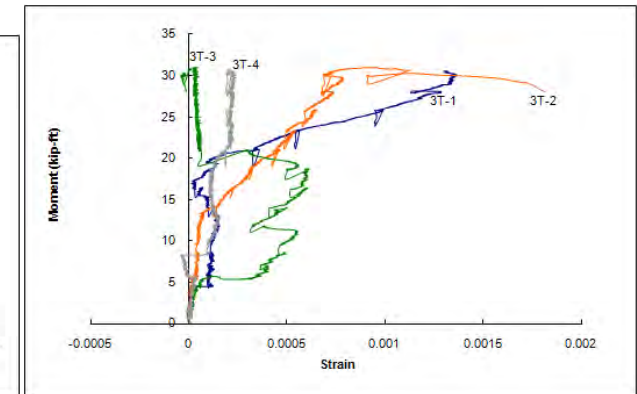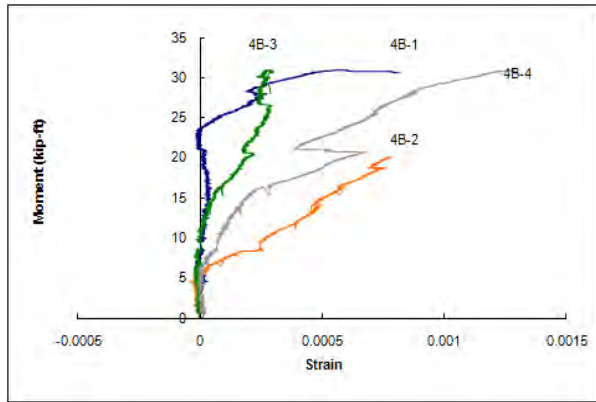
(e) Bottom of U-bar 4 (Specimen WB-1)
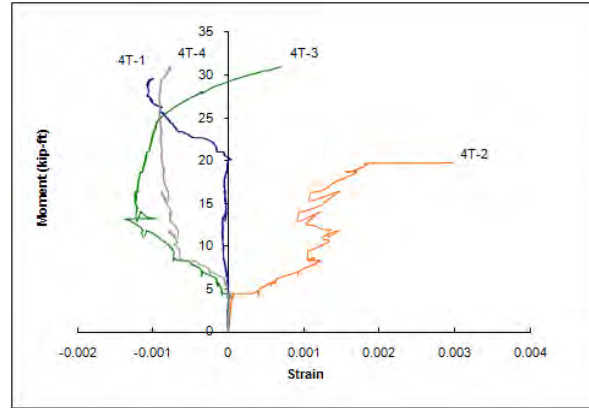
(f) Top of U-bar 4 (Specimen WB-1)
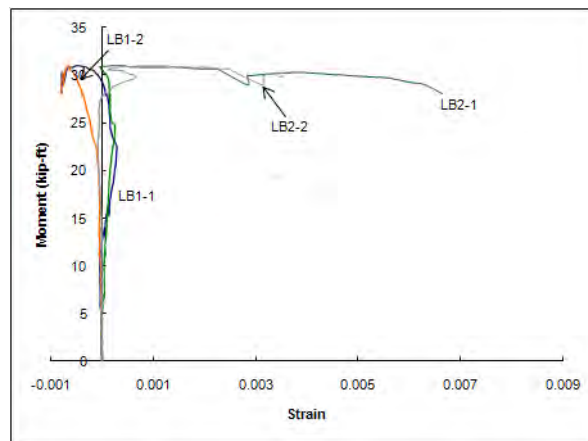
(g) Lacer Bars 1 and 2 (Specimen WB-1)

Figure 9.1.24: Moment versus rebar strain curves for WB-1
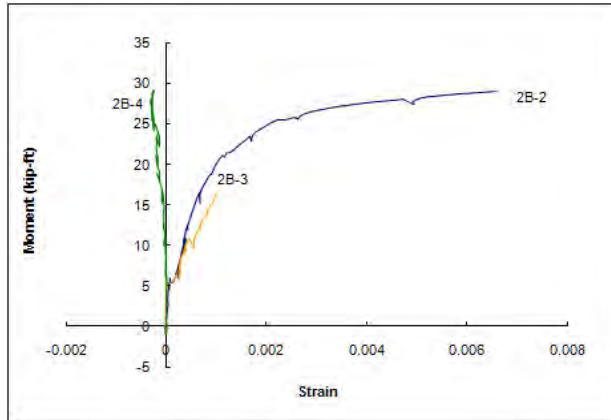
(a) Bottom of U-bar 2 (Specimen HB-1)
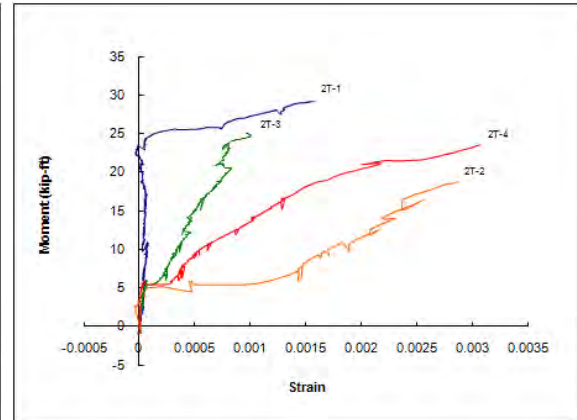
(b) Top of U-bar 2 (Specimen HB-1)
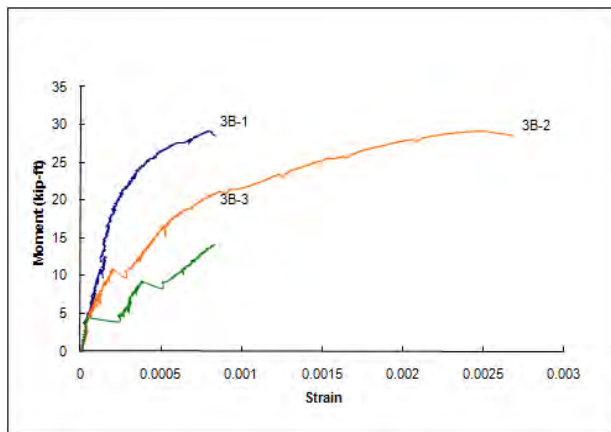
(c) Bottom of U-bar 3 (Specimen HB-1)
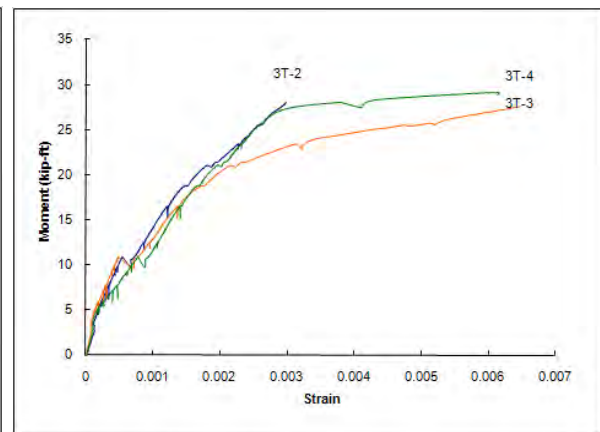
(d) Top of U-bar 3 (Specimen HB-1)
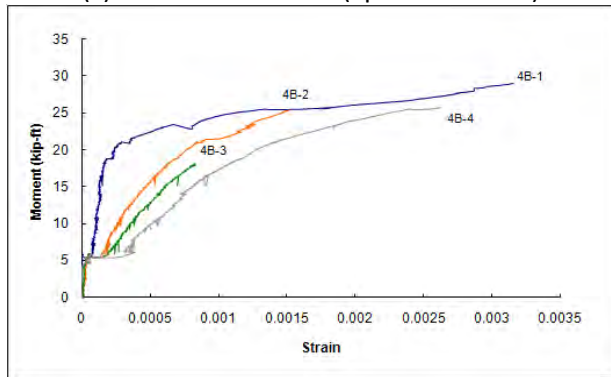
(e) Bottom of U-bar 4 (Specimen HB-1)

(f) Top of U-bar 4 (Specimen HB-1)

283
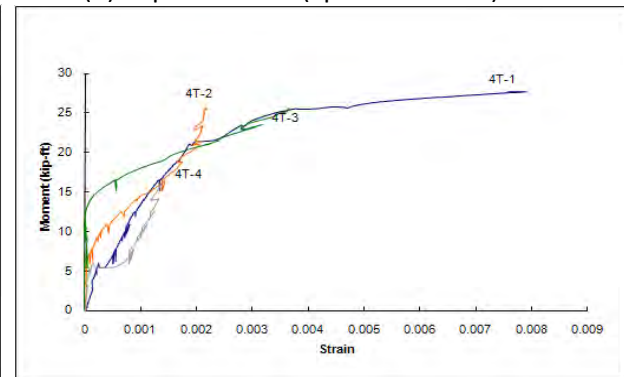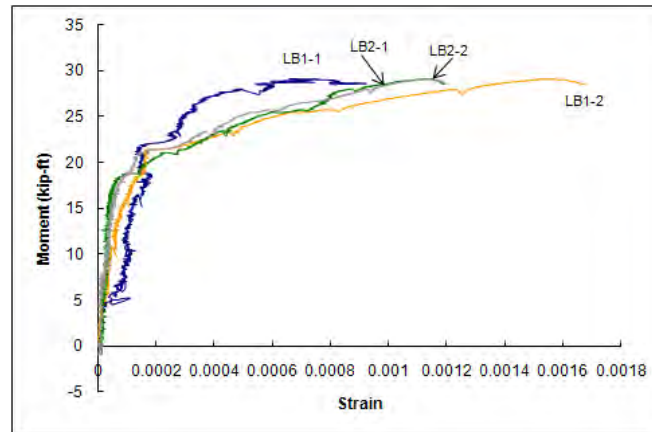
(g) Lacer Bars 1 and 2 (Specimen HB-1)

Figure 9.1.25: Moment versus rebar strain curves for HB-1

Tensile Capacity (Transverse Joint Behavior)

Specimens ST-1, WT-1 and HT-1 were tested in tension to simulate the conditions in the deck at a transverse joint where the compression forces were assumed to be resisted by the girder. As mentioned in the section on *Flexural Capacity (Longitudinal Joint Behavior)*, the specimen naming convention indicated the type of reinforcement detail investigated (i.e., S=stainless steel; W=deformed wire; H=headed bar); the "T" stands for tension test, and the "1," indicates the specimen number of that type. Specimen HT-1 utilized a headed bar joint detail made of conventional reinforcement. Specimens ST-1 and WT-1 both utilized the U-bar joint detail. The reinforcement used in ST-1 was stainless steel, and the reinforcement used in specimen WT-1 was deformed wire reinforcement (DWR).

The largest tension capacity that was expected from the tension specimens was the force determined by multiplying the area of steel of the lightly reinforced side of the specimens by the appropriate rebar yield strength. HT-1 was reinforced with conventional rebar with a nominal yield strength of 60 ksi and was expected to have a maximum tensile capacity of 74.4 kips. The maximum capacity of HT-1 was calculated considering the four #5 bars comprising the lightly reinforced side of the specimen and the rebar yield strength. The U-bar specimens both used reinforcement that had a nominal yield strength of 75 ksi, considering the yield strength of the reinforcement and the area of the four #5 bars in the lightly reinforced side of the specimen, the maximum expected tensile capacity of the U-bar specimens was 93.0 kips.

All specimens produced similar tensile capacities. HT-1 produced the lowest tensile capacity, which was 89.81 kip. This was to be expected because HT-1 contained conventional rebar with the lowest nominal rebar yield strength. The second highest tensile capacity was produced by the U-bar detail using stainless steel reinforcement (ST-1). ST-1 produced a tensile capacity of 91.8 kip. The largest tensile capacity was produced by WT-1, which was 93.3 kips.

Both WT-1 and HT-1 exceeded the expected tensile capacity. The additional capacity of specimens WT-1 and HT-1 might be attributed to the actual yield strength being higher than the nominal design yield strength or the steel may have developed strain hardening. However, specimen ST-1 did not meet the expected capacity of 93 kips, it only had a capacity of 91.78 kips. ST-1 had a capacity that was 1.3 percent

284

less than the expected tensile capacity. The low capacity could have been due to the fact that the welds broke during testing at a load of approximately 65 kips. The specimen was rewelded and tested to failure, but the specimen may have been damaged during the first unsuccessful test. ST-1 may have experienced damage that could have affected its behavior and tensile capacity during the second successful test.

Load deflection curves were constructed for the test specimens. During the second test of ST-1, no strain gage or LMT data was collected. The only data collected from the second test were the applied load and actuator displacement. The actuator displacement allowed for the determination of the total specimen deflection. The data collected from both tests were spliced together to form a complete load versus deflection curve. Load versus deflection curves were also constructed for specimens HT-1 and WT-1. The applied load was determined from the load data from the MTS actuator system. The total specimen deflection was used in the construction of the curves; these data were taken from the LMT that was attached to the bottom of the specimens. The load versus deflection curves for specimens HT-1, WT-1 and ST-1 were plotted together and can be seen in Figure 9.1.26. The end of the bold line for specimen ST-1 signifies where the data from the first test ends and where the data from the second test begins.
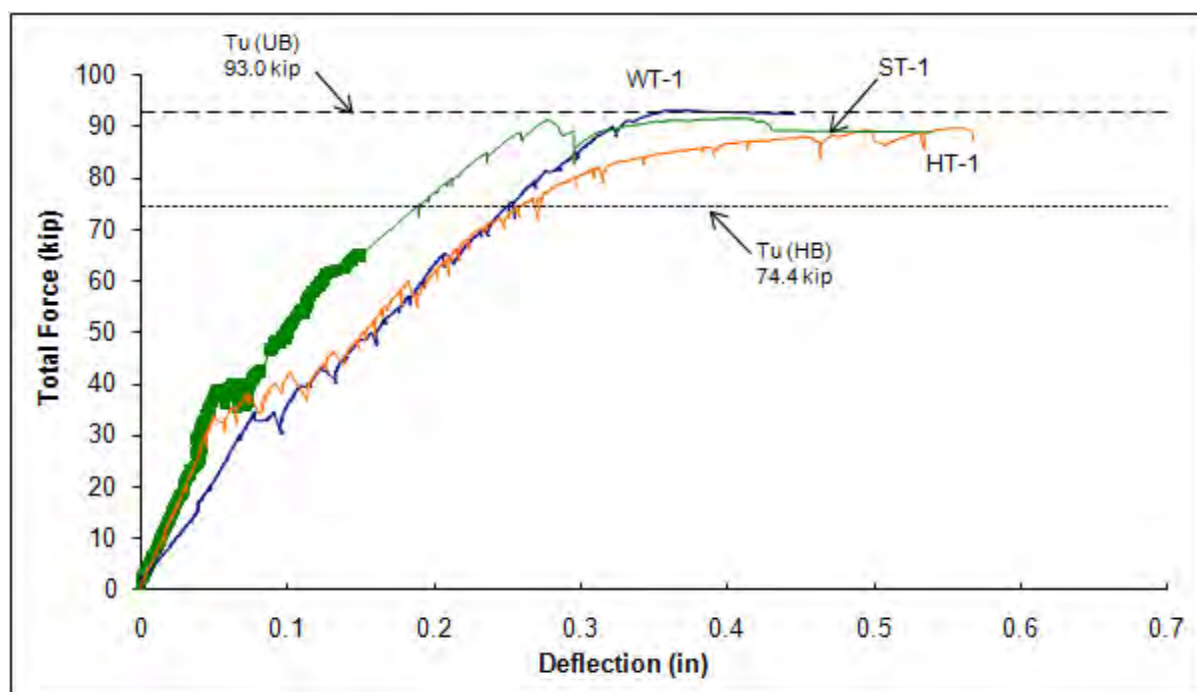
Figure 9.1.26: Total applied force versus deflection curves

Figure 9.1.26 shows the load deflection curves of all the specimens leveling off at approximately the force required to yield the reinforcement as determined from the nominal capacities. The increase in deflection while holding constant load signifies that the reinforcement in the specimens was yielding. Both the shape of the load versus deflection curves and the capacities of the specimens indicate that it can be assumed that the reinforcement in all the specimens yielded. The behavior of the specimens shows that the U-bar and the headed bar joint details can successfully yield the joint reinforcement without brittle failure. This

285

result shows that both joint details could effectively be used as a transverse joint in a negative moment region, which would mainly produce global tension in the deck.

Tension Specimen Behavior (Transverse Joint Behavior)

All specimens produced similar crack patterns up to and beyond the service loading. The tensile service load was calculated by using the service level negative moment found in design example 9.6 of the PCI Bridge Design Manual (PCI 2003). The neutral axis was then found for the cracked composite cross section, which was then used in conjunction with the service level negative moment to determine the total tensile service load. The area of steel in the specimens was compared to the total required area of steel to determine the tensile service loads for the specimens. The tensile service load for HT-1 was determined to be 44.1 kips (i.e., 35.6 ksi stress times the reinforcement area of 1.24 in.^{2}), and the tensile service load for ST-1 and WT-1 was determined to be 44.1 x (75/60) = 55.1 kips. Different tensile service loads were determined for the U-bar and headed bar specimens because of the different nominal yield strengths of their reinforcing materials.

The first cracks to appear were transverse cracks evenly spaced along the length of the specimens. The joint zone usually experienced transverse cracking after several other transverse cracks had already formed in other locations. Delayed transverse cracking in the joint zone may have been due to the larger area of reinforcement in the joint region compared to that of the body of the specimens. The transverse cracks initially were found only on the surface of the concrete, and as the loading progressed the cracks propagated through the entire thickness of the specimens. Additional loading produced longitudinal cracks that appeared above the main longitudinal reinforcement in the specimens. These longitudinal cracks appeared above the longitudinal reinforcement that comprised the lightly reinforced half of the specimen, or the top half of the specimens in this particular set-up. When approaching the capacities of the specimens, diagonal cracks appeared close to the sides of the specimens. These diagonal cracks would usually propagate toward a transverse crack in the joint zone and cause the failure surface for the specimens. Figure 9.1.24 shows the crack patterns at failure for specimens ST-1, WT-1 and HT-1. The numbers written by the cracks in Figure 9.1.27 represent the total force applied in kips when the crack was formed.

286

(a) Specimen ST-1   (b) Specimen WT-1
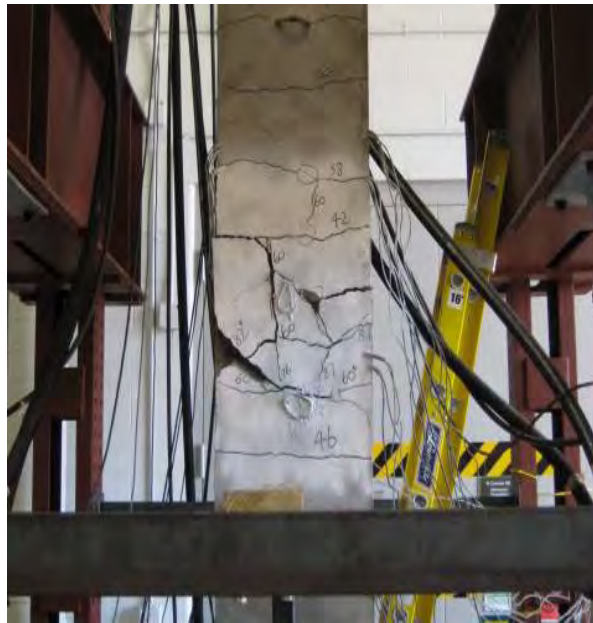
(c) Specimen HT-1

Figure 9.1.27: Tension crack patterns at failure

Tensile Crack Widths at Service Level Loading (Transverse Joint Behavior)

Crack widths in the tension specimens were measured in the same way as in the flexural specimens. A crack width gage was used to visually determine the widths of the specimens. Crack widths were measured

287

systematically throughout the testing of HT-1 and ST-1, but only two crack widths were measured at two different loads for specimen WT-1.

The average crack width of all cracks within the joint zone at 55 kips (estimated service load level for ST-1 and WT-1) was found to be 0.010 in for ST-1 (a comparable crack width measurement was taken at 45 kips for specimen ST-1, and the average crack width was found to be 0.006 in.). The average crack width at 44 kips (estimated service load level for HT-1) for specimen HT-1 was determined to be 0.012 in. The last crack width measurement for specimen WT-1 was taken at 40 kips and the average crack width was found to be 0.0079 in. Comparing the crack widths of the two joint details, one can see that the headed bar detail of specimen HT-1 generated the largest crack widths at approximately 40 kips and at its service level loading, compared to the crack widths created by the U-bar details of specimens ST-1 at its service level loading and WT-1 at approximately 40 kips.

Strain Gage Data (Transverse Joint Behavior)

Strain gages were installed on the specimen reinforcement in the configurations shown in Figures 9.1.7 and 9.1.8. Figures 9.1.28 and 9.1.29 show the total force versus reinforcement strain curves for specimens WT-1 and HT-1, respectively. The strain gage data for ST-1 were unfortunately lost for this specimen which suffered a weld failure. The strain gage data show that both joint details allow the reinforcement to develop large strains, and the required forces were transferred across the joints.

288
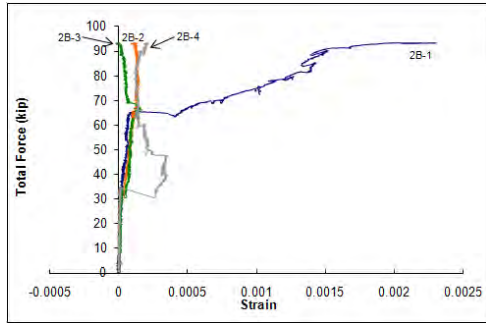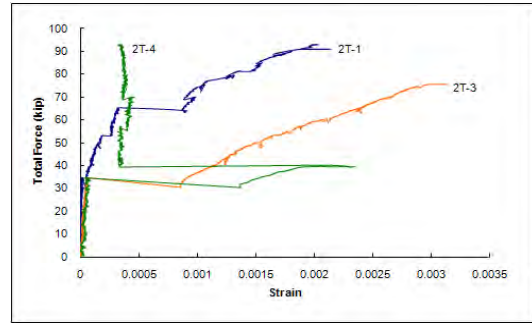
(a) Bottom of U-bar 2

(b) Top of U-bar 2
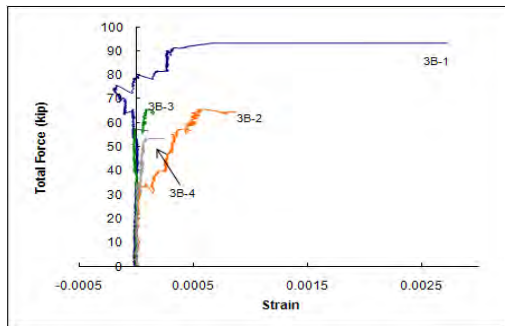
(c) Bottom of U-bar 3
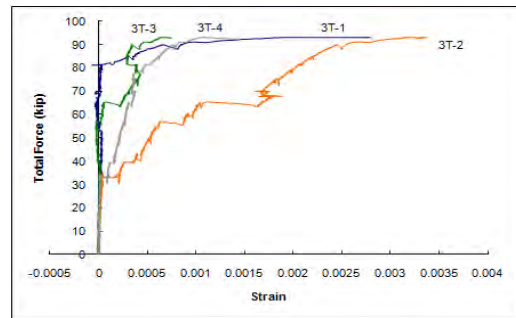
(d) Top of U-bar 3
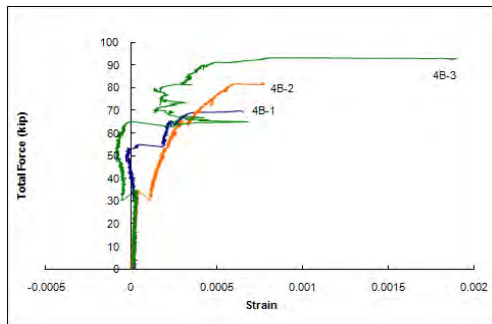
(e) Bottom of U-bar 4
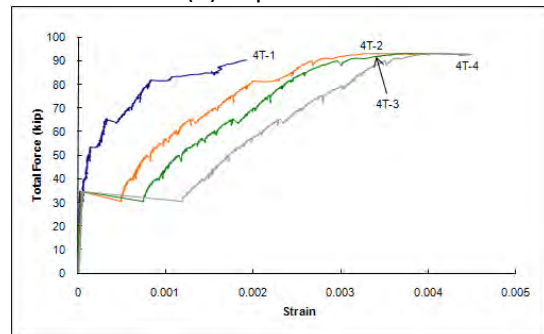
(f) Top of U-bar 4
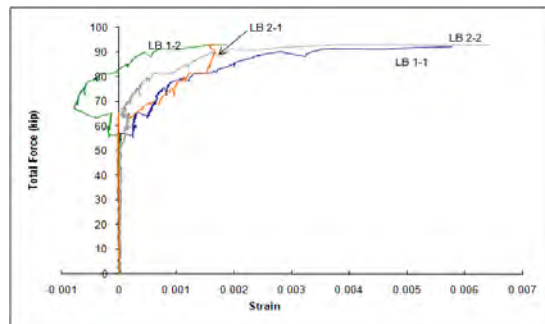
(g) Transverse Lacer Bars 1 and 2

Figure 9.1.28: Total force versus rebar strain for WT-1

289
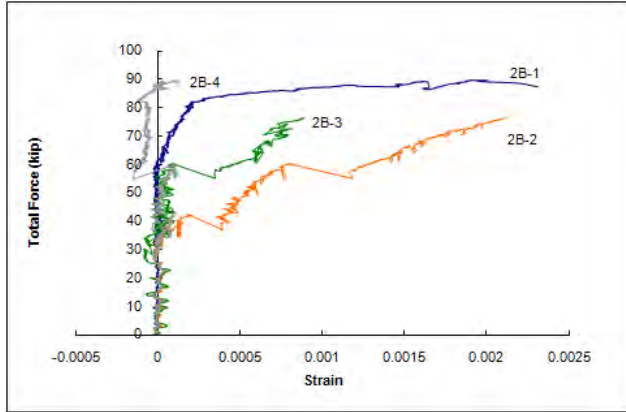
(a) Bottom Bar of Headed Bar Set 2 (Specimen HT-1)
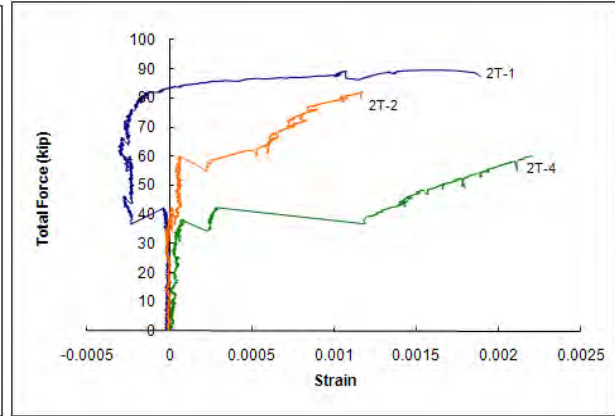
(b) Top Bar of Headed Bar Set 2 (Specimen HT-1)
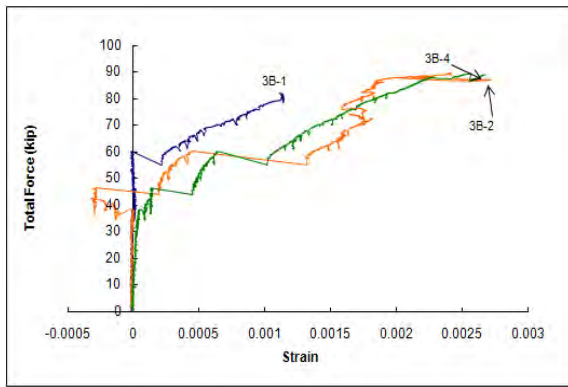
(c) Bottom Bar of Headed Bar Set 3 (Specimen HT-1)
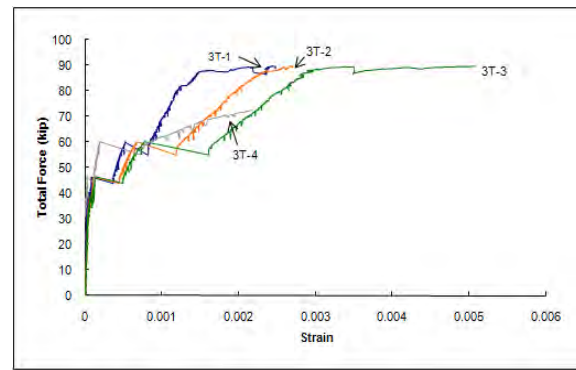
(d) Top Bar of Headed Bar Set 3 (Specimen HT-1)
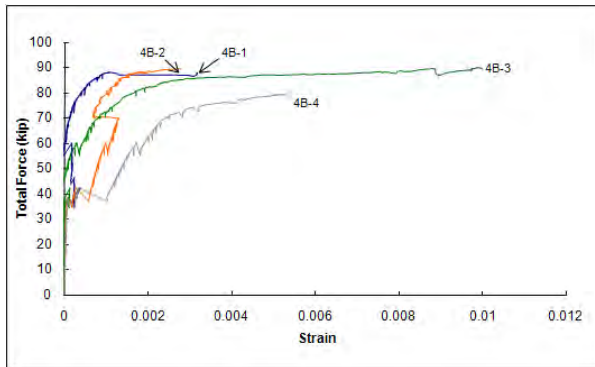
(e) Bottom Bar of Headed Bar Set 4 (Specimen HT-1)
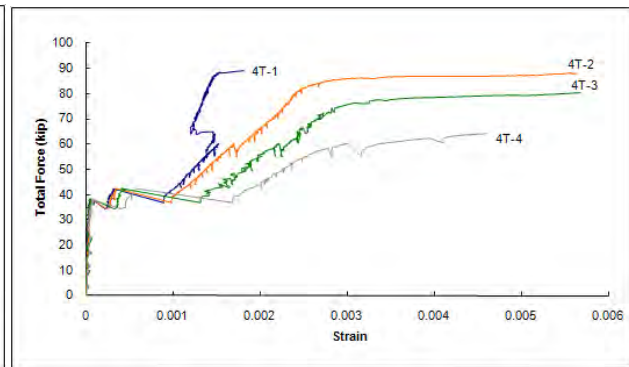
(f) Top Bar of Headed Bar Set 4 (Specimen HT-1)

290
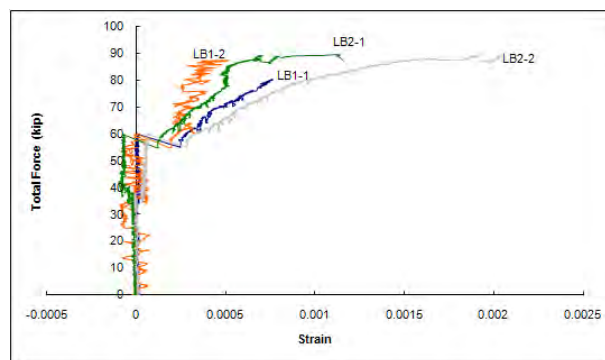
(g) Transverse Lacer Bars 1 and 2

Figure 9.1.29: Total force versus rebar strain for HT-1

9.1.6. Conclusions for Phase I U-Bar (SS, DWR) and Headed Bar (HB) Tests

As stated previously, the main objective of this research was to test two joint details (i.e., U-bar and headed bar details) and select the best performing joint detail for further testing. The additional testing of the best performing detail described in Section 9.2 to investigate variations in parameters was the first step toward the development of design guidelines and standard details for longitudinal and transverse precast deck joints.

Specimens containing both headed bar and U-bar joint details were tested in tension and in flexure to simulate the loading conditions in transverse and longitudinal joints, respectively, to ensure that the proposed joints could produce a precast deck system that would act monolithically. The behavior and capacities of the joint details were compared to select the best performing joint detail. All joint details produced adequate capacities and ductility in both the tension and flexure tests. Specimens containing the U-bar joint detail produced the largest capacities in both the bending and tension tests, as expected because they were fabricated with a higher grade of steel. Specimen WT-1 produced the largest tensile capacity which was 93.24 kips, and specimen SB-1 produced the largest flexural capacity which was 31.88 kip-ft. The U-bar detail produced the largest capacities without compromising ductility. Smaller crack widths at service level loading were also produced by the U-bar detail compared to the headed bar detail. The development of small crack widths increase durability by decreasing reinforcement corrosion, thus leading to longer deck life.

The constructability and reinforcement costs of the joint details were also compared. The U-bar detail created a less congested joint, which made it the easiest to construct. The bearing heads of the headed bar detail require more space to accommodate the larger diameter of the rebar heads. This extra space would reduce construction tolerances and could therefore cause problems in placement of precast deck components. The U-bars can also be easily tied together to form a rebar cage, which would allow for easy construction in the precast yard when compared to the two single layers of reinforcement in the headed bar detail. The lowest material cost was the conventional rebar used for the headed bars. The material costs were competitive between the conventional rebar used in the headed bars and the deformed wire reinforcement. The cost for conventional reinforcement was approximately 800 dollars a ton with an additional cost of 25 dollars for the installation of each Lenton Terminator bearing head. The deformed wire reinforcement cost was 850-900 dollars a ton for single fabricated cut wires or 900-1000 dollars a ton for

291

fabricated wire mesh. The stainless steel reinforcement had the highest cost of 5000 dollars a ton including fabrication. Even though the initial cost of stainless steel is high, it should still be considered due to the potential to increase the life span of the structure.

After consideration of capacity, service level crack widths, constructability, and cost, the U-bar detail constructed of deformed wire reinforcement was chosen for further testing. This detail produced adequate capacities in both the tension and flexural testing, while still producing adequate ductility. The constructability of the U-bar detail as well as the cost of the deformed wire reinforcement made this detail an economical choice. It should be noted however, that none of the reinforcement studied in the NCHRP 10-71 project was coated reinforcement. If the reinforcement were protected with epoxy coating, it may have an impact on the required length to transfer forces across the joint. Because the objectives of the project were to minimize the joint thickness, in regions where reinforcement protection is required, it is recommended that deformed wire reinforcement be used.

The Phase I experiments showed that the U-bar detail could develop adequate capacity with an overlap length of 6 in., a rebar spacing of 4.5 in. and two transverse lacer bars, but the Phase I tests did not provide a sense of how variations in these parameters would affect the behavior of the joint. The Phase II tests, discussed in the next section, provided insight regarding the effects of these parameters.

9.2. Test Phase II

Testing Parameters

Based on the test results from Phase I, U-bar details with deformed wire reinforcement were selected for further testing in Phase II. The testing parameters of the U-bar joint detail are listed in Table 9.2.1. As discussed earlier, each specimen is labeled where the "W" represents deformed wire reinforcement, the "B" represents bending test, the "T" represents tension test, and the number represents the specimen number tested in chronological order. WB-1 was the first specimen to be tested in flexure, which was completed in Test Phase I. The testing parameters for WB-2, WB-3 and WB-4 were then specified based on testing results of WB-1. Also, WT-1 was the first specimen to be tested in pure tension, which was conducted as part of the Phase I tests. The testing parameters for WT-2, WT-3, and WT-4 were specified based on the testing results of WT-1.

292

Table 9.2.1: Testing parameters

Specimen ID		Concrete Strength	Bar Spacing	Joint Overlap Length
		(ksi)	*(in)*	*(in)*
WB-1	WT-1	10.0	4.5	6.0
WB-2	WT-2	**7.0**	4.5	6.0
WB-3	WT-3	10.0	4.5	**4.0**
WB-4	WT-4	10.0	**6.0**	6.0

As shown in Table 9.2.1, two different concrete strengths (10 and 7 ksi), two different rebar spacings (4.5 and 6 in.), and two different overlap lengths (6 and 4 in.) were considered in this second phase tests. The details of the longitudinal joint test specimens are provided in Figures 9.2.1 through 9.2.4. And details of the transverse joint test specimens are provided in Figures 9.2.5 through 9.2.8.
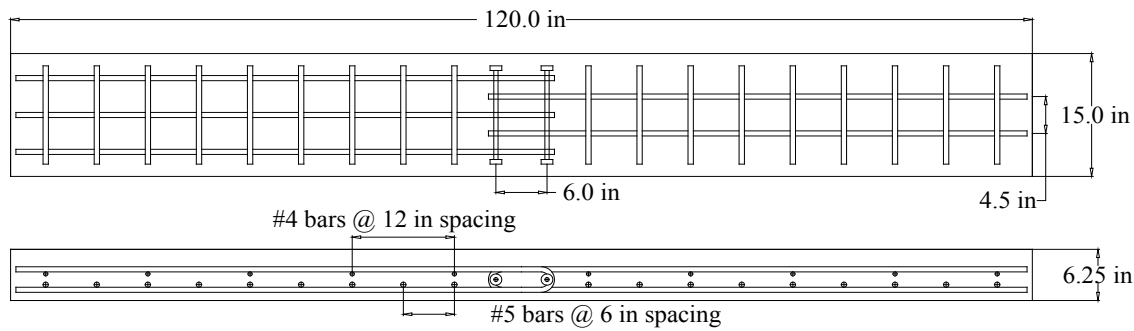
Figure 9.2.1: WB-1 longitudinal joint specimen (Tested in Phase I)
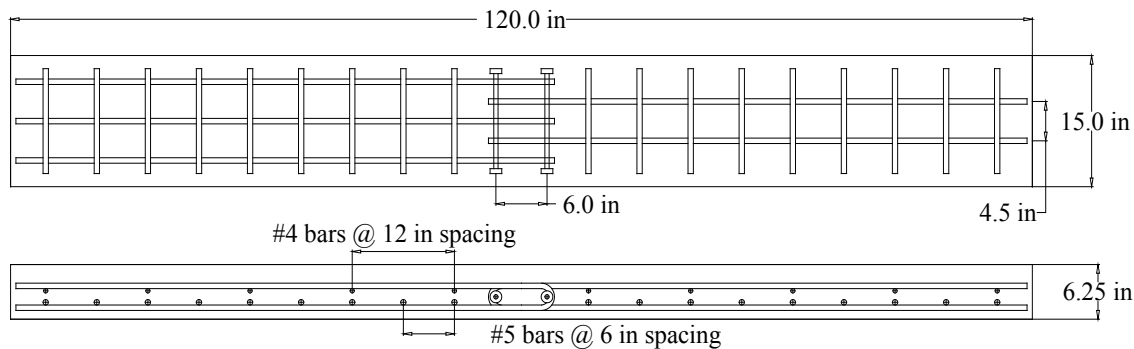
Figure 9.2.2: WB-2 longitudinal joint specimen

293
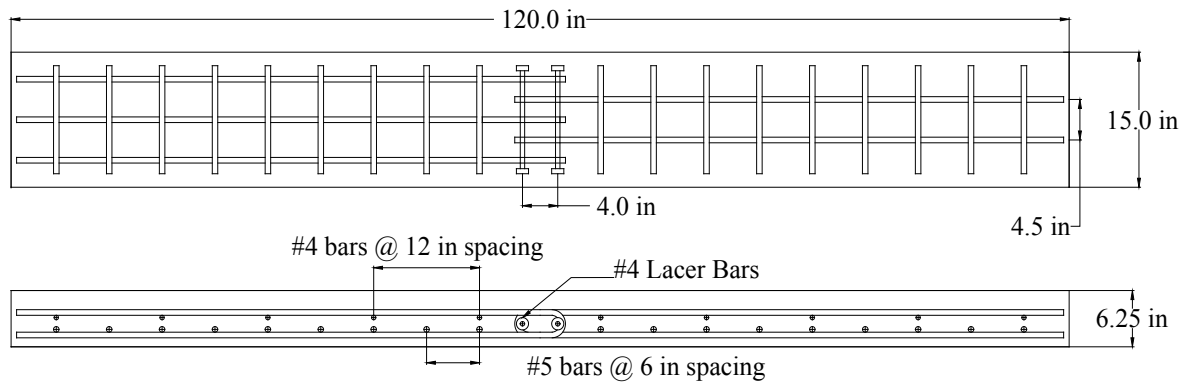
Figure 9.2.3: WB-3 longitudinal joint specimen
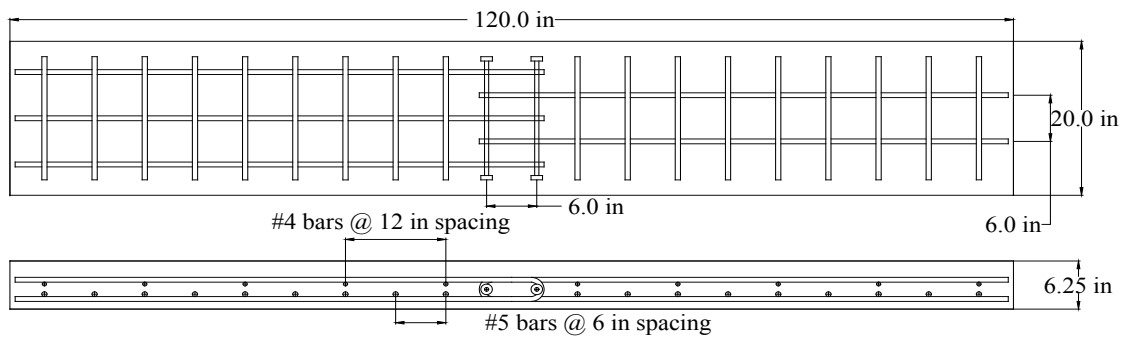
Figure 9.2.4: WB-4 longitudinal joint specimen
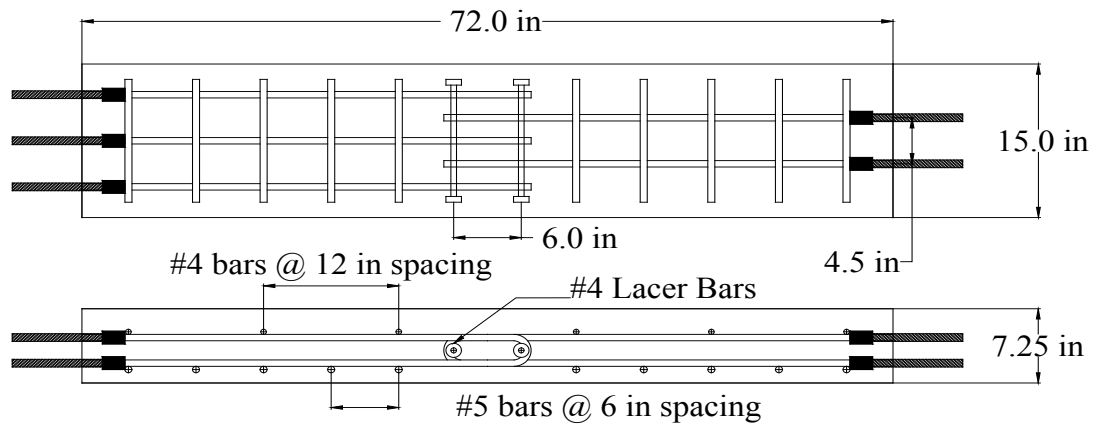
Figure 9.2.5: WT-1 transverse joint specimen (Tested in Phase I)

294
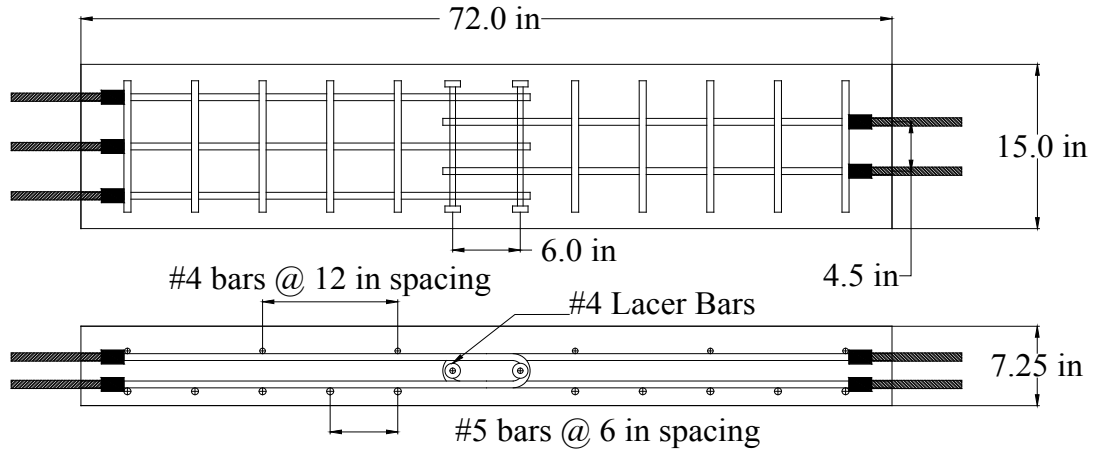
Figure 9.2.6: WT-2 transverse joint specimen
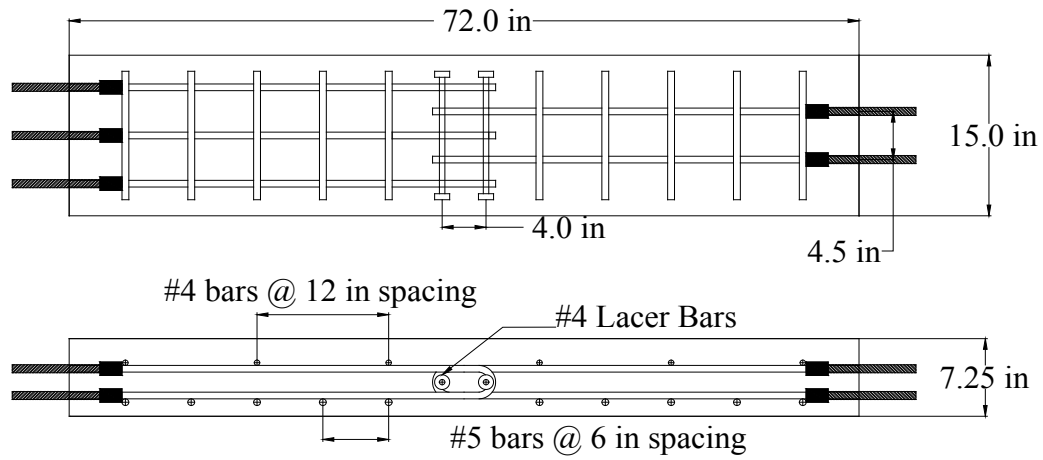
Figure 9.2.7: WT-3 transverse joint specimen

295
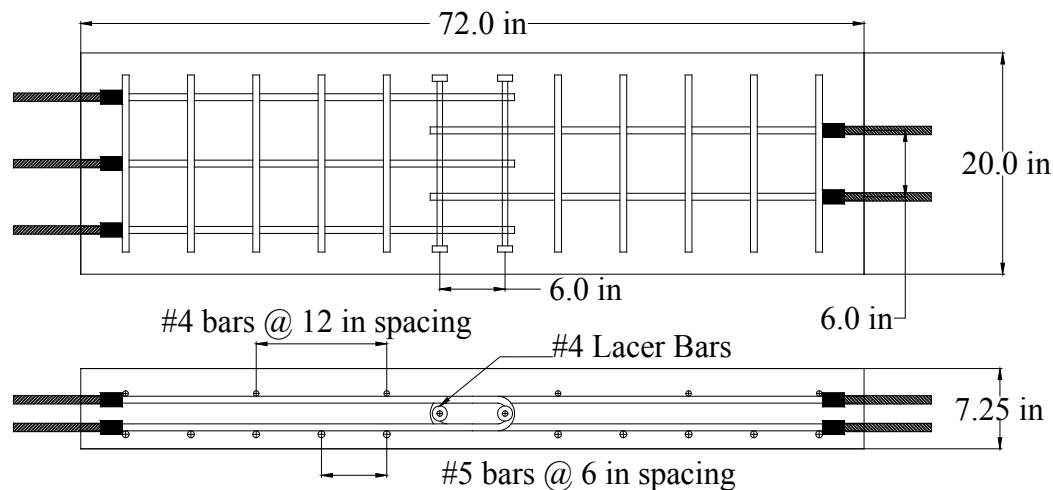
Figure 9.2.8: WT-4 transverse joint specimen

9.2.1. Experimental Setup and Instrumentation

The Phase I test setups and instrumentation described in Section 9.1.2 were also used for the Phase II test series. The only change was that the strain gage configuration was modified based on the test results obtained for WB-1 and WT-1during the first phase of testing. In Phase II, gages were placed on either side of the expected development length location so that the region of yielding in the bar could be identified. In Phase I, the gages were placed on both the top layer and the bottom layer of the U-bar in WB-1 and WT-1. In Phase II, the gages were placed only on the bottom layer of the U-bar. For WB-3 and WT-3, the specimens with a 4 in. joint overlap length, gages were placed at 4, 6, and 8 in. away from the bend of the U-bar. For WB-2, WT-2, WB-4 and WT-4, the specimens with a 6 in. joint overlap length, gages were placed at 6, 8, and 10 in. away from the bend of the U-bar. Figures 9.2.9 and 9.2.10 show the strain gage configurations for each joint overlap length of the specimens tested during Phase II.

The strain gage diagrams have notations indicating the U-bar identifier and the location of the gage on the bar. The U-bars are represented by "UB" and the lacer bars are indicated by "LB." The distance from the bend of the U-bar to each gage is shown at the bottom of the diagram. All distances indicated on the diagrams are in inches and measured from center-to-center. A gage was placed on one lacer bar at 1 in. from the bearing surface of the head and a second gage was placed at the midpoint of the lacer bar. The strain gage configuration of the lacer bar is shown previously in Figure 9.1.9.

296
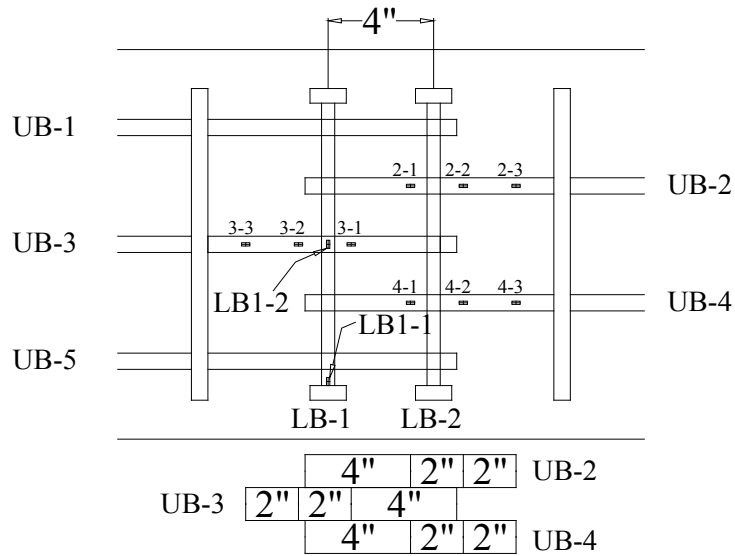
Figure 9.2.9: Strain gage configuration for WB-3 and WT-3
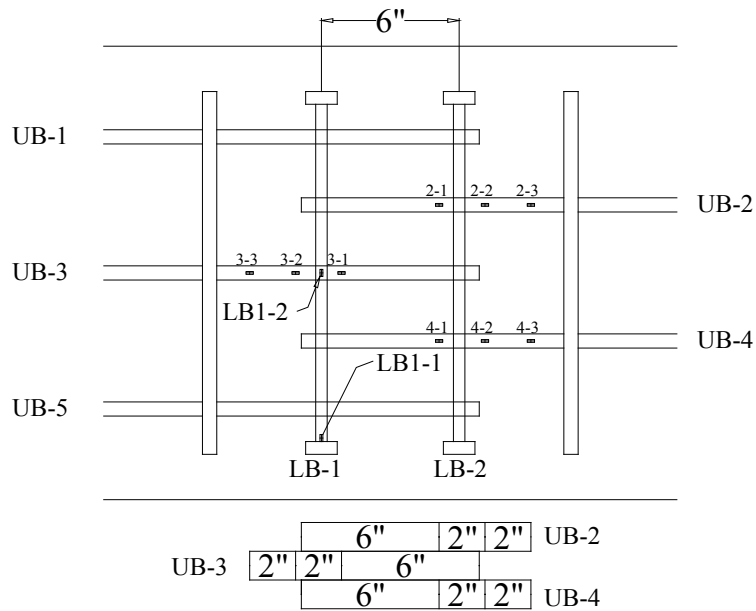
Figure 9.2.10: Strain gage configuration for WB-2, WT-2, WB-4, and WT-4

297

9.2.2. Material Testing

Concrete Testing

The longitudinal joint specimens were cast on September 16, 2009. When these three specimens were poured, fifteen companion cylinders were also cast. To get accurate concrete compressive strengths, three cylinders were cast for each specimen to be tested on the day of the actual flexural test conducted in the laboratory. Three cylinders were also cast for 7-day and 28-day compressive strength measurements. Fifteen companion cylinders were also cast with the transverse joint specimens which were poured on November 3, 2009. All cylinder tests complied with the ASTM C 39 standards when tested to determine the concrete compressive strength (ASTM C 39, 2005). The cylinders were loaded as specified in the standards and within the limit of 35±7 psi/s. The cylinder's compressive forces were recorded at failure. Due to a machine malfunction, some cylinders were not able to be tested at the 7-day benchmark, as denoted by "n/a" in Table 9.2.2. The compressive strength test results are recorded in Tables 9.2.2 and 9.2.3.

Table 9.2.2: Concrete compressive strengths (longitudinal joint specimens)

	Cylinder ID	7-Day Test (psi)	Day of Test (psi)	28-Day Test (psi)
WB-1	1	8710	Ages exceeded 28 days. Results from "28-Day Test" were used.	10350
	2	9753		11651
	3	9820		11575
	Average	**9428**		**11192**
WB-2	1	8323	9359	10743
	2	8780	9308	10504
	3	8989	9103	11220
	Average	*8697*	*9257*	*10822*
WB-3	1	n/a	10544	10743
	2	n/a	10385	10464
	3	n/a	10180	10265
	Average	*n/a*	*10370*	*10491*
WB-4	1	n/a	9759	10743
	2	n/a	11711	10464
	3	n/a	10097	10265
	Average	*n/a*	*10522*	*10491*

298

Table 9.2.3: Concrete compressive strengths (transverse joint specimens)

	Cylinder ID	7-Day Test (psi)	Day of Test (psi)	28-Day Test (psi)
WT-1	1	8301	Ages exceeded 28 days. Results from "28-Day Test" were used.	9948
	2	8068		9383
	3	8114		9416
	Average	**8161**		**9582**
WT-2	1	7600	7600	9231
	2	7958	7958	9111
	3	7600	7600	8992
	Average	*7719*	*7719*	*9111*
WT-3	1	9072	9629	10743
	2	9390	9231	10265
	3	9231	9629	10743
	Average	*9231*	*9496*	*10584*
WT-4	1	9072	9589	10743
	2	9390	9152	10265
	3	9231	9987	10743
	Average	*9231*	*9576*	*10584*

9.2.3. Results and Discussion

Flexural Capacity (Longitudinal Joint Behavior)

The four longitudinal joint specimens, WB-1, WB-2, WB-3, and WB-4, were tested in flexure. As stated before, the "W" represented deformed wire reinforcement, the "B" represented bending test, and the number identified the specimen tested in chronological order.

The service level moments were calculated for WB-1 based on the AASHTO service limit states. WB-1, as well as WB-2 and WB-3, had a width of 15 in., therefore the service moments were be the same for those specimens. However, the width of WB-4 was 20 in., so the service moments increased by the width ratio of 1.33. The results of these moment calculations are presented in Table 9.2.4.

Table 9.2.4: Service moments

M+		M-	
WB-1, WB-2, WB-3	WB-4	WB-1, WB-2, WB-3	WB-4
(kip-ft)	(kip-ft)	(kip-ft)	(kip-ft)
10.1	13.4	8.3	11.0

To compare the behavior among the specimens, moment versus deflection and moment-versus-curvature plots were created, as shown in Figures 9.2.11 and 9.2.12, respectively. The deflection measurements were obtained from the LMT's placed at the center location and end locations on the tension side of the specimen. Because padding was secured between the specimen and the supports, the LMT's could have given an inaccurate value for the total deflection. To improve the accuracy of the data, the deflection readings of the LMT's at both ends of the specimen were averaged together. The averaged end deflections and the middle deflection were combined to obtain the total deflection of each specimen. The curvature values were derived based on the data provided by the horizontally placed LMT's across the joint zone on the tension and compression side of the specimen. The moment capacities were derived from the forces applied by the MTS actuators.

As the loading increased toward ultimate capacity, the deflection LMT's were removed in order to prevent damage. By removing these LMT's, the data was not completely representative of the behavior of the specimen. The moment versus deflection curves should reach a peak and then taper off to ultimate failure. This tapering effect was evident in WB-1 and WB-4. However, the deflection readings were not available at ultimate for WB-2 and WB-3. These trends can be viewed in Figure 9.2.11.

The curvature LDVT's were also removed as the loading increased to ultimate capacity. As the cracks propagated and the crack widths increased, the LMT on the top of the specimen was removed because the measuring device went out of range. The LMT located on the bottom of the specimen was removed when the concrete began to spall due to high compressive stresses. The moment-versus-curvature curves should also taper off toward ultimate. The data for WB-1 and WB-2 displayed this tapering effect, but the top and bottom LMT's were removed before adequate data could be recorded for WB-3 and WB-4. These trends are displayed in Figure 9.2.12.

300
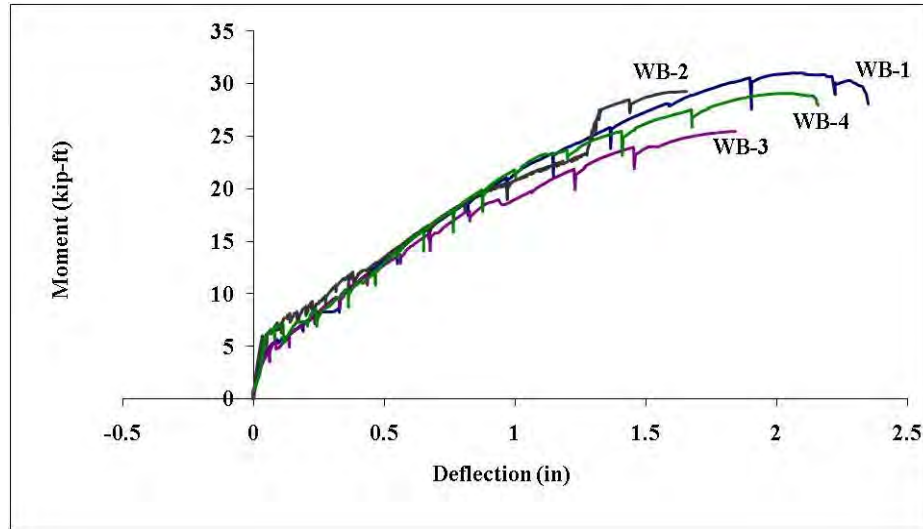
Figure 9.2.11: Moment versus deflection
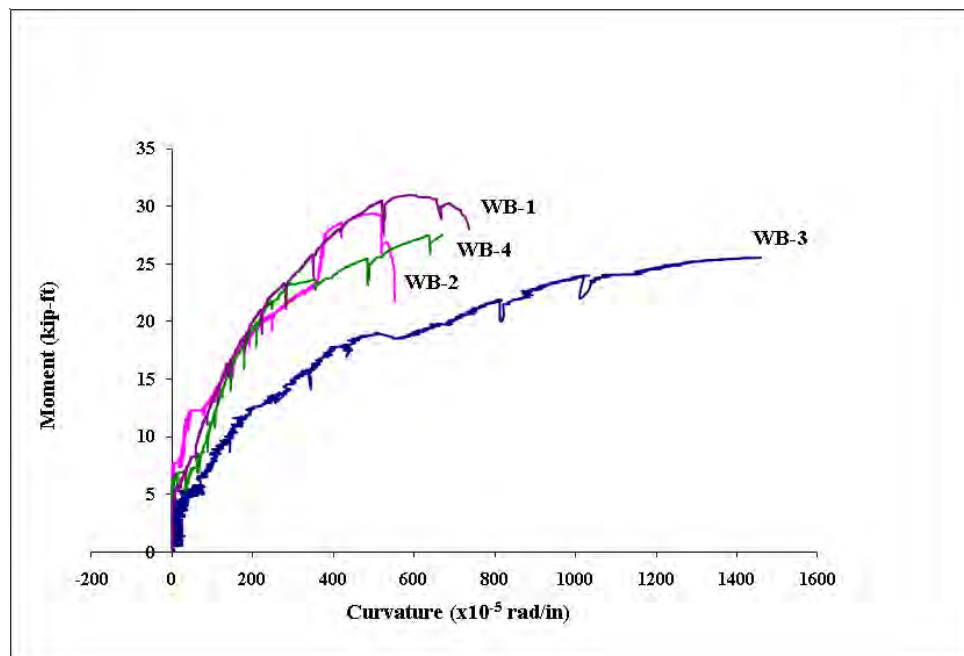
Figure 9.2.12: Moment-versus-curvature

From Figures 9.2.11 and 9.2.12, the behavior of each specimen can be compared to one another. Because ACI 318-08 does not provide a specific method for calculating the moment capacity for a staggered U-bar detail at the joint, two continuously reinforced beam sections were analyzed using two different steel reinforcement patterns: (1) cross-section with A_s=1.24 in^2 representing the side of the longitudinal joint specimen with two U-bars and (2) cross-section with A_s=1.86 in^2 representing the other side of the

301

longitudinal joint specimen with three U bars. The cross-sections used in theoretical calculations are displayed in Figures 9.2.13 and 9.2.14. In order to observe the behavior of each test specimen in comparison to the continuously reinforced cross sections, the moment versus deflection and moment-versus-curvature curves of each specimen were plotted along with the continuously reinforced calculated curves in Figures 9.2.15 and 9.2.16, respectively. The curves relating to the continuously reinforced cross sections were plotted using analysis software called Response 2000. This program was used to predict the moment curvature behavior of a continuously reinforced specimen with either 15 in wide or 20 in wide cross section. The nominal yield stress of 75ksi, steel elastic modulus of 29000ksi and concrete strength of 10ksi or 7ksi were used in the Response 2000 analysis. The material properties used in Response 2000 are shown in Figure 9.2.17.
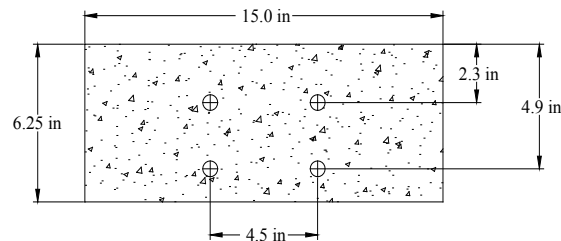
(a) WB-1, WB-2, and WB-3
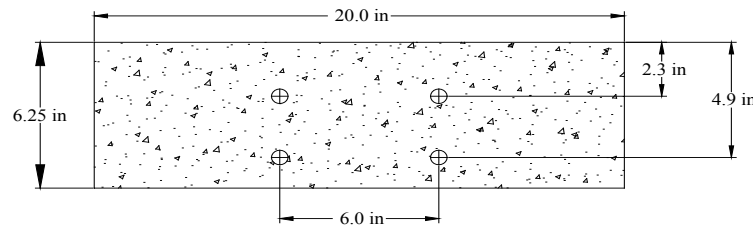
(b) WB-4

Figure 9.2.13: Cross sections, A_s of 1.24 in^2

302
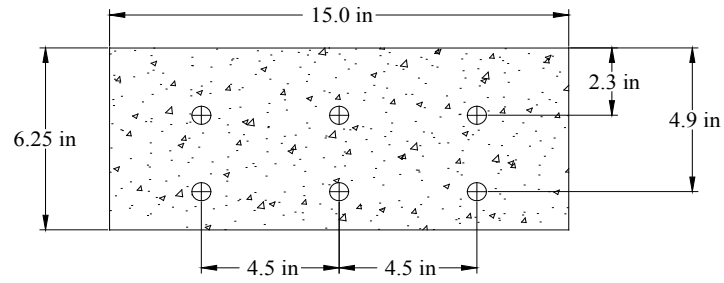
(a) WB-1, WB-2, and WB-3
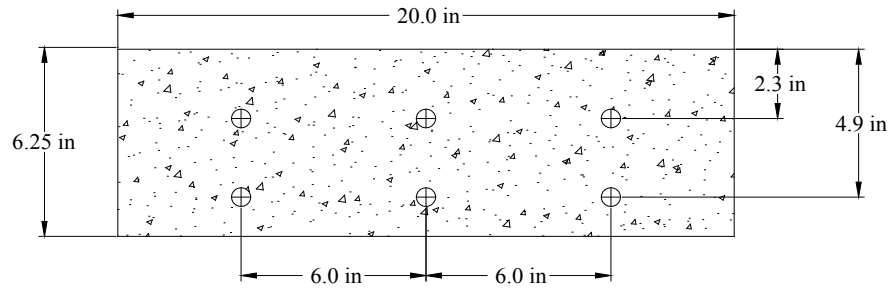
(b) WB-4

Figure 9.2.14: Cross sections, A_s of 1.86 in^2

303

(a) WB-1

(b) WB-2

304
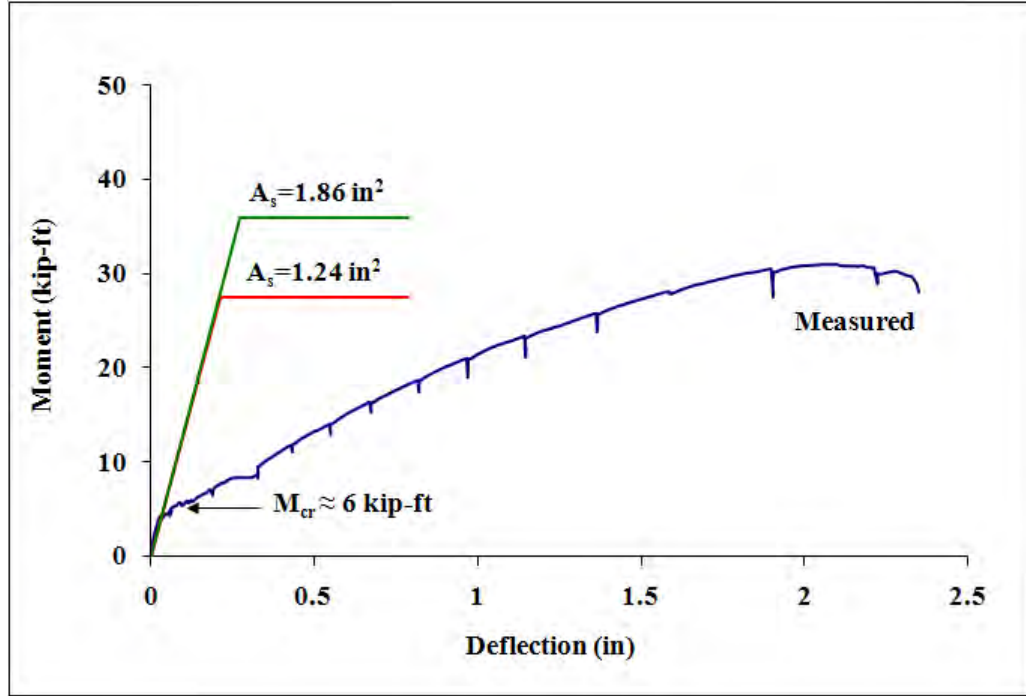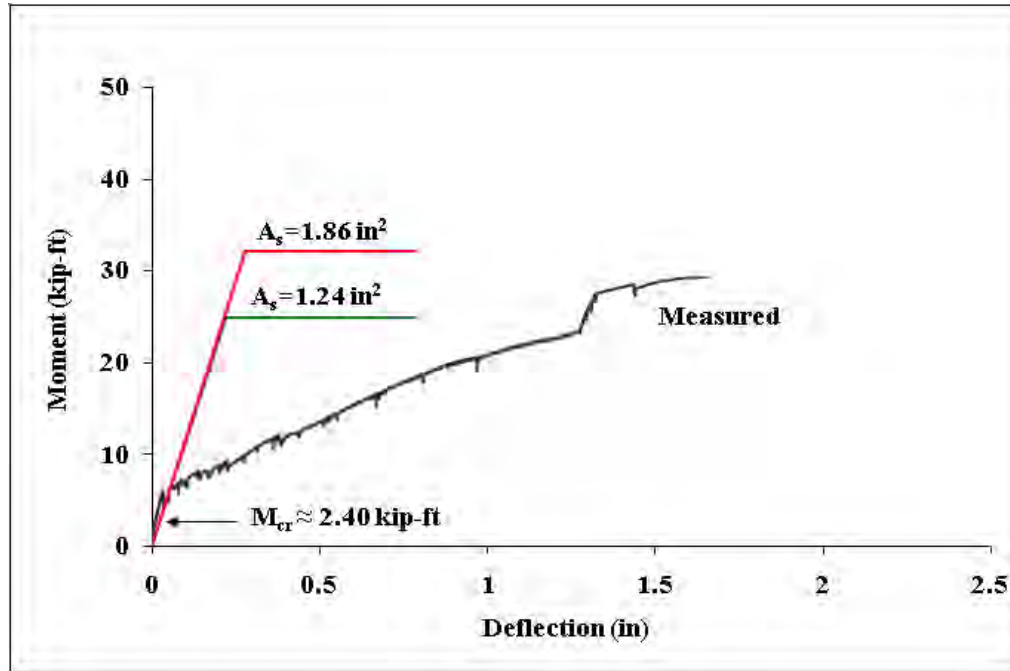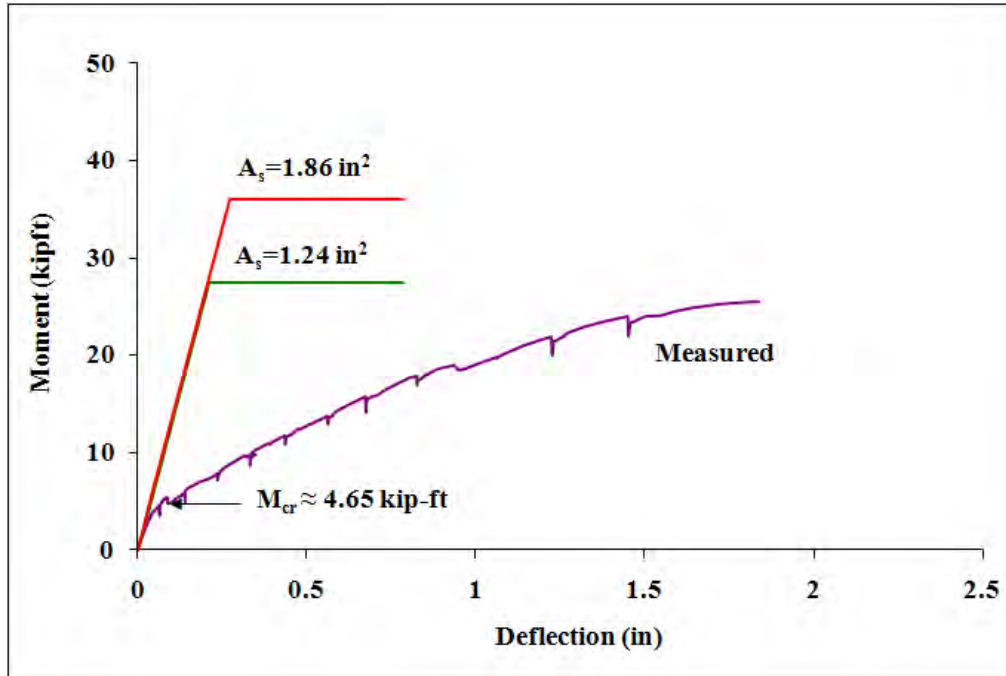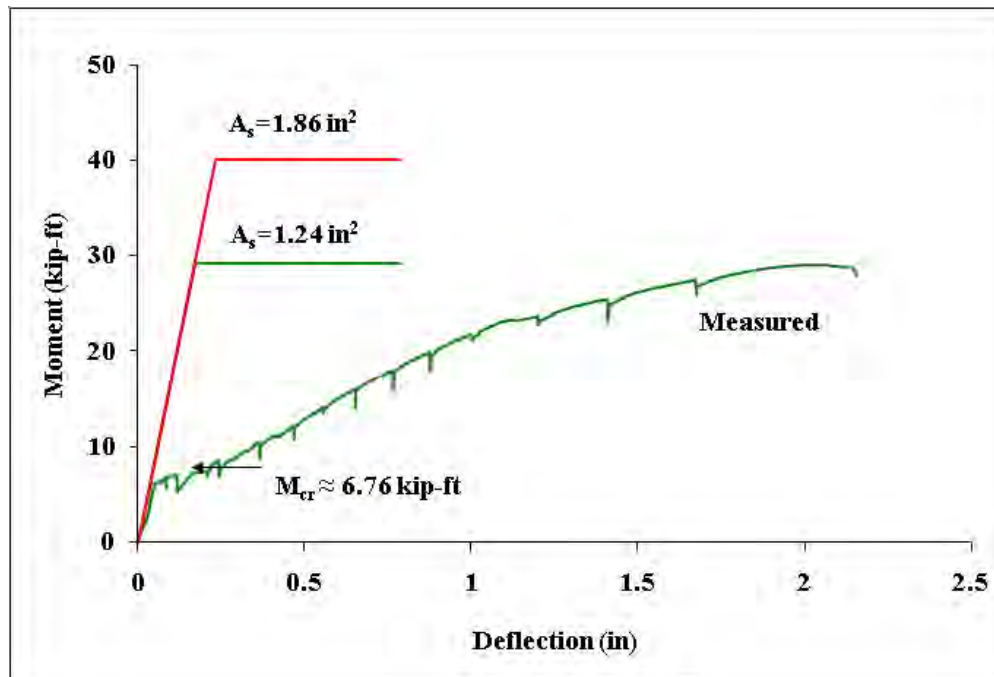
(c) WB-3

(d) WB-4

Figure 9.2.15: Measured and calculated moment versus deflection

305

(a) WB-1

(b) WB-2

306
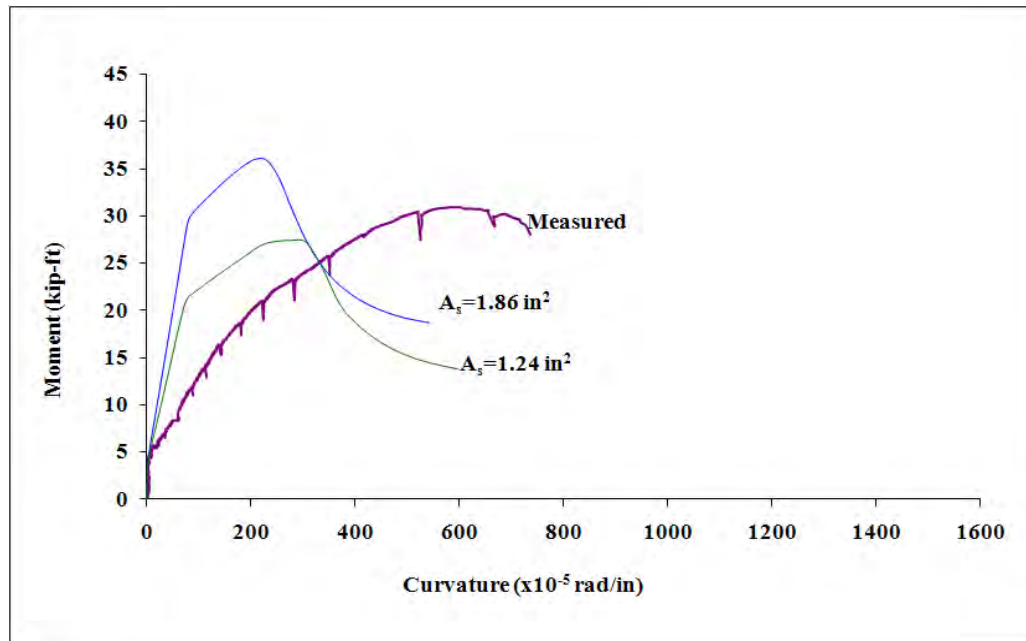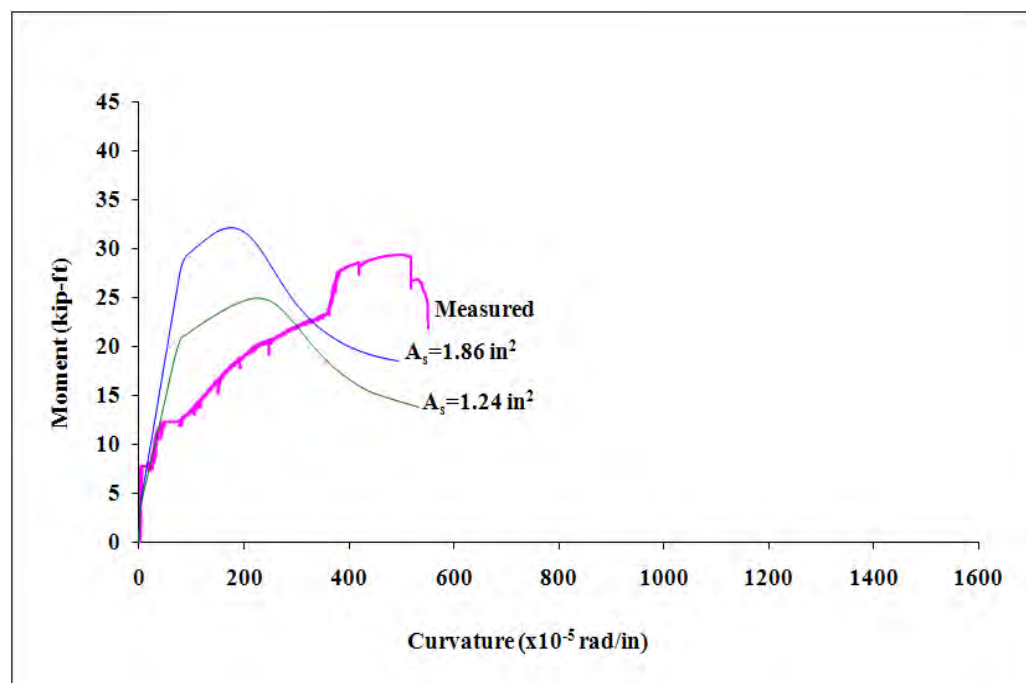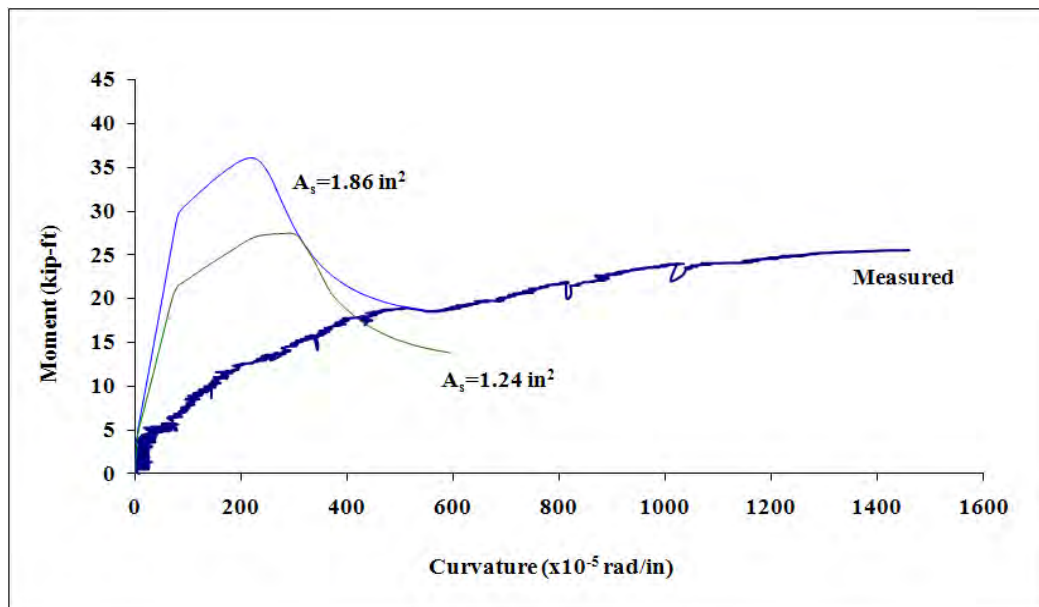
(c) WB-3
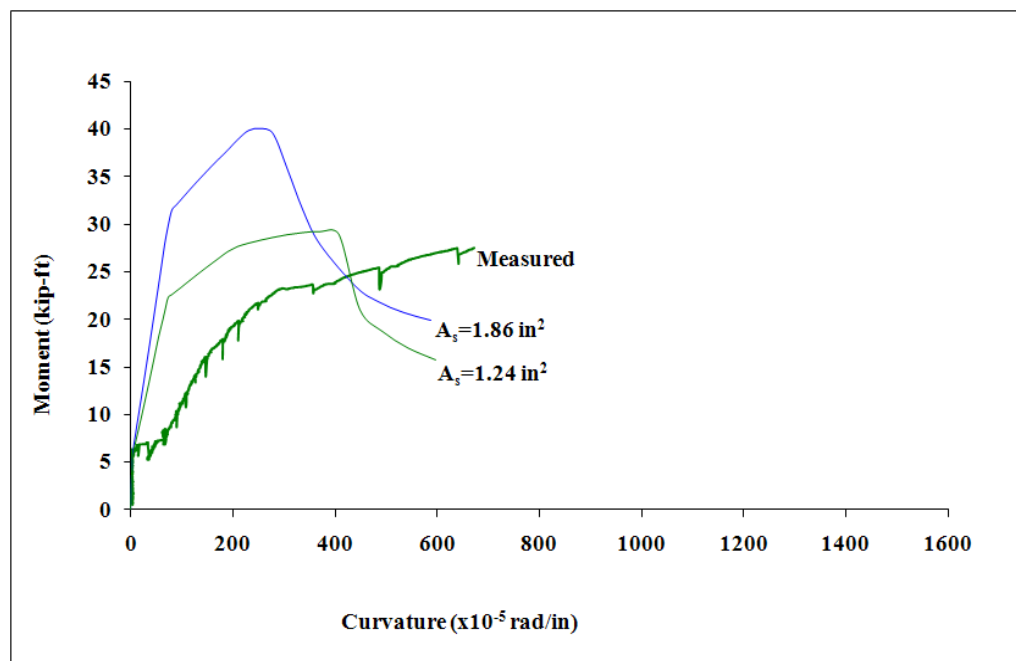
(d) WB-4

Figure 9.2.16: Measured and calculated moment-versus-curvature

307
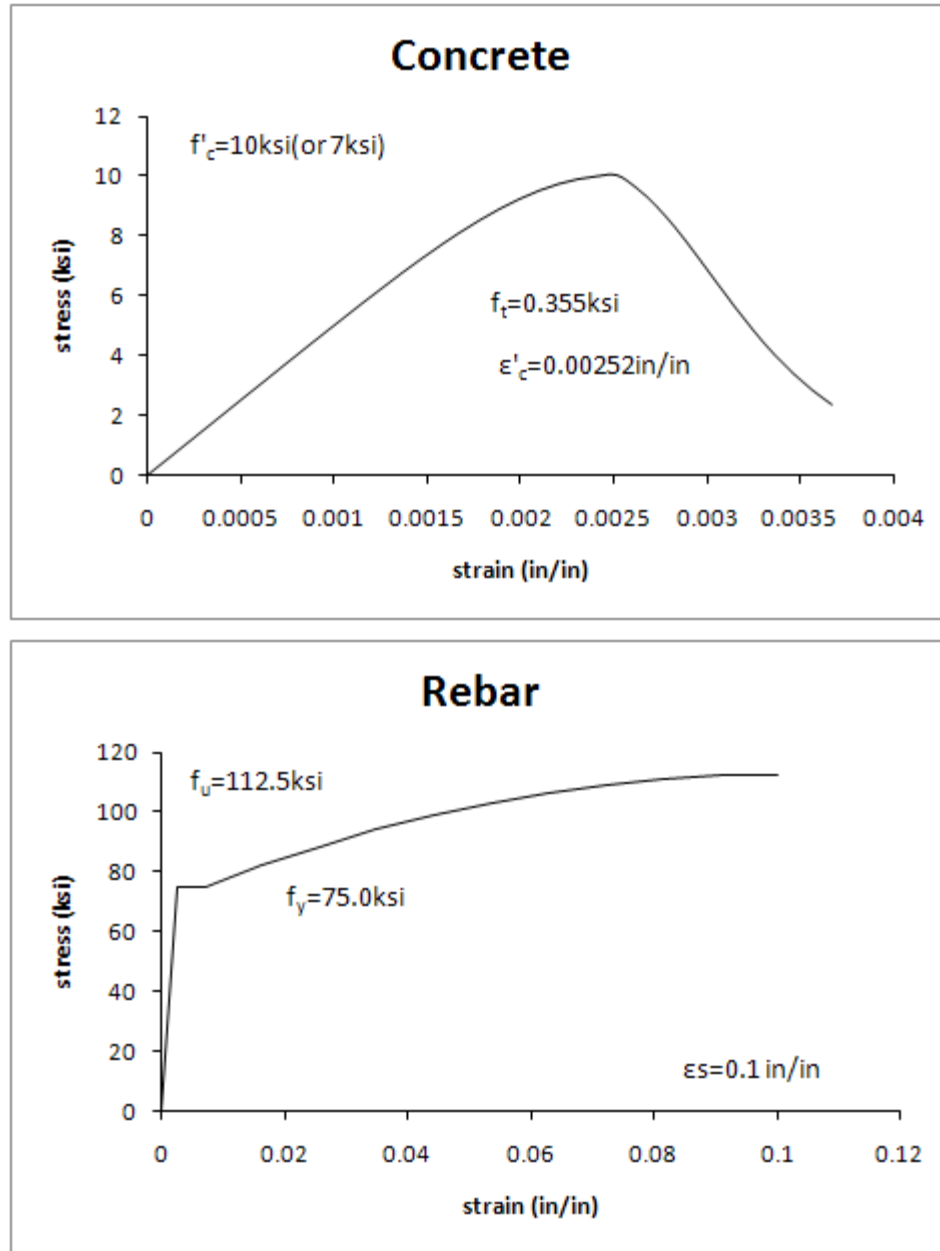
Figure 9.2.17: Material properties used in Response 2000

Because the U-bars were staggered in the test specimens, the moment capacities, curvatures, and deflections differed from a continuously reinforced section. The joint was a combination of two U-bars, A_s=1.24 in^2, and three U-bars, A_s=1.86 in^2. Ideally the measured moment versus deflection curve would fall in between the two continuously reinforced calculated curves. The results of the flexural tests are shown in Tables 9.2.5 and 9.2.6.

308

Table 9.2.5: Flexural test results, nominal moments (M_n)

Specimen ID	M_n (kip-ft)		
	Test	Calculation	
		2 Bars	3 Bars
WB-1	31.05	27.48	36.00
WB-2	29.31	24.93	32.20
WB-3	25.50	27.48	36.00
WB-4	29.09	29.22	40.05

Table 9.2.6: Flexural test results, curvatures (Φ_n)

Specimen ID	Φ_n ($x10^{-5}$ 1/in)		
	Test	Calculation	
		2 Bars	3 Bars
WB-1	736.9	595.9	541.8
WB-2	550.4	532.6	492.3
WB-3	1459.2	595.9	541.8
WB-4	670.8	595.9	586.0

From Tables 9.2.5 and 9.2.6, WB-1, WB-2 and WB-4 produced adequate capacities in comparison to a continuously reinforced beam with A_s=1.24 in². WB-3 did not produce adequate moment capacity. WB-3 had the reduced joint overlap length of 4 in. All four U-bar detailed specimens were extremely flexible in comparison to what would be expected from a continuously reinforced section.

309

Flexural Specimen Behavior (Longitudinal Joint Behavior)

According to the data, each specimen cracked at the following moments: WB-1 cracked at approximately 5.9 kip-ft; WB-2 cracked at 2.4 kip-ft; WB-3 cracked at 4.7 kip-ft; and WB-4 cracked at 6.8 kip-ft. Early in the loading, transverse cracks appeared during the flexural tests, as expected, on the tension side of the specimens. As the loading slowly increased, longitudinal cracks began to form inside the joint zone. These longitudinal cracks corresponded to the transverse joint reinforcement within the bridge deck. The longitudinal cracks in the joint did not appear until the following: 7.6 kip-ft for WB-2; 19.9 kip-ft for WB-3; and 18.0 kip-ft for WB-4. After the longitudinal cracks formed, the cracks continued to propagate deeper in the longitudinal and transverse directions until diagonal cracks appeared over the joint zone. Each specimen displayed the same diagonal crack patterns on the heavier-reinforced side of the joint. These diagonal cracks appeared near the failure point of each specimen. WB-3 produced the widest crack width in the center of the joint at failure. Also, as the specimen neared ultimate failure, the concrete on the compression side began to crush and fall to the ground. The cracks at failure can be seen in Figure 9.2.18. The numbers written on the specimens represent the forces that were applied when the cracks occurred.

(a) WB-1

(b) WB-2

(c) WB-3

(d) WB-4
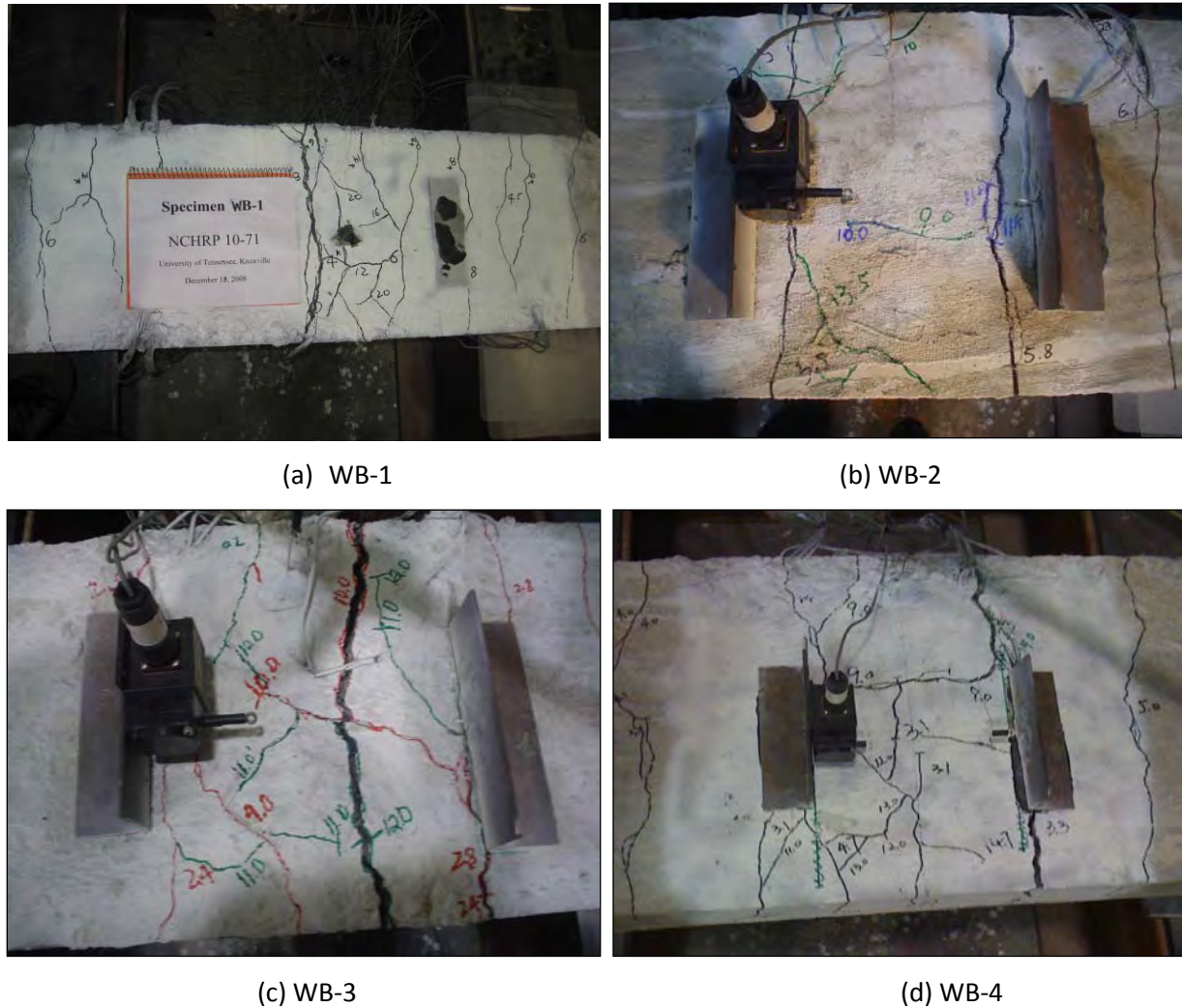
Figure 9.2.18: Flexural cracks at failure

Flexural Crack Widths at Service Level Loading (Longitudinal Joint Behavior)

Cracks are a concern for several reasons. The appearance of cracks in a structure causes public concern, and deterioration of concrete and corrosion of reinforcement is a major concern among engineers. As discussed earlier in this chapter, the service level positive moment was 10.1 kip-ft for WB-2 and WB-3 and 13.4 kip-ft for WB-4. Because the longitudinal joint in a bridge deck would primarily resist positive bending, the service level positive moment of 10.1 kip-ft was used to compare crack widths. For WB-1, which was tested as part of Phase I, a crack width ruler was used to measure the crack widths. At service level loading, the crack width for WB-1 was 0.01 in. The crack widths were measured incrementally while the test was conducted; therefore the crack widths at the service level loading were interpolated values. At service level loading, the crack width for WB-2 was 0.009''. The other crack widths were as follows: 0.006 in. for WB-3; and 0.003 in. for WB-4.

311

Strain Gage Data (Longitudinal Joint Behavior)

As discussed in Section 9.2.1, strain gages were applied to the reinforcement to determine whether the reinforcement yielded within the overlap length. Several of the strain gages were destroyed during either transport or casting, so they were not able to be used for testing.

For the longitudinal joint tests, moment-versus-strain curves for each gage location are plotted in Figure 9.2.19. Note that the strain gages for the WB-1 specimen shown in Figure 9.2.19 are actually gages 2-2, 2-3, 2-4, 3-2, 3-3, 3-4, 4-2, 4-3, 4-4 for comparison due to different gage configurations in Phases I and II. Theoretically, as the loading increases, the gages should indicate increasing strains in the reinforcement due to the increased strains in the reinforcement. For the longitudinal joint tests, most of the data proved this to be true and all the U-bars were observed to yield on the tension side of the specimen. Due to cracking of the concrete at some of the gage locations, a few of the strain gage readings produced noisy data and were discarded. The strain gages were placed near the approximate development length of the U-bars. Because of cracks occurring over some of the gages, no consistent data was present throughout all four specimens to verify the development length. However, the data was consistent in showing that the reinforcement developed large strains where diagonal cracks occurred.

312
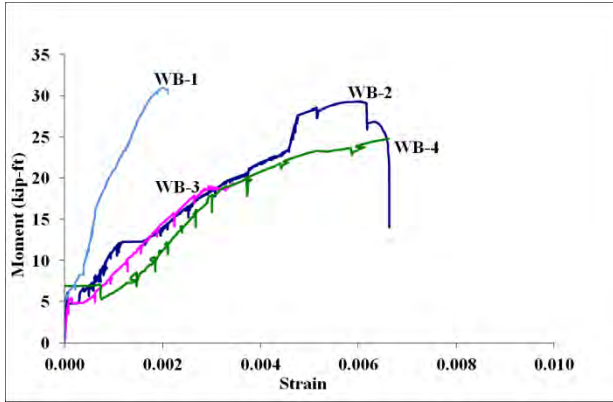
(a) Gage 2-1
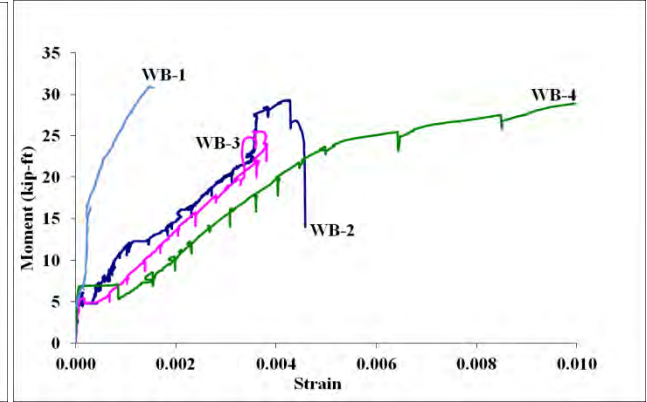
(b) Gage 2-2
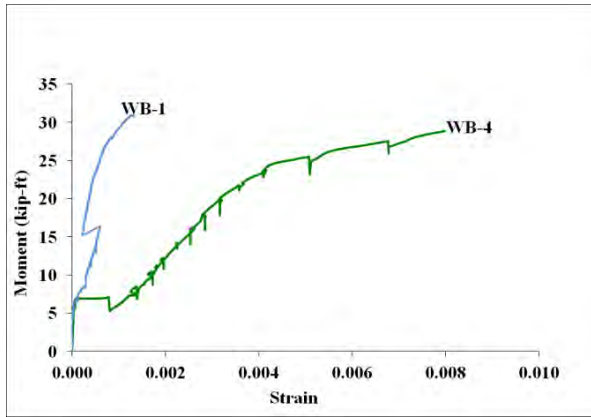
(c) Gage 2-3
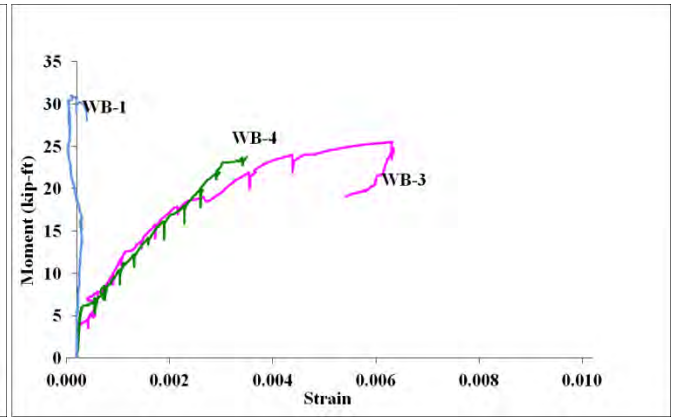
(d) Gage 3-1

(e) Gage 3-2

(f) Gage 3-3

313

(g) Gage 4-1

(h) Gage 4-2

(i) Gage 4-3

(j) Gage LB 1-2
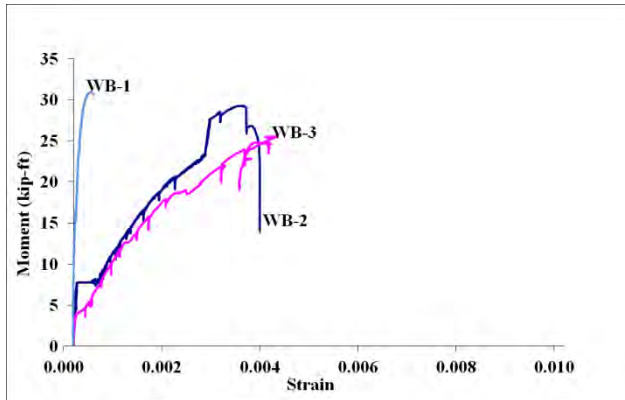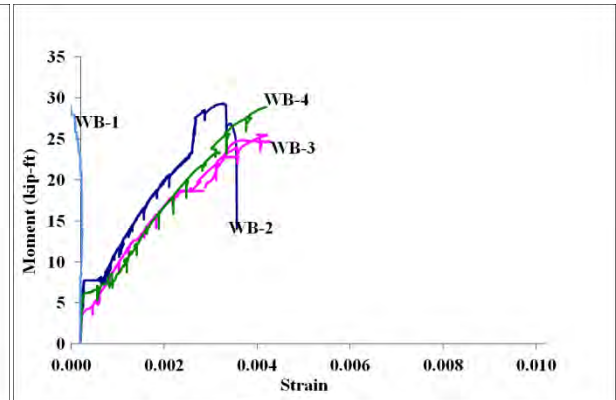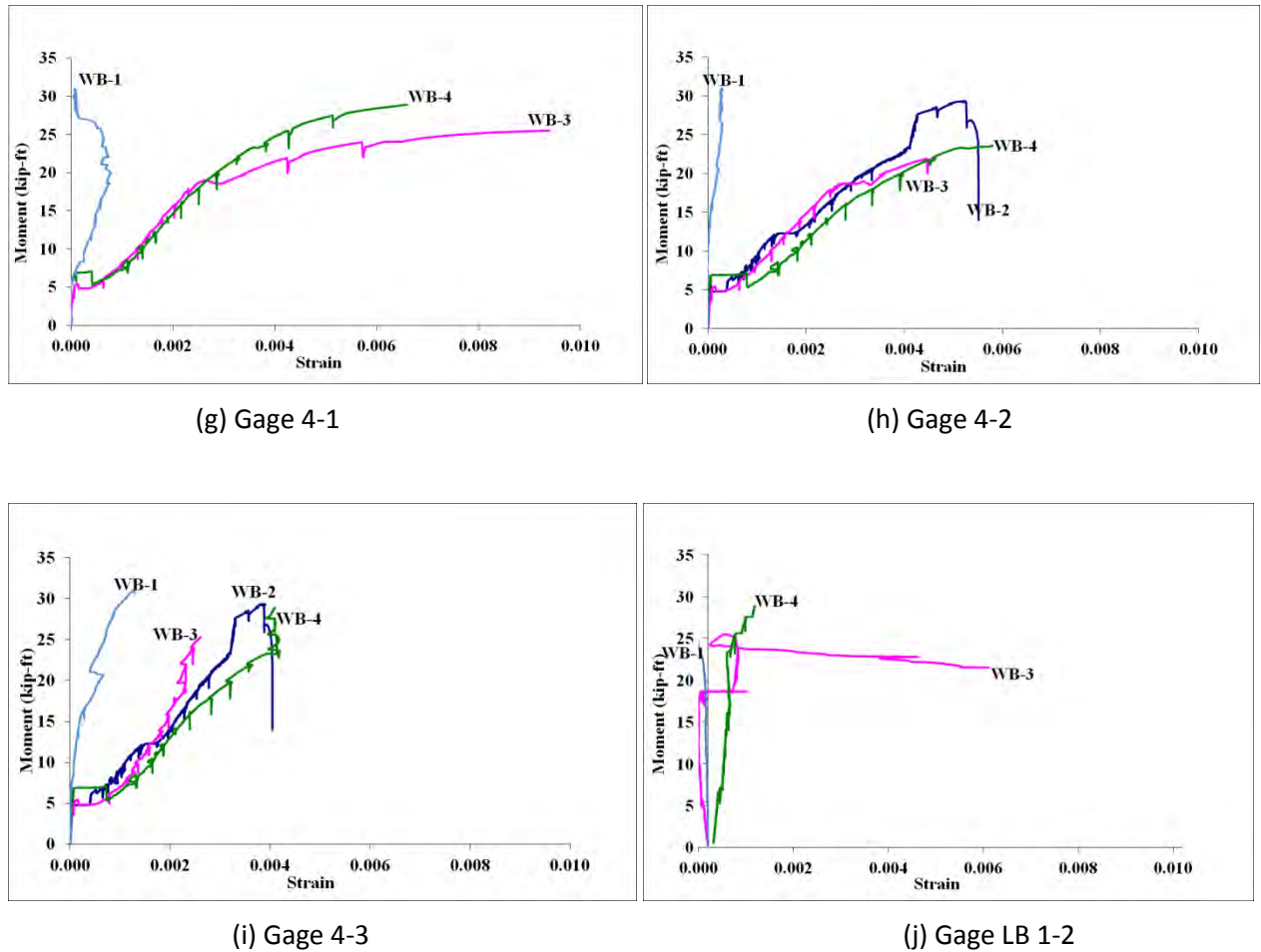
Figure 9.2.19: Moment versus rebar strain for longitudinal joint tests

Tensile Capacity (Transverse Joint Behavior)

The four transverse joint specimens, WT-1, WT-2, WT-3, and WT-4, were tested in tension. As stated before, the "W" represented deformed wire reinforcement, the "T" represented tension test, and the number identified the specimen tested in chronological order.

The tensile capacity of the U-bar specimen was calculated as the product of the lightly reinforced area of steel, A_s=1.24 in^2, and the nominal U-bar yield strength of 75 ksi. The expected nominal tensile capacity of the specimens was 93 kips. The service level was determined earlier. The results of the tests are tabulated below in Table 9.2.7.

314

Table 9.2.7: Tensile test results

Specimen ID	Tensile Capacity (kip)		Deflection (in)
	Test	Calculation	Test
		Nominal	
WT-1	93.2	93.0	0.446
WT-2	88.7	93.0	0.411
WT-3	75.6	93.0	0.295
WT-4	106.6	93.0	0.350

Typically, the tensile capacity of a specimen under pure tension is a function of the amount and strength of steel if the steel is continuous. All four specimens exceeded the service level load. However, only two of the specimens, WT-1 and WT-4, exceeded the theoretical tensile capacity. Because the amount of steel was not varied among the test specimens, the tensile capacity must be attributed to the interaction between the concrete and steel as well as the steel arrangement.

The tensile capacity of WT-2, which had a decrease in f'_c from 10 to 7 ksi, was 4.6% less than the expected capacity based on nominal properties, and the tensile capacity of WT-3, which had a decrease in joint overlap length from 6 to 4 in., was 18.7% less than the expected capacity based on nominal properties. In the joint zone, the staggered U-bars tied with two lacer bars created a truss-like model. This truss model can also be considered a strut-and-tie model where the compression in the concrete represents the strut and the tension in the reinforcement represents the tie.

As a test specimen reaches failure, the load will begin to decrease while the displacement continues to increase. During the WT-4 test, the actuators did not display this behavior. The actuators would reach about 92 kips, and then the load and displacement would level off due to a problem with the system hydraulic pressure. After the system was back in full operating mode, the tension test was completed, but the only data collected beyond 92 kips were the forces and displacements of the actuators, because the other instrumentation had been removed anticipating specimen failure.

Once all the transverse joint tests were completed, load versus deflection curves were plotted. The LMT, placed at the bottom of the specimen, recorded the total deflection of the specimen under the tensile loading. Specimens had similar slopes after cracking of the concrete. As the loading increased beyond theoretical tensile capacity, the concrete began to form large cracks and crumble at the joint zone. To avoid damaging the deflection measuring device below the joint zone, the LMT was removed as the loading caused this crumbling effect. Figure 9.2.20 displays the load versus deflection curves of all four tension specimens prior to the removal of the LMT's. In the case of WT-3 where the joint overlap length was reduced from 6 to 4 in., the specimen was observed to fail at a load that was almost 20% less than the expected failure load of 93 kips.

315
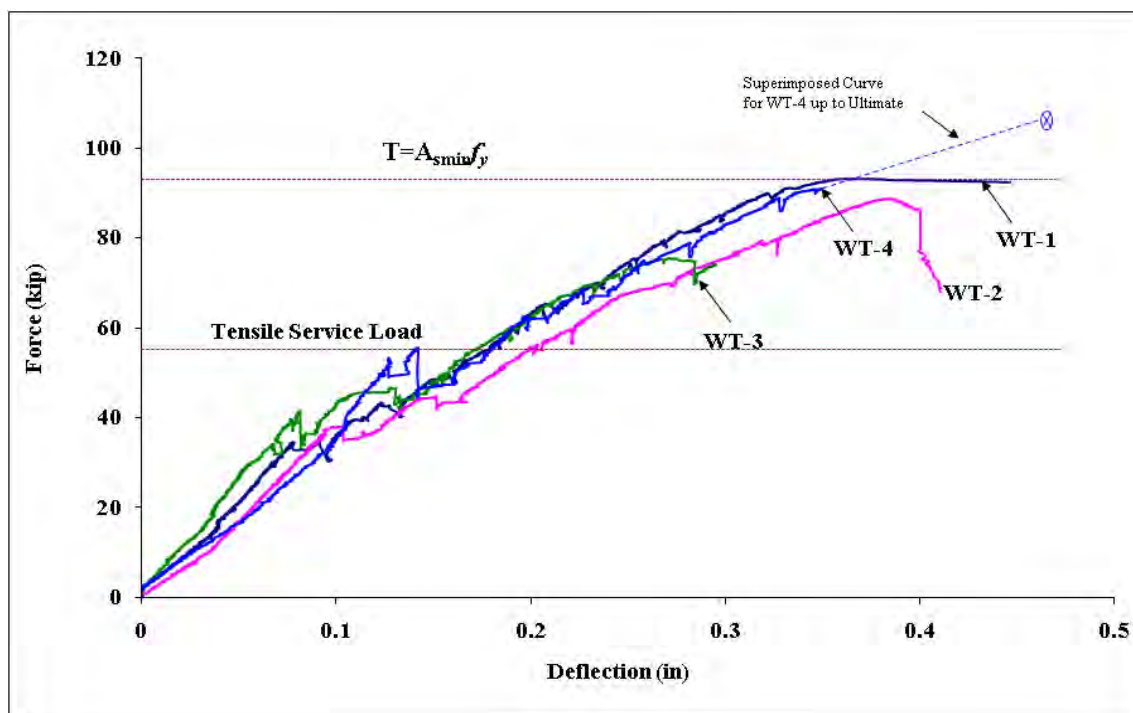
Figure 9.2.20: Load versus deflection

Tensile Specimen Behavior (Transverse Joint Behavior)

For all specimens, the first visible surface cracks developed in the transverse direction and were located outside the joint zone. As the tension loading increased, transverse cracks continued to appear in various locations outside the joint zone. For WT-1, the first cracks to appear were transverse cracks evenly spaced along the length of the specimens. The transverse cracks initially were found only on the surface of the concrete, and as the loading progressed the cracks propagated through the entire thickness of the specimens. For WT-2, the first transverse crack to develop at the joint occurred at approximately 28 kips, which was at about 30% of the nominal tensile capacity. For WT-3, the first transverse crack occurred at nearly 34 kips, at about 45% of the nominal tensile capacity. For WT-4, the first transverse crack to develop near the joint occurred at 54 kips, at about half of the nominal tensile capacity. All initial transverse cracks occurred on the side of the specimen that had a 2 in. cover measured from the reinforcement surface to the surface of concrete (the cover on the other face was 1 in. as shown in Fig. 9.2.14). As testing progressed, the cracks began to form throughout the thickness of the specimen.

For WT-1, additional loading produced longitudinal cracks that appeared above the main longitudinal reinforcement in the specimen. These longitudinal cracks appeared above the longitudinal reinforcement that comprised the lightly reinforced half of the specimen, or the top half of the specimens in this particular set-up. Longitudinal cracks began forming inside the joint zone at the following loads: 60 kips for WT-2, 44 kips for WT-3, and 70 kips for WT-4. The longitudinal cracks formed above the longitudinal reinforcement in the specimen, which relates to the longitudinal reinforcement that crosses the transverse joint in the deck of precast bridge deck system.

316

Diagonal cracks appeared in the joint as the specimens approached capacity. These diagonal cracks propagated toward the first transverse cracks that developed in the joint. The concrete could be easily removed from the specimen where the diagonal and transverse cracks met. The crack patterns at tensile failure for WT-1, WT-2, WT-3, and WT-4 can be seen in Figure 9.2.21.

The lacer bars provided confinement of concrete within the joint and served as restraints for the U-bars. The lacer bars allowed ductile failure in all four specimens (compared to the behavior of the headed bar specimens discussed earlier). An example of the deformation of the lacer bars can be seen in Figure 9.2.22. Please note that the location of the lacer bar in reference to the U-bars; the lacer bar also serves as bearing to U-bars. These "bearing" forces caused the lacer bar to bend. This interaction between the lacer bar and U-bars helps to explain the more ductile failure mode observed in the U-bar tests.

317

(a) WT-1

(b) WT-2

(c) WT-3

(d) WT-4

Figure 9.2.21: Tensile cracks at failure

318

Figure 9.2.22: Deformation of lacer bar

Tensile Crack Widths at Service Level Loading (Transverse Joint Behavior)

As calculated in Section 9.1, the tensile service load for the U-bar detail was determined to be 55.1 kips if the yield strength of reinforcement was 75.0 ksi. For the tension tests, the crack widths were measured using a crack comparator, as shown in Figure 9.2.23. However, the crack widths inside the joint zone were measured incrementally as for the flexural tests. To determine the crack widths at service-level loading, the values were interpolated as described earlier. For each specimen, the first transverse cracks that developed in the joint zone, as discussed above, were the ones measured throughout the tension tests for crack widths. The crack widths for WT-2 and WT-4 at service level were 0.020 and 0.008 in., respectively. For WT-3, the crack width at service- level loading had exceeded the limits of the comparator of 0.050 in. WT-3, with the joint overlap length of 4 in., created the largest crack width at service-level loading.

319
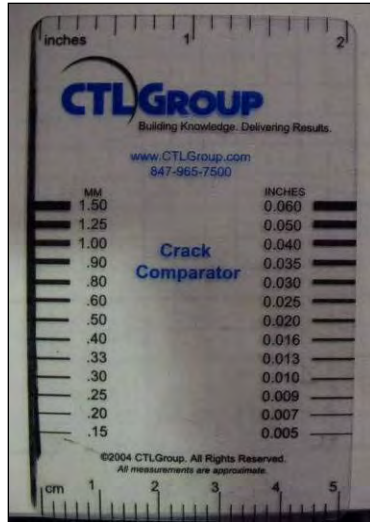
Figure 9.2.23: Crack comparator used to measure tension crack widths

Strain Gage Data (Transverse Joint Behavior)

In Figure 9.2.24, the total applied force versus strain curves for each gage location were plotted for the transverse joint tests. For the transverse joint tests, the data provided by the strain gages was not as consistent in proving increasing strain in the reinforcement. Also, the strains were smaller at each gage located further from the bearing surface in the joint. According to the strain data, only a couple of U-bars in WT-2 and WT-4 yielded at failure which was observed at the strain gage closest to the bend. As in the longitudinal joint tests, the data from the transverse joint tests were consistent in showing that the reinforcement developed large strains where diagonal cracks occurred.

320
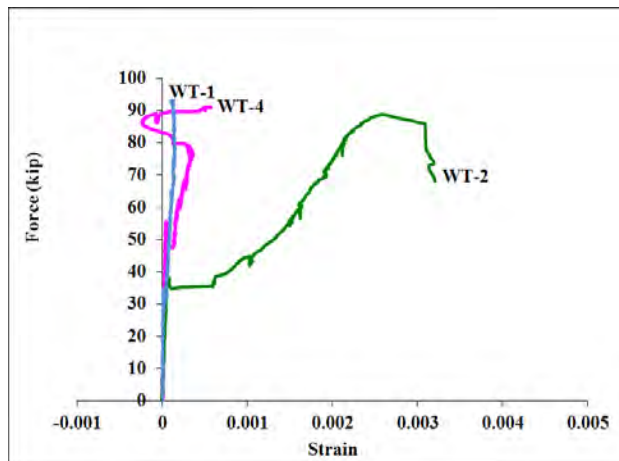
(a) Gage 2-1
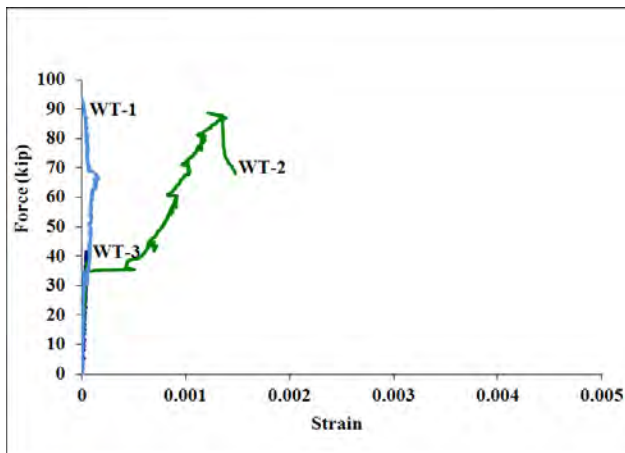
(b) Gage 2-2
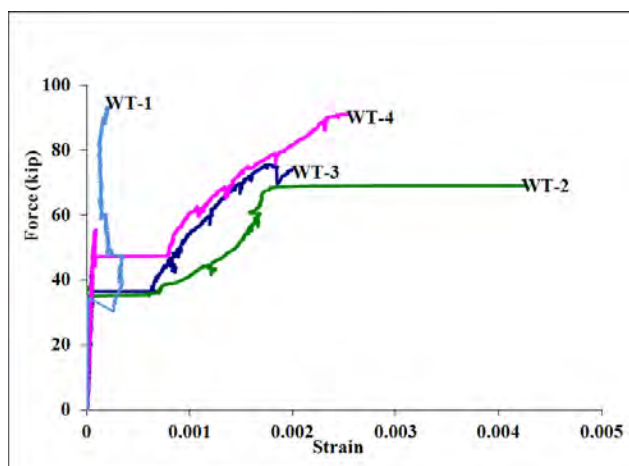
(c) Gage 2-3
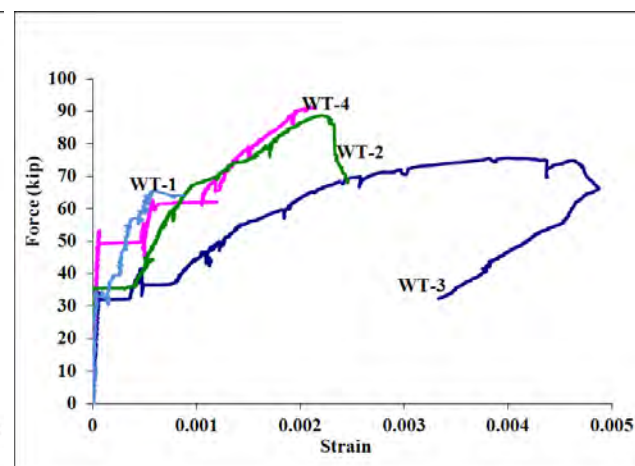
(d) Gage 3-1

321
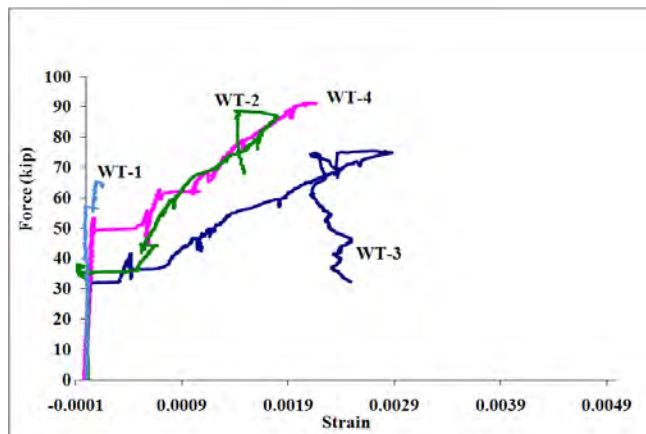
(e) Gage 3-2
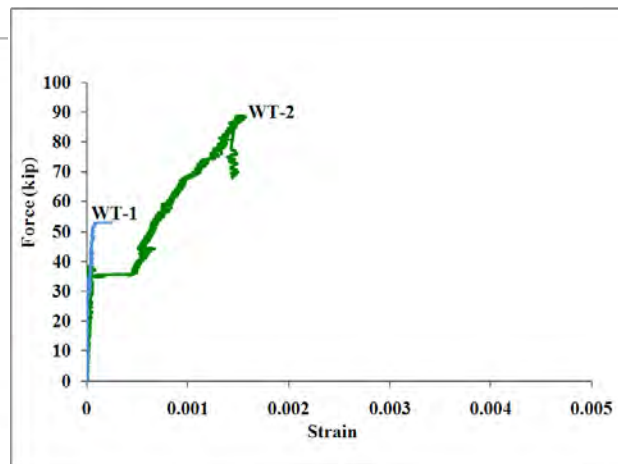
(f) Gage 3-3

(g) Gage 4-1

(h) Gage 4-2

322
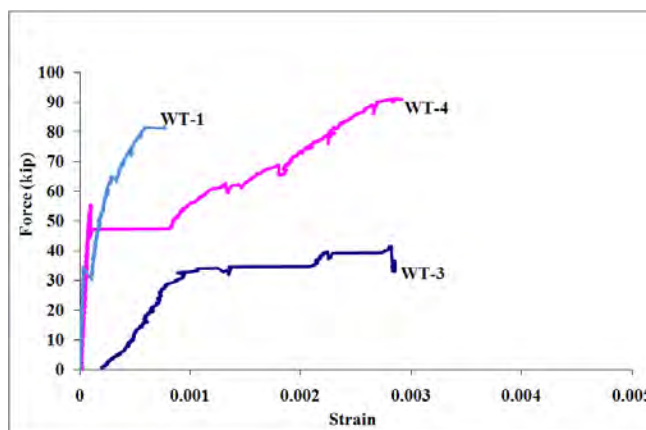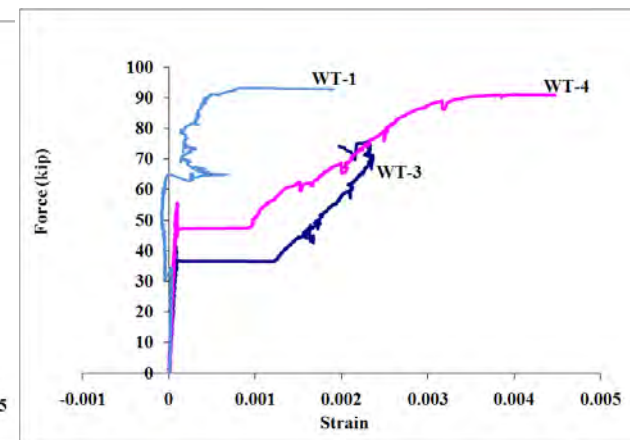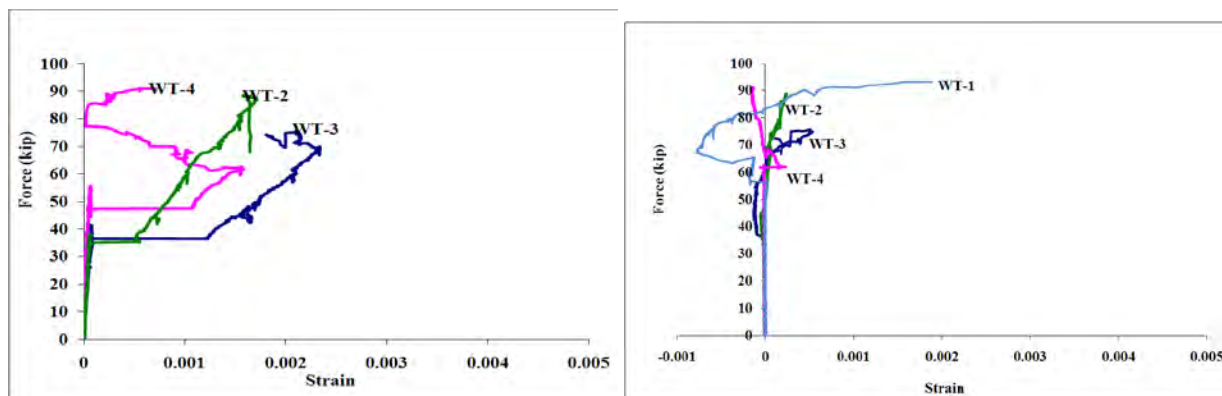
(i) Gage 4-3   (j) Gage LB 1-2

Figure 9.2.24: Force versus rebar strain for transverse joint tests

9.2.4. Conclusions for Phase II Tests

The purpose of the research in Phase II was to test variations in U-bar joint details to identify the most influential variables. Once the significance of the variables was identified, the best performing U-bar detail could be fabricated for large-scale jointed tests used to develop the design guidelines and details for both longitudinal and transverse joints in precast bridge deck systems.

The longitudinal and transverse joint specimens with a U-bar joint detail were tested in flexure and tension to represent the behavior of a precast bridge deck system. Based on the testing results of WB-1 and WT-1 of the Phase I test series, the variables considered in Phase II included concrete strength, joint overlap length, and spacing between the U-bar reinforcement. A summary of the tested variables is given in Table 9.2.8.

Table 9.2.8: Summary of tested parameters

Specimen ID		Testing Parameter	Concrete Strength	Bar Spacing	Joint Overlap Length
			(ksi)	(in)	(in)
WB-1	WT-1	Original Test Specimen	10	4.5	6
WB-2	WT-2	Decreased f'_c	7	4.5	6
WB-3	WT-3	Decreased Joint Overlap Length	10	4.5	4
WB-4	WT-4	Increased Longitudinal Reinforcement Spacing	10	6.0	6

By reducing the concrete strength, both the flexural and tensile capacities were reduced. When decreasing the joint overlap length from 6 to 4 in., the crack widths were observed to be significantly larger, the

323

flexural capacity was decreased by 17.8%, and the tensile capacity was decreased by 18.9%. Increasing the spacing of the U-bar reinforcement from 4.5 to 6 in. did not change the behaviors of longitudinal and transverse joints very much in terms of crack width, flexural capacity, or tensile capacity.

In summary, to provide adequate ductility without significant loss of strength at ultimate, the joint overlap length should not be less than 6 in. where using #5 joint reinforcement. The #4 lacer bars were observed to provide restraint to help facilitate anchorage of the U-bar details for the joint zones in both flexure and in tension, and should be included in the joint detail. It is important that the lacer bars be located at the bearing face of the U-bar.

9.3.   Conclusions

Chapter 9 presents the results of a study that assessed potential alternate details for longitudinal and transverse joints based on constructability, performance and cost. In the Phase I test series, six reinforced concrete specimens were tested. Three of the specimens represented longitudinal joint connections (flexural specimens) and three represented transverse joint connections (tension specimens). The three joint details investigated included (1) lapped headed reinforcement, (2) lapped U-bar reinforcement fabricated with deformed wire, and (3) lapped U-bar reinforcement fabricated with stainless steel. The three specimens tested in flexure were subjected to forces that would be experienced in a longitudinal deck joint, and three specimens tested in tension were subjected to forces that would be experienced in a transverse joint over an interior pier.

The capacities of the joint details were used for comparison and the selection of the best performing joint detail. All joint details produced adequate capacities and ductility in both the tension and flexural tests. Specimens with U-bar details and headed bar details both produced a capacity corresponding to their respective nominal design yield strengths. Because the U-bars had a higher nominal design yield strength (i.e., 75 ksi) than the headed bars (i.e., Grade 60), specimens containing the U-bar joint detail produced the largest capacities in both the bending and tension tests without compromising ductility. Smaller crack widths at service-level loading were also produced by the U-bar detail when compared to the headed bar detail.

The constructability and reinforcement costs of the joint details were also compared. The U-bar detail created a less congested joint, which made it the easiest to construct. The bearing heads of the headed bar detail require more space due to the larger diameter of the rebar heads. This extra space reduces construction tolerances and could therefore cause problems in placement of precast deck components. The U-bars can also be easily tied together to form a rebar cage, which would allow for easy construction in the precast yard when compared to the two single layers of reinforcement in the headed bar detail. The lowest material cost was the conventional rebar used for the headed bars. The material costs were competitive between the conventional rebar used in the headed bars and the deformed wire reinforcement. The stainless steel reinforcement had the highest cost.

After consideration of capacity, service level crack widths, constructability, and cost, the U-bar detail, with an overlap length of 6 in., a rebar spacing of 4.5 in. and two transverse lacer bars, constructed of deformed wire reinforcement was recommended for the Phase II tests.

In the Phase II tests, another six specimens with the U-bar detail were tested, three in flexure and three in tension, to investigate effects of variables including overlap lengths, rebar spacings, and concrete strengths. Based on results of the Phase II tests, the following conclusions can be made.

By reducing the concrete strength, both the flexural and tensile capacities are reduced. When decreasing the joint overlap length from 6 to 4 in., the crack widths were significantly enlarged, the flexural capacity was decreased by 17.8%, and the tensile capacity was decreased by 18.9%. Increasing the spacing of the U-bar reinforcement from 4.5 to 6.0 in. was not observed to significantly change the behaviors of longitudinal and transverse joints in terms of their crack widths, flexural capacities, and tensile capacities. In order to provide adequate ductility without significant loss of strength at ultimate, the joint overlap length should not be less than 6 in. and #4 lacer bars should be provided to enhance the mechanical anchorage of the U-bars.

325

Chapter 10 Flange/Deck Connection: Numerical Studies to Determine Forces to be Applied in Large-Scale Tests

10.1. Investigation of Maximum Forces in the Longitudinal Joints

10.1.1. Introduction

The objective of the numerical study described in this chapter was to develop a database of maximum forces for determination of the loading demand on the longitudinal joints due to service live loads. This information was subsequently used in the large-scale laboratory investigations to evaluate the performance of the joints. The effects of individual variables were researched by performing parametric studies using ABAQUS. The following variables were considered:

- Girder geometry including depth, span, and spacing
- Single-lane loading and multi-lane loading
- Bridge Skew
- Impact of cracking of joints

The decked bulb-T (DBT) girder was chosen for this study. Table 10.1.1 summarizes the practical span ranges for typical girder sections (i.e., girder depths of 41, 53 and 65 in.). The girder section was named by the girder depth, such as section "DBT41" referring to a DBT girder with 41 in. depth. For each girder section, there were three different girder spacings investigated: 4, 6 and 8 ft. Figure 10.1.1 shows the cross section of the DBT girder.

Table 10.1.1: Practical span ranges for optimized DBT girders

Section	Spacing (ft)	Span (ft)	
		Minimum	Maximum
DBT41	4	84	124
	6	72	130
	8	64	118
DBT53	4	98	150
	6	84	156
	8	76	148
DBT65	4	108	172
	6	94	180

326

	8	84	176
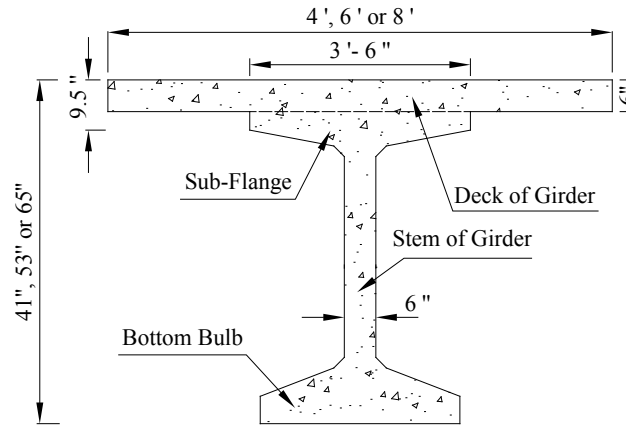
Figure 10.1.1: Cross section of optimized DBT girder

10.1.2. Description of Bridge Parameters

Table 10.1.2 summarizes the seven bridge models with different girder geometry and bridge skew developed for the parametric study. Bridges A, B, C and D were straight bridges with various girder geometry (depth, spacing and span). Bridges D, E, F and G had the same girder geometry with different bridge skews.

Table 10.1.2: Summary of the seven bridge models

Bridge	Girder		Span	Skew
	Depth (inch)	Spacing (ft)	(ft)	(degree)
A	65	8	134	0
B	65	8	84	0
C	65	4	108	0
D	41	8	118	0
E	41	8	118	45
F	41	8	118	30
G	41	8	118	15

327

All seven bridges were simply supported. The use of diaphragms between adjacent girders, as shown in Figure 10.1.2, would decrease the load transferred across the longitudinal joint. Consequently, only a single diaphragm (i.e., the minimum diaphragm configuration that would be used in practice) was assumed in the models to maximize the loads on the longitudinal joint. The single intermediate steel diaphragm (ISD) was assumed at midspan of the bridge to connect the web and bottom flange of the girders. Both the inclined member and horizontal member of the ISD used L 3x3x3/8 in. steel angles which had a cross-sectional area of 2.11 in^2. The deck of the adjacent girders was connected by the proposed continuous longitudinal joint shown in Figure 10.1.3 as discussed in Chapter 9.
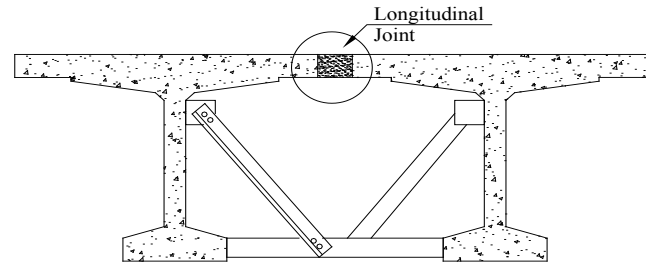
Figure 10.1.2: Steel diaphragm connecting adjacent girders at midspan
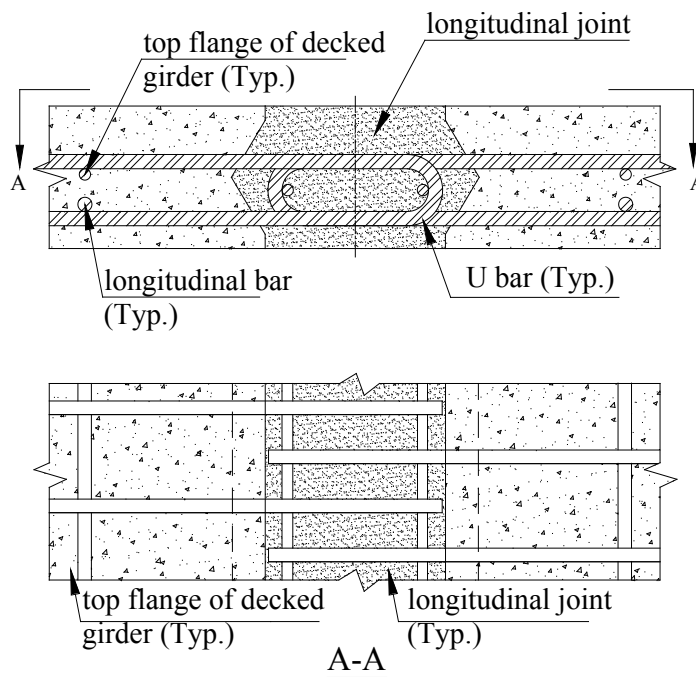
Figure 10.1.3: Proposed continuous longitudinal joint

All of the bridge models in Table 10.1.2 had the same bridge width of 40 ft; a modified version of bridge model B was later added to investigate the effect of bridge width. Figure 10.1.4-(a) to Figure 10.1.4-(d) show the cross-sectional views of the four straight bridges and Figure 10.1.5-(a) to Figure 10.1.5-(c) show the plan views of the three skew bridges. The joints between girders were labeled as "Joint 1", "Joint 2" and so on from left to right. Because of the symmetry of each bridge in the width direction, the forces in the joints located in the left half of each bridge were studied. The metal railing was not shown in these sketches because only the live load was considered in the study, and the railing was assumed to have a negligible effect on the bridge stiffness.

(a) Bridge A (65 in. deep; 96 in. spacing; 134 ft span)

(b) Bridge B (65 in. deep; 96 in. spacing; 84 ft span)

(c) Bridge C (65 in. deep; 48 in. spacing; 108 ft span)

(d) Bridge D (41 in. deep; 96 in. spacing; 118 ft span)
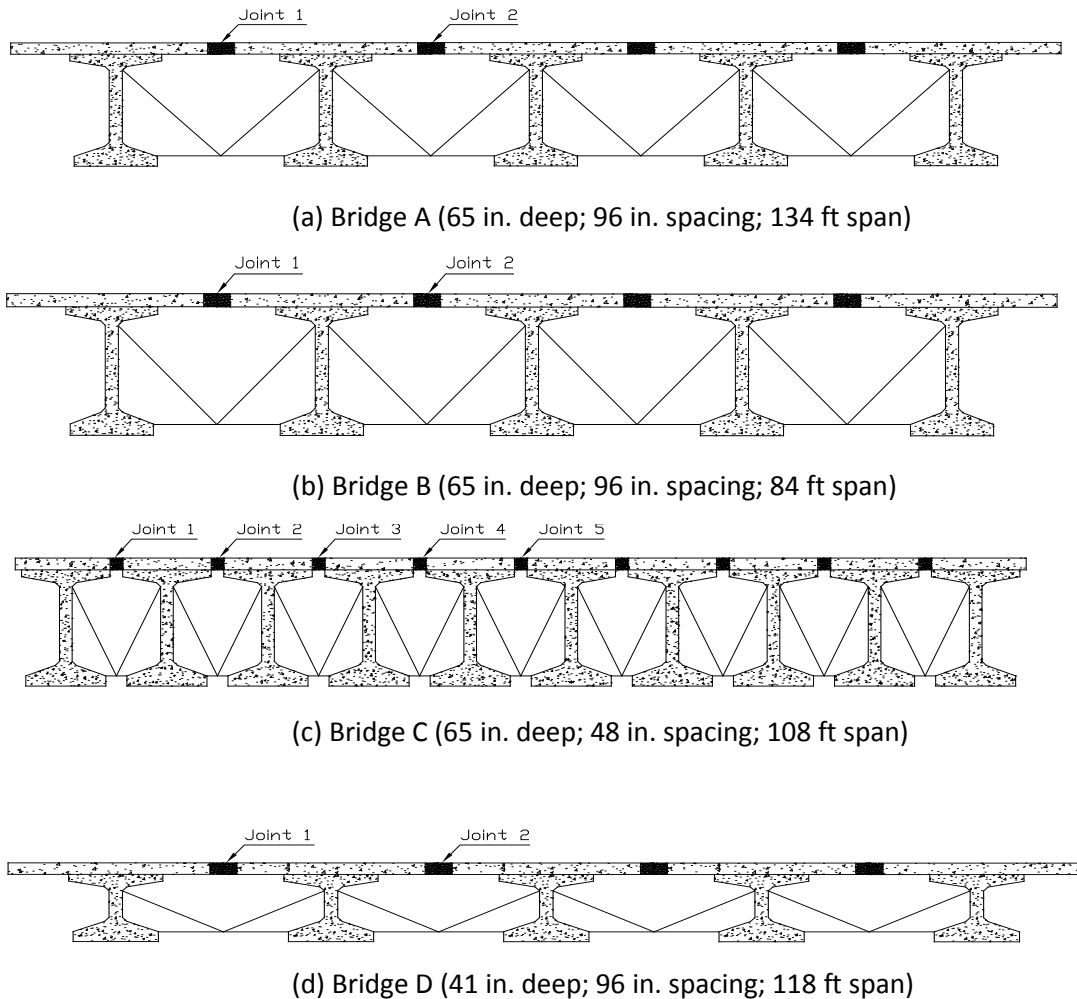
Figure 10.1.4: Cross section of bridge models

329

(a) Bridge E   (b) Bridge F   (c) Bridge G
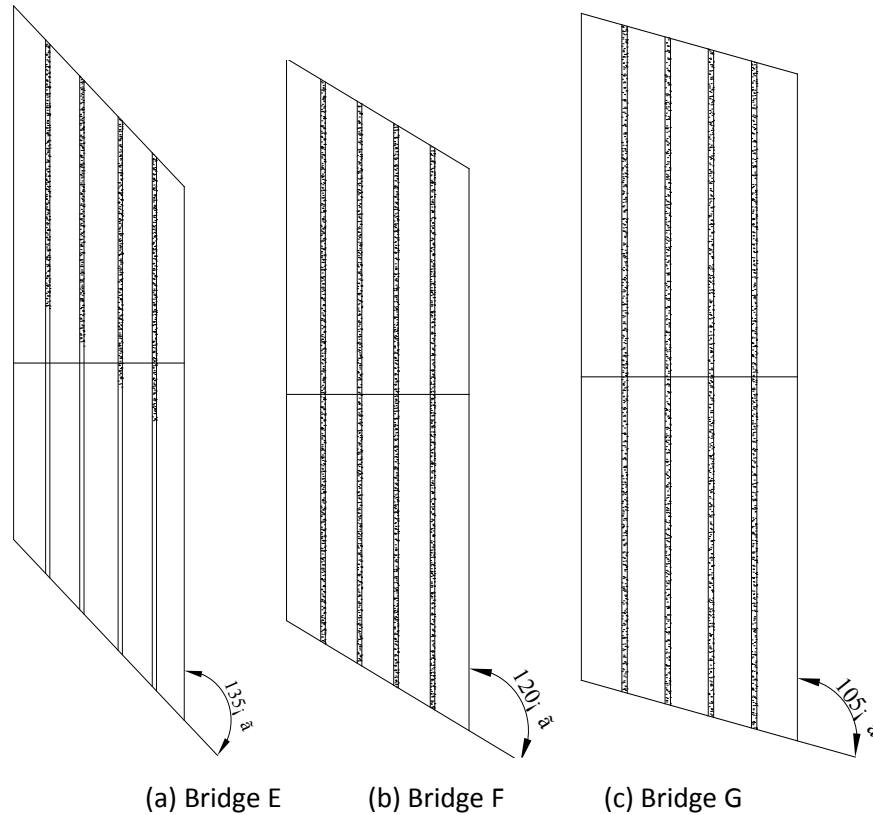
Figure 10.1.5: Plan view of skewed bridge models

10.1.3. Description of Loadings

The AASHTO LRFD Bridge Design Specification HL-93 live load was used in the study. The HL-93 live load consisted of a design vehicle load and lane load. The design vehicle was either a design truck or design tandem whichever could produce the larger forces. Figure 10.1.6 shows the dimensions and wheel weights of the HL-93 live load. The tire contact area for the design vehicle was 10 by 20 in. The dynamic load allowance was applied to the design vehicle load but not to the lane load. The length of the lane load was varied to produce the largest load effects. The distance between middle wheel and rear wheel of the truck load could vary from 14 ft to 30 ft to produce the largest load effects. In the parametric study, multiple presence factors of 1.2 and 1.0 were used for single-lane loading and multi-lane (i.e., two-lane) loading, respectively.

330
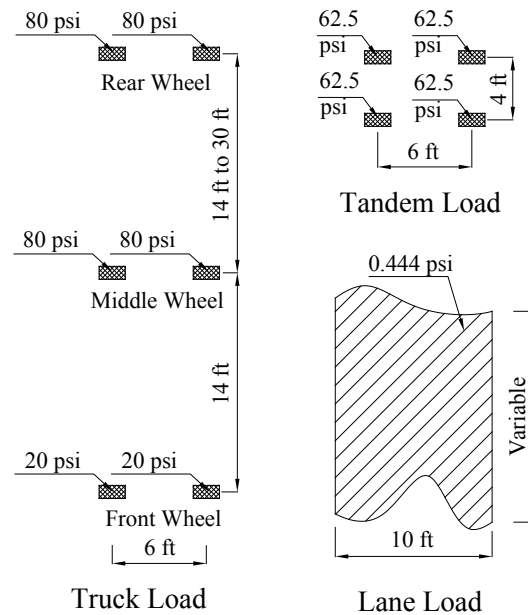
Figure 10.1.6: Dimensions and wheel weights of the HL-93 live load

10.1.4. Development of Finite Element Models

Three-dimensional (3D) finite element (FE) modeling was completed using ABAQUS 6.7.1. The bridge modeling consisted of three main components: intermediate steel diaphragms at midspan, DBT girders, and the continuous longitudinal joint connection between the top flanges of adjacent girders (Figure 10.1.7). The inclined members of the steel diaphragm were modeled using 3D two-node truss elements (T3D2); the horizontal member was modeled using 3D two-node beam elements (B31) as shown in Figure 10.1.7-a. The angle between the inclined member and horizontal member was dependent on the depth and the spacing of the girder. The major portion of the DBT girder, including the bottom bulb, stem, sub-flange, and the deck directly above the sub-flange, was modeled using 3D twenty-node solid elements (C3D20) as shown in Figure 10.1.7-b.

The remainder of the model consisted of the longitudinal joint that provided continuity of the deck between the DBTs by connecting the outer edges of the girder flanges shown in Figure 10.1.2. This was the main area of interest in this study. Sensitivity analyses were carried out to compare results using various modeling approaches for this area of the deck. Shell elements were used in lieu of solid elements in the sensitivity analyses to facilitate the determination of moments and shear forces in the longitudinal joint. Based on the results of the analyses (i.e., moments and shears compared at the longitudinal joints of bridges assuming only one interior transverse diaphragm at midspan), this area of the deck, including the continuous longitudinal joint connection, was modeled using 3D eight-node thick shell elements (S8R), as shown in Figure 9.1.7-c.

331
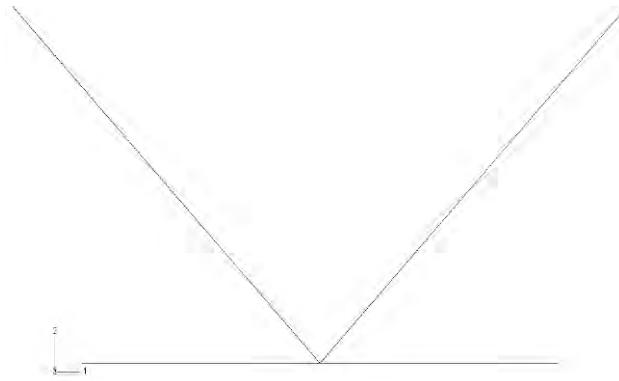
(a) Intermediate steel diaphragm
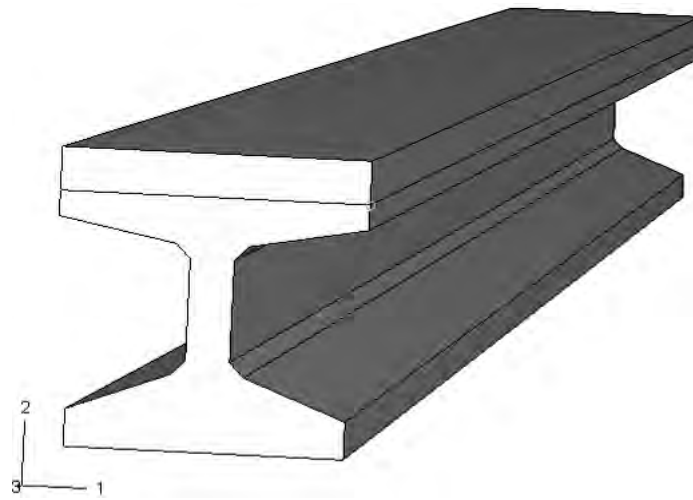
(b) Decked bulb-T (DBT) girder
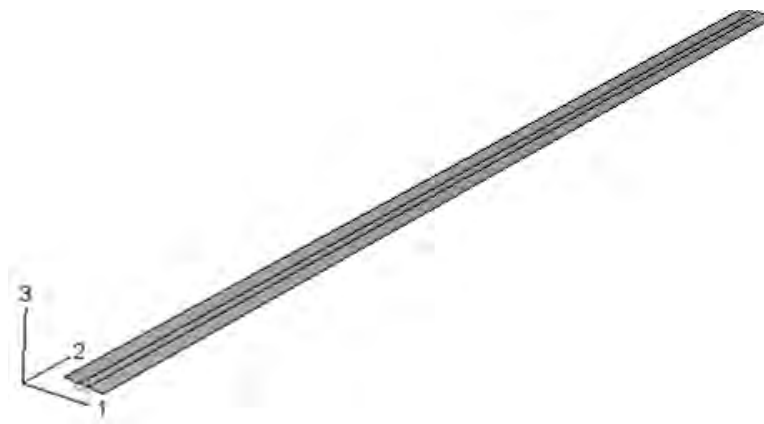
(c) Continuous longitudinal joint connection

Figure 10.1.7: Bridge components modeled by 3D finite elements

Different material properties were assigned to different bridge components. The Young's modulus for the stem of the girder including the bottom bulb and sub-flange was 4,769 ksi (based on 7 ksi compressive strength), the modulus for the deck of the girder was 3,605 ksi (based on 4,000 psi compressive strength), and the modulus for the steel diaphragm was 29,000 ksi. The Poisson's ratios for the concrete and steel were taken as 0.18 and 0.3, respectively. A sufficiently refined mesh was used to ensure the results from the 3D FE models were adequate.

The bridge models were assumed to be simply supported at the ends. In the 3D FE models (Figure 10.1.8), a roller support was modeled at one end by restraining the vertical movement (direction 3) of the bottom flange of the girders. The pinned support at the other end was modeled by restraining the movements of girder bottom flanges in both the girder length and vertical directions (direction 2 and 3). In the transverse direction (direction 1), both end sections of the girder were restrained to simulate concrete end diaphragms. The developed 3D FE models were calibrated and discussed in detail by Ma et al. 2007.
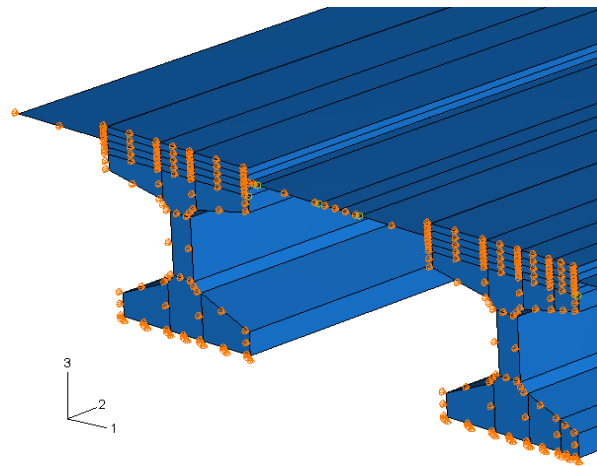
Figure 10.1.8: Boundary conditions at pinned end

10.1.5. Parametric Study

Based on the bridge models and vehicle loading discussed above, parametric studies were conducted to determine the maximum forces in the longitudinal joint. The following parameters were considered: different loading locations, effect of bridge width, combination of design truck and lane loading versus combination of design tandem and lane loading, girder geometry (depth, spacing and span), bridge skew, single-lane loading versus multi-lane loading, and impact of cracking of the joints. The maximum bending moment and maximum vertical shear in the longitudinal joints were the focus of the study.

10.1.5.1.　　　Effect of Loading Locations

Lane Loading. The effect of the extent of the lane loading on the maximum moments and shear in Joint 1 were studied with bridge model A (see Figure 10.1.4), considering its wider girder spacing and longer span.

The combination of design truck load and lane load was chosen to produce the maximum forces in the joint, the extreme condition of the design truck load with 14 ft between the middle wheel and rear wheel was applied in the study. Figure 10.1.9 shows the loading positions for the study of bending moment in Joint 1. The design truck was positioned at the same location in the two cases. In the longitudinal direction, the truck was located to produce the maximum moment in the bridge, and in the transverse direction, the center of the left wheels of the truck was located directly on top of Joint 1 to produce the maximum bending moment in the joint according to the influence line analysis. The length of lane load was varied. In case (a), the lane load was terminated at the center of the rear wheel of the truck while in case (b), the lane load was fully applied along the bridge in the longitudinal direction. The maximum bending moments with the corresponding vertical shear in the Joint 1 are shown in Table 10.1.3.

Table 10.1.3: Forces in Joint 1 due to loads applied in accordance with Figure 10.1.9

Load Positions	Forces in Joint 1	
	Maximum Moment (kip-ft/ft)	Corresponding Shear (kip/ft)
Case (a)	5.34	0.09
Case (b)	5.50	0.11

As shown in Table 10.1.3, the maximum moment in the two cases were very close which meant the position of lane load had little effect on the moment in the joint. The values of the corresponding vertical shear were very small and close to zero indicating that there was almost no shear while the maximum moment was produced in the joint.

334
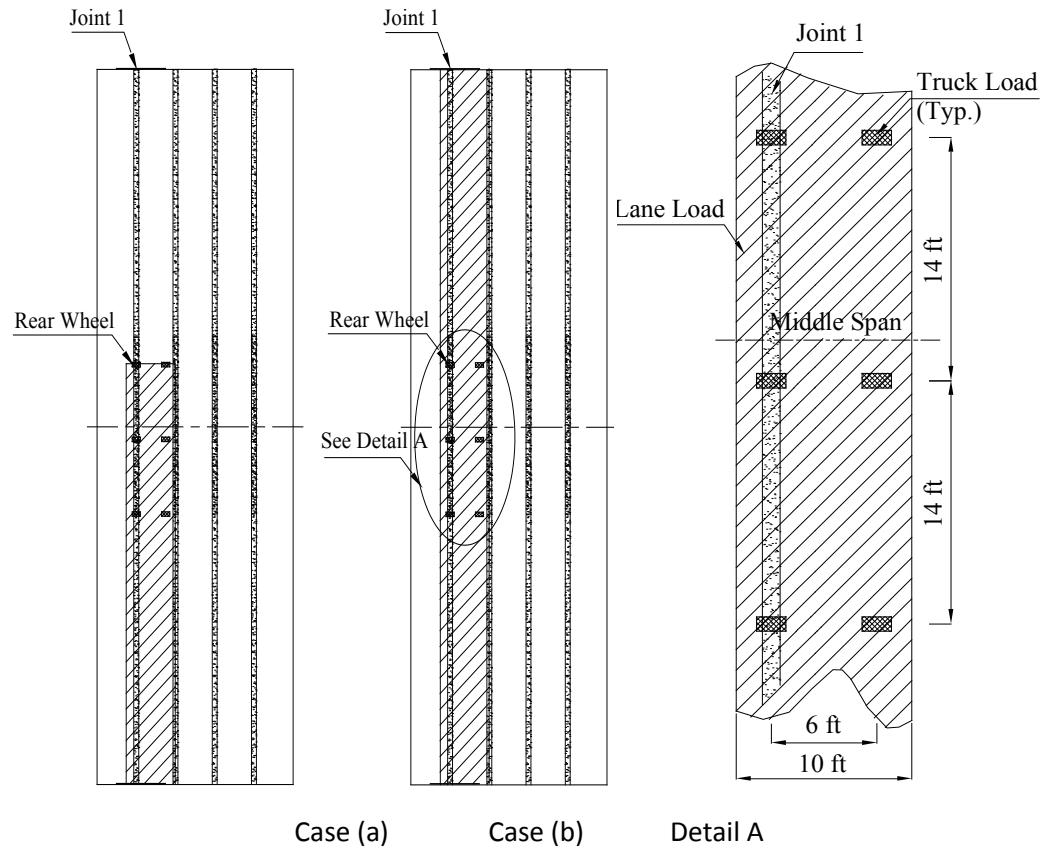
Figure 10.1.9: Lane loading positions for moment

Figure 10.1.10 shows the loading positions for the study of vertical shear. In the longitudinal direction, the design truck load was located at the same position as for the case of the moment study. In the transverse direction, the left edge of left wheels was located directly on top of Joint 1 to produce the maximum vertical shear in the joint according to the influence line analysis. There were three different lane loads investigated as shown in cases (a) through (c), respectively: fully along the bridge; terminated at the center of the middle wheels; and terminated at the center of the rear wheels. The maximum shear with the corresponding moment for each load case is presented in the Table 10.1.4.

335
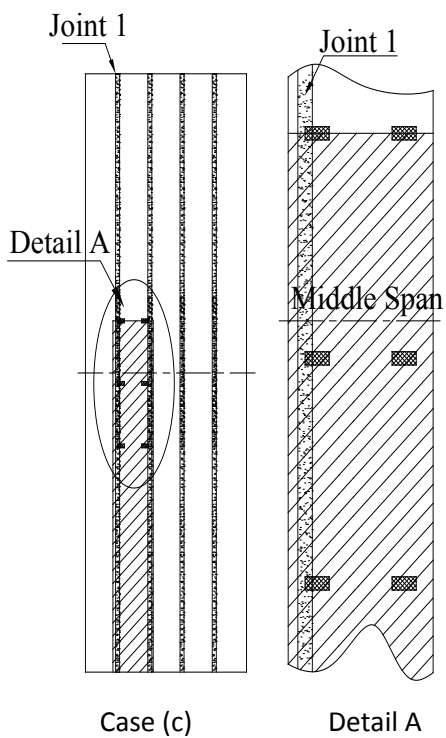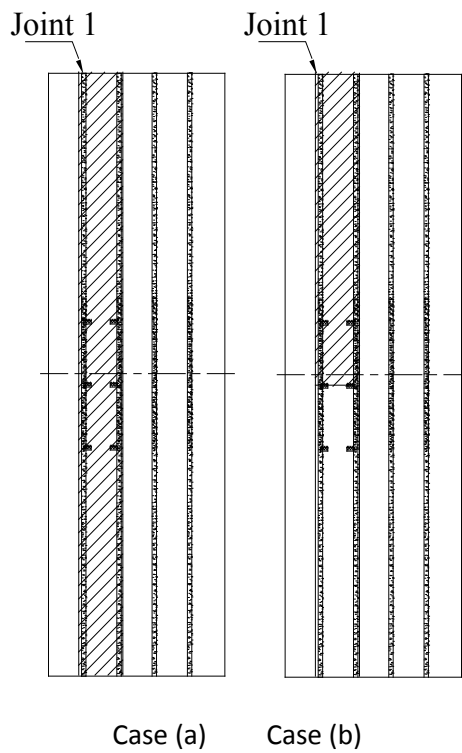
Figure 10.1.10: Lane loading positions for shear

336

Table 10.1.4: Forces in Joint 1 due to loads applied in accordance with Figure 10.1.10

Load Positions	Forces in Joint 1	
	Corresponding Moment (kip-ft/ft)	Maximum Shear (kip/ft)
Case (a)	3.76	4.93
Case (b)	3.60	5.92
Case (c)	3.72	6.02

From Table 10.1.4, it can be seen that cases (b) and (c) produced larger maximum shears than case (a); however, the difference was not significant. As long as the lane load was terminated at the heavy truck wheel (middle wheel or rear wheel), the difference of the maximum shear in the two cases was negligible.

In summary, the lane load which was fully applied along the bridge length direction produced the largest moment in the joint while the lane load that terminated at the center of the rear truck wheel produced the largest shear in the joint.

Truck/Tandem Loading Positions The effects of the truck and tandem loading positions on the maximum moments and shear generated in Joint 1 were also studied with the bridge model A. Figure 10.1.11 shows the loading positions for the study of bending moment. In all six cases, the lane load was fully applied along the bridge length direction. For the truck load, the center of the left wheel was located directly on top of Joint 1 (Figure 10.1.9-detail A) in the transverse direction. In the longitudinal direction, the truck positions were specified by the distance between the center of the front wheel and the midspan of the bridge. The results of maximum moment in Joint 1 and the corresponding shear are given in Table 10.1.5.

337
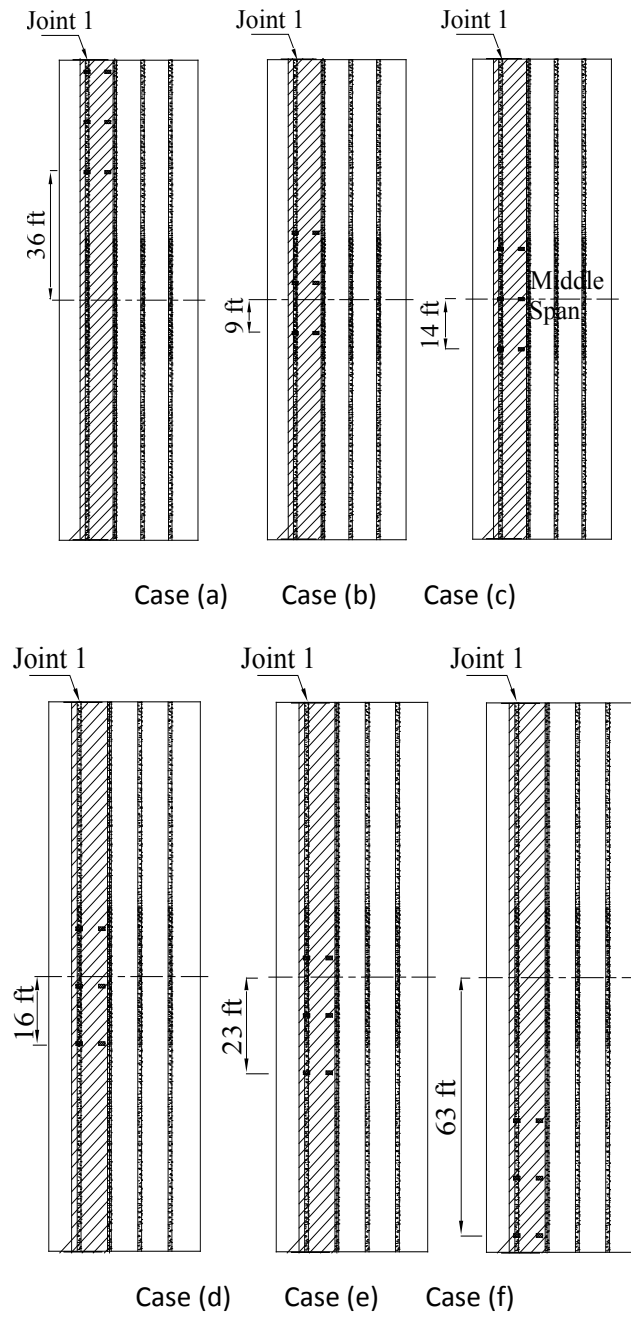
Figure 10.1.11: Truck load positions for moment

338

Table 10.1.5: Forces in Joint 1 due to loads applied in accordance with Figure 10.1.11

Load Positions	Forces in Joint 1	
	Maximum Moment (kip-ft/ft)	Corresponding Shear (kip/ft)
Case (a)	5.39	0.04
Case (b)	5.50	0.05
Case (c)	5.50	0.09
Case (d)	5.50	0.11
Case (e)	5.49	0.14
Case (f)	5.49	0.07

As shown in Table 10.1.5, all six cases produced approximately the same maximum moment in Joint 1. Truck loads with heavy wheels (middle wheels and rear wheels) located near midspan (Cases b-e) produced 2% more moment than the truck loads with heavy wheels located farthest from midspan (Cases a and f). Consequently, while load case (d) produced the largest maximum moment, the influence of the truck load position on the maximum moment was negligible.

Figure 10.1.12 shows the loading positions for the study of vertical shear. In all four cases, the lane load was terminated at the center of truck rear wheel. For the truck load, the left edge of the left wheel was located directly on top of Joint 1 (Figure 10.1.10-detail A) in the transverse direction. In the longitudinal direction, the truck positions were specified by the distance between the center of the front wheel and the midspan of the bridge. The maximum shears and corresponding moments obtained in Joint 1 are given in Table 10.1.6.

339
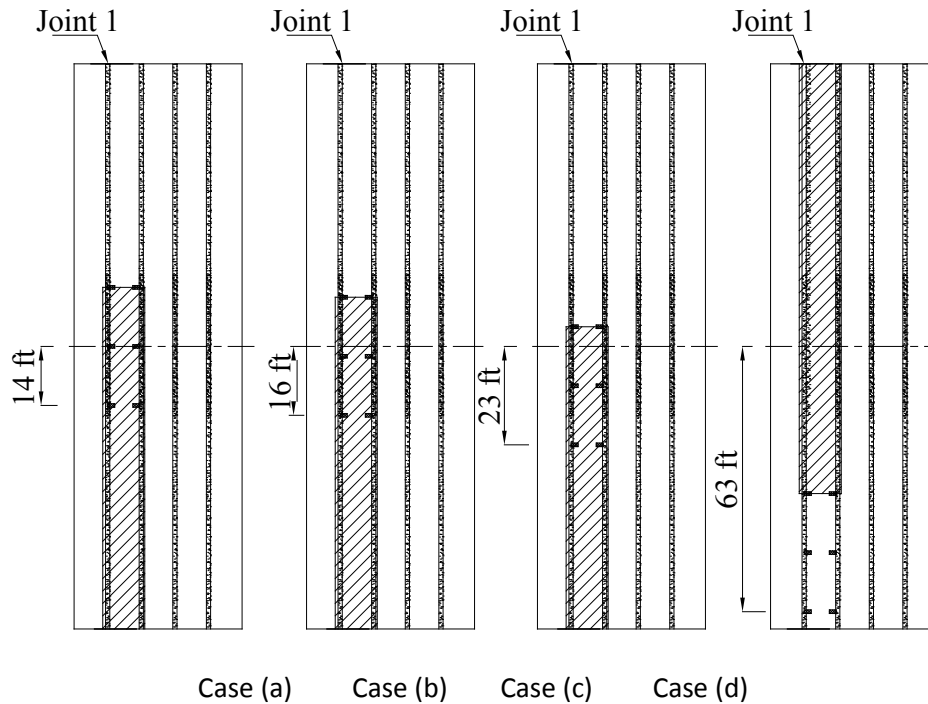
Figure 10.1.12: Truck load positions for shear

Table 10.1.6: Forces in Joint 1 due to loads applied in accordance with Figure 10.1.12

| Load Cases | Forces in Joint 1 | |
	Corresponding Moment (kip-ft/ft)	Maximum Shear (kip/ft)
a	3.82	5.81
b	3.72	6.02
c	3.61	5.95
d	2.80	5.39

As shown in Table 10.1.6, truck loads with heavy wheels (middle wheels and rear wheels) located near midspan (Cases a- c) produced larger shear forces than truck loads with the heavy wheels located further away from midspan (Case d). For truck loads with the heavy wheels located near midspan, the variation in maximum shear force in the joint was only 3%.

As for the investigation of the truck load position, bridge model A was also used to investigate the effect of the tandem loading position on the maximum moment and shear in Joint 1. Figure 10.1.13 shows the locations of the tandem load combined with the lane load to produce the maximum moment or shear in

340

the joint. In Figure 10.1.13-a, the tandem was located to produce maximum moment in the longitudinal direction of the bridge, while in the transverse direction, the center of left wheels of the tandem was located directly on top of Joint 1. The lane load was applied fully along the bridge length. In Figure 10.1.13-b to determine maximum shear, the tandem was positioned at the same location in the longitudinal direction, while in the transverse direction; the left edge of the left wheels was located directly on top of Joint 1. The lane load terminated at the center of the rear tandem wheel.

In summary, the influence of truck load position in the longitudinal direction on the maximum moment and shear in the joint was not significant while truck loads with heavy wheels located near midspan produced the largest maximum moment and shear.

In summary, the influence of the location of the vehicle load (truck or tandem) in the longitudinal direction on the maximum forces in the joint was not significant. The truck with heavy wheels (middle wheel or rear wheel) or the tandem located around midspan of the bridge produced a slightly larger moment and shear than the other locations.

341

Joint 1

Joint 1

Lane Load

See Detail A

Middle Span

4 ft

Tandem Load
(Typ.)

6 ft

10 ft

Detail A

(a): Maximum Moment

Joint 1

Joint 1

Tandem Load
(Typ.)

See Detail B

Middle Span

4 ft

Lane Load

6 ft

10 ft

Detail B
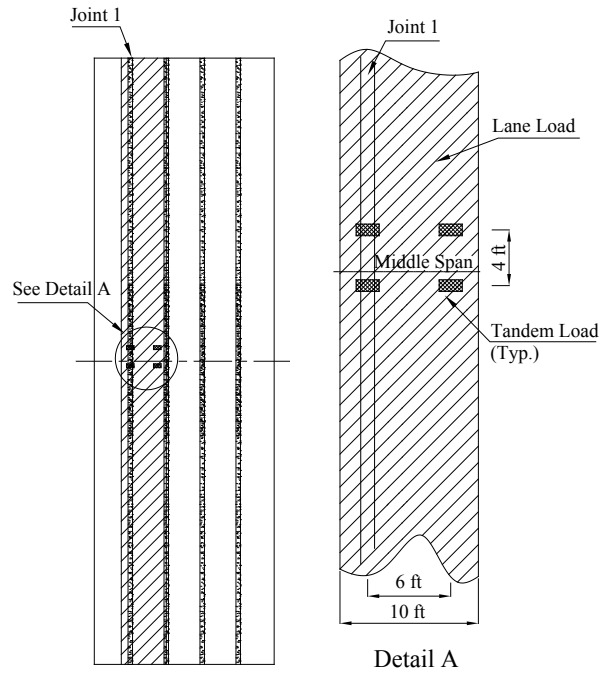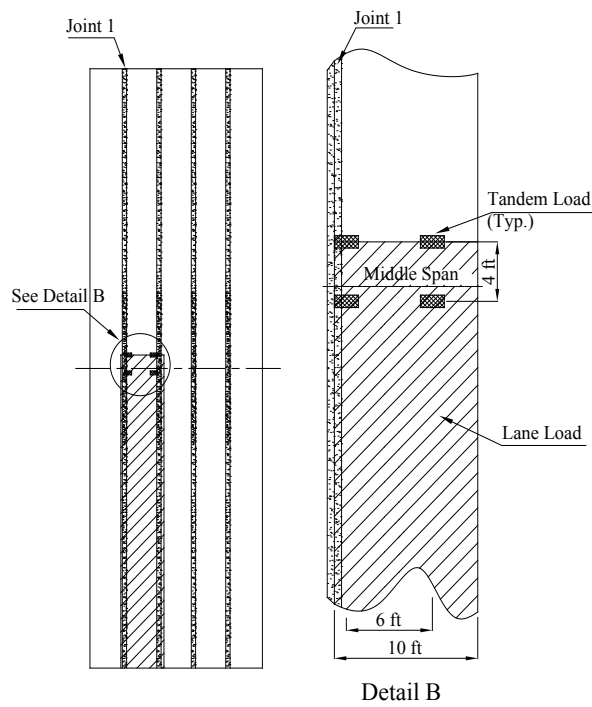
(b): Maximum Shear

Figure 10.1.13: Tandem load positions for maximum moment and shear

342

10.1.5.2.   Effect of Bridge Width

Figure 10.1.14 shows the effect of the bridge width on the maximum negative moment in Joint 2 of bridge model B. Joint 2 was studied because joints closer to the middle of the bridge deck will experience larger negative moments when loads are applied closer to the edge of the deck. The position for the left loading was the same for all three cases (i.e., the left edge of the left lane loading was 2 ft away from the left edge of the bridge based on the requirement specified in the AASHTO LRFD (2010)). The position of the right loading was varied. The right edge of the right lane loading was 10, 6 and 2 ft away from the right edge of the bridge for Cases (a) through (c), respectively. Table 10.1.7 summarizes the results for the maximum negative moment under the three loading cases.
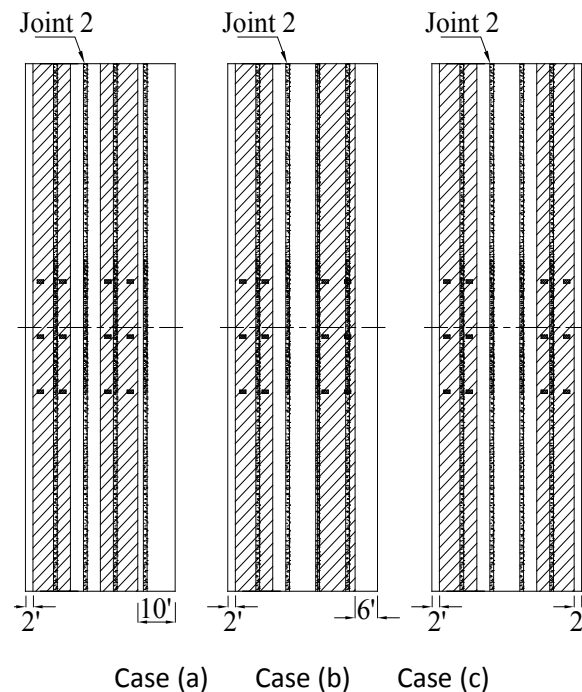
Figure 10.1.14: Load positions for negative moment on bridge model B

Table 10.1.7: Negative moment in Joint 2 due to loads applied in accordance with Figure 10.1.14

Load Positions	Maximum Negative Moment (kip-ft/ft)
Case a	-0.66
Case b	-1.00
Case c	-1.03

343

As shown in Table 10.1.7, it appeared that the maximum negative moment increased with the increase in distance between the two loadings in the transverse direction such that a larger negative moment would be expected to be produced in a wider bridge. In order to study the impact of bridge width on the negative moment, a "modified bridge B" (adding one more girder) was developed in the study. Figure 10.1.15 shows the cross section of the modified bridge model B.
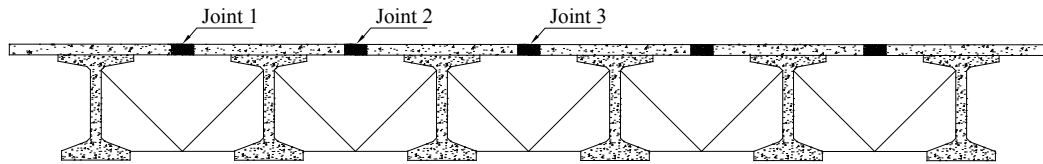
Figure 10.1.15: Cross section of Modified Bridge B

Figure 10.1.16 shows the multi-lane loading positions on the modified bridge model B to produce negative moment in Joints 2 and 3. The left edge of the left lane loading was 2 ft away from the left edge of the bridge while the right edge of the right lane loading was 2 ft away from the right edge of the bridge. The maximum negative moments in Joints 2 and 3 are summarized in Table 10.1.8.
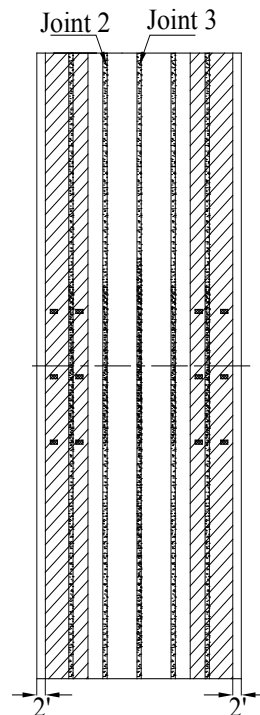
Figure 10.1.16: Loading positions for negative moment on modified bridge model B

344

Table 10.1.8: Negative moment in Joints 2 and 3 due to loads applied in accordance with Figure 10.1.16

Modified Bridge B	Maximum Negative Moment (kip-ft/ft)
Joint 2	-0.67
Joint 3	-0.87

The maximum negative moment in modified bridge model B, given in Table 10.1.8, was less than that of bridge model B, given in Table 10.1.7.

The maximum positive moment and shear were also studied between bridge B and modified bridge B. The maximum forces under different loading locations are presented in Table 10.1.9.

Table 10.1.9: Maximum positive moment and shear comparison between bridge B and modified bridge B

	Bridge B		Modified Bridge B	
	Moment (kip-ft/ft)	Shear (kip/ft)	Moment (kip-ft/ft)	Shear (kip/ft)
Joint 1	5.03	5.65	5.03	5.63
Joint 2	5.23	5.90	5.15	5.69
Joint 3			5.10	5.69

From Table 10.1.9, the maximum positive moment and shear in the modified bridge model B were less than those found for bridge model B; however, the difference was negligible. In summary, increasing the bridge width decreased the maximum negative moment in the joints while it had a negligible effect on the maximum positive moment and the maximum shear.

10.1.5.3. Truck and Lane Loading versus Tandem and Lane Loading

The HL-93 live load has two different loading combinations: one combination was truck load plus lane load; the other combination was tandem load plus lane load. Generally, the truck and lane load combination produce larger forces on long-span bridges; while the tandem and lane load combination produce larger forces on short-span bridges (where the span of the bridge is comparable to the distance from the front wheel to the rear wheel of the truck). In order to determine the effect of different loading combinations on the maximum forces in the joint for practical span ranges of DBT girders, the maximum forces under two

345

loading combinations both for the long-span bridge (bridge model A) and the short-span bridge (bridge model B) were studied.

Figure 10.1.17 shows a comparison of the maximum moment and shear in Joints 1 and 2 produced by different loading combinations in the long-span bridge (bridge model A). The label "Truck" means truck and lane load combination while "Tandem" refers to the tandem and lane load combination.
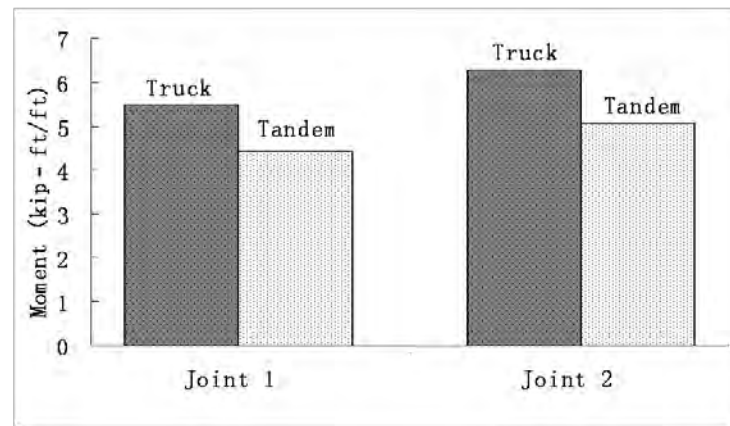
(a) Moment
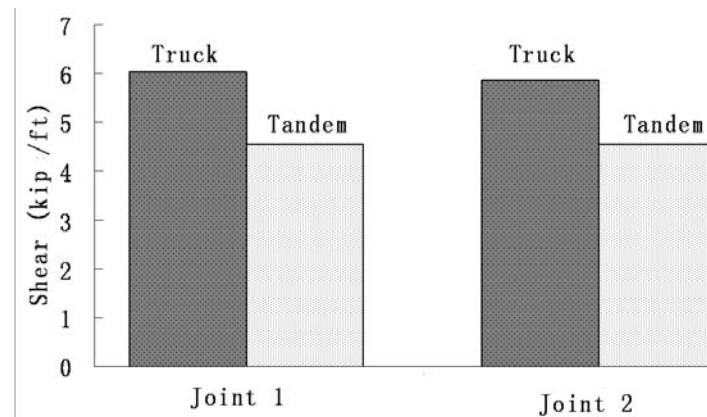
(b) Shear

Figure 10.1.17: Moment and shear comparison in long-span bridge (A)

Figure 10.1.18 shows a comparison of the maximum moment and shear in Joints 1 and 2 produced by different loading combinations in the short-span bridge (bridge model B).

346
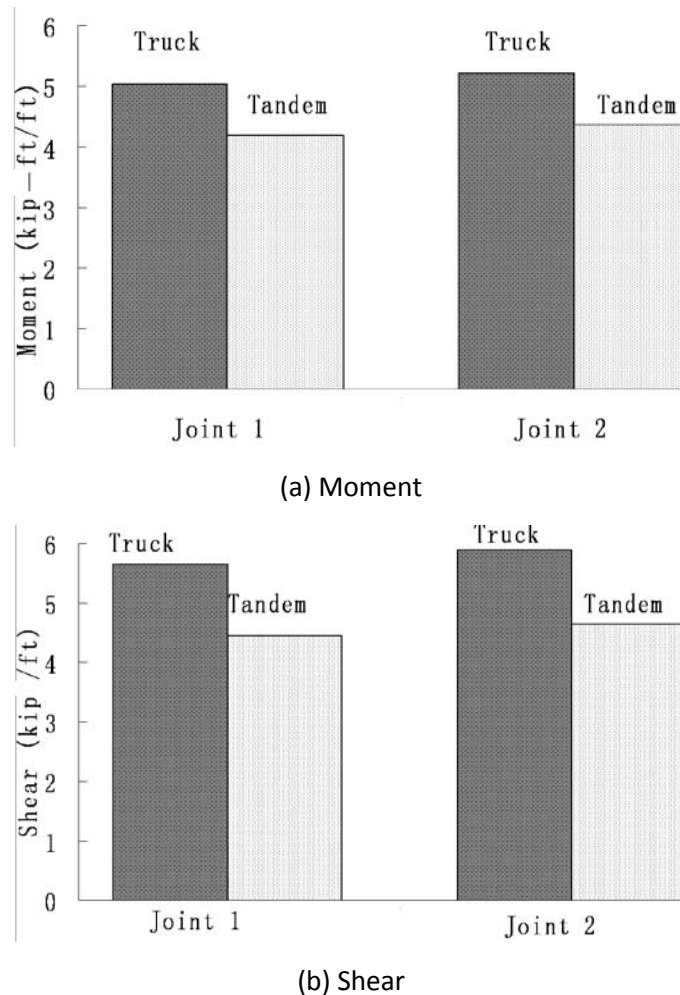
(a) Moment

(b) Shear

Figure 10.1.18: Moment and shear comparison in short-span bridge (B)

It can be seen that the truck and lane load combination produced larger maximum forces than the tandem and lane load combination in both the long- and short-span bridges investigated. This occurred because the practical span range of DBT girders is much longer than the truck length which makes the truck and lane load dominate the loading.

10.1.5.4. Effect of Girder Span

The effect of girder span on the maximum forces in the joints was studied between bridge model A and bridge model B. Both bridge models had the same girder cross-sectional geometry. Bridge model A had a long girder span while bridge model B had a short girder span. Figure 10.1.19 compares the maximum forces in the joint between the long-span bridge model A and the short-span bridge model B.

347
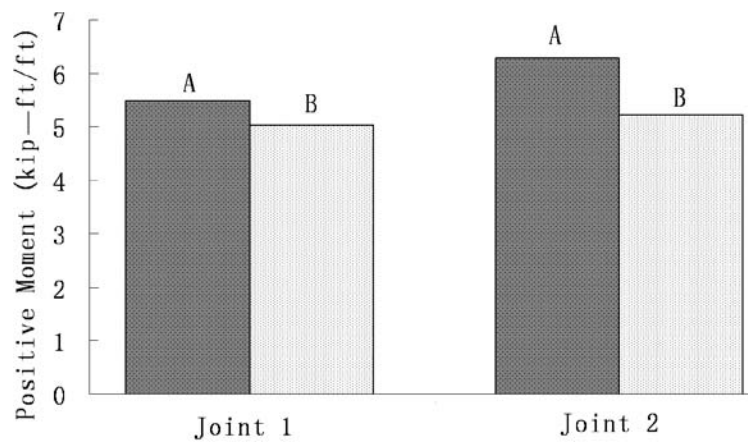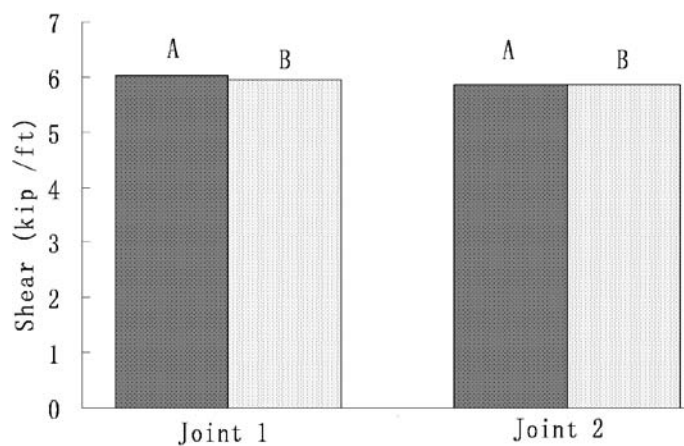
(a) Positive Moment

(b) Shear
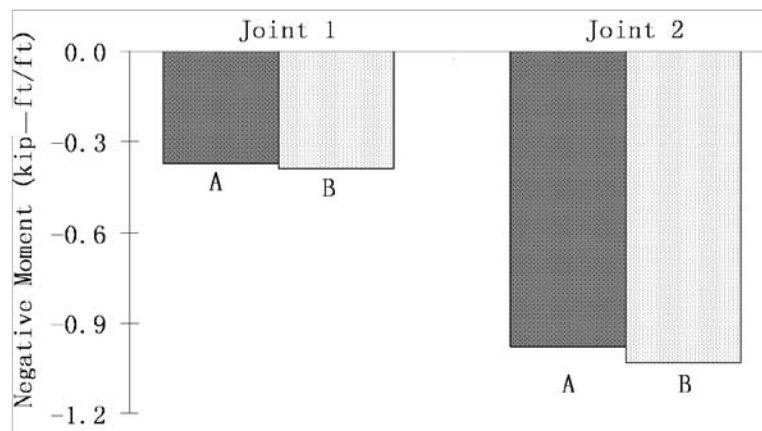
(c) Negative Moment

Figure 10.1.19: Span effect on forces in joint

348

It can be seen that the girder span had some effect on the maximum positive moment in the joint. The longer span produced larger positive moments. However, the influence was not significant. For the shear and negative moment, there was little difference between the results of the two models which means the span had a negligible effect on the maximum shear and negative moment in the joint

10.1.5.5.　　　Effect of Girder Depth

The DBT girder family investigated had three different girder depths: 41, 53, and 65 in. The effect of girder depth on the maximum forces in the joint was studied by comparing the results for the 41 in. girder depth using bridge model D and the 65 in. girder depth using bridge model A. The results are shown in Figure 10.1.20.

349

(a) Positive Moment

(b) Shear

(c) Negative Moment
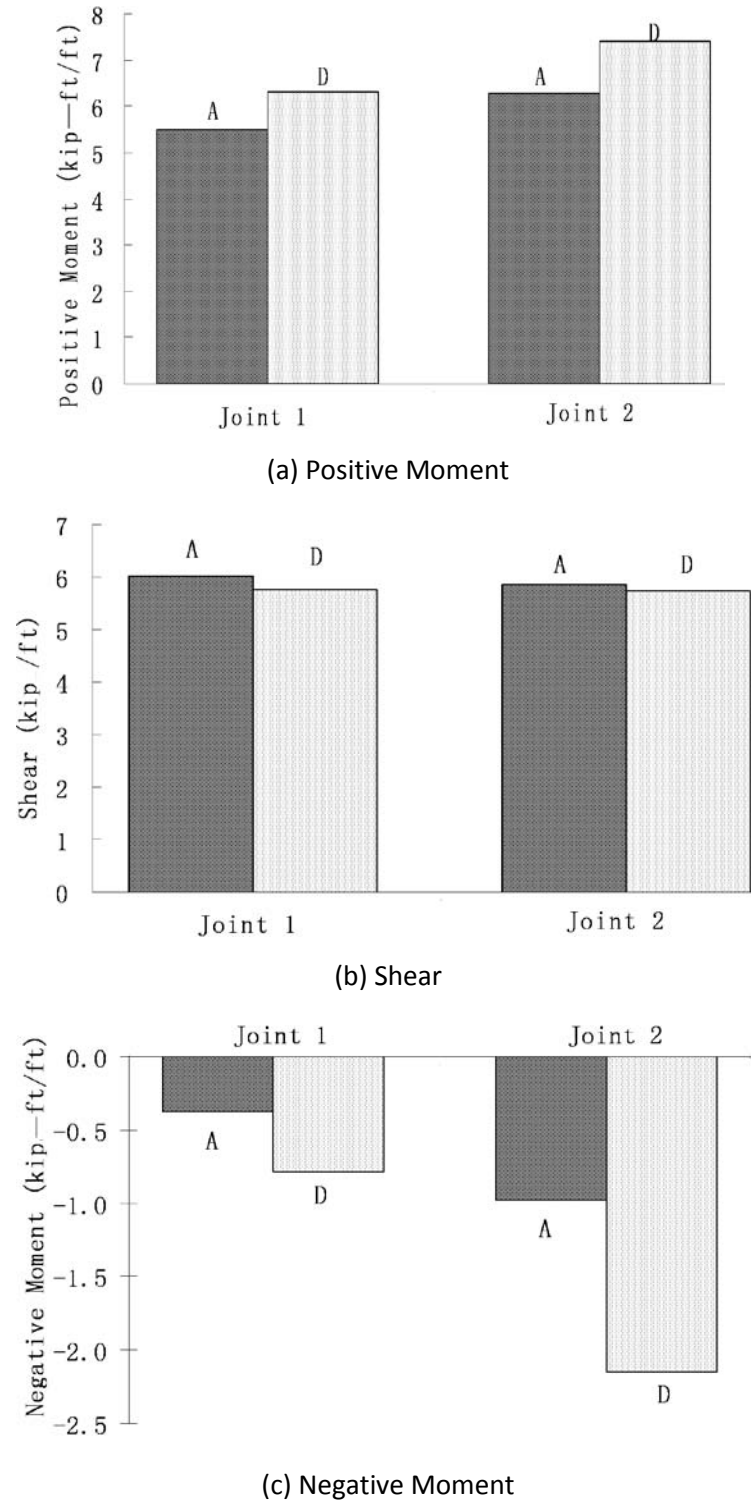
Figure 10.1.20: Effect of girder depth on forces in joint

The girder depth had an influence on the maximum forces in both joints. The influence was found to be larger on the moment than on the shear. Decreasing the girder depth caused an increase in the magnitude of the positive and negative moments of up to 58 and 120%, respectively, while the shear decreased 4%.

10.1.5.6.   Effect of Girder Spacing

The DBT girder family investigated had three different girder spacings: 4, 6, and 8 ft. The effect of girder spacing on the maximum forces in the joint was studied by comparing the results for the 4 ft girder spacing using bridge model C and the 8 ft girder spacing using bridge model A. The results are shown in Figure 10.1.21 where it can be seen that the girder spacing had a significant influence on the forces in the joints. Decreasing the girder spacing reduced both the moment and shear. For the bridges with the same width, decreasing the girder spacing meant adding more girders to resist the loading. The bridge with more girder members produced less force in the joint but might cost more.

351
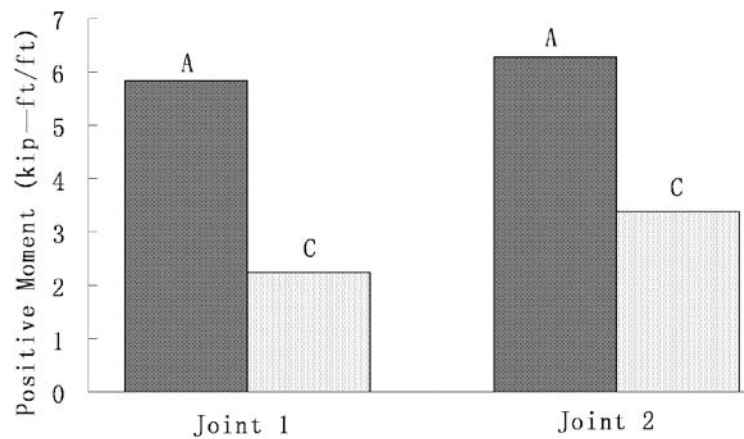
(a) Positive Moment
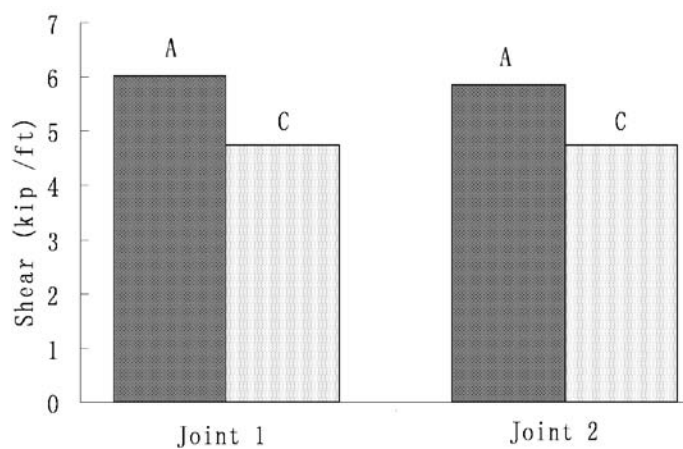
(b) Shear
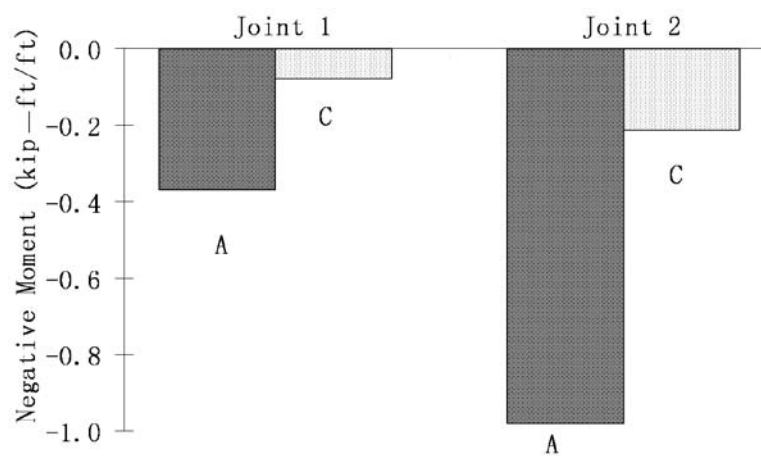
(c) Negative Moment

Figure 10.1.21: Effect of girder spacing on forces in joint

352

10.1.5.7.　　Effect of Bridge Skew

The effect of bridge skew on the maximum forces in the joints was studied using bridge models D through G (Figure 10.1.22). They each had the same girder cross-sectional geometry while the girder skew varied between 0 and 45 degrees.

It can be seen that the bridge skew had an influence on the maximum moment in the joints while it had no influence on the shear. For bridge models with different skews, the maximum shear forces were almost the same in each joint. However, the effect of skew on the maximum moment depended on the loading positions related to the joint of interest. To maximize the positive moment in Joints 1 and 2, the single-lane loadings were applied, which made the moment increase with increasing skew. To maximize the magnitude of the negative moment in Joints 1 and 2, multi-lane loadings were applied. The multi-lane loading positioned on the same side of Joint 1 made the magnitude of the negative moment increase with increasing skew. However, the multi-lane loading located on each side of Joint 2 made the magnitude of the negative moment decrease with increasing skew.

353
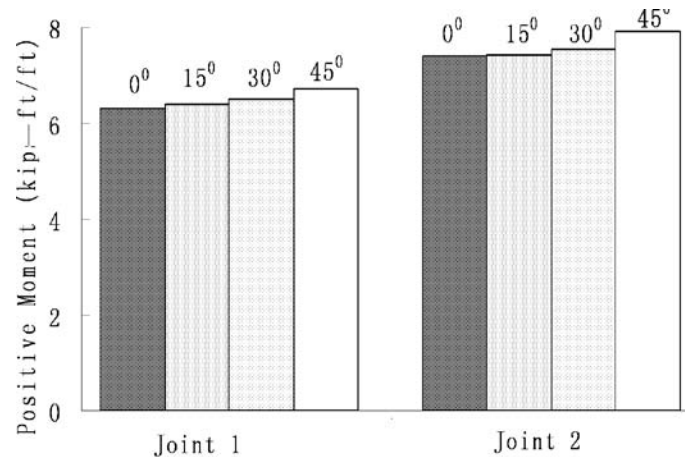
(a) Positive Moment
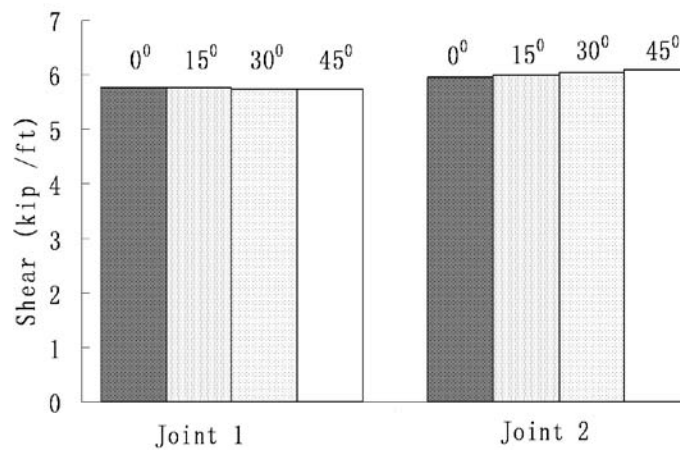
(b) Shear
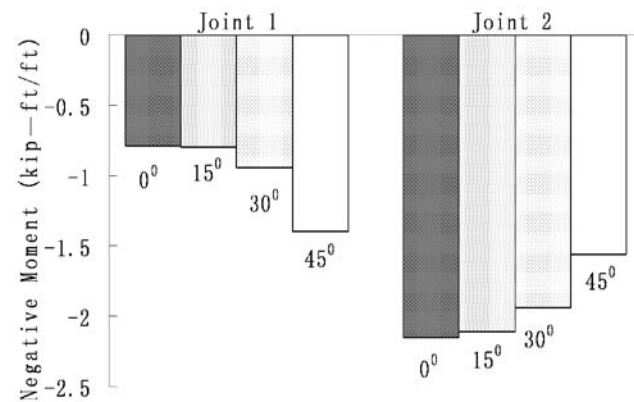
(c) Negative Moment

Figure 10.1.22: Effect of bridge skew on forces in joint

354

10.1.5.8.   Single-lane Loading versus Multi-lane Loading

Figure 10.1.23 compares the effect of the number of loaded lanes on the maximum forces in the joints among the bridge models. The left column of each model represents the single-lane loading and the right column of each model represents the multi-lane loading. Note that the data includes multiple presence factors of 1.2 and 1.0 for the single- and multi-lane (two-lane) loading, respectively, based on Article 3.6.1.1.2 in AASHTO LRFD 2010.

(a) Joint 1-Moment   (b) Joint 1- Shear

(c) Joint 2-Moment   (d) Joint 2-Shear
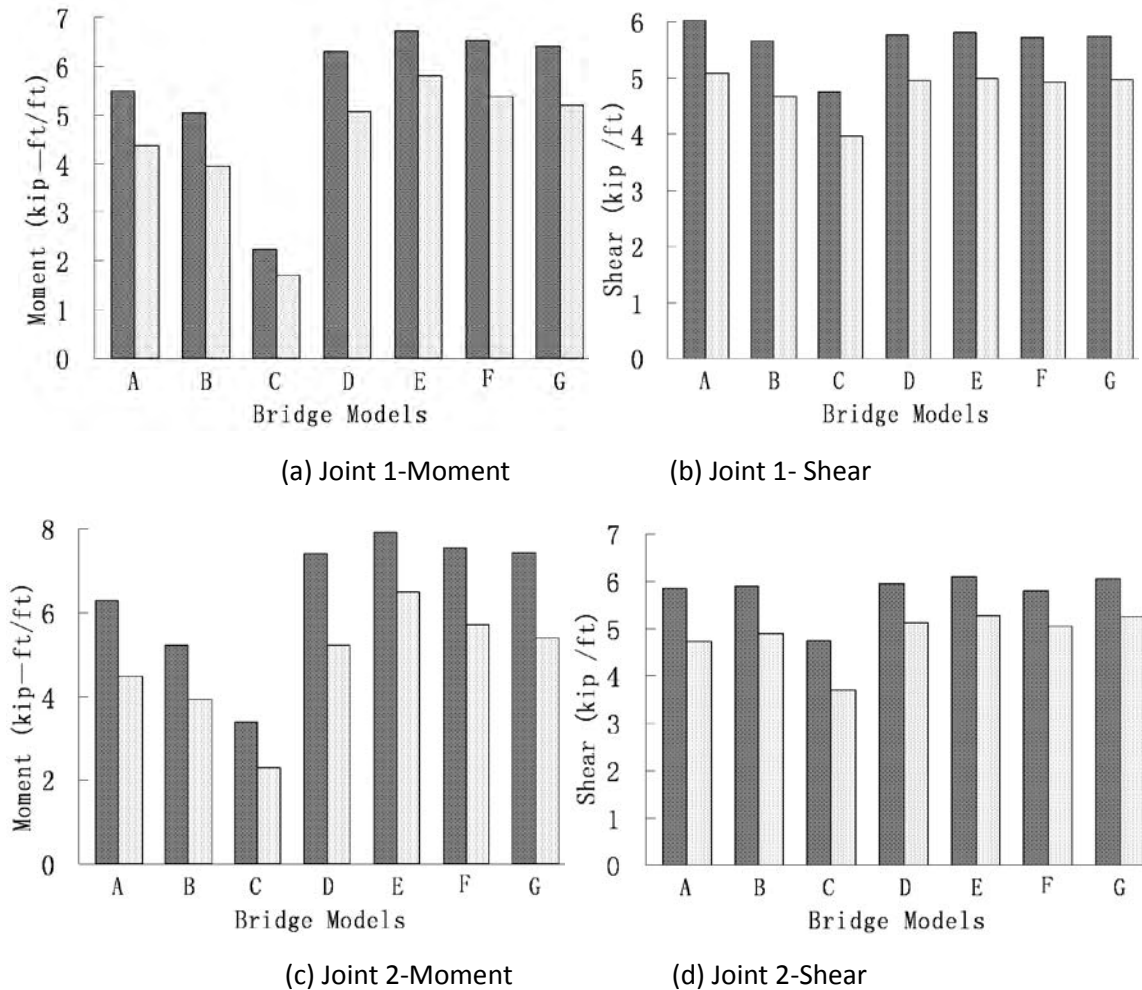
Figure 10.1.23: Effect of number of loaded lanes (single-lane loading (left column bar for each model) versus multi-lane loading (right column bar for each model))

From Figure 10.1.23, it can be concluded that the different number of loaded lanes produced different maximum forces in the joint. Both moment and shear under single-lane loadings were larger than those under multi-lane loading in both joints. So the single-lane loading was observed to dominate the loading.

Table 10.1.10 to Table 10.1.14 summarize the maximum forces in the joints of the seven bridge models under different loading locations. Table 10.1.10 to Table 10.1.13 include the maximum positive moment (M) with corresponding shear (CS) and the maximum shear (S) with corresponding moment (CM).

Table 10.1.10: Maximum positive moment (+Moment) and shear in Joint 1 under single-lane loading

Bridge Models	Maximum +Moment		Maximum Shear	
	M (kip-ft/ft)	CS (kip/ft)	CM (kip-ft/ft)	S (kip/ft)
A	5.50	0.11	3.72	6.02
B	5.03	0.09	3.37	5.65
C	2.24	0.03	1.67	4.75
D	6.30	0.23	4.49	5.77
E	6.71	0.14	5.03	5.70
F	6.51	0.18	4.69	5.72
G	6.40	0.20	4.59	5.75

Table 10.1.11: Maximum positive moment (+Moment) and shear in Joint 2 under single-lane loading

Bridge Models	Maximum +Moment		Maximum Shear	
	M (kip-ft/ft)	CS (kip/ft)	CM (kip-ft/ft)	S (kip/ft)
A	6.29	0.11	4.21	5.86
B	5.23	0.05	3.44	5.90
C	3.39	0.30	2.43	4.74
D	7.39	0.35	5.29	5.95
E	7.92	0.42	5.46	6.09
F	7.53	0.36	5.37	6.05
G	7.43	0.35	5.31	6.04

356

Table 10.1.12: Maximum positive moment (+Moment) and shear in Joint 1 under multi-lane loading

Bridge	Maximum +Moment		Maximum Shear	
Models	M (kip-ft/ft)	CS (kip/ft)	CM (kip-ft/ft)	S (kip/ft)
A	4.38	0.23	2.96	5.07
B	3.93	0.04	2.62	4.67
C	1.72	0.02	1.25	3.96
D	5.06	0.39	3.52	4.96
E	5.79	0.29	4.36	4.91
F	5.37	0.32	3.80	4.93
G	5.19	0.36	3.60	4.94

Table 10.1.13: Maximum positive moment (+Moment) and shear in Joint 2 under multi-lane loading

Bridge	Maximum +Moment		Maximum Shear	
Models	M (kip-ft/ft)	CS (kip/ft)	CM (kip-ft/ft)	S (kip/ft)
A	4.47	0.10	2.83	4.72
B	3.94	0.06	2.53	4.89
C	2.29	0.23	2.20	3.70
D	5.22	0.52	3.49	5.13
E	6.48	0.57	4.07	5.27
F	5.70	0.51	3.76	5.22
G	5.39	0.52	3.58	5.17

357

Table 10.1.14: Maximum negative moment in Joints 1 and 2 under multi-lane loading

Bridge Models	Joint 1 (kip-ft /ft)	Joint 2 (kip-ft/ft)
A	-0.37	-0.98
B	-0.39	-1.03
C	-0.08	-0.22
D	-0.79	-2.15
E	-1.40	-1.56
F	-0.94	-1.94
G	-0.82	-2.11

In summary, the maximum positive moment, negative moment and shear in the longitudinal joint under the HL-93 live load were 7.92 kip-ft/ft, -2.15 kip-ft/ft and 6.09 kip/ft, respectively. Based on the AASHTO Table A4-1 Deck Slab Design Table, the maximum positive live load moment in the bridge deck supported by girders spaced at 8 ft was 5.69kip-ft/ft. Table A4-1 was used to determine the design moments for the bridge deck. Specified assumptions and limitations were used in developing this table that should be considered when used for design. Among bridge models A, B, D-G, which had 8 ft spacings, models E and F had greater maximum positive moments than those from the AASHTO table.

10.1.5.9. Impact of Cracking

Based on the results of the analyses discussed above using uncracked sections for the longitudinal joints, it was anticipated that the joints would be cracked under service loading. Therefore, the forces in the joint would be expected to be reduced compared with the forces calculated assuming uncracked sections. The difference in structural behavior before and after cracking resulted from a change in the joint stiffness.

In the FE models where the largest maximum forces in the joint were found, the impact of cracking of the joint was studied by changing the modulus of elasticity (E) in the joint while keeping the moment of inertia (I) the same. The FE model for bridge model E considering cracking of the joint is shown in Figure 10.1.24. In Figure 10.1.24-(a), the lane with the arrows, which are for the lane load, is where the lane load placed; the circles indicate the position of the truck loads. Figure 10.1.25-(a) and Figure 10.1.25-(b) show the impact of cracking on the maximum moment (positive moment and negative moment) and maximum shear, respectively.

358
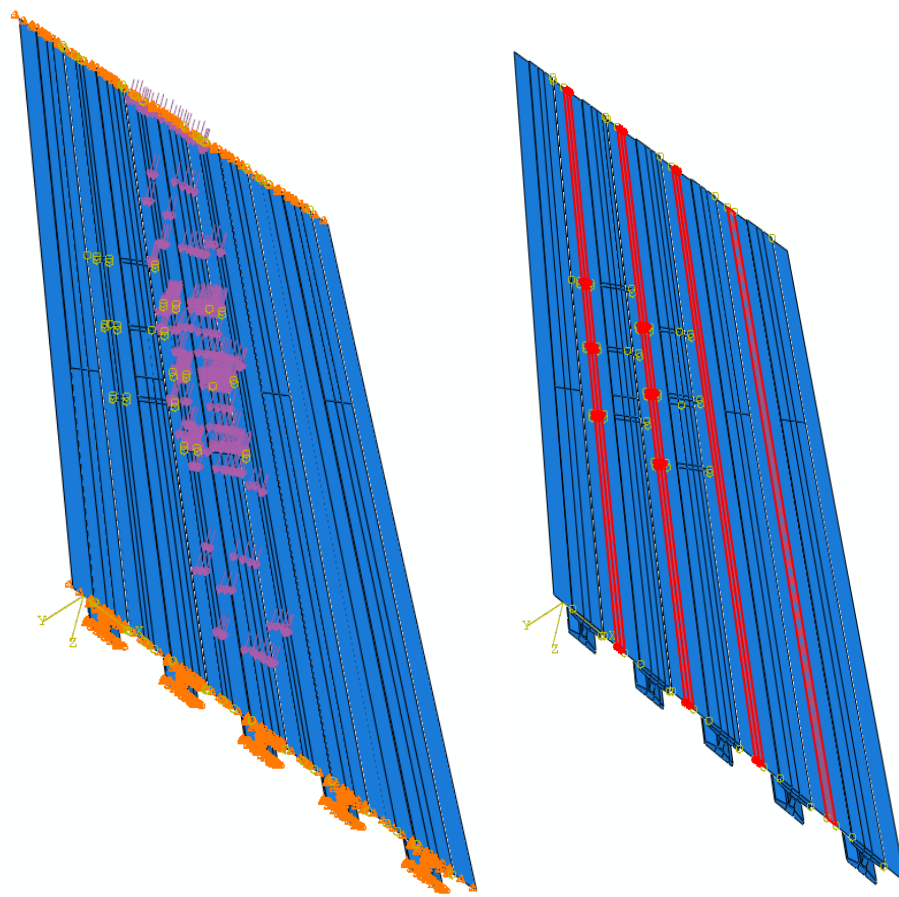
(a) Loading for the Maximum Positive Moment   (b) Cracked Joints

Figure 10.1.24: FE Model

359

(a) Moment

(b) Shear
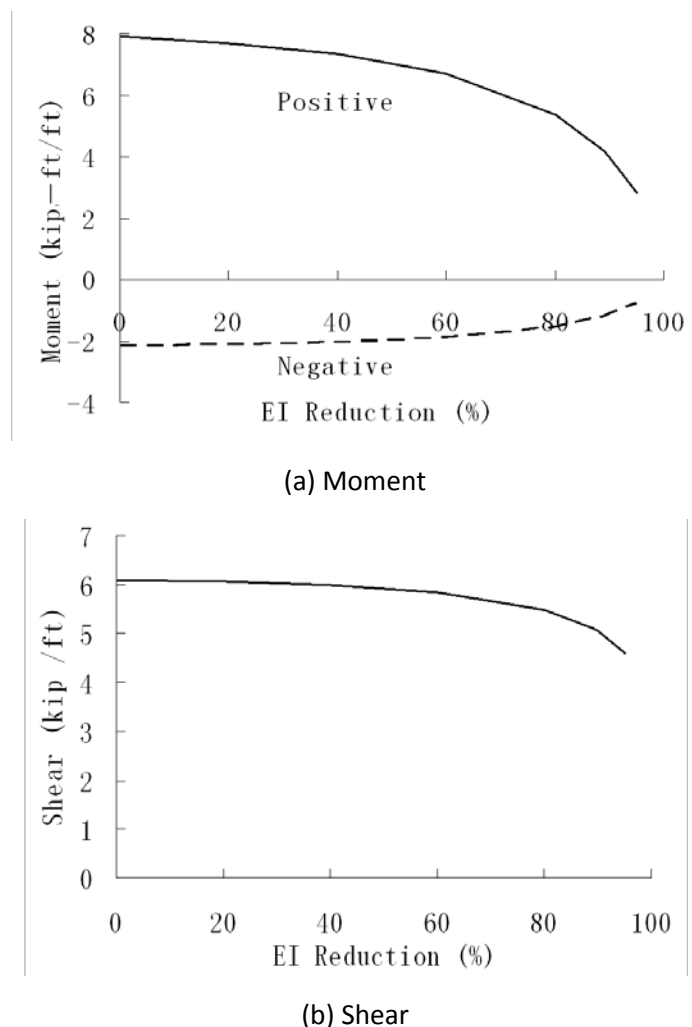
Figure 10.1.25: Impact of cracking on forces

From Figure 10.1.25, it can be seen that cracking had an influence on the maximum forces in the joints. As the section was cracked (modeled as a reduction in stiffness (EI)), the joint forces decrease. The rate of decrease in force increased dramatically for large reductions in stiffness; as the stiffness reduced to zero, the joint resistance would converge to zero. The reduction in stiffness had a greater influence on moment than on shear. At a stiffness reduction of 95%, the moment and shear resisted by the joint were 35% and 76% of the values, respectively, of the values calculated assuming uncracked section properties. To estimate the expected stiffness reduction of the joint as a result of cracking, the theoretical results for flexural specimen WB-1 described in Chapter 9 were used. For this specimen the theoretical reduction in stiffness due to cracking was estimated to be on the order of 84%, as discussed in Section 9.1.5.

Based on the estimated 84% reduction in stiffness from the theoretical calculations associated with WB-1 to account for the effects of joint cracking, the maximum positive moment, negative moment and shear in the

longitudinal joint under live load HL-93 were expected to be 4.55 kip-ft/ft, -1.40 kip-ft/ft and 5.34 kip/ft respectively. The corresponding moment (CM) occurring with the maximum shear was 3.37 kip-ft/ft. The estimated 84% reduction in stiffness from the theoretical calculations associated with WB-1 was used because: 1) the point when the first crack occurred was not observed in the WB-1 test and calculation of the stiffness change based on the test may not be accurate; 2) the WB-2 test had not yet been performed at the time of the force analysis.

10.1.5.10.   Fatigue Loading

The Articles in AASHTO LRFD (2010) referenced to the fatigue loading are listed below:

> 3.4.1 FATIGUE-Fatigue and fracture load combination relating to repetitive gravitational vehicular live load and dynamic responses under a single design truck having the axle spacing specified in Article 3.6.1.4.1
>
> 3.4.1 A load factor of 0.75 (Table 3.4.1-1) shall be applied to fatigue load combination
>
> 3.6.1.2.1 Vehicular live loading on the roadways of bridges or incidental structures, designated HL-93, shall consist of a combination of the design truck or design tandem, and design lane load.
>
> 3.6.1.4.1 The fatigue load shall be one design truck or axles thereof specified in Article 3.6.1.2.2, but with a constant spacing of 30.0 feet between the 32.0-kip axles.
>
> 3.6.2.1 The static effects of the design truck or tandem shall be increased by 15% (fatigue and fracture limit state) for dynamic load allowance (Table 3.6.2.1-1). The dynamic load allowance shall not be applied to pedestrian loads or to the design lane load.

Revisions to fatigue loading were accepted by AASHTO Bridge Committee, Technical Committees T-5 Loads, and T-14 Steel in May of 2008. The revisions consisted of inclusion of two levels of fatigue load in Table 3.4.1-1. These were Fatigue I and Fatigue II. Fatigue II retained the current Load Factor of 0.75 and was to be applied to represent an effective stress range caused by the fatigue truck with respect to a large but finite number of stress range cycles. Fatigue I had a Load Factor of 1.5 (or 2 times 0.75) and was to be applied to the stress range caused by the fatigue truck with respect to an infinite number of stress range cycles.

Using the Load Factor of 0.75 for Fatigue II and not including the Lane Load (i.e., 0.75 [1.15 (Fatigue Truck Load)], resulted in maximum positive moment, negative moment and shear in the longitudinal joint under fatigue live load HL-93 for finite life of 1.99 kip-ft/ft, -0.35 kip-ft/ft and 2.34 kip/ft, respectively. The forces associated with the Fatigue Load were analyzed using the same FE models discussed in Section 10.1.5.9 with the fatigue load factor and dynamic load allowance considered. These values were used to determine the fatigue loading in the large-scale tests.

A separate analytical parametric study was carried out using SAP2000 to determine the shear force assumed to be transferred across the joint due to the leveling of differential camber during construction. Based on that study, a shear force 0.5 kip/ft was determined as a reasonable upper bound to consider in the test specimens. The combination of the fatigue shear of 2.34 kip/ft plus camber leveling shear of 0.5 kip/ft, 2.844 kip/ft, was used to determine the fatigue loading in the large-scale fatigue-shear tests.

10.2. Maximum Forces in the Transverse Joints

The decked bulb-T girder family was chosen for the study of the live load forces in the transverse joint. This decked bulb-T girder family had the same girder cross sections as those used for the parametric study of the live load forces in the longitudinal joint. Table 10.1.1 summarized the practical span ranges for these girder sections.

The transverse joints over the piers experience negative moment under service live load. The maximum negative moment in the transverse joint was studied using QConBridge™, which is a live load (AASHTO LRFD HL-93, 2010) analysis program for continuous bridge frames developed by WSDOT. Two types of bridge systems were developed: (1) two-span continuous bridge and (2) three-span continuous bridge.

According to AASHTO LRFD (2010), the HL-93 loading consists of the combination of the design vehicle load and the design lane load. The design vehicle load is either a truck or tandem with dynamic allowance of 1.33. The design truck is specified in Article 3.6.1.2.2 while the design tandem is specified in Article 3.6.1.2.3. The practical span ranges used in the study were much larger than those controlled by the tandem loading, so the truck loading controlled the vehicle load in the analyses. The design lane load was 0.64 kip/ft without dynamic allowance.

Based on Article 3.6.1.3.1, for negative moment between points of dead load contra-flexure, and reactions at interior piers only, 90% of the effect of two design trucks spaced at a minimum of 50 ft between the lead axle of one truck and the rear axle of the other truck, combined with 90% of the effect of the design lane load should be considered. The distance between the 32 kip axles of each truck should be taken as 14 ft.

Considering the practical span range of the decked bulb-T girder family, Table 10.2.1 lists the bridge span length in each bridge model and shows the maximum negative moment in the transverse joint over the piers for each bridge model under service live load HL-93.

Table 10.2.1: Negative moment over piers in bridge models

Bridge Model	Bridge System	Span (ft)			Moment (kip-ft)	
		First	Second	Third	Design Load	Fatigue Load
1	Two-Span	64	64		-1153	-323
2		180	180		-4700	-1048
3		180	94		-4870	-1377
4		176	84		-4780	-1385
5	Three-Span	64	64	64	-1064	-320
6		176	176	176	-4523	-1091
7		94	180	94	-3786	-1093
8		84	176	84	-3671	-1094

From the analysis results, it can be seen that the span length of the bridge had the largest positive effect on the maximum negative moment in the transverse joint. Generally speaking, the bridge model with the longer span length produced the larger maximum negative moment. For the bridge model with the same span length, the difference of the maximum negative moment between the two-span bridge systems and three-span bridge systems was negligible. In the case of the two-span bridge systems, the bridge model with different span lengths produced larger moments than the bridge model with the same span lengths.

The decked bulb-T girder section (DBT65) and the bulb-T girder section (BT72) were chosen for the study of the maximum loads including the design loading and the fatigue loading in the transverse joints. Table 10.2.2 and Table 10.2.3 summarize the maximum moment in the transverse joint over the piers for girder sections DBT65 and BT72, respectively, under the HL-93 service live load. The calculated moments in Table 10.2.2 and Table 10.2.3 represent the loadings per lane. The first bridge model in Table 10.2.2 is a two-span bridge with a span of 176 ft and one of 84 ft.

363

Table 10.2.2: Moment over piers in bridge models with DBT65

Bridge System	DBT 65 Span (ft)			Moment (kip-ft)			
	First	Second	Third	Design (-)	Fatigue (-)	Design (+)	Fatigue (+)
Two-Span	176	84		-4780	-1385		
Three Span	176	176	176	-4523	-1091	689	268

Table 10.2.3: Moment over piers in bridge models with BT72

Bridge System	BT 72 Span (ft)			Moment (kip-ft)			
	First	Second	Third	Design (-)	Fatigue (-)	Design (+)	Fatigue (+)
Two-Span	105	70		-2067	-679		
Three Span	105	105	105	-2333	-603	346	147

In order to determine the distribution factor for a typical interior girder by the simplified distribution factor formulas (AASHTO LRFD 4.6.2.2), the following conditions must be met:

1. Number of beams, Nb $\geq$ 4
2. Width of deck is constant
3. Beams are parallel and approximately of the same stiffness
4. Roadway part of overhang $\leq$ 3 ft
5. Curvature < Limit of AASHTO 4.6.1.2.4
6. For precast concrete T-section with shear keys and with or without transverse post-tensioning, the bridge type is (j)
7. For precast concrete I or Bulb-Tee section, the bridge type is (k)

The BT72 and DBT65 were classified by type and the distribution factors were determined accordingly.

Bridge Type (K) or Type (J) if sufficiently connected to act as a unit: BT72

For one design lane loaded,

$$DFM = 0.06 + (\frac{S}{14})^{0.4}(\frac{S}{L})^{0.3}(\frac{K_g}{12Lt_s^3})^{0.1}$$

(10.2.1)

For two or more design lanes loaded,

364

$$DFM = 0.075 + (\frac{S}{9.5})^{0.6} (\frac{S}{L})^{0.2} (\frac{K_g}{12Lt_s^3})^{0.1}$$

(10.2.2)

where:

DFM = distribution factor for moment for interior beam

S = beams spacing, ft

L = beam span, ft

t_s = depth of deck, in.

Kg = longitudinal stiffness parameter, in.^{4}, = n (I+Ae$_g^2$)

n = modular ratio between beam and deck materials

$$= \frac{E_c(beam)}{E_c(deck)} = \frac{4769}{3605} = 1.32$$

A = cross-sectional area of the beam, in.^{2}

I = moment of inertia of the beam, in.^{4}

e_g = distance between the centers of gravity of the beam and deck, in.

The parameters were determined as follows for the BT72:

S = 12 ft

L = 70 ft

t_s = 6 in.

Kg=n (I+Ae$_g^2$) = (1.3229) (545894+767x38.4^2) = 2218347 in.^{4}

For one design lane loaded,

$$DFM = 0.06 + (\frac{12}{14})^{0.4} (\frac{12}{70})^{0.3} (\frac{2218347}{12 \times 70 \times 6^3})^{0.1} = 0.772$$

For two or more design lanes loaded,

$$DFM = 0.075 + (\frac{12}{9.5})^{0.6} (\frac{12}{70})^{0.2} (\frac{2218347}{12 \times 70 \times 6^3})^{0.1} = 1.114$$

Thus, for the case of where two or more design lanes loaded control, DFM=1.114 lanes/beam.

365

The maximum moment in the transverse joint over the interior piers with girder section BT72 due to the HL-93 service live load was determined as:

negative design load: M=-(0.9)(1.114)(2333)=-2339 kip-ft/beam

negative fatigue load: M=-(0.9)(1.114)(679)=-681 kip-ft/beam

positive design load: M=(1.114)(346)=385 kip-ft/beam

positive fatigue load: M=(1.114)(147)=164 kip-ft/beam

Bridge Type (J) if connected only enough to prevent relative vertical displacement at the interface: DBT65

Regardless of number of loaded lanes,

$$DFM = S/D \tag{10.2.3}$$

where:

D= $11.5-N_L + 1.4N_L (1-0.2C)^2$ where $C \leq 5$

D=$11.5-N_L$ where C > 5

C=K (W/L) ≤K

$$K = \sqrt{\frac{(1+\mu)I}{J}}$$

DFM = distribution factor for moment for interior beam

S = beams spacing, ft

D = width of distribution per lane ft

N_L= number of design lanes as specified in Article 3.6.1.1.1

C = stiffness parameter

K = constant for different types of construction

W = edge to edge width of bridge, ft

L = beam span, ft

μ = Poisson's ratio

I = moment of inertia of the beam, in.4

J = St. Venant's torsional inertia, in.4

For thin-walled open beam, J=(1/3) (Σbt^3)

366

The parameters were determined as follows for the DBT65:

S = 8 ft

W = 40 ft

N_L= 3

L = 84 ft to 176 ft

μ = 0.18

I = 835069 in.4

J = 190789 in.4

$$K = \sqrt{\frac{(1+0.18) \times 835069}{190789}} = 5.16$$

C=5.16(40/176) = 1.173<K

D=11.5-3+1.4x 3x (1-0.2x1.173)^2=10.96

DFM=8/10.96=0.73

The maximum moment in the transverse joint over the interior piers with girder section DBT65 due to the HL-93 service live load was determined by:

negative design load: M= -(0.9) (0.73) (4780)=-3140 kip-ft/beam

negative fatigue load: M=-(0.9)(0.73)(1385)=-910 kip-ft/beam

positive design load: M=(0.73)(689)=503 kip-ft/beam

positive fatigue load: M=(0.73)(268)=196 kip-ft/beam

In summary, the maximum moments in the transverse joint over the interior piers with girder section DBT65 were larger than the maximum moments in the girder section BT72 due to the HL-93 service live load. For girder section DBT65, the negative design moment was -3140 kip-ft/beam; the negative fatigue moment was -910 kip-ft/beam; the positive design moment was 503 kip-ft/beam; and the positive fatigue moment was 196 kip-ft/beam.

Assuming uncracked sections, the resulting extreme fiber stresses at the top of the girder over the interior piers in the transverse joint associated with the maximum moments were -1.06 ksi, -0.31 ksi, 0.17 ksi, and 0.07 ksi under the negative design load, negative fatigue load, positive design load, and positive fatigue

367

load, respectively. The negative design stress (-1.06 ksi) under the design load (-3140 kip-ft) was greater than the modulus of rupture of concrete. Thus, the transverse joint was reanalyzed assuming cracked section properties. Based on the cracked section analysis, the stresses of the U-bar in girder DBT65 were determined to be 35.6 ksi and 10.3 ksi under the negative design load (-3140 kip-ft) and negative fatigue load (-910kip-ft), respectively.

10.3. Conclusions

For the longitudinal joints, a total of seven bridge models with different girder geometries were developed and subjected to the HL-93 live load in the parametric study. The purpose of the study was to provide a database of maximum forces in the longitudinal joints for determination of loadings for the static and fatigue tests described in Chapters 12 and 13 to determine the serviceability, static load strengths, and fatigue characteristics for the selected longitudinal/transverse joints. The following parameters were considered: different loading locations, effect of bridge width, design truck and lane loading versus design tandem and lane loading, girder geometry (depth, spacing and span), bridge skew, single-lane loading versus multi-lane loading, and impact of cracking of the joints. Based on the parametric study discussed above, the following findings are summarized below:

1. The position of lane load had little effect on the maximum forces in the joint. Typically, the lane load which was fully applied along the bridge length direction produced the largest moment in the joint while the lane load terminated at the center of rear truck wheel produced the largest shear in the joint.
2. While the influence of truck load position in the longitudinal direction on the maximum moment and shear in the joint was not significant, truck loads with heavy wheels located near midspan produced the largest maximum moment and shear.
3. The truck and lane load combination produced larger maximum forces than the tandem and lane load combination in both the long and short span bridges. This occurred because the practical span range of the DBT girders was much longer than the truck length which made the truck and lane load dominate the loading.
4. Increasing the bridge width decreased the maximum negative moment in the joints while it had a negligible effect on the maximum positive moment and maximum shear.
5. The effect of girder span on the maximum forces in the joints was not significant. However, the maximum forces were influenced significantly by the spacing and depth of the girder. Girders with larger spacings and shallower depths produced larger moments and shears.
6. The bridge skew had an influence on the maximum moment in the joints while it had no influence on the shear. However, the effect of skew on the maximum moment depended on the loading positions related to the joint of interest.
7. Single-lane loading was observed to dominate the loading compared to multi-lane loading. Both moment and shear under single-lane loadings were larger than those under multi-lane loading in the two joints investigated.

368

8. The maximum forces in the joints decreased after the joint cracking. However, the impact of cracking had more effect on moment than on shear.

9. Before cracking, the maximum positive moment was 7.92 kip-ft/ft; the maximum negative moment was -2.15 kip-ft/ft; the maximum shear was 6.09 kip/ft. After cracking, the maximum positive moment was 4.55 kip-ft/ft; the maximum negative moment was -1.40 kip-ft/ft; the maximum shear was 5.34 kip/ft, based on the estimated 84% reduction in stiffness from the theoretical calculations associated with WB-1 to account for the effects of joint cracking. The maximum forces before and after cracking were subsequently used to determine the static loading demand for the test specimens described in Chapters 12 and 13 to investigate serviceability (including crack control), static load strengths, and fatigue characteristics for the selected longitudinal/transverse joint.

10. The maximum positive moment, negative moment and shear in the longitudinal joint under fatigue live load HL-93 was determined to be 1.99 kip-ft/ft, -0.35 kip-ft/ft and 2.34 kip/ft respectively. These forces were subsequently used to determine the fatigue loading demand for the test specimens described in Chapters 12 and 13.

To determine the controlling load case for a transverse joint, the transverse joint should be positioned over an interior support in a continuous span bridge system. In this case, if the deck was compositely connected to the girder, the deck would have to resist large tensile forces that would be produced by the negative moment developed there. Conservatively it was assumed that all the tension force created by the negative moment would be resisted by the deck.

The decked bulb-T girder section (DBT65) and the bulb-T girder section (BT72) were chosen for the study of the maximum loads including the design loading and the fatigue loading in the transverse joints. The following findings are summarized below:

1. The maximum moments in the transverse joint over the interior piers with girder section DBT65 were larger than the maximum moments in the girder section BT72 due to the HL-93 service live load. For girder section DBT65, the negative design moment was -3140 kip-ft/beam; the negative fatigue moment was -910 kip-ft/beam; the positive design moment was 503 kip-ft/beam; and the positive fatigue moment was 196 kip-ft/beam.

2. Assuming uncracked sections, the resulting extreme fiber stresses at the top of the girder in the transverse joint associated with the maximum moments were -1.06 ksi, -0.31 ksi, 0.17 ksi, and 0.07 ksi under the negative design load, negative fatigue load, positive design load, and positive fatigue load, respectively. The negative design stress (-1.06 ksi) under the design load (-3140 kip-ft) was greater than the modulus of rupture of concrete. Thus, the transverse joint was reanalyzed assuming cracked section properties. Based on the cracked section analysis, the stresses of the U-bar in girder DBT65 were determined to be 35.6 ksi and 10.3 ksi under the negative design load (-3140 kip-ft) and negative fatigue load (-910kip-ft), respectively.

369

Chapter 11 Selection of Durable Closure Pour Materials for Accelerated Bridge Construction

11.0   Introduction

For precast bridge deck systems with cast-in-place (CIP) connections, precast elements are brought to the construction site ready to be set in place and quickly joined together. Then, a concrete closure pour (CP) completes the connection. The performance of the CP material is one of the key parameters affecting the overall performance of the bridge system.

Longitudinal connections between the flanges of DBTs and between precast panels between girders require that the joints must be able to transfer shear and moment induced by vehicular loads. Shrinkage of CP materials and transverse shortening of precast members further subject the joints to direct tension. Freeze-thaw resistance and low permeability of joints are also important. An ideal CIP connection detail emulates monolithic behavior and results in a more durable and longer lasting structure.

Traditionally, different types of grouts have been used as CP materials for precast bridge deck systems with CIP connections. Mrinmay (1986) documented a wide variety of materials used after 1973 to avoid joint failure in closure pours. These materials included sand-epoxy mortars, latex modified concrete, cement-based grout, non-shrink cement grout, epoxy mortar grout, calcium aluminate cement mortar and concrete, methylmethacrylate polymer concrete and mortar, and polymer mortar. Epoxy or polymer modified grouts can have significant advantages, such as a high strength of 10 ksi in 6 hours, better bond, reduced chloride permeability, and lower shrinkage (Issa et al 2003) than different MAP grouts. However, they are often significantly more expensive and less compatible with surrounding concrete. In addition, if the resin is used in too large of a volume, the heat of reaction may cause it to boil, and thereby develop less strength and lose bond. Cementitious grouts have been used more in precast construction than have epoxy or polymer-modified grouts (Matsumoto et al. 2001). A primary disadvantage of cementitious grouts is the shrinkage and cracking that result from the use of hydraulic cement. Non-shrink grout compensates for the shrinkage by incorporating expansive agents into the mix. With non-shrink grout, the effects of shrinkage cracks or entrapped air on the transfer of forces and bond are minimized, though not eliminated. ASTM C 1107 establishes strength, consistency, and expansion criteria for prepackaged, hydraulic-cement, non-shrink grout.

Nottingham (1996) reported that the very nature of Portland cement grouts virtually assures some shrinkage cracks in grout joints, regardless of quality control. Prepackaged magnesium ammonium phosphate (MAP) based grout often extended with pea gravel can meet requirements, like high quality, low shrinkage, impermeable, high bond, high early strength, user friendly and low temperature curing ability (Nottingham 1996; Issa et al. 2003). Gulyas et al. (1995) undertook a laboratory study to compare composite grouted keyway specimens using two different grouting materials: non-shrink grouts and magnesium ammonium phosphate (MAP) mortars, in which MAP materials performed better than non-shrink grouts. Gulyas and Champa (1997) further examined inadequacies in the selection of a traditional

non-shrink grout for use in shear keyways. The MAP grout outperformed the non-shrink grout in all areas tested, including direct vertical shear, direct tension, longitudinal shear, bond, shrinkage, etc. Menkulasi and Roberts-Wollmann (2005) presented a study of the horizontal shear resistance of the connection between full-depth precast concrete bridge deck panels and prestressed concrete girders. Two types of grout were evaluated: a latex modified grout and a MAP grout. For both types of grout, an angular pea gravel filler was added. The MAP grout developed slightly higher peak shear stresses than the latex modified grout.

Grout without coarse aggregate extension is usually referred to as neat grout, while grout with coarse aggregate extension, typically 1/2 or 3/8 in. coarse aggregate, is extended grout. Compared with neat grout, extended grout has the following potential benefits: (1) more compatible with concrete; (2) better interlock between connection components; (3) denser, less permeable; (4) less drying shrinkage and creep; and (5) larger grout volume per bag, hence less expensive. However, it was pointed out by Matsumoto et al. (2001) that the extended grout required more cement paste than available in prepackaged bags, leading to lower strengths and poor workability.

As discussed above, numerous products are available for CP materials, and various materials were studied. However, limited research had been previously conducted to provide consistent comparison among a large number of different types of CP materials. Also adequate performance-based criteria need to be developed to ensure appropriate selection of CP materials, particularly for accelerated bridge construction, which is the subject of this chapter. Performance-based specifications focus on properties such as consistency, strength, durability, and aesthetics. They reward quality, innovation, and technical knowledge, in addition to promoting better use of materials, and present an immense opportunity to optimize the design of materials.

As part of the process of developing the performance criteria, eight candidate CP materials were selected and evaluated with respect to their potential effectiveness in accelerated bridge construction. In this chapter, accelerated bridge construction is defined with respect to two categories: overnight cure of CP materials and 7-day cure of CP materials. For the overnight cure, published performance data from different grout materials were collected through contacts with material suppliers and users. For the 7-day cure, standard or special concrete mixtures and their performance data were collected through contacts with HPC (High Performance Concrete) showcase states as well as with material suppliers. Based on these initial collected data, four grouts were first selected as candidate overnight cure materials, and four special concrete mixes as candidate 7-day cure materials. The preliminary selection was based on strength tests of selected materials or prediction models to narrow the candidate materials down to two materials in each of the two categories. Then long-term tests were performed on the four final selected materials, including freezing-and-thawing durability, shrinkage, bond, and permeability tests. The final performance criteria for selecting durable CP materials were developed based on results of these long-term tests.

11.1. Preliminary Performance Criteria

Performance characteristics, compressive strength, shrinkage, chloride penetration, freezing-and-thawing durability and bond strength, were investigated as performance criteria. For the closure pour/precast unit interface, the focus must be on minimizing cracking in this location to reduce intrusion of water that may result in corrosion. And thus, shrinkage, chloride penetration, freezing-and-thawing durability and bond strength need be investigated to control cracking and corrosion. An extensive literature review was performed to develop preliminary performance criteria of overnight and 7-day cure CP materials.

The FHWA defined a set of concrete performance characteristics for long-term concrete durability and strength of highway structures. Standard laboratory tests, specimen preparation procedures, and grades of performance were suggested for each characteristic. Because standard test methods sometimes offer different options, Russell and Ozyildirim (2006) modified the FHWA definition. The modified performance characteristic grades for high-performance structural concrete are given in Table 11.1.1. Tepke and Tikalsky (2007) provided a working guide to the design and construction of concrete structures using attainable high standards rather than common practice. An engineering design tool for the development of performance specifications for reinforced concrete highway structures was developed and performance characteristic grades for HPC are given in Table 11.1.2. As shown in Tables 11.1.1 and 11.1.2, the same or similar standard laboratory tests were recommended. Also three grades were suggested in both criteria. The performance criteria identified in Table 11.1.2 have lower requirements for compressive strength and chloride penetration, and higher requirements for shrinkage than the criteria in Table 11.1.1 in all three grades. They have similar grade limits for freezing-and-thawing durability. Both criteria were developed generally for bridges including girders and decks.

Table 11.1.1: Proposed performance characteristic grades by Russell and Ozyildirim (2006)

Performance characteristic*	Test Method	Grade 1	Grade 2	Grade 3
Compressive Strength** (CS), ksi	AASHTO T22 ASTM C 39	8≤CS<10	10≤CS<14	14≤CS
Shrinkage*** (S), με	AASHTO T160 ASTM C157	600≤S<800	400≤S<600	S<400
Chloride Penetration (ChP), coulombs	AASHTO T277 ASTM C1202	1500<ChP≤2500	500<ChP≤1500	ChP≤500
Freezing-and-thawing Durability (F/T) (relative dynamic modulus of elasticity after 300 cycles)	AASHTO T161 ASTM C666 Procedure A	70%≤ F/T<80%	80%≤ F/T<90%	90%≤ F/T

*All tests to be performed on concrete samples moist- or submersion-cured for 56 days until otherwise specified.

**The 56-day strength is recommended.

*** Shrinkage measurements are to start 28 days after moist curing and be taken for a drying period of 180 days.

Table 11.1.2: Performance characteristic grades by Tepke and Tikalsky (2007)

Performance Characteristic	Test Method	Grade 1	Grade 2	Grade 3
Compressive Strength (CS), ksi	AASHTO T22	3.5≤CS<8.0 @ 28 days	8.0≤CS @ 28 days	3.5≤CS @ early ages
Shrinkage (S), με	ASTM C157	S≤600 @ 56 days	S≤400 @ 56 days	S≤200 @ 56 days
Chloride Penetration (ChP), coulombs	AASHTO T277	ChP≤4000 @ 56 days	ChP≤1500 @ 56 days	ChP≤800 @ 56 days
Freezing-and-thawing Durability (F/T) (relative modulus after 300 cycles)	AASHTO T161 Proc. A after 28 days moist curing and 7 days air drying	60%≤F/T	80%≤F/T	90%≤F/T

There exist some practical difficulties in implementing the above performance criteria. For example, MAP grouts like EUCO-SPEED MP and Set® 45 HW should be air cured for 8 hours, as overnight cure materials, while HPC should be cured for 7 days, as 7-day cure materials, by both the membrane-forming compound method and the water method with burlap. However, proposed test methods in Table 11.1.1 and 11.1.2 have a very different curing scheme. The test methods need also be modified based on the following considerations. For the shrinkage, when shrinkage occurs after initial moist curing, concrete starts to develop stiffness as measured by the modulus of elasticity. High performance concretes often have low w/cm (water to cementitious materials ratios) and high stiffness as a result. If the shrinkage strains are high enough, they simply crack due to the restraint, the stiffness, and the drying shrinkage. For CP materials in floor systems, the restraint is developed due to the internal reinforcing steel, especially the steel that runs through the construction joint in the existing concrete member into the next cast adjacent concrete member or section. This creates a tremendous "racking restraint" that does not allow the second adjacent slab to shorten during cooling from hydration heat and also due to later developing drying shrinkage. The AASHTO PP34-99 (1998) restrained shrinkage ring test can test the crack potential, and should be used instead of the ASTM C157 test. There are also issues with the ASTM C1202 rapid chloride permeability test (RCPT). The RCPT has some interference problems with materials such nitrate corrosion inhibitors and even Set® 45. Part of the problem is the epoxy coating that must be bonded to the exterior side walls of the core. The coating does not work well with the material and cannot block the chloride from running through the specimen. To avoid this issue, the ASTM C1543 ponding test is recommended to be used to determine the chloride gradient.

To aid in the selection of candidate CP materials for long-term durability tests, reasonable preliminary performance limits were specified first based on extensive literature reviews as well as the following considerations. To expedite construction and reduce cost, it is desirable to minimize the width of the joint zone. The headed bar detail with a 6 in. lap length was recommended as the improved longitudinal joint detail for DBT bridges by Li et al. (2010). And it was found that a certain compressive strength was needed to develop the headed bars within a short overlap length (Li et al. 2010). A criterion of 6 ksi was proposed for the compressive strength of the CP materials. CDOT Specifications Committee (2005) specified Class H concrete used for bare concrete bridge decks must not exhibit a crack at or before 14 days in the cracking tendency test (AASHTO PP 34). For the chloride threshold level (CTL) for steel corrosion in concrete, Glass and Buenfeld (1995) summarized various research studies and found CTLs to vary from 0.17 to 2.5% (by mass of cement) with a value of 0.2% chosen as a good prediction of CTL for harsh environments. A depth of 1.5 in., corresponding to the minimum concrete cover for #5 and smaller bars cast in CIP concrete exposed to earth or weather by ACI 318-08, was proposed as the maximum depth of chloride penetration for percent chloride of 0.2% by mass of cement after 90-day ponding. To determine the required bond strength, results of the parametric study on joints of DBT bridges described in Chapter 10 was used. In that study, it was found that the maximum shear stress at joints due to live loads was 84 psi (6.09 kip/ft). Thus, a higher limit of 200 psi was proposed for bond strength. For freezing-and-thawing durability, performance characteristic grades by Russell and Ozyildirim (2006) were used; that is, the relative dynamic modulus of

374

elasticity after 300 cycles was required to be greater than 70, 80, and 90%, for Grades 1, 2 and 3, respectively, as shown in Table 11.1.1.

Based on these performance criteria, a preliminary selection was made to narrow down the choices of CP materials in the study from the candidate materials to two different materials in each of the two joint material classifications (i.e., overnight and 7-day cure). Further long-term tests, including freezing-and-thawing durability, shrinkage, bond, and permeability tests, were performed to evaluate the selected four joint materials (two for each cure) in order to validate or finalize the proposed preliminary performance criteria.

11.2. Selection of Candidate Materials for Long-Term Tests

11.2.1. Overnight Cure Materials and Their Preliminary Selection

For the overnight cure, different grout materials were considered as candidate materials. As discussed earlier, published performance data from different grout materials were collected through contacts with material suppliers and users. Based on their potentials to meet the proposed preliminary performance criteria, candidate overnight cure materials were selected as shown in Table 11.2.1 with the mixing information. Five Star® Patch was cement-based, while EUCO-SPEED MP, Set® 45 and Set® 45 Hot Weather were all magnesium-phosphate based. Water and aggregate extension amounts used were based on manufacturer recommendations. The aggregate used was 3/8 in. pea gravel, which was tested for fizzing with 10% HCL to avoid calcareous aggregate made from soft limestone.

375

Table 11.2.1:   Candidate overnight cure materials including mix proportions

Product Name		Mixing Quantities per 50-lb, Bag				
		Initial Water, pints	Additional Water, pints	Aggregate Extension, % by weight	Aggregate Extension, lb	Yield Volume, cu. ft.
Neat Grout	EUCO-SPEED MP	3.1	0.5	0	0	0.42
	Five Star® Patch	5.00	1.00	0	0	0.40
	Set® 45	3.25	0.50	0	0	0.39
	Set® 45 HW	3.25	0.50	0	0	0.39
Extended Grout	EUCO-SPEED MP	3.1	0.5	60	30	0.57
	Five Star® Patch	5.00	1.00	80	40	0.66
	Set® 45	3.25	0.50	60	30	0.58
	Set® 45 HW	3.25	0.50	60	30	0.58

The preliminary selection was based on strength tests of selected materials to narrow the choices down to two different materials in the overnight cure material classification. For neat grouts, the compressive strength was tested per ASTM C 109 modified. Both ASTM C 109 modified and ASTM C 39 modified were used to obtain the compressive strength for extended grouts to get both the cube strength and the cylinder strength. Both ASTM C 109 and ASTM C 39 required moist curing. However, the manufacturers for EUCO-SPEED MP, Set® 45 and Set® 45 HW did not recommend wet curing their products. Thus two normally used curing methods, air curing and moist curing, were investigated. The compressive strengths using these two curing methods are compared in Figure 11.2.1. The reported strength was the average of three specimens. As shown in Figure 11.2.1, the extended grouts gained strength slower than the corresponding neat grouts. Also, for the extended grouts, there was no significant difference between the strengths achieved by the two curing methods, although for neat grouts, there was a difference for the 4-hour strengths when comparing two curing methods except for Five Star® Patch.

376
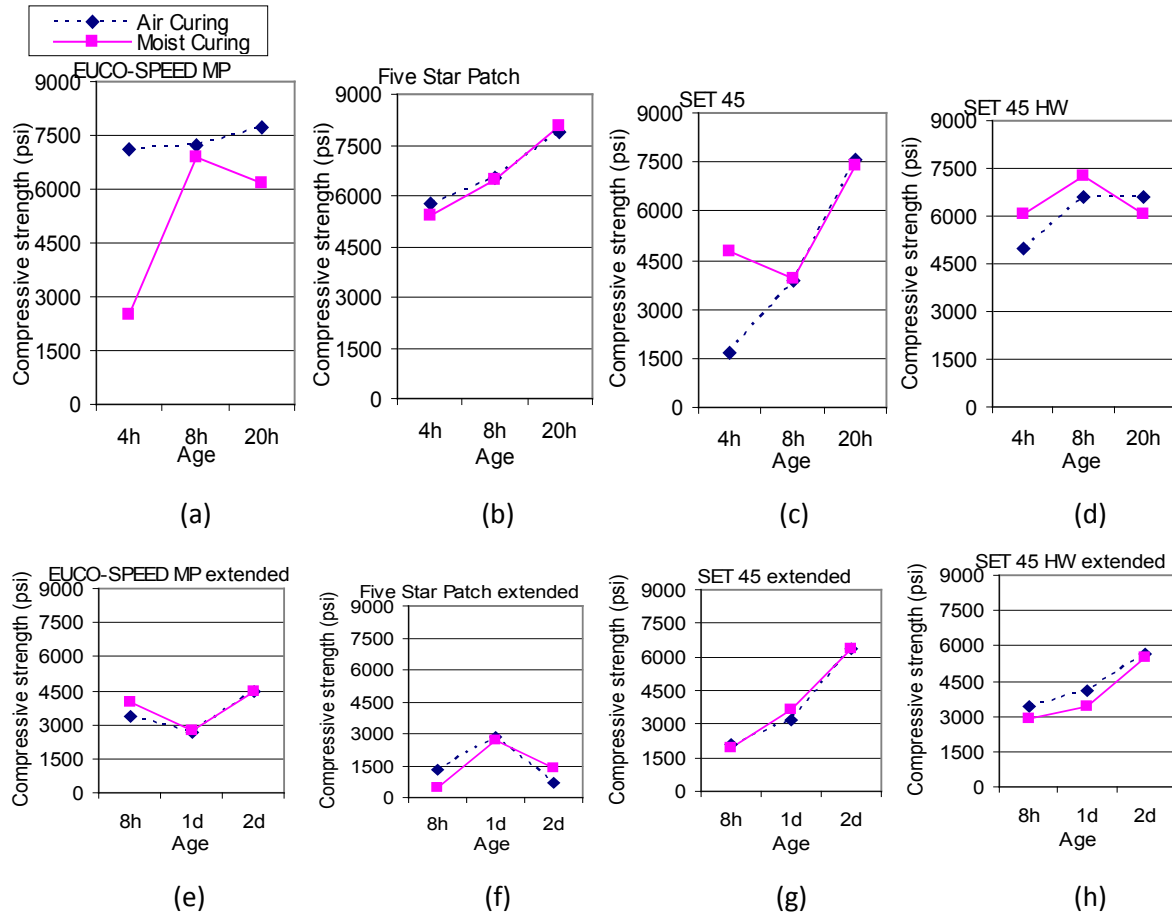
Figure 11.2.1: Compressive strength development of the neat grouts per ASTM C 109 and extended grouts per ASTM C 39. ("h"=hour; "d"=day)

Flow characteristics for each grout were measured in accordance with ASTM C 1437 modified. Specifications for the flow table and truncated flow cone were found in ASTM C 230. In these tests, the table was dropped 10 times within 15 seconds instead of 25 drops within 15 seconds according to the standard test method. The modification was needed to consider the fact that these particular types of grouts tend to flow better than the average mortars for which this test method was intended. Twenty-five drops would result in the grout spreading across the entire 10 in. diameter of the table and the purpose of the test would be lost. Flow results are presented in Figure 11.2.2. Observations were made regarding the workability of each grout based on the degree of effort required to mix each product as well as their work time and initial set time, as given in Table 11.2.2. Work time was measured from the start of mixing until workability began to decrease. Decreased workability was defined by the inability to move the grout with vibration, or easily finish a surface. Initial set time was measured from the start of mixing until the product showed resistance to the penetration of a thin rod or trowel edge.

377
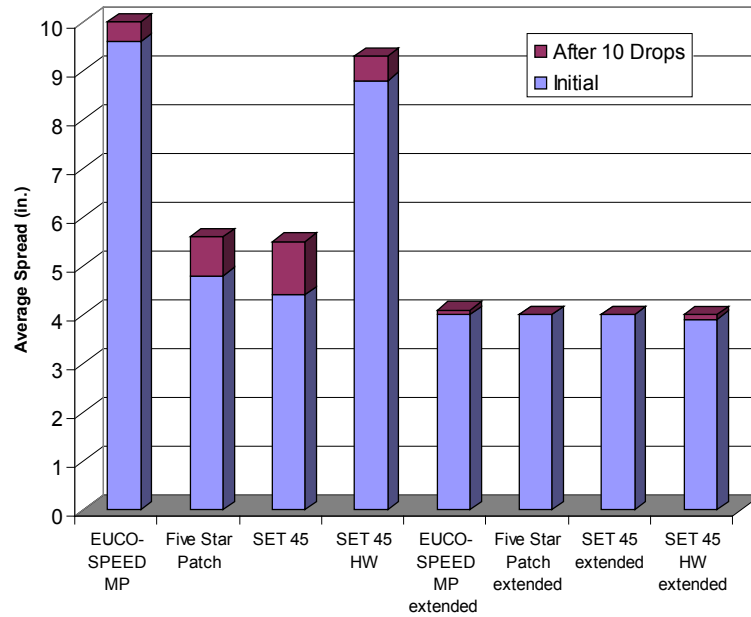
Figure 11.2.2: Truncated flow cone spread values per ASTM C 1437 for neat gouts and extended gouts

Table 11.2.2 Candidate grout workability observations for neat gouts and extended grouts

Grout	Work Time, min.	Initial Set Time, min.	Consistency
EUCO-SPEED MP	8	14	medium
Five Star® Patch	18	32	medium
Set® 45	6	10	medium
Set® 45 HW	32	47	runny
EUCO-SPEED MP extended	16	21	thick
Five Star® Patch extended	13	27	thick
Set® 45 extended	10	18	thick
Set® 45 HW extended	30	45	thick

Among the grout candidates, EUCO-SPEED MP and Set® 45 HW performed better than the remaining grouts based on the flow and workability performance. All of the extended grouts did not perform well in the flow cone spread testing. With regard to the workability, only Set® 45 HW extended had favorable workability results. Five Star® Patch extended 80% and Set® 45 extended 60% were almost impossible to mix with such a high recommended aggregate extension. Their flow suffered because of this. All the extended grouts exhibited lower strength than the corresponding neat grouts at an age of 8 hours. A lower aggregate

378

extension ratio would be more suitable for use in a precast deck panel system. Comparing the compressive strength and flow and workability performance of both neat and extended grouts, EUCO-SPEED MP and Set® 45 HW were selected for further evaluation.

11.2.2. 7-Day Cure Materials and Their Preliminary Selection

For the 7-day cure materials, standard or special concrete and mortar mixtures, including five HPC mixtures, Emaco® T430 mix with latex, LMC-VE and two RSLP mixes, were considered as candidate materials. The candidate HPC mix designs are listed in Table 11.2.3. Mixes 1 to 3 were selected from Russell et al. (2006), and Mix 4 and 5 were developed by working with River Region Cement Division of Lafarge. Emaco® T430 mix with latex was developed by working with BASF Construction Chemicals, LLC, LMC-VE by working with the Virginia DOT, and RSLP mixes by the Virginia DOT and CTS Cement Manufacturing Corporation. The mix designs are given in Table 11.2.4.

379

Table 11.2.3: Candidate HPC mixes and mix proportions

MIX NUMBER	MIX 1	MIX 2	MIX 3	MIX 4		MIX 5	
W/CM Ratio	0.31	0.35	0.31	0.32		0.35	
Cement Type	I	I	II	I / II (Lafarge Sugar Creek SF)		I / II (Lafarge Sugar Creek SF)	
Cement Quantity, lb/yd^3	750	474	490	563*		431*	
Fly Ash Type C Quantity, lb/yd^3	75	221	210	75		58	
Slag Quantity, lb/yd^3				113		86	
Fine Aggregate, lb/yd^3	1400	1303	1365	1161		1308	
Coarse Aggregate Maximum Size, in	0.5	1	1.25	1.5	0.5	1.5	0.5
Coarse Aggregate Quantity, lb/yd^3	1400	1811	1900	1530	270	1520	380
Air Entrainment, fl oz/yd^3	5		3.1	3		2.3	
Water reducer, fl oz/yd^3	30						
Retarder, fl oz/yd^3		22	28				
High-Range Water Reducer, fl oz/yd^3	135	122	156	60		46	
Shrinkage Reducing Admixture, fl oz/yd^3				32		24.7	

* 7% of silica fume is included in blended cement.

380

Table 11.2.4: 7-day cure mixes and mixture proportions, lb/yd^3

Mixture	Emaco® T430 mix with latex	LMC-VE	RSLP Mix 1	RSLP Mix 2
Cement/Mortar Type	Emaco® T430	CTS Rapid Set® cement	CTS RSLP	CTS RSLP
Cement/Mortar Quantity	2530	658	665	658
Fine Aggregate	---	1600	1200	1695
Coarse Aggregate* Quantity	1380	1168	1800	1454
Latex	30	205	---	---
Water	170	137	280	263

* Coarse aggregate maximum size is 0.5 in.

Three HPC mix proportions were first selected from the five candidate HPC mixes in Table 11.2.3 using the worksheet developed by Lawler et al. (2007). A statistically based experimental methodology was used in the worksheet to identify the optimum concrete mixture proportions for a specific set of conditions, as well as to predict performances of hydraulic cement concrete mixtures incorporating supplementary cementitious materials. In the worksheet, "desirability" was introduced. Desirability is a function that converts any test result into a value between "0" and "1", where "0" means the result is unacceptable, and "1" means the result needs no improvement. Intermediate values show the level of acceptability (desirability) of the result. The overall desirability for each mixture is the geometric mean of the individual desirability for that mixture for each test. "Response" is the measured value from a performance test. According to the criteria employed for the study, the four responses were associated with the compressive strength at 7 day, shrinkage, chloride penetration and freezing-and-thawing durability. The corresponding desirability functions of the four "responses" were selected. Using standard linear regression analysis to obtain the response of a given mix that best fit the testing data, a model was developed by Lawler et al. (2007), which can be used to predict the desirability functions of an untested mixture. Based on this procedure, Mix 1, 4 and 5 were selected, comparing the predicted overall desirability and 7-day compressive strength desirability of the five HPC mixes based on the model.

Compressive strength tests were performed on the remaining seven 7-day cure materials, HPC Mix 1, Mix 4 and Mix 5 and Emaco® T430 mix with latex, LMC-VE, RSLP Mix 1 and RSLP Mix 2, for further selection. The compressive strengths at 7 days and 28 days of the remaining seven 7-day cure materials are listed in Table 11.2.5. The reported strength was the average of three cylinders. Based on the compressive strengths, HPC Mix 1 and RSLP Mix 2 were selected as the two 7-day cure materials for the long-term tests.

Table 11.2.5: Compressive strengths (psi) per ASTM C 39 Modified

	HPC Mix 1	HPC Mix 4	HPC Mix 5	Emaco T430 mix	LMC-VE	RSLP Mix 1	RSLP Mix 2
7-day Compressive Strength	6494	4112	5058	1470	4404	3820	10564
28-day Compressive Strength	8895	5269	7309	2307	4389	4232	11262

11.3. Long-Term Tests

Long-term tests were performed on the four candidate materials selected (i.e., EUCO-SPEED MP and Set® 45 HW for the overnight cure materials, and HPC Mix 1 and RSLP Mix 2 for the 7-day cure materials). The long-term tests included freezing-and-thawing durability, shrinkage, bond, and permeability tests.

11.3.1. Bond Strength Test

The bond strength test was conducted per ASTM C 882 modified. Scholz et al. (2007) investigated slant cylinder bond strength of eight grouts with varying concrete surface preparations: a) smooth, b) exposed aggregate, c) raked, and d) raked and sandblasted. There was not a particular preparation found that consistently provided the best bond strength for all of the tested grouts. Scholz et al. (2007) concluded that the smooth interface performed better than anticipated, providing the worst or second worst bond strength for only half of the candidate grouts. For the cost involved with the other surface preparations (i.e., exposed aggregate, raked and sand blasting), the smooth interface was used for the NCHRP 10-71 study.

The concrete half-cylinders were made using the mold and dummy section shown in Figure 11.3.1-a. After curing for at least 28 days, the half cylinders were inserted into a whole 4 in. by 8 in. cylinder mold. Then for the overnight cure materials, the grout was poured into the mold to complete the cylinder (see Figure 11.3.1-b). For the 7-day cure materials, a layer of cement paste was first applied onto the slanted face of the half-cylinder and then the test material was poured into the mold to complete the cylinder. Specimens for two overnight cure materials were air cured for 8 hours, while specimens for two 7-day cure materials were cured for 7 days by both the membrane-forming compound method and the water method with burlap, a typical practice for curing bridge decks.

After curing, cylinders were tested in compression to investigate the bond strength of each material. The test setup is shown in Figure 11.3.1-c. Observations were made to determine whether the cylinders failed along the shear plane or if failure was due to significant cracking in the grout or concrete. The failure modes are shown in Figure 11.3.2 and described in Table 11.3.1. In each case, the maximum load was recorded and converted to stress by dividing by the elliptical area of the bonded interface, as suggested by Scholz et al. (2007). The maximum load was multiplied by the cosine of 30° to obtain the true shear stress component

382

acting along the bonded interface. Results for the slant cylinder tests are presented in Table 11.3.1. The strength results represent the average of three cylinders. All the materials had bond strengths greater than 300 psi, and the lower-bound of the criterion was subsequently increased from 200 to 300 psi.

(a)   (b)   (c)
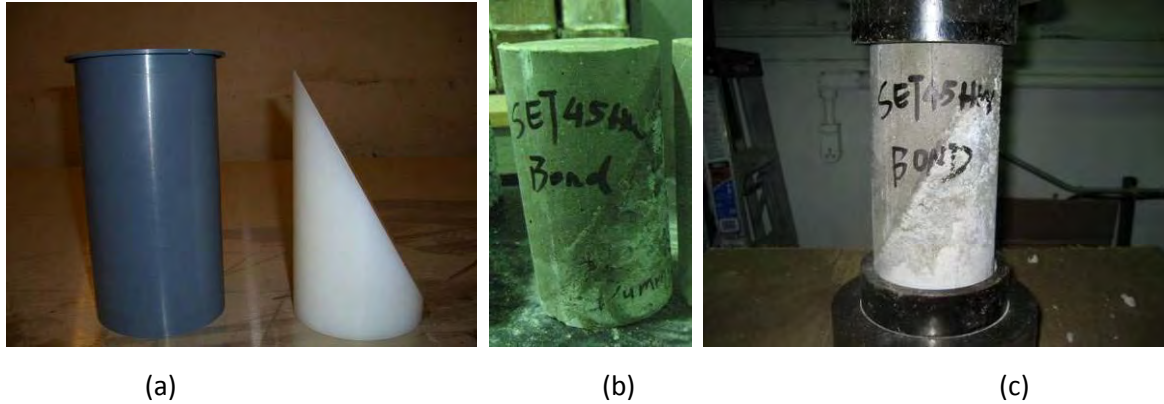
Figure 11.3.1: ASTM C882 Test: (a) Test mold and dummy section (b) Completed slant shear cylinders ready for testing (c) Test setup

(a)   (b)   (c)
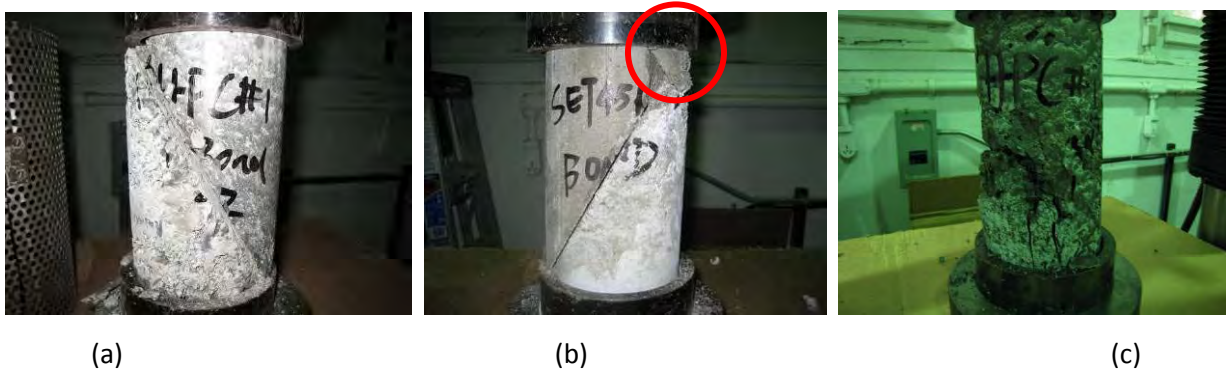
Figure 11.3.2: ASTM C882 Test Failure Modes (a), (b) and (c)[*]

[*]Descriptions of the three types of failure modes a-c are provided in footnotes to Table 11.3.1

Table 11.3.1 Slant cylinder bond strength and failure mode

Material Type	Specimen Number	Test Age	Shear Stress (psi)	Average Shear Stress (psi)	Mode of Failure*
EUCO-SPEED MP	1	8 hours	456	397	b
	2		159		b
	3		576		b
Set® 45 HW	1	8 hours	1161	1176	b
	2		1121		b
	3		1240		b
HPC Mix 1	1	7 days	1607	1817	c
	2		1917		a
	3		1925		a
RSLP Mix 2	1	7 days	659	705	a
	2		634		a
	3		823		a

*a) clean shearing of bond along slanted interface (Figure 11.3.2-a)

b) grout and/or concrete cracking before interface bond failure. However, it was possible to load the specimen until the bonded interface failed. (Figure 11.3.2-b)

c) grout cracked and split in a vertical manner so that it was not possible to continue loading the specimen (Figure 11.3.2-c)

11.3.2. Permeability Test

As discussed earlier, the ponding test was prepared in accordance with ASTM C 1543 modified instead of the ASTM C1202 test. Three specimens (10×10×3 in.) for each of the selected overnight cure materials, EUCO-SPEED MP and Set® 45 HW, and 7-day cure materials, HPC Mix 1 and RSLP Mix 2, were cast. Specimens for the two overnight cure materials were air cured for 8 hours, while the two specimens for the 7-day cure materials were cured for 7 days by both the membrane-forming compound method and the water method with burlap. After curing, the sides of the specimens were coated with the rubber coating

384

material, 1 in. high closed-cell polystyrene foams were bonded to the specimens with silicone sealant, and then the specimen were subjected to continuous ponding with a 3% sodium chloride solution to a depth of approximate 0.8 in for 90 days, as shown in Figure 11.3.3-a. The specimen surfaces were then brushed with a wire brush to remove the salt, and 4 in. cores were taken as shown in Figure 11.3.3-b. The core cylinders were then cut into slices. Four slices were cut from different depths (Layer 1: 0-0.25 in.; Layer 2: 0.25-0.75 in.; Layer 3: 0.75-1.25 in. and Layer 4: 1.25-1.75 in). The concrete slices were then dried at 105 °C to constant mass and ground with a pulverizer to pass an 850-µm sieve [No. 20] sieve. So for each specimen, powder samples were obtained at four corresponding depths. A solution was made with each powder sample following the ASTM C 1152 modified procedure.

| (a) Ponding of specimens | (b) Specimen coring |

Figure 11.3.3: Specimen preparation per ASTM C 1543

Figure 11.3.4: Chloride concentration determination with ISE

The titration test was introduced in the ASTM C 1152 to determine the chloride concentration. However, this method was very time-consuming. The tests by Ghanem et al. (2008) showed that the chloride ion selective electrode (ISE) matched titration readings, and suggested that the chloride concentration can be

385

taken directly using the ISE. Consequently, the chloride ISE was used rather than the titration test. The ISE was calibrated using chloride solutions with five different concentrations. These solutions were obtained by diluting a 100 ppm solution two, five, ten, and 100 times to get solutions with concentrations ranging from 1 to 100 ppm. A calibration curve was constructed with the measured electrode potential in mV (linear axis) plotted against the concentration (log axis). The mV readings of the sample solutions were taken, as shown in Figure 11.3.4, and the concentration was then determined from the calibration curve. The chloride concentrations were analyzed and are shown in Figure 11.3.5.
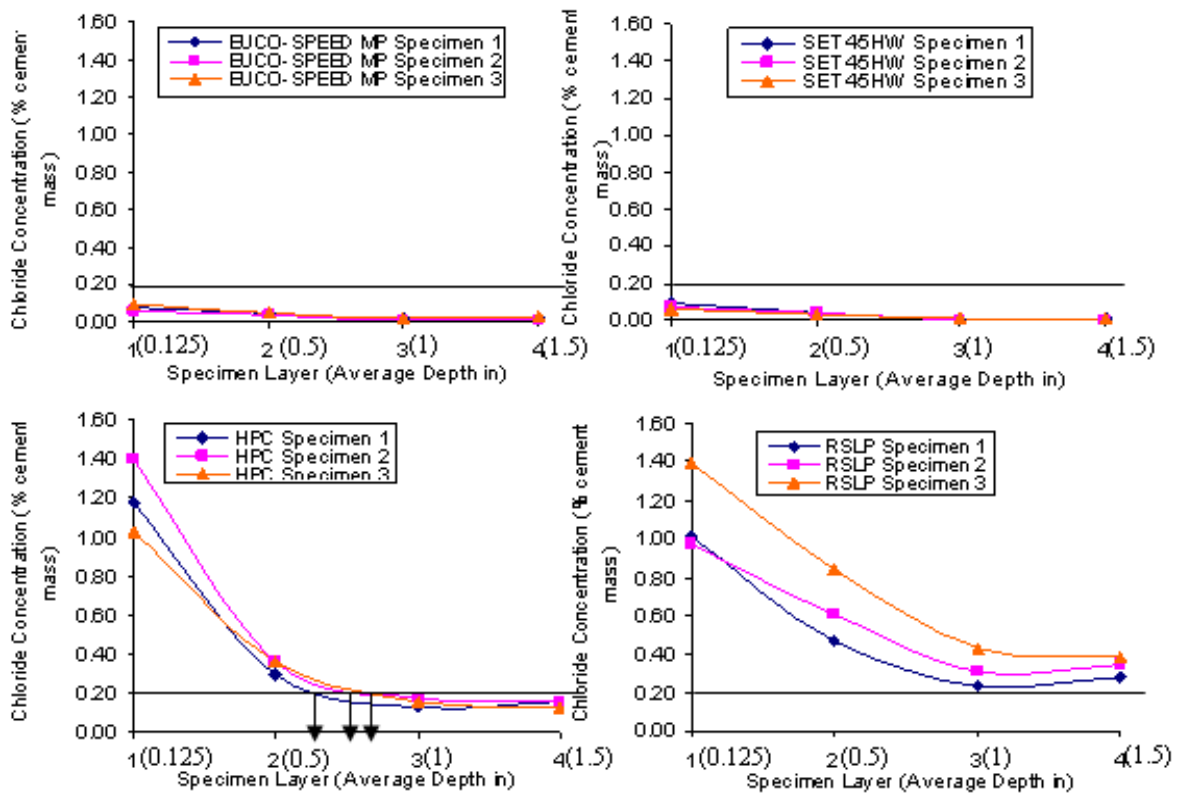
Figure 11.3.5: Chloride content profile after 90-day ponding test

(Layer 1: 0-0.25 in.; Layer 2: 0.25-0.75 in.; Layer 3: 0.75-1.25 in. and Layer 4: 1.25-1.75 in.)

Table 11.3.2: Depths (in.) for 0.2% chloride content (by mass of cement)

Materials	Sample		
	1	2	3
EUCO-SPEED MP	<0.125	<0.125	<0.125
Set® 45 HW	<0.125	<0.125	<0.125
HPC Mix 1	<1	<1	<1
RSLP Mix 2	>1.5	>1.5	>1.5

The depths for the 0.2% chloride content (by mass of cement) for the four materials were calculated based on Figure 11.3.5, as listed in Table 11.3.2. Note that the "down arrows" in Figure 11.3.5 for the HPC mixes indicate the depths at which the 0.2% chloride content (by mass of cement) threshold was exceeded. For calculating the depths, average depths of 0.125, 0.5, 1.0, and 1.5 in. were assigned to the respective layers (Layers 1-4). The two overnight cure CP materials had depths for 0.2% chloride content less than 0.125 in. For the 7-day cure CP materials, HPC Mix 1 was less than 1.0 in, and the RSLP Mix 2 was greater than 1.5 in. The two overnight cure and one of the 7-day cure materials, HPC Mix 1, met the criterion (i.e., 0.2% chloride content was not exceeded at a depth of 1.5 in.).

11.3.3. Freezing-and-Thawing Test

The freezing-and-thawing test was prepared in accordance with ASTM C 666 Procedure A modified. Specimens for two overnight cure materials were air cured for 8 hours, while specimens for the two 7-day cure materials were cured for 7 days by both the membrane-forming compound method and the water method with burlap. After curing, specimens were moisture-conditioned in saturated lime water at $23.0\pm2^{o}C$ ($73.4\pm3^{o}F$) for 48 hours prior to testing, as specified by ASTM C 666 for specimens sawed from hardened concrete. After curing and 48-hour moisture-conditioning, the test was started as shown in Figure 11.3.6. After 76 cycles, the RSLP Mix 2 specimens failed as shown in Figure 11.3.6-c. The relative dynamic modulus of elasticity after 300 cycles was 92% for EUCO-SPEED MP, 96% for Set® 45 HW, and 96% for HPC Mix 1. Each result was the average of three specimens. EUCO-SPEED MP, Set® 45 HW and HPC Mix 1 performed very well, exceeding the preliminary criterion (i.e., the relative dynamic modulus of elasticity after 300 cycles was greater than 70%, 80%, and 90%, for Grades 1, 2 and 3, respectively).

<center>(a)   (b)   (c)</center>
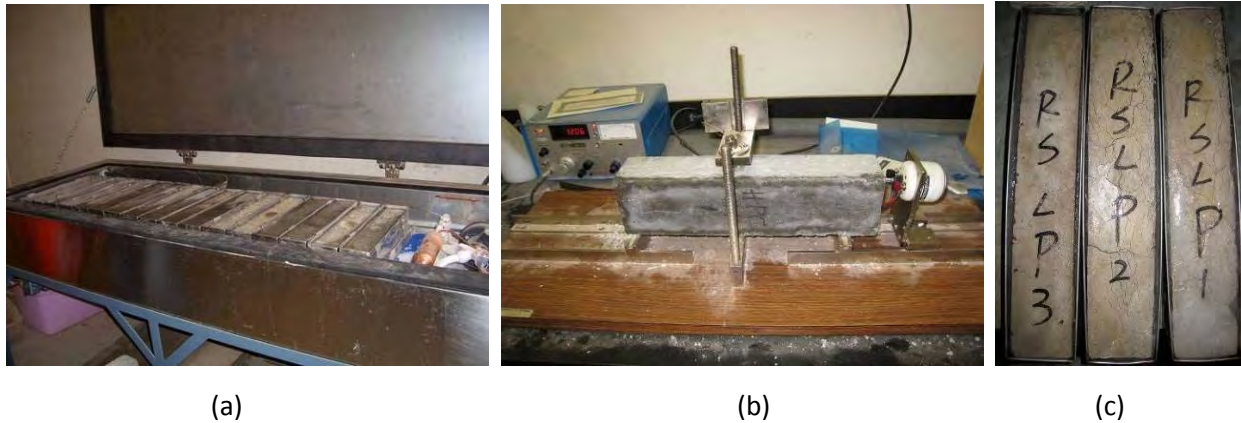
Figure 11.3.6: ASTM C666 Freezing-and-Thawing Durability Test: (a) Freezing-and-thawing apparatus, (b) Fundamental transverse frequency test, (c) Failure of RSLP Mix 2 specimens

11.3.4. Shrinkage Test

For shrinkage, as discussed earlier, the steel ring test was prepared in accordance with AASHTO PP34 (1998) modified as shown in Figure 11.3.7. Strain gages were bonded at four equidistant mid-height locations on the interior of the steel ring and were oriented to measure strain in the circumferential direction. Three ring specimens were fabricated for each material, and were immediately transferred to the curing room with a constant air temperature of 21.0±1.7^{o}C (73.4±3°F) and a relative humidity of 50±4 percent after completion of casting. The strain gages were connected to the data acquisition system to start monitoring the strain development in the steel ring. Specimens for the two overnight cure materials were air cured, while specimens for the two 7-day cure materials were cured by both the membrane-forming compound method and the water method with burlap till the age of 24 hours ± 1 hour. Then the outer ring was removed and the top surface was sealed. The strain development of one specimen is shown in Figure 11.3.8.

Cracks were found for specimens of the HPC Mix 1 at the age of 20.5 days. No crack was observed to occur for the EUCO-SPEED MP, Set® 45 HW and RSLP Mix 2 throughout the tests which were terminated at the ages of 58, 62 and 61 days, respectively. All materials met the criterion (i.e., to not exhibit a crack at or before 14 days).

Figure 11.3.7: AASHTO PP34 test setup
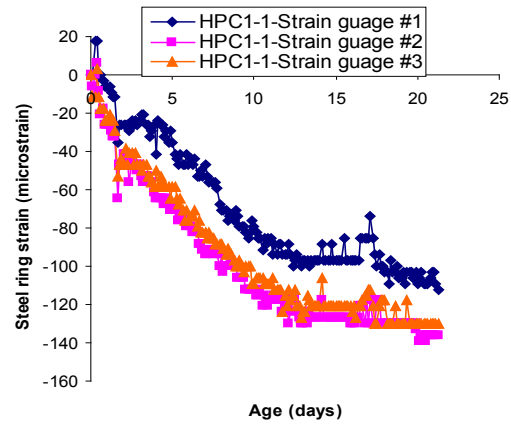
Figure 11.3.8: Steel ring strain versus specimen age for HPC Mix 1

389

11.4. Proposed Performance Criteria and Conclusions

For accelerated bridge construction, both transverse and longitudinal joints in decks may be required. Appropriate selection of CP materials for these deck-joints is critical for long-term durability considerations. Two categories of CP materials, overnight cure and 7-day cure, were proposed and studied. Candidate materials were compared by laboratory tests and software analysis, and two CP materials were selected for each category, as discussed in Section 11.2. Based on extensive literature reviews and the experimental investigation carried out on the selected candidate materials in association with NCHRP 10-71, performance criteria for selecting durable CP materials were developed as listed in Tables 11.4.1 and 11.4.2. Durability tests used to establish the performance criteria with the selected candidate materials included freezing-and-thawing durability, shrinkage, bond, and permeability tests.

Table 11.4.1: Proposed performance criteria of CP materials

Performance Characteristic	Test Method	Performance Criteria		
Compressive Strength (CS), ksi	ASTM C39 modified	6.0≤CS @ 8 hours (overnight cure) @ 7 days (7-day cure)		
Shrinkage[a](S), (Crack age, days)	AASHTO PP34 modified	20<S		
Bond Strength (BS), psi	ASTM C882 modified	300<BS		
Chloride Penetration[b](ChP), (Depth for Percent Chloride of 0.2% by mass of cement after 90-day ponding, in.)	ASTM C1543 modified	ChP<1.5		
Freezing-and-thawing Durability (F/T), (relative modulus after 300 cycles)	ASTM C666 Procedure A modified	Grade[c] 1	Grade 2	Grade 3
		70%≤F/T	80%≤F/T	90%≤F/T

a: No S criterion need be specified if the CP material is not exposed to moisture, chloride salts or soluble sulfate environments.

b: No ChP criterion need be specified if the CP material is not exposed to chloride salts or soluble sulfate environments.

c: Grades are defined in Table 11.4.2.

390

Table 11.4.2: Application of CP material grades for freezing-and-thawing durability

Freezing-and-thawing Durability (F/T)	Is the concrete exposed to freezing-and-thawing environments?	Yes	Is the member exposed to deicing salts?	Yes	Will the member be saturated during freezing?	Yes. Specify F/T-Grade 3
						No. Specify F/T-Grade 2
				No. Specify F/T- Grade 1		
		No. F/T grade should not be specified.				

391

Chapter 12 Longitudinal Joint Details for Accelerated Bridge Construction: Fatigue Evaluation

12.0   Introduction

Chapter 9 presented results of a preliminary study that assessed potential longitudinal and transverse joint connection details for CIP joints between DBTs or full-depth precast panel to panel connections. The investigation was conducted in two phases. During Phase I, lapped headed reinforcement and two kinds of lapped U-bar reinforcement (i.e., deformed wire (DWR) and stainless steel (S)) were tested to determine the most promising connector. Monolithic reinforced concrete flexural specimens were constructed for each of the three types of connections to simulate the forces that would be experienced in a longitudinal deck joint, and monolithic reinforced concrete tension specimens were fabricated for each of the three types of connections to simulate the forces that would be experienced in a transverse joint over an interior pier. Based on that study, the DWR U-bar detail was deemed the most promising in terms of overall performance, constructability and cost. In the second phase of experiments, six specimens with the DWR U-bar detail were tested, three in flexure and three in tension, to investigate effects of variables including overlap lengths, rebar spacings, and concrete strengths. A DWR U-bar detail with a 6 in. overlap length and 4.5 in spacing was selected for additional testing to further investigate replacing the current welded steel connector detail. This chapter describes the test program and presents results of this additional testing to investigate its feasibility for the longitudinal joint, and Chapter 13 investigates the U-bar detail for the transverse joint.

Four pairs of large-scale slabs were fabricated to investigate the flexure and flexure-shear behavior of the longitudinal joints fabricated using the DWR U-bar detail with a 6 in. overlap length. Two closure pour (CP) materials were investigated based on the most promising overnight and 7-day cure CP materials summarized in Chapter 10: SET® 45 HW without extension for the overnight cure and HPC Mix1 for the 7-day cure material. In the longitudinal joint study, two of the specimens incorporating CP overnight-cure materials were fabricated with grout SET® 45 HW with 60% extension.

A total of eight tests were conducted, which required the reuse of the four pairs of large-scale slabs. Each slab had U-bars and shear keys along two opposite edges, so after completing tests on the first joint, the panels were separated and another joint was assembled by using the other two edges of the slabs to create a second specimen. The eight tests consisted of static flexure (SF), static shear (SS), fatigue flexure (FF) and fatigue shear (FS) tests conducted on longitudinal joints with two different types of closure pour (CP) materials (overnight and 7-day cure materials).

The loads applied to the joints were based on the analytical parametric study summarized in Chapter 10, which was conducted to provide a database of maximum forces used to determine the service live and fatigue loading demand for the slab tests described in this and the subsequent chapter. The results of the static and fatigue tests under four-point pure-flexural loading, as well as three-point flexural-shear loading, are described in this chapter. The test results were evaluated based on flexural capacity, curvature

392

behavior, cracking, deflection and steel strain. Based on these test results, the U-bar detail was deemed to be a viable connection system for the longitudinal joint.

12.1.   Experimental Program

12.1.1. Slab Dimension

A total of eight slabs with the same dimensions were fabricated for the static and fatigue testing, with two different closure pour materials used in the longitudinal joint. Each specimen consisted of two panels connected by a longitudinal joint as shown in Figure 12.1.1. Each panel was 72 in. wide, 64 in. long and 6-¼ in. deep. The female-to-female shear key was provided at the vertical edge of both ends in the specimen length direction. This allowed each slab to be used for two tests.
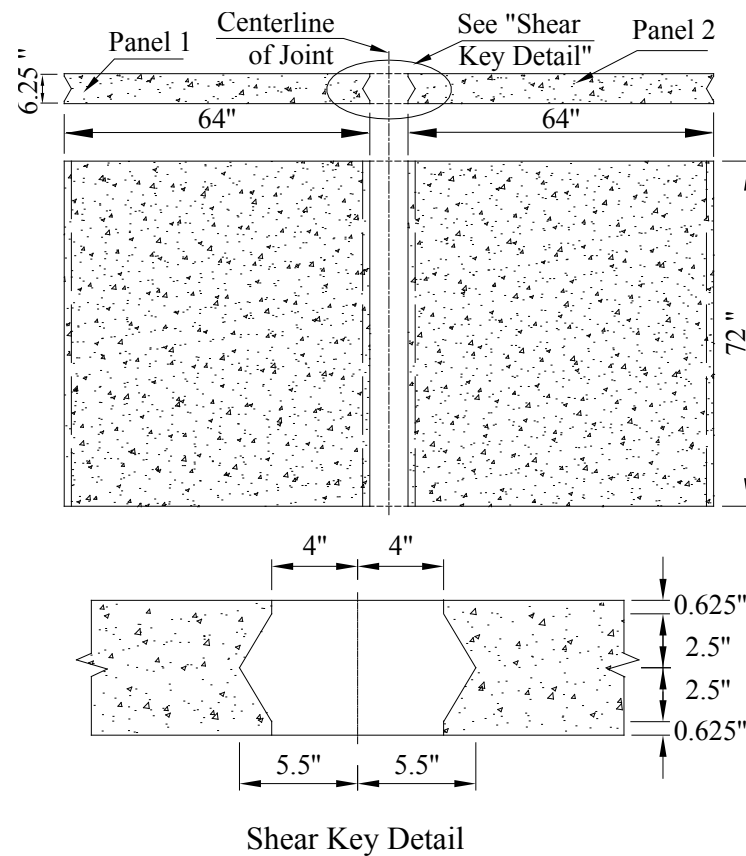
Figure 12.1.1: Dimensions of longitudinal joint specimen

12.1.2. Reinforcement Layout and Strain Gage Instrumentation

Figure 12.1.2 displays the reinforcement layout used in the longitudinal joint specimen. There were four layers of reinforcement in each panel along the specimen depth direction with 2 in. cover at the top and 1

393

in. cover at the bottom. The straight bars simulated longitudinal reinforcement while the U-bars simulated the transverse reinforcement in the bridge deck. The reinforcement details in the specimen were as follows: #5 straight bar spaced at 6 in. at the bottom along the slab length direction; #4 straight bar spaced at 12 in. at the top along the slab length direction. Note that the longitudinal reinforcement was located within the U-bars to enable the largest diameter bend as possible for the U-bar while still meeting concrete cover requirements. The #5 U- bars projected out of the panel to splice with the U-bars in the adjacent panel in the longitudinal joint. The spacing of the U-bars was 4.5 in. and the overlap length (the distance between bearing surfaces of adjacent U-bars) was 6 in. The interior diameter of bend of the U-bar was $3d_b$.
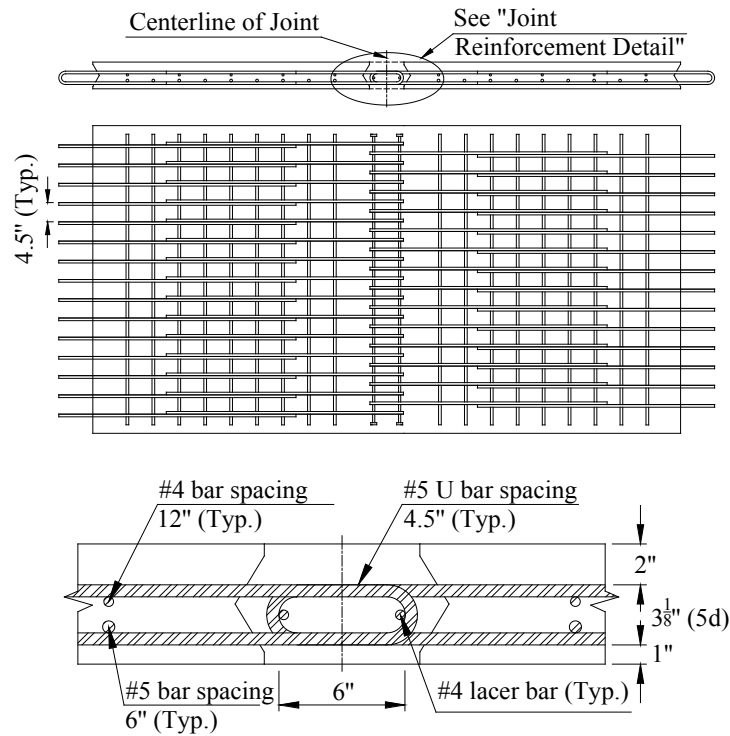
Figure 12.1.2: Reinforcement layout in longitudinal joint specimen

The U-bars around the joint zone were instrumented with strain gages to gain an understanding of the behavior of the slab connected by the longitudinal joint. Figure 12.1.3 depicts the strain gage layout in the slab for the four-point pure-flexure test and the three-point flexure-shear test.

(a) Bars instrumented with strain gages (marked with red)

(b) Strain gage locations for Bar L1 and R1   (c) Strain gage locations for Bar L5 and R4

(d) Strain gage locations for Bar L8 and R7   (e) Strain gage locations for Lacer Bar a
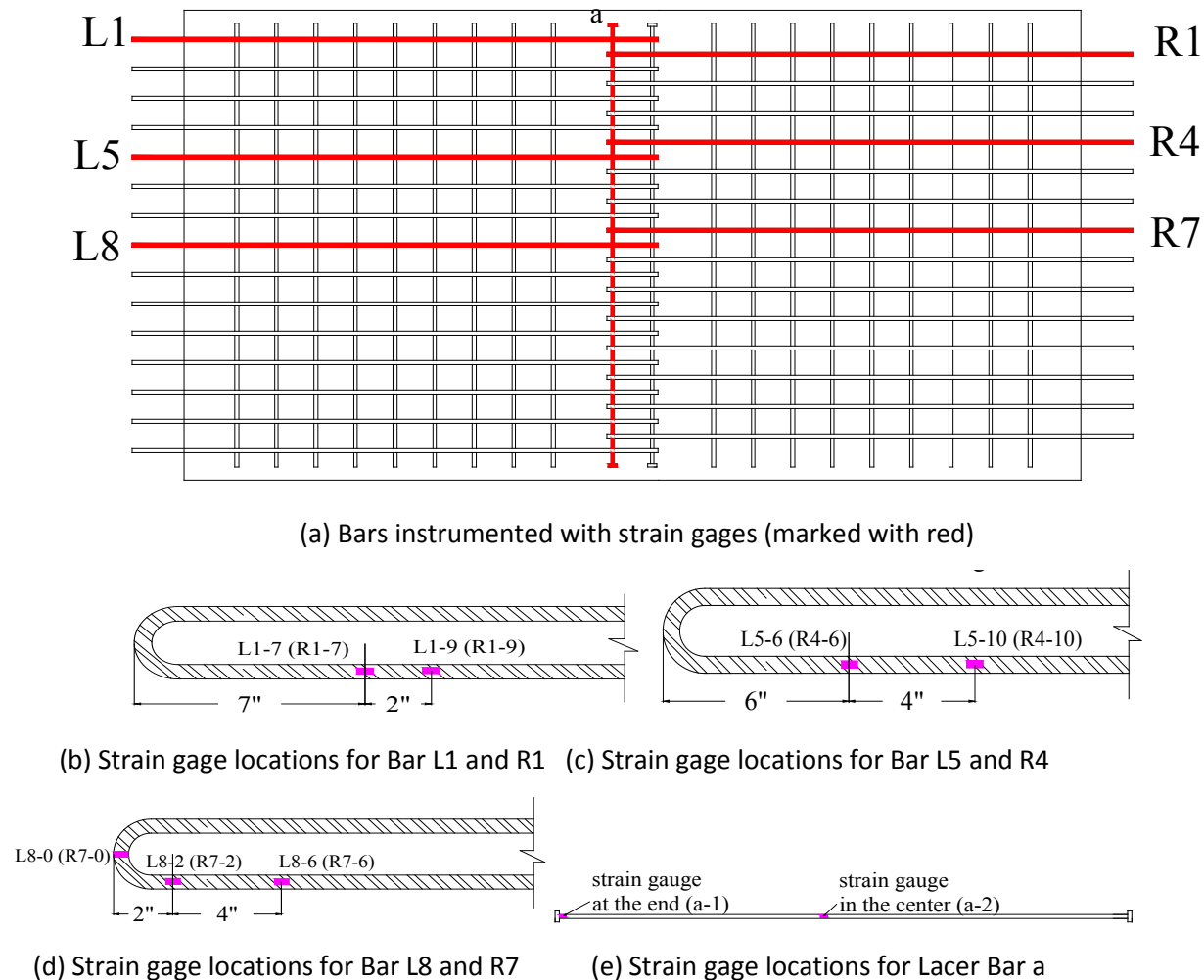
Figure 12.1.3: Strain gage layout

There were six U-bars with installed strain gages. The U-bars were numbered from the edge of the slab (number 1) to the middle (number 8) along the slab width direction. Strain gages were labeled to identify whether it was attached to a U-bar in the left (L) or right (R) slab, the U-bar designator (1-8), and the distance from the outside bend of the bar. For example, strain gage "L1-7" meant the strain gage on U-bar #1 of the left slab, located 7 in. away from the outside bend of the bar. Two strain gages were also placed at the end and middle of the lacer bar, labeled as a-1 and a-2 respectively.

12.1.3. Panel Fabrication

The concrete panels were fabricated locally at Ross Prestressed Concrete Inc. in Knoxville, TN. Figure 12.1.4-a and c show the panel reinforcement before placement of the concrete. The two ends of the wood form, in

395

the length direction, were slotted at a spacing of 6 in. to fix the U-bars in place. Foam wedges were used to form the configuration of the shear key at the vertical edge of the panel. The design concrete compressive strength at 28 days was 7000 psi. Companion concrete cylinders were cast with the panels (Figure 12.1.4-b and d).

| (a) Before pouring (FS & SS Specimens) | (b) After pouring (FS & SS Specimens) |

| (c) Before pouring (FF & SF Specimens) | (d) After pouring (FF & SF Specimens) |

Figure 12.1.4: Panel fabrication

12.1.4. Joint Surface Preparation

The surfaces of the shear key were sandblasted to prepare the joint for the closure pour. The purpose of the surface preparation was to remove all contaminants that could interfere with adhesion and to develop a surface roughness to promote mechanical bond between the CP material and panel concrete. After the

396

removal of the deteriorated concrete, proper preparation should provide a dry, clean and sound surface offering a sufficient profile to achieve adequate adhesion. There were many methods of surface preparation considered such as chemical cleaning, mechanical cleaning and blast cleaning. Sandblasting was chosen, which uses compressed air to eject a high speed stream of sand onto the surface which needed to be prepared. This method is very effective to process the surface of precast members under industrial conditions. Black Beauty 2050 sand was chosen for sandblasting to prepare the surface in this study. The profiles of the surface before and after sandblasting are shown in Figure 12.1.5.

(a) Before sandblasting   (b) After sandblasting

Figure 12.1.5: Profile of joint surface

12.1.5. Closure Pour (CP) Materials

The longitudinal joint was filled with closure pour (CP) material to complete the connection which simulated the longitudinal joint connection at the interface of the top flange of adjacent DBT girders or full-depth precast panel to panel connections, considered to be the structural element of the bridge deck. To facilitate accelerated bridge construction, it is important for the selected CP material to reach its design compressive strength in a relatively short period of time. In this study, it was decided to use two primary CP materials, SET® 45 HW for overnight cure and HPC Mix1 for 7 day cure, selected in Chapter 11. The grout SET® 45 HW used in the longitudinal joint study was investigated both without extension in two joints and with 60% extension in two joints for comparison. The uniform-sized sound 0.25-0.5 in. round pea gravel used to extend the grouts was tested with 10% HCL to confirm that it was not calcareous.

12.1.6. Testing Plan and Setup

397

A total of eight slab specimens were made. Each slab specimen consisted of two concrete panels connected with an overlapping U-bar detail and one of the selected closure pour (CP) materials. During the test setup, each panel was placed on a steel I-beam, which was leveled to ensure that the two panels were on the same plane. At the joint zone, the two panels were positioned to satisfy the 6 in. overlap length and the 4.5 in. spacing of the U-bar (Figure 12.1.6-a). A wood form was use at the bottom and at both ends of the joint to prevent leakage when casting the CP joint. After the CP material was placed, the longitudinal joint slab specimen consisting of 2 panels connected by the joint was ready for testing (Figure 12.1.6-b). Because each panel had U-bars and shear keys along two edges, each set of two panels was used to fabricate two test specimens. After completion of testing the first joint, the panels were separated, and then another joint was reassembled by the other two edges to create the second test specimen.

(a) Before grouting   (b) After grouting
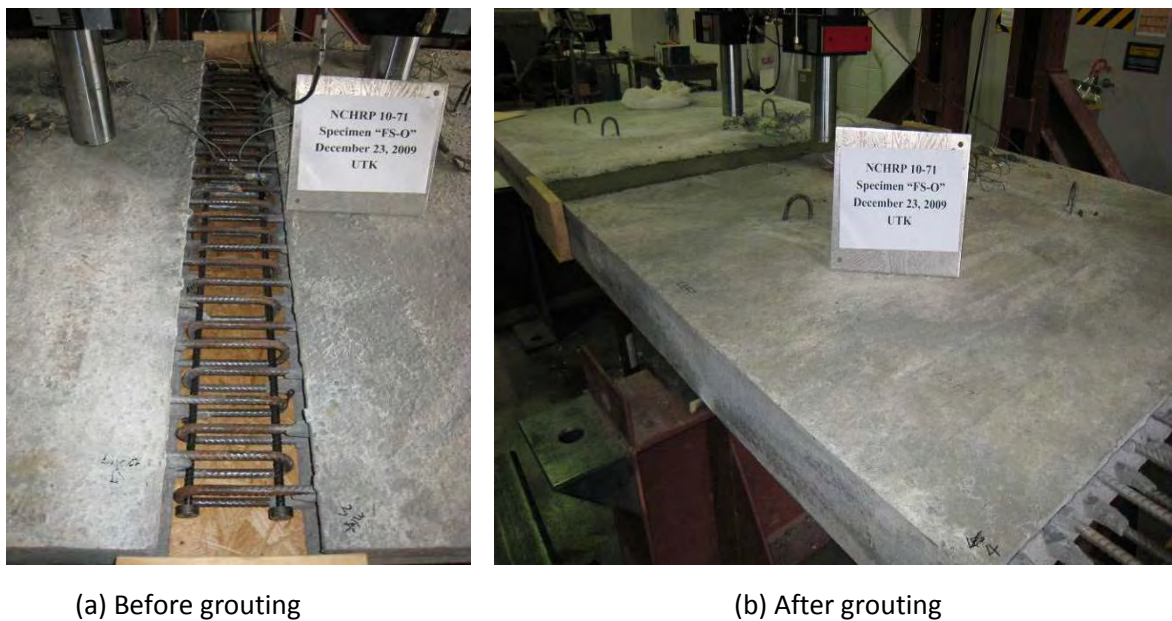
Figure 12.1.6: Longitudinal joint specimen before and after grouting

Eight slab specimens (four for each of two selected CP materials) were tested under different parameters: 1) static flexure (SF) test; 2) static shear (SS) test; 3) fatigue flexure (FF) test, and 4) fatigue shear (FS) test. Table 12.1.1 presents the loading matrix for the eight specimens. Figure 12.1.7 shows the testing setup and the linear motion transducer (LMT) instrumentation layout for each test. All slab specimens were simply supported with a 72 in. span and the joint zone located in the center of the span. A neoprene pad, with two layers of plastic sheets placed between the pad and slab bottom, was used at one end; only the neoprene pad was used at the other end, as shown in Figure 12.1.8. A 10 in. by 20 in. neoprene pad and steel plate were used to simulate the truck tire contact area and the pressure loading. The LMT's were used to measure the specimen deflection, settlement and curvature. Four LMT's (Nos. 4-7 in Figure 12.1.7) were

398

used to measure the vertical deflection along the joint. LMT's 4, 6 and 7 were placed along the centerline of the joint while LMT 5 was placed at the panel edge off the interface of the joint. In this way, the relative deflection between the side of the joint interface and joint center could be measured. LMT's 1-3 and 8-10 were used to measure potential support settlement. Two LMT's, placed horizontally across the top and bottom of the joint, were used to measure the average curvature of the joint zone. DEMEC points were used to measure the width of crack opening at the joint interface with a DEMEC mechanical strain gage. The DEMEC points were glued onto the slab, as shown in Figure 12.1.9.

Table 12.1.1: Slab specimen loading matrix

Overnight Cure				7 Day Cure			
Flexure		Flexure-Shear		Flexure		Flexure-Shear	
Static	Fatigue	Static	Fatigue	Static	Fatigue	Static	Fatigue
SET® 45 HW extended	SET® 45 HW	SET® 45 HW	SET® 45 HW extended	HPC Mix 1			

399

(a) Static Flexure (SF) test

(b) Static Shear (SS) test

(c) Fatigue Flexure (FF) test

(d) Fatigue Shear (FS) test
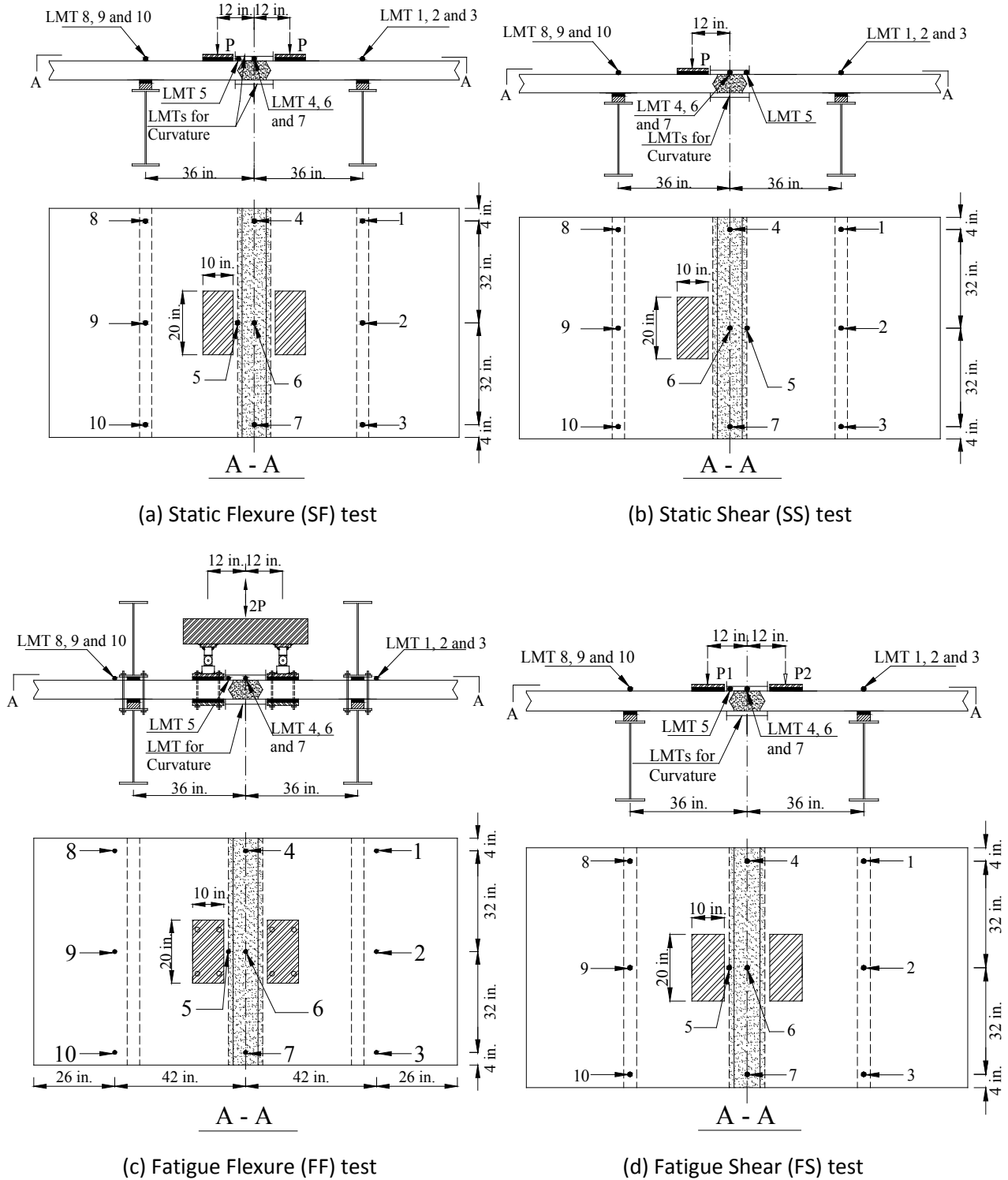
Figure 12.1.7: Longitudinal joint specimen test setup

400

Figure 12.1.8: Simple support boundary condition at edge of longitudinal joint specimen

A - A
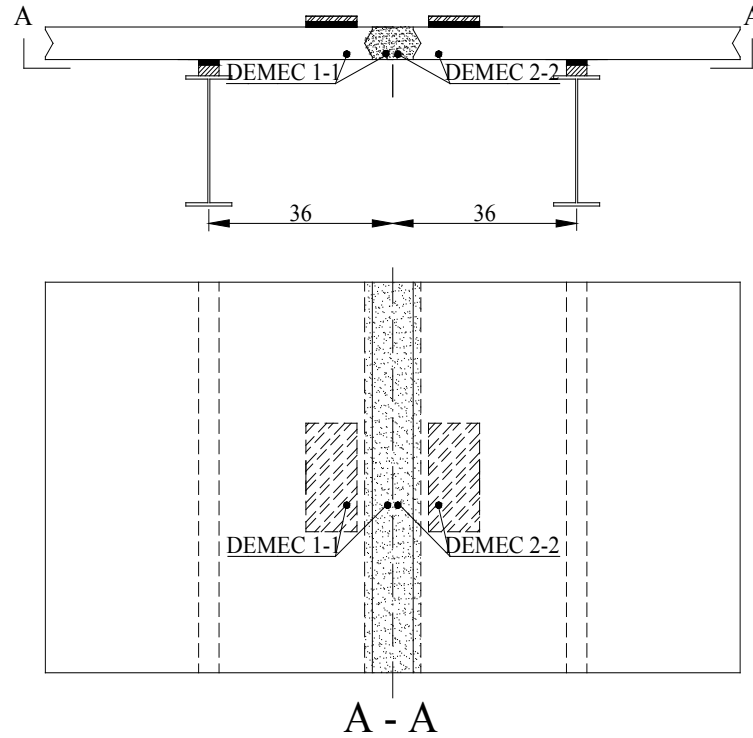
(a) DEMEC points for SF, SS, FS tests

401
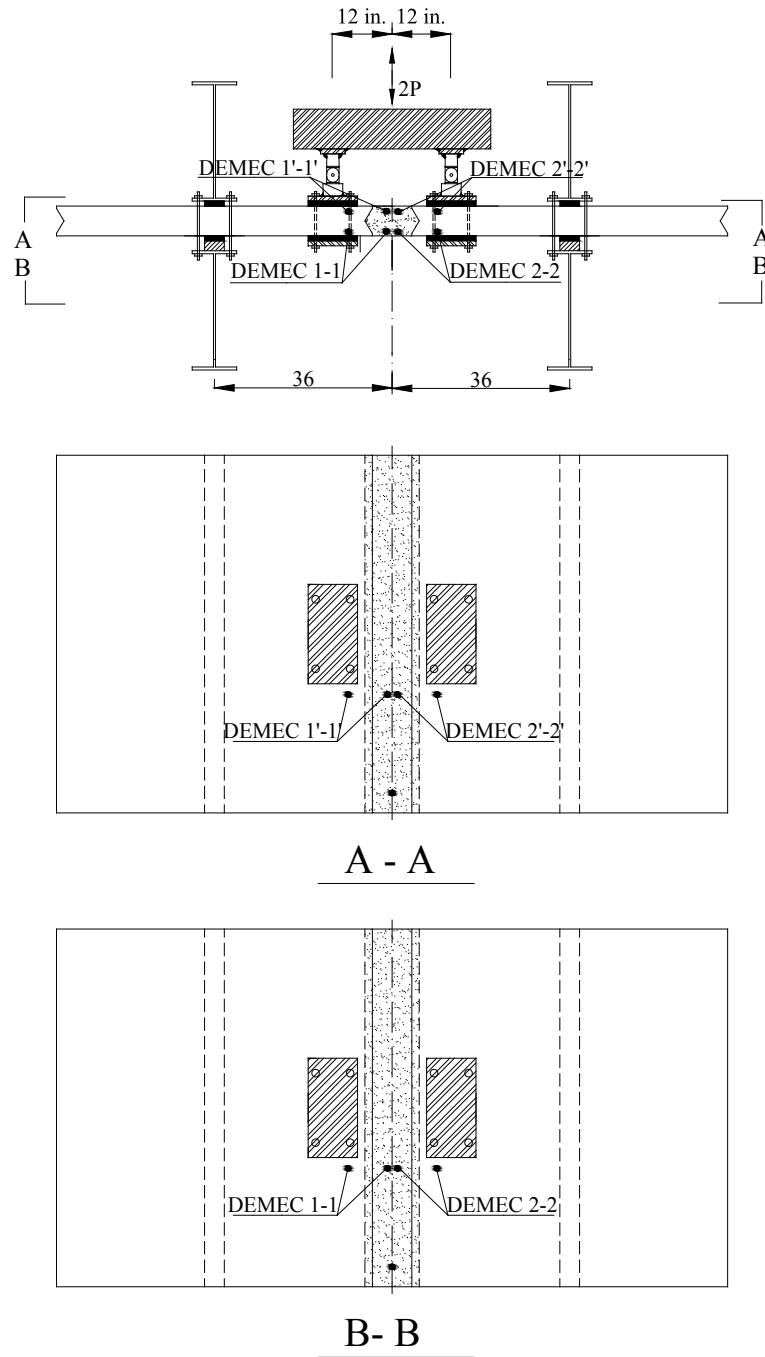
(b) DEMEC points for FF Tests

Figure 12.1.9: DEMEC points

402

The static flexural (SF) test specimens were loaded with two equal loads spaced at 12 in. about the center of the span using Material Test System (MTS) actuators until the specimen failed. The joint zone experienced the maximum constant moment without shear. The static shear (SS) test specimens were loaded with one load located at 12 in. off the center of the span until the specimen failed. The joint zone experienced a combination of moment and shear. Similar to the SF test specimens, the fatigue flexural (FF) test specimens were loaded with two equal loads spaced at 12 in. about the center of the span. Figure 12.1.10 shows the apparatus used to apply the fatigue forces to the joint zone of the specimen.
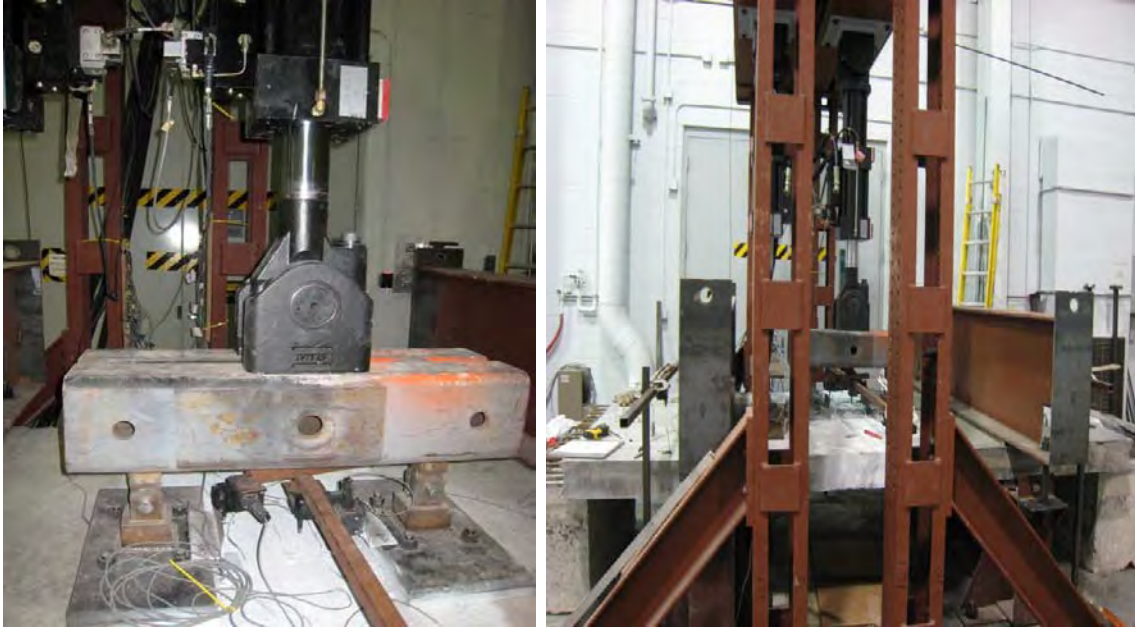
Figure 12.1.10: Test setup for applying fatigue forces

One side of the swivel rod end was screwed to the actuator tightly while the other side was bolted to the load spreader (i.e., spread tube) at midspan by four steel rods. The spread tube was soldered to two steel hinges, which were located 12 in. away from the middle of the spread tube. The other end of each steel hinge was soldered to the 10 in. by 20 in. steel plate. The use of steel hinges between the spread tube and the steel plates was intended to eliminate any extra moment from being applied to the slab specimen produced by the bending of the spread tube. The steel plate and neoprene pad at the bottom of the slab were bolted to the correspondent top steel plate and neoprene pad through the slab by 4 steel rods, which applied the fatigue forces to the slab. The boundary condition was provided by the steel girder below the slab and by the steel girder above the slab. The two steel girders at each support-end (one below the slab and the other above the slab) were connected by bolts. The steel girder below the slab was fixed to the strong floor as shown in Figure 12.1.10. A neoprene pad, with two layers of plastic sheets placed between the pad and slab surface, was used at one end above and below the slab; only the neoprene pad was used

403

at the other end above and below the slab. The two loads spaced at 12 in. about the center of the span in the FS specimens, designated P1 and P2, were applied out-of-phase on each side of the joint during the fatigue test. For example, when "P1" reached the maximum force, "P2" was zero. The joint zone experienced fatigue shear by applying load reversals at the single point load (i.e., reversing the loading directions).

The compressive strength of concrete panel (f'_c) and the compressive strength of grouted joint (f'_{cj}) at the time of testing for each specimen are given in Table 12.1.2. The specimens were designated based on the type of test (e.g., static flexure (SF), fatigue flexure (FF), static shear (SS) and fatigue shear (FS)) followed by the type of cure material used (e.g., overnight cure (O) and 7-day cure (7)). For example, "SS-O" denoted the static shear longitudinal joint connection test with the overnight cure closure pour (CP) material. The joint concrete compressive strength used in the FE models in Chapter 9 to develop a database of maximum forces was 4000 psi.

404

Table 12.1.2: Compressive strength of concrete panel and grouted joint

Specimen	Panel (psi)		Joint (psi)	
	Start of Test	End of Test	Start of Test	End of Test
SS-O	11512*		7586	
SS-7	11512*		8740	
FS-O	10687	11512*	6321	6572
FS-7	11512*	11512*	7861	9417**
SF-O	12441		5939	
SF-7	12441		6966	
FF-O	11711	11632	4592	5345
FF-7	11035	11711	10796***	12361

* The panels for FS-O, FS-7, SS-O, and SS-7 were fabricated with the same batch of concrete and were tested or the test was finished more than 120 days after the panels were fabricated. The 148-day concrete compressive strength of 11,512 psi is the reported strength.

** The test for FS-7 started 5 days after the joint was cast, and finished 13 days after the joint was cast. The strength reported here is the 21-day joint strength.

*** The FF-7 test started at the age of 22 days, and the joint strength reported in the table is the 8-day strength.

12.1.7. Fatigue Loading Determination

FE models of the test specimens (Figure 12.1.11) were developed to determine the loadings to be used in the fatigue tests in order to produce the maximum moment or the maximum shear in the joint zone corresponding to the results from the previous parametric studies summarized in Chapter 10. Figure 12.1.11-b shows the moment distribution for the model loaded at one pad to produce an average moment along the joint of 10.0 kip-ft/ft. Figure 12.1.11-c shows the shear distribution and average shear for the same loading. These plots indicate that the moment was not expected to vary significantly from the average or nominal moment as compared to the shear which varied significantly along the joint length.

405
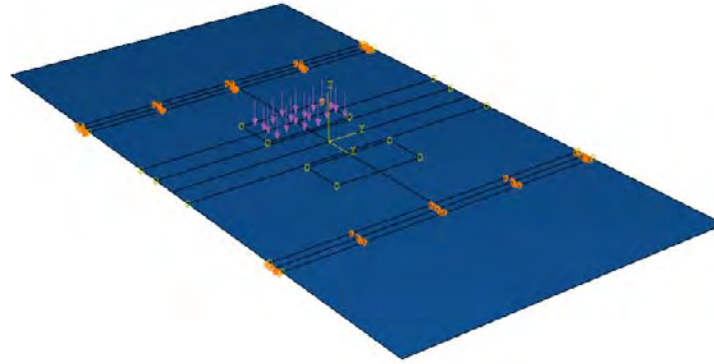
(a) Static shear test (FE Model)
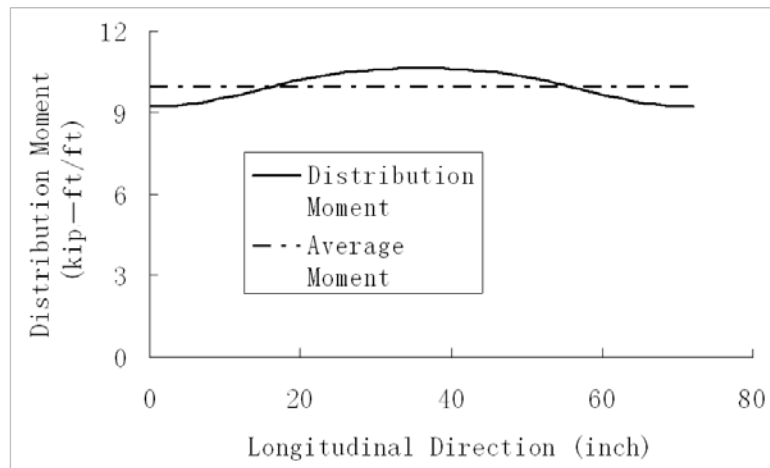
(b) Moment distribution along Joint
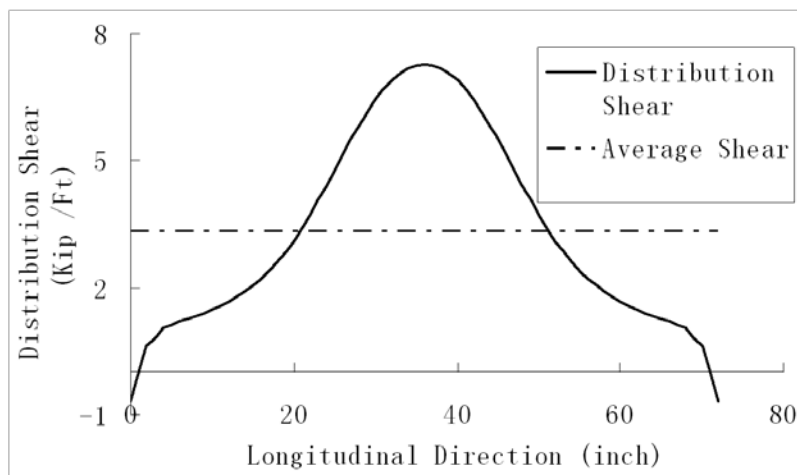
(c) Distribution and average vertical shear along joint

Figure 12.1.11: FE model for load determination

406

For the FF specimen, static loading was applied with the two patch loads on either side of the joint in several increments up to 44.6 kips (22.3 kips on each pad) in order to produce the maximum positive moment of 7.92 kip-ft per unit length (Section 10.1.5.8) in the joint to crack the joint (see Section 10.3, bullet point 9, for a summary of the sources of these applied moments). After unloading to zero, a negative static load of -12.0 kips (-6.0 kips on each pad), corresponding to a negative moment of -2.15 kip-ft per unit length (as determined to crack the joint in negative bending) was applied and unloaded to zero.

During the fatigue test, the applied load was cycled between 11.4 kips (5.7 kips on each pad) corresponding to a positive moment of 1.99 kip-ft per unit length and -2.0 kips (-1.0 kips on each pad) corresponding to a negative moment of -0.35 kip-ft per unit length for a total of 2 million cycles at a frequency of 4Hz. At the end of 0.5, 1.0, 1.5, and 2.0 million cycles, an interim static loading test was conducted. During each of these static tests, the static loading was applied in several increments up to 26.2 kips (13.1 kips on each pad) corresponding to a positive moment of 4.55 kip-ft per unit length after cracking. After unloading to zero, a negative static load of -8.0 kips (-4.0 kips on each pad) corresponding to a negative moment of -1.40 kip-ft per unit length after cracking was applied and unloaded to zero. Finally, the slab specimen was loaded to failure.

For the FS test, fatigue loads "P1" and "P2" were applied by the two MTS rams having the same frequency but out-of-phase, as discussed in Section 12.1.6. Before applying cyclic loading, static loading was applied through P1 in several increments up to 49.9 kips in order to produce the maximum shear of 6.091 kips per unit length in the joint to crack the joint. After unloading to zero, a static load of -49.9 kips was applied through P2, corresponding to a negative shear of -6.091 kips per unit length, then the specimen was unloaded to zero.

Figure 12.1.12 shows the first few cycles of the fatigue loading history for the FS specimen. As discussed earlier, fatigue loads "P1" and "P2" were applied by the two MTS actuators at the same frequency but out-of-phase. The slab was subjected to fatigue loading with the resultant magnitude of "P1+P2" as shown in Figure 12.1.12.

The peak P1 was 25.0 kips, corresponding to a positive shear of 2.84 kips per unit length, which was the combination of the fatigue shear of 2.34 kips/ft plus the camber leveling shear of 0.5 kips/ft. The "Average" value of "P1+P2" of 4.4 kips provided the camber leveling shear of 0.5 kips/ft at the middle of the joint zone all the time. Consequently, the maximum value of P2 was equal to 4.4 kips × 2 – P1= -16.2 kips. An interim static loading test (applying "P1" and "P2" separately) was conducted at the end of 0.5, 1.0, 1.5, and 2.0 million cycles. During each of these static tests, the static loading P1 was applied in several increments up to 46.9 kips corresponding to a positive shear of 5.34 kips per unit length after cracking. After unloading to zero, a static load P2 of -46.9 kips corresponding to a negative shear of -5.34 kips per unit length after cracking was applied and unloaded to zero. The specimen was loaded to failure after the fatigue cycles.

407
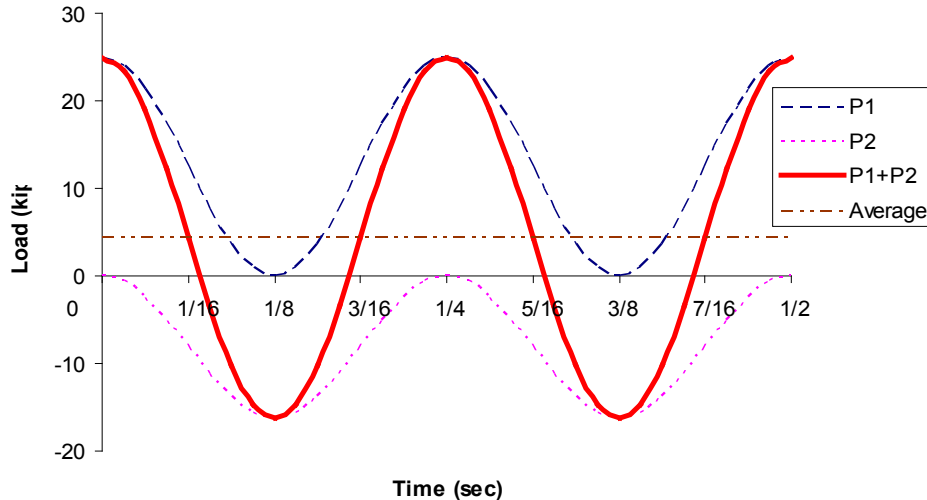
Figure 12.1.12: First two cycles of fatigue shear (FS) loading applied

12.1.8. Moment Capacity and Curvature

Figure 12.1.13 shows the curvature versus the number of fatigue cycle curves (C-N) for the fatigue tests. The curvature represents the average curvature of the joint zone under a specific loading and is plotted relative to the number of fatigue cycles completed. For example, the curve labeled with "M=4.0 k-ft/ft" in Figure 12.1.13-a represents the change in the curvature of the joint zone for the FF-O specimen with respect to the numbers of fatigue cycles completed, where the curvature was measured at the loading level corresponding to a moment of 4.0 kip-ft/ft during each of the interim static load tests.

As shown in Figure 12.1.13, the curvature increased with increasing joint moment for all specimens. There were problems with the initial curvature measurements for the FS-7 (under P1 loading) specimen before fatigue cycling, so the initial results for this specimen are not included in Figure 12.1.13-e. Comparing the results among the different joint moment levels, the impact of fatigue on the curvature was observed to be similar for all loading levels in each of the specimens. It appeared that the fatigue loading had little effect on the curvature for the FF-O and FS-O (under P1 or P2 loading) specimens while initial increases in curvature were observed for the FF-7 and FS-7 (under P2 loading) specimens during the first set of 0.5-million cycles, after which the damage accumulations due to fatigue ceased and the curvatures stabilized for the last 1.5-million cycles. Because the initial data was missing for the FS-7 (under P1 loading) specimen, no conclusions can be made with respect to its fatigue behavior relative to its initial performance. In general, there was no significant influence of fatigue cycles on the curvature for joints fabricated with the overnight CP material, and no significant influence after the first 0.5-million cycles for the 7-day cure CP material.

408
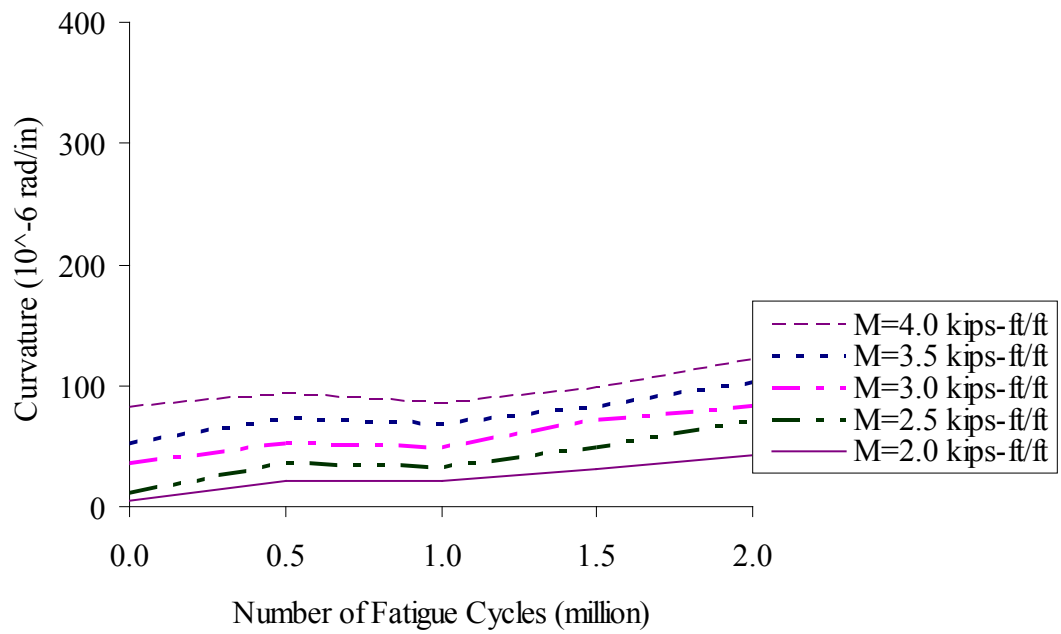
(a) FF-O Specimen

(b) FF-7 Specimen

409
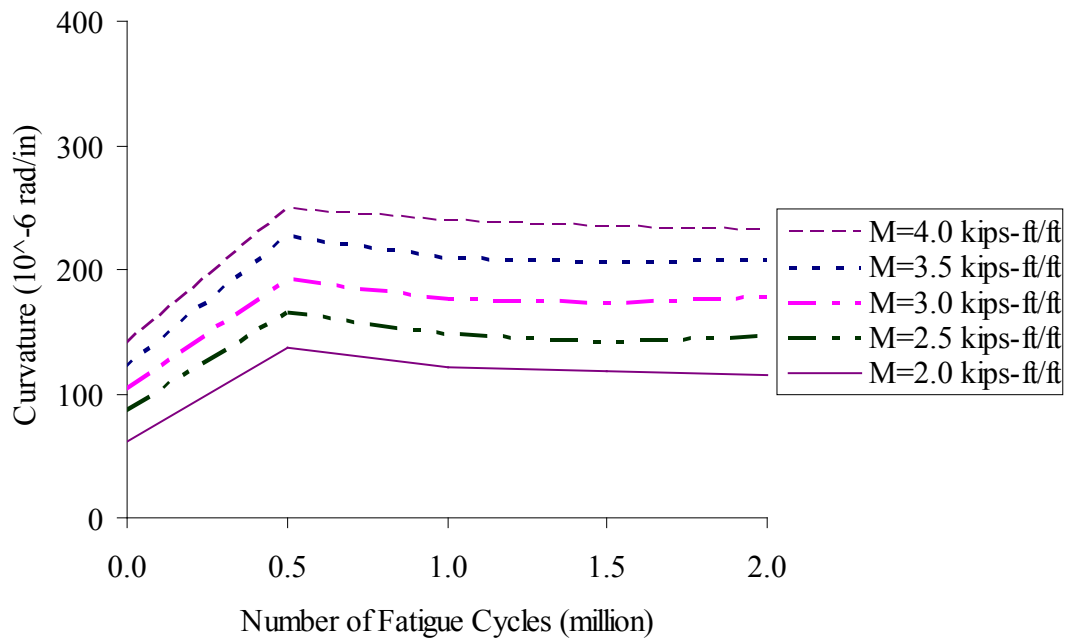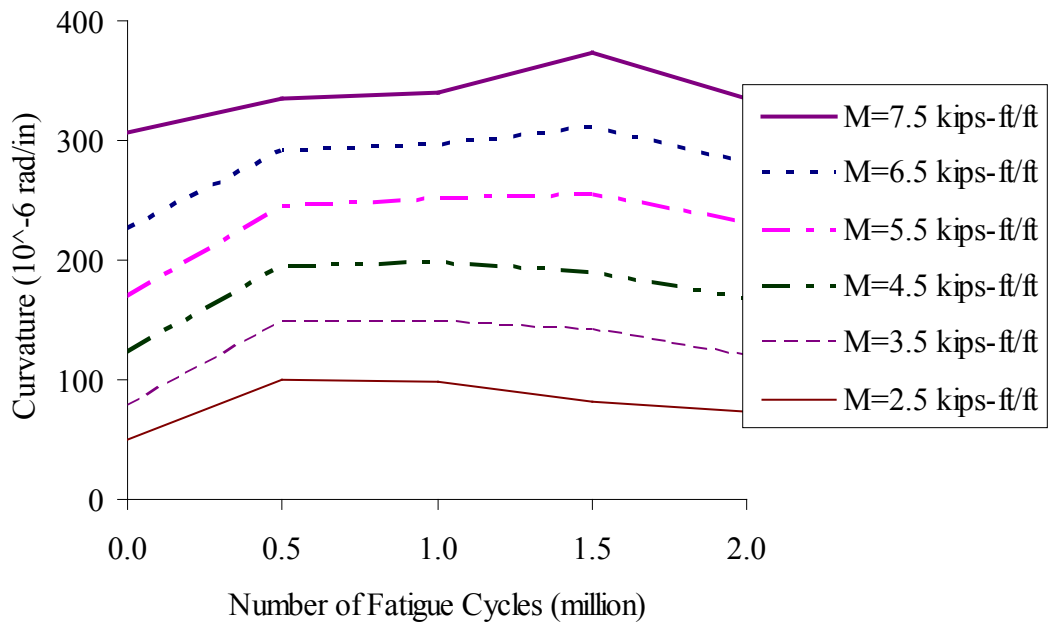
(c) FS-O Specimen under P1
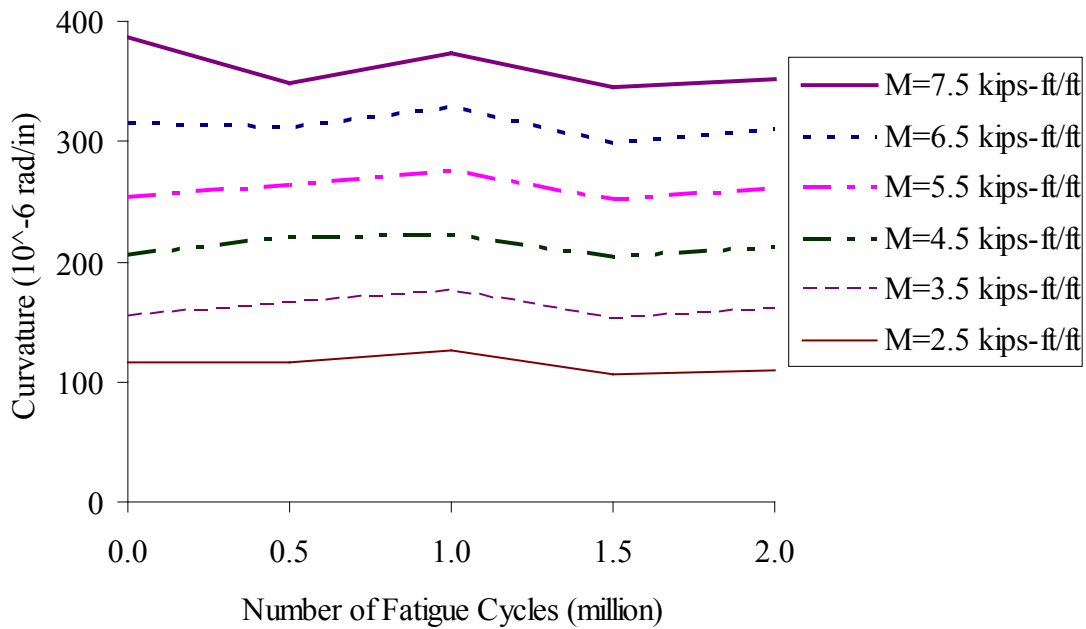
(d) FS-O Specimen under P2

410
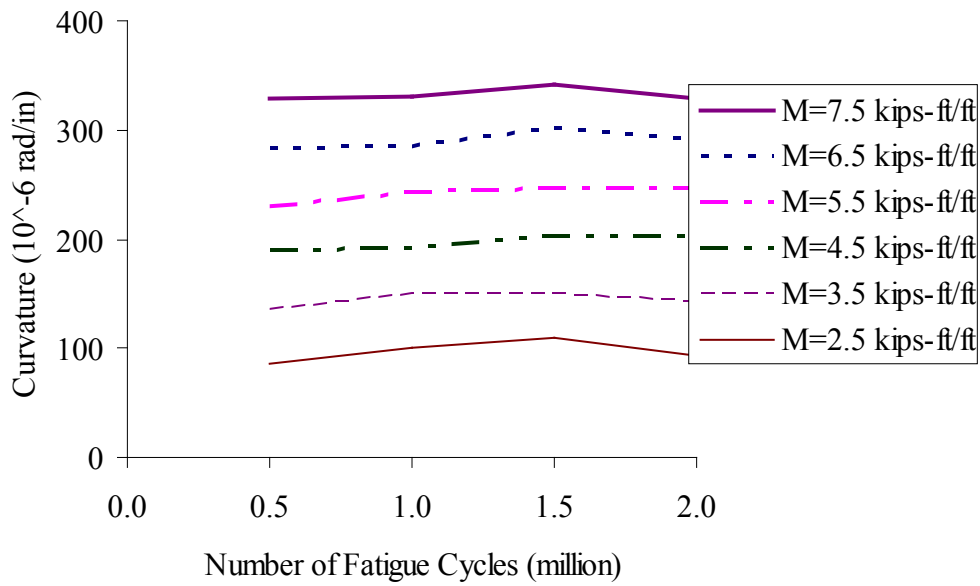
(e) FS-7 Specimen under P1
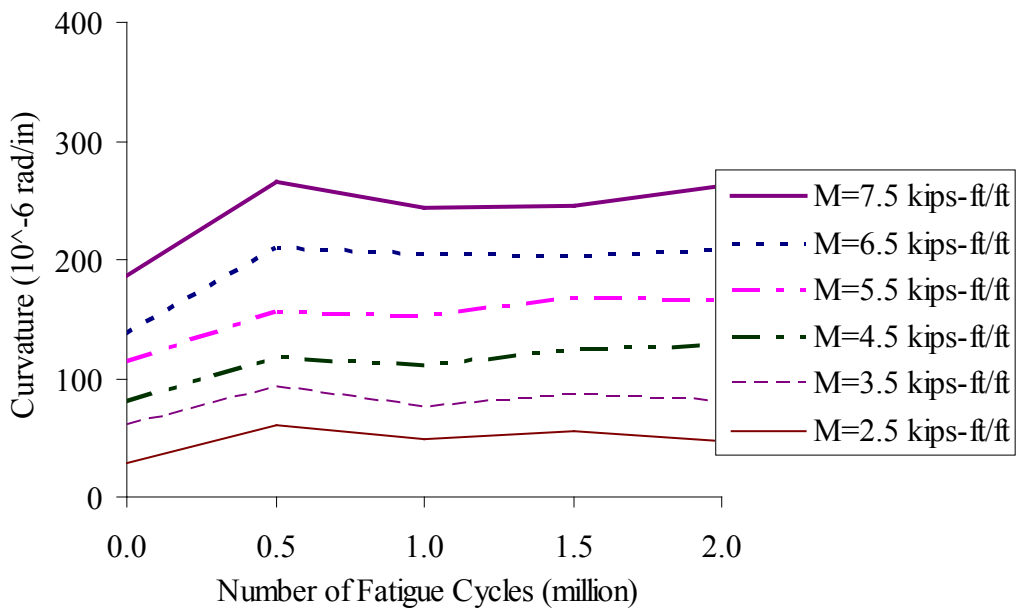
(f) FS-7 Specimen under P2

Figure 12.1.13: C-N curves for flexure and flexure-shear specimens

411

The test results for the moment capacity are compared with the calculated values in Table 12.1.3. The strengths shown in the table for the fatigue tests, FS and FF, were the cylinder strengths measured at the end of the tests, and Table 12.1.2 presents detailed information about the compressive strengths. The service live load was the maximum positive calculated moment after cracking of 4.546 kip-ft/ft reported in Section 10.1.5.9 for the flexure tests; for the flexure-shear tests the service live load was the corresponding moment (CM) that occurred with the maximum shear, which was 3.372 kip-ft/ft after cracking reported in Section 10.1.5.9.

Table 12.1.3: Measured and calculated loading capacity

Specimen	Measured			Calculated	
	Panel Compressive Strength (f'_c) (psi)	Joint Compressive Strength (f'_{cj}) (psi)	Failure Load (kip-ft/ft)	Service Live Load (kip-ft/ft)	Ultimate Load (kip-ft/ft)
SS-O	11512	7586	19.34	3.37	19.31
FS-O	11512	6572	22.18	3.37	19.31
SS-7	11512	8740	25.44	3.37	19.31
FS-7	11512	9417	23.30	3.37	19.31
SF-O	12441	5939	24.21	4.55	19.31
FF-O	11632	5345	19.39	4.55	19.31
SF-7	12441	6966	31.5*	4.55	19.31
FF-7	11711	12361	31.5*	4.55	19.31

* SF-7 and FF-7 specimens were beyond the MTS capacity (31.5 kip-ft/ft) and couldn't be failed by MTS.

The measured ultimate capacities of all of the specimens obtained following the service fatigue loading cycles exceeded their calculated capacities. The joints with the overnight cure materials had lower capacities than those with the 7-day cure, due to the lower strength of the joint material.

Figure 12.1.14-a compares the moment-curvature curves obtained for the specimens tested in flexure under static loading (FS) with those tested in flexure following 2.0 million cycles of fatigue loading (FF).

412

Figure 12.1.14-b compares the moment-curvature curves obtained for the specimens tested in flexure-shear under static loading (SS) with those tested in flexure-shear following 2.0 million cycles of fatigue loading (SF). The vertical axis labeled "Moment/Joint Length" represents the applied moment assumed to be uniformly distributed along the joint (i.e., applied moment divided by the length of the joint). Both the SF and SS specimens were loaded with applied moments assuming uncracked sections while the FF and FS specimens were loaded with applied moments assuming cracked sections after 2.0 million fatigue cycles. As a result, the slope of the curves (i.e., stiffnesses of the specimens) for SF and SS were steeper (larger) than those of the FF and FS specimens at the beginning of the plots. After the applied moment exceeded the cracking moment level, the slopes of the two curves were similar, indicating that the fatigue cycles had no significant effect on the curvature development, as discussed earlier.

In Figure 12.1.14-a, the strengths of SF-7 and FF-7 specimens were beyond the MTS capacity (31.5 kip-ft/ft) and as a consequence could not be tested to failure. The maximum curvature for FF-7 cannot be reported because the LMT's were removed during the test. At service loading, the SF-O and FF-O specimens had about the same curvature, while FF-7 had more curvature than SF-7. FF-O had a similar failure load and curvature as calculated, while SF-O, SF-7 and FF-7 had higher failure loads and curvatures than calculated. When comparing overnight cure and 7-day cure CP materials, SF-7 had higher failure load and curvature than SF-O, and FF-7 performed better than FF-O. This was because 7-day cure material developed higher strength than the overnight cure material in the tests, as shown in Table 12.1.2.

In Figure 12.1.14-b, SS-7 had a higher failure load and more curvature than FS-7, so the fatigue cycles had some influence on the failure load of the joint with the 7-day cure CP material. The failure load for FS-O was higher than that of SS-O. The maximum curvature for SS-O and FS-O cannot be reported, because the LMT's were removed during the tests. As shown in Figure 12.1.14-b, for the range of loading for which curvature was measured, SS-O and FS-O developed almost the same curves after the service load. The influence of fatigue cycles on the joint with the overnight cure CP material was not significant. At service loading, the SS-O and FS-O specimens had essentially the same curvature, and it was the same for the SS-7 and FS-7 specimens. When comparing with the calculation, SS-7 and FS-7 had higher failure loads and curvatures than the calculated, while SS-O and FS-O had similar failure loads as the calculated. Comparing between different CP materials, the joints with the 7-day cure CP material developed higher strength capacity and more curvature, due to the higher strength developed by the 7-day cure material.
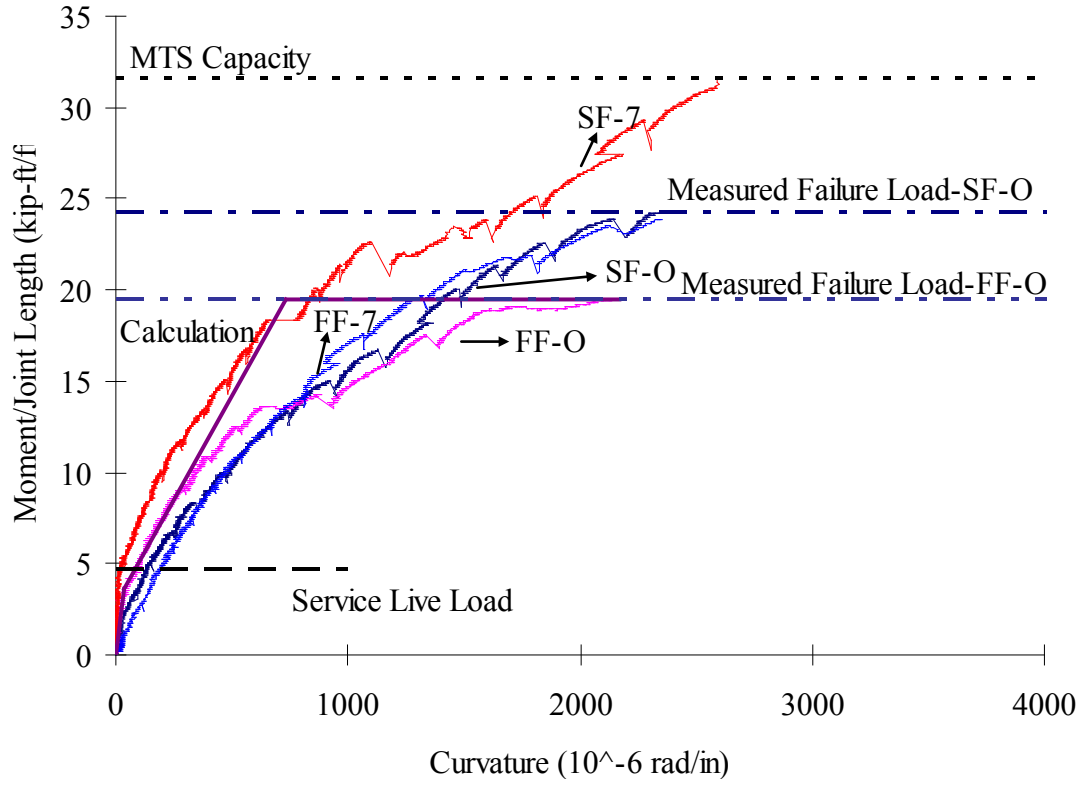
(a) Flexure tests
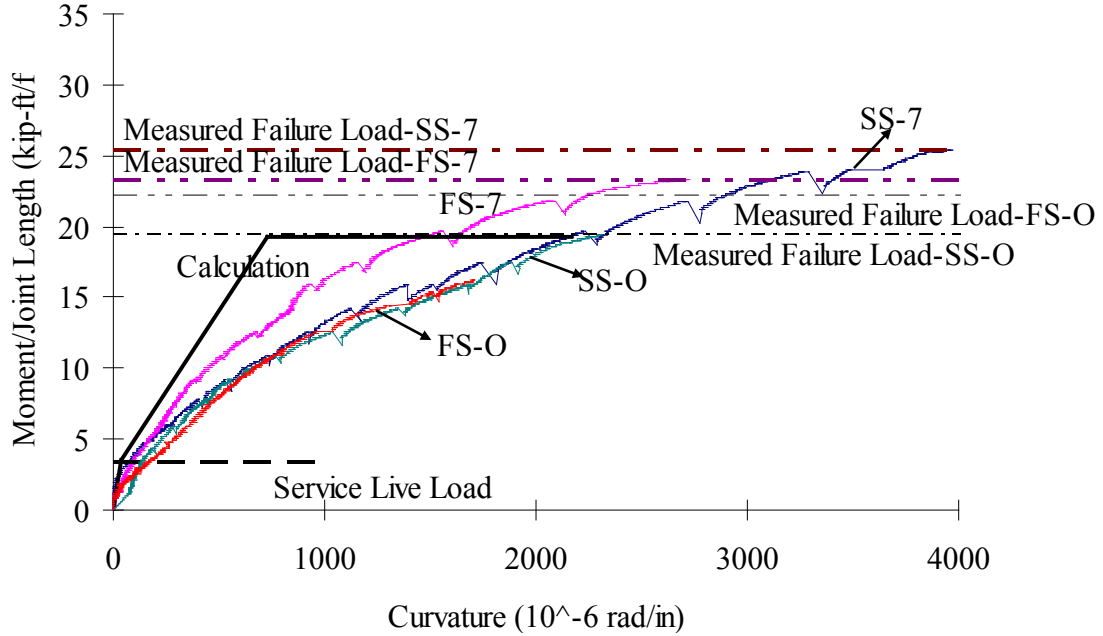
(b) Flexure-Shear tests

Figure 12.1.14: Moment-curvature curves for flexure and flexure-shear specimens

414

12.1.9. Deflection Development

Figure 12.1.15-a and b show a comparison of the load-deflection curves of the fatigue specimens after 2 million cycles and the specimens subjected to static loading without fatigue cycles, for the flexure and flexure-shear tests, respectively. The vertical axis labeled "Load/Joint Length" represents the nominal distributed load along the joint, which was the applied load, P, divided by the width of the specimen (i.e., length of the joint). Note that the load P was the load applied to one loading pad as shown in Figure 12.1.7. The LMT's were removed from the specimen for their protection before the specimens reached their maximum capacities.

a.   Flexure tests

415
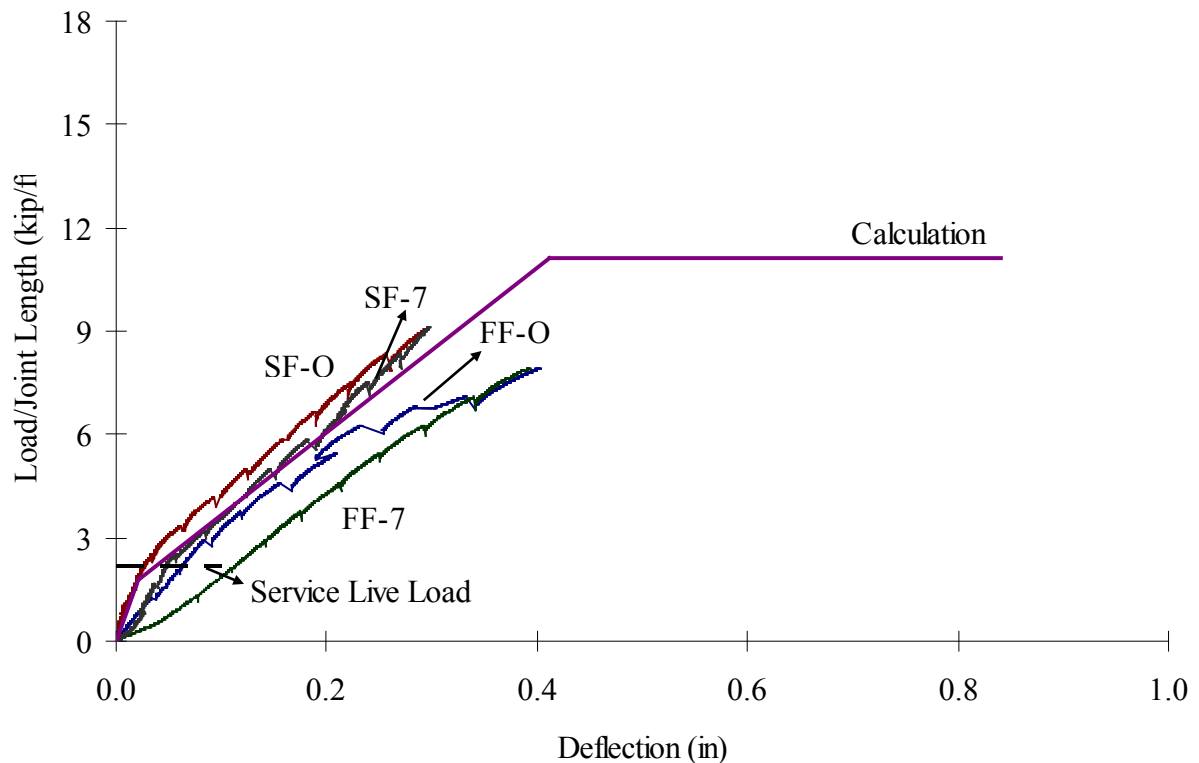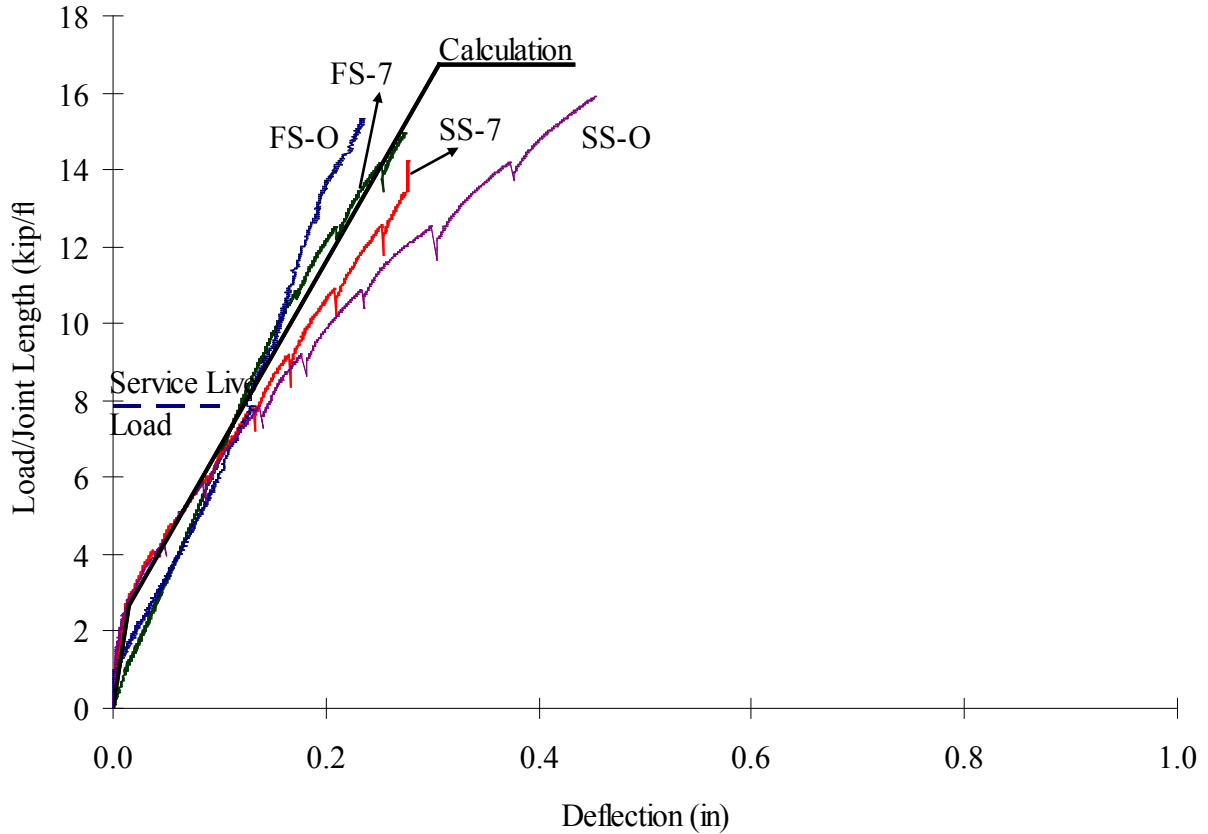
b. Flexure-Shear tests

Figure 12.1.15: Load-deflection curves of flexure and flexure-shear specimens

The calculated response in the plots represents the expected load-deflection curve before cracking, after cracking to reinforcement yield, and the stage of plastic hinge development at midspan after reinforcement yielding. Similar to Figure 12.1.14, the slopes of the SF and SS curves were steeper than the slopes of the curves for the FF and FS specimens from the initial loading until the cracking load was reached. After cracking, the load-deflection behavior for the statically-loaded specimen was similar to that of the fatigue-loaded specimens, except for SS-O and FS-O. This indicates that the fatigue cycles had no significant effect on the deflection at that stage.

The service live load shown in Figure 12.1.15-a was the Load/Joint Length of 2.18 kips/ft which corresponded to the maximum positive calculated moment of 4.55 kip-ft/ft after cracking reported in Section 10.1.5.9. The service live load shown in Figure 12.1.15-b was the Load/Joint Length of 7.82 kips/ft, which corresponded to the maximum calculated shear near the pad load of 5.34 kips/ft based on analyses using the finite element model shown in Figure 12.1.11.

During the shear tests, differential vertical deflection was observed at the interface of the CP and precast panel. Figure 12.1.16 shows the relative displacement (RD) measured between the side of the joint

416

interface and joint center versus fatigue-cycle (N) curves for FS under specific loading levels during interim static load tests. For the FF specimens, the relative displacement of the joint interface was zero under service live load and thus was not studied here.

From Figure 12.1.16, it can be seen that the relative displacement was dependent upon the applied load. As expected, the relative displacement increased with increasing applied load. The change in relative displacement observed over the course of the fatigue tests was not significant, so it was concluded that the fatigue cycles did not have an impact on the performance of the joints subjected to service live load.
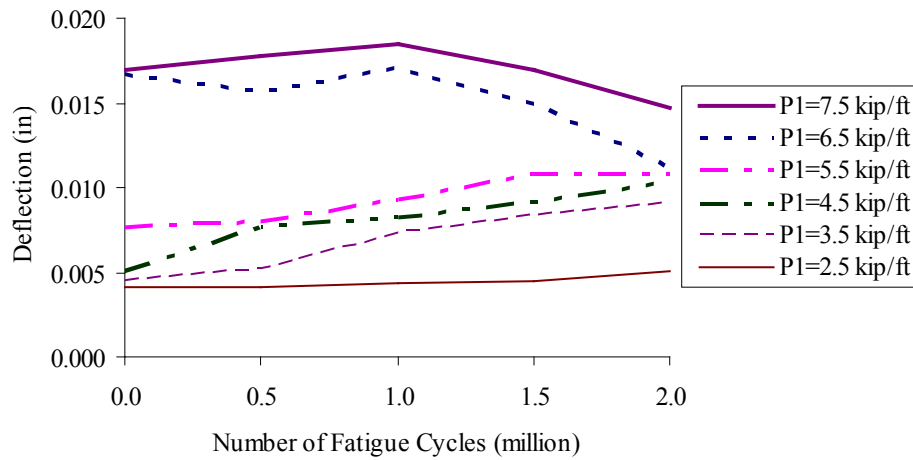
(a) FS-O Specimen under P1

417
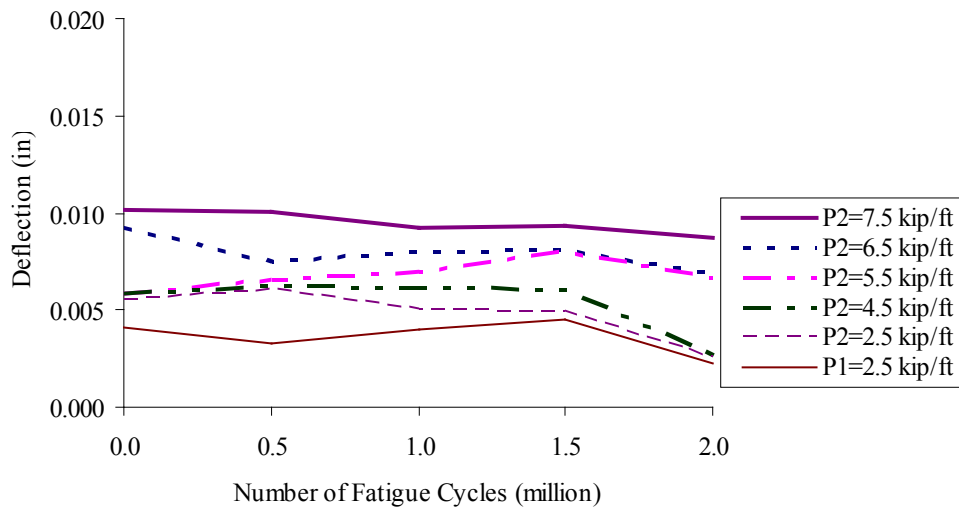
(b) FS-O Specimen under P2
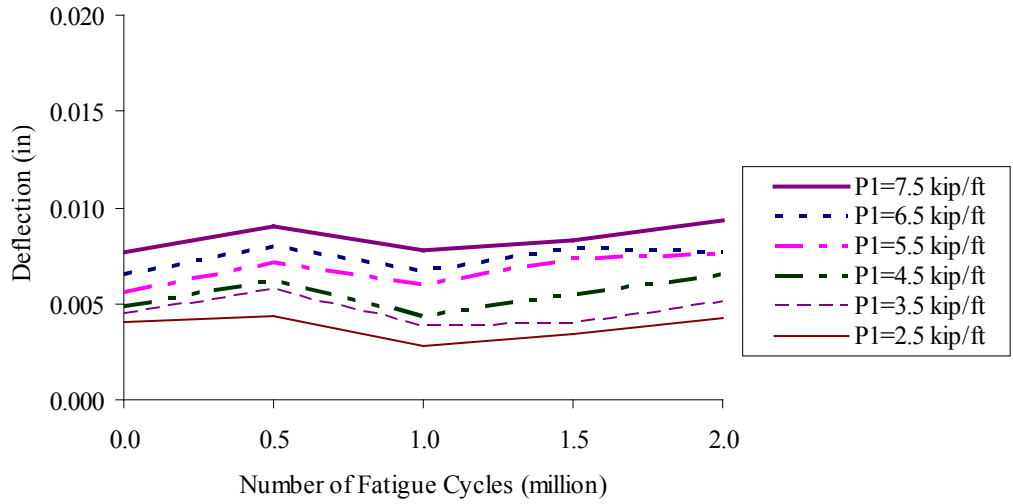
c.   FS-7 Specimen under P1
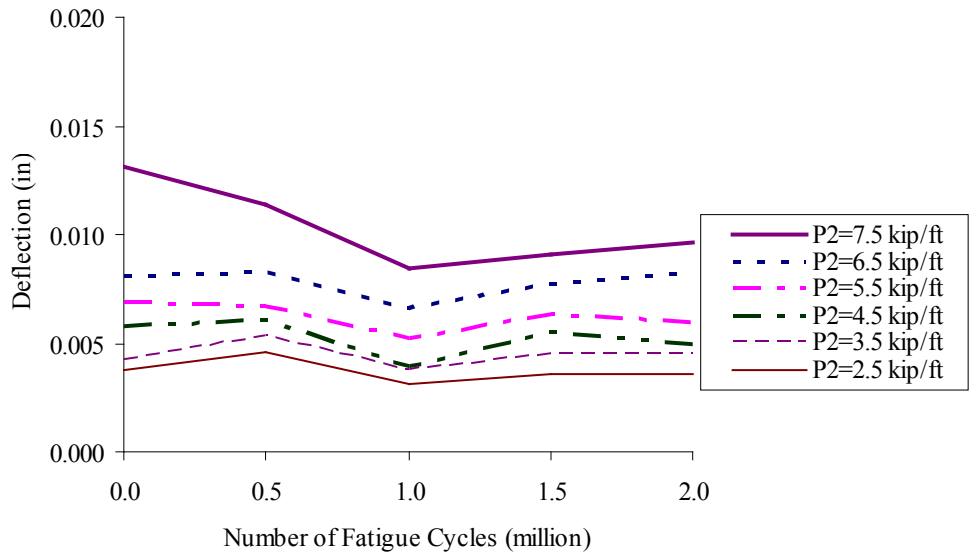
d.   FS-7 Specimen under P2

Figure 12.1.16: RD-N curves for flexure and flexure-shear specimens

418

12.1.10. Crack Width Development

During the tests, the cracks at the interface between the grouted joint and the concrete panel were measured. The two cracks marked as "①" and "②" shown in Figure 12.1.17 show the locations of "Crack 1" and "Crack 2," respectively.
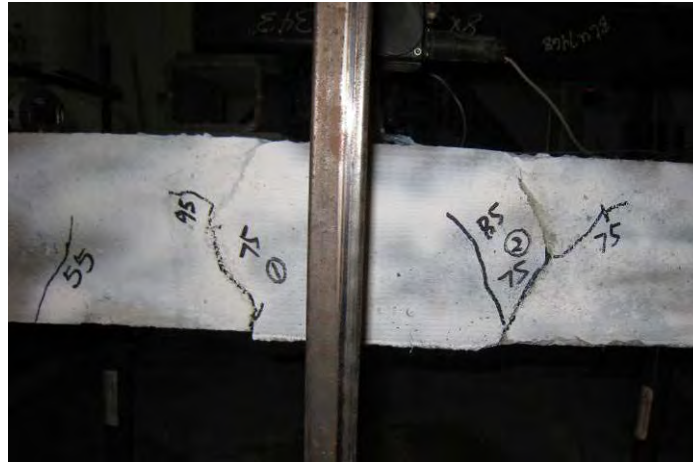
Figure 12.1.17: Cracks at joint-panel interface

Figure 12.1.18 shows the moment-crack width relationship for the SF and SS specimens. The service live load shown in Figure 12.1.18-a was the maximum positive calculated moment of 4.55 kip-ft/ft, after cracking, reported in Section 10.1.5.9. The service live load shown in Figure 12.1.18-b was 3.37 kip-ft/ft, which was the corresponding moment (CM) occurring with the maximum shear of 5.34 kips/ft after cracking based on analyses using the finite element model discussed in Section 10.1.5.9.

The crack width was measured using a Crack Comparator, and represents the maximum width along the crack. From Figure 12.1.18-a, it can be seen that the width of the two cracks monitored during the tests of SF-O and SF-7 developed at different rates. The width of "Crack 1" grew faster than that of "Crack 2" due to the reinforcement yielding that developed at the joint interface of the "Crack 1" location. The crack widths at the service live load level were relatively small compared to the cracks that developed after that. At the same load level, the crack widths of SF-O were greater than those of SF-7, but the difference was not significant. The crack widths of SF-7 at failure were larger than those of SF-O, because SF-7 had a higher failure load.

In Figure 12.1.18-b, the two cracks of the same test, SS-O or SS-7, widened at approximately the same rate with the increasing level of the loading. The crack widths at the service live load level were relatively small compared to the cracks that developed after that. At the same load level, the crack widths of SS-O and SS-7 were similar. The crack widths of SS-7 at failure were larger than those of SS-O, because SS-7 had a higher failure load.

(a) SF Specimens

421
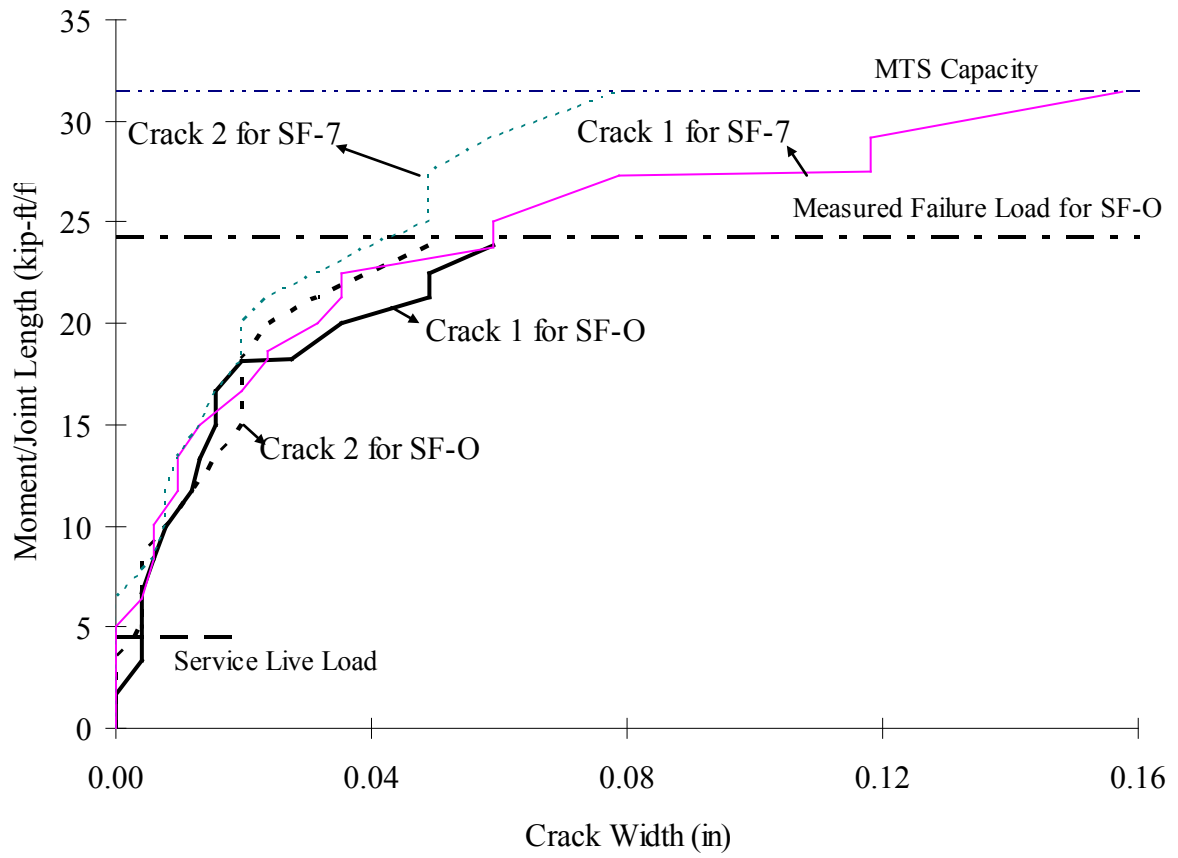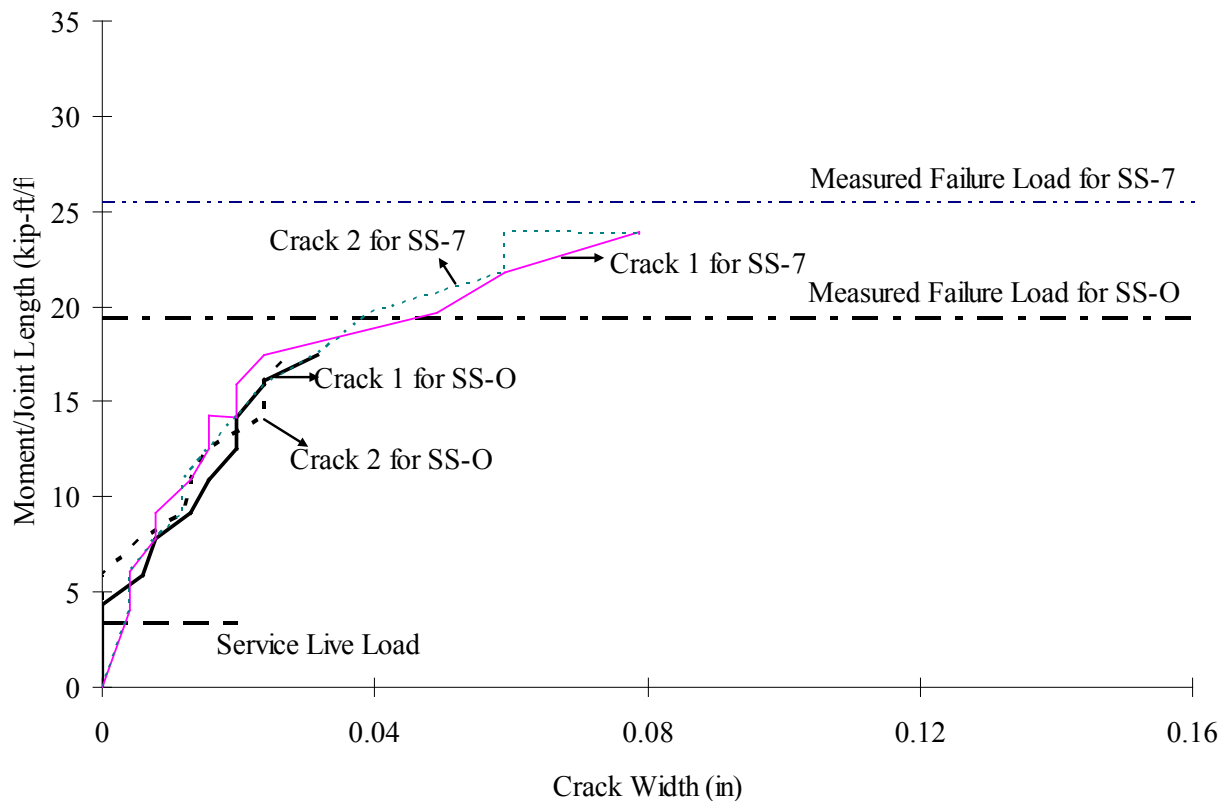
(b) SS Specimens

Figure 12.1.18: Moment-crack width curves for static flexure and static flexure-shear specimens

Figure 12.1.19 shows the crack width-fatigue cycle curves (CW-N) for the fatigue tests. The crack widths represent the maximum crack widths (Crack 1 or Crack 2) measured within the joint at specified load levels after various numbers of fatigue cycles were completed. For the FF tests, 2.18 kips /ft corresponded to the maximum static loading of 26.2 kips (13.1 kips on each pad) during the interim static loading tests, as discussed in Section 12.1.7. And 1.25 kips /ft corresponded to the static loading of 15 kips (7.5 kips on each pad). For the FS tests, 5.83 kips /ft and 4.17 kips /ft corresponded to the static loading of 35 kips and 25 kips, respectively, applied during the interim static loading tests.

From Figure 12.1.19, it can be seen that the crack widths measured within the joint were dependent upon the applied load, as would be expected. At similar levels of load, changes in crack widths were not significant, except for specimen FF-7. So the influence of fatigue cycles on the crack width within the joint was concluded to be negligible under service live load for the joints with overnight cure materials, while fatigue cycles had an influence on the joint with the 7-day cure material. For FF-7, a transverse crack was observed to develop at the middle of the joint length, shown circled in Figure 12.1.20; this was the largest

422

crack measured under service live load, 0.012 in. compared with 0.008 in. for Crack 1 and 2, and as the load was approaching the failure, this crack was getting smaller and Crack 1 and 2 kept increasing and had the largest crack widths. For FF-O, a transverse crack was observed to develop at a similar location to that of FF-7; however, in the case of FF-O, the transverse crack width was similar in size to the cracks observed along the joint interfaces under service live load. For FS-O and FS-7, the crack along the joint interface, Crack 1 or 2 as shown in Figure 12.1.17, had the maximum width under service live load. Under P1 loading, Crack 1 was the widest crack, while Crack 2 had the maximum crack width under P2 loading. This resulted because P1 and Crack 1 were on the same side of the joint and P2 and Crack 2 were on the other side. In the fatigue flexure tests (FF), the joint with 7-day cure material developed larger crack widths than those of the overnight cure material, while in the fatigue shear tests (FS) the crack width of the joint with the 7-day cure material was similar to that of the overnight cure material.
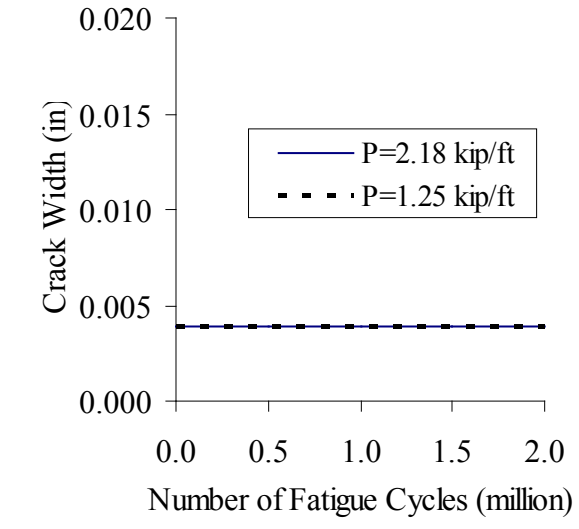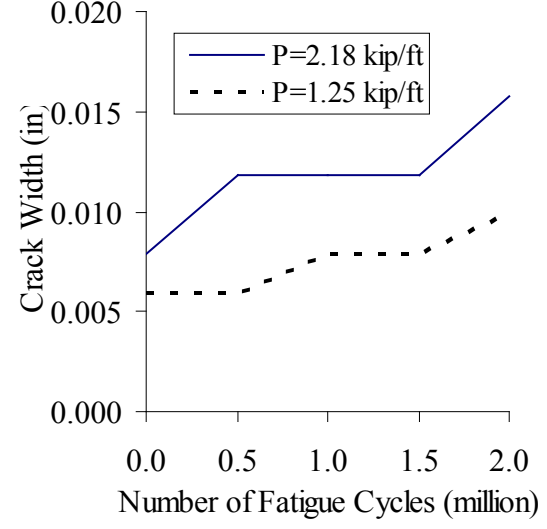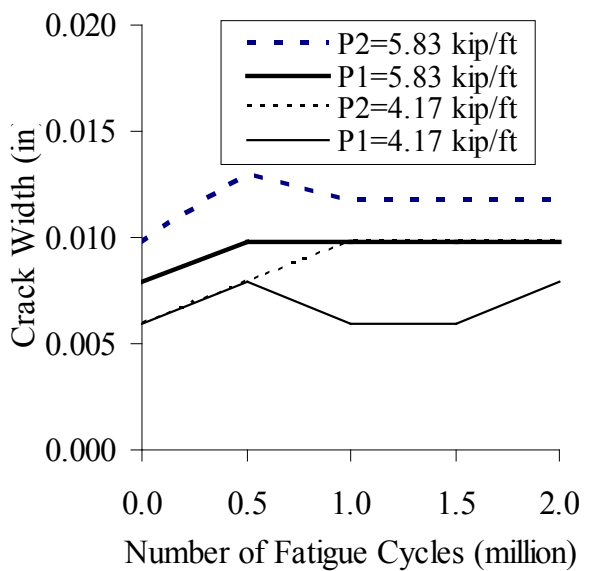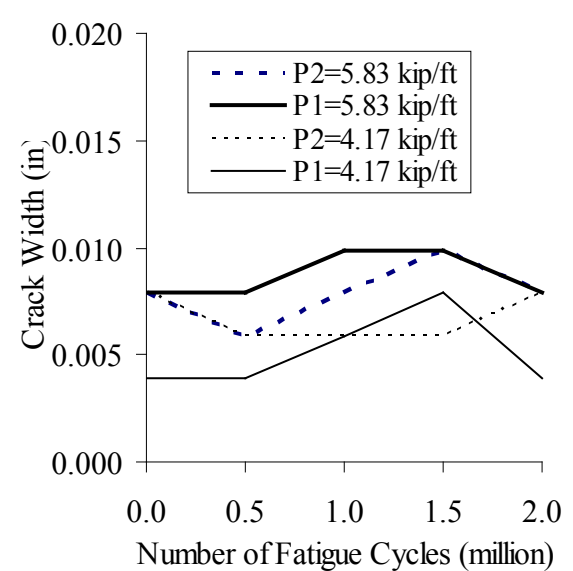
Figure 12.1.19: CW-N curves for fatigue flexure and fatigue flexure-shear specimens

424

Figure 12.1.20: Transverse crack in FF-7 test (circled in red)

12.1.11.   Strain Development

Figure 12.1.21 shows the strain-fatigue cycle curves (MS-N) for the fatigue tests representing the reinforcement strain in the joint measured during intermittent static tests conducted over the course of the fatigue cycles under service live load. The strain gage number and the loading are shown in the figure. For example, "R1-9" denotes the strain gage on U-bar #1 of the right slab that was located 7 in. away from the outside bend of the bar, as shown in Figure 12.1.3. The loading denoted "M = 4 k-ft/ft" signifies the moment applied to the joint per unit length.

From Figure 12.1.21, it can be seen that negligible variations in reinforcement strain were observed at the peak static loads applied intermittently during the course of the fatigue tests. Strain increases were observed with increase in distance from the bend of the U-bars, as shown in Figure 12.1.21. The R4-10 and L5-10 strains were exceptions, because they were located outside of the joint.

Figure 12.1.22 shows the moment-strain curves representing the maximum strain values in the joint zone for each specimen, which also show the variation of the reinforcement strain after fatigue cycles is not significant.

425
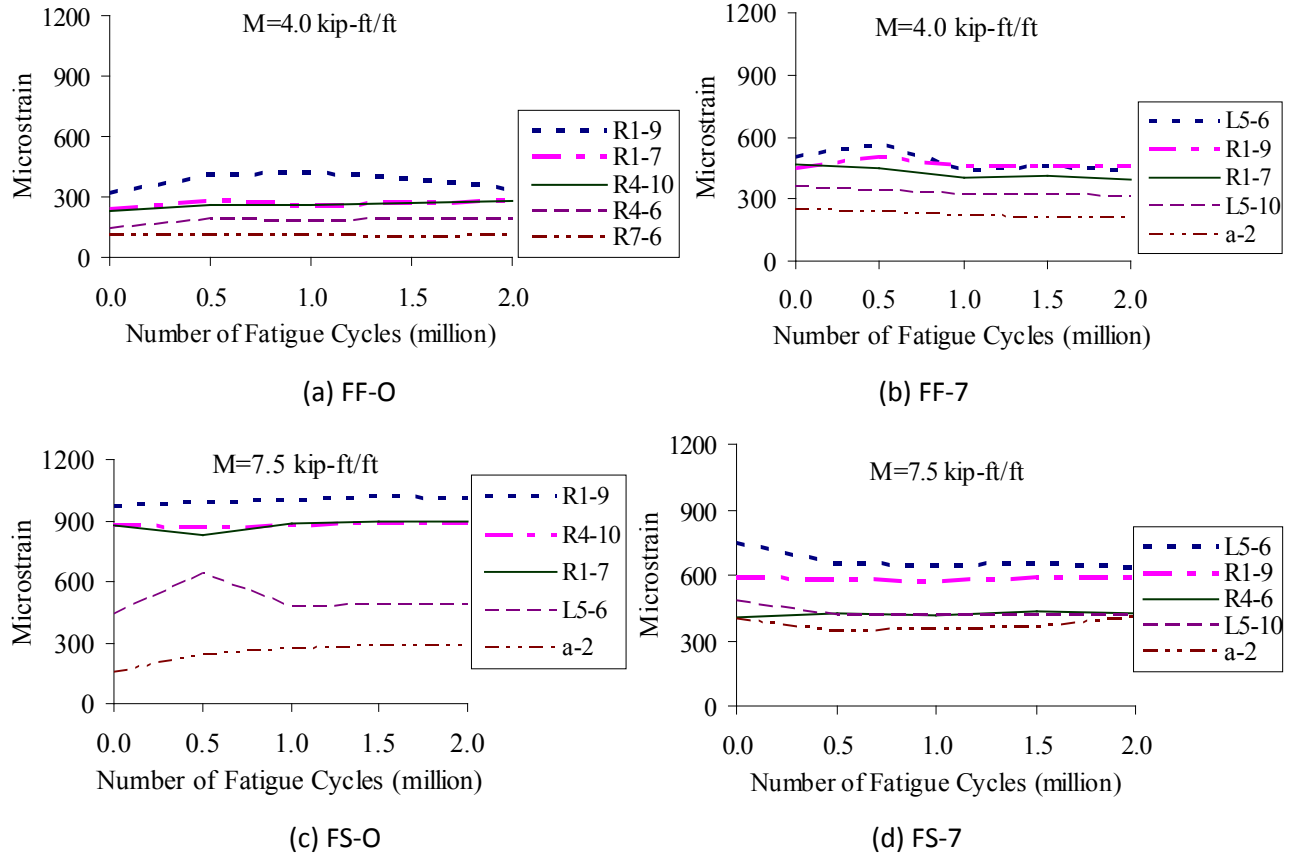
Figure 12.1.21: MS-N curves for fatigue flexure and fatigue flexure-shear specimens

426
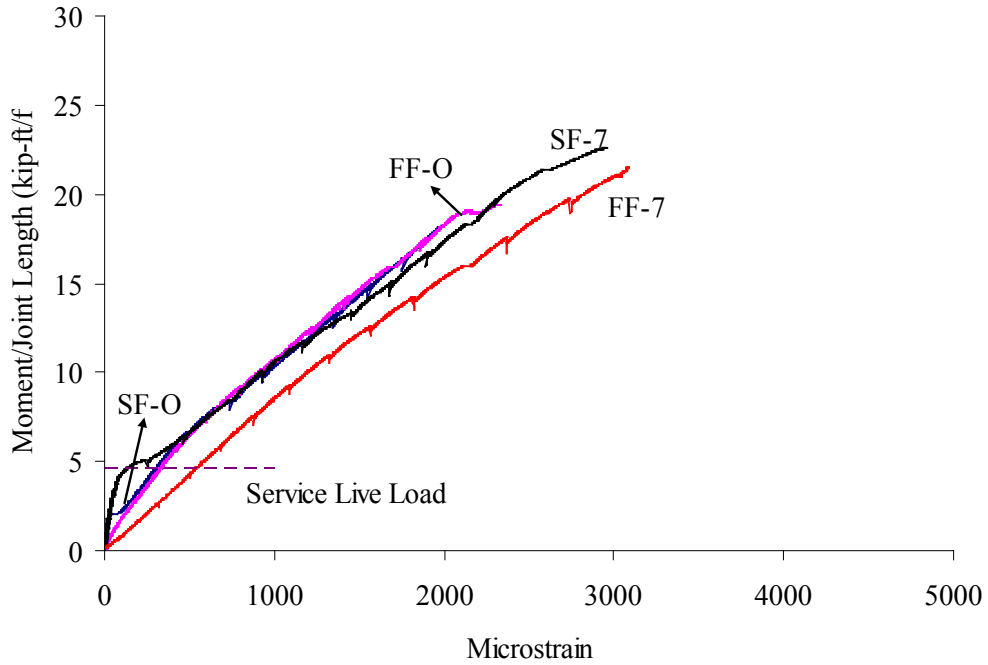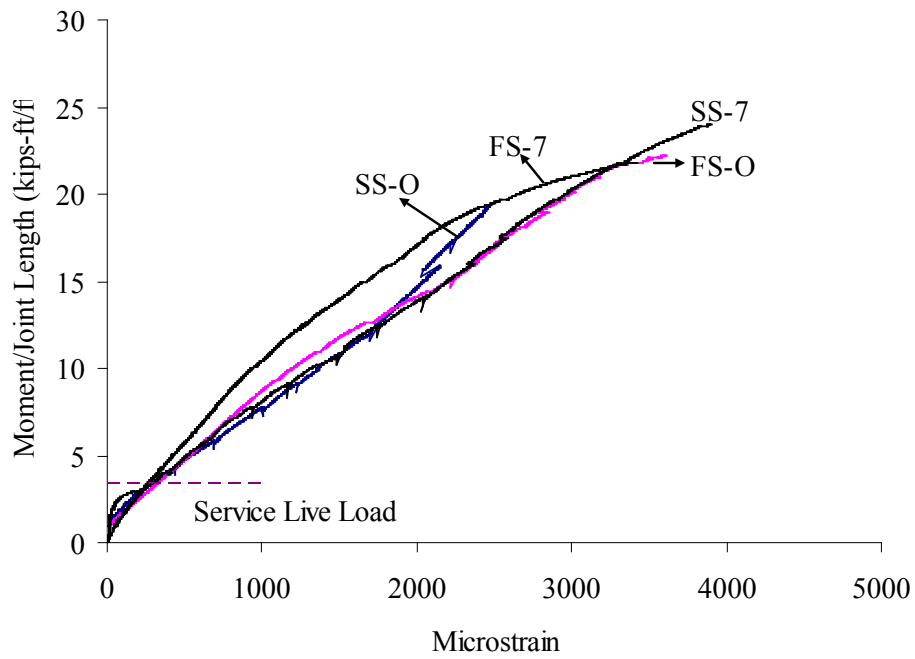
(a) Flexure tests

(b) Flexure-shear tests

Figure 12.1.22: Moment-strain curves for flexure and flexure-shear specimens

427

12.1.12.   Failure of Specimen

As shown in Figure 12.1.23, the failure modes exhibited by the SF-O and FF-O specimens were typical flexural failures. After the U-bar reinforcement yielded, the CP material in the joint zone eventually crushed at the top. Two large cracks developed along the two interfaces of the joint during the tests and two developed within the joint at the bottom of the slab, as shown in Figure 12.1.24-a and b. The widths of the two large cracks within the joint increased significantly when the load was large at approximately 18 kip-ft/ft. The two cracks along the interfaces of the joint had the largest crack widths through the flexural failure tests. The flexure specimens experienced a ductile failure (i.e. The U-bars yielded and then concrete or grout at the top of the joint crushed). After reaching peak loads, ductile specimens can develop large displacements. It was not possible to fail specimens SF-7 and FF-7 due to the limiting capacity of the MTS testing equipment. In specimens SF-7 and FF-7, a horizontal crack was observed to develop at the bottom of the slab starting from the edges of the slab, as shown in Figure 12.1.24-c and d, which increased significantly at the end of the test, when the load was close to the capacity of the MTS equipment.

Flexure-shear failure modes were observed in specimens SS-O, FS-O and SS-7, FS-7. A shear crack developed across the joint zone when the specimen failed, as shown in Figure 12.1.25. For SS-O and FS-O specimens, a crack along the joint interface at the loading side developed though the specimen thickness, and the CP material crushed at the top along the joint interface at failure. For SS-7 and FS-7 specimens, a crack developed from the lower part of the joint interface at the loading side and then propagated vertically, not following the interface. The grout also crushed at the top along the joint interface at failure. For SS-O, FS-O and SS-7, FS-7 specimens, one horizontal crack within the joint, as shown in Figure 12.1.26, increased tremendously at the bottom when the slabs were close to failure.
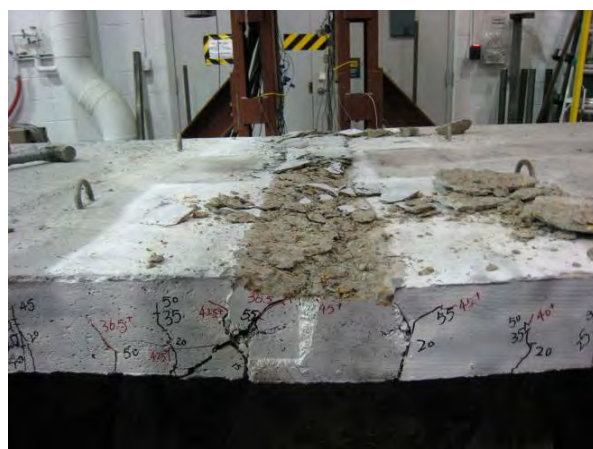
| (a) SF-O | (b) FF-O |

Figure 12.1.23: Specimen failures for flexure specimens

428

(a) SF-O

(b) FF-O

(c) SF-7

(d) FF-7

Figure 12.1.24: Cracks at the bottom of the flexure specimens (the joint interfaces are marked with dashed lines)

429

(a) SS-O

(b) FS-O

(c) SS-7

(d) FS-7

Figure 12.1.25: Specimen failures for flexure-shear specimens

430

(a) SS-O

(b) FS-O

(c) SS-7

(d) FS-7
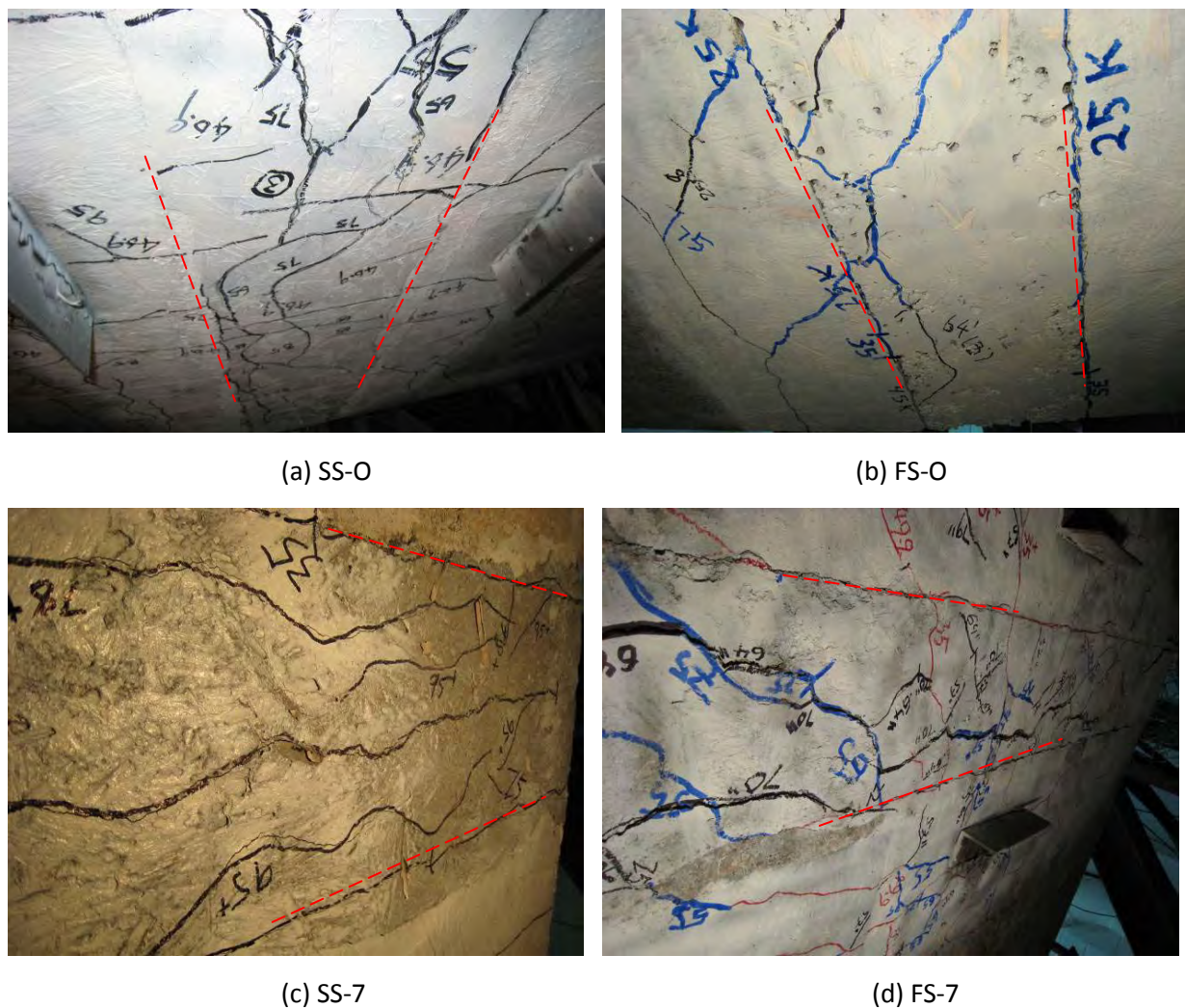
Figure 12.1.26: Cracks at the bottom of the flexure-shear specimens (the joint interfaces are marked with dashed lines)

12.2. Conclusions

Based on the parametric study and the experimental program, the following conclusions can be made:

1. Fatigue loading had little influence on the behavior of the longitudinal joints (flexure and flexure-shear test specimens) in terms of average curvature of the joint, deflection at midspan, relative displacement of the joint interface and joint center as well as reinforcement strain under service live load.

2. Fatigue loading was observed to have an effect on the loading capacity of the flexure specimens using the overnight cure material. After 2 million cycles, the specimens fabricated with the overnight cure material had less load capacity than the corresponding specimens subjected to the

431

static load tests. For the specimens with 7-day cure material in the joint, fatigue loading had negligible effect on the results for the flexure-shear tests. In the case of the flexure tests, the failure load was not reached due to limitations of the MTS test equipment.

3. Joints with the 7-day cure material performed better than those with the overnight cure material in some cases. Examples included the flexure-shear tests, SS and FS, where the joints with the 7-day cure material had larger failure loads and curvatures than those of the specimen with the overnight cure material. This was because the 7-day cure material used developed higher strengths than could be achieved with the overnight cure material in the tests.

Based on these tests, the U-bar detail was deemed to be a viable connection system for longitudinal joints between full-depth precast deck panels and decked bulb-Ts.

432

Chapter 13 Transverse Joint Details for Accelerated Bridge Construction: Fatigue Evaluation

13.0   Introduction

This chapter presents a summary of the investigation of the U-bar detail used for the transverse joint (i.e., tension tests). In this study, eight specimens connected by a U-bar detail utilizing a 6 in. lap length were fabricated and tested. The analytical parametric study conducted to provide the database of tension forces to be applied to specimen was summarized in Chapter 10. The forces applied to the tension specimens were intended to simulate the service live load demand anticipated in the transverse joint at a pier in a continuous decked bulb-T bridge or full-depth precast panel on girder bridge. Static and fatigue tests under tension loading were conducted. Test results were evaluated based on tensile capacity, cracking, displacement and steel strain. Based on these test results, the U-bar detail was deemed to be a viable connection system for the transverse joint.

13.1.   Experimental Program

13.1.1. Specimen Dimension

A total of four specimens were fabricated for the static and fatigue testing, with two different closure pour materials used in the transverse joint. Each specimen consisted of two panels (Part 1 and Part 2 in the figure) connected by one of the closure pour materials (overnight and 7-day cure) as shown in Figure 13.1.1. Each panel was 15 in. wide, 32 in. long and 7.25 in. deep. The female-to-female shear key was provided at the vertical edge of the end with the U-bar extended in the specimen length direction.

433
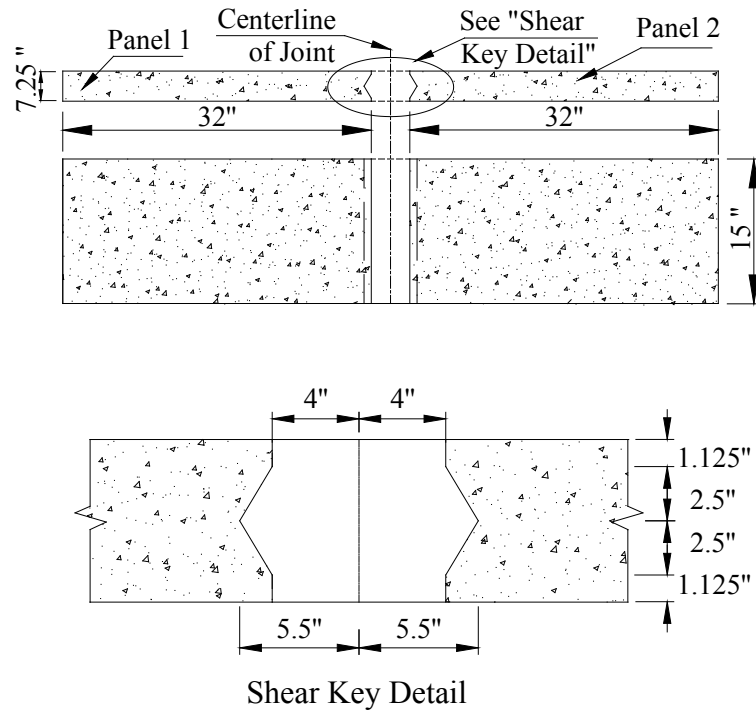
Figure 13.1.1: Dimension of transverse joint (tension) specimen

13.1.2. Reinforcement Layout and Strain Gage Instrumentation

Figure 13.1.2 displays the reinforcement layout used in the tension specimens. The reinforcement layout was the same as that used in WT-1 and WT-2, discussed in Chapter 9, except that the welded joints connecting the threaded rods to the U-Bars were kept outside of the concrete specimen. This facilitated repair of the welded connection if it were to fail before the specimen. There were four layers of reinforcement in each panel along the specimen depth direction with a 2 in. cover at the top and 1 in. cover at the bottom. The straight bars simulated the transverse reinforcement while the U-bars simulated the longitudinal reinforcement that comprised the transverse joint connection reinforcement in the bridge deck. The reinforcement details in the specimen were as follows: #5 straight bar spaced at 6 in. at the bottom along the specimen width direction; #4 straight bar spaced at 12 in. at the top along the specimen width direction. The #5 U-bars projected out of the panel to splice with the U-bars in the adjacent panel in the transverse joint. The spacing of the U-bars was 4.5 in. and the overlap length (the distance between bearing surfaces of adjacent U-bars) was 6 in. The interior diameter of bend of the U-bar was $3d_b$.

434
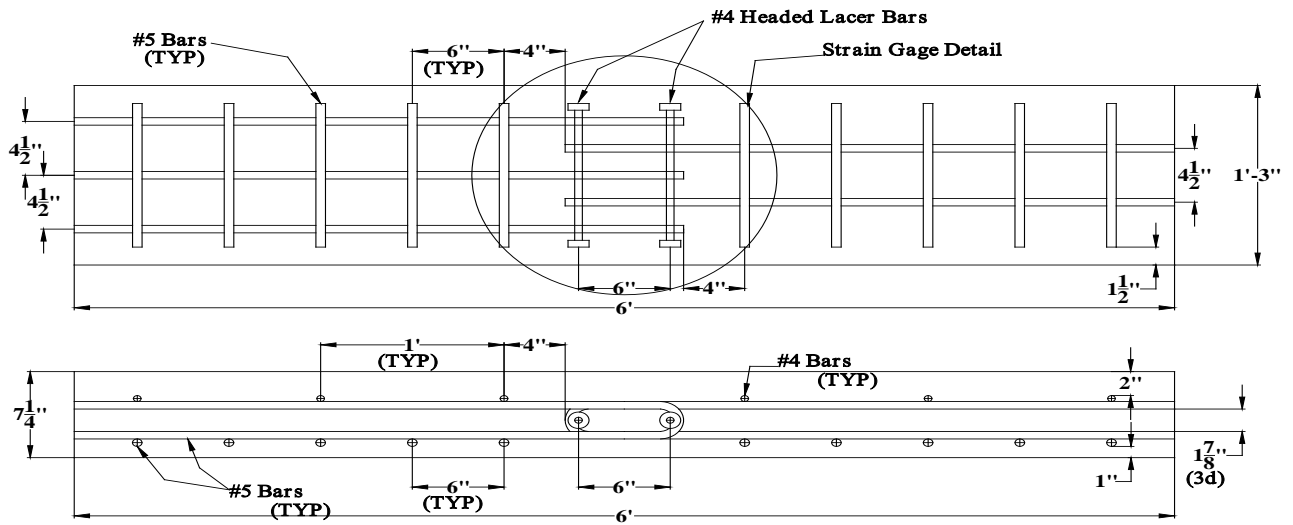
Figure 13.1.2: Reinforcement layout in transverse joint (tension) specimen

The strain gage configuration was modified based on the test results described in Chapter 9. Figure 13.1.3 depicts the strain gage layout in the specimen for the tension test. Gages were placed at 2 and 6 in. away from the bend of the U-Bar. The strain gage diagrams have notations indicating the U-Bar identifier and the location on the bar. The U-Bars are represented by "UB" and the lacer bars are indicated by "LB." The distance from the bend of the U-Bar to each gage is shown at the bottom of the diagram. All distances indicated on the diagrams are in inches and measured from center-to-center. A gage was placed at the midpoint of the lacer bar.

435
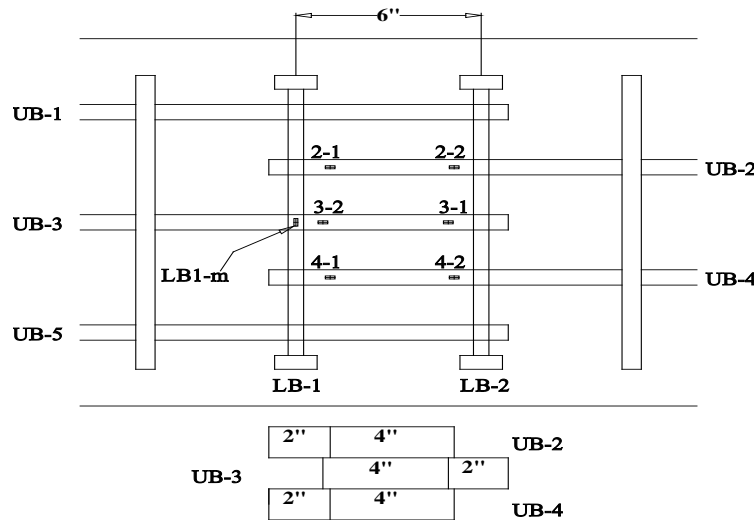
(a) Strain gage configuration for U-bars
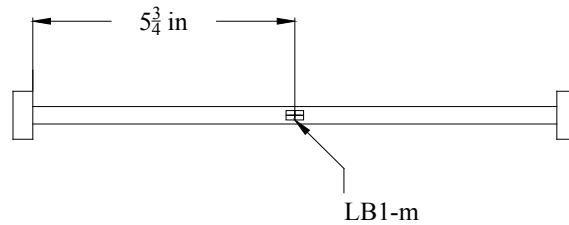
(b) Strain gage configuration for Lacer Bar

Figure 13.1.3: Strain gage configuration for transverse joint (tension) specimen

13.1.3. Specimen Fabrication

The specimens were fabricated at Ross Prestressed Concrete Inc. in Knoxville, TN. Figure 13.1.4-a shows the panel reinforcement before placement of the concrete. One end of the wood form, in the length direction, was slotted at a spacing of 6 in. to fix the U-bars in place, and foam wedges were used to form the configuration of the shear key at the vertical edge of the panel. Holes were drilled in the other end of the form, so that the threaded rods attached to the reinforcement could be extended out of the specimen. The design concrete compressive strength at 28 days was 7000 psi. Companion concrete cylinders were cast with the panels.

436

| (a) Before pouring | (b) After pouring and curing |

Figure 13.1.4: Panel fabrication

13.1.4. Joint Surface Preparation

The surfaces of the shear keys were sandblasted to prepare the joints for the closure pours. The purpose of the surface preparation was to remove all contaminants that might interfere with adhesion and to develop a surface roughness to promote a mechanical bond between the grout and the panel. After the removal of the deteriorated concrete, proper preparation provided a dry, clean and sound surface, which offered a sufficient profile to achieve adequate adhesion. As discussed in Chapter 12, there were many available methods to prepare the surface including chemical cleaning, mechanical cleaning and blasting cleaning. Sandblasting, which uses compressed air to eject the high speed stream of sand onto the surface, was used because it is a very effective method to process the surface of precast members under industrial conditions. Black Beauty 2050 sand was chosen for sandblasting to prepare the surface in this study. The profile of the surface after sandblasting is shown in Figure 13.1.5.

437

Figure 13.1.5: Profile of joint surface after sandblasting

13.1.5. Closure-Pour Materials

The longitudinal joint, which is filled with closure-pour (CP) materials connecting the top flange of the adjacent DBT girders, is considered to be the structural element of the bridge deck. It is important for the selected CP material to reach its design compressive strength in a relatively short time for the purpose of accelerated bridge construction. In this study, it was decided to use two closure-pour materials, SET® 45 HW for overnight cure and HPC Mix1 for 7 day cure, as described in Chapter 11.

13.1.6. Testing Plan and Setup

A total of four specimens were made, where each specimen consisted of two concrete panels connected with an overlapping U-bar detail and one of the selected closure pour materials. When grouting, two panels were positioned to satisfy the 6 in. U-bar overlap length and the 4.5 in. spacing of the U-bars in the joint zone (Figure 13.1.6-a). The wood form was provided at the bottom and at both ends of the joint to prevent leakage. After grouting, the transverse joint (tension) specimen consisting of 2 panels connected by the joint was ready for testing (Figure 13.1.6-b).

438

(a) Before grouting   (b) After grouting
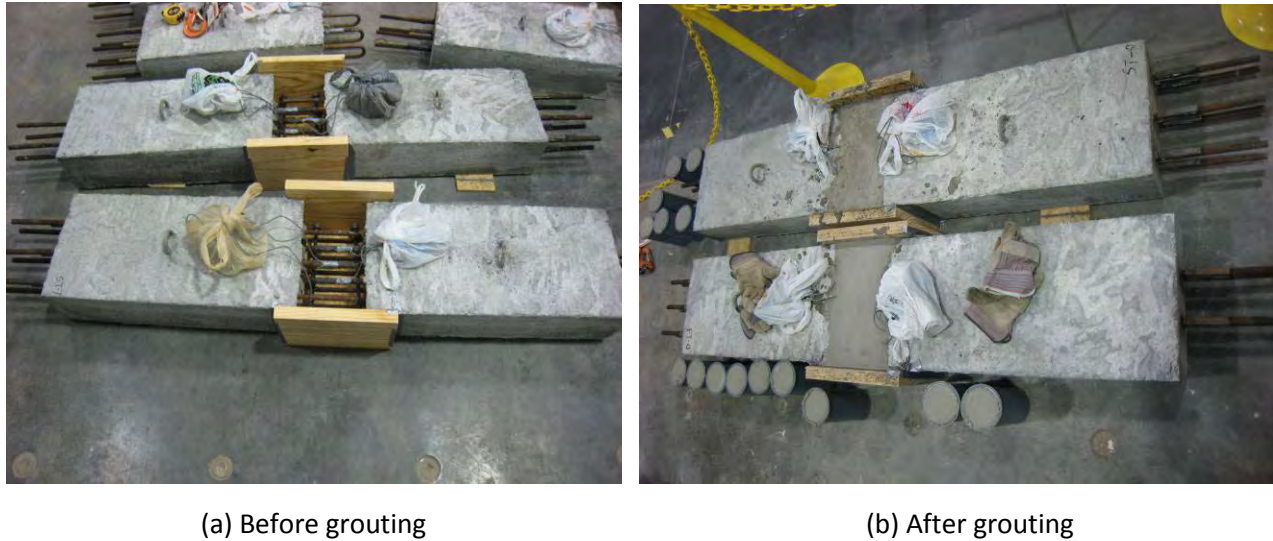
Figure 13.1.6: Transverse joint (tension) specimen before and after grouting

Two of the four specimens (two for each of the two selected CP materials) were tested under static tension (ST), and correspondingly, two of the four specimens were tested under fatigue tension (FT). Table 13.1.1 presents the loading matrix for the four specimens. Figure 13.1.7 shows the test setup and the linear voltage displacement transducers (LMT) instrumentation for each test. The same test setup and LMT instrumentation were employed as used in the tension tests described in Chapter 9. The Crack Comparator was used to measure the crack width.

Table 13.1.1: Transverse joint (tension) specimen loading matrix

Overnight Cure		7 Day Cure	
Static	Fatigue	Static	Fatigue
SET® 45 HW	SET® 45 HW	HPC Mix 1	HPC Mix 1

439

Figure 13.1.7: Tension test setup

The compressive strength of the concrete panel f'_c and the compressive strength of grouted joint f'_{cj} at the time of testing for each specimen are given in Table 13.1.2.

440

Table 13.1.2: Compressive strength of concrete panel and grouted joint

Specimen	Panel (psi)		Joint (psi)	
	Start of Test	End of Test	Start of Test	End of Test
ST-O	8462		4649	
ST-7	8886		9974	
FT-O	8462	8216	3994	4982
FT-7	8462	9162	9470	9505

13.1.7. Fatigue Loading Determination

As discussed in Section 10.2, the resulting extreme fiber stresses at the top of the girder in the transverse joint associated with the maximum moments were -1.056 ksi, -0.306 ksi, 0.169 ksi, and 0.066 ksi under the negative design load, negative fatigue load, positive design load, and positive fatigue load, respectively, assuming uncracked sections. The negative design stress (-1.056 ksi) under the design load (-3140 kip-ft) was greater than the modulus of rupture of concrete. Thus, the transverse joint was reanalyzed assuming cracked section properties. Based on the cracked section analysis, the stresses of the U-bar in girder DBT65 were determined to be 35.6 ksi and 10.3 ksi under the negative design load (-3140 kip-ft) and negative fatigue load (-910kip-ft), respectively.

The static and fatigue loadings during the test were determined as follows:

Static Tension: P=2×2×0.31×35.6=44.1 kips

Fatigue Tension: P=2×2×0.31×10.3=12.8 kips

Static Compression: P=7.25×15×0.169=18.4 kips

Fatigue Compression: P=7.25×15×0.066=7.2 kips

In the determination of the tension loads, on one side of the joint there were three sets of #5 U-bars, on the other side of the joint, there were two sets of #5 U-bars, as shown in Figure 13.1.2. The tension load was determined by multiplying the desired stress (i.e., 35.6 ksi or 10.3 ksi, for the static and fatigue tests, respectively) by total cross-sectional area of the fewest number of bars crossing the joint (i.e., two sets of U-bars, which was two sets of two bars multiplied by the cross-sectional area of a #5 bar of 0.31 in.[2]). The compression load was found by multiplying the concrete cross-sectional area by the desired compressive stress.

441

In the tests, the compression load was not applied to be conservative. During the fatigue test, the applied tension load was cycled between 12.8 kips (6.4 kips on each actuator) corresponding to a negative fatigue load of -910 kip-ft and 0 kips for a total of 2 million cycles at a frequency of 4Hz.

Before the cycling and at the end of 0.5, 1.0, 1.5, and 2.0 million cycles, a static test was conducted. A static tension loading was applied in several increments up to 44.1 kips (22.1 kips on each actuator) in order to produce the negative design load of -3140kip-ft, and unloaded to zero. Finally, the specimen was loaded to failure.

13.1.8. Tensile Capacity

The tensile capacity was calculated as the product of the lightly reinforced area of steel, As=1.24 in^2, and the U-Bar nominal yield strength of 75 ksi, as discussed in Chapter 9. The service live load was also determined in Chapter 9. The test results are compared with the calculation in Table 13.1.3. The strengths for the fatigue tests, FT-O and FT-7, shown in the table are strengths at end of the tests.

Table 13.1.3: Tensile capacity

Specimen	Measured			Calculated		
	Panel Strength (psi)	Joint Strength (psi)	Failure Load (kip)	Service Live Load (kip)	Ultimate Load (kip)	
					75 ksi (U-Bar Nominal Yield Strength)	60 ksi (U-Bar Nominal Yield Strength)
WT-2	7719		88.70	44.14	93.00	74.40
ST-O	8462	4649	67.85	44.14	93.00	74.40
FT-O	8216	4982	65.21	44.14	93.00	74.40
ST-7	8886	9974	93.49	44.14	93.00	74.40
FT-7	9162	9505	101.15	44.14	93.00	74.40

WT-2, discussed in Chapter 9, had the same reinforcement layout as the tension specimens tested in this phase. The difference was that WT-2 was poured as a monolithic specimen, while ST-O, FT-O, ST-7 and FT-7 were fabricated by joining two panels with one of the CP materials as shown in Figure 13.1.6. All of the specimens exceeded the nominal service live load capacity. However, only ST-7 and FT-7 exceeded the

442

calculated tensile capacity. In Section 9.2.4, it was concluded that tensile capacities were reduced by reducing the concrete strength. Please note that the longitudinal reinforcement is not continuous in the U-bar detail. And one reason that ST-O and FT-O have lower capacities is due to the lower strength of the joint material. Attention needs be paid to the moisture loss during the first 3 hours after placement, which may have caused the lower strengths in the tests.

13.1.9. Load Deflection Relationships

Figure 13.1.8 compares the load-deflection curves of the fatigue specimens after 2 million cycles with those of the specimens subjected to static loading without fatigue cycles. The vertical axis labeled "Load" represents the total applied tension load, and the horizontal axis "Deflection" represents the relative displacement between the two joint interfaces.
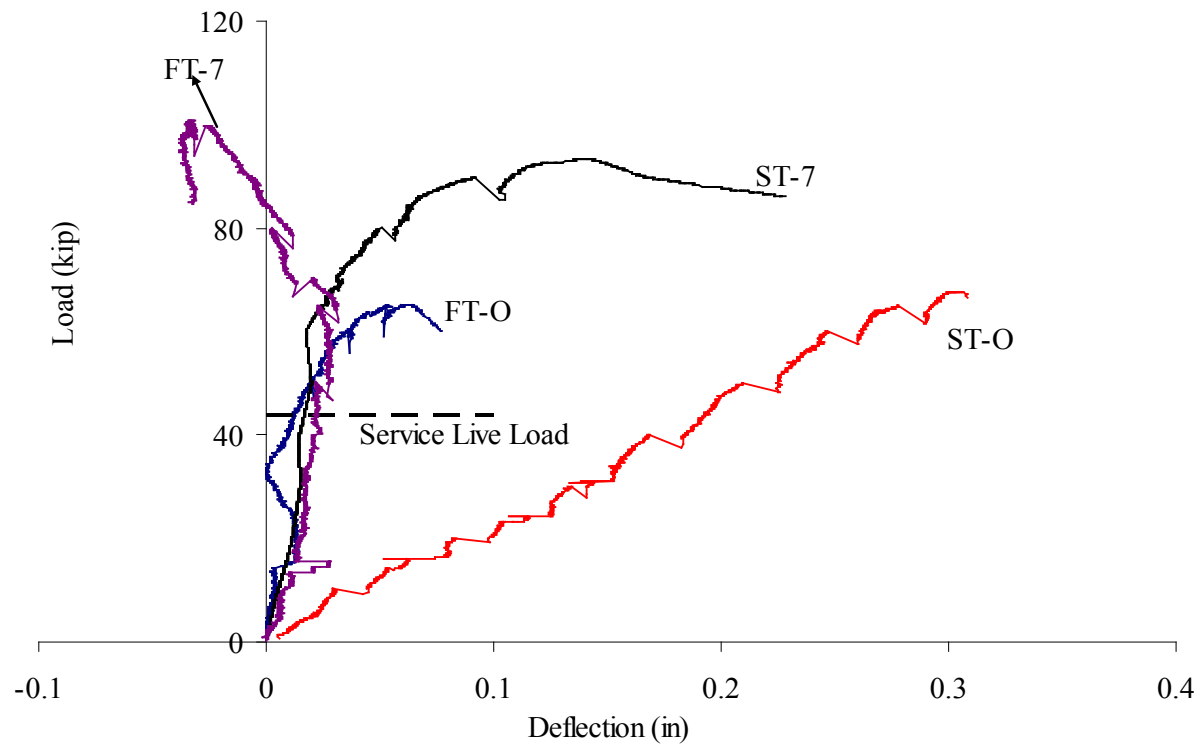
Figure 13.1.8: Load-deflection curves of the tension specimens

The slopes for ST-7, FT-O and FT-7 were large, because the specimens deflected out of phase at the beginning of the load, and the FT-7 specimen had this out-of-phase problem through the test. ST-O developed more deflection than FT-O. After reaching the peak load, ST-7 exhibited more ductility than FT-7. The fatigue cycles had an effect on the deflection of joints.

443

13.1.10.　　　Crack Width Development

During the tests, the entire specimen was monitored for crack development, and crack widths were measured. The crack development within the joint zone is presented in Figure 13.1.9. "Crack 1", "Crack 2", "Crack 3", and "Crack 4" are shown in Figure 13.1.10, marked as "①", "②", "③" and "④," respectively.

Cracks 1 and 2 were cracks along the upper and lower joint interfaces, respectively. Crack 3 was a longitudinal crack observed within the joint, and Crack 4 referred to the diagonal or transverse cracks within the joint.

The crack development observed in ST-O and ST-7 was similar. From Figure 13.1.9, the width of "Crack 1" grew faster among all of the cracks due to the less reinforcement at the joint interface of the "Crack 1" location. There were two U-bars that crossed the joint interface at the "Crack 1" location and three that crossed the joint at the "Crack 2" location. Crack 2 had the smallest measured crack widths throughout the tests as would be expected.

For all four specimens, the first crack developed along the joint interfaces with less U-bars, Crack 1 as shown in the figures. As the tension loading was increased, transverse cracks continued to appear in various locations within and outside the joint zone. For ST-O, the first transverse crack occurred at approximately 20 kips, which was about 30% of the tensile capacity. For FT-O, the first transverse crack occurred at nearly 10 kips, about 15% of the tensile capacity. For ST-7, the first transverse crack developed at 30 kips, 32% of tensile capacity, and for FT-7, the first transverse crack developed at 30 kips.

Longitudinal cracks began forming inside the joint zone at the following loads: 40 kips for ST-O, 20 kips for FT-O before cycling, 40 kips for ST-7, and 44.1 kips for FT-7 after 0.5 million cycles. The longitudinal cracks formed above the longitudinal reinforcement in the specimen, which relates to the longitudinal reinforcement in the deck of precast bridge deck system crossing the transverse joint. Such cracks initiate splitting cracks associated with bond failure.

Diagonal cracks appeared in the joint, as the specimens approached capacity.

(a) ST-O
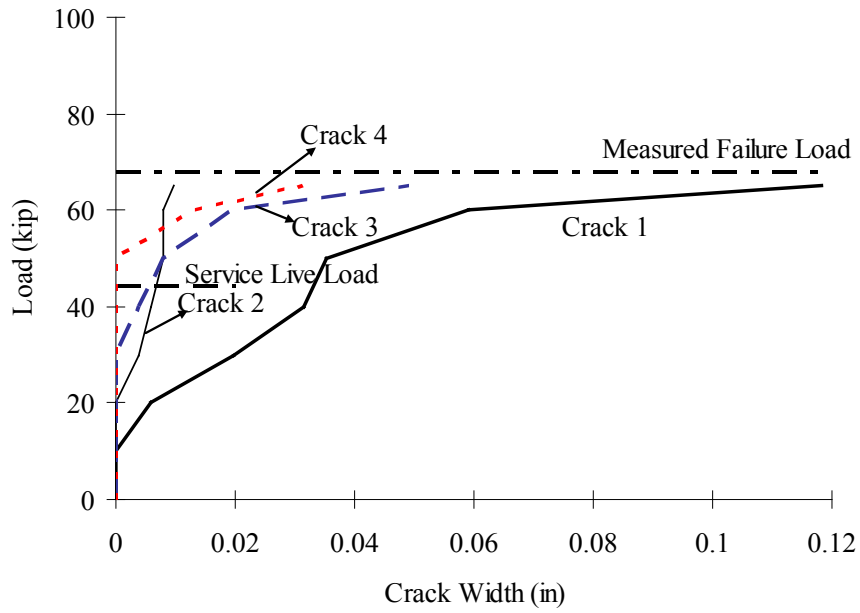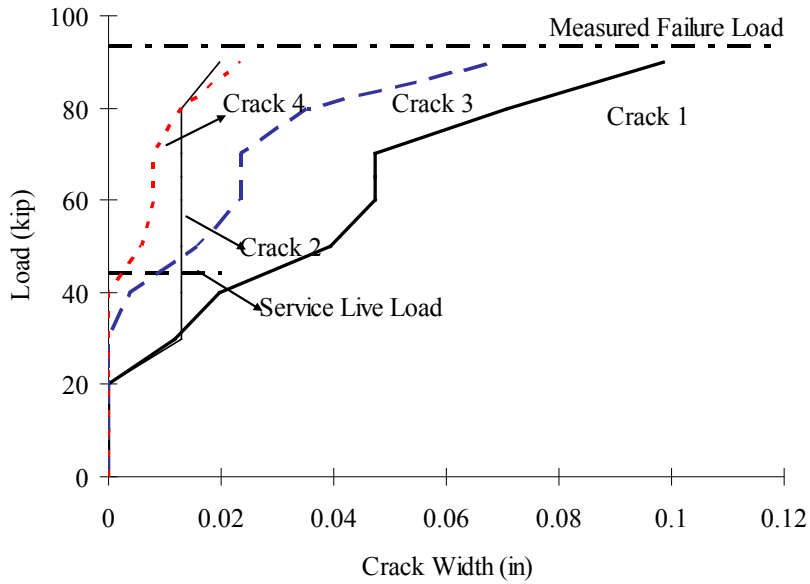
(b) ST-7

Figure 13.1.9: Load-crack width curves of static tension specimens

445

(a) ST-O   (b) ST-7
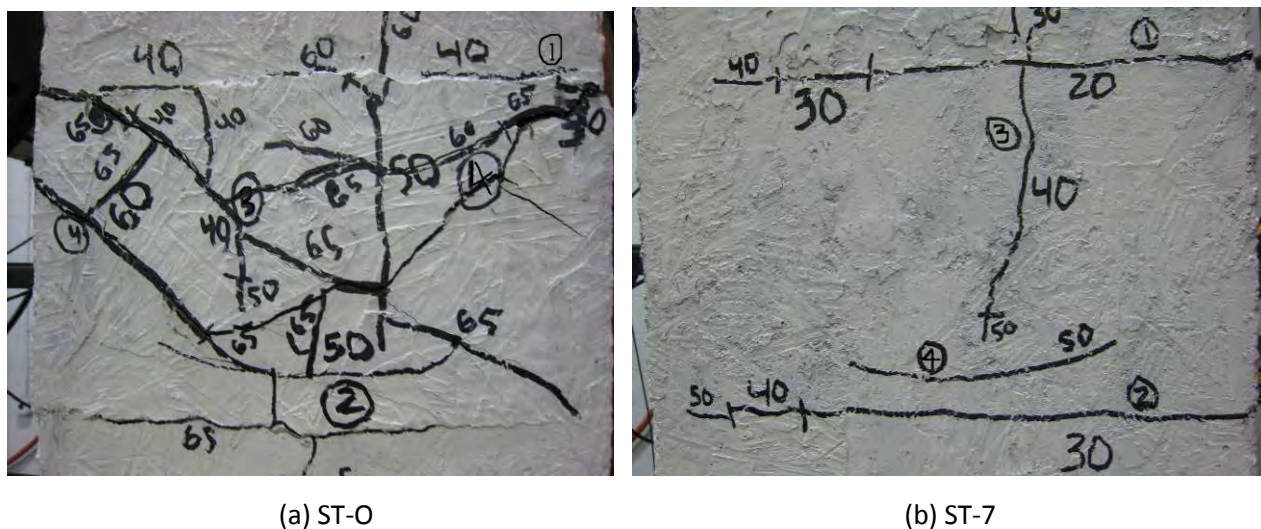
Figure 13.1.10: Cracks within the Joint

Figure 13.1.11 shows the crack width-fatigue cycle curve (CW-N) for the fatigue tests representing the maximum crack width within the joint after various number of fatigue cycles under specified loadings. For FT-7, Crack 1 and 2 along the joint interfaces developed before the fatigue cycling, and one longitudinal crack developed in the static test after 0.5 million cycles. The longitudinal crack width was less than 0.008 in. all through the cycling. For FT-O, seven cracks developed during the static test before the fatigue cycling, including two cracks along the joint interfaces, two transverse cracks and three longitudinal cracks in the joint. No new crack occurred in the interim static tests. Crack 1 along the joint interface with two U-bars had the largest width all through the fatigue cycling, while all the other cracks had widths less than 0.008 in.

From Figure 13.1.11, it can be seen that the width of the cracks within the joint was dependent upon the applied load. The crack widths increased with increased loads, as expected. Under the same loading, the crack widths were observed to increase with increasing numbers of fatigue cycles, particularly for the specimens with the overnight cure material. The joint with the 7-day cure material developed smaller crack widths than the overnight cure material, and the cracks in the joint with the 7-day cure material tended to stabilize under fatigue loads.

446

(a) FT-O

(b) FT-7
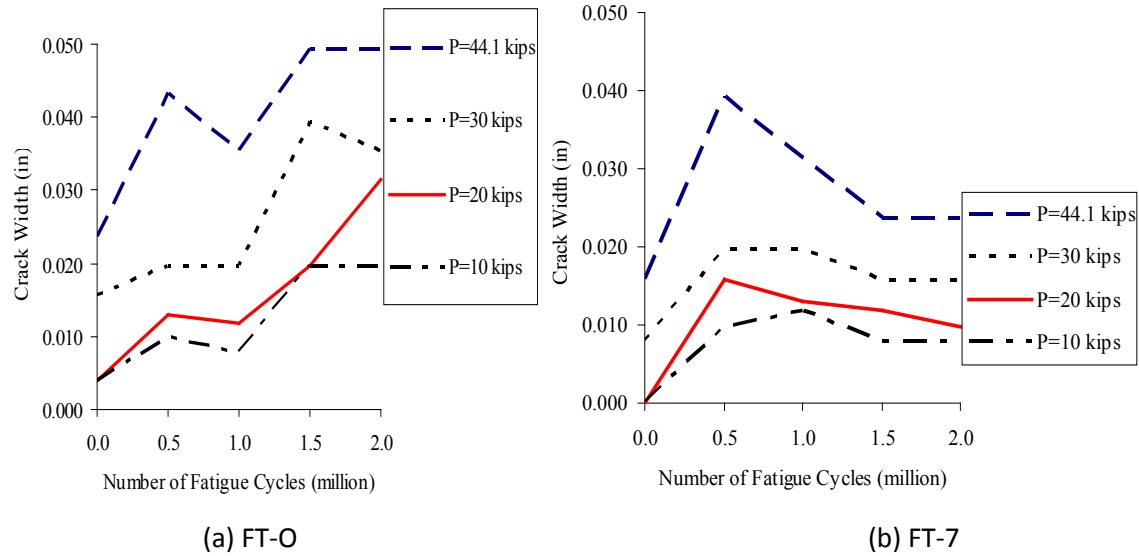
Figure 13.1.11: CW-N curve

13.1.11. Strain Development

Figure 13.1.12 shows the strain-fatigue cycle curves (MS-N) for the fatigue tests representing the reinforcement strain in the joint after various number of fatigue cycles under service live load. The strain gage number and the loading are shown in the figure. The strain gage layout is shown in Figure 13.1.3. "P = 44.1 kips" means the specimen was subjected to a tension load of 44.1 kips in total when the strain measurement was taken.

From Figure 13.1.12, it can be seen that the variation of the reinforcement strain after different fatigue cycles was not significant. The strains were larger in the two U-bar reinforcement (see gage numbers 2-# and 4-#) compared with the strains in the three U-bar reinforcement (see gage number 3-#). The strain was observed to increase with increase in distance from the bend of the U-bars. The lacer bar experienced low axial strains; it served to provide mechanical anchorage to the U-bars through dowel action.

447
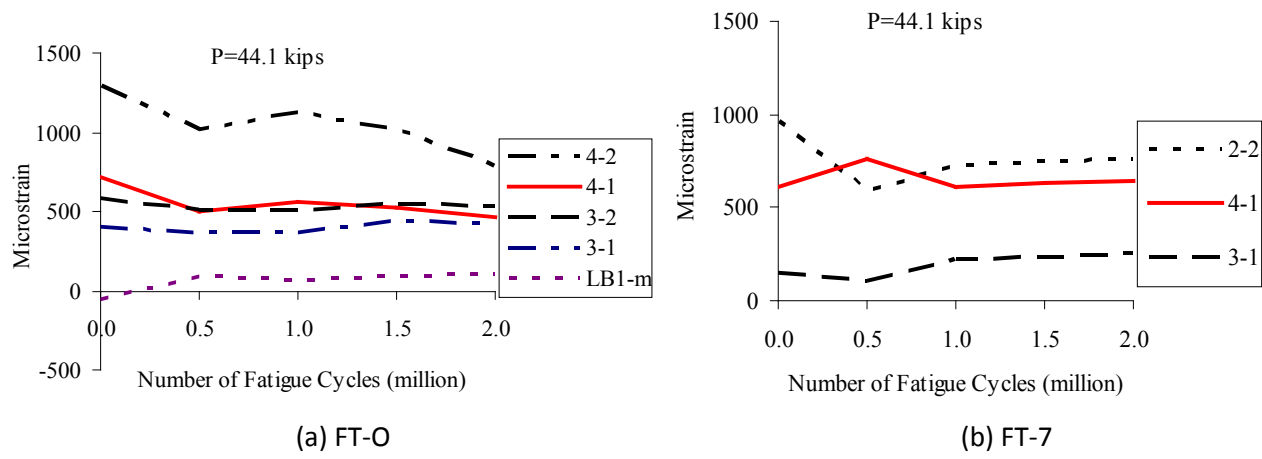
Figure 13.1.12: MS-N curves of fatigue tension specimens

Figure 13.1.13 shows the load-strain curves representing the strain values in the joint zone (Strain gage 3-1 shown in Figure 13.1.3) for each specimen, which also show that the variation in the reinforcement strain observed after fatigue cycles was not significant in comparing ST-O to FT-O and ST-7 to FT-7.

448
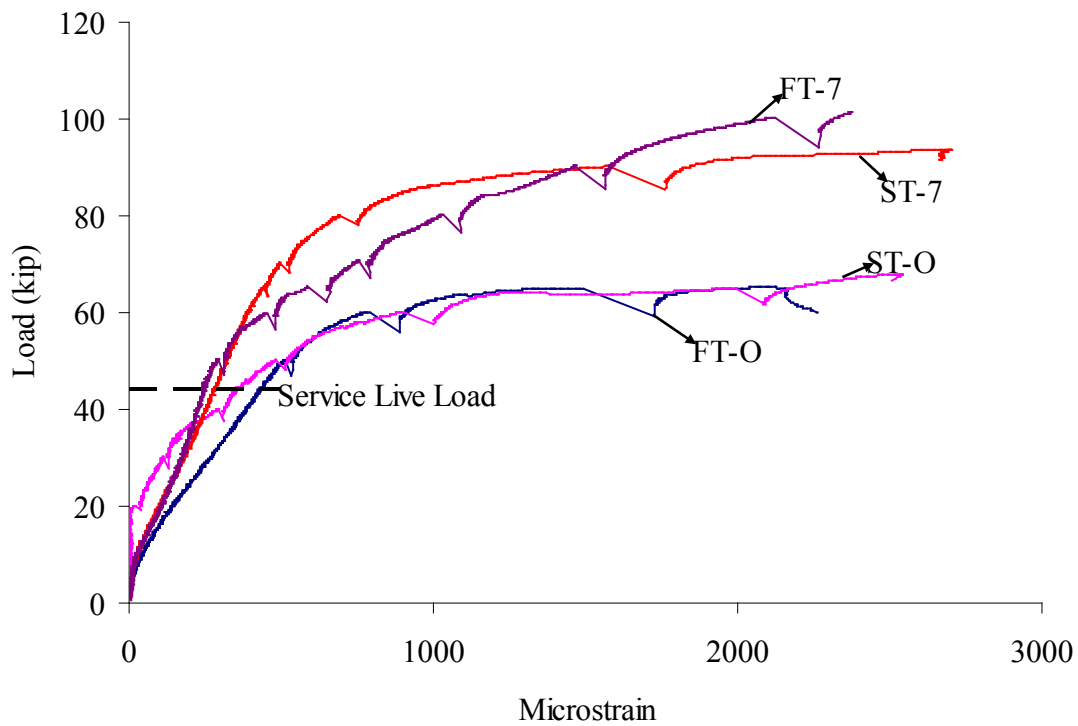
Figure 13.1.13: Load-strain curve

13.1.12. Failure of Specimen

The crack patterns at tensile failure for ST-O, FT-O, ST-7 and FT-7 are shown in Figure 13.1.14. The diagonal cracks propagated toward the first transverse cracks that developed along the joint interface. The concrete could be easily removed from the specimen where the diagonal and transverse cracks met.

The lacer bars were intended to serve as restraints for the U-Bars to facilitate ductile failure in the specimens. An example of the deformation of the lacer bars can be seen in Figure 13.1.15.

(a) ST-O (1 in. cover side)

(b) ST-O (2 in. cover side)
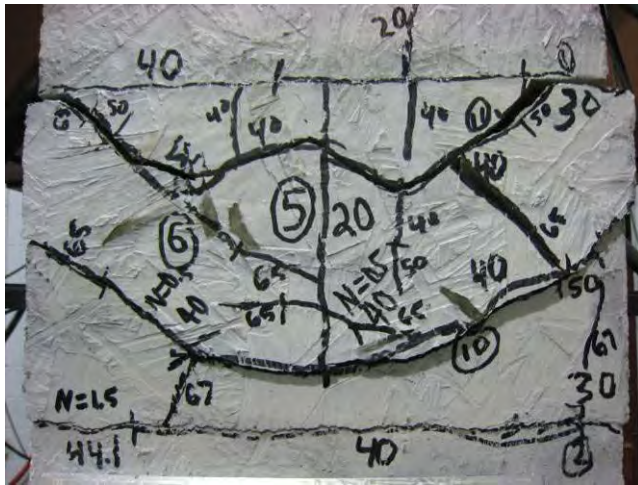
(c) FT-O (1 in. cover side)

(d) FT-O (2 in. cover side)

450

(e) ST-7 (1 in. cover side)

f) ST-7 (2 in. cover side)
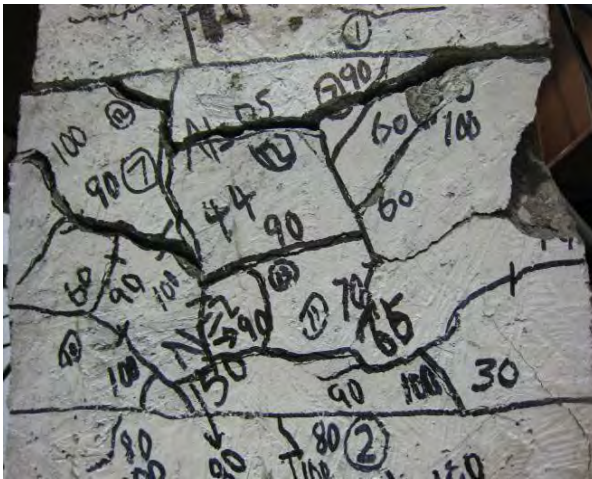
(g) FT-7 (1 in. cover side)
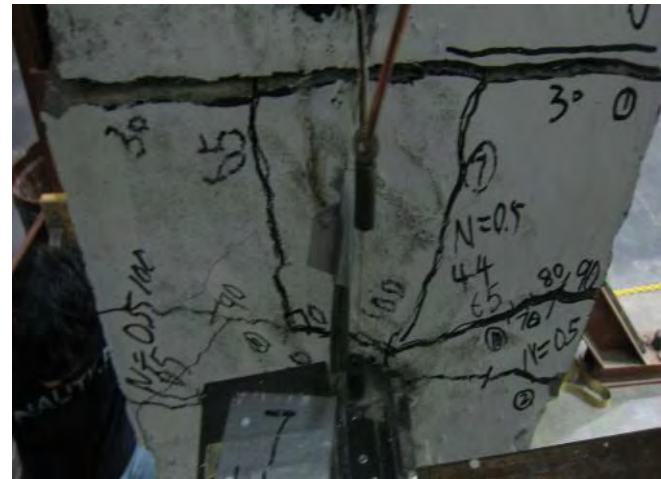
(h) FT-7 (2 in. cover side)

Figure 13.1.14: Cracking in transverse joint (tension) specimens

451

Figure 13.1.15: Deformation of lacer bar

13.2. Conclusions

Based on the parametric study and the experimental program, the following conclusions can be made:

1. The fatigue loading had no significant influence on the tensile capacity and reinforcement strains.
2. The fatigue loading was observed to have an effect on the deflection development, particularly for the joints with the 7-day cure material.
3. The fatigue loading had some effect on the measured crack widths in the specimens with the overnight cure material. Under the same loading, the crack widths were observed to increase after the fatigue cycles.
4. Undesirable wider crack widths will be developed at service load levels in transverse joints designed with higher grades of steel (e.g., 75 ksi compared to 60ksi) because smaller amounts of reinforcement can provide the required nominal strength. Under service loads, larger stresses would be expected in the smaller bars, which lead to wider cracks at service. It is recommended that 60 ksi nominal yield strength be used in the design of transverse joints, or that stresses in the reinforcement are limited at service.
5. Based on these tests and with the aforementioned caveats, the U-bar detail may be considered a viable connection system for transverse joints in continuous decked bulb-T and full-depth precast deck panel on girder bridges.

452

Chapter 14 Full-Depth Deck Panel and Decked Bulb-T: Summary

14.1. Summary

Speed of construction, particularly for bridge replacement and repair projects, has become a critical issue to minimize disruption of traffic and commerce. Promising systems for rapid construction include precast bridge systems fabricated using decked bulb-T (DBT) concrete girders or full-depth precast deck panels on girders. One of the hurdles that must be overcome to enable a wider use of this technology is the development of design guidelines and standard details for the joints used in these systems, which must produce full strength joints, but still allow for accelerated construction. The focus of NCHRP 10-71 was to develop specifications, guidelines, and examples for the design and construction of durable cast-in-place (CIP) reinforced concrete connections for precast deck systems that emulate monolithic construction, considering issues including speed of construction, durability, and fatigue. Chapters 8 through 14 summarize the research effort conducted by the University of Tennessee at Knoxville (UTK) research team, associated with the development of longitudinal and transverse connection concepts between full-depth deck panels and decked bulb-T flanges including the development of durable closure pour materials for accelerated bridge construction. The following provides a summary and conclusions of that study.

1) The analytical parametric study, considering parameters such as different loading locations, effect of bridge width, design truck and lane loading versus design tandem and lane loading, girder geometry (depth, spacing and span), bridge skew, single-lane loading versus multi-lane loading, and impact of cracking of the joints, was conducted to provide the database of maximum forces in the joint. These forces were subsequently used to determine the fatigue loading demand for the large-scale longitudinal joint specimen (flexure and shear-flexure) tests and the large-scale transverse joint specimen (tension) tests.

2) Initial tests were conducted using monolithic specimens that contained details to simulate longitudinal and transverse joint connection concepts (i.e., flexural and tension test specimens, respectively). The connection concepts consisted of two types of U-bar details (i.e., deformed wire reinforcement (DWR) and stainless steel (SS)) and a headed bar detail. Based on the performance of the initial tests, the most promising connection concept in terms of behavior, constructability and cost, was investigated in additional tests where parameters were varied to refine the proposed connection concepts. The results of these tests indicated that a U-bar detail with #5 equivalent deformed wire reinforcement at 4.5 in. spacing with 6 in. overlap length provided a viable detail.

3) Two categories of closure pour (CP) materials, overnight cure and 7-day cure, were proposed and studied. Based on extensive literature reviews and the experimental investigation, performance criteria for selecting durable CP materials were developed as listed in Tables 14.1.1 and 14.1.2.

Table 14.1.1: Proposed performance criteria of CP materials

Performance Characteristic	Test Method	Performance Criteria		
Compressive Strength (CS), ksi	ASTM C39 modified	6.0≤CS @ 8 hours (overnight cure) @ 7 days (7-day cure)		
Shrinkage[a](S), (Crack age, days)	AASHTO PP34 modified	20<S		
Bond Strength (BS), psi	ASTM C882 modified	300<BS		
Chloride Penetration[b](ChP), (Depth for Percent Chloride of 0.2% by mass of cement after 90-day ponding, in)	ASTM C1543 modified	ChP<1.5		
Freezing-and-thawing Durability (F/T), (relative modulus after 300 cycles)	ASTM C666 Procedure A modified	Grade[c] 1 70%≤F/T	Grade 2 80%≤F/T	Grade 3 90%≤F/T

a: No S criterion need be specified if the CP material is not exposed to moisture, chloride salts or soluble sulfate environments.

b: No ChP criterion need be specified if the CP material is not exposed to chloride salts or soluble sulfate environments.

c: Grades are defined in Table 14.1.2.

Table 14.1.2: Application of CP material grades for freezing-and-thawing durability

Freezing-and-thawing Durability (F/T)	Is the concrete exposed to freezing-and-thawing environments?	Yes	Is the member exposed to deicing salts?	Yes	Will the member be saturated during freezing?	Yes. Specify F/T-Grade 3
						No. Specify F/T-Grade 2
				No. Specify F/T- Grade 1		
		No. F/T grade should not be specified.				

4)   The final test series included large-scale tests of jointed specimens including static and fatigue flexure and flexure-shear loading of the longitudinal joint details shown in Figures 14.1.1 and 14.1.2. These studies indicated that the proposed longitudinal joint detail has sufficient strength, fatigue characteristics, and crack control for the maximum service loads determined from the analytical

454

studies and was deemed to be a viable connection system to provide continuity in jointed deck systems over piers.
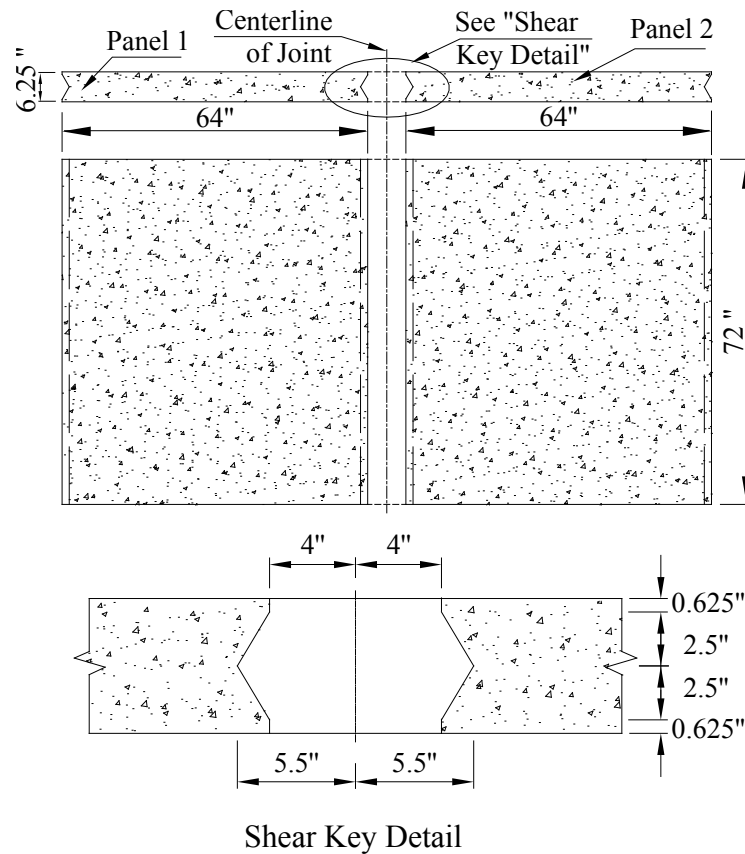
Figure 14.1.1: Dimension of Slab Specimen

5) Static and fatigue tests under tension loading were also conducted to simulate transverse joints intended to provide continuity through the deck at bridge piers. It was assumed that at the pier in negative bending, the deck would transmit tension equilibrated by compression in the girder. Test results were evaluated based on tensile capacity, cracking, displacement and steel strain. Based on these test results, the U-bar detail was deemed a viable connection system for the transverse joint. The joint with the 7-day cure material was able to achieve higher strengths which might be attributed to the section with the lower strength overnight cure material being unable to fully develop the reinforcement. To reduce the crack sizes in the joints, it is proposed to reduce the service stresses in the joints. This could be accommodated economically by using more lower-grade reinforcement (i.e., Grade 60 rather than Grade 75 bars).

Effects of variables including overlap lengths, rebar spacings, and concrete strengths were investigated. Based on capacity, service level crack widths, constructability, and cost, the U-bar detail, with an overlap length of 6 in., a rebar spacing of 4.5 in. and two transverse lacer bars, constructed of deformed wire reinforcement was recommended as an alternate detail for longitudinal and transverse joints. The tests were based on uncoated reinforcement. If epoxy-coated reinforcement were used, larger joint widths

455

may be required to develop the reinforcement across the joint. An alternative is to use stainless steel reinforcement which performed well in the initial study, but was an expensive alternative.
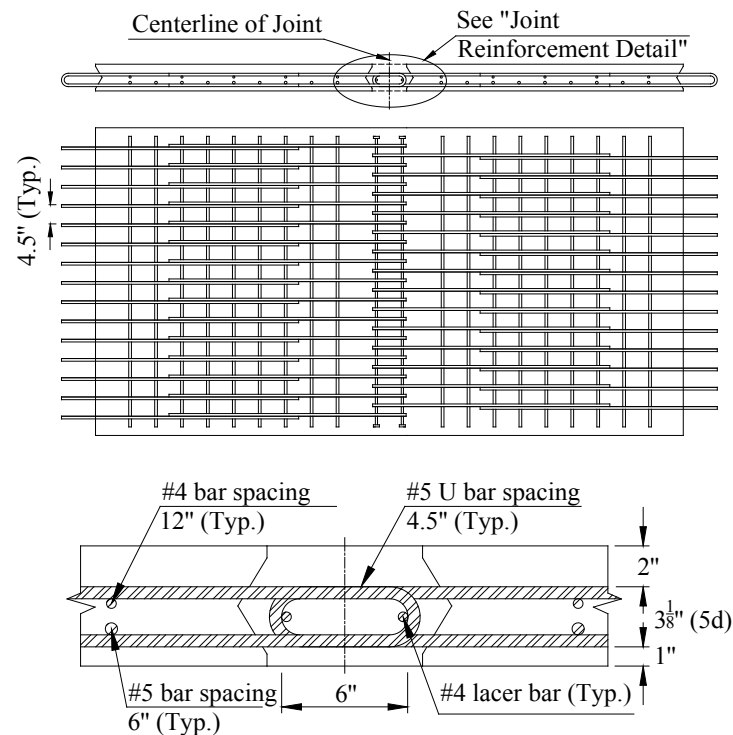
Figure 14.1.2: Reinforcement Layout in Slab

14.2.   Full Depth Deck Panel and Decked Bulb T Design Recommendations:

The research completed during the NCHRP 10-71 study resulted in the development of a comprehensive design guide for the design and construction of longitudinal and transverse joints for full depth deck panels and decked bulb T's (DBTs). The design guide covers the detailing requirements for both loop bar and headed bar details. Adequate performance of these systems requires the use of lacer bars which improve the mechanical anchorage of these systems. Tests were conducted to investigate the behavior of these systems in shallow decks to emulate the flanges of DBTs. These shallow deck thicknesses required the use of tighter bends than presently allowed by AASHTO (2010) and thus the recommendations are restricted to wire reinforcement and stainless steel reinforcement which may accommodate tighter bends due to their higher levels of ductility. Another important feature of these joints is the performance of the closure pour materials, which was also investigated through a series of laboratory tests that included an evaluation of the shrinkage and freeze-thaw durability characteristics of candidate overnight-cure and 7-day cure materials which might be considered in rapid construction applications. The proposed modifications to the AASHTO LRFD 2010 Bridge Design Specification, as well as the AASHTO LRFD Bridge Construction Specifications are included in Appendix A, and corresponding design examples showing recommended details for the longitudinal and transverse joints are included in Appendix B.

456

References for PCSSS Study

AASHTO, 1961, *Interim Specifications: Standard Specifications for Highway Bridges*, Washington, DC

AASHTO, 1994, *AASHTO LRFD Bridge Design Specifications 1st Edition,* Washington, DC

AASHTO, 1997, *Standard Specifications for Highway Bridges 16th Edition*, American Association of State Highway Officials, Washington, DC

AASHTO, 2005, *AASHTO LRFD Bridge Design Specifications 3rd Edition,* Washington, DC

AASHTO, 2010, *AASHTO LRFD Bridge Design Specifications 5th Edition*, Washington, DC

ACI 308.1, 1998, *Standard Specification for Curing Concrete*. American Concrete Institute (ACI), Farmington Hills, MI

ACI 224, 2001, *Control of Cracking in Concrete Structures*. American Concrete Institute (ACI) Committee 224, Farmington Hills, MI

ACI 318, 2008, *Building Code Requirements for Structural Concrete and Commentary*, Farmington Hills, MI

Anderson, A.R., *Systems Concepts for Precast and Prestressed Concrete Bridge Construction*, Highway Research Board Special Report, Issue No. 132. 1972. Highway Research Board, Washington D.C., pp. 9-21

ASTM C36, 2009, *Test Method for Compressive Strength of Cylindrical Concrete Specimens*. American Society for Testing Materials, West Conshohocken, PA

ASTM C78, 2009, *Standard Test Method for Flexural Strength of Concrete (Using Simple Beam with Third-Point Loading)*. American Society for Testing Materials, West Conshohocken, PA

ASTM C469, 2002, *Standard Test Method for Static Modulus of Elasticity and Poisson's Ratio of Concrete in Compression*. American Society of Testing Materials, West Conshohocken, PA

Barker, R., and Puckett, J., *Design of Highway Bridges: An LRFD Approach, 2nd Edition*, 2007. Wiley and Sons, NJ

Base, B.D., *An Investigation of Transmission Length in Pre-tensioned Concrete*. Portland Cement Association Research Report No. 5, 1958

Bell, C., Shield, C.K., French. C.W., *Application of Precast Decks and other Elements to Bridge Structures*. Mn/DOT Technical Report No. MN/RC 2006-37, 2006. Minnesota Department of Transportation, Saint Paul, MN

Blackman, D., *Evaluation of Design Methods for the Control of Early Age Bridge Deck Cracking,* Master's Thesis, 2002, Purdue University, West Lafayette, IN

Endicott, W.A., *'Instant' Bridges Keep Traffic on the Move*, Ascent. 1993. Precast/Prestressed Concrete Institute, Chicago, IL, pp. 26-28

Erikkson, W.D., *Vertical Tensile Stresses in End Regions of Precast Composite Slab-Span Systems and Restraint Moments,* Master's Thesis, May 2008. University of Minnesota-Twin Cities Graduate School, Minneapolis, MN

Freyermuth, C.L., *Design of Continuous Highway Bridges with Precast, Prestressed Concrete Girders*. Journal of the Prestressed Concrete Institute 14(2), 1969. pp. 14-39

Fountain, R.S., *A Field Inspection of Prestressed Concrete Bridges*. Portland Cement Association (PCA), 1963

Frosch, R.J., Bice, J.K., Erickson, J.B., *Field Investigation of a Concrete Deck Designed by the AASHTO Empirical Method: The Control of Deck Cracking,* Indiana Department of Transportation Technical Report FHWA/IN/JTRP-2006/32. September 2006. Indiana Department of Transportation, Indianapolis, IN

Gergely, P., Sozen, M.A., Seiss, C.P., *The Effect of Reinforcement on Anchorage Zone Cracks in Prestressed Concrete Members,* Structural Research Series No. 271, 1963. University of Illinois

Hagen, K. "Development and Construction of Mn/DOT Precast Slab System." PCI National Bridge Conference. October 18, 2005

Hawkins, N.M., Shahawy, M., *Anchorage Zone Stresses in Prestressed Concrete Beams,* Structural Research Series No. 207, 1960. University of Illinois

INDOT, 1999, *Standard Specifications*, Indiana Department of Transportation, Indianapolis, IN

Issa, M.A., Yousif, A.A., Kaspar, I.I., Khayyat, S.Y., *Field Performance of Full Depth Precast Concrete Panels in Bridge Deck Reconstruction,* PCI Journal, Vol. 40, No. 1, May-June 1995. Precast/Prestressed Concrete Institute, Chicago, IL, pp. 82-105

Le, Quoc Thanh Chau, "Transverse Cracking in Bridge Decks: Parametric Study." Master's Thesis, 1998. University of Minnesota-Twin Cities Graduate School, Minneapolis, MN

Marshall, W.T., Mattock, A.H., *Control of Horizontal Cracking in Ends of Pretensioned Prestressed Concrete Girders,* Journal of the Prestressed Concrete Institute, 7(5), 1962, pp. 56-74

Merwin, D.P., *Prestressed Concrete Bridge Built in One Weekend*, Ascent, Vol. 13(3). August 2003. Precast/Prestressed Concrete Institute, Chicago, IL., pp. 32-34

Molnau, K., Dimaculangan, M.C., "Inverted T Design." LRFD Bridge Design Workshop, June 12, 2007

Naito, C., Deschenes, D., *Horizontal Shear Capacity of Composite Concrete Beams without Ties,* Proceedings, Prestressed/Precast Concrete Institute (PCI) National Bridge Conference, 2006. Grapevine, TX

Park, R., Priestley, M.J.N., Gill, W.D., "Ductility of Square Confined Concrete Columns." *Journal of the Structural Division*, ASCE, Vol. 108, No. ST4, April 1982, pp. 929-950

Radabaugh, R.D., *Investigation of Early Age Bridge Deck Cracking*, Master's Thesis, 2001. Purdue University, West Lafayette, IN

Saenz, L.P., "Equations for the Stress-Strain Curve of Concrete." *ACI Journal Proceedings*, Vol. 61, No. 22, September 1964, pp. 1229-1235

SAS Inc., 2004, *ANSYS Version 9.0*, Swanson Analysis Systems, Houston, PA

Smith, M.J., Eriksson, W.D., Shield, C.K., French, C.W., *Monitoring and Analysis of Mn/DOT Precast Composite Slab Span System (PCSSS),* Mn/DOT Technical Report No. MN/RC 2008-41. September 2008. Minnesota Department of Transportation, Saint Paul, MN

Suttikan, C., "A Generalized Solution for Time-Dependent Response and Strength of Noncomposite and Composite Prestressed Concrete Beams." University of Texas at Austin, 1978

Tadros, M.K., Baishya, M.C., *Rapid Replacement of Bridge Decks,* NCHRP Report No. 407, National Cooperative Highway Research Program, Transportation Research Board, Washington, DC, 1998

Tokerud, R., *Precast Prestressed Concrete Bridges for Low-volume Roads*, PCI Journal. 1979. Precast/Prestressed Concrete Institute, Chicago, IL

Uijl, J.A.d., *Tensile Stresses in the Transmission Zones of Hollow-Core Slabs Prestressed with Pretensioned Strands Report 5-83-10*, The Netherlands: Delft University of Technology Department of Civil Engineering, 1983

Wallace, J.W., BIAX – *A Computer Program for the Analysis of Reinforced Concrete Sections*. University of California at Berkeley, 1989

Zia, P., Preston, H.K., Scott, N.L., and Workman, E.B., *Estimating Prestress Losses*. Concrete International, June 1979. pp. 32-38

References for Full-Depth Deck Panel and Decked Bulb-T Study

AASHTO Designation: PP 34-99 (1998), "Standard Practice for Estimating the Cracking Tendency of Concrete," American Association of State and Highway Transportation Officials, June 1998, pp199-202

AASHTO LRFD (2010). "*Bridge Design Specifications.*" Fourth Edition, American Association for State Highway and Transportation Officials, Washington, DC

American Concrete Institute. (2008). "Building Code Requirements for Structural Concrete and Commentary," ACI Committee 318, Farmington Hills, MI

Bentz, E. C., and Collins, M.P. (2000). *Response-2000 Reinforced Concrete Sectional Analysis*. A software downloaded http://www.ecf.utoronto.ca/~bentz/r2k.htm (2006)

Colorado DOT's 2005 Standard Specifications for Road and Bridge Construction, CDOT Specification Committee, Denver, CO

Dragosavic, M.; van den Beukel, A.; Gijsbers, F.B.J., (1975) "Loop Connections between Precast Concrete Components Loaded in Bending," Heron, Vol. 20, No. 3, pp. 3-35

Einea, A., Yehia, S. and Tadros, M. K. (1999) "Lap Splices in Confined Concrete" ACI Structural Journal, 96(6), 947-956

Ghanem, H., Phelan, S., Senadheera, S., and Pruski, K. (2008), "Chloride Ion Transport in Bridge Deck Concrete Under Different Curing Durations", ASCE Journal of Bridge Engineering, Vol. 13, No. 3, May 1, pp. 218-225

Glass, G.K. and Buenfeld, N.R. (1995), "Chloride threshold levels for corrosion induced deterioration of steel in concrete," Chloride Penetration into Concrete, International RILEM Workshop, St. Remy-Les Chevreuse

Gordon, S. R.; May, I. M., (2005) "Development of In Situ Joints for Pre-Cast Bridge Deck Units," Bridge Engineering 000, Issue BEO, pp. 1-14

461

Gulyas, R. J. and Champa, J. T. (1997), "Use of Composite Testing for Evaluation of Keyway Grout for Precast Prestressed Bridge Beams," American Concrete Institute (ACI) Materials Journal, Technical Paper, V. 94, No. 3, May-June, pp. 244-250

Gulyas, R. J., Wirthlin G. J. and Champa, J. T. (1995), "Evaluation of Keyway Grout Test Methods for Precast Concrete Bridges," Precast/Prestressed Concrete Institute (PCI) Journal, V. 40, No. 1, January-February, pp. 44-57

Issa, M. A., Cyro do V., Abdalla, H., Islam, M. S., and Issa, M. A. (2003), "Performance of Transverse Joint Grout Materials in Full-Depth Precast Concrete Bridge Deck Systems," Precast/Prestressed Concrete Institute (PCI) Journal, V. 48, no. 4, July-August, pp. 92-103

Lawler, J. S., Connolly, J. D., Krauss, P. D., Tracy, S. L., and Ankenman, B. E. (2007), "Guidelines for Concrete Mixtures Containing Supplementary Cementitious Materials to Enhance Durability of Bridge Decks," NCHRP Project 18-08A Report 566, Transportation Research Board, Washington, DC

Li, L., Ma, Z., Griffey, M. E., and Oesterle, R. G. (2010), "Improved Longitudinal Joint Details in Decked Bulb Tees for Accelerated Bridge Construction: Concept Development," ASCE Journal of Bridge Engineering, 15(3), 327-336

Li, L. (2009), "Development of Continuous Longitudinal Joints and Optimization of Intermediate Diaphragms in Decked Bulb Tee Girder Bridges for Accelerated Construction," Ph. D. Dissertation, University of Tennessee, Knoxville

Li, L., Ma, Z., and Oesterle, R. G. (2010a), "Improved Longitudinal Joint Details in Decked Bulb Tees for Accelerated Bridge Construction: Fatigue Evaluation," ASCE Journal of Bridge Engineering, 15(5)

Ma, Z. et al (2007), "Field Test and 3D FE Modeling of Decked Bulb-Tee Bridges," ASCE Journal of Bridge Engineering, 12(3), 306-314

Martin, L.D., and Osborn, A.E.N. (1983), "Connections for Modular Precast Concrete Bridge Decks," Report No. FHWA/RD-82/106, US DOT, Federal Highway Administration

Matsumoto, E., Waggoner, M. C., Sumen G., Kreger, M. E., and Breen, J. E. (2001), "Development of a Precast Bent Cap System," University of Texas Austin, Project summary report 1748-S, March

Menkulasi, F. and Roberts-Wollmann, C. L. (2005), "Behavior of Horizontal Shear Connections for Full-Depth Precast Concrete Bridge Decks on Prestressed I-Girders," Precast/Prestressed Concrete Institute (PCI) Journal, V. 50, No. 3, May-June, pp. 60-73

Mrinmay B. (1986), "Precast Bridge Deck Design System," Prestressed/Precast Concrete Institute (PCI) Journal, V. 31, No. 2, March-April, pp. 40-86

Nottingham, D. (1996), "Joints Grouting in Alaskan Bridges and Dock Decks," Concrete International, V. 18, No. 2, February, pp.45-48

Precast Prestressed Concrete Institute, (2003) "Precast Prestressed Concrete Bridge Design Manual," Chicago, IL., Sections 9.6 and 9.8

Ralls, M. L., et al. (2005), "Prefabricated Bridge Elements and Systems in Japan and Europe," FHWA-PL-05-003, March, 48pp

Russell, H. G., Miller, R. A., Ozyildirim, H. C., and Tadros, M. K. (2006), "Compilation and Evaluation of Results from HPC Bridge Projects, Volume 1: Final Report," Report No. FHWA-HRT-05-056, Federal Highway Administration, October

Russell, H. G. and Ozyildirim, H. C. (2006), "Revising high performance concrete classifications" Concrete International, August, pp.43-49

Scholz, D.P., Wallenfelsz, J. A., Lijeron, C., Roberts-Wollmann, C. L., and Davis, R. T. (2007), "Recommendations for the connection between full-depth precast bridge deck panel systems and precast I-beams", Report No. FHWA/VTRC 07-CR17, June

Stanton, J., and Mattock, A.H. (1986) "Load distribution and connection design for precast stemmed multibeam bridge superstructures" NCHRP Rep. 287

Tepke, D. G. and Tikalsky, P. J. (2007), "Best Engineering Practices Guide for Bridge Deck Durability Report" February 24

Thompson, M.K., et al. (2006) "Behavior and Capacity of Headed Reinforcement" ACI Structure Journal, 103(4), 522-530

Treece, R.A.; Jirsa, J. O., (1987) "Bond Strength of Epoxy-Coated Reinforcing Bars," Reinforced Concrete Research Council-Project 50, PMFSEL Report No. 87-1

Zhu, P. and Ma, Z. (2010a), "Selection of Durable Closure Pour Materials for Accelerated Bridge Construction," ASCE Journal of Bridge Engineering, 15(6)

Appendix A

NCHRP 10-71 Design Guide

ACKNOWLEDGMENTS

Foreword

Strong momentum exists for the growing use of precast elements in bridge construction as a means to speed construction and minimize disruption to traffic and commerce. Precast construction also offers higher quality control compared to on-site concrete casting and can reduce the impact of bridge construction on the environment through the elimination of formwork. Two recent NCHRP projects have focused on the investigation of precast decked systems: NCHRP 12-65 Full-Depth, Precast-Concrete Bridge Deck Panel Systems and NCHRP 12-69 Design and Construction Guidelines for Long-Span Decked Precast, Prestressed Concrete Girder Bridges. NCHRP 12-65 addressed the development of transverse and longitudinal connections between full-depth, precast-concrete bridge deck panels, with emphasis on systems without overlays and without post tensioning through the connection. NCHRP 12-69 addressed I-beam, bulb-tee, or multi-stemmed girders with integral decks cast and prestressed with the girder.

This report contains the design recommendations which have been developed as an outcome of project NCHRP 10-71 Cast-in-Place Reinforced Connections for Precast Deck Systems. The focus of this project has been the development of specifications, guidelines, and examples for the design and construction of durable cast-in-place (CIP) reinforced concrete connections for precast deck systems that emulate monolithic construction. The typical sequence of erecting bridge superstructures in the United States is to erect the precast prestressed concrete or steel beams, place either temporary formwork or stay-in-place formwork such as steel or concrete panels, place deck reinforcement, cast deck concrete, and remove formwork if necessary. This project focused on systems that eliminate the need to place and remove formwork thus accelerating on-site construction and improving safety.

The three systems considered in NCHRP 10-71 to accomplish these objectives were identified during the 2004 Prefabricated Bridge Elements and Systems International Scanning tour (International Scanning Study Team, 2005). The scanning tour visited France, Belgium, Japan, and the Netherlands with eleven participants representing FHWA, State Departments of Transportation, National Association of County Engineers, industry, and academia. The study team developed a series of recommendations related to prefabricated elements and systems to be used for superstructure systems, along with substructure systems and movement systems for rapid replacement and construction. Three of the superstructure systems were identified to be specifically addressed in NCHRP 10-71. These systems included: (1) a precast composite slab-span system (PCSSS) for short to moderate span structures, (2) full depth prefabricated concrete decks, and (3) deck joint closure details (e.g., bulb-tee flange connections) for precast prestressed concrete girder systems for long span structures. Each system uses precast elements that are brought to the construction site ready to be set in place and quickly joined together. Depending on the system, the connections are either transverse (across the width of the bridge) or longitudinal (along the length of the bridge); however, practices differ in detailing the transverse and longitudinal connections.

The design recommendations contained herein are divided into two sections. Section 1 contains the recommendations for precast composite slab-span system (PCSSS) bridges. These recommendations encompass the entire design of the system, as the connections are integral with the performance of the entire composite system. Section 2 contains the recommendations for the longitudinal and transverse

joints of the decked bulb-tee and precast panel systems. This study was focused only on the design of the cast-in-place joints within these systems, rather than the systems themselves. The design recommendations for the systems have been covered elsewhere through recommendations developed in conjunction with NCHRP 12-65 and 12-69 and are not repeated herein. In addition to the detailing requirements for these connections, however, performance requirements were developed for the closure pour materials to be used with these connections, which are included herein.

A-vi

Table of Contents

List of Figures

viii

List of Tables

Section 1: Precast Composite Slab-Span System

1.0   Introduction to Design Recommendations for PCSSS Bridge Systems

This section contains design recommendations to facilitate the adaptation and use of precast composite slab span system (PCSSS) bridges. The Minnesota Department of Transportation (Mn/DOT) developed the initial implementation of PCSSS bridges in the US as an outcome of a *2004 Prefabricated Bridge Elements and Systems International Scanning Tour* (International Scanning Study Team, 2005). The PCSSS, based on the French Poutre Dalle system, is an efficient section for short to moderate span structures. Precast inverted-T panel elements are readily assembled at the construction site and serve as formwork for the cast-in-place concrete which acts compositely with the panels. Transverse reinforcement protruding from the precast webs serves as transverse load distribution reinforcement and also serves as crack control reinforcement in conjunction with a drop-in cage that is placed in the trough over the longitudinal joint between adjacent precast webs.

The recommendations contained herein are based on a comprehensive study that includes information from the field performance of PCSSS bridges and the results of the NCHRP 10-71 study on *Cast-in-Place Concrete Connections for Precast Deck Systems*. The NCHRP study included large-scale laboratory tests on two-span and simple-span PCSSS bridges, as well as, seven subassemblage tests. The two-span and simple-span large-scale bridge specimens provided an opportunity to investigate different cross-sectional details and associated aspects of bridge behavior. These include the effect of flange thickness and type and quantity of transverse joint reinforcement on reflective crack control; horizontal shear transfer reinforcement on composite action; and bursting reinforcement on crack control at release. The seven subassemblages provided an opportunity to investigate variations in crack control reinforcement across the longitudinal joint between the precast flanges.

1.1.   Design Recommendations

The proposed design recommendations for the PCSSS are outlined in the following sections based on the controlling behavior. Significant research effort was concentrated on systems constructed using a 12 in. deep precast inverted T-section panel with cast-in-place (CIP) topping measuring 6 in. deep on top of the precast webs. This composite system provides an efficient design for spans in the range of 20 ft. to 31 ft. While the proposed design recommendations herein are generally applicable to sections of all depths, sample calculations included in this discussion refer to sections constructed with a 12 in. deep precast panel; Figure 1.1.1 shows a cross section of a single 12 in. deep precast member with all relevant dimensions required for calculations contained herein. The maximum span length for efficient application of PCSSS bridges is just over 60 ft.
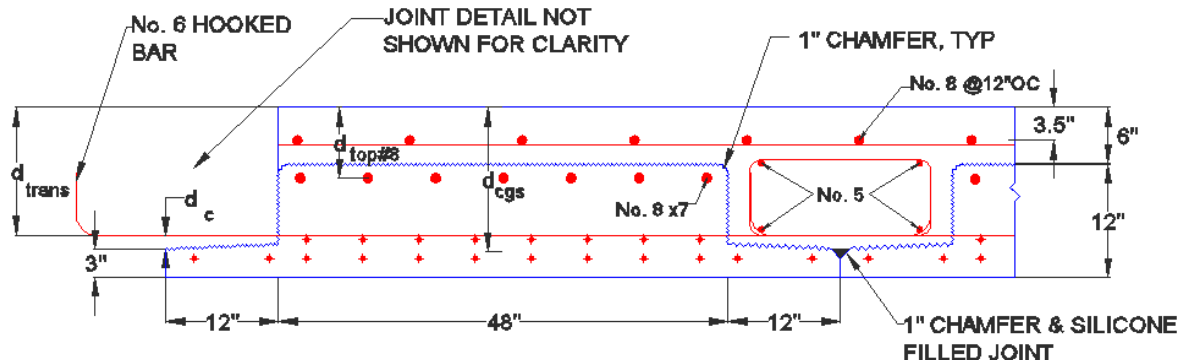
A-1

Figure 1.1.1: Typical 18 in. total depth PCSSS cross section and relevant dimensions

Because of the jointed nature of the precast portion of the PCSSS system created by the discontinuity between flanges of adjacent inverted shallow T-sections, and because the continuity of the PCSSS system is provided by cast-in-place (CIP) concrete, rather than through the use of post-tensioning, it is recognized that cracking will likely be initiated in these systems through restrained shrinkage and environmental effects. Consequently, it is important to recognize the existence of such cracking for all design parameters. An important aspect of the design is the control of such cracking through transverse reinforcement located across the joint region in the trough between adjacent precast web sections. It should be noted that CIP systems, which the PCSSS is intended to emulate, are also expected to develop cracks due to restrained shrinkage and environmental effects, as well as due to load effects. In the case of PCSSS bridges, it may be possible to more readily predict locations where cracking due to restraint is likely to occur and apply reinforcement in those regions to control the cracking.

The following design recommendations consist of both proposed modifications to current specifications, generally defined in the 2010 AASHTO LRFD Bridge Design Specifications (5th Edition), as well as general design and construction practices that should be observed by the designer. Anytime AASHTO (2010) is shown in the text, it is meant to reference the 2010 AASHTO LRFD Bridge Design Specifications, unless otherwise noted. Other specifications used in this document include the 2008 ACI 318 Building Code Requirement for Structural Concrete, which is referenced as ACI 318-08 in the text. In the case of modifications to current AASHTO (2010) specifications, proposed additions and deletions to the specification are shown with underline and strikethrough notation, respectively.

It is proposed that a new definition be added for Precast Composite Slab Span Systems in AASHTO (2010) 5.2 as shown below:

AASHTO (2010) Article **5.2 DEFINITIONS**

> *Post-Tensioning Duct*—A form device used to provide a path for post-tensioning tendons or bars in hardened concrete.
> .
> .
> .
> <u>*Precast Composite Slab Span System*— A type of superstructure in which shallow precast prestressed inverted T-sections are made composite with cast-in-place concrete to form a composite slab bridge. The individual precast prestressed inverted T-sections are considered beam elements until made composite with the cast-in-place concrete and are joined transversely with spliced bars that extend from the precast webs. The spliced bars also provide crack control reinforcement in conjunction with a supplemental cage.</u>
>
> *Precast Members*—Concrete elements cast in a location other than their final position.
> .
> .
> .

1.1.1. Precast Prestressed Inverted-T Design

To better address the design of precast prestressed inverted T-sections incorporated in PCSSS bridges, specifications suggested for modification include AASHTO (2010) Articles 5.14.1.2.2, C5.14.1.2.2, and 5.14.1.2.4

In the initial implementation of PCSSS bridges in the State of Minnesota, the flanges of the precast inverted T-sections were 5.25 in. deep. In the next generation of PCSSS bridges, it was recommended that the flange thickness be decreased to 3 in. for two reasons: (1) to reduce the discontinuity between the adjacent flanges (which acts like a crack between adjacent panels); and (2) to lower the transverse reinforcement that crosses the interface between adjacent panels which better facilitates crack control and the effectiveness of the reinforcement for transverse load transfer. The reduced 3 in. flange depth was deemed to be sufficiently robust for transportation and handling purposes during construction. To investigate the effect of the flange thickness in the NCHRP 10-71 study, the flange thickness was 5.25 in. in one span of the Concept 1 laboratory bridge specimen and 3 in. in the other span as well as in the Concept 2 bridge and the subassemblage specimens.

The flange thickness is measured at the longitudinal joint, while a taper increases the thickness by 1/4 in. at the vertical web. The flange must provide adequate flexural capacity to hold the wet CIP concrete during construction and associated construction loads. A practical upper bound can be investigated with the 22 in. deep precast section with a 6 in. deep CIP deck, the 3 in. thick flange provides sufficient flexural and shear capacity during construction when the compressive strength of the precast concrete at erection is taken to be 6,000 psi. For this reason, it is recommended that the flange thickness provided for the inverted-T precast sections be 3 in. at the joint, and taper to 3 1/4 in. at the precast web.

A-3

A 1 in. 45 degree chamfer shall be included in the top of the flanges at the precast joint, to provide a channel for a silicone caulk to be applied prior to placement of the CIP concrete. The silicone provides an elastic interface between the PC and CIP concrete at the discontinuity created by the precast joint, and seals the joint so wet concrete doesn't leak through the joint. In addition, a 1 in. chamfer shall be included on the top web corners of the PC member, which removes the potential for a sharp, 90 degree corner at that location. Figure 1.1.1 illustrates the chamfer locations.

Two geometric design constraints that should remain fixed for the design of the precast prestressed inverted-T sections, irrespective of the span length, include the thickness of the flange (i.e., 3 in. tapered up to 3 1/4 in.), and the width of the flange (i.e., 12 in.). Changes to the width of the web of the precast inverted-T section may be required depending on the constraints of a specific project. Issues to consider in selecting the web width include hauling and crane limitations in transporting and placing the precast elements, as well as the availability of appropriate formwork from the precast Fabricator. Longer spans (in excess of 31 ft.) would require deeper precast sections and additional prestress. A precast section thinner than 12 in. should be used with caution, as the investigation of thinner sections was not completed during the NCHRP 10-71 study.

To address these issues associated with the design of the precast inverted-T portion of the PCSSS, the following recommendations in AASHTO (2010) should be modified as indicated below.

AASHTO (2010) Article **5.14.1.2 Precast Beams**

5.14.1.2.1 Preservice Conditions

The preservice conditions of prestressed girders for shipping and erection shall be the responsibility of the contractor.

5.14.1.2.2 Extreme Dimensions

The thickness of any part of precast concrete beams shall not be less than:

top flange……………………………………………………………………………2.0 in.
web, non post-tensioned……………………………………………………………5.0 in.
web, post-tensioned…………………………………………………………………6.5 in.
bottom flange, non inverted-T……………………………………………………..5.0 in.
bottom flange, inverted-T for precast composite slab-span system………3.0 in.

The width of the bottom flange extension of precast concrete inverted-T beams used for precast composite slab-span systems shall be 12.0 in., unless it can be shown that the distance between webs in the precast composite slab-span system is sufficient to accommodate the development of the spliced transverse reinforcement, the supplemental cage for crack control, and the spacing of the bottom longitudinal bars in

A-4

the case of continuous span systems that require reinforcement for positive restraint moment.

The maximum dimensions and weight of precast members manufactured at an offsite casting yard shall conform to local hauling restrictions.

C5.14.1.2.2

The 2.0-in. minimum dimension relates to bulb-T and double-T types of girders on which cast-in-place decks are used. The 5.0-in and 6.5-in. web thicknesses have been successfully used by contractors experienced in working to close tolerances. The 5.0-in. limit for bottom flange thickness normally relates to box-type sections, while the 3.0-in. limit for bottom flange thickness specifically relates to inverted-T type sections with 12.0-in. wide flange extensions for use in precast composite slab-span systems. It is suggested that the bottom flange be tapered from 3.0-in. at the joint to 3.25-in. at the vertical web face of the precast member for precast concrete inverted-T beams used for precast composite slab-span systems to facilitate form removal.

The width of the bottom flange for inverted-T type sections is specified at 12.0-in. to ensure (1) adequate development of the transverse reinforcement spliced in the longitudinal closure joint, (2) adequate space to accommodate cage for supplemental crack control reinforcement, and (3) adequate spacing to accommodate longitudinal reinforcement located in single layer in bottom of cage to provide resistance to positive restraint moments in continuous systems where necessary. Increases in the bottom flange width are not recommended, because the minimum thickness of 3.0-in. of the bottom flange may not be adequate to resist construction loads when the flange is wider than 12.0-in. Increasing the thickness of the bottom flange of inverted-T type sections is not recommended as close proximity of the transverse reinforcement to the bottom of the section is preferred.

…

Total structure depth for the PCSSS shall conform to Article 2.5.2.6.3 of the AASHTO (2010) specification without modification, which provides minimum section depths for serviceability requirements. The PCSSS shall be considered a prestressed concrete slab superstructure, as specified in Table 2.5.2.6.3-1 of the specification. As given by AASHTO (2010), for precast concrete slab superstructures, the minimum depths, including the deck, are $0.030L$ and $0.027L$ for simple and continuous spans, respectively. Furthermore, both equations are capped at 6.5 in. and the span length, L, and resulting section depth are both in units of ft. For a simple span, the required minimum section depth for a 31 ft. and 65 ft. span would be 11.2 in. and 23.4 in., respectively, which are smaller than the required section dimensions for strength.

A-5

Furthermore, the designer should specify a smooth flange surface. As observed in the second control subassemblage specimen, the smooth flange performed better than many of the other specimens. The smoothness of the flange may help to distribute the transverse loads more uniformly over the width of the longitudinal closure joint. The smooth flange also facilitates the removal of formwork for the precast Fabricator.

The reinforcement provided for confinement of the tendons shall conform to AASHTO (2010) Article 5.10.10.2 as written.

The design of the bearing and connection details at both the end and continuous supports for the PCSSS was motivated by three primary characteristics. First, the PCSSS should be designed such that even and uniform bearing across the full width of the precast inverted-T panel is achieved at the ends of the members, ideally through an elastomeric bearing pad as defined by *AASHTO 2009 Interim LRFD Bridge Construction Specifications Article 18.2* and of sufficient dimension to support the factored loads. The bearing pad should extend across the full width of the PCSSS bridge system, less 6 in. to provide a drip setback. Second, a method for relieving restrained shrinkage at the supports should be considered, such as through the use of a bond breaker between the pier cap and CIP closure pour. Finally, a means of transferring the compression force effectively between adjacent spans at a continuous support should be considered. During the current study, a 10 in. flange blockout was utilized near the continuous support to facilitate the development of negative moment at the pier by providing integral CIP concrete within the compression zone of the beam in the joint regions. The 10 in. flange blockout is illustrated in a plan and cross-sectional view of a continuous pier in Figures 1.1.2 and 1.1.3, respectively. The bearing pads are shown in Figure 1.1.2 with diamond hatching, and are not included below the 24 in. trough region, thereby allowing the CIP concrete to be placed directly against the pier cap in these locations, though a bond breaker, when utilized, would separate the interface between the pier cap and CIP concrete.
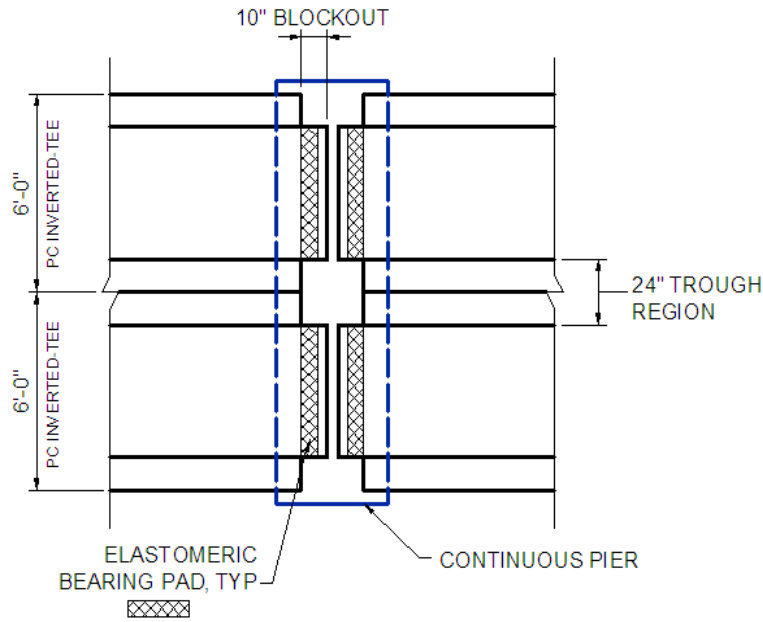
Figure 1.1.2: Plan view of a PCSSS flange blockout at a continuous pier to facilitate the development of negative moment at the pier

A cross-sectional view of the PCSSS and support at a continuous pier is shown in Figure 1.1.3. As in the previous figure, the bearing pad material is shown with a diamond hatching. Also shown is a polystyrene foam in the regions between the precast inverted-T members and the pier, which provided containment for the CIP concrete during the closure pour, but was relatively crushable and was therefore not expected to significantly affect the location of center of bearing.

A-7
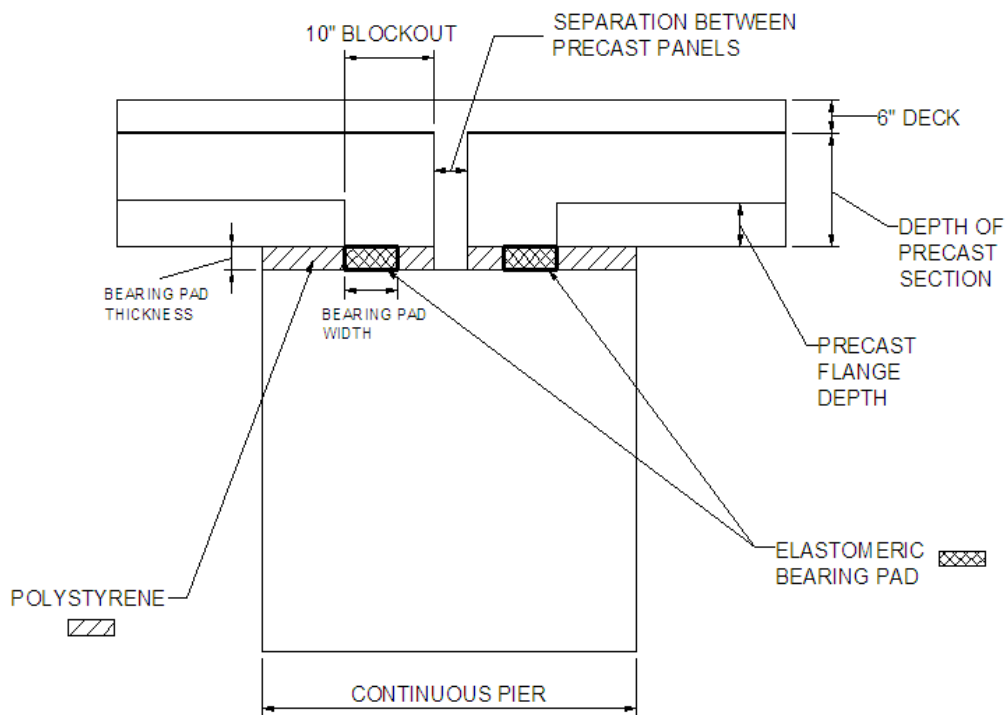
Figure 1.1.3: Cross-sectional view of a PCSSS and support at a continuous pier illustrating the 10 in. flange blockout and general bearing details

Vertical dowels shall be installed in the pier cap and embedded in the CIP closure pour to provide a positive connection between the superstructure and substructure. The ideal location of the vertical dowels is such that they lie in a line along the length of the pier cap that bisects the area created between the ends of longitudinally adjacent precast panels at a continuous pier. Where there is insufficient clearance between adjacent precast panels for the installation of the vertical reinforcement, the dowels may be placed in the area created by the flange blockouts in the trough area between inverted-T members. A review of the PCSSS construction documents utilized in the construction of Mn/DOT Bridge 13004 in Center City, Minnesota revealed that the vertical dowels consisted of No. 5 bars at 12 in. on center, although an equal area of reinforcement grouped in the blockout locations was expected to be a satisfactory alternative where there was insufficient clearance between the ends of the precast members. It is recommended that the dowels be stainless steel for durability, and that they be wrapped (e.g., with ½ in. pipe insulation) above the pier or abutment cap to reduce the amount of restrained shrinkage in the transverse direction.

To address these issues associated with the bearing detail under the precast beam at the abutment and pier of the PCSSS, the following recommendations in AASHTO (2010) should be modified as indicated below.

A-8

AASHTO (2010) Article *5.14.1.2.4 Detail Design*

All details of reinforcement, connections, bearing seats, inserts, or anchors for diaphragms, concrete cover, openings, and fabrication and erection tolerances shall be shown in the contract documents. For any details left to the Contractor's choice, such as prestressing materials or methods, the submittal and review of working drawings shall be required.

For precast composite slab span construction, continuous bearing shall consist of an elastomeric bearing device of sufficient dimension to support the factored loads.

The effects of restrained shrinkage in the transverse direction on the CIP closure pour shall be considered, and where feasible, a means of relieving restrained shrinkage at the supports shall be employed.

At continuous supports of precast composite slab span bridge construction, a means of facilitating the development of negative moment at the pier by providing integral CIP concrete within the compression zone of the beam in the joint region shall be provided.

Vertical dowels, or equivalent, shall be installed in the pier cap and embedded within the CIP closure pour to provide a positive connection between the superstructure and substructure, and where surface cracking near the continuous piers it to be expected, the dowel reinforcement shall be fabricated from a corrosion resistant material.

C5.14.1.2.4

AASHTO LRFD Bridge Construction Specifications include general requirements pertaining to the preparation and review of working drawings, but the contract documents should specifically indicate when they are required.

Article 18.2 of the *AASHTO 2009 Interim LRFD Bridge Construction Specifications* provides information relevant to the properties of the elastomeric bearing pad.

Restrained shrinkage caused by restraint at the supports may increase the transverse tensile stresses near the precast joint region and subsequently promote or advance reflective cracking. A bond breaker (i.e., plastic sheet) provided between the pier cap and CIP closure pour may reduce the restrained shrinkage near the joint region. The application of foam pipe insulation to vertical dowels emanating from the pier cap and embedded in the CIP concrete is expected to reduce the effects of restrained shrinkage due to the dowel reinforcement and should also be considered.

A flange block out at the end of precast composite slab span members at continuous piers offers a means of providing contiguous CIP concrete in the joint region to facilitate the compressive reaction in the negative moment region of a PCSSS bridge. Research and current design methodology suggest that a 10 in. blockout, measured from the end of the beam was sufficient to accommodate the development of negative

A-9

> moment at the continuous pier. The blockout shall be incorporated into the precast
> member during fabrication, and not by means of cutting after fabrication of the
> members.

1.1.2. Bursting, Splitting and Spalling Forces

An evaluation of the end zone forces in the prestressed inverted T-section was completed by Eriksson (2008) which resulted in suggested modifications to AASHTO (2010) Article 5.10.10.1.

For years, the AASHTO specification included requirements for reinforcement to control "bursting" at the ends of prestressed beams due to the effects of the transfer of prestress from the reinforcement into the concrete. The original specifications were developed to control "spalling" stresses in I-girders, and were mislabeled in the code as "bursting" stresses. The guidelines required the placement of large amounts of vertical reinforcement within a distance of $h/4$ from the end of the member, where h is the depth of the member. The shallow section depths of inverted-T precast beams result in limited area for the placement of vertical reinforcement, which leads to significant congestion.

Experimental and numerical studies were completed to investigate the effects of spalling and bursting on the inverted-T sections used in PCSSS. The experimental tests on 12 in. deep inverted T-sections used indicated that the concrete had sufficient strength to resist tensile stresses induced in the transfer zone at release regardless of the reinforcement provided, suggesting that vertical reinforcement was not required in the end zones of those specimens.

Furthermore, numerical studies conducted as part of the investigation supported that certain inverted-T members did not require spalling or bursting reinforcement, specifically those with member depths less than 22 in. and which satisfied the expectation that the concrete tensile strength was larger than the stress developed due to the transfer of prestress. Through the numerical studies, vertical reinforcement was found to be required to control the spalling stresses in deeper sections. The requirement for the vertical reinforcement to be provided within $h/4$ from the end of the member (where h is the depth of the member) was determined to be the most critical region for the reinforcement to be located.

In the current AASHTO (2010) provisions, the term "bursting" has been replaced with "splitting," although the correct terminology that should be used is "spalling." Bursting and splitting stresses occur along the transfer length of the strand, whereas spalling stresses tend to occur at the end of the member. Although not specifically addressed in AASHTO, the confinement requirements of AASHTO (2010) 5.10.10.2 should help control the bursting and splitting stresses that develop in the transfer length region.

AASHTO (2010) Article **5.10.10 Pretensioned Anchorage Zones**

5.10.10.1 ~~Splitting~~ Spalling Resistance

For all sections other than rectangular slabs and shallow inverted-T sections with heights less than 22 in, the ~~splitting~~ spalling resistance of pretensioned anchorage zones provided by reinforcement in the ends of pretensioned beams shall be taken as:

$$P_r = f_s A_s \qquad (5.10.10.1\text{-}1)$$

where:

f_s = stress in steel not to exceed 20 ksi

A_s = total area of reinforcement located within the distance h/4 from the end of the beam (in.^{2})

h = overall dimension of precast member in the direction in which ~~splitting~~ spalling resistance is being evaluated (in.)

The resistance shall not be less than four percent of the total prestressing force at transfer.

For pretensioned I-girders or bulb tees, …

.
.
.

… from the end of each web.

In pretensioned anchorage zones of rectangular slabs and shallow inverted-T sections with heights less than 22 in., vertical reinforcement in the end zones is not required if:

$$\sigma_s < f_r \qquad (5.10.10.1\text{-}2)$$

where:

$$\sigma_s = \frac{P}{A}\left(0.1206\,\frac{e^2}{h\,d_b} - 0.0256\right) \geq 0$$

$$f_r = 0.23\,\sqrt{f_{ci}'}$$

σ_s = maximum spalling stress on the end face (ksi)

f_r = direct tensile strength as defined by Article C5.4.2.7 (ksi)

P = prestressing force at transfer (kip)

A = gross cross-sectional area of concrete (in.^{2})

e = strand eccentricity (in.)

h = overall depth of precast member (in.)

d_b = prestressing strand diameter (in.)

f_{ci}' = concrete compressive strength at transfer (ksi)

Where end zone vertical reinforcement is required, it shall be located within the horizontal distance h/4 from the end of the beam, and shall be determined as:

$$A_S = \frac{P\left(0.02\frac{e^2}{h\,d_b} - 0.01\right)}{f_s} \qquad \text{(5.10.10.1-3)}$$

_____

where:

A_s = total area of reinforcement located within the distance h/4 from the end of the beam (in.^{2})

The resistance shall not be less than four percent of the total prestressing force at transfer.

In all cases, t~~T~~he reinforcement shall be as close to the end of the beam as practicable.

Reinforcement used to satisfy this requirement can also be used to satisfy other design requirements.

C5.10.10.1

The primary purpose of the choice of the 20-ksi steel stress limit for this provision is crack control.

Spalling ~~Splitting~~ resistance is of prime importance in relatively thin portions of pretensioned members that are tall or wide, such as the webs of I-girders and the webs and flanges of box and tub girders. ~~Prestressing steel that is well distributed in such portions will reduce the splitting forces, while steel that is banded or concentrated at both ends of a member will require increased splitting resistance.~~
For pretensioned slab members with well-distributed prestressing steel across the width of the member, tensile zones can form in the vertical direction of the member due to strand eccentricity.

Numerical studies (*French et al. 2011*) indicate that in shallow precast inverted-T sections (no greater than 22 in. deep), the concrete tensile strength is able to resist the spalling stresses due to the small eccentricities. For deeper sections, with larger strand eccentricities, the numerical studies indicate that reinforcement is required to resist the larger spalling stresses. ~~the width of the member is greater than the depth. A tensile zone is then formed in the horizontal direction perpendicular to the centerline member.~~

For tub and box girders, prestressing strands are located in both the bottom flange and webs. Tensile zones are then formed in both the vertical and horizontal directions in the webs and flanges. Reinforcement is required in both directions to resist ~~the~~ spalling and splitting forces, respectively. Prestressing steel that is well distributed in such portions will reduce the splitting forces, while steel that is banded or concentrated at both ends of a member will require increased splitting resistance.

Experience has shown that the provisions of this article generally control cracking in the end regions of pretensioned members satisfactorily; however, more reinforcement than required by this Article may be necessary under certain conditions. Figures C5.10.10.1-1 and C5.10.10.1-2 show examples of spalling and splitting reinforcement for tub girders and voided slabs.

Changes should be made to the labeling in Figures C5.10.10.1-1 and C5.10.10.1-2 to denote reinforcement which is providing spalling resistance and reinforcement which is providing splitting resistance. Note that the tensile stresses due to bursting/splitting occur along the transfer length region and thus the location of the reinforcement to handle these stresses may need to be distributed differently from that used to resist spalling stresses.

1.1.3. Restraint Moment

Specifications suggested for modification to address restraint moment issues for continuous PCSSS bridges include AASHTO (2010) Article 5.14.1.4.2, 5.14.1.4.4

Restraint moments can be generated in continuous composite systems due to differential time-dependent effects (i.e., creep and shrinkage) between the precast and CIP topping and thermal gradient effects through the cross section due to solar radiation. The effects of both positive and negative restraint moments must be considered for the PCSSS. When CIP is cast on a precast element that is relatively old (i.e., may have been stored in a precasting yard for several months before being placed), much of the creep and shrinkage of the precast element will have occurred prior to casting the CIP topping. In this case, negative restraint moments would be expected to result due to the shrinkage of the CIP placed on the seasoned precast element. Negative restraint moments will cause cracking at the top of the section at the pier, and can therefore be controlled through longitudinal reinforcement near the top of the member which is generally supplied by the deck, and possibly supplemental, reinforcement. When the CIP is cast on a young element, the shrinkage of the CIP and precast may be

A-13

expected to be relatively similar; however, the precast section will undergo shortening due to creep effects that generally result in positive restraint moments. Cracking due to positive restraint moment will occur near the bottom of the section at the pier. The reinforcement provided to resist positive restraint moment in the PCSSS must be provided in the trough area between precast panels, which limits the available area and disbursement (i.e., the reinforcement must be grouped in the troughs and not be spread out over the width of the system) of reinforcement to resist positive restraint moments.

Significant research was completed by Smith et al. (2008) and Eriksson (2008) on the restraint moment effects for continuous precast composite slab span systems. Smith et al. (2008) monitored the restraint moment in the Concept 1 laboratory bridge for a period of 250 days after continuity was made by determining the reactions measured with load cells at the outside piers of the specimen. In addition, Smith monitored one of the initial implementations of the PCSSS in Minnesota, the Center City Bridge, which was instrumented by Mn/DOT to investigate load distribution and the potential development of reflective cracking. Gages located at the pier indicated that cracking initiated due to the effects of positive restraint moment. The crack was observed to occur as the bridge underwent its first large thermal gradient effects due to solar radiation in the spring. As a consequence, it was suspected that the behavior was driven by thermal gradients in the bridge superstructure where the solar radiation heated the top of the bridge. This caused the individual spans of the bridge to camber which generated positive restraint moments. Eriksson (2008, pp. 56) stated, "Because [the] time-dependent effects on [the day the crack was observed] should not have varied significantly from the previous day, researchers speculated thermal effects may have played a role in the crack development. Based on this conjecture, both time-dependent and thermal gradient effects on restraint moment were investigated analytically." Eriksson (2008) completed a parametric study to investigate the effects of differential shrinkage, creep, and thermal gradient effects on the development of restraint moments.

In an effort to predict the restraint moment in a section based on the time-dependent properties of the system, Eriksson completed a numerical parametric study using Pbeam, which is a fiber-based finite element code developed by Suttikan at the University of Texas in 1978 (Suttikan, 1978). The program allows for inputs including material strength, age, creep, shrinkage, steel relaxation, dead loads and support conditions. The program provides output in the form of stresses, strains, reactions and deformations at user specified time intervals (Suttikan 1978). Furthermore, Eriksson utilized a modified version of Pbeam created by Le (1998), called TPbeam, which incorporates thermal gradient in the analysis. After finding that, when using functions based on measured quantities for the input values (i.e., creep, shrinkage, concrete strength gain with age, etc.), Pbeam predicted restraint moments that corresponded reasonably well with the measured results from the Concept 1 laboratory specimen, Eriksson utilized both Pbeam and TPbeam to conduct a parametric study to determine reasonable bounds for expected restraint moments in PCSSS bridges. In general, the purpose of the parametric study was to predict the maximum positive and negative restraint moments that would be expected in PCSSS bridges. Precast strengths of 6 ksi and 12.9 ksi were used with assumed continuity dates of 7, 28, 60, and 90 days to develop an expected envelope of the positive and negative restraint moments.

Because of the difficulty in providing reinforcement for positive restraint moment due to the geometry of the PCSSS, the necessity to design for such moments was of interest. Eriksson found that, "positive restraint moment cracking due to time-dependent effects is not expected [for PCSSS] for spans between

20 and 50 ft." This conclusion was based on a finite element study that considered only time-dependent effects. It should be noted in design that AASHTO (2010) 5.14.1.4.5 requires that the stress at the bottom of the diaphragm be compressive in order to take advantage of full continuity, considering all load effects. The check is made assuming that the concrete section cannot carry any tension (i.e., section may already be cracked at the pier due to positive moment).

Eriksson found that positive restraint moment generally induced at the pier was due to creep of the precast member, therefore increasing the age of the precast member at continuity will reduce the positive restraint moment due to time-dependent effects in the section. The thermal gradient due to solar radiation has the same effect as placing CIP on a young precast section. Eriksson (2008) found that the positive restraint moments caused by thermal effects induced restraint moments that were two to seven times larger than the positive restraint moments caused by time-dependent effects. As a consequence, positive restraint moment cracking due to thermal gradient effects was expected to occur in nearly all of the designs studied.

Based on the findings by Eriksson (2008), it is important to consider the effects of thermal gradient in the positive restraint moment design for continuous PCSSS bridges. Because the use of Pbeam or TPbeam by bridge designers would be impractical, an analytical method is described below which should be applied to calculate the restraint moment caused by a temperature gradient as defined by AASHTO LRFD (2010) Article 3.12.3. The total restraint moment at a given pier should be calculated as the sum of restraint moments generated by a thermal gradient and time-dependent effects.

AASHTO (2010) Article 3.12.3 provides general guidelines for design of thermal gradients based on regional zones, but indicates temperature gradient should be evaluated on a project specific basis. Judgment is reserved for experienced designers indicating thermal gradient can be neglected if previous structures have not experienced distress. These basic guidelines provide little guidance regarding when thermal gradients are important. Based on the fiber-based finite element model results from Pbeam and TPbeam and the suspected positive moment crack in the Center City Bridge, thermal effects have a significant effect on the development of positive restraint moments and should be considered in the restraint moment design.

Restraint moment design for time-dependent properties is complicated by the need to investigate the interaction of the variation in time-dependent effects over time. The PCA and P-method both provide options for how to design for restraint moments due to time-dependent effects. However, design for restraint moments caused by thermal effects does not include the time variation and should be summed with restraint moments due to time-dependent effects.

Barker and Puckett (2007) provide a hand calculation for determining the restraint moment due to the thermal effects. Assuming the beam is a simple span between supports, apply the design thermal gradient to the section and calculate the resulting curvature in the beam. The curvature from a temperature gradient can be expressed as

$$\varphi = \frac{\alpha}{I} \int T(y) \cdot y \cdot dA \qquad (1.1.1)$$

where α is the coefficient of thermal expansion, $T(y)$ is the temperature gradient (°F) through the depth y of the member (in.), and I is the moment of inertia of the entire cross section (in.[4]) (Barker and Puckett, 2007) This equation is also found in AASHTO (2010) Article C4.6.6.

The end rotation (θ) can be found by integrating the curvature over half the length of the span. Then, the restraint moment, or the moment restraining the rotation, can be found using the three-moment equation. The equation assumes pinned end supports and is expressed as

$$M = 3 \cdot \theta \cdot \frac{E \cdot I}{L} \tag{1.1.2}$$

where θ is the rotation, E is the elastic modulus (for the composite system), and L is the span length.

The moment, M, is the restraint moment at the pier of a continuous system to resist the rotations induced by the thermal gradient. If the span lengths on each side of the pier are not equal, then the different spans will induce different moments at the pier (i.e., the rotation would be different, leading to different moments). To use this analysis method, continuity of slope at the pier is necessary. The restraint moments induced by thermal gradients in each span can be calculated using Equation (1.1.2) and the design should be for the largest restraint moment. The effects of thermal gradients and time-dependent effects can be calculated independently and then combined with the appropriate load factors.

Using the above methodology for prediction of the thermally induced restraint moments in the 20 ft. and 50 ft. span beams in the parametric study conducted by Eriksson (2008) provided conservative results as compared to the TPbeam results. The hand calculations overpredicted the calculated positive restraint moment by a range of 20 to 40 percent. The calculations agreed with TPbeam results that the highest ratio of positive restraint moment induced by a thermal gradient to the cracking moment (i.e., 2.9) was for the 20 ft. span with 12.9 ksi concrete. The shorter span with greater strength had the greatest stiffness and the least flexibility of the sections studied. Consequently, the 50 ft. span with 6 ksi concrete, the most flexible section studied had the lowest ratio of positive restraint moment induced by thermal gradient to cracking moment (i.e., 0.95).

If the above design method provides undesirable results, there are a few other options to decrease the positive restraint moment effects. By decreasing time-dependent effects, the combination of thermal effects and time dependent effects would be reduced. Increasing the specified concrete compressive strength of the precast member would increase the stiffness and decrease the creep in the member, which would decrease the positive restraint moments. Providing 90-day girder age at continuity would decrease the time-dependent effects of the positive restraint moment and eliminate the need for calculation of positive restraint moment due to time-dependent effects based on AASHTO (2010) Article 5.14.1.4.4.

For all cases of PCSSS design, the effectiveness of the continuity connection at the pier must be checked according to AASHTO 5.14.1.4.5. This continuity check requires that the sum of all post-continuity dead loads, restraint moments, half live load, and half thermal gradient, result in net compression at the bottom of the diaphragm. It is recommended that the live load stress used in this check be the stress at the pier associated with the maximum positive moment on the live load envelope. If the continuity check is not satisfied, the system is not fully effective and partial continuity must be considered.

If the above methods do not provide a reasonable design, then the benefits from continuity should be neglected in design and the system should be designed as a series of simple spans. The design of the PCSSS as a simple span while still providing reinforcing steel in the trough region over the pier would not be conservative. The positive moment reinforcement over the pier would generate restraint effects that must be considered in design.

AASHTO (2010) Article 5.14.1.4.2 provides guidance in the design of restraint moments for bridges composed of simple span precast girders made continuous. In addition to changes in association with the code and commentary of 5.14.1.4.2, a change is proposed to the commentary of 5.14.1.4.1

AASHTO (2010) *C5.14.1.4.1 General*

.

.

.

Positive moment connections improve the structural integrity of a bridge, increasing its ability to resist extreme event and unanticipated loadings. These connections also control cracking that may occur in the continuity diaphragm. Therefore, it is recommended that positive moment connections be provided in all bridges detailed as continuous for live load. If such reinforcement is provided, the effect of positive restraint moments that may be generated should not be neglected.

AASHTO (2010) Article *5.14.1.4.2 Restraint Moments*

The bridge shall be designed for restraint moments that may develop because of time-dependent, thermal gradient, or other deformations, except as allowed in Article 5.14.1.4.4.

Restraint moments shall not be included in any combination when the effect of the restraint moment is to reduce the total moment.

For precast composite slab span construction made continuous, reinforcement provided for positive restraint moment must be included in the longitudinal trough region across the pier.

AASHTO (2010) Article *5.14.1.4.4 Age of Girder When Continuity Is Established*

The minimum age of the precast girder when continuity is established should be specified in the contract documents. This age shall be used for calculating restraint moments due to creep and shrinkage. If no age is specified, a reasonable, but conservative estimate of the time continuity is established shall be used for all calculations of restraint moments.

A-17

The following simplification may be applied if acceptable to the Owner and if the contract documents require a minimum girder age of at least 90 days when continuity is established:

- Positive restraint moments caused by girder creep and shrinkage and deck slab shrinkage may be taken to be zero.

- Computation of <u>time-dependent</u> restraint moments shall not be required.

- <u>Positive restraint moments caused by thermal gradients must be taken into consideration for PCSSS bridges made continuous.</u>

- A positive moment connection shall be provided with a factored resistance, φMn, ~~not less than 1.2 M_{cr},~~ as specified in Article 5.14.1.4.9. <u>For all systems with the exception of PCSSS, the factored resistance, φMn, shall not be not less than 1.2 M_{cr}.</u>

For other ages at continuity, the age-related design parameters should be determined from the literature, approved by the Owner, and documented in the contract documents.

C5.14.1.4.4

.

.

.

Even if the girders are 90 days old or older when continuity is established, some positive moment may develop at the connection and some cracking may occur. Research (Miller, et al. 2004) has shown that if the connection is designed with a capacity of 1.2 M_{cr}, the connection can tolerate this cracking without appreciable loss of continuity.

<u>For PCSSS bridges, research has shown (French, et al. 2011) that positive restraint moments caused by thermal gradients are more significant than those due to time-dependent effects, and should not be ignored. Because the continuity in PCSSS bridges is achieved by continuous reinforcement over the piers in the trough region, it is not practical to fit sufficient reinforcement in that region to achieve 1.2 Mcr.</u>

This provision provides a simplified approach to design of precast girder bridges made continuous that eliminates the need to evaluate restraint moments <u>due to time-dependent effects</u>. Some states allow design methods where restraint moments are...

.

.

.

A-18

1.1.4. Live Load Distribution Factors and Skew Effects

The applicability of the current live load distribution factors, specifically those designated for cast-in-place slab span bridges, to the PCSSS was investigated during the NCHRP 10-71 study. Numerical modeling was combined with observations from a live load truck test on the Center City Bridge along with load distribution tests on the laboratory bridge specimens.

Numerical models were run to investigate the effect of potential discontinuities generated in PCSSS bridges due to the development of precast-CIP interface separation or reflective cracks on live load distribution relative to the live load distribution obtained for monolithic slab-span systems for single tandem and double tandem loading cases. In the case of the double tandem loading, the load scenario was an extreme case, where a double wheel patch load was placed over the joint (i.e., tandems were assumed to be spaced much closer together than physically constitutes two 12ft. lanes of loading.

The PCSSS cases investigated included CIP bonded only to the sides and top of the panel webs (i.e., the CIP was left unbonded from the panel flanges) to simulate the separation of the flanges from the CIP above the longitudinal joints. In addition, runs were conducted to investigate the effect of the discontinuity along the longitudinal joint between the precast flanges, with the CIP assumed to be bonded to the top of the flanges. A model was also run to investigate the effect of a potential reflective crack that extended to approximately the elastic neutral axis depth of the section in transverse bending (i.e., 3 in. below the top surface of the CIP in an 18 in. deep PCSSS).

Although the curvatures obtained for the PCSSS models were larger than those obtained for the corresponding CIP slab-span models, the design curvatures predicted using AASHTO LRFD (2010) exceeded those obtained from the finite element models for all cases. The numerical models illustrated that even in the case of the PCSSS with a reflective crack assumed to extend to within 3 in. of the extreme compression fiber and tandem load greater than could be physically applied to the lane, the longitudinal curvatures were only 84 percent of the longitudinal curvatures predicted using the AASHTO LRFD (2010) load distribution factors for monolithic concrete slab-span bridges. This suggests that the live load distribution factors for PCSSS type superstructures could reasonably and conservatively be designed using the current live load distribution factors for monolithic slab span bridges.

Furthermore, the live load truck tests on the Center City Bridge suggested that the measured longitudinal curvatures were approximately three times less than those calculated using the monolithic slab span equations. Additionally, the measured longitudinal curvatures were consistently conservative when compared to monolithic slab span FEM models.

Because the numerical study and laboratory results consistently suggested that the PCSSS could be conservatively designed as a solid slab-span bridge system, as specified in AASHTO (2010) Article 4.6.2.3., it is recommended that the PCSSS be designed according to the slab-span effective lane width provisions for determination of the longitudinal design moments.

Numerical modeling was also utilized to investigate the effects of skew on PCSSS bridges through a simply-supported bridge model with skewed supports ranging from 0 to 45 degrees. The primary behavior under investigation was the maximum horizontal shear induced above the precast joint. Three load cases were considered with patch loads centered along the outside panel: midspan, quarter span near acute angle, quarter span near obtuse angle. The longitudinal stress measured in the jointed and monolithic models remained relatively constant through the range of skew angles considered. For lower angles or no skew, the load at the obtuse quarter span controlled among the tested load cases, while for larger skew angles, the midspan load case controlled. Differences between the results for the PCSSS and monolithic CIP case were subtle. At no skew, the horizontal shear stress in the precast joint model was slightly higher than that of the monolithic section, likely due to the reduction in sectional area to carry the shear; while at higher skews, the monolithic model horizontal shear stress was higher than that of the PCSSS, possibly due to better load transfer across the longitudinal joint of the monolithic system.

The small variation and consistency between the models considering a 3 in. joint between the flanges in the PCSSS and a monolithic structure suggest that the effect of the precast joint in PCSSS construction was not expected to significantly affect the performance of the system in skewed applications. The design of skewed PCSSS bridges may be completed assuming a monolithic slab-span system in accordance with AASHTO LRFD (2010), where the longitudinal force effects for slab-span bridges can be reduced by a factor of *r* given a skew angle θ by Eq. 4.6.2.3-3. This relationship has been shown to perform well for monolithic slab-span systems.

Because the precast joint detail of the PCSSS does not significantly change the load transfer across the width of the bridge, it is recommended that the AASHTO LRFD (2010) skew design for slab-span systems be applied to PCSSS.

AASHTO (2010) Article **4.6.2.3 Equivalent Strip Widths for Slab Type Bridges**

This Article shall be applied to the types of cross sections shown schematically in Table 1. For the purpose of this Article, cast-in-place voided slab and precast composite slab-span system (PCSSS) bridges may be considered as slab bridges.

The equivalent width of longitudinal strips per lane for both shear and moment with one lane, i.e., two lines of wheels, loaded may be determined as:

$$E = 10.0 + 5.0\sqrt{L_1 W_1} \qquad\qquad (4.6.2.3\text{-}1)$$

The equivalent width of longitudinal strips per lane for both shear and moment with more than one lane loaded may be determined as:

$$E = 84.0\,0 + 1.44\sqrt{L_1 W_1} \le \frac{12.0W}{N_L} \qquad\qquad (4.6.2.3\text{-}2)$$

where:

E = equivalent width (in.)

L_1 = modified span length taken equal to the lesser of the actual span length or 60.0 (ft.)

A-20

W_1 = modified edge-to-edge width of bridge taken to be equal to the lesser of the actual width or 60.0 for multilane loading, or 30.0 for single-lane loading (ft.)

W = physical edge-to-edge width of bridge (ft.)

N_L = number of design lanes as specified in Article 3.6.1.1.1

For skewed bridges, the longitudinal force effects may be reduced by the factor r:

$$r = 1.05 - 0.25\tan\theta \leq 1.00 \qquad\qquad\qquad (4.6.2.3\text{-}3)$$

where:

θ = skew angle (degrees)

1.1.5. Transverse Load Distribution

To address transverse load distribution requirements for PCSSS bridges, suggested specification modifications include AASHTO (2010) Article 5.14.4.3.3e.

To emulate the satisfactory performance of CIP slab-span systems, precast composite slab-span systems require load transfer between adjacent precast panels. The nature of the design of the precast system, specifically the presence of the discontinuity produced at the flange interfaces, creates a longitudinal joint between panels and requires that adequate transverse load transfer be provided across the joint. The effectiveness of the transverse reinforcement is improved if the flange thickness of the precast sections is minimized. This enables the transverse reinforcement to be placed lower within the cross section increasing its effective depth.

In the case of transverse load distribution, as well as crack control, it is prudent to define the reinforcement ratio based on the amount of concrete near the transverse load distribution reinforcement. In the NCHRP 10-71 study, the depth of concrete considered in the definition of the transverse load distribution reinforcement ratio included the CIP concrete between the top of the precast flanges and the top of the deck. In the case of the 12 in. deep precast section, the depth considered was 15 in. (i.e., 12 in. deep precast section + 6 in. thick deck - 3 in. flange thickness). The total area of reinforcement used in the reinforcement ratio determination should include only the transverse reinforcement terminating in 90^0 hooks that extend through the precast webs and lap with companion hooked bars protruding from the adjacent precast webs. This lapped reinforcement provides continuity across the longitudinal joints. A single bar should be used in the transverse load distribution reinforcement calculation because the lapped bars must transfer load to each other between the adjacent panels. The reinforcement and depth of concrete considered in the calculation of the reinforcement ratio for load transfer per unit length is highlighted in yellow in Figure 1.1.2.
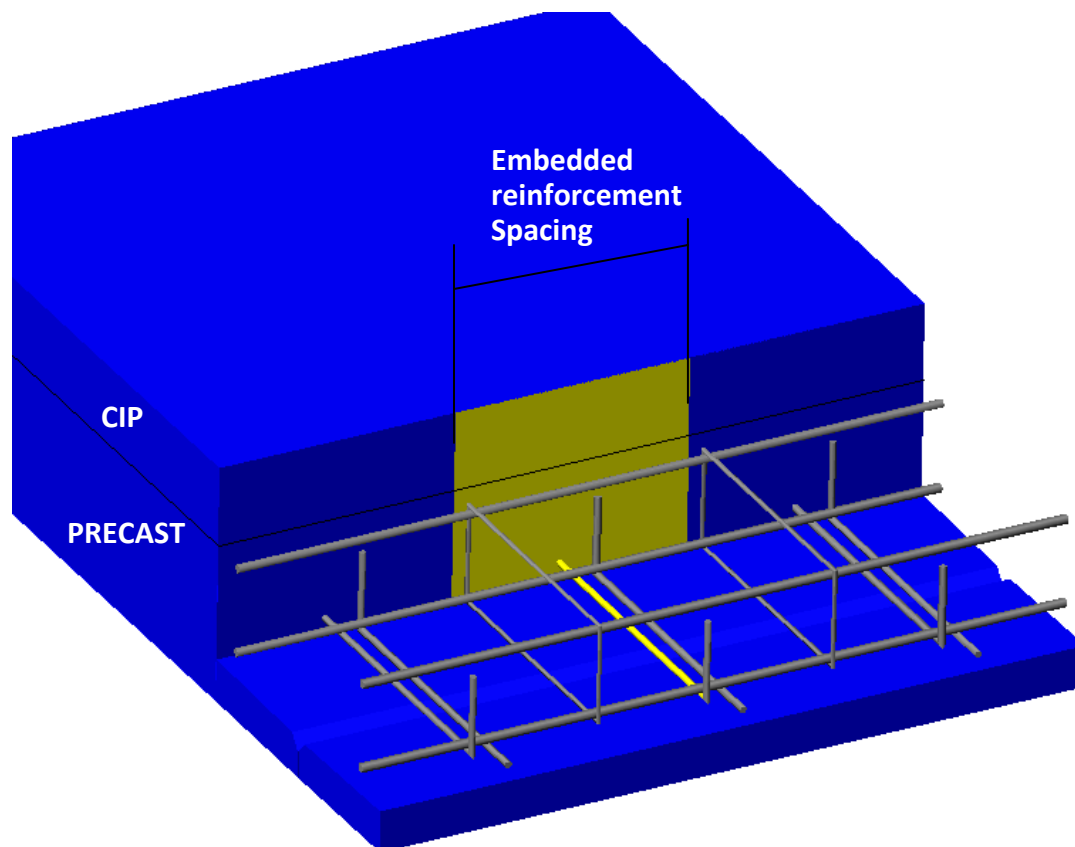
Figure 1.1.2: reinforcement and depth of concrete considered in calculation of the reinforcement ratio for transverse load transfer (highlighted in yellow)

The AASHTO 2010 LRFD Bridge Design Specifications provide guidance in the design of reinforcement for the transverse load distribution in CIP concrete bridge superstructures. Article 5.14.4.1 states that the transverse reinforcement be selected based on the longitudinal flexural reinforcement and the span length. Specifically, the transverse mild reinforcement is computed as a percentage of the total longitudinal flexural reinforcement considering both mild and prestressed longitudinal reinforcement. In the case of prestressed construction, the ratio of the strand stress to the mild reinforcement strength (taken to be 60 ksi in the specification) is taken into account. The calculation for the transverse load reinforcement for mild and prestressed reinforcement is given in AASHTO (2010) equations 5.14.4.1-1 and 5.14.4.1-2, respectively shown below.

- For longitudinal reinforced concrete construction:

$$k_{mild} = \frac{100}{\sqrt{L}} \leq 50\% \qquad \text{(LRFD 5.14.4.1-1)}$$

- For longitudinal prestressed construction

$$k_{ps} = \frac{100}{\sqrt{L}} * \frac{f_{pe}}{60} \leq 50\% \qquad \text{(LRFD 5.14.4.1-2)}$$

where:

k_{mild} = percent of longitudinal mild flexural reinforcement

A-22

k_{ps} = percent of longitudinal prestressed flexural reinforcement

L = span length [ft]

f_{pe} = effective stress in prestressing strand [ksi]

The application of equation 5.14.4.1-2 to spans in the range of 20 ft. to 31 ft. resulted in required transverse reinforcement proportions of 65 percent and 52 percent, respectively, when the effective strand stress was taken to be 175 ksi. In both cases, the proportion of transverse reinforcement would be capped at 50 percent.

The amount of longitudinal reinforcement to be considered in proportioning the transverse reinforcement shall include only the primary prestressing strand unless longitudinal mild reinforcement is included as the primary tensile reinforcement; longitudinal mild reinforcement located in the precast flanges may be neglected when present.

A primary disparity in the application of AASHTO (2010) Article 5.14.4.1 to the PCSSS is the difference in depth of the longitudinal and transverse reinforcement. In CIP slab systems, the transverse reinforcement is generally located immediately above the single longitudinal reinforcement layer. In contrast, the PCSSS is constructed such that the centroid of the longitudinal reinforcement may be significantly different than that of the transverse reinforcement. The longitudinal strands are usually located as low as possible within the section depth to maximize strand eccentricity and effectiveness in providing positive moment resistance, whereas the depth of the transverse reinforcement is constrained by requiring sufficient clearance below the bar and the top surface of the flange which limits its effective depth.

The difference between the effective depths of the longitudinal and transverse reinforcement layers is dependent on the number of layers of prestressing strand used in the design and the thickness of the flange. For this reason, it is suggested that the reduction in the effectiveness of the transverse reinforcement be taken into consideration through increasing the required transverse reinforcement by the ratio of the longitudinal to transverse reinforcement effective depths. Because only the prestressing reinforcement is likely to have a larger effective depth compared to that of the transverse reinforcement, an adjustment to increase the required transverse reinforcement for this effect need only be considered for the tendons; the larger effective depth of the transverse reinforcement relative to the centroid of the longitudinal mild reinforcement is conservatively ignored. In the case of a typical 12 in. deep section, the ratio of the effective depth of longitudinal to transverse reinforcement is 1.13 [i.e., (depth of center of gravity of strand)/(effective depth of transverse reinforcement)= 15.2 / 13.5 = 1.126 ≈ 1.13]. The required transverse load distribution reinforcement can be calculated by combining the separate proportions determined relative to the prestressed longitudinal reinforcement and mild longitudinal reinforcement, respectively. The relationship between the longitudinal flexural reinforcement and transverse load distribution reinforcement for the PCSSS can be defined based on the AASHTO (2010) requirement, as shown in equation 1.1.3.

$$A_{tld} = k_{mild} A_{l-mild} + \alpha \, k_{ps} A_{l-ps} \tag{1.1.3}$$

A-23

where:

A_{tld} = area required for transverse load distribution reinforcement [in^2]

$A_{l\text{-}mild}$ = area of longitudinal mild flexural reinforcement [in^2]

$A_{l\text{-}ps}$ = area of longitudinal prestressed flexural reinforcement [in^2]

$\alpha = d_{cgs} / d_{trans} \geq 1.0$

d_{cgs} = depth of center of gravity of prestressed reinforcement [in.]

d_{trans} = depth of center of gravity of transverse reinforcement [in.]

For transverse bar spacing between 12 in. and 18 in., the required bar sizes to satisfy the demands outlined in the previous paragraph would be No. 5 or No. 6 bars for a 12 in. deep precast section with spans between 20 ft. and 31 ft., which are reasonably acceptable bar sizes for bridge construction.

The transverse bars must be designed to be continuous throughout the width of the bridge. The continuity of the reinforcement through the width of the precast member can be achieved either through the use of embedded hooked reinforcement extending through the width of the precast member and protruding across the longitudinal joints, or by separate embedded reinforcement and hooked bars mechanically anchored to the precast member. The transverse bars should terminate with a standard hook, as specified in AASHTO (2010) Article 5.10.2.1 (hook extension of 12 times diameter of the bar), and the hook should extend vertically upward. The transverse reinforcement should extend through the trough area such that the reinforcement terminates as near to the vertical web face of the adjacent precast member as possible, and should never terminate farther than 2.0 in. clear from the vertical precast web of an adjacent panel. For a No. 6 standard hook developed in tension in 4 ksi concrete, the development length is 11.9 in., suggesting that the 22 in. (24 in. width joint – 2.0 in. maximum clear distance) is sufficient to fully develop the reinforcement.

The adjacent transverse load distribution reinforcement was considered to be most accurately represented in the current specification by a contact lap splice. Therefore, the maximum stagger between adjacent transversely load distribution reinforcement should be limited by AASHTO (2010) Article 5.11.5.2, which limits the transverse spacing to one fifth of the lap splice length or 6 in., whichever is less.

Both the Concept 1 and Concept 2 laboratory bridges displayed good load distribution characteristics before and after the introduction of a reflective crack near the precast joint. The 18 in. maximum spacing and reinforcement ratio of 0.0007 (No. 4 bars at 18 in. spacing = .2in^2/ft * 12in/18in / (15in * 12in)) of the transverse bars in the Concept 2 specimen provided a more economical design compared to the Concept 1 specimen, with a maximum spacing of 12 in. and reinforcement ratio of 0.0024 (No. 6 bars at 12 in. spacing = .44in^2/ft / (15in * 12in)). The 18 in. transverse hook spacing may be preferred by fabricators because it requires fewer perforations of their formwork to allow for the embedded transverse bars.

A-24

Article 5.14.4.3.3 of the 2010 Interim LRFD Design Specification specifically addresses shear-flexure transfer joints in precast deck bridges; for CIP closure joints, part 'e' of this Article applies.

AASHTO (2010) *Article 5.14.4.3.3e* Load Transfer in *Cast-in-Place Closure Joint*

Concrete in the closure joint should have strength comparable to that of the precast components; however, this need not be the case in precast-composite slab-span systems. The width of the longitudinal closure joint shall be large enough to accommodate development of the reinforcement in the joint, but in no case shall the width of the joint be less than 12.0 in.

The following additional requirements apply to precast-composite slab-span systems:
 The transverse reinforcement for load transfer shall be adequately embedded or mechanically anchored and continuously extend through the supporting precast component.
The amount of bottom transverse load distribution reinforcement per unit length of span shall be determined as in Article 5.14.4.1 by combining the percentages calculated based on longitudinal reinforcing steel and longitudinal prestressing steel divided by the precast inverted-T member width. The percentage based on the longitudinal prestressing steel shall be adjusted by the factor α. The longitudinal mild steel reinforcement in the precast flanges need not be included in the percentage calculation based on longitudinal mild reinforcement.
where:

$$\alpha = d_{cgs} / d_{trans} \geq 1.0$$

d_{cgs} = depth of center of gravity of prestressed reinforcement (in.)

d_{trans} = depth of transverse reinforcement (in.)

The transverse reinforcement shall be provided such that all load developed in the closure pour can be fully transferred to either, or both, of the adjacent precast sections; therefore the calculated required transverse reinforcement must be provided in each precast section. The transverse load distribution reinforcement shall be installed such that lapping bars from adjacent precast panels in a common closure joint be laterally spaced with a minimum nominal clear spacing of the greater of (1 in., d_b, 4/3 * aggregate size) between the lapped bars. A tolerance in the lateral placement of the transverse hooks of 1/4 in. is acceptable.
The transverse load distribution reinforcement shall be considered to be a lap splice, and thereby conform to Article 5.11.5.2.
The transverse load distribution reinforcement shall be evenly distributed throughout the span, with the reinforcement protruding from a given precast unit spaced at no more than 18.0 in.

A-25

Research on precast-composite slab-span systems has shown adequate performance where typical concrete deck mixes are cast on the precast inverted-T sections. The CIP concrete provides the closure pour material in the trough region above the adjacent precast flanges and is contiguously cast the thickness of a typical deck across the bridge to encase the deck reinforcement.

1.1.6. Reflective Crack Control

Suggested specifications to be modified to address reflective crack control include AASHTO (2010) Article 5.7.3.4, 5.14.4.3.3f, 5.14.4.3.3g.

Reflective cracking originating at the longitudinal joint between adjacent precast flanges can be controlled through the addition of a drop-in reinforcing cage in combination with the transverse load distribution reinforcement. It is to be noted that the drop-in cage is only effective in controlling cracks that develop in the vicinity over the longitudinal joint. Cracks that might form at the interface between the CIP and precast web interface would only be restrained by the reinforcement provided for transverse load distribution (i.e., hooked bars protruding from the precast webs). In the vicinity of the longitudinal joint, the reinforcement ratio and spacing required for crack control is based on the sum of the two types of reinforcement (i.e., drop-in reinforcing cage and transverse hooked bars protruding from the precast webs). The reinforcement ratio provided for crack control considers the lower leg of the cage hoops as well as both of the adjacent lapped transverse bars provided for load transfer. The reinforcement and depth of concrete considered in the calculation of the reinforcement ratio for crack control is highlighted in Figure 1.1.3.

The reinforcement spacing provided for crack control is defined as the maximum spacing between the reinforcement crossing the joint, regardless of whether it is part of the drop-in cage or the transverse hooked bars. Therefore, offsetting of the reinforcement cage from the transverse bars wherever possible will reduce the reinforcement spacing provided for crack control; reduction in the spacing of the transverse reinforcement provided an observed benefit in the crack control capabilities of the subassemblage specimens in the NCHRP 10-71 study.

A-26
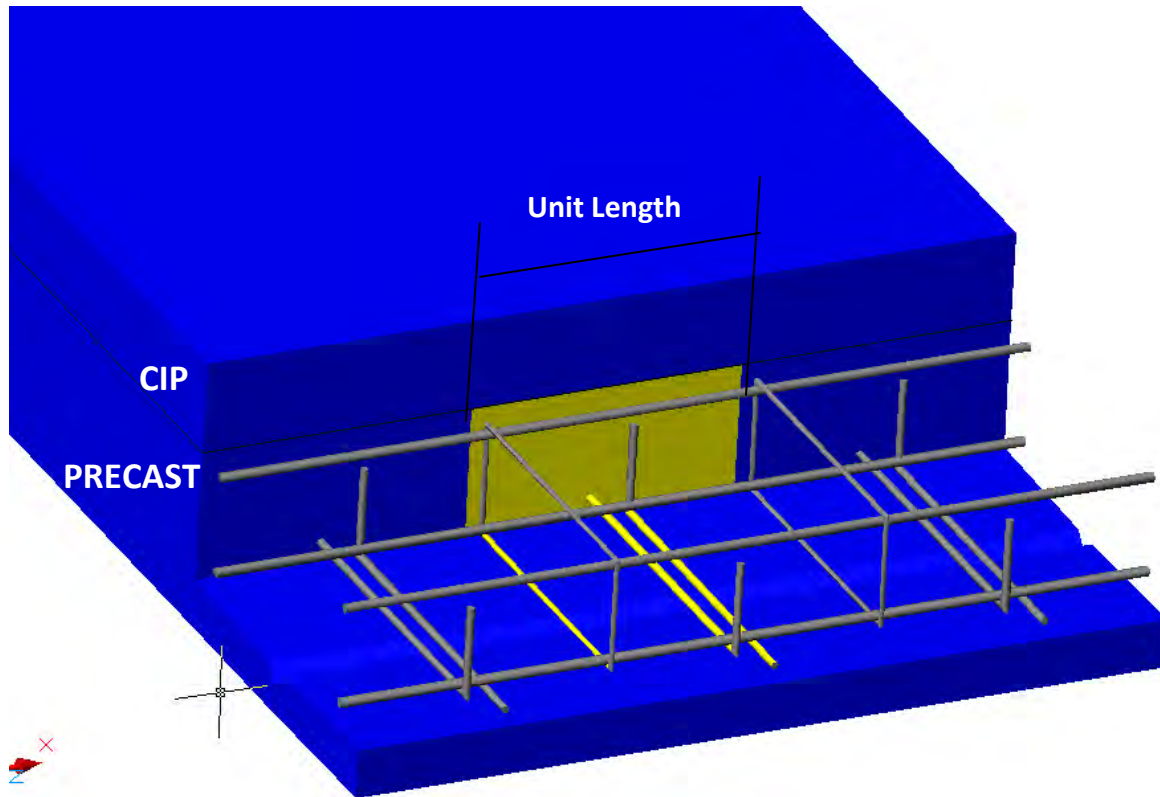
Figure 1.1.3: Reinforcement and depth of concrete considered in the calculation of the reinforcement ratio for crack control (highlighted in yellow)

Three useful resources that provide insight into the design of reinforcement for crack control include AASHTO (2010), ACI 318-08, and Frosch et al. (2006) The AASHTO (2010) and ACI 318-08 specifications provide spacing requirements for flexural reinforcement and shrinkage and temperature reinforcement. Frosch, et al. provides guidelines for the spacing and reinforcement ratio required for crack control in bridge decks. The design requirements for each are summarized in

Table 1.1.1. Both AASHTO (2010) and ACI 318-08 provide maximum spacing of 18 in. and a minimum ratio of the area of flexural and shrinkage and temperature reinforcement to the area of the gross section of 0.0018.

A-27

Table 1.1.1[1]: Spacing and reinforcement ratio limits for flexural and crack control reinforcement

Reinforcement Type	Reinforcement Design Limits	Source	Article in Spec.
Crack control and shrinkage and temperature	$s < \dfrac{700\gamma_e}{\beta_s * f_{ss}} - 2 * d_c, \quad where \quad \beta_s = 1 + \dfrac{d_c}{0.7 * (h - d_c)}$	AASHTO (2010)	5.7.3.4
	$s \leq \min(1.5h, 18\ in.)$		5.10.3.2
Shrinkage and temperature	$A_{sAASHTO} \geq \dfrac{1.30\ bh}{2(b + h)f_y}; \quad 0.11 \leq A_{sAASHTO} \leq 0.60$		5.10.8
Crack control and shrinkage and temperature	$s < 15 * \dfrac{40000}{f_s} - 2.5 * c_c$	ACI 318-08	10.6.4
Shrinkage and temperature	$A_{sACI} = 0.0018bh \quad (when\ using\ Gr.\ 60\ bars)$		7.12.2.1
	$s \leq \min(5h, 18\ in.)$		7.12.2.2
Crack control	$s < 9 * \left(2.5 - \dfrac{c_c}{2}\right) \leq 9in$	Frosch et al. (2006)	
	$\rho_{Frosch} = 6\dfrac{\sqrt{f_c'}}{f_y}$		

[1]Variables in
Table 1.1.1 are defined as follows:
$\gamma_e = 1.0$ for Class 1(No corrosion concerns); 0.75 for Class 2 (Corrosion concerns)
$f_{ss} = $ Stress in reinforcement at service [ksi]
$d_c = $ Depth of concrete cover measured from tension fiber of concrete to center of
     reinforcement, defined by AASHTO (2010)Section 5.7.3.4 [in.]
$c_c = $ Depth of concrete cover measured from tension fiber of concrete to face of
     reinforcement, defined by ACI 318 − 08 Section 10.6.4 [in.]
$h = $ Total section depth [in]
$A_{sAASHTO} = $ Area of reinforcement in each direction and each face [in.^{2}/ft.]
$A_{sACI} = $ Area of shrinkage and temperature reinforcement [in.^{2}]
$b = $ Least width of component section [in.]
$f_s = $ Stress in reinforcement at service [psi]
$f_c' = 28 − $ day concrete compressive strength [psi]
$f_y = $ Reinforcement yield strength [psi]
$\rho_{Frosch} = $ Reinforcement ratio defined by Frosch et al. (2006). Equivalent to:
     area of reinforcement /gross area of section [dim]

The spacing requirements outlined in

Table 1.1.1 depend on the depth of cover provided. AASHTO (2010) defines the depth of cover, d_c, as the distance between the extreme tension fiber of concrete to the center of the flexural reinforcement located closest thereto, while ACI 318-08 defines the depth of concrete cover, c_c, as the distance from the tension fiber of concrete to the face of the reinforcement. Furthermore, Frosch et al. define the depth of cover analogously to ACI 318-08, with the clear distance to the face of the reinforcement. In the case of the transverse reinforcement used for crack control, the depth of cover can be defined in two reasonable ways, depending on whether or not the thickness of the precast flange is considered, as illustrated in Figure 1.1.4. The depth of cover is always measured at the precast joint. The depth of cover for the reference section illustrated in Figure 1.1.1, defined by AASHTO (2010) and ACI 318-08 is 4.6 in. (3.25 in. + 1 in. clear + 0.3125 in.) and 4.25 in. (3.25 in. + 1 in. clear) when the flange is included in the calculation, respectively. When the flange is excluded in the calculation, the depth of cover is 1.6 in. (4.6 in. − 3 in.) and 1.25 in. (4.25 in. − 3 in.) as defined by AASHTO (2010) and ACI 318-08, respectively. When the precast flange is included in the calculation, the spacing requirements are difficult to satisfy, with spacing values ranging from negative values calculated via the AASHTO (2010) equation to 4.4 in. using the equation provided by ACI 318-08. Excluding the flange produces more reasonable spacing values, ranging from 8.3 in. (assuming Class 2 corrosion concerns) to 11.9 in. based on the AASHTO (2010) and ACI 318-08 equations, respectively. Because the crack control reinforcement is located in the CIP above the gap between the adjacent precast flanges, it could be reasoned, that the depth of the flange should not be considered in the calculation of the crack control reinforcement spacing.
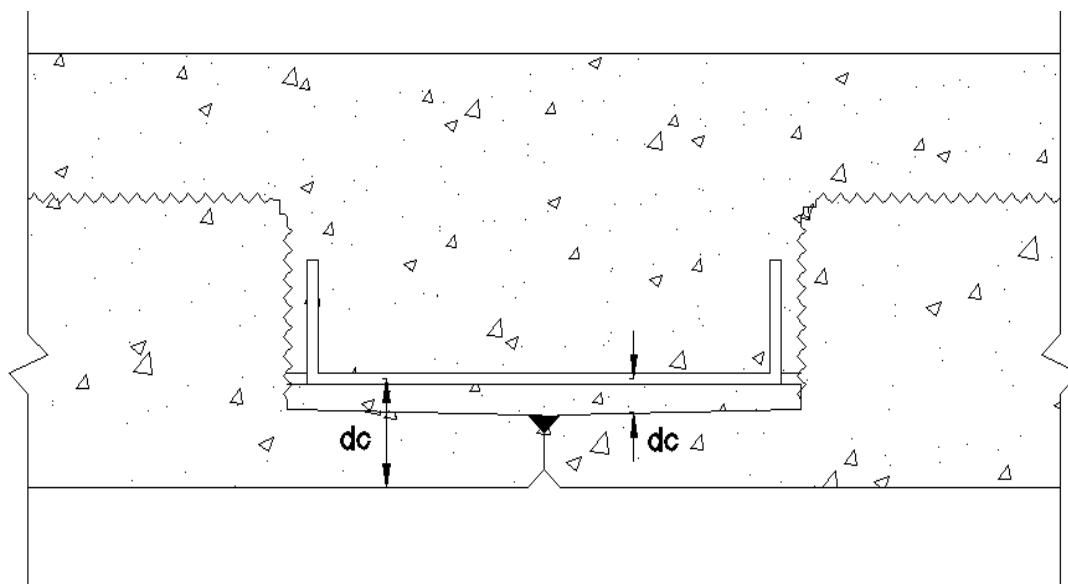
Figure 1.1.4[1]: Variation in magnitude of assumed depth of cover depending on inclusion/exclusion of precast flange measured to center of reinforcement, as defined by AASHTO (2010)

[1]The depth of cover is always measured at the joint; the annotations in Figure 1.1.4 are shown offset for clarity.

Several variations in the spacing and reinforcement ratio provided for crack control were considered in the NCRHP 10-71 study. In the Concept 1 large-scale laboratory bridge specimen, the transverse crack control reinforcement was designed to reflect that of the original Mn/DOT implementation of the PCSSS in Center City, MN. One of the two spans had the same flange depth as the Center City Bridge (i.e., 5.25 in.), and the other span had a reduced flange thickness to reduce the discontinuity between the precast flanges (i.e., 3 in.). The Concept 2 large-scale simply-supported bridge specimen and subassemblage tests were designed to investigate variations in the reinforcement spacing and reinforcement ratios for crack control. The selected configurations, summarized in Table 1.1.2 for each of the laboratory test specimens, provided an opportunity to investigate the range of requirements specified among the three design guidelines outlined above. The smallest reinforcement ratio selected for the study was 0.0025 (among the 12 in. deep sections), which was associated with the maximum spacing and minimum reinforcement size for the transverse hooks (i.e., No. 4 bars) considered to be feasible from a constructability standpoint. The cage reinforcement was fabricated with No. 3 closed stirrups which represented a practical lower bound reinforcement size for the cage.

Table 1.1.2: Crack control reinforcement parameters in the laboratory test specimens

Specimen	Transverse Bar Spacing [in.]	Cage Spacing [in.]	Reinforcement Ratio[1] [%]	Effective Maximum Bar Spacing[2] [in.]
Concept 1, Span 1	12	12	0.0110	12
Concept 1, Span 2	12	12	0.0147	12
Concept 2 Bridge	18	18	0.0031	9
SSMBLG1-Control1	18	18	0.0031	9
SSMBLG2-NoCage	18	NA	0.0025	18
SSMBLG3-HighBars	18	18	0.0031	9
SSMBLG4-DeepSection	18	18	0.0022	9
SSMBLG5-No.6Bars	18	18	0.0061[3]	9
SSMBLG6-Frosch	18	4.5	0.0052[3]	4.5
SSMBLG7-Control2	18	18	0.0031	9

[1]This is the reinforcement ratio defined for crack control
[2]The effective maximum bar spacing is based on the combined transverse bar and cage configuration.
[3]Note that the reinforcement ratio for the SSMBLG5-No.6Bars was actually closer to that of the Frosch et al. (2006) requirements than was the reinforcement ratio for the SSMBLG6-Frosch specimen.

Both the Concept 1 and Concept 2 laboratory bridge specimens provided sufficient crack control throughout the duration of all laboratory testing. Both specimens performed relatively similarly, with comparable increases in the transverse strain over the joint before and after cracking, as well as before and after cycling. In the continuous Concept 1 bridge, cracking in the exterior half span of the test span

was always greater than on the interior half span towards the center support. The interior half span was supported on 15 in. of a 42 in. wide concrete pier and the exterior half spans were supported on 12 in. of a 12 in. wide flange section. Due to the continuous nature of the two-span Concept 1 bridge, this phenomenon was expected (i.e., the center pier provided greater restraint to the transverse cracking).

Because both laboratory bridge specimens provided adequate crack control through the duration of testing, both configurations can reasonably be utilized in future designs. The AASHTO (2010) equation provides an adequate measure of the required reinforcement spacing for crack control, however an upper limit is recommended. The good crack control performance of the Concept 1 bridge suggests that the 12 in. maximum spacing is known to produce good results. Therefore, it is recommended that the AASHTO (2010) equation be bounded to a maximum spacing of 12 in.

It is suggested that all transverse bars protruding from the precast members terminate in standard hook, as specified in Section 1.1.5.

AASHTO (2010) **Article 5.7.3.4 Control of Cracking by Distribution of Reinforcement**

The provisions specified herein shall apply to the reinforcement of all concrete components, except that of deck slabs designed in accordance with Article 9.7.2, in which tension in the cross-section exceeds 80 percent of the modulus of rupture, specified in Article 5.4.2.6, at applicable service limit state load combination specified in Table 3.4.1-1.

The spacing s of mild steel reinforcement in the layer closest to the tension face shall satisfy the following:

$$s \leq \frac{700\, \gamma_e}{\beta_s\, f_{ss}} - 2d_c \qquad (5.7.3.4\text{-}1)$$

in which:

$$\beta_s = 1 + \frac{d_c}{0.7(h - d_c)}$$

where:

γ_e = exposure factor
    = 1.00 for Class 1 exposure condition
    = 0.75 for Class 2 exposure condition

d_c = thickness of concrete cover measured from extreme tension fiber to center of the flexural reinforcement located closest thereto (in.)

f_{ss} = tensile stress in steel reinforcement at the service limit state (ksi)

h = overall thickness or depth of the component (in.)

Class 1 exposure condition applies when cracks can be tolerated due to reduced concerns of appearance and/or corrosion. Class 2 exposure condition applies to transverse design of segmental concrete box girders for any loads applied prior to attaining full nominal concrete strength and when there is increased concern of appearance and/or corrosion.

In the computation of d_c, the actual concrete cover thickness is to be used. For the design of the transverse reinforcement located in the longitudinal closure joint of precast composite slab-span superstructures, d_c shall be taken as the distance between the extreme tension fiber of the cast-in-place concrete in the trough and the center of the transverse reinforcement in the closure joint, thereby neglecting the thickness of the precast flange.

When computing the actual stress in the steel reinforcement, axial tension effects shall be considered, while axial compression effects may be considered.

The minimum and maximum spacing of reinforcement shall also comply with the provisions of Articles 5.10.3.1 and 5.10.3.2, respectively.

…

The reinforcement ratio presented by Frosch provides a good basis for the development of an adequate reinforcement ratio for crack control in the longitudinal joint region of precast slab span bridge systems. Frosch et al. (2006) suggests that at the initiation of cracking in the section, adequate reinforcement should be provided to transfer all load from the concrete to the reinforcement.

The presence of a reinforcing cage located in the longitudinal trough between inverted-T sections shall be required in all PCSSS bridge systems. The lack of a cage was investigated during the subassemblage tests and was found to perform poorly relative to the other specimens tested, especially in terms of crack widths and lengths measured on the faces of the specimen. Furthermore, all PCSSS bridges constructed in the field have been built with cage reinforcement, and therefore no information regarding the large-scale in-service performance of a bridge system without a cage was available. Therefore, cage reinforcement shall be provided in each trough region between each precast member, and the transverse reinforcement in the cage shall consist of no less than No. 4 bars spaced at 12 in.

The cage stirrups may be designed in two primary configurations, but in both cases the bottom of the stirrup shall coincide with the depth of the transverse reinforcement for load transfer. The depth of the stirrup may be such that the top horizontal leg is flush with the top of the precast web, or preferably, the depth of the stirrup is minimized (i.e., the depth of the stirrup is the minimum bend diameter for the bar size used or is such to provide adequate room to tie the four longitudinal No. 5 bars inside the stirrup). The minimized stirrup depth allows the top horizontal leg of the stirrup increased potential to intercept a reflective crack earlier. The width of the stirrup in the trough shall be similar to the width of the precast hooks, and shall be as wide as possible while allowing for adequate clearance for the longitudinal cage reinforcement inside of the transverse hooks.

A-32

It is suggested that a separate section is designated for reinforcement requirements for crack control, which will be designated as AASHTO (2010) Article 5.14.4.3.3f. The current Article 5.14.4.3.3f shall be moved to 5.14.4.3.3g.

AASHTO (2009) Article ~~5.14.4.3.3f~~ *5.14.4.3.3g Structural Overlay*

Where a structural overlay is used to qualify for improved load distribution as provided in Articles 4.6.2.2.2 and 4.6.2.2.3, the thickness of structural concrete overlay shall not be less than 4.5 in. An isotropic layer of reinforcement shall be provided in accordance with the requirements of Article 5.10.8. The top surface of the precast components shall be roughened.

AASHTO (2010) *Article 5.14.4.3.3f Reflective Crack Control in Cast-in-Place Closure Joint for Precast Composite Slab-Span Systems*

Transverse reinforcement for crack control shall be placed near the extreme tension face in the cast-in-place closure joint. Transverse reinforcement may be provided by both the reinforcement present for transverse load transfer, as specified in Article 5.14.4.3.3e, as well as through the use of a reinforcing cage consisting of vertical closed stirrups. Transverse reinforcement shall be provided to satisfy:

$$\rho_{cr} = \frac{6\sqrt{f_c'}}{f_y} \qquad\qquad (5.14.4.3.3\text{f-1})$$

where:

ρ_{cr} = reinforcement ratio of the section for crack control (%)

f_c' = 28 – day concrete compressive strength (psi)

f_y = yield stress in the reinforcement (psi)

The reinforcement ratio of the section for crack control, ρ_{cr}, shall be calculated considering all load transfer reinforcement and the lower horizontal leg of the cage stirrup crossing the longitudinal joint. The area of concrete considered in the calculation shall be only the cast-in-place concrete between the top of the precast flange and the top of the precast web. The reinforcement ratio for crack control shall be taken as:

$$\rho_{cr} = \frac{A_{trans-cr}}{12(h_{pc}-d_{flange})} \qquad\qquad (5.14.4.3.3\text{f-2})$$

where:

$A_{trans-cr}$ = area of transverse reinforcement for crack control. Consists of all reinforcement

A-33

traversing the longitudinal joint per unit length (in^2./ft.)

h_{pc} = overall depth of the precast section (in.)

d_{flange} = depth of the precast flange (in.)

A minimum reinforcing cage is required in all sections, and shall consist of no less than No. 4 closed stirrups spaced at 12 in. One longitudinal bar shall be provided in each interior corner of the stirrup for anchorage.

C5.14.4.3.3f

The vertical closed stirrups provided in the reinforcement cage should be configured such that the bottom horizontal stirrup leg is located at approximately the same depth as the transverse load distribution reinforcement. The vertical depth of the top horizontal stirrup leg should be minimized where possible, as the minimized stirrup depth allows the top horizontal leg to intercept potential reflective cracking at a lower depth. The width of the stirrups in the reinforcement cage should be maximized while ensuring minimum bar spacing clearances are met between the cage and the vertical precast web faces.

1.1.7. Composite Action

To address composite action in PCSSS, specifications suggested for modification include AASHTO (2010) Articles 5.8.4.3, and 5.8.4.4

Composite action was maintained throughout the extent of the ultimate loading tests on each of the two spans of the Concept 1 laboratory bridge specimen and the simple-span Concept 2 laboratory bridge specimen. It should be noted that in the Concept 2 bridge, the section relied on only the composite action of the roughened concrete surface; there was no horizontal shear steel that crossed the interface. Both bridge specimens had a standard raked finish on the top horizontal surface of the precast web. Furthermore, each specimen had a roughened diamond pattern with approximately 1/8 in. to 1/4 in. perturbations on the vertical web surfaces of the precast panels. Likewise, the East span of the Concept 1 bridge, which was constructed with the 5 1/4 in. thick precast flange, also had the tops of the precast flanges roughened with the same diamond pattern. The ability of the Concept 2 specimen to maintain composite action suggests that PCSSS bridges can provide adequate horizontal shear strength in the absence of supplemental reinforcement across the precast-CIP concrete interface. The wide precast web sections provided a sufficiently large area such that horizontal forces could be effectively transferred between the CIP and precast units. Furthermore, Kovach and Naito (2008) suggested that concrete beams without horizontal shear reinforcement can conservatively provide 300 psi of horizontal shear resistance at service conditions with a broom or rake finish. The 2010 AASHTO LRFD specification suggests that an intentionally roughened surface can be expected to achieve 240 psi of horizontal shear

resistance, which was increased from 100 psi in the 2005 specification. However, the 2010 specification still requires minimum horizontal shear reinforcement.

The compressive force that was transferred between the CIP and precast sections was measured to be 2088 kips in the Concept 2 bridge at the maximum load available to be applied to the section by integrating the strain from three longitudinal strain gages between the neutral axis and the top of the section. The stress in the section was calculated using the modified Kent-Park concrete stress-strain relationship assuming no confinement reinforcement, while using measured values for the maximum concrete compressive strength and a corresponding concrete strain assumed to be 0.002 at the maximum compressive stress. The horizontal shear stress developed at this condition was calculated by dividing the total compressive force at mid-span by the full width of the deck and half of the center to center of bearing span length, resulting in a measured horizontal shear stress of 135 psi. The width of the deck was taken as 10 ft., and included the area above the precast trough.

Because the Concept 2 bridge specimen, which had no horizontal shear reinforcement, developed a horizontal shear stress of 135 psi, it is recommended that the specification allow for sections to develop a horizontal shear stress of 135 psi with no horizontal shear reinforcement. The K_1 and K_2 values, which provide upper bound estimates of the horizontal shear capacity of a given section, selected to be used in the proposed specification modifications are simply the smallest, or most conservative of the existing K_1 and K_2 values. Because these were developed specifically for composite beams with horizontal shear reinforcement, even the selected values may not be appropriate. However, these values provide a maximum horizontal shear force that is at least a factor of two larger than the horizontal shear force that would be developed by the full 6 in. deep deck constructed with 10 ksi concrete at ultimate (i.e., assuming that the section were reinforced such that it were required to fully transfer Whitney's stress block through the full 6 in. depth of the CIP deck).

AASHTO (2010) Article **5.8.4 Interface Shear Transfer – Shear Friction**

    5.8.4.1 General

        Interface shear transfer shall be considered across a given plane at:

- An existing or potential crack,

- An interface between dissimilar materials,

- An interface between two concretes cast at different times, or

- The interface between different elements of the cross-section

   …

        The nominal shear resistance of the interface plane shall be taken as:

$$V_{ni} = c\,A_{cv} + \mu(A_{vf}\,f_y + P_c) \qquad\qquad (5.8.4.1\text{-}3)$$

A-35

where:

A_{cv} = area of concrete considered to be engaged in interface shear transfer (in.^{2})

A_{vf} = area of interface shear reinforcement crossing the shear plane within the area A_{cv} (in.^{2})

c = cohesion factor specified in Article 5.8.4.3 (ksi)

μ = friction factor specified in Article 5.8.4.3 (dim.)

f_y = yield stress of reinforcement but design value not to exceed 60 (ksi)

P_c = permanent net compressive force normal to the shear plane; if force is tensile, P_c = 0.0 (kip)

…

5.8.4.3 Cohesion and Friction Factors

The following values shall be taken for cohesion, c, and friction factor, μ:

…

For normal-weight concrete placed against a clean concrete surface, free of laitance, with surface intentionally roughened to an amplitude of 0.25 in.:

c = 0.24 ksi
μ = 1.0
K_1 = 0.25
K_2 = 1.5 ksi

For concrete placed against a clean concrete surface, free of laitance, but not intentionally roughened:

c = 0.075 ksi
μ = 0.6
K_1 = 0.2
K_2 = 0.8 ksi

For normal-weight concrete placed against a clean concrete surface, free of laitance, with surface intentionally roughened to an amplitude of 0.25 in. and no interface shear reinforcement provided crossing the shear plane up to the minimum required A_{vf} in Eq. 5.8.4.4-1:

c = 0.135 ksi
μ = 1.0

K$_1$ = 0.2
K$_2$ = 0.8 ksi

…

5.8.4.4 Minimum Area of Interface Shear Reinforcement

Except as provided herein, the cross-sectional area of the interface shear reinforcement, A_{vf}, crossing the interface area, A_{cv}, shall satisfy:

$$A_{vf} \geq \frac{0.05\, A_{cv}}{f_y}$$ (5.8.4.4-1)

For a cast-in-place concrete slab on clean concrete girder surfaces free of laitance, the following provisions shall apply:

The minimum interface shear reinforcement, A_{vf}, need not exceed the lesser of the amount determined using Eq. 1 and the amount needed to resist $1.33V_{ui}$ / ϕ as determined using Eq. 5.8.4.1-3.

The minimum reinforcement provisions specified herein shall be waived for girder/slab interfaces with surface roughened to an amplitude of 0.25 in. where the factored interface shear stress, v_{ui} of Eq. 5.8.4.2-1, is less than 0.210 ksi, and all vertical (transverse) shear reinforcement required by the provisions of Article 5.8.1.1 is extended across the interface and adequately anchored in the slab.

For the cast-in-place concrete of precast-composite slab-span systems that is cast on clean precast inverted-T surfaces free of laitance, with a surface intentionally roughened to an amplitude of 1/4 in., the minimum reinforcement provisions specified herein shall be waived.

C5.14.4.3.3f

.
.
.

With respect to a girder/slab interface, the intent is that the portion of the reinforcement required to resist vertical shear which is extended into the slab also serves as interface shear reinforcement.

In the case of precast-composite slab-span systems, research (*French et al. 2010*) has shown that transverse reinforcement was not required across the CIP-precast interface in order to achieve composite action. Similar results were obtained in studies by Naito et al. (2008).

1.2. Construction Specification Recommendations

The 2009 Interim AASHTO LRFD Bridge Construction Specification (AASHTO 2009) provides guidance for the construction of most bridge superstructures and supporting elements. The PCSSS requires a

somewhat unique method of construction and erection which are important to achieve the desired performance of the system. The following sections outline changes to the AASHTO construction specifications in the same manner as utilized in the sections above; proposed modifications to the specification are shown with additions and deletions shown in underline and strikethrough notation, respectively.

1.2.1. Sequence of Placement

Suggested specifications to be modified to address sequence of placement include AASHTO Construction Specification (2009) Article 8.7.2.2

The CIP portion of the inverted-T sections should be poured in a single lift. It is likely that if, for whatever reason, the CIP was placed in two pours, a construction joint would be created in the trough area flush with the top of the precast webs; this type of joint will limit the ability for the section to maintain composite action, as this coincides with the plane separating the precast and CIP concrete.

> **8.7.2.2 Superstructures**
>
> Unless otherwise permitted, no concrete shall be placed …
>
> …
>
> Concrete for box girders may be placed in two or three separate operations consisting of the bottom slab, girder stems, and top slab. In either case, the bottom slab shall be placed first and, unless otherwise permitted by the Engineer, the top slab shall not be placed until the girder stems have been in place for at least five days.
> Cast-in-place concrete for the closure pour and deck of composite inverted-T precast slab span structures shall be placed in a single operation.

1.2.2. Construction Joints

There are two primary contact surfaces in the joints of PCSSS bridges. These are the horizontal and vertical surfaces of the precast web and flanges that are in contact with the CIP concrete. All surfaces that will be in contact with CIP concrete during a closure pour must be pre-wetted prior to the placement of concrete, as described in Article 8.8.2, to ensure adequate bond will be achieved between the precast and CIP surfaces. No changes to this section are required; however, to reduce the stress discontinuity at the longitudinal joint between the precast elements, consideration can be given to debonding or "softening" a portion of the CIP-precast flange interface in the vicinity of the longitudinal joint. Extending the debonding across the entire flange width should be avoided as it could lead to reflective cracks initiating at the CIP-precast web interface where the crack control reinforcement consists of only the transverse load distribution reinforcement (i.e., the crack would miss the cage in the trough).

A-38

8.8.2 Bonding

Unless otherwise specified in the contract documents, horizontal joints may be made without keys, and vertical joints shall be constructed with shear keys. …

…

All construction joints shall be cleaned of surface laitance, curing compound, and other foreign materials before fresh concrete is placed against the surface of the joint. Abrasive blast or other approved methods shall be used to clean horizontal construction joints to the extent that clean aggregate is exposed. All construction joints shall be flushed with water and allowed to dry to a surface dry condition immediately prior to placing concrete.

1.2.3. Special Requirements for PCSSS Bridges

Specifications suggested for modification to address PCSSS construction include AASHTO Construction Specification (2009) Article 8.17

There are several special requirements unique to PCSSS construction that must be considered. It is useful to provide a new Article in the bridge construction specifications that specifically addresses PCSSS construction. It is recommended that this be Article 8.17: Special Requirements for PCSSS Bridges.

8.17.1 Sequence of Placement

The PCSSS system shall conform to Article 8.7.2.2.

8.17.2 Construction Joints

All construction joints shall be prepared pursuant to Article 8.8.2.

8.17.2.1 Longitudinal Precast Construction Joint

The top longitudinal edge of the precast flanges shall be formed with a 1 in. 45 degree chamfer (measured along the length of the chamfer) to produce a channel 1.4 in. wide by 0.7 in. deep at the precast joint. A silicone caulk, or bonding agent, must be utilized to fill the chamfer between adjacent precast panels. The agent must provide adequate ductility such that cracking does not initiate in the silicone when the panels separate by a total of 1/4 in. at the joint and must remain adequately bonded to the precast members.

The bonding agent must be placed in the chamfer of the joint sufficiently early such that it has fully cured based on Manufacturer's specifications prior to the

A-39

application of CIP concrete.

8.17.3 Transverse Load Distribution Reinforcement

Transverse reinforcement must be provided to ensure load transfer between adjacent precast panels. All reinforcement for load transfer must be securely anchored or embedded to the respective precast panel. Furthermore, the transverse reinforcement must extend completely through the width of the precast member.

In the case of transverse load distribution reinforcement terminating in a standard hook, the hook shall be oriented vertically regardless of whether the bar is embedded or mechanically to the precast member.

Transverse load distribution reinforcement protruding from adjacent precast panels shall be nominally spaced to provide a minimum clear spacing of the greater of (1 in., d_b, 4/3 * aggregate size) between lapped bars, after erection, with a maximum allowable lateral tolerance of 1/2 in. at each set of transverse bars.

8.17.4 Reinforcing Cage

The reinforcing cage shall be constructed such that the stirrups are oriented vertically after construction. The stirrups shall be installed such that the overlapping closed loop portion of the stirrup alternates between the left and right side of the trough area.

Unless otherwise specified in the contract documents, the reinforcing cage shall be offset from the embedded transverse hooks such that the maximum spacing between transverse reinforcement is minimized.

8.17.5 Bearing Devices

Uniform bearing shall be provided under the full area of contact between the precast composite beams and the pier caps by means of an elastomeric bearing pad of sufficient dimension to support the factored loads in accordance with Article 18.2. The bearing pad should extend along the full width of the PCSSS bridge system, less 6 in. for a drip setback. A crushable membrane shall be provided in areas directly between the precast member and pier cap not supported by the elastomeric bearing pad to prevent the egress of CIP concrete during the closure pour. When the CIP concrete and pier cap are to be separated by a bond breaker to reduce the potential for restrained shrinkage, a layer of plastic sheeting can be used to provide the bond breaker.

Details at continuous piers must be provided to ensure proper construction practices. Longitudinally adjacent precast members meeting at continuous piers must be sufficiently separated such that CIP

concrete can be placed between the end faces of the members. A minimum separation of 4 in. is recommended, which provides adequate clearance for placement and vibration of the CIP concrete. Furthermore, vertical dowels, adequately embedded in the pier cap, shall be provided in the area between longitudinally adjacent members to provide a pin connection with the piers. No. 5 vertical dowels spaced at 12 in. were provided in the Mn/DOT implementation of the PCSSS bridge in Center City; no problems have been observed in the connection between the pier caps and superstructure. It should be noted that more reinforcement may be required to ensure integrity of the connection at the pier for PCSSS bridges located in seismic regions. The use of PCSSS bridges in seismic regions was out of the scope of the NCHRP 10-71 project.

These connection details might be revisited in the future to investigate whether separation of the PCSSS with the bridge pier might be desirable to reduce the potential effects of restrained shrinkage in the longitudinal joint between the precast flanges across the width of the bridge.

8.17.6 Connections at Continuous Piers

Vertical dowels, or equivalent, shall be installed in the pier cap and embedded in the CIP closure pour to provide a positive connection between the superstructure and substructure, and when surface cracking near the continuous piers it to be reasonably expected, the dowel reinforcement shall be fabricated from a corrosion resistant material.

Longitudinally adjacent precast panels meeting at a continuous pier shall be installed such that there is a space no less than 4.0 in. between the beam ends of the adjacent panels, and shall be located equidistant from the vertical dowels. The elastomeric bearing pad is not to be present in the space between adjacent panels, thereby allowing the CIP concrete to fill that region.

References for Precast Slab Span System

AASHTO (2010), *AASHTO LRFD Bridge Design Specifications,* 5th edition, Washington D.C.

AASHTO (2009), *AASHTO LRFD Bridge Construction Specifications,* 2nd edition, Washington D.C., 2009 Interim

ACI 318-08. *Building Code Requirements for Structural Concrete (ACI318-08) and Commentary (ACIR-08).* Farmington Hills, MI. 2008.

Barker, R., and Puckett, J. *Design of Highway Bridges: An LRFD Approach*, 2nd edition, New Jersey: Wiley and Sons, 2007.

Eriksson, W., "Vertical Tensile Stresses in End Regions of Precast Composite Slab-Span Systems and Restraint Moments". M.S., University of Minnesota, 2008

Frosch, R.J., Bice, J.K., Erickson, J.B. "Field Investigation of a Concrete Deck Designed by the AASHTO Empirical Method: The Control of Deck Cracking". *Indiana Department of Transportation Technical Report FHWA/IN/JTRP-2006/32*. September 2006.

International Scanning Study Team, Ralls, M., Tang, B., Bhide, S., Brecto, B., Calvert, E., Capers, H., Dorgan, D., Matsumoto, E., Napier, C., Nickas, W., Russell, H., "Prefabricated Bridge Elements and Systems in Japan and Europe". Federal Highway Administration Report Number FHWA-PL-05-003, 2005

Kovach, J.D., Naito, C. "Horizontal Shear Capacity of Composite Concrete Beams without Interface Ties". *Advanced Technology for Large Structural Systems (ATLSS) Report No. 08-05.*June, 2008.

Le, Quoc Thanh Chau, "Transverse cracking in bridge decks: Parametric study." M.S., University of Minnesota, 1998.

Smith, M., Eriksson, W., Shield, C., French, C., "Monitoring and Analysis of Mn/DOT Precast Composite Slab Span System (PCSSS)". *Minnesota Department of Transportation Technical Report No. MN/RC 2008-41.* September 2008

Suttikan, C., "A Generalized Solution for Time-Dependent Response and Strength of Noncomposite and Composite Prestressed Concrete Beams." University of Texas at Austin, 1978.

Section 2: Connection Concepts between Precast Flanges and Panels

2.0 Introduction to Design Recommendations for Longitudinal and Transverse Joints between Decked Bulb Tees (DBTs) and Precast Panels

This section contains design recommendations for cast-in-place (CIP) connections between the flanges of decked bulb tee's (DBTs) and between precast panels used to form the deck of girder bridges. A "decked" bulb tee (DBT) is defined as a precast, prestressed concrete "I," bulb-tee, multiple stemmed or single-tee girder with an integral deck that is cast and prestressed with the girder for bridge applications. DBTs are erected so that the flanges of adjacent units abut through "longitudinal joints." Where DBTs are made continuous through the deck in the longitudinal direction, "transverse joints" are required. The top surface of the precast DBT flange becomes the vehicle driving surface.

The precast deck panels used on girder bridges considered in the study were assumed to be full-depth panels (i.e., top surface of the precast deck panel serves as driving surface without the use of cast-in-place topping). The plan dimensions of the panels are determined by the specific bridge geometry, and the panel depth (i.e., thickness) is determined by structural design. For bridges less than 50 ft in width, full-depth precast deck panels can typically extend across the entire bridge width and adjacent panels along the span length are connected with "transverse joints" at approximately 8 to 12 ft intervals. For bridges wider than 50 ft, panels designed for half the bridge width are typically considered. Partial panel widths are also used in bridge replacement projects with construction phasing requirements. In these latter cases, the panels must be joined together in the width direction through "longitudinal joints."

The NCHRP 10-71 study on *Cast-in-Place Concrete Connections for Precast Deck Systems* focused on the development of cast-in-place (CIP) connections for both DBTs and full-depth precast panels. The CIP connections were developed so that the precast decks could emulate the performance of monolithic CIP deck construction. The connections were required to transfer the load to the adjacent elements through a combination of bending and shear across the longitudinal joints, and through tension and/or compression across the transverse joints. The design of the DBTs and precast deck panels themselves were out of scope of this study. The design recommendations contained herein focus on the requirements associated with the connection details including the type of reinforcement and configuration, required lap length for the transfer of forces across the joints, minimum joint widths, and performance requirements for the closure pour materials.

2.1. Design Recommendations

In earlier applications of DBTs, load transfer between adjacent units has typically been provided by longitudinal joints (parallel to traffic direction) with welded steel connectors and grouted shear keys (Stanton and Mattock 1986, Ma et al. 2007). In order to reduce the total DBT weight, the thickness of the deck is typically limited to 6 in. Welded steel connectors are typically spaced at 4 ft. on center. The

A-43

current longitudinal joint has the strength needed to transfer shear and limited moment from one girder to adjacent girders. However, because welded steel plates are located 4 ft. from each other and at mid-depth of the flange, they cannot help to control flexural cracks along the longitudinal joint.

As alternatives to the welded steel plate detail, two types of connection details were investigated in NCHRP 10-71 to provide two layers of reinforcement in the joint to facilitate moment as well as shear transfer. The details consisted of U-bar details and headed-bar details, discussed in Sections 2.1.1 and 2.1.2, respectively. These details are also applicable to precast panel to panel connections where the panels are made to act compositely with steel or prestressed concrete girders. To determine the moments and shears to design the connection reinforcement, the strip method may be used.

2.1.1. U-Bar Details

To improve the current joint detail of DBTs, one concept is to replace the current welded steel connectors with distributed U-bars, as shown in Figure 2.1.1, to provide moment transfer as well as shear transfer across the joint. The U-bar details are oriented vertically in the joint to provide two layers of reinforcement fabricated with a single rebar. The U-bars provide continuity of the deck reinforcement across the joint by lapping with the U-bars from the adjacent flanges. The 180° bend of the U-bar, embedded in the joint, provides mechanical anchorage to the detail necessary to minimize the required lap length. The extended reinforcement of the U-bar details is staggered (i.e., out of phase) with the adjacent lapped U-bar to facilitate constructability in the field. The stagger cannot be too large, or the transfer of forces across the joint would be difficult to achieve.

The U-bar details are designed to minimize deck thickness. This is accomplished by using a small bend diameter for the U-bar detail. The inside bend diameter that was used in the testing program was three times the diameter of the bar (i.e., $3d_b$), which resulted in an inside bend diameter of 1-7/8 in. for the No. 5 bars used in the study. Minimum bend diameters are established primarily for two reasons, feasibility of bending the reinforcement without breaking it and possible crushing of the concrete within the tight bend. To ensure that the reinforcement would not be broken while bending, two ductile reinforcing materials were used in the testing program, deformed wire reinforcement and stainless steel reinforcement in order to achieve these tight bend diameters, which are much smaller than those of the current AASHTO LRFD (2010) Specifications given in Article 5.10.2.3. As shown in Figure 2.1.1, a minimum depth of the top flange of DBTs of 6-1/8 in. using the U-bar detail with No. 5 bars can be achieved.

For precast deck panels, the researchers recommend a minimum panel thickness of 7-3/8 in. to accommodate both longitudinal and transverse joints in the precast panels containing orthogonal double layers of reinforcement. The increased thickness accommodates the orthogonal arrangements of U-bars with the inner layer oriented in the longitudinal direction, and the outer layer oriented in the transverse direction. The recommendation of orienting the outer layers of reinforcement in the transverse direction provides increased flexural capacity across the longitudinal joints. As the transverse joints are required to carry primarily tension or compression forces in the longitudinal direction due to the composite action of the precast panel with the girders, the reinforcement in that direction is

A-44

suggested to be located in the inner layer. It may be possible to use a single layer of reinforcement in that direction, in which case the depth of the precast panels can be further minimized.

The deck components in either the DBTs or precast deck panel systems would then be placed so that the rebar in the joint would have a specified overlap length and spacing. The overlap length is the distance between bearing surfaces of adjacent reinforcing bars and the spacing is the center to center distance of adjacent bars. The figure shows the bar spacing at 4.5 in.; however, this distance was further increased to 6 in. in the NCHRP 10-71 study, and the joint was still found to perform adequately. The joint would then be completed after the addition of transverse lacer bars and grout. The bearing surface of the U-bar is the inside of the bend, and the addition of transverse lacer bars tied to the inside of the bend adds confinement and increases the bearing resistance to the joint.

A-45

(a) Shear Key Detail

(b) Joint Reinforcement Detail
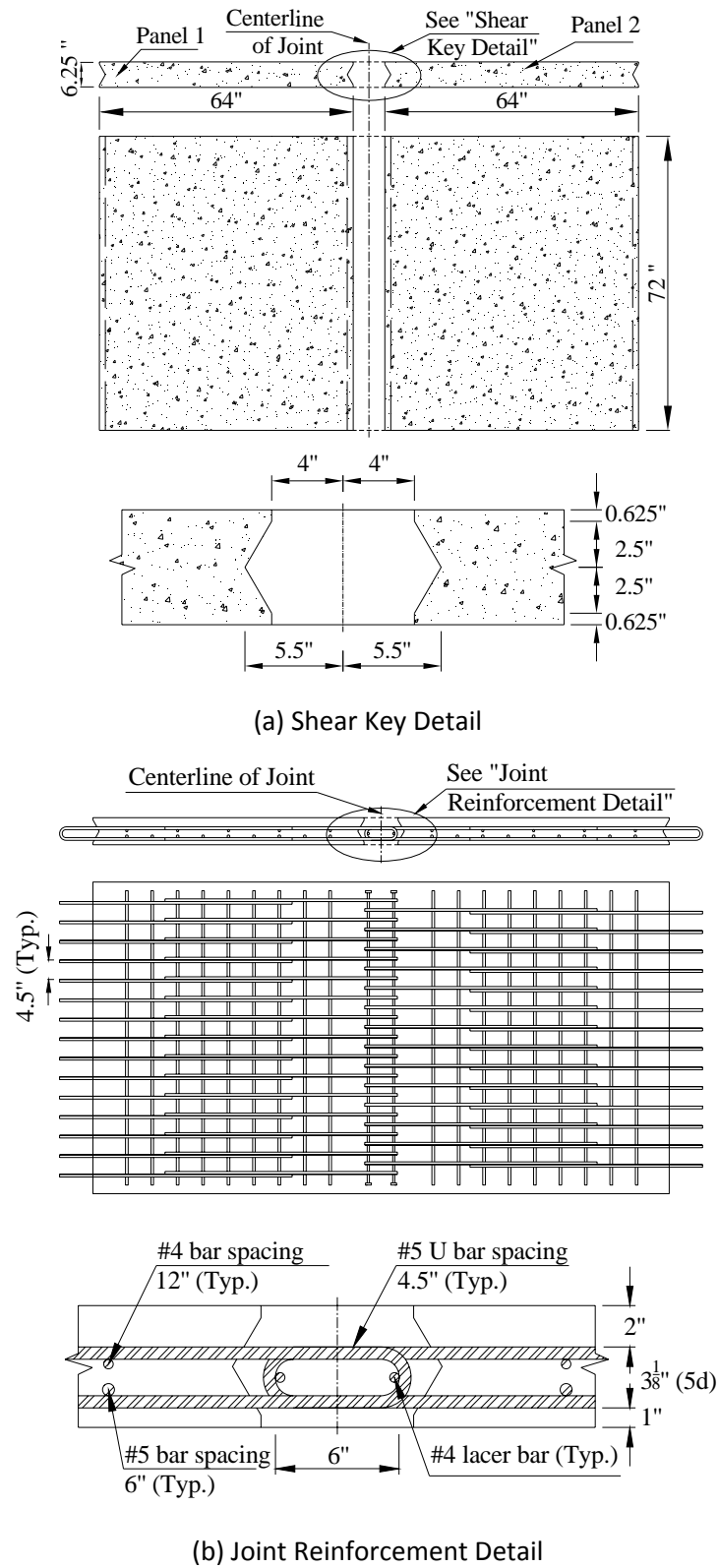
Figure 2.1.1: Longitudinal U-Bar joint details

A-46

The joint overlap length, which is the distance between the reinforcement bearing surfaces, was determined based on the expected development length of a U-bar. The ACI equation for determining the development length of a standard hook in tension was used to calculate the approximate development length of a U-bar. This equation does not directly apply to the U-bars that were used, because the U-bars do not meet the dimensional requirements for a standard hook, namely the $3d_b$ bend diameter used in the U-bar fabrication violates the minimum $6d_b$ bend diameter specified in ACI 318-08. Eq. 2.1.1 shows the ACI development length equation for a standard hook in tension.

$$l_{dh} = \left[\frac{.02 \Psi_e \lambda f_y}{\sqrt{f'_c}} \right] d_b \text{ (ACI 12.5.2)} \tag{2.1.1}$$

where l_{dh} represents the development length from the tail of the hook, in.; Ψ_e is the epoxy coating factor; λ is the lightweight concrete factor; f_y is the reinforcement yield strength; $\sqrt{(f'c)}$, the square root of the concrete compressive stress, is expressed in psi; and d_b is the diameter of the bar, in. The terms, Ψ_e and λ, were both set equal to one in Eq. 2.1.1, because the rebar that was used was not epoxy coated and the concrete was not lightweight. It should be noted that a number of states do not use epoxy-coated reinforcement in their decks, 4 of 38 states surveyed by Russell (2004) indicated that they do not specify epoxy-coated deck reinforcement. In addition, 14 of the 38 states surveyed, indicated that they specify a metallic coating for the deck reinforcement, and 7 of the 38 states indicated that they were beginning to use solid stainless steel. In order to minimize the joint width between the precast flanges or panels, it is desirable to avoid epoxy-coated reinforcement because that may require a longer lap length to develop the reinforcement. In addition, tighter bend diameters are feasible with stainless steel reinforcement than with ordinary mild reinforcement.

Using Eq. 2.1.1, the development length was calculated for a No. 5 bar, assuming a concrete compressive strength of 6.0 ksi and a steel yield strength of 75 ksi, because deformed wire reinforcement and stainless steel were materials used for this joint detail. The ACI 318-08 development length modification factor of 0.7 was used, because the specimens met the bar cover perimeters of having not less than 2.5 in. of side cover and not less than 2 in. of cover beyond the extension of the bar. The development length of a standard hook bar in tension for this situation was calculated to be 8.5 in. In the testing program, an overlap length of 6 in. was used for the U-bar detail, as shown in Figure 2.1.1. Where the overlap length is taken from the inside bend of the adjacent hooks. This would be 7.25 in. to the outside of the hooks, less than the 8.5 in. specified by ACI 318-08, but lacer bars were also used in the connection to enhance the mechanical anchorage.

The experiments in first phase of the NCHRP 10-71 study showed that the U-bar detail could develop adequate capacity with an overlap length of 6 in., a rebar spacing of 4.5 in., and two transverse lacer bars. In the second phase of the NCHPR 10-71 study, additional tests were conducted with varying overlap lengths, rebar spacings, and concrete strengths. Based on a comparison of tests with overlaps of 4.0 in. and 6 in., a minimum overlap length of 6 in. was recommended for the No. 5 bars. The size for the lacer bars is recommended to be the same as the top distributed reinforcement in the deck. Two lacer bars are required to be tied to the inside bend of the U-bars, one on each side, as shown in Fig 2.1.1.

A-47

2.1.2. Headed-Bar Details

As an alternative to the U-bar details, two layers of headed bars can be used to provide continuity of the top and bottom deck steel through the joint. The previous NCHRP 12-69 project explored the use of single large-headed bars to provide continuity across the joint (Li et al. 2010, Li et al. 2010a). In that project, Headed Reinforcement Corporation (HRC) provided the headed reinforcement, which consisted of a No. 5 bar with a standard 2.0 in. diameter circular friction welded head with a head thickness of 0.5 in. Large-headed bars such as these with the bearing area (A_{brg}) exceeding nine times the area of the bar (A_b), are assumed to be able to develop the bar force through bearing at the head. Bars with smaller heads, (e.g., $A_{brg}/A_b \geq$ 4) are assumed to be able to develop the force in the bar through a combination of mechanical anchorage and bond, where the development length for these bars is less than that required to develop a hooked bar (ACI 318-08). In the NCHRP 10-71 study, the headed reinforcement used was No. 5 bar with Lenton Terminator® bearing heads. The diameter of the head was 1.5 in., and the thickness of the head was 7/8 in., which gave A_{brg}/A_b of 4.76. The smaller head dimension was necessary in order to fit the two layers of reinforcement within the deck while minimizing the deck thickness. The large-headed bars in two layers would have resulted in a much thicker, uneconomical deck system.

Based on Li et al. (2010), headed bar details with varying overlap lengths, 2.5 in., 4 in. and 6 in., were tested and compared, and the lap length for the headed bar detail was also recommended to be 6.0 in. Compared to the headed bar details (Li et al. 2010), the U-bar detail created a less congested joint, which made it the easier to construct. The bearing heads of the two-layer headed bar detail require more space in a given rebar spacing, due to the larger diameter of the rebar heads. This would reduce construction tolerances and may therefore cause problems in placement of precast deck components. The U-bars can also be easily tied together to form a rebar cage, which would allow for easy construction in the precast yard when compared to the two layers of reinforcement of the headed bar detail.

For the case of the No. 5 headed bars, with the small head size, the overlap length is recommended to be 6.0 in., as shown in Figure 2.1.2. Consequently, the joint width is the same as that shown in Figure 2.1.1 for the U-bar detail.
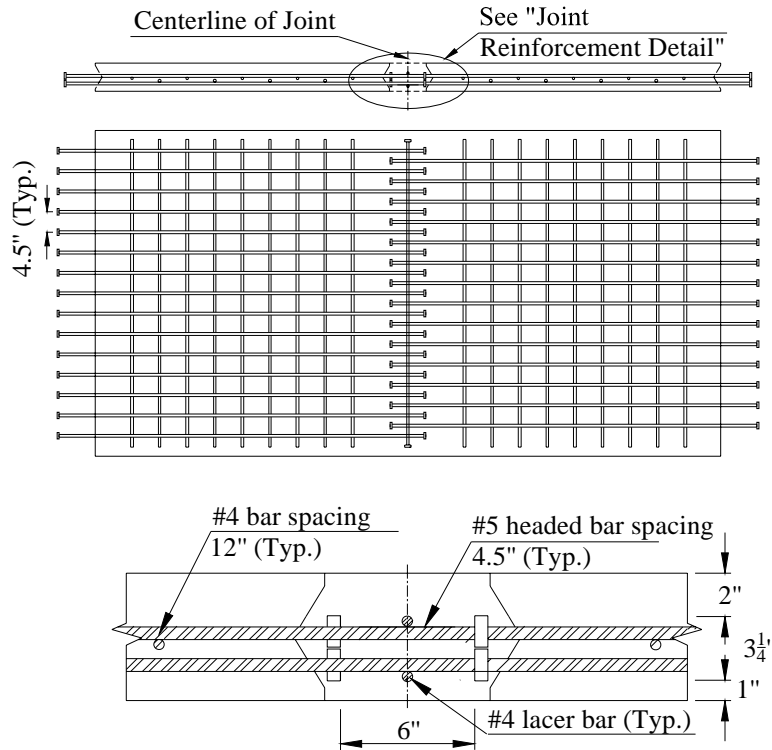
Joint Reinforcement Detail

Figure 2.1.2: Longitudinal Headed-Bar joint details

Based on these investigations, the following sections outline the proposed changes to the AASHTO LRFD (2010) specifications.

2.1.3. Minimum Bar Bend

To better address the tighter bend diameters required for the economical construction of bulb-tee flanged decks and precast deck panels, specifications suggested for modification include AASHTO (2010) Articles 5. 10.2.3 and C5.10.2.3.

AASHTO (2010) Article 5.10.2.3 **Minimum Bend Diameters**

> The diameter of a bar bend, measured on the inside of the bar, shall not be less than that specified in Table 5.10.2.3-1, unless otherwise noted.

A-49

Table 5.10.2.3-1 **Minimum Diameters of Bend.**

Bar Size and Use	Minimum Diameter
No. 3 through No. 5—General	$6.0\ d_b$[1]
No. 3 through No. 5—Stirrups and Ties	$4.0\ d_b$
	$6.0\ d_b$
No. 6 through No. 8—General	$8.0\ d_b$
No. 9, No. 10, and No. 11	$10.0\ d_b$
No. 14 and No. 18	

[1]For Grade 75 stainless steel and deformed wire reinforcement , the minimum bend diameter shall be taken as $3.0 d_b$ for use in longitudinal and transverse cast-in-place joints of precast deck and bulb-tee girder systems.

The inside diameter of bend for stirrups and ties in plain or deformed welded wire fabric shall not be less than $4.0 d_b$ for deformed wire larger than D6 and $2.0\ d_b$ for all other sizes. Bends with inside diameters of less than $8.0\ d_b$ shall not be located less than $4.0\ d_b$ form the nearest welded intersection.

C.5.10.2.3

The higher ductility of Grade 75 stainless steel and deformed wire reinforcement enables the achievement of tighter bend diameters for these types of reinforcement. For No. 5 and smaller bars, the minimum bend diameter of $3\ d_b$ has shown to be effective.

Note that the CRSI Manual currently limits the minimum bend diameters to those given in AASHTO Table 5.10.2.3-1 and will require a change working in conjunction with AASHTO to facilitate the use of tighter bend diameters in state and federal projects. It should be cautioned that higher strength carbon reinforcement with strengths in the 80 to 100ksi range, may not have the elongation required to allow for tighter bends.

2.1.4. Minimum Depth and Cover

To economically construct bulb-tee flanged decks and precast deck panels, the deck thickness should be minimized which is achievable through the use of U-bars made of No. 5 bars and smaller with tight minimum bend diameters (i.e., 3 d_b) or through the use of two layers of headed reinforcement. Specifications suggested for modification with regard to the deck thickness include AASHTO (2010) Article 9.7.1.1 and C9.7.1.1. Specifications to be modified to address cover issues include AASHTO (2010) Article 5.12.3.

AASHTO (2010) Article 9.7.1.1 **Minimum Depth and Cover**

Unless approved by the Owner, the depth of a concrete deck, excluding any provision for grinding, grooving, and sacrificial surface, should not be less than 7.0 in., except in the case of precast flanges for bulb-tee girders used as the riding surface or in the case of precast deck panels. The depth of a precast concrete deck in these circumstances should not be less than 6-1/8 in.

Minimum cover shall be in accordance with the provisions of Article 5.12.3
C.9.7.1.1

For slabs of depth less than 1/20 of the design span consideration should be given to prestressing in the direction of that span in order to control cracking.

Construction tolerances become a concern for thin decks; however, the high quality control achieved in precast plants and the crack control achieved by prestressing can enable the fabrication of decks with smaller minimum thicknesses. The thickness of the decks should be controlled by considerations of minimum cover and either (a) minimum bend diameters for U-bars, or (b) allowances for headed bar dimensions, where used as top and bottom deck reinforcement. In the case of precast panels that may have both longitudinal and transverse joints with double layers of reinforcement, the minimum deck thickness will increase to accommodate the required clearances.

Minimum cover requirements…

The only proposed changes to the cover requirements in AASHTO LRFD (2010) Article 5.12.3 are to address reduced cover requirements for stainless steel reinforcement. In the case of epoxy-coated reinforcement (which was not included in this investigation), the minimum cover to the main bars is 1.0 in. The cover should be at least 2.5 in. for unprotected main reinforcing steel if exposed to deicing salts. In areas where deicing salts are not used, this cover can be reduced to 2.0 in. In the case of cast-in-place slabs, the bottom cover for bars up to No. 11 is a minimum of 1 in. In the NCHRP 10-71 study, uncoated reinforcement was used for the U-bar and headed-bar details with minimum concrete covers of 2 in. top and 1 in. bottom. This would correspond to an exterior exposure environment where the deck would not be exposed to deicing salts. Larger covers, and consequently thicker decks, would be required in environments where the deck could be exposed to deicing salts. Where stainless steel reinforcement is used, the smaller cover requirements allowed for epoxy-coated reinforcement should be applicable.

A-51

If the unprotected reinforcement is replaced by epoxy-coated reinforcement, wider joints may be required to accommodate increased development lengths of epoxy-coated reinforcement.

AASHTO (2010) Article 5.12.3 **Concrete Cover**

Cover for unprotected prestressing and reinforcing steel….

.

.

.

Minimum cover to main bars, including <u>stainless steel reinforcement or</u> bars protected by epoxy coating, shall be 1.0 in.

2.1.5. Live Load Distribution factors for Moment and Shear

There are two basic approaches to computing the live load distribution factor in accordance with the AASHTO LRFD (2010) Specifications: the approximate method and the refined method of analysis. The approximate method is treated in Article 4.6.2, including specifics on conditions of its use, which is the most typical approach used in engineering practice. DBT bridges are designated as Bridge Type "j" in which the supporting components are precast concrete tee sections with shear keys, with or without transverse post-tensioning, and the deck type is integral concrete. Separate treatments are given for moment and shear, for interior and exterior beams, for single lane loaded and multiple lanes loaded cases, and for "sufficiently connected" or "not sufficiently connected" cases. The conventional DBT construction with welded shear connections is considered "not sufficiently connected". Construction with the proposed alternate longitudinal joint with spliced U-bars is considered "sufficiently connected." Further detail is provided below as the provisions also relate to precast panel systems.

AASHTO (2010) Table 4.6.2.2.1-1 Common Deck Superstructures Covered in Articles 4.6.2.2.2 and 4.6.2.2.3 identify typical cross sections of deck superstructures. There are three cases identified in that figure that address the precast concrete decks systems covered in NCHRP 10-71. They are: Case (a) Steel beam with cast-in-place concrete slab, precast concrete slab, steel grid, glued/spiked panels and stressed wood deck; Case (j) Precast Concrete Tee Section with Shear Keys and with or without Transverse Post-Tensioning with integral concrete deck; and Case (k) Precast Concrete I or Bulb-Tee Sections with cast-in-place concrete or precast concrete deck. Cases (a) and (k) cover precast panels on steel or prestressed concrete girders, and Case (j) covers the decked bulb-tee system.

The AASHTO Articles that address the live load distribution factors for moment in interior beams (Table 4.6.2.2.2b-1) and exterior beams (Table 4.6.2.2.2d-1), respectively, and those that address the live load distribution factors for shear in interior beams (Table 4.6.2.3a-1)and exterior beams (Table 4.6.2.2.3b-1), respectively, refer to the (a) through (l) systems identified in AASHTO (2010) Table 4.6.2.2.1-1. The precast deck panels and decked bulb tee flanges connected with the U-bar details or two-layer headed

A-52

bar details investigated through NCHRP 10-71 provide both shear and moment transfer across the joints to emulate cast-in-place construction. Consequently, these systems described as (a), (j) and (k), can be considered "sufficiently connected to act as a unit" in determining the appropriate distribution factors to be applied. No changes need to be made to the AASHTO specifications to address live load distribution factors for these systems.

It should be noted that NCHRP 10-71 addressed the precast panel-to-panel connections, but did not include the investigation of the panel-to-girder connections required for composite design. The latter details have been investigated and reported in other studies including NCHRP 12-41 *Rapid Replacement of Bridge Decks* (Tadros et al. 2002).

2.1.6. Precast Deck Slabs on Girders with Longitudinal and Transverse Joints

To better address precast deck slabs that provide both shear and moment transfer across the joints, modifications are required for AASHTO (2010) Article 9.7.5 and its subsections.

AASHTO (2010) Article 9.7.5 **Precast Deck Slabs on Girders**

9.7.5.1 General

Both reinforced and prestressed precast concrete slab panels may be used. The depth of the slab excluding any provision for grinding, grooving, and sacrificial surface, shall not be less than 7.0 in. For precast panels designed with shear and flexural continuity in two directions (transversely and longitudinally joined panels) using U-bar details, the depth of the slab shall not be less than 7-3/8 in., and shall include consideration for the required minimum bar bend diameter of and the provision of two layers of reinforcement in both directions, in addition to the cover requirements of Articles 5.12.3 and 9.7.1.1.

9.7.5.2 Transversely Joined Precast Decks

9.7.5.2.1 Flexurally Discontinuous Decks

Flexurally discontinuous decks made from precast panels and joined together by shear keys may be used. The design of the shear key and the grout used in the key shall be approved by the Owner.

9.7.5.2.2 Flexurally Continuous Decks Provided by Cast-in-Place Connections

Flexurally continuous decks made from precast panels and joined together by shear keys with U-bar or double layer headed-bar details to provide continuity may be used as identified for the connection of decked-bulb-tee flange connections in Article 9.7.7. The design of the shear key and the grout used in the key shall be approved by the Owner.

9.7.5.3 *9.7.5.2.3* Longitudinally Post-Tensioned Precast Decks

The precast components may be placed on beams and joined together by longitudinal post-tensioning. The minimum average effective prestress shall not be less than 0.25 ksi.

The transverse joint between the components and the block-outs at the coupling of post-tensioning ducts shall be specified to be filled with a nonshrink grout having a minimum compressive strength of 5.0 ksi at 24 hours.

Block-outs shall be provided in the slab around the shear connectors and shall be filled with the same grout upon completion of post-tensioning.

9.7.5.3 Longitudinally Joined Precast Decks

9.7.5.3.1 Flexurally Continuous Decks Provided by Cast-in-Place Connections

Flexurally continuous decks made from precast panels and joined together by shear keys with reinforced connection details to provide continuity may be used as identified for the connection of decked-bulb-tee flange connections in Article 9.7.7. Depending on whether flexure needs to be transmitted through the section or pure tension or compression as required for flexural continuity of a composite section in the longitudinal direction, double layers or single layers of reinforcement should be used. To achieve flexural continuity where double layers of reinforcement are required, U-bar or double layer headed-bar details shall be used. To achieve continuity where pure tension is required, as would be the case at a joint over a support, a single layer of headed-bar details may be used. The design of the shear key and the grout used in the key shall be approved by the Owner. The provisions of Article 9.7.4.3.4 may be applicable for the design of the bedding.

2.1.7. Longitudinal and Transverse Joints between Decked Bulb Tees

To address the design of decked-bulb-tee flanges that are detailed to provide both shear and moment transfer across the joints, new specifications are proposed to be added to AASHTO (2010) Article 9.7 following the provisions for "Deck Slabs in Segmental Construction" and its subsections.

AASHTO (2010) Article 9.7.7 **Decked-Bulb-Tee Decks**

9.7.7.1 General

The depth of the precast decked-bulb-tee flange to be used as a driving surface in members with longitudinal joints detailed to provide shear and flexure continuity, excluding any provision for grinding, grooving, and sacrificial surface, shall not be less than 6-1/8 in. For precast decked-bulb-tee flange connections designed with shear and flexural continuity in two directions (transversely and longitudinally joined flanges) using U-bar details, the depth of the flange shall include consideration for the required minimum bar bend diameter of and the provision of two layers of reinforcement in both directions, in addition to the cover requirements of Articles 5.12.3 and 9.7.1.1.

9.7.7.2 Transversely Joined Decked Bulb Tees made Flexurally Continuous with Cast-in-Place Connections

Flexurally continuous decks made from decked bulb tees joined together by shear keys with U-bar or double layer headed-bar details to provide continuity may be used. The design of the shear key and the grout used in the key shall be approved by the Owner. The provisions of Article 9.7.4.3.4 may be applicable for the design of the bedding.

9.7.7.2.1 Required Concrete Compressive Strength

For overnight and 7-day cure, the minimum specified concrete compressive strength shall be 6000psi.

9.7.7.2.2 Reinforcement Details

Where two layers of reinforcement are required, continuity shall be provided by U-bar details or two layers of headed-bar details. To achieve continuity where pure tension is required, as would be the case at a joint over a support, a single layer of headed-bar details may be used.

The U-bar details shall be fabricated with No. 5 Grade 75 or less uncoated deformed wire or stainless steel with a minimum bend diameter as prescribed in Article 5.10.2.3.

The No. 5 bars shall have a minimum overlap length (measured from inside of bearing surfaces of the bend or head) of 6 in.

The spacing of the connection reinforcement extending from the faces of adjacent flanges shall not exceed 6 in.

Lacer bars shall be provided in the connection tied to the inside bend in the case of the U-bar details.

Where the joint reinforcement is made with epoxy-coated reinforcement, the overlap length should be increased to account for the increased development length associated with epoxy-coated reinforcement.

9.7.7.2.3 Minimum Joint Width

To accommodate the required uncoated deformed wire or stainless steel reinforcement details described in Article 9.7.5.2.2 requires a minimum joint width of 8.0 in.

Where the joint reinforcement is made with epoxy-coated reinforcement, the minimum joint width should be increased to account for the increased overlap length associated with the epoxy-coated reinforcement.

9.7.7.3 Longitudinally Joined Decked Bulb Tees made Flexurally Continuous with Cast-in-Place Connections

Flexurally continuous decks made from decked bulb tees and joined together by shear keys with reinforced connection details to provide continuity may be used. Depending on whether flexure needs to be transmitted through the deck section or pure tension or compression in the longitudinal direction, double layers or single layers of reinforcement should be used in the deck joint. To achieve continuity where double layers of reinforcement are required, U-bar or double layer headed-bar details shall be used. To achieve continuity where pure tension is required, as would be the case at a joint over a support, a single layer of headed-bar details may be used. The design of the shear key and the grout used in the key shall be approved by the Owner. The provisions of Article 9.7.4.3.4 may be applicable for the design of the bedding.

The detailing of the joint shall be in accordance with the transversely joined decked-bulb-tee flange connections given in Articles 9.7.7.2.1 through 9.7.7.2.3.

C.9.7.7

The provisions contained herein are provided for the design of decked-bulb-tee flanges that emulate cast-in-place deck construction. Double layers of reinforcement are provided across the joint provide moment transfer across the joint.

C.9.7.7.2.1

The minimum concrete strengths facilitate the speed of fabrication of the system.

C.9.7.7.2.2

The specific detailing requirements for the minimum bar bend of the U-bar details require ductile reinforcement, thereby the specification requires deformed wire reinforcement

A-56

or stainless steel of Grade 75 or lower. Higher grades of steel or other types of reinforcement may not achieve the minimum bend diameters.

The required overlap length is based on the assumption of No. 5 uncoated reinforcement. Larger size bars or coated reinforcement would require increased overlap lengths, where the overlap length is defined as the length between the bearing surfaces of the bars (180° hooks) protruding from adjacent panels.

The lacer bars are required to enhance the development of the bars by improving the concrete confinement and bearing.

The maximum spacing of 6 in. should not be exceeded in order to ensure adequate force transfer to the adjacent bars across the joint.

C. 9.7.7.2.3

The joint width must be able to accommodate the clearances required for the overlap length, diameter of the bar at each end across the width of the connection in the case of the U-bar detail or the thickness of the head at each across the width of the connection in the case of the headed bar detail, and sufficient clearance for casting the concrete around the detail.

2.2.   Construction Specification Recommendations

This section describes the details of the construction joint, its preparation, and the material requirements developed in the NCHRP 10-71 project for cast-in-place connections between precast deck panels and flanges of decked bulb tees. As shown in Figure 2.1.1 above, the minimum joint width for connections is 8.0 in. This is based on using No. 5 uncoated reinforcement in the joints with an overlap length of 6 in. The use of larger bars or epoxy-coated reinforcement would require a larger joint width. Figure 2.1.1 also shows the shape of the shear key recommended by Stanton and Mattock (1986). Foam wedges can be used to form the configuration of the shear key at the vertical edge of the panel, as shown in Figure 2.2.1.

Figure 2.2.1: Foam wedges for the configuration of the shear key

A-57

The surfaces of the shear key should be thoroughly cleaned to remove all contaminants that can interfere with adhesion and to develop a surface roughness to promote a mechanical bond between the grout and base concrete. Methods of surface preparation include chemical cleaning or sand blasting. Sandblasting using Black Beauty 2050 sand was chosen for sandblasting to prepare the surfaces of the test specimens in the testing program. The profiles of the surface before and after sandblasting are shown in Figure 2.2.2 (Li et al. 2010a) in association with project NCHRP 12-69. Typically, sand blasting the joint surfaces would be accomplished in the fabrication plant prior to hauling. During the sandblasting procedure, the contractor was asked not to sandblast coated bars in association with the NCHRP 12-69 research effort; no special protection was provided.

(a): Before Sandblasting   *(b): After Sandblasting*
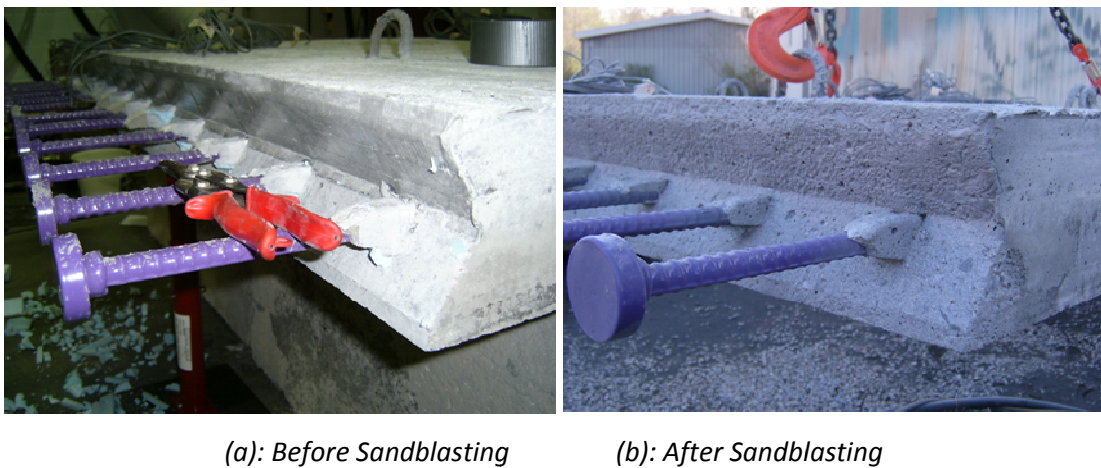
Figure 2.2.2: Profile of joint surface before and after sandblasting

Because of the width of the joint, formwork is required to support the joint grout. The longitudinal joint, which is filled with closure-pour materials connecting adjacent precast deck panels or the top flange of the adjacent DBT girders, is considered to be the structural element of the bridge deck. Therefore, it is important for the selected closure-pour material to reach its design compressive strength in a relatively short time for the purpose of accelerated bridge construction. To quantify "relatively short time," it is proposed to use the terminology "overnight cure" and "7-day cure" closure pour materials.

The performance criteria for (i) overnight cure and (ii) 7-day cure including the compressive strength are shown in Tables 2.2.1 and 2.2.2 below. The criteria listed in Table 2.2.2 were based on those developed by Tepke and Tikalsky (2007).

Table 2.2.1: Proposed performance criteria of closure pour materials

Performance Characteristic	Test Method	Performance Criteria		
Compressive Strength (CS), ksi	ASTM C39 modified	6.0≤CS @ 8 hours (overnight cure) @ 7 days (7-day cure)		
Shrinkage[a] (S), (Crack age, days)	AASHTO PP34 modified	20<S		
Bond Strength (BS), psi	ASTM C882 modified	300<BS		
Chloride Penetration[b] (ChP), (Depth for Percent Chloride of 0.2% by mass of cement after 90-day ponding, in)	ASTM C1543 modified	ChP<1.5		
Freezing-and-thawing Durability (F/T), (relative modulus after 300 cycles)	ASTM C666 Procedure A modified	Grade[c] 1 70%≤F/T	Grade 2 80%≤F/T	Grade 3 90%≤F/T

a: No S criterion need be specified if the closure pour material is not exposed to moisture, chloride salts or soluble sulfate environments.

b: No ChP criterion need be specified if the closure pour material is not exposed to chloride salts or soluble sulfate environments.

c: Grades are defined in Table 2.2.2.

Table 2.2.2: Application of closure pour material grades for freezing-and-thawing durability

Freezing-and-thawing Durability (F/T)	Is the concrete exposed to freezing-and-thawing environments?	Yes	Is the member exposed to deicing salts?	Yes	Will the member be saturated during freezing?	Yes. Specify F/T-Grade 3
						No. Specify F/T-Grade 2
				No. Specify F/T- Grade 1		
	No. F/T grade should not be specified.					

The candidate overnight cure and 7-day cure materials listed in Tables 2.2.3 and 2.2.4, respectively, were selected for further investigation in the NCHRP 10-71 project after a preliminary selection from a broader set of mixes based on strength tests and prediction models as discussed by Zhu and Ma (2008). These materials were subjected to a battery of tests to investigate their performance criteria relative to those outlined in Tables 2.2.1 and 2.2.2. Of the several grout materials investigated for the overnight cure, two grout materials, SET 45 HW (SET) and EUCO-SPEED MP (EUCO), were selected based on

comparison of their performance in terms of compressive strength and flow and workability of both neat and extended grouts. Both of these grouts were found to perform satisfactorily relative to the performance criteria. For the 7-day cure material, high-performance concrete (HPC) "Mix 1" and RSLP 2 "Mix 2" were selected for further investigation. Of these, HPC "Mix 1" was selected as the best performing mix. The RSLP 2 "Mix 2" did not perform satisfactorily with regard to the ponding and freeze-thaw tests.

The two grout materials were magnesium phosphate-based materials that can be used with a 60% extension of pea gravel. A thoroughly washed and dried uniform-sized sound 0.25 in. - 0.5 in. round pea gravel was used to extend the grouts. The pea gravel was tested with 10% HCL to confirm that it was not calcareous. The compressive strengths of the grout SET and EUCO, tested with 60% extension, reached at least 5670 psi compressive strength within one day. For grout SET, the initial setting time and final setting time were 15-20 minutes and 45-60 minutes, respectively. For grout EUCO, the initial setting time and final setting time were 6-10 minutes and 15-20 minutes, respectively. The two grouts were air cured for eight hours. The 7-day cure materials were cured for 7 days by both the membrane-forming compound method and the water method with burlap.

Table 2.2.3: Candidate overnight cure materials and mixing information

Product Name	Mixing Quantities per 50-lb, Bag				
	Initial Water, pints	Additional Water, pints	Aggregate Extension, % by weight	Aggregate Extension, lb	Yield Volume, cu. ft.
EUCO-SPEED MP	3.10	0.50	0	0	0.42
Set® 45 HW	3.25	0.50	0	0	0.39

Table 2.2.4: Candidate 7-day cure materials mix proportions

MIX NUMBER	HPC Mix 1	RSLP Mix 2
W/CM Ratio	0.31	0.40
Cement Type	I	CTS RSLP
Cement Quantity, lb/yd^3	750	658
Fly Ash Type	C	
Fly Ash Type Quantity, lb/yd^3	75	
Fine Aggregate, lb/yd^3	1400	1695
Coarse Aggregate	#8	#8
Coarse Aggregate Quantity, lb/yd^3	1400	1454
Water, lb/yd^3	255	263
Air Entrainment, fl oz/yd^3	5	
Water reducer, fl oz/yd^3	30	
High-Range Water Reducer, fl oz/yd^3	135	

Grouts used as closure pour materials for the precast bridge deck system with CIP connections, like cement-based grout, non-shrink cement grout, epoxy mortar grout, magnesium ammonium phosphate (MAP) based grout, etc., should be added in AASHTO LRFD Construction Specifications Article 8.2.4. Grouts for closure pour materials shall be selected based on the performance criteria in Article. 8.4. In Article 8.4.1.1, the performance criteria for selecting durable closure pour materials listed in Tables 2.2.1 and 2.2.2 should be provided.

A-61

2.2.1. Classes of Concrete

To enable the use of overnight cure grout materials, grouts for closure pour materials should be added to AASHTO Construction Specification (2009) in Article 8.2.4, and the title of 8.2 should be modified.

AASHTO (2009) Article 8.2 CLASSES OF CONCRETE AND GROUT

AASHTO (2009) Article **8.2.4 Grouts for overnight cure**

> Grouts used as closure pour materials for the precast bridge deck system with CIP connections, like cement-based grout, non-shrink cement grout, epoxy mortar grout, magnesium ammonium phosphate (MAP) based grout shall conform to the requirements specified in the contract documents and shall satisfy the special performance requirements outlined in 8.4.1.1.

2.2.2. Performance Criteria

To ensure the satisfactory performance of closure pour materials, the performance requirements listed in Tables 2.2.1 and 2.2.2, above, should be added to Article 8.4.1.1 in the AASHTO Construction Specification (2009).

AASHTO (2009) Article **8.4.1.1 Responsibility and Criteria**

> The Contractor shall design and be responsible for the performance of all concrete and grout mixes used in structures. The mix proportions selected shall produce concrete that is sufficiently workable and finishable for all uses intended and shall conform to the requirements in Table 8.2.2-1 and all other requirements of this Section.
> For normal-weight…
>
> The mix design shall be based on the specified properties….that complies with the specified concrete properties.
>
> Overnight and 7-day closure pour materials for use in longitudinal and transverse joints between decked bulb tees and precast panels to emulate cast-in-place construction for moment and shear transfer shall also comply with the performance criteria outlined in Tables 8.2.2-2 and 8.2.2-3.

[Note Table 8.2.2.-2 corresponds to Table 2.2.1 above, and Table 8.2.2.-3 corresponds to Table 2.2.2 above.]

C.8.4.1.1

Closure pour materials for use in cast-in-place connections between precast deck panels and flanges of decked bulb tees to be used as the driving surface in bridge decks are required to achieve performance requirements at early ages (overnight or 7-day) to ensure adequate performance of these systems throughout their service life. The performance characteristics evaluated include compressive strength, shrinkage, chloride penetration, freezing-and-thawing durability and bond strength. Careful attention should be paid to appropriate curing of these materials.

A-63

References for Longitudinal and Transverse Joints between Decked Bulb Tees (DBTs) and Precast Panels

AASHTO (2010), *AASHTO LRFD Bridge Design Specifications,* 5th edition, Washington D.C.

ACI 318-08. *Building Code Requirements for Structural Concrete (ACI318-08) and Commentary (ACIR-08).* Farmington Hills, MI. 2008.

Li, L., Ma, Z., Griffey, M. E., and Oesterle, R. G., "Improved Longitudinal Joint Details in Decked Bulb Tees for Accelerated Bridge Construction: Concept Development," ASCE Journal of Bridge Engineering, Vol. 15, No. 3, 2010.

Li, L., Ma, Z., and Oesterle, R. G., "Improved Longitudinal Joint Details in Decked Bulb Tees for Accelerated Bridge Construction: Fatigue Evaluation," ASCE Journal of Bridge Engineering, DOI: 10.1061/(ASCE)BE.1943-5592.0000097, 2010a.

Ma, Z., Chaudhury, S., Millam, J. L., Hulsey, J. L., "Field Test and 3D FE Modeling of Decked Bulb-Tee Bridges" ASCE Journal of Bridge Engineering, 12(3), 306-314, 2007.

Russell, H. G., "Concrete Bridge Deck Performance: *A Synthesis of Highway Practice,*" NCHRP Report 333, 2004.

Stanton, J., and Mattock, A.H. , "Load distribution and connection design for precast stemmed multibeam bridge superstructures" NCHRP Report 287, 1986.

Tadros, M. K., Badie, S. S., and Kamel, M. R., Girder/Deck Connection for Rapid Removal of Bridge Decks, PCI Journal, Vol. 47, No. 3, May-June, 2002, pp. 58-69.

Tepke, D. G. and Tikalsky, P. J. (2007), "Best Engineering Practices Guide for Bridge Deck Durability Report" February 24.

Zhu, P. and Ma, Z**.,** "Selection of Closure Pour Materials for CIP Connection of the Precast Bridge Deck Systems," Proceedings of the National Concrete Bridge Conference, October 2008, Orlando, Florida.

Appendix B

NCHRP 10-71 Design Examples

Foreword

The NCHRP 10-71 study involved the development of design recommendations and details for *Cast-in-Place Concrete Connections for Precast Deck Systems*. The project covered two very different systems: (1) the precast composite slab-span system (PCSSS), which is an entire bridge system, and (2) transverse and longitudinal cast-in-place connection concepts between the flanges of precast decked bulb-Ts and full-depth precast deck panels on girders. In the case of the longitudinal connections, flexure and flexure-shear are to be transferred across the joint. In the case of the transverse joints, tension or compression is to be transferred across the joint depending upon the location of the joint along the span. The most critical location for the transverse connection would be at a pier in a continuous system, where the connection would be required to transmit tension, equilibrated by compression in the girder.

The five design examples presented in this appendix are separated according to the connection concepts, and the level of detail and complexity in the examples is commensurate with the type of connection concept. The first two examples represent a 50 ft. simply-supported PCSSS bridge (Example 1) and a 40-50-40 ft. three-span continuous PCSSS bridge (Example 2). Because these examples cover the design of complete systems, they have a significant level of detail. The latter three examples provide guidance on the detailing of longitudinal and transverse connection concepts. Example 3 details the design of a longitudinal joint between decked bulb-T members, while the design of a transverse joint over the piers of a continuous bulb-T girder bridge that incorporates full-depth deck panels is presented in Example 4. Finally, Example 5 illustrates the longitudinal connection between two full-depth deck panels. The connection in the latter example is required where the width of the bridge exceeds the practical span of a single full-depth deck panel. Because Examples 3 through 5 cover the longitudinal (flexure or flexure-shear) or transverse joints (tension) that transfer flexure, flexure-shear, or tension, the level of detail In the examples is restricted to the detailing of the connections themselves, rather than the entire bridge systems.

Each of the five examples illustrates the use of the recommendations from the design guide provided in Appendix A.

Example Problem 1

1.1 Introduction

This example covers the design of the primary load-carrying superstructure elements of a precast composite slab-span system (PCSSS) bridge. The structural system is single span, simple-span beam with a 50' design span. The steps required to design a representative composite panel are illustrated. The design is generally carried out in accordance with the *AASHTO LRFD Bridge Design Specifications,* 5th Edition, plus interim revisions through 2010.

1.2 Materials, Geometry, Loads and Load Factors

Units:

$kcf := kip \cdot ft^{-3}$ Defined unit: kips per cubic foot

$ksf := kip \cdot ft^{-2}$ Defined unt: kips per square foot

Materials:

Concrete:

$f'_c := 7.0 \cdot ksi$	Strength of beam concrete at 28 days
$f'_{ci} := 5.5 \cdot ksi$	Strength of beam concrete at transfer of prestressing force
$w_c := 0.150 \cdot kcf$	Density of beam concrete
$f'_{ct} := 4.0 \cdot ksi$	Strength of CIP concrete at 28 days
$w_{ct} := 0.15 \cdot kcf$	Density of CIP concrete
$H := 70$	Average ambient relative humidity
$\alpha := 0.000006 \, /^oF$	Coefficient of thermal expansion

Strand:

$A_{strand} := 0.217 \cdot in^2$	Area of one prestressing strand.
$d_b := 0.6 \cdot in$	Nominal diameter of prestressed strand.
$f_{pu} := 270 \cdot ksi$	Tensile strength of prestressing steel
$E_p := 28500 \cdot ksi$	Modulus of elasticity of prestressing steel
$f_{py} := 0.9 \cdot f_{pu}$	Yield strength of prestressing steel
$Pull := 0.75$	Pull of strands expressed as a fraction of f_{pu}
$t := 18 \cdot hr$	Time from tensioning to detensioning of strands

Rebar:

$f_y := 60 \cdot ksi$	Yield stress of ordinary rebar
$E_s := 29000 \cdot ksi$	Modulus of elasticity of non-prestressed reinforcement

Geometry:

Beam:

$Section := \text{"IT"}$	Precast section name
$h := 18.0 \cdot in$	Height of precast
$A := 936.0 \cdot in^2$	Gross area of precast section
$I := 27120 \cdot in^4$	Gross moment of inertia of precast cross section about centroidal x-x axis
$y_b := 8.42 \cdot in$	Center of gravity of gross precast cross section
$b_f := 72.0 \cdot in$	Width of bottom flange of precast section
$t_{flg} := 3.00 \cdot in$	Effective thickness of bottom flange

B1-1

	$b_v := 72.00 \cdot in$	Shear width of precast section (web and longitudinal trough width)
	$A_c := 450 \cdot in^2$	Area of concrete on flexural tension side of member (see LRFD B5.2-3)
	$VS_b := 5.2 \cdot in$	Volume to surface ratio of precast section
	$VS_d := 6.0 \cdot in$	Volume to surface ratio of CIP slab
Slab:	$t_{slab} := 6.00 \cdot in$	Thickness of CIP slab above precast beam
	$t_h := 15.00 \cdot in$	Thickness of CIP region between precast beams
	$b_h := 24.00 \cdot in$	Width of CIP region between precast units.
	$t_{ws} := 0.0 \cdot in$	Thickness of portion of CIP slab assumed to be wear
Span:	$L_{ovr} := 50.0 \cdot ft$	Overall length of precast section
	$L_{des} := 49.0 \cdot ft$	Design span of precast section
	$L_{pad} := 12 \cdot in$	Length of bearing pad
Bridge:	$S := 6.00 \cdot ft$	Beam spacing
	$N_g := 8$	Number of precast sections in bridge cross section
	$Width_{overall} := 47.5 \cdot ft$	Overall width of bridge
	$Width_{ctc} := 44.0 \cdot ft$	Curb to curb width of bridge
	$N_l := 2$	Number of lanes

Loads:

Dead:	$N_{barriers} := 2$	Number of barriers
	$w_{barrier} := 0.300 \cdot klf$	Weight of single barrier
	$w_{fws} := 0.023 \cdot ksf$	Weight of future wearing surface allowance
Live:	HL-93	Notional live load per LRFD Specs
	$w_{lane} := 0.64 \cdot klf$	Design lane load
	$w_{const} := 10 \cdot psf$	Construction live load

Construction Timing:

	$t_{transfer} := 1.00 \cdot day$	Time from release tensioning of strands to release of prestress
	$t_{deck} := 90 \cdot day$	Time to placement of superimposed dead load (SDL)
	$t_{final} := 20000 \cdot day$	Time final

Load & Resistance Factors:

	ϕ_f	Resistance factor for flexure
	$\phi_v := 0.90$	Resistance factor for shear
	$DLA := 0.33$	Dynamic load allowance (LRFD 3.6.2.1-1)

1.3 Plan, Elevation, and Typical Section
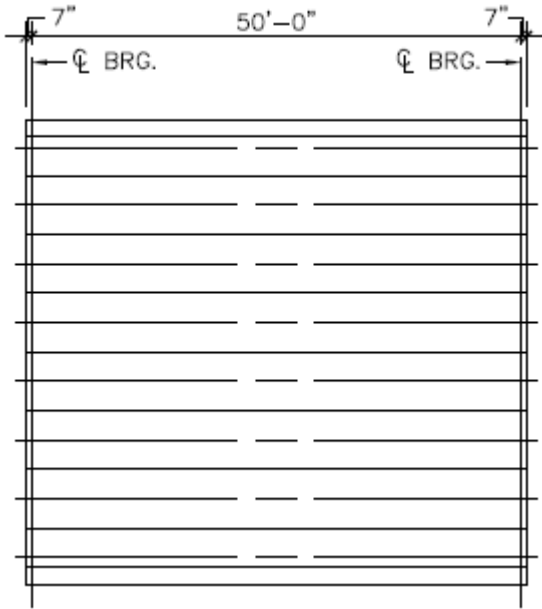
Figure 1: General plan of bridge.
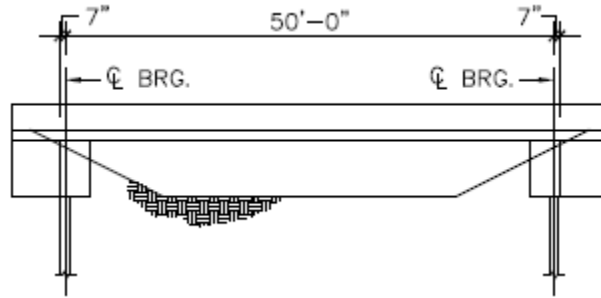
Figure 2: General elevation of bridge.
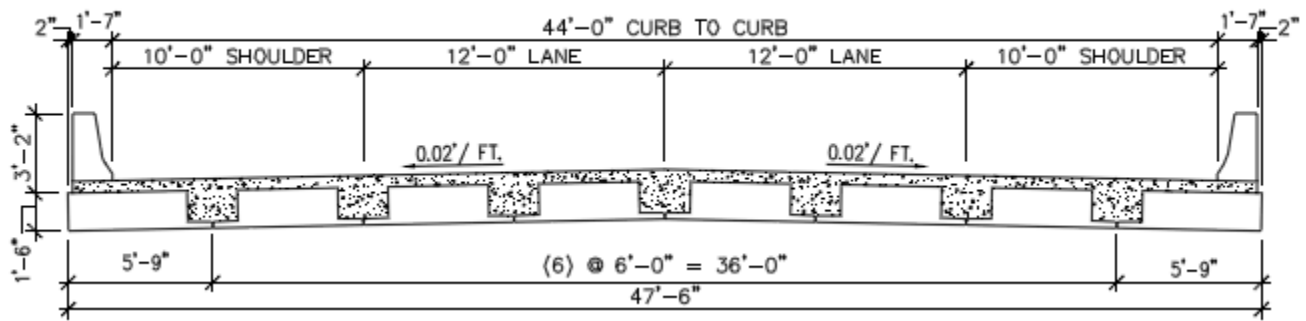
Figure 3: Typical cross section of bridge.

Strand Pattern:

No, Strands   Elevation (in)

$$\text{Pat\_n} := \begin{pmatrix} 0 \\ 0 \\ 12 \\ 12 \end{pmatrix} \qquad \text{Pat\_h} := \begin{pmatrix} 16 \\ 6 \\ 4 \\ 2 \end{pmatrix} \cdot \text{in}$$

B1-3

1.4 Section Properties

Figure 4: Precast slab dimensions.
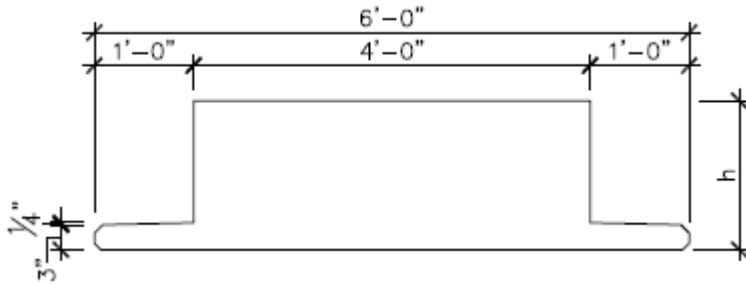
Note: Flange assumed to be a constant thickness of 3" for computation of section properties.

Non-Composite Section Properties:

$$S_b := \frac{I}{y_b} \qquad\qquad S_b = 3220.9 \cdot in^3$$

$$y_t := h - y_b \qquad S_t := \frac{I}{y_t} \qquad S_t = 2830.9 \cdot in^3$$

Effective Width: (LRFD 4.6.2.6.1)

The effective width of the composite section may be taken as 1/2 the distance to the adjacent beam.

$$b_{eff} := \frac{S}{2} + \frac{S}{2} \qquad b_{eff} = 72 \cdot in$$

$$n := \sqrt{\frac{f'_{ct}}{f'_c}} \qquad n = 0.7559 \qquad b_{tran} := n \cdot b_{eff} \qquad b_{tran} = 54.4269 \cdot in$$

Composite Section Properties:

$$A_{slab} := b_{tran} \cdot (t_{slab} - t_{ws}) \qquad A_{slab} = 326.6 \cdot in^2 \qquad A_h := n \cdot t_h \cdot b_h \qquad A_h = 272.1 \cdot in^2$$

$$A_{comp} := A + A_h + A_{slab} \qquad A_{comp} = 1534.7 \cdot in^2$$

$$y_{bc} := \frac{A \cdot y_b + A_h \cdot \left(t_{flg} + \frac{t_h}{2}\right) + A_{slab} \cdot \left(h + \frac{t_{slab} - t_{ws}}{2}\right)}{A_{comp}} \qquad y_{bc} = 11.466 \cdot in$$

$$h_c := h + t_{slab} - t_{ws} \qquad h_c = 24 \cdot in$$

$$y_{tc} := h_c - y_{bc} \qquad y_{tc} = 12.53 \cdot in$$

$$I_{slab} := \frac{b_{tran} \cdot (t_{slab} - t_{ws})^3}{12} \qquad I_{slab} = 979.7 \cdot in^4 \qquad I_h := \frac{n \cdot b_h \cdot t_h^3}{12} \qquad I_h = 5102.5 \cdot in^4$$

$$I_c := I + A \cdot (y_b - y_{bc})^2 + I_h + A_h \cdot \left(t_{flg} + \frac{t_h}{2} - y_{bc}\right)^2 + I_{slab} + A_{slab} \cdot \left(h + \frac{t_{slab} - t_{ws}}{2} - y_{bc}\right)^2$$

$$I_c = 71824 \cdot in^4$$

$$S_{bc} := \frac{I_c}{y_{bc}} \qquad S_{bc} = 6264.3 \cdot in^3 \qquad\qquad S_{tc} := \frac{I_c}{y_{tc} \cdot n} \qquad S_{tc} = 7580.3 \cdot in^3$$

B1-4

Composite section modulus at the top of the prestressed beam:

$$y_{tcb} := h - y_{bc} \qquad S_{tcb} := \frac{I_c}{y_{tcb}} \qquad S_{tcb} = 10991.8 \cdot in^3$$

1.5 Strand Pattern Properties
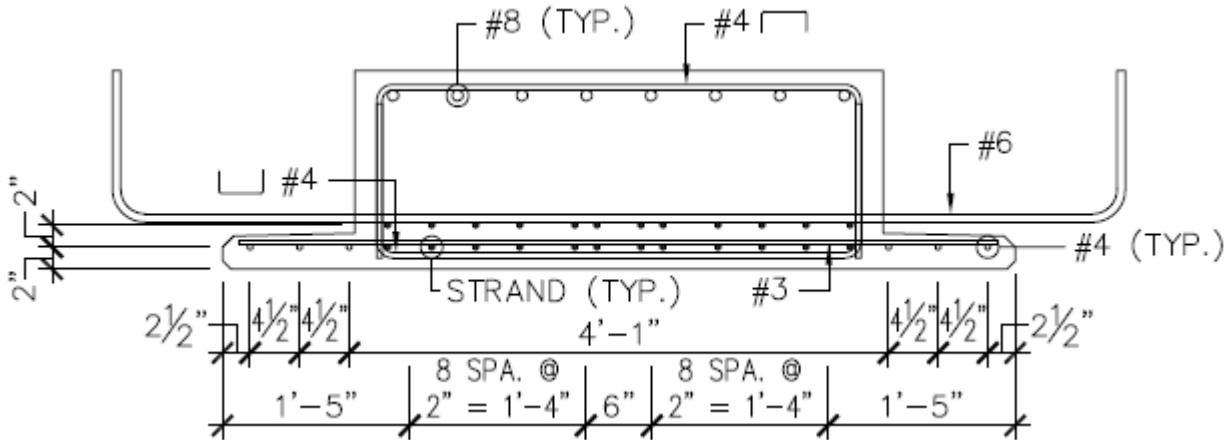
Figure 5: Cross section with reinforcement.

$$No\_Strands := \sum Pat\_n \qquad No\_Strands = 24$$

$$i := 1 .. last(Pat\_n)$$

$$y_{cg} := \frac{\sum_i \left(Pat\_n_i \cdot Pat\_h_i\right)}{No\_Strands} \qquad y_{cg} = 3 \cdot in$$

$$ecc := y_b - y_{cg} \qquad ecc = 5.42 \cdot in$$

1.6 Moments and Shears

At Release:

Self-weight of beam at release:

At transfer, there are two locations along the beam that are of interest:

1. Transfer point of strands: $\quad x_{r_1} := 60 \cdot d_b$ (LRFD 5.8.2.3)

2. Midspan of beam: $\quad x_{r_2} := \dfrac{L_{ovr}}{2}$

$$x_r^T = (3 \quad 25) \cdot ft$$

$$w_{sw} := w_c \cdot A \qquad w_{sw} = 0.975 \cdot klf$$

$$i := 1 .. 2$$

$$M_{swr_i} := \frac{w_{sw} \cdot x_{r_i}}{2} \cdot \left(L_{ovr} - x_{r_i}\right) \qquad\qquad M_{swr}^T = (68.7 \quad 304.7) \cdot kip \cdot ft$$

B1-5

At Final Conditions:

Beam self-weight at final:

At final conditions, there are also two points of interest:

1. The critical section for shear is d_v from the face of the support, with d_v taken as 0.72h (see discussion in Theory section).

$$x_{f_1} := 0.72 \cdot h_c + \frac{L_{pad}}{2}$$

2. Midspan of beam: $x_{f_2} := 0.5 \cdot L_{des}$ $x_f^T = (1.94 \quad 24.5) \cdot ft$

$j := 1 .. 2$

$$M_{swf_j} := \frac{w_{sw} \cdot x_{f_j}}{2} \cdot \left(L_{des} - x_{f_j}\right)$$ $M_{swf}^T = (44.5 \quad 292.6) \cdot kip \cdot ft$

$$V_{swf_j} := w_{sw} \cdot \left(\frac{L_{des}}{2} - x_{f_j}\right)$$ $V_{swf}^T = (22 \quad 0) \cdot kip$

Deck Weight:

$$w_d := \left[\left(t_{slab} - t_{ws}\right) \cdot S + t_h \cdot b_h\right] \cdot w_{ct}$$ $w_d = 0.825 \cdot klf$

$$M_{deck_j} := \frac{w_d \cdot x_{f_j}}{2} \cdot \left(L_{des} - x_{f_j}\right)$$ $M_{deck}^T = (37.7 \quad 247.6) \cdot kip \cdot ft$

$$V_{deck_j} := w_d \cdot \left(\frac{L_{des}}{2} - x_{f_j}\right)$$ $V_{deck}^T = (18.6 \quad 0) \cdot kip$

Barrier Weight (Composite Dead Load):

$w_{barrier} = 0.3 \cdot klf$ Per barrier: $w_b := \dfrac{N_{barriers} \cdot w_{barrier}}{N_g}$ $w_b = 0.075 \cdot klf$

$$M_{barrier_j} := \frac{w_b \cdot x_{f_j}}{2} \cdot \left(L_{des} - x_{f_j}\right)$$ $M_{barrier}^T = (3.4 \quad 22.5) \cdot kip \cdot ft$

$$V_{barrier_j} := w_b \cdot \left(\frac{L_{des}}{2} - x_{f_j}\right)$$ $V_{barrier}^T = (1.7 \quad 0) \cdot kip$

Future Wearing Surface:

$w_{fws} = 0.023 \cdot ksf$ Per Beam: $w_f := \dfrac{Width_{ctc} \cdot w_{fws}}{N_g}$ $w_f = 0.1265 \cdot klf$

$$M_{fws_j} := \frac{w_f \cdot x_{f_j}}{2} \cdot \left(L_{des} - x_{f_j}\right)$$ $M_{fws}^T = (5.8 \quad 38) \cdot kip \cdot ft$

$$V_{fws_j} := w_f \cdot \left(\frac{L_{des}}{2} - x_{f_j}\right)$$ $V_{fws}^T = (2.9 \quad 0) \cdot kip$

Live Load:

Live Load Distribution Factors:

Assume superstructure acts like a slab-type bridge. Utilize provisions of LRFD Art. 4.6.2.3 to compute width of equivalent strip to resist lane load.

Single-Lane Loading:

$$L_1 := if\left(L_{des} > 60 \cdot ft, 60 \cdot ft, L_{des}\right) \qquad L_1 = 49.00\,ft$$

$$W_{1\_1} := if\left(Width_{overall} > 30 \cdot ft, 30 \cdot ft, Width_{overall}\right) \qquad W_{1\_1} = 30.00\,ft$$

$$E_{strip1} := 10 \cdot in + 5.0 \cdot in \cdot \sqrt{\frac{L_1}{ft} \cdot \frac{W_{1\_1}}{ft}} \qquad E_{strip1} = 202 \cdot in \qquad E_{strip1} = 16.8\,ft$$

Put in terms of fraction of one lane to be distributed to one precast unit:

$$DF_{1lane} := \frac{b_f}{E_{strip1}} \qquad DF_{1lane} = 0.357$$

Double-Lane Loading:

$$W_{1\_2} := if\left(Width_{overall} > 60 \cdot ft, 60 \cdot ft, Width_{overall}\right) \qquad W_{1\_2} = 47.50\,ft$$

$$E_{strip2} := 84 \cdot in + 1.44 \cdot in \cdot \sqrt{\frac{L_1}{ft} \cdot \frac{W_{1\_2}}{ft}} \qquad E_{strip2} = 153 \cdot in \quad E_{strip2} = 12.8\,ft$$

$$DF_{2lane} := \frac{b_f}{E_{strip2}} \qquad DF_{2lane} = 0.4691$$

Governing Case:

$$DF := if\left(DF_{1lane} > DF_{2lane}, DF_{1lane}, DF_{2lane}\right) \qquad DF = 0.4691$$

This distribution factor is applicable to both shear and moment:

$$DF_m := DF$$

$$DF_v := DF$$

Live Load Moments (HL-93):

Maximum Moments Due to Design Truck and Design Lane:

Due to the Design Truck:

A closed-form solution for the maximum moment at any point along a simply-supported beam due to the LRFD design truck is given below. There are two formulae, one which is valid for the region between the support and the L/3 point of the beam, and the other which is valid between L/3 and midspan. These two formulae correspond to different orientations of the truck (i.e., when it faces one way or the other).

$$L := L_{des} \qquad \text{(purely to condense the expression)}$$

$$M_{truck_j} := if\left[x_{f_j} \le \frac{L}{3}, \frac{8 \cdot kip \cdot x_{f_j}}{L} \cdot \left(9 \cdot L - 9 \cdot x_{f_j} - 84 \cdot ft\right), \frac{8 \cdot kip}{L} \cdot \left[-9 \cdot \left(x_{f_j}\right)^2 + 9 \cdot x_{f_j} \cdot L - 42 \cdot ft \cdot x_{f_j} - 14 \cdot ft \cdot L\right]\right]$$

$$M_{truck}^T = (107.5 \quad 602) \cdot kip \cdot ft$$

B1-7

Due to the Design Lane:

$$M_{lane_j} := \frac{w_{lane} \cdot x_{f_j}}{2} \cdot \left(L - x_{f_j}\right) \qquad\qquad M_{lane}{}^T = (29.2 \quad 192.1) \cdot kip \cdot ft$$

Maximum Service Live Load Moments (HL-93):

The dynamic load allowance (DLA) is applied to the truck portion only: (LRFD 3.6.2.1-1)

$$M_{LL_j} := DF_m \cdot \left[M_{lane_j} + (1 + DLA) \cdot M_{truck_j}\right] \qquad\qquad M_{LL}{}^T = (80.8 \quad 465.7) \cdot kip \cdot ft$$

Live Load Shears:

$$V_{truck_j} := \frac{8 \cdot kip}{L} \cdot \left(9 \cdot L - 9 \cdot x_{f_j} - 84 \cdot ft\right) \qquad\qquad V_{truck}{}^T = (55.4 \quad 22.3) \cdot kip$$

$$V_{lane_j} := \frac{w_{lane} \cdot \left(L - x_{f_j}\right)^2}{2 \cdot L} \qquad\qquad V_{lane}{}^T = (14.5 \quad 3.9) \cdot kip$$

$$V_{LL_j} := DF_v \cdot \left[V_{lane_j} + (1 + DLA) \cdot V_{truck_j}\right] \qquad\qquad V_{LL}{}^T = (41.4 \quad 15.7) \cdot kip$$

Thermal Gradient: (LRFD 3.12.3)

$\gamma_{TG} := 1.0 \qquad$ (no live live)

$\gamma_{TG\_L} := 0.5 \qquad$ (with live load)

Effects due to uniform temperature change:

Since superstructure is not restrained axially, uniform temperature change causes no internal stress.

Effects due to temperature gradient:

Fig. 6: Positive temperature gradient (from LRFD 3.12.3-2)

Assume AASHTO temperature Zone 1:

$T_1 := 54 \qquad$ (deg F)

$T_2 := 14$

$T_3 := 0$
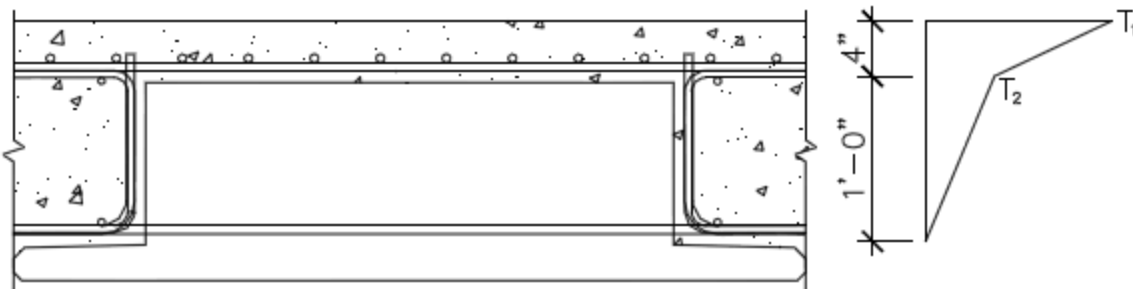
$A_{temp} := if\left(h_c \geq 16 \cdot in, 12 \cdot in, h_c - 4 \cdot in\right) \qquad A_{temp} = 12.00 \cdot in$

$A_1 := 4 \cdot in$

$A_2 := A_{temp} \qquad A_2 = 1 \, ft$

B1-8

Compute gradient-induced curvature:

$$\psi = \frac{\alpha}{I}\cdot\Sigma\left(T_{ai}\cdot y_i\cdot A_i + \frac{\Delta T_i}{d_i}\cdot I_i\right)$$

(LRFD C4.6.6)

$\text{Area}_1 := A_1\cdot b_f \qquad \text{Area}_1 = 288\cdot in^2$

$I_1 := \dfrac{b_f\cdot A_1^{\;3}}{12} \qquad I_1 = 384\cdot in^4$

$\text{Area}_2 := A_2\cdot b_f \qquad \text{Area}_2 = 864\cdot in^2$

$I_2 := \dfrac{b_f\cdot A_2^{\;3}}{12} \qquad I_2 = 10368\cdot in^4$

$\varepsilon_{gr} := \dfrac{\alpha}{A}\cdot\left(T_1\cdot \text{Area}_1 + T_2\cdot \text{Area}_2\right) \qquad \varepsilon_{gr} = 0.000177$

$E_{pr} := 33000\cdot w_c^{1.5}\cdot kcf^{-1.5}\cdot\sqrt{f'_c}\cdot ksi^{.5} \qquad E_{pr} = 5072\cdot ksi$

$F_{gr} := E_{pr}\cdot A_c\cdot\varepsilon_{gr} \qquad F_{gr} = 404.5\cdot kip$

$y_1 := y_{tc} - \dfrac{A_1}{2} \qquad y_1 = 10.53\cdot in$

$y_2 := y_{tc} - \left(A_1 + \dfrac{A_2}{2}\right) \qquad y_2 = 2.53\cdot in$

$$\psi := \frac{\alpha}{I_c}\cdot\left[\left(\frac{T_1 - T_2}{2}\right)\cdot y_1\cdot\text{Area}_1 + \frac{\left(T_1 - T_2\right)}{\frac{A_1}{2}}\cdot I_1 + \left(\frac{T_2}{2}\right)\cdot y_2\cdot\text{Area}_2 + \frac{\left(T_2\right)}{\frac{A_2}{2}}\cdot I_2\right]$$

$\psi = 0.000108\,ft^{-1}$

Only the internal stress component affects the unrestrained simple span:

$$\sigma_E = E\cdot\left(\alpha\cdot T_G - \alpha\cdot T_{uG} - \psi\cdot z\right)$$

(LRFD C4.6.6-6)

Evaluate at top and bottom of precast:

$$f_{TGt} := E_{pr}\cdot\left[\alpha\cdot T_2\cdot\left(\frac{A_1 + A_2 - t_{slab}}{A_2}\right) - \psi\cdot y_{tcb}\right]$$

$f_{TGt} = 0.0564\cdot ksi$

$$f_{TGb} := E_{pr}\cdot\psi\cdot y_{tcb}$$

$f_{TGb} = 0.2987\cdot ksi$

$$f_{TGtt} := E_{pr}\cdot\left(\alpha\cdot T_1 - \psi\cdot y_{tc}\right)$$

$f_{TGtt} = 1.0705\cdot ksi$

1.7 Flexural Stresses

At Release:

Beam Self-Weight Stresses:

$$f_{swrt_j} := \frac{M_{swr_j}}{S_t} \qquad f_{swrt} = \begin{pmatrix} 0.291 \\ 1.292 \end{pmatrix} \cdot ksi \qquad f_{swrb_j} := -\frac{M_{swr_j}}{S_b} \qquad f_{swrb} = \begin{pmatrix} -0.256 \\ -1.135 \end{pmatrix} \cdot ksi$$

At Final Conditions:

Note: Since for a simple-span structural system of this type, it is unlikely that compression at the top of the deck at a given section would exceed its allowable value, calculation of those stresses will be omitted for simplicity. Only the stresses at the bottom and top of the precast beam itself will be computed.

The precast weight and CIP deck weight are carried by the precast section only. Additional loads (i.e. barrier, overlay, live load) are carried by the composite section.

Self-Weight:

$$f_{swt_j} := \frac{M_{swf_j}}{S_t} \qquad f_{swt} = \begin{pmatrix} 0.189 \\ 1.24 \end{pmatrix} \cdot ksi \qquad f_{swb_j} := -\frac{M_{swf_j}}{S_b} \qquad f_{swb} = \begin{pmatrix} -0.166 \\ -1.09 \end{pmatrix} \cdot ksi$$

Deck Weight:

$$f_{deckt_j} := \frac{M_{deck_j}}{S_t} \qquad f_{deckt} = \begin{pmatrix} 0.16 \\ 1.05 \end{pmatrix} \cdot ksi \qquad f_{deckb_j} := -\frac{M_{deck_j}}{S_b} \qquad f_{deckb} = \begin{pmatrix} -0.14 \\ -0.922 \end{pmatrix} \cdot ksi$$

Barriers:

$$f_{barriert_j} := \frac{M_{barrier_j}}{S_{tcb}} \qquad f_{barriert} = \begin{pmatrix} 0.004 \\ 0.025 \end{pmatrix} \cdot ksi \qquad f_{barrierb_j} := -\frac{M_{barrier_j}}{S_{bc}} \qquad f_{barrierb} = \begin{pmatrix} -0.007 \\ -0.043 \end{pmatrix} \cdot ksi$$

$$f_{barriertt_j} := \frac{M_{barrier_j}}{S_{tc}} \qquad f_{barriertt} = \begin{pmatrix} 0.005 \\ 0.036 \end{pmatrix} \cdot ksi \qquad \text{(top of topping)}$$

Future Wearing Surface:

$$f_{fwst_j} := \frac{M_{fws_j}}{S_{tcb}} \qquad f_{fwst} = \begin{pmatrix} 0.006 \\ 0.041 \end{pmatrix} \cdot ksi \qquad f_{fwsb_j} := -\frac{M_{fws_j}}{S_{bc}} \qquad f_{fwsb} = \begin{pmatrix} -0.011 \\ -0.073 \end{pmatrix} \cdot ksi$$

$$f_{fwstt_j} := \frac{M_{fws_j}}{S_{tc}} \qquad f_{fwstt} = \begin{pmatrix} 0.009 \\ 0.06 \end{pmatrix} \cdot ksi \qquad \text{(top of topping)}$$

Live Load:

$$f_{LLt_j} := \frac{M_{LL_j}}{S_{tcb}} \qquad f_{LLt} = \begin{pmatrix} 0.088 \\ 0.508 \end{pmatrix} \cdot ksi \qquad f_{LLb_j} := -\frac{M_{LL_j}}{S_{bc}} \qquad f_{LLb} = \begin{pmatrix} -0.155 \\ -0.892 \end{pmatrix} \cdot ksi$$

$$f_{LLtt_j} := \frac{M_{LL_j}}{S_{tc}} \qquad f_{LLtt} = \begin{pmatrix} 0.128 \\ 0.737 \end{pmatrix} \cdot ksi \qquad \text{(top of topping)}$$

Prestress Losses

At Release:

At release, two components of prestress loss are significant: relaxation of the prestressing steel and elastic shortening. Elastic shortening is the loss of prestress that results when the strands are detensioned and the precast beam shortens in length due to the applied prestress. When the strands are tensioned in the prestress bed and anchored at the abutments, the steel gradually begins to relax as a function of time. By the time the strands are detensioned a small, but measurable, loss due to steel relaxation has occurred.

Steel Relaxation (short term):

$$f_{pj} := Pull \cdot f_{pu} \qquad f_{pj} = 202.5 \cdot ksi \qquad f_{py} = 243 \cdot ksi$$

$$\Delta f_{pR1} := \frac{\log\left(\frac{t}{hr}\right)}{40.0} \cdot \left(\frac{f_{pj}}{f_{py}} - 0.55\right) \cdot f_{pj} \qquad \Delta f_{pR1} = 1.801 \cdot ksi \qquad \text{(LRFD 5.9.5.4.4b-2)}$$

Elastic Shortening:

$$E_{ci} := 33000 \cdot w_c^{1.5} \cdot kcf^{-1.5} \cdot \sqrt{f'_{ci}} \cdot ksi^{.5} \qquad E_{ci} = 4496 \cdot ksi \qquad \text{(LRFD 5.4.2.4-1)}$$

$$A_{ps} := No\_Strands \cdot A_{strand} \qquad A_{ps} = 5.208 \cdot in^2 \qquad \text{(Area of strand at midspan)}$$

$$f_{pbt} := f_{pj} - \Delta f_{pR1} \qquad f_{pbt} = 200.7 \cdot ksi$$

$$\Delta f_{pES} := \frac{A_{ps} \cdot f_{pbt} \cdot \left(I + ecc^2 A\right) - ecc \cdot M_{swr_2} \cdot A}{A_{ps} \cdot \left(I + ecc^2 A\right) + \frac{A \cdot I \cdot E_{ci}}{E_p}} \qquad \Delta f_{pES} = 8.986 \cdot ksi$$

Total Prestress Loss at Release:

$$\Delta f_{sr} := \Delta f_{pES} + \Delta f_{pR1} \qquad \Delta f_{sr} = 10.786 \cdot ksi$$

$$\%Loss := \frac{\Delta f_{sr}}{Pull \cdot f_{pu}} \cdot 100 \qquad \%Loss = 5.3264$$

$$f_{per} := f_{pj} - \Delta f_{pES} - \Delta f_{pR1} \qquad f_{per} = 191.7 \cdot ksi$$

$$P_r := f_{per} \cdot No\_Strands \cdot A_{strand} \qquad P_r = 998.4 \cdot kip$$

At Final Conditions:

Total Loss of Prestress:

$$\Delta f_{pT} = \Delta f_{pES} + \Delta f_{pLT} \qquad \text{(LRFD 5.9.5.1-1)}$$

where:

Δf_{pES} = Sum of all losses due to elastic shortening at time of application of prestress load (ksi).

Δf_{pLT} = Total loss due to long-term effects, which include shrinkage and creep of the concrete and relaxation of the prestressing steel (ksi).

In pretensioned bridge girder design, stresses have traditionally been assessed at two timeframes: at release of prestress (i.e., when the prestress force is applied to the girder) and at final (long-term) conditions. Therefore, loss of prestress has been evaluated at these two periods in the life of the girder. However, with the new prestress loss procedure introduced in the 2005 Interim Revisions, long-term losses are computed in two steps: (a) The time period between prestress transfer and placement of the cast-in-place concrete deck and (b) the time period between deck placement and the end of the service life of the girder. These two periods correspond to the non-composite and composite phases of the structural system. The rate of stress change in the strands can differ significantly in each phase, hence the need to subdivide the long-term losses into two components.

Loss at Release:

The principal component of prestress loss when the strands are released and the prestress force in the strands is imparted into the girder is elastic shortening. This reduction in prestress (prestress loss) occurs essentially instantaneously.

Loss at Final Conditions:

The time-dependent loss of prestress consists of three distinct components. Loss due to:

1. Creep of girder concrete,
2. Relaxation of prestressing strands, and
3. Shrinkage of girder concrete.

These are computed in two stages:

1. From time prestress force is imparted to the girder to the time the girder is erected and
2. From the time the CIP deck is placed to final time.

Mathematically, this is expressed as:

$$\Delta fpLT = (\Delta f_{pSR} + \Delta f_{pCR} + \Delta f_{pR1})_{id} + (\Delta f_{pSD} + \Delta f_{pCD} + \Delta f_{pR2} - \Delta f_{pSS})_{df}$$ (LRFD 5.9.5.4.1-1)

Material Properties:

The shrinkage and creep properties of the girder and deck need to be computed in preparation for the prestress loss computations. These are addressed in LRFD Article 5.4.2.3. Creep coefficients are computed in accordance with Article 5.4.2.3.2 and shrinkage strains are computed in accordance with Article 5.4.2.3.3.

Creep Coefficients

Girder creep coefficient at final time due to loading at transfer:

$$\psi_b(t_f, t_i) = 1.9 \cdot k_{vs} \cdot k_{hc} \cdot k_f \cdot k_{td} \cdot t_i^{-0.118}$$ (LRFD Eq. 5.4.2.3.2-1)

where:

ψ_b = Ratio of creep strain to elastic strain.

k_{vs} = Factor for the effect of volume to surface ratio.

k_{hc} = Humidity factor for creep.

k_f = Factor for strength of concrete.

k_{td} = Factor for time development.

$$k_{vs} := 1.45 - 0.13 \frac{VS_b}{in} \qquad k_{vs} = 0.774 \qquad \text{Note: } k_{vs} \text{ must be greater than 1.0.} \qquad \text{(LRFD 5.4.2.3.2-1)}$$

$$k_{vs} := 1.000$$

$$k_{hc} := 1.56 - 0.008H \qquad k_{hc} = 1.000 \qquad \text{(LRFD Eq. 5.4.2.3.2-3)}$$

$$k_f := \frac{5}{1 + \dfrac{f'_{ci}}{ksi}} \qquad k_f = 0.769 \qquad \text{(LRFD 5.4.2.3.2-4)}$$

$$t_f := t_{final} \qquad t_i := t_{transfer}$$

$$t := t_f - t_i \qquad t = 19999 \cdot day$$

$$k_{td} := \frac{\dfrac{t}{day}}{61 - \dfrac{4 \cdot f'_{ci}}{ksi} + \dfrac{t}{day}} \qquad k_{td} = 0.998 \qquad \text{(LRFD 5.4.2.3.2-5)}$$

$$\psi_{bfi} := 1.9 \cdot k_{vs} \cdot k_{hc} \cdot k_f \cdot k_{td} \cdot \left(\frac{t_i}{day}\right)^{-0.118} \qquad \psi_{bfi} = 1.459$$

Girder creep coefficient at time of CIP placement due to loading at transfer:

$$t_i := t_{transfer} \qquad t_d := t_{deck}$$

$$t := t_d - t_i \qquad t = 89 \cdot day$$

$$k_{td} := \frac{\dfrac{t}{day}}{61 - \dfrac{4 \cdot f'_{ci}}{ksi} + \dfrac{t}{day}} \qquad k_{td} = 0.695$$

$$k_{vs} := 1.45 - 0.13 \frac{VS_b}{in} \qquad k_{vs} = 0.774 \qquad \text{Note: } k_{vs} \text{ must be greater than 1.0.} \qquad \text{(LRFD 5.4.2.3.2-1)}$$

$$k_{vs} := 1.000$$

$$k_{hc} := 1.56 - 0.008H \qquad k_{hc} = 1.000 \qquad \text{(LRFD Eq. 5.4.2.3.2-3)}$$

$$k_f := \frac{5}{1 + \dfrac{f'_{ci}}{ksi}} \qquad k_f = 0.769 \qquad \text{(LRFD 5.4.2.3.2-4)}$$

$$\psi_{bdi} := 1.9 \cdot k_{vs} \cdot k_{hc} \cdot k_f \cdot k_{td} \cdot \left(\frac{t_i}{day}\right)^{-0.118} \qquad \psi_{bdi} = 1.016$$

B1-13

Girder creep coefficient at final time due to loading at CIP placement:

$t_i := t_{deck}$

$t := t_f - t_i$ $\qquad t = 19910 \cdot day$

$$k_{td} := \dfrac{\dfrac{t}{day}}{61 - \dfrac{4 \cdot f'_{ci}}{ksi} + \dfrac{t}{day}} \qquad k_{td} = 0.998$$

$k_{vs} := 1.45 - 0.13 \dfrac{VS_b}{in}$ $\qquad k_{vs} = 0.774$ $\qquad$ Note: k_{vs} must be greater than 1.0. $\qquad$ (LRFD 5.4.2.3.2-1)

$k_{vs} := 1.000$

$k_{hc} := 1.56 - 0.008H$ $\qquad k_{hc} = 1.000$ $\qquad\qquad\qquad\qquad$ (LRFD Eq. 5.4.2.3.2-3)

$$k_f := \dfrac{5}{1 + \dfrac{f'_{ci}}{ksi}} \qquad k_f = 0.769 \qquad\qquad\qquad\qquad\text{(LRFD 5.4.2.3.2-4)}$$

$$\psi_{bfd} := 1.9 \cdot k_{vs} \cdot k_{hc} \cdot k_f \cdot k_{td} \cdot \left(\dfrac{t_i}{day}\right)^{-0.118} \qquad \psi_{bfd} = 0.858$$

CIP concrete creep coefficient from time of casting to final:

$k_{hc} := 1.56 - 0.008 \cdot H$ $\qquad k_{hc} = 1.000$

$$k_f := \dfrac{5}{1 + \dfrac{0.8 \cdot f'_{ct}}{ksi}} \qquad k_f = 1.19$$

$k_{vs} := 1.45 - 0.13 \dfrac{VS_d}{in}$ $\qquad k_{vs} = 0.670$ $\qquad$ Note: k_{vs} must be greater than 1.0.

$k_{vs} := 1.000$

$k_{hc} := 1.56 - 0.008H$ $\qquad k_{hc} = 1.000$

$t := t_f - t_{deck}$ $\qquad t = 19910 \cdot day$

$$k_{td} := \dfrac{\dfrac{t}{day}}{61 - \dfrac{4 \cdot f'_{ci}}{ksi} + \dfrac{t}{day}} \qquad k_{td} = 0.998$$

$$\psi_{dfd} := 1.9 \cdot k_{vs} \cdot k_{hc} \cdot k_f \cdot k_{td} \cdot \left(\dfrac{t_{deck}}{day}\right)^{-0.118} \qquad \psi_{bfd} = 0.858$$

B1-14

Shrinkage Strains

Girder concrete shrinkage strain between transfer and final time:

The concrete shrinkage strain, ε_{bid}, is computed in accordance with Art. 5.4.2.3.3:

$$\varepsilon_{sh} = -k_{vs} \cdot k_{hs} \cdot k_f \cdot k_{td} \cdot 0.48 \cdot 10^{-3} \qquad \text{(LRFD 5.4.2.3.3-1)}$$

where:

k_{vs} = Factor for the effect of volume to surface ratio.

k_{hs} = Factor for humidity.

k_f = Factor for strength of concrete.

k_{td} = Factor for time development.

$$k_{vs} := 1.45 - 0.13 \frac{VS_b}{in} \qquad k_{vs} = 0.774 \qquad \text{Note: kvs must be greater than 1.0} \qquad \text{(LRFD 5.4.2.3.2-1)}$$

$$k_{vs} := 1.000$$

$$k_{hs} := 2.00 - 0.014 \cdot H \qquad k_{hs} = 1.020 \qquad \text{(LRFD 5.4.2.3.3-2)}$$

$$k_f := \frac{5}{1 + \dfrac{f'_{ci}}{ksi}} \qquad k_f = 0.769 \qquad \text{(LRFD 5.4.2.3.2-4)}$$

$$t_f := t_{final} \qquad t_i := t_{transfer}$$

$$t := t_f - t_i \qquad t = 19999 \cdot day$$

$$k_{td} := \frac{\dfrac{t}{day}}{61 - \dfrac{4 \cdot f'_{ci}}{ksi} + \dfrac{t}{day}} \qquad k_{td} = 0.998 \qquad \text{(LRFD 5.4.2.3.2-5)}$$

$$\varepsilon_{bif} := -k_{vs} \cdot k_{hs} \cdot k_f \cdot k_{td} \cdot 0.48 \cdot 10^{-3} \qquad \varepsilon_{bif} = -376 \times 10^{-6}$$

Girder concrete shrinkage strain between transfer and CIP placement:

$$k_{vs} := 1.45 - 0.13 \frac{VS_b}{in} \qquad k_{vs} = 0.774 \qquad \text{Note: kvs must be greater than 1.0} \qquad \text{(LRFD 5.4.2.3.2-1)}$$

$$k_{vs} := 1.000$$

$$k_{hs} := 2.00 - 0.014 \cdot H \qquad k_{hs} = 1.020 \qquad \text{(LRFD 5.4.2.3.3-2)}$$

$$k_f := \frac{5}{1 + \dfrac{f'_{ci}}{ksi}} \qquad k_f = 0.769 \qquad \text{(LRFD 5.4.2.3.2-4)}$$

$$t := t_d - t_i \qquad t = 89 \cdot day$$

B1-15

$$k_{td} := \frac{\dfrac{t}{day}}{61 - \dfrac{4 \cdot f'_{ci}}{ksi} + \dfrac{t}{day}}$$
$k_{td} = 0.695$ (LRFD 5.4.2.3.2-5)

$$\varepsilon_{bid} := -k_{vs} \cdot k_{hs} \cdot k_f \cdot k_{td} \cdot 0.48 \cdot 10^{-3}$$ $\varepsilon_{bid} = -262 \times 10^{-6}$

CIP concrete shrinkage from deck placement to final:

$$k_{vs} := 1.45 - 0.13 \frac{VS_d}{in}$$ $k_{vs} = 0.670$ Note: kvs must be greater than 1.0   (LRFD 5.4.2.3.2-1)

$$k_{vs} := 1.000$$

$$k_{hs} := 2.00 - 0.014 \cdot H$$ $k_{hs} = 1.020$ (LRFD 5.4.2.3.3-2)

$$k_f := \frac{5}{1 + \dfrac{f'_{ci}}{ksi}}$$ $k_f = 0.769$ (LRFD 5.4.2.3.2-4)

$$t_f := t_{final} \qquad t_i := t_{deck}$$

$$t := t_f - t_i \qquad t = 19910 \cdot day$$

$$k_{td} := \frac{\dfrac{t}{day}}{61 - \dfrac{4 \cdot f'_{ci}}{ksi} + \dfrac{t}{day}}$$
$k_{td} = 0.998$ (LRFD 5.4.2.3.2-5)

$$\varepsilon_{ddf} := -k_{vs} \cdot k_{hs} \cdot k_f \cdot k_{td} \cdot 0.48 \cdot 10^{-3}$$ $\varepsilon_{ddf} = -376 \times 10^{-6}$

Girder concrete shrinkage strain between CIP placement and final time:

The girder concrete shrinkage between deck placement and final time is the difference between the shrinkage at time of deck placement and the total shrinkage at final time.

$$\varepsilon_{bdf} := \varepsilon_{bif} - \varepsilon_{bid} \qquad \varepsilon_{bdf} = -114 \times 10^{-6}$$

Loss from Transfer to CIP Placement:

The prestress loss from transfer of prestress to placement of CIP consists of three loss components: shrinkage of the girder concrete, creep of the girder concrete, and relaxation of the strands. That is,

Time-Dependent Loss from Transfer to CIP Placement = $\Delta f_{pSR} + \Delta f_{pCR} + \Delta f_{pR1}$

B1-16

Shrinkage of Concrete Girder:

$$\Delta f_{pSR} = \varepsilon_{bid} \cdot E_p \cdot K_{id}$$

(LRFD5.9.5.4.2a-1)

where:

ε_{bid} = Concrete shrinkage strain of girder between transfer and CIP placement. Computed using LRFD Eq. 5.4.2.3.3-1

E_p = Modulus of elasticity of prestressing strand (ksi).

K_{id} = Transformed steel coefficient that accounts for time-dependent interaction between concrete and bonded steel in the section being considered for the time period between transfer and CIP placement.

The transformed section coefficient, k_{id}, is computed using:

$$K_{id} = \frac{1}{1 + \dfrac{E_p}{E_{ci}} \cdot \dfrac{A_{ps}}{A} \cdot \left(1 + \dfrac{A \cdot e_{pg}^2}{I_g}\right) \cdot \left(1 + 0.7 \cdot \psi_b(t_f, t_i)\right)}$$

(LRFD Eq. 5.9.5.4.2a-2)

where:

e_{pg} = Eccentricity of strands with respect to centroid of girder (in).

$\psi_b(t_f, t_i)$ = Creep coefficient at final time due to loading introduced at transfer.

$e_{pg} := ecc$ $e_{pg} = 5.42 \cdot in$ $I = 27120 \cdot in^4$ $A = 936 \cdot in^2$

$$K_{id} := \frac{1}{1 + \dfrac{E_p}{E_{ci}} \cdot \dfrac{A_{ps}}{A} \cdot \left(1 + \dfrac{A \cdot e_{pg}^2}{I}\right) \cdot \left(1 + 0.7 \cdot \psi_{bfi}\right)}$$ $K_{id} = 0.8745$

Therefore, the prestress loss due to shrinkage of the girder concrete between time of transfer and CIP placement is:

$$\Delta f_{pSR} := -\varepsilon_{bid} \cdot E_p \cdot K_{id}$$ $\Delta f_{pSR} = 6.526 \cdot ksi$

Creep of Concrete Girder:

$$\Delta f_{pCR} = \frac{E_p}{E_{ci}} \cdot f_{cgp} \cdot \psi_b(t_d, t_i) K_{id}$$

(LRFD 5.9.5.4.2b-1)

where:

f_{cgp} = Concrete stress at cg of prestress pattern due to the prestressing force immediately after transfer and the self-weight of the girder at the section of maximum moment (ksi).

Section modulus at cg of strand pattern:

$e_{pti} := ecc$ $e_{pti} = 5.42 \cdot in$

$$S_{cgp} := \frac{I}{e_{pti}}$$ $S_{cgp} = 5004 \cdot in^3$

B1-17

.

Initial prestress force:

$$f_{pj} := Pull \cdot f_{pu}$$

$$P_{init} := f_{pj} \cdot A_{ps} \qquad\qquad P_{init} = 1054.6 \cdot kip$$

$$f_{cgp} := P_{init} \cdot \left(\frac{1}{A} + \frac{e_{pti}}{S_{cgp}} \right) - \frac{M_{swf_2}}{S_{cgp}} \qquad\qquad f_{cgp} = 1.567 \cdot ksi$$

$$\Delta f_{pCR} := \frac{E_p}{E_{ci}} \cdot f_{cgp} \cdot \psi_{bdi} K_{id} \qquad\qquad \Delta f_{pCR} = 8.829 \cdot ksi$$

For this example, it will be assumed to be equal to 1.2 ksi (Article 5.9.5.4.2b permits this).

$$\Delta f_{pR1} := 1.2 \cdot ksi$$

Total prestress loss at time of CIP placement:

$$\Delta f_{pLTid} := \Delta f_{pSR} + \Delta f_{pCR} + \Delta f_{pR1}$$

Calculated above:

$$\Delta f_{pSR} = 6.53 \cdot ksi \qquad \Delta f_{pCR} = 8.83 \cdot ksi \qquad \Delta f_{pR1} = 1.20 \cdot ksi$$

$$\Delta f_{pLTid} = 16.555 \cdot ksi$$

Loss from CIP Placement to Final:

The prestress loss from placement of CIP to final conditions consists of four loss components: shrinkage of the girder concrete, creep of the girder concrete, and relaxation of the strands. That is,

Time-Dependent Loss from CIP Placement to Final = $\Delta f_{pSD} + \Delta f_{pCD} + \Delta f_{pR2} - f_{ss}$

Shrinkage of Concrete Girder:

$$\Delta f_{pSD} = \varepsilon_{bdf} \cdot E_p \cdot K_{df} \qquad\qquad\qquad \text{(LRFD5.9.5.4.3a-1)}$$

where:

ε_{bdf} = Concrete shrinkage strain of girder between time of CIP placement and final time. Computed using LRFD Eq. 5.4.2.3.3-1

K_{df} = Transformed steel coefficient that accounts for time-dependent interaction between concrete and bonded steel in the section being considered for the time period between the time of CIP placement and final time.

Compute K_{df}:

$$K_{df} = \frac{1}{1 + \dfrac{E_p}{E_{ci}} \cdot \dfrac{A_{ps}}{A_c} \cdot \left(1 + \dfrac{A_c \cdot e_{pc}^2}{I_c} \right) \cdot \left(1 + 0.7 \, \psi_b(t_f, t_i) \right)} \qquad\qquad \text{(LRFD 5.9.5.4.3a-2)}$$

where:

e_{pc} =   Eccentricity of strands with respect to centroid of composite section

A_c =   For composite sections, the gross area of the composite section should be used. However, since this girder is non-composite, the gross area of the non-composite section is used.

I_c =   Gross area of composite section for composite systems, gross area of bare beam for non-composite systems.

$\psi_b(t_f, t_i)$ =   Girder creep coefficient

$e_{pc} := ecc$ $e_{pc} = 5.42 \cdot in$

$A_c:$ $A = 936 \cdot in^2$

$I_c:$ $I = 27120 \cdot in^4$

$$K_{df} := \frac{1}{1 + \dfrac{E_p}{E_{ci}} \cdot \dfrac{A_{ps}}{A} \cdot \left(1 + \dfrac{A \cdot e_{pc}^2}{I}\right) \cdot \left(1 + 0.7\psi_{bfi}\right)}$$ $K_{df} = 0.874$

Therefore, prestress loss due to shrinkage of girder concrete between CIP placement and final is:

$\Delta f_{pSD} := -\varepsilon_{bdf} \cdot E_p \cdot K_{df}$ $\Delta f_{pSD} = 2.842 \cdot ksi$

Creep of Concrete Girder:

$$\Delta f_{pCD} = \frac{E_p}{E_{ci}} \cdot f_{cgp} \cdot \left(\psi_b(t_f, t_i) - \psi_b(t_d, t_i)\right) \cdot K_{df} + \frac{E_p}{E_c} \cdot \Delta f_{cd} \cdot \psi_b(t_f, t_d) \cdot K_{df} \geq 0.0$$ (LRFD5.9.5.4.3b-1)

where:

Δf_{cd} =   Change in concrete stress at centroid of prestressing strands due to long-term losses between transfer and CIP placement combined with superimposed loads (ksi).

$\psi_b(t_f, t_d)$ =   Girder creep coefficient at final time due to loading at CIP placement per Eq. 5.4.2.3.2-1.

Let:

$$\Delta f_{pCD} = \Delta f_{pCD1} + \Delta f_{pCD2}$$

compute Δf_{pCD1}:

$$\Delta f_{pCD1} := \frac{E_p}{E_{ci}} \cdot f_{cgp} \cdot \left(\psi_{bfi} - \psi_{bdi}\right) \cdot K_{df}$$ $\Delta f_{pCD1} = 3.844 \cdot ksi$

compute Δf_{pCD2}:

compute Δf_{cd}:

$$\Delta f_{cd} = \Delta P \cdot \left(\frac{1}{A_g} + \frac{e_{pg}^2}{I_g}\right) - \left(\frac{M_{fws} + M_{barrier} + M_{deck}}{S_{cgp}}\right)$$

$\Delta P := -\Delta f_{pLTid} \cdot A_{ps}$ $\Delta P = -86.2 \cdot kip$

$e_{pg} := y_b - y_{cg}$ $e_{pg} = 5.42 \cdot in$

B1-19

$$\Delta f_{cd} := \Delta P \cdot \left(\frac{1}{A} + \frac{e_{pg}^2}{I} \right) - \left(\frac{M_{fws_2} + M_{barrier_2} + M_{deck_2}}{S_{cgp}} \right) \qquad \Delta f_{cd} = -0.924 \cdot ksi$$

$$E_c := 33000 \cdot 1.0 \cdot \left(0.14 + \frac{f'_c}{1000 \cdot ksi} \right)^{1.5} \cdot \sqrt{\frac{f'_c}{ksi}} \cdot ksi \qquad E_c = 4921 \cdot ksi$$

$$\Delta f_{pCD2} := \frac{E_p}{E_c} \cdot \Delta f_{cd} \cdot \psi_{bfd} \cdot K_{df} \qquad \Delta f_{pCD2} = -4.016 \cdot ksi$$

Therefore,

$$\Delta f_{pCD} := \Delta f_{pCD1} + \Delta f_{pCD2} \qquad \Delta f_{pCD} = -0.171 \cdot ksi$$

Shrinkage of the CIP deck:

$$A_d := \frac{A_{slab}}{n} \qquad\qquad\qquad A_d = 432 \cdot in^2$$

$$E_{cd} := 33000 \cdot w_c^{1.5} \cdot kcf^{-1.5} \cdot \sqrt{f'_{ct}} \cdot ksi^{.5} \qquad E_{cd} = 3834 \cdot ksi$$

$$e_d := \frac{h}{2} \qquad\qquad\qquad e_d = 9 \cdot in$$

$$\Delta f_{cdf} := \frac{\varepsilon_{ddf} \cdot A_d \cdot E_{cd}}{\left(1 + 0.7 \cdot \psi_{dfd} \right)} \cdot \left(\frac{1}{A_c} - \frac{e_{pc} \cdot e_d}{I_c} \right) \qquad \Delta f_{cdf} = -0.498 \cdot ksi$$

$$\Delta f_{pSS} := \frac{E_p}{E_c} \cdot \Delta f_{cdf} \cdot K_{df} \cdot \left(1 + 0.7 \cdot \psi_{bfd} \right) \qquad \Delta f_{pSS} = -4.0364 \cdot ksi$$

Relaxation of Prestressing Strands:

$$\Delta f_{pR2} := \Delta f_{pR1} \qquad \Delta f_{pR2} = 1.2 \cdot ksi \qquad\qquad\qquad \text{(LRFD 5.9.5.4.3c-1)}$$

Total prestress loss from CIP placement to final, therefore, is:

$$\Delta f_{pLTdf} := \Delta f_{pSD} + \Delta f_{pCD} + \Delta f_{pR2} - \Delta f_{pSS}$$

Calculated above:

$$\Delta f_{pSD} = 2.84 \cdot ksi \quad \Delta f_{pCD} = -0.17 \cdot ksi \quad \Delta f_{pR2} = 1.2 \cdot ksi \qquad \Delta f_{pSS} = -4.0364 \cdot ksi$$

$$\Delta f_{pLTdf} = 7.907 \cdot ksi$$

Summary of Time-Dependent Losses

Losses from Transfer to CIP Placement

Girder shrinkage: $\Delta f_{pSR} = 6.53 \cdot ksi$

Girder creep: $\Delta f_{pCR} = 8.83 \cdot ksi$

Strand relaxation: $\Delta f_{pR1} = 1.2 \cdot ksi$

Total = $\Delta f_{pLTid} = 16.555 \cdot ksi$

B1-20

<u>Losses from CIP Placement to Final</u>

Girder shrinkage: $\Delta f_{pSD} = 2.84 \cdot ksi$

Girder creep: $\Delta f_{pCD} = -0.17 \cdot ksi$

Strand relaxation: $\Delta f_{pR2} = 1.2 \cdot ksi$

Differential Shrinkage: $\Delta f_{pSS} = -4.0364 \cdot ksi$

Total = $\Delta f_{pLTdf} = 7.907 \cdot ksi$

$\Delta f_{pLT} := \Delta f_{pLTid} + \Delta f_{pLTdf}$ $\quad\quad \Delta f_{pLT} = 24.46 \cdot ksi$

$\Delta f_{PT} := \Delta f_{pES} + \Delta f_{pLT}$ $\quad\quad \Delta f_{PT} = 33.45 \cdot ksi$

$\%Loss := \dfrac{\Delta f_{PT}}{Pull \cdot f_{pu}} \cdot 100$ $\quad\quad \%Loss = 16.52$

Check effective stress after losses:

$f_{pe} := Pull \cdot f_{pu} - \Delta f_{PT}$ $\quad\quad f_{pe} = 169.1 \cdot ksi$

$f_{allow} := 0.80 \cdot f_{py}$ $\quad\quad f_{allow} = 194.4 \cdot ksi$ $\hfill$ (LRFD 5.9.3-1)

Stresses Due to Prestress at End of Transfer Length and Midspan

At Release Conditions:

$j := 1 .. 2$

$f_{psrb_j} := P_r \cdot \left(\dfrac{1}{A} + \dfrac{ecc}{S_b} \right)$ $\quad\quad f_{psrb}{}^T = (2.747 \quad 2.747) \cdot ksi$

$f_{psrt_j} := P_r \cdot \left(\dfrac{1}{A} - \dfrac{ecc}{S_t} \right)$ $\quad\quad f_{psrt}{}^T = (-0.845 \quad -0.845) \cdot ksi$

At Final Conditions:

$dist_j := x_{f_j} + \dfrac{L_{ovr} - L_{des}}{2}$ $\quad\quad dist^T = (2.44 \quad 25) \, ft$

$L_t := 60 \cdot d_b$ $\quad\quad L_t = 36 \cdot in$

$dt_j := if\left(dist_j > L_t, 1.0, \dfrac{dist_j}{L_t} \right)$ $\quad\quad dt^T = (0.8133 \quad 1)$ (Fraction strands are transferred.)

$j := 1 .. 2$

$P_{f_j} := f_{pe} \cdot dt_j \cdot No\_Strands \cdot A_{strand}$ $\quad\quad P_f{}^T = (716.1 \quad 880.4) \cdot kip$

$f_{psb_j} := P_{f_j} \cdot \left(\dfrac{1}{A} + \dfrac{ecc}{S_b} \right)$ $\quad\quad f_{psb} = \begin{pmatrix} 1.97 \\ 2.422 \end{pmatrix} \cdot ksi$ $\quad\quad f_{pst_j} := P_{f_j} \cdot \left(\dfrac{1}{A} - \dfrac{ecc}{S_t} \right)$ $\quad\quad f_{pst} = \begin{pmatrix} -0.606 \\ -0.745 \end{pmatrix} \cdot ksi$

B1-21

Service Stress Check

At Release Conditions:

Top of precast section (tension):

$$f_{rt_j} := f_{psrt_j} + f_{swrt_j} \qquad\qquad f_{rt}^{\mathsf{T}} = (-0.554 \quad 0.447) \cdot ksi$$

$$f_{allow\_rt} := -0.24 \cdot \sqrt{f'_{ci}} \cdot \sqrt{ksi} \qquad f_{allow\_rt} = -0.563 \cdot ksi$$

$$Status\_ServiceLSrt_j := if\left(f_{rt_j} \geq f_{allow\_rt}, "OK", "NG"\right) \qquad Status\_ServiceLSrt^{\mathsf{T}} = ("OK" \quad "OK")$$

Bottom of precast section (compression):

$$f_{rb_j} := f_{psrb_j} + f_{swrb_j} \qquad\qquad f_{rb}^{\mathsf{T}} = (2.491 \quad 1.612) \cdot ksi$$

$$f_{allow\_rc} := 0.6 \cdot f'_{ci} \qquad f_{allow\_rc} = 3.3 \cdot ksi$$

$$Status\_ServiceLSrc_j := if\left(f_{rt_j} \leq f_{allow\_rc}, "OK", "NG"\right) \qquad Status\_ServiceLSrc^{\mathsf{T}} = ("OK" \quad "OK")$$

Compute required amount of top tension steel at transfer point:

$$x_{tt} := h \cdot \left(\frac{f_{rt_1}}{f_{rt_1} + f_{rb_1}}\right) \qquad x_{tt} = -5.14 \cdot in \qquad\qquad \text{(LRFD C5.9.4.1.2)}$$

$$T_{tt} := \frac{f_{rt_1}}{2} \cdot b_v \cdot x_{tt} \qquad T_{tt} = 102.49 \cdot kip$$

$$A_{tt} := \frac{T_{tt}}{30 \cdot ksi} \qquad A_{tt} = 3.4162 \cdot in^2$$

Assume #8 bars will be used as top tension steel. Required number of bars:

$$N_{tt} := \frac{A_{tt}}{0.79 \cdot in^2} \qquad N_{tt} = 4$$

At Final Conditions:

Check Service Limit States:

Service III Limit State (Tensile Stresses in Bottom of Beam):

$$f_{IIIb_j} := f_{psb_j} + f_{swb_j} + f_{deckb_j} + f_{barrierb_j} + f_{fwsb_j} + 0.8 \cdot f_{LLb_j} + 0.5 \cdot f_{TGb} \qquad f_{IIIb}^{\mathsf{T}} = (1.672 \quad -0.271) \cdot ksi$$

$$f_{allow\_ft} := -0.19 \cdot \sqrt{f'_c} \cdot \sqrt{ksi} \qquad f_{allow\_ft} = -0.503 \cdot ksi \qquad\qquad \text{(LRFD 5.9.4.2.2b)}$$

$$Status\_ServiceLSft_j := if\left(f_{IIIb_j} \geq f_{allow\_ft}, "OK", "NG"\right) \qquad Status\_ServiceLSft^{\mathsf{T}} = ("OK" \quad "OK")$$

Service I (Compressive Stresses in Top of Beam):

Compressive Stress Due to Permanent Loads:

$$f_{Idt_j} := f_{pst_j} + f_{swt_j} + f_{deckt_j} + f_{barriert_j} + f_{fwst_j} + f_{TGt} \qquad f_{Idt}^{\mathsf{T}} = (-0.1912 \quad 1.6673) \cdot ksi$$

$$f_{allow\_fcd} := 0.45 \cdot f'_c \qquad f_{allow\_fcd} = 3.15 \cdot ksi \qquad\qquad \text{(LRFD 5.9.4.2.1)}$$

$$Status\_ServiceLSfcd_j := if\left(f_{Idt_j} \leq f_{allow\_fcd}, "OK", "NG"\right) \qquad Status\_ServiceLSfcd^{\mathsf{T}} = ("OK" \quad "OK")$$

Compressive Stress Due to Full Dead Load + Live Load:

$$f_{llt_j} := f_{pst_j} + f_{swt_j} + f_{deckt_j} + f_{barriert_j} + f_{fwst_j} + f_{LLt_j} + 0.5 \cdot f_{TGt}$$

$$f_{llt}^T = (-0.1312 \quad 2.1476) \cdot ksi$$

$$f_{allow\_fcl} := 0.6 \cdot f'_c \qquad\qquad f_{allow\_fcl} = 4.2 \cdot ksi \qquad\qquad \text{(LRFD 5.9.4.2.1)}$$

$$\text{Status\_ServiceLSfcl}_j := if\left(f_{llt_j} \le f_{allow\_fcl}, \text{"OK"}, \text{"NG"}\right) \qquad \text{Status\_ServiceLSfcl}^T = (\text{"OK"} \quad \text{"OK"})$$

Service I (Compressive Stresses in Top of Topping):

Only loads acting on composite section cause stresses in the topping.
Since flange slenderness ratio is less than 15, set $\phi_w = 1$.

Compressive Stress Due to Permanent Loads:

$$f_{ldtt_j} := f_{barriertt_j} + f_{fwstt_j} + f_{TGtt} \qquad\qquad f_{ldtt}^T = (1.085 \quad 1.1662) \cdot ksi$$

$$\text{Status\_ServiceLSfcdt}_j := if\left(f_{ldtt_j} \le f_{allow\_fcd}, \text{"OK"}, \text{"NG"}\right) \qquad \text{Status\_ServiceLSfcdt}^T = (\text{"OK"} \quad \text{"OK"})$$

Compressive Stress Due to Full Dead Load + Live Load:

$$f_{lltt_j} := f_{barriertt_j} + f_{fwstt_j} + f_{LLtt_j} + 0.5 \cdot f_{TGtt} \qquad\qquad f_{lltt}^T = (0.6777 \quad 1.3682) \cdot ksi$$

$$\text{Status\_ServiceLSfclt}_j := if\left(f_{lltt_j} \le f_{allow\_fcl}, \text{"OK"}, \text{"NG"}\right) \qquad \text{Status\_ServiceLSfclt}^T = (\text{"OK"} \quad \text{"OK"})$$

1.8 Flexural Strength Check

$$M_{u_j} := 1.25 \cdot \left(M_{swf_j} + M_{deck_j} + M_{barrier_j}\right) + 1.5 \cdot M_{fws_j} + 1.75 \cdot M_{LL_j} \qquad\qquad M_u^T = (257 \quad 1575) \cdot kip \cdot ft$$

$$\beta_1 := if\left[f'_{ct} \le 4 \cdot (ksi), 0.85, if\left[f'_{ct} \ge 8 \cdot (ksi), 0.65, 0.85 - \left[\frac{f'_{ct} - 4 \cdot (ksi)}{1 \cdot (ksi)} \cdot 0.05\right]\right]\right] \qquad \beta_1 = 0.85 \qquad \text{(LRFD 5.7.2.2)}$$

Preliminary estimate of L_d: $\qquad L_d := \left(270.0 \cdot ksi - \frac{2}{3} \cdot f_{pe}\right) \cdot d_b \cdot ksi^{-1} \qquad L_d = 94.38 \cdot in \qquad$ (LRFD Eq. 5.11.4.2-1)

$$K_{ld} := if(h \le 24 \cdot in, 1.0, 1.6) \qquad K_{ld} = 1$$

$$df_j := if\left[dist_j < L_t, \frac{dist_j}{L_t} \cdot \frac{f_{pe}}{f_{pu}}, if\left[dist_j < K_{ld} \cdot L_d, \frac{f_{pe} + \left(\frac{dist_j - L_t}{K_{ld} \cdot L_d - L_t}\right) \cdot \left(f_{pu} - f_{pe}\right)}{f_{pu}}, 1.0\right]\right]$$

$$df^T = (0.5092 \quad 1) \qquad \text{(fraction strands are developed)}$$

$$A_{ps_j} := No\_Strands \cdot df_j \cdot A_{strand} \qquad\qquad A_{ps}^T = (2.6522 \quad 5.208) \cdot in^2$$

$$b := b_{eff}$$

$$d_p := h + t_h + t_{slab} - t_{ws} - y_{cg}$$

$$k := 2 \cdot \left(1.04 - \frac{f_{py}}{f_{pu}}\right) \qquad\qquad k = 0.28$$

$$\qquad\qquad\qquad\qquad\qquad\qquad\qquad\qquad\qquad\qquad\qquad\qquad \text{(LRFD 5.7.3.1.1-2)}$$

$$h_f := t_{slab}$$

B1-23

$$c_j := \frac{A_{ps_j} \cdot f_{pu}}{0.85 \cdot f'_{ct} \cdot \beta_1 \cdot b + k \cdot A_{ps_j} \cdot \frac{f_{pu}}{d_p}}$$

$$c^T = (3.35 \quad 6.42) \cdot in$$

(LRFD 5.7.3.1.1-4)

$$b_{w_j} := if\left(c_j \le h_f, b, b_v\right)$$

$$b_w^T = (72 \quad 72) \cdot in$$

$$c_j := \frac{A_{ps_j} \cdot f_{pu} - 0.85 \cdot f'_{ct} \cdot \left(b - b_{w_j}\right) \cdot h_f}{0.85 \cdot f'_{ct} \cdot \beta_1 \cdot b_{w_j} + k \cdot A_{ps_j} \cdot \frac{f_{pu}}{d_p}}$$

$$c^T = (3.35 \quad 6.42) \cdot in$$

(LRFD 5.7.3.1.1-3)

$$f_{ps_j} := f_{pu} \cdot \left(1 - k \cdot \frac{c_j}{d_p}\right)$$

$$f_{ps}^T = (263 \quad 256.5) \cdot ksi$$

(LRFD 5.7.3.1.1-1)

$$a_j := \beta_1 \cdot c_j$$

$$a^T = (2.8489 \quad 5.4573) \cdot in$$

$$L_d := \left(f_{ps_1} - \frac{2}{3} \cdot f_{pe}\right) \cdot d_b \cdot ksi^{-1}$$

$$L_d = 90.16 \cdot in$$

(LRFD 5.11.4.1-1)

$$dist_j := x_{f_j} + \frac{L_{ovr} - L_{des}}{2}$$

$$dist^T = (2.44 \quad 25) \, ft$$

$$df_j := if\left[dist_j < L_t, \frac{dist_j}{L_t} \cdot \frac{f_{pe}}{f_{ps_j}}, if\left[dist_j < K_{ld} \cdot L_d, \frac{f_{pe} + \left(\frac{dist_j - L_t}{K_{ld} \cdot L_d - L_t}\right) \cdot \left(f_{ps_j} - f_{pe}\right)}{f_{ps_j}}, 1.0\right]\right]$$

$$df^T = (0.5229 \quad 1)$$ (fraction strands are developed)

$$A_{ps_j} := No\_Strands \cdot df_j \cdot A_{strand}$$

$$A_{ps}^T = (2.7231 \quad 5.208) \cdot in^2$$

$$M_{n_j} := A_{ps_j} \cdot f_{ps_j} \cdot \left(d_p - \frac{a_j}{2}\right) + 0.85 \cdot f'_c \cdot \left(b - b_{w_j}\right) \cdot h_f \cdot \left(\frac{a_j}{2} - \frac{h_f}{2}\right)$$

(LRFD 5.7.3.2.2-1)

$$M_n^T = (2063 \quad 3704) \cdot kip \cdot ft$$

Compute phi for each section:

$$\phi_{f_j} := 0.583 + 0.25 \cdot \left(\frac{d_p}{c_j} - 1\right)$$

$$\phi_f^T = (3.02 \quad 1.73)$$

(LRFD Eq. 5.5.4.2.1-1)

$$\phi_{f_j} := if\left(\phi_{f_j} \le 0.75, 0.75, if\left(\phi_{f_j} > 1.0, 1.0, \phi_{f_j}\right)\right)$$

$$\phi_f^T = (1.00 \quad 1.00)$$

$$\phi M_{n_j} := \phi_{f_j} \cdot M_{n_j} \qquad M_{r_j} := \phi M_{n_j}$$

$$M_r^T = (2063 \quad 3704) \cdot kip \cdot ft \qquad \qquad M_u^T = (257 \quad 1575) \cdot kip \cdot ft$$

$$Status\_StrengthLS_j := if\left(M_{u_j} \le M_{r_j}, "OK", "NG"\right)$$

$$Status\_StrengthLS^T = ("OK" \quad "OK")$$

B1-24

Maximum Steel Check:

Note: The provisions contained in Art. 5.7.3.3.1 to check maximum reinforcement were deleted in 2005. This check is now effectively handled by varying phi, depending upon whether the section is compression or tension controlled. See Art. 5.5.4.2.1.

Minimum Steel Check:

Compute Cracking Moment at Midspan:

$$f_r := 0.37 \cdot \sqrt{f'_c} \cdot \sqrt{ksi} \qquad f_r = 0.979 \cdot ksi$$

$$M_{cr} := S_{bc} \cdot \left(f_r + f_{psb_2}\right) - \left(M_{swf_2} + M_{deck_2}\right) \cdot \left(\frac{S_{bc}}{S_b} - 1\right)$$

$$M_{cr} := if\left(M_{cr} < S_{bc} \cdot f_r, S_{bc} \cdot f_r, M_{cr}\right) \qquad M_{cr} = 1265 \cdot kip \cdot ft$$

$$1.2 \cdot M_{cr} = 1518 \cdot kip \cdot ft \qquad \text{Ref:} \quad M_{r_2} = 3704.1 \cdot kip \cdot ft$$

$$1.33 \cdot M_{u_2} = 2095.3 \cdot kip \cdot ft$$

$$M_{min} := if\left(1.2 \cdot M_{cr} < 1.33\, M_{u_2}, 1.2 M_{cr}, 1.33 \cdot M_{u_4}\right) \qquad M_{min} = 1518 \cdot kip \cdot ft$$

$$Status\_MinStl := if\left(M_{min} < M_{r_2}, \text{"OK"}, \text{"NG"}\right) \qquad \qquad Status\_MinStl = \text{"OK"}$$

1.9 Vertical Shear Design

At each section the following must be satisfied for shear:

$$V_u \le V_r \qquad\qquad \text{(LRFD 5.8.2.1-2)}$$

$$V_r = \phi V_n$$

$$V_n = V_c + V_s + V_p \qquad\qquad \text{(LRFD 5.8.3.3-1)}$$

Critical Section for Shear: (LRFD 5.8.3.2)

The critical section for shear near a support in which the reaction force produces compression in the end of the member is, from the face of support (Fig. 2), the greater of:
   a. $0.5 d_v \cot(\theta)$, or
   b. d_v

where,
   d_v = Effective shear depth = Distance between resultants of tensile and compressive forces = d_e - a/2

Compute A_{ps} & d_p

Note that A_{ps} in the equation used to compute ε_x is the area of the prestressing steel on the flexural tension side only. It is not the total area of strands. The variable A_{ps_ex} is introduced below to handle this.

B1-25

$$\text{No}_{\text{Aps\_ft}}(\text{Pat\_n}, \text{Pat\_h}, \text{hc\_2}) := \begin{array}{|l} j \leftarrow \text{last}(\text{Pat\_n}) \\ N \leftarrow 0 \\ \text{while } \text{Pat\_h}_j \leq \dfrac{\text{hc\_2}}{2} \\ \quad \begin{array}{|l} N \leftarrow N + \text{Pat\_n}_j \\ j \leftarrow j - 1 \\ \text{break if } j = 0 \end{array} \\ N \end{array}$$

$$N_{\text{Aps\_ft}} := \text{No}_{\text{Aps\_ft}}(\text{Pat\_n}, \text{Pat\_h}, h_c) \qquad N_{\text{Aps\_ft}} = 24$$

$$\text{CG}_{\text{Aps\_ft}}(\text{Pat\_n}, \text{Pat\_h}, \text{hc\_2}) := \begin{array}{|l} j \leftarrow \text{last}(\text{Pat\_n}) \\ N \leftarrow 0 \\ N\_cg \leftarrow 0 \\ \text{while } \text{Pat\_h}_j \leq \dfrac{\text{hc\_2}}{2} \\ \quad \begin{array}{|l} N \leftarrow N + \text{Pat\_n}_j \\ N\_cg \leftarrow N\_cg + \text{Pat\_n}_j \cdot \text{Pat\_h}_j \\ j \leftarrow j - 1 \\ \text{break if } j = 0 \end{array} \\ \dfrac{N\_cg}{N} \end{array}$$

$$\text{CG}_{\text{Aps\_ft}} := \text{CG}_{\text{Aps\_ft}}(\text{Pat\_n}, \text{Pat\_h}, h_c) \qquad \text{CG}_{\text{Aps\_ft}} = 3 \cdot \text{in}$$

$$d_{pv} := h + t_h + t_{slab} - t_{ws} - \text{CG}_{\text{Aps\_ft}} \qquad d_{pv} = 36 \cdot \text{in}$$

$$A_{ps\_ex} := dt_1 \cdot N_{\text{Aps\_ft}} \cdot A_{strand} \qquad A_{ps\_ex} = 4.236 \cdot \text{in}^2 \qquad dt_1 = 0.8133$$

Compute "a" based on Aps on Flexural-Tension Side:

$$A_{ps\_a} := df_1 \cdot N_{\text{Aps\_ft}} \cdot A_{strand} \qquad A_{ps\_a} = 2.723 \cdot \text{in}^2 \qquad df_1 = 0.5229$$

$$c_v := \dfrac{A_{ps\_a} \cdot f_{pu}}{0.85 \cdot f'_{ct} \cdot \beta_1 \cdot b + k \cdot A_{ps\_a} \cdot \dfrac{f_{ps_1}}{d_{pv}}} \qquad c_v = 3.44 \cdot \text{in}$$

$$b_{wv} := \text{if}(c_v \leq h_f, b, b_v) \qquad b_{wv} = 72 \cdot \text{in}$$

$$c_v := \dfrac{A_{ps\_a} \cdot f_{pu} - 0.85 \cdot f'_{ct} \cdot (b - b_{wv}) \cdot h_f}{0.85 \cdot f'_{ct} \cdot \beta_1 \cdot b_{wv} + k \cdot A_{ps\_a} \cdot \dfrac{f_{ps_1}}{d_{pv}}} \qquad c_v = 3.44 \cdot \text{in}$$

$$a_v := \beta_1 \cdot c_v \qquad a_v = 2.9252 \cdot \text{in}$$

$$M_{nv} := A_{ps\_a} \cdot f_{ps_1} \cdot \left(d_{pv} - \dfrac{a_v}{2} \right) + 0.85 \cdot f'_c \cdot (b - b_{wv}) \cdot h_f \cdot \left(\dfrac{a_v}{2} - \dfrac{h_f}{2} \right)$$

$$M_{nv} = 2061 \cdot \text{kip} \cdot \text{ft}$$

B1-26

Compute d_v:

$$d_v := \frac{M_{nv}}{A_{ps\_a} \cdot f_{ps_1}} \qquad d_v = 34.537 \cdot in$$

(LRFD C5.8.2.9-1)

But d_v need not be taken less than the greater of $0.9d_e$ and $0.72h$. Thus,

$$0.9 \cdot d_p = 32.4 \cdot in \qquad\qquad 0.72 \cdot h_c = 17.28 \cdot in$$

$$Min\_d_v := if\left(0.9 \cdot d_p \geq 0.72 \cdot h_c, 0.9 \cdot d_p, 0.72 \cdot h_c\right) \qquad Min\_d_v = 32.4 \cdot in$$

$$d_v := if\left(d_v < Min\_d_v, Min\_d_v, d_v\right) \qquad d_v = 34.537 \cdot in$$

To compute critical section, assume: $\qquad \theta := 20.8 \cdot deg$

$$0.5 \cdot d_v \cdot \cot(\theta) = 45.4602 \cdot in$$

$$Crit\_sec := if\left(d_v > 0.5 \cdot d_v \cdot \cot(\theta), d_v, 0.5 \cdot d_v \cdot \cot(\theta)\right)$$

(LRFD 5.8.2.7)

$$Crit\_sec = 45.46 \cdot in \qquad Crit\_sec = 3.788\,ft$$

Assuming that the distance from the face of support to the centerline of bearing is half the bearing pad length, the critical section for shear is:

$$x_{f_1} := Crit\_sec + \frac{L_{pad}}{2} \qquad x_{f_1} = 4.288\,ft \qquad \text{(Note: Compare this to previous assumption)}$$

At the critical section, the factored shear is:

$$V_u := 1.25 \cdot \left(V_{swf_1} + V_{deck_1} + V_{barrier_1}\right) + 1.5 \cdot V_{fws_1} + 1.75 \cdot V_{LL_1}$$

$$V_u = 129.6 \cdot kip$$

Since the pattern profile for PCSSS beams will always be straight, there will be no vertical component of the prestressing force, V_p:

$$V_p := 0.0 \cdot kip$$

Compute maximum permissible shear capacity at a section:

$$V_{r\_max} := \phi_v \cdot \left(0.25 \cdot f'_c \cdot b_v \cdot d_v + V_p\right) \qquad\qquad V_{r\_max} = 3917 \cdot kip$$

(LRFD 5.8.3.3-2)

$$Status\_V_{rmax} := if\left(V_u \leq V_{r\_max}, \text{"OK"}, \text{"NG"}\right)$$

$$Status\_V_{rmax} = \text{"OK"}$$

The shear contribution from the concrete, V_c, is given by:

$$V_c = 0.0316 \cdot \beta \cdot \sqrt{f_c} b_v \cdot d_v$$

(LRFD 5.8.3.3-3)

To calculate β, first compute f_{po}:

This can be taken as $0.70f_{pu}$ per the 2000 Interim Specifications:

$$f_{po} := 0.75 \cdot f_{pu} \qquad f_{po} = 202.5 \cdot ksi$$

(LRFD 5.8.3.4.2)

In the 2008 Interim the procedure for the calculation of θ and β was moved to an appendix. The new procedure for the calculation of these two values involves a new value, ε_s.

Check lower bound for Mu:

$$M_{uLB} := if\left[M_{u_1} < d_v \cdot \left(V_u - V_p\right), d_v \cdot \left(V_u - V_p\right), M_{u_1}\right] \qquad M_{uLB} = 372.9 \cdot kip \cdot ft$$

$$\varepsilon_s := \frac{\dfrac{M_{uLB}}{d_v} + \left(V_u - V_p\right) - A_{ps\_ex} \cdot f_{po}}{E_p \cdot A_{ps\_ex}} \qquad \varepsilon_s = -0.00495882$$

(LRFD 5.8.3.4.2-4)

B1-27

If ε_s is less than zero, it can be taken equal to zero:

$$\varepsilon_s := \text{if}\left(\varepsilon_s < 0, 0.0, \varepsilon_s\right) \qquad\qquad\qquad \varepsilon_s = 0$$

$$\beta := \frac{4.8}{1 + 750 \cdot \varepsilon_s} \qquad\qquad\qquad \beta = 4.8 \qquad\qquad\qquad \text{(LRFD 5.8.3.4.2-1)}$$

$$\theta := 29 + 3500 \cdot \varepsilon_s \qquad\qquad\qquad \theta = 29 \qquad\qquad\qquad \text{(LRFD 5.8.3.4.2-3)}$$

New value for V_c

$$V_c := 0.0316 \cdot \beta \cdot \sqrt{f'_c} \cdot \sqrt{ksi} \cdot b_v \cdot d_v \qquad\qquad\qquad V_c = 997.9 \cdot kip$$

Required V_s is, therefore:

$$V_s := \frac{V_u}{\phi_v} - V_c - V_p \qquad\qquad\qquad V_s = -854 \cdot kip$$

Assuming two vertical legs of No. #4 bars:

$$A_v := \frac{V_s}{f_y \cdot d_v \cdot \cot(\theta)} \qquad\qquad A_v = -4.387 \cdot \frac{in^2}{ft} \qquad\qquad\qquad \text{(LRFD C5.8.3.3-1)}$$

$$\text{Spac} := \frac{2 \cdot 0.2 \cdot in^2}{A_v} \qquad\qquad \text{Spac} = -1.1 \cdot in \qquad\qquad \text{(stirrup spacing)}$$

Check minimum transverse reinforcement:

$$A_{v\_min} := 0.0316 \cdot \sqrt{f'_c} \cdot \sqrt{ksi} \cdot \frac{b_v}{f_y} \qquad\qquad A_{v\_min} = 1.2 \cdot \frac{in^2}{ft} \qquad\qquad \text{(LRFD 5.8.2.5-1)}$$

Check maximum stirrup spacing:

$$\text{(LRFD 5.8.2.7-2)}$$

$$V_{spc} := 0.1 \cdot f'_c \cdot b_v \cdot d_v \qquad\qquad V_{spc} = 1740.7 \cdot kip$$

Ref: $\quad V_u = 129.6 \cdot kip \qquad\qquad d_v = 34.54 \cdot in$

$$\text{Max\_spac} := \text{if}\left(V_u < V_{spc}, \text{if}\left(0.8 \cdot d_v < 24 \cdot in, 0.8 \cdot d_v, 24 \cdot in\right), \text{if}\left(0.4 \cdot d_v < 12 \cdot in, 0.4 \cdot d_v, 12 \cdot in\right)\right)$$

$$\text{Max\_spac} = 24 \cdot in$$

1.10 Longitudinal Reinforcement Check

LRFD requires that the longitudinal steel be checked at all locations along the beam. This requirement is made to ensure that the longitudinal reinforcement is sufficient to develop the required tension tie, which is required for equilibrium. Equation 5.8.3.5-1 is the general equation, applicable at all sections. However, for the special case of the inside edge of bearing at simple-end supports, the longitudinal reinforcement must be able to resist a tensile force of $(V_u/\phi - 0.5V_s - V_p)\cot(\theta)$. Note that when pretensioned strands are used to develop this force, only a portion of the full prestress force may be available near the support due to partial transfer. Additionally, only those strands on the flexural tension side of the member contribute to the tension tie force.

<u>Required Tension Tie Force:</u>

If only the minimum amount of transverse reinforcement that is required by design is provided, the required tension tie force is:

$$F_{L\_reqd} := \left(\frac{V_u}{\phi_v} - 0.5 \cdot V_s - V_p\right) \cdot \cot(\theta) \qquad\qquad F_{L\_reqd} = 643.6 \cdot kip \qquad\qquad \text{Eq. 5.8.3.5-2}$$

However, a greater amount of stirrup reinforcement is typically provided than is required, which increases the actual V_s. Note that by Eq. 5.8.3.5-2, increasing V_s decreases the required tension tie force. Hence, it is helpful to use the computed value of V_s that results from the transverse reinforcement detailed in the design. In this case, the required tension tie force is:

    Assume 2 legs of No. 4 bars at 12" on center (amount of steel at the critical section for shear):

$$A_{v\_actual} := 0.4 \cdot in^2$$

$$V_{s\_actual} := \frac{A_{v\_actual} \cdot f_y \cdot d_v \cdot \cot(\theta)}{12 \cdot in} \qquad\qquad V_{s\_actual} = 77.9 \cdot kip$$

    Check the upper limit of V_s:

$$V_{s\_actual\_max} := \frac{V_u}{\phi_v} \qquad\qquad V_{s\_actual\_max} = 144 \cdot kip \qquad\qquad \text{LRFD 5.8.3.5}$$

    Adopt the lesser of provided V_s and the upper limit of V_s:

$$V_{s\_actual} := if\left(V_{s\_actual} < V_{s\_actual\_max}, V_{s\_actual}, V_{s\_actual\_max}\right)$$

$$V_{s\_actual} = 77.9 \cdot kip$$

    The revised value of the required tension tie force is:

$$F_{L\_reqd} := \left[\left(\frac{V_u}{\phi_v}\right) - 0.5 \cdot V_{s\_actual} - V_p\right] \cdot \cot(\theta) \qquad F_{L\_reqd} = 118.4 \cdot kip$$

<u>Provided Tension Tie Force:</u>

The longitudinal reinforcement that contributes to the tension tie are strands that are on the flexural tension side of the precast section. Near the ends of the precast section, the strands are typically only partially effective. C5.8.3.5 of the 2006 Interim Revisions permits the strand stress in regions of partial development to be estimated using a bilinear variation, as shown in Fig. 4.
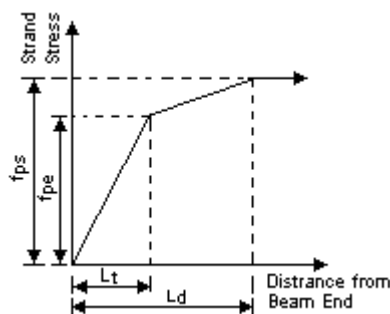
Figure 6: Variation in strand stress in relation to distance from beam end.

The stress in the strands at a given section depends on the location of the section with respect to the end of the precast section. If the section is between the end of the beam and L_t (see Fig. 5), a linear interpolation is performed using a stress variation of 0.0 at the end of the beam to f_{pe} at a distance of L_t from the end of the precast section. If the section is to the right of L_t but to the left of L_d, then the stress is interpolated between f_{pe} and f_{ps}. If the section is to the right of L_d, then the stress is assumed to be a constant value of f_{ps}.

At the face of bearing, the stress in the effective strands is:

$$x_{FB} := \frac{L_{ovr} - L_{des}}{2} + \frac{L_{pad}}{2} \qquad x_{FB} = 1.00\,\text{ft} \qquad \text{(Distance from physical end of beam to face of bearing)}$$

$$A_{str} := A_{strand}$$

$$F_{L\_prov} := if\left[x_{FB} < L_t, N_{Aps\_ft} \cdot A_{str} \cdot f_{pe} \cdot \frac{x_{FB}}{L_t}, if\left[x_{FB} < K_{ld} \cdot L_d, N_{Aps\_ft} \cdot A_{str} \cdot \left[f_{pe} + \left(\frac{x_{FB} - K_{ld} \cdot L_d + L_t}{K_{ld} \cdot L_d - L_t}\right) \cdot (f_{ps} - f_{pe})\right], N_{Aps\_ft} \cdot A_{str} \cdot f_{pe}\right]\right]$$

$$F_{L\_prov} = 293.5 \cdot \text{kip}$$

$$\text{Status\_V}_I := if\left(F_{L\_prov} \geq F_{L\_reqd}, \text{"OK"}, \text{"NG"}\right) \qquad\qquad \boxed{\text{Status\_V}_I = \text{"OK"}}$$

Refined Estimate of Provided Tension Tie Force:

If it is assumed that the point of intersection of the bearing crack (at angle theta) and c.g. of the strands is where the force in the strands is computed, then additional tensile capacity from the strands can be utilized.
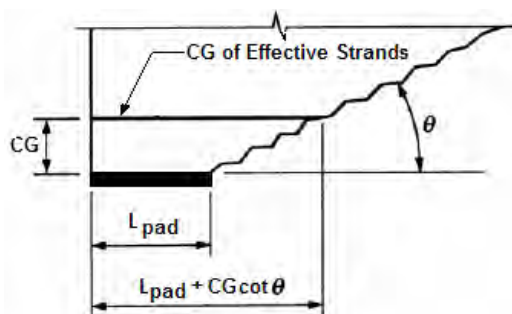
Figure 7: Elevation view of end of beam showing location where assumed failure crack crosses the c.g. of that portion of the strand pattern that is effective for resisting tensile forces caused by moment and shear.

Distance from end of beam to point of intersection of assumed crack and center of gravity of effective strands:

$$x_c := \left(\frac{L_{pad}}{2}\right) + CG_{Aps\_ft} \cdot \cot(\theta) \qquad\qquad x_c = 0.8 \cdot \text{ft} \qquad \text{(Measured from L face of bearing)}$$

$$x_c := \left(\frac{L_{ovr} - L_{des}}{2}\right) + \left(\frac{L_{pad}}{2}\right) + CG_{Aps\_ft} \cdot \cot(\theta) \qquad x_c = 1.3 \cdot \text{ft} \qquad \text{(Measured from L end of beam)}$$

$$F_{L\_prov} := if\left[x_c < L_t, N_{Aps\_ft} \cdot A_{str} \cdot f_{pe} \cdot \frac{x_c}{L_t}, if\left[x_c < K_{ld} \cdot L_d, N_{Aps\_ft} \cdot A_{str} \cdot \left[f_{pe} + \left(\frac{x_c - K_{ld} \cdot L_d + L_t}{K_{ld} \cdot L_d - L_t}\right) \cdot (f_{ps} - f_{pe})\right], N_{Aps\_ft} \cdot A_{str} \cdot f_{pe}\right]\right]$$

$$F_{L\_prov} = 376.2 \cdot \text{kip}$$

$$\text{Status\_V}_I := if\left(F_{L\_prov} \geq F_{L\_reqd}, \text{"OK"}, \text{"NG"}\right) \qquad\qquad \boxed{\text{Status\_V}_I = \text{"OK"}}$$

1.11 Interface Shear Design

The ability to transfer shear across the interface between the top of the precast beam and the cast-in-place deck must be checked. This check falls under the interface shear or shear friction section of LRFD (5.8.4). Recall that under the *Standard Specs*, this check falls under the horizontal shear section.

Little guidance is offered by the LRFD Specs on how to compute the applied shear stress at the strength limit state. The procedure presented here uses the approach recommended by the *PCI Bridge Design Manual,* which is a strength limit state approach.

Applied Factored Shear: $V_u = 129.6 \cdot kip$

$$v_{uh\_s} := \frac{V_u}{d_v \cdot b_v} \qquad\qquad v_{uh\_s} = 0.052 \cdot ksi$$

$$v_{nh\_reqd} := \frac{v_{uh\_s}}{\phi_v} \qquad\qquad v_{nh\_reqd} = 0.0579 \cdot ksi$$

$$A_{cv} := b_v \cdot 1.0 \cdot ft \qquad A_{cv} = 864 \cdot in^2$$

$$V_{nhr} := v_{nh\_reqd} \cdot A_{cv} \qquad V_{nhr} = 50 \cdot kip$$

Nominal Shear Resistance of the Interface (Capacity):

$$V_n = c A_{cv} + \mu \left(A_{vf} \cdot f_y + P_c \right) \qquad\qquad \text{(LRFD 5.8.4.1-2)}$$

Interface is CIP concrete slab on clean, roughened beam surface, no reinforcement crossing shear plane: (LRFD 5.8.4.3)

$c := 0.135 \cdot ksi$ (cohesion factor)

$\mu := 1.000$ (friction factor)

$K_1 := 0.2$ (fraction of concrete strength available to resist interface shear)

$K_2 := 0.8 \cdot ksi$ (limiting interface shear resistance)

Since there is no permanent net compressive stress normal to shear plane, $P_c = 0$.   (LRFD 5.8.4.2)

Check Maximum Allowable Shear:

$$V_{ni\_max1} := K_1 \cdot f'_{ct} \cdot A_{cv} \qquad V_{ni\_max1} = 691 \cdot kip \qquad\qquad \text{(LRFD 5.8.4.1-4)}$$

$$V_{ni\_max2} := K_2 \cdot A_{cv} \qquad V_{ni\_max2} = 691 \cdot kip \qquad\qquad \text{(LRFD 5.8.4.1-5)}$$

$$V_{nh\_max} := if \left(V_{ni\_max1} \le V_{ni\_max2}, V_{ni\_max1}, V_{ni\_max2} \right) \qquad\qquad \text{(LRFD 5.8.4.1-2,3)}$$

$$V_{nh\_max} = 691 \cdot kip$$

$$V_{nh\_reqd} := v_{nh\_reqd} \cdot A_{cv} \qquad\qquad V_{nh\_reqd} = 50 \cdot kip$$

$$\text{Status\_V}_{uh\_max} := if \left(V_{nh\_reqd} < V_{nh\_max}, \text{"OK"}, \text{"NG"} \right) \qquad\qquad \text{Status\_V}_{uh\_max} = \text{"OK"}$$

Assuming no horizontal shear reinforcement crossing the shear plane, provided horizontal shear resistance is:

$$V_{nh\_prov} := c \cdot A_{cv} \qquad V_{nh\_prov} = 116.6 \cdot kip$$

$$\text{Status\_V}_{nh\_prov} := if \left(V_{nhr} < V_{nh\_prov}, \text{"OK"}, \text{"NG"} \right) \qquad\qquad \text{Status\_V}_{nh\_prov} = \text{"OK"}$$

B1-31

1.12 Spalling Forces

If the maximum spalling stress on the end face of the girder is less than the direct tensile strength of the concrete, then spalling reinforcement is not required when the member depth is less than 22 in. The maximum spalling stress is estimated as:

$$\sigma_s = \frac{P}{A}\left(0.1206 \cdot \frac{e^2}{h \cdot d_b} - 0.0256\right) \geq 0$$

And the direct tensile strength is computed as:

$$f_{r\_dts} := -0.23 \cdot \sqrt{f'_c} \cdot \sqrt{ksi} \qquad f_{r\_dts} = -0.609 \cdot ksi \qquad\qquad \text{(LRFD C5.4.2,7)}$$

Check reinforcement requirement:

$$\text{Ref:} \quad A = 936 \cdot in^2 \quad h = 18 \cdot in \quad ecc = 5.42 \cdot in \quad d_b = 0.6 \cdot in$$

$$P_{jack} := A_{ps_2} \cdot f_{pj} \qquad P_{jack} = 1 \times 10^3 \cdot kip$$

$$\sigma_s := \frac{-P_{jack}}{A}\left(0.1206 \cdot \frac{ecc^2}{h \cdot d_b} - 0.0256\right) \qquad \sigma_s = -0.341 \cdot ksi$$

Check whether spalling stress is below threshold and thus is spalling/busting reinforcement is needed:

$$\text{Status\_Spalling} := if\left(\sigma_s > f_{r\_dts}, \text{"OK"}, \text{"NG"}\right) \qquad\qquad \text{Status\_Spalling} = \text{"OK"}$$

1.13 Transverse Load Distribution

The transverse load distribution reinforcement is computed by:

$$A_{tld} = k_{mild} \cdot A_{l\_mild} + \alpha \cdot k_{ps} \cdot A_{l\_ps}$$

where:

$$\alpha = \frac{d_{cgs}}{d_{trans}}$$

$$k_{ps} = \frac{100}{\sqrt{L}} \cdot \frac{f_{pe}}{60} \leq 50\%$$

$$k_{mild} = \frac{100}{\sqrt{L}} \leq 50\%$$

$$d_{cgs} := h_c - y_{cg} \qquad d_{cgs} = 21.0 \cdot in$$

Compute d_{trans}:

$$d_{trans} := h_c - 4in - \frac{d_b}{2} - \frac{0.75 \cdot in}{2} \qquad d_{trans} = 19.3 \cdot in$$

$$\alpha := \frac{d_{cgs}}{d_{trans}} \qquad \alpha = 1.0867$$

Assume there is no mild longitudinal reinforcement A_{l_mild} in tension at the strength limit state.

$$A_{l\_mild} := 0.0 \cdot in^2$$

$$k_{mild} := \frac{\dfrac{100 \cdot \sqrt{ft}}{\sqrt{L_{des}}}}{100} \qquad k_{mild} = 14.29 \cdot \%$$

B1-32

$$k_{ps} := \frac{\dfrac{100 \cdot \sqrt{ft}}{\sqrt{L_{des}}} \cdot \dfrac{f_{pe}}{60 \cdot ksi}}{100} \qquad k_{ps} = 40.25 \cdot \%$$

$$A_{l\_ps} := A_{ps_2} \qquad\qquad A_{l\_ps} = 5.208 \cdot in^2$$

Total amount of transverse load distribution is:

$$A_{tld} := k_{mild} \cdot A_{l\_mild} + \alpha \cdot k_{ps} \cdot A_{l\_ps} \qquad A_{tld} = 2.28 \cdot in^2$$

Since the longitudinal reinforcement is per beam width, the area of distribution reinforcement per foot is:

$$A_{tld\_per\_ft} := \frac{A_{tld}}{S} \qquad A_{tld\_per\_ft} = 0.38 \cdot \frac{in^2}{ft}$$

Assuming transverse bars are #6, maximum spacing is:

Set transverse load distribution reinforcement spacing at 12 in.:

$$S_{ld\_spac\_max} := \frac{0.44 \cdot in^2}{A_{tld\_per\_ft} \cdot ft} \cdot ft \qquad S_{ld\_spac\_max} = 13.9 \cdot in \qquad S_{ld\_spac} := 12 in$$

1.14 Reflective Crack Control Reinforcement

Reflective crack control reinforcement is provided from both the transverse load distribution reinforcement as well a drop in cage consisting of vertical stirrups. The total amount of reflective crack control reinforcement required is given as follows:

$$\rho_{cr\_req} := \frac{6 \sqrt{f'_{ct}} \cdot \sqrt{psi}}{f_y} \qquad \rho_{cr\_req} = 0.00632 \qquad\qquad \text{(LRFD 5.14.4.3.3f-1)}$$

The crack control reinforcement ratio is defined, per unit length of span, as follows:

$$\rho_{cr} = \frac{A_{scr}}{(h - t_{flg}) \cdot 1 ft} \qquad\qquad \text{(LRFD 5.14.4.3.3f-2)}$$

The required area of reinforcement of reflective crack control is therefore calculated, per unit length of span, as:

$$A_{scr\_req} := \rho_{cr\_req} \cdot (h - t_{flg}) \cdot 1 ft \qquad A_{scr\_req} = 1.1384 \cdot in^2$$

The required area of cage reinforcement is subsequently calculated, per unit length of span, as the difference between the total required area of crack control reinforcement and that provided by the reinforcement for transverse load distribution; both transverse bars are effective in providing crack control, however only the lower horizontal legs of the stirrups are considered in the calculation. All calculations are per unit length of span:

$$A_{ld} := \frac{2 S_{ld\_spac} \cdot .44 in^2}{1 ft} \qquad\qquad A_{ld} = 0.88 \cdot in^2$$

$$A_{cr\_cage\_req} := A_{scr\_req} - A_{ld} \qquad A_{cr\_cage\_req} = 0.2584 \cdot in^2$$

B1-33

Provide No. 5 stirrups at 12 in. on center:

$S_{cage\_spac} := 12 in$ $A_{scage} := 0.31 in^2$

$A_{cr\_cage\_prov} := A_{scage} \cdot \left(\dfrac{1 ft}{S_{cage\_spac}} \right)$ $A_{cr\_cage\_prov} = 0.31 \cdot in^2$

$A_{scr\_prov} := A_{ld} + A_{cr\_cage\_prov}$

$Status\_A_{scrack} := if \left(A_{scr\_req} < A_{scr\_prov}, "OK", "NG" \right)$ $Status\_A_{scrack} = "OK"$

Figure 8: Cross section of bridge showing CIP regions.
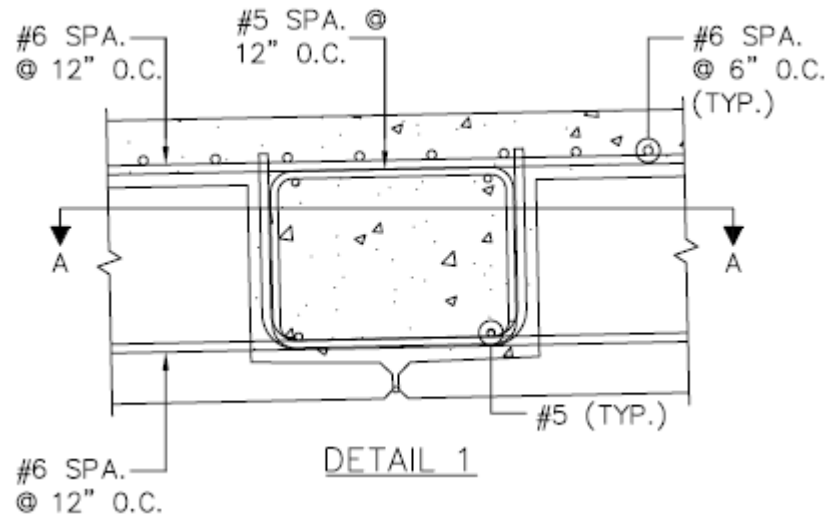
Figure 9: Detail of drop-in cage.
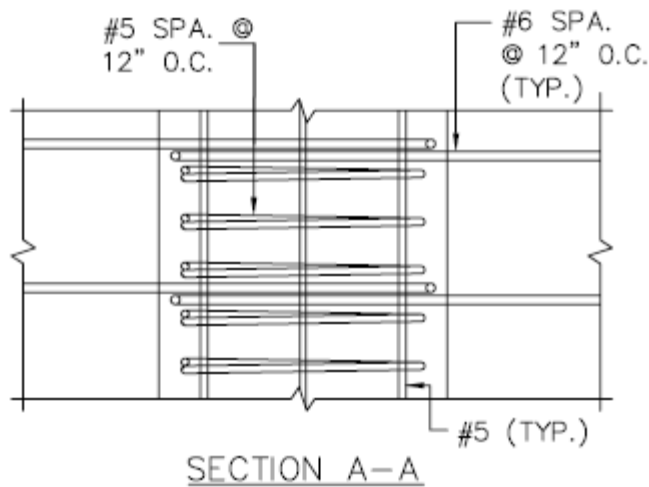
Figure 10: Plan view of drop-in cage.

1.14 Bottom Flange Reinforcement

Determine steel required to resist construction loads on bottom flange:

Assume a 1' wide strip:

Loads:

Self-weight of flange:

$$w_{flng\_sw} := t_{flg} \cdot 12 \cdot in \cdot w_{ct} \qquad\qquad w_{flng\_sw} = 0.0375 \cdot klf$$

CIP weight:

$$w_{flng\_cip} := (h - t_{flg}) \cdot 12 \cdot in \cdot w_{ct} \qquad w_{flng\_cip} = 0.1875 \cdot klf$$

Construction live load (assume 10 psf):

$$w_{flng\_LL} := w_{const} \cdot 12 \cdot in \qquad\qquad w_{flng\_LL} = 0.0100 \cdot klf$$

Moments:

$$b_{cant} := \frac{b_h}{2} \qquad\qquad b_{cant} = 1.00\,ft \qquad \text{(Length of cantilever)}$$

$$M_{flng\_sw} := \frac{w_{flng\_sw} \cdot b_{cant}^2}{2} \qquad M_{flng\_sw} = 0.0187 \cdot kip \cdot ft$$

$$M_{flng\_cip} := \frac{w_{flng\_cip} \cdot b_{cant}^2}{2} \qquad M_{flng\_cip} = 0.0937 \cdot kip \cdot ft$$

$$M_{flng\_LL} := \frac{w_{flng\_LL} \cdot b_{cant}^2}{2} \qquad M_{flng\_LL} = 0.005 \cdot kip \cdot ft$$

Strength Limit State I:

$$M_{u\_flng} := 1.25 \cdot (M_{flng\_sw} + M_{flng\_cip}) + 1.75 \cdot M_{flng\_LL} \qquad\qquad M_{u\_flng} = 0.15 \cdot kip \cdot ft$$

B1-35

Try #3 bars at 12" o.c:

$$A_{s\_flng} := 0.11 \cdot in^2 \qquad\qquad A_{s\_flng} = 0.11 \cdot in^2$$

$$c_{flng} := \frac{A_{s\_flng} \cdot f_y}{0.85 \cdot f'_c \cdot \beta_1 \cdot 12 \cdot in} \qquad c_{flng} = 0.11 \cdot in$$

$$\beta_{1p} := if\left[f'_c \le 4 \cdot (ksi), 0.85, if\left[f'_c \ge 8 \cdot (ksi), 0.65, 0.85 - \left[\frac{f'_c - 4 \cdot (ksi)}{1 \cdot (ksi)} \cdot 0.05\right]\right]\right] \qquad \beta_{1p} = 0.70$$

$$a_{flng} := \beta_{1p} \cdot c_{flng} \qquad\qquad a_{flng} = 0.0761 \cdot in$$

$$d_s := t_{flg} - 1 \cdot in - 0.5 \cdot in - \frac{0.5 \cdot in}{2} \qquad d_s = 1.25 \cdot in$$

$$M_{n\_flng} := A_{s\_flng} \cdot f_y \cdot \left(d_s - \frac{a_{flng}}{2}\right) \qquad M_{n\_flng} = 0.67 \cdot kip \cdot ft$$

$$\phi_{f\_flng} := 0.65 + 0.15 \cdot \left(\frac{d_s}{c_{flng}} - 1\right) \qquad \phi_{f\_flng} = 2.22$$

$$\phi_{f\_flng} := if\left(\phi_{f\_flng} \le 0.75, 0.75, if\left(\phi_{f\_flng} > 0.9, 0.9, \phi_{f\_flng}\right)\right) \qquad \phi_{f\_flng} = 0.9$$

$$M_{r\_flng} := \phi_{f\_flng} \cdot M_{n\_flng} \qquad M_{r\_flng} = 0.60 \cdot kip \cdot ft$$

$$Status\_StrengthLS_{flng} := if\left(M_{u\_flng} \le M_{r\_flng}, "OK", "NG"\right) \qquad Status\_StrengthLS_{flng} = "OK"$$

Use: Minimum #3 bars @ 12" o.c. in bottom flange.

Example Problem 2

2.1 Introduction

This example covers the design of the multi-span continuous bridge superstructure consisting of precast composite slab span system (PCSSS) elements. The structural system is a three-span, continuous structure with a 40'-50'-40' span layout. The steps required to design representative composite slab of the center span are illustrated. The design is carried out in accordance with the *AASHTO LRFD Bridge Design Specifications,* 5th Edition (2010).

2.2 Materials, Geometry, Loads and Load Factors

Units:

$kcf := kip \cdot ft^{-3}$ Defined unit: kips per cubic foot

Materials:

Concrete:

$f'_c := 7.0 \cdot ksi$ Strength of beam concrete at 28 days

$f'_{ci} := 5.0 \cdot ksi$ Strength of beam concrete at transfer of prestressing force

$w_c := 0.150 \cdot kcf$ Density of beam concrete

$f'_{ct} := 4.0 \cdot ksi$ Strength of CIP concrete at 28 days

$w_{ct} := 0.15 \cdot kcf$ Density of CIP concrete

$H := 70$ Average ambient relative humidity

$\phi_u := 2.1$ Ultimate creep coefficient

$\varepsilon_{shp\_u} := 0.00056$ Ultimate shrinkage strain in precast concrete

$\varepsilon_{shc\_u} := 0.00069$ Ultimate shrinkage strain in CIP concrete

$\alpha := 0.000006$ /°F   Coefficient of thermal expansion

Strand:

$A_{strand} := 0.217 \cdot in^2$ Area of one prestressing strand.

$d_b := 0.6 \cdot in$ Nominal diameter of prestressed strand.

$f_{pu} := 270 \cdot ksi$ Tensile strength of prestressing steel

$E_p := 28500 \cdot ksi$ Modulus of elasticity of prestressing steel

$f_{py} := 0.9 \cdot f_{pu}$ Yield strength of prestressing steel

$Pull := 0.75$ Pull of strands expressed as a fraction of f_{pu}

$t := 18 \cdot hr$ Time from tensioning to detensioning of strands

Rebar:

$f_y := 60 \cdot ksi$ Yield stress of ordinary rebar

$E_s := 29000 \cdot ksi$ Modulus of elasticity of non-prestressed reinforcement

Geometry:

Beam:

$Section := "IT"$ Precast section name

$h := 18.0 \cdot in$ Height of precast

$A := 936.0 \cdot in^2$ Gross area of precast section

$I := 27120 \cdot in^4$ Gross moment of inertia of precast cross section about cenroidal x-x axis

$y_b := 8.42 \cdot in$ — Center of gravity of gross precast cross section

$b_f := 72.0 \cdot in$ — Width of bottom flange of precast section

$t_{flg} := 3.00 \cdot in$ — Effective thickness of bottom flange

$b_v := 72.00 \cdot in$ — Shear width of precast section (web and longitudinal trough width)

$A_c := 450 \cdot in^2$ — Area of concrete on flexural tension side of member (see LRFD B5.2-3)

$VS_b := 5.2 \cdot in$ — Volume to surface ratio of precast section

$VS_d := 6.0 \cdot in$ — Volume to surface ratio of CIP slab

Slab:

$t_{slab} := 6.00 \cdot in$ — Thickness of CIP slab above precast beam

$t_h := 15.00 \cdot in$ — Thickness of CIP region between precast beams

$b_h := 24.00 \cdot in$ — Width of CIP region between precast units.beams

$t_{ws} := 0.0 \cdot in$ — Thickness of portion of CIP slab assumed to be wear

Span:

$L_{p2p} := 50.0 \cdot ft$ — Centerline of pier to centerline of pier dimension

$L_{ovr} := 49.0 \cdot ft$ — Overal length of precast section

$L_{des} := 48.0 \cdot ft$ — Design span of precast section

$L_{pad} := 12 \cdot in$ — Length of bearing pad

$Pier_{offset} := 0.5 \cdot ft$ — Distance from centerline of pier to end of beam

$Brng_{offset} := 0.5 \cdot ft$ — Distance from end of beam to centeriline of bearing

Bridge:

$S := 6.00 \cdot ft$ — Beam spacing

$N_g := 8$ — Number of precast sections in bridge cross section

$Width_{overall} := 47.5 \cdot ft$ — Overall width of bridge

$Width_{ctc} := 44.0 \cdot ft$ — Curb to curb width of bridge

$N_l := 2$ — Number of lanes

Loads:

Dead:

$N_{barriers} := 2$ — Number of barriers

$w_{barrier} := 0.300 \cdot klf$ — Weight of single barrier

$w_{fws} := 0.023 \cdot ksf$ — Weight of future wearing surface allowance

Live:

HL-93 — Notional live load per LRFD Specs

$w_{lane} := 0.64 \cdot klf$ — Design lane load

Construction Timing:

$t_{transfer} := 1.00 \cdot day$ — Time from release tensioning of strands to release of prestress

$t_{deck} := 7 \cdot day$ — Time when continuity is established

$t_{final} := 20000 \cdot day$ — Assumed end of service life of bridge (time final)

Load & Resistance Factors:

ϕ_f — Resistance factor for flexure

$\phi_v := 0.90$ — Resistance factor for shear

$DLA := 0.33$ — Dynamic load allowance (LRFD 3.6.2.1-1)
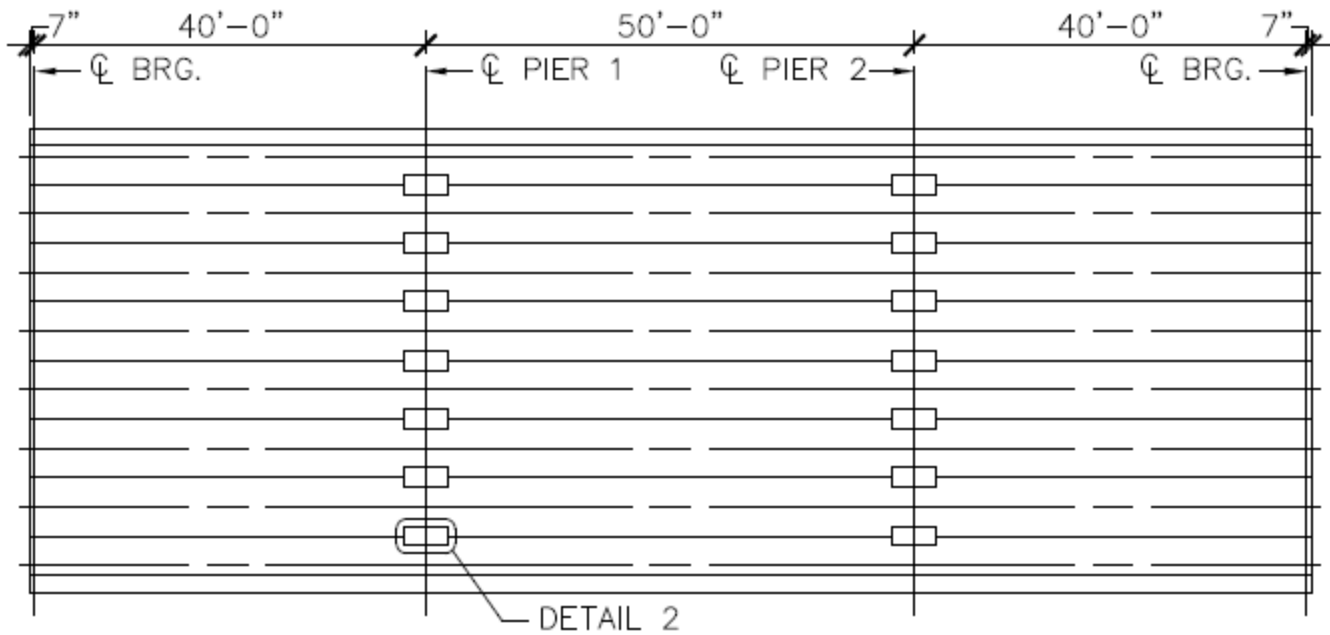
Figure 1: Plan view of bridge.
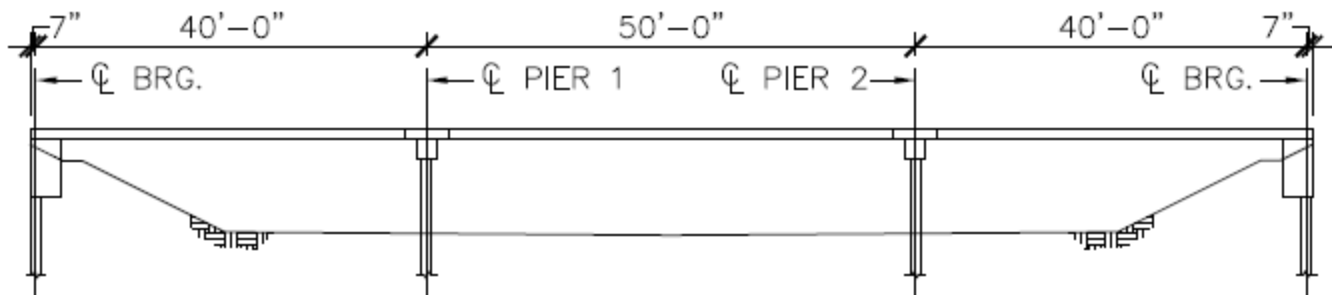
Figure 2: ELevation view of bridge.
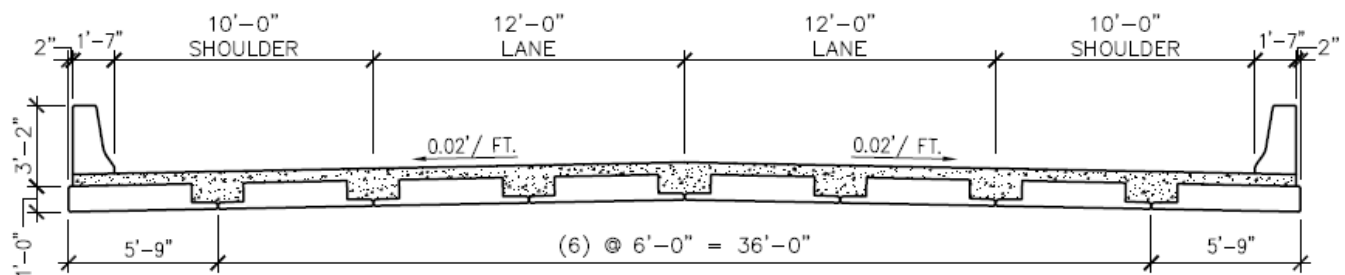
Figure 3: Cross section of bridge.

Loads:

<u>Composite Dead Load:</u>

Future Wearing Surface:

$$w_{fws} := 0.025 \cdot ksf \qquad w_{fws} := w_{fws} \cdot \frac{Width_{ctc}}{N_g} \qquad w_{fws} = 0.1375 \cdot klf \quad \text{(per beam)}$$

The moments and shears shown below were manually entered into this template. They represent 10th-point values of Span 2 that were generated by a 2-D continuous beam program using the model given in Fig. 5 along with the uniform load given above applied to all spans. All similarly highlighted regions represent manually entered values that were generated in a similar fashion.

Span 2:

$$M_{fws\_c} := \begin{pmatrix} -30.4 \\ -13.8 \\ -0.8 \\ 8.5 \\ 14.0 \\ 15.9 \\ 14.0 \\ 8.5 \\ -0.8 \\ -13.9 \\ -30.4 \end{pmatrix} \cdot kip \cdot ft \qquad V_{fws\_c} := \begin{pmatrix} 3.7 \\ 3.0 \\ 2.2 \\ 1.5 \\ 0.7 \\ 0 \\ -0.7 \\ -1.5 \\ -2.2 \\ -3.0 \\ -3.7 \end{pmatrix} \cdot kip$$

Barrier Loads:

$$w_{barrier} := 0.300 \cdot klf \qquad w_{barrier} := \frac{N_{barriers} \cdot w_{barrier}}{N_g} \qquad w_{barrier} = 0.075 \cdot klf \quad \text{(per beam)}$$

Span 2:

$$M_{barrier\_c} := \begin{pmatrix} -15.4 \\ -7.0 \\ -0.4 \\ 4.3 \\ 7.1 \\ 8.0 \\ 7.1 \\ 4.3 \\ -0.4 \\ -7.0 \\ -15.4 \end{pmatrix} \cdot kip \cdot ft \qquad V_{barrier\_c} := \begin{pmatrix} 1.9 \\ 1.5 \\ 1.1 \\ 0.8 \\ 0.4 \\ 0 \\ -0.4 \\ -0.8 \\ -1.1 \\ -1.5 \\ -1.9 \end{pmatrix} \cdot kip$$

B2-4

<u>Live Load:</u>   HL-93

As with the composite dead load moments and shears, the moments and shears for each component of the HL-93 live load were manually entered below.

Design Truck, Span 2, +M:

$$M_{truck\_pc} := \begin{pmatrix} 57.9 \\ 79.3 \\ 189.1 \\ 299.1 \\ 365.7 \\ 377.9 \\ 365.7 \\ 299.9 \\ 189.1 \\ 79.7 \\ 57.6 \end{pmatrix} \cdot kip \cdot ft \qquad V_{truck\_pc} := \begin{pmatrix} 59.6 \\ 52.7 \\ 45.2 \\ 37.2 \\ 29.3 \\ 21.0 \\ 15.1 \\ 9.0 \\ 5.3 \\ 5.3 \\ 5.3 \end{pmatrix} \cdot kip$$

Design Truck, Span 2, -M:

$$M_{truck\_nc} := \begin{pmatrix} -277.4 \\ -181.9 \\ -155.3 \\ -128.6 \\ -121.3 \\ -121.3 \\ -124.7 \\ -128.6 \\ -155.3 \\ -181.9 \\ -277.4 \end{pmatrix} \cdot kip \cdot ft \qquad V_{truck\_nc} := \begin{pmatrix} -5.3 \\ -5.3 \\ -5.3 \\ -9.0 \\ -15.1 \\ -21.9 \\ -29.3 \\ -37.2 \\ -45.2 \\ -52.7 \\ -59.6 \end{pmatrix} \cdot kip$$

Design Tandem, Span 2, +M:

$$M_{tandem\_pc} := \begin{pmatrix} 50.8 \\ 86.1 \\ 206.0 \\ 299.9 \\ 357.6 \\ 373.8 \\ 357.6 \\ 299.9 \\ 206.0 \\ 86.1 \\ 50.8 \end{pmatrix} \cdot kip \cdot ft \qquad V_{tandem\_pc} := \begin{pmatrix} 48.6 \\ 44.6 \\ 39.8 \\ 34.4 \\ 28.6 \\ 22.6 \\ 16.8 \\ 11.3 \\ 6.3 \\ 4.7 \\ 4.7 \end{pmatrix} \cdot kip$$

Design Tandem, Span 2, -M:

$$M_{tandem\_nc} := \begin{pmatrix} -216.9 \\ -159.4 \\ -136.1 \\ -112.7 \\ -89.4 \\ -66.0 \\ -89.4 \\ -112.7 \\ -136.1 \\ -159.4 \\ -216.9 \end{pmatrix} \cdot kip \cdot ft \qquad V_{tandem\_nc} := \begin{pmatrix} -4.7 \\ -4.7 \\ -5.4 \\ -10.2 \\ -15.6 \\ -21.4 \\ -27.4 \\ -33.2 \\ -38.7 \\ -43.7 \\ -47.9 \end{pmatrix} \cdot kip$$

Design Lane, Span 2, +M

$$M_{lane\_pc} := \begin{pmatrix} 17.1 \\ 17.9 \\ 42.7 \\ 81.0 \\ 105.0 \\ 113.0 \\ 105.0 \\ 81.0 \\ 42.7 \\ 17.9 \\ 17.1 \end{pmatrix} \cdot kip \cdot ft \qquad V_{lane\_pc} := \begin{pmatrix} 17.6 \\ 14.5 \\ 11.7 \\ 9.1 \\ 7.0 \\ 5.2 \\ 3.8 \\ 2.7 \\ 2.1 \\ 1.7 \\ 1.6 \end{pmatrix} \cdot kip$$

Design Lane, Span 2, -M

$$M_{lane\_nc} := \begin{pmatrix} -148.6 \\ -77.3 \\ -46.2 \\ -44.5 \\ -40.1 \\ -40.1 \\ -40.1 \\ -44.5 \\ -46.2 \\ -77.3 \\ -148.6 \end{pmatrix} \cdot kip \cdot ft \qquad V_{lane\_nc} := \begin{pmatrix} -1.7 \\ -1.6 \\ -2.1 \\ -2.7 \\ -3.8 \\ -5.2 \\ -7.0 \\ -9.1 \\ -11.7 \\ -14.5 \\ -17.6 \end{pmatrix} \cdot kip$$

B2-5

Load & Resistance Factors:

<u>Load Factors:</u> $\gamma_{pDC} := 1.25$ $\gamma_{pDW} := 1.5$ $\gamma_{LL} := 1.75$

<u>Resistance Factors:</u>   Flexure: (variable) $\phi_{fn} := 1.00$ Shear: $\phi_v := 0.90$

Strand Pattern:

$$Pat\_n := \begin{pmatrix} 0 \\ 0 \\ 12 \\ 14 \end{pmatrix} \qquad Pat\_h := \begin{pmatrix} 16 \\ 6 \\ 4 \\ 2 \end{pmatrix} \cdot in$$

$A_s := 8 \cdot 0.79 \cdot in^2$

$A_{s\_top} := 12 \cdot 0.44 \cdot in^2$ (longitudinal rebar in slab)

No, Strands   Elevation (in)

2.3 Section Properties
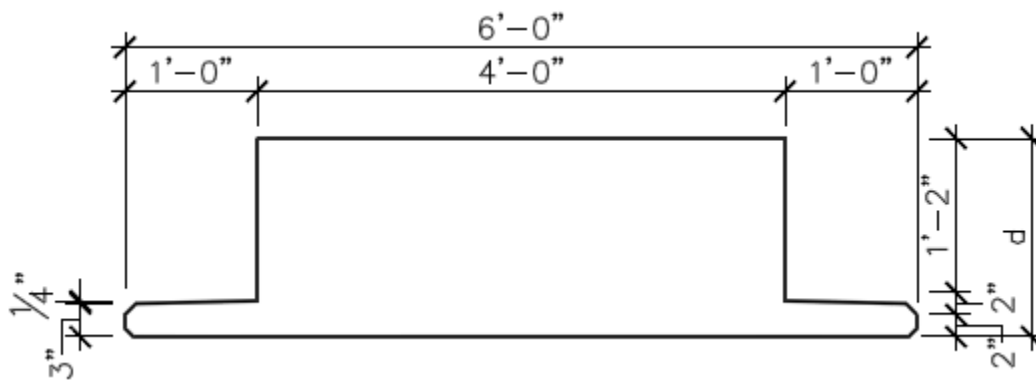
Figure 4: Section dimensions.

Non-Composite Section Properties:

$$S_b := \frac{I}{y_b} \qquad\qquad S_b = 3220.9 \cdot in^3$$

$$y_t := h - y_b \qquad S_t := \frac{I}{y_t} \qquad S_t = 2830.9 \cdot in^3$$

Effective Width: (LRFD 4.6.2.6.1)

The effective width of the composite section may be taken as 1/2 the distance to the adjacent beam

$$b_{eff} := \frac{S}{2} + \frac{S}{2} \qquad b_{eff} = 72 \cdot in$$

$$n := \sqrt{\frac{f'_{ct}}{f'_c}} \qquad n = 0.7559 \qquad b_{tran} := n \cdot b_{eff} \qquad b_{tran} = 54.43 \cdot in$$

Composite Section Properties:

$$A_{slab} := b_{tran} \cdot (t_{slab} - t_{ws}) \qquad A_{slab} = 326.6 \cdot in^2 \qquad A_h := n \cdot t_h \cdot b_h \qquad A_h = 272.1 \cdot in^2$$

$$A_{comp} := A + A_h + A_{slab} \qquad A_{comp} = 1534.7 \cdot in^2$$

$$y_{bc} := \frac{A \cdot y_b + A_h \cdot \left(t_{flg} + \frac{t_h}{2}\right) + A_{slab} \cdot \left(h + \frac{t_{slab} - t_{ws}}{2}\right)}{A_{comp}} \qquad y_{bc} = 11.466 \cdot in$$

$$h_c := h + t_{slab} - t_{ws} \qquad h_c = 24 \cdot in$$

$$y_{tc} := h_c - y_{bc} \qquad y_{tc} = 12.53 \cdot in$$

$$I_{slab} := \frac{b_{tran} \cdot (t_{slab} - t_{ws})^3}{12} \qquad I_{slab} = 979.7 \cdot in^4 \qquad I_h := \frac{n \cdot b_h \cdot t_h^3}{12} \qquad I_h = 5102.5 \cdot in^4$$

$$I_c := I + A \cdot (y_b - y_{bc})^2 + I_h + A_h \cdot \left(t_{flg} + \frac{t_h}{2} - y_{bc}\right)^2 + I_{slab} + A_{slab} \cdot \left(h + \frac{t_{slab} - t_{ws}}{2} - y_{bc}\right)^2$$

$$I_c = 71824 \cdot in^4$$

$$S_{bc} := \frac{I_c}{y_{bc}} \qquad S_{bc} = 6264.3 \cdot in^3 \qquad S_{tc} := \frac{I_c}{y_{tc} \cdot n} \qquad S_{tc} = 7580.3 \cdot in^3$$

Composite section modulus at the top of the prestressed beam:

$$y_{tcb} := h - y_{bc} \qquad S_{tcb} := \frac{I_c}{y_{tcb}} \qquad S_{tcb} = 10991.8 \cdot in^3$$

2.4 Strand Pattern Properties
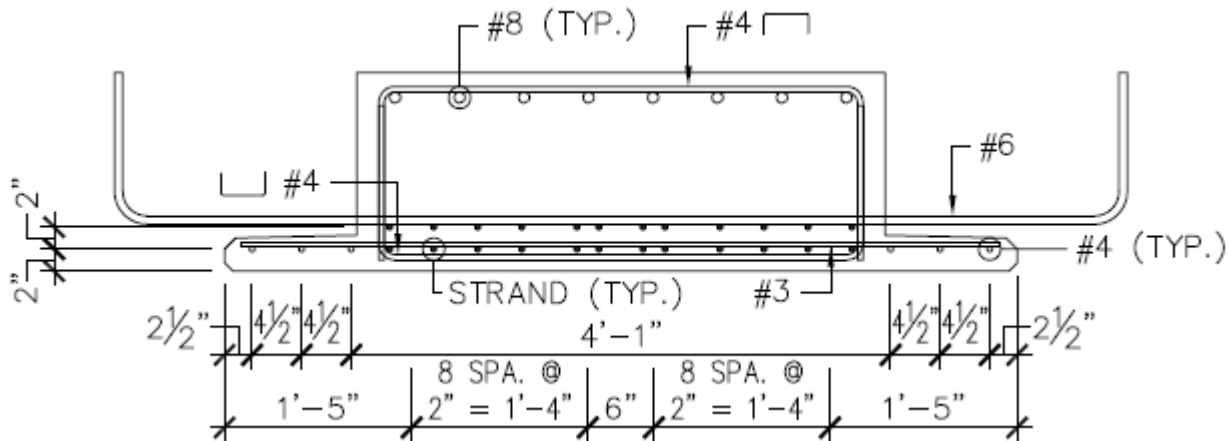
Figure 5: Strand pattern.

$$No\_Strands := \sum Pat\_n \qquad No\_Strands = 26$$

$$i := 1 .. last(Pat\_n)$$

$$y_{cg} := \frac{\sum_i \left(Pat\_n_i \cdot Pat\_h_i\right)}{No\_Strands} \qquad y_{cg} = 2.9231 \cdot in$$

$$ecc := y_b - y_{cg} \qquad ecc = 5.50 \cdot in$$

2.5 Moments and Shears

At Release:

At release, when the prestress force is transferred to the beam, the structural model is a simple-span beam. The assumed length of the beam can be the overall length of the beam, or it can be somewhat less than the overall length to model supports that are located some distance in from the ends of the beam. For this example, the effective beam length at release will be assumed to be the overall length of the precast beam.

While the beam is in the prestress yard, there are two locations along the beam that are potentially of interest: the transfer point of the strands and the midspan of the beam. For beams with no debonding, the net stress due to prestress and beam self-weight will achieve maximum and minimum values at one or more of these locations .

1. Transfer point of strands:

$$L_t := 60 \cdot d_b \qquad L_t = 36 \cdot in \qquad x_{r_1} := L_t \qquad\qquad \text{(LRFD 5.8.2.3)}$$

2. Midspan of beam: $\qquad\qquad x_{r_2} := \dfrac{L_{ovr}}{2}$

$$x_r^T = (3 \quad 24.5) \cdot ft$$

beam self-weight at release:

$$w_{sw} := w_c \cdot A \qquad w_{sw} = 0.975 \cdot klf$$

$$i := 1 .. 2$$

$$M_{swr_i} := \dfrac{w_{sw} \cdot x_{r_i}}{2} \cdot \left(L_{ovr} - x_{r_i} \right) \qquad M_{swr}^T = (67.3 \quad 292.6) \cdot kip \cdot ft$$

At Final Conditions:

<u>Check Points:</u>

At final conditions, there are two structural models that are required to perform the analysis. For a composite system, such as this one, some of the loads act on the bare precast beam and some of the loads act on the continuous, multi-span system. Using the principle of superposition, the effects of the loads that act on the simple-span model can be added to the moments, shears, and stresses caused by loads that act on the continuous system.

Two frames of reference are convenient for locating checkpoints at final conditions on a continuous structure. For checking stresses in the beam, for checking the positive flexural capacity, and for computing the required transverse reinforcement (i.e., stirrups), the centerline of the left bearing of the beam will be the reference point and will be designated x_f. For computing gross moments and shears acting on the continuous system and for assessing the negative flexural capacity of the system, the centerline of the left pier of the span will be used as the point of reference and will be designated x_{fc}.

For this particular structure, for the first frame of reference, there are four points of interest in Span 2 at final conditions:

1. Centerline of left bearing $\qquad x_{f_1} := 0.0 \cdot ft \qquad$ (Note: All final checkpoints are referenced to L. bearing)

2. Left transfer point of strands: $\qquad x_{f_2} := L_t - \dfrac{L_{ovr} - L_{des}}{2}$

3. Left critical section for shear.

   The critical section for shear is d_v from the face of the support. This can be conservatively assumed to be 0.72h.

   $$x_{f_3} := 0.72 \cdot h_c + \dfrac{L_{pad}}{2}$$

4. Midspan of beam:

$$x_{f_4} := \frac{L_{des}}{2}$$

$$x_f^T = (0 \quad 2.5 \quad 1.94 \quad 24) \cdot ft$$

For the second frame of reference there are eleven points of interest in Span 2 at final conditions, which correspond to tenth points of Span 2, measured from centerline of the left pier (Pier 2) to the centerline of the right pier (Pier 3) :

$$k := 1 .. 11 \qquad L_{p2p} = 50\,ft$$

$$x_{fc_k} := \frac{k-1}{10} \cdot L_{p2p}$$

$$x_{fc}^T =$$

	1	2	3	4	5	6	7	8	9	10	11	ft
1	0	5	10	15	20	25	30	35	40	45	50	

Loads Acting on Simple-Span Model

beam self-weight at final:

$$j := 1 .. 4$$

$$M_{swf_j} := \frac{w_{sw} \cdot x_{f_j}}{2} \cdot \left(L_{des} - x_{f_j}\right) \qquad M_{swf} = \begin{pmatrix} 0 \\ 55.5 \\ 43.6 \\ 280.8 \end{pmatrix} \cdot kip \cdot ft \qquad V_{swf_j} := w_{sw} \cdot \left(\frac{L_{des}}{2} - x_{f_j}\right) \qquad V_{swf} = \begin{pmatrix} 23.4 \\ 21 \\ 21.5 \\ 0 \end{pmatrix} \cdot kip$$

CIP Weight:

$$w_d := \left[\left(t_{slab} - t_{ws}\right) \cdot S + t_h \cdot b_h\right] \cdot w_{ct} \qquad w_d = 0.825 \cdot klf$$

$$M_{deck_j} := \frac{w_d \cdot x_{f_j}}{2} \cdot \left(L_{des} - x_{f_j}\right) \qquad M_{deck} = \begin{pmatrix} 0 \\ 46.9 \\ 36.9 \\ 237.6 \end{pmatrix} \cdot kip \cdot ft \qquad V_{deck_j} := w_d \cdot \left(\frac{L_{des}}{2} - x_{f_j}\right) \qquad V_{deck} = \begin{pmatrix} 19.8 \\ 17.7 \\ 18.2 \\ 0 \end{pmatrix} \cdot kip$$

Loads Acting on Continuous Model

For beam design itself, the results of the continuous structure (10th points, measured from centerline of pier to centerline of pier) must be mapped onto the checkpoints of the beam. The following function maps the results from the continuous beam analysis to the beam check points at final using linear iterpolation.

$$\text{Map}\left(PO, BO, x_f, x_{fc}, MVc\right) := \begin{vmatrix} j_{max} \leftarrow \text{last}\left(x_{fc}\right) \\ \text{for } i \in 1 .. \text{last}\left(x_f\right) \\ \begin{vmatrix} j \leftarrow 1 \\ \text{while } \left(PO + BO + x_{f_i}\right) > x_{fc_j} \\ \begin{vmatrix} j \leftarrow j + 1 \\ \text{break if } j > j_{max} \end{vmatrix} \\ C \leftarrow \dfrac{PO + BO + x_{f_i} - x_{fc_{j-1}}}{x_{fc_j} - x_{fc_{j-1}}} \\ MV_i \leftarrow MVc_{j-1} + C \cdot \left(MVc_j - MVc_{j-1}\right) \end{vmatrix} \\ MV \end{vmatrix}$$

Barrier Weight (composite, continuous structure):

$$M_{barrier} := Map(Pier_{offset}, Brng_{offset}, x_f, x_{fc}, M_{barrier\_c}) \qquad M_{barrier}^T = (-13.72 \quad -9.52 \quad -10.4608 \quad 8) \cdot kip \cdot ft$$

$$V_{barrier} := Map(Pier_{offset}, Brng_{offset}, x_f, x_{fc}, V_{barrier\_c}) \qquad V_{barrier}^T = (1.82 \quad 1.62 \quad 1.6648 \quad 0) \cdot kip$$

Future Wearing Surface (composite, continuous structure):

$$M_{fws} := Map(Pier_{offset}, Brng_{offset}, x_f, x_{fc}, M_{fws\_c}) \qquad M_{fws}^T = (-27.1 \quad -18.8 \quad -20.6 \quad 15.9) \cdot kip \cdot ft$$

$$V_{fws} := Map(Pier_{offset}, Brng_{offset}, x_f, x_{fc}, V_{fws\_c}) \qquad V_{fws}^T = (3.6 \quad 3.2 \quad 3.3 \quad 0) \cdot kip$$

Live Load:

Dynamic Load Allowance (impact):

$$DLA := 0.33 \qquad DLA_f := 0.15 \qquad\qquad\qquad\qquad\qquad\qquad\qquad \text{(LRFD 3.6.2.1-1)}$$

Distribution Factors:

Assume superstructure acts like a slab-type bridge. Utilize provisions of LRFD Art. 4.6.2.3 to compute width of equivalent strip to resist lane load.

Single-Lane Loading:

$$L_1 := if(L_{des} > 60 \cdot ft, 60 \cdot ft, L_{des}) \qquad L_1 = 48.00\, ft$$

$$W_{1\_1} := if(Width_{overall} > 30 \cdot ft, 30 \cdot ft, Width_{overall}) \qquad W_{1\_1} = 30.00\, ft$$

$$E_{strip1} := 10 \cdot in + 5.0 \cdot in \cdot \sqrt{\frac{L_1}{ft} \cdot \frac{W_{1\_1}}{ft}} \qquad E_{strip1} = 200 \cdot in \qquad E_{strip1} = 16.6\, ft$$

Put in terms of fraction of one lane to be distributed to one precast unit:

$$DF_{1lane} := \frac{b_f}{E_{strip1}} \qquad DF_{1lane} = 0.3605$$

Double-Lane Loading:

$$W_{1\_2} := if(Width_{overall} > 60 \cdot ft, 60 \cdot ft, Width_{overall}) \qquad W_{1\_2} = 47.50\, ft$$

$$E_{strip2} := 84 \cdot in + 1.44 \cdot in \cdot \sqrt{\frac{L_1}{ft} \cdot \frac{W_{1\_2}}{ft}} \qquad E_{strip2} = 153 \cdot in \qquad E_{strip2} = 12.7\, ft$$

$$DF_{2lane} := \frac{b_f}{E_{strip2}} \qquad DF_{2lane} = 0.4713$$

Governing Case:

$$DF := if(DF_{1lane} > DF_{2lane}, DF_{1lane}, DF_{2lane}) \qquad DF = 0.4713$$

This distribution factor is applicable to both shear and moment:

$$DF_m := DF$$

$$DF_v := DF$$

Live Load (HL-93) Moments & Shears:

Positive Moment Envelope:

$$\text{Max\_Vehicle}\left(\text{Vehicle}_1, \text{Vehicle}_2\right) := \begin{array}{|l} \text{for } i \in 1 .. \text{last}\left(\text{Vehicle}_1\right) \\ \qquad \begin{array}{|l} \text{Vehicle}_i \leftarrow \text{Vehicle}_{1_i} \quad \text{if } \text{Vehicle}_{1_i} > \text{Vehicle}_{2_i} \\ \text{Vehicle}_i \leftarrow \text{Vehicle}_{2_i} \quad \text{otherwise} \end{array} \\ \text{Vehicle} \end{array}$$

$$M_{\text{Vehicle\_pc}} := \text{Max\_Vehicle}\left(M_{\text{truck\_pc}}, M_{\text{tandem\_pc}}\right)$$

$M_{\text{Vehicle\_pc}}^T =$

	1	2	3	4	5	6	7	8	9	10	11
1	58	86	206	300	366	378	366	300	206	86	58

$\cdot \text{kip·ft}$

$$M_{\text{vehicle\_p}} := \text{Map}\left(\text{Pier}_{\text{offset}}, \text{Brng}_{\text{offset}}, x_f, x_{fc}, M_{\text{Vehicle\_pc}}\right) \qquad M_{\text{vehicle\_p}}^T = (64 \quad 78 \quad 74 \quad 378) \cdot \text{kip·ft}$$

$$M_{\text{lane\_p}} := \text{Map}\left(\text{Pier}_{\text{offset}}, \text{Brng}_{\text{offset}}, x_f, x_{fc}, M_{\text{lane\_pc}}\right) \qquad M_{\text{lane\_p}}^T = (17 \quad 18 \quad 18 \quad 113) \cdot \text{kip·ft}$$

$$M_{\text{LL\_p}_j} := DF_m \cdot \left[M_{\text{lane\_p}_j} + (1.0 + DLA) \cdot M_{\text{vehicle\_p}_j}\right] \qquad M_{\text{LL\_p}}^T = (48 \quad 57 \quad 55 \quad 290) \cdot \text{kip·ft}$$

$$V_{\text{Vehicle\_pc}} := \text{Max\_Vehicle}\left(V_{\text{truck\_pc}}, V_{\text{tandem\_pc}}\right)$$

$V_{\text{Vehicle\_pc}}^T =$

	1	2	3	4	5	6	7	8	9	10	11
1	60	53	45	37	29	23	17	11	6	5	5

$\cdot \text{kip}$

$$V_{\text{vehicle\_p}} := \text{Map}\left(\text{Pier}_{\text{offset}}, \text{Brng}_{\text{offset}}, x_f, x_{fc}, V_{\text{Vehicle\_pc}}\right) \qquad V_{\text{vehicle\_p}}^T = (58.2 \quad 54.8 \quad 55.5 \quad 22.6) \cdot \text{kip}$$

$$V_{\text{lane\_p}} := \text{Map}\left(\text{Pier}_{\text{offset}}, \text{Brng}_{\text{offset}}, x_f, x_{fc}, V_{\text{lane\_pc}}\right) \qquad V_{\text{lane\_p}}^T = (17 \quad 15.4 \quad 15.8 \quad 5.2) \cdot \text{kip}$$

$$V_{\text{LL\_p}_j} := DF_v \cdot \left[V_{\text{lane\_p}_j} + (1.0 + DLA) \cdot V_{\text{vehicle\_p}_j}\right] \qquad V_{\text{LL\_p}}^T = (44.5 \quad 41.6 \quad 42.3 \quad 16.6) \cdot \text{kip}$$

Negative Moment Envelope:

$$\text{Min\_Vehicle}\left(\text{Vehicle}_1, \text{Vehicle}_2\right) := \begin{array}{|l} \text{for } i \in 1 .. \text{last}\left(\text{Vehicle}_1\right) \\ \qquad \begin{array}{|l} \text{Vehicle}_i \leftarrow \text{Vehicle}_{1_i} \quad \text{if } \text{Vehicle}_{1_i} < \text{Vehicle}_{2_i} \\ \text{Vehicle}_i \leftarrow \text{Vehicle}_{2_i} \quad \text{otherwise} \end{array} \\ \text{Vehicle} \end{array}$$

$$M_{\text{Vehicle\_nc}} := \text{Min\_Vehicle}\left(M_{\text{truck\_nc}}, M_{\text{tandem\_nc}}\right)$$

$M_{\text{Vehicle\_nc}}^T =$

	1	2	3	4	5	6	7	8	9	10	11
1	-277	-182	-155	-129	-121	-121	-125	-129	-155	-182	-277

$\cdot \text{kip·ft}$

$$M_{\text{vehicle\_n}} := \text{Map}\left(\text{Pier}_{\text{offset}}, \text{Brng}_{\text{offset}}, x_f, x_{fc}, M_{\text{Vehicle\_nc}}\right) \qquad M_{\text{vehicle\_n}}^T = (-258 \quad -211 \quad -221 \quad -121) \cdot \text{kip·ft}$$

$$M_{\text{lane\_n}} := \text{Map}\left(\text{Pier}_{\text{offset}}, \text{Brng}_{\text{offset}}, x_f, x_{fc}, M_{\text{lane\_nc}}\right) \qquad M_{\text{lane\_n}}^T = (-134 \quad -99 \quad -107 \quad -40) \cdot \text{kip·ft}$$

$$M_{LL\_n_j} := DF_m \cdot \left[M_{lane\_n_j} + (1.0 + DLA) \cdot M_{vehicle\_n_j} \right] \qquad M_{LL\_n}^T = (-225 \quad -179 \quad -189 \quad -95) \cdot kip \cdot ft$$

$$V_{Vehicle\_nc} := Min\_Vehicle(V_{truck\_nc}, V_{tandem\_nc})$$

$V_{Vehicle\_nc}^T =$

	1	2	3	4	5	6	7	8	9	10	11
1	-5	-5	-5	-10	-16	-22	-29	-37	-45	-53	-60

· kip

$$V_{vehicle\_n} := Map(Pier_{offset}, Brng_{offset}, x_f, x_{fc}, V_{Vehicle\_nc}) \qquad V_{vehicle\_n}^T = (-5 \quad -5 \quad -5 \quad -22) \cdot kip$$

$$V_{lane\_n} := Map(Pier_{offset}, Brng_{offset}, x_f, x_{fc}, V_{lane\_nc}) \qquad V_{lane\_n}^T = (-2 \quad -2 \quad -2 \quad -5) \cdot kip$$

$$V_{LL\_n_j} := DF_v \cdot \left[V_{lane\_n_j} + (1.0 + DLA) \cdot V_{vehicle\_n_j} \right] \qquad V_{LL\_n}^T = (-4 \quad -4 \quad -4 \quad -16) \cdot kip$$

Positive Restraint Moment: (Peterman, 1998)

Restraint moments are calculated using the Peterman Method (P-Method)
Compute restraint moments at the piers due to shrinkage and creep effects at the
end of the service life of the bridge, assumed to be time t_{final}. Continuity is
established at time t_{deck}.

Calculate the moment due to eccentric prestressing:

Estimate stress in prestressing strands at time of continuity as:

$$f_{pe} := 185 \cdot ksi$$

$$P_{ps} := No\_Strands \cdot f_{pe} \cdot A_{strand} \qquad P_{ps} = 1.0 \times 10^3 \cdot kip$$

$$M_p := P_{ps} \cdot (ecc) \quad M_p = 478.1 \cdot kip \cdot ft$$

Dead load moments for Span 2:

$$M_{dp2} := M_{swf_4} \qquad M_{dp2} = 280.8 \cdot kip \cdot ft \qquad M_{dd2} := M_{deck_4} \qquad M_{dd2} = 237.6 \cdot kip \cdot ft$$

Dead load moments for Span 1 are assumed to be 70% of those of Span 2:

$$M_{dp1} := 0.70 \cdot M_{dp2} \qquad M_{dp1} = 196.6 \cdot kip \cdot ft \qquad M_{dd1} := 0.70 \cdot M_{dd2} \qquad M_{dd1} = 166.32 \cdot kip \cdot ft$$

Estimate differential shrinkage at end of service life of bridge:

$$\varepsilon_{sh} = -k_{vs} \cdot k_{hs} \cdot k_f \cdot k_{td} \cdot 0.48 \cdot 10^{-3} \qquad \text{(LRFD 5.4.2.3.3-1)}$$

where:
- k_{vs} = Factor for the effect of volume to surface ratio.
- k_{hs} = Factor for humidity.
- k_f = Factor for strength of concrete.
- k_{td} = Factor for time development.

Shrinkage strain in precast at time continuity is established:

$$k_{vs} := 1.45 - 0.13 \frac{VS_b}{in} \qquad k_{vs} = 0.774 \qquad \text{Note: } k_{vs} \text{ must be greater than 1.0.} \qquad \text{(LRFD 5.4.2.3.2-1)}$$

$$k_{vs} := 1.000$$

$$k_{hs} := 2.00 - 0.014 \cdot H \qquad k_{hs} = 1.020 \qquad \text{(LRFD 5.4.2.3.3-2)}$$

$$k_f := \frac{5}{1 + \dfrac{f'_{ci}}{ksi}} \qquad k_f = 0.833 \qquad \text{(LRFD 5.4.2.3.2-4)}$$

$$t_d := t_{deck} \qquad t_d = 7 \cdot day$$

$$t_i := t_{transfer} \qquad t_i = 1 \cdot day$$

$$t := t_d - t_i \qquad t = 6 \cdot day$$

$$k_{td} := \frac{\dfrac{t}{day}}{61 - \dfrac{4 \cdot f'_{ci}}{ksi} + \dfrac{t}{day}} \qquad k_{td} = 0.128 \qquad \text{(LRFD 5.4.2.3.2-5)}$$

$$\varepsilon_{bid} := -k_{vs} \cdot k_{hs} \cdot k_f \cdot k_{td} \cdot 0.48 \cdot 10^{-3} \qquad \varepsilon_{bid} = -52 \times 10^{-6}$$

Shrinkage strain in precast at time final:

$$k_{vs} := 1.45 - 0.13 \frac{VS_b}{in} \qquad k_{vs} = 0.774 \qquad \text{Note: } k_{vs} \text{ must be greater than 1.0.} \qquad \text{(LRFD 5.4.2.3.2-1)}$$

$$k_{vs} := 1.000$$

$$k_{hs} := 2.00 - 0.014 \cdot H \qquad k_{hs} = 1.020 \qquad \text{(LRFD 5.4.2.3.3-2)}$$

$$k_f := \frac{5}{1 + \dfrac{f'_{ci}}{ksi}} \qquad k_f = 0.833 \qquad \text{(LRFD 5.4.2.3.2-4)}$$

$$t_f := t_{final} \qquad t_i := t_{transfer}$$

$$t := t_f - t_i \qquad t = 19999 \cdot day$$

$$k_{td} := \frac{\dfrac{t}{day}}{61 - \dfrac{4 \cdot f'_{ci}}{ksi} + \dfrac{t}{day}} \qquad k_{td} = 0.998 \qquad \text{(LRFD 5.4.2.3.2-5)}$$

$$\varepsilon_{bif} := -k_{vs} \cdot k_{hs} \cdot k_f \cdot k_{td} \cdot 0.48 \cdot 10^{-3} \qquad \varepsilon_{bif} = -407 \times 10^{-6}$$

Net precast shrinkage strain:

$$\varepsilon_{shp} := \varepsilon_{bif} - \varepsilon_{bid} \qquad \varepsilon_{shp} = -0.000355$$

Shrinkage strain in CIP at time final:

$$\varepsilon_{sh} = -k_{vs} \cdot k_{hs} \cdot k_f \cdot k_{td} \cdot 0.48 \cdot 10^{-3} \qquad \text{(LRFD 5.4.2.3.3-1)}$$

where:

$k_{vs} = $ Factor for the effect of volume to surface ratio.

$k_{hs} = $ Factor for humidity.

$k_f = $ Factor for strength of concrete.

$k_{td} = $ Factor for time development.

$$k_{vs} := 1.45 - 0.13 \frac{VS_d}{in} \qquad k_{vs} = 0.670 \qquad \text{Note: } k_{vs} \text{ must be greater than 1.0.} \qquad \text{(LRFD 5.4.2.3.2-1)}$$

$$k_{vs} := 1.000$$

$$k_{hs} := 2.00 - 0.014 \cdot H \qquad k_{hs} = 1.020 \qquad \text{(LRFD 5.4.2.3.3-2)}$$

$$k_f := \frac{5}{1 + \dfrac{0.8 \cdot f'_{ct}}{ksi}} \qquad k_f = 1.190 \qquad \text{(LRFD 5.4.2.3.2-4)}$$

$$t_f := t_{final} \qquad t_i := t_{deck}$$

$$t := t_f - t_i \qquad t = 19993 \cdot day$$

$$k_{td} := \frac{\dfrac{t}{day}}{61 - \dfrac{4 \cdot 0.8 \cdot f'_{ct}}{ksi} + \dfrac{t}{day}} \qquad k_{td} = 0.998 \qquad \text{(LRFD 5.4.2.3.2-5)}$$

$$\varepsilon_{ddf} := -k_{vs} \cdot k_{hs} \cdot k_f \cdot k_{td} \cdot 0.48 \cdot 10^{-3} \qquad \varepsilon_{ddf} = -581 \times 10^{-6}$$

Differential shrinkage:

$$\varepsilon_{sh} := \varepsilon_{ddf} - \varepsilon_{shp} \qquad \varepsilon_{sh} = -0.000226$$

Calculate the uniform shrinkage moment:

$$E_d := 33000 \cdot w_c^{1.5} \cdot kcf^{-1.5} \cdot \sqrt{f'_{ct}} \cdot ksi^{.5} \qquad E_d = 3834 \cdot ksi$$

$$e_e := y_{tcb} \qquad e_e = 6.5343 \cdot in$$

$$E_{pr} := 33000 \cdot w_c^{1.5} \cdot kcf^{-1.5} \cdot \sqrt{f'_c} \cdot ksi^{.5} \qquad E_{pr} = 5072 \cdot ksi$$

$$A_d := \frac{A_{slab}}{n} \qquad A_d = 432 \cdot in^2$$

$$\eta := \left(\frac{1}{1 + \dfrac{E_{pr} \cdot A}{E_d \cdot A_d}}\right) \cdot \left[\frac{1}{\left(1 + \dfrac{E_s \cdot A_{s\_top}}{E_d \cdot A_d}\right)}\right] \qquad \eta = 0.2368$$

$$M_s := \varepsilon_{sh} \cdot E_d \cdot A_d \cdot \left(e_e + \frac{t_{slab}}{2}\right) \cdot \eta \qquad M_s = -70.5 \cdot kip \cdot ft$$

Creep effects on precast M_p and M_d:

Creep in precast at continuity:

$$t_i := t_{transfer} \qquad t_d := t_{deck}$$

$$t := t_d - t_i \qquad t = 6 \cdot day$$

$$k_{td} := \frac{\dfrac{t}{day}}{61 - \dfrac{4 \cdot f'_{ci}}{ksi} + \dfrac{t}{day}} \qquad k_{td} = 0.128$$

B2-14

$$k_{vs} := 1.45 - 0.13 \frac{VS_b}{in} \qquad k_{vs} = 0.774 \qquad \text{Note: } k_{vs} \text{ must be greater than 1.0.} \qquad \text{(LRFD 5.4.2.3.2-1)}$$

$$k_v := 1.000$$

$$k_{hc} := 1.56 - 0.008H \qquad k_{hc} = 1.000 \qquad \text{(LRFD Eq. 5.4.2.3.2-3)}$$

$$k_f := \frac{5}{1 + \dfrac{f'_{ci}}{ksi}} \qquad k_f = 0.833 \qquad \text{(LRFD 5.4.2.3.2-4)}$$

$$\psi_{bdi} := 1.9 \cdot k_{vs} \cdot k_{hc} \cdot k_f \cdot k_{td} \cdot \left(\frac{t_i}{day}\right)^{-0.118} \qquad \psi_{bdi} = 0.156$$

Creep in precast at time final:

$$k_{vs} := 1.45 - 0.13 \frac{VS_b}{in} \qquad k_{vs} = 0.774 \qquad \text{Note: } k_{vs} \text{ must be greater than 1.0.} \qquad \text{(LRFD 5.4.2.3.2-1)}$$

$$k_{vs} := 1.000$$

$$k_{hc} := 1.56 - 0.008H \qquad k_{hc} = 1.000 \qquad \text{(LRFD Eq. 5.4.2.3.2-3)}$$

$$k_f := \frac{5}{1 + \dfrac{f'_{ci}}{ksi}} \qquad k_f = 0.833 \qquad \text{(LRFD 5.4.2.3.2-4)}$$

$$t_f := t_{final} \qquad t_i := t_{transfer}$$

$$t := t_f - t_i \qquad t = 19999 \cdot day$$

$$k_{td} := \frac{\dfrac{t}{day}}{61 - \dfrac{4 \cdot f'_{ci}}{ksi} + \dfrac{t}{day}} \qquad k_{td} = 0.998 \qquad \text{(LRFD 5.4.2.3.2-5)}$$

$$\psi_{bfi} := 1.9 \cdot k_{vs} \cdot k_{hc} \cdot k_f \cdot k_{td} \cdot \left(\frac{t_i}{day}\right)^{-0.118} \qquad \psi_{bfi} = 1.580$$

Creep effects on CIP M_d and M_s:

$$t_i := t_{deck}$$

$$t := t_f - t_i \qquad t = 19993 \cdot day$$

$$k_{td} := \frac{\dfrac{t}{day}}{61 - \dfrac{4 \cdot f'_{ci}}{ksi} + \dfrac{t}{day}} \qquad k_{td} = 0.998$$

$$k_{vs} := 1.45 - 0.13 \frac{VS_b}{in} \qquad k_{vs} = 0.774 \qquad \text{Note: } k_{vs} \text{ must be greater than 1.0.} \qquad \text{(LRFD 5.4.2.3.2-1)}$$

$$k_{vs} := 1.000$$

$$k_{hc} := 1.56 - 0.008H \qquad k_{hc} = 1.000 \qquad \text{(LRFD Eq. 5.4.2.3.2-3)}$$

$$k_f := \frac{5}{1 + \dfrac{f'_{ci}}{ksi}} \qquad k_f = 0.833 \qquad \text{(LRFD 5.4.2.3.2-4)}$$

$$\psi_{bfd} := 1.9 \cdot k_{vs} \cdot k_{hc} \cdot k_f \cdot k_{td} \cdot \left(\frac{t_i}{day}\right)^{-0.118} \qquad \psi_{bfd} = 1.256$$

Compute M_r at interior face of Pier 1:

Factors:

$$F_1 := \left(1 - e^{-\psi_{bfi}}\right) - \left(1 - e^{-\psi_{bdi}}\right) \qquad F_1 = 0.6492$$

$$F_2 := 1 - e^{-\psi_{bfd}} \qquad F_2 = 0.7152$$

Using moment distribution, the following values were obtained:

Moment at inside face of Pier 1 due to prestress:

$$M_{rp} := 462 \cdot kip \cdot ft$$

Moment at inside face of Pier 1 due to differential shrinkage:

$$M_{rs} := -68 \cdot kip \cdot ft$$

Moments due to superimposed dead load:

$$M_{rdp} := -182 \cdot kip \cdot ft \qquad M_{rdd} := -153 kip \cdot ft$$

Calculated restraint moment:

$$M_{rm} := \left(M_{rp} + M_{rdp}\right) \cdot F_1 + M_{rdd} \cdot F_2 + M_{rs} \cdot \left(\frac{F_2}{\psi_{bfd}}\right) \qquad M_{rm} = 34 \cdot kip \cdot ft$$

Thermal Gradient: (LRFD 3.12.3)

$$\gamma_{TG} := 1.0 \qquad \text{(no live live)}$$

$$\gamma_{TG\_L} := 0.5 \qquad \text{(with live load)}$$

Effects due to uniform temperature change:

Since superstructure is not restrained axially, uniform temperature change causes no internal stress.

Effects due to temperature gradient:

Fig. 6: Positive temperature gradient (from LRFD 3.12.3-2)

Assume AASHTO temperature Zone 1:

$$T_1 := 54 \qquad \text{(deg F)}$$

$$T_2 := 14$$

$$T_3 := 0$$

$$A_{temp} := if\left(h_c \geq 16 \cdot in, 12 \cdot in, h_c - 4 \cdot in\right) \qquad A_{temp} = 12.00 \cdot in$$

$$A_1 := 4 \cdot in$$

B2-16

$$A_2 := A_{temp} \qquad A_2 = 1 \text{ ft}$$

Compute graident-induced curvature:

$$\psi = \frac{\alpha}{I} \cdot \Sigma\left(T_{ai} \cdot y_i \cdot A_i + \frac{\Delta T_i}{d_i} \cdot I_i\right)$$

(LRFD C4.6.6-3)

$$Area_1 := A_1 \cdot b_f \qquad Area_1 = 288 \cdot in^2$$

$$I_1 := \frac{b_f \cdot A_1^3}{12} \qquad I_1 = 384 \cdot in^4$$

$$Area_2 := A_2 \cdot b_f \qquad Area_2 = 864 \cdot in^2$$

$$I_2 := \frac{b_f \cdot A_2^3}{12} \qquad I_2 = 10368 \cdot in^4$$

$$\varepsilon_{gr} := \frac{\alpha}{A} \cdot \left(T_1 \cdot Area_1 + T_2 \cdot Area_2\right) \qquad \varepsilon_{gr} = 0.000177$$

$$F_{gr} := E_{pr} \cdot A_c \cdot \varepsilon_{gr} \qquad F_{gr} = 404.5 \cdot kip$$

$$y_1 := y_{tc} - \frac{A_1}{2} \qquad y_1 = 10.53 \cdot in$$

$$y_2 := y_{tc} - \left(A_1 + \frac{A_2}{2}\right) \qquad y_2 = 2.53 \cdot in$$

$$\psi := \frac{\alpha}{I_c} \cdot \left[\left(\frac{T_1 - T_2}{2}\right) \cdot y_1 \cdot Area_1 + \frac{\left(T_1 - T_2\right)}{\frac{A_1}{2}} \cdot I_1 + \left(\frac{T_2}{2}\right) \cdot y_2 \cdot Area_2 + \frac{\left(T_2\right)}{\frac{A_2}{2}} \cdot I_2\right] \qquad \psi = 0.000108 \, ft^{-1}$$

Compute graident-induced fixed-end moment:

$$FEM_{gr} := E_{pr} \cdot I_c \cdot \psi \qquad FEM_{gr} = 274 \cdot kip \cdot ft$$

From moment distribution, the moment in Span 2 was calculated:

$$M_{gr} := 265 kip \cdot ft$$

Compute graident-induced internal stresses:

$$\sigma_E = E \cdot \left(\alpha \cdot T_G - \alpha \cdot T_{uG} - \psi \cdot z\right)$$

(LRFD C4.6.6-6)

Evaluate at top and bottom of precast:

$$f_{ist} := E_{pr} \cdot \left[\alpha \cdot T_2 \cdot \left(\frac{A_1 + A_2 - t_{slab}}{A_2}\right) - \psi \cdot y_{tcb}\right] \qquad f_{ist} = 0.0564 \cdot ksi$$

$$f_{isb} := E_{pr} \cdot \psi \cdot y_{tcb} \qquad f_{isb} = 0.2987 \cdot ksi$$

$$f_{istt} := E_{pr} \cdot \left(\alpha \cdot T_1 - \psi \cdot y_{tc}\right) \qquad f_{istt} = 1.0705 \cdot ksi$$

2.6 Flexural Stresses

Note: Since for a structural system of this type, it is unlikely that compression at the top of the deck at a given section would exceed its allowable value, calculation of those stresses will be omitted for simplicity. Only the stresses at the bottom and top of the precast beam itself will be computed.

The precast weight and CIP deck weight are carried by the precast section only. Additional loads (i.e. barrier, overlay, live load) are carried by the composite section.

At Release $\quad j := 1 .. 2$

$$f_{swrt_j} := \frac{M_{swr_j}}{S_t} \qquad f_{swrt} = \begin{pmatrix} 0.285 \\ 1.24 \end{pmatrix} \cdot ksi \qquad\qquad f_{swrb_j} := -\frac{M_{swr_j}}{S_b} \qquad f_{swrb} = \begin{pmatrix} -0.251 \\ -1.09 \end{pmatrix} \cdot ksi$$

At Final Conditions

Self-Weight: $\quad j := 1 .. 4$

$$f_{swt_j} := \frac{M_{swf_j}}{S_t} \qquad f_{swt} = \begin{pmatrix} 0 \\ 0.235 \\ 0.185 \\ 1.19 \end{pmatrix} \cdot ksi \qquad f_{swb_j} := -\frac{M_{swf_j}}{S_b} \qquad f_{swb} = \begin{pmatrix} 0 \\ -0.207 \\ -0.162 \\ -1.046 \end{pmatrix} \cdot ksi$$

Deck Weight:

$$f_{deckt_j} := \frac{M_{deck_j}}{S_t} \qquad f_{deckt} = \begin{pmatrix} 0 \\ 0.199 \\ 0.156 \\ 1.007 \end{pmatrix} \cdot ksi \qquad f_{deckb_j} := -\frac{M_{deck_j}}{S_b} \qquad f_{deckb} = \begin{pmatrix} 0 \\ -0.175 \\ -0.137 \\ -0.885 \end{pmatrix} \cdot ksi$$

Barriers:

$$f_{barriert_j} := \frac{M_{barrier_j}}{S_{tcb}} \qquad f_{barriert} = \begin{pmatrix} -0.015 \\ -0.01 \\ -0.011 \\ 0.009 \end{pmatrix} \cdot ksi \qquad f_{barrierb_j} := -\frac{M_{barrier_j}}{S_{bc}} \qquad f_{barrierb} = \begin{pmatrix} 0.026 \\ 0.018 \\ 0.02 \\ -0.015 \end{pmatrix} \cdot ksi$$

$$f_{barriertt_j} := \frac{M_{barrier_j}}{S_{tc}} \qquad f_{barriertt} = \begin{pmatrix} -0.022 \\ -0.015 \\ -0.017 \\ 0.013 \end{pmatrix} \cdot ksi \qquad \text{(top of topping)}$$

Future Wearing Surface:

$$f_{fwst_j} := \frac{M_{fws_j}}{S_{tcb}} \qquad f_{fwst} = \begin{pmatrix} -0.03 \\ -0.021 \\ -0.023 \\ 0.017 \end{pmatrix} \cdot ksi \qquad f_{fwsb_j} := -\frac{M_{fws_j}}{S_{bc}} \qquad f_{fwsb} = \begin{pmatrix} 0.052 \\ 0.036 \\ 0.04 \\ -0.03 \end{pmatrix} \cdot ksi$$

$$f_{fwstt_j} := \frac{M_{fws_j}}{S_{tc}} \qquad f_{fwstt} = \begin{pmatrix} -0.043 \\ -0.03 \\ -0.033 \\ 0.025 \end{pmatrix} \cdot ksi \qquad \text{(top of topping)}$$

Live Load:

Positive Moment Envelope:

$$f_{pLLt_j} := \frac{M_{LL\_p_j}}{S_{tcb}} \qquad\qquad f_{pLLt}^T = (0.052 \quad 0.062 \quad 0.06 \quad 0.317) \cdot ksi$$

$$f_{pLLb_j} := -\frac{M_{LL\_p_j}}{S_{bc}} \qquad\qquad f_{pLLb}^T = (-0.092 \quad -0.109 \quad -0.105 \quad -0.556) \cdot ksi$$

$$f_{pLLtt_j} := \frac{M_{LL\_p_j}}{S_{tc}} \qquad\qquad f_{pLLtt}^T = (0.076 \quad 0.09 \quad 0.087 \quad 0.459) \cdot ksi \qquad \text{(top of topping)}$$

Negative Moment Envelope:

$$f_{nLLt_j} := \frac{M_{LL\_n_j}}{S_{tcb}} \qquad\qquad f_{nLLt}^T = (-0.246 \quad -0.195 \quad -0.206 \quad -0.104) \cdot ksi$$

$$f_{nLLb_j} := -\frac{M_{LL\_n_j}}{S_{bc}} \qquad\qquad f_{nLLb}^T = (0.431 \quad 0.342 \quad 0.362 \quad 0.182) \cdot ksi$$

$$f_{nLLtt_j} := \frac{M_{LL\_n_j}}{S_{tc}} \qquad\qquad f_{nLLtt}^T = (-0.357 \quad -0.283 \quad -0.299 \quad -0.15) \cdot ksi \qquad \text{(top of topping)}$$

Restraint Moment:

Note: For the center span, restraint moments are constant across the span. For the end spans, restraint moment will vary linearly to zero at the abutments. Also, using the P-method, the restraint moment at the pier on the end span will be larger than the restraint moment at the same pier on the center span.

$$f_{rmt} := \frac{M_{rm}}{S_{tcb}} \qquad\qquad f_{rmt} = 0.0367 \cdot ksi$$

$$f_{rmb} := -\frac{M_{rm}}{S_{bc}} \qquad\qquad f_{rmb} = -0.0644 \cdot ksi$$

$$f_{rmtt} := \frac{M_{rm}}{S_{tc}} \qquad\qquad f_{rmtt} = 0.0532 \cdot ksi$$

Thermal Gradient:

$$f_{grt} := \frac{M_{gr}}{S_{tcb}} + f_{ist} \qquad\qquad f_{grt} = 0.3457 \cdot ksi$$

$$f_{grb} := -\frac{M_{gr}}{S_{bc}} + f_{isb} \qquad\qquad f_{grb} = -0.209 \cdot ksi$$

$$f_{grtt} := \frac{M_{gr}}{S_{tc}} + f_{istt} \qquad\qquad f_{grtt} = 1.49 \cdot ksi$$

Continuity Check:

The continuity check from LRFD 5.14.1.4.5 is required for all simply-supported beams made continuous. The sum of stresses due to post-continuity dead load, restraint moment, 50% live load, and 50% thermal gradient at the bottom of the diaphragm must have no net tension:

$$f_{barrier} + f_{rm} + 0.5 \cdot f_{LL} + 0.5 \cdot f_{TG} \geq 0 \qquad \text{(LRFD 5.14.1.4.5)}$$

The live load stress used in the continuity check can be taken as that which exists when the effect of continuity is most needed (i.e.- when the maximum positive moment in the continuous live load envelope occurs). Using the vehicle position that creates the maximum positive live load moment at midspan, the negative moment at the pier is evaluated and the corresponding stress at the bottom of the section is determined:

$$f_{barrierc} := f_{barrierb_1} \qquad\qquad\qquad f_{barrierc} = 0.0263 \cdot ksi$$

$$f_{pLLc} := 0.247 ksi \qquad\qquad\qquad \text{Generated by the 2D live load model and entered manually}$$

$$f_{rmc} := f_{rmb} \qquad\qquad\qquad f_{rmc} = -0.0644 \cdot ksi$$

$$f_{grc} := f_{grb} \qquad\qquad\qquad f_{grc} = -0.209 \cdot ksi$$

$$f_c := f_{barrierc} + f_{rmc} + 0.5 \cdot f_{pLLc} + 0.5 f_{grc} \qquad\qquad f_c = -0.0191 \cdot ksi$$

There is net tension at the bottom of the diaphragm, and the continuity check fails. The stresses at the diaphragm from Span 1 would also need to be checked for continuity. However, the continuity check fails for Span 2 and will be used to evaluate partial continuity.

The continuous live load positive moment envelop cannot be used in design and a partial continuity envelope must be calculated. Partial continuity is a nonlinear load redistribution through an inhomogeneous cross section that requires FE modeling for an exact analysis. An approximate method can be used for a rational design approach. The following is a simplified, linear-elastic method that is reasonable, though there are other ways to model partial continuity:

A portion of the live load is required to satisfy the continuity check (i.e.- close the assumed cracks from the bottom tension). This portion is calculated below:

$$LL_{req} := \frac{-\left(f_{barrierc} + f_{rmc} + 0.5 \cdot f_{grc}\right)}{f_{pLLc}} \qquad\qquad LL_{req} = 0.5774$$

Therefore, 57.7% of the live load is used to obtain a continuous system, applied on a simple span. The remaining 42.3% is applied on a continuous span. The two live load envelopes are proportioned as such, and a new partial continuity live load envelope is formed:

Simple span live load moment envelope:
$$M_{LLs} := \begin{pmatrix} 0 \\ 90 \\ 76 \\ 355 \end{pmatrix} \cdot kip \cdot ft$$

Continuous system live load positive moment envelope:
$$M_{LL\_p} = \begin{pmatrix} 48 \\ 57 \\ 55 \\ 290 \end{pmatrix} \cdot kip \cdot ft$$

$$M_{LLpar} := LL_{req} \cdot M_{LLs} + \left(1 - LL_{req}\right) \cdot M_{LL\_p}$$

$$M_{LLpar}^T = \begin{pmatrix} 20 & 76 & 67 & 328 \end{pmatrix} \cdot kip \cdot ft$$

$$M_{LL\_p} := if\left(LL_{req} < 0.5, M_{LL\_p}, M_{LLpar}\right)$$

$$M_{LL\_p}^T = \begin{pmatrix} 20 & 76 & 67 & 328 \end{pmatrix} \cdot kip \cdot ft$$

Computing partial continuity live load stresses:

$$f_{pLLt_j} := \frac{M_{LL\_p_j}}{S_{tcb}} \qquad\qquad f_{pLLt}^T = (0.022 \quad 0.083 \quad 0.073 \quad 0.358) \cdot ksi$$

$$f_{pLLb_j} := -\frac{M_{LL\_p_j}}{S_{bc}} \qquad\qquad f_{pLLb}^T = (-0.039 \quad -0.146 \quad -0.129 \quad -0.628) \cdot ksi$$

$$f_{pLLtt_j} := \frac{M_{LL\_p_j}}{S_{tc}} \qquad\qquad f_{pLLtt}^T = (0.032 \quad 0.12 \quad 0.106 \quad 0.519) \cdot ksi \qquad \text{(top of topping)}$$

2.7 Prestress Losses

At Release:

At release, two components of prestress loss are significant: relaxation of the prestressing steel and elastic shortening. Elastic shortening is the loss of prestress that results when the strands are detensioned and the precast beam shortens in length due to the applied prestress. When the strands are tensioned in the prestress bed and anchored at the abutments, the steel gradually begins to relax as a function of time. By the time the strands are detensioned a small, but measurable, loss due to steel relaxation has occurred.

Steel Relaxation (short term):

$$f_{pj} := Pull \cdot f_{pu} \qquad f_{pj} = 202.5 \cdot ksi \qquad f_{py} = 243 \cdot ksi$$

$$\Delta f_{pR1} := \frac{\log\left(\frac{t}{hr}\right)}{40.0} \cdot \left(\frac{f_{pj}}{f_{py}} - 0.55\right) \cdot f_{pj} \qquad\qquad \Delta f_{pR1} = 8.149 \cdot ksi \qquad\qquad \text{(LRFD 5.9.5.4.4b-2)}$$

Elastic Shortening:

$$E_{ci} := 33000 \cdot w_c^{1.5} \cdot kcf^{-1.5} \cdot \sqrt{f'_{ci}} \cdot ksi^{.5} \qquad\qquad E_{ci} = 4287 \cdot ksi \qquad\qquad \text{(LRFD 5.4.2.4-1)}$$

$$A_{ps} := No\_Strands \cdot A_{strand} \qquad A_{ps} = 5.642 \cdot in^2 \qquad \text{(Area of strand at midspan)}$$

$$f_{pbt} := f_{pj} - \Delta f_{pR1} \qquad f_{pbt} = 194.4 \cdot ksi$$

$$\Delta f_{pES} := \frac{A_{ps} \cdot f_{pbt} \cdot \left(I + ecc^2 A\right) - ecc \cdot M_{swr_2} \cdot A}{A_{ps} \cdot \left(I + ecc^2 A\right) + \frac{A \cdot I \cdot E_{ci}}{E_p}} \qquad\qquad \Delta f_{pES} = 10.333 \cdot ksi$$

Total Prestress Loss at Release:

$$\Delta f_{sr} := \Delta f_{pES} + \Delta f_{pR1} \qquad\qquad \Delta f_{sr} = 18.482 \cdot ksi$$

$$\%Loss := \frac{\Delta f_{sr}}{Pull \cdot f_{pu}} \cdot 100 \qquad\qquad \%Loss = 9.1268$$

$$f_{per} := f_{pj} - \Delta f_{pES} - \Delta f_{pR1} \qquad\qquad f_{per} = 184 \cdot ksi$$

$$P_r := f_{per} \cdot No\_Strands \cdot A_{strand} \qquad P_r = 1038.2 \cdot kip$$

At Final Conditions:

<u>Total Loss of Prestress:</u>

$$\Delta f_{pT} = \Delta f_{pES} + \Delta f_{pLT}$$

(LRFD 5.9.5.1-1)

where:

Δf_{pES} = Sum of all losses due to elastic shortening at time of application of prestress load (ksi).

Δf_{pLT} = Total loss due to long-term effects, which include shrinkage and creep of the concrete and relaxation of the prestressing steel (ksi).

The shrinkage and creep properties of the girder need to be computed in preparation for the prestress loss computations. These are addressed in LRFD Article 5.4.2.3. Creep coefficients are computed in accordance with Article 5.4.2.3.2 and shrinkage strains are computed in accordance with Article 5.4.2.3.3.

Creep Coefficients

Girder creep coefficients were calculated previously for restraint moments

Girder creep coefficient at final time due to loading at transfer:

$\psi_{bfi} = 1.580$

Girder creep coefficient at time of CIP placement due to loading at transfer:

$\psi_{bdi} = 0.156$

Girder creep coefficient at final time due to loading at CIP placement:

$\psi_{bfd} = 1.256$

CIP deck creep coefficient at final time due to loading at CIP placement:

$t_f := t_{final}$

$t_i := t_{deck}$

$t := t_f - t_i$ $\qquad t = 19993 \cdot day$

$$k_{td} := \frac{\dfrac{t}{day}}{61 - \dfrac{4 \cdot (0.8 \cdot f'_{ct})}{ksi} + \dfrac{t}{day}} \qquad\qquad k_{td} = 0.998$$

$$k_{vs} := 1.45 - 0.13 \frac{VS_d}{in} \qquad\qquad k_{vs} = 0.670 \qquad \text{Note: } k_{vs} \text{ must be greater than 1.0.}$$

$$k_{vs} := 1.000$$

$$k_{hc} := 1.56 - 0.008 H \qquad\qquad k_{hc} = 1.000$$

$$k_f := \frac{5}{1 + \dfrac{(0.8 \cdot f'_{ct})}{ksi}} \qquad\qquad k_f = 1.19$$

$$\psi_{dfd} := 1.9 \cdot k_{vs} \cdot k_{hc} \cdot k_f \cdot k_{td} \cdot \left(\frac{t_i}{day}\right)^{-0.118} \qquad\qquad \psi_{dfd} = 1.794$$

B2-22

<u>Shrinkage Strains</u>

Shrinkage strains were calculated previously for restraint moment.

Girder concrete shrinkage strain between transfer and final time:

$$\varepsilon_{bif} = -407 \times 10^{-6}$$

Girder concrete shrinkage strain between transfer and CIP placement:

$$\varepsilon_{bid} = -52 \times 10^{-6}$$

Girder concrete shrinkage strain between CIP placement and final time:

> The girder concrete shrinkage between deck placement and final time is the difference between the shrinkage at time of deck placement and the total shrinkage at final time.

$$\varepsilon_{bdf} := \varepsilon_{bif} - \varepsilon_{bid} \qquad \varepsilon_{bdf} = -355 \times 10^{-6}$$

CIP concrete shrinkage strain between CIP placement and final time:

$$\varepsilon_{ddf} = -581 \times 10^{-6}$$

<u>Loss from Transfer to CIP Placement:</u>

The prestress loss from transfer of prestress to placement of CIP consists of three loss components: shrinkage of the girder concrete, creep of the girder concrete, and relaxation of the strands. That is,

> Time-Dependent Loss from Transfer to CIP Placement = $\Delta f_{pSR} + \Delta f_{pCR} + \Delta f_{pR1}$

Shrinkage of Concrete Girder:

$$\Delta f_{pSR} = \varepsilon_{bid} \cdot E_p \cdot K_{id} \qquad\qquad\qquad\text{(LRFD5.9.5.4.2a-1)}$$

where:

ε_{bid} = Concrete shrinkage strain of girder between transfer and CIP placement. Computed using LRFD Eq. 5.4.2.3.3-1

E_p = Modulus of elasticity of prestressing strand (ksi).

K_{id} = Transformed steel coefficient that accounts for time-dependent interaction between concrete and bonded steel in the section being considered for the time period between transfer and CIP placement.

The transformed section coefficient, k_{id}, is computed using:

$$K_{id} = \frac{1}{1 + \dfrac{E_p}{E_{ci}} \cdot \dfrac{A_{ps}}{A} \cdot \left(1 + \dfrac{A \cdot e_{pg}^2}{I_g}\right) \cdot \left(1 + 0.7 \cdot \psi_b(t_f, t_i)\right)} \qquad\text{(LRFD Eq. 5.9.5.4.2a-2)}$$

where:

e_{pg} = Eccentricity of strands with respect to centroid of girder (in).

$\psi_b(t_f, t_i)$ = Creep coefficient at final time due to loading introduced at transfer.

Note: The eccentricity of the strand pattern is stored in the vectors ecc_r and ecc_f. Vector

B2-23

ecc_r contains values at check points relative to release (i.e., the end of the girder), and vector ecc_r is relative to final check points (i.e., relative to the left bearing of the girder). The eccentricity at the midspan of the girder is the value of interest.

$$e_{pg} := ecc \qquad e_{pg} = 5.5 \cdot in \qquad I = 27120 \cdot in^4 \qquad A = 936 \cdot in^2$$

$$K_{id} := \frac{1}{1 + \dfrac{E_p}{E_{ci}} \cdot \dfrac{A_{ps}}{A} \cdot \left(1 + \dfrac{A \cdot e_{pg}^2}{I}\right) \cdot (1 + 0.7 \cdot \psi_{bfi})} \qquad\qquad K_{id} = 0.8529$$

Therefore, the prestress loss due to shrinkage of the girder concrete between time of transfer and CIP placement is:

$$\Delta f_{pSR} := -\varepsilon_{bid} \cdot E_p \cdot K_{id} \qquad \Delta f_{pSR} = 1.266 \cdot ksi$$

Creep of Concrete Girder:

$$\Delta f_{pCR} = \frac{E_p}{E_{ci}} \cdot f_{cgp} \cdot \psi_b(t_d, t_i) \, K_{id} \qquad\qquad\qquad \text{(LRFD 5.9.5.4.2b-1)}$$

where:

f_{cgp} = Concrete stress at cg of prestress pattern due to the prestressing force immediately after transfer and the self-weight of the girder at the section of maximum moment (ksi).

Section modulus at cg of strand pattern:

$$e_{pti} := y_b - y_{cg} \qquad\qquad e_{pti} = 5.5 \cdot in$$

$$S_{cgp} := \frac{I}{e_{pti}} \qquad\qquad S_{cgp} = 4934 \cdot in^3$$

Initial prestress force:

$$f_{pj} := Pull \cdot f_{pu}$$

$$P_{init} := f_{pj} \cdot A_{ps} \qquad\qquad P_{init} = 1142.5 \cdot kip$$

$$f_{cgp} := P_{init} \cdot \left(\frac{1}{A} + \frac{e_{pti}}{S_{cgp}}\right) - \frac{M_{swf_2}}{S_{cgp}} \qquad\qquad f_{cgp} = 2.359 \cdot ksi$$

$$\Delta f_{pCR} := \frac{E_p}{E_{ci}} \cdot f_{cgp} \cdot \psi_{bdi} \, K_{id} \qquad\qquad \Delta f_{pCR} = 2.092 \cdot ksi$$

Relaxation of Prestressing Strands:

Since, according to LRFD C5.9.5.4.2c, the second equation is the more accurate equation, Δf_{pR1} should be computed using the second. However, for this example, it will be assumed to be equal to 1.2 ksi (Article 5.9.5.4.2b permits this).

$$\Delta f_{pR1} := 1.2 \cdot ksi$$

Total prestress loss at time of CIP placement:

$$\Delta f_{pLTid} := \Delta f_{pSR} + \Delta f_{pCR} + \Delta f_{pR1}$$

Calculated above:

$$\Delta f_{pSR} = 1.27 \cdot ksi \qquad \Delta f_{pCR} = 2.09 \cdot ksi \qquad \Delta f_{pR1} = 1.20 \cdot ksi$$

$$\Delta f_{pLTid} = 4.559 \cdot ksi$$

B2-24

Loss from CIP Placement to Final:

The prestress loss from placement of CIP to final conditions consists of four loss components: shrinkage of the girder concrete, creep of the girder concrete, and relaxation of the strands. That is,

Time-Dependent Loss from CIP Placement to Final = $\Delta f_{pSD} + \Delta f_{pCD} + \Delta f_{pR2}$

Shrinkage of Concrete Girder:

$$\Delta f_{pSD} = \varepsilon_{bdf} \cdot E_p \cdot K_{df} \qquad\qquad \text{(LRFD5.9.5.4.3a-1)}$$

where:

ε_{bdf} =   Concrete shrinkage strain of girder between time of CIP placement and final time. Computed using LRFD Eq. 5.4.2.3.3-1

K_{df} =   Transformed steel coefficient that accounts for time-dependent interaction between concrete and bonded steel in the section being considered for the time period between the time of CIP placement and final time.

Compute K_{df}:

$$K_{df} = \cfrac{1}{1 + \cfrac{E_p}{E_{ci}} \cdot \cfrac{A_{ps}}{A_c} \cdot \left(1 + \cfrac{A_c \cdot e_{pc}^2}{I_c}\right) \cdot \left(1 + 0.7\,\psi_b(t_f, t_i)\right)} \qquad\qquad \text{(LRFD 5.9.5.4.3a-2)}$$

where:

e_{pc} =   Eccentricity of strands with respect to centroid of composite section

A_c =   For composite sections, the gross area of the composite section should be used. However, since this girder is non-composite, the gross area of the non-composite section is used.

I_c =   Gross area of composite section for composite systems, gross area of bare beam for non-composite systems.

$\psi_b(t_f, t_i)$ =   Girder creep coefficient

$e_{pc} := y_b - y_{cg}$ $e_{pc} = 5.4969 \cdot in$

A_c: $A = 936 \cdot in^2$

I_c: $I = 27120 \cdot in^4$

$$K_{df} := \cfrac{1}{1 + \cfrac{E_p}{E_{ci}} \cdot \cfrac{A_{ps}}{A} \cdot \left(1 + \cfrac{A \cdot e_{pc}^2}{I}\right) \cdot \left(1 + 0.7\psi_{bfi}\right)} \qquad\qquad K_{df} = 0.853$$

Therefore, prestress loss due to shrinkage of girder concrete between CIP placement and final is:

$\Delta f_{pSD} := -\varepsilon_{bdf} \cdot E_p \cdot K_{df}$ $\Delta f_{pSD} = 8.632 \cdot ksi$

Creep of Concrete Girder:

$$\Delta f_{pCD} = \frac{E_p}{E_{ci}} \cdot f_{cgp} \cdot \left(\psi_b(t_f, t_i) - \psi_b(t_d, t_i) \right) \cdot K_{df} + \frac{E_p}{E_c} \cdot \Delta f_{cd} \cdot \psi_b(t_f, t_d) \cdot K_{df} \geq 0.0 \qquad \text{(LRFD5.9.5.4.3b-1)}$$

where:

$\Delta f_{cd} =$ Change in concrete stress at centroid of prestressing strands due to long-term losses between transfer and CIP placement combined with superimposed loads (ksi).

$\psi_b(t_f, t_d) =$ Girder creep coefficient at final time due to loading at CIP placement per Eq. 5.4.2.3.2-1.

Let:

$$\Delta f_{pCD} = \Delta f_{pCD1} + \Delta f_{pCD2}$$

compute Δf_{pCD1}:

$$\Delta f_{pCD1} := \frac{E_p}{E_{ci}} \cdot f_{cgp} \cdot \left(\psi_{bfi} - \psi_{bdi} \right) \cdot K_{df} \qquad\qquad \Delta f_{pCD1} = 19.041 \cdot ksi$$

compute Δf_{pCD2}:

    compute Δf_{cd}:

$$\Delta f_{cd} = \Delta P \cdot \left(\frac{1}{A_g} + \frac{e_{pg}^2}{I_g} \right) - \left(\frac{M_{fws_7} + M_{barrier_7}}{S_{cgp}} \right)$$

$$\Delta P := -\Delta f_{pLTid} \cdot A_{ps} \qquad\qquad \Delta P = -25.7 \cdot kip$$

$$e_{pg} := y_b - y_{cg} \qquad\qquad e_{pg} = 5.497 \cdot in$$

$$\Delta f_{cd} := \Delta P \cdot \left(\frac{1}{A} + \frac{e_{pg}^2}{I} \right) - \left(\frac{M_{fws_2} + M_{barrier_2}}{S_{cgp}} \right) \qquad\qquad \Delta f_{cd} = 0.013 \cdot ksi$$

$$E_c := 33000 \cdot 1.0 \cdot \left(0.14 + \frac{f'_c}{1000 \cdot ksi} \right)^{1.5} \cdot \sqrt{\frac{f'_c}{ksi}} \cdot ksi \qquad\qquad E_c = 4921 \cdot ksi$$

$$\Delta f_{pCD2} := \frac{E_p}{E_c} \cdot \Delta f_{cd} \cdot \psi_{bfd} \cdot K_{df} \qquad\qquad \Delta f_{pCD2} = 0.079 \cdot ksi$$

Therefore,

$$\Delta f_{pCD} := \Delta f_{pCD1} + \Delta f_{pCD2} \qquad\qquad \Delta f_{pCD} = 19.12 \cdot ksi$$

Relaxation of Prestressing Strands:

$$\Delta f_{pR2} := \Delta f_{pR1} \qquad\qquad \Delta f_{pR2} = 1.2 \cdot ksi \qquad\qquad\qquad \text{(LRFD 5.9.5.4.3c-1)}$$

Shrinkage of the CIP deck:

$$A_d := \frac{A_{slab}}{n} \qquad\qquad\qquad\qquad A_d = 432 \cdot in^2$$

$$E_{cd} := 33000 \cdot w_c^{1.5} \cdot kcf^{-1.5} \cdot \sqrt{f'_{ct}} \cdot ksi^{.5} \qquad\qquad E_{cd} = 3834 \cdot ksi$$

$$e_d := \frac{h}{2} \qquad\qquad\qquad\qquad e_d = 9 \cdot in$$

B2-26

$$\Delta f_{cdf} := \frac{\varepsilon_{ddf} \cdot A_d \cdot E_{cd}}{(1 + 0.7 \cdot \psi_{dfd})} \cdot \left(\frac{1}{A_c} - \frac{e_{pc} \cdot e_d}{I_c} \right) \qquad\qquad \Delta f_{cdf} = -0.6548 \cdot ksi$$

$$\Delta f_{pSS} := \frac{E_p}{E_c} \cdot \Delta f_{cdf} \cdot K_{df} \cdot (1 + 0.7 \cdot \psi_{bfd}) \qquad\qquad \Delta f_{pSS} = -6.0784 \cdot ksi$$

Total prestress loss from CIP placement to final, therefore, is:

$$\Delta f_{pLTdf} := \Delta f_{pSD} + \Delta f_{pCD} + \Delta f_{pR2} + \Delta f_{pSS}$$

Calculated above:

$\Delta f_{pSD} = 8.63 \cdot ksi$ $\Delta f_{pCD} = 19.12 \cdot ksi$ $\Delta f_{pR2} = 1.2 \cdot ksi$ $\Delta f_{pSS} = -6.0784 \cdot ksi$

$\Delta f_{pLTdf} = 22.873 \cdot ksi$

Summary of Time-Dependent Losses

Losses from Transfer to CIP Placement

Girder shrinkage:	$\Delta f_{pSR} = 1.27 \cdot ksi$
Girder creep:	$\Delta f_{pCR} = 2.09 \cdot ksi$
Strand relaxation:	$\Delta f_{pR1} = 1.2 \cdot ksi$
Total =	$\Delta f_{pLTid} = 4.559 \cdot ksi$

Losses from CIP Placement to Final

Girder shrinkage:	$\Delta f_{pSD} = 8.63 \cdot ksi$
Girder creep:	$\Delta f_{pCD} = 19.12 \cdot ksi$
Strand relaxation:	$\Delta f_{pR2} = 1.2 \cdot ksi$
Differential Shrinkage:	$\Delta f_{pSS} = -6.0784 \cdot ksi$
Total =	$\Delta f_{pLTdf} = 22.873 \cdot ksi$

$$\Delta f_{pLT} = 10.0 \cdot \frac{f_{pj} \cdot A_{psm}}{A} \cdot \gamma_h \cdot \gamma_{st} + 12.0 \cdot ksi \cdot \gamma_h \cdot \gamma_{st} + \Delta f_{pR} \qquad\qquad \text{(LRFD 5.9.5.3-1)}$$

$$\gamma_h := 1.7 - 0.01 \cdot H \qquad\qquad \gamma_h = 1.00 \qquad\qquad\qquad \text{(LRFD 5.9.5.3-2)}$$

$$\gamma_{st} := \frac{5 \cdot ksi}{1 \cdot ksi + f'_{ci}} \qquad\qquad \gamma_{st} = 0.833 \qquad\qquad\qquad \text{(LRFD 5.9.5.3-3)}$$

$$\Delta f_{pR} := 2.4 \cdot ksi$$

$$\Delta f_{pLT} := \Delta f_{pLTid} + \Delta f_{pLTdf} \qquad\qquad \Delta f_{pLT} = 27.43 \cdot ksi$$

$$\Delta f_{PT} := \Delta f_{pES} + \Delta f_{pLT} \qquad\qquad \Delta f_{PT} = 37.77 \cdot ksi$$

$$\%Loss := \frac{\Delta f_{PT}}{Pull \cdot f_{pu}} \cdot 100 \qquad\qquad \%Loss = 18.65$$

Check effective stress after losses:

$$f_{pe} := Pull \cdot f_{pu} - \Delta f_{PT} \qquad\qquad f_{pe} = 164.7 \cdot ksi$$

$$f_{allow} := 0.80 \cdot f_{py} \qquad\qquad f_{allow} = 194.4 \cdot ksi \qquad\qquad\qquad \text{(LRFD 5.9.3-1)}$$

B2-27

2.8 Stresses Due to Prestress at End of Trnasfer Length and Midspan

At Release:

$P_r := f_{per} \cdot No\_Strands \cdot A_{strand}$ $\qquad$ $P_r = 1038.2 \cdot kip$

$j := 1 .. 2$

$f_{psrb_j} := P_r \cdot \left(\dfrac{1}{A} + \dfrac{ecc}{S_b} \right)$ $\qquad$ $f_{psrb}^T = (2.881 \quad 2.881) \cdot ksi$

$f_{psrt_j} := P_r \cdot \left(\dfrac{1}{A} - \dfrac{ecc}{S_t} \right)$ $\qquad$ $f_{psrt}^T = (-0.907 \quad -0.907) \cdot ksi$

At Final Conditions:

$j := 1 .. 4$

$dist_j := x_{f_j} + \dfrac{L_{ovr} - L_{des}}{2}$ $\qquad$ $dist^T = (0.5 \quad 3 \quad 2.44 \quad 24.5) \, ft$

$dt_j := if\left(dist_j > L_t, 1.0, \dfrac{dist_j}{L_t} \right)$ $\qquad$ $dt^T = (0.1667 \quad 1 \quad 0.8133 \quad 1)$ $\quad$ (Fraction strands are transferred.)

$P_{f_j} := f_{pe} \cdot dt_j \cdot No\_Strands \cdot A_{strand}$ $\qquad$ $P_f^T = (154.9 \quad 929.4 \quad 755.9 \quad 929.4) \cdot kip$

$ecc = 0.4581 \, ft$

$f_{psb_j} := P_{f_j} \cdot \left(\dfrac{1}{A} + \dfrac{ecc}{S_b} \right)$ $\qquad$ $f_{psb}^T = (0.43 \quad 2.579 \quad 2.098 \quad 2.579) \cdot ksi$ $\qquad$ $S_b = 1.8639 \, ft^3$

$A = 6.5 \, ft^2$

$f_{pst_j} := P_{f_j} \cdot \left(\dfrac{1}{A} - \dfrac{ecc}{S_t} \right)$ $\qquad$ $f_{pst}^T = (-0.135 \quad -0.812 \quad -0.66 \quad -0.812) \cdot ksi$

2.9 Service Stress Check

At Release:

$j := 1 .. 2$

Bottom of beam (compression):

$f_{rb_j} := f_{psrb_j} + f_{swrb_j}$ $\qquad$ $f_{rb}^T = (2.63 \quad 1.791) \cdot ksi$

$f_{allow\_rc} := 0.6 \cdot f'_{ci}$ $\qquad$ $f_{allow\_rc} = 3 \cdot ksi$

$Status\_ServiceLSrc_j := if\left(f_{rb_j} \le f_{allow\_rc}, "OK", "NG" \right)$ $\qquad$ <mark>$Status\_ServiceLSrc^T = ("OK" \quad "OK")$</mark>

Top of beam (tension):

$f_{rt_j} := f_{psrt_j} + f_{swrt_j}$ $\qquad$ $f_{rt}^T = (-0.622 \quad 0.334) \cdot ksi$

$f_{allow\_rt} := -0.0948 \cdot \sqrt{f'_{ci}} \cdot \sqrt{ksi}$ $\qquad$ $f_{allow\_rt} = -0.212 \cdot ksi$

$Status\_ServiceLSrt_j := if\left(f_{rt_j} \ge f_{allow\_rt}, "OK", "NG" \right)$ $\qquad$ <mark>$Status\_ServiceLSrt^T = ("NG" \quad "OK")$</mark>

Since top tension exceeds limit, compute required amount of top tension steel at transfer point:

$x_{tt} := h \cdot \left(\dfrac{f_{rt_1}}{f_{rt_1} + f_{rb_1}} \right)$ $\qquad$ $x_{tt} = -5.57 \cdot in$ $\qquad$ (LRFD C5.9.4.1.2)

$$T_{tt} := \frac{f_{rt_1}}{2} \cdot b_v \cdot x_{tt} \qquad T_{tt} = 124.64 \cdot kip$$

$$A_{tt} := \frac{T_{tt}}{30 \cdot ksi} \qquad A_{tt} = 4.1545 \cdot in^2$$

Assume #8 bars will be used as top tension steel:

$$N_{tt} := \frac{A_{tt}}{0.79 \cdot in^2} \qquad N_{tt} = 5 \quad \text{#8 bars}$$

At Final Conditions:

<u>Positive Moment Envelope</u>

Service III Limit State (Tensile Stresses in Bottom of Beam):

$$j := 1 .. 4$$

$$f_{pAllb_j} := f_{psb_j} + f_{swb_j} + f_{deckb_j} + f_{barrierb_j} + f_{fwsb_j} + \left(0.8 \cdot f_{pLLb}\right)_j + f_{rmb} + 0.5 \cdot f_{grb}$$

$$f_{pAllb}^T = (0.308 \quad 1.967 \quad 1.586 \quad -0.069) \cdot ksi$$

$$f_{allow\_ft} := -0.19 \cdot \sqrt{f'_c} \cdot \sqrt{ksi} \qquad f_{allow\_ft} = -0.503 \cdot ksi \qquad \text{(LRFD 5.9.4.2.2b)}$$

$$\text{Status\_ServiceLSft}_j := if\left(f_{pAllb_j} \geq f_{allow\_ft}, \text{"OK"}, \text{"NG"}\right) \qquad \text{Status\_ServiceLSft}^T = (\text{"OK"} \quad \text{"OK"} \quad \text{"OK"} \quad \text{"OK"})$$

Service I (Compressive Stresses in Top of Beam):

Compressive Stress Due to Permanent Loads:

$$f_{pPermt_j} := f_{pst_j} + f_{swt_j} + f_{deckt_j} + f_{barriert_j} + f_{fwst_j} + f_{rmt} + f_{grt}$$

$$f_{pPermt}^T = (0.203 \quad -0.026 \quad 0.029 \quad 1.794) \cdot ksi$$

$$f_{allow\_fcd} := 0.45 \cdot f'_c \qquad f_{allow\_fcd} = 3.15 \cdot ksi \qquad \text{(LRFD 5.9.4.2.1)}$$

$$\text{Status\_ServiceLSfcd}_j := if\left(f_{pPermt_j} \leq f_{allow\_fcd}, \text{"OK"}, \text{"NG"}\right) \qquad \text{Status\_ServiceLSfcd}^T = (\text{"OK"} \quad \text{"OK"} \quad \text{"OK"} \quad \text{"OK"})$$

Compressive Stress Due to Full Dead Load + Live Load:

$$f_{allow\_fcl} := 0.6 \cdot f'_c \qquad f_{allow\_fcl} = 4.2 \cdot ksi \qquad \text{(LRFD 5.9.4.2.1)}$$

$$f_{pAllt_j} := f_{pst_j} + f_{swt_j} + f_{deckt_j} + f_{barriert_j} + f_{fwst_j} + f_{pLLt_j} + f_{rmt} + 0.5 \cdot f_{grt}$$

$$f_{pAllt}^T = (0.052 \quad -0.116 \quad -0.07 \quad 1.979) \cdot ksi$$

$$\text{Status\_ServiceLSfcl}_j := if\left(f_{pAllt_j} \leq f_{allow\_fcl}, \text{"OK"}, \text{"NG"}\right) \qquad \text{Status\_ServiceLSfcl}^T = (\text{"OK"} \quad \text{"OK"} \quad \text{"OK"} \quad \text{"OK"})$$

<u>Negative Moment Envelope</u>

Compressive Stress Due to Full Dead Load + Live Load:

$$f_{nAllb_j} := f_{psb_j} + f_{swb_j} + f_{deckb_j} + f_{barrierb_j} + f_{fwsb_j} + f_{nLLb_j} + f_{rmb} + 0.5 \cdot f_{grb}$$

$$f_{nAllb}^T = (0.771 \quad 2.425 \quad 2.051 \quad 0.615) \cdot ksi$$

$$f_{allow\_fcn} := 0.6 \cdot f'_c \qquad f_{allow\_fcn} = 4.2 \cdot ksi \qquad \text{(LRFD 5.9.4.2.1)}$$

$$\text{Status\_ServiceLSfnc}_j := if\left(f_{nAllb_j} < f_{allow\_fcn}, \text{"OK"}, \text{"NG"}\right) \qquad \text{Status\_ServiceLSfnc}^T = (\text{"OK"} \quad \text{"OK"} \quad \text{"OK"} \quad \text{"OK"})$$

2.10 Flexural Strength Check

Positive Moment Envelope

$$M_{u_j} := 1.25 \cdot \left(M_{swf_j} + M_{deck_j} + M_{barrier_j} \right) + 1.5 \cdot M_{fws_j} + 1.75 \cdot M_{LL\_p_j} + M_{rm}$$

$$M_u^T = (11 \quad 255 \quad 208 \quad 1289) \cdot kip \cdot ft$$

$$\beta_1 := if\left[f'_{ct} \le 4 \cdot (ksi), 0.85, if\left[f'_{ct} \ge 8 \cdot (ksi), 0.65, 0.85 - \left[\frac{f'_{ct} - 4 \cdot (ksi)}{1 \cdot (ksi)} \cdot 0.05 \right] \right] \right] \qquad \beta_1 = 0.85 \qquad \text{(LRFD 5.7.2.2)}$$

$$L_d := \left(270.0 \cdot ksi - \frac{2}{3} \cdot f_{pe} \right) \cdot d_b \cdot ksi^{-1} \qquad L_d = 96.11 \cdot in \qquad \text{(Preliminary estimate of } L_d\text{)}$$

$$K_{ld} := if(h \le 24 \cdot in, 1.0, 1.6) \qquad K_{ld} = 1 \qquad\qquad\qquad \text{(LRFD Eq. 5.11.4.2-1)}$$

$$df_j := if\left[dist_j < L_t, \frac{dist_j}{L_t} \cdot \frac{f_{pe}}{f_{pu}}, if\left[dist_j < K_{ld} \cdot L_d, \frac{f_{pe} + \left(\frac{dist_j - L_t}{K_{ld} \cdot L_d - L_t} \right) \cdot (f_{pu} - f_{pe})}{f_{pu}}, 1.0 \right] \right]$$

$$df^T = (0.1017 \quad 0.6101 \quad 0.4962 \quad 1) \qquad \text{(Preliminary estimate of fraction strands are developed)}$$

$$A_{ps_j} := No\_Strands \cdot df_j \cdot A_{strand} \qquad A_{ps}^T = (0.5737 \quad 3.4423 \quad 2.7998 \quad 5.642) \cdot in^2$$

$$b := b_{eff} \qquad b = 72 \cdot in$$

$$d_p := h + t_{slab} - t_{ws} - (y_{cg}) \qquad d_p = 21.08 \cdot in$$

$$k := 2 \cdot \left(1.04 - \frac{f_{py}}{f_{pu}} \right) \qquad k = 0.28 \qquad\qquad\qquad \text{(LRFD 5.7.3.1.1-2)}$$

$$c_j := \frac{A_{ps_j} \cdot f_{pu}}{0.85 \cdot f'_{ct} \cdot \beta_1 \cdot b + k \cdot A_{ps_j} \cdot \frac{f_{pu}}{d_p}} \qquad c^T = (0.74 \quad 4.22 \quad 3.47 \quad 6.67) \cdot in \qquad \text{(LRFD 5.7.3.1.1-4)}$$

$$h_f := t_{slab} \qquad \text{(Height of flange is slab thickness since this is a composite section)}$$

$$b_{w_j} := if(c_j \le h_f, b, b_v) \qquad b_w^T = (72 \quad 72 \quad 72 \quad 72) \cdot in$$

$$c_j := \frac{A_{ps_j} \cdot f_{pu} - 0.85 \cdot f'_{ct} \cdot \left(b - b_{w_j} \right) \cdot h_f}{0.85 \cdot f'_{ct} \cdot \beta_1 \cdot b_{w_j} + k \cdot A_{ps_j} \cdot \frac{f_{pu}}{d_p}} \qquad c^T = (0.74 \quad 4.22 \quad 3.47 \quad 6.67) \cdot in \qquad \text{(LRFD 5.7.3.1.1-3)}$$

$$a_j := \beta_1 \cdot c_j \qquad a^T = (0.627 \quad 3.584 \quad 2.946 \quad 5.671) \cdot in$$

$$f_{ps_j} := f_{pu} \cdot \left(1 - k \cdot \frac{c_j}{d_p} \right) \qquad f_{ps}^T = (267.4 \quad 254.9 \quad 257.6 \quad 246.1) \cdot ksi \qquad \text{(LRFD 5.7.3.1.1-1)}$$

$$L_d := \left(f_{ps_1} - \frac{2}{3} \cdot f_{pe} \right) \cdot d_b \cdot ksi^{-1} \qquad L_d = 94.52 \cdot in \qquad \text{(LRFD 5.11.4.1-1)}$$

B2-30

$$df_j := if\left[dist_j < L_t, \frac{dist_j}{L_t}\cdot\frac{f_{pe}}{f_{ps_j}}, if\left[dist_j < K_{ld}\cdot L_d, \frac{f_{pe} + \left(\frac{dist_j - L_t}{K_{ld}\cdot L_d - L_t}\right)\cdot\left(f_{ps_j} - f_{pe}\right)}{f_{ps_j}}, 1.0\right]\right]$$

$df^T = (0.1027 \quad 0.6463 \quad 0.5202 \quad 1)$ (fraction strands are developed)

$A_{ps_j} := No\_Strands \cdot df_j \cdot A_{strand}$ $\qquad A_{ps}^T = (0.5794 \quad 3.6466 \quad 2.9349 \quad 5.642)\cdot in^2$

$$c_j := \frac{A_{ps_j} \cdot f_{pu}}{0.85 \cdot f'_{ct} \cdot \beta_1 \cdot b + k \cdot A_{ps_j} \cdot \frac{f_{pu}}{d_p}}$$

$b_{w_j} := if\left(c_j \le h_f, b, b_v\right)$ $\qquad\qquad b_w^T = (72 \quad 72 \quad 72 \quad 72)\cdot in$

$$c_j := \frac{A_{ps_j} \cdot f_{pu} - 0.85 \cdot f'_{ct} \cdot \left(b - b_{w_j}\right)\cdot h_f}{0.85 \cdot f'_{ct} \cdot \beta_1 \cdot b_{w_j} + k \cdot A_{ps_j} \cdot \frac{f_{pu}}{d_p}}$$ $\qquad c^T = (0.74 \quad 4.45 \quad 3.62 \quad 6.67)\cdot in$

$$M_{n_j} := df_j \cdot A_{ps_j} \cdot f_{ps_j} \cdot \left(d_p - \frac{a_j}{2}\right) + 0.85 \cdot f'_{ct} \cdot \left(b - b_{w_j}\right)\cdot h_f \cdot \left(\frac{a_j}{2} - \frac{h_f}{2}\right)$$ $\qquad$ (LRFD 5.7.3.2.2-1)

$M_n^T = (28 \quad 965 \quad 642 \quad 2110)\cdot kip\cdot ft$

Compute phi for each section:

$\phi_{f_j} := 0.583 + 0.25\cdot\left(\frac{d_p}{c_j} - 1\right)$ $\qquad\qquad \phi_f^T = (7.41 \quad 1.52 \quad 1.79 \quad 1.12)$ $\qquad$ (LRFD Eq. 5.5.4.2.1-1)

$\phi_{f_j} := if\left(\phi_{f_j} \le 0.75, 0.75, if\left(\phi_{f_j} > 1.0, 1.0, \phi_{f_j}\right)\right)$ $\qquad \phi_f^T = (1.00 \quad 1.00 \quad 1.00 \quad 1.00)$

$M_{r_j} := \phi_{f_j} \cdot M_{n_j}$

$M_r^T = (28 \quad 965 \quad 642 \quad 2110)\cdot kip\cdot ft$ $\qquad\qquad M_u^T = (11 \quad 255 \quad 208 \quad 1289)\cdot kip\cdot ft$

$Status\_StrengthLS_j := if\left(M_{u_j} \le M_{r_j}, "OK", "NG"\right)$ $\qquad Status\_StrengthLS^T = ("OK" \quad "OK" \quad "OK" \quad "OK")$

<u>Maximum Steel Check:</u>

> Note: The provisions contained in Art. 5.7.3.3.1 to check maximum reinforcement were deleted in 2005. This check is now effectively handled by varying phi, depending upon whether the section is compression or tension controlled. See Art. 5.5.4.2.1.

<u>Minimum Steel Check:</u>   (LRFD 5.7.3.3.2)

Compute Cracking Moment at Midspan:

$$f_r := 0.37 \cdot \sqrt{f'_c} \cdot \sqrt{ksi} \qquad\qquad f_r = 0.979 \cdot ksi$$

$$M_{cr} := S_{bc} \cdot \left(f_r + f_{psb_4} \right) - \left(M_{swf_4} + M_{deck_4} \right) \cdot \left(\frac{S_{bc}}{S_b} - 1 \right)$$

$$M_{cr} := if\left(M_{cr} < S_{bc} \cdot f_r, S_{bc} \cdot f_r, M_{cr} \right) \qquad\qquad M_{cr} = 1367.6 \cdot kip \cdot ft$$

$$1.2 \cdot M_{cr} = 1641.1 \cdot kip \cdot ft \qquad\qquad \text{Ref:} \quad M_{r_4} = 2110.4 \cdot kip \cdot ft$$

$$1.33 \cdot M_{u_4} = 1714.1 \cdot kip \cdot ft$$

$$M_{min} := if\left(1.2 \cdot M_{cr} < 1.33 \, M_{u_4}, 1.2 M_{cr}, 1.33 \cdot M_{u_4} \right) \qquad M_{min} = 1641.1 \cdot kip \cdot ft$$

$$Status\_MinStl := if\left(M_{min} < M_{r_4}, \text{"OK"}, \text{"NG"} \right) \qquad\qquad \boxed{Status\_MinStl = \text{"OK"}}$$

Negative Moment Envelope

$$M_{LL\_nc} := DF_m \cdot \left[M_{lane\_nc_1} + (1.0 + DLA) \cdot M_{Vehicle\_nc_1} \right] \qquad\qquad M_{LL\_nc} = -244 \cdot kip \cdot ft$$

$$M_{un} := 1.25 \cdot \left(M_{barrier\_c_1} \right) + 1.5 \cdot M_{fws\_c_1} + 1.75 \cdot M_{LL\_nc} \qquad\qquad M_{un} = -492 \cdot kip \cdot ft$$

$$\beta_{1n} := if\left[f'_c \le 4 \cdot (ksi), 0.85, if\left[f'_c \ge 8 \cdot (ksi), 0.65, 0.85 - \left[\frac{f'_c - 4 \cdot (ksi)}{1 \cdot (ksi)} \cdot 0.05 \right] \right] \right] \qquad \beta_{1n} = 0.7 \qquad\qquad \text{(LRFD 5.7.2.2)}$$

$$c_n := \frac{A_s \cdot f_y}{0.85 \cdot f'_c \cdot \beta_{1n} \cdot b_f} \qquad c_n = 1.26 \cdot in \qquad\qquad A_s = 6.32 \cdot in^2 \;\text{(Reinforcement at the top of the precast)} \quad \text{(LRFD 5.7.3.1.1-4)}$$

$$b_{wn} := if\left(c_n \le t_{flg}, b_f, b_v \right) = 6 \, ft \qquad b_{wn} = 72 \cdot in$$

$$c_n := \frac{A_s \cdot f_y - 0.85 \cdot f'_{ct} \cdot \left(b_f - b_{wn} \right) \cdot h_f}{0.85 \cdot f'_c \cdot \beta_{1n} \cdot b_{wn}} \qquad\qquad c_n = 1.26 \cdot in$$

$$a_n := \beta_{1n} \cdot c_n \qquad a_n = 0.885 \cdot in \qquad\qquad\qquad \text{(LRFD 5.7.3.1.1-3)}$$

Compute phi for each section:

$$\phi_{f_j} := 0.583 + 0.25 \cdot \left(\frac{d_p}{c_j} - 1 \right) \qquad\qquad\qquad \phi_f^T = (7.41 \quad 1.52 \quad 1.79 \quad 1.12) \qquad\qquad \text{(LRFD Eq. 5.5.4.2.1-1)}$$

$$\phi_{f_j} := if\left(\phi_{f_j} \le 0.75, 0.75, if\left(\phi_{f_j} > 1.0, 1.0, \phi_{f_j} \right) \right) \qquad \phi_f^T = (1.00 \quad 1.00 \quad 1.00 \quad 1.00)$$

$$d_s := h_c - \frac{t_{slab}}{2}$$

$$M_{rn} := \phi_{f_4} \cdot A_s \cdot f_y \cdot \left(d_s - \frac{a_n}{2} \right) + 0.85 \cdot f'_c \cdot \left(b_f - b_{wn} \right) \cdot b_f \cdot \left(\frac{a_n}{2} - \frac{t_{flg}}{2} \right) \qquad\qquad \text{(LRFD 5.7.3.2.2-1)}$$

$$M_{rn} = 650 \cdot kip \cdot ft \qquad Status\_StrengthLSn := if\left(-M_{un} \le M_{rn}, \text{"OK"}, \text{"NG""} \right) \qquad \boxed{Status\_StrengthLSn = \text{"OK"}}$$

2.11 Vertical Shear Design

At each section the following must be satisfied for shear:

$V_u \le V_r$

Note: Evaluation has been disabled for these three equations (as indicated by the small boxes) to enable them to be shown without first evaluating their parameters.

(LRFD 5.8.2.1-2)

$V_r = \phi V_n$

$V_n = V_c + V_s + V_p$

(LRFD 5.8.3.3-1)

Critical Section for Shear: (LRFD 5.8.3.2)

The critical section for shear near a support in which the reaction force produces compression in the end of the member is, from the face of support (Fig. 2), the greater of:

   a. $0.5 d_v \cot(\theta)$, or
   b. d_v

where,

   d_v = Effective shear depth = Distance between resultants of tensile and compressive forces = d_e - a/2

$d_v := d_s - \dfrac{a_n}{2}$ $\qquad d_v = 20.557 \cdot in$ $\qquad\qquad a_n = 0.885 \cdot in$

But d_v need not be taken less than the greater of $0.9 d_e$ and 0.72h. Thus,

$d_e := d_s$ $\qquad 0.9 \cdot d_e = 18.9 \cdot in$ $\qquad 0.72 \cdot h_c = 17.28 \cdot in$

$Min\_d_v := if(0.9 \cdot d_e \ge 0.72 \cdot h_c, 0.9 \cdot d_e, 0.72 \cdot h_c)$ $\qquad Min\_d_v = 18.9 \cdot in$

$d_v := if(d_v < Min\_d_v, Min\_d_v, d_v)$ $\qquad d_v = 20.557 \cdot in$

To compute critical section, assume: $\qquad \theta := 32.3 \cdot deg$

$0.5 \cdot d_v \cdot \cot(\theta) = 16.2593 \cdot in$

$Crit\_sec := if(d_v > 0.5 \cdot d_v \cdot \cot(\theta), d_v, 0.5 \cdot d_v \cdot \cot(\theta))$ $\qquad Crit\_sec = 20.56 \cdot in$ $\qquad$ (LRFD 5.8.2.7)

Assuming that the distance from the face of support to the centerline of bearing is half the bearing pad length, the critical section for shear is:

$Crit\_sec := Crit\_sec + \dfrac{L_{pad}}{2}$ $\qquad Crit\_sec = 2.213\,ft$

The above calculations for determining the location of the critical section for shear per LRFD are for illustrative purposes. PSBeam uses a conservative approach to estimating the location of the critical section that is consistent with the LRFD provisions, but which requires no assumptions and no iteration.

PSBeam assumes the critical section to be located at 0.72h from the face of bearing. The logic of this is as follows: since d_v need not be lower than the greater of $0.9 d_e$ and 0.72h, either of these two values is permissible. And since the greater of the two values may be used, either value may be used since adopting the lesser value is conservative since the design shear is higher closer to the support.

Recall that 0.72h from the face of the support was computed earlier as: $\qquad x_{f_3} = 1.94\,ft$

At the critical section, the factored shear is:

$V_u := 1.25 \cdot \left(V_{swf_3} + V_{deck_3} + V_{barrier_3}\right) + 1.5 \cdot V_{fws_3} + 1.75 \cdot V_{LL\_p_3}$ $\qquad V_u = 130.6 \cdot kip$

Compute maximum permissible shear capacity at a section:

$V_{r\_max} := \phi_v \cdot \left(0.25 \cdot f'_c \cdot b_v \cdot d_v + 0.0 \cdot kip\right)$ $\qquad\qquad V_{r\_max} = 2331.2 \cdot kip$ $\qquad$ (LRFD 5.8.3.3-2)

$Status\_V_{rmax} := if(V_u \le V_{r\_max}, "OK", "NG")$ $\qquad\qquad Status\_V_{rmax} = "OK"$

The shear contribution from the concrete, V_c, is given by:

$$M_{uv} := 1.25 \cdot \left(M_{swf_3} + M_{deck_3} + M_{barrier_3} \right) + 1.5 \cdot M_{fws_3} + 1.75 \cdot M_{LL\_n_3} \qquad M_{uv} = -274 \cdot kip \cdot ft$$

In the 2008 Interim the procedure for the calculation of θ and β was moved to an appendix. The new procedure for the calculation of these two values involves a new value, ε_s.

Check lower bound for Mu:

$$M_{uLB} := if\left[\left| M_{uv} \right| < d_v \cdot \left(V_u \right), d_v \cdot \left(V_u \right), \left| M_{uv} \right| \right] \qquad M_{uLB} = 274.2 \cdot kip \cdot ft$$

$$\varepsilon_s := \frac{\dfrac{M_{uLB}}{d_v} + \left(V_u \right)}{E_s \cdot A_s} \qquad\qquad \varepsilon_s = 0.00158587 \qquad\qquad \text{(LRFD 5.8.3.4.2-4)}$$

If ε_s is less than zero, it can be taken equal to zero:

$$\varepsilon_s := if\left(\varepsilon_s < 0, 0.0, \varepsilon_s \right) \qquad\qquad \varepsilon_s = 0.00158587$$

$$\beta := \frac{4.8}{1 + 750 \cdot \varepsilon_s} \qquad\qquad \beta = 2.1924 \qquad\qquad \text{(LRFD 5.8.3.4.2-1)}$$

$$\theta := 29 + 3500 \cdot \varepsilon_s \qquad\qquad \theta = 34.5505 \qquad\qquad \text{(LRFD 5.8.3.4.2-3)}$$

New value for V_c

$$V_c := 0.0316 \cdot \beta \cdot \sqrt{f'_c} \cdot \sqrt{ksi} \cdot b_v \cdot d_v \qquad\qquad V_c = 271.3 \cdot kip$$

Required V_s is, therefore:

$$V_s := \frac{V_u}{\phi_v} - V_c \qquad\qquad V_s = -126.2 \cdot kip$$

Assuming two vertical legs of No. #4 bars:

$$A_v := \frac{V_s}{f_y \cdot d_v \cdot \cot(\theta \cdot deg)} \qquad A_v = -0.845 \cdot \frac{in^2}{ft} \qquad\qquad \text{(LRFD C5.8.3.3-1)}$$

$$Spac := \frac{2 \cdot 0.2 \cdot in^2}{A_v} \qquad Spac = -5.7 \cdot in \qquad \text{(stirrup spacing)}$$

Check minimum transverse reinforcement:

$$A_{v\_min} := 0.0316 \cdot \sqrt{f'_c} \cdot \sqrt{ksi} \cdot \frac{b_v}{f_y} \qquad A_{v\_min} = 1.204 \cdot \frac{in^2}{ft} \qquad\qquad \text{(LRFD 5.8.2.5-1)}$$

Check maximum stirrup spacing:

$$\text{(LRFD 5.8.2.7-2)}$$

$$V_{spc} := 0.1 \cdot f'_c \cdot b_v \cdot d_v \qquad V_{spc} = 1036.1 \cdot kip$$

Ref: $\quad V_u = 130.6 \cdot kip \qquad\qquad d_v = 20.56 \cdot in$

$$Max\_spac := if\left(V_u < V_{spc}, if\left(0.8 \cdot d_v < 24 \cdot in, 0.8 \cdot d_v, 24 \cdot in \right), if\left(0.4 \cdot d_v < 12 \cdot in, 0.4 \cdot d_v, 12 \cdot in \right) \right)$$

$$Max\_spac = 16.4 \cdot in$$

2.12 Longitudinal Reinforcement Check

LRFD requires that the longitudinal steel be checked at all locations along the beam. This requirement is made to ensure that the longitudinal reinforcement is sufficient to develop the required tension tie, which is required for equilibrium. Equation 5.8.3.5-1 is the general equation, applicable at all sections. However, for the special case of the inside edge of bearing at simple-end supports, the longitudinal reinforcement must be able to resist a tensile force of $(V_u/\phi - 0.5V_s - V_p)\cot(\theta)$. Note that when pretensioned strands are used to develop this force, only a portion of the full prestress force may be available near the support due to partial transfer. Additionally, only those strands on the flexural tension side of the member contribute to the tension tie force.

Required Tension Tie Force:

If only the minimum amount of transverse reinforcement that is required by design is provided, the required tension tie force is:

$$V_p := 0 \cdot kip$$

$$F_{L\_reqd} := \left(\frac{V_u}{\phi_v} - 0.5 \cdot V_s - V_p\right) \cdot \cot(\theta \cdot deg) \qquad\qquad F_{L\_reqd} = 302.4 \cdot kip \qquad\qquad \text{Eq. 5.8.3.5-2}$$

However, a greater amount of stirrup reinforcement is typically provided than is required, which increases the actual V_s. Note that by Eq. 5.8.3.5-2, increasing V_s decreases the required tension tie force. Hence, it is helpful to use the computed value of V_s that results from the transverse reinforcement detailed in the design. In this case, the required tension tie force is:

Assume 2 legs of No. 4 bars at 12" on center (amount of steel at the critical section for shear):

$$A_{v\_actual} := 0.4 \cdot in^2$$

$$V_{s\_actual} := \frac{A_{v\_actual} \cdot f_y \cdot d_v \cdot \cot(\theta \cdot deg)}{12 \cdot in} \qquad\qquad V_{s\_actual} = 59.7 \cdot kip$$

Check the upper limit of V_s:

$$V_{s\_actual\_max} := \frac{V_u}{\phi_v} \qquad\qquad V_{s\_actual\_max} = 145.1 \cdot kip \qquad\qquad \text{LRFD 5.8.3.5}$$

Adopt the lesser of provided V_s and the upper limit of V_s:

$$V_{s\_actual} := if\left(V_{s\_actual} < V_{s\_actual\_max}, V_{s\_actual}, V_{s\_actual\_max}\right)$$

$$V_{s\_actual} = 59.7 \cdot kip$$

The revised value of the required tension tie force is:

$$F_{L\_reqd} := \left[\left(\frac{V_u}{\phi_v}\right) - 0.5 \cdot V_{s\_actual} - V_p\right] \cdot \cot(\theta) \qquad\qquad F_{L\_reqd} = -1.7 \times 10^4 \cdot kip$$

Provided Tension Tie Force:

The longitudinal reinforcement that contributes to the tension tie are strands that are on the flexural tension side of the precast section. Near the ends of the precast section, the strands are typically only partially effective. C5.8.3.5 of the 2006 Interim Revisions permits the strand stress in regions of partial development to be estimated using a bilinear variation, as shown in Fig. 4.
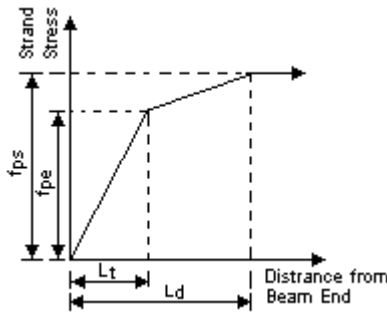
Figure 7: Variation in strand stress in relation to distance from beam end.

The stress in the strands at a given section depends on the location of the section with respect to the end of the precast section. If the section is between the end of the beam and L_t (see Fig. 5), a linear interpolation is performed using a stress variation of 0.0 at the end of the beam to f_{pe} at a distance of L_t from the end of the precast section. If the section is to the right of L_t but to the left of L_d, then the stress is interpolated between f_{pe} and f_{ps}. If the section is to the right of L_d, then the stress is assumed to be a constant value of f_{ps}.

At the face of bearing, the stress in the effective strands is:

$$x_{FB} := \frac{L_{ovr} - L_{des}}{2} + \frac{L_{pad}}{2} \qquad x_{FB} = 1.00\,\text{ft} \qquad \text{(Distance from physical end of beam to face of bearing)}$$

$$A_{str} := No\_Strands \cdot A_{strand} \qquad A_{str} = 5.642 \cdot in^2$$

$$F_{L\_prov} := if\left[x_{FB} < L_t, A_{str} \cdot f_{pe} \cdot \frac{x_{FB}}{L_t}, if\left[x_{FB} < K_{ld} \cdot L_d, A_{str} \cdot \left[f_{pe} + \left(\frac{x_{FB} - K_{ld} \cdot L_d + L_t}{K_{ld} \cdot L_d - L_t} \right) \cdot \left(f_{ps} - f_{pe} \right) \right], A_{str} \cdot f_{pe} \right] \right]$$

$$F_{L\_prov} = 309.8 \cdot kip$$

$$Status\_V_I := if\left(F_{L\_prov} \geq F_{L\_reqd}, \text{"OK"}, \text{"NG"} \right) \qquad \qquad Status\_V_I = \text{"OK"}$$

<u>Refined Estimate of Provided Tension Tie Force:</u>

If it is assumed that the point of intersection of the bearing crack (at angle theta) and c.g. of the strands is where the force in the strands is computed, then additional tensile capacity from the strands can be utilized.
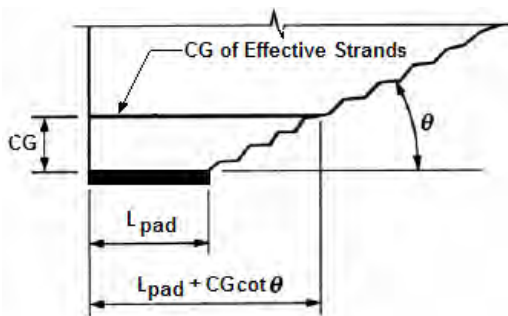
Figure 8: Elevation view of end of beam showing location where assumed failure crack crosses the c.g. of that portion of the strand pattern that is effective for resisting tensile forces caused by moment and shear.

Distance from end of beam to point of intersection of assumed crack and center of gravity of effective strands:

$$x_c := \left(\frac{L_{pad}}{2}\right) + ecc \cdot \cot(\theta \cdot deg)$$

$x_c = 1.2 \cdot ft$ (Measured from L face of bearing)

$$x_c := \left(\frac{L_{ovr} - L_{des}}{2}\right) + \left(\frac{L_{pad}}{2}\right) + ecc \cdot \cot(\theta \cdot deg)$$

$x_c = 1.7 \cdot ft$ (Measured from L end of beam)

$$F_{L\_prov} := if\left[x_c < L_t, A_{str} \cdot f_{pe} \cdot \frac{x_c}{L_t}, if\left[x_c < K_{ld} \cdot L_d, A_{str} \cdot \left[f_{pe} + \left(\frac{x_c - K_{ld} \cdot L_d + L_t}{K_{ld} \cdot L_d - L_t}\right) \cdot (f_{ps} - f_{pe})\right], A_{str} \cdot f_{pe}\right]\right]$$

$F_{L\_prov} = 515.9 \cdot kip$

$Status\_V_l := if\left(F_{L\_prov} \geq F_{L\_reqd}, "OK", "NG"\right)$

$Status\_V_l = "OK"$

2.13 Interface Shear Design

The ability to transfer shear across the interface between the top of the precast beam and the cast-in-place deck must be checked. This check falls under the interface shear or shear friction section of LRFD (5.8.4). Recall that under the *Standard Specs*, this check falls under the horizontal shear section.

Little guidance is offered by the LRFD Specs on how to compute the applied shear stress at the strength limit state. The procedure presented here uses the approach recommended by the *PCI Bridge Design Manual,* which is a strength limit state approach.

Applied Factored Shear: $V_u = 130.6 \cdot kip$

$$v_{uh\_s} := \frac{V_u}{d_v \cdot b_v}$$

$v_{uh\_s} = 0.088 \cdot ksi$

$d_v = 20.56 \cdot in$

$x_{FB} = 1.00 \, ft$ (Distance from physical end of beam to face of bearing)

$$v_{nh\_reqd} := \frac{v_{uh\_s}}{\phi_v}$$

$v_{nh\_reqd} = 0.098 \cdot ksi$

$A_{cv} := b_v \cdot 1.0 \cdot ft$ $A_{cv} = 864 \cdot in^2$

$V_{nhr} := v_{nh\_reqd} \cdot A_{cv}$ $V_{nhr} = 84.7 \cdot kip$

Nominal Shear Resistance of the Interface (Capacity):

$Status\_V_l := V_n = cA_{cv} + \mu\left(A_{vf} \cdot f_y + P_c\right)', "NG"\right)$ (LRFD 5.8.4.1-2)

Interface is CIP concrete slab on clean, roughened beam surface, no reinforcement crossing shear plane: (LRFD 5.8.4.3)

$c := 0.135 \cdot ksi$ (cohesion factor)

$\mu := 1.000$ (friction factor)

$K_1 := 0.2$ (fraction of concrete strength available to resist interface shear)

$K_2 := 0.8 \cdot ksi$ (limiting interface shear resistance)

Since there is no permanent net compressive stress normal to shear plane, $P_c = 0$. (LRFD 5.8.4.2)

Check Maximum Allowable Shear:

$V_{ni\_max1} := K_1 \cdot f'_{ct} \cdot A_{cv}$ $V_{ni\_max1} = 691 \cdot kip$ (LRFD 5.8.4.1-4)

$V_{ni\_max2} := K_2 \cdot A_{cv}$ $V_{ni\_max2} = 691 \cdot kip$ (LRFD 5.8.4.1-5)

$V_{nh\_max} := if\left(V_{ni\_max1} \le V_{ni\_max2}, V_{ni\_max1}, V_{ni\_max2}\right)$ (LRFD 5.8.4.1-2,3)

$V_{nh\_max} = 691 \cdot kip$

$V_{nh\_reqd} := v_{nh\_reqd} \cdot A_{cv}$ $V_{nh\_reqd} = 84.7 \cdot kip$

$Status\_V_{uh\_max} := if\left(V_{nh\_reqd} < V_{nh\_max}, "OK" , "NG"\right)$

Assuming no horizontal shear reinforcement crossing the shear plane, provided horizontal shear resistance is:

$V_{nh\_prov} := c \cdot A_{cv}$ $V_{nh\_prov} = 116.6 \cdot kip$

$Status\_V_{nh\_prov} := if\left(V_{nhr} < V_{nh\_prov}, "OK" , "NG"\right)$ $Status\_V_{nh\_prov} = "OK"$

2.14 Spalling Forces

If the maximum spalling stress on the end face of the girder is less than the direct tensile strength of the concrete, then spalling reinforcement is not required when the member depth is less than 22 in. The maximum spalling stress is estimated as:

$$\sigma_s = \frac{P}{A}\left(0.1206 \cdot \frac{e^2}{h \cdot d_b} - 0.0256\right) \ge 0$$

And the direct tensile strength is computed as:

$f_{r\_dts} := -0.23 \cdot \sqrt{f'_c} \cdot \sqrt{ksi}$ $f_{r\_dts} = -0.609 \cdot ksi$ (LRFD C5.4.2,7)

Check reinforcement requirement:

Ref: $A = 936 \cdot in^2$ $h = 18 \cdot in$ $ecc = 5.4969 \cdot in$ $d_b = 0.6 \cdot in$

$P_{jack} := A_{ps_4} \cdot f_{pj}$ $P_{jack} = 1142.5 \cdot kip$

$\sigma_s := \frac{-P_{jack}}{A}\left(0.1206 \cdot \frac{ecc^2}{h \cdot d_b} - 0.0256\right)$ $\sigma_s = -0.381 \cdot ksi$

Check whether spalling stress is below threshhold and thus is spalling/busting reinforcement is needed:

$Status\_Spalling := if\left(\sigma_s > f_{r\_dts}, "OK" , "NG"\right)$ $Status\_Spalling = "OK"$

2.15 Transverse Load Distribution

The transverse load distribution reinforcement is computed by:

$$A_{tld} = k_{mild} \cdot A_{l\_mild} + \alpha \cdot k_{ps} \cdot A_{l\_ps}$$

where:

$$\alpha = \frac{d_{cgs}}{d_{trans}}$$

$$k_{ps} = \frac{100}{\sqrt{L}} \cdot \frac{f_{pe}}{60} \leq 50\%$$

$$k_{mild} = \frac{100}{\sqrt{L}} \leq 50\%$$

$$d_{cgs} := h_c - y_{cg} \qquad d_{cgs} = 21.1 \cdot in$$

Compute d_{trans}:

$$d_{trans} := h_c - 4in - \frac{d_b}{2} - \frac{0.75 \cdot in}{2} \qquad d_{trans} = 19.3 \cdot in$$

$$\alpha := \frac{d_{cgs}}{d_{trans}} \qquad \alpha = 1.0907$$

Assume there is no mild longitudinal reinfocement A_{l_mild} in tension at the strength limit state.

$$A_{l\_mild} := 0.0 \cdot in^2$$

$$k_{mild} := \frac{\dfrac{100 \cdot \sqrt{ft}}{\sqrt{L_{des}}}}{100} \qquad k_{mild} = 14.43 \cdot \%$$

$$k_{ps} := \frac{\dfrac{100 \cdot \sqrt{ft}}{\sqrt{L_{des}}} \cdot \dfrac{f_{pe}}{60 \cdot ksi}}{100} \qquad k_{ps} = 39.63 \cdot \%$$

$$A_{l\_ps} := A_{ps_2} \qquad A_{l\_ps} = 3.6466 \cdot in^2$$

Total amount of transverse load distribution is:

$$A_{tld} := k_{mild} \cdot A_{l\_mild} + \alpha \cdot k_{ps} \cdot A_{l\_ps} \qquad A_{tld} = 1.58 \cdot in^2$$

Since the longitudinal reinforcement is per beam width, the area of distribution reinforcement per foot is:

$$A_{tld\_per\_ft} := \frac{A_{tld}}{S} \qquad A_{tld\_per\_ft} = 0.26 \cdot \frac{in^2}{ft}$$

Assuming transverse bars are #6, maximum spacing is:

Set transverse load distribution reinforcement spacing at 12 in.:

$$S_{ld\_spac\_max} := \frac{0.44 \cdot in^2}{A_{tld\_per\_ft} \cdot ft} \cdot ft \qquad S_{ld\_spac\_max} = 20.1 \cdot in$$

$$S_{ld\_spac} := 12in$$

2.16 Reflective Crack Control Reinforcement

Reflective crack control reinforcement is provided from both the transverse load distribution reinforcment as well as drop in cage consisting of vertical stirrups. The total amount of reflective crack control reinforcement required is given as follows:

$$\rho_{cr\_req} := \frac{6\sqrt{f'_{ct}} \cdot \sqrt{psi}}{f_y} \qquad \rho_{cr\_req} = 0.00632 \qquad\qquad \text{(LRFD 5.14.4.3.3f-1)}$$

The crack control reinforcement ratio is defined, per unit length of span, as follows:

$$\rho_{cr} = \frac{A_{scr}}{(h - t_{flg}) \cdot 1ft} \qquad\qquad \text{(LRFD 5.14.4.3.3f-2)}$$

The required area of reinforcement of reflective crack control is therefore calculated, per unit length of span, as:

$$A_{scr\_req} := \rho_{cr\_req} \cdot (h - t_{flg}) \cdot 1ft \qquad A_{scr\_req} = 1.1384 \cdot in^2$$

The required area of cage reinforcement is subsequently calculated, per unit length of span, as the difference between the total required area of crack control reinforcement and that provided by the reinforcement for transverse load distribution; both transverse bars are effective in providing crack control, however only the lower horizontal legs of the stirrups are considered in the calculation. All calculations are per unit length of span:

$$A_{ld} := \frac{2 S_{ld\_spac} \cdot .44in^2}{1ft} \qquad\qquad A_{ld} = 0.88 \cdot in^2$$

$$A_{cr\_cage\_req} := A_{scr\_req} - A_{ld} \qquad\qquad A_{cr\_cage\_req} = 0.2584 \cdot in^2$$

Provide No. 5 stirrups at 12 in. on center:

$$S_{cage\_spac} := 12in \qquad\qquad A_{scage} := 0.31in^2$$

$$A_{cr\_cage\_prov} := A_{scage} \cdot \left(\frac{1ft}{S_{cage\_spac}}\right) \qquad\qquad A_{cr\_cage\_prov} = 0.31 \cdot in^2$$

$$A_{scr\_prov} := A_{ld} + A_{cr\_cage\_prov}$$

$$\text{Status\_A}_{scrack} := if(A_{scr\_req} < A_{scr\_prov}, \text{"OK"}, \text{"NG"}) \qquad\qquad \text{Status\_A}_{scrack} = \text{"OK"}$$
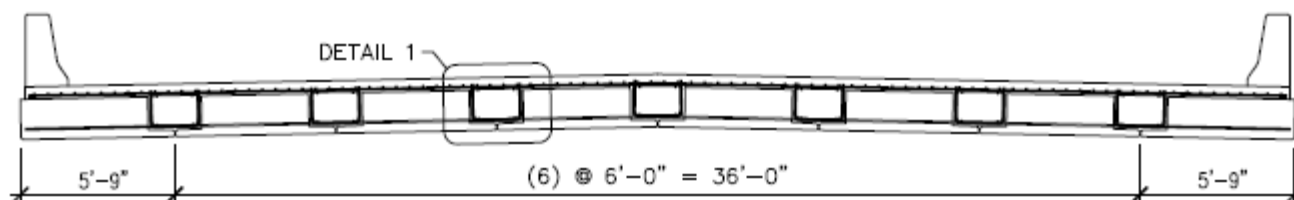
Figure 9: Cross section of bridge showing CIP regions.
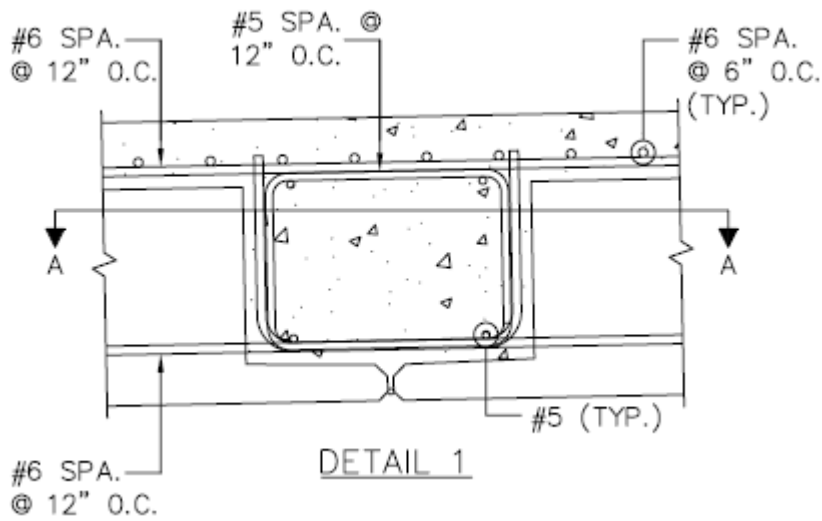
Figure 10: Detail of drop-in cage.
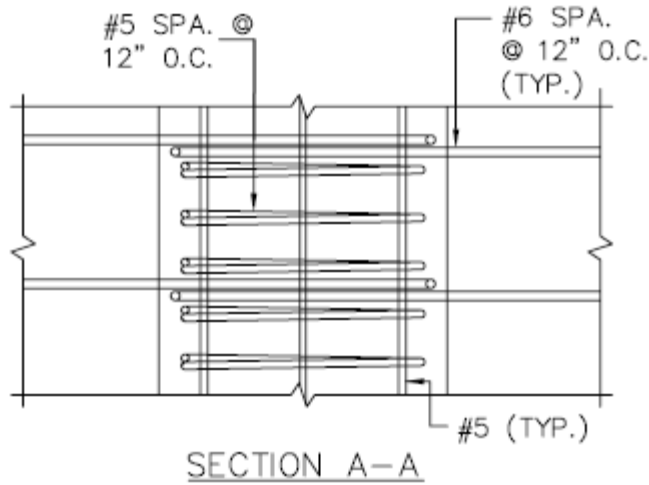
Figure 11: Plan view of drop-in cage.

2.17 Bottom Flange Reinforcement

Determine steel required to resist construction loads on bottom flange:

Assume a 1' wide strip:

Loads:

Self-weight of flange:

$$w_{flng\_sw} := t_{flg} \cdot 12 \cdot in \cdot w_{ct} \qquad w_{flng\_sw} = 0.0375 \cdot klf$$

CIP weight:

$$w_{flng\_cip} := \left(h - t_{flg}\right) \cdot 12 \cdot in \cdot w_{ct} \qquad w_{flng\_cip} = 0.1875 \cdot klf$$

Construction live load (assume 10 psf): $\quad w_{const} := 10psf$

$$w_{flng\_LL} := w_{const} \cdot 12 \cdot in \qquad w_{flng\_LL} = 0.0100 \cdot klf$$

Moments:

B2-41

$$b_{cant} := \frac{b_h}{2} \qquad\qquad b_{cant} = 1.00\,\text{ft} \qquad\qquad \text{(Length of cantilever)}$$

$$M_{flng\_sw} := \frac{w_{flng\_sw} \cdot b_{cant}^2}{2} \qquad M_{flng\_sw} = 0.0187 \cdot \text{kip} \cdot \text{ft}$$

$$M_{flng\_cip} := \frac{w_{flng\_cip} \cdot b_{cant}^2}{2} \qquad M_{flng\_cip} = 0.0937 \cdot \text{kip} \cdot \text{ft}$$

$$M_{flng\_LL} := \frac{w_{flng\_LL} \cdot b_{cant}^2}{2} \qquad M_{flng\_LL} = 0.005 \cdot \text{kip} \cdot \text{ft}$$

Strength Limit State I:

$$M_{u\_flng} := 1.25 \cdot \left(M_{flng\_sw} + M_{flng\_cip}\right) + 1.75 \cdot M_{flng\_LL} \qquad M_{u\_flng} = 0.15 \cdot \text{kip} \cdot \text{ft}$$

Try #3 bars at 12" o.c:

$$A_{s\_flng} := 0.11 \cdot \text{in}^2 \qquad\qquad A_{s\_flng} = 0.11 \cdot \text{in}^2$$

$$c_{flng} := \frac{A_{s\_flng} \cdot f_y}{0.85 \cdot f'_c \cdot \beta_1 \cdot 12 \cdot \text{in}} \qquad c_{flng} = 0.11 \cdot \text{in}$$

$$\beta_{1p} := \text{if}\left[f'_c \le 4 \cdot (\text{ksi}), 0.85, \text{if}\left[f'_c \ge 8 \cdot (\text{ksi}), 0.65, 0.85 - \left[\frac{f'_c - 4 \cdot (\text{ksi})}{1 \cdot (\text{ksi})} \cdot 0.05 \right] \right] \right] \qquad \beta_{1p} = 0.70$$

$$a_{flng} := \beta_{1p} \cdot c_{flng} \qquad\qquad a_{flng} = 0.0761 \cdot \text{in}$$

$$d_s := t_{flg} - 1 \cdot \text{in} - 0.5 \cdot \text{in} - \frac{0.5 \cdot \text{in}}{2} \qquad d_s = 1.25 \cdot \text{in}$$

$$M_{n\_flng} := A_{s\_flng} \cdot f_y \cdot \left(d_s - \frac{a_{flng}}{2} \right) \qquad M_{n\_flng} = 0.67 \cdot \text{kip} \cdot \text{ft}$$

$$\phi_{f\_flng} := 0.65 + 0.15 \cdot \left(\frac{d_s}{c_{flng}} - 1 \right) \qquad \phi_{f\_flng} = 2.22$$

$$\phi_{f\_flng} := \text{if}\left(\phi_{f\_flng} \le 0.75, 0.75, \text{if}\left(\phi_{f\_flng} > 0.9, 0.9, \phi_{f\_flng} \right) \right) \qquad \phi_{f\_flng} = 0.9$$

$$M_{r\_flng} := \phi_{f\_flng} \cdot M_{n\_flng} \qquad M_{r\_flng} = 0.60 \cdot \text{kip} \cdot \text{ft}$$

$$\text{Status\_StrengthLS}_{flng} := \text{if}\left(M_{u\_flng} \le M_{r\_flng}, \text{"OK"}, \text{"NG"} \right) \qquad\qquad \text{Status\_StrengthLS}_{flng} = \text{"OK"}$$

Use: Minimum #3 bars @ 12" o.c. in bottom flange.

2.18 Reinforcement for Positive Restraint Moment at Pier

Load factors for each load component are derived from AASHTO (2009) Table 3.4.1-2. Because dead loads induce negative moments at the piers, they were underestimated by 10 percent (i.e.: $\gamma_p = 0.9$). The moments due to creep, shrinkage, and prestress force were designed with a load factor (γ_{RM}) of 1.0, as given by AASHTO (2009) Table 3.4.1-3.

$$\gamma_p := 0.9 \qquad \gamma_{RM} := 1.0$$

From Section 2.5:

The design restraint moment due to the time depenent effects of prestress, creep, and shrinkage have been included. Postive restraint moments due to the design thermal gradient have been calculated (Section 2.5) based on AASHTO (2009) Temperature Zone 1, though will not be specifically designed for in this example because of the difference in the relative magnitude of the restraint moment due to thermal gradients and the remaining time dependent effects.

$$M_{rm} = 34 \cdot kip \cdot ft \qquad\qquad M_{gr} = 265 \cdot ft \cdot kip$$

$$M_{uprm} := \gamma_p \cdot M_{barrier\_c_1} + \gamma_p \cdot M_{fws\_c_1} + M_{rm} \qquad\qquad M_{uprm} = -8 \cdot ft \cdot kip$$

All reinforcement provided to resistive positive restraint moments is located in the 24 in. wide trough region between precast panels. The reinforcement is located immediately above the precast flange. Assume No. 4 bars are used for positive continuity reinforcement, and (4) bars are used in each 24 in. trough region:

$$d_{No4} := 0.5in \qquad\qquad A_s := 0.2in^2 \qquad\qquad A_{sRM\_prov} := 4 \cdot A_s \quad A_{sRM\_prov} = 0.8 \cdot in^2$$

$$d_{s\_RM} := h + 6in - 3.25in - 1in - \frac{d_{No4}}{2} \qquad\qquad d_{s\_RM} = 19.5 \cdot in$$

The reinforcement required is calculated at the ultimate limit state (i.e.: assuming Whitney's stress block)

$$a := \frac{A_{sRM\_prov} \cdot f_y}{0.8 \cdot f'_{ct} \cdot 72in} \qquad\qquad a = 0.21 \cdot in$$

$$A_{sRM\_req} := \frac{M_{uprm}}{f_y \cdot \left(d_{s\_RM} - \frac{a}{2}\right)} \qquad\qquad A_{sRM\_req} = -0.08 \cdot in^2$$

$$Status\_A_{sRM} := if\left(A_{sRM\_req} < A_{sRM\_prov}, "OK", "NG"\right) \qquad\qquad \boxed{Status\_A_{sRM} = "OK"}$$

B2-43
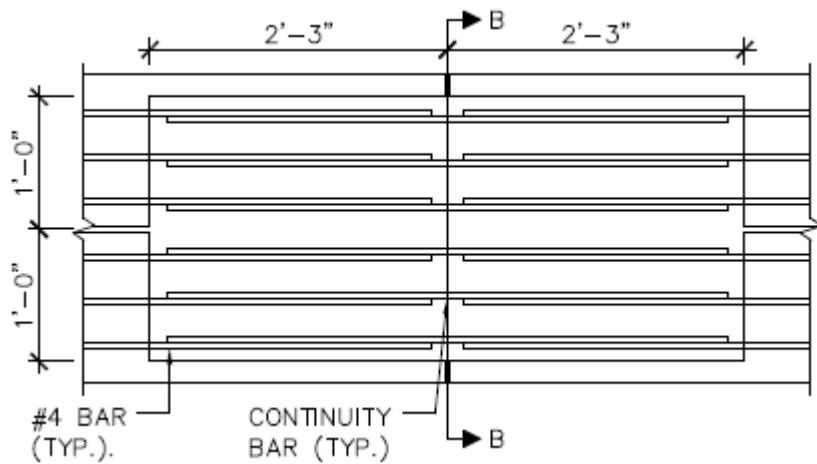
Figure 12: Detail of the positive restraint moment reinforcement
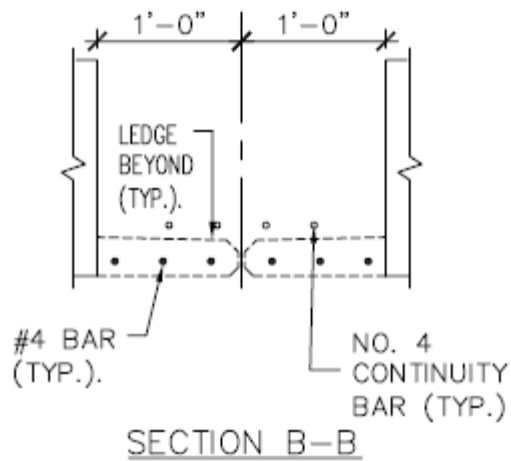
Figure 13: Cross section of the positive restraint moment reinforcement

References

Peterman, R. and Ramirez, J., "Restraint Moments in Bridges with Full-Span Prestressed Concrete Form Panels", *PCI Journal*, V. 43, No. 2, Jan.-Feb. 1998, pp. 54-73.

Example Problem 3

3.1 Introduction

The design of the longitudinal joint between decked bulb tee members is illustrated in this example.

3.2 Materials, Geometry, Loads and Load Factors

Units:

$kcf := kip \cdot ft^{-3}$ Defined unit: kips per cubic foot

$ksf := kip \cdot ft^{-2}$ Defined unt: kips per square foot

Materials:

$f'_c := 7.0 \cdot ksi$ Strength of beam concrete at 28 days

$f'_{ci} := 6.0 \cdot ksi$ Strength of beam concrete at transfer of prestressing force

$w_c := 0.150 \cdot kcf$ Density of beam concrete

$E_s := 29000 \cdot ksi$ Modulus of elasticity of non-prestressed reinforcement

$f_y := 60.0 \cdot ksi$ Yield stress of stainless steel rebar

Geometry:

$L_{ovr} := 141.0 \cdot ft$ Overal length of girder

$L_{des} := 140.0 \cdot ft$ Design span of girder

$S := 7.00 \cdot ft$ Girder spacing

$N_g := 4$ Number of girders in bridge cross section

$Width_{overall} := 28.00 \cdot ft$ Overall width of bridge

$Width_{ctc} := 25.5 \cdot ft$ Curb to curb width of bridge

$N_l := 2$ Number of lanes

$t_{flng} := 6.25 \cdot in$ Thickness of girder flange

$Width_{barrier} := 1.25 \cdot ft$ Assumed width of a typical barrier

Loads:

$N_{barriers} := 2$ Number of barriers (assumed typical weight)

$w_{barrier} := 0.300 \cdot klf$ Weight of single barrier

$w_{fws} := 0.025 \cdot ksf$ Weight of future wearing surface allowance

HL-93   Notional live load per LRFD Specs

$w_{lane} := 0.64 \cdot klf$ Design lane load

Factors:

ϕ_f Resistance factor for flexure

$\phi_v := 0.90$ Resistance factor for shear

$DLA := 0.33$ Dynamic load allowance (LRFD 3.6.2.1-1)

3.3 Plan, Elevation, and Typical Section
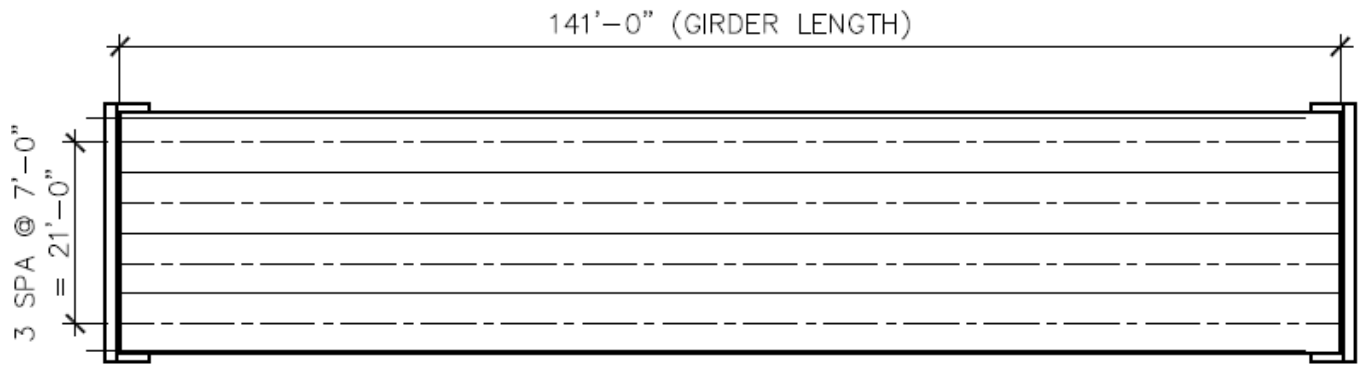
Fig. 1: Framing plan of bridge.
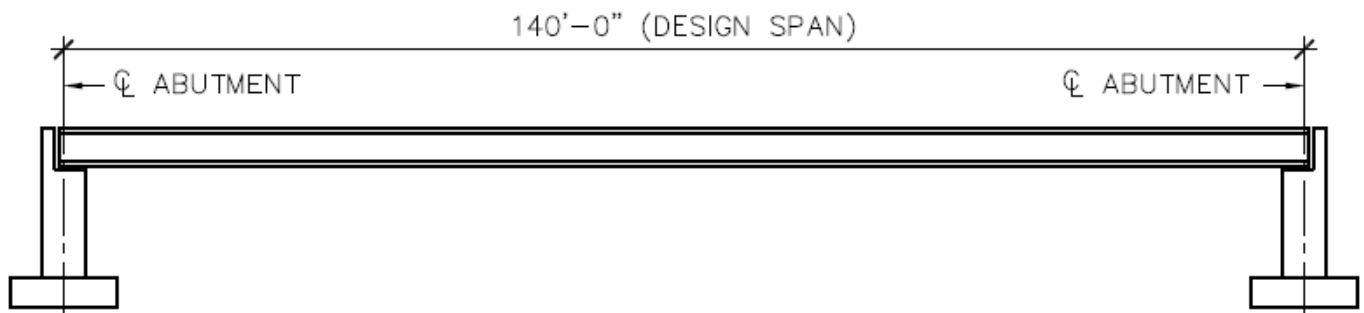
Fig. 2: Elevation view of girder layout.

Fig. 3: Typical section.

B3-2
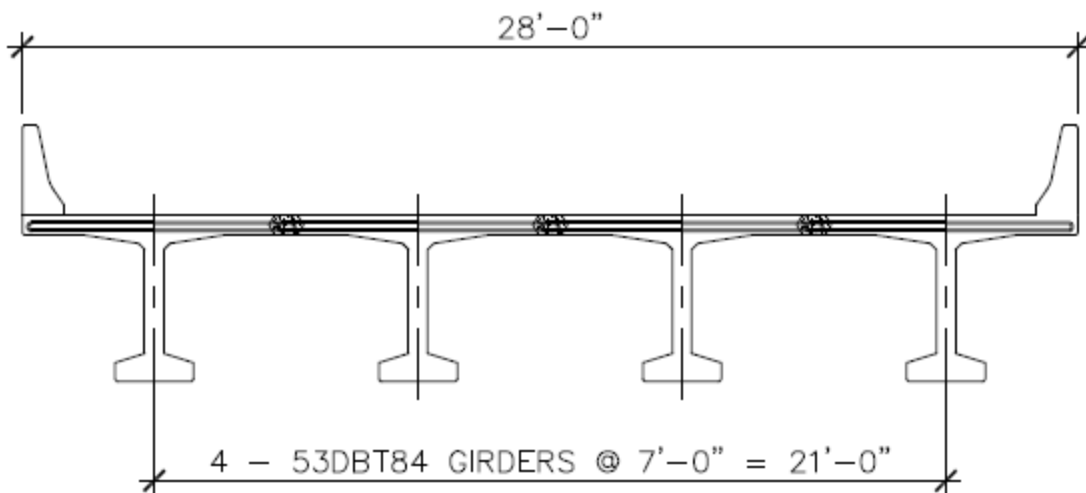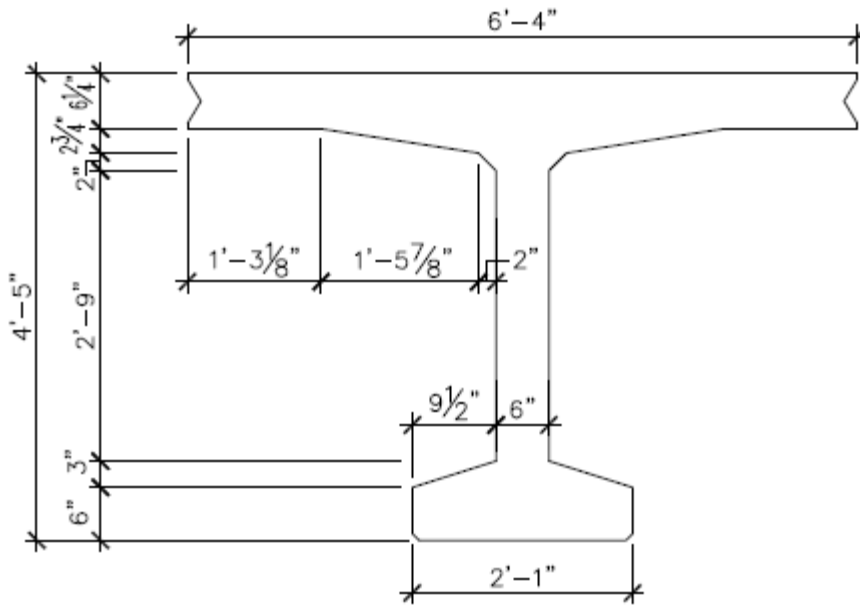
Fig. 4: Girder dimensions.

3.4 Strip Widths
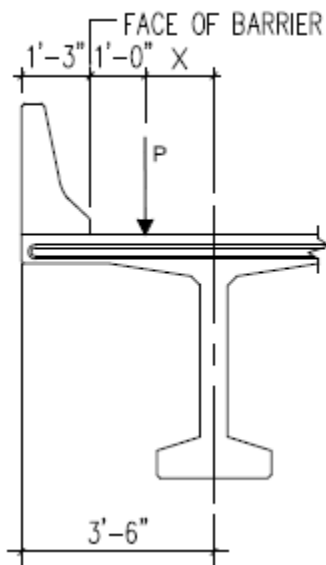
Fig. 5: Geometry of exterior girder and wheel load.

Overhang:

(LRFD 4.6.2.1)

$$X_{overhang} := \frac{\left[Width_{overall} - (N_g - 1)\cdot S\right]}{2} - Width_{barrier} - 1.00\cdot ft = 1.25\,ft$$

$$E_{overhang} := 45.0\cdot in + 10.0\cdot \frac{X_{overhang}}{12} \qquad E_{overhang} = 57.5\cdot in$$

B3-3

+Moment:

$\quad X_{pM} := 7.0 \cdot ft$

$\quad E_{pM} := 26.0 \cdot in + 6.6 \cdot \dfrac{X_{pM}}{12} \qquad E_{pM} = 72.2 \cdot in$

-Moment:

$\quad X_{nM} := 7.0 \cdot ft$

$\quad E_{nM} := 48.0 \cdot in + 3.0 \cdot \dfrac{X_{nM}}{12} \qquad E_{nM} = 69.0 \cdot in$

3.4 Analysis

Dead Load:

Self-weight:

Assume dead load acts on simple span, Use 1-ft strip:

$\quad w_{sw} := t_{flng} \cdot 12 \cdot in \cdot w_c \qquad w_{sw} = 0.0781 \cdot klf$

$\quad M_{sw} := \dfrac{w_{sw} \cdot (7 \cdot ft)^2}{8} \qquad M_{sw} = 0.4785 \cdot kip \cdot ft$

Barriers:

Use continuous beam model with barriers modeled as point loads at each cantilever.

$\quad M_{barrier} := 1.0 \cdot kip \cdot ft$

Future wearing surface:

Use continuous beam model with FWS modeled as uniform load:

$\quad M_{FWS} := 0.020 \cdot kip \cdot ft$

Live Load:

Use mulit-span continous model to assess live load moments:
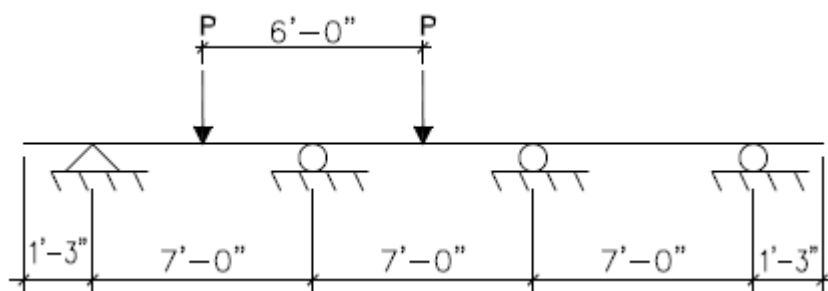
Fig. 6: Conitnuous beam model of live load analysis of panel strip.

Maximum live load moment:

$\quad M_{pLL} := 21.2 \cdot kip \cdot ft$

$\quad M_{LL\_perfoot} := \dfrac{M_{pLL}}{\dfrac{E_{pM}}{ft}} \qquad M_{LL\_perfoot} = 3.52 \cdot kip \cdot ft$

B3-4

3.5 Load Combintations

Use Strength Limit State I:

$$M_u := 1.25 \cdot \left(M_{sw} + M_{barrier} \right) + 1.5 \cdot M_{FWS} + 1.75 \cdot M_{LL\_perfoot} \qquad M_u = 8.04 \cdot kip \cdot ft$$

3.6 Flexural Analysis

Lap Length Sufficient to Develop 180° Hook
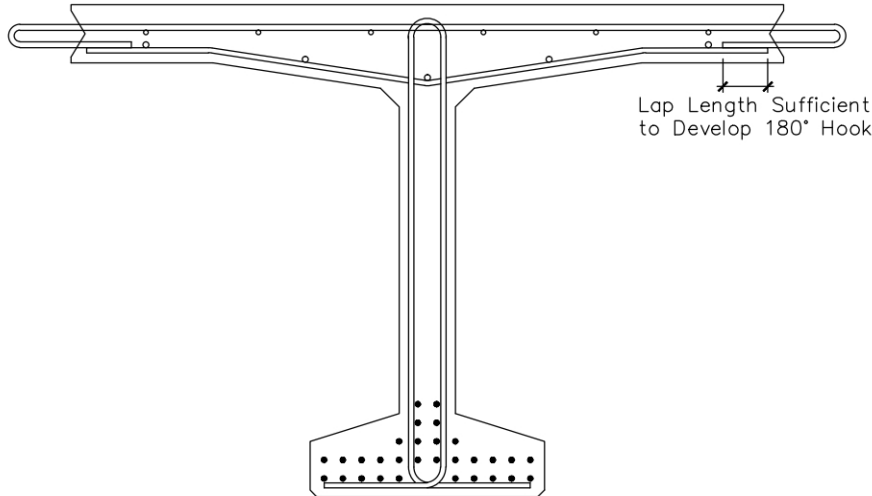
Fig. 7: Girder reinforcement layout.

11"

8"

6"

#4 @ 1'-0" O.C. (TYP.)

#5 UBAR @ 4½" O.C.

#4 LACER BAR (TYP.)

#5 @ 6" O.C. (TYP.)
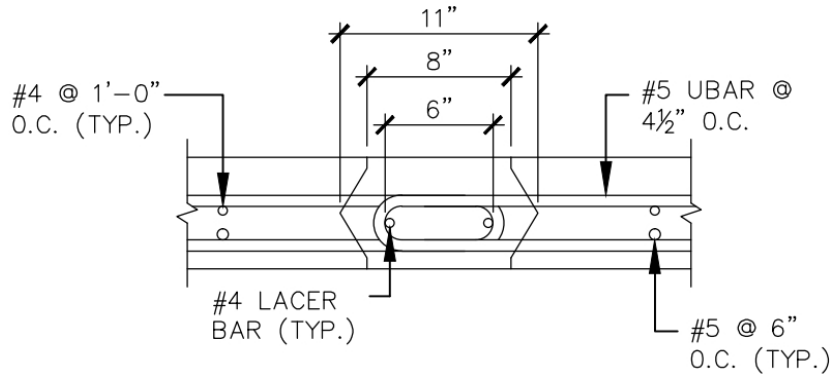
Fig. 8: Joint reinforcement and geometry. Closure pour material should be based on recommended performance criteria from NCHRP 10-71 design recommendations.

$D \geq 3d_b$
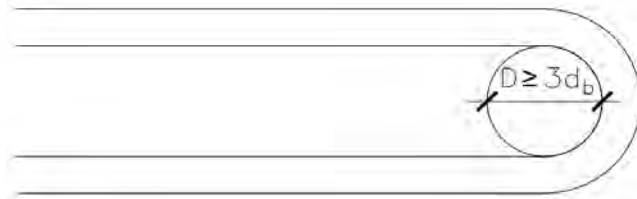
Fig. 9: Bend diameter of U bars. Note: This is a different than the $6d_b$ requirement in AASHTO, but acceptable because of the additional ductility of stainless steel.

B3-5

$$M_n := \phi \cdot A_s \cdot f_y \cdot \left(d_s - \frac{a}{2} \right)^{\blacksquare}$$

$$\phi := 0.90$$

Check #5 bars at 9" o.c.

$$Area_{bar} := 0.31 \cdot in^2 \qquad Spacing_{bar} := 9 \cdot in$$

$$A_s := Area_{bar} \cdot \frac{12 \cdot in}{Spacing_{bar}} \qquad A_s = 0.41 \cdot in^2$$

$$a := \frac{A_s \cdot f_y}{0.85 \cdot f'_c \cdot 12 \cdot in} \qquad a = 0.35 \cdot in$$

$$d_s := t_{flng} - 1 \cdot in - \frac{0.625 \cdot in}{2} \qquad d_s = 4.9375 \cdot in$$

$$M_n := \phi \cdot A_s \cdot f_y \cdot \left(d_s - \frac{a}{2} \right) \qquad M_n = 8.9 \cdot kip \cdot ft$$

Distribution reinforcement:

$$A_{s\_dist\_pct} := \frac{100}{\sqrt{\dfrac{S}{ft}}} \qquad (< 50\%) \hspace{4cm} \text{(LRFD 5.14.4.1-1)}$$

$$A_{s\_dist\_pct} = 37.8 \text{ (percent of primary reinforcement)}$$

$$A_{s\_dist} := \frac{A_{s\_dist\_pct}}{100} \cdot A_s \qquad A_{s\_dist} = 0.16 \cdot in^2$$

B3-6

Example Problem 4

4.1 Introduction

The design of the transverse joint over the piers of a girder bridge that incorporates full-depth deck panels is presented.

4.2 Materials, Geometry, Loads and Load Factors

Units: $kcf := kip \cdot ft^{-3}$

Materials:

Concrete:	$f'_c := 7.0 \cdot ksi$	Strength of beam concrete at 28 days
	$w_c := 0.150 \cdot kcf$	Density of beam concrete
	$f_y := 60 \cdot ksi$	Yield stress of stainless steel rebar

Geometry:

Beam:	$h := 72.0 \cdot in$	Height of girder
	$b_f := 26.0 \cdot in$	Width of bottom flange of precast section
	$t_f := 10.50 \cdot in$	Thickness of bottom flange of girder
	$S_{beam} := 12.00 \cdot ft$	Beam spacing
Deck:	$t_{slab} := 6.00 \cdot in$	Thickness of precast deck panel

4.3 Plan, Elevation, and Typical Section

Fig. 1: Plan view of bridge.

Fig. 2: Elevation view of bridge.

B4-1
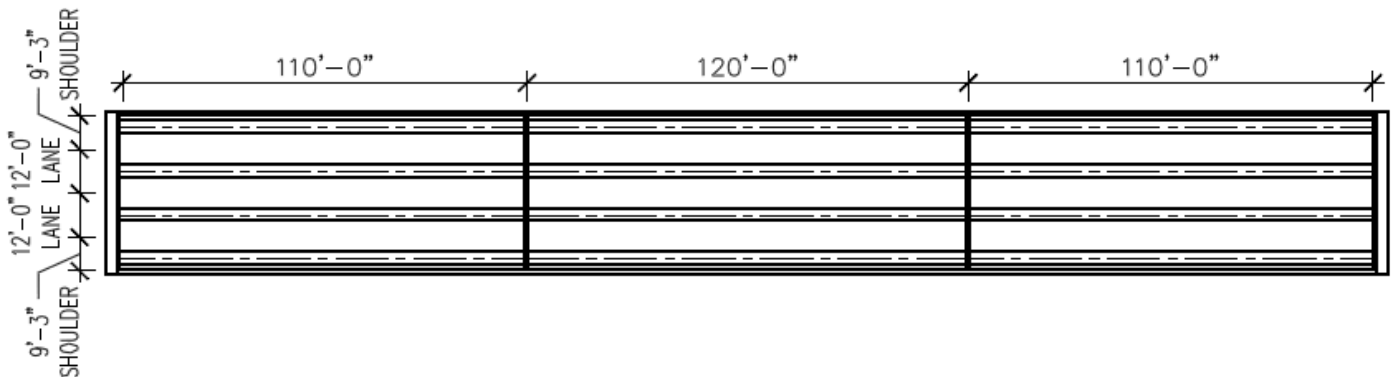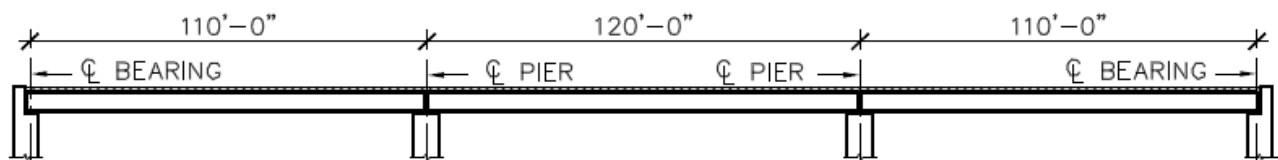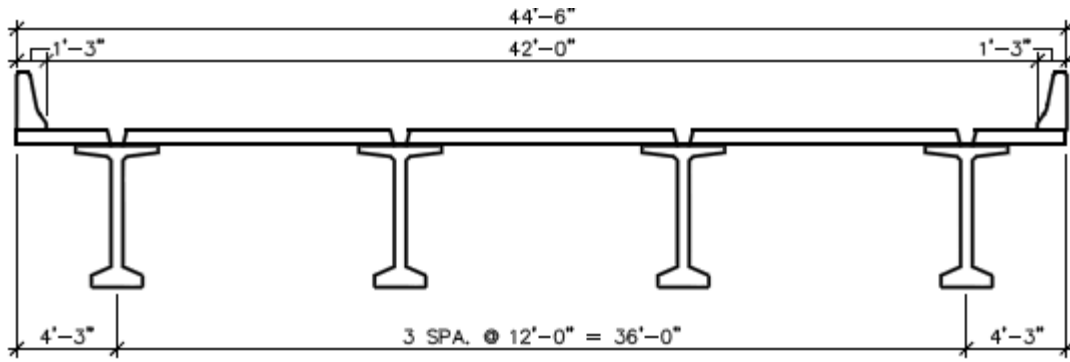
Fig. 3: Typical section of bridge.

Fig. 4: Girder dimensions.

B4-2
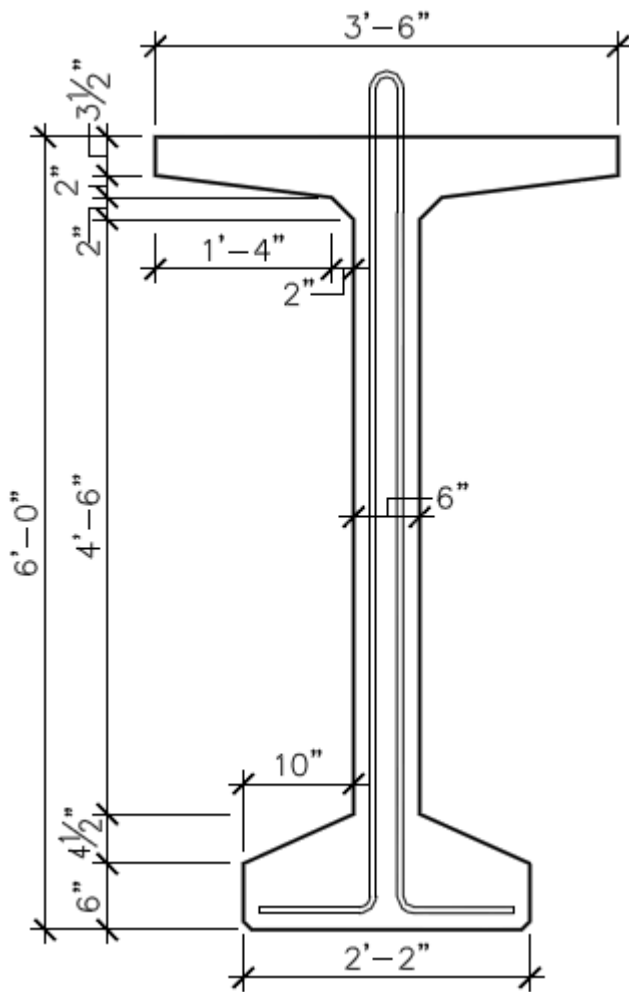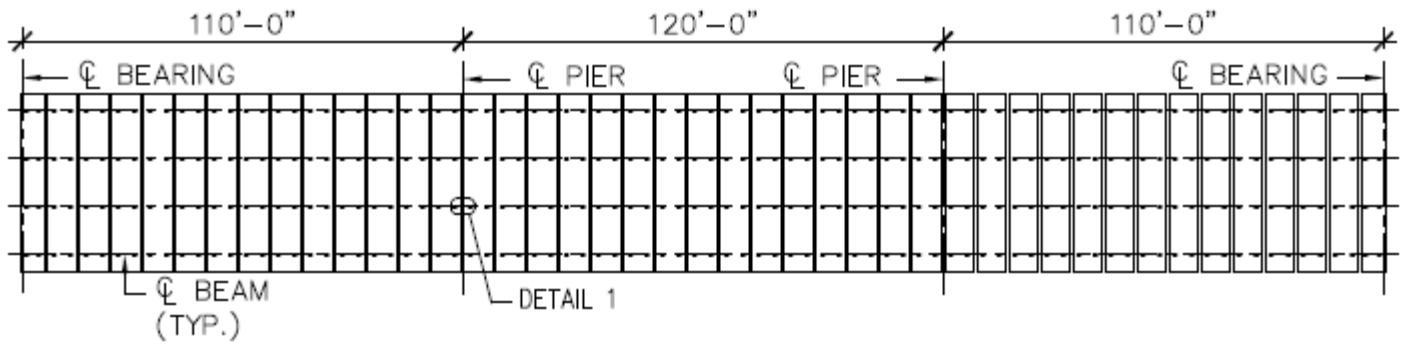
Fig. 5: Panel layout.
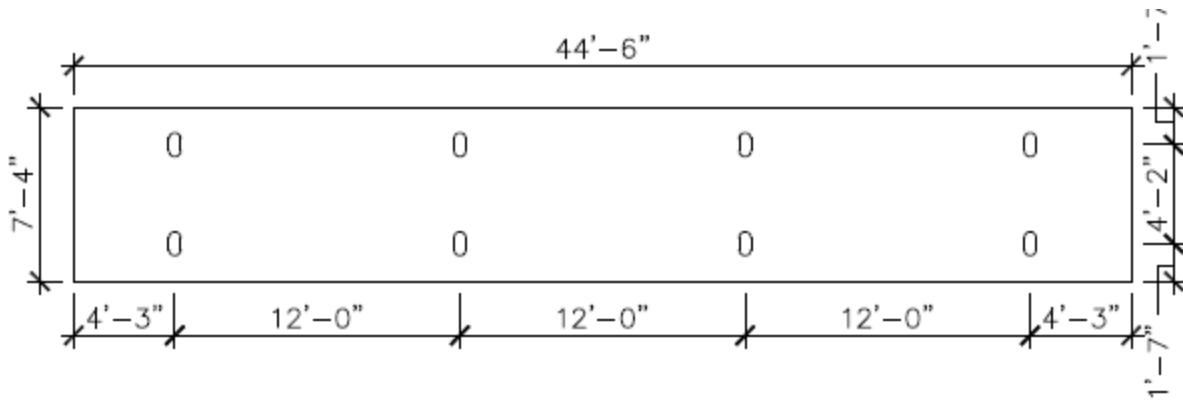
Fig. 6: Panel dimensions.

Fig. 7: Transverse panel section.
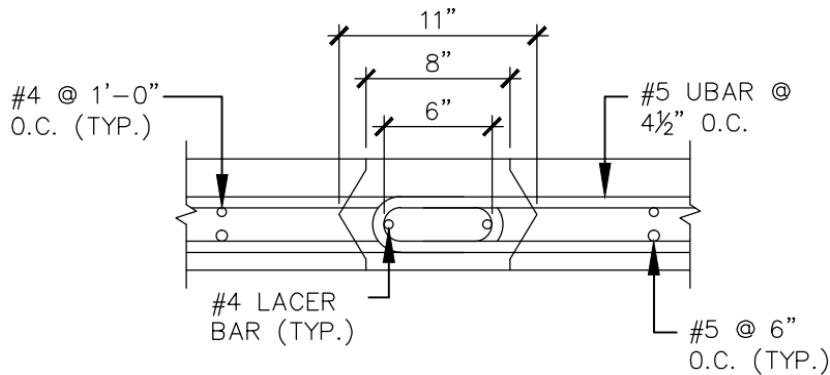
Fig. 8: Detail of panel-to-panel connection.

B4-3
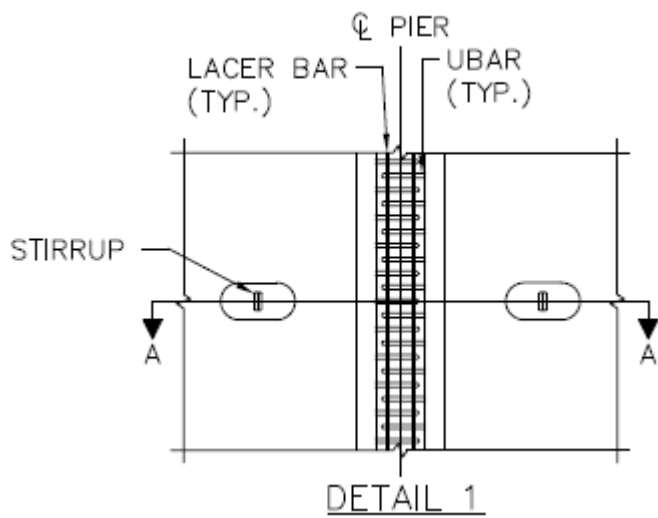
Fig. 9: Detail panel-to-panel connection over piers (see Fig. 5).
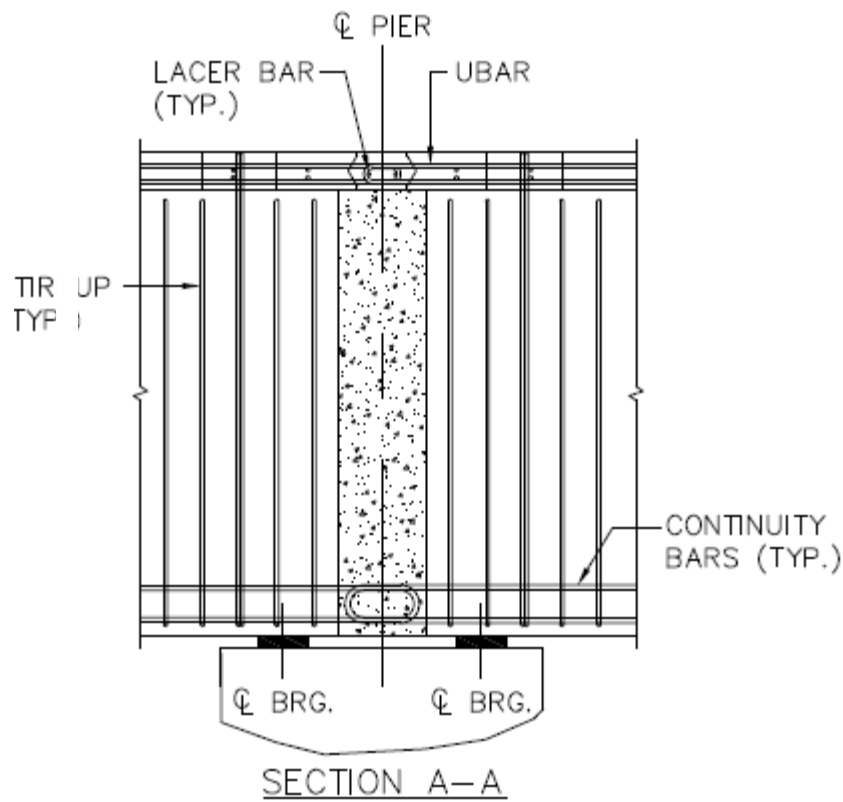
Fig. 10: Section through girders at pier.

4.3 Analysis

Only loads that act on the composite section cause negative moment over the piers.

Barrier Weight:

$$M_{barrier} := -213.1 \cdot kip \cdot ft$$

Future Wearing Surface:

$$M_{FWS} := -248.6 \cdot kip \cdot ft$$

Live Load:

$$M_{Design\_Truck} := -1265 \cdot kip \cdot ft$$

$$M_{Design\_Lane} := -843 \cdot kip \cdot ft$$

Fraction of live load moment for one design lane distributed to girder:

$$DF_m := 0.7404$$

Dynamic load allowance (applied to truck only):

$$DLA := 0.33$$

Effective Negative Live Load Moment:

$$M_{LL} := DF_m \cdot \left[M_{Design\_Lane} + (1 + DLA) \cdot M_{Design\_Truck} \right] \qquad M_{LL} = -1869.8 \cdot kip \cdot ft$$

4.4 Load Combinations

Use Strength Limit State I

$$M_u := 1.25 \cdot \left(M_{barrier} + M_{FWS} \right) + 1.75 \cdot \left(M_{LL} \right) \qquad M_u = -3849.4 \cdot kip \cdot ft$$

$$M_{u\_per\_ft} := \frac{M_u}{\frac{S_{beam}}{ft}} \qquad M_{u\_per\_ft} = -320.8 \cdot kip \cdot ft \quad \text{(per foot)}$$

4.5 Reinforcement

$$M_n := \phi \cdot A_s \cdot f_y \cdot \left(d_s - \frac{a}{2} \right)^{\blacksquare}$$

Try #5 bars at 6" o.c (2 legs of u-bar):

$$Area_{bar} := 2 \cdot 0.31 \cdot in^2 \qquad Spacing_{bar} := 6 \cdot in$$

$$A_s := Area_{bar} \cdot \frac{12 \cdot in}{Spacing_{bar}} \qquad A_s = 1.24 \cdot in^2$$

$$c := \frac{A_s \cdot f_y}{0.85 \cdot f'_c \cdot 12 \cdot in} \qquad c = 1.04 \cdot in \quad \text{(< 10.5 in OK)}$$

$$\beta_1 := \text{if}\left[f'_c \le 4 \cdot (ksi), 0.85, \text{if}\left[f'_c \ge 8 \cdot (ksi), 0.65, 0.85 - \left[\frac{f'_c - 4 \cdot (ksi)}{1 \cdot (ksi)} \cdot 0.05 \right] \right] \right] \qquad \beta_1 = 0.7$$

$$a := \beta_1 \cdot c \qquad a = 0.729 \cdot in$$

B4-5

Center of gravity of deck reinforcement lies at mid-height of deck.

$$d_s := h + \frac{t_{slab}}{2}$$

$$d_s = 75 \cdot in$$

$$\phi_f := 0.65 + 0.15 \cdot \left(\frac{d_s}{c} - 1 \right)$$

$$\phi_f := if\left(\phi_f \le 0.75, 0.75, if\left(\phi_f > 0.9, 0.9, \phi_f \right) \right)$$

$$\phi_f = 0.9$$

$$M_n := -\phi_f \cdot A_s \cdot f_y \cdot \left(d_s - \frac{a}{2} \right) \qquad M_n = -416.5 \cdot kip \cdot ft \quad \textbf{OK}$$

B4-6

Example Problem 5

5.1 Introduction

The required width of a bridge can exceed the practical length of a full-depth deck panel. To accommodate this, a longitudinal joint must be introduced into the cross section of the bridge. The joint can occur between girders or, preferably, over the centerline of a girder. This example provides typical details for making such connections. Previously presented methods for designing the joints apply.

5.2 Materials, Geometry, and Loads

Units: $kcf := kip \cdot ft^{-3}$

Materials:

Concrete:	$f'_c := 7.0 \cdot ksi$	Strength of beam concrete at 28 days
	$w_c := 0.150 \cdot kcf$	Density of beam concrete
	$f_y := 60.0 \cdot ksi$	Yield stress of stainless steel rebar

Geometry:

Beam:	$h := 72.0 \cdot in$	Height of girder
	$b_f := 26.0 \cdot in$	Width of bottom flange of precast section
	$t_f := 10.50 \cdot in$	Thickness of bottom flange of girder
	$S_{beam} := 10.30 \cdot ft$	Beam spacing
Deck:	$t_{slab} := 6.00 \cdot in$	Thickness of precast deck panel

5.3 Plan, Elevation, and Typical Section

Fig. 1: Plan view of bridge.

Fig. 2: Elevation view of bridge.

B5-1
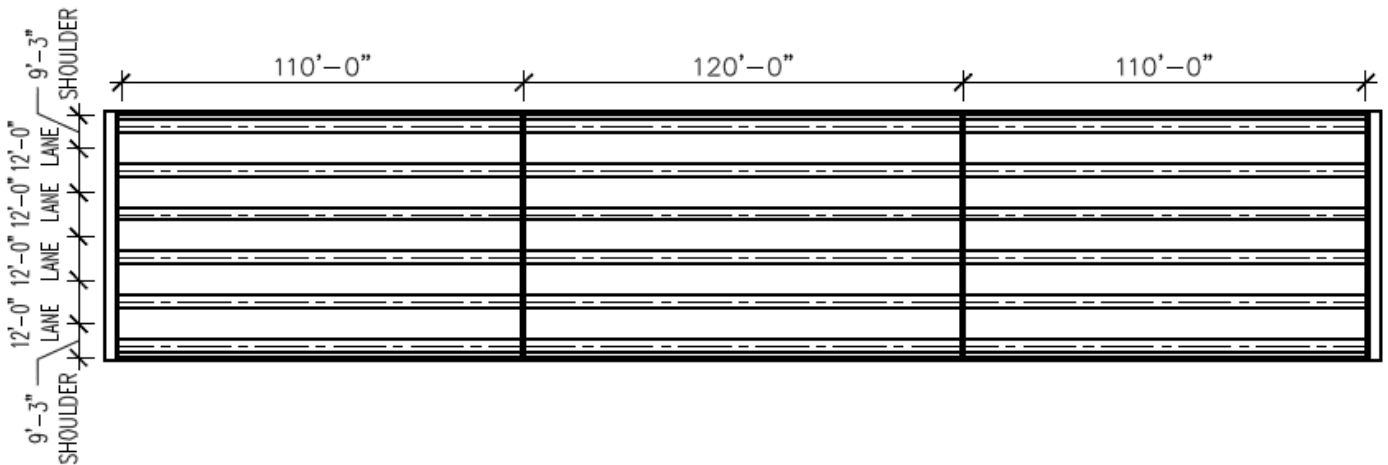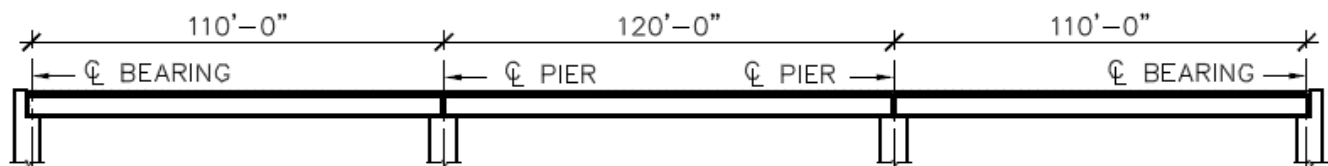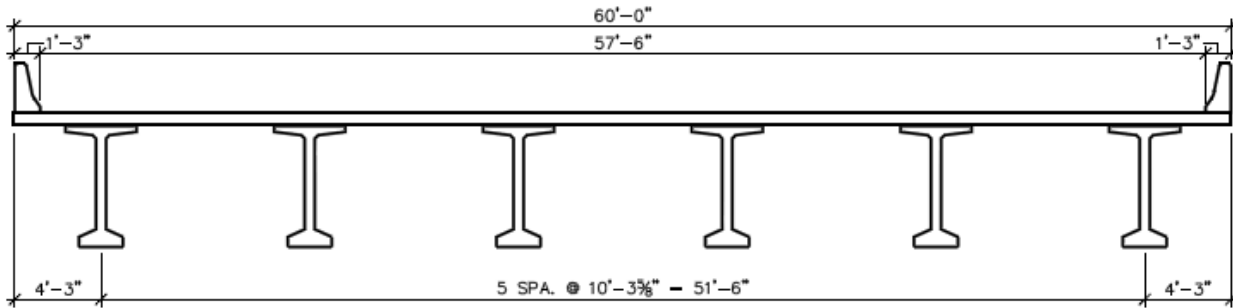
Fig. 3: Bridge cross section.
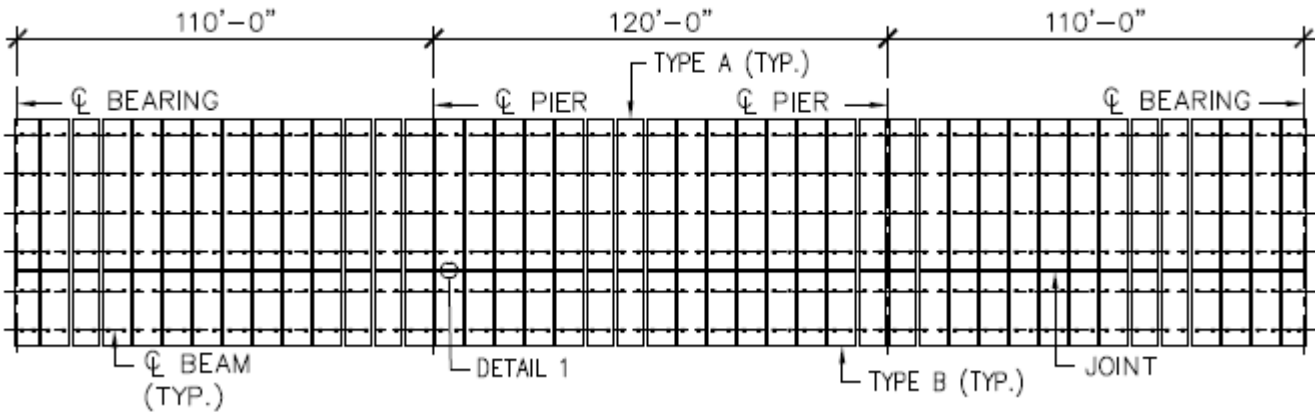
Fig. 4: Panel layout with joint between girders.

Fig. 5: Girder cross section.

B5-2

Fig. 6: Type "A" panel (see Fig. 4). Connection bars in the longitudinal direction should be outside the connection bars in the transverse direction through the section depth.
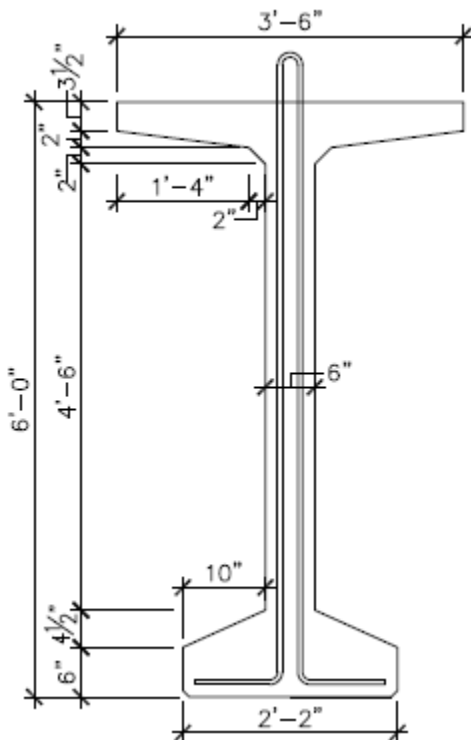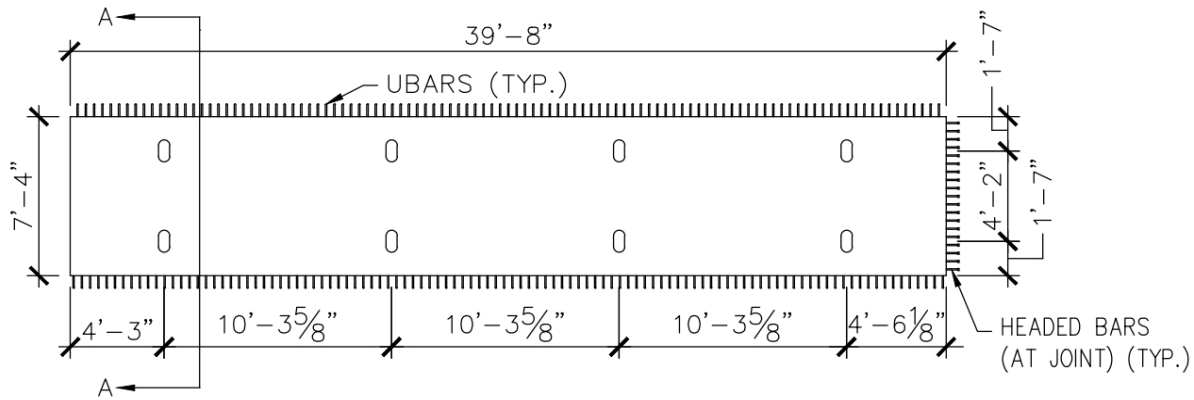
Fig. 7: Section A-A through Type "A" panel.
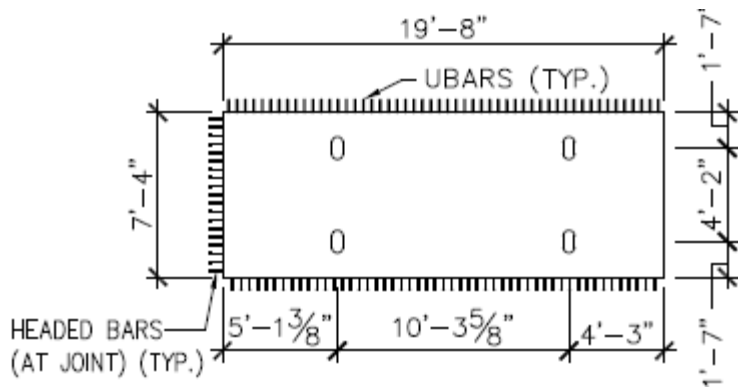
Fig. 8: Type "B" panel (see Fig. 4).
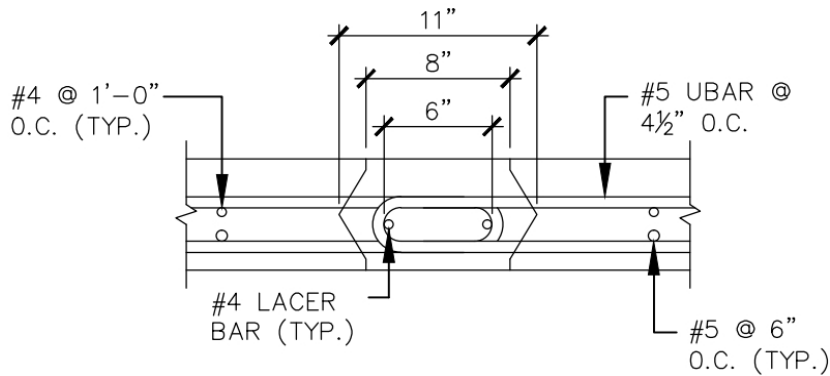
Fig. 9: Typical transverse joint between panels.

B5-3
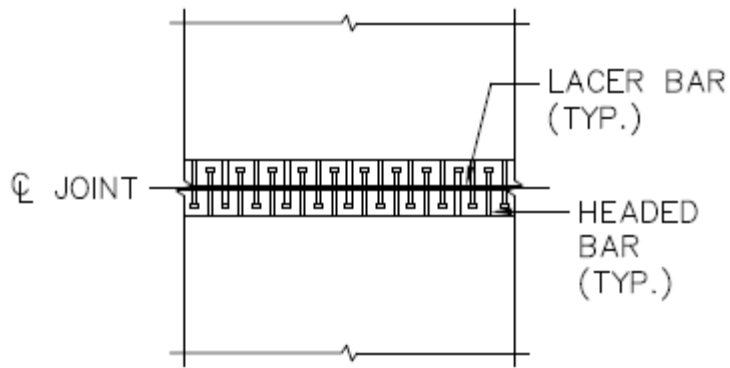
Fig. 10: Typical longitudinal joint between panels.This joint is used for cases where the length of a panel exceeds the the limit for shipping or hauling of a panel, which requires that the panel be subdivided into two or more panels of shorter length.
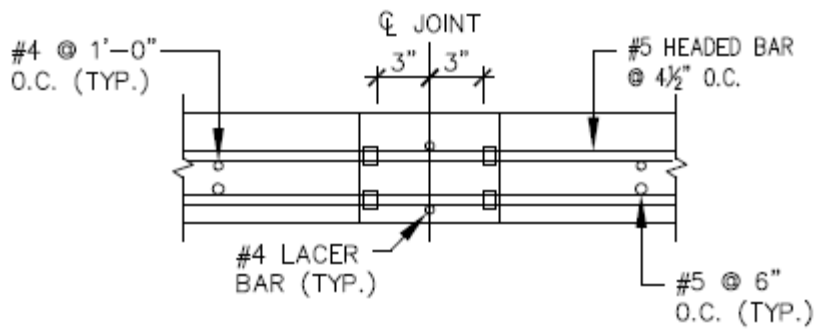
Fig. 11: Section through longitudinal joint.

B5-4

Appendix C

Phone Survey Results

C.1   Introduction to Phone Survey

This appendix provides a synthesis of the comments received from the individual respondents who participated in the phone survey that was used to gather information including the respondents' experience with similar systems, their input on important performance criteria, and their feedback on proposed connection concepts.

Nearly 60 people were interviewed during the phone surveys which were conducted in partial fulfillment of project Tasks 1 and 2. The individuals interviewed were selected through consultation with the project team, David Beal, and interviewees who recommended others who should be contacted. The respondents represent bridge engineers (including many individuals who serve as State Bridge Engineers), consulting engineers, fabricators, material suppliers, industry representatives, and technical committee contacts. The distribution is presented in Table C.1.1.

Table C.1.1: Distribution of phone survey respondents

Bridge Engineer	Material Specialist	Fabricator	Researcher	Industry Rep	Contractor	Other
36	9	6	13	3	0	3

A few survey respondents were identified under multiple categories in Table C.1.1, so the total number in the table (70) exceeds the number of survey respondents (59). Also note, that although there are no individuals listed under the "contractor" category, a number of bridge engineers and fabricators were able to provide firsthand experience on constructability issues encountered in the field. Attempts were made to include contractors in the survey, but because of the high level of activity with the contractors in the field towards the end of the construction season, and the difficulty in reaching the individuals in the field, this was not possible. The contractor on site during construction of the MnDOT implementation of the Poutre Dalle (PD) concept was queried by members of the project team regarding constructability issues, which influenced some of the decisions made in the concept development implemented in the University of Minnesota laboratory specimens described in Chapters 5 and 6. A complete list of the phone survey participants is included in Table C.1.2.

Prior to being interviewed, the participants who agreed to be surveyed were sent a packet that is included at the end of this appendix. The package included brief background information, figures of proposed concepts, and sample questions to be posed during the call. Participants were told that information hoped to be gained from the survey included:

- Details of similar precast bridge deck systems in use or under consideration, including experience with the systems and issues encountered during design, fabrication, construction and service.

- Input on key performance criteria to be used to evaluate proposed concepts, and

- Feedback on concepts considered by the research team for investigation as part of NCHRP 10-71.

Table C.1.2: List of Phone Survey Participants

First Name	Last Name	Bridge Engineer	Material Specialist	Fabricator	Researcher	Industry Rep	Contractor	Other	Employer
Sameh	Badie				X				George Washington U
Shri	Bhide		X			X			Portland Cement Association
Gregg	Blaszak		X	X					Tech Fab
Hank	Bonstedt	X							PCA Pennsylvania
Jimmy	Camp	X							P.E., New Mexico DOT
Reid	Castrodale	X	X						Carolina Stalite Co.
Vijay	Chandra	X							Parsons Brinckerhoff
Ned	Cleland							X	Blue Ridge Design, Inc.
Mike	Culmo	X							CME Associates
John	Dick				X				Director, Transportation Systems PCI
Dan	Dorgan	X							MN DOT
Marc	Eberhard				X				U of Washington
Al	Eriksson		X						Splice Sleeve North America
Merv	Eriksson	X							USFS
Roy	Eriksson	X							Eriksson Technologies, Inc.
Sam	Fallaha	X							Nebraska Dept. of Roads
James	Flynn	X							NYDOT
Ajit	Gokhale	X							FLUOR-OBDP - Salem, OR
Jon	Grafton	X		X					Pomeroy (producers)
Robert	Gulyas		X						Master Builders
Joey	Hartmann	X			X				FHWA
Neil	Hawkins				X				Prof. Emeritus University of Illinois
Mark	Henderson	X							LJB Engineers and Architects
Finn	Hubbard	X							Wisconsin DOT
Michael	Hyzak	X							TX DOT
Mohsen	Issa				X				University of Illinois - Chicago
Steve	Johnson	X							South Dakota DOT
Keith	Kaufman			X					Morse Brothers, Inc.
Bijan	Khalegi	X							WS DOT
Tom	Koch	X							NC DOT
Mervyn	Kowalsky				X				NC State Univ. Dept of Civil Engineering
Jim	Ma	X							CalTrans
Kevin	MacDonald		X						CEMSTONE
Lee	Marsh	X							Berger/ABAM Engineers
Elmer	Marx	X							Alaska DOT
Norm	McDonald	X							Iowa DOT
Don	Meinheit				X			X	Wiss Janney Elstner Associates
Rich	Miller				X				University of Cincinnati
William	Nickas	X							FL DOT
Mike	Oliva				X				University of Wisconsin
Vic	Perry		X						DUCTAL
Charles	Powell		X						ThermalChem
Chuck	Prussack			X					Central Pre-Mix Prestress
Basile	Rabbat					X			Portland Cement Association
MaryLou	Ralls	X							former TX DOT
Russell	Robertson	X							FHWA
Carin	Roberts-Wollmann				X				Virginia Tech Dept. of Chem. Eng.
Hugh	Ronald	X							HDR Engineered Structures
Henry	Russell		X		X			X	Henry Russel Inc.
Andrea	Schokker				X				Penn State University
David	Scott	X							NH DOT
Steve	Seguirant	X		X					Concrete Technology Corp.
Larbi	Sennour	X							Consulting Engineers Group
Peter	Smith	X		X					Fort Miller Company, Inc.
Maher	Tadros	X			X				U of Nebraska, Lincoln
Benjamin	Tang	X							FHWA (NY)
Julius	Volgyi	X							VA DOT
RIch	Zeldenrust	X							Washington State DOT
Steve	Zendegui	X							Jacobs Civil, Tampa
	TOTAL	36	9	6	13	3		3	

C.2 Performance Requirements/Specifications

The respondents were asked to comment on design/fabrication/construction/performance criteria that must be satisfied to provide adequate performance of key parameters to be included for consideration on this project (listed below). The parameters listed in parentheses are sample issues that must be addressed.

- Durability (Cracking; Corrosion resistance)
- Strength (Static strength; Continuity for live load; Load distribution)
- Fatigue resistance
- Seismic resistance (Strength; Ductility)
- Constructability (Transportability including minimization of thin sections and size of precast concrete pieces; Ease of installation including accommodation of differential camber; Adaptability including skew or transverse slopes and ability to accommodate future expansion)
- Rapid construction (Speed of erection; Reduction of formwork; Field placement of reinforcement)
- Serviceability/Performance (Rideability)
- Economy (Construction, Life-cycle operations/maintenance)

Respondents were first asked to indicate whether or not they thought anything was missing from list. They were then asked to rank, in order of importance for the project, the key parameters identified above.

Regarding whether or not anything was missing from the list, most respondents thought that all of the key parameters were identified. A few of the respondents listed additional issues of concern. These are summarized in the following section.

C.2.1 Additional issues identified for consideration

Associated with durability, staining was listed as an issue of concern that is a result of cracking and subsequent leakage through connection regions.

Regarding the issue of fatigue, M. Eriksson [USFS] indicated that for the systems to be considered on low volume roads, fatigue should not be considered as a criterion of concern.

Under the category of constructability, it was suggested to consider two components: (1) access to site (e.g., in remote areas, bulb-Ts may be preferred because they are durable and robust in transport, and accessibility to CIP on site may be impossible or outrageously expensive); and (2) reducing construction time in field, which though broadly applicable, has dramatic implications at remote locations or regions with short construction seasons. It was suggested that consideration should be given to developing systems that put more time into fabrication at the plant to reduce the fabrication time required in the field.

Under the category of economy, many respondents indicated that everyone talks about the importance of life cycle costs, but in reality, initial cost is what is important to state DOTs, because of limited

budgets and numerous projects that must be funded. Culmo indicated that it should be noted that rapid construction automatically adds 15-25 percent increase in cost.

Matching the joint color with the precast so the systems do not appear jointed was suggested as an added criterion by Bhide and Ralls.

Culmo [CT, NH] also suggested including inspectability and tolerances (including sweep and camber) in the list of performance criteria. He felt that the tolerances issue needed to be a major bullet item and should include vertical and horizontal adjustability that must be built into the system.

Tolerances

In addition to the comments by Culmo, several other respondents commented on tolerances. Dick (PCI) indicated that tolerances, alignment and fragility all needed to be evaluated. Flynn (NY) indicated that tight tolerances are needed. Most states have specific girder tolerances and total out-to-out tolerances. Tolerances include sweep, width, depth, flange thickness, etc. (e.g., specifications can be found on AK website). Tolerances in PA were initially based on PCI product tolerances; however, when the state experiences a new problem with a product, they will generate a new tolerance requirement (e.g., plumbness of web). Some states (e.g., NM) have had problems with tolerances in terms of camber and sweep [Camp]. Tang (NYDOT) indicated that sections often have a lot of sweep which makes forming joints in the field difficult. Ralls indicated that it would be desirable to have more tolerances in the field (e.g., FL built a 143 ft. span that had to be placed with just 1 in. to spare on each side). Roberts-Wollman indicated that issues associated with tolerances are exacerbated if the systems do not incorporate overlays.

In addition to consideration as a performance criterion, Smith stated that tolerances are needed in the specification. He believed the loop bar detail would be good for longitudinal joints because he thought it could readily accommodate tolerance issues. He also indicated that wider joints (e.g., $\geq$12 in.) can make up the difference in camber among adjacent precast elements.

C.2.2   Rank ordering

Several of the respondents were asked to rank order the performance criteria in order of importance (with "1" being highest), assuming that the proposed connection concepts satisfied at least the minimum acceptable criteria in each category. In other words, all things being equal, respondents were asked whether they would prefer a system that provided a slight edge on durability or a slight edge on speed of construction, for example.

Table C.2.1 contains the number of responses for each ranking value for each of the performance criterion. As noted below the table, if the respondents listed multiple performance criteria as equally important, those criteria were given the same ranking (e.g., if durability, strength, and seismic were selected as top choice, they would all be designated with a "1," the next choice that would follow would be designated "4;" there would not be a listing with a "2" or "3" for that individual). Of the 59 interviews, 15 did not rank order the criteria. Of the 44 individuals who did offer ranking, it is clear that

C-4

durability was considered of greatest importance, as it was mentioned by 40 of the 44 individuals who ranked the criteria, and of those, 75 percent of them ranked it as the top priority.

Besides durability, other issues considered of great importance were constructability and rapid construction; followed by economy and serviceability/performance. In reviewing some of the comments of the survey respondents, they felt that if the sections were not durable, none of the other criteria mattered. That is, although it is desirable to have bridges that can be constructed rapidly, if the bridges do not last, it creates more problems in the long run than if they had taken longer to construct a more durable structure in the first place.

Strength was listed on the lower end of the spectrum, because many respondents indicated that they could always design the structure to ensure that it had adequate strength or find a means to achieve the required strength. So it was not that strength was not necessarily a primary concern, it was felt that it was not an issue.

The lowest ranked criteria were fatigue and seismic resistance, in fact for these categories, fatigue and seismic were listed by 6 and 11 individuals, respectively, as either low or not applicable. In the case of fatigue, one of the individuals who ranked fatigue as a high priority (i.e., rating = "2") was concerned with the potential fatigue resistance of the WWR connection detail in particular.

Some of the respondents amplified their responses with additional comments on their selections. The following selected comments provide insight into some of the rank ordering. This is followed by some grouping of comments associated with particular topics (e.g., seismic, rapid construction, etc.) in cases where a number of people provided input on similar issues.

Table C.2.1: Rank ordering of performance criteria

Rank Order	Durability	Strength	Fatigue	Seismic	Constructability	Rapid Construction	Serviceability/ Performance	Economy
1-highest	30	3	1	0	13	9	8	6
2	4	3	1	0	9	8	2	4
3	4	5	1	0	7	3	2	3
4	1	3	2	2	0	0	5	3
5	1	0	2	3	1	3	0	2
6	0	1	0	2	0	2	1	1
7	0	0	1	2	0	0	1	1
8-lowest	0	0	1	0	0	0	0	0
SUM	40	15	9	9	30	25	19	20
% of respondents	91	34	20	20	68	57	43	45

[1]If the respondents listed multiple performance criteria as equally important, those criteria were given the same ranking (e.g., if durability and strength were selected as top choice, they would both be designated with a "1," the next choice would be designated "3"…there would not be a listing with a "2" for that example).

General comments associated with performance criteria

The following is a list of comments which amplify the respondents ranking. The comments are ordered alphabetically by State DOTs, followed by alphabetical listing of other respondents.

AK indicated that as part of the durability criterion, crack width (see AASHTO serviceability), coulomb resistance to chlorides, elasticity of grouts, greater ductility and resistance to abrasion are important. Rapid construction is important to Alaska because of the short construction season (March-October).

CA believes durability (including cracking and corrosion resistance) is an issue of particular importance for joints. CATrans has closure pours when widening bridges and cracking and corrosion that can occur at those locations is of concern. Rob Chai (UCDavis) is currently conducting research related to these issues. They have discussed using stainless steel, FRP and configuring steel layout to achieve minimum width of closure pour.

IA DOT considers that if economy is not there, it is hard to justify any of the proposed systems. IA does not have a concern for rapid construction [McDonald].

Dorgan (MnDOT) indicated durability and low or minimal long term maintenance go hand-in-hand. With limited budgets, first costs have a huge impact on the choice of system. For rapid construction definition, on local roads, it means cutting construction time in half. For interstate highway bridges, rapid construction could mean a weekend. Although fatigue may not be a big concern, it should be considered with regard to breaking up grouted keyways and effects of differential deflection on further breakup.

NYDOT considers constructability and durability as top priorities. They use stainless steel where they require better corrosion resistance and longer life. They also use corrosion inhibitors with HPC in precast elements for good long term performance, and seal decks with a silane sealer.

PA does not do continuity for live load. Criteria such as strength/fatigue/seismic are engineering requirements that must be met by all systems (they are overarching, rather than fitting them into rank order scheme of priorities) [Bonstedt]. Rideability is a criterion that can be fixed (i.e., you can overlay or grind it).

TX is not in extreme corrosive environment except the panhandle. The important performance criteria for TX include constructability and transportability [Hyzak]. Keep widths of sections down for transportability. Durability is also important for the joints. They will be the "weak link." Ralls mentioned staining and rideability as important issues. She indicating cracking is a problem, but the real issue is corrosion. Rather than using corrosion resistant materials, she would rather have the focus on high performance concrete. For rapid construction, Ralls indicated the less concrete the better. For serviceability, a wider joint width helps rideability and grinding can be used. When all is said and done, economy (initial cost) is still the driver. Strength and lateral load transfer can be achieved.

Robertson (UT) indicated that constructability issues to be considered included traffic, availability of CIP, room to build (i.e., right-of-way).

Volgyi (VADOT) indicated the top priority would be cost (like it or not first cost controls). Durability is also a top priority. He has concerns whether or not the systems can hold up without PT.

Zeldenrust (WSDOT) listed performance/durability high on the list. Cheaper and faster are not always best. Regarding durability, the concern is whether or not the system is leakproof. It must behave well in the long term and at least as good as monolithic—that should be the standard.

Shipping and transportation is important. Initially fabrication will cost more in development of new form, but afterward, costs should level out.

Bhide indicated that the priorities for the project research should be different than the priorities of bridge engineers which are (1-safety; 2-economy; 3-aesthetics).

Castrodale indicated that issues related to serviceability include differential camber and camber growth. He also indicated that rapid construction is sometimes considerably slowed by requiring screeding, it is better to fill the joint and subsequently grind if necessary to achieve rapid construction. It is important to be aware of capacity of equipment needed (due to weight and size of pieces); availability of CIP due to distance from plant.

Chandra indicated that durability is a concern when CIP is used. Type A cement is expensive and sometimes hard to find.

Eriksson stated that it is a given connections must have durability/strength/serviceability/performance. Consider bridges for life (i.e., 75 year lifespan is desired); consider making quantitative crack width requirements; use better materials (i.e., good detailing and better grouts); and consider rethinking how live load is distributed within the system.

Hartmann indicated all systems developed as part of this program must meet the objectives of rapid construction and economy. If they do not meet these objectives, it does not matter if they meet the second objectives (durability/constructability) because they would not be competitive.

Hawkins indicated that constructability also involves adaptability (e.g., can the proposed system accommodate skews).

Oliva indicated that flexural strength is not a key issue at joints, because most decks fail in punching shear. Other aspects to be included in criteria include surface roughness on girders and bond that can be developed.

Prussack emphasized the importance of durability. If the bridge is put into service, and needs replacement a couple of years later, the speed of construction was not worth it. It is difficult to achieve, good, fast, and economical simultaneously. In considering speed of construction, the amount of time it takes grout to cure must be considered. It is important to know the objectives of the project. One-day installation might require magnesium phosphate grout. In order to move to a new system, the entire mindset must be changed.

Rabbat thought that "leakage" should be considered under category of durability. Need to pay attention to type of grout chosen. Grout needs shrinkage resistance and workability (which are often competing parameters).

It is extremely hard, if not impossible, to avoid cracking. Roberts-Wollman suggests figuring out what is causing cracking and find a way to eliminate corrosion. Freeze-thaw is probably not a top priority. She also indicated that serviceability and performance should include rideability.

C-8

The system has to be easy to use and result in reduction in labor if trying to compete with CIP [Ronald]. Use these criteria to screen out potential systems. If the potential systems satisfy these, then make them work to satisfy the other criteria (e.g., serviceability, strength, durability). Also consider climate as a criterion. If one system requires good weather and another is not as restrictive, the system which can be built in any environment is the preferred option.

Russell commented that in Miller's research on boxes, his conclusion was that temperature effects on the joints was significant. Precast systems should be designed to be placed at the site without concern for particular orientation—the installation should be fool-proof. If a section can be put in wrong, it is likely that it will occur in the field at some point. The majority of the work should be done in the plant off site such that limited work is required in the field. Initial cost is also important because of DOT limited annual budgets.

Scott (NH) stated that all of the criteria are essential in design; fatigue and strength cannot be compromised.

Seguirant indicated that durability is the primary concern with the systems. However, it is less of a concern with the PD system because of the thickness of the CIP over the joint which is likely to mitigate reflective cracking. Durability will likely be improved if joints are enlarged and filled with concrete instead of grout. Seigurant also indicated issues such as load distribution need to be addressed for some of the systems. AASHTO provides a simple calculation for decked bulb-Ts, which may not be very accurate. Regarding other criteria, constructability is a big issue. Transportability will vary from state to state because of equipment availability and permit requirements. Differential camber can be dealt with using leveling techniques. Decked bulb-Ts must be adaptable to different bridge geometries because the precast is the final bridge grade. Decked bulb-Ts have been manufactured to varying vertical curvatures by varying the thickness of the flange (although this adds weight and has practical limitations). Concrete Tech Corp has deflected forms to change profile of girder to achieve up to 2 ft. of vertical curvature. Skews and cross slopes are generally not a problem, although combined vertical curvatures and skew can lead to flange match-up problems.

Smith indicated that under the criteria of durability, both cracking and corrosion resistance are important. The slab strength should be carefully analyzed as this has not been done in the case of the two bridges with loop bar details that Smith described; neither deck was analyzed for bending strength which may be an issue for the larger girder spacing. Regarding constructability, Smith did not see a need to get by without a form system. For the loop bar detail shown in the survey, he was more concerned with spalling chunks of concrete from the thin sections that butt; construction ease is not worth the risk. Smith also indicated that it is not wise to have a large percentage of deck area done with grout; it is difficult to do it right and achieve good durability. Smith does not like about transverse joints.

Tadros stated that transverse jointed systems should be designed to provide adequate live load distribution. Without PT, he is concerned that the system will have transverse cracking. Reinforcement is required for crack control and corrosion protection. Poutre Dalle system may need to address fatigue for the joint over the pier. Joints should not be weaker than the rest of the system. Reinforcement should be placed as close to the top surface as allowed for crack control.

C-9

With regard to durability, Tang (NYDOT) suggests a "nested system" approach (i.e., epoxy-coated bar or stainless steel with HPC). Avoid forming in the field—make pieces that butt.

Rapid

Respondents had many comments on rapid construction. Rapid meant different things to different people. Simply shortening the typical time span would be desirable (e.g., instead of constructing bridge over one construction season, cut down time by half). Tadros believes that the primary performance criteria to be addressed is rapid construction/speed of erection. He also noted that when CIP is required, placing, finishing, curing take time—it should be avoided. He indicated deck bulb-Ts have a good future for rapid construction. He recommended keeping things simple. Ronald indicated that the concern should be on cutting the schedule of a conventional job. If it is an emergency repair, it is not unusual to pay a premium for such a system. Rather than focusing on niche markets (e.g., remote areas where CIP is expensive) develop systems that are competitive in regular market. Issues that speed erection include reduction or elimination of formwork, CIP, or onsite bar placement.

C.3   Comments on Precast Slab Span Superstructure Concepts (e.g. Poutre Dalle System)

The survey included renderings of the Poutre-Dalle concept and the MnDOT implementation of a Poutre Dalle concept as examples of precast slab-span superstructure concepts. Many of the respondents liked the Poutre Dalle concept, particularly the MnDOT implementation of it. Many mentioned potential applications for the system especially on low-volume roads. A few individuals recommended considering the use of voids or lightweight aggregate concrete (LWAC) to achieve longer spans with the PD system; however, a number of other individuals were strongly opposed to voids and LWAC due to problems encountered in the past. An issue that was noted several times in relation to the PD system is that the use of CIP makes this system less rapidly constructable. It was not necessarily the quantity of the CIP, but rather that it was used with the system at all, that they found would slow the construction time due to the need for curing and strength development. The following are some of the comments in alphabetical order in terms of the state agencies represented, followed by alphabetical listing of others who provided comment.

Marx (AKDOT) liked the shallow span-to-depth ratio of the PD system. He thought it provides economy by requiring less fill in overpasses. In AK, however, CIP should be avoided because of its high cost in remote areas.

Ma (CalTrans) was very interested in composite slab span systems. Standard details would be helpful to them for this type of system. He thought the PD looked attractive with the bottom flanges abutting. For short spans, he indicated the differential camber of the PD system should be small and there may be no need to debond strands at the ends. He did not see how the short clearance of the bars protruding from the web could provide horizontal shear transfer—it was not clear how they could be developed.

Nickas (FL) had seen longer versions of the PD bridge. He thought the vertical upright bars in the MnDOT implementation would pose a safety issue. Inspectors in FL request bending all vertical bars down. He was also concerned with potential interference with the protruding bars. He thought that it could have

potential problems orienting the pieces in the field. In the range of 50-60 ft., FL is using the NE inverted Ts. Nickas would be interested in using the PD system in spans of less than 35 ft. He does not see a need to add wire mesh in the tips of the PD; bulb-T systems have larger areas without rebar than the PD detail and Nickas does not have memory of losing a chunk of concrete after construction was completed.

McDonald (IA) thought that the PD system looked better than current inverted-T system they are using. For longer spans he recommended trying to reduce dead weight by considering voids. In addition, he recommended considering changing some reinforcement to make the precast section more constructable (e.g., change S1608E bars to two C-shaped bars).

Kaufman (Morse Brothers, Inc., OH) had concern with PD handling skew and staged construction. Flange could be decreased down to 3 in. He did not think that making the flanges thinner would help with reflective cracking, to avoid reflective cracking he recommended putting a lot of reinforcement across the joint.

Dorgan of MN is a proponent of the system. He favored working to further reduce mild reinforcement which would ease congestion. He preferred a roughened top surface of bottom flange as the system in the field currently appeared to be performing well.

Falhalla of NE liked the uniform slab which is good for traffic.

Scott (NH) was concerned whether precasters would buy into building new forms for the PD system. He was also concerned with so much CIP that the system would not be rapid. He wondered what the advantage of this system was over a butted box beam.

Camp of NM saw a real advantage to the PD. He thought that it looked attractive and could be competitive with a large inventory of slab bridges NM builds in the range of 40-45 ft. Advantages include the need to pour less concrete and the elimination of formwork. He thought the change to 90 degree bends in the bars lapping in the adjacent sections was a great way to ease construction in the field compared with the original 180 degree bends used in the French implementation.

Flynn (NY) did not see much of an advantage with the PD system. Complications of the system include the single protruding bar. He indicated that mechanical connectors should be explored; however, he preferred not to "spin" the bars on in the field.

Koch (NC) thought the PD system would be a harder sell than most common precast systems because it appears to be more "exotic." NC likes to try less exotic systems, however he thought the PD system looked innovative. He favored the shallowness of the section. They have used voided slabs on short span structures (e.g., 40-60 ft.) with a 2 in. asphalt or concrete overlay; most of these systems have performed well. Of 100 bridges reviewed, the ones with poor drainage issues (e.g., without grade or cross slope) had problems where water either sat or filtered down. Koch suggested LWAC might be used to lighten up the section.

Bonstedt of PA liked the PD system, but thought it looked heavy. He thought the bars protruding from the form may be difficult to accommodate in the plant, but installation in the field did not seem difficult. He suggested laying out the reinforcement to avoid bars interfering in the field.

The PD system looked like much more work in field compared to double-Ts with weld plates that SD is currently using [Johnson]. PD looked good for its load transfer. If it could be used on state highways, it would be a benefit. Advantages include the elimination of formwork and good riding surface. They appear more expensive than their typical bridges. If the system is heavy, it would require more support at the abutment and piers than their conventional systems.

Hyzak (TX) thought application of the PD system was limited because of short span lengths. Competition is prestressed slab systems. Likely applications for PD systems include stream crossings and locations where shallow clearances are required.

Ralls thought the PD system could be improved if the pieces could be set straight down without sliding them under adjacent pieces. TXDOT has done some similar new shapes. The PD system is also more conventional than rapid, but allows for rapidity of construction through precast while including more conventional CIP.

Volgyi (VA) stated that if rapid is the desire, then avoid use of CIP. He did not think that the PD system went far enough toward rapid construction with the CIP component.

Zeldenrust thought the PD system had its applications, but it is limited in span length. A standard element used by WSDOT is a 2 ft.-2 in. voided slab. Khalegi of WS indicated MnDOT modified original PD in logical ways, except he did not favor the protruding bars. To increase potential span length, WSDOT proposes a voided system without protruding bars. WSDOT uses a solid slab system up to 50 ft. on local roads.

WI also sees PD applicability for short spans, and would likely use it on local roads. Hubbard indicated lightening up the section while maintaining strength would be a good goal.

Eriksson (USFS) thought PD looked like interesting concept but appeared heavy. He thought it might be difficult to compete economically. Also in remote areas CIP is not readily available.

Bhide agreed the PD system looked good but heavy. In addition to considering voids, he recommended reducing the web width or using LWAC. Bhide also commented on the voided slab system developed by Tadros at UNE.

Castrodale indicated that CIP of PD system hurts its efficiency; must wait 28 days for it to cure.

Chandra was concerned with connection between the bottom flanges.

Culmo liked the concept. He had some concerns with reflective cracking and the time required in the field for reinforcement and concrete placement. He recommended making the web full depth and pouring the joint above the flange in the field to eliminate the need for screed rails. A float finish should be all that is required. A watertight membrane and overlay on top would help deal with differential camber issues. Culmo believed this double field system would be faster than a single cast. He did not recommend the system for highway bridges.

Dick was concerned with the weight of the system and thought that the proposed section was unnecessarily wide. He recommended modifying the bottom flange to be a SIP form rather than keeping the web as part of the system.

Ericson thought the system was a perfect example of an emulative design.

C-12

Eriksson stated that the section seemed highly erectable and efficient; the drawback was the large amount of CIP.

Gokhale, who participated in the PD showcase, did not see any advantage of this system to voided slabs. He thought voided slab construction would be quicker and there would usually be an asphalt overlay with a membrane or thick HPC deck on the top which he thought would require less effort than pouring the CIP portion of the PD.

Grafton (Pomeroy) indicated the only change he would make to the PD system would be to eliminate the projection of the bar beyond the edge of the flange. The current configuration requires "drifting in" the precast pieces laterally in the field. He also suggested a flat seal or T-seal over the joint between the abutting edges. This system would be in direct competition with other short span bridges (e.g., voided slabs) in the range of 30-50 ft.

Hartmann thought the MnDOT "drop-in" cage was a great improvement over the original concept. The section looked appropriate for the span range.

Henderson and Sletten thought that the PD system would be very "doable." They indicated that it was similar to box beam systems with a CIP deck on top. They thought the system would perform well, but may develop some reflective cracking.

Issa thought the system looked good, but would not be rapid because of the CIP. He thought all of the suggested variations of the PD, described in the survey handout, would work.

Marsh liked the MnDOT adjustments to the PD system. If it were curved or corded, it would be difficult to thread the bars through in the French system. Its weight will limit its use to short spans. A system that may compete with the PD would be a tub or short span box section which has deeper more effective shapes. The advantage of the PD system is its short profile which is advantageous for bridges with vertical clearance limits. Voids may help lighten the system. Marsh recommended keeping the top of the bottom flange of the PD roughened or it may curl or pull away from the CIP.

Oliva thought that the PD system looked good and would be something that would be considered in WI. A void should be considered to reduce the shipping weight. Regarding a smooth surface at the top of the bottom flange, FHWA research has indicated that a smooth surface can help to avoid concrete fatigue issues. Because a crack will pre-exist or will develop at joints, designer should purposely design the system so that crack is likely to occur at location with higher reinforcement content.

Prussack felt the PD was a robust system and had no doubt it would perform well. He thought the protruding rebar made things complicated in that forming would not be so easy, but he did not think it would be very expensive to build. He suggested avoiding voids. He thinks they are a pain to build. They need to be restrained to stay in place. Economically he said it would be cheaper to add a few more strands to carry the larger self weight than to use voids. Problems go up exponentially with size of voids. He stated every precaster has problems with them and often find that they move when casting.

Rabbat commented that no matter how much CIP is required for the PD system, placing and finishing equipment would still be needed on site. A modification Rabbat suggested for the PD system would be to have one protruding hook a few inches above the other so the longitudinal bar could be slipped and

dropped into the joint which would make it easier for the longitudinal bars to be tied in place. [Although, note that currently, the longitudinal bars are dropped in place in a prefabricated cage.]

Roberts-Wollman thought the PD system had promise for short span bridges. The thick CIP can help control reflective cracking. Potential issues of concern include differential shrinkage. Load induced cracking should not be a problem, but she expected that the system would crack.

Ronald (HDR Engineered Structures) did not care for the PD system because of the field labor involved and the need to cast CIP in addition to providing precast. He did not feel that there was enough time savings with this system. He suggested considering PT with a threaded bar through the PD system.

Russell liked the drop-in cage in the MnDOT implementation of the PD system. He commented on the closeness of the horizontal shear reinforcement to the surface (i.e., difficult to get concrete underneath). He also commented that most designers detail bars in the corner (i.e., extend S1609E closer to corner of concrete). He recommended concrete covers of 2 to 2½ in. on top and 1 in. on bottom from NCHRP study recommendations. He recommended going with LWAC if the CIP exceeds 8 in. in thickness.

Seigurant thought that the PD systems may prove to be economical and assembled quickly as have the decked bulb-Ts. When given a choice between full depth deck systems and CIP, contractors often choose CIP as more economical. If speed of construction is an issue, the cost premium may be acceptable. Two comments on the system developed by MnDOT: 1) avoid stirrups protruding horizontally; enable vertical drop of the precast pieces into position; and 2) horizontal shear reinforcement should project out of the piece far enough to develop into the topping.

Sennour felt the PD system looked promising, and would be a great solid span useful for county bridges. In response to those who think there is too much CIP in the PD system, he indicated that as long as CIP is being used, the thickness does not matter. He recommended a smooth top surface on the bottom flange as well as a flange that was as thin as possible.

Smith did not care for the PD system, but thought it would be adequate for short spans. In terms of importance, he would place it at the low end of the spectrum. He thought it looked rigid and put a lot of dead load in the wrong places. Besides proposing voids, other suggestions Smith proposed from a fabricator's perspective included using dowel bar stubs rather than having transverse bars protruding from the forms. The protruding bars can then be screwed into the couplers in the field.

Tadros indicated the PD system had a limited place; he did not particularly care for it. He described the NE Inverted-T section which can span to 100 ft. He recommended avoiding situations where two torsionally stiff elements are connected. Anytime that is done, if they are not connected well enough, torsional cracks will develop (e.g., box beams). It is difficult to achieve longer spans with the PD system without a void (he recommended Chapter 8 of PCI Bridge Design Manual for guidance on design of transverse sections of adjacent boxes to make the deck width act as a plate). He recommended changing the top surfaces of the bottom flange to smooth.

Tang really liked the PD and saw its potential on multispan and continuous bridges. He would like to see minimal CIP (just fill in voids between the webs and use precast top of web as riding surface). Also consider stronger joint connection details and LWAC. He was not sure if voids would work with the

system. He did not think that it mattered whether or not the top of the bottom flange was rough or smooth because any crack that would form should be arrested by the reinforcement. He recommended considering mechanical connectors as a means of connecting the reinforcement (e.g., screw-in or clip/swage together).

Zendegui thought that rideability should be good with the PD system. He thought that the vertical bars in the PD system could result in many small cracks due to shrinkage resistance (may be better than one large crack). He also recommended avoiding the use of the bars protruding laterally, as they may cause forming problems (contractor refused to use them in their application because they did not want to damage the forms).

C.4   Comments on Potential Means to Lighten the Precast Slab Span Superstructure Concepts

A number of individuals surveyed indicated that means should be investigated to lighten the precast slab span system. Two options were mentioned: use of voids and lightweight aggregate concrete. This section summarizes these comments.

Comments on use of voids

Grafton (Pomeroy) indicated adding voids would be an option. In CA the ceiling is 48 kip on a flatbed truck (with up to 55 ft. length) without having to go to a more elaborate trucking unit. If the system is heavier than that, he suggests looking into the use of voids. If voids are required, look into using Styrofoam or cardboard. Corrugated metal can be used for voids up to 18-20 in. in diameter. If moisture gets into the voids, he suggests including a drain in the bottom and seals at the ends. If you can load the system on a truck without voids—avoid them.

TX has good control over voids in forms; they sometimes pour in two sections [Hyzak]. WSDOT developed PD proposal with voids [Khalegi]. Culmo and Hawkins recommend looking into using voids if the system becomes deeper than 18 in. Issa built models with voids and tested them in the laboratory. He did not see a problem with constructing the PD with voids. Roberts-Wollman thought that voids could work if precasters can be convinced to use them. Tadros indicated that the PD system needed voids to span longer lengths. The NE Inverted-T section has voids made by topping the web with a timber form and casting the top flange. They have had no problem with floating voids with this construction concept and have experienced little leakage. The contractors also like it. Smith would recommend the use of voids to lighten the dead weight of the PD system. He is a fan of Tadros' NE Inverted-T system; it is basic and easy to construct. Smith likes to patent products, and considered building Tadros' system, but thought it would be difficult to patent.

Ralls thought the PD system looked heavy without voids; however she indicated states like MD have changed from voided to solid systems due to voids popping up during casting. Dick opposed the use of voids as it increases complexity and adds new problems. MN and SD are opposed to voids because of previous durability issues experienced with voids.

C-15

Nickas did not recommend using voids because the forms float and end up costing more than a solid slab. Sennour also thought that voids could be problematic because of floating. If the system becomes very popular, he indicated that voids could be formed mechanically (as done in box beam systems). Russell thought that in general voids are fine; if they float then they were not tied down.

Comments on use of LWAC

Advantages that LWAC provides include cost savings on transportation and required crane needs. Grafton (Pomeroy) has used LWAC commercially but not for bridges. CA is interested in lightweight boxes for reduced superstructure mass and therefore reduced inertial forces created in response to seismic loading [Marx]. Although CalTrans is interested in LWAC, they have not yet used it that much (maybe less than 1 percent LWAC).WI is interested in lightweight. They have learned a lot over the last few years and think it looks promising [Hubbard]. Smith has had a lot of success with LWAC. Culmo associated with CT DOT and NH DOT is a big fan of LWAC. They used LWAC in SD in the '60's and did not have problems with it, although cost may be an issue, Johnson thought it may be o.k. Prussack thought LWAC should be looked at as a tool, like magnesium phosphate grout. If it is possible to ship out more pieces with adjusted density of mix, he is for it. Back-calculate required density based on trucking limitations. Ralls indicated that individuals at TXDOT think that LWAC is the way to go for precast deck panels. She thinks that LWAC now has similar properties to NWC and good abrasion resistance. Breen at UT-Austin is doing some work in this area. Some DOTs have had disastrous results however.

Lightweight concrete has performed poorly in AK and TX decks in past [Marx, Hyzak]. Marx indicated AK is hesitant because of poor experience in the past even though the problems were identified (i.e., reactive aggregate was detrimental to the mix). Material shortages have also been a problem in the past. TX would be interested in using it if research could provide success stories. IADOT has not had a reason to use it [McDonald]. Eriksson (USFS) had problems with LWAC in the past. Decks with estimated service lives of 20-25 years showed problems within 5 years.

Castrodale, who is now with Stalite, indicated that LWAC is very viable. It has abrasion resistance that is suitable for a driving surface. It is also possible to get more uniform mix with LWAC compared with NWC. Many have had problems with LWAC in past, one of the lessons learned is the need to qualify the aggregate. Its reduced tensile capacity may lead to problems with the shear keys. Advantages include the ability to haul more pieces. It also can be used to span longer lengths. The aggregate/paste has better bond and with its lower stiffness is more forgiving than NWC and may lead to less cracking. Marsh suggested trying LWAC, but was concerned with aggregate segregation and lower strength of the material. He also noted that shear keys may not be as effective if made with LWAC.

Russell and Sennour encouraged the use of lightweight materials in the project; Sennour uses it as often as possible. Abrasion tests indicate that LWAC is an acceptable material. The correct modulus needs to be used which affects the stiffness of the system including live load recovery and continuity. He does not think the freeze-thaw or chloride penetration issues are any more of a problem for LWAC than NSC.

C.5   Comments on Longitudinal and Transverse Connection Concepts between Precast Panels and Bulb-T Flanges

Survey respondents provided some general comments on longitudinal and transverse joint connection concepts. These comments are summarized first, followed by comments specific to the five joint connection concepts identified in the survey: loop bar (U-bar) detail, straight bar detail with spiral to reduce lap length, headed bar detail, welded wire reinforcement (WWR) detail, and structural tube detail. These details are sometimes identified in the comments below as 5a-5e, respectively. The numbers correspond to the figure numbers in the handout distributed to the survey participants that described the connection concepts.

C.5.1   General Comments on Longitudinal and Transverse Connection Concepts

Culmo indicated that cross slope is always an issue in bridges that must be considered in developing connection concepts. CA is interested in the design of longitudinal and transverse jointed systems, along with the types of grouting available.

Eriksson (USFS) thought all of the concepts looked more difficult than the weld tie system. Prussack is involved with NCHRP 12-69 with bulb-T flange connectors. Prussack and Rabbat would be interested in knowing how weld plate system would test out. Seigurant thinks that their welded connections with grouted shear keys work well. The weld plates also help correct for differential camber. With the connections shown, it is not clear how the leveling forces will be held until the grout/concrete achieves some level of strength, which is possible but will delay the introduction of traffic on the bridge. He thought that connections other than the loop bar detail are possible, but involve tight tolerances and difficult forming schemes.

Grafton (Pomeroy) commented that most DOTs are used to CIP on prestressed I-girders. These jointed systems will be a new way of thinking for many DOTs. Ralls indicated the simpler the better regarding connection details. Issa thought that all of the proposed details would work. Zeldenrust thought some of the connections would require thicker decks (e.g., 10-11 in.); he would prefer 7½ in. decks. With higher dead loads, more girders may be needed. Kaufman (Morse Brothers Inc., OH) thought any reinforcement coming out of form would add cost. Straight bars sticking out of form (5b-e) create a safety hazard. Other than the looped bar detail and possibly the spiral detail, Oliva thought that the other connections would be difficult to form in the plant with the elements sticking out. Kowalsky thought the benefit of the spiral (5b), headed bar (5c) and steel tube (5e) was the rapidity of construction. For the transverse joint, he thought that the loop bar detail looked best followed by the spiral because of the capability to transfer moment. Marsh indicated that the joints may not provide the out-of-plane (vertical) shear capacity necessary to make the precast units share load, which needs further consideration before testing.

Hawkins stated that it is desirable to have the reinforcement as close as possible to the surface for crack control and moment transfer, however joints may be lost quickly by corrosion attack.

Koch (NC) indicated that the bulb-T system is a nice option to have, however, they would not use it on everyday bridges because they are expensive and less durable. It introduces joints that they have been

trying to eliminate for years. The place for these systems is with rapid construction. Ronald indicated that where there is differential camber, a haunch should be used on the girder. The flange-to-flange connection has too many drawbacks including the potential camber differential and large longitudinal joints.

Henderson and Sletten have not used details like those proposed. They indicated that the connections are similar to closure pour details when the deck is cast on girders during phased construction. They have closure pours as narrow as 2ft.-6in. and recommend using mechanical connectors to develop the reinforcement. They suggested two websites for ideas: www.exodermic.com (contains details as to how their firm, LJB Engineers & Architects, have approached transverse and longitudinal joint details) and www.barsplice.com (for ideas of mechanical connectors). Perry thought that any joint detail would work with Ductal and not much space would be required in the joints because of the high bond strength and fluidity of the Ductal. Connections must be able to transfer moment if diaphragms are not used; Chandra recommended considering connection details used in cable-stayed bridges.

Ericson with Splice Sleeve North America has experience with emulative details. He served as the chair of ACI 550 *Precast Concrete Structures* which produced report ACI 550.1R-01 on emulative detailing. Emulative detailing involves connecting adjacent precast segments bar-by-bar in concrete or grout, thus simulating CIP. Ericson discussed two systems that could be used to connect jointed precast elements: (1) NMB Splice-Sleeve® which is an oversized ductile cast iron tube which allows the rebar to fit inside even with minor misalignment; and (2) "Kwik Joint" developed by Al Yee. The bars are placed at middepth of the panel and dropped into couplers (open at the top) in adjacent panels.

Tadros indicated that CIP should be avoided, because it slows down the construction. He recommended bolting things together to create a dry mechanical connection or a connection that is grouted later. Remove CIP from the critical path. If an overlay is included in the detailing, the CIP aspect is still included. The challenge is to execute the systems without CIP. I-beams with precast panels can be fit up with a built-in haunch and the top surface of the section could be ground if necessary.

Potential barriers to the use of these systems where guidance is needed includes the 24 in. spacing of studs connecting panels to the girders [Volgyi]. It is difficult to judge the constructability of the proposed systems looking at the survey, would need to see field installation. Volgyi recommended getting contractor input.

Badie recommended developing new connection concepts that do not protrude from the forms.

C.5.2 Specific Comments on Five Originally Proposed Longitudinal and Transverse Connection Concepts

The following summaries present comments from the respondents specific to the five connection concepts distributed to the survey respondents for their input. The general format of the summaries is to list the positives of the details, followed by the concerns.

C-18

Looped bar (U-bar) detail (5a)

Bhide commented that the loop bar detail system has been successful in Japan [although in correspondence with some Japanese colleague there was some concern expressed in using these systems in high seismic regions]. Tang indicated that the loop bar detail was specifically developed for seismic regions. Oliva mentioned a similar loop system developed in Yugoslavia for seismic design in '80's for wall system and wall/floor joint system. With this system you can force the crack through the overlapped reinforcement. A negative is that it requires a depth of deck which can be a problem for bulb-Ts. It may be possible to look into varying the deck thickness, but this may cause problems with differences in camber and sweep. Eriksson thought that this detail should be investigated further, and indicated that it would be the most seismically capable. Issa noted that the Koreans are also using a similar system, and he thought it was a good option. Chandra, Johnson, and Ma believed that this detail will work. Scott (NH) indicated that the looped bar detail was the one that interested him; Volgyi thought the detail looked "bullet proof." Marx (AK) and Prussack felt this detail was the most promising, but Marx thought it may require a thicker deck which would be a negative in terms of added weight in transporting members, particularly bulb-Ts. Prussack noted that a similar detail was used in shear wall panels to link walls; he also saw some advantages to a thicker deck because it is hard to fit the loop bar detail into a bulb-T flange. Prussack did not think forming should be an issue, once the fabricator understands the detail, they can gear up. Prussack did not prefer use of stainless steel, he preferred a thicker deck (e.g., 8 in. think) or smaller bar (e.g., No. 4) to accomplish the detail. Tadros indicated the key to this detail was to get a waiver on the bend radius. He also mentioned wire can have a tighter bend radius because of the lower carbon content. Zendegui though that the loop bar detail looked promising for the use in the top of girders and for panel-to-panel connections. Forms can be built around the protruding loops. He thought potential problems would be with leveling and getting the shear connection. In addition, he thought there was too much steel inside the loops.

Falhalla mentioned that they have had a similar detail in NE which has been in service for three years and has performed perfectly. He emphasized the concrete connection must be either nonshrink or expansive to ensure cracking does not occur and to avoid allowing moisture into the joint. In their project they required a Type-K cement, he recommends specifying material in a more generic way (e.g., expansive cement). Perry thought that the loop bar detail would work fine using Ductal®. Nickas thought the looped bar detail was pretty standard. He thought that the loops did not need to be side by side, that they required staggering. Constructability of the system is fairly routine, and the top and bottom longitudinal bars are not included. FL contractors have lots of experience with this detail and recommend it. Ralls thought the detail looked attractive and indicated TXDOT is using something similar without the lip on the shear key. Seigurant mentioned that they have used a similar detail to join wall panels in precast floating structures and it has worked well. He thought that durability of the system can be improved if the joint is enlarged (as shown in Fig. 5a) and filled with concrete instead of grout. Sennour (CEG) indicated that the loop bar detail is used often in vertical joints of wall panels as a seismic detail He had a complaint with the rendering in terms of the number and size of bars. It looks very labor intensive. With a 6 in. bend radius, should not exceed No. 4 or No. 5 bar. In addition, he thought that 2 in. clear cover for precast should be plenty. Smith had experience with the loop bar detail, and thought

that it performed well. For the loop bar detail shown in the survey (Fig. 5a) he was more concerned with spalling chunks of concrete from the thin sections that butt; construction ease is not worth the risk.

Culmo indicated that this connection would be the best detail for a moment connection in the longitudinal and transverse directions; however others questioned its capability. Rabbat questioned the ability of the looped bar detail to transfer moment. He thought it looked more like a hinge. He was concerned that there was very little straight bar to develop stress before the bend; however, he urged testing of this detail. Also Koch and Ronald were not certain about the transfer of moment without testing the detail. Miller thought this detail was simple, but when looking at positive moment development, must be able to mesh bars. Trying to position girders and get bars to mesh in, would be complicated. He has done work with bent bars and bent strands and believes that the bent prestressed strands worked best. The problem with the bent bars was that the bars could not be prebent before placing in the field.

Several respondents were concerned with threading the longitudinal bars through and size of closure pour [Camp, Hyzak, Hubbard, Khalegi, Koch, Marsh]; other than constructability issue Culmo and McDonald (IADOT) indicated the detail looked promising. Culmo questioned whether longitudinal bars are needed in loops. R. Eriksson, on the other hand, indicated that must ensure enough longitudinal reinforcement within the loop to make the noncontact lap splice of the hoops effective.

Tang thought the detail had potential constructability issues with the longitudinal bars. He was also concerned with the thin flange sections that abut and may have Q/C issues in handling/transport. In addition, radius of Japanese shear key poses constructability issues, he recommended straight edge with grooved interface. He preferred opening up the detail as was done in Mn/DOT implementation of PD. Kaufman was concerned with how to deal with skew with this system. In addition, he, Dick (PCI), Marsh saw a potential concern with breaking off flange tip (see *Shape of Keyway* section for proposed modification); Johnson (SD) did not have a concern with spalling off the flange tip. Ronald had experience with the loop bar system with mixed success. Unless it is constructed well, this joint will be the weak link; problems include loops not fitting right, interference, longitudinal bars not fitting through the loops. He also noticed the system, as proposed (5a), had potential for spalling off the thin flange under the joint. As noted above, Ronald also did not believe the detail would provide full moment transfer. Badie (NCHRP 12-65) is concerned with the tight bend radius of the system. To achieve tight bends, he believed the bars would have to be heated, which would increase the cost.

Grafton (Pomeroy) indicated that the loop bar detail can be somewhat painful with the forms. It should be kept standard (e.g., at 6 or 8 in.) or as multiple (e.g., 4 in. spacing where unused holes could be taped). NYDOT used the loop bar detail but found it to be a fabrication nightmare in the precast plant [Flynn]. Part of the problem occurred because it was not in the contract to draw up details for the fabricator. There have been noticeable problems with the system in the field. Bonstedt thought that fabrication would be easy (sufficient development length, sturdy, forms easily on bottom), but constructability would be complex. Castrodale, Dorgan, Eriksson (USFS), and Zeldenrust indicated that it would be hard to fit the looped bar detail in the thickness of the deck; Castrodale and R. Eriksson indicated one way to fit the looped bar detail in the thickness of the deck would be to tilt the bars—but this would increase problems with fabrication including dropping the precast pieces in place. Eriksson

(USFS) also indicated the longitudinal bars would need to be flexible to fit into the system. Roberts-Wollman thought that the loop bar detail was a "pain" to use while trying to maintain the cover that DOTs require. She liked the idea of using stainless steel as an alternative but cautioned against the use of dissimilar metals.

Straight bar with spiral reinforcement to reduce lap length detail (5b)

Khalegi of WSDOT and Hawkins favored this detail of the jointed systems. Falhalla, Ma, Marsh, Prussack thought that this detail, as the loop bar detail (5a), looked like a good positive connection. Zendegui thought that the spiral detail, as well as the headed bar and WWR details, would work out fine for transverse connections. One concern is potential alignment problems. Issa favored this detail, but thought it would be more costly. Ronald also thought the detail looked expensive just to get a shorter lap splice; he also did not like the additional field labor required and potential alignment issues. Miller liked this detail, but thought it would require a large joint and would be expensive. Castrodale and Oliva thought the spiral detail may be o.k. Looks reasonable if spiral is small enough to compress easily for construction [Hyzak]. Stretching the spring would be labor intensive [Hubbard]. Johnson (SD), Koch (NC), Nickas (FL) thought that the system looked complex with the coil. Ericson indicated that this system was similar to Al Yee's initial design to reduce splice lengths by 1/3 (predecessor to NMB splice sleeve). The system can be constructed by sliding the spirals to one side (need to be flexible). Mechanical connector is the next step beyond the spiral if it is required to reduce the width of the closure pour. McDonald (IADOT) indicated the connection looked reasonable but would have higher field labor costs than the other details. Badie thinks that this is a reasonable connection. He personally fabricated 3-4 panels with spirally confined joints at UNE and had no problems. Bonstedt thought that this system looked similar to one proposed by Tadros. His comments were that it would be difficult to construct, congested, and expensive (requires a lot of steel). Tadros indicated that this detail works very well and has been used previously in NE. He envisions the spirals would come to the jobsite precompressed and slid on the bars on one side of the precast. After the pieces are set, the spirals would be released and extended across the spliced reinforcement.

Others with reservations about the splice detail included Hartmann (FHWA), Smith, and Sennour with comments related to the detail being congested and difficult to fabricate. Camp of NM and Dorgan of Mn/DOT thought that placement of the spiral would be difficult. Culmo thought this detail was complicated because it would have to be formed—he thinks PT could be done faster. Russell thought the detail was too labor intensive.

Perry thought that the spiral detail would be redundant with Ductal, because the fiber in Ductal already provides confinement. Ralls indicated TX awarded a project in August '04 with a similar detail. Roberts-Wollman indicated they attempted to use a similar detail on a precast panel—she suggested discussing it with contractors.

C-21

Headed bar detail (5c)

Several respondents thought the headed bar detail had promise and preferred it over some of the other details. Bonstedt preferred this option over the spiral detail. Hubbard preferred it to the loop bar detail. Russell liked the headed bar and WWR details the best. Issa thought this system looked good, and this system like the WWR detail, would come to the field nearly completed. Sennour thought the headed bar detail was ideal (second only to the WWR if it could work), but would need testing. Marsh liked this detail better than the WWR detail; he thought that there would be more positive transfer for in-plane shear. Shear transfer, transverse to load is needed to hold the section together for flexure. For shear transfer in the vertical plane, the shape of the shear key is important. Dorgan thought this system might be the easiest to fabricate, but would have to be tested. As for the spiral and WWR details, Zendegui thought that the headed bar detail would work out fine for transverse connections. Falhalla has not had much experience with headed bars in NE, but thought that the detail looked fine. Ma (CA) and Nickas (FL) thought it could be used to reduce the development length, and consequently joint width. Others who thought the detail may have some advantages included Johnson (SD) and McDonald (IADOT). A few respondents indicated that his connection looked similar to one investigated in 12-69 [Hyzak, Prussack].

Culmo thought the detail would work but would be difficult to fabricate. Marx (AK) thought that both this and the WWR detail would be hard to line up. Camp, Khalegi and Koch thought it would be difficult to place the longitudinal steel under the headed bars; however other than that, Koch thought that this detail was the simplest. Castrodale thought it may be possible to tie the longitudinal bars to the underside of the headed bar on one panel and then position them in the field. Hartmann was concerned with the legs of the shear key potentially breaking off. Miller and Roberts-Wollman questioned whether this system could get the necessary development; Roberts-Wollman thought that otherwise it looked like a good detail "theoretically." Miller thought the headed bar detail might be expensive.

Welded wire reinforcement (WWR) detail (5d)

Of the respondents who commented on this detail, Hubbard, Johnson, and Prussack indicated that it looked like it would be rapid to construct and doable. Bonstedt, Koch, and Nickas also thought that this connection would work. Issa also thought this system looked good, and this system like the headed bar detail, would come to the field nearly completed. Roberts-Wollman and Ronald thought the WWR detail had merit; Ronald thought it was more "fool proof" than the other details. Russell liked the WWR and headed bar details the best. Dorgan (Mn/DOT) thought the detail may be fine but emphasized that welding in the field should be avoided [note WWR would not require field welding]. As for the spiral and headed-bar details, Zendegui thought that the WWR detail would work out fine for transverse connections. Culmo thought it would work but would be difficult to fabricate.

Sennour was uncertain about the WWR detail. It would need testing and he had a difficult time believing that the development is achieved and the section satisfies AASHTO requirements. If these are not factors, this would be his first choice because of the ease of constructability. Miller thought this detail may not be able to be fully developed. In addition to having trouble developing capacity; Camp, Hyzak and McDonald thought it would be difficult to fit two layers in the deck thickness. Marx (AK) thought

C-22

that both this and the headed bar detail would be hard to line up. Hartmann was concerned with the legs of the shear key potentially breaking off with this detail as well as in the cases of the other concepts. In addition, he had concerns with potential for fatigue, but was not certain whether that suspicion was justified. Ma indicated that WWR was not allowed in CA; he indicated that it may be a fatigue issue. He mentioned the work of Tadros on WWR, and although CA does not allow it now, manufacturers are pushing it. Marsh (Berger/ABAM) has never been enamored with WWR; it takes two cross wires to develop the tensile wire. Perry thought that it would be better to overlap alternating protruding bars and then drop in longitudinal bars rather than having the perpendicular bars coming from precast sections.

Structural tube detail (5e)

Koch (NC) thought contractors would like this detail the most of all. Marsh thought this detail looked "bomb proof," provided there would be enough space; reflective cracking potential above the steel tube should be investigated. Dick (PCI) also thought the detail looked robust. Hubbard indicated that the detail looked unique and expensive [Hubbard]. Culmo thought the detail was worth consideration. Camp thought that this system required testing to ensure that the transfer of bar forces would be achieved. Perry and Ronald liked the tube detail; the heads on the bars should be large enough. Tang liked the tube detail and suggested an "L-shaped" slot to keep the bars in place, and noted that it would be difficult to place this detail in narrow joints. Sennour liked the tube detail; he thought this mechanical connection looked much better than trying to fit the bars through the loop detail; however tolerance may be an issue. He indicated that because DOTs typically have their own quality control personnel monitoring the fabrication of their products, it may be possible to achieve better tolerances. He indicated that one might expect that ½ to ¾ in. tolerances may be required, whereas for commercial use, attainable tolerances might be on the order of 2 in. A few respondents indicated this detail looked similar to one investigated in 12-65 [Hyzak, Ma].

Dorgan (Mn/DOT) and Bondstedt thought the system looked simple but may have alignment issues; Roberts-Wollman (VATech) and Hartmann (FHWA) were also concerned with alignment/constructability issues. Zendegui thought that this detail should have reinforcement running perpendicular to the tube and was concerned with alignment issues. Johnson liked this detail less than the others. Zeldenrust thought the tube detail would require tight control; it looks interesting, but difficult. McDonald (IADOT) and Nickas (FL) saw potential issues with sloppy field work and tube not filled with grout. Nickas also thought that the system had potential for lots of cracking before it engaged the bars. Russell thought that the detail would work, but if bars the bars were epoxy-coated, the tube would need to be coated. He was concerned with cracking with a whole row of these tubes within the joint. Badie indicated that the tube in Figure 5e looked too thick. Castrodale indicated that the detail may result in reflective cracking with the very stiff spot created by the tube. Bonstedt and Miller thought this system would be expensive and more difficult to place. Prussack did not care for this detail.

C.5.3   Comments on Common Issues of Concern with Connection Concepts

Spalling of lip of joint (5a)

Ronald, Smith, and Tang had concerns that the thin lip of concrete forming the bottom of the joint may spall; Smith stated that construction ease associated with butting the adjacent flanges is not worth the risk. Hartmann was also concerned that the concrete tips might crack off at the bottom of the shear keys in several of the other connection concepts, as well. Hubbard indicated that such spalling does not happen too much and WI would not have fear of it; their biggest concern would be rust prying off the piece. Johnson (SD) and Prussack also did not have a concern with spalling of the tip. Marsh indicated that keyways have performed well in the field. In cases where they have broken, he attributed it to large overloads. He noted that the joints of untopped panels leak occasionally, especially if the grout mix design, joint preparation, or grout placement are not done correctly.

Form below joint in field

A number of respondents indicated that requiring a form below joint in field should be avoided [Hubbard, WI, Prussack, Ronald]. R. Eriksson suggested that forming should be minimized. Ronald stated that anything that requires labor in the field adds cost and is problematic; all important quality control issues should be addressed in the fabricating plant. Ralls suggests minimizing closure joint width. However, rideability is a huge issue (especially for motorcyclists); if joint is 18 in. wide it may be possible to smooth out differences in elevation in adjacent pieces. Russell would like to keep the two interfaces as close together as possible.

C.6   Comments on New Materials

Many states are open to the use of new materials. Camp of NM is open to grouts with fibers, FRP and stainless steel bars. Prussack does not see much motivation for stainless and FRP because he has not seen problems with current systems and the new systems are costly. TXDOT is looking at HPC, corrosion inhibitors, SCC, FRP decks, LWAC [Ralls]. The following is a summary of the comments associated with a number of different proposed new materials.

C.6.1   High Performance Steels (e.g., Stainless Steel, MMFX)

Meinheit (WJE) recommended either epoxy-coated or stainless-steel clad rebar for use in CIP joints in precast decks to minimize or eliminate corrosion problems. He also suggested looking into ZBar stainless steel clad bars (www.gerdauameristeel.com). Volgyi indicated VADOT is leaning toward using stainless steel or MMFX. They have had lots of problems with epoxy-coated bar where the coating debonds. They initially used epoxy-coating on the top mat, but two years after implementation, they used it on both layers. NYDOT uses epoxy coated bar, but galvanized steel or stainless steel are options. Within the last year, NYDOT made change to require both top and bottom mat of steel to be epoxy-coated. Prior to that just the top layer was coated. NYDOT uses stainless steel where there is extra concern about durability

or if longer life is needed, or if where it would be costly to shut down the bridge. AK has used galvanized steel and had discussions regarding stainless clad steel. They are not opposed to trying new materials; the downside is the cost, Nickas concurred. WI has done two stainless clad projects but they needed to get material from England [Hubbard]. MMFX is more locally available. Stainless or MMFX may be more acceptable than FRP because they fit with current code requirements [Hubbard]. Castrodale thought both stainless steel and MMFX were reasonable options. Culmo, McDonald (IADOT), Koch (NC), and Johnson (SDDOT) were concerned with cost of stainless steel; McDonald and Tadros were also concerned with the lack of ductility of MMFX. Although Bonstedt indicated that he did not have much experience with stainless steel bars, he thought they would be harder to bend. He recommended investigating new materials to target 100 year design life. With current conventional materials (e.g., epoxy coated bars, HPC, SCC, etc.) may only be able to get 60-70 yr. life. Culmo had issues with the cost of these materials. Russell thought that stainless steel would be a good material to try. Zeldenrust (WSDOT) was not opposed to stainless steel or A706. Scott (NH) likes stainless steel, but has not seen recent cost estimates. Dick would consider stainless steel but indicated cracks would still be a problem in the long term for freeze-thaw issues. Ericson (Splice Sleeve North America) indicated that with stainless steel clad, roller is shallow and rounded which affects development in a deleterious way. Eriksson indicated that stainless steel has high elongations and suggested looking at Pfeiffer's research from WJE. Hawkins indicated that it was a good idea to use new materials (e.g., stainless steel or MMFX). The FHWA IBRC program enables innovative things and one of the most common has involved use of stainless steel. Ronald did not think that stainless steel was necessary for this project. The introduction of stainless steel would mean the problem is unique to this specific precast system; as such it would not be a good job of emulation.

Dissimilar metals

In exploring the possibility of using stainless steel to achieve tighter bend radii or using the tube detail for the connection, several respondents raised concern that the use of dissimilar metals in the system could lead to the promotion of corrosion cells. The following is a brief summary of the comments. Meinheit (WJE) and Russell cautioned about the use of dissimilar metals as there would be danger of setting up a corrosion cell. Tadros stated dissimilar metals should be avoided. WI would have a concern with dissimilar metals [Hubbard]; they had a problem with single top layer of epoxy bars corroding. Ericson with Splice Sleeve North America would not recommend combining dissimilar metals because of the potential for a galvanic reaction. MacDonald indicated that when dissimilar metals are in contact it causes a problem; he indicated that if they were not in contact, he did not think it would be a problem. Schokker also commented on the potential to develop corrosion cells when using dissimilar materials in the joint (i.e., grout) with respect to the adjacent precast concrete panels; this is discussed further in Section C.6.3.

C.6.2 Fiber Reinforced Polymer (FRP) Reinforcement

Bhide recommended looking at nonmetallic reinforcement in the systems. Russell thought that FRP was worth looking into but was unsure about the ability to bend it. WI is very interested in FRP. They have used grids and bars [Hubbard]. In NC there are two regions where corrosion is a concern, and in those regions, GFRP has given them good results. They have also used FRP wrap, but it is difficult for the inspectors to know what to look for in those cases. FRP is an option for SD, however they have not had much experience with it yet. Eriksson thinks FRPs are an option even though they are more expensive. Sometimes contractors just need to get used to new materials and with experience they may be strong proponents. Scott (NH) indicated that NH has built a bridge sing FRP grids made by Autocon in Ontario. Goodspeed oversaw the design, the deck is bare and there is no cracking; he indicated that "the bridge is beautiful." He also noted that Goodspeed considered using epoxy in the joints on the project. TX has built bridges with FRP structural members and reinforcement; Hyzak expressed concerns with cost and flexibility. Culmo also had issues with the cost.

Blaszak with TechFab is a structural engineer with many years of experience with FRP. He recommended considering FRP grid in place of WWR detail (5d). Advantages of the FRP include reduced cover and good crack control. He does not believe FRPs would be an option for the loop bar detail (5a).

Dick would consider FRPs but as the case for stainless steel, he indicated cracks would still be a problem in the long term for freeze-thaw issues. Castrodale indicated that FRP may have stiffness issues. Oliva concurred. Upon cracking, FRP bars tend to be "softer" due to the reduced modulus. As a consequence there is likely to be more deterioration at the cracks with these bars [Oliva]. Flynn (NY) is interested in FRP, however the system cannot be designed in the same way. Because of the brittle nature of FRP, there is not a one-for-one swap with conventional rebar. Hartmann was concerned with out-of-plane distortion of FRP and fatigue. Marsh thought that the joints would not be wide enough to accommodate the development of FRP.

Henderson and Sletten did not think that any of the connection details proposed looked like potential candidates for using FRP. They believe that the emphasis should be on grout materials. Sennour (CEG) strongly believed in exploring FRP for reinforcement—it is the way of the future.

C.6.3 Grouts

This section summarizes comments on materials to use within the connection regions. Most of the comments were on grouts, however, Badie and others also recommend investigating the use of ultra high performance concrete (UHPC) to reduce the development length of the reinforcement in the joints. Smith indicated that HPC was a good idea, but stated that it would not work for overnight construction. Smith also noted that it is not desirable to have a large percentage of deck area made with grout as it is difficult to get it done right and achieve good durability; therefore, minimize the use of grout. Ronald indicated that grout materials must be cost effective. The girder haunch material must be pumped in place and consequently needs a long pot life and must be flowable. New cementitious grouts (still very expensive) are being developed for PT that are just short of going to zero slump concrete.

C-26

Gulyas (former chair of ACI 223 Shrinkage-Compensating Concrete) has had a great deal of experience with grouts and epoxies including magnesium ammonium phosphate. Because something is called "nonshrink" does not mean it will not change dimension. Nonshrink grouts are evaluated in a sealed environment and "nonshrink" refers to the grout not undergoing settlement issues where water and vapor rise to the top and cause shortening. "Nonshrink" grouts are still susceptible to drying shrinkage. Cementitious grouts must be kept continuously wet to keep them from shrinking which is impossible. The use of less Portland cement and more aggregate is desirable, but it still does not stop shrinkage. Gulyas indicated one means of reducing the amount of shrinkage is to control the rate and amount of ettringite formed. Gulyas also mentioned interaction of reinforcement and grout related to restraint issues. Grout materials that do not shrink (as opposed to Portland cement grouts) include magnesium phosphate. It is a rapid set grout and can be used over a wide range of temperatures. If magnesium phosphate is used, surface preparation is very important (i.e., cannot have carbonation at interface). Some concern was expressed with the pot life of magnesium phosphate [Hyzak]. It may be sensitive to proportioning and mix temperature. Contractors may wish to work with grouts that are more forgiving (e.g., nonshrink cementitious grouts).

Ericson with Splice Sleeve of North America indicated that if the grout layer is small (~½ in. to ¾ in.), sand would be used in the system and in the case of coupling columns, the grout layer is required to be ~2ksi stronger than the connecting elements. If the grout layer is thicker (e.g., 2 to 4 in.) pea gravel would be used in the mix. In Badie's project, they are using Dayton Superior product (SS mortar) similar to that used in NMB Splice Sleeve. With this high performance grout they are able to reduce the anchorage lengths of their connection reinforcement. They estimate development lengths using ACI 318-05 equations assuming confined concrete compressive strengths.

To avoid cracking in grout, MacDonald recommended maximizing the use of fly ash or slag. With the use of these materials, he indicated that cracks that would occur due to shrinkage could be plugged or would self-heal. Grout specifications should include a limitation on shrinkage (0.025 percent grout) or w/c max (0.220-0.225). He also indicated that there are a number of effective, but expensive, shrinkage reducing admixtures that reduce the surface tension of the water and thus reduce shrinkage. MacDonald proposed another option of filling the joints with an expansive material like Type A cement and add fiber to provide restraint. There is a 40 year track record of its use. Organic VMAs stabilize bleeding on a microscopic scale and have good results with reducing shrinkage. Tests to consider include ASTM C157 for shrinkage or ASTM C845 for expansive materials. Also look at permeability of the materials without fibers. Consider also freeze-thaw testing (although, if air entrained, it should not be a problem). Other materials to consider include self consolidating concrete (perform both U-box and L-box, filling and passing ability tests, respectively).

Meinheit (WJE) developed specifications for the concrete mix used in the Wacker Driver reconstruction in Chicago. The role of WJE included designing the specifications for the concrete, conducting QC testing of the concrete during placement, and developing a method for fogging and blanketing after placement. The mix is a dense quaternary cementitious mix to avoid problems with freeze-thaw deterioration and alkali aggregate reactivity. He supports the use of shrinkage-compensated grouts (or grouts with controlled expansion). An alternative is to pre-place the aggregate and then pump the grout; in this case mechanical interlock between aggregate particles prevents global shrinkage. Fibers in the grout may

also be an option. Meinheit strongly cautions against using grouts with significantly different properties from the adjacent precast concrete (e.g., modulus of elasticity); however, he sees advantages to polymer modified grouts because they provide better bond to hardened concrete surfaces.

Miller stated epoxy grout is not thermally compatible with the girder and will start peeling off the end of the girder. Another problem is a chemical solvent (e.g., Methyl ethyl ketone (MEK)) is needed to clean grout off surfaces, which may create personal and environmental safety concerns. Miller has used every type of non-shrink grout available, some bridges get cracking, some do not. His experience with nonshrink grout leads him to believe that non-shrink grout is rarely placed correctly. ODOT has had problems with placement of grout. Just because it comes in a bag does not mean it is easy to use. He suggests using a grout mix that can be delivered in a ready mix truck.

Perry described the advantages of the Ductal system which is a high strength ultra high performance concrete. It might be used to reduce the joint widths. Ductal can also be dyed to any color to match precast systems. Perry indicated that is also good in seismic performance. It is strong and has shown good results in fatigue tests. Roberts-Wollman indicated that Ductal shrinks a lot; she indicated that using Ductal with FRP is a possibility.

Regarding fibers in the grouts, Gulyas indicated that they tend to stick up and are not great for tires as concrete wears away. He suggested putting on metallic "dry shake" and troweling surface to bury the fibers. Marx (AK) indicated that fibers would not help resist a crack that would form at the interface between the grout and the precast.

AK has used high performance prepacked nonshrink grouts including Set 45 [Marx]. They have also used epoxy-based grout supplied by ThermalChem. Flynn (NY) indicated that they use corrosion inhibitors (e.g., calcium nitrate in their grouts). They also seal the system with silane sealers. It is difficult to stop the closure pours from cracking, but they have had some success with a nonshrink grout with an elastomeric seal on top. Preventing moisture from getting into the grout has helped a lot. ThermalChem has experience in producing grouts (e.g., Product 3). By their very nature of being epoxy (i.e., nonhydrating material) they do not shrink. Product 3 also has a higher compressive and tensile strength than concrete. The biggest issue is the potential difference in coefficient of thermal expansion between the grout and adjacent material. This difference can cause the concrete to break around patches. They recommend mixing sand with the epoxy. A pourable system is a 4½ :1 ratio by weight (sand:epoxy). Temperatures can play havoc with the viscosity.

Prussack indicated owner/agency handles grout specifications. He provides input along the lines of ASBI or provides specifications if asked (e.g., require high quality, prepackaged, non-shrink grout, with specified minimum strength of 4ksi and 5-6ksi as desirable range). They used to add aluminum powder (~2tsp) which provided non-shrink grout characteristics due to gaseous reaction of aluminum powder. Prussack indicates that non-shrink grouts today are vastly superior.

Roberts-Wollman did research on grouts. They constructed 12x12x4 in. thick slabs with hole in middle filled with grout. The surface of the hole was moistened before filling with grout. The slabs were ponded regularly and after 6 mos., four of eight joints had cracks and started leaking. She did not necessarily think the problem was associated with shrinkage or cohesion. She suggested trying grout with pea

C-28

gravel instead of cement material. Adding fibers to the grout might help reduce cracking at places other than the interface. High flowability of the grout is sometimes important.

Schokker stated that CIP must have similar properties to precast or a corrosion cell could be created. If the joint is more durable than precast and salts and water permeate the precast, major corrosion problems can occur. She stated that polymer or epoxy grouts should be avoided and suggested reviewing repair literature on polymer and epoxy grouts. Schokker recommended investigating different grout materials to show different consequences of not using durable materials. She also thought that freeze-thaw issues should probably be examined. High flowability grout may be needed. If corrosion/durability test procedures are proposed for use in the project, Schokker expressed willingness to review the proposed tests. Schokker indicated that expansive grouts should be investigated to counteract settlement, but indicated that if it is an additive, rather than bagged material, caution and high degree of quality control would be needed at site.

Sennour believed in exploring high strength grouts; he thought it would be desirable to move the potential for cracking out of the joint region and into the concrete (consider two part sand to one part epoxy). Regular grout makes the joint the weak zone. Also consider shrinkage compensating or nonshrink grout that is Portland cement based.

Shape of keyway A number of respondents commented on the importance of the shape of the keyway. Hyzak indicated the keyway shape shown in Figure C.6.1 would be effective in accommodating the transmission of compression struts across the joint. Marsh indicated that larger loads may require a sawtooth connection which could engage more struts. Tang was concerned with the shape of the keyway with the Japanese detail (5a). He suggested using a straight edge for the keyway with a grooved interface.
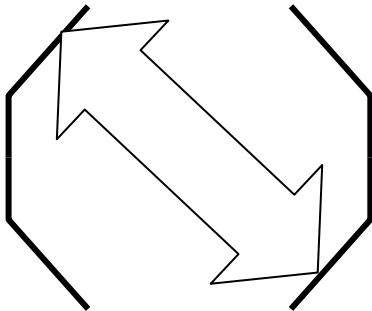
Figure C.6.1: Effective shape of keyway

Miller indicated that through FEM, he determined that full-depth shear keys are better than partial depth shear keys. For full-depth keys, the principle stress under load becomes longitudinal, while for a partial depth shear key, it becomes transverse. Ideally, Miller stated that a shear key would not be

poured all the way to the top, but would have a sealant on top; however, this then becomes a maintenance issue. Kaufman's suggestion was to provide a ¾ in. chamfer, then a minimum 1 in. vertical, then start the shear key. Bhide indicated that the project should investigate whether there was a significant advantage to wider CIP joints as opposed to traditional female-female shear pocket grouted joints.

Preparation of joint prior to grouting

Nickas (FL) indicated that when replacing an old concrete deck, it is so dry, it drains the moisture from the new concrete. Consequently they require 4 hours of soaking before new deck is placed on top. On precast SIP, they require 12 hours of sprinkling with soaker hoses prior to placing the CIP.

In TX, they usually pressure wash rather than sand blast the joints. They get the precast surface saturated surface dry (SSD) prior to grouting or use appropriate bonding agents [Hyzak]. Gulyas mentioned that hardened concrete should be presoaked or surface should be coated with epoxy (on dry concrete) so water cannot leave grout into the hardened material. If this procedure is not followed could experience curling. If epoxy is used, the epoxy should not be "too cured" prior to placement or could exacerbate formation of a crack. Good bond and well distributed reinforcement will distribute the stresses and control cracking.

Prussack (Central Pre-Mix Prestress) emphasized the importance of surface preparation. Before a precast element leaves the plant, the outer surfaces (where form was attached) are sandblasted to remove surface paste and to create a texture for enhancement of bond. The precast is brought to SSD before grouting. The grout is then poured and cured with spray film or wet burlap. Prussack was not convinced that magnesium phosphate grouts work that much better than regular Portland cement based grout. The magnesium phosphate grout is more tolerant of cold weather and cures and sets faster—so it has an advantage in situations where bridge would have to otherwise be heated.

MacDonald indicated that as long as the precast is clean, the CIP should bond with the precast. Sandblasting is good, but preferred close to time of placement of CIP. Wetting the surface without standing water is also effective. Culmo recommended sandblasting the keyways ahead of time and only using prepackaged grouts. Grafton (Pomeroy) indicated the shear key is sandblasted in the plant to take off form residue.

Curing

Keeping the time between casting and curing short to alleviate shrinkage was recommended. Hyzak also commented that raking the surface increases the surface area which causes even great moisture loss.

Grinding

In FL and TX, sections are made ½ in. thicker to accommodate grinding. Hubbard indicated that approximately ¼ in. should be ground from surface to accommodate roadways with faster speeds;

C-30

rideability would be problem without grinding. Koch (NC) prefers adding ½ in. extra cover to facilitate grinding, than adding asphalt. Grinding is not a problem, they typically grind and prior to putting on an overlay. Smith and Tadros did not have a problem with grinding. Tadros preferred it to CIP. Roberts-Wollman indicated that grinding and grooving are doable alternatives to overlays.

WSDOT does not consider grinding an option because of reduction in potential cover. Dick suggested providing a surface that does not require grinding. Ralls also suggested avoiding grinding; it is done a lot in TX and is acceptable as long as extra cover is provided.

C.7   Other Issues of Concern Related to Development of Connection Concepts

This section summarizes additional comments that were provided related to the investigation of connection concepts. Some of the comments that were provided were general in nature. The following sections present the additional comments that are grouped into categories including differential camber, rideability, deck thickness, two layers of reinforcement, and skew. This is followed by a section of the more general comments.

C.7.1   Differential Camber

Bhide and Tang expressed concern with differential camber between pieces. Composite decks are used in PA to deal with any differential alignment issues; Bonstedt does not favor varying flange thicknesses to accommodate superelevations or connections at joints. R. Eriksson indicated that CIP overlays can cure a lot of problems such as differential cambers and cross slopes. Ronald indicated that in the case of differential camber, a haunch should be used on the girder. He thought the flange-to-flange system had too many drawbacks including the potential camber differential. Seigurant concurred that differential camber was the most concerning issue with respect to decked bulb-T construction.

Koch (NC) did not think differential camber was much of a problem, but NC was wary about it. They installed inserts in the center of the girders at mid-span so that they could pull/pushdown the beams to match the panels. Smith in discussing tolerances indicated that joints ≥12 in. wide can also make up difference in camber, in addition grinding can be done if necessary.

C.7.2   Superelevation

Tang believes that proposed systems need to provide a means to accommodate crown and superelevation. Smith stated that for transverse panels, superelevation needs to be accommodated in a single plane. Thickening the deck is a "slippery slope." It is not desirable for the bottom form to be on a different plane than the top plane.

C.7.3   Rideability

Rideability is an important issue for FL, NH, PA, and VA. Contractors are penalized in PA if the surface does not meet the International Roughness Index (IRI). Contractors sometimes need to grind even CIP

decks to meet contract obligations. Castrodale indicated that the ability to remove differential camber is important to rideability. Koch (NC) stated that PT and segmental bridges have lots of problems with rideability. Ronald indicated another drawback to the bulb-T, besides differential camber, is the complication associated with trying to achieve a smooth ride (e.g., profiling the surface of the bulb-T is heading in the wrong direction). Zendegui concurred that good rideability was difficult to achieve with deck bulb-Ts, but noted that the PD system would have good Rideability. NH prefers not to use bare decks [Scott]; however maintenance crews prefer them.

C.7.4   Deck thickness

The range in deck thicknesses commonly used in the different states varied. A few of the respondents provided information on the common deck thicknesses they use. CA uses 6.5 to 8 in. decks with a 1 to 3 in. asphalt overlay. FL uses a minimum of 8 ½ in. deck for CIP. MN uses 8 to 9 in. deck. PA always uses a composite deck, sometimes with SIP forms. The deck thickness is 6 to 8 in. depending on girder spacing. Zeldenrust (WSDOT) prefers a 7½ in. deck and expressed concern that some of the proposed connection concepts looked like they may require 10 to 11 in. thick decks. Eriksson (USFS) uses minimum deck thickness of 6 ½ in. including the ½ in. wearing course. For larger loads (i.e., U80) the deck is ½ in. thicker.

A related issue is concrete cover (also see Section 3.6.3 for comments on grinding). For untopped panels, Marsh stated that it is desirable to have generous cover. Prussack indicated cover was traditionally 2 to 2 ½ in. on precast elements.

C.7.5   Two layers of reinforcement in joint

Regarding the ability to emulate CIP and to transfer moment effectively through the joint, several respondents commented on the issue of two layers of reinforcement in the joint. Johnson (SD) thought one would be fine, two would be better. Marsh (Berger/ABAM) thought that a single layer of steel for shear transfer is adequate, but he recommended two layers of steel for crack control and durability. In the case of a single layer of steel, if the joint is located over the web (e.g. precast deck panels with longitudinal joints), the single layer of steel should be skewed upward to provide negative moment capacity. Russell preferred two layers of reinforcement in the joint for bending resistance rather than a single layer near the middle. Prussack thought it may be difficult to get two layers of steel into many of the proposed details.

C.7.6   Skew

Some respondents indicated that connection concepts considered should be able to accommodate up to 30 degree skew; 90 percent of the bridges in FL have skews less than 30 degree. Hartmann concurred that skews up to 30 degree should be readily accommodated by the systems; he suggested that the panels be aligned normal to the beams and adjusted at the ends with special panels. Koch suggested investigating skews up to 45 degree. Tang recommended considering accommodating skews up to 15 to

20 degree; he indicated consideration should be given regarding how to place/connect panels (i.e., parallel to skew or use trapezoidal sections at ends). Curved bridges should be avoided.

C.7.7 General Comments

This section contains a number of general comments which did not fit into a specific category. They are organized here in alphabetical order of the respondents surveyed.

Bhide thought that companion monolithic tests should be considered to validate the performance of the emulative systems. Marsh believed that it is more important to look in detail at new emulative systems rather than testing companion CIP systems. Need to define loads to be transferred, look at concentrated wheel effects. Also need tests for shear strength transfer in plane.

Bhide also mentioned that issues related to design/detailing/construction of nonsymmetrical end pieces with integral crash barriers should be considered.

Bondstedt indicated that one of the biggest problems with these precast systems is the crash barrier. There was a fatality in PA when a parapet broke off the bridge. If proposed systems do not corrode, can handle skew and superelevations, they would be sellable to PA DOT. Bonstedt also commented that there are regional issues to consider. In NE labor is expensive relative to materials, whereas in SW situation may be the opposite. For NE, innovations should be made on the precast elements to save labor in the field (and plant if possible).

Chandra recommended the use of STM modeling to develop the details. He also recommended studying additional connections including foundation or pile connections to precast slab and column to cap connections. The investigation should also include a number of different ways of avoiding reflective cracking; ways of improving durability (e.g., SCC); different types of reinforcement; admixtures for precast and CIP closure joint to help with durability. He also indicated that in the past he had a problem with a microsilica overlay because the material had a higher modulus than the deck concrete; this was a problem in a long span structure where compression was introduced into the deck. Chandra also indicated the effect of traffic vibrations on green concrete may be of concern.

Henderson and Sletten emphasized the importance of keeping water from collecting which would cause premature deterioration.

Issa indicated that contractors do not like composite systems because they cannot make as much money when part of the cost of the project goes to the precaster, they prefer CIP.

Khalegi of WSDOT suggests using anchor bars to fabricate system without protruding bars.

MacDonald recommended considering performing a test of the bond between the concrete and the grout.

Marsh recommended STM method for evaluating force transfer though the connection (see his comments on individual survey contained in Appendix B). He suggested that it may be possible to use a shear friction connection to transfer the shear in the connections; consequently, just need something to hold the joint together (i.e., compression from the diaphragm action or tension steel across the joint).

C-33

Ralls indicated UTDOT will use a new system as long as the cost does not exceed 30 percent more than the conventional method. IBRC/IBRD funds are a way to get innovative projects built. TX is interested in developing a system that can be constructed quickly with tolerance for camber mismatch. Their main concern is with durability.

Russell suggested casting some of the specimens outside to investigate temperature effects on the joints.

Schokker recommended investigating durability as it is a key issue. She indicated that good standard durability tests do not exist, but she recommended ponding saltwater on key connection details.

Other issues that should be considered include those that drive the prices of precast include lifting weights and volume of use. McDonald, Tadros and several others strongly advocated for saving time in the field and doing most of work in precast plant.

C.8   Issues to be Considered in Development of Guidelines

This section summarizes some of the comments related to design issues and the development of guidelines. It includes general comments for consideration, as well as specific comments on issues such as restraint moments and bursting reinforcement requirements.

C.8.1   General Comments for Consideration

Eriksson recommends the use of detailed FEM models and STM calibrated with measurements to determine the capacity of the details. Simple rules for design (e.g., formulas, table) should be developed. Geometry will not vary much, so STM can be used for a parametric study to develop simple guidelines for practical design.

Grafton (Pomeroy) suggested developing a catalog of standard details with provided design methodology.

Hyzak suggested that an empirical method be provided for design. Once settled on a detail, it is convenient to apply it from project to project. Prescriptive specifications are desirable until achieve a comfort level with new systems [Hubbard].

Hartmann suggested relooking at bursting steel requirements for appropriateness. Also look at developing crack width limitations.

Koch (NC) gave an example of useful specifications for full-depth precast deck slabs PT together. FHWA website provides prescriptive guidance on grouting and PT. Koch found this information helpful.

Meinheit recommended that the selection and design of precast should strive for crack free superstructures for which the most effective technique is PT. As an alternative, cracks can be maintained tightly closed if sufficient reinforcing steel crosses potential crack surfaces. He recommends steel reinforcement twice the ACI (318-08) recommended minimums (i.e., at least twice 0.0018*Ag). This amount keeps cracks closed tight enough to minimize moisture penetration. Any cracks that form could be "self-repaired" by formation of calcium carbonate within the crack.

C-34

Ronald identified road blocks in the code to getting precast deck systems to be economical. These include AASHTO recommendations for cohesion and shear friction mechanisms for load transfer across the panel (e.g., shear studs placed at less than 2 ft. on center). In a bulb-T system with a 4 to 5 ft. wide flange, shear studs are not needed except at the ends where the rate of change of moment is high (i.e., maybe last 10 ft. of span) where shear is high. Other road blocks can be avoided by applying provisions of the code to a system that works. Areas where the code needs clarification includes required PT force between panels (e.g., 250 psi) to keep the joints from separating. An analysis should be done to determine if this amount of PT is necessary. In the case of joints that span transversely, the 250 psi may not be appropriate particularly where tension occurs. A 10 psi tension may not detrimentally affect the monolithic nature of the joint.

Russell did not think that any specification covered the proposed systems adequately. The material obtained from this study would be useful in any format including AASHTO bridge specification, guide specification or guideline/drawing. He also recommended the development of a catalog of details as a starting point with suggestions for innovative opportunities. For initial installations, guidance on acceptable span lengths, specific requirements, are needed.

Sennour stated that the main problem with bridge deck systems is that DOTs have gone to a "one design fits all" system (i.e., there is no variation in deck associated with different girder spacings). This limits the allowable girder spacing that can be used; girder spacing, deck thickness and strand number could be optimized to save money.

Smith stated that guidelines on tolerances need to be developed. In addition, the design and bending capacity of decks connected with details such as the loop bar detail need to be determined.

Tang suggested developing a catalog of 2-3 acceptable, standardized details. Provide a couple of options to deal with each different design situation. Try to eliminate interior joints on the deck, consider systems that are integral or semi-integral.

Tadros indicated that there are specifications available for similar systems; however, they need improvement. Depending on the specification used (e.g., AASHTO Standard/LRFD, Ontario) different amounts of longitudinal steel are needed in the deck. Determine whether or not reinforcement needs to be distributed all over, is 250 psi minimum PT required, does shrinkage and temperature steel need to be distributed, is it additive to other reinforcement, etc.

C.8.2   Restraint moments

Restraint moments are an issue where CIP is cast onto a precast section. The moments are generated due to the differential movements (i.e., shrinkage and creep) between the composite materials. Hawkins said this issue was regional (e.g., Western Washington this is not a problem because of the moderate moist environment. Ma (CA) and Tang thought that restraint moments would not be a problem for shorter spans (i.e., situations where the PD system would be used).

Oliva and Tang suggested specifying age of precast to avoid problems with restraint moments; Tang suggested 30 days as an example. Tadros also thought a waiting period would be ideal; otherwise he suggested that empirical details be developed rather than requiring calculations to deal with restrain

moment issues. Castrodale mentioned Miller's NCHRP project (5-19) which included investigation of restraint moments. Miller's work indicates that if a member is aged to 90 days, there is not an issue with restraint moments; whereas if the member is younger than 90 days, the designer needs to calculate restraint moments (see NCHRP 12-53). In AK sections sit for at least 90 days or more (sometimes 9 mos.) so restraint moments have not been a problem. AK is a zero tension state. If continuity for live load does not occur, they allow 3 to $6\sqrt{f'_c}$ tension. Grafton thought that restraint moment issues could be avoided with letting the product age (7 days is too young, 90 days is excessive and would hurt the industry). Prussack concurred. He indicated most jobs are only 90 days from design to finish. Need a more forgiving option than waiting 90 days. NYDOT requires precast beams to be in storage for a minimum of 60 days prior to placement. They also use HPC for its qualities of lower shrinkage and creep.

IADOT mainly uses prestressed beams with CIP pier diaphragms and restraint moments have not been an issue. Khalegi of WSDOT suggests extending strands into diaphragms to accommodate restraint moments (also helps for moment reversals due to seismic loading). WI has not considered restraint moments nor have they been concerned with restraint moment issues until 3-4 years ago with likelihood of change in specifications resulting from U of Cincinnati [Hubbard]. Systems (other than steel bridges) designed in TX as simply-supported, therefore they are not concerned with restraint moments [Hyzak]. R. Eriksson recommended addressing restraint moment issues and their transmission along the longitudinal joints. Consider using strands to establish resistance. Nickas prefers a simple solution (e.g., putting in reinforcement for worst case).

C.8.3   Bursting

Hawkins indicated that shear stresses being developed at end of beam need to be considered with respect to the development of bursting stresses. Sennour and Tadros saw no problem with bursting steel in deck panels. Culmo indicated that bursting is an area that could be addressed in AASHTO. Current requirements do not make sense for box beams or PD system, Oliva and Roberts-Wollman concurred. AK follows AASHTO Section 1301 which requires 4 percent reinforcement and 20 ksi. STM is used to model anchor regions. Tang stated that current specifications require too much reinforcement. This should be studied and reduced for appropriate situations. IA DOT uses debonded strands at ends of inverted T's WI has not had problems [Hubbard]. WSDOT submitted a change to AASHTO relating to bursting steel requirements for a slab on a U-shaped member.

C.8.4   Color between Joint and Precast

Some of the respondents indicated that joints between the precast elements might create a driving hazard because drivers may tend to follow joint lines rather than striping. This section summarizes some of the comments on this issue.

AK has not had a problem with joint lines. Koch, Smith, and Tang also did not see any drivers following joint lines as a major issue. Prussack indicated that he had never considered joints as confusing to drivers on well-traveled roads especially because of presence of fog lines and reflectors on busy roads. It does not seem that this has been an issue in Japan. Also deck surface may discolor from normal oils, etc.

In TX, they carefully tried to address color difference between grout and precast in Waco bridge. They were not successful. The color mismatch is noticeable and adversely affects safety—it may be necessary to use an asphalt overlay [Hyzak]. Falhalla concurred that it is important to require a uniform color so that drivers do not get confused. NB has required overlays so the appearance would be uniform, but would prefer being able to achieve a uniform appearance without an overlay. Falhalla thought it may be reasonable to strategically place the joints. Gulyas stated that grout will not match color of concrete but brooming in same direction as precast may help to hide the difference. In WS, drivers following grout joints rather than roadway striping is a concern. Falhalla of NB indicated that it is especially a problem in longer bridges. Hartmann concurred that he has heard of problems with drivers following joints, but he believes that it should be dealt with by others (e.g., DOTs). McDonald (IADOT) thought issue of joint lines confusing drivers was a minor issue. Bhide indicated that matching the joint color with the precast so the systems do not appear jointed should be added as a criterion (see above). Chandra also preferred matching the colors of the CIP to the precast. Mn/DOT has used overlays so this has not been an issue, Dorgan indicated that getting the precast system and grout to match would be ideal. Ma discourages the promotion of untopped diaphragms. He believes that it makes it difficult to distinguish lane lines. Sometimes decks are ground, but Ma prefers topping.

Appendix D

Center City Field Bridge Instrumentation Designation, Nominal, and Measured Locations

The instrumentation in the Center City Bridge was documented in MnDOT Report 2006-37 (Bell et al. 2006). However, the instrument locations given were nominal, and the measured instrument locations are given in Table D.1. The measurements that differed from the MnDOT report are highlighted, italicized, and bold. The instrument designation convention is given in Figure D.1. The origin and sign convention of the strain gage measurements is given in Figure D.2. Web #1 was located between Joints #1 and 2, and Web #2 was located between Joints #2 and 3. The center of Joints 1, 2, and 3 were located at 128.5, 200.5 and 272.2 in., respectively from the parapet (i.e., measured distance "Y" in Figure D.1).

Type of VW Strain Gage:
➢C = VW Embedment Strain Gage (Concrete)
➢S = VW Spot-weldable Strain Gage (Steel Reinforcement)

Location of Gage (Longitudinal):
➢1 = Adjacent to E Abutment
➢2 = Midspan of E Span
➢3 = Eastern Side of E Pier Cap
➢C = Center of E Pier Cap
➢ 4 = Western Side of E Pier Cap
➢5 = Midspan of Center Span

Location of Gage (Transverse):
Indicates the number of the gage at that location (longitudinal) of the bridge and height (within depth of cross section). Numbering increases from south to north.

CJ1-51-1

Proximity of Gage:
➢J# = Gage is installed above Longitudinal Joint
    ➢1 = Long. Joint #1
    ➢2 = Long. Joint #2
    ➢3 = Long. Joint #3
➢W# = Gage is installed above Web of a Precast Section
    ➢1 = Web #1
    ➢2 = Web #2

Location of Gage (Within Depth of the Cross Section):
"C" Gages-
➢1 = Directly Above Long. Joint
➢2 = Above Precast Section Web Corners
"S" Gages-
➢T = Transverse Hook
➢1 = Bottom Long. R/F of R/F Cage
➢2 = Top Long. R/F of R/F Cage
➢3 = Long. Deck R/F

Figure D.1: Center City Bridge instrumentation designation

D-1
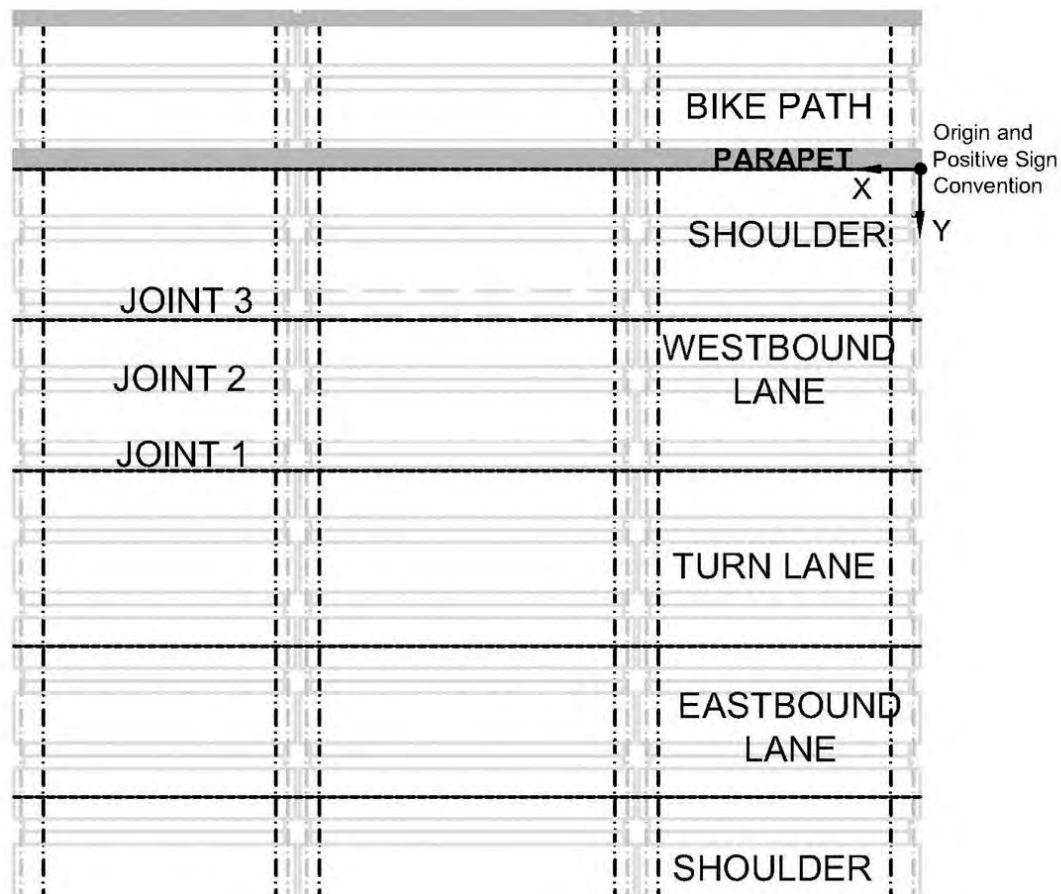
Figure D.2: Center City Bridge measurement origin and sign convention

Table D.1: Nominal and measured locations of longitudinal spot-weldable strain gages in the Center City Bridge

Instrument	Nominal (Mn/DOT 2006-37)			Measured		
	X	Y	Z	X	Y	Z
SJ1-51-1	429	264	9	429.00	*263.25*	*8.75*
SJ1-52-1	429	264	12.5	429.00	*263.25*	*12.00*
SJ1-53-1	427.5	276.5	15.5	427.50	*276.25*	*15.00*
SJ1-53-2	427.5	263.5	15.5	427.50	*264.50*	*15.00*
SJ1-41-1	290	268.5	9	290.00	*268.75*	9.00
SJ1-43-1	290	280	15.5	290.00	280.00	*15.00*
SJ1-43-2	290	268.5	15.5	290.00	268.50	*15.00*
SJ1-C1-1	271	268.5	9	271.00	*269.50*	9.00
SJ1-C3-1	271	268.5	15.5	271.00	268.50	*14.00*
SJ1-C3-2	271	296	15.5	271.00	296.00	*14.00*
SJ1-31-1	252	268.5	9	252.00	268.50	9.00
SJ1-33-1	251	280	15.5	*250.00*	280.00	*15.00*
SJ1-33-2	250	269.5	15.5	*249.00*	269.50	*15.00*
SJ1-21-1	128.5	264	9	128.50	264.00	9.00
SJ1-22-1	128.5	264	12.5	128.50	264.00	*13.00*
SJ1-23-1	130	261.5	15.5	130.00	261.50	15.50
SJ1-11-1	22	264	9	22.00	*264.25*	9.00
SJ1-12-1	22	264	12.5	22.00	*264.25*	*13.00*
SJ1-13-1	21	261.5	15.5	21.00	261.50	15.50
SJ2-51-1	427.5	192	9	427.50	*191.50*	9.00
SJ2-52-1	427.5	192	12.5	427.50	*191.50*	12.50
SJ2-53-1	426.5	193.5	15.5	426.50	193.50	*14.75*
SJ2-41-1	289.5	198	9	289.50	*198.25*	9.00
SJ2-43-1	291.5	197	15.5	291.50	197.00	*15.25*
SJ3-41-1	287	124.5	9	*287.50*	124.50	9.00
SJ3-43-1	286	124	15.5	*285.00*	124.00	*15.00*
SW1-43-1	292.5	249.5	15.5	292.50	249.50	*14.50*
SW1-43-2	292.5	236	15.5	292.50	236.00	*14.50*
SW1-43-3	292.5	225	15.5	*292.00*	225.00	*14.50*
SW2-43-1	291	177.5	15.5	*291.50*	*177.75*	*14.50*
SW2-43-2	291	165.5	15.5	291.00	165.50	*14.50*
SW2-43-3	291	154.5	15.5	291.00	*154.25*	*14.50*

D-3

Table D.2: Nominal and measured locations of transverse spot-weldable strain gages in the Center City Bridge

Instrument	Nominal (Mn/DOT 2006-37)			Measured		
	X	Y	Z	X	Y	Z
SJ1-5T-1	434	278.5	7	434.00	278.50	7.00
SJ1-5T-2	432.5	276.5	7	*432.25*	276.50	7.00
SJ1-5T-3	434	274.5	7	434.00	274.50	7.00
SJ1-5T-4	432.5	272.5	7	*432.25*	272.50	7.00
SJ1-5T-5	434	270.5	7	434.00	270.50	7.00
SJ1-5T-6	432.5	268.5	7	*432.25*	268.50	7.00
SJ1-5T-7	434	266.5	7	434.00	266.50	7.00
SJ2-5T-1	434	206.5	7	434.00	206.50	7.00
SJ2-5T-2	432.5	204.5	7	*433.00*	204.50	7.00
SJ2-5T-3	434	202.5	7	434.00	202.50	7.00
SJ2-5T-4	432.5	200.5	7	*433.00*	200.50	7.00
SJ2-5T-5	434	198.5	7	434.00	198.50	7.00
SJ2-5T-6	432.5	196.5	7	*433.00*	196.50	7.00
SJ2-5T-7	434	194.5	7	434.00	194.50	7.00
SJ3-5T-1	434	134.5	7	434.00	134.50	7.00
SJ3-5T-2	432.5	132.5	7	432.50	132.50	7.00
SJ3-5T-3	434	130.5	7	434.00	130.50	7.00
SJ3-5T-4	432.5	128.5	7	432.50	128.50	7.00
SJ3-5T-5	434	126.5	7	434.00	126.50	7.00
SJ3-5T-6	432.5	124.5	7	432.50	124.50	7.00
SJ3-5T-7	434	122.5	7	434.00	122.50	7.00

Table D.3: Nominal and measured locations of transverse concrete embedment strain gages in the Center City Bridge

Instrument	Nominal (Mn/DOT 2006-37)			Measured		
	X	Y	Z	X	Y	Z
CJ1-51-1	438	278.5	8.5	438.00	278.50	*8.25*
CJ1-51-2	438	275.5	8.5	438.00	275.50	*8.25*
CJ1-51-3	438	272.5	8.5	438.00	272.50	*8.25*
CJ1-51-4	438	269.5	8.5	438.00	269.50	*8.25*
CJ1-51-5	438	266.5	8.5	438.00	266.50	*8.25*
CJ2-51-1	438	206.5	8.5	*439.00*	206.50	*8.25*
CJ2-51-2	438	203.5	8.5	*439.00*	203.50	*8.25*
CJ2-51-3	438	200.5	8.5	*439.00*	200.50	*8.25*
CJ2-51-4	438	197.5	8.5	*439.00*	197.50	*8.25*
CJ2-51-5	438	194.5	8.5	*439.00*	194.50	*8.25*
CJ3-51-1	438	134.5	8.5	*438.50*	134.50	*8.25*
CJ3-51-2	438	131.5	8.5	*438.50*	131.50	*8.25*
CJ3-51-3	438	128.5	8.5	*438.50*	128.50	*8.25*
CJ3-51-4	438	125.5	8.5	*438.50*	125.50	*8.25*
CJ3-53-5	438	122.5	8.5	*438.50*	122.50	*8.25*
CJ1-53-1	438	293	13.5	*437.00*	293.00	13.50
CJ1-53-2	438	288.5	13.5	*437.00*	288.50	13.50
CJ1-53-3	438	284	13.5	*437.00*	284.00	13.50
CJ1-53-4	438	279.5	13.5	*437.00*	279.50	13.50
CJ1-53-5	438	275	13.5	*437.00*	275.00	13.50
CJ1-53-6	438	270.5	13.5	*437.00*	270.50	13.50
CJ1-53-7	438	266	13.5	*437.00*	266.00	13.50
CJ1-53-8	438	261.5	13.5	*437.00*	261.50	13.50
CJ1-53-9	438	257	13.5	*437.00*	257.00	13.50
CJ1-53-10	438	252.5	13.5	*437.00*	252.50	13.50
CJ2-53-1	438	221	13.5	438.00	221.00	13.50
CJ2-53-2	438	216.5	13.5	438.00	216.50	13.50
CJ2-53-3	438	212	13.5	438.00	212.00	13.50
CJ2-53-4	438	207.5	13.5	438.00	207.50	13.50
CJ2-53-5	438	203	13.5	438.00	203.00	13.50
CJ2-53-6	438	198.5	13.5	438.00	198.50	13.50
CJ2-53-7	438	194	13.5	438.00	194.00	13.50
CJ2-53-8	438	189.5	13.5	438.00	189.50	13.50
CJ2-53-9	438	185	13.5	438.00	185.00	13.50
CJ2-53-10	438	180.5	13.5	438.00	180.50	13.50
CJ3-53-1	438	149	13.5	*439.00*	149.00	13.50
CJ3-53-2	438	144.5	13.5	*439.00*	144.50	13.50
CJ3-53-3	438	140	13.5	*439.00*	140.00	13.50
CJ3-53-4	438	135.5	13.5	*439.00*	135.50	13.50
CJ3-53-5	438	131	13.5	*439.00*	131.00	13.50
CJ3-53-6	438	126.5	13.5	*439.00*	126.50	13.50
CJ3-53-7	438	122	13.5	*439.00*	122.00	13.50
CJ3-53-8	438	117.5	13.5	*439.00*	117.50	13.50
CJ3-53-9	438	113	13.5	*439.00*	113.00	13.50
CJ3-53-10	438	108.5	13.5	*439.00*	108.50	13.50

Appendix E

Concept 1 Large-Scale Laboratory Bridge Instrumentation Designation and Measured Locations

E.1 Concept 1 Laboratory Specimen Instrumentation Designation

The instrumentation for the concept 1 laboratory specimen was labeled as described in this section as documented by Smith et al. (2008). An example designation is given in Figure E.1.

1. The first character indicated the type of gage.

- C = VW concrete embedment gage
- F = Strand resistive gage
- M = Polyester Mold concrete resistive gage
- P = Polyester Wire surface resistive gage
- R = Rosette concrete resistive gage
- S = VW spot-weldable gage
- V = 120Ω waterproof resistive gage
- W = 350Ω waterproof resistive gage

2. The second character indicated the span in which the gage was located.

- 1 = West span
- 2 = East span
- D = CL Pier

3. The third character indicated the precast section within the span in which the gage was located.

- N = North precast section
- S = South precast section
- J = Joint

There was a hyphen after the third character.

4. The fourth character indicated the position of the gage along the precast section.

- 1 = Pinned end of the beam
- 2 = Outer quarter point
- 3 = Midspan
- 4 = Inner quarter point
- 5 = Continuous end of the beam

E-1

5. The fifth character indicated where the gage was located in the depth of the cross section.

Longitudinal Curvature Gages:

Flange Region

- 1 = Gage on strand
- 2 = Gage at bottom of R/F cage
- 3 = Gage on deck steel

Web Region

- 1 = Gage on strand
- 2 = Gage on mild R/F in beam
- 3 = Gage on deck steel

Composite Action Gages (Additional to those used for longitudinal curvature):

Flange Region

- 5 = Gage at top of R/F cage

Web Region

- 4 = Gage half-way between strand and mild R/F

Prestress Loss Gages:

- 1 = Center of Gravity of Strands

Transverse Gages:

- 1 = Gage over flange
- 2 = Gage over web corner

Bursting Gages:

- M = Mid-height of web

6. The sixth character indicated the orientation of the gage.

- L = Longitudinal
- T = Transverse
- V = Vertical

There was a hyphen after the sixth character.

E-2

7. The seventh character indicated the number of the gage at that position.   For transverse gages, the numbering increased from south to north. For longitudinal gages, the numbering increased from the outside of the specimen to the middle of the specimen. For bursting rebar gages, the numbering increased from the stirrup closest to the face of the beam toward the center of the precast section.

Type of Gage:
350Ω Waterproof Gage

Location Along the Span:
Midspan

Orientation of Gage:
Longitudinal

W1N-33L-1

Span Location:
West Span

North/South Location:
North Precast Section

Location within the Depth:
Gage on Deck Steel

Gage Number:
Furthest Gage from
Longitudinal C.L.
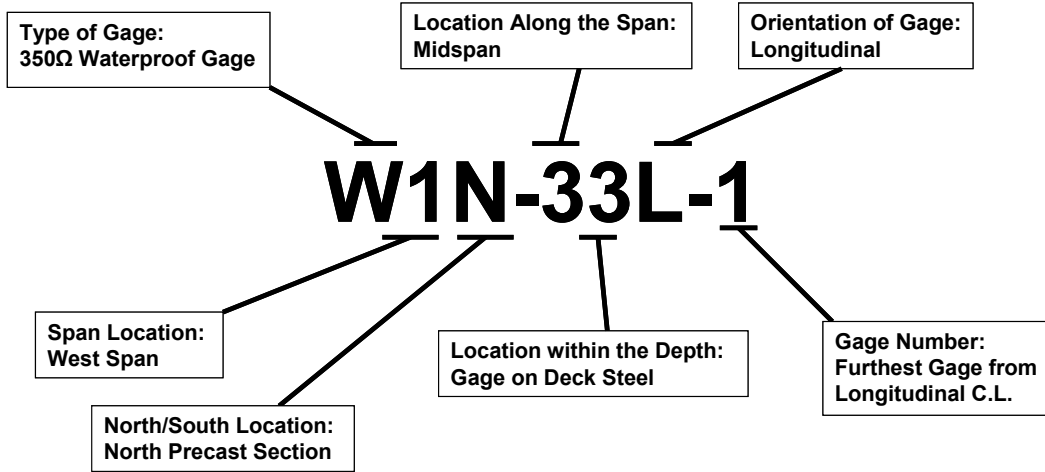
Figure E.1: Concept 1 Laboratory specimen strain gage designation example (Smith et al., 2008)

E.2 Measured Locations of Concept 1 Laboratory Specimen Instrumentation

All of the instrumentation in the laboratory specimen was measured to the nearest ¼ in. The sign convention of the gage ordinates is shown in Figure E.2. The X axis was measured in the E-W direction from the centerline of the pier (E positive); Y was measured in the N-S direction from the joint (N positive); the Z axis was measured in the vertical direction from the bottom of the precast sections (upward positive). The measurements are given in Table E.1.
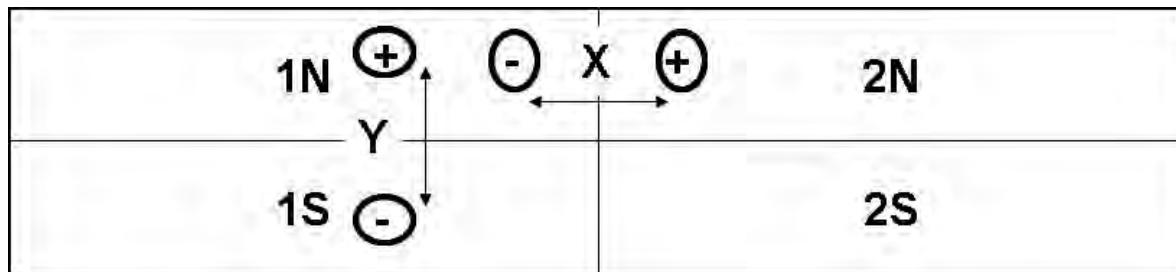
Figure E.2: Sign convention for the strain gage location measurements in the Concept 1 Laboratory Bridge (Smith et al., 2008)

Table E.1: Measured global gage locations for instruments in the concept 1 laboratory bridge specimen (in.)

X from CL pier (E+);Y from joint (N+); Z from top of flange/web			
Gage	X	Y	Z
M1J-11T-1	-255	-9.5	3
M1J-11T-2	-257.5	-5.5	3
M1J-11T-3	-255	0	3
M1J-11T-4	-257.5	5.5	3
M1J-11T-5	-255	9.5	3
M1J-12T-1	-253.5	-18.5	11.25
M1J-12T-2	-251	-14.5	11.25
M1J-12T-3	-253.5	-10.5	11.25
M1J-12T-4	-251	-6.5	11.25
M1J-12T-5	-253.5	-2.5	11.25
M1J-12T-6	-251	2.5	11.25
M1J-12T-7	-253.5	6.5	11.25
M1J-12T-8	-251	10.5	11.25
M1J-12T-9	-253.5	14.5	11.25
M1J-12T-10	-251	18.5	11.25
M1J-21T-1	-194.5	-9.5	4
M1J-21T-2	-197.5	-5.5	4
M1J-21T-3	-194.5	0	4
M1J-21T-4	-197.5	5.5	4
M1J-21T-5	-194.5	9.5	4
M1J-31T-1	-134	-9.5	3
M1J-31T-2	-136.5	-5.5	3

X from CL pier (E+);Y from joint (N+); Z from top of flange/web			
Gage	X	Y	Z
M1J-31T-3	-134	0	3
M1J-31T-4	-136.5	5.5	3
M1J-31T-5	-134	9.5	3
M1J-32T-1	-134.5	-18.5	11
M1J-32T-2	-132	-14.5	11
M1J-32T-3	-134.5	-10.5	11
M1J-32T-4	-132	-6.5	11
M1J-32T-5	-134.5	-2.5	11
M1J-32T-6	-132	2.5	11
M1J-32T-7	-134.5	6.5	11
M1J-32T-8	-132	10.5	11
M1J-32T-9	-134.5	14.5	11
M1J-32T-10	-132	18.5	11
M1J-41T-1	74	-9.5	3
M1J-41T-2	76.5	-5.5	3
M1J-41T-3	74	0	3
M1J-41T-4	76.5	5.5	3
M1J-41T-5	74	9.5	3
M1J-51T-1	26	-9.5	3
M1J-51T-2	29	-5.5	3
M1J-51T-3	26	0	3
M1J-51T-4	29	5.5	3

E-5

X from CL pier (E+);Y from joint (N+); Z from top of flange/web			
Gage	X	Y	Z
M1J-51T-5	26	9.5	3
M1J-52T-1	-27.5	-18.5	11
M1J-52T-2	-25	-14.5	11
M1J-52T-3	-27.5	-10.5	11
M1J-52T-4	-25	-6.5	11
M1J-52T-5	-27.5	-2.5	11
M1J-52T-6	-25	2.5	11
M1J-52T-7	-27.5	6.5	11
M1J-52T-8	-25	10.5	11
M1J-52T-9	-27.5	14.5	11
M1J-52T-10	-25	18.5	11
M2J-11T-1	257.75	-9.5	2
M2J-11T-2	255	-5.5	2
M2J-11T-3	257.75	0	2
M2J-11T-4	255	5.5	2
M2J-11T-5	257.75	9.5	2
M2J-12T-1	255	-18.5	8.5
M2J-12T-2	257.5	-14.5	8.5
M2J-12T-3	255	-10.5	8.5
M2J-12T-4	257.5	-6.5	8.5
M2J-12T-5	255	-2.5	8.5
M2J-12T-6	257.5	2.5	8.5

X from CL pier (E+);Y from joint (N+); Z from top of flange/web			
Gage	X	Y	Z
M2J-12T-7	255	6.5	8.5
M2J-12T-8	257.5	10.5	8.5
M2J-12T-9	255	14.5	8.5
M2J-12T-10	257.5	18.5	8.5
M2J-21T-1	198	-9.5	1.25
M2J-21T-2	195.5	-5.5	1.25
M2J-21T-3	198	0	1.25
M2J-21T-4	195.5	5.5	1.25
M2J-21T-5	198	9.5	1.25
M2J-31T-1	147.5	-9.5	2
M2J-31T-2	145	-5.5	2
M2J-31T-3	147.5	0	2
M2J-31T-4	145	5.5	2
M2J-31T-5	147.5	9.5	2
M2J-32T-1	134	-18.5	8.25
M2J-32T-2	136.5	-14.5	8.25
M2J-32T-3	134	-10.5	8.25
M2J-32T-4	136.5	-6.5	8.25
M2J-32T-5	134	-2.5	8.25
M2J-32T-6	136.5	2.5	8.25
M2J-32T-7	134	6.5	8.25
M2J-32T-8	136.5	10.5	8.25

X from CL pier (E+);Y from joint (N+); Z from top of flange/web			
Gage	X	Y	Z
C1J-11T-1	-243.5	0	3
C1J-21T-1	-183.5	0	3.5
C1J-31T-1	-123.5	0	3
C1J-41T-1	-64.5	0	3
C1J-51T-1	-15	0	3.5
C2J-11T-1	244.5	0	2
C2J-21T-1	207.5	0	2
C2J-31T-1	134.5	-8.5	1.75
C2J-31T-2	136.5	-5.5	1.75
C2J-31T-3	134.5	0	1.75
C2J-31T-4	136.5	5.5	1.75
C2J-31T-5	134.5	8.5	1.75
C2J-41T-1	87.5	0	2
C2J-51T-1	16.5	0	2
S1J-21T-1	-192	0	3.5
S1J-31T-1	-132.5	0	2.75
S1J-41T-1	-72.5	0	3.75
S1J-51T-1	-24	0	3.5
S2J-21T-1	202	0	1.75
S2J-31T-1	141.5	0	1.75
S2J-41T-1	81.5	0	1.75

E-8

X from CL pier (E+);Y from joint (N+); Z from top of flange/web			
Gage	X	Y	Z
M2J-32T-9	134	14.5	8.25
M2J-32T-10	136.5	18.5	8.25
M2J-41T-1	77.75	-9.5	2.25
M2J-41T-2	75	-5.5	2.25
M2J-41T-3	77.75	0	2.25
M2J-41T-4	75	5.5	2.25
M2J-41T-5	77.75	9.5	2.25
M2J-51T-1	30	-9.5	1.5
M2J-51T-2	27	-5.5	1.5
M2J-51T-3	30	0	1.5
M2J-51T-4	27	5.5	1.5
M2J-51T-5	30	9.5	1.5
M2J-52T-1	25	-18.5	8.5
M2J-52T-2	27.5	-14.5	8.5
M2J-52T-3	25	-10.5	8.5
M2J-52T-4	27.5	-6.5	8.5
M2J-52T-5	25	-2.5	8.5
M2J-52T-6	27.5	2.5	8.5
M2J-52T-7	25	6.5	8.5
M2J-52T-8	27.5	10.5	8.5
M2J-52T-9	25	14.5	8.5
M2J-52T-10	27.5	18.5	8.5

E-9

X from CL pier (E+);Y from joint (N+); Z from top of flange/web			
Gage	X	Y	Z
W1N-22L-3	-196.5	8	8
W1N-23L-1	-196	45.5	14.5
W1N-23L-2	-195	20.5	14.5
W1N-23L-3	-195	3.75	15
W1N-32L-3	-137.5	8	8
W1N-33L-1	-138	45.25	14.5
W1N-33L-2	-137	20.5	14.25
W1N-33L-3	-137	4	14.75
W1N-42L-3	-77.5	8	7.5
W1N-43L-1	-79	44.75	14.5
W1N-43L-2	-78	19.75	14.25
W1N-43L-3	-78	3.5	14.75
W1N-52L-4	-20.5	3.25	5
W1N-53L-1	-20.5	2.25	14.25
W1N-53L-2	-20.5	2.25	14.25
W1N-53L-3	-20.5	2.5	14.5
W1N-53L-4	-20.5	12	15
W1S-22L-3	-196.5	-8	8
W1S-23L-1	-196	-42.5	14.5
W1S-23L-2	-196	-18.5	14.5
W1S-23L-3	-195	-4.5	15
W1S-32L-3	-137.5	-8.5	8

E-10

X from CL pier (E+);Y from joint (N+); Z from top of flange/web			
Gage	X	Y	Z
W2N-43L-2	79	20.5	14.25
W2N-43L-3	79	2.75	14
W2N-52L-4	19	3	8.25
W2N-53L-1	20	56.75	14
W2N-53L-2	19	39	14.25
W2N-53L-3	21	19.5	14.5
W2N-53L-4	21	2.75	14.5
W2S-22L-3	197.5	6.5	8.75
W2S-23L-1	196	-42.5	14.5
W2S-23L-2	195	-18.5	14.75
W2S-23L-3	195	-5	14.5
W2S-32L-3	137.5	-8	9
W2S-33L-1	137	-42	14.5
W2S-33L-2	137	-18	14.5
W2S-33L-3	137	-5	14
W2S-42L-3	77.5	7.5	8.25
W2S-43L-1	78	-41.5	14.5
W2S-43L-2	78	-17.5	14.5
W2S-43L-3	79	-4.5	14.25
W2S-52L-4	19	-2.5	8.25
W2S-53L-1	22	-58.25	14.5
W2S-53L-2	22	-37.5	14.25

E-11

X from CL pier (E+);Y from joint (N+); Z from top of flange/web			
Gage	X	Y	Z
W1S-33L-1	-138	-42.75	14.25
W1S-33L-2	-138	-18.5	14.25
W1S-33L-3	-138	-4.5	14.75
W1S-42L-3	-77.5	-8	7
W1S-43L-1	-79	-42.5	14.5
W1S-43L-2	-79	-19	14.25
W1S-43L-3	-78	-4.5	114.5
W1S-52L-4	-20.5	-2.25	7.75
W1S-53L-1	-17	-58.25	14.25
W1S-53L-2	-17	-38	14.25
W1S-53L-3	-17	-22	14.25
W1S-53L-4	-19	-4.5	15
W2N-22L-3	197.5	-8.75	9
W2N-23L-1	196	44.5	14.5
W2N-23L-2	196	20	14.5
W2N-23L-3	196	2.25	14.25
W2N-32L-3	137.5	-9	9
W2N-33L-1	137	45	14.5
W2N-33L-2	138	20	14
W2N-33L-3	138	2.5	14
W2N-42L-3	77.5	-8	8.75
W2N-43L-1	79	45	14.5

X from CL pier (E+);Y from joint (N+); Z from top of flange/web			
Gage	X	Y	Z
W2S-53L-3	24	-21.5	14.25
W2S-53L-4	19	-4	14.75
W1N-35L-3	-137.5	8	15.25
W1S-35L-3	-137.5	-8.5	15.25
W2N-35L-3	137.5	-9	15.25
W2N-35L-3	137.5	8.5	11.75

E-13

X from CL pier (E+);Y from joint (N+); Z from bottom of section			
Gage	X	Y	Z
F2N-21L-1	198	44	1.75
F2N-21L-2	199	21	1.75
F2N-21L-3	198	3.5	2
F2N-31L-1	136.75	45	1.75
F2N-31L-2	136.5	21	1.75
F2N-31L-3	136.5	3.75	2
F2N-41L-1	79.5	44.25	2
F2N-41L-2	80	21.25	1.75
F2N-41L-3	78.5	3.75	2
F2N-51L-1	21	57	2.25
F2N-51L-2	19.5	39	2
F2N-51L-3	20.25	21	2
F2N-51L-4	20.75	3.5	2
M2N-52-1	22	53	8.5
M2N-52-2	22.5	39.5	9
M2N-52-3	22.5	17.75	9.25

E-14

X from CL pier (E+);Y from joint (N+); Z from bottom of section			
Gage	X	Y	Z
M1N-34L-2	-136	22	6.25
C1N-31L-1	-137.5	36	2.5
C1N-31L-2	-134	7	1.5
F1N-1MV-1a	-269.5	58.25	6.75
F1N-1MV-2a	-267.5	58.25	6.75
W1N-5MV-1b	-4.75	57.5	6.5
W1N-22L-1	-197	42.5	9.5
W1N-22L-2	-197	21.5	9.5
W1N-32L-1	-137	43	9
W1N-32L-2	-136	22	9.25
W1N-42L-1	-80	42.5	9.25
W1N-42L-2	-80	21.5	9.5
W1N-52L-1	-22.5	55	9.5
W1N-52L-2	-21.5	36	9.5
W1N-52L-3	-23	22	9.25

E-15

X from CL pier (E+);Y from joint (N+); Z from bottom of section			
Gage	X	Y	Z
F1S-21L-1	-196.5	-44	1.75
F1S-21L-2	-197	-21	1.75
F1S-21L-3	-196.5	-3	2
F1S-31L-1	-138.5	-44.5	1.75
F1S-31L-2	-138	-21	1.75
F1S-31L-3	-138	-3	2
F1S-41L-1	-78.5	-39.25	1.75
F1S-41L-2	-79.5	-21	1.75
F1S-41L-3	-79	-3	2
F1S-51L-1	-21	-57	2.25
F1S-51L-2	-20	-38.5	2
F1S-51L-3	-21	-21	1.75
F1S-51L-4	-19	-3	2
W1S-1MV-1c	-269	-49.5	7.5
W1S-1MV-1d	-269.25	-58	5.5
W1S-1MV-2c	-267	-49.5	7.5
W1S-1MV-2d	-267.25	-58	5.5
W1S-5MV-1a	-4.75	-58	5.75
W1S-5MV-2a	-6	-58	5.75

X from CL pier (E+);Y from joint (N+); Z from bottom of section			
Gage	X	Y	Z
W1S-22L-1	-197	-42.25	9
W1S-22L-2	-197	-21.5	9.25
W1S-32L-1	-139	-42.5	8.75
W1S-32L-2	-137.5	-21.5	9.25
W1S-42L-1	-78.75	-43	8.75
W1S-42L-2	-79.75	-21.5	9.5
W1S-52L-1	-20	-55.5	9
W1S-52L-2	-19.5	-36	9.25
W1S-52L-3	-18.5	-21.5	9.5
M1S-34L-2	-137.5	-21	7
C1S-31L-1	-139	-36	2.75
C1S-31L-2	-143	-6.75	1.75
M1S-52L-1	-20.5	-52.5	9
M1S-52L-2	-20.5	-39.5	9.25
M1S-52L-3	-18.5	-19	9.25

X from CL pier (E+);Y from joint (N+); Z from bottom of section			
Gage	X	Y	Z
F2N-21L-1	198	44	1.75
F2N-21L-2	199	21	1.75
F2N-21L-3	198	3.5	2
F2N-31L-1	136.75	45	1.75
F2N-31L-2	136.5	21	1.75
F2N-31L-3	136.5	3.75	2
F2N-41L-1	79.5	44.25	2
F2N-41L-2	80	21.25	1.75
F2N-41L-3	78.5	3.75	2
F2N-51L-1	21	57	2.25
F2N-51L-2	19.5	39	2
F2N-51L-3	20.25	21	2
F2N-51L-4	20.75	3.5	2
M2N-52-1	22	53	8.5
M2N-52-2	22.5	39.5	9
M2N-52-3	22.5	17.75	9.25

E-18

X from CL pier (E+);Y from joint (N+); Z from bottom of section			
Gage	X	Y	Z
W2N-22L-1	198	43	10
W2N-22L-2	198	22	10
W2N-32L-1	135.5	43	9.5
W2N-32L-2	135.75	21.5	9.5
W2N-42L-1	80	41.75	9.5
W2N-42L-2	79.5	21.25	9.5
W2N-52L-1	21.5	55.5	9.5
W2N-52L-2	22.75	35.25	9.5
W2N-52L-3	24	20.5	9.5
M2N-34L-2	136.5	21.5	6
W2N-5MV-1a	3.5	58	5.5
W2N-5MV-2a	7.5	58	5.5
W2N-1MV-1b	269.5	58	6
C2N-31L-1	136.75	36.5	2.75
C2N-31L-2	136.75	7	2.75

E-19

X from CL pier (E+);Y from joint (N+); Z from bottom of section			
Gage	X	Y	Z
F2S-21L-1	197.5	-45	1.75
F2S-21L-2	198.5	-21	1.75
F2S-21L-3	199	-3.5	2
F2S-31L-1	139.5	-45	2
F2S-31L-2	140	-21	1.75
F2S-31L-3	141.5	-3.25	2
F2S-41L-1	79	-44.75	1.75
F2S-41L-2	79.5	-21	1.75
F2S-41L-3	79.5	-3	2
F2S-51L-1	23	-57	2
F2S-51L-2	22.5	-45.25	2
F2S-51L-3	22.5	-21.25	1.75
F2S-51L-4	22.5	-3	2
W2S-22L-1	198	-43	9
W2S-22L-2	197.75	-22	9.25
W2S-32L-1	138.5	-42.25	9.25
W2S-32L-2	139.5	-21.5	9.25
W2S-42L-1	19	-42	9.25
W2S-42L-2	79.5	-21.25	9.5
W2S-52L-1	23.5	-56	9.25
W2S-52L-2	23.5	-36	9.5
W2S-52L-3	23.5	-21.5	9.5

X from CL pier (E+);Y from joint (N+); Z from bottom of section			
Gage	X	Y	Z
M2S-34L-2	138.5	-21.5	5.5
C2S-31L-1	140.5	-36	2.75
C2S-31L-2	141	-7	2.5
W2S-1MV-1a	168.5	-58	6
W2S-1MV-2a	266.5	-58	6.25
W2S-5MV-1c	5.25	-49	7
W2S-5MV-1d	5.5	-58	7.25
W2S-5MV-2c	7.5	-49	7
W2S-5MV-2d	7.5	-58	7.25
M2S-52L-1	20	-53.5	9.25
M2S-52L-2	20	-39.5	9.5
M2s-52L-3	20	-18.5	9.5

X from pier end of beam; Y from joint side of beam; Z from bottom of beam			
Gage	X	Y	Z
R1N-11L-1	266.25	60	7
R1N-11V-1	266.25	60	7
R1N-11S-1	266.25	60	7
R1N-51L-1	2.75	60	6.5
R1N-51V-1	2.75	60	6.5
R1N-51S-1	2.75	60	6.5
R1S-11L-1	266.75	60	6.25
R1S-11V-1	266.75	60	6.25
R1S-11S-1	266.75	60	6.25
R1S-51L-1	3.25	60	6.25
R1S-51V-1	3.25	60	6.25
R1S-51S-1	3.25	60	6.25
R2N-51L-1	2.5	60	7.5
R2N-51V-1	2.5	60	7.5
R2N-51S-1	2.5	60	7.5
R2N-11L-1	267.5	60	7
R2N-11V-1	267.5	60	7
R2N-11S-1	267.5	60	7
R2S-11L-1	265	60	7
R2S-11V-1	265	60	7
R2S-11S-1	265	60	7
R2S-51L-1	2.75	60	7.25
R2S-51V-1	2.75	60	7.25
R2S-51S-1	2.75	60	7.25

E-22

X from pier end of beam; Y from joint side of beam; Z from bottom of beam			
Gage	X	Y	Z
F1N-1MV-1a	267	58.25	6.75
F1N-1MV-2a	265	58.25	6.75
W1N-5MV-1b	2.25	57.5	6.5
W1S-1MV-1c	266.5	49.5	7.5
W1S-1MV-1d	266.75	58	5.5
W1S-1MV-2c	264.5	49.5	7.5
W1S-1MV-2d	264.75	58	5.5
W1S-5MV-1a	2.25	58	5.75
W1S-5MV-2a	3.5	58	5.75
W2N-5MV-1a	1	58	5.5
W2N-5MV-2a	5	58	5.5
W2N-1MV-1b	267	58	6
W2S-1MV-1a	266	58	6
W2S-1MV-2a	264	58	6.25
W2S-5MV-1c	2.75	49	7
W2S-5MV-1d	3	58	7.25
W2S-5MV-2c	5	49	7
W2S-5MV-2d	5	58	7.25

Appendix F

Concept 2 Large-Scale Laboratory Bridge Instrumentation Designation, Nominal, and Measured Locations

F.1 Concept 2 Laboratory Specimen Instrumentation Designation

The instrumentation for the concept 2 laboratory specimen was labeled as described in this section. An example designation is given in Figure F.1.

1. The first character indicated the type of gage.

- C = VW concrete embedment gage
- T = Strand resistive gage
- M = Polyester Mold concrete resistive gage
- P = Polyester Wire surface resistive gage
- S = VW spot-weldable gage
- V = 120Ω waterproof resistive gage
- W = 350Ω waterproof resistive gage

2. The second character indicated the span number. There was only one span in this bridge, however this digit was maintained to facilitate comparison with the instrumentation in the Concept 1 bridge. This value was 1 for every instrument in the Concept 2 bridge.

3. The third character indicated the precast section within the span in which the gage was located.

- N = North precast section
- S = South precast section
- J = Joint

There was a hyphen after the third character.

4. The fourth character indicated the position of the gage along the precast section.

- 1.0 = East end of span
- 1.5 = $1/8^{th}$ point of the span
- 2.0 = 1/4 point of the span
- 2.5 = $3/8^{th}$ point of the span
- 3.0 = 1/2 point, or mid-span
- 3.5 = $5/8^{th}$ point of the span
- 4.0 = 3/4 point of the span
- 4.5 = $7/8^{th}$ point of the span
- 5.0 = West end of the span

There was a hyphen separating the fourth and fifth characters

F-1

5. The fifth character indicated where the gage was located in the depth of the cross section. Numerical values representing the depth start at the bottom of the section and increase towards the top of the section.

a.)　　For longitudinal instrumentation:

      i.　0.5 = Gage was located on the bottom face of the precast unit

      ii.　1.0 = Gage was located on the bottom prestressing strand

      iii.　2.0 = Gage was located above the precast flange

      iv.　2.5 = Gage was located below the precast web

      v.　3.0 = Gage was located above the precast web

      vi.　3.5 = Gage was located near the top surface of the member

b.)　　For transverse instrumentation:

      i.　1.0 = Gage was located above precast flange at same depth as transverse hooked reinforcement

      ii.　1.5 = Gage was located at mid-height of cage stirrup

      iii.　2.0 = Gage was located above precast web

6. The sixth character indicated the orientation of the gage.

- L = Longitudinal
- T = Transverse

There was a hyphen after the sixth character.

7. The seventh character indicated the number of the gage at that position.

a.)　　For longitudinal instrumentation

      i.　1 = For gages located closest to the outside flange (farthest away from the interior precast joint)

⋮

      iii.　n = For gages located nearest to the inside joint

b.)　　For transverse instrumentation

      i.　1 = For gage located farthest south in gage group

⋮

      iii.　n = For gage located farthest north in gage group

F-2
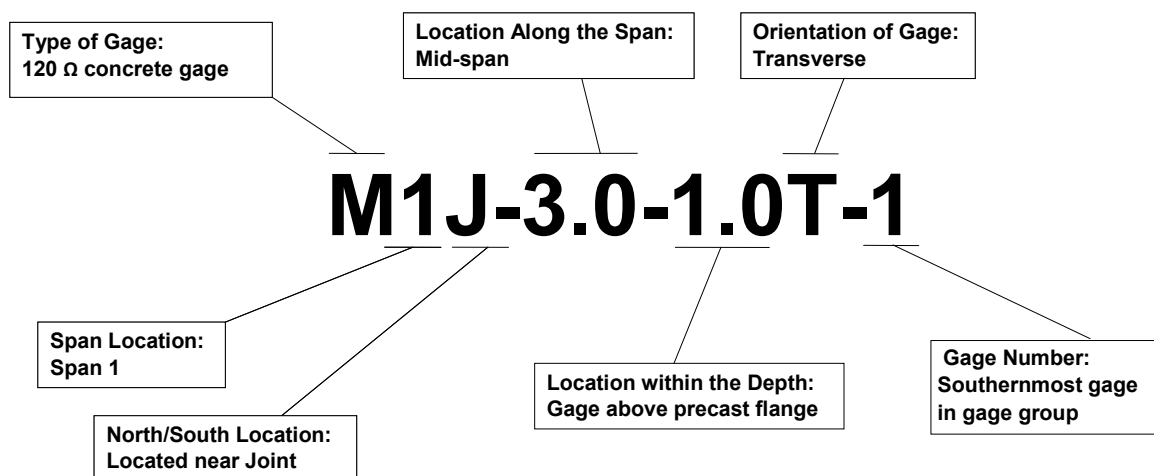
Figure F.1: Concept 2 Laboratory specimen strain gage designation example

F.2 Measured Locations of Concept 2 Laboratory Specimen Instrumentation

All of the instrumentation in the laboratory specimen was measured to the nearest ¼ in. The sign convention of the gage ordinates is shown in Figure F.2. The X axis was measured in the E-W direction from the centerline of the pier (E positive), which was located 2 in. from the end face of the precast unit and corresponded to the center of the concrete pier. The instrumentation in the Concept 2 bridge was designed to correspond with the naming convention utilized in the Concept 1 bridge, where there was a 4 in. gap between the two spans at the concrete pier. The Y ordinate was measured in the N-S direction from the joint (N positive); the Z axis was measured in the vertical direction from the bottom of the precast sections (upward positive). The measurements are given in Table F.1.

CENTERLINE OF PIER
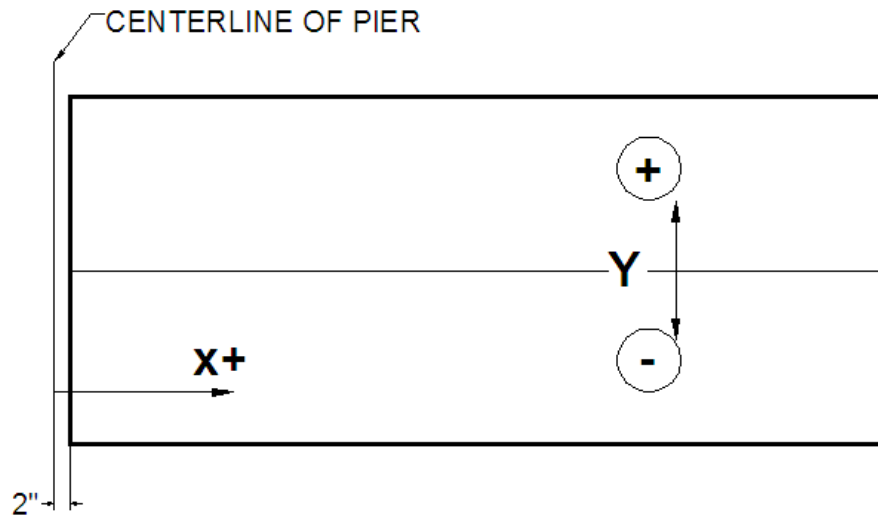
Figure F.2: Sign convention for the strain gage location measurements in the Concept 1 Laboratory Bridge

Table F.1: Global gage locations for instruments in the Concept 2 laboratory bridge specimen (in.)

X from CL pier (E+); Y from joint (N+); Z from bottom of section						
	Nominal Locations			Measured Locations		
Gage	X	Y	Z	X	Y	Z
7/8th point of the span						
T1J-4.5a-1.0T-1	51.75	0	4.5	52.25	0	4.75
M1J-4.5b-1.0T-1	49	0	4.5	49.25	0	4.75
M1J-4.5c-1.0T-1	45	-4.5	4.5	46	-4.5	4
M1J-4.5c-1.0T-2	42.5	0	4.5	42.25	0	4.75
M1J-4.5c-1.0T-3	45	4.5	4.5	45.75	4.5	4.25
M1J-4.5c-1.5T-1	45	-4.5	8.0	46	-4.5	8.25
M1J-4.5c-1.5T-2	42.5	0	8.0	42.25	0	8.5
M1J-4.5c-1.5T-3	45	4.5	8.0	46.25	4.5	8.5
M1J-4.5d-1.0T-1	38.75	0	4.5	39.25	0	4.25
T1J-4.5e-1.0T-1	35.75	0	4.5	34.5	0	4.75
3/4 point of the span (west quarter point)						
M1J-4.0-1.0T-1	81	-4.5	4.5	81.25	-4.5	4
M1J-4.0-1.0T-2	78.5	0	4.5	77.75	0	4
M1J-4.0-1.0T-3	81	4.5	4.5	81.5	4.5	4.25
M1J-4.0-1.5T-1	81	-4.5	8.0	81.5	-4.5	7.25
M1J-4.0-1.5T-2	78.5	0	8.0	78.25	0	7.75
M1J-4.0-1.5T-3	81	4.5	8.0	80.75	4.5	7.75
M1J-4.0-2.0T-1	81	-4.5	14.0	81.5	-4.5	13.75
M1J-4.0-2.0T-2	78.5	0	14.0	78.25	0	13.5
M1J-4.0-2.0T-3	81	4.5	14.0	81.75	4.5	13.75
S1J-4.0-1.0T-1	70.5	0	4.5	75.25	0	4.75
C1J-4.0-1.0T-1	75	0	4.5	76.5	0	4.5
5/8th point of the span						
T1J-3.5a-1.0T-1	105.75	0	4.5	105.75	0	4.75
M1J-3.5b-1.0T-1	103	0	4.5	103.25	0	4.5
M1J-3.5c-1.0T-1	99	-4.5	4.5	99.75	-4.5	4.25
M1J-3.5c-1.0T-2	96.5	0	4.5	96.75	0	4
M1J-3.5c-1.0T-3	99	4.5	4.5	99.5	4.5	4.25
M1J-3.5c-1.5T-1	99	-4.5	8.0	100	-4.5	7.5
M1J-3.5c-1.5T-2	96.5	0	8.0	96.5	0	7.5
M1J-3.5c-1.5T-3	99	4.5	8.0	100	4.5	8.5
M1J-3.5d-1.0T-1	92.75	0	4.5	92.5	0	4
T1J-3.5e-1.0T-1	89.75	0		89.75	0	4.75

X from CL pier (E+); Y from joint (N+); Z from bottom of section						
	Nominal Locations			Measured Locations		
Gage	X	Y	Z	X	Y	Z
1/2 point of the span (midspan)						
M1J-3.0-1.0T-1	135.75	-4.5	4.5	136.5	-4.5	4.5
M1J-3.0-1.0T-2	133.25	0	4.5	133.25	0	4.5
M1J-3.0-1.0T-3	135.75	4.5	4.5	136.5	4.5	4.75
M1J-3.0-1.5T-1	135.75	-4.5	8.0	136.75	-4.5	7.75
M1J-3.0-1.5T-2	133.25	0	8.0	133.25	0	8.25
M1J-3.0-1.5T-3	135.75	4.5	8.0	136.75	4.5	8
M1J-3.0-2.0T-1	135.75	-4.5	14.0	136.75	-4.5	13.5
M1J-3.0-2.0T-2	133.25	0	14.0	133.5	0	14
M1J-3.0-2.0T-3	135.75	4.5	14.0	136.25	4.5	13.5
S1J-3.0-1.0T-1	141.75	0	4.5	139.5	0	5
C1J-3.0-1.0T-1	137.5	0	4.5	134.5	0	4.25
3/8th point of the span						
T1J-2.5a-1.0T-1	177.75	0	4.5	178.25	0	4.75
M1J-2.5b-1.0T-1	175	0	4.5	175.5	0	4.5
M1J-2.5c-1.0T-1	171	-4.5	4.5	171	-4.5	4.25
M1J-2.5c-1.0T-2	168.5	0	4.5	168	0	4.5
M1J-2.5c-1.0T-3	171	4.5	4.5	171	4.5	4.5
M1J-2.5c-1.5T-1	171	-4.5	8.0	171	-4.5	8
M1J-2.5c-1.5T-2	168.75	0	8.0	167.75	0	8.5
M1J-2.5c-1.5T-3	171	4.5	8.0	170.75	4.5	8.25
M1J-2.5d-1.0T-1	164.75	0	4.5	165	0	4.75
T1J-2.5ae-1.0T-1	161.75	0	4.5	162	0	4.75
1/4 point of the span (east quarter point)						
M1J-2.0-1.0T-1	189	-4.5	4.5	189.25	-4.5	4
M1J-2.0-1.0T-2	186.5	0	4.5	187.75	0	4.25
M1J-2.0-1.0T-3	189	4.5	4.5	189.25	4.5	4.25
M1J-2.0-1.5T-1	189	-4.5	8.0	189.25	-4.5	8
M1J-2.0-1.5T-2	186.5	0	8.0	186.75	0	8
M1J-2.0-1.5T-3	189	4.5	8.0	189.5	4.5	7.5
M1J-2.0-2.0T-1	189	-4.5	14.0	190.5	4.5	13.75
M1J-2.0-2.0T-2	186.5	0	14.0	187	0	13.75
M1J-2.0-2.0T-3	189	4.5	14.0	190.25	-4.5	13.5
S1J-2.0-1.0T-1	196	0	4.5	200.75	0	5
C1J-2.0-1.0T-1	193	0	4.5	185	0	4.25

X from CL pier (E+); Y from joint (N+); Z from bottom of section						
	Nominal Locations			Measured Locations		
Gage	X	Y	Z	X	Y	Z
1/8th point of the span						
T1J-1.5a-1.0T-1	232.25	0	4.5	233.5	0	4.75
M1J-1.5b-1.0T-1	229	0	4.5	229.25	0	4
M1J-1.5c-1.0T-1	225	-4.5	4.5	226.5	-4.5	4.25
M1J-1.5c-1.0T-2	222.5	0	4.5	222.5	0	4.5
M1J-1.5c-1.0T-3	225	4.5	4.5	226.25	4.5	4.25
M1J-1.5c-1.5T-1	225	-4.5	8.0	227	-4.5	8.5
M1J-1.5c-1.5T-2	222.5	0	8.0	222.5	0	8.75
M1J-1.5c-1.5T-3	225	4.5	8.0	226.75	4.5	8
M1J-1.5d-1.0T-1	218.75	0	4.5	219.25	0	4.5
T1J-1.5e-1.0T-1	215.5	0	4.5	215.75	0	4.75

X from CL pier (E+); Y from joint (N+); Z from bottom of section						
	Nominal Locations			Actual Locations		
Gage	X	Y	Z	X	Y	Z
M1N-3.5-3.0L-2	104.5	21	14.0	110	23	13.75
M1N-3.5-3.5L-2	104.5	21	16.0	111.5	23	15.5
M1N-3.5-2.0L-2	104.5	21	5.0	108	22.5	4.75
M1N-3.5-2.5L-2	104.5	21	9.5	108.75	22.25	9.5
M1N-3.5-3.0L-1	106	44	14.0	110.5	44.5	13.5
M1N-3.5-3.5L-1	106	44	16.0	110.5	44.5	15.5
M1N-3.5-2.0L-1	106	44	5.0	107.75	44.25	4.75
M1N-3.5-2.5L-1	106	44	9.5	108	44	9.75
M1N-3.5-2.0L-3	106	3	4.5	106.5	4	6
M1N-3.5-2.5L-3	106	3	8.0	106.5	4	10.5
M1N-3.5-3.0L-3	106	3	14.0	109.5	4	14
M1N-3.5-3.5L-3	106	3	16.0	110	4	15.5
M1N-2.0-3.0L-2	181.5	21	14.0	181.75	21.5	13.5
M1N-2.0-3.5L-2	181.5	21	16.0	181.75	21.5	15.5
M1N-2.0-2.0L-2	181.5	21	5.0	182	21	4.5
M1N-2.0-2.5L-2	181.5	21	9.5	182.5	21	9.25
M1N-2.0-3.0L-1	181.5	45	14.0	182	45.75	13.5
M1N-2.0-3.5L-1	181.5	45	16.0	182.5	45.75	15.5
M1N-2.0-2.0L-1	181.5	45	5.0	182.25	45.25	4.75
M1N-2.0-2.5L-1	181.5	45	9.5	182.5	45	9.5
M1N-2.0-2.0L-3	181.5	3	4.5	182.5	1.75	6.25
M1N-2.0-2.5L-3	181.5	3	8.0	182.5	2.25	10.25
M1N-2.0-3.0L-3	181.5	3	14.0	182.5	3	14
M1N-2.0-3.5L-3	181.5	3	16.0	182.5	3	15.5
M1S-3.5-3.0L-2	107.5	21	14.0	111	22.75	13.25
M1S-3.5-3.5L-2	107.5	21	16.0	111	22.75	15.25
M1S-2.0-2.0L-2	107.5	21	5.0	107	21.25	5.5
M1S-2.0-2.5L-2	107.5	21	9.5	107.75	21.75	9.75

Appendix G

Large-Scale Laboratory Bridge and Subassemblage Core Analysis

G.1 Introduction to Coring Analysis

Several core samples were removed from the large-scale bridge and subassemblage specimens to investigate the presence of internal reflective cracking. The cores were analyzed initially by the naked eye, and subsequently with the aid of a microscope. Prior to being examined, the cores were prepped, which included rinsing them lightly under water, wiping them gently to remove any remaining sludge from the coring process, and patting them dry with paper towels. The cores were reassembled if broken in multiple sections, and the general characteristics of the core were documented (e.g. core height, diameter, and number of sections). The cores were initially examined without the use of the stereomicroscope. Any readily visible cracks observed using only a magnifying glass and a bright light were marked, which will be described later in this section. When it became too difficult to observe the crack by this method, the cores were placed under the viewing objective of the stereomicroscope and examined further for cracks.

The stereomicroscope employed to examine the cores was an Olympus Stereomicroscope SZX12, made available for use by the University of Minnesota's Institute of Technology Characterization Facility. In addition, an Olympus DP10 digital camera was used to take photos of specimens under the viewing objective. The stereomicroscope level of magnification used to examine the cores ranged between 2.1X to 27X magnification. The cores were first typically examined using a magnifying glass before being placed under the stereomicroscope. When a crack was identified, the core was placed under the microscope and the entire visible length of the crack was located using a magnification anywhere from 10X to 27X. To assist in locating the cracks, telescoping lights were positioned such that the cracks were easier to locate. Figure G.1 shows the stereomicroscope and indicates where the digital camera and telescoping lights were mounted.

Once a crack was identified under the microscope, it was marked using a dotted line of red ink along the visible length of the crack, as shown in Figure G.2. A crack gage was used to measure the crack widths along the length of the crack. The measured crack widths were indicated on the surface of the core with pencil, as shown in Figure G.3, along the length of the crack according to the crack width classification categories defined in Table G.1. The orientation, depth, and type of the crack were documented on a supplementary form. During examination of the cores, visible cracks were the only item of the core that was located and marked. In addition, the examination also included looking for indications of potential crack location. Most commonly, these notes referred to location and orientation of an inclined plane between two sections of a broken core because these planes may indicate that a crack was present prior to the sections breaking apart.

Figure G1: Photograph of Olympus Stereomicroscope SZX12 used for core analysis

Figure G2: Identified crack marked on core specimen using red ink

G-2

Figure G3: Crack widths marked on core specimen in pencil

Table G1: Crack width classification categories

Crack Classification	Crack Width (W)
0.002[1]	W < 0.002"
A	0.002" ≤ W < 0.008"
B	0.008" ≤ W < 0.023"
C	0.023" ≤ W < 0.200"
D	W ≥ 0.200"

[1]Cracks classified as having width < 0.002" are shown simply with a "2" in Table G2.

G2:   Tabulation of Cracking in Cores

Cracking was tabulated for each core specimen. Reflective cracking was measured from a reference line that corresponded with the precast flange – CIP interface, as shown in Figure G4. The tabulated crack measurements are outlined in Table G2.
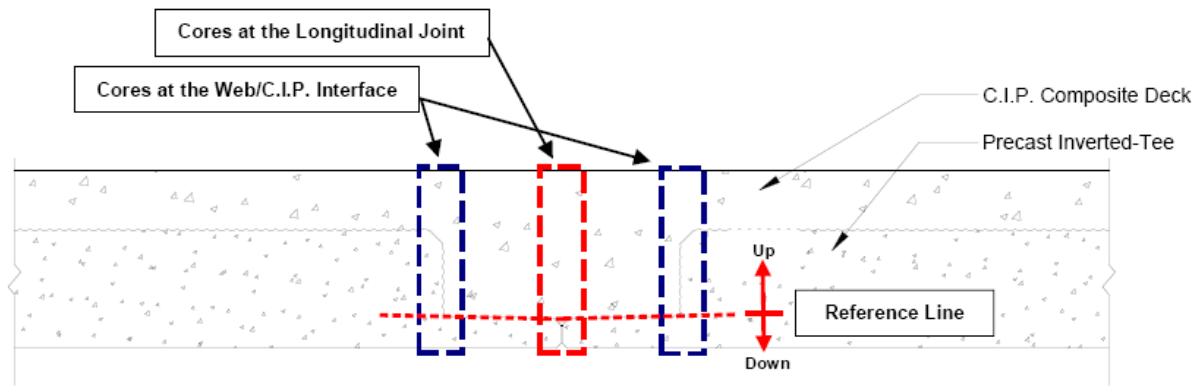
Figure G4: Location of reference line for measurement of vertical location of cracking in core specimens

Table G2: Tabulation of characteristics of core samples

Core Designation					Core Characteristics	Reflective Crack Characteristics			
Specimen[1]	X-Coord.[2]	Y-Coord.[3]	Location of Core	Side of Longitudinal Joint	Core Diameter	Distance from Longitudinal Joint or Web/C.I.P. interface	Side of Core	Depth of Crack[4]	Width of Crack[5]
C1-S1	26	0	Longitudinal Joint	N/A	2 ¾" S.C.[6]	N.O.[7]	N.O.[7]	N.O.[7]	N.O.[7]
C1-S1	134	0	Longitudinal Joint	N/A	2 ¾" S.C.[6]	N.O.[7]	N.O.[7]	N.O.[7]	N.O.[7]
C1-S1	192	2	Longitudinal Joint	North	2 ¾" S.C.[6]	N.O.[7]	N.O.[7]	N.O.[7]	N.O.[7]
C1-S1	197.5	0	Longitudinal Joint	N/A	2 ¾" S.C.[6]	1/8" South 1/8" South	West East	2 ¾" (up) 1 ¼" (up)	**A**: 0"-1 ¼"; **2**: 1 ¼"-2 ¾" **2**: 0"-1 ¼"
C1-S1	-194.5	0	Longitudinal Joint	N/A	1 ¾"	½" North ½" North	West East	Undefined[8]	Undefined[8]
C1-S2	74	0	Longitudinal Joint	N/A	1 ¾"	N.O.[7]	N.O.[7]	N.O.[7]	N.O.[7]
C1-S2	146	0	Longitudinal Joint	N/A	1 ¾"	N.O.[7]	N.O.[7]	N.O.[7]	N.O.[7]
C1-S2	195.5	0	Longitudinal Joint	N/A	1 ¾"	N.O.[7]	N.O.[7]	N.O.[7]	N.O.[7]
C1-S2	198	0	Longitudinal Joint	N/A	1 ¾"	N.O.[7]	N.O.[7]	N.O.[7]	N.O.[7]
C2-2.0	193	0	Longitudinal Joint	N/A	3 ¾"	N.O.[7]	N.O.[7]	N.O.[7]	N.O.[7]
C2-2.0	193	12	Web/C.I.P. Interface	North	3 ¾"	0" 0"	West East	3 ½" 1 ½"	**2**: ¼"-1"; **A**: 1"-2 ¼"; **2**: 2 ¼"-3 ½" **2**: 1 ¼" – 1 ½"
C2-2.0	193	12	Web/C.I.P. Interface	South	3 ¾"	0"	North	(0")[9]	**2**: (entire length)
C2-4.0	76	0	Longitudinal Joint	N/A	3 ¾"	N.O.[7]	N.O.[7]	N.O.[7]	N.O.[7]
C2-4.0	76	12	Web/C.I.P. Interface	North	3 ¾"	N.O.[7]	N.O.[7]	N.O.[7]	N.O.[7]
C2-4.0	76	12	Web/C.I.P. Interface	South	3 ¾"	N.O.[7]	N.O.[7]	N.O.[7]	N.O.[7]

G-5

Core Designation					Core Characteristics	Reflective Crack Characteristics			
Specimen[1]	X-Coord.[2]	Y-Coord.[3]	Location of Core	Side of Longitudinal Joint	Core Diameter	Distance from Longitudinal Joint or Web/C.I.P. interface	Side of Core	Depth of Crack[4]	Width of Crack[5]
SSMBLG 1	31.5	0	Longitudinal Joint	N/A	2 ¾"	¾" East 1 ¼" East	North South	7 ½" (up) 6" (up)	(North) **C**: 0"-1"; **B**: 1"-2"; **A**: 2"-3 ½"; **B**: 3 ½"-4 ½"; **A**: 4 ½"-5"; **2**: 5"-7 ½" (South) **C**: 0"-1"; **B**: 1"-1 ¼"; **2**: 1 ¼"-1 ½"; **A**: 1 ½"-1 ¾"; **C**: 1 ¾"-2 ¼"; **B**: 2 ¼"-2 ¾"; **A**: 2 ¾"-3 ½"; **B**: 3 ½"-4 ½"; **A**: 4 ½"-5"; **2**: 5"-6"
SSMBLG 1	31.5	12	Web/C.I.P. Interface	East	2 ¾"	0" 0"	North South	7" (up); 3"(down) 7" (up); 3"(down)	**A**: 0"-¾"; **2**: ¾"-7" (up); **A**: 0"-1"; **B**: 1"-3" (down) **A**: 0"-1"; **2**: 1"-7" (up); **B**: 0"-3" (down)
SSMBLG 1	31.5	12	Web/C.I.P. Interface	West	2 ¾"	N.O.[7]	N.O.[7]	N.O.[7]	N.O.[7]
SSMBLG 2	33.5	0	Longitudinal Joint	N/A	2 ¾"	¾" West ¾" West	North South	7 ¼" 7"	**B**: 0"-2 ¼"; **A**: 2 ¼"-3 ¼"; **2**: 3 ¼"-4"; **A**: 4"-7 ¼" **B**: 0"-2" **A**: 2"- 2 ¾"; **B**: 2 ¾"-3 ¼"; **A**: 3 ¼"-5 ¾"; **2**: 5 ¾"-7"
SSMBLG 2	33.5	12	Web/C.I.P. Interface	East	2 ¾"	N.O.[7]	N.O.[7]	N.O.[7]	N.O.[7]
SSMBLG 2	33.5	12	Web/C.I.P. Interface	West	2 ¾"	N.O.[7]	N.O.[7]	N.O.[7]	N.O.[7]
SSMBLG 3	28	0	Longitudinal Joint	N/A	2 ¾"	¾" (West) 1" (West)	North South	9 ½" 9 ¼"	*B.P.*[10]: 0"-6 ½"; **A**: 6 ½"- 8 ½"; **2**: 8 ½"- 9 ½" *B.P.*[10]: 0"-6 ½"; **A**: 6 ½"- 7"; **B**: 7"-8 ½"; **A**: 8 ½"- 8 ¾"; **2**: 8 ¾"- 9 ¼"
SSMBLG 3	28	12	Web/C.I.P. Interface	West	2 ¾"	N.O.[7]	N.O.[7]	N.O.[7]	N.O.[7]
SSMBLG 4	31.5	0	Longitudinal Joint	N/A	2 ¾"	1" West 1 ¾" West	North South	11 ½" 10 ¾"	(North) **A**: 0"- ½"; **B**: ½"-1 ½"; **A**: 1 ½"-3 ½"; **B**: 3 ½"-7 ¼"; **2**: 7 ¼"-8 ¼"; **A**: 8 ¼"-9"; **2**: 9"-11 ½" (South) **B**: 0"-1 ¼"; **A**: 1 ¼"-1 ¾"; **B**: 1 ¾"-5"; **A**: 5"-5 ½"; **B**: 5 ½"-7 ¼"; **2**: 7 ¼"-8"; **A**: 8"-8 ¼"; **2**: 8 ¼"-10 ¾"
SSMBLG 4	31.5	12	Web/C.I.P. Interface	East	2 ¾"	¼" West ¼" West	North South	10 ¼" (up); 3" (down) 10 ¾" (up); 3" (down)	*BP*[10]: 0"-6"; **A**: 6"-6 ½"; **2**: 6 ½"-10 ¼" (up); *B.P.*[10]: 0"-3"; **B**: 1"-2 ½" (down) *B.P.*[10]: 0"-6"; **A**: 6"-7 ¾"; **2**: 7 ¾"-10 ¾" (up); *B.P.*[10]: 0"-3" (down)
SSMBLG 4	31.5	12	Web/C.I.P. Interface	West	2 ¾"	0" 0"	North South	10 ¾" 10 ¾"	*B.P.*[10]: 0"-10 ¼"; **2**: 10 ¼"-10 ¾" *B.P.*[10]: 0"-9 ½"; **A**: 9 ½"-10"; **2**: 10"-10 ¾"
SSMBLG 5	28	1	Longitudinal Joint	East	2 ¾"	1 ½" East 1 ¼" East	North South	7 ½" 4"	**B**: 0"- ½"; **A**: ½"-1 ¼"; **B**: 1 ¼"-1 ¾"; **A**: 1 ¾"-4"; **2**: 4"-7 ½" **A**: 0"- ½"; **B**: ½"-1 ½"; **A**: 1 ½"-2 ¾"; **2**: 2 ¾"-4"
SSMBLG 5	31.5	0	Longitudinal Joint	N/A	2 ¾"	N.O.[7]	N.O.[7]	N.O.[7]	N.O.[7]
SSMBLG 5	31.5	12	Web/C.I.P. Interface	East	2 ¾"	0" 0"	North South	7" (up); 1 ½" (down) 7" (up); ¾" (down)	**2**: 0"-7" (up); **2**: 0"-1 ½" (down) **2**: 0"-7" (up); **2**: 0"-¾" (down)
SSMBLG 5	31.5	12	Web/C.I.P. Interface	West	2 ¾"	0" 0"	North South	1" (down) 1" (down)	**A**: 0"- ½"; **2**: ½"-1" **A**: 0"- ½"; **2**: ½"-1"

G-6

Core Designation					Core Characteristics	Reflective Crack Characteristics			
Specimen[1]	X-Coord.[2]	Y-Coord.[3]	Location of Core	Side of Longitudinal Joint	Core Diameter	Distance from Longitudinal Joint or Web/C.I.P. interface	Side of Core	Depth of Crack[4]	Width of Crack[5]
SSMBLG 6	32	0	Longitudinal Joint	N/A	2 ¾"	¾" East 1 ½" East	North South	1 ¾" 2 ¼"	**2**: 0"-1 ¾" **A**: 0"-1 ¾"; **2**: 1 ¾"-2 ¼"
SSMBLG 6	32	12	Web/C.I.P. Interface	East	2 ¾"	0" 0"	North South	8" (up); 2" (down) 7" (up); 1 ½" (down)	(North) **B**: 0"-2 ½"; **A**: 2 ½"-4 ½"; **2**: 4 ½"-8" (up); **B**: 0"-1 ½"; **2**: 1 ½"-2" (down) (South) **B**: 0"-1 ¼"; **A**: 1 ¼"-4 ¼"; **2**: 4 ¼"-7" (up); **B**: 0"-1 ½" (down)
SSMBLG 6	32	12	Web/C.I.P. Interface	West	2 ¾"	0" 0"	North South	¾" ¼"	**2**: 0"- ¾" **2**: 0"- ¼"
SSMBLG 7	28.5	0	Longitudinal Joint	N/A	2 ¾"	N.O.[7]	N.O.[7]	N.O.[7]	N.O.[7]
SSMBLG 7	31.5	0	Longitudinal Joint	N/A	2 ¾"	N.O.[7]	N.O.[7]	N.O.[7]	N.O.[7]
SSMBLG 7	31.5	12	Web/C.I.P. Interface	East	2 ¾"	N.O.[7]	N.O.[7]	N.O.[7]	N.O.[7]
SSMBLG 7	31.5	12	Web/C.I.P. Interface	West	2 ¾"	N.O.[7]	N.O.[7]	N.O.[7]	N.O.[7]

[1]"C1" represents "Concept 1 Bridge Specimen"; "S1" represents "Span 1"; "S2" represents "Span 2"; SSMBLG" represents "Subassemblage Bridge Specimen"

[2]Distance along the longitudinal joint referenced from side of specimen, (inches)

[3]Distance perpendicular to and referenced from the longitudinal joint (inches)

[4]Depth of crack measured up (unless specified otherwise) from the reference line indicated in the Longitudinal Joint Elevation Figure.

[5]Width of crack, classifications (bold font) defined by Table XY, ranging between depths from the reference point defined on the Bridge Specimen - Longitudinal Joint Elevation Figure.

[6]"S.C." indicates that core was split into two half-diameter cores due to a "Saw Cut" made during the demolition of the bridge specimen

[7]"N.O." represents "No Reflective Cracks Observed"

[8]Reflective crack is continuous with shrinkage crack from surface, so beginning and end points are undefined

[9]Reflective crack lies along precast flange/C.I.P. interface (i.e. reflective crack has no vertical depth)

[10]"B.P." represents that this is actually a "Break Plane" between two sections of the core that is likely to have been a reflective crack prior to breaking apart. It is not an in-situ reflective crack.

Appendix H
Subassemblage Sectional Calculations and Analyses

H.1: Subassemblage Specimen Design Calculations and Analyses

The subassemblage specimens utilized during the current study were primarily considered to provide a comparison of the benefits of particular crack control details relative to one another. To provide an understanding of the expected behavior of each specimen based on its individual measured material properties, geometry, and reinforcement details, a detailed analytical investigation was completed. The relevant calculations are outlined below.

Sectional calculations for subassemblage specimens

Specimen dimensions and variables are defined in plan and elevation views of the subassemblage specimens in Figures H.1 and H.2, respectively. As shown in Figure H.1, each subassemblage specimen was 120 in. "long", which corresponded with the span length during the load tests while the width of each specimen, which was measured parallel to the longitudinal precast joint, ranged from 62.75 in. to 67.25 in. The origin of each specimen, for reference regarding the instrumentation and reinforcement placement, as well as general documentation, was located on the bottom of the section, directly at the precast joint. The origin corresponded with the end of each specimen nearest the embedded transverse reinforcement that was spaced a clear distance of 3 in. from the face, which was consistent among each of the seven subassemblage specimens, and is also shown in Figure H.2.

As illustrated in Figure H.2, the total section depth is composed of the precast member depth, which was either 12 in. or 16 in., plus a 2 in. thick deck for all specimens other than SSMBLG3-HighBars, which had a 2 in. thick deck near the joint region, and tapered to 3-1/2 in. a distance of 15 in. in either direction from the joint.
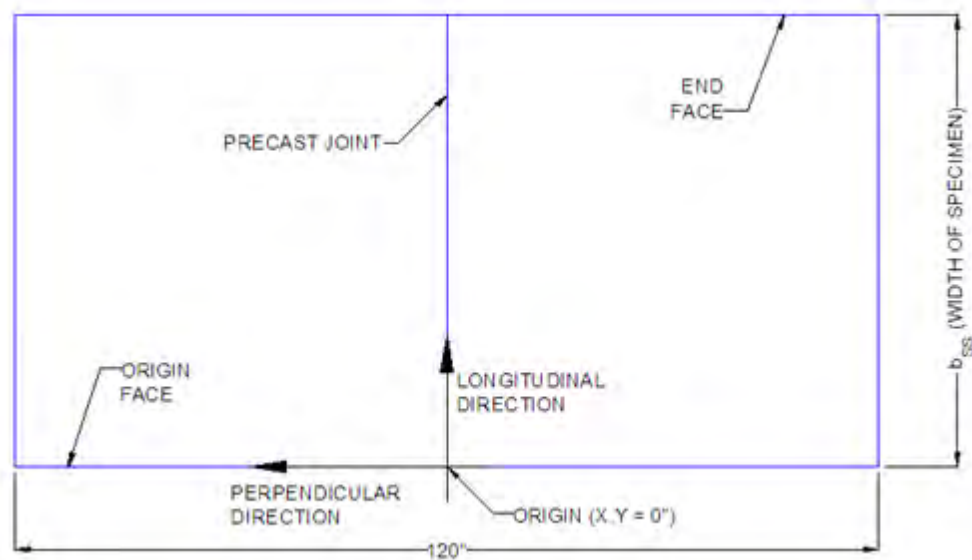
Figure H.1: Plan view of subassemblage specimens

H-1
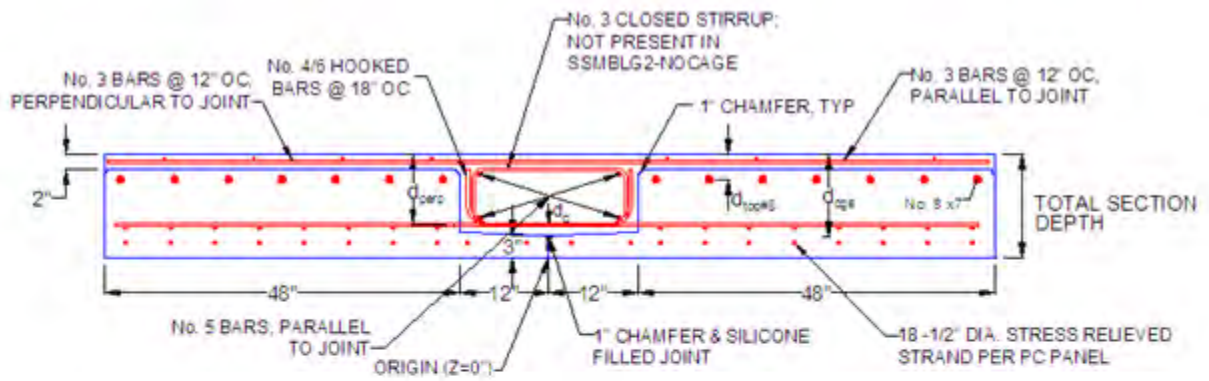
(a) Subassemblage section view perpendicular to joint
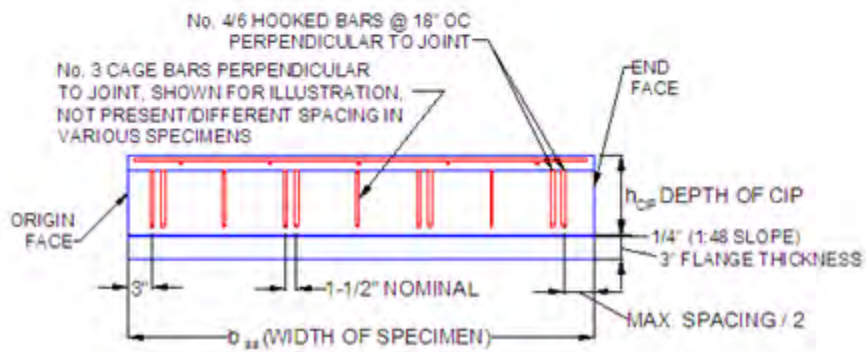
(b) Subassemblage section view parallel to joint

Figure H.2: Subassemblage specimen section views

Note: The index number in each array represents the subassemblage specimen number. For example, subassemblage 1 will always be represented as the first entry in any array variable

Useful units:

$$kip := 1000lbf \qquad\qquad ksi := \frac{kip}{in^2} \qquad\qquad \text{Specimen range variable:} \qquad i := 1..7$$

Specimen naming includes specimen number - description - maximum distance between perpendicular reinforcement immediately above the precast joint

$Specimens_i :=$

"1-Control1-9in."
"2-NoCage-18in."
"3-HighBars-9in."
"4-Deep-9in."
"5-No.6Bars-9in."
"6-Frosch-4.5in."
"7-Control2-9in."

Material Properties

Measured material properties have been documented herein. Values were measured on the first day of laboratory testing for each specimen

CIP Elastic modulus: tensile strength via 3 point beam test: concrete compressive strength:

E_{cSS_i}	f_{t_i} :	f_{c_i} :
4740ksi	.840ksi	6552psi
5633ksi	.746ksi	6577psi
3933ksi	.678ksi	4726psi
4703ksi	.757ksi	7151psi
4112ksi	.609ksi	5204psi
5270ksi	.806ksi	6898psi
4194ksi	.732ksi	7005psi

Steel elastic modulus: $E_s := 29000ksi$

H-3

Specimen and reinforcement geometry and layout

A_{shook} equals the area of a single perpendicular hooked bar

A_{scage} equals the area of all horizontally oriented legs of the stirrups in the cage at a given level, i.e.: all the horizontal legs of the stirrups at the bottom of the trough

b_{ss} equals nominal width, perpendicular to joint, of specimen

h_{cip} equals the nominal depth of CIP concrete between top of precast flange at the joint and the top of the specimen

d_{shook} equals the nominal depth of the hooks oriented perpendicular to joint, measured from top of specimen to center of reinforcement, also used as depth of lower horizontal leg of cage reinforcement

$d_{toplegofcage}$ equals the nominal depth of the center of the top horizontal leg of the cage reinforcement from the top of the specimen

d_{sdeck} equals the nominal depth of the center of the deck reinforcement oriented perpendicular to the joint from the top of the specimen

A_{shook_i}

$.2in^2$
$.2in^2$
$.2in^2$
$.2in^2$
$.44in^2$
$.2in^2$
$.2in^2$

A_{scage_i}

$.33in^2$
$0in^2$
$.33in^2$
$.33in^2$
$.33in^2$
$1.43in^2$
$.33in^2$

Area of No. 3 mild reinforcement:

$$A_3 := 0.11in^2$$

b_{ss_i}	h_{cip_i}	d_{shook_i}
62.75in	11in	9.75in
67.25in	11in	9.75in
62.75in	11in	7in
62.75in	15in	13.75in
62.75in	11in	9.6875in
64.0in	11in	9.75in
62.75in	11in	9.75in

$$d_{sdeck} := 1.5625in$$

$$d_{toplegofcage} := 2.25in$$

H-4

Location of uncracked and cracked neutral axis

Method of transformed sections is utilized to calculate neutral axis (NA) location, the modular ratio is the ratio of the elastic modulus of the steel to the elastic modulus of the concrete

$$n_i := \frac{E_s}{E_{cSS_i}} \qquad\qquad n = \begin{pmatrix} 6.1 \\ 5.1 \\ 7.4 \\ 6.2 \\ 7.1 \\ 5.5 \\ 6.9 \end{pmatrix}$$

Depth of neutral axis is measured from top surface of each specimen, as follows:

$$A_{total} \cdot \bar{x} = \sum_i \left[(n-1)A_s \cdot d_s + A_{concrete} \cdot d_{concrete} \right]^{\blacksquare}$$

Black box in upper right corner of equation indicates that the equation is not evaluated; only shown for illustration of method of calculation

Uncracked

$$x_{uncracked_i} := \frac{\dfrac{b_{ss_i} \cdot \left(h_{cip_i} \right)^2}{2} + \left(n_i - 1 \right) \cdot \left[\left(8A_{shook_i} + A_{scage_i} \right) \cdot d_{shook_i} + A_{scage_i} \cdot d_{toplegofcage} \cdots \right. }{b_{ss_i} \cdot h_{cip_i} + \left(n_i - 1 \right) \cdot \left(8A_{shook_i} + 2A_{scage_i} + 5A_3 \right)}$$

$$x_{uncracked} = \begin{pmatrix} 5.54 \\ 5.53 \\ 5.5 \\ 7.54 \\ 5.61 \\ 5.54 \\ 5.54 \end{pmatrix} \cdot in$$

Cracked

Neutral axis depth is calculated as above; the depth of the concrete in compression is equal to the neutral axis depth, therefore a quadratic equation must be solved. The coefficients of the quadratic equation are as follows:

The cracked transformed section is shown in Figure H.3:
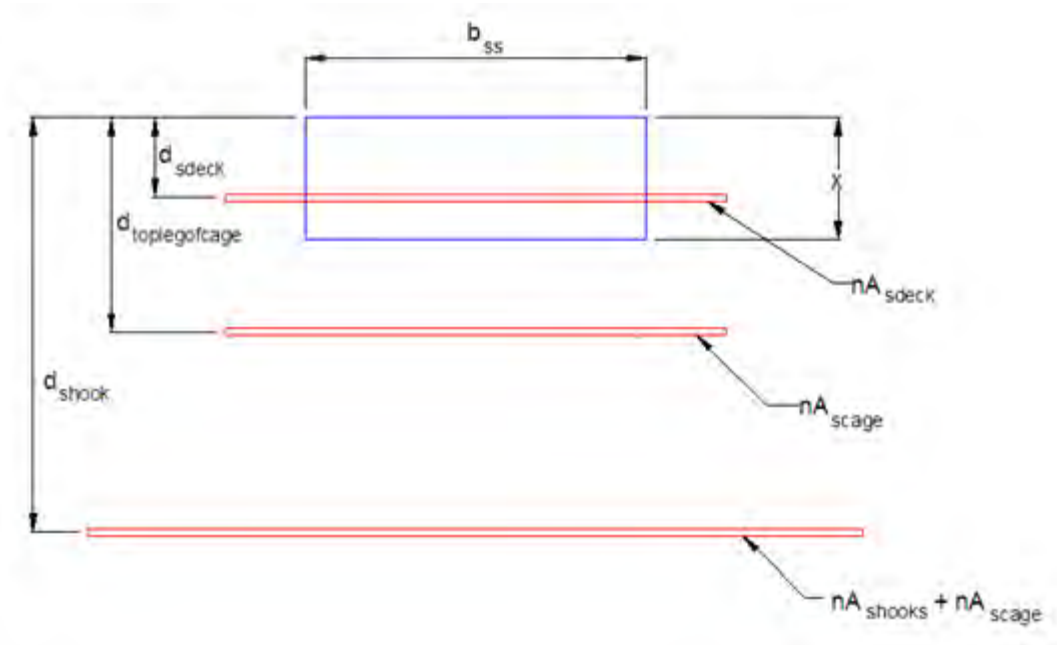
Figure H.3: Cracked transformed section, with neutral axis, x, measured from top of section

The area of the deck reinforcement should be subtracted from the total area of the section by multiplying by (n-1) if x is greater than d_{sdeck}, but should not be subtracted if x less than d_{sdeck}.

Assume that the neutral axis is larger than the depth of the deck reinforcement:

quadratic equation for neutral axis depth (x): $\qquad Ax^2 + Bx + C = 0$

$$A = \frac{b_{ss_i}}{2}$$

$$B = n_i \cdot \left(8 A_{shook_i} + 2 A_{scage_i}\right) + \left(n_i - 1\right) \cdot 5 \cdot A_3$$

$$C = -\left[n_i \cdot \left(8 A_{shook_i} + A_{scage_i}\right) \cdot d_{shook_i} + n_i \cdot A_{scage_i} \cdot d_{toplegofcage} + \left(n_i - 1\right) \cdot 5 \cdot A_3 \cdot d_{sdeck}\right]$$

H-6

The polyroots function is used to evaluate the parabolic function for each specimen. The polyroots function takes the coefficients A,B, and C and returns, for a parabolic function, two roots. Let the matrix *Coeffs* be the matrix of coefficients, with each column representing a subassemblage specimen:

$$\text{Coeffs} := \begin{vmatrix} M \leftarrow 0 \\ \text{for } i \in 1..7 \\ \quad M_{3,i} \leftarrow \dfrac{b_{ss_i}}{2} \\ \quad M_{2,i} \leftarrow \left[n_i \cdot \left(8 A_{shook_i} + 2 A_{scage_i} \right) + \left(n_i - 1 \right) \cdot \left(5 A_3 \right) \right] \cdot \dfrac{1}{in} \\ \quad M_{1,i} \leftarrow -\left[n_i \cdot \left[\left(8 A_{shook_i} + A_{scage_i} \right) \cdot d_{shook_i} \right] + n_i \cdot \left(A_{scage_i} \cdot d_{toplegofcage} \right) \cdots \right. \\ \left. \qquad + \left(n_i - 1 \right) \cdot 5 A_3 \cdot d_{sdeck} \right] \cdot \dfrac{1}{in^2} \\ \text{return } M \end{vmatrix}$$

$$\text{Coeffs} = \begin{pmatrix} -124.1 & -83.9 & -110.6 & -172.7 & -273.5 & -184.1 & -140.3 \\ 16.6 & 10.5 & 20.2 & 16.8 & 32.8 & 27 & 18.9 \\ 31.4 & 33.6 & 31.4 & 31.4 & 31.4 & 32 & 31.4 \end{pmatrix} \cdot in$$

<-- constant term
<-- linear term
<-- parabolic term

Evaluating the polyroots function returns two roots, the second root, denoted by the subscript 2 after the polyroots function, is the positive root for each case, which is saved to the variable $x_{cracked}$

$$x_{cracked_i} := polyroots\left(\text{Coeffs}^{\langle i \rangle} \right)_2 \cdot in$$

$$x_{cracked} = \begin{pmatrix} 1.74 \\ 1.43 \\ 1.58 \\ 2.09 \\ 2.48 \\ 2.01 \\ 1.84 \end{pmatrix} \cdot in$$

Check assumption that the depth of the deck reinforcement is less than the depth of the neutral axis:

$$NAcheck_i := \begin{vmatrix} \text{"OK"} & \text{if } x_{cracked_i} > d_{sdeck} \\ \text{"NG"} & \text{if } x_{cracked_i} < d_{sdeck} \end{vmatrix}$$

$$d_{sdeck} = 1.563 \cdot in$$

$$NAcheck = \begin{pmatrix} \text{"OK"} \\ \text{"NG"} \\ \text{"OK"} \\ \text{"OK"} \\ \text{"OK"} \\ \text{"OK"} \\ \text{"OK"} \end{pmatrix}$$

H-7

Recalculate the depth of the neutral axis with the area of the deck reinforcement not subtracted from the total area of the section when the deck reinforcement is below the neutral axis depth

$$
\text{Coeffs} := \quad
\begin{aligned}
&M \leftarrow 0 \\
&\text{for } i \in 1..7 \\
&\qquad M_{3,i} \leftarrow \frac{b_{ss_i}}{2} \\[6pt]
&\qquad M_{2,i} \leftarrow \left[n_i \cdot \left(8 A_{shook_i} + 2 A_{scage_i} \right) + \left| \begin{aligned} &\left(n_i \cdot 5 A_3 \right) \text{ if } x_{cracked_i} < d_{sdeck} \\ &\left[\left(n_i - 1 \right) \cdot 5 \cdot A_3 \right] \text{ if } x_{cracked_i} > d_{sdeck} \end{aligned} \right. \right] \cdot \frac{1}{\text{in}} \\[6pt]
&\qquad M_{1,i} \leftarrow -\left[n_i \cdot \left[\left(8 A_{shook_i} + A_{scage_i} \right) \cdot d_{shook_i} \right] + n_i \cdot \left(A_{scage_i} \cdot d_{toplegofcage} \right) \dots \right. \\
&\qquad \qquad \left. + \left| \begin{aligned} &\left(n_i \cdot 5 \cdot A_3 \cdot d_{sdeck} \right) \text{ if } x_{cracked_i} < d_{sdeck} \\ &\left[\left(n_i - 1 \right) \cdot 5 \cdot A_3 \cdot d_{sdeck} \right] \text{ if } x_{cracked_i} > d_{sdeck} \end{aligned} \right. \right] \cdot \frac{1}{\text{in}^2} \\[6pt]
&\text{return } M
\end{aligned}
$$

$$
\text{Coeffs} = \begin{pmatrix} -124.1 & -84.7 & -110.6 & -172.7 & -273.5 & -184.1 & -140.3 \\ 16.6 & 11.1 & 20.2 & 16.8 & 32.8 & 27 & 18.9 \\ 31.4 & 33.6 & 31.4 & 31.4 & 31.4 & 32 & 31.4 \end{pmatrix} \cdot \text{in}
$$

                             <-- constant term

                             <-- linear term

                             <-- parabolic term

Evaluating the polyroots function returns two roots, the second root, denoted by the subscript 2 after the polyroots function, is the positive root for each case, which is saved to the variable $x_{cracked}$

$$
x_{cracked_i} := polyroots \left(\text{Coeffs}^{\langle i \rangle} \right)_2 \cdot \text{in}
$$

$$
x_{cracked} = \begin{pmatrix} 1.74 \\ 1.43 \\ 1.58 \\ 2.09 \\ 2.48 \\ 2.01 \\ 1.84 \end{pmatrix} \cdot \text{in}
$$

Moment of Inertia

The moment of inertia of the section is the moment of inertia of the individual components about centroid of component plus area of component multiplied by the distance to centroid of section squared (parallel axis theorem). Assume reinforcement contributes only the portion defined by the parallel axis theorem:

$$I_{section} = \sum_{components} I_{component} + A_{component} \cdot distance^2$$

Uncracked

$$I_{uncracked_i} := \frac{1}{12} b_{ss_i} \cdot \left(h_{cip_i}\right)^3 + b_{ss_i} \cdot h_{cip_i} \cdot \left(\left|\frac{h_{cip_i}}{2} - x_{uncracked_i}\right|\right)^2 \dots$$
$$+ \left(n_i - 1\right) \left[8 A_{shook_i} \cdot \left(\left|d_{shook_i} - x_{uncracked_i}\right|\right)^2 + A_{scage_i} \cdot \left(\left|d_{shook_i} - x_{uncracked_i}\right|\right)^2 \dots \right.$$
$$\left. + A_{scage_i} \cdot \left(\left|d_{toplegofcage} - x_{uncracked_i}\right|\right)^2 + 5 \cdot A_3 \cdot \left(\left|d_{sdeck} - x_{uncracked_i}\right|\right)^2 \right]$$

$$I_{uncracked} = \begin{pmatrix} 7199 \\ 7614 \\ 7064 \\ 18184 \\ 7433 \\ 7450 \\ 7236 \end{pmatrix} \cdot in^4$$

H-9

Cracked

$$
\begin{aligned}
I_{cracked_i} := {} & \frac{1}{12} b_{ss_i} \left(x_{cracked_i}\right)^3 + b_{ss_i} \cdot x_{cracked_i} \cdot \left(\left|\frac{x_{cracked_i}}{2} - x_{cracked_i}\right|\right)^2 \cdots \\
& + n_i \cdot \left[8 A_{shook_i} \cdot \left(\left|d_{shook_i} - x_{cracked_i}\right|\right)^2 + A_{scage_i} \cdot \left(\left|d_{shook_i} - x_{cracked_i}\right|\right)^2 \cdots \right] \cdots \\
& \qquad \left. + A_{scage_i} \cdot \left(\left|d_{toplegofcage} - x_{cracked_i}\right|\right)^2 \right] \\
& + \left| \begin{array}{l} \left[n_i \cdot 5 \cdot A_3 \cdot \left(\left|d_{sdeck} - x_{cracked_i}\right|\right)^2 \right] \text{ if } x_{cracked_i} < d_{sdeck} \\ \left[\left(n_i - 1\right) \cdot 5 \cdot A_3 \cdot \left(\left|d_{sdeck} - x_{cracked_i}\right|\right)^2 \right] \text{ if } x_{cracked_i} > d_{sdeck} \end{array} \right.
\end{aligned}
$$

$$
I_{cracked} = \begin{pmatrix} 868 \\ 636 \\ 502 \\ 1810 \\ 1732 \\ 1173 \\ 966 \end{pmatrix} \cdot in^4
$$

Curvature

$$
M_{crack_i} := \frac{f_{t_i} \cdot I_{uncracked_i}}{h_{cip_i} - x_{uncracked_i}}
$$

$$
M_{crack} = \begin{pmatrix} 1107 \\ 1038 \\ 870 \\ 1845 \\ 840 \\ 1099 \\ 970 \end{pmatrix} \cdot in \cdot kip
$$

Flexural capacity of specimen. Because the transverse hooks are not continuous into both adjacent precast sections, consider only half of the transverse hooks and none of the reinforcing cage

Calculate β_1 for each specimen, β_1 is a function of the concrete strength, rounded to the nearest thousand:

$$
rounded\_f_{c_i} := round\left(f_{c_i} \cdot \frac{1}{psi}, -3 \right)
\qquad
rounded\_f_{c_i} = \begin{pmatrix} 7000 \\ 7000 \\ 5000 \\ 7000 \\ 5000 \\ 7000 \\ 7000 \end{pmatrix}
$$

H-10

$$\beta_{1_i} := \begin{vmatrix} 0.85 & \text{if } \text{rounded\_f}_{c_i} \leq 4000 \\ \left[0.85 - 0.05 \cdot \dfrac{\left(\text{rounded\_f}_{c_i} - 4000 \right)}{1000} \right] & \text{if } \text{rounded\_f}_{c_i} > 4000 \\ 0.65 & \text{if } \text{rounded\_f}_{c_i} > 8000 \end{vmatrix} \qquad \beta_1 = \begin{pmatrix} 0.70 \\ 0.70 \\ 0.80 \\ 0.70 \\ 0.80 \\ 0.70 \\ 0.70 \end{pmatrix}$$

$$M_{flexure_i} := 4\,A_{shook_i} \cdot 60\text{ksi} \cdot \left(d_{shook_i} - \frac{\beta_{1_i} \cdot x_{cracked_i}}{2} \right) \qquad M_{flexure} = \begin{pmatrix} 439 \\ 444 \\ 306 \\ 625 \\ 918 \\ 434 \\ 437 \end{pmatrix} \cdot \text{in} \cdot \text{kip}$$

$$\phi_{uncracked_i} := \frac{M_{crack_i}}{E_{cSS_i} \cdot I_{uncracked_i}} \qquad \phi_{uncracked} = \begin{pmatrix} 0.000032 \\ 0.000024 \\ 0.000031 \\ 0.000022 \\ 0.000027 \\ 0.000028 \\ 0.000032 \end{pmatrix} \cdot \frac{1}{\text{in}}$$

The same moment is applied immediately before and after cracking:

$$\phi_{cracked_i} := \frac{M_{crack_i}}{E_{cSS_i} \cdot I_{cracked_i}} \qquad \phi_{cracked} = \begin{pmatrix} 0.000269 \\ 0.00029 \\ 0.000441 \\ 0.000217 \\ 0.000118 \\ 0.000178 \\ 0.00024 \end{pmatrix} \cdot \frac{1}{\text{in}}$$

H-11

Compare results, normalized by the Control 1 specimen:

$$\frac{x_{uncracked_i}}{x_{uncracked_1}} = \begin{pmatrix} 1.000 \\ 0.998 \\ 0.993 \\ 1.362 \\ 1.013 \\ 1.000 \\ 1.001 \end{pmatrix} \qquad \frac{x_{cracked_i}}{x_{cracked_1}} = \begin{pmatrix} 1.000 \\ 0.822 \\ 0.909 \\ 1.203 \\ 1.422 \\ 1.157 \\ 1.054 \end{pmatrix}$$

$$\frac{I_{uncracked_i}}{I_{uncracked_1}} = \begin{pmatrix} 1.000 \\ 1.058 \\ 0.981 \\ 2.526 \\ 1.032 \\ 1.035 \\ 1.005 \end{pmatrix} \qquad \frac{I_{cracked_i}}{I_{cracked_1}} = \begin{pmatrix} 1.000 \\ 0.732 \\ 0.578 \\ 2.084 \\ 1.995 \\ 1.351 \\ 1.112 \end{pmatrix}$$

$$\frac{\phi_{uncracked_i}}{\phi_{uncracked_1}} = \begin{pmatrix} 1.000 \\ 0.746 \\ 0.966 \\ 0.665 \\ 0.847 \\ 0.863 \\ 0.986 \end{pmatrix} \qquad \frac{\phi_{cracked_i}}{\phi_{cracked_1}} = \begin{pmatrix} 1.000 \\ 1.077 \\ 1.641 \\ 0.806 \\ 0.438 \\ 0.661 \\ 0.891 \end{pmatrix}$$

H-12

Because the instrumentation utilized during the subassemblage specimens tests was zeroed at the start of each load step, the effects of self weight was not included in the relative strains measured with the embedment resistive gages. The predicted increase in the transverse stress in the hooked bars was calculated as shown below:

The yield strength of a representative piece of the mild steel reinforcement was measured in the laboratory to be approximately 70 ksi. Therefore the predicted steel stresses are below the yield and are assumed to be linear elastic.

$$q := .15 \frac{kip}{ft^3} \qquad\qquad w_i := q \cdot b_{ss_i} \cdot \left(h_{cip_i} + 3in \right) \qquad\qquad \text{(3" is added for flange depth)}$$

Steel members used for clamping apparatus; 2 of each member were used in the setup

$$\text{L8x8x1-1/18} \qquad w_{L8} := 56.9 \frac{lbf}{ft} \qquad L_{L8} := 84in \qquad W_{L8} := 2 \cdot w_{L8} \cdot L_{L8} = 796.6\,lbf$$

$$\text{W8x35} \qquad L_{W8x35} := 68.5in \qquad W_{W8x35} := 2 \cdot 35 \frac{lbf}{ft} \cdot L_{W8x35} = 399.583\,lbf$$

SW = self weight

$$M_{SW_i} := \frac{w_i \cdot L_{span}^2}{8} + \frac{\left(W_{L8} + W_{W8x35} \right) \cdot L_{span}}{4} \qquad\qquad M_{SW} = \begin{pmatrix} 158.0 \\ 166.9 \\ 158.0 \\ 193.4 \\ 158.0 \\ 160.4 \\ 158.0 \end{pmatrix} \cdot in \cdot kip$$

$$\varepsilon_{sSW_i} := \frac{n_i \cdot M_{SW_i} \cdot \left(d_{shook_i} - x_{cracked_i} \right)}{E_{cSS_i} I_{cracked_i}} \cdot 10^6 \qquad\qquad \varepsilon_{sSW} = \begin{pmatrix} 1.881 \times 10^3 \\ 1.995 \times 10^3 \\ 3.198 \times 10^3 \\ 1.633 \times 10^3 \\ 1.128 \times 10^3 \\ 1.105 \times 10^3 \\ 2.134 \times 10^3 \end{pmatrix} \mu\varepsilon$$

H-13

The strain in the transverse hooks due to self weight and the weight of the clamping system was between 1105 and 3198με. The largest transverse strain measured in the hooks was approximately 1455με in SSMBLG1-Control1, in which case the state of strain near that gage was expected to be closer to 3336με. The onset of strain hardening was measured to occur at a strain of approximately 6000με, which suggested that strain hardening was not expected in the reinforcement at the locations that were instrumented, however because the locations of the strain gages on the steel bars were localized over the joint, and were unlikely to coincide with the location of cracking, the strain in the reinforcement at the location of the crack may have been larger.

Appendix I

Subassemblage Instrumentation Designation, Nominal, and Measured Locations

I.1 Subassemblage Specimen Instrumentation Designation

The instrumentation for the subassemblage specimens was labeled as described in this section. An example designation is given in Figure I.1.

1. The first character indicated the specimen and type of gage. The specimen was labeled as SSLGX, where 'X' was the specimen number. The gage types are listed below:

- C = VW concrete embedment gage
- T = Steel resistive gage
- M = Polyester Mold concrete resistive gage
- S = VW spot-weldable gage

There was a hyphen after the first character.

2. The second character indicated the position of the gage along the length of the precast joint

- 2.0 = Origin face of specimen
- 3.0 = 1/2 point, or middle of specimen measured along length of joint

There was a hyphen separating the fourth and fifth characters

3. The third character indicated where the gage was located in the depth of the cross section. Numerical values representing the depth start at the bottom of the section and increase towards the top of the section.

    i.   1.0 = Gage was located above precast flange at same depth as transverse hooked reinforcement
    ii.   1.5 = Gage was located at mid-height of cage stirrup
    iii.   2.0 = Gage was located above precast web

4. The fourth character indicated the orientation of the gage. All gages were oriented transversely, or perpendicular to the precast joint.

- T = Transverse

There was a hyphen after the sixth character.

7. The seventh character indicated the number of the gage at that position.

    ii.   1 = For gage located farthest south in gage group

    iv.   n = For gage located farthest north in gage group

I-1

Type of Gage:
120 Ω concrete gage

Location along the PC Joint:
Middle of specimen along joint

Orientation of Gage::
Transverse

SSLG1M-3.0-1.0T-1

Specimen Number:
Subassemblage 1

Location within the Depth::
Gage above precast flange

Gage Number::
Southernmost gage
in gage group
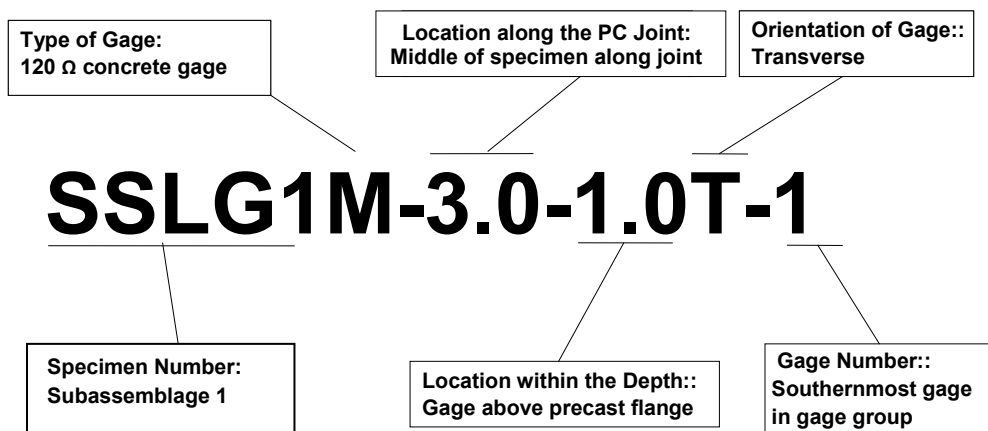
Figure I.1: Subassemblage specimen strain gage designation example

I.2 Measured Locations of Subassemblage Specimen Instrumentation

All of the instrumentation in the subassemblage specimens was measured to the nearest ¼ in. The sign convention of the gage ordinates is shown in Figure I.2. The X axis (which was defined to be the North direction) was measured along the length of the precast joint from the origin face, which was defined to be the face where the transverse hooked reinforcement was always 3 in. away; Y was measured in the E-W direction from the joint (W positive); the Z axis was measured in the vertical direction from the bottom of the precast sections (upward positive). The measurements are given in Table I.1.
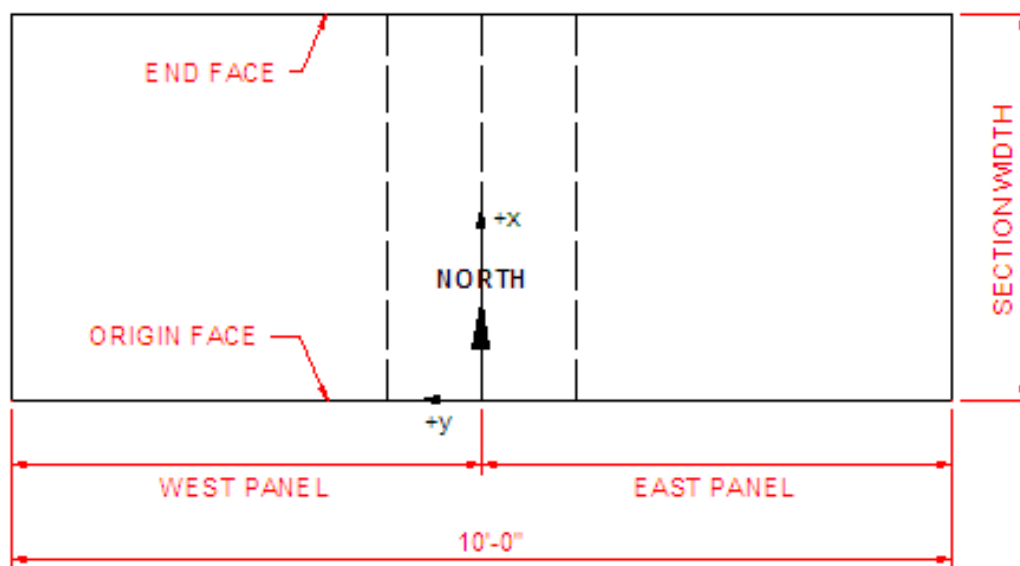
Figure I.2: Sign convention for the strain gage location measurements in the Concept 1 Laboratory Bridge

Table I.1: Nominal and measured instrumentation locations in the subassemblage specimens

Gage	Nominal Locations			Measured Locations		
	X	Y	Z	X	Y	Z
X from edge (N+); Y from joint (W+); Z from bottom of section						
Resistive gages located near middle cross section						
SSLG1M-3.0-1.0T-1	33.5	-4.5	4.5	33.25	-4.5	4.25
SSLG1M-3.0-1.0T-2	30.5	0	4.5	29.5	0	4.25
SSLG1M-3.0-1.0T-3	33.5	4.5	4.5	33	4.5	4
SSLG1M-3.0-1.5T-1	33.5	-4.5	8	33.5	-4.5	9
SSLG1M-3.0-1.5T-2	30.5	0	8	29.5	0	9.25
SSLG1M-3.0-1.5T-3	33.5	4.5	8	33.25	4.5	9.25
SSLG1M-3.0-2.0T-1	33.5	-4.5	14	33.5	-4.5	11.75
SSLG1M-3.0-2.0T-2	30.5	0	14	28.75	0	12
SSLG1M-3.0-2.0T-3	33.5	4.5	14	33.5	4.5	12
Resistive gages located near origin cross section						
SSLG1Ta-2.0-1.0T-1	23	0	4.5	23	0	4
SSLG1Mb-2.0-1.0T-1	18	0	4.5	18	0	4.25
SSLG1Mc-2.0-1.0T-1	15.5	-4.5	4.5	16.25	-4.5	4.25
SSLG1Mc-2.0-1.0T-2	12.5	0	4.5	12.75	0	4.25
SSLG1Mc-2.0-1.0T-3	15.5	4.5	4.5	16.25	4.5	4.25
SSLG1Mc-2.0-1.5T-1	15.5	-4.5	8	16.75	-4.5	8.25
SSLG1Mc-2.0-1.5T-2	12.5	0	8	12.5	0	9.25
SSLG1Mc-2.0-1.5T-3	15.5	4.5	8	16.5	4.5	8.5
SSLG1Md-2.0-1.0T-1	9	0	4.5	9	0	4.25
SSLG1Te-2.0-1.0T-1	5	0	4.5	5	0	4
Vibrating wire gage located near middle cross section						
SSLG1C-3.0-1.0T-1	34	0	4.5	34.25	0	4.5

X from edge (N+); Y from joint (W+); Z from bottom of section						
Gage	Nominal Locations			Measured Locations		
	X	Y	Z	X	Y	Z
Gages located near middle cross section						
SSLG2M-3.0-1.0T-1	33.5	-4.5	4.5	33.75	-4.5	4.5
SSLG2M-3.0-1.0T-2	30.5	0	4.5	30.75	0	4.75
SSLG2M-3.0-1.0T-3	33.5	4.5	4.5	33.5	4.5	4.5
SSLG2M-3.0-1.5T-1	33.5	-4.5	8	33.5	-4.5	6.75
SSLG2M-3.0-1.5T-2	30.5	0	8	30.5	0	6.25
SSLG2M-3.0-1.5T-3	33.5	4.5	8	33.5	4.5	6.5
SSLG2M-3.0-2.0T-1	33.5	-4.5	14	33.75	-4.5	9.75
SSLG2M-3.0-2.0T-2	30.5	0	14	21	0	9.5
SSLG2M-3.0-2.0T-3	33.5	4.5	14	33.5	4.5	9.5
Gages located near origin cross section						
SSLG2Ta-2.0-1.0T-1	23	0	4.5	22.75	0	4
SSLG2Mb-2.0-1.0T-1	18	0	4.5	18.75	0	4.25
SSLG2Mc-2.0-1.0T-1	15.5	-4.5	4.5	15.5	-4.5	4.5
SSLG2Mc-2.0-1.0T-2	12.5	0	4.5	12.25	0	4.25
SSLG2Mc-2.0-1.0T-3	15.5	4.5	4.5	15	4.5	4.25
SSLG2Mc-2.0-1.5T-1	15.5	-4.5	8	15.75	-4.5	7.25
SSLG2Mc-2.0-1.5T-2	12.5	0	8	12.5	0	7.25
SSLG2Mc-2.0-1.5T-3	15.5	4.5	8	15.25	4.5	7.25
SSLG2Md-2.0-1.0T-1	9	0	4.5	8.75	0	4.5
SSLG2Te-2.0-1.0T-1	5	0	4.5	4.75	0	4
Vibrating wire gage located near middle cross section						
SSLG2C-3.0-1.0T-1	34	0	4.5	35.5	0	4.5

Gage	Nominal Locations			Measured Locations		
X from edge (N+); Y from joint (W+); Z from bottom of section						
	X	Y	Z	X	Y	Z
Gages located near middle cross section						
SSLG3M-3.0-1.0T-1	33.5	-4.5	4.5	33.5	-4.5	4.25
SSLG3M-3.0-1.0T-2	30.5	0	4.5	29.75	0	4
SSLG3M-3.0-1.0T-3	33.5	4.5	4.5	33	4.5	4.25
SSLG3M-3.0-1.5T-1	33.5	-4.5	8	33.25	-4.5	7.5
SSLG3M-3.0-1.5T-2	30.5	0	8	30.75	0	8.25
SSLG3M-3.0-1.5T-3	33.5	4.5	8	31.75	4.5	8.25
SSLG3M-3.0-2.0T-1	33.5	-4.5	14	33.25	-4.5	13.5
SSLG3M-3.0-2.0T-2	30.5	0	14	29.5	0	14.25
SSLG3M-3.0-2.0T-3	33.5	4.5	14	33.5	4.5	15
Gages located near origin cross section						
SSLG3Ta-2.0-1.0T-1	23	0	4.5	22.5	0	4
SSLG3Mb-2.0-1.0T-1	18	0	4.5	18	0	4.25
SSLG3Mc-2.0-1.0T-1	15.5	-4.5	4.5	15	-4.5	4
SSLG3Mc-2.0-1.0T-2	12.5	0	4.5	13.25	0	4.5
SSLG3Mc-2.0-1.0T-3	15.5	4.5	4.5	15.75	4.5	4.25
SSLG3Mc-2.0-1.5T-1	15.5	-4.5	8	15.5	-4.5	7.75
SSLG3Mc-2.0-1.5T-2	12.5	0	8	13.25	0	8.25
SSLG3Mc-2.0-1.5T-3	15.5	4.5	8	15.75	4.5	8
SSLG3Md-2.0-1.0T-1	9	0	4.5	8.25	0	4.25
SSLG3Te-2.0-1.0T-1	5	0	4.5	5	0	4
Vibrating wire gage located near middle cross section						
SSLG3C-3.0-1.0T-1	34	0	4.5	33.5	0	4.25

I-5

Gage	Nominal Locations			Measured Locations		
X from edge (N+); Y from joint (W+); Z from bottom of section						
	X	Y	Z	X	Y	Z
Gages located near middle cross section						
SSLG4M-3.0-1.0T-1	33.5	-4.5	4.5	33.25	-4.5	4.5
SSLG4M-3.0-1.0T-2	30.5	0	4.5	30.5	0	4
SSLG4M-3.0-1.0T-3	33.5	4.5	4.5	33	4.5	4
SSMBLG4M-3.0-1.25T-2a	33.5	0	8	33.5	0	8.25
SSMBLG4M-3.0-1.25T-2b	30.5	0	8	29.75	0	8.25
SSLG4M-3.0-1.5T-1	33.5	-4.5	8	33.5	-4.5	10
SSLG4M-3.0-1.5T-2	30.5	0	8	30	0	10.25
SSLG4M-3.0-1.5T-3	33.5	4.5	8	33.25	4.5	9.75
SSLG4M-3.0-2.0T-1	33.5	-4.5	14	33.25	-4.5	15.5
SSLG4M-3.0-2.0T-2	30.5	0	14	29.75	0	15.74
SSLG4M-3.0-2.0T-3	33.5	4.5	14	33.5	4.5	15.5
Gages located near origin cross section						
SSLG4Ta-2.0-1.0T-1	23	0	4.5	23	0	4.25
SSLG4Mb-2.0-1.0T-1	18	0	4.5	18	0	4.5
SSLG4Mc-2.0-1.0T-1	15.5	-4.5	4.5	15.5	-4.5	4.25
SSLG4Mc-2.0-1.0T-2	12.5	0	4.5	12	0	4.5
SSLG4Mc-2.0-1.0T-3	15.5	4.5	4.5	15.25	4.5	4.5
SSLG4Mc-2.0-1.5T-1	15.5	-4.5	8	16	-4.5	10
SSLG4Mc-2.0-1.5T-2	12.5	0	8	11.25	0	10.5
SSLG4Mc-2.0-1.5T-3	15.5	4.5	8	15.75	4.5	9.75
SSLG4Md-2.0-1.0T-1	9	0	4.5	6.25	0	4.25
SSLG4Te-2.0-1.0T-1	5	0	4.5	4.75	0	4
Vibrating wire gage located near middle cross section						
SSLG4C-3.0-1.0T-1	34	0	4.5	34.75	0	4.5

X from edge (N+); Y from joint (W+); Z from bottom of section						
Gage	Nominal Locations			Measured Locations		
	X	Y	Z	X	Y	Z
Gages located near middle cross section						
SSLG5M-3.0-1.0T-1	33.5	-4.5	4.5	32.75	-4.5	4.25
SSLG5M-3.0-1.0T-2	30.5	0	4.5	31	0	4.25
SSLG5M-3.0-1.0T-3	33.5	4.5	4.5	32.5	4.5	4
SSLG5M-3.0-1.5T-1	33.5	-4.5	8	32.75	-4.5	8.5
SSLG5M-3.0-1.5T-2	30.5	0	8	30.25	0	8.25
SSLG5M-3.0-1.5T-3	33.5	4.5	8	32.5	4.5	8.5
SSLG5M-3.0-2.0T-1	33.5	-4.5	14	32.5	-4.5	13.75
SSLG5M-3.0-2.0T-2	30.5	0	14	29.75	0	14.5
SSLG5M-3.0-2.0T-3	33.5	4.5	14	33.25	4.5	14.5
Gages located near origin cross section						
SSLG5Ta-2.0-1.0T-1	23	0	4.5	23.75	0	4.25
SSLG5Mb-2.0-1.0T-1	18	0	4.5	18.5	0	4.25
SSLG5Mc-2.0-1.0T-1	15.5	-4.5	4.5	15.5	-4.5	4
SSLG5Mc-2.0-1.0T-2	12.5	0	4.5	12.25	0	4.5
SSLG5Mc-2.0-1.0T-3	15.5	4.5	4.5	15.25	4.5	4.25
SSLG5Mc-2.0-1.5T-1	15.5	-4.5	8	15.25	-4.5	8
SSLG5Mc-2.0-1.5T-2	12.5	0	8	12.75	0	8.25
SSLG5Mc-2.0-1.5T-3	15.5	4.5	8	16	4.5	8.25
SSLG5Md-2.0-1.0T-1	9	0	4.5	8.25	0	4.25
SSLG5Te-2.0-1.0T-1	5	0	4.5	4.5	0	4.25
Vibrating wire gage located near middle cross section						
SSLG5C-3.0-1.0T-1	34	0	4.5	34.5	0	4.25

X from edge (N+); Y from joint (W+); Z from bottom of section						
Gage	Nominal Locations			Measured Locations		
	X	Y	Z	X	Y	Z
Gages located near middle cross section						
SSLG6M-3.0-1.0T-1	33.5	-4.5	4.5	34.5	-4.5	4.5
SSLG6M-3.0-1.0T-2	30.5	0	4.5	30.5	0	4.25
SSLG6M-3.0-1.0T-3	33.5	4.5	4.5	34.75	4.5	4.25
SSLG6M-3.0-1.5T-1	33.5	-4.5	8	34.75	-4.5	6
SSLG6M-3.0-1.5T-2	30.5	0	8	30.25	0	7.5
SSLG6M-3.0-1.5T-3	33.5	4.5	8	34.75	4.5	6
SSLG6M-3.0-2.0T-1	33.5	-4.5	14	35	-4.5	11.75
SSLG6M-3.0-2.0T-2	30.5	0	14	31	0	11.75
SSLG6M-3.0-2.0T-3	33.5	4.5	14	35	4.5	11.5
Gages located near origin cross section						
SSLG6Ta-2.0-1.0T-1	23	0	4.5	23	0	4
SSLG6Mb-2.0-1.0T-1	18	0	4.5	18.5	0	4
SSLG6Mc-2.0-1.0T-1	15.5	-4.5	4.5	15	-4.5	4
SSLG6Mc-2.0-1.0T-2	12.5	0	4.5	13	0	4
SSLG6Mc-2.0-1.0T-3	15.5	4.5	4.5	15.25	4.5	4.25
SSLG6Mc-2.0-1.5T-1	15.5	-4.5	8	15.25	-4.5	7.25
SSLG6Mc-2.0-1.5T-2	12.5	0	8	12.5	0	7.5
SSLG6Mc-2.0-1.5T-3	15.5	4.5	8	15.25	4.5	7.75
SSLG6Md-2.0-1.0T-1	9	0	4.5	9.25	0	4
SSLG6Te-2.0-1.0T-1	5	0	4.5	5.25	0	4
Vibrating wire gage located near middle cross section						
SSLG6C-3.0-1.0T-1	34	0	4.5	32.5	0	4.5

X from edge (N+); Y from joint (W+); Z from bottom of section						
Gage	Nominal Locations			Measured Locations		
	X	Y	Z	X	Y	Z
Gages located near middle cross section						
SSLG7M-3.0-1.0T-1	33.5	-4.5	4.5	32.5	-4.5	4.25
SSLG7M-3.0-1.0T-2	30.5	0	4.5	30.25	0	4.5
SSLG7M-3.0-1.0T-3	33.5	4.5	4.5	32.5	4.5	4.25
SSLG7M-3.0-1.5T-1	33.5	-4.5	8	33	-4.5	7.5
SSLG7M-3.0-1.5T-2	30.5	0	8	30.75	0	8.25
SSLG7M-3.0-1.5T-3	33.5	4.5	8	32.5	4.5	8.25
SSLG7M-3.0-2.0T-1	33.5	-4.5	14	32	-4.5	11.75
SSLG7M-3.0-2.0T-2	30.5	0	14	30.5	0	12.25
SSLG7M-3.0-2.0T-3	33.5	4.5	14	32	4.5	12
Gages located near origin cross section						
SSLG7Ta-2.0-1.0T-1	23	0	4.5	23	0	4.25
SSLG7Mb-2.0-1.0T-1	18	0	4.5	17.75	0	4.25
SSLG7Mc-2.0-1.0T-1	15.5	-4.5	4.5	16	-4.5	4.25
SSLG7Mc-2.0-1.0T-2	12.5	0	4.5	12.25	0	4.5
SSLG7Mc-2.0-1.0T-3	15.5	4.5	4.5	16	4.5	4.25
SSLG7Mc-2.0-1.5T-1	15.5	-4.5	8	15.75	-4.5	8
SSLG7Mc-2.0-1.5T-2	12.5	0	8	12.5	0	7.5
SSLG7Mc-2.0-1.5T-3	15.5	4.5	8	16	4.5	7.5
SSLG7Md-2.0-1.0T-1	9	0	4.5	9	0	4.5
SSLG7Te-2.0-1.0T-1	5	0	4.5	5.25	0	4.5
Vibrating wire gage located near middle cross section						
SSLG7C-3.0-1.0T-1	34	0	4.5	34.5	0	4.25